NASA Conference Publication 3317

Upper Atmosphere Research Satellite Validation Workshop III: Temperature and Constituents Validation

Edited by
William L. Grose and John Gille

Proceedings of a workshop sponsored by the
National Aeronautics and Space Administration,
Washington, D.C., and held in
Atlanta, Georgia
September 20–23, 1993

November 1995

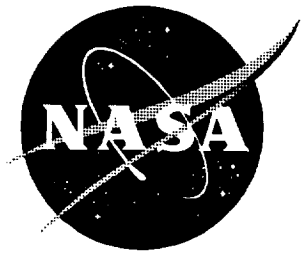

NASA Conference Publication 3317

Upper Atmosphere Research Satellite Validation Workshop III: Temperature and Constituents Validation

Edited by
William L. Grose
Langley Research Center • Hampton, Virginia

John Gille
National Center for Atmospheric Research • Boulder, Colorado

Proceedings of a workshop sponsored by the
National Aeronautics and Space Administration,
Washington, D.C., and held in
Atlanta, Georgia
September 20–23, 1993

National Aeronautics and Space Administration
Langley Research Center • Hampton, Virginia 23681-0001

November 1995

This publication is available from the following sources:

NASA Center for AeroSpace Information
800 Elkridge Landing Road
Linthicum Heights, MD 21090-2934
(301) 621-0390

National Technical Information Service (NTIS)
5285 Port Royal Road
Springfield, VA 22161-2171
(703) 487-4650

PREFACE

The Upper Atmosphere Research Satellite (UARS) was launched in September 1991. Since that time data have been retrieved continuously from the various instruments on the UARS spacecraft. These data have been processed by the respective instrument science teams and subsequently archived in the UARS Central Data Handling Facility (CDHF) at the NASA Goddard Space Flight Center, Greenbelt, Maryland.

Prior to use of the UARS data for scientific investigations, an extensive data validation effort was organized and has been active continuously to ensure reliability of the data. Shortly after establishment of the UARS Science Team, a data validation plan was formulated. It was decided that responsibility for validation of the data from any individual instrument would not rest solely with that instrument team. Rather, the validation would be accomplished by the UARS Science Team as a whole, including both the instrument and theoretical science teams. In practice, the validation of the data from the various instruments has been accomplished through (1) intercomparison of like quantities amongst the UARS instruments; (2) comparison of UARS data with correlative (non-UARS) data obtained during the UARS mission; (3) comparison of UARS data with existing data; and (4) comparison of UARS data with results from atmospheric simulation models.

This report contains the proceedings from one of the three workshops held to evaluate the progress in validating UARS constituents and temperature data and to document the quality of that data. The first workshop was held in Oxford, England, in March 1992, five and one-half months after UARS launch. The second workshop was held in Boulder, Colorado, in October 1992. Since launch, the various data have undergone numerous revisions. In many instances these revisions are a result of data problems identified during the validation workshops. Thus, the formal validation effort is a continually ongoing process.

William L. Grose
NASA Langley Research Center

CONTENTS

1. INTRODUCTION

The Upper Atmosphere Research Satellite (UARS) was launched on Sptember 12, 1991. Within a month of launch the observatory began to acquire data from the various instruments on board. Since that time, the data has been processed into geophysical quantities and archived at the Central Data Handling Facility (CDHF) at the NASA Goddard Space Flight Center, Greenbelt, Maryland.

From the moment of data capture, an enormous amount of effort and resources has been expended on evaluation and validation of the data. An initial workshop was hosted at Oxford University, England in March 1992 to begin the formal process of validation and intercomparison of temperature and constituent data from the CLAES, HALOE, ISAMS, and MLS instruments on UARS. Consideration was initially restricted to temperature and those constituents (ozone, water vapor, methane, and nitrous oxide) thought to be in a satisfactory status to begin validation. Two periods (December 9-11, 1991 and January 9-11, 1992) were chosen corresponding to periods in which the four instruments were in normal operating modes and looking nortward into the winter hemisphere. Participants included representatives frm both the UARS instrument teams and theory teams. The workshop concentrated on intercomparison of data from the various UARS instruments and comparison with a few correlative sets and other existing data. The results of that workshop focused upon evaluating the quality of the data and identifying discrepancies and problems requiring future attention.

A second validation workshop was hosted at the National Center of Atmospheric Research (NCAR) in Boulder, Colorado in October 1992. All retrieved temperature and constituents were evaluated at this workshop. Additional validation periods were selected in addition to the periods chosen for the Oxford workshop. The period of April 15-20, 1992 was chosen as a time when the instruments would be observing the Southern Hemisphere. A third period, August 8-11, 1992, was chosen to correspond to a time when data was available from the Observatoire de Haute Provence, France. A final period, August 25-30, 1992, was chosen when the instruments would be looking into the Southern Hemisphere and might be expected to observe interesting features associated with development of the Antarctic ozone hole. Comparisons were also done for specific periods when correlative data were available which would be of unique interest to one or more of the instruments.

The results presented in this document derive from the third UARS validation workshop which was hosted at Georgia Tech in Atlanta, Georgia on September 20-23, 1993. The workshop adopted the format of the two previous ones. By this time, the various data sets had gone through a number of changes as problems were identified and retrieval algorithms were improved. These results are applicable to the data version which were available at the date of the workshop and will become obsolete as the data are continually improved. This report is primarily intended for the UARS science team, but may be helpful as well to the general scientific community as they use the UARS data products.

The work contained herein is the product of the entire UARS science team and would have been impossible without their dedication and diligence. Special thanks are due John Gille, William Grose, Derek Cunnold, James Holton, Donald Wuebbles, Steven Massie, and Gary Thomas who coordinated the various working groups who assembled the chapters of this report and to P. Newman and L. Coy who prepared the meteorological overview.

2 CALIBRATION, ALGORITHM, AND PROCESSING STATUS

2.1 HALOE Version 12 Calibration, Algorithm, and Processing Status

2.1.1 Overview

The HALOE Version 12 processing produces retrieved profiles of temperature, pressure, HF, HCl, CH_4, NO, NO_2, O_3, and H_2O. In addition, aerosol extinction profiles are retrieved for each modulation channel wavelength (2.45, 3.4, 3.47, and 5.26 μm) and the CO_2 channel wavelength of 2.8 μm. Although significant improvements are still to come (many already verified in our experimental code and scheduled for future release), current results for all products are suitable for research use, if quality and error estimates are noted.

Error estimates in the data set currently do not include systematic components. Only noise and error due to aerosol correction are considered, thereby underestimating errors where these two mechanisms are not the dominant error source. At the completion of the validation effort, systematic components will be reported in validation papers and software tools for adding systematic error to the random component will be made available. To date the systematic sources are still being accurately quantified. The following gives a brief status review for each retrieved parameter.

2.1.2 Temperature and Pressure

CURRENT RESULTS

A pressure reference is obtained by matching a simulated signal, using NMC or UKMO data, to a measured signal at 2.8 μm. A temperature and pressure profile is then retrieved from 35 km up to the S/N limits (about 80 km). Statistically, errors range from 3 to 10 K over those altitudes. These errors add only a small contribution to the species retrieval error for an occultation experiment. A high altitude model (MSIS) is used above, with NMC used below retrieved results (< 35 km). There does appear to be a 4 to 5-K cold bias in the upper stratosphere that leads to lower pressure values, as a function of altitude, at high altitudes through hydrostatic build-up of pressure. This effect is still being investigated, but it appears to result in pressures that are about 10 to 15% low, inducing 10 to 15% high mixing ratios above 50 km. Density as a function of altitude, inferred from mixing ratio, pressure and temperature, will not be affected by this problem.

FUTURE IMPROVEMENTS

The above problems will be addressed, plus other enhancements are to be included. Iterative correction for aerosol to allow retrievals to lower altitudes is planned. At present aerosol interference limits temperature retrievals to 35 km and above. Higher resolution retrievals will be implemented using all the oversampled data.

2.1.3 Hydrogen Fluoride (HF)

CURRENT RESULTS

The HF results are very good. The first year of data has some sunspot contamination in the signal that degrades results for 5 to 10% of the data. This is flagged in the data, so the user must take note. Low altitudes (below 20 km) are quite noisy but appear to be statistically good. Correlative comparisons indicate ± 15% accuracy.

FUTURE IMPROVEMENTS

Higher resolution is planned using all of the oversampled data. This procedure has been demonstrated to achieve better results, sensing small-scale wave structure much more faithfully. Computational resources have prevented implementation to date, but this limitation is being alleviated.

2.1.4 Hydrogen Chloride (HCl)

CURRENT RESULTS

HCl results are very good. Both quality and problems are nearly identical to those for HF. However, an additional incorrect 15 to 20% variation with orbital beta angle is observed at high altitudes (above the 1 mbar level). The HCl signal is the most complex to model, due to strong CH_4 interference, which is most likely the source of the difficulty. The problem is being vigorously pursued. Nevertheless, correlative comparisons at stratospheric levels show a statistical accuracy of ± 15%.

FUTURE IMPROVEMENTS

The expected improvements are identical to those for HF, except for the beta angle dependence. It is expected that the beta dependence will be corrected for releases in the coming year.

2.1.5 Methane (CH_4)

CURRENT RESULTS

Methane retrievals appear to be of excellent quality. Results indicate nearly the identical tracer behavior as for HF (only in a negative sense, due to opposite vertical slope). Good results are retrieved up to 70 km and higher, with very minimal error due to sunspots. Errors over the stratosphere are ± 15%, as inferred from correlative measurements.

FUTURE IMPROVEMENTS

As with HCl and HF, multiple pass retrievals at high resolution appear to improve the results through the aerosol layers.

2.1.6 Nitrogen Oxide (NO)

CURRENT RESULTS

From all indications, the NO results are very good. Retrievals extend from the tropopause to 130 km and show the morphology, magnitude, and solar activity dependence that is expected. Total NO_x comparisons with LIMS data and old 1985 ATMOS comparisons indicate ± 15% accuracy in the stratosphere, degrading as expected with noise at higher altitude. Often, mixing ratios drop below instrument sensitivity in the mesosphere between 60 and 85 km, but increase to detectable levels again above those altitudes. The user should ignore values below the error estimates contained in the data.

FUTURE IMPROVEMENTS

As with the other gas correlation measurements (HF, HCl, and CH_4), NO will show substantial improvement with multiple pass retrievals that use more of the data in the densely sampled signal profiles.

2.1.7 Ozone (O_3)

CURRENT RESULTS

Ozone results have shown excellent agreement with correlative data. In the stratosphere below 20 km the agreement is within 5%. Below 20 km, aerosol correction, signal model accuracy, and gradient and tracking errors quickly degrade the results. At high altitudes (up to 90 km), the results are statistically very good, but noise limited, so the estimated errors should be noted.

FUTURE IMPROVEMENTS

Refraction scintillation of the solar edge, used for tracking, has limited profile fidelity in the troposphere. Better processing techniques, using gimbal position data, show promise for greatly improving these lower-altitude data. Correction methods for gradients along the line of sight are being explored. This error mechanism is not a problem above 20 km and is still being quantified below 20 km.

2.1.8 Water Vapor (H_2O)

CURRENT RESULTS

Current results are excellent, as inferred from correlative comparisons with balloon and microwave data. Statistically, errors throughout the stratosphere appear to be ± 10%, with profiles continuing up to 80 km. At high altitudes, the error increases as expected with decreasing S/N. Tracking fidelity, clouds, and variation of aerosol along the viewing track quickly degrade the results in the troposphere.

FUTURE IMPROVEMENTS

H_2O results will benefit from the same processing improvements noted for ozone, although lower opacity and less aerosol extinction has allowed better results in the lower stratosphere.

2.1.9 Nitrogen Dioxide (NO_2)

CURRENT RESULTS

NO_2 results show excellent agreement with correlative measurements, ± 10% (± 0.5 ppb), statistically. When sunset values are combined with NO, the data show remarkable consistency with LIMS morphology. Aerosol correction uncertainty can cause as much as ± 1 ppb error in the lower stratosphere. A first-order correction for diurnal effects is applied using estimated relative line-of-sight gradients. Simulations have shown that the error due to this mechanism is less than 5% in the mid-stratosphere and above.

FUTURE IMPROVEMENTS

No substantial improvement is expected.

2.1.10 Aerosol

CURRENT RESULTS

The aerosol retrievals at the gas correlation and CO_2 channel wavelengths are producing excellent results, as evidenced from correlative comparisons and the ability to make corrections to the radiometer signals. The noise level for all of the channels is approximately 2×10^{-6} km^{-1}, limited by the signal digitization. The systematic errors appear to be less than 10%, judging from the success in correcting the radiometer results.

FUTURE IMPROVEMENTS

No major improvement is expected.

2.1.11 General Planned Improvements

The following planned enhancements to the algorithm should yield significant improvements to the already good results:

- A more comprehensive error estimate.
- Higher resolution multipass retrievals of gas correlation signals.
- Vertical-tracking error corrections at lower altitudes.
- Enhanced temperature and pressure retrievals.
- Horizontal gradient modeling. (Ignoring horizontal gradients induces very little error for occultation measurements.)
- Improved spectroscopy in the HCl and CH_4 channels.
- Identification and removal of beta angle dependence mechanism in the HCl results.
- Optimization of the retrieval smoothing constraints for improved resolution.

2.1.12 Conclusion

The HALOE processing algorithm is currently giving good results for all channels. Although significant improvements will be realized in the coming year, all data products are now suitable for use in research activities, if error estimates are observed and validation results noted.

The error estimates listed above are for altitudes with good experimental sensitivity, unless otherwise noted, and are meant only as a rough guide to current understanding. The user should observe random error estimates included in the data set and refer to other sections of this document as well as future validation papers for more detailed estimates of error. There is always the possibility of uncovering error components yet to be recognized, which could alter these estimates.

2.2 CLAES Calibration, Algorithm, and Processing Status

2.2.1 Processing Status: CLAES Data Versions (Past, Present, and Future)

Several CLAES data versions have been produced and catalogued on the UARS Central Data Handling Facility (CDHF). The version V0006 is the version that was evaluated during the UARS Validation Workshop activities held in Atlanta on 20–24 September 1993. It is this version that is discussed in this report.

An improved instrument science mode was implemented beginning in early January 1992. The V0006 retrieval can process data from this mode only. Later software versions will be capable of processing data obtained prior to 9 January 1992.

Previous CLAES data versions have been processed and catalogued on the UARS CDHF. None will be transferred to the DAAC, but for historic interest these are:

- Data Version V0003
  24 days in November and December 1991.
  This data version was evaluated at the UARS Oxford Validation Workshop held in March 1992.
- Data Version V0004
  75 days from January 92 through 12 September 92 were processed to V0004.
  This data version was partially evaluated at the Aix-En-Provence UARS Science Team Meeting held in June 1992.
- Data Version V0005
  231 days from January 92 through April 93 were processed to V0005.
  This data version was evaluated at the UARS Boulder validation workshop held in October 1992 and discussed in the report *Upper Atmosphere Research Satellite Validation Workshop II Report: Temperature and Constituents.*

Plans are to implement processing software improvements that are described in sections 2.2.11 and 2.2.3.2 below into a version that will go into production approximately February 1994.

2.2.2 Calibration

2.2.2.1 Review of CLAES Spectral Regions

Various spectral regions of 5 to 15 cm^{-1} in width have been selected for geophysical parameter retrieval. Blocker filters transmit light in these regions and serve as order sorters for much higher resolution (of the order 0.2 to 0.6 cm^{-1}) tilt tuned Fabry-Perot etalons. In operation of the CLAES standard science mode, data are obtained at etalon resolution in several spectral channels in each of these blocker regions. In order to provide retrieval stability, data are obtained in more spectral channels than there are species contributing to radiance in that blocker region. For example, in the 790-cm^{-1} region, the blocker filter is approximately 4 cm^{-1} wide and centered on 791 cm^{-1}. Three species contribute significantly to the radiance, CO_2, O_3, and aerosol, but nine spectral channels of about 0.2 cm^{-1} in width are used. The blocker filter regions and the species (subtypes to search for when using the UCSS query system) to be retrieved from data obtained in each of these regions are given in Table 2.2–1 below.

Table 2.2–1—Blocker Filter Regions and Subtypes of Retrieved Parameters

Blocker Filter Band Center	Blocker Number	Subtypes of Retrieved Parameters
790	8	TEMP (from CO_2 radiance), O3B8 (ozone), AERO790
780	9	O3B9 (ozone), CLONO2, AERO780
843	7	CFCL3*
880	6	HNO3, AERO880
925	5	CF2CL2, AERO925
1257	4	CH4, N2O, N2O5*, AERO1257
1605	3	H2O, NO2, AERO1605
1897	2	NO, AERO1897

The blocker filter number designation is included in Table 2.2–1 for future reference.

The "*" beside the species $CFCl_3$ and N_2O_5 calls attention to the fact that the state of the retrieval is so preliminary for these species that they are not deemed useful enough for science purposes. They have been catalogued on the UARS CDHF to provide a baseline to compare against future improved versions. Ozone retrieved in blocker filter 9 (O3B9) is recommended over that retrieved in blocker filter 8 (O3B8).

There is an additional CLAES blocker filter region near 2843 cm^{-1} where data have been obtained, but to date no retrieval has been incorporated in the production processing software. Data in this region are to be used for retrieval of HCl, aerosol and for properties of OH chemiluminescence emissions. Data have been obtained in this short wave region by use of special detectors as described by Roche et al. (1993) and require specialized processing by comparison to data obtained in the other eight CLAES blocker regions. Since HCl is not designated a primary measurement for CLAES, processing of data obtained in this region has not been given high priority.

In the blocker region 7 there is the possibility to retrieve NO_2 and O_3, but this has not been attempted in the data version V0006.

2.2.2.2 Radiometric Calibration

An aperture-sized blackbody calibrator is mounted on the inside of the CLAES door. When the door is closed the blackbody calibrator fills the instrument FOV and CLAES is operated in the radiometric calibration mode 2. In this mode every other EMAF is identical with the operation of the CLAES nominal science mode 1.

CLAES radiometric calibration parameters are obtained by a least squares fit of count rate to blackbody radiance as the door-mounted blackbody calibrator cools to equilibrium each time the door is shut. Calibration parameters are obtained in this way for 20 detectors and more than 50 spectral channels. The RMS difference between the fit and the data provides a noise estimate.

When the door is open the calibrator equilibrates at approximately 245 K. When the door is closed the calibrator cools down to equilibration of about 160 K. However, early in the mission when the cryogen was colder than its equilibrium temperature, this number was more like 145 K.

Early in the mission the gains of the detectors were set for atmospheric measurement during the blackbody cool down and this procedure worked well. However, as the equilibrium temperature for the closed-door blackbody increased with time, tserious problems developed in that the atmospheric gains were so high that for some detectors and channels the blackbody never reached a low enough temperature for the detector to come out of saturation. This problem was fixed early in 1992 by using smaller gains during cool down than for atmospheric observations. However, considerable effort is required in the calibration and retrieval software to compensate for the problem and the change in operations. Although a stop-gap approach to solve the problem has been implemented, manifestations still remain in the CLAES data. The largest impact was on ozone retrievals from blocker 9. There has been essentially no impact on retrievals from blockers 8, 4, 3, and 2. In the final processing software, we expect to practically eliminate problems due to this effect.

A second and less serious problem with the radiometric calibration is associated with channels for which relatively few points free of saturation are obtained on a door blackbody calibrator cool down. These cases occur most frequently for the long wave blocker regions. These cases do not occur for blocker region 2 for example. In these cases the current software essentially linearly connects the region where data exists to where it is zero. However, we know by looking at the short wave cases (less photons at a given temperature) that there is some nonlinearity in the calibration curve at low photon illumination, where the linear assumption is made for the long wave channels. This known error is present in the V0006, but algorithms that use the nonlinear characteristic curves as observed in the short-wave regions to extrapolate to zero in the long-wave cases are in development, and this error will be fixed in the next version. The magnitude of the error may be such to help account for CLAES temperature retrieval being systematically a degree or so cooler than other UARS instruments in the 1–10 mbar region, for example.

2.2.2.3 Zero Level Subtraction

CLAES was designed so that a positive count rate of several hundred counts would be output when observing a zero radiance level. In the mission it has turned out that there are two problems with the zero level that were not readily observable in ground tests. The ground tests had to contend with significant 60-cycle interference that masked these problems.

The first of these problems involves an approximate 0.38-Hz modulation in the zero level which was erroneously thought to be a part of the 60-Hz problem during ground test. Therefore, it was thought this effect would disappear in orbit. The amplitude and phase of this effect varies from detector to detector, as functions of gain and integration time. It also varies slowly with time.

The second of these problems is more subtle. For some of the detectors the DC component of the zero level apparently changes somewhat as the radiance level approaches zero. Thus, if the zero level DC component is calibrated from the zero radiance case, it results in subtraction of an incorrect zero level in the case where radiance is present. This effect is small enough that it presents no problem for moderately large signals. However, at high altitudes the problem is present in the current

version V0006 and leads to systematic detector-to-detector pattern error in low signal cases. We now believe that we understand this problem. It is associated with the AC coupling scheme utilized for main array detectors.

To deal with these problems we have developed and implemented special instrument calibration modes in order to obtain data to characterize these effects over the time period of the mission. The approach has been to include a short "zero level" calibration period into each EMAF. In this period light is blocked off from reaching the detectors so that the zero level ripple and DC component can be calibrated. In the science mode this procedure is done for one combination of the four that are used for gain and integration time. A special calibration mode that was run for several EMAFs each day was also implemented to ensure the zero level information is accurately extrapolated to the remaining three gain and integration time combinations.

Preliminary algorithms have used the data from these modes to apply first order corrections for the version V0006. We are currently developing improved algorithms to apply the corrections. These improvements will primarily benefit low signal-to-noise cases such as those occurring in the short wave blocker region 2, and at high altitudes in blocker regions 3, 4, 5, 6, and 7.

2.2.2.4 Spiking

A rudimentary despike algorithm has been developed and implemented in the production of V0006. This algorithm deals specifically with short period spikes of duration 128 ms (this is the basic time interval for which CLAES obtains a data sample). A task remains to develop algorithms for spikes of longer time periods.

2.2.2.5 Spectral Calibration

CLAES uses a special mode 3 to obtain spectral calibration data to verify and fine tune the characterization of blocker filter and etalon spectral transmission. Sensitivity studies of the impact of spectral characterization are also in progress. Revised spectral characteristics have been developed for all blocker regions. These spectral characteristics were used in computing revised EGA (Emissivity Growth Approximation) coefficients to be used in the next production version.

2.2.2.6 Potential Off-Axis and Out-of-Field Effects

In collaboration with NCAR (National Center for Atmospheric Research), we have been studying the data for indications of out-of-field effects that may be due to scattering, BRDF, or even out-of-band spectral effects. Data have been obtained in spacecraft roll-up maneuvers, and special off-axis calibration instrument modes have been run to better define the problem. At this point analysis is difficult due to uncertainties introduced by zero-level subtraction as discussed above. It is expected that more can be learned about potential off-axis and out-of-field effects once the zero-level problem has been fixed. Analysis of the off-axis and roll-up data may then be expected to better define the problem and eventually permit retrievals to higher altitudes and from weaker signals.

2.2.2.7 HCl Detectors

CLAES has a special detector array dedicated to HCl measurement that are DC-coupled (the main array detectors are AC coupled) and have unique problems. We have developed algorithms to subtract zero-level and despike these HCl detector data, but have not included these in the software that produces V0006. These algorithms need further development including capability for zonal mean averaging and improved despiking. The HCl data will be processed in future CLAES versions.

Preliminary results in calibrating and despiking HCl detector data show that HCl radiance can be observed routinely in the sunlit atmosphere due to resonance scattering of sunlight, and that this effect might be used for HCl retrieval. Also, it can be observed in thermal emission in the case of strong stratospheric warmings. For one such event the effect has been successfully modeled using the CLAES retrieved stratospheric warming temperature profile and a near coincidence HALOE HCl retrieval. The data also show a very prominent OH chemiluminescent emission feature, and strong aerosol signal due to both thermal emission and scattering of sunlight. Absorption of the aerosol scattered light by HCl seems to be present in the data, raising the possibility that this effect might also be used for HCl retrieval.

2.2.2.8 Saturations

In cases of large radiances the fourth detector from the bottom of the CLAES array will saturate. This detector and its electronics have a defect in that it has only one-half the dynamic range of the other 19 detectors on the main CLAES detector array. This problem had been noted, and corrected, in the methane channel in blocker 4 prior to release of the software to produce version V0006. The extent of the problem for other blocker regions was not fully appreciated however until many CLAES days had been processed to version V0006. In particular it was also seen to become a considerable problem for the January, southern polar summer case for the blocker 8 CO_2 q-branch channel that is used for temperature retrieval. Since this discovery, the effect has been corrected in development software, but will not be included in production software until the next release.

2.2.2.9 High Altitude Artifacts

These effects have been noted in radiance data at high altitudes. They are an artifact of the process of subtracting telescope thermal emission from atmospheric radiances in high altitude regions where the former is much larger than the latter, and can have uncertainty due to digitization granulation of the temperature of the telescope. This problem will be corrected in the next release.

2.2.2.10 Improvements to Be Implemented in Calibration

Improvements that are planned for future versions include:

- Software upgrades to find and compensate for saturations in atmospheric radiance data;
- Correction of artifacts due to subtraction of thermal telescope emission;
- Improved algorithm for zero level subtraction.
- Use of a nonlinear characteristic curve for calibration of long wave channels;
- Upgrade to utilize improved calibration mode 2 data in the production processing environment;
- Improved spectral filter functions for EGA coefficients;
- Further modifications so that software can handle all versions of the nominal science mode 1, radiometric calibration mode 2, and the zero-level calibration mode 4F;
- Improved despiking algorithm for main array detectors;
- Improved cross-talk/off-axis model (if appropriate, pending analysis);
- Improved HCl radiance despiking and calibration;
- Zonal mean averaging of NO and HCl radiances.

2.2.3 Level 1 → Level 3 Processing

2.2.3.1 Status

The CLAES L3 version V0006 products include the subtypes CLONO2, O3B9, TEMP, O3B8, CFCL3, HNO3, CF2CL2, CH4, N2O, NO2, H2O, NO, and the aerosols AERO780, AERO790, AERO880, AERO925, AERO1257, AERO1605, and AERO1897. The species and the aerosols are ordered by the wavelength region in which the radiance they are retrieved from is obtained, going from long wave to short. The status of these retrieved parameters is summarized in the subsections 2.2.4–2.2.16.

2.2.3.2 Further Improvements Required for the L1 → L3 Software

- Improve approach for regions with more than one continuum emitter such as N_2O_5; and AERO1257 in Blocker region 4, and CFC 11 and AERO843 in Blocker region 7;
- Utilization of upgraded EGA coefficients and generation of additional coefficient sets for use with data obtained in 1991;
- Implement horizontal temperature gradients into temperature retrieval and horizontal species gradients into species retrieval;
- Fine tune utilization of forward radiance model;
- Improved approach to extrapolation into regions where the signal-to-noise ratio is less than or approximately equal to one;
- Improve error estimation procedure;
- Test utility of retrieving O_3 and NO_2 from Blocker region 7 data;
- Comparison exercise to verify production processing forward radiance model;
- Upgrade L1 → L3 algorithms to deal with 1991 data;
- Fine tune pressure registration;

- Improved despiking routines for L2 data;
- An improved approach to dealing with high altitude NO and HCl non-LTE emission;
- Retrievals from zonally averaged radiances of NO and HCl;
- Investigate possibility of retrieving HCl from absorption for the lowest HCl detector for the sunlit aerosol cases;
- Analyze the utility of CO_2 laser line emissions on blocker region 5 for backup temperature retrieval;
- Ongoing comparison with correlative data to guide algorithm fine tuning.

2.2.3.3 CLAES Error Bars

The error estimation procedure for the CLAES version V0006 data is described in a report (Kumer, 1992) that may be obtained from CLAES personnel on request. In summary, the CLAES version V0006 error bars are generally larger than would be predicted from random noise alone. This result occurs because systematic effects render the radiance residuals larger than random noise in the multiple channels in which CLAES measurements are obtained. It is the radiance residuals, rather than the estimated instrument noise, that are used to calculate the CLAES error bars. With this approach enhanced error bars will also be reported for cases where undetected noise spikes have inadvertently been allowed to remain in the level 1 data, or where emitters that are not modeled adequately are contributing significantly to the CLAES data. The error estimation procedure takes account of loss of tangent point sensitivity due to saturation of the target species spectral lines and/or strong vertical gradients. It does not propagate errors in the temperature profile used for the retrieval.

The version V0006 procedure is not the result of a final effort at definitive error estimation. Future CLAES production software versions will use a more mature approach. At this point in algorithm development, the CLAES science team philosophy is that it is more important to concentrate on making the error as small as possible, than it is to concentrate on rigorous error determination.

2.2.4 Temperature

In general the CLAES retrieved temperature has good profile-to-profile consistency along the measurement track, shows no apparent aerosol degradation, shows good day-to-day consistency in zonal mean cross-sections and other mapped products.

A large number of comparisons have been done with lidars, rocketsondes, various balloon-borne instruments, NMC data, and other UARS instruments. These comparisons show the CLAES V0006 retrieved temperatures to have a mean bias of 1-2K (warm) from 100-10 mb and 2-5K (cold) from 10-0.1 mb. The CLAES data tends to agree better with the data from the other UARS sensors than with the NMC data. While CLAES and NMC data show similar features in mapped fields, those from CLAES are generally stronger.

Independent determination of repeatability in the CLAES data, based on statistical analysis, indicates about 1-2K precision in the 100-0.2 mb range which is in reasonable agreement with the reported CLAES L3 data quality error bars. We note that the

independent determination does not discriminate against natural short-scale atmospheric sItructure and is therefore an upper limit.

The major caveats on the use of CLAES V0006 temperature data are:

- CLAES temperatures are still cold with respect to NMC analysis inside the southern polar winter vortex (i. e. poleward of about 65S), especially near 46 mb. Differences average about 5K, but can reach as much as 10K;
- Occasional saturation effects distort temperature profiles in the southern polar summer;
- Occasional spikes are still seen in the profiles.

2.2.5 Aerosol

Aerosol extinction coefficients are being retrieved in seven spectral regions for all latitudes between 80S and 80N. The precision, accuracy, and caveats are discussed in detail in Chapter 3. The seven CLAES spectral regions for which aerosol is retrieved include 1897 cm^{-1}, 1605 cm^{-1}, 1257 cm^{-1}, 925 cm^{-1} 880 cm^{-1}, 790 cm^{-1} and 780 cm^{-1}. The data are suitable for studying the evolution of the Pinatubo cloud, aerosol microphysics, and polar stratospheric clouds.

The measurement accuracy is estimated at between 20 and 30% for the 780 and 790-cm^{-1} channels for moderate and heavy aerosol loading. The range of pressures where the error bars indicate high quality data is between 20 and 68 mbar, although this varies with aerosol loading. The profiles for the 790-cm^{-1} channels agree well with the ISAMS 12.1-μm measurement and with scaled SAGE II measurements within this pressure range. Comparisons with HALOE for the 1897-cm^{-1} measurement are shown to agree to within 20% between 20 and 30 mbar for a selected set of measurements in April, 1992.

Major caveats for data use are:

- the 1257-cm^{-1} measurements are best for daytime conditions because there are algorithmic problems associated with distinguishing nearly continuous N_2O_5 emission from the aerosol continuum at night;
- the 1605-cm^{-1} aerosol absorption coefficients contain a contribution from O_2 pressure-induced absorption which can be corrected by the user;
- the daytime 1897-cm^{-1} aerosol absorption coefficients contain a significant contribution from solar scattering, and there is less data in this spectral region due to frequent profile processing failures (for nighttime data),;
- there is a 20% difference between aerosol extinction measured in the 790-cm^{-1} region and that measured at 780 cm^{-1}, while theory would suggest a maximum difference of 3%. Work is ongoing to correct these problems in the next version.

2.2.6 Ozone (O_3)

As stated above, the CLAES O3B9 subtype of version V0006 ozone is recommende, and it was this data that was considered in the validation activities of this workshop. An overall accuracy of the order of 10–15% for the CLAES B9 channel can be deduced from comparisons with the available correlative data and other UARS instruments. The systematic nature of this error is manifest in a vertical oscillation in the difference

between CLAES and comparison data that is a minimum at approximately 0.68, 3.2, and 10 to 15 mb. The CLAES V0006 ozone retrievals have standard deviations of approximately 15%, and there are spikes in time-tracks and maps. Despite all this, when vertically averaged, the percentage differences with the correlative measurements are generally less than about 10%. Sensitivity studies show no effect on retrieval initializatio

The consensus from this workshop is a recommendation to wait for future versions of the CLAES data for most research studies. For the next version, systematic errors and spikes need to be removed, and more realistic error bars are required.

2.2.7 Water Vapor (H_2O)

The comparisons with correlative data suggest an overall H_2O accuracy of the order of 15% from about 46 to 10 mbar. At high latitudes in winter, however, especially in the south, CLAES mixing ratios increase rapidly with latitude compared with climatology and the MLS data, and are probably unrealistically high, perhaps due to effects of large vertical temperature gradients on the retrieval.

Above 10 mb the comparisons with correlative data suggest accuracy of the order of 25 -30%, with CLAES data generally being lower than the correlative data and that from the other UARS instruments. Also, in the 4.6-0.46 mb range, the CLAES daytime values are 1-2 ppmv higher than nighttime values, with solar zenith angle dependence, suggesting a non-LTE effect.

The data show reasonable qualitative agreement with climatology and the other instruments with respect to zonal mean pressure-latitude cross-sections and longitude-pressure structure. Especially when compared to MLS, time-track data at constant pressure level show good consistency over many orbits. In addition, the good day-to-day repeatability in zonal mean and profile data, lead us to believe that the data precision is of the order of 15%, somewhat better than the error bars would indicate, except in the cold polar regions mentioned previously.

The consensus of this workshop is that CLAES version V0006 H_2O retrievals have deficiencies that might make them difficult for use in scientific investigations.

The main issues to be addressed in future retrieval versions include:

- the high values in the polar winter regions;
- the bias (low) with respect to correlative data;
- day-night differences;
- apparent spiking in some of the high latitude data;
- some low-level dependence on initialization;
- and in general, more correlative comparisons.

2.2.8 Methane (CH_4)

CH_4 is being retrieved at all latitudes between 80S and 80N from about 100 mbar to 0.1 mbar. Our best confidence is from 40 mbar to 0.2 mbar, or where the CH_4 mixing ratio is less than 1.35 ppmv. Our confidence in this range is based on examination of altitude profile data in comparison with correlative data, and investigation of daily zonal mean cross-sections in comparison with ISAMS and climatology. In our good confidence range, CH_4 retrieval appears to be independent of retrieval initialization.

ALTITUDE PROFILES

The suite of available correlative data sets occur between March 1992 and March 1993, at altitudes mainly from 50 to 0.1 mbar, and latitudes from 35N to 50S. Mean differences between CLAES and the correlative data ranged between 10 and 20% above the 40-mbar surface, in many cases comparable with the error estimates provided by the correlative investigators. Overall, this agreement leads us to assign a 20% systematic error to the CH_4 data being retrieved by the current data processing algorithm for the altitude range 40 to 0.2 mbar. The profile-to-profile repeatability (or precision), which is altitude dependent, varies from about 50 ppbv RMS at 1 mbar to 100 ppbv RMS at 40 mbar.

ZONAL MEANS

The only global zonal mean cross-sections available for comparisons with the CLAES data were those from the ISAMS instrument for altitudes above 10 mbar. The instrument data fields are in good structural agreement for the periods examined, and both are in reasonable structural agreement with 2-D models, especially from tropical to middle latitudes. (Note the caveats discussed below, however). The zonal mean profiles show a lot of variability and unusual structure at altitudes below 40 mbar, which is part of the reason for assigning less confidence to this low altitude region.

CAVEATS

The possible effects which may contribute to errors in the altitude region below 40 mbar include insensitivity of the current retrieval to the tangent point radiance variance when the mixing ratio exceeds about 1.35 ppmv, and perhaps some small residual interference from the Pinatubo aerosol cloud in the tropics.

A weak local maximum appears in the CLAES CH_4 data between 10 and 5 mbar at the equator, not seen in the ISAMS data nor in the models A somewhat similar feature appears in the N_2O data, but at a lower altitude (15 mb). These features can persist for many weeks in a particular period, but in other periods virtually disappear. They are being investigated.

There is an issue with respect to differential behavior of CH_4 and N_2O, primarily near the south winter pole. This issue is summarized in the following N_2O section.

2.2.9 Nitrous Oxide (N_2O)

N_2O is being retrieved at all latitudes between 80S and 80N from about 100 mbar to 0.15 mbar. Our best confidence exists from 40 mbar to 0.3 mbar, or where the N_2O mixing ratio is less than 220 ppbv. Our confidence in this range is based on examination of altitude profile data in comparison with correlative data and investigation of daily zonal

mean cross-sections in comparison with ISAMS and climatology. In our good confidence range, N_2O retrieval appears to be independent of retrieval initialization.

ALTITUDE PROFILES

The suite of available correlative data sets covered periods between March 1992 and March 1993, at altitudes mainly from 60 to 0.1 mbar and latitudes from 76N to 50S. Mean differences between CLAES and the correlative data ranged between 10 and 20% above the 40-mbar surface, in many cases comparable with the error estimates provided by the correlative investigators. For surfaces below 60 mbar the mean differences had a considerably wider spread. Overall, we assign a 20% systematic error to the N_2O data being retrieved by the current data-processing algorithm for the altitude range 40 to 0.2 mbar. The profile-to-profile repeatability (or precision), which is altitude dependent, varies from about 7 ppbv RMS at 1 mbar to about 20 ppbv RMS at 40 mbar.

ZONAL MEANS

The only global zonal mean cross-sections available for comparisons with the CLAES data were those from the ISAMS instrument for altitudes above 10 mbar. The instrument data fields are in good structural agreement for the periods examined, and both are in reasonable structural agreement with 2-D models, especially from tropical to middle latitudes. (Note the caveats discussed below, however). The zonal mean profiles show a lot of variability and unusual structure at altitudes below 40 mbar, which is part of the reason for assigning less confidence to this low altitude region.

CAVEATS

The possible effects which may contribute to errors in the altitude region below 40 mbar include insensitivity of the current retrieval to the tangent point radiance variance when the mixing ratio exceeds about 220 ppbv and perhaps some residual interference from the Pinatubo aerosol cloud in the tropics.

A weak local maximum appears in the CLAES N_2O data near 15 mbar at the equator, not seen in the ISAMS data and nor in the models. This feature can persist for many weeks in a particular period, but in other periods virtually disappears. It is being investigated.

As noted in section 2.2.8 above, and discussed in section 7, there is an issue with respect to differential behavior of CH_4 and N_20, primarily near the southern winter pole. From about 55S to 80S in winter, the CH_4 isopleths descend much more steeply than those for N_2O, between about 20 and 2 mbar. Dynamical models would predict that both fields should behave similarly, and the CH_4 data seems in closer agreement with the models. As part of the effort to determine whether this behavior is real or otherwise, the retrieval algorithms for both constituents are being investigated to look for possible differential interference or temperature sensitivity effects.

2.2.10 Chlorine Nitrate ($CLONO_2$)

Chlorine nitrate is being retrieved at all latitudes and all times. At the time of this validation meeting, there were three correlative measurements with which to compare as detailed in Section 8.2. The CLAES measurements agree well within about 30% with the correlative data in terms of the mixing ratio profile at the profile peak. Good agreement is shown with the only high latitude winter correlative measurement of $ClONO_2$

available. There isn't a direct comparison with tight enough error bars to be certain, but an overall comparison between CLAES and other measurements from the midlatitudes, particularly the G. Toon (1992) measurements, suggest that the CLAES mixing ratio is suppressed in the vicinity of 10 mbar. This result is perhaps due to use of a climatology at higher altitudes which is too large, but could also be related to the pattern noise identified in the ozone mixing ratio profiles retrieved from blocker 9.

The uncertainty indicated by the error bars is less than about 30% for the highest quality retrievals and pertains to a majority of the data in the altitude range from 20 to 68 mbar. The error bars on the CLAES retrieved mixing ratios are a good indicator of whether the particular datum is truly retrieved, or is closely related to the UARS climatology. If the error bars are large, as one frequently finds at pressures below 6 mbar or so, the profile is dominated by climatology. At high pressures, approximately above 68 mbar, the profile also may be influenced heavily by climatology, again indicated by large error bars which show an uncertainty of 100% or more.

Observed diurnal variations qualitatively agree with photochemical model simulations. Chlorine nitrate zonal features appear to be independent of retrieval initialization and show similarity with the LLNL 2-D model. Column densities in the Arctic winter agree with columnar measurements made from aircraft in 1989.

Future improvements will include:

- an improved filter function which may change retrievals at the 5% level;
- temperature-dependent chlorine nitrate absorption cross- sections (we now use cross-sections representative of 223 K);
- elimination of the pattern noise in blocker 9 through improvement in the use of calibration data.

The use of a better upper boundary condition for $ClONO_2$ than currently provided by the UARS climatology, or a better implementation of the climatology will be investigated.

2.2.11 Nitrogen Dioxide (NO_2)

NO_2 is being retrieved at all latitudes between 80S and 80N and reported on the nominal pressure range from about 100 mbar to 0.1 mbar. In most cases we have good confidence in the range from 100 mbar to approximately 0.3 mbar. Our confidence in this range is based mainly on comparison with daily zonal mean cross-sections from LIMS data and climatology. There are also some limited profile comparisons as discussed in section 10.2.1 below. Direct comparison with solar occultation instruments such as SAGE are limited, but are consistent. Comparisons with other UARS instruments, ISAMS and HALOE, confirm reasonable diurnal, seasonal and regional structure. However, HALOE comparisons have the same problems as with SAGE.

In general, the CLAES NO_2 data: show good resemblance to climatological zonal mean structure from approximately 0.3 mbar to greater than 100 mbar; are approximately 20% less than climatology; have good day-to-day consistency in zonal mean maps; show physically realistic diurnal dependence; show no apparent aerosol degradation; and are insensitive to a priori information.

ZONAL MEANS

General zonal mean structure is in reasonable agreement with LIMS and/or climatology, although the CLAES values are smaller than LIMS by roughly 20%. There is good day-to-day consistency in the CLAES zonal mean maps. Day and night maps show the expected diurnal variation. There is no apparent aerosol degradation. There are features in the CLAES southern polar zonal means that are not directly comparable to LIMS data.

PROFILES

For this validation exercise there weretwo directly comparable data sets (from the FIRS–2 and BLISS, see sections 10.1.2 and 10.1.3 below) available. CLAES data agree within a few percent of the BLISS data, but were considerably smaller than the FIRS–2 data. For that case, scaled LIMS data more closely resembled CLAES than FIRS–2 data.

TIME-TRACK COMPARISONS

The CLAES and ISAMS data are highly correlated in time-track comparisons. The ISAMS data are about a factor of two greater than CLAES, while CLAES is of the order 20% less than corresponding LIMS data. The time-tracks show the expected diurnal and latitudinal variations.

ERROR DISCUSSION

Based on the comparisons cited above, we believe, conservatively, that CLAES NO_2 systematic error is of the order of 30% for all cases, except perhaps polar winter conditions involving large vertical temperature gradients. In atmospherically quiet regions, including almost all conditions except polar winter, production software error estimates (as discussed in section 2.2.3.3) represent a worst case limit on precision, typically of the order of several tenths of a ppbv near 46 mbar, about 10% of the reported value near the peak, and indicate significant results to levels well above 1 mbar in most nighttime cases.

In the polar winter cases involving large vertical temperature gradients the error can become very large, especially at altitudes below the stratopause. The problem is associated with large temperature gradients between a relatively high altitude tropopause and low altitude stratopause. For example, the zonal mean temperature changes by more than 70 K (i.e., from < 196 K to > 266 K) between 32 to 47 km (i.e., ≈ 10 to 1.0 mbar) at 76S on 8/23/92. For this example, errors of the magnitude of the retrieved data are reported in the CLAES data below 32 km. Degradation in the accuracy begins at about 44 km.

2.2.12 Nitric Acid (HNO3)

HNO_3 is being retrieved at all latitudes between 80S and 80N and is reported on the nominal pressure range from about 100 mbar to 0.1 mbar. Our best confidence is from 100 to 3 mbar. Our confidence in this range is based on examination of altitude profile data in comparison with correlative data, and investigation of daily zonal mean cross-sections in comparison with LIMS data and climatology. As described below, we lose confidence in the retrieval values of about 8 ppbv or more, which we intend to correct in subsequent versions. In our good confidence range, HNO_3 retrieval appears to be independent of retrieval initialization.

ZONAL MEANS

General zonal mean structure is in reasonable agreement with LIMS data and/or climatology, although maximum mixing ratios at high north winter polar latitudes are sometimes lower in altitude. There is no data base for these comparisons in southern polar winter conditions with de-nitrification and relatively large descent. There is good day-to-day consistency in the CLAES zonal mean maps. There is no apparent aerosol degradation.

PROFILES

In general CLAES shows good agreement with correlative profile data from several data sources as described in Chapter 9. Agreement in peak amount is better than 10% on the average. There may be a trend for the CLAES data to be registered to lower altitudes, sometimes by as much as 1.5 km, than the correlative data, though several cases can be found where the CLAES might be registered slightly higher. Due to the steep slopes in HNO_3 mixing ratio below and above the peak value, misregistration can result in apparently large errors at such altitudes, which we conservatively estimate to be of the order of 30%. Profile-to-profile variability, and production software error estimates (as discussed in section 2.2.3.3), suggest precision of the order 1.0 and 0.3 ppbv at 46 and 4.6 mbar respectively.

CAVEATS

Studies of the CLAES Data Version V0006 HNO_3 retrieval sensitivity to variations in the iteration procedure that is used, the number of iterations used, and the a priori data have been conducted. These studies show that the retrieval is reasonably robust and insensitive to variations in these parameters for retrieved mixing ratio levels that are less than approximately 8 ppbv and agree well with correlative data and LIMS data. For larger values of the mixing ratio the retrieval becomes unstable, and in some cases , unreasonably large values of mixing ratio are rètrieved.

We are studying the possibility that part of the problem involves the forward model. Spectral parameters and/or error in implementing the forward model are suspect. When the problem occurs the channels are very near to saturation, and the use of temperatures that are too low might also be involved. Spectral registration has been verified in a preliminary sense, but this will need further study. Resolution of these difficulties is a priority for our next software version.

UTILITY

In spite of these difficulties we expect the HNO_3 V0006 results will be very useful for cases where the mixing ratios are less than 8 ppbv. These results should be able to support studies of de-nitrification in the polar region winters, for example. But it must be emphasized that quantitative values for HNO_3 mixing ratios that are greater then 8 ppbv are suspect. Also, any results at altitudes lower than the highest altitude where the mixing ratio is 8 ppbv are also suspect.

2.2.13 CFC 12

We are currently retrieving CFC 12 from about 100 to 2 mbar, but have our best confidence from 50-5 mb, based on comparisons with limited correlative profile data and 2-D model simulations. There is no significant retrieval initialization effect.

ALTITUDE PROFILES

At the time of this workshop, only one direct correlative comparison was available, a balloon-borne interferometer flown September 15, 1992, at 35N. A comparison reveals differences between 25 and 10% from 40 to 5 mb with the CLAES values being larger. A comparison with a 1985 ATMOS profile, with tropopause mixing ratio scaled to recent measurements shows mean differences between 10 and 20% from 60 to 20 mb. Based upon this comparison, we assign an overall systematic error of 20% to the retrievals between 50 and 5 mb. We note however, that the ATMOS data is restricted to 35N. There is some indication that the CLAES data at low altitudes in the tropics can be higher than the climatology by more than 20%, at least in the early part of the mission.

The precision estimates generated by the algorithm typically vary between 0.15 ppbv rms at 50 mb and 0.12 ppbv rms at 10 mb. However, in the case of the direct comparison with the balloon data, the standard deviation of the difference between the data sets from 50 to 5 mb is of the order of 0.05 ppbv, and a similar number is seen for the comparison with the scaled ATMOS data. Examination of many adjacent profiles also indicates a repeatability of better than 0.05 ppbv. The listed precision estimates are probably unrealistically large , and therefore need to be investigated. Pending further correlative comparisons, we estimate a precision of the order of 0.05 ppbv to be appropriate for the range 50 to 5 mb, noting the caveats listed below.

ZONAL MEAN CROSS_SECTIONS

Zonal mean cross-sections were compared with the Lawrence Livermore National Laboratory (LLNL) 2-D model. Reasonable structural agreement is seen for all periods except for polar latitudes in southern winter. In absolute values the data and the model simulated values are in best agreement outside a latitude band of 20S to 20N. Within this tropical band below about 20 mb, the CLAES values are significantly higher than those from the model in January, but less so as the year progresses. During southern polar winter the data fields deviate from those produced by the model by indicating an upwelling near the pole. There is also some indication of this behavior (much weaker) in April 1992 near the south pole.

CAVEATS

Further analysis of the reliability of high values below 20 mb in the tropics is required. This issue may involve some residual from incomplete removal of the effect of the Mt. Pinatubo aerosol cloud. Additional correlative comparisons will be especially important in resolving possible retrieval problems.

2.2.14 DINITROGEN PENTOXIDE (N_2O_5)

The CLAES V0006 N_2O_5 are too preliminary to be used for any scientific purpose. It has been catalogued on the CDHF to provide a baseline for measuring progress in future versions. It is not recommended for transfer to the DAAC.

The N_2O_5 is one of four species to be retrieved from data obtained in five high resolution (≈ 0.3 cm^{-1}) radiance channels in the CLAES blocker region 4 which is centered at approximately 1257 cm^{-1}. These species are CH_4, N_2O, aerosol, and N_2O_5. One radiance channel centered at 1259.66 cm^{-1} targets a well-resolved CH_4 line, and two channels centered at 1257.36 and 1258.28 cm^{-1}, respectively, target two well-resolved N_2O lines. The two remaining channels centered at 1256.99 and 1257.77 cm^{-1}, respectively, are located in between the lines of CH_4 and N_2O for the purpose of retrieval of continuum emitting species such as N_2O_5 and aerosol. Thus, in this blocker region there is good spectral contrast for the line emitting species CH_4 and N_2O, but practically no contrast between the N_2O_5 and the aerosol. The N_2O_5 retrieval is further complicated in that it contributes only very weakly to the total measured radiance, even in the two continuum channels, for those altitudes, latitudes and times for which N_2O_5 could be expected to be contributing the most. By contrast, the aerosol contributes very significantly in certain altitude and latitude regions. The retrieval scheme attempts to exploit the dissimilar spatial distributions of N_2O_5 and aerosol to overcome the spectral contrast problem, but has achieved no success in this preliminary version of the retrieval. It is not clear at this point if this result is due to error in implementation, or if it is basically not possible to retrieve the N_2O_5 and the aerosol simultaneously, due to the lack of spectral contrast between the two and the relatively weak contribution due to N_2O_5. If the latter is the case, it still may be possible to attempt to retrieve N_2O_5 alone, and model the aerosol contribution to radiance in this region on the basis of aerosol retrieval in other CLAES blocker regions.

2.2.15 Nitric Oxide (NO)

In general the CLAES NO data show: a resemblance to climatological zonal mean structure, although becoming unrealistically large for altitudes above about 1 mbar; reasonable day-to-day consistency in zonal mean maps; no apparent aerosol degradation; and are not particularly sensitive (of the order 10% for a zonal mean on doubling the profile) to a priori information. There is no retrieval for nighttime conditions.

To the limited extent possible, the comparisons with HALOE appear reasonable. Other comparisons, and potential correlative data sources are discussed below in the main section on NO.

ERROR DISCUSSION

Examination of CLAES production software error estimates indicates best confidence in the region from roughly 5 to 1 mbar. in general. This conclusion is supported by comparison of CLAES zonal means with climatology. Below 5 mbar the climatology, scaled by the data in the 1 to 5 mbar region, is reported. Above 1 mbar the retrieval is unrealistically large, probably due to inadequate compensation for high altitude non-LTE NO emission.

Based on the comparisons with our nighttime NO_2, and a potential systematic error as discussed in section 2.2.11 above, we estimate the systematic error in our NO of about 30% too large at 2.2 mbar. The assumption that NO_y is mostly NO_2 by night, and mostly NO by day, at 2.2 mbar is used in this first order analysis. Repeatability in the daily zonal mean sense at 2.2 mbar is also about 30%. Error bars on individual profiles can be considerably larger.

CAVEATS

The NO spectral region is at relatively short wavelength, and the radiance data are therefore relatively noisy. There is considerable work to be done in optimizing the CLAES NO retrieval which is at present in a relatively immature state. Work that remains includes:

- Improvement of DC zero-level component subtraction which is an electronics problem that can be solved by the processing software in future versions;
- Subtraction of high-altitude non-LTE NO radiance, which is still very crude;
- Evaluation of non-LTE effects in the stratosphere, which may be important and may be responsible for apparent systematic error to the high side;
- Develop the capability to average zonal mean radiances and retrieve from these.

2.2.16 Hydrogen Chloride (HCl)

In our current software version, HCl is not retrieved. However, our radiance data indicate that we should be able to retrieve HCl once some special processing software is developed and in place. In this section we describe some CLAES radiances obtained with the special HCl array of oversized DC coupled detectors. For this example we use data taken on Jan. 10, 1992. In addition to HCl retrieval, these data should be useful for retrieving aerosol physical properties, further understanding of OH chemiluminescent emissions, including some very interesting structure, and perhaps for back up CH_4 retrieval.

The CLAES HCl array consists of three detectors. Nominally, detector 23 detects radiance from altitudes 14 to 28 km, detector 22 detects radiance from 28 to 43 km, and detector 21 detects radiance from 43 to 58 km. These numbers can vary up or down by a few kilometers depending on where CLAES is pointing.

Figures 2.2.16–1 to 2.2.16–3 show the radiances for detectors 21, 22, and 23, respectively, for slightly over one orbit of data on January 10, 1992. One orbit is approximately 88 EMAFs. In normal operation, each detector on the HCl array produces a value for each EMAF for each of three channels responding primarily to aerosol, HCl and OH emissions. In each figure, radiances are shown for the aerosol, HCl and OH channels. Also shown are the sun elevation and latitude at the tangent point. For the last two quantities the scale must be divided by 5, that is, a reading of 200 is actually 40 degrees. The results for detector 23 show a very pronounced enhancement for EMAFs 520 through to 560. This period corresponds to the interval between sunrise to sunset at the observation tangent point with the highest radiance at EMAF 5[illegible]6. This maximum coincides with the thickest part of the Pinatubo aerosol cloud, in the vicinity of the equator, and is just before the maximum solar elevation (at EMAF 540). These observations are consistent with the hypothesis that the enhancement is due to the

scattering of incident solar radiation by aerosols in the field of view of this detector which extends approximately from 14 to 28 km. It will be seen that there is considerable structure in this enhancement and that the results for the three channels are highly correlated. This structure is probably due to changes in the position of the mirror that keeps CLAES pointed to the correct altitude in the atmosphere, but may also be related to changes in aerosol scattering. The correlation between the three channels is expected since they are very close together in wavelength, and aerosol scattering will not change much in this interval. The corresponding enhancement for detector 22 is much smaller than that for detector 23, and the enhancement for detector 21 is smaller still. This result occurs because there are fewer aerosols higher in the atmosphere. Also, part of these enhancements for these higher altitude detectors may be due to the scattering of light from the field of view of detector 23 by optical elements and surfaces in the instrument.

During sunlit hours, for detector 23, the aerosol radiance is larger than the radiance for the other two channels. This difference is probably due to more absorption of the outgoing scattered radiation in the HCl and OH channels than in the aerosol channel. Absorption in the OH channel is mostly due to CH_4 in this altitude region. For detectors 22 and 21 during sunlit hours the effect is opposite; that is, the radiance for HCl and OH is larger than the aerosol radiance (points where the aerosol radiance is larger are believed to be spikes in the data which will be removed with further processing). The difference varies between 0–5 radiance units (RU), where one RU is $10^{-7}\,W{\cdot}m^{-2}{\cdot}sr^{-1}{\cdot}(cm^{-1})^{-1}$. The average value is about 3 RU for both HCl and OH for both detectors. This can be compared with previous daytime estimates made by Mergenthaler and Kumer (1986). These estimates give about 1.5 RU for HCl and 15 RU for OH at 30, 40, and 50 km. Thus, the CLAES values appear to be of the same order of magnitude as the Mergenthaler-Kumer (M-K) estimates for both detectors, although HCl is enhanced by a factor of two and OH is decreased by a factor of five. Explanations for the enhanced HCl could include: more HCl present than used for the M-K prediction; a smaller quenching coefficient for HCl ($v = 1$) than used by M-K; or additional daytime non-LTE mechanisms for exciting HCl ($v = 1$) that were not considered by M-K. As for OH, the M-K estimates were for the upper limit that could be determined from the low S/N and low resolution SPIRE data. Therefore, it is not surprising that the OH radiance observed by CLAES is lower than the M-K estimate.

At about the time the sun comes up in many of the orbits on January 10, there is a very large increase in atmospheric temperature in the 30 to 60-km region corresponding to the "hot spot" in the minor stratospheric warming event that occurred on that day. There are enhancements in the detector 22 radiance that correspond with these hot spot coincidences. The highest temperature during the day, as measured by CLAES at a level of 2.154 mbar (near the top of detector 22), was 320 K and occurred near EMAF 521 in Figure 2.2.16–2. By using the CLAES retrieved temperature and CH_4, and the HALOE retrieved HCl, we were able to model the observed 15-RU enhancement in detector 22 emission to within a few percent. Note that this enhancement is of the order of 36 times the nominal atmospheric thermal radiance on detector 22 because the ratio of 3.5-μm blackbody emission at the enhanced temperature of 320 K to emission at the nominal temperature of 250 K is approximately 36. This fact suggests that we are indeed measuring HCl thermal emission and not just seeing aerosol scattering (there is no similar

increase in the aerosol channel radiance for these EMAFs). Similar peaks in the HCl radiance are seen on other orbits at the same EMAFs as the temperature peaks. No enhancement in HCl emission is seen for orbits where temperatures are nominal.

During the night, the HCl radiance is about the same as the aerosol radiance for all three detectors, indicating that the radiance is mainly from aerosol emission. For detector 23, the radiances are low for northern latitudes, but reach as high as 150 RU for equatorial latitudes due to thermal emission of the Pinatubo aerosol cloud. For detectors 22 and 21 the high and low latitudes are not noticeably different and mostly vary between 2-6 RU.

During the night we observe a relatively high OH emission of 5–10 RU in each channel which subsides during the day. This effect is probably a result of chemiluminescence at night. There seems to be a slight increase in emission with altitude as would be expected. In the M-K paper mentioned above, estimates of nighttime OH radiance are for 33 RU at 30 km and 38 RU at 40 km. Thus, the CLAES results are lower than the M-K estimates by a factor of 3–7, but the factor of 3 in night versus day enhancement of OH, as predicted by M-K, is observed in the CLAES data.

CONCLUSIONS

Our radiance data suggest:

- HCl retrieval from resonance scattering of sunlight by HCl molecules may be possible for detector 21 and 22 data.
- HCl retrieval from thermal emission observed in stratospheric warmings may be possible for detector 22 data.
- HCl retrieval from absorption in aerosol scattered sunlight may be possible for detector 23 data.

FUTURE TASKS

- Do more work on despiking data.
- Get improved calibration with full cooldown.
- Map zonal mean averages of radiance and use in retrievals to provide an alternative to L3 for altitudes greater than 28 km.
- Use CLAES data to monitor HCl in regions where there is no HALOE coverage.
- Combine the OH measurements with WINDII, SIRRIS, etc., to improve the chemiluminescence OH models.
- Look for mesosphere wave structure in OH.
- Investigate possibility of backup CH_4 retrieval based on CH_4 absorption of scattered sunlight in the OH channel for detector 23.

2.2.17 CFC11

CLAES version V0006 retrievals of CFC11 are too preliminary to be used for any scientific purpose. The data has been catalogued on the CDHF to provide a baseline for measuring progress in future versions.

2.3 ISAMS Algorithm Description and Status

ISAMS version 8 data processing produces retrieved profiles of temperature, pressure, H_2O, O_3, CH_4, N_2O, NO_2, CO and aerosol at 12.1 μm and 6.2 μm. There is a total of 179 days of ISAMS data available since the start of the UARS mission which have been processed with version 8 of the software suite, producing V0008 data files. These data will in due course be replaced by V0009 data, but it is only version 8 that is described here. The remaining ISAMS gases, NO, N_2O_5 and HNO_3, are either not retrieved in version 8, or are unsuitable for scientific use. These data will appear in future processings.

A description of the instrument can be found in Taylor et al. (1993), and a full description of the methods used to retrieve temperature and constituents from ISAMS measurements can be found in Dudhia (in preparation) and Marks and Rodgers (1993).

2.3.1 Algorithm Overview

The heart of the retrieval method is a forward model which describes how the measured radiance depends on the atmospheric state. A retrieval is obtained by adjusting an estimated state using optimal estimation methods (Rodgers 1976) until convergence and appropriate agreement with the corresponding measurements is obtained.

We first retrieve the temperature and pressure distribution using a Kalman filter along the measurement track, using a method similar to that described for SAMS (Rodgers, Jones, and Barnett 1984). Radiances are measured at intervals of 2.048 seconds. For each measurement time, an a priori profile is constructed, based on the profile retrieved at the previous measurement time. This profile is then updated using the measurement to produce an optimal estimate of for the current measurement time. The filter is run in both the forward and backward directions, and the two estimates are combined. The state vector that is estimated each time comprises temperatures on the measurement grid, together with the pressure at one grid element.

The grid on which the retrievals are carried out is neither a height nor a pressure grid, but is the set of tangent points corresponding to the nominal set of directions that the ISAMS scan mirror can view. These points are separated by 0.05 degrees in elevation angle, (approximately 2.46 km), but can drift vertically on the limb with variations in the spacecraft attitude and the figure of the earth. Retrieved profiles are interpolated onto the UARS pressure surfaces for the level 3 archival data.

For constituents, two approaches have been developed. The first approach ("LV2CON") is to grid the radiances to produce vertical profiles at regular intervals along the measurement track, and then to retrieve constituent profiles for each of these locations individually. The gridding technique uses a Kalman filter, essentially retrieving the two dimensional radiance distribution from the particular scan pattern in use. The individual retrieval method uses optimal estimation to derive profiles, either in a full "vector-vector" mode, or in an "onion-peeling" mode. In the case of more difficult, non-linear problems, the vector-vector retrieval can use an enhancement based on the Marquardt method (e.g., Press et al., 1989) to ensure convergence. The more recent second approach ("LV2VMR"), which is more computer intensive, is more akin to the temperature retrieval. This approach uses a Kalman filter, updating a running estimate of

the profile for every radiance measured. The quantity retrieved is the logarithm of mixing ratio on the measurement grid which is interpolated onto UARS surfaces for the level 3 archive data. For further details, see the description below of N_2O_5, which is the only constituent where LV2VMR has been used in version 8.

2.3.2 Temperature

The retrieved temperature profile spans 35 levels of the measurement grid, nominally covering the range 100-0.01 mbar. The reference pressure is at level 11, close to 3 mbar. The CIRA climatology is used as a priori data, assuming a 20 K standard deviation. No spectral contaminants are included in version 8. This procedure causes a systematic error of a few degrees relative to version 9, which will include ozone and nitrous oxide.

Spectral contamination by aerosol is included, by carrying out a retrieval of the 12.1 μm aerosol extinction in parallel with the temperature retrieval, and using a factor of 1.98 to estimate the extinction in the temperature channel. Separate retrievals are used later to produce the final aerosol products.

The useful range of the version 8 temperatures is 100-0.1 mbar. Above 0.1 mbar the product is largely climatology, as reflected in the negative value assigned to the profile error bars. The error bars associated with the stratospheric temperatures are clearly too large, on comparison with other measurements, but the mesospheric values seem reasonable.

2.3.3 Constituents

Not all of the ISAMS constituents are available in version 8. The missing ones, which will become available in future versions are nitric oxide, nitric acid and nitrogen pentoxide. Almost all of the constituents are affected by the Mt. Pinatubo aerosol, and as a result the lowest level retrieved is generally 10 mbar. The exceptions are aerosol itself and nitrogen dioxide. Except where stated, the constituent retrievals have used the LV2CON program..

2.3.3.1 Aerosol, 12.1 μm, 100-5 mbar

The V0008 aerosol retrieval uses the Marquardt vector-vector method (see above) with a nominal retrieval range from 100 mbar to 5 mbar. The standard UARS climatologies used are O_3, CO_2, H_2O and F11. A seasonal 2-D climatology has been used for O_3, and a single profile for the other gases. $ClONO_2$ has not been included in V0008 . The a priori aerosol profile consists of a single profile and because of the large variability of the aerosol extinction a very large a priori uncertainty (1000%) is used to ensure that the retrieval is only loosely constrained.

The natural extinction unit for ISAMS is the cross-section per mole of air (m^2mol^{-1}) which, like mixing ratio is conserved under changes of atmospheric pressure in the absence of aerosol formation or loss. It is related to the more commonly used unit of extinction per unit length (km^{-1}) by the local molar air density (p/RT, mol m^{-3}). The ISAMS level 2 processing produces aerosol extinction in both units, but only the extinction per km is produced at level 3.

There is an anomaly in the retrieved 12.1 μm aerosol in the height range 19 to 25 km, because of an interaction between a change in operational mode and the method used for

dealing with the field of view function. Retrieved aerosol in this range is higher before April 11, 1992 than after that date by up to 20%. It is likely that the earlier data is overestimated.

2.3.3.2 Water Vapor, 10-0.05 mbar

The H_2O retrieval uses the vector-vector scheme, retrieving between 10 and 0.05 mbar using the wideband channel only. Radiances from the PM channel are not used in the production retrievals because of the uncertainty in the partial pressure of H_2O in the PMC. A reliable retrieval can be performed using the wideband radiances because they are relatively insensitive to the contents of the PMC. Emission due to aerosol is not included in the forward model calculation so the lower limit of the range is set to be above the worst of the aerosol contamination (10 mbar), although aerosol contamination is apparent in the water vapor retrievals near the equator at around 10 mbar.

The a priori data used to constrain the H_2O retrieval is a climatological profile with a standard deviation of 75% and a correlation length scale of 5 km. The profile is an ATMOS model profile. Climatologies for contaminants CH_4 and O_2 are based on the UARS climatologies. The CH_4 climatology has been averaged to provide zonal mean seasonal climatologies in six latitude bands. The O_2 climatology is a single profile.

There is no non-LTE included in the forward model calculation for the H_2O retrieval, so daytime retrievals are not performed.

The constituent retrievals use ISAMS retrieved temperature and pressure in the forward model calculation, so errors in these quantities are included in the error budget of the constituent retrievals. For the H_2O retrieval, an (over)estimate of this error in radiance terms was added to the radiance measurements as an additional 'forward model error'.

2.3.3.3 Ozone, (O3), 10-0.2 mbar

Ozone is retrieved using the optimal onion-peeling technique described by Connor and Rodgers (1988). Compared to simple onion-peeling, the use of the optimal estimation formulation provides a great reduction in noise sensitivity. While the full-blown vector optimal estimation technique is slightly better in this regard, it also allows systematic errors in the lower part of the profile (e.g. due to the aerosol correction) to propagate upwards. Since the ozone radiances have both high signal-to-noise and significant aerosol contamination, we have adopted the optimal onion-peeling approach.

In version 8, aerosol retrieved from the 12.1 μm channel and CO_2 from climatology are used as contaminants. As with all ISAMS measurements, the ISAMS retrieved temperature is used to calculate radiances. No correction is applied for non-LTE radiation.

Retrievals are carried out at 100-0.2 mbar. The high altitude cutoff is dictated by the accuracy of calibration. The lower limit, 100 mbar, is what was expected for ISAMS before the Pinatubo eruption. Subsequent experience has shown that residual aerosol effects, acting indirectly via the temperature retrieval, make ozone values below the 10 mbar surface suspect. Data above 1 mbar are suspect and should be used only with caution, because daytime data are influenced by non-LTE processes, and nighttime data

are biased by the use of a daytime a priori profile, so that the day/night variation will be poorly represented.

2.3.3.4 Methane (CH_4), 10-0.2 mbar and Nitrous Oxide (N_2O), 10-0.8 mbar

In V0008, CH_4 and N_2O were retrieved jointly using three channels: 20P (N_2O pressure modulated signal); 60P (CH_4 pressure modulated signal); and 60W (CH_4 wideband signal). An onion-peeling retrieval was used since vector-vector retrievals had difficulties with convergence, possibly due to some mismatch between the channels (see below). There is reasonable separation in the retrieval so that 20P provides most of the information on N_2O, and 60W and 60P provide most of the information on CH_4 (but see below). The errors on the input radiances to the retrieval scheme were a combination of random error estimates from the gridding of the radiances and estimated forward model errors. The forward model error treatment consisted of a single profile of radiance errors calculated at the equator from estimated uncertainties in the temperatures of about 5 K (4-6 K in the retrieval range) with a lower limit of 2% of the climatological radiance at that location to account for other uncertainties in the forward model calculation. These errors are considerably overestimated and will be better described in future versions. Errors on the a priori estimates were set to 75% for both products, so an error of 53% on the output products indicates that the a priori estimates and the measurements have contributed equally to the retrieved value.

In V0008, CH_4 is retrieved between 10 mbar and 0.2 mbar, the lower altitude limit being imposed by aerosol contamination, and the upper altitude limit by the estimated forward model errors. The data are reasonable between 5 mbar and 0.2 mbar, the region between 10 mbar and 5 mbar often being contaminated by aerosol in the tropics. From December through to April, there are pronounced features in the tropics between 10 mbar and 2 mbar which may be due to increased aerosol contamination at these altitudes. As noted before, most of the information in the CH_4 retrieval comes from 60P and 60W, but the retrieval tends to follow 60P more closely at altitudes above 5 mbar. Tests indicate that the CH_4 amounts retrieved independently from 60P are about 20% higher than those retrieved from 60W. This result implies that there is a small error in characterization of the CH_4 pressure modulator cell in which case the wideband retrieved amounts should be more believable and might explain why ISAMS measurements of CH_4 tend to be higher than those by CLAES and HALOE.

In V0008, N_2O is retrieved between 10 mbar and 0.8 mbar for similar reasons to those discussed above for CH_4. Since N_2O mixing ratio decreases rapidly with height, the upper altitude is not expected to change significantly even with lower estimates for the radiance errors. The N_2O results are contaminated by aerosol in a similar manner to the CH_4 data. Apart from this, relative N_2O values are good and less noisy than the equivalent CH_4 data. There is however a problem with the N_2O absolute values which is believed to be due to problems of the pressure modulator cell (PMC) characterization. This possibility is being investigated, but comparisons with CLAES data and climatology indicate that the ISAMS values could be too large by about a factor of two. Our current understanding of the N_2O PMC problem indicates that changes in values of ISAMS N_2O on a timescale of months may have a component due to changing PMC conditions which are not being adequately modelled. Changes over a few days should be believable and

comparisons of tracer data among the UARS instruments show good agreement in 3-D fields.

2.3.3.5 Nitric Oxide (NO)

The nitric oxide channel has proved difficult to calibrate due to emission from thermospheric NO in the region of the limb scan used for a space view in the other channels. A calibration scheme had not been developed in time for the version 8 processing, but will be implemented in version 10. It is not expected that validated NO will be available until version 11.

2.3.3.6 Nitrogen Dioxide (NO_2) and 6.2 μm Aerosol, 100-0.1 mbar

The method used for the retrieval is optimal estimation using the vector-vector scheme with the Marquardt enhancement to aid rapid convergence. Channel 5 wide-band (50W) and pressure modulator (50P) radiances are inverted simultaneously to retrieve both NO_2 volume mixing ratio and the aerosol extinction in the band (referred to hereafter as 62X). Both signals are affected by three spectral contaminants, H_2O, O_2 and CH_4, and are accounted for using climatological fields. Any deviation from these climatological states (relevant for H_2O and CH_4) will manifest itself in one of the products, primarily in the aerosol product rather than the NO_2. Water and methane are of course also ISAMS operational products, and their use as contaminants in the NO_2/62X retrieval is anticipated in the future. The retrieval range is 100 to 0.32 mbar for the version 8 delivery, extended up to 0.1 mbar in version 9, thus covering the full range of useful information from the instrument.

The a priori estimates for the products are simple single profiles (separate day and night for NO_2), so that these may not introduce large-scale structures in synoptic fields. The associated standard deviations are set at 75% for NO_2 and 200% for 62X with vertical correlation scale-lengths l (the correlation falls off as $e^{-(dz/l)^2}$), of 5 km.

The patterns shown by the retrieved NO_2 distribution look reasonable, but the absolute values are a little high. It is suspected that our measurement of the amount of NO_2 in the pressure modulator cell is in error. The distribution of aerosol does not agree in detail with that at 12.1 μm. This result is partly artificial, due to the bias in the NO_2 retrieval, and partly real, due to spectral differences in the aerosol between the two wavelengths.

2.3.3.7 Dinitrogen Pentoxide (N_2O_5)

V0008 N_2O_5 is the first operational product generated by a new ISAMS retrieval algorithm, LV2VMR. This algorithm assimilates the Level 1 radiances directly at their measurement time and location, performing a retrieval every ISAMS Measurement Period (IMP=2.048s, or about 15 km along-track) to update the estimated profile. The standard optimal estimation equations are used (Rodgers, 1976), simplified for a single iteration. It is assumed that the measurement errors are uncorrelated (probably unrealistic if calibration errors dominate the random noise), so that the measurement covariance is a simple diagonal matrix.

For the first retrieval in a 'mode' (a period of continuous ISAMS viewing to either the +Y or -Y side, or an entire day, whichever is shorter), the a priori estimate and its

covariance are taken from climatology. For subsequent retrievals, the a priori estimate is constructed from the previous retrieval, relaxed slightly towards climatology. Thus, after a few retrievals, the a priori estimate is largely determined by the previous retrievals rather than climatology, and it is assumed that this will be close enough to the next solution so that only a single iteration is required.

The N_2O_5 climatology is represented by a single profile, assumed applicable to all latitudes, times of day and seasons. While this is clearly unrealistic, it does guarantee that any observed structure in the retrieved N_2O_5 is not created by the climatology (although it may be influenced by the contaminant climatologies, which do include latitudinal/seasonal factors). The profile was that used in the FASCODE transmission program, representing typical noon concentrations. The climatological covariance matrix contains diagonal elements based on a 1σ uncertainty of 1000% in the climatology, and off-diagonal elements falling off as $e^{-|dz/l|}$, where l is 5 km.

Profiles of temperature, pressure and aerosol extinction come from the ISAMS Level 2 products, the latter obtained by scaling the retrieved 12.1 μm extinction by a suitable constant to estimate the 8.1 μm extinction. For other spectral contaminants (CO_2, H_2O, CH_4, N_2O, O_3), climatological values are used.

The retrieval is performed both forward and backward through the mode, and at selected times the result of the forward a priori estimate is combined with the backward retrieval to generate a merged estimate. This technique is the same Kalman filter approach used in the ISAMS temperature/pressure retrieval. The merged estimates form the level 2 profiles, with the "quality" values taken from the square-roots of the corresponding diagonal elements of the covariance matrix, converted from ln(vmr) to vmr (volume mixing ratio). At profile levels where this covariance exceeds 50% of the climatological covariance, the quality value is made negative to indicate that most of the information comes from the climatology rather than the measurements. To conform to other ISAMS products, level 2 profiles are generated twice per UARS minute, i.e., every 200 km along-track, although it should be remembered that there is only one profile of 72W measurements per UARS minute.

The error analysis indicates that N_2O_5 errors in version 8 are greater than 100% at all levels. This data should not be used except with great caution, and consultation with the ISAMS team.

2.3.3.8 Nitric Acid (HNO_3)

The nitric acid channel is heavily contaminated with aerosol emission. The retrieval in the presence of this contamination has proved difficult to the accuracy required for public release of the data. Consequently nitric acid is not available in version 8 or 9. It is expected that it will become available in version 10 of the data processing.

2.3.3.9 Carbon Monoxide (CO), 10-0.03 mbar

The V0008 retrieval of CO uses the vector-vector scheme and CO is retrieved between 10 and 0.03 mbar (31 and 74 km approx). The CO a priori climatology consists of a single profile, taken from Allen et al., 1981, with a standard deviation of 75% of the CO value. The three molecular contaminant species CO_2, N_2O and O_3, included in the retrieval are

taken from the ISAMS climatology. In version 8, the forward model errors at every altitude were assumed equal to 2% of a climatological radiance profile, which is unrealistically small. The retrieval lower limit has been set up at 10 mbar, since aerosol contamination is present in the 00P signal, but no correction for aerosol emission has been included yet operationally. No line-of-sight correction is made in Version 8. The statistics of the retrieval shows, typically, an average number of iterations for convergence of about 4.7 , and 99% of the retrievals converge.

It is important to note the greater ability of the retrieval scheme to sound the mesospheric CO during daytime than at night. As a consequence of the enhanced non-LTE emission in the mesosphere during daytime, the 00P level 2 radiances have a larger signal to noise than at night. During nighttime, the radiance noise is similar to the radiance value above about the stratopause and, consequently, the retrieved CO tends to the climatology in the mesosphere. Note also that the effect of mesospheric emissions at stratospheric altitudes is important during daytime. In summary, the user must be aware of the generally different values of CO for day and night at collocated geographical points in the mesosphere in version 8. The nighttime retrieved CO is more biassed towards the a priori estimate in the nighttime case, while the larger daytime S/N relation makes the effect of the a priori estimate smaller in this case. Mesospheric nighttime CO should be disregarded on this basis.

Generally, the version 8 CO retrievals look reasonable, but validation is problematical owing to lack of correlative data.

2.4 MLS Algorithm Status

Currently MLS is producing version 0003 files using its version 412 software. All MLS data since launch have been reprocessed to version 3, and older versions should not be used. An error was found in the L3AL longitude field after reprocessing began. A patch to the software was delivered, and higher-cycle L3AL files were generated. Lower -cycle files should not be used.

A fatal failure occurred in the 183-GHz radiometer in April of 1993. The last good full day of data was April 15, 1993 (UARS Day 582), for ozone from 183-GHz band and for H_2O retrievals. Although Level 3 files for these two species were produced until August 8, 1993 (UARS Day 697), the period after April 15 gave climatological fields rather than MLS information about these fields. Therefore, only fields for O3_183 and H_2O prior to April 16, 1993 should be used for scientific purposes.

Occasional interference effects (induced by the switching mirror stepper motor at low spacecraft battery voltage) can perturb the radiances and retrieved parameter values. This problem started in mid-October 1992, and typically occurs just before sunrise (at the satellite location) for a few minutes. Some diagnostics are sensitive to this effect (quality fields in the Level 3 parameter files show a degradation for ClO and O3_205), but the predictive capabilities of the current software did not allow for this effect to be reflected in the error bars (quality values) given in the Level 3A files. The MLS team plans to document in more detail the specific times/locations of these interference effects, which can lead to occasional bad profiles, especially for those parameters derived from the weakest signals.

The V0003 MLS files for temperature, ozone (both from the 205-GHz band retrievals and the 183-GHz band retrievals), water vapor, chlorine monoxide, and sulfur dioxide

contain generally reliable and useful information about the global distribution and variability (spatial and temporal) of these fields. However, the error bars (quality fields in the files) and other diagnostic information need to be examined for optimum use of these fields in scientific analyses. A summary of useful vertical ranges, precision and accuracy estimates, caveats, and known systematic effects is provided below for each retrieved parameter. This summary will be detailed further and updated in published work. Current issues and future goals, in terms of retrieval algorithms for each parameter, are also summarized.

The next significant upgrade in software (for full reprocessing) is not expected until late 1994.

2.4.1 Temperature

CHANGES FROM PREVIOUS VERSION

Temperatures in the V0003 files are very similar to the previous version, except in the mesosphere. The retrieval software includes in the error budget, a term for field of view (FOV) calibration uncertainty. Temperatures in the mesosphere are closer to climatology and have larger errors. Temperature differences (RMS) between versions V0002 and V0003 are 1 K from 22 mbar to 2.2 mbar, 2.5 K at 1 mbar and 5 K at 0.46 mbar.

CURRENT STATUS

UARS Level	Standard Pressure (mbar)	Estimated Single Profile 1σ Precision[1] (K)	Estimated Accuracy[2] (K)
20	0.46	3	7
18	1.0	2.5	5
16	2.2	1.5	5
14	4.6	1.5	5
12	10	1.5	4
10	22	1.5	4

[1] The precisions are estimated from RMS differences between near collocated measurements on adjacent orbits (1.5 hours separated) at the orbit turn-around points.

[2] The accuracies are obtained from RMS differences between the MLS profiles and the NMC daily analyses interpolated onto the MLS orbit tracks. The numbers should be interpreted as preliminary upper bounds on the 1σ accuracy.

RESOLUTION

The retrieved vertical resolution is two UARS pressure surfaces ($\Delta\log_{10}(p) = 0.33$, or about 6 km). The retrieved temperature profile is represented as a piecewise-linear function with break points at alternate (even-numbered) UARS pressure surfaces (e.g., 10, 4.6, 2.2, 1 mbar). The temperatures on the even-numbered surfaces (level 3AT files only) are the retrieved break-point values, while those on the odd-numbered surfaces (e.g., 6.8, 3.2, 1.5 mbar) are averages of the temperatures on adjacent even-numbered surfaces. The level 3AL profiles have an additional linear interpolation with respect to latitude to generate an evenly spaced latitude grid.

SYSTEMATIC EFFECTS

Orbit and yaw period dependencies are observed in the temperature field. Zonal mean differences and zonal RMS differences between the MLS temperature field and the NMC analysis show biases which depend on: whether the data is obtained during the ascending or descending sides of the UARS orbit, whether MLS is looking north or south, and when during a yaw period the measurements are taken. These systematic errors are 1–3 K in the stratosphere, but can be as much as 10 K in the lower mesosphere. Comparisons of zonal mean cross-sections , before and after yaw maneuvers suggest that the north-looking cross-sections may be shifted northward 1–3 degrees in latitude relative to the south-looking cross-sections.

MLS temperatures are biased 1–2 K lower than NMC temperatures between 22 mbar and 1 mbar.

Lapse rates in the mesosphere are too negative due to decreasing sensitivity. A notch, usually negative, is observed in many MLS temperature profiles at 0.22 mbar.

CAVEATS

The retrieval is based on the sequential estimation algorithm with an a priori estimate containing both the NMC daily analysis (when available) and a month-dependent, latitude-dependent climatology developed by the UARS science team. Although the profiles extend from 1000 mbar to 0.0001 mbar, useful information is provided by MLS only between 22 mbar and 0.46 mbar. Above 0.22 mbar the profiles relax slowly to the climatology. Below 22 mbar, the profiles are linearly interpolated from NMC daily analyses (or climatology when necessary) onto even-numbered surfaces. Temperatures outside the range, 22 mbar to 0.4 mbar should not be used without the endorsement of the MLS team.

Currently a linearized forward model is used to fit radiances in a one-pass retrieval through the data. In the winter at high latitudes, the atmosphere may differ from the linearization point by more than 20 K, especially when wave activity is enhanced. During these periods, systematic errors from nonlinearities may be of the order of 5–10 K. Wave amplitudes may be misrepresented during periods of large wave activity.

The "quality" field in the level 3A files is the retrieval's estimated uncertainty, includes random and systematic components, and is obtained by propagating precisions of the radiance measurements, estimates of constrained parameter uncertainties, forward model inaccuracies, and some calibration uncertainties through the retrieval software. The quality should be interpreted as a lower bound on the accuracy.

At the conclusion of the retrieval, the estimated uncertainty is compared with the a priori uncertainty. When the ratio is greater than 0.5, or the temperature is more than 25% climatology, the quality is set negative to flag the dependence of the retrieved temperature on the a priori knowledge. Profiles with all qualities negative were usually not retrieved and are the a priori estimates; including these profiles in scientific analyses is not recommended.

The level 3 parameter files (described in the "Standard Formatted Data Units, MLS Level 3TP Parameter File" and "Standard Formatted Data Units, MLS Level 3LP Parameter File" documents) contain the diagnostic flag "MMAF_STAT." For optimal use of the MLS data, the parameter files should be examined, and profiles with MMAF_STAT not set to "G," "T," or "t" should be disregarded.

ISSUES AND FUTURE GOALS

- Continued investigation into sources of orbit and yaw period dependency of temperature field.
- Improve winter polar temperature retrievals where the atmosphere is further from retrieval linearization point by including a fully nonlinear radiance model.
- Improve temperature sensitivity in the mesosphere by using the three magnetic center channels, adjust retrieval grid to better reflect actual sensitivity, and fold tangent point pressure differences and geodetic altitude into the temperature retrievals.
- Extend MLS temperatures profiles lower into the stratosphere by incorporating a nonlinear retrieval scheme. Useful range should be extended to 46 or 68 mbar.

2.4.2 Ozone (O_3)

CHANGES FROM PREVIOUS VERSION

V0003 files for O3_205 give data values which are very close to the previous version, except in the lower stratosphere. A general increase in ozone occurred at 100 mbar, with some decrease at 46 mbar; this led to much fewer negative values at 100 mbar, where an overall negative bias existed before. The previous bias was largely caused by the inclusion of radiances for scan positions with tangent pressures larger than 100 mbar. However, small biases still persist, as discussed above.

Also, an adjustment was made in the pointing angle of the 183-GHz radiometer field of view (FOV), based on a comparison between the two ozone retrievals and independent moon scans to check the relative pointing between the 205-GHz and 183-GHz radiometer FOVs. This brought the two ozone retrievals in reasonable agreement, but a refinement in this approach is to be expected.

CURRENT STATUS

This information is for O3_205 (ozone retrieved from 205-GHz radiometer radiances).

UARS Level	Standard Pressure (mbar)	Estimated Single Profile 1σ Precision[1] (ppmv)	Estimated Accuracy[2] (%)
20	0.46	0.5	10
18	1.0	0.3	7
16	2.2	0.3	7
14	4.6	0.3	5
12	10	0.2	5
10	22	0.2	7
8	46	0.2	30
6	100	0.5	> 50

[1] The estimated precisions are based on observed variability in latitude bands where meteorological variability is small, hence the true precisions may be somewhat better than these estimates. These numbers are 1σ (RMS) precisions and are consistent with theoretical estimates obtained by propagating the radiance measurement precisions through a sequential estimation retrieval algorithm.

[2] The accuracy estimates are based on statistical comparisons with other data sets (including SAGE II, ozonesonde, and balloon correlative data) and are preliminary.

RESOLUTION

The retrieved vertical resolution is two UARS pressure surfaces ($\Delta \log_{10}(p) = 0.33$, or about 6 km). The retrieved ozone volume mixing ratio profile is represented as a piecewise-linear function with break points at alternate (even-numbered) UARS pressure surfaces (e.g., 100, 46, 22, 10 mbar). The mixing ratios on the even-numbered surfaces (level 3AT files only) are the retrieved break-point values, while those on the odd-numbered surfaces (e.g., 68, 32, 15 mbar) are averages of the mixing ratios on adjacent even-numbered surfaces. The level 3AL profiles have an additional linear interpolation with respect to latitude to generate an evenly spaced latitude grid.

SYSTEMATIC EFFECTS

The 46-mbar ozone mixing ratios usually have a negative bias (in comparison with other data sets) of approximately a few tenths of a ppmv, whereas the 100-mbar ozone mixing ratios generally have a positive bias of approximately 0.1 to 0.2 ppmv; these biases account for most of the accuracy figures at 46 and 100 mbar.

A small (approximately 5%) positive bias relative to SAGE II measurements exists in the middle and upper stratosphere. Similar biases are seen in other (but not all) comparisons near the ozone volume mixing ratio profile maximum. Integrated column ozone using data at 100 mbar and above tend to be biased high compared to estimated columns from other data sets (TOMS or ozonesondes); these biases may be caused by inadequate vertical resolution.

A cyclic O3_205 fluctuation synchronized to the UARS yaw period (roughly every 36 days) is present primarily in the tropics at the lowest altitudes, and affects column ozone by approximately 5 to 10 percent. The zonal mean O3_205 trend shows small "jumps" coincident with some satellite yaw maneuvers.

CAVEATS

O3_205 has received greater scrutiny than O3_183 and is currently the recommended ozone for stratospheric studies. It has consistently agreed with other data sets better than O3_183, and the 205-GHz radiances show better radiance residual closure than the 183-GHz radiances. However, O3_183 is better for mesospheric studies (up to 0.05 mbar) where the 205-GHz radiances lose sensitivity. The two fields are in good agreement in the upper stratosphere where both 183 and 205-GHz radiances have similar sensitivities.

The retrieval is based on the sequential estimation algorithm with an a priori estimate based on a month-dependent and latitude-dependent climatology developed by the UARS science team. While the O3_205 profiles have 37 grid points extending from 464 mbar to 4.6×10^{-4} mbar, the values at pressures outside the range 100 mbar to 0.46 mbar are mostly climatological. O3_205 at 100 mbar currently exhibits some large biases and therefore has limitations for use in scientific studies. Mixing ratios at pressures larger than 100 mbar or smaller than 0.46 mbar should not be used for scientific studies, and values at 100 mbar should not be used without consulting the MLS team.

The "quality" field in the level 3A files is the retrieval's estimated uncertainty. It includes random and systematic components, and is obtained by propagating precisions of the radiance measurements, estimates of constrained parameter uncertainties and

forward model inaccuracies through the retrieval software. The quality should be interpreted as a lower bound on the accuracy.

At the conclusion of the retrieval, the estimated uncertainty is compared with the a priori uncertainty. When the ratio is greater than 0.5, or the estimated mixing ratio is more than 25% climatology, the quality is set negative to flag the dependence of the retrieved mixing ratio on the a priori knowledge (note that the 100-mbar and 0.2-mbar levels are generally flagged with negative quality). Profiles with all qualities negative were usually not retrieved and are climatology; including these profiles in scientific analyses is not recommended.

The level 3 parameter files (described in the "Standard Formatted Data Units, MLS Level 3TP Parameter File" and "Standard Formatted Data Units, MLS Level 3LP Parameter File" documents) contain the diagnostic flag "MMAF_STAT." For optimal use of the MLS data, the parameter files should be examined and profiles with MMAF_STAT not set to "G," "T," or "t" should be disregarded.

CURRENT STATUS

This information is for O3_183 (ozone retrieved from 183-GHz radiometer radiances).

UARS Level	Standard Pressure (mbar)	Estimated Single Profile 1σ Precision[1] (ppmv)	Estimated Accuracy[2] (%)
26	0.046	0.4	—
24	0.10	0.3	—
22	0.22	0.2	—
20	0.46	0.2	—
18	1.0	0.2	—
16	2.2	0.3	—
14	4.6	0.3	—
12	10	0.2	—
10	22	0.2	—
8	46	0.2	—

[1] The estimated precisions are based on observed variability in latitude bands where meteorological variability is small, hence the true precisions may be somewhat better than these estimates. These numbers are 1σ (RMS) precisions and are consistent with theoretical estimates obtained by propagating the radiance measurement precisions through a sequential estimation retrieval algorithm.

[2] The accuracy estimates for O3_183 should be similar to, but somewhat larger than those for O3_205 based on comparisons of the two products.

RESOLUTION

The retrieved vertical resolution is two UARS pressure surfaces ($\Delta \log_{10}(p) = 0.33$, or about 6 km). The retrieved ozone volume mixing ratio profile is represented as a piecewise linear function with break points at alternate (even-numbered) UARS pressure surfaces (e.g., 10, 4.6, 2.2, 1 mbar). The mixing ratios on the even-numbered surfaces (level 3AT files only) are the retrieved break-point values, while those on the odd-numbered surfaces (e.g., 6.8, 3.2, 1.5 mbar) are averages of the mixing ratios on adjacent even-numbered surfaces. The level 3AL profiles have an additional linear interpolation with respect to latitude to generate an evenly-spaced latitude grid.

SYSTEMATIC EFFECTS

O3_183 may be biased high by 5 to 10 percent (based on what is known for O3_205 and limited comparisons between the O3_205 and O3_183 fields).

CAVEATS

The O3_183 data have not been scrutinized as critically as the O3_205 data because of efforts to resolve observed postlaunch biases. O3_205 has consistently agreed with other data sets better than O3_183, and the 205-GHz radiances show better radiance residual closure than the 183-GHz radiances. Although reasonable consistency exists with the O3_205 data, detailed studies of possible systematic effects have not been completed. This should be kept in mind when attempting to analyze O3_183 data.

O3_183 is better than O3_205 for mesospheric studies (up to 0.05 mbar) where the 205-GHz radiances lose sensitivity. The two fields are in good agreement in the upper stratosphere where both 183 and 205-GHz radiances have similar sensitivities.

The retrieval is based on the sequential estimation algorithm with an a priori estimate based on a month-dependent latitude-dependent climatology developed by the UARS science team. While the O3_183 profiles have 37 grid points, extending from 464 mbar up to 4.6×10^{-4} mbar, the mixing ratios at pressures outside the range 46 mbar to 0.046 mbar are mostly climatological and should not be used for scientific studies.

The "quality" field in the level 3A files is the retrieval's estimated uncertainty. It includes random and systematic components, and is obtained by propagating precisions of the radiance measurements, estimates of constrained parameter uncertainties and forward model inaccuracies through the retrieval software. The quality should be interpreted as a lower bound on the accuracy.

At the conclusion of the retrieval, the estimated uncertainty is compared with the a priori uncertainty. When the ratio is greater than 0.5, or the estimated mixing ratio is more than 25% climatology, the quality is set negative to flag the dependence of the retrieved mixing ratio on the a priori knowledge. Profiles with all qualities negative were usually not retrieved and are climatology; including these profiles in scientific analyses is not recommended.

The level 3 parameter files (described in the "Standard Formatted Data Units, MLS Level 3TP Parameter File" and "Standard Formatted Data Units, MLS level 3LP Parameter File" documents) contain the diagnostic flag "MMAF_STAT." For optimal use of the MLS data, the parameter files should be examined and profiles with MMAF_STAT not set to "G," "T," or "t" should be disregarded.

ISSUES AND FUTURE GOALS

- Improved accuracy and further extension of the useful vertical ranges through the use of a nonlinear, iterative retrieval scheme, which makes optimum use of all channels at all scan positions.
- Increased vertical resolution (in the retrieval grid), particularly in the lower stratosphere.
- Elimination of possible "small" biases in the O3_205 profiles. This includes refinement of simulation tests, and is tied to the previous two items.

- Elimination of the artificial cyclic behavior (within yaw periods) for O3_205 (and O3_183 if present there as well). This effect may be tied to the band 1 retrievals (temperature and tangent pressure).
- Elimination of small jumps in the zonal mean values (studied only for O3_205 so far) across yaw days. This effect may be tied to the band 1 retrievals (temperature and tangent pressure).
- Improved radiance fits for the 183-GHz ozone in particular.
- Refinements in the postlaunch determination of radiometer pointing differences (this effect has an impact on the retrievals).
- Better agreement between the two independent ozone retrievals, particularly in the lower stratosphere (with the possible generation of one common ozone field, for the period when both radiometers were operational).

2.4.3 Water Vapor (H_2O)

CHANGES FROM PREVIOUS VERSION

Improvement of the 183-GHz radiometer calibration (see comments on MLS O_3) has resulted in a reduction of retrieved MLS H_2O stratospheric values (using V0003) of about 5–10% (in comparison to versions V0001 and V0002, which were used at the Oxford and Boulder data validation meetings). A reduction in the mesospheric temperature spikes (systematic effect) in V0003 files has helped reduce the extent of H_2O spikes, although some effect still exists.

Upper tropospheric H_2O retrievals using band 3 are being produced routinely at JPL and analyzed as a research product.

CURRENT STATUS

UARS Level	Standard Pressure (mbar)	Estimated Single Profile 1σ Precision[1] (ppmv)	Estimated Accuracy[2] (%)
22	0.22	0.4	15–30
20	0.46	0.4	15–30
18	1.0	0.3	15–30
16	2.2	0.2	15–30
14	4.6	0.2	15–30
12	10	0.1	15–20
10	22	0.2	15–20
8	46	0.2	15–20

[1] The estimated precisions are based on observed variability in latitude bands where meteorological variability is small, hence the true precisions may be somewhat better than these estimates.

[2] These accuracies are first-order estimates based on comparisons of MLS H_2O data with other UARS and/or correlative measurements.

RESOLUTION

The retrieved vertical resolution is two UARS pressure surfaces ($\Delta\log_{10}(p) = 0.33$, or about 6 km). The retrieved water vapor volume mixing ratio profile is represented as a piecewise-linear function with break points at alternate (even-numbered) UARS pressure surfaces (e.g., 10, 4.6, 2.2, 1 mbar). The water vapor mixing ratios on the even-numbered

surfaces (level 3AT files only) are the retrieved break-point values, while those on the odd-numbered surfaces (e.g., 6.8, 3.2, 1.5 mbar) are averages of the mixing ratios on adjacent even-numbered surfaces. The level 3AL profiles have an additional linear interpolation with respect to latitude to generate an evenly spaced latitude grid.

SYSTEMATIC EFFECTS

At high latitudes, especially in winter, the estimated uncertainty (see below) can increase to 1.8 ppmv at 46 mbar, and to 1 ppmv at 22 mbar, whereas the low latitude uncertainties are around 0.9 ppmv and 0.8 ppmv. At these pressures, the a priori uncertainty is 2 ppmv, so that for these estimated uncertainties, the estimated mixing ratios are more than 80% or 25% climatology. Detailed studies suggest that this is due to a combination of the atmosphere being optically thick and very low temperatures (especially during winter), resulting in a loss of information content.

A "notch" of high H_2O values appears in the lower mesosphere (in the region near 0.1 mbar) which is thought to be unreal and needs further study.

Comparisons with other UARS data and/or correlative data suggest that MLS H_2O may be roughly 10–30% too high in the range 46 mbar to 0.2 mbar.

CAVEATS

The "quality" field in the level 3A files, the retrieval's estimated uncertainty, includes random and systematic contributions, and is obtained by propagating precisions of the radiance measurements, estimates of constrained parameter uncertainties, and forward model inaccuracies through the retrieval software. The quality should be interpreted as a lower bound on the accuracy.

The useful vertical range for MLS H_2O is 46 mbar to 0.2 mbar. At 46 mbar there is a loss of information at high latitudes. H_2O values at 46 mbar should not be used in scientific studies without the endorsement of the MLS team.

The retrieval is based on the sequential estimation algorithm and uses an a priori estimate based on a month-dependent latitude-dependent climatology developed by the UARS science team. At the conclusion of the retrieval, the estimated uncertainty is compared with the a priori uncertainty. When the ratio is greater than 0.5, or the mixing ratio is more than 25% climatology, the quality is set negative to flag the dependence of the retrieved mixing ratio on the a priori estimate. Only data having positive quality should be used for scientific purposes.

The level 3 parameter files (described in the "Standard Formatted Data Units, MLS Level 3TP Parameter File" and "Standard Formatted Data Units, MLS Level 3LP Parameter File" documents) contain the diagnostic flag "MMAF_STAT." For optimal use of the MLS data, the parameter files should be examined and profiles with MMAF_STAT not set to "G" should be disregarded.

ISSUES AND FUTURE GOALS

- Improved accuracy and further extension of the useful vertical ranges through the use of a nonlinear, iterative retrieval scheme, which makes optimum use of all channels at all scan positions.

- Increased vertical resolution (in the retrieval grid), particularly in the lower stratosphere.
- Further investigation of any possible systematic effects in the profiles, such as the notch in mesospheric H_2O, and elimination of such effects.
- Further investigation of any possible systematic effects in the temporal evolution of zonal mean fields (such as the effects observed in temperature and O3_205), and elimination of such effects.
- Improved radiance fits.
- Refinements in the postlaunch determination of radiometer pointing differences (this has an impact on the retrievals).

2.4.4 Chlorine Monoxide (ClO)

The latest MLS production data-processing algorithms were implemented in software delivered to the CDHF in December 1992, and all MLS data have been reprocessed with this software. These algorithms corrected all ClO problems mentioned in the report from the previous October 1992 UARS Validation Workshop held in Boulder.

CURRENT STATUS

UARS Level	Standard Pressure (mbar)	Estimated Single Profile 1σ Precision[1] (ppbv)	Estimated Accuracy[2]
20	0.46	1.6	0.15 ppbv and 30%
18	1.0	1.3	0.10 ppbv and 20%
16	2.2	0.8	0.10 ppbv and 15%
14	4.6	0.5	0.10 ppbv and 15%
12	10	0.4	0.15 ppbv and 15%
10	22	0.4	0.20 ppbv and 15%
8	46	0.5	0.50 ppbv and 15%
6	100	1.5	0.70 ppbv and 40%

[1] The estimated precisions given here are typical values obtained by propagating yhe radiance precisions through the retrieval algorithm and are consistent with the observed variance in situations where ClO is below the instrument noise level. The quality field in the level 3A files give the estimated precisions on individual profiles. Precision can be improved by averaging together individual profiles.

[2] The estimated accuracies are a root sum square of a bias error (accuracy given in ppbv) plus a scaling error (the product of the fractional accuracy and the estimated mixing ratio). These accuracies do not include the random noise which, for a single profile, is the estimated precision..

USEFUL VERTICAL RANGE

The useful vertical range is 100 to 0.46 mbar. As with other MLS data in Version 3 files, ClO is retrieved only on "even" UARS surfaces (100, 46, 22, ... mbar); values given on the "odd" UARS surfaces (68, 32, 15, ... mbar) are averages of the values retrieved on the two adjacent surfaces. Only data having positive values of the quality indicator in the Level 3 data files should be used for scientific purposes. Additional quality indicators in the Level 3 parameter files should also be examined, and only data having MMAF_STAT=G and QUALITY_CLO=4 should be used for scientific studies.

Individual ClO profiles generally have poor signal-to-noise ratios and most scientific uses of these data will require averaging.

CAVEATS

The data contain known systematic errors which are described in section 2.5.4, and these should be accounted for when scientific studies are performed with the data. Of particular note is that the enhanced abundances of lower stratospheric polar winter vortex ClO are expected to be overestimated by approximately 0.4 ppbv when HNO_3 abundances are near zero. Also, the 100 mbar ClO retrievals are still under investigation and should not be used in scientific investigations without endorsement by the MLS team. ClO values appear in the data files for pressures greater than 100 mbar, but should not be used for scientific purposes: these are strongly affected by the a priori estimate and are used to provide suitable "boundary conditions" outside the region where useful retrievals are obtained. MLS measures only the ^{35}ClO isotope. Retrieved ^{35}ClO mixing ratios are multiplied by 1.32 to give the estimated total ClO mixing ratio in both ^{35}ClO and ^{37}ClO isotopes, and this total is stored in the Version 3 data files. References for the chlorine isotopic abundances are given in Waters (1993).

CURRENT ISSUES

There is a possible discrepancy between MLS and ground-based September 1992 measurements of upper stratospheric ClO over Antarctica, and more work is needed to resolve this discrepancy. More work is also needed to quantify the uncertainties (both random noise and systematic effects) in the 100-mbar ClO values, and the extent to which these values can be generally used in scientific studies. Improvements in the MLS retrieval algorithms are planned for future reprocessing(s) to further improve the quality of the ClO product.

It must be emphasized that the ClO values given in the MLS data files represent a "best fit" profile which is piecewise linear in ClO mixing ratio versus $\log_{10}(p)$. The break points of this piecewise linear representation occur at even UARS pressure surfaces (100, 46, 22, ..., 0.46 mbar), corresponding to a vertical resolution of about 5 km. Vertical structure finer than 5 km, as expected to be significant during polar stratospheric cloud processing, is not resolved and errors can result if the MLS values are interpreted only as "abundances at that pressure." The proper interpretation is that the values describe the vertical profile which best fits the MLS measurements under the limitations of the current algorithms and vertical representation.

Averaging kernels (Rodgers 1990), which describe the vertical smearing of the Version 3 ClO data, are shown in Figure 2.4.4–1. The a priori profile used in the ClO retrievals is from the UARS "climatology," and includes no heterogeneous chemistry enhancements of lower stratospheric ClO, so as to eliminate possibility of an a priori positive bias on the enhanced ClO values retrieved in the polar winter vortices. An a priori uncertainty of 3 ppbv (1σ) is used for ClO at all pressures from 100 to 0.46 mbar.

An important aspect of validating the MLS ClO measurement is examination of the radiances from the instrument, and the extent to which these radiances are "fit" by the radiances calculated from the retrieved profiles. A linear "spectral baseline" is retrieved for each measured spectrum, so that only the spectrally varying component of the

measured radiances affects the retrieved atmospheric parameters. There are 30 spectral channels (in MLS spectral bands 2 and 3) which are used for retrieving ClO. These channels resolve the ClO emission line at all altitudes throughout the stratosphere, allowing clear identification of the ClO signal. An independent retrieval (with no "memory" of the previous retrieved profile) is performed on each 65-s limb scan with approximately 18 measured spectra used in each retrieval. Thus, approximately 500 spectral measurements in each limb scan are used to retrieve the profile. Since there are many more spectral measurements than retrieved parameters, examination of the residuals is a meaningful exercise. A quality indicator for each ClO retrieval (QUALITY_CLO) is calculated and placed in the Level 3 Parameter files on the CDHF; this includes information on the quality of radiances used in the retrievals, and the quality of the retrieval "fit" to the radiances. As mentioned earlier, only retrievals having ClO quality indicator of 4 (good radiances, and good fit to within the expected noise) should be used for scientific analyses.

Figure 2.4.4–2 shows averages of measured lower stratospheric radiances and residuals for conditions of enhanced lower stratospheric ClO in the Arctic vortex (see discussion in Waters et al. 1993). Figure 2.4.4–3 shows similar quantities for upper stratospheric radiances. The measured ClO signal is well fit by the signal calculated from the retrieved profiles, and the fits shown here are typical. Note the narrower spectral line for the upper stratospheric ClO signal as expected due to decreased pressure broadening in the upper stratosphere. Figure 2.4.4–4 shows spectra taken from tangent heights above approximately 65 km. Negligible ClO signal is expected at these altitudes and the spectra illustrate residual instrumental artifacts in the measured radiances. These artifacts are at the 0.05-K brightness temperature level, which correspond to ClO abundances at approximately 0.05 ppbv. They appear sufficiently stable that day-night differences (of data taken within a period of a few days) should reduce the instrumental artifacts to a level corresponding to ClO abundances of approximately 0.01 ppbv.

2.4.4.1 Chlorine Monoxide Error Estimates

Errors in the retrieved ClO profiles are conveniently grouped into three categories: Figure 2.4.4.1-1 shows the contributions from:

(1) Noise - a random contribution which can be reduced by averaging;
(2) Scaling - a multiplicative uncertainty which gives a percentage uncertainty in the measurements;
(3) Bias - an additive uncertainty which can be reduced by taking appropriate differences.

Figure 2.4.4.1-1 shows contributions to the MLS errors using the formalism developed by Rodgers (1990). The curve labeled "a priori error" is what has sometimes previously been called the null space error, and we use the new terminology per the recommendation of Marks and Rodgers (1993). The a priori error can be considered a scaling error, as will be discussed later. The " measurement error" curve shown in the figure is due to the instrument hoise for a single profile. The "residual error" is the error associated with the lack of a complete fit to the radiances and should be considered a bias error. It is an aggregate measure of any errors which prevents fitting the measured radiances by the forward model and retrieval scheme. Values shown in Figure 2.4.4.1-1 were determined by averaging measurements so that instrument noise did not contribute significantly. The residual error can vary, depending upon the particular situation, but we believe the values

shown adequately represent mid-latitude situations. More details on bias uncertainties for conditions of enhanced ClO in the polar vortex are discussed in Section 2.5.4.3

Figure 2.4.4.1-2 summarizes estimates for these three types of uncertainties for the ClO data in the MLS Version 3 files on the CDHF. The following subsections describe how these estimates were obtained.

2.4.4.2 ClO Noise Errors

The noise uncertainty (+/- one signal) associated with each retrieved profile is computed by the retrieval algorithms and stored with the retrieved values in the CDHF files as a quality indicator. The algorithms which calculate it include the effects of uncertainties in temperature, pointing (pressure), water vapor, fitted spectral baseline, and other parameters which are part of the overall state vector for the MLS retrievals. The uncertainty is made negative if the a priori error (a constant 3 ppbv for ClO) is not reduced by at least a factor of two (corresponding to less than 75% of the information in the retrieved profile being from the MLS measurements and more than 25% being from the a priori).

Figure 2.4.4.2-1 compares the noise uncertainties produced by the retrieval algorithms and the observed standard deviation in the retrieved ClO values. Each of the plots is for a full UARS month (summer in each hemisphere) of retrievals made for data at night with local solar times between midnight and 6 am (no retrievals were included for which the solar zenith angle was less than 95°) when stratospheric ClO is expected to be a minimum and variations in the retrieved profiles are expected to be dominated by the instrument noise. More than 10,000 independent retrievals were included for each of the two months. The standard deviation of the measurements agrees closely with the predicted one sigma noise, except at 100 mb. Part of the discrepancy at 100 mb is due to the fact that the uncertainties predicted by the retrieval algorithms include a contribution due to the assigned 3 ppbv a priori uncertainty, while a constant a priori value (essentially a value of zero at 100 mb) with no noise is actually used during the retrievals. This effect is easily calculated, and the predicted noise at 100 mb should be reduced from 1.7 to 1.4 ppbv with no actual noise on the a priori. The remaining discrepancy of approximately 0.4 ppbv is under investigation. Note that the formal error estimates in Figure 2.4.4.1-1 also show smaller errors than predicted by the production processing algorithms at 100 mb and even smaller than the observed variations. Further investigations of the 100 mb noise estimates are needed.

Figure 2.4.4.2-2 shows the distribution on each retrieval pressure surface of values of the nighttime ClO retrievals which were included in Figure 2.4.4.2-1 (a total of more than 20,000 retrievals). The distribution is seen to be Gaussian, as expected. A similar distribution for nighttime MLS ClO in northern 1992 winter was found in the analyses of Schoeberl et al. (1993). These results indicate that analyses based on Gaussian noise statistics are justified for the MLS ClO data.

2.4.4..3 ClO Scaling Errors

Figure 2.4.4.3-1 summarizes the estimated scaling uncertainties associated with the Version 3 ClO data files. The basis for these estimates is described below.

ClO is retrieved from optically-thin radiance measurements, and there is, to within a good approximation, a linear relationship between the ClO abundances, the ClO spectral line strength, and the radiances. The same scaling uncertainties in radiances and ClO line strength thus apply to the retrieved ClO abundances.

An instrument calibration uncertainty of 3% is assigned (MLS Instrument Calibration Report, Jarnot and Cofield, 1991). Calibration uncertainty is defined as the combination of uncertainty in the calibrated radiances from each instrument channel and the uncertainties introduced by instrument parameters in the forward model calculations of radiance. The forward model uses measured instrument spectral and field-of-view responses to account for instrumental effects on the calculated atmospheric radiances. A linearized version of the forward model is used in the retrieval algorithms producing MLS Version 3 data.

Uncertainties in the ClO line strength are due to uncertainties in the measured dipole moment of ClO and in the calculated matrix element for the particular rotational transition observed by MLS. The dipole moment has been measured (Yaron et al., 1988) with 0.1% accuracy, which introduces a 0.2% error since the square of the dipole moment appears in the relevant expressions. The uncertainty in the calculation of the transition matrix element is estimated to be 0.5% (H. M. Pickett, private communication).

MLS resolves the ClO spectral line, and these measurements provide information on the line shape and width. An off-line retrieval scheme was implemented which allowed retrieval of the ClO collisional linewidth, simultaneously with the other parameters that are normally retrieved. Results gave a linewidth parameter somewhat smaller than the nominal N_2 broadening value measured by Pickett et al. (1981). The ClO linewidth due to both N_2 and O_2 (and the respective temperature dependencies) were then measured in the JPL laboratory by J. J. Oh and E. A. Cohen. These new laboratory measurements (with an accuracy of 3%) gave a value consistent (within the error bars) with the earlier N_2 value of Pickett et al. (1981), but with smaller broadening by O_2, which produced an overall atmospheric linewidth consistent with that retrieved from the MLS data. The new linewidth has been used in the production of the MLS Version 3 data files. The effect was to reduce the retrieved values of lower stratospheric ClO by 10-20% from the values obtained using the earlier value for the linewidth. The effect of the estimated 3% uncertainty of this linewidth parameter on the retrieved profiles was determined by propagating the uncertainty through the retrieval algorithms, which resulted in the curve included in Figure 2.4.4.3-1. Additional uncertainties (such as errors in the assumed line shape function) can cause lack of closure in the retrievals, and these should already be accounted for in the residual errors shown in Figure 2.4.4.1.-1.

Figures 2.4.4.3-2(a), (b) show results of simulations where the "true" ClO was made to cycle between 0, 1, and 2 ppbv at all retrieval surfaces. Except at 100mb (and to some extent at 0.46 mb) where effects of the a priori are expected, the retrieval closure is seen to be within 10%. A worst case scaling error of approximately 30% due to the a priori influence is calculated for 100 and 0.46 mb and less than 3% between 4.6 and 46 mb. For the closure errors shown in the above figures, we assume the worst case of the lack of closure shown in the simulations and that expected due to the a priori.

2.4.4.4 ClO Bias Errors

Bias errors can be introduced in the retrievals due to lack of adequately fitting the radiances (the residual error curve in Figure 2.4.4.1-1) and by errors due to interfering species which are not adequately accounted for in the retrieval scheme. Molecules which have a small effect on the ClO signal and which are not adequately accounted for in the current algorithms include HNO_3 and N_2O.

Figure 2.4.4.4-1 shows results of simulation tests for enhanced lower stratospheric ClO, where both day and night conditions are simulated. Each curve is the result of approximately 40 retrievals. Curve 1 (dashed) is "truth), and curve 2 (solid) gives results from the algorithms producing Version 3 data. The results agree to within 0.1 ppbv. However, with a change from climatological to zero HNO_3 or N_2O.(as can effectively happen in the polar vortex), the ClO retrieval is affected in this simulation by up to 0.25 ppbv at 46 and 100 mb as shown by curves 3 and 4. Curves 3 and 4 are results obtained by averaging radiances before doing retrievals and including iterations in the retrieval process. The bottom panel in Figure 2.4.4.4-1 shows that taking day-night differences removes the bias introduced by changing to zero HNO_3 and N_2O in these simulations.

Figure 2.4.4.4-2 and 2.4.4.4-3 show results from different retrieval schemes used on real data taken in the Antarctic vortex on August 17 and September 17, 1992, respectively. The two days were chosen for examination because in mid-August, MLS measured greatly enhanced ClO on both the 22 and 46 mb retrieval surfaces, whereas in mid-September enhanced ClO does not appear at 22 mb (Waters et al., 1993b). Results from approximately 20 retrievals with the Version 3 production algorithms (curve 1) are included for August 17 and approximately 49 for September 17. Curve 2 gives results from a retrieval in which the radiances are averaged before doing the retrievals and the retrievals are iterated. Peak values of ClO are reduced by 0.1-0.2 ppbv from the production algorithm values, and the 100 mb value is increased by about 0.7 ppbv on both days. Reasons for the large effect at 100 mb include the fact that th radiance-averaging scheme uses radiances from higher pressure levels than does the production algorithms. The results indicate that the Version 3 ClO values at 100 mb should only be used with caution and only with endorsement by the MLS team. Curves 3 and 4 show the effects of changing HNO_3 and N_2O from the climatological values (assumed by the current algorithms) to zero. Taking day-night differences appears to remove the effects of HNO_3 and N_2O at 46 mb and above, but with the production algorithms still giving approximately 0.1 ppbv more peak ClO than the radiance-averaging iterative algorithm results. This test indicates that when HNO_3 is near zero, the enhanced lower stratospheric ClO values in the Version 3 data files will be approximately 0.4 ppbv high. The tests indicate that day-night differences (bottom panel) can remove the error to within approximately +/- 0.1 ppbv. The day-night difference does not necessarily reduce the difference at 100 mb (as shown in the August 17 results), which emphasizes the uncertainties in the 100 mb ClO values in the Version 3 data files.

Bias errors in the ClO retrievals can be determined empirically by using the diurnal variation in ClO. ClO is a photolytic product which decays at night. At pressures greater than approximately 10 mb, the time constants are sufficiently short that negligible ClO is expected at night for gas-phase chemistry. In the lower polar stratosphere where enhanced levels of ClO may occur as a result of heterogeneous processes, thermal

decomposition of ClOOCl at temperatures above 200-210K can result in significant levels of nighttime ClO. Figures 2.4.4.4-4 and 2.4.4.4-5 show averages of ClO retrievals made at night (solar zenith angle greater than 95°) and only between midnight and 6 am when ClO is expected to be a minimum. The negative values between 10 and 100 mb indicate a bias error of 0.1-0.2 ppbv. Note that the shape and range of values are obtained in all the latitude bins considered for both hemispheres. Future versions of the algorithms are expected to remove this bias. At altitudes above about 3 mb, positive values of ClO are retrieved at night. The corresponding radiances at these altitudes, given in Figure 2.4.4.4-6, show a clear ClO spectral line at night, indicating the presence of ClO. The ClO spectral line calculated from the retrieved profiles agrees with the measured spectral line, indicating a discrepancy of less than 0.1 ppbv. These nighttime ClO values are qualitatively consistent with model predictions (e. g. Ko and Sze, 1984) that ClO should be present at night in the upper stratosphere.

Figure 2.4.4.4-7 summarizes the estimated bias uncertainties for the Version 3 ClO data files. The values at higher altitudes (pressures below about 10 mb) were obtained from the residual error curve in Figure 2.4.4.1-1. The values at lower altitudes were obtained empirically from the nighttime retrievals, and the tests performed for conditions of enhanced ClO in the lower stratospheric polar vortex.

2.4.5 Sulfur Dioxide (SO_2)

SO_2 was not an original MLS measurement objective, but an unanticipated and significant spectral feature located in the edge of the MLS ClO spectral band was evident in tropical radiances beginning with the first day of measurements on 19 September 1991 (Read et al., 1993). This feature, shown in Figure 2.4.5–1, exhibited no diurnal variation and is assignable to the SO_2 $18_{3,16} \rightarrow 18_{2,15}$ rotational transition at 204.247 GHz. The radiance residuals, also given in Figure 2.4.5–1, show that the feature is well fit by the radiances calculated from the retrieved SO_2 profile. Confirmation of the signal being due to SO_2 is obtained by another spectral feature which appears in the radiance residuals for the MLS 205-GHz O_3 band. That feature is shown in Figure 2.4.5–2 which, because of the much greater strength of the O_3 line, is evident only in residuals after the O_3 contribution is removed. This second feature is assignable to the SO_2 $24_{3,21} \rightarrow 24_{2,22}$ rotational transition at 200.287 GHz.

MLS has, to date, detected SO_2 from the Pinatubo and Lascar eruptions. The Lascar eruption (20 April 1993) actually produced a stronger SO_2 signal for MLS, but this was highly localized.

SO_2 is routinely retrieved in MLS Level 2 processing, and placed in the Level 2 files on the CDHF. Only a limited number of Level 3 files have been created. These include UARS days 54–124, 157–193, 278–305, 338–375, and 415–581. Additional Level 3 files can be produced from the Level 2 files if scientific interest arises.

USEFUL VERTICAL RANGE

The useful vertical range is 46 to 2.2 mbar. Retrievals over this range are useful within their stated uncertainties. The 100-mbar coefficient is retrieved, but its precision of 20–30 ppbv is only marginally useful except during the largest injections of SO_2 by volcanic eruptions.

CURRENT ISSUES

SO_2 is only detectable by MLS following volcanic injections, and this makes it difficult to obtain SO_2 correlative measurements. The measurements available for comparison, although indirect, support the quality of the MLS SO_2 measurements within the uncertainties stated above, and there are no current issues which require resolution.

2.4.5.1 Sulfur Dioxide Error Estimates

Sulfur dioxide error estimates are obtained in a manner similar to that discussed for ClO. The SO_2 precision at 46 mb is 7 ppbv, at 22 mb is 4.5 ppbv, and at 10-2.2 mb is 3.0-3.5 ppbv. The SO_2 retrievals also have sytematic errors or uncertainties which can produce additive shifts (bias errors) and multiplicative effects (scaling errors). SO_2 is measured in the same spectral region as ClO, and the bias and scaling errore for ClO previously discussed should be generally applicable to SO_2. The current estimated bias error for SO_2 is based on SO_2 retrievals on data taken more than one and one-half years after the Pinatubo eruption. These data show a steady non-decaying value of approximately 3 ppbv between 46 and 10 mb, and this is attributed to bias in the retrievals. The ClO scaling error of approximately 10-15% should apply to SO_2. Thus, at 46 mb and above, the accuracy of SO_2 in the CDHF Version 3 files is believed to be the rss of 3ppbv and 15% of the retrieved SO_2, in addition to the noise values in the data files. The 100 mb level has not been studied in detail.

REFERENCES

Allen, M., Y. L. Yung and J. W. Waters, "Vertical Transport and Photochemistry in the Terrestrial Mesosphere and Lower Thermosphere (50-120 km)", *J. Geophys. Res.*, **86**, pp 3617-3627, 1981.

Connor, B. J., and C. D. Rodgers, "A Comparison of Retrieval Methods: Optimal Estimation, Onion-Peeling, and a Combination of the Two" , RSRM '87: *Advances in Remote Sensing Retrieval Methods*, pp. 271-281, A. Deepak, H.E. Fleming, and J. S. Theon, eds., A. Deepak Publishing, 1989.

Kumer, J. B. , "CLAES Error Bar Discussion for Software Version 4.10," Lockheed Palo Alto internal report, 1992.

Marks, C. J. and C. D. Rodgers, "A Retrieval Method for Atmospheric Composition from Limb Emission Measurements", *J. Geophys. Res.*, **98**, pp 14939-14953, 1993.

Mergenthaler, J. L., and Kumer, J. B., "An Assessment of OH Airglow Interference on the Remote Sensing of Stratospheric HCl via Limb Sounding in the Near-Infrared," *Int. J. Remote Sensing*, **7**, pp 1203-1211, 1986.

Press, W. H., Flannery, B. P., Teukolsky, S. A., Vetterling, W. T., *Numerical Recipes*, Cambridge University Press, 702 , 1989.

Read, W. G., Friideveaux, L., and Waters, J. W., "Microwave Limb Sounder (MLS) Measurements of SO_2 from Mt. Pinatubo Volcano," *Geophys. Res. Lett.*, **20**, pp. 1299-1302, 1993.

Roche, A. E., Kumer, J. B., Mergenthaler, J. L., Ely, G. A., Uplinger, W. G., Potter, J. F., James, T. C., and Sterritt, L. W. 1993, "The Cryogenic Limb Array Etalon Spectrometer (CLAES) on UARS: Experiment Description and Performance," *J. Geophys. Res.*, **98**, 10763.

Rodgers, C. D., "Retrieval of Atmospheric Temperature and Composition from Remote Measurements of Thermal Radiation. " *Revs. Geophys. Space. Phys.*, **14**, pp 609-624, 1976.

Rodgers, C. D., Jones, R. L., Barnett, J. J., "Retrieval of Temperature and Composition from NIMBUS 7 SAMS Measurements", *J. Geophys. Res.*, **89**, pp 5280-5286, 1984.

Taylor, F.W., C. D. Rodgers, J. G. Whitney, S. T.Werrett, J. J. Barnett, G. D.Peskett, P. Venters, J. Ballard, C. W. P. Palmer, R. J. Knight, P. Morris, T. Nightingale, A. Dudhia, "Remote Sensing of Atmospheric Structure and Composition by Pressure Modulator Radiometry from Space: The ISAMS Experiment on UARS", *J. Geophys. Res.*, **98**, 10799-10814, 1993.

Waters, J. W., "Microwave Limb Sounding" in *Atmospheric Remote Sensing by Microwave Radiometry,* (M. A. Janssen, ed.), New York, John Wiley and Sons, 1993.

Waters, J. W., Froideveaux, L., Read, W. G., Manney, G. L., Elson, L. S., Flower,, D. A., Jarnot, R. F., and Harwood, R. S., "Stratospheric ClO and Ozone from the Microwave Limb Sounder on the Upper Atmospheric Research Satellite," *Nature,* **362,** pp. 597-602, 1993.

Yaron, D., K. Peterson, and W. Klemperer, "On the Dipole Moment Functions of ClO and OH", *J. Chem. Phys..,* **88**, pp. 4702-4710, 1988.

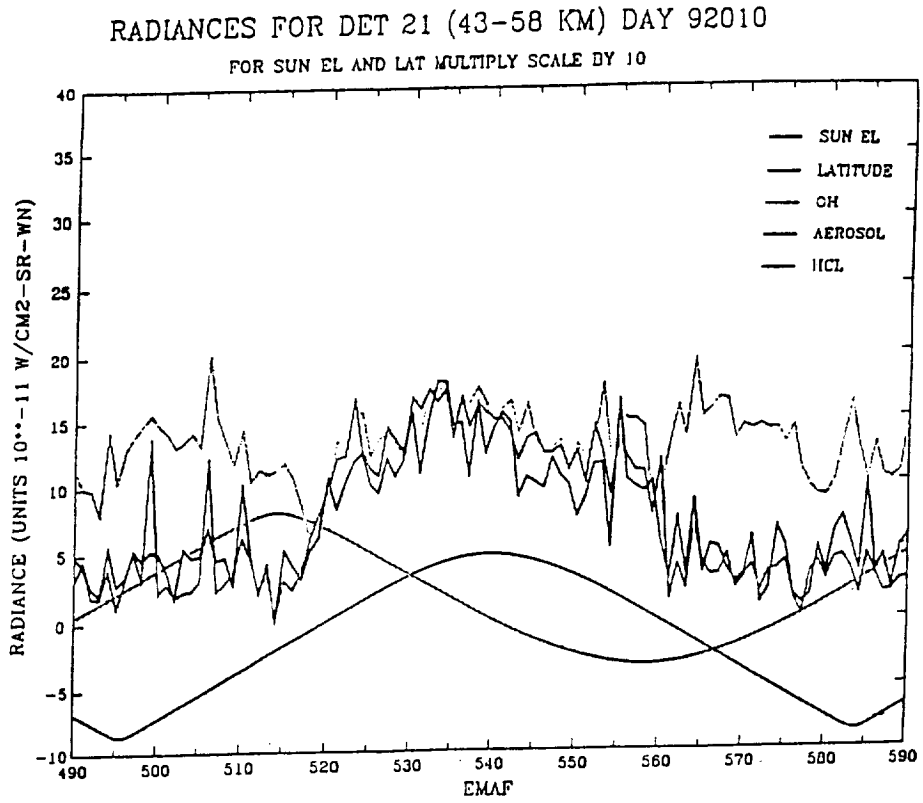

Figure 2.2.16–1. Radiances for detector 21, for one orbit of data on January 10, 1992.

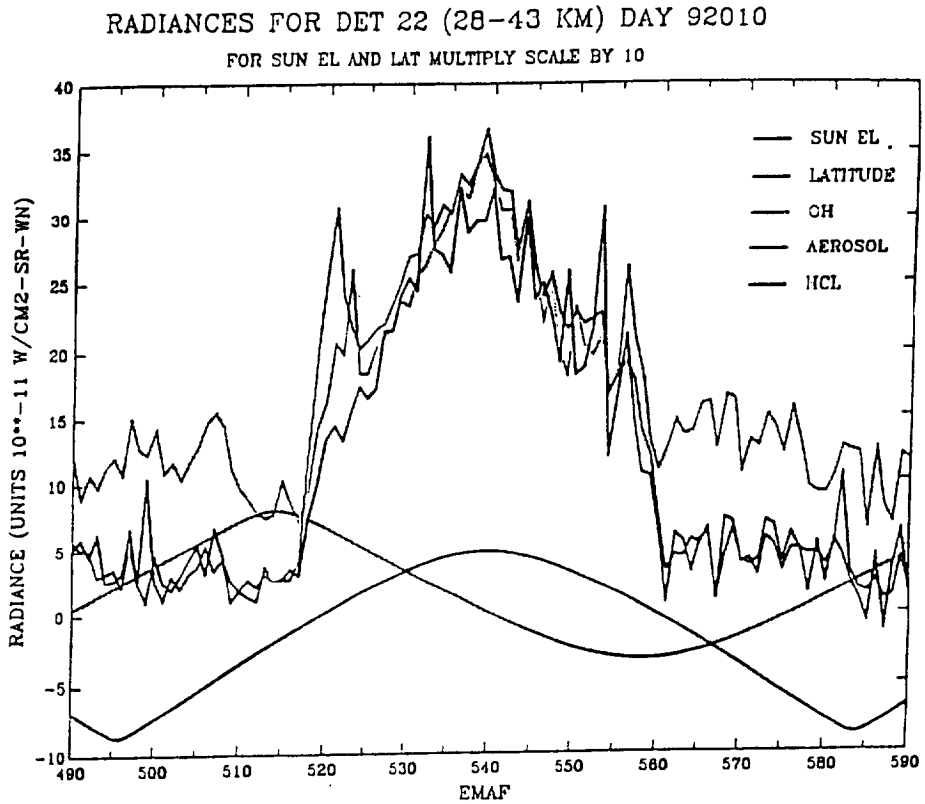

Figure 2.2.16–2. Radiances for detector 22, for one orbit of data on January 10, 1992.

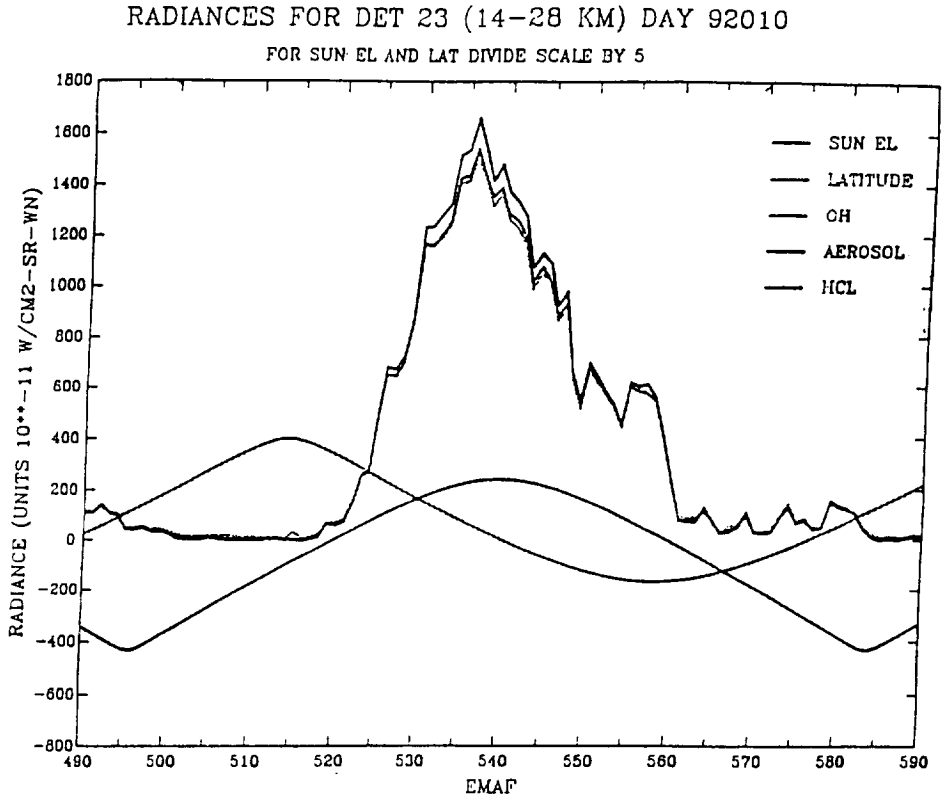

Figure 2.2.16–3. Radiances for detector 23, for one orbit of data on January 10, 1992.

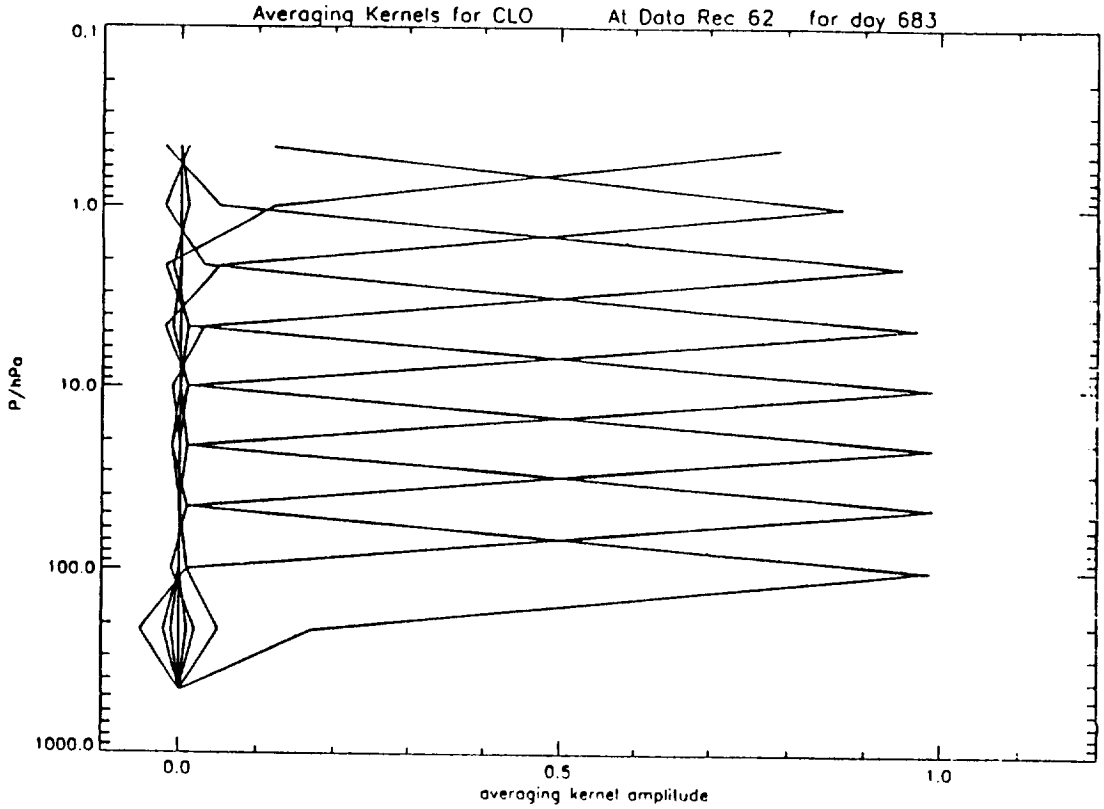

Figure 2.4.4–1. MLS ClO averaging kernels.

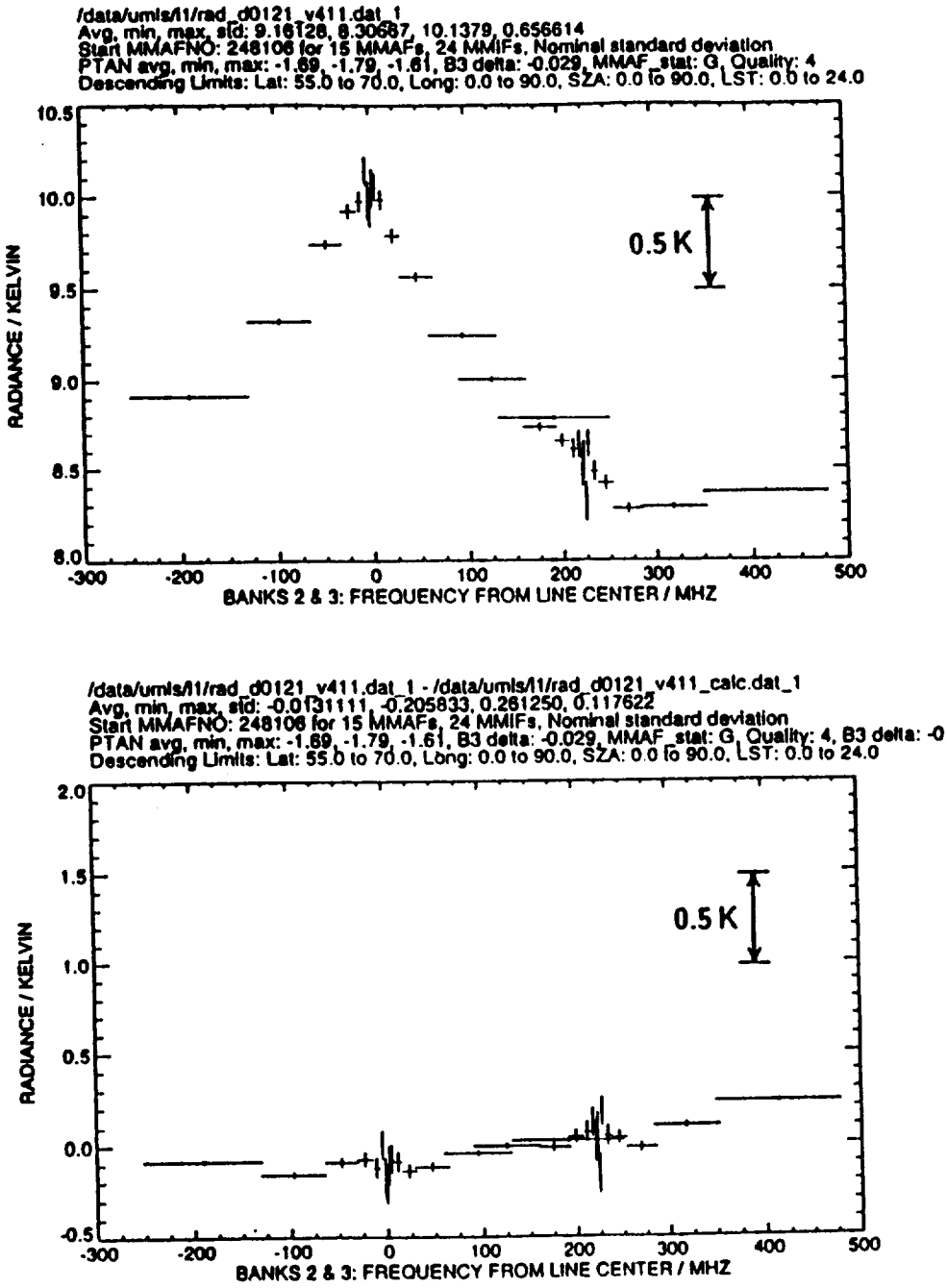

Figure 2.4.4–2. MLS measured radiances (top) and residuals (bottom) for enhanced lower stratospheric ClO. The radiances shown here are an average of measurements made during daytime on 10 January 1992, having inferred tangent pressures between 40 and 60 mbar and at locations in the arctic vortex where enhanced ClO was retrieved from the MLS data. The radiance measurements were averaged over both latitude and longitude, namely, 55–70°N and 0–90°E. The residuals are the average of all individual differences between the measured radiances and the radiances that were calculated from the individually retrieved ClO profiles. Only MLS data with a ClO quality indicator of 4 (good radiances and fits) and MMAF_STAT=G (good) were included in the averages; this amounted to 24 individual measurements of the radiance spectrum.

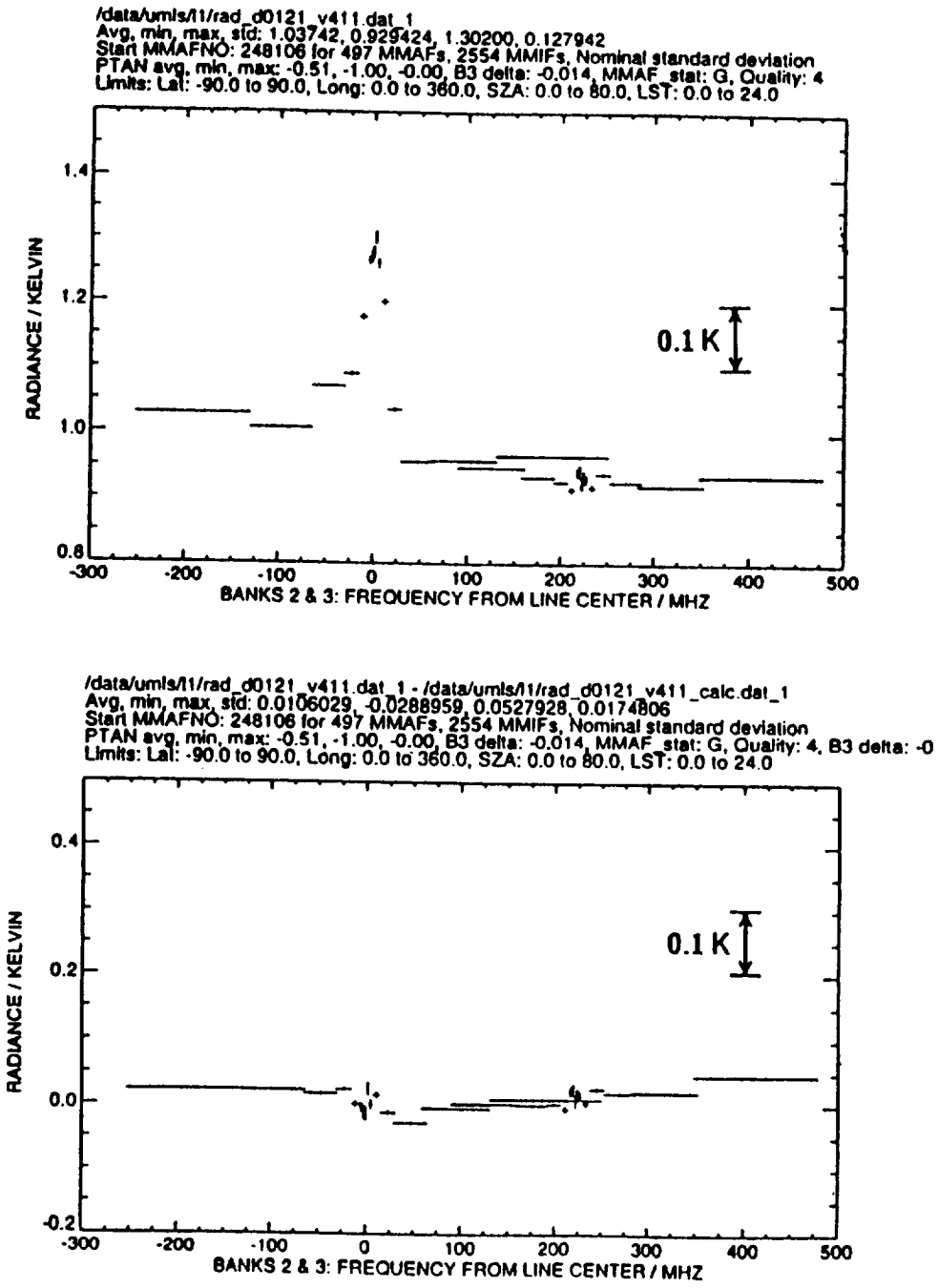

Figure 2.4.4–3. MLS measured radiances (top) and residuals (bottom) for upper stratospheric ClO. The radiances shown here are an average of all of the measurements that were made during the daytime on 10 January 1992, with inferred tangent pressures between 1 and 10 mbar and solar zenith angles (at the measurement location) less than 80°. The residuals are the average of all of the individual differences between the measured radiances and the radiances that were calculated from the retrieved ClO profiles. Only MLS data with a ClO quality indicator of 4 (good radiances and fits) and MMAF_STAT=G (good) were included in the averages; this amounted to 2554 individual measurements of the radiance spectrum.

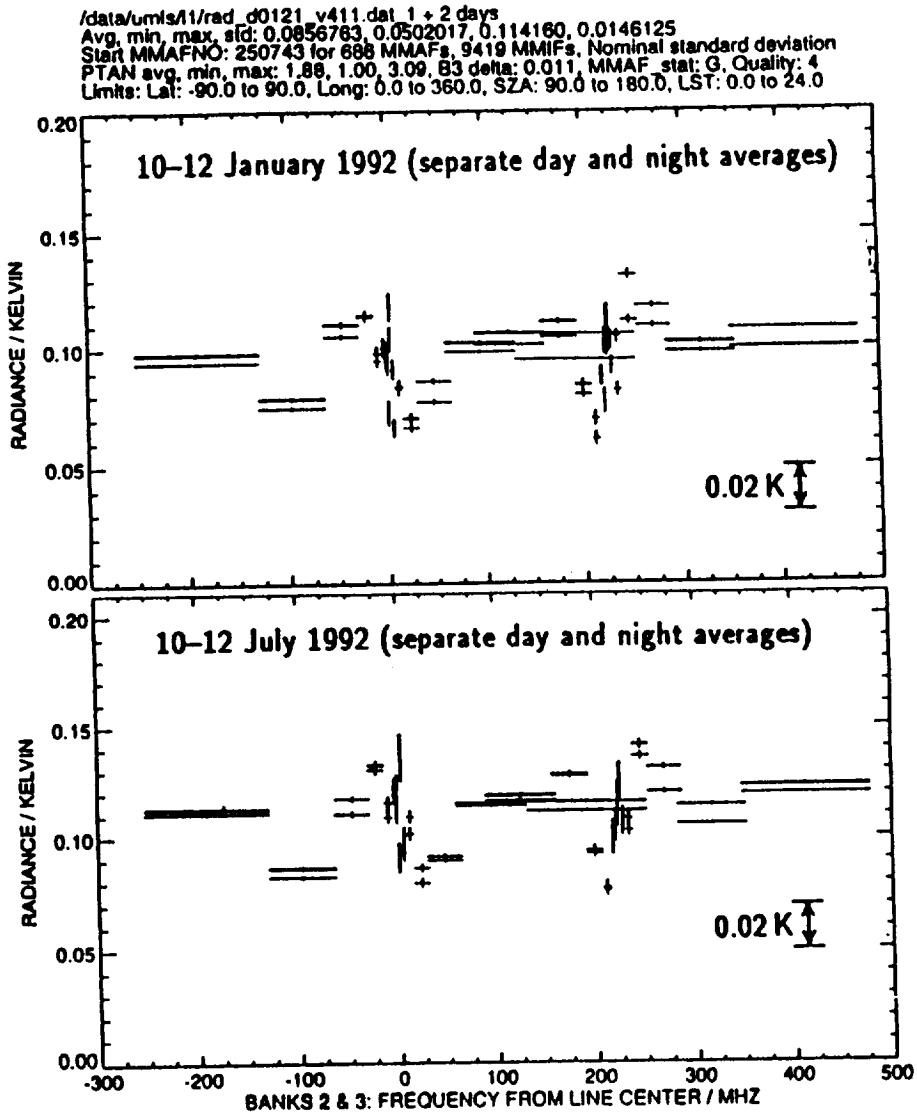

Figure 2.4.4–4. MLS "space radiances" for two 3-day periods, averaged separately for day and night. Only radiances with an inferred tangent pressure less than 0.1 mbar (heights above about 65 km) are included in the average. The top panel is for January 10–12, 1992 (north looking), and the bottom panel is for July 10–12, 1992 (south looking). The two spectra in each panel are the separate averages for "day" (solar zenith angle less than 90°) and "night" (solar zenith angle greater than 90°). The spectral pattern for the high altitudes that are shown here is thought to be due to residual instrumental artifacts. Note that the peak-to-peak variation in its amplitude is approximately 0.05 K in brightness temperature, which corresponds to the amplitude of a signal from a ClO abundance of approximately 0.05 ppbv. Also note that the pattern between day and night repeats to within about 0.01 K in brightness temperature, which corresponds to the amplitude of a signal from a ClO abundance of approximately 0.01 ppbv. Roughly 9000 individual spectra, each measured with an instrument integration time of 2 s, were included in these averages. Only data that corresponds to ClO retrievals with a quality indicator of 4 (good radiances and fits) and MMAF_STAT=G (good) were included in the averages.

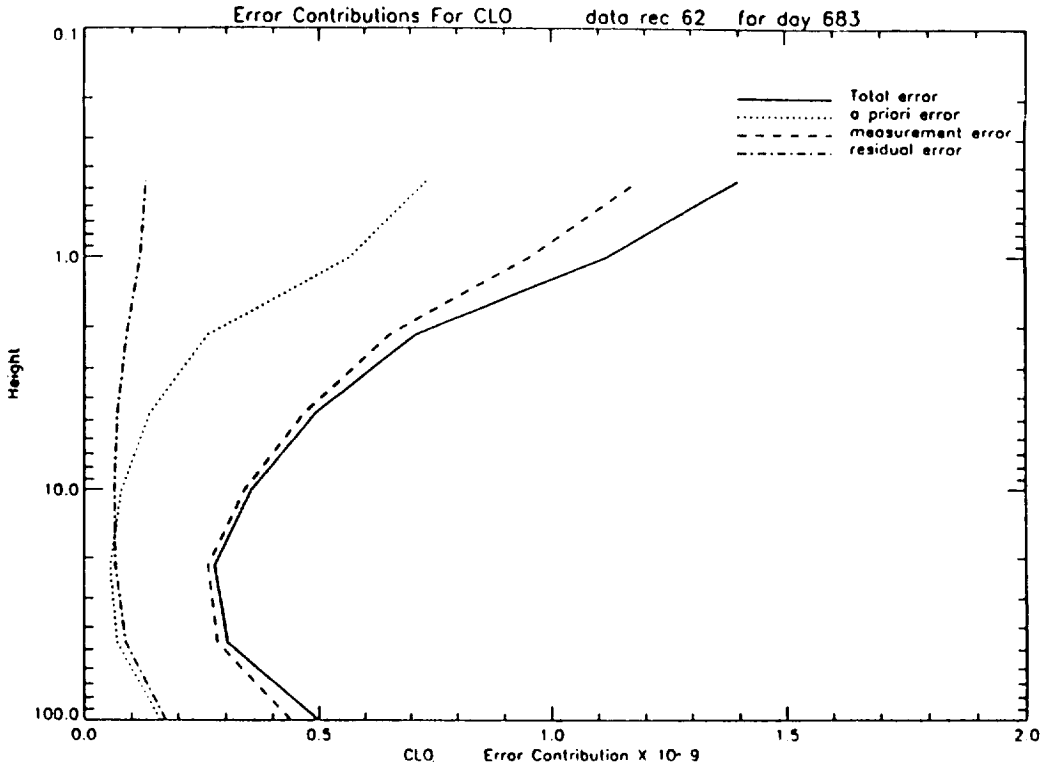

Figure 2.4.4.1-1. Contributions to errors in MLS ClO retrievals.

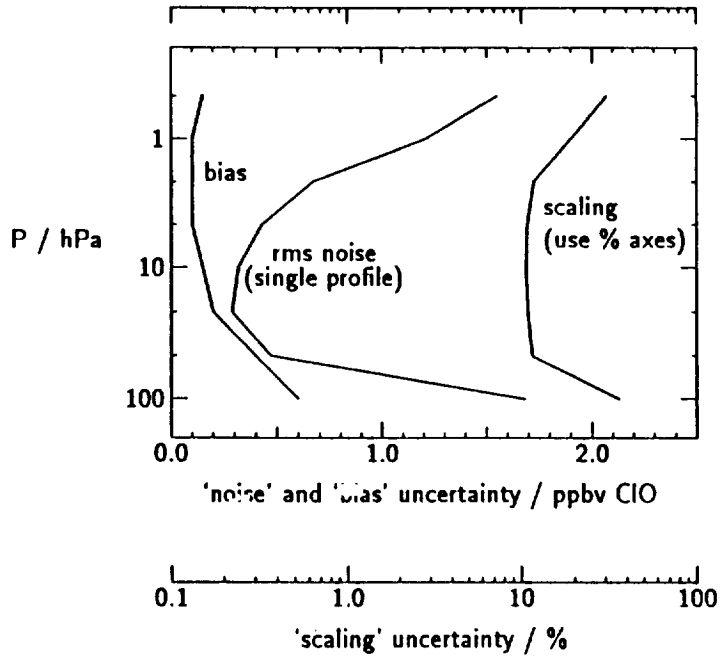

Figure 2.4.4.1-2. Summary of estimated uncertainties for the ClO values in the MLS Version 3 CDHF data files. The curve here for the "noise" uncertainty gives typical values; quantities in the data files should be used for the noise on any specific profile. The noise component can be reduced by taking averages. The "bias" component can be reduced by taking appropriate (day-night, for example) differences.

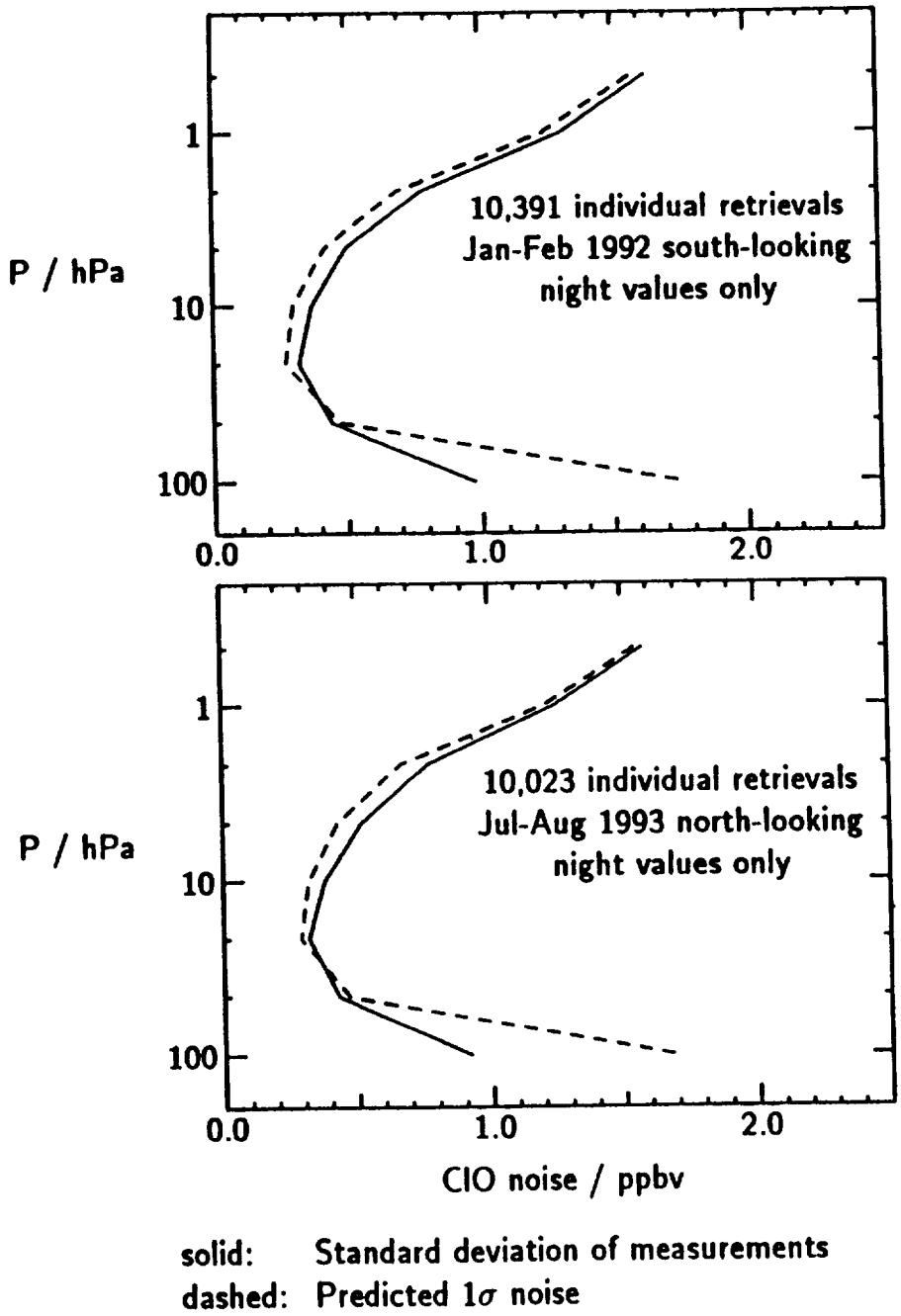

Figure 2.4.4.2-1. Measured and predicted noise in individual MLS ClO retrievals. The data sample here included only retrievals made in early morning (solar zenith angles greater than 95° and local solar times between midnight and 6 am) during January 15 to February 14, 1992 south-looking summer (top) and July 9 to August 8, 1993 north-looking summer (bottom. This sample covers times when ClO is expected to be a minimum, and variations in the retrieved values are expected to be dominated by measure noise. The predicted 1 sigma noise shown by the dashed curves is the average value for each dat ensemble of the values produced by the algorithms for the Version 3 data.

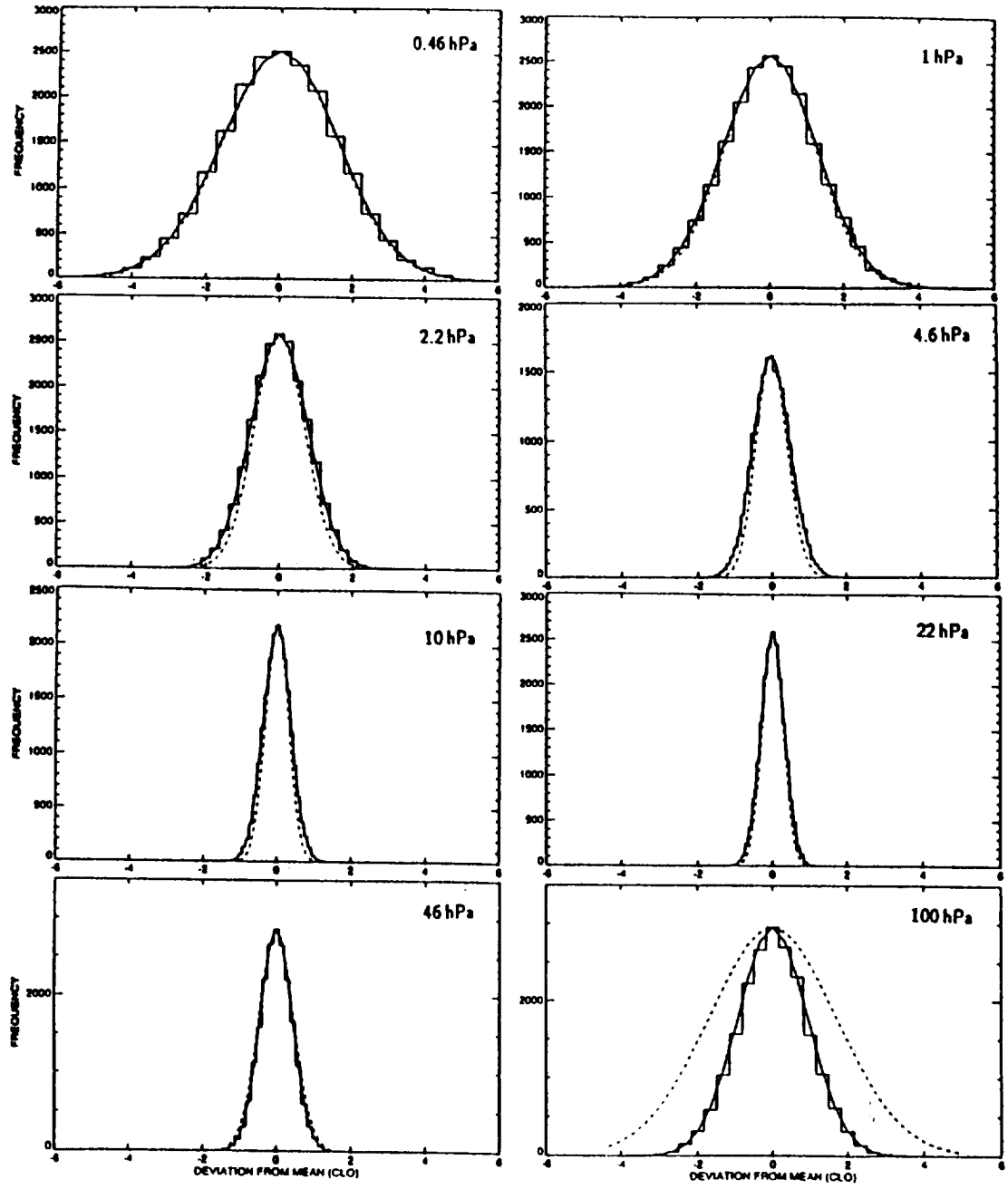

Figure 2.4.4.2-2. The distribution of nighttime ClO profiles retrieved from MLS. The data ensemble used here includes 20,414 individual profiles retrieved between midnight and 6 am for the UARS months of January-February 1992 (south-looking summer) and July-August 1993 (north-looking summer) when stratospheric ClO is expected to be a minimum, and the retrieved distribution is expected to be dominated by measurement noise. The "staircase" histograms in each panel show the measured distribution of the retrieved values. The smooth solid curve is a Gaussian having width equal to the measured standard deviation of the data. The dashed curve is a Gaussian having width equal to the average (for this data ensemble) of the absolute value of the estimated uncertainties in the MLS Version 3 data files. The horizontal axis is deviation from the mean (in ppbv) and the vertical axis is the number of points with the incremental values indicated by the histogram.

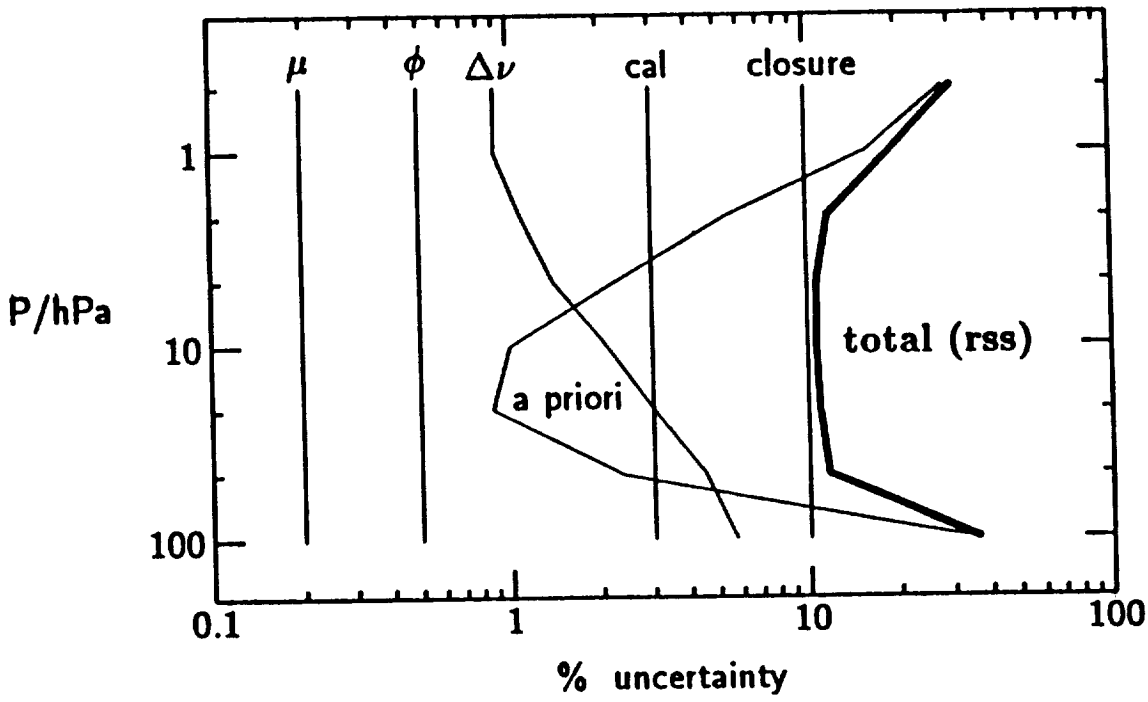

μ	due to molecular dipole moment
ϕ	due to transition matrix element
$\Delta\nu$	due to linewidth
cal	due to instrument calibration
closure	due to lack of retrieval closure
a priori	maximum effect of a priori

Figure 2.4.4.3-1. Estimated scaling error for ClO in the MLS Version 3 CDHF files.

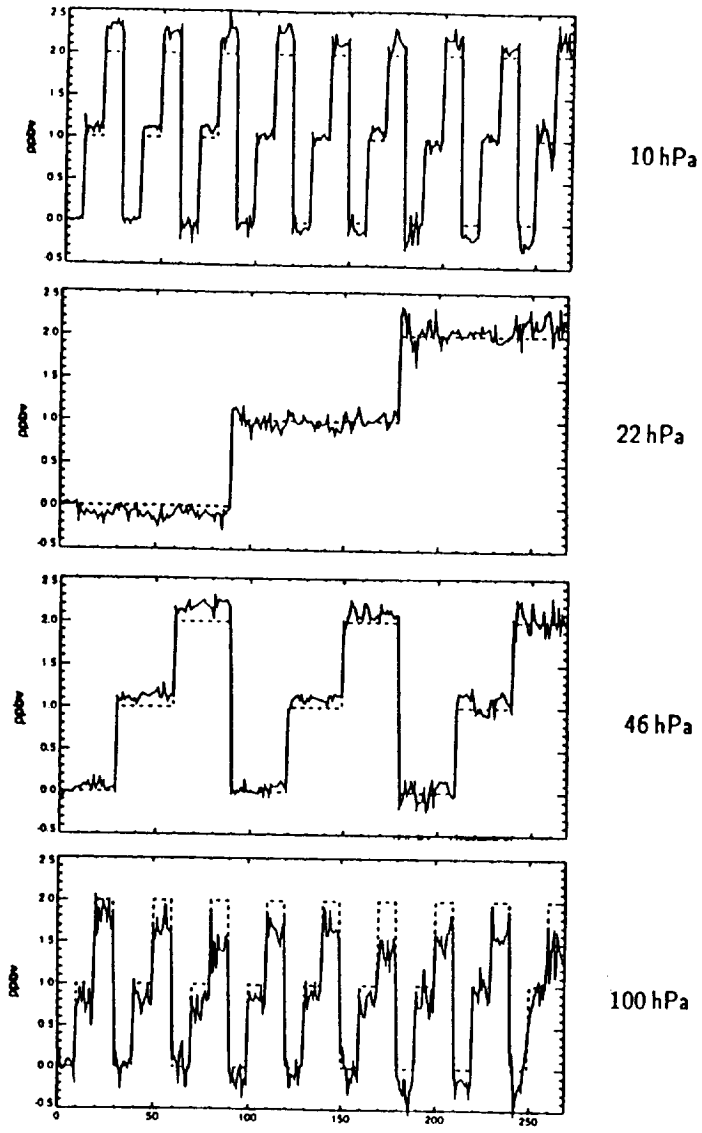

Figure 2.4.4.3-2a. Results of simulations using the algorithms producing ClO values in the Version 3 CDHF files. A total of 270 simulations were performed for this test, and the horizontal axis gives the index of the individual retrievals. The dashed lines are the "truth" and the solid lines are the simulated retrieval results. The "truth" was made to cycle between 0, 1, and 2 ppbv ClO at the various levels. The "noise" in the retrievals is due to other than measurement noise, as noise was not added to the simulated radiances used in these tests (although nominal radiance uncertainties were assumed by the algorithms) in order to see the effects more precisely. Underestimates of ClO at 100 hPa are expected due to effects of the a priori.

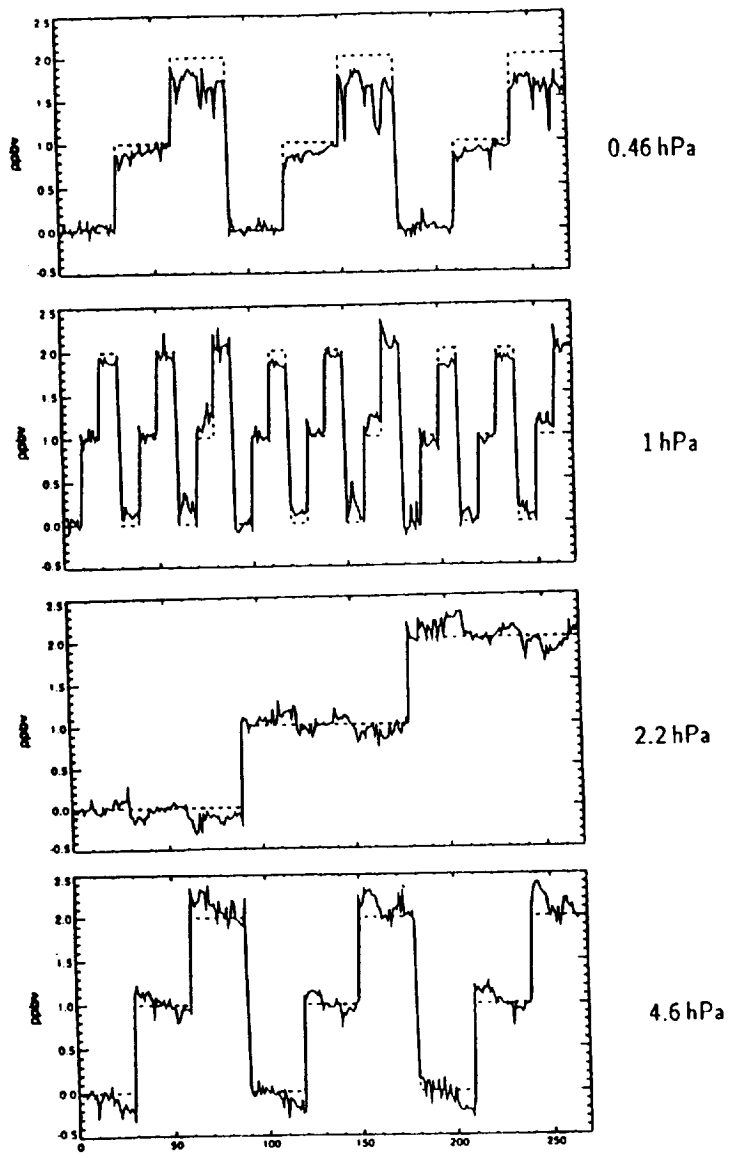

Figure 2.4.4.3-2b. Results of simulations using the algorithms producing ClO values in the Version 3 CDHF files. A total of 270 simulations were performed for this test, and the horizontal axis gives the index of the individual retrievals. The dashed lines are the "truth" and the solid lines are the simulated retrieval results. The "truth" was made to cycle between 0, 1, and 2 ppbv ClO at the various levels. The "noise" in the retrievals is due to other than measurement noise, as noise was not added to the simulated radiances used in these tests (although nominal radiance uncertainties were assumed by the algorithms) in order to see the effects more precisely. Underestimates of ClO at 0.46 hPa are expected due to effects of the a priori.

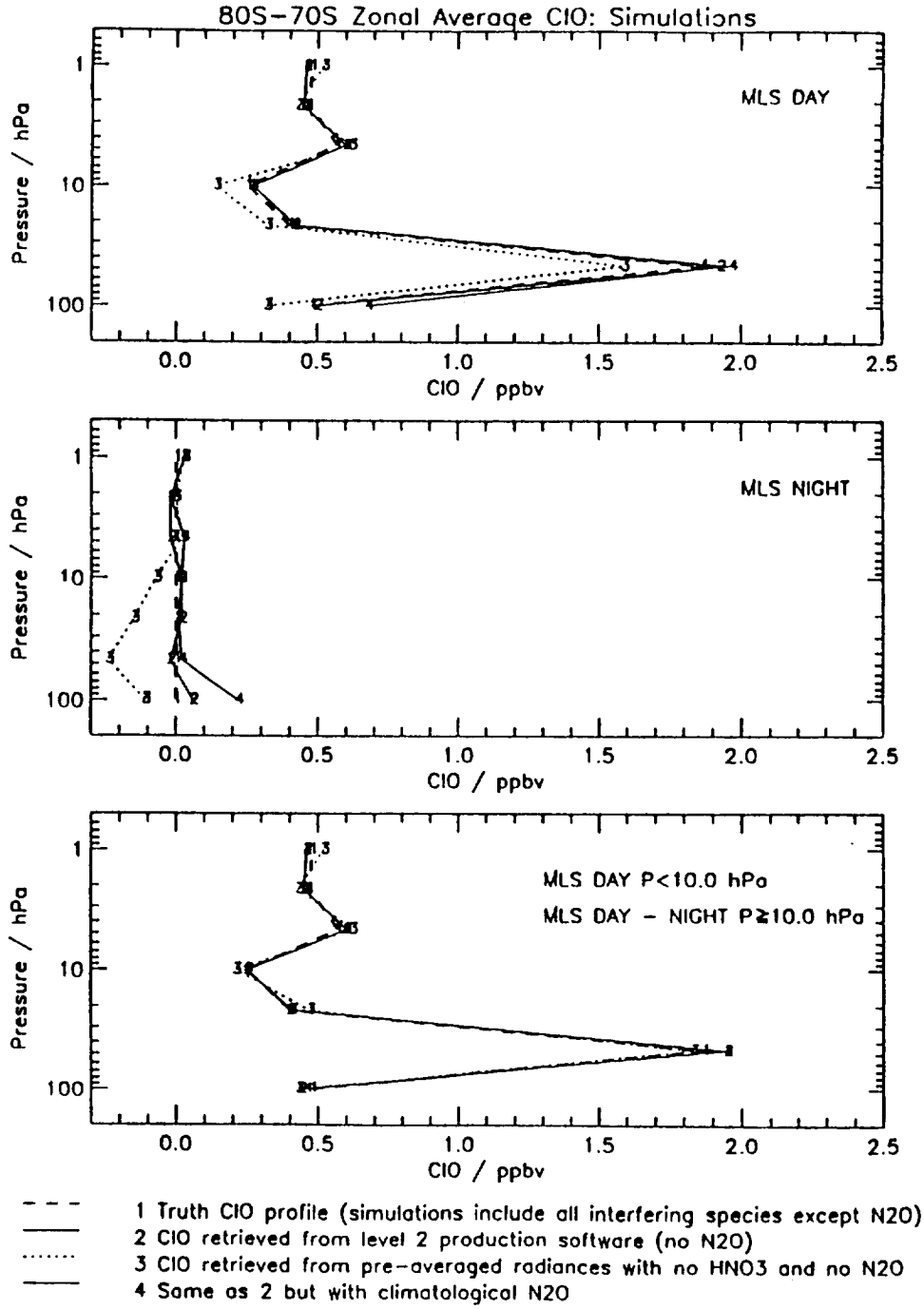

Figure 2.4.4.4-1. Results of ClO retrieval simulations for conditions of enhanced ClO in the lower stratosphere. "True profiles" are the dashed curves. Curves labeled "2" give results from algorithms producing the MLS Version 3 data files on the CDHF. Curves 3 and 4 show the effects of HNO_3 and N_2O. The results shown here are the averages of approximately 40 individual retrievals for both day and night conditions.

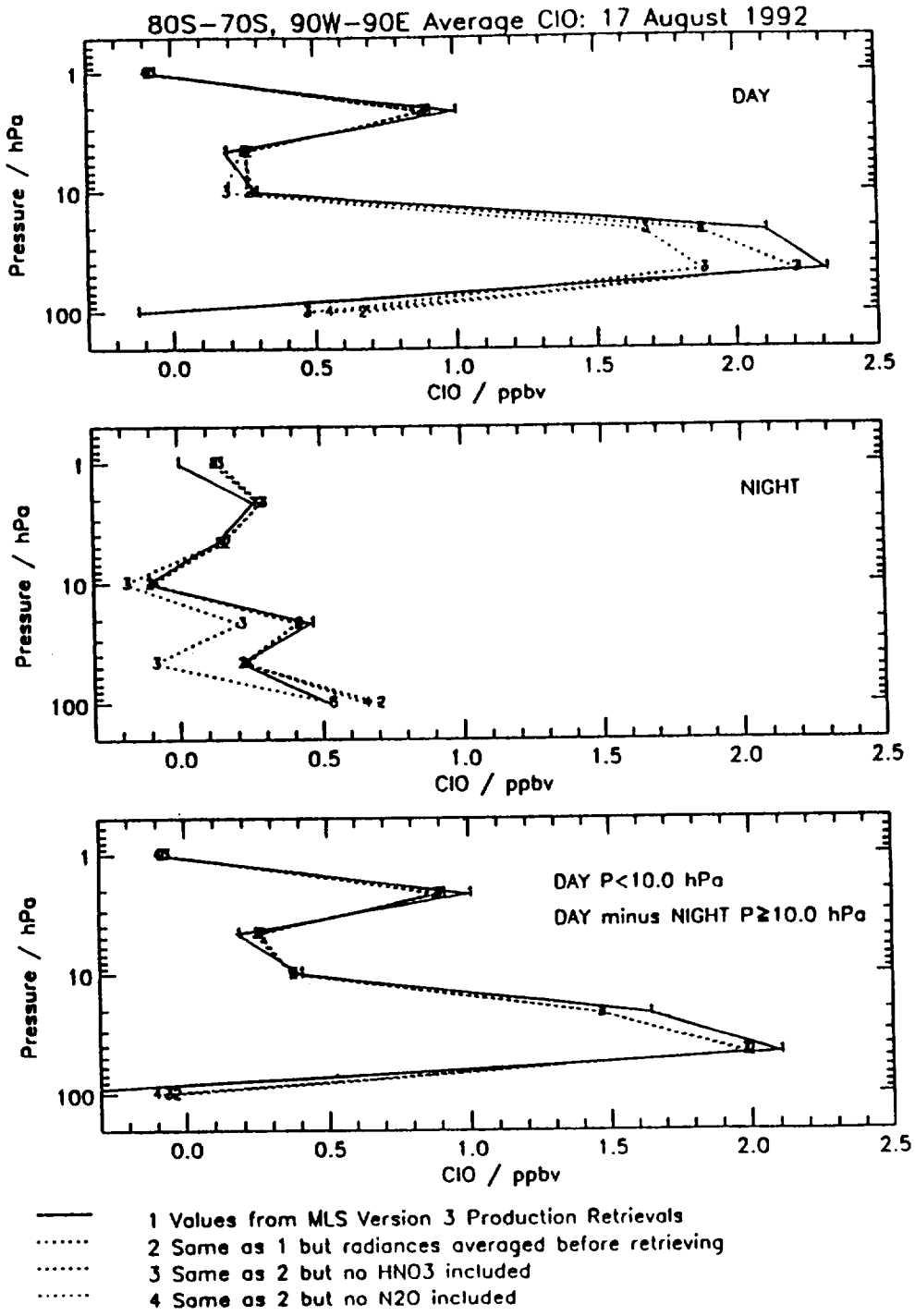

Figure 2.4.4.4-2. Results from different retrieval schemes used on August 17, 1992 MLS data taken over Antarctica. These are the averages of approximately 20 individual retrievals. The solid curves are from the algorithms producing the MLS Version 3 data files on the CDHF. Curves 2 are retrievals made with an iterative scheme which averages radiances before doing retrievals, but which handles HNO_3 and N_2O in the same way as the production algorithms. Curves 3 and 4 show the effects of changing from climatological to zero values of HNO_3 and N_2O.

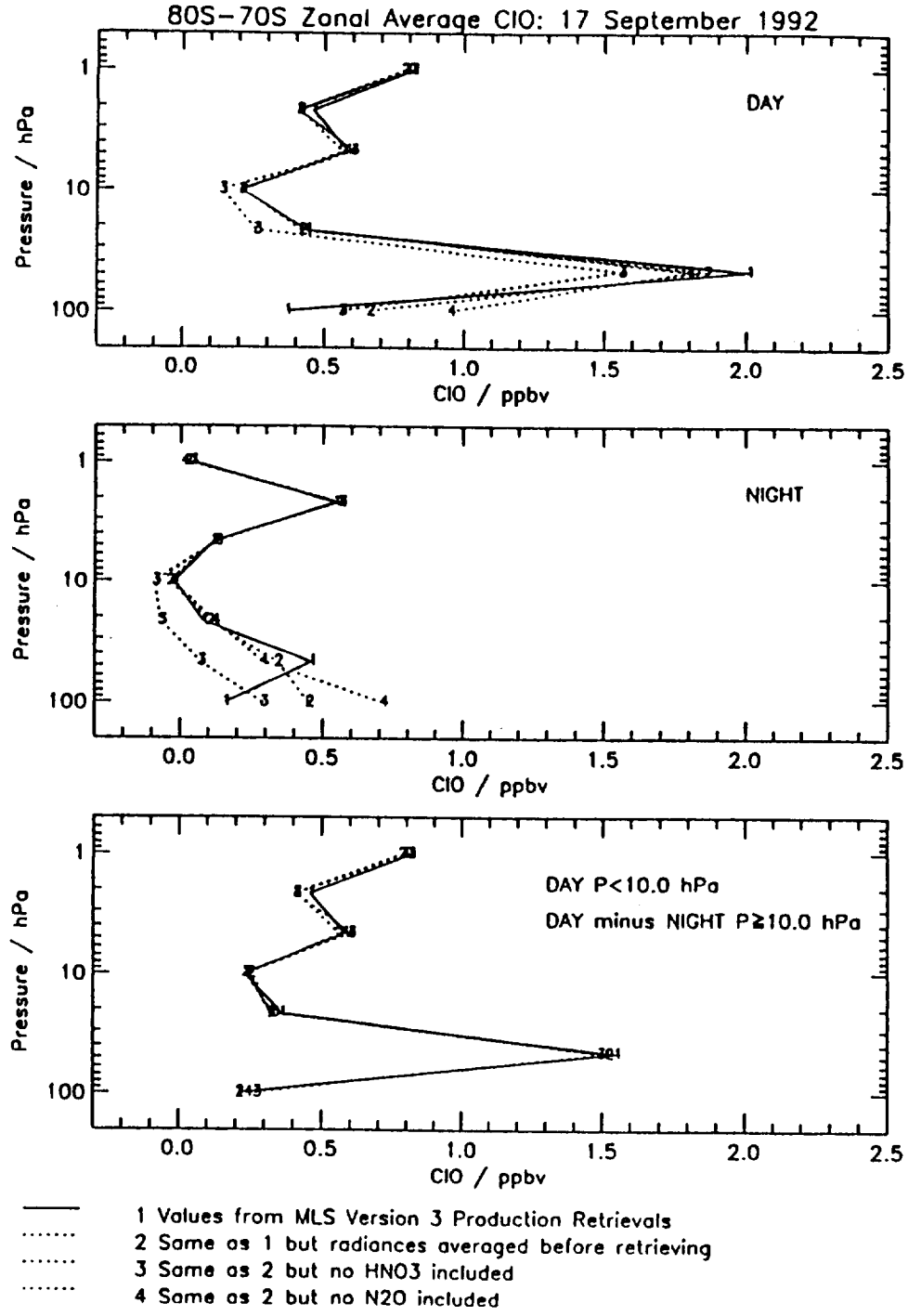

Figure 2.4.4.4-3. Results from different retrieval schemes used on September 17, 1992 MLS data taken over Antarctica. These are the averages of approximately 20 individual retrievals. The solid curves are from the algorithms producing the MLS Version 3 data files on the CDHF. Curves 2 are retrievals made with an iterative scheme which averages radiances before doing retrievals, but which handles HNO_3 and N_2O in the same way as the production algorithms. Curves 3 and 4 show the effects of changing from climatological to zero values of HNO_3 and N_2O.

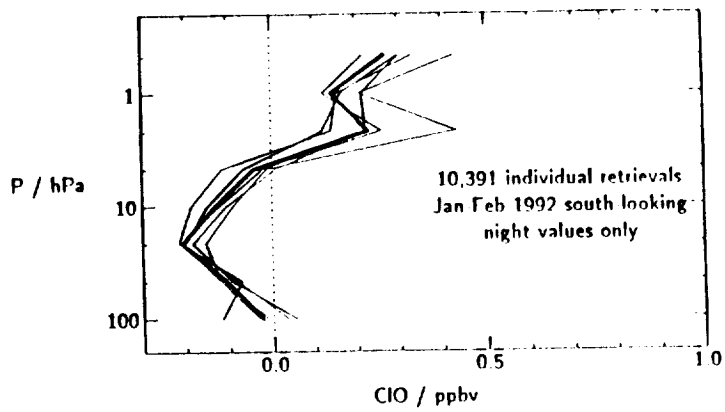

thick: average of all data (10,391 profiles)
thin: averages in following latitude bins:

(1)	34–10° N	5146 profiles
(2)	10° N – 10° S	1877 profiles
(3)	10–30° S	1384 profiles
(4)	30–50° S	980 profiles
(5)	50–70° S	403 profiles

Figure 2.4.4.4-4. Nighttime MLS ClO retrievals. The data ensemble used here includes 10,023 independent retrievals of measurements made in early morning (solar zenith angles greater than 95° and local solar times between midnight and 6 am) during the January 15 to February 14, 1993 south-looking (southern summer) UARS month. This sample covers times when ClO is expected to be a minimum. Only MLS data having ClO quality indicator of 4 (good radiances and fits) and MMF_STAT=G (good) have been included in the averages.

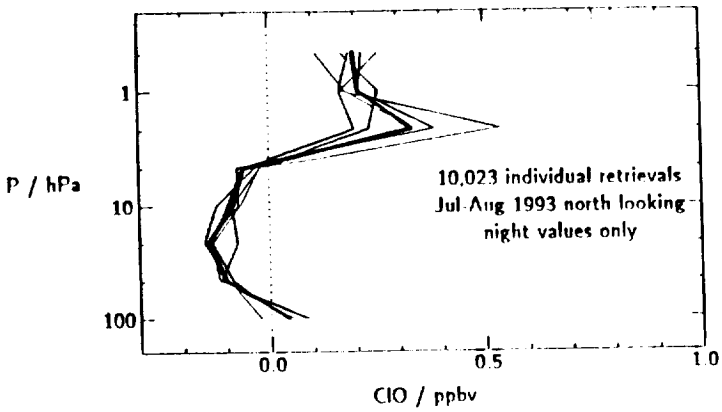

thick: average of all data (10,023 profiles)
thin: averages in following latitude bins:

(1)	50–70° N	234 profiles
(2)	30–50° N	817 profiles
(3)	10–30° N	1256 profiles
(4)	10° N – 10° S	1857 profiles
(5)	10–34° S	5859 profiles

Figure 2.4.4.4-5. Nighttime MLS ClO retrievals. The data ensemble used here includes 10,391 independent retrievals of measurements made in early morning (solar zenith angles greater than 95° and local solar times between midnight and 6 am) during the July 9 to August 7, 1993 north-looking (nortthern summer) UARS month. This sample covers times when ClO is expected to be a minimum. Only MLS data having ClO quality indicator of 4 (good radiances and fits) and MMF_STAT=G (good) have been included in the averages.

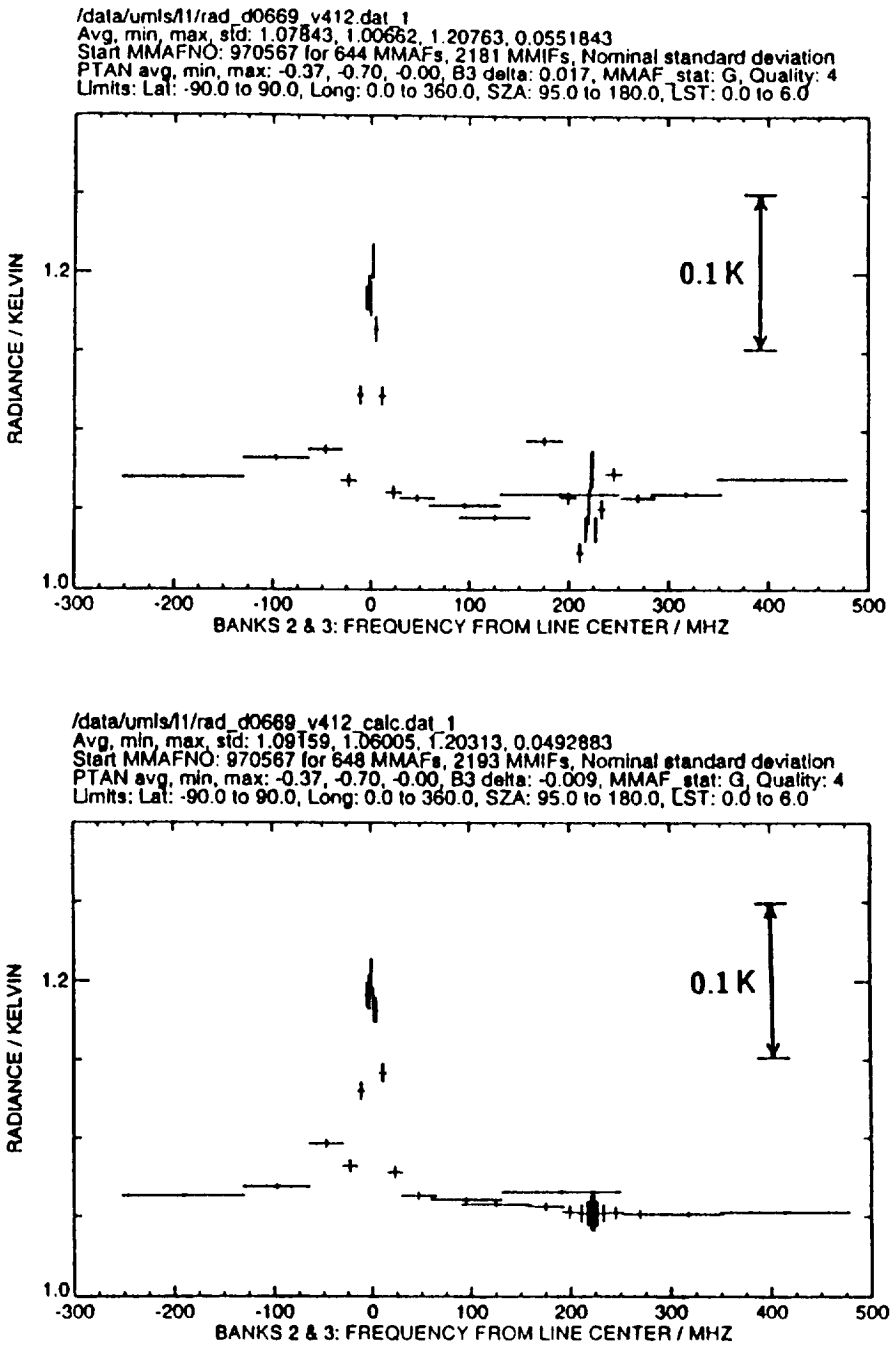

Figure 2.4.4.4-6. Nighttime emission spectrum of ClO: measured (top) and calculated from retrieved profiles (bottom). The measured spectrum is an average of all upper stratospheric spectra (having inferred tangent pressures between 1 and 5 hPa) taken at night (solar zenith angles greater than 95°) between local solar times of midnight and 6 am on July 11, 1993. The calculated spectrum is the average of all calculations using individually retrieved profiles corresponding to the spectra in the top panel. Only spectra corresponding to retrieved ClO quality indicator of 4 (good radiances and fits) and MMF_STAT=G (good) have been included in the averages. The nighttime ClO signal is evident.

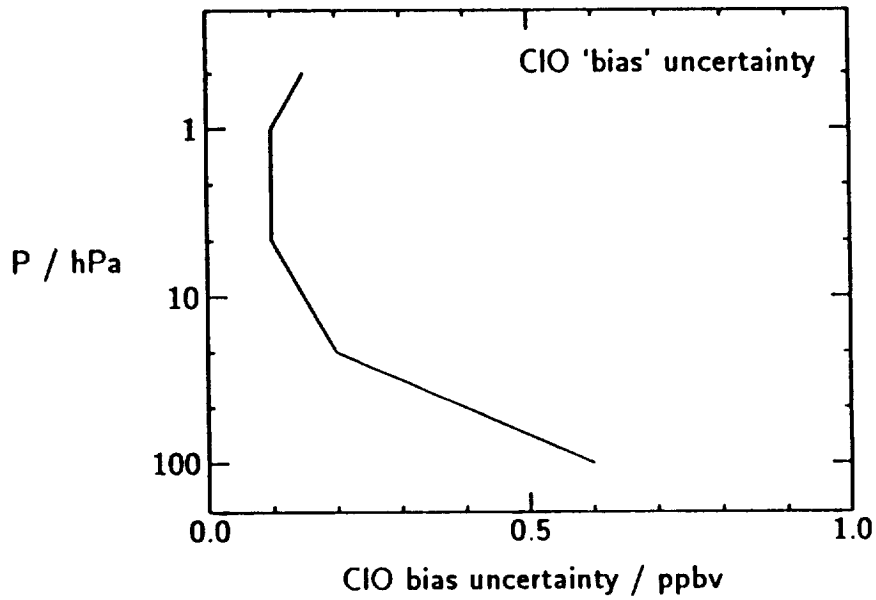

Figure 2.4.4.4-7. Estimated bias uncertainty in MLS ClO profiles. This uncertainty will not "average-down", but can be reduced by taking appropriate differences (day-night, for example).

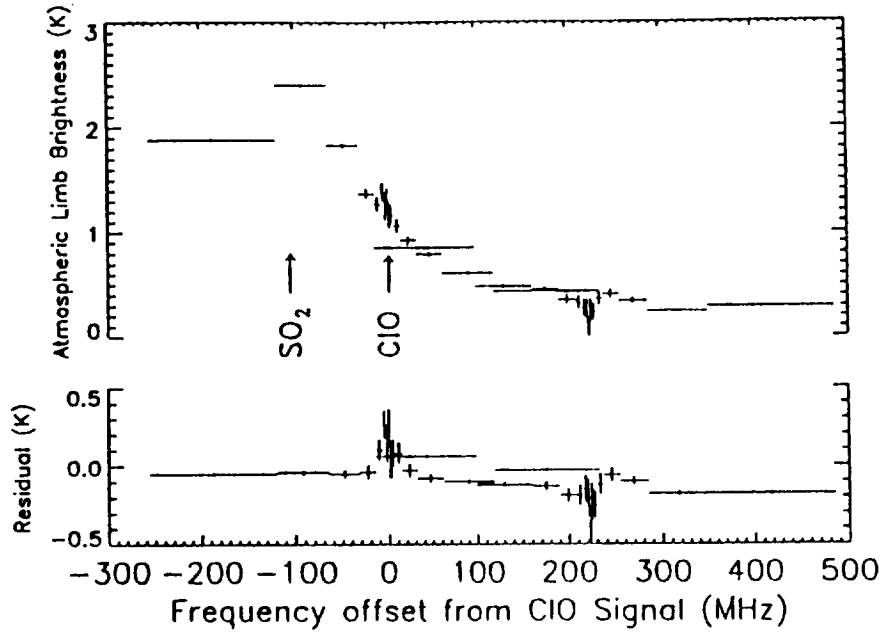

Figure 2.4.5–1. Top: A 5–10°S zonal average of MLS nighttime radiances at a tangent height of approximately 26 km, showing the SO_2 line at 204.247 GHz. Bottom: The radiance residuals after fitting ClO and SO_2. The ClO signal does not appear prominently at night, because ClO is a photolytic product.

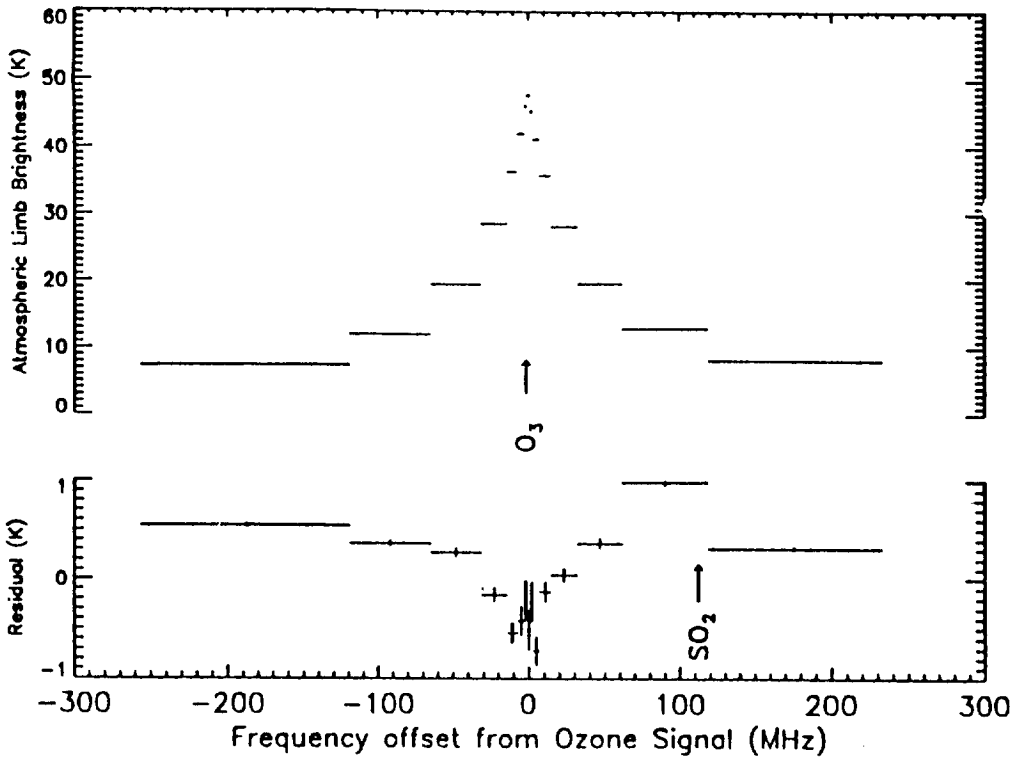

Figure 2.4.5–2. Top: A 5–10°S zonal average of MLS radiances at a tangent height of approximately 26 km, from the 206-GHz spectral band that is used to measure O_3. Bottom: The spectral difference after retrieving O_3 (but not retrieving SO_2). The line positions of O_3 and SO_2 are shown.

3 AEROSOLS

Aerosol extinction is not regularly measured by satellites throughout the infrared spectrum. UARS instruments are making pioneering observations of aerosol in the infrared and near-visible wavelength regions. These observations are of interest for several reasons. Retrievals of gaseous constituents and temperature are impacted by the presence of stratospheric aerosol. Of particular importance to the UARS launch in September 1991 was the increased burden of aerosol deposited by the eruption of Mt. Pinatubo in June 1991. Global distributions of aerosol can be used to test the transport in atmospheric simulation models. The aerosol extinction is also of interest to provide estimates of aerosol parameters used in theoretical studies of heterogeneous chemical processes related to reactions on sulfate aerosols.

3.1 UARS Aerosol Measurement Techniques

HALOE, ISAMS, CLAES, and HRDI all measure global aerosol distributions. The first three of these instruments report infrared extinction in units of km^{-1}. HRDI reports visible aerosol scattering in km^{-1}. Since the absorption coefficients at the HRDI observation wavelengths are very small, HRDI effectively measures the extinction coefficient.

3.1.1 HALOE

Haloe uses four gas filter channels to measure mixing ratio profiles of the molecular species HF, HCl, CH_4, and N_2O, in addition to aerosol extinction at each channel's center wavelength (2.45, 3.40, 3.46, and 5.6 microns, respectively). Four broad band radiometer channels measure profiles of the molecular species CO_2,, NO_2, H_2O, and O_3, in addition to the aerosol extinction at the CO_2 channel center wavelength (2.80 microns). The technique used to infer aerosol extinction relies on the ability to simulate a broad band signal without aerosol absorption. For the gas filter channels, the gas mixing ratio retrieval is unaffected by aerosol and the retrieved mixing ratios are used to simulate the broad band signals. For the CO_2 channel, a constant mixing ratio (352 ppmv) is used to simulate the broad band signal. The ratio of measured signal, which contains aerosol absorption, to the simulated signal without aerosol, yields the aerosol transmission. The transmission profiles are used to retrieve profiles of aerosol extinction coefficient. The current retrieval algorithm provides 3 km vertical resolution for the 2.45, 3.40, 3.46, and 5.26 μ measurements (gas filter channels) and 0.6 km resolution for the 2.80 μ measurement (CO_2 channel). An algorithm has been developed which retrieves on the over-sampled 0.3 km vertical grid spacing. A profile interleave method provides stability in the high resolution retrievals, and the actual vertical resolution of the measurements will be improved from 3 to 2 km. This version of the data is not yet available.

3.1.2 ISAMS

ISAMS measures emission in eleven spectral regions, of which the 12.1 μ channel was intended for aerosol detection. The 6.2 channel was designed for measurement of NO_2, but because both wide band and gas correlation signals are obtained, it has proved feasible to retrieve both NO_2 and aerosol at that wavelength. The wide band signal depends mostly on aerosol, while the gas correlation signal depends mostly on NO_2. Both are affected by water vapor, but H_2O is measured separately in the 6.2 μ channel. A joint retrieval is carried out to separate them. It is hoped to extend this approach to

other channels in future versions of the data processing, notably to the 4.6 μ (CO) and 5.3 μ channels.

3.1.3 CLAES

The CLAES experiment measures emission using a blocker filter (of approximately 10 cm^{-1} width) in conjunction with a tilting Fabry-Perot etalon. There are nine blocker filters and four etalons. Each radiance profile samples the infrared spectrum with a resolution between 0.20 and 0.65 cm^{-1}, dependent upon the etalon used for the observation. Blocker regions 1, 2, 3, 4, 5, 6, 7, 8, and 9 correspond to observations centered near 2844, 1897, 1605, 1257, 923, 880, 840, 790, and 780 cm^{-1}. These wave numbers correspond to wavelengths of 3.52, 5.27, 6.23, 7.95, 10.83, 11.36, 11.90, 12.65, and 12.82 μ, respectively. Aerosol extinction is reported for the 5.27, 6.23, 7.95, 10.83, 11.36, 12.65, and 12.82 μ blocker regions. For blocker regions 2-9, spectra are sensed by 20 detectors, each which span 2.5 km in the vertical.

Simultaneous retrievals of temperature, gaseous constituents and continua are conducted for the 5.27, 6.23, 11.36, and 12.65 μ blocker regions. For the 10.83 and 12.82 μ observations, the retrieval process solves for the scaling parameters whch best scale the 12.65 μ aerosol extinction profile to the 10.83 and 12.82 μ data (i. e. the retrieval solves for the aerosol scaling factors, and the mixing ratio profiles of the gaseous constituents, for the two blocker regions).

The continua are due to aerosol, cloud opacity, and to the pressure induced absorption (PIA) in the 6.23 μ blocker. The version V0006 data set reports the extinction coefficient due to all continua in the 6.23 μ blocker region. For the blocker 4 data near 7.95 μ, an attempt has been made to subtract the influence of N_2O_5 (so that the 7.95 μ extinction is due to aerosol). A climatological amount of N_2O_5 is used in the subtraction process for the daytime aerosol data, while a simultaneous retrieval for N_2O_5 and aerosol is carried out for the nighttime data.

3.2 Comparisons with Particle Size Measurements

Most groups have used the particle size measurements of T. Deshler (University of Wyoming), obtained on balloon flights near Laramie, Wyoming, to predict the aerosol extinction retrieved from UARS observations. The theoretical predictions then were used to compare theory and observations for cases where the UARS instruments were viewing near Laramie (41N and 254E). Some details of the theoretical Mie calculation will be mentioned, since the validation exercise methodology has not been used in previous studies. Input to the theoretical Mie calculation , for a specific altitude level, is the measured particle size distribution, temperature, and water vapor pressure. The Mie calculation assumes that the sulfuric acid particles are spherical in shape (a reasonable assumption). The temperature and water vapor pressure values are used to calculate an equilibrium H_2SO_4 concentration (by weight), which determines the indices of refraction used in the theoretical calculation. The UARS groups use the Palmer and Williams indices (measured at room temperature). The Lorentz-Lorenz relationship can be used to predict the indices at lower temperatures, though further laboratory study is necessary to quantify the indices at stratospheric temperatures. Thus, the theoretical procedure has some uncertainty. Also, keep in mind that the satellite observations average over a horizontal path length, while the balloon measurement samples locally.

Some differences in comparing theory and observations are therefore expected, even for perfect measurements.

Figures 3.2-1 to 3.2-8 present comparisons of UARS extinction profiles with theoretical predictions. In figure 3.2-1, HALOE and theoretical profiles at 3.46 μ are presented for September 3, 1992. The HALOE and Deshler measurements were obtained a day apart and are separated by 1.7 degrees in latitude and 10 degrees in longitude. The aerosol peaks differ by 20% in pressure andagree well in absolute magnitude. The HALOE values become larger than tha predicted values for pressures less than 20 mb.

Figure 3.2-2 displays comparisons between ten HALOE extinction profiles and predictions at 3.4 μ. Near the peak of the aerosol layer, between 40 and 80 mb, the mean HALOE value is within 15% of the mean predicted value (see the right panel). This level of agreement holds for all five HALOE channels at 2.45, 2.80, 3.40, 3.46, and 5.26 μ. RMS differences are on the order of 50 percent. Above and below the aerosol peak, the mean HALOE extinction values are greater than the predicted values by about 50 percent.

Figures 3.2-3 and 3.2-4 present pressure versus time cross-sectios for October 1991 to January 1993 for the HALOE 3.46 μ data and theoretical calculations based upon the Deshler particle size distributions. The balloon flights were made at about two week intervals above Laramie. HALOE sampling provides coverage at 41N at about three to four week intervals. The HALOE observations shown occur within 3 degrees latitude and 20 degrees longitude of Laramie. Arrival of the Mt. Pinatubo aerosol cloud is evident in the balloon data as enhanced extinction at 50 mb near UARS day 80. HALOE observes the enhanced layer 25 days later at 40 mb. The layer of peak extinction decreases in altitude from 50 mb to about 100 mb in both data sets and are in agreement in the general morphology of the cloud. Many features are more accurately resolved by the balloon sampling with its better time and height resolution (1km). The balloon data show a region of enhanced extinction at 60 mb near ady 430, a feature not apparent in the HALOE cross-sections. Days shortly after the Mt. pinatubo eruption were characterized by patchy aerosol structure, which may account for the differences in figures 3.2-3 and 3.2-4 near UARS day 50.

Figures 3.2-5 and 3.2-6 present comparisons of CLAES and theory for August 8, 1992. In the geographical maps, triangles mark the location of Laramie, and circles mark the tangent points of the CLAES observations. For the aerosol profiles, the theory values are denoted by triangles and the CLAES values by solid lines (the dashed lines indicating error bars). General agreement is apparent at the aerosol peak for blockers 4, 5, and 6. For blockers 2, 3, 8, and 9, the CLAES extinction is larger than the predicted values at the aerosol peak. For blocker 3 the difference is in part due to the presence of pressure induced absorption of molecular oxygen (which increases as a function of pressure squared at lower altitudes). For blocker 2 there is likely to be a large solar scattering component in the data.

Figure 3.2-7 compares ISAMS data for April 17, 1992, May 8, 1992, and May 29, 1992 with predicted values. The + signs are theoretical values calculated for 59 and 86% H_2SO_4 (with larger values corresponding to the 59% case). There is general agreement with the 59% case, although such a composition is unlikely at altitudes below 20 mb. Use of a more typical acidity is consistent with ISAMS values being too high by about 30%.

It is apparent for all three instruments that theoretical profiles of aerosol extinction fall off with increasing altitude at a arte faster than observations for pressure less than 20 mb. UARS extinction values are generally larger in magnitude than those of the correlative measurement for pressures less than 20 mb. This situation is apparent in figure 3.2-8 in which HALOE and CLAES 5.2 μ data are compared with the theoretical profile. The CLAES and Wyoming balloon measurement are nearly coincident, and the HALOE data are for one day later (August 9, 1992). The reason for this disagreement is at present unknown.

3.3 Comparisons with SAGE II Data

Another correlative data set is the extinction measured by the SAGE II (Stratospheric Aerosol and Gas Experiment) experiment. Sage II, retrieves aerosol extinction at 0.385, 0.453, 0.525, and 1.02 μ, using the Sun in an occultation measurement. To compare the SAGE II data in the visible with UARS infrared data, it is necessary to scale the data. The scaling is done by theoretically calculating ratios of extinction at the CLAES wavelengths to that at 0.525 μ. Figure 3.3-1 presents scaling factors, based on Mie theory, which scales the SAGE II data at 0.525 μ to the CLAES wavelengths. These scaling factors are averages based on many individual Mie theoretical ratios. The calculations used Deshler's size distributions extending from a month before to 580 days after the Mt. Pinatubo eruption. The calculations used particle size distributions for altitudes between 18 and 24 km. Individual calculations for the 12.82 and to 0.525 μ aerosol extinction ratio are presented in figure3.3-2. The spread in the ratios indicates that the values in figure 3.3-1 are approximate to ± 50%, that is the ratios in figure 3.3-2 vary from 0.01 to 0.03. Two extinction profile comparisons for January 8,1992, at 8N and 319E, are presented in figure 3.3-3. The dashed line represents CLAES data with superimposed error bars, and the solid line represents scaled SAGE II data. For pressures greater than 10 mb, the two profiles agree well. Figure 3.3-4 displays similar comparisons for 112 profiles averaged for the period January 9-11, 1992. For the case of perfect extinction data and theoretical Mie scaling ratios without any variation, the ratio profile in figure 3.3-4 would have a value of unity. Values of unity are not expected since the extinction data have some error, and the scaling factors used to scale the SAGE II and CLAES data are averages. In figure 3.3-4 the ratios for blocker regions 3, 4, 5, 6, 8, and 9 for the range 20 to 50 mb are within a factor of two of unity. At pressures less than 10 mb, the CLAES extinction is much larger than the scaled SAGE II data. However, the extent of the CLAES error bars suggest caution with respect to any conclusion.

3.4 Instrument-Instrument Profile Comparisons

Figures 3.4-1 to 3.4-7 present profile comparisons for several of the instruments. Figure 3.4-1 shows single profile data at 6.25 μ for HALOE, CLAES, and ISAMS. HALOE and ISAMS are near-coincident (5 hours in time, 0.3 degrees in latitude, and 3.5 degrees in longitude), while the CLAES data is from the previous day, January 9, 1992. The CLAES data has additional opacity as a result of 6.23 μ pressure-induced absorption, so it is expected to be larger than that for the other two instruments at lower altitudes. The measurements generally agree for pressure levels between 20 and 40 mb. Figure 3.4-2 presents CLAES (12.65 μ) and ISAMS (12.1 μ) profile comparisons on January 9, 1992, over the Pacific Ocean. Both instruments retrieve similar profile shapes between 20 and 50 mb. Figures 3.4-3 to 3.4-5 display CLAES (with error bars superimposed) and ISAMS individual profiles for low, medium and heavy aerosol loading cases. It is readily apparent that both instruments retrieve a similar vertical profile structure.

Statistical averaging of profile-profile comparisons is shown in Figures 3.4-6 and 3.4-7. In Figure 3.4-6, HALOE/ISAMS (6.25 μ) mean extinction, mean difference, and rms differences are presented for 45 cases for the period April 18-20, 1992. The HALOE mean values are larger than the ISAMS values above 30 mb (70 percent) and smaller below 30 mb. Rms differences are on the order of 70 percent. For the same time and geographical range, HALOE/CLAES means and differences are shown in Figure 3.4-7. CLAES extinction is likely high at the lower altitudes because of the pressure-induced continuum of O_2. CLAES means are larger than the HALOE means above 20 mb. Rms differences are on the order of 50 percent between 20 and 50 mb.

3.5 Instrument-Instrument Cross-Section Comparisons

Comparison of the longitudinal structure retrieved by CLAES and ISAMS is illustrated in Figures 3.5-1 to 3.5-6. ISAMS (12.1 μ) and CLAES (12.65 μ) data are displayed at 72S and at the Equator for April 18, 1992. At 72S both instruments suggest enhanced extinction at longitudes 60 and 300 degrees, although the details in the overall structure differ. Figure 3.5-3 presents a difference map for the data shown in the previous two figures. The differences range from -4 to+120 percent (plus values denote CLAES values larger than ISAMS values). Figures 3.5-4 to 3.5-6 present a similar perspective at the Equator. Theoretical calculations of extinction using the Deshler size distributions predict a value of 0.91 for the ratio of extinction at 12.65 and 12.1 μ . In Figure 3.5-6, the differences are in the 25 to 50 percent range. Performing rms averages with respect to longitude at each standard pressure level (latitudes 80S and 28N) for April 18, 1992, results in values of 28, 42, 48, and 55 percent at 68, 46, 31, and 22 mb, respectively.

Longitudinal cross-sections (21S) of extinction at 6.25 μ for April 18-20, 1992, for the HALOE, CLAES, and ISAMS instruments are presented in Figures 3.5-7 to 3.5-9. Best agreement is apparent between 20 and 30 mb. Above 10 mb, the CLAES extinction is larger than that for HALOE and ISAMS by an order of magnitude. Undulations in the lines of constant extinction amount do not have the same structure in the three maps. The difference maps for the HALOE comparisons with CLAES and ISAMS are shown in Figures 3.5-10 and 3.5-11.

3.6 Scatter Diagrams

Scatter diagrams of ISAMS and CLAES data for 12.1 and 12.65μ are presented in Figure 3.6-1 for April 17, 1992, at 68, 46, 31, and 21 mb. The CLAES values are larger than those for ISAMS. The scatter plots also show that there is a 60 percent spread in the two data sets, which is consistent with the 40 to 50 percent rms values discussed in the previous section.

Diagrams comparing CLAES 12.82 and 12.65 μ data reveal that the two channels differ by 15 to 25 percent. By Mie theory, the ratio of extinction is expected to be in the range 1.00 to 1.03, based upon calculations using Deshler's particle size distributions. Scatter diagrams for HALOE data are presented in Figures 3.6-2 and 3.63. In Figure 3.6-2, HALOE 3.40 and 3.45 μ data are displayed for a wide range of extinction. For these two wavelengths, the extinction values are expected to be close. This expectation is borne out by the data points that fall along the solid line. The diagram illustrates that for over 1600 data points, there are few outlyers. The diagram also illustrates that the retrieval of extinction becomes uncertain for extinction values less than 1.0×10^{-5} km^{-1}. A comparison of extinction from the HALOE instrument at 3.46 and 5.26 μ is given in

Figure 3.6-3. For these two wavelengths, the Mie theory predicts that the ratio of extinction should be 0.7 and 0.3 for 50 and 90 percent H_2SO_4, respectively. Slope one data would fall along the solid line. The locus of points below this line (fitted by the dashed line) confirms the theoretical expectation, in that the observed ratios varied between 0.71 and 0.48. As with Figure 3.6-2, the scatter diagram shows that extinction values below 1.0×10^{-5} km^{-1} are becoming uncertain. There is additional information in this diagram. For large extinction values, there is a set of points for which the extinction ratios are close to unity (see the data points greater than 1.0×10^{-3} km^{-1}, along the solid line). These data points are likely due to ice crystals, since the wavelength dependence of the extinction is expected to be small for the 3.46 and 5.26μ HALOE wavelengths.

3.7 Aerosol Properties Inferred from Multi-Wavelength Extinction Data

Aerosol properties (total number density, particle size distribution parameters, and surface area) were retrieved from the HALOE spectral extinction data in a research study. The aerosol size distribution was assumed to have a single mode log-normal form. Model inputs were adjusted using non-linear least squares until simulated and measured spectral extinctions matched. The aerosol properties retrieved from HALOE were then compared with the Deshler size distribution data. The results of this comparison are presented in Figures 3.7-1 to 3.7-4.. Figures 3.7-1 to 3.7-3 show comparisons for a single profile on August 9, 1992. The solid lines are the HALOE results, and the dashed lines are the Deshler measurements. Though the Deshler size distributions are bi-modal, the stratospheric sulfate particle size distribution can be well represented by a single mode. The HALOE retrieval, based upon a single mode analysis, does quite well in representing the Deshler data. In Figure 3.7-4, a comparison of the surface area density (μ^2/cm^{-3}) is given for HALOE, SAGE II, and dustsonde measurements (the Deshler data) for April 3, 1992 over Laramie. The agreement is seen to be very encouraging.

3.8 Caveats and Recommendations

Each instrument group forwarded caveats and recommendations which complement the preceding discussion, along with a table of accuracies and precision for the extinction data.

ISAMS Archived data: Version 8 aerosol extinction (km^{-1}) at 12.1 and 6.25μ .

Pressure mb	Bias %	Precision %	Accuracy %	Resolution km
68	3	23	26	2.5
46	-1	15	23	2.5
32	-1	18	21	2.5
21	-4	35	37	2.5
15	-4	88	89	2.5

Internal comparisons show that the precision of the ISAMS Version 8 aerosol retrievals is better than 25 percent in the altitude range of 19 to 25 km. However, the aerosol data in Version 8 from launch until April 11, 1992, may be overestimated by 20-30 percent in the altitude range 19-25 km because of an error in the radiometric calibration. There is an anomaly in the radiance in the height range 19-25 km which is under investigation. The

symptom is that the retrieved aerosol in this range is higher before April 11, 1992, than after that date by 20-30%. It is likely that the earlier data is overestimated. This problem is not included in the above table.

HALOE Archived data: The HALOE aerosol extinction (km^{-1}) data are available from the Level 2 files. Level 3 aerosol files are not being produced.

Pressure mb	Wavelength (μ)				
	2.45	2.80	3.40	3.46	5.26
	Uncertainty (%)				
< 1	>100	>100	>100	>100	>100
8-1	50-100	>100	50-100	50-80	50-100
15-8	20-50	35-100	15-50	15-50	15-50
100-15	10-20	20-35	10-15	10-15	10-15

The vertical resolution is 3.0 km for this pressure range at all wavelengths.

The current Version 12 aerosol data should not be used at pressures less than 10 mb for any investigation. The files do not at present contain error estimates, but they will be added in the next version. A good conservative estimate of the measurement uncertainty (precision+accuracy) can be taken from the above table. The 2.8μ measurement is done differently from the other channels, and some systematic differences may be observed when compared to the other channels. In general, the HALOE channels are internally consistent in that the wavelength dependence of the measurements is consistent with theory for extinction values greater than about 1.0×10^{-5} km^{-1}.

CLAES Archived data: Version 6 aerosol extinction (km^{-1}) at 12.82, 12.65, 11.36, 10.83, 7.95, 6.23, and 5.27μ.

The precision, accuracy, and vertical resolution of the aerosol measurements depends upon the magnitude of the aerosol extinction, and on its uniformity. The following tables are based upon work with aerosol data for January 9, 1992, for a period of heavy volcanic aerosol loading. Data above 10 mb have large error bars and are not recommended for use. The precision numbers contain some component attributable to spatial variation of the aerosol and were determined by measuring the statistical spread in the ratios of aerosol extinction relative to the 12.6μ extinction in the same engineering major frame.

(a) Blocker 9 (12.82 μ, 780 cm^{-1})

Pressure mb	Bias %	Precision %	Accuracy %	Based on average extinction of km^{-1}
10	3	25	TBD	1.0×10^{-5}
32	3	20	20	1.0×10^{-3}
46	3	10	20	1.0×10^{-3}
68	3	14	20	6.3×10^{-4}
100	3	80	TBD	1.5×10^{-4}

Other biases may be present, based upon estimates of calibration and etalon characterization uncertainties.

(b) Blocker 8 (12.65 μ, 790 cm^{-1})

Pressure mb	Bias %	Precision %	Accuracy %	Based on average extinction of km^{-1}
10	3	25	TBD	1.0×10^{-5}
32	3	20	20	1.2×10^{-3}
46	3	10	20	1.2×10^{-3}
68	3	12	30	6.3×10^{-4}
100	3	80	TBD	1.5×10^{-4}

Of the seven blocker regions for which aerosol extinction is reported, most confidence is placed in the 12.65μ data, since the spectral contrast between the line emitters (CO_2 and O_3) and the continuum aerosol is good. However, there is a 20% discrepancy between the aerosol extinction measured at 12.82 and 12.65μ, while the theoretical difference, based upon published optical constants for sulfuric acid aerosol, is on the order of 2%. The 12.82μ profile contains a small component from CCl_4 which contributes as a continuum source of opacity and has not been subtracted. At 100 mb this extinction is estimated to be about 1.0×10^{-4} km^{-1} and drops off with increasing altitude.

(c) Blocker 6 (11.36 μ, 880 cm^{-1})

Pressure mb	Bias %	Precision %	Accuracy %	Based on average extinction of km^{-1}
10	3	>100	TBD	3.0×10^{-5}
32	3	20	25	1.2×10^{-3}
46	3	15	20	1.0×10^{-3}
68	3	37	40	4.0×10^{-4}
100	3	80	TBD	1.5×10^{-4}

(d) Blocker 5 (10.83 μ, 925 cm^{-1})

Pressure mb	Bias %	Precision %	Accuracy %	Based on average extinction of km^{-1}
10	3	>100	TBD	3.0×10^{-5}
32	3	25	25	1.5×10^{-3}
46	3	15	40	1.7×10^{-3}
68	3	33	60	1.0×10^{-3}
100	3	>100	TBD	5.0×10^{-4}

(e) Blocker 4 (7.95 μ, 1257 cm^{-1})

Pressure mb	Bias %	Precision %	Accuracy %	Based on average extinction of km^{-1}
10	-33	50	TBD	4.0×10^{-5} nighttime
32	- 33	27	TBD	1.5×10^{-3} nighttime
32	3	16	20	5.6×10^{-3} daytime
46	3	15	80	3.2×10^{-3} daytime
68	3	20	>100	3.1×10^{-3} daytime
68	-33	25	TBD	1.6×10^{-3} nighttime
100	-33	95	TBD	1.0×10^{-3} nighttime

In the Version 6 aerosol data for the 7.95μ region, climatological amounts of N_2O_5 are assumed during the day, and the production software retrieves the daytime aerosol extinction. For the nighttime, a simultaneous retrieval of N_2O_5 and aerosol is performed. The daytime aerosol is roughly 33% larger than the nighttime amounts. It is believed that too much signal is being attributed to N_2O_5 at night, and thus the nighttime aerosol extinction is on the low side. The daytime values are probably more accurate because the effect of subtracting the climatological N_2O_5 values in the daytime data is small. It is recommended that the daytime data be used for scientific studies.

(f) Blocker 3 (6.23 μ, 1605 cm^{-1})

Pressure mb	Bias %	Precision %	Accuracy %	Based on average extinction of km^{-1}
10	0.15	75	TBD	4.0×10^{-5}
32	1.5	28	30	1.6×10^{-3}
46	3.0	32	35	3.2×10^{-3}
68	7.0	33	60	1.0×10^{-3}
100	15.0	>100	TBD	1.0×10^{-3}

Bias at 10 mb is 0.15×10^{-4} km^{-1} and results from the pressure-induced absorption of molecular oxygen.

The aerosol, along with the O_2 pressure-induced absorption (PIA), are lumped together as a continuum. The contribution of the O_2 PIA can be easily evaluated and subtracted from the data. The low altitude data appear to be too small much of the time to allow for subtraction of the PIA. This result may arise because the tangent-point signal at these levels is dominated by the aerosol a priori, which does not contain the PIA component.

(g) Blocker 2 (5.27 μ, 1897 cm^{-1})

Pressure mb	Bias %	Precision %	Accuracy %	Based on average extinction of km^{-1}
10	3	75	TBD	4.0×10^{-5} nighttime
10	(*)	>100	(*)	4.0×10^{-5} daytime
32	3	30	30	2.0×10^{-3} nighttime
32	(*)	36	(*)	4.0×10^{-3} daytime
46	3	60	60	1.3×10^{-3} nighttime
46	(*)	60	(*)	8.3×10^{-3} daytime
68	3	55	60	1.3×10^{-3} nighttime
68	(*)	60	(*)	3.1×10^{-3} daytime
100	3	125	(*)	8.0×10^{-4} nighttime

(*) the daytime extinction is roughly twice as large as the nighttime extinction and has a large component due to solar scattering.

Possible sunlight scattering from the aerosol at 5.27 μ may result in a large diurnal variation in the retrieved extinction coefficient. Simce the scattered solar radiation is artificially boosting the retrieved extinction coefficient for the day, it is recommended that the nighttime values be used in scientific studies. However, because of algorithm problems, there are fewer nighttime profiles than for the other blocker regions.

3.9 Conclusions

From the above studies, several conclusions can be made. HALOE, CLAES, and ISAMS generally retrieve similar aerosol profile shapes. Channels from each instrument can be chosen from which the aerosol peak is similar in altitude (when individual profiles are intercompared). To within a factor of two, theoretical Mie profiles (based upon the Deshler size distribution measurements), scaled SAGE profiles and retrieved aerosool profiles agree in magnitude for pressure levels in the range 20-68 mb. Above 20 mb, the HALOE, CLAES, and ISAMS profiles have gradients which are not as steep as that of the SAGE data or the theoretical predictions based upon the Deshler data. The reason for this disagreement is not known. Expressed differently, the uars extinction values are greater than those of the correlative measurements above 20 mb. HALOE mean extinction values agree with theoretically derived values to the 15 percent level for an average over ten coincident profiles. Rms differences for the comparison between theory and observation are on the order of 50 percent. Rms differences between instruments (using longitudinal cross-sections) are on the order of 40-50 percent for the 20 to 68 mb range. The stated percent accuracies for the ISAMS and CLAES extinction values are smaller than the percent differences in the instrument intercomparisons. Generally, the HALOE, ISAMS, and CLAES data sets can be jointly used in the range 20 to 68 mb, while data error bars caution against usage at other pressure levels. Improvement in the accuracy of the aerosol extinction data is expected. Finally, encouraging results of application of the HALOE data, used to retrieve particle size distribution information, has produced estimates of surface area for sulfate aerosol, which compares well with correlative measurements.

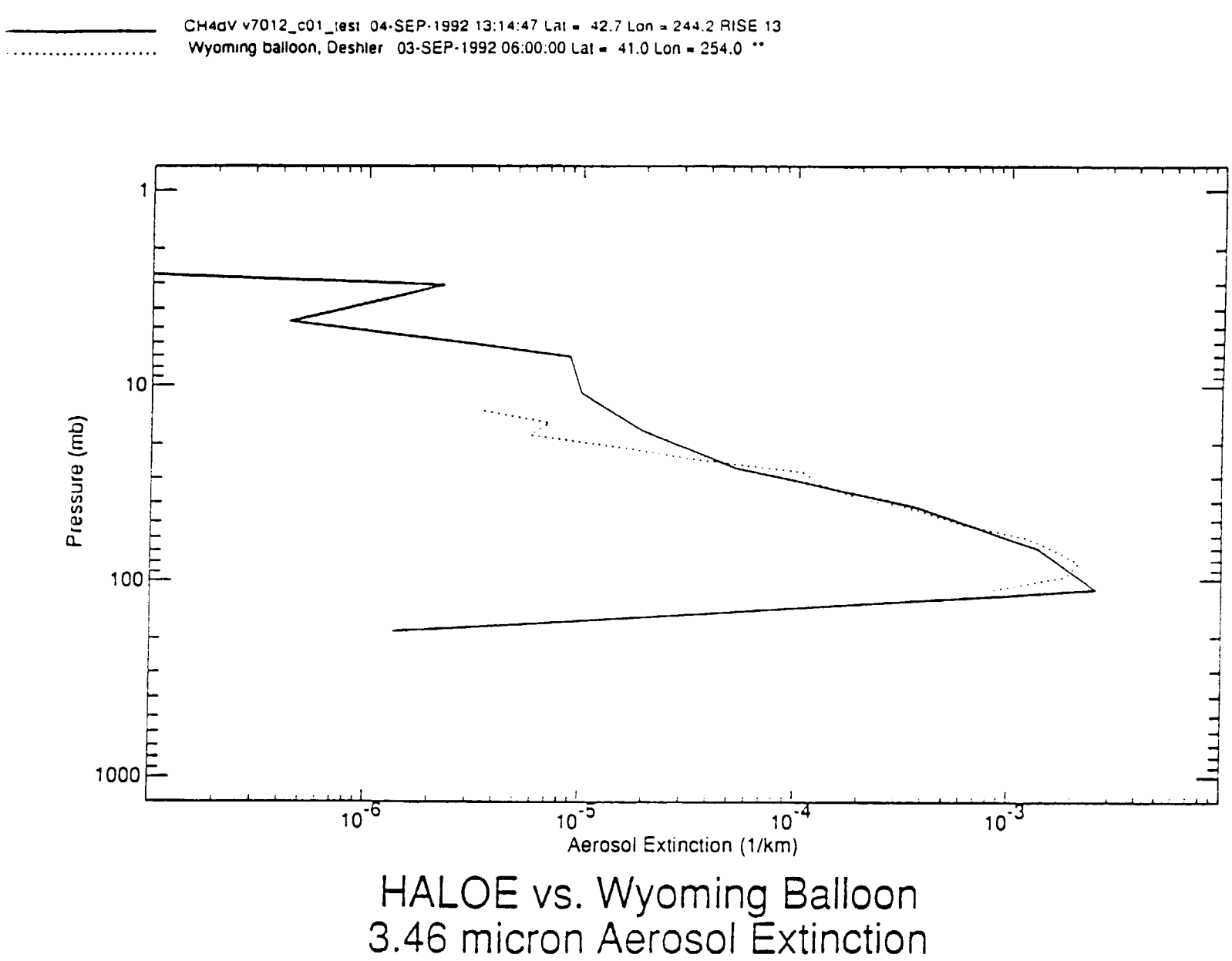

Figure 3.2-1 HALOE (——) and theoretical (- - -) 3.46 μ extinction profile for Sept. 3 - 4 , 1992.

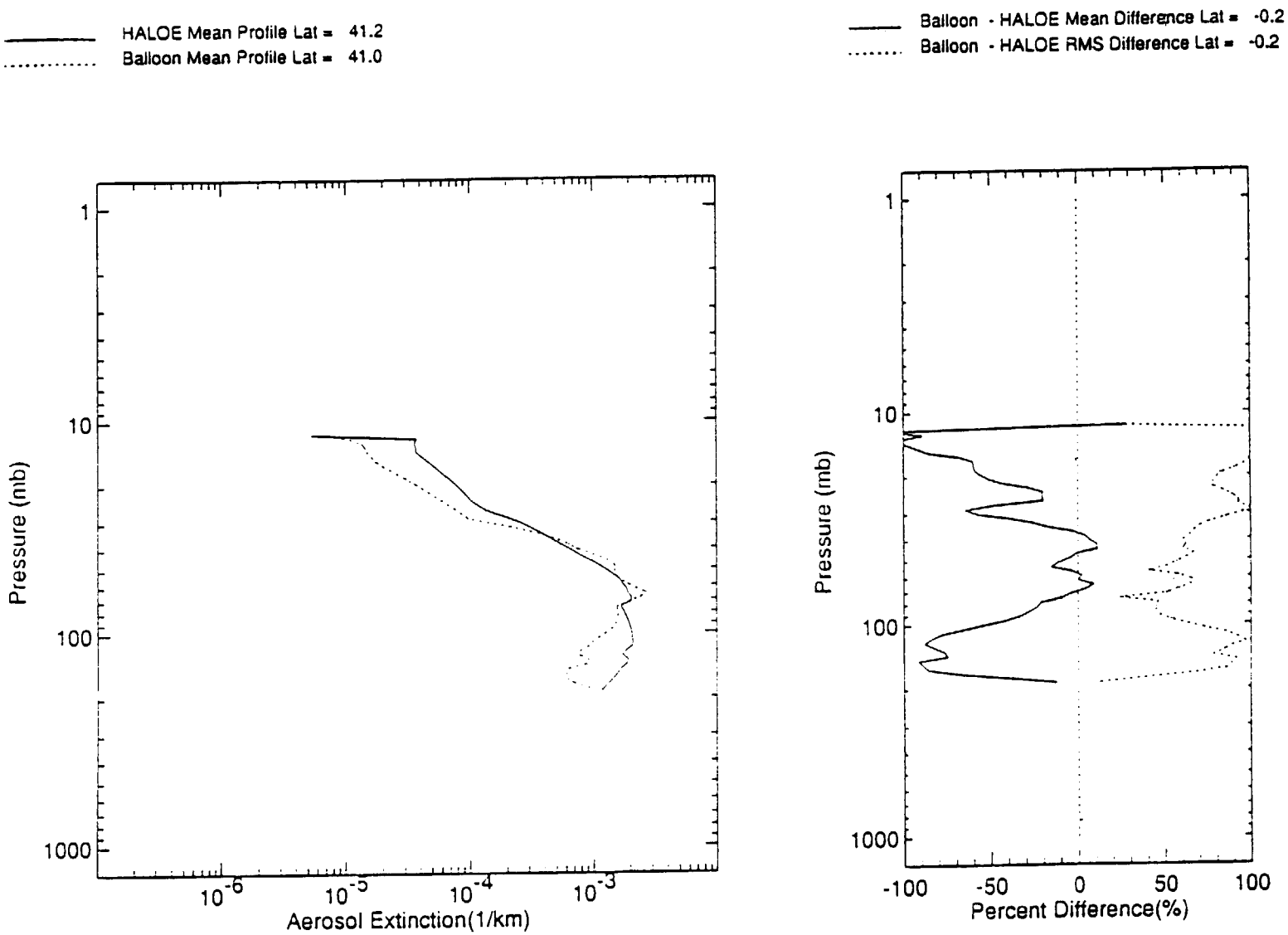

Figure 3.2-2 Left panel: Mean of ten HALOE (——) and ten theoretical (- - -) 3.46 μ extinction profiles. Right panel: Mean (——) and rms differences (- - -).

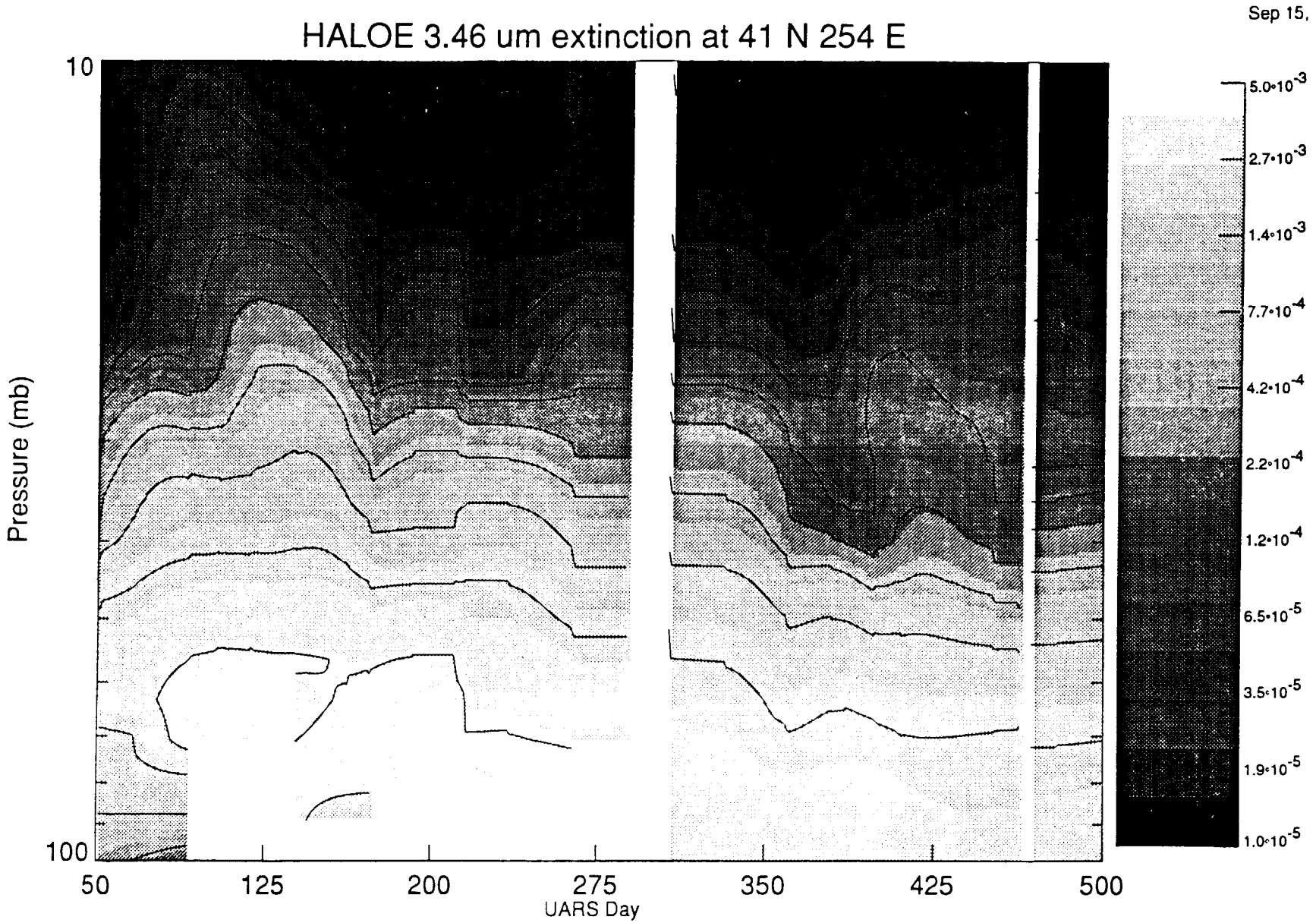

Figure 3.2-3 HALOE 3.46 μ extinction as a function of pressure and time for Oct. 26, 1991 to Jan. 29, 1993.

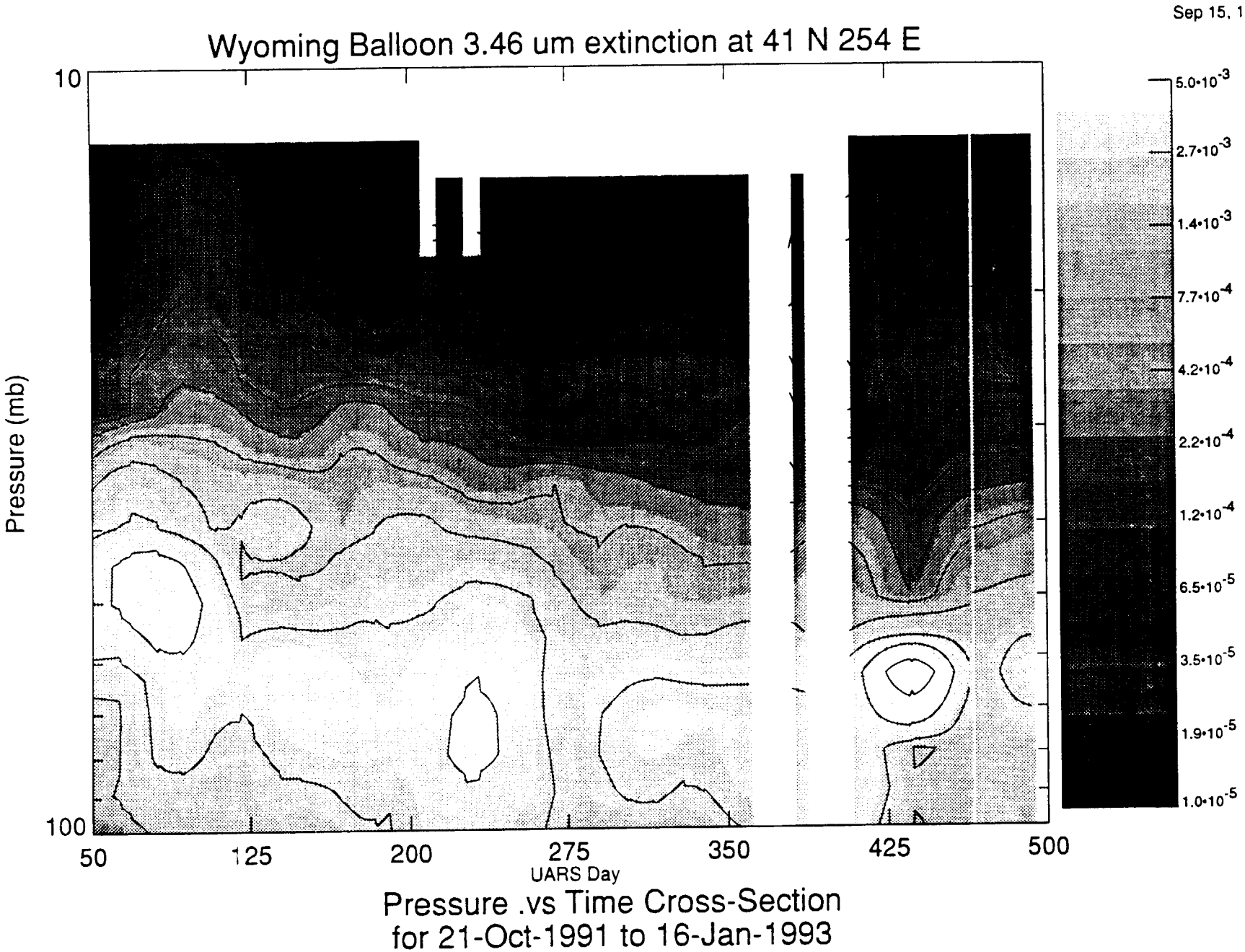

Figure 3.2-4 Theoretical 3.46 μ extinction as a function of pressure and time for Oct. 26, 1991 to Jan. 29, 1993.

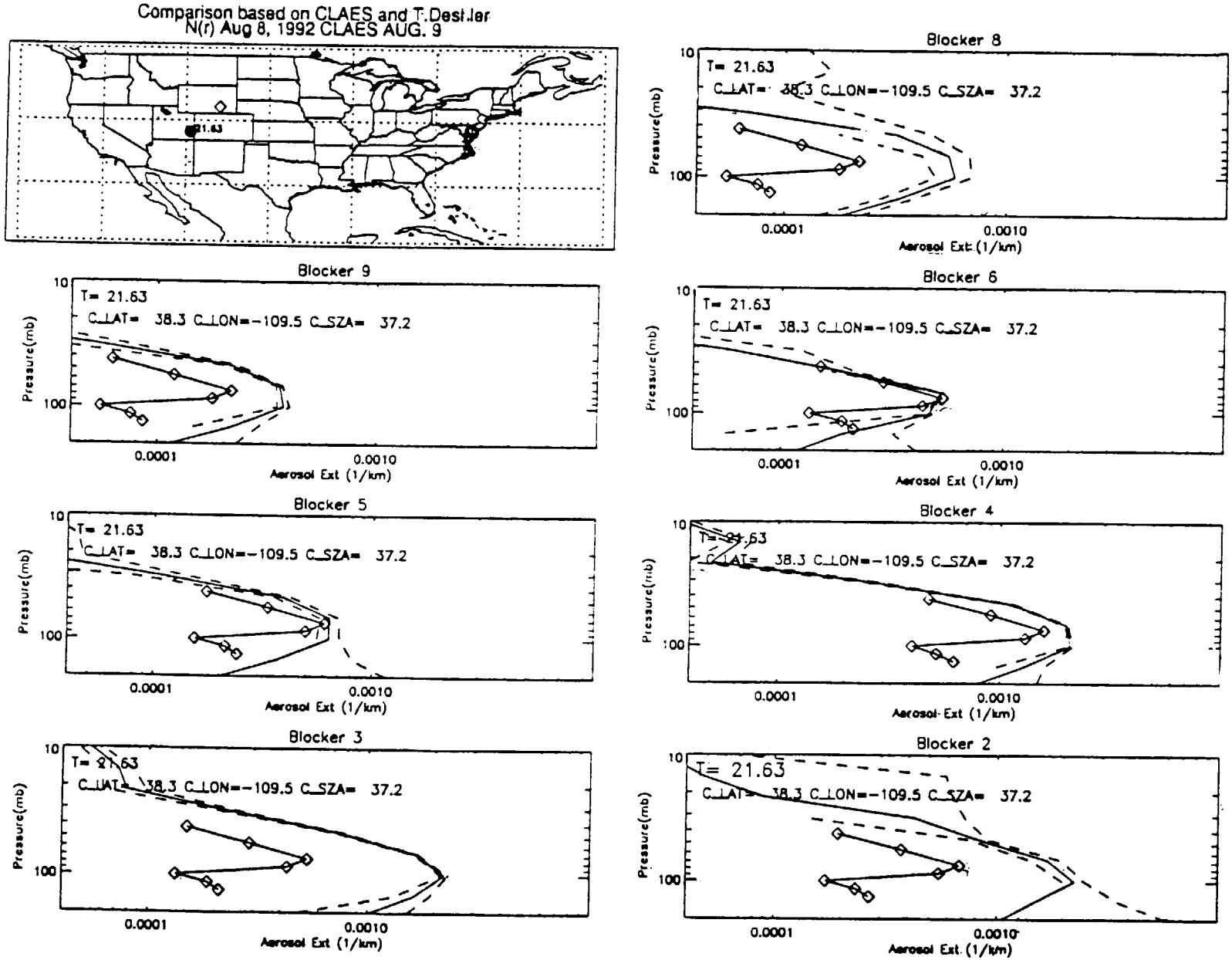

Figure 3.2-5 Comparison of CLAES and theoretical extinction profiles for Aug. 8, 1992 at 38.3 N and 109.5 W.

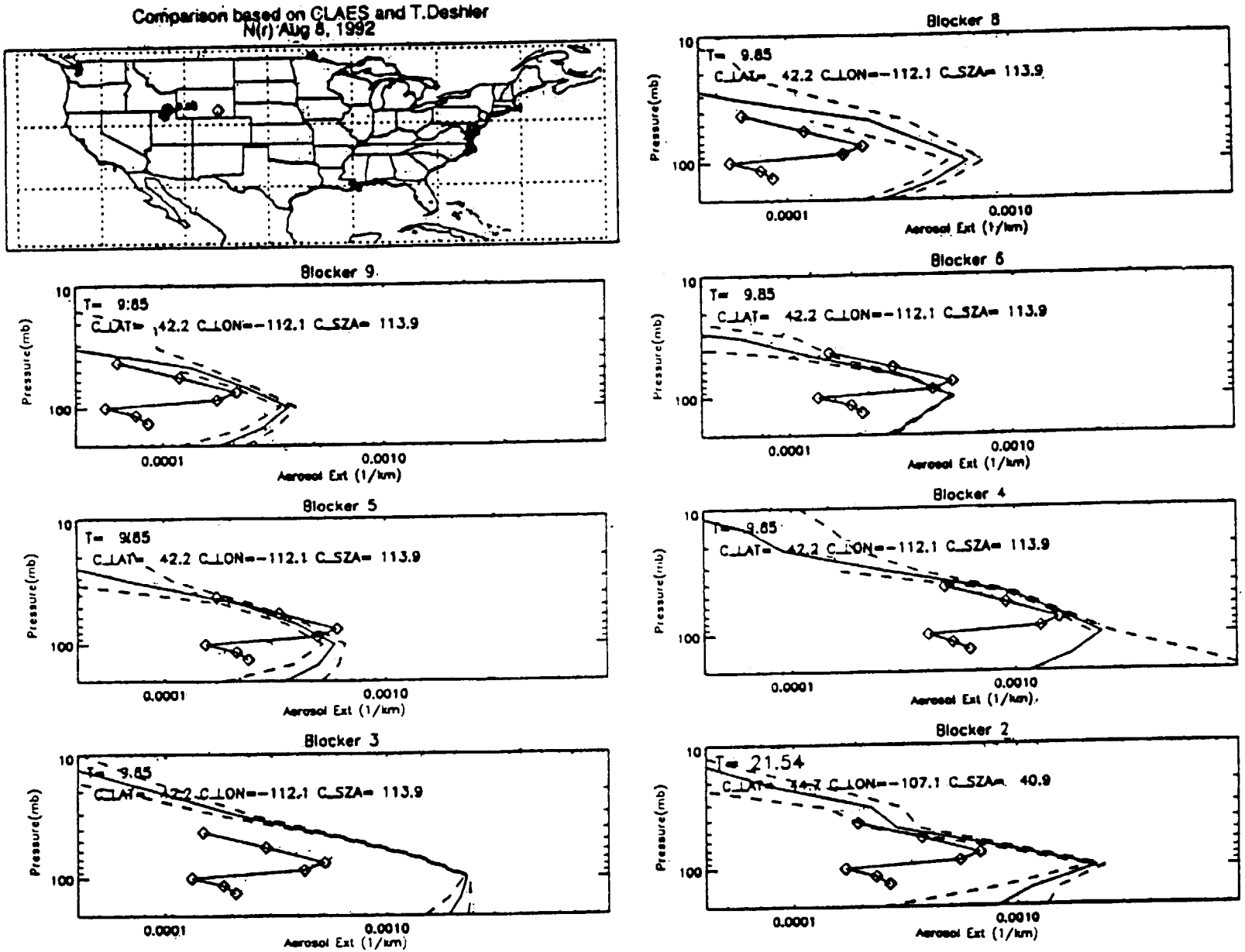

Figure 3.2-6 Comparison of CLAES and theoretical extinction profiles for Aug. 8, 1992 at 42.2 N and 112.1 W.

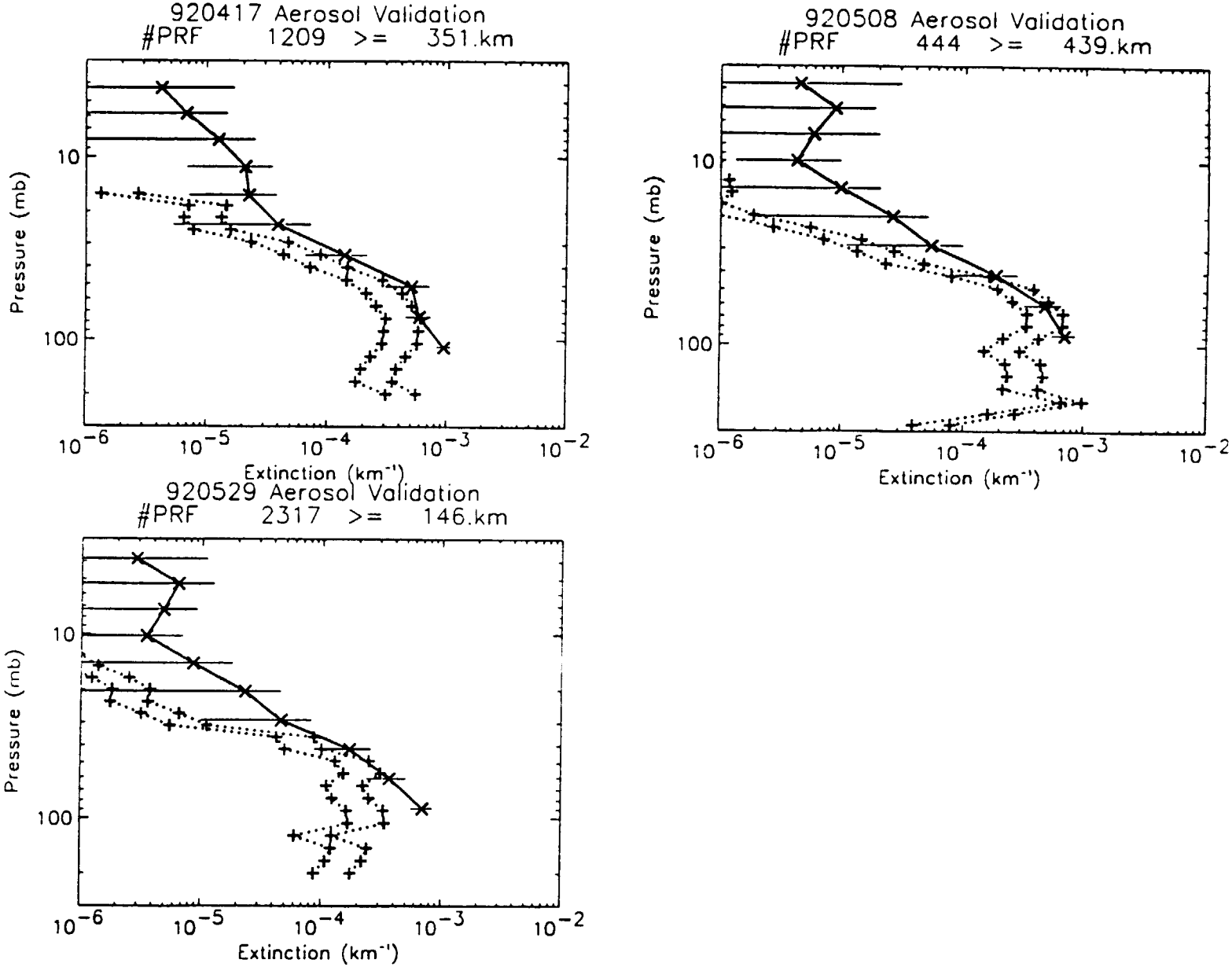

Figure 3.2-7 Comparison of ISAMS (——) and theoretical extinction profiles (- - -) on May 29, 1992. Left and right theory curves are for 59 and 86 percent H_2SO_4, respectively.

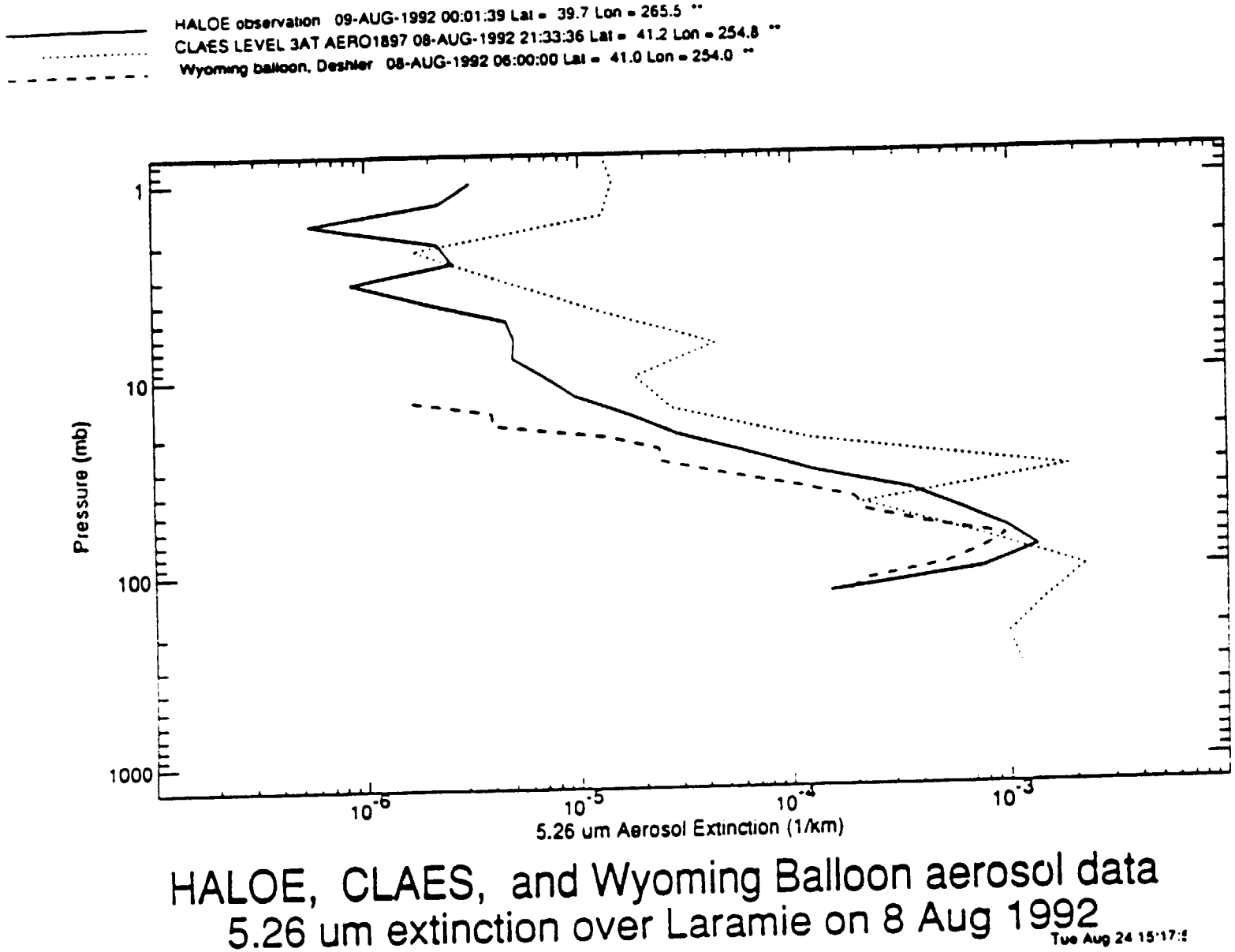

Figure 3.2-8 Comparison of HALOE, CLAES, and a theoretical prediction of 5.26 μ extinction on Aug. 8, 1992.

SAGE and CLAES intercomparison

Formed ratios of CLAES and SAGE extinction (km^{-1}) for 112 profiles for pressures between 100 and 3 mb for January 9-11, 1992. The latitude range was from -3 S to +34 N. Version 6 CLAES data is used.

The SAGE extinction was scaled by theoretical ratios of extinction (based upon Mie calculations calculated using Terry Deshler's size distributions). Ratios refer to the 0.525 micron observation of SAGE, e.g. (CLAES 780 km^{-1}) / (SAGE 0.525 micron km^{-1}) is 2.32e-2.

cm^{-1}	ratio
780	2.32e-2
790	2.34e-2
840	2.87e-2
880	5.23e-2
925	5.33e-2
1257	1.41e-1
1605	5.26e-2

Figure 3.3-1 Theoretical ratios of extinction based upon Mie calculations.

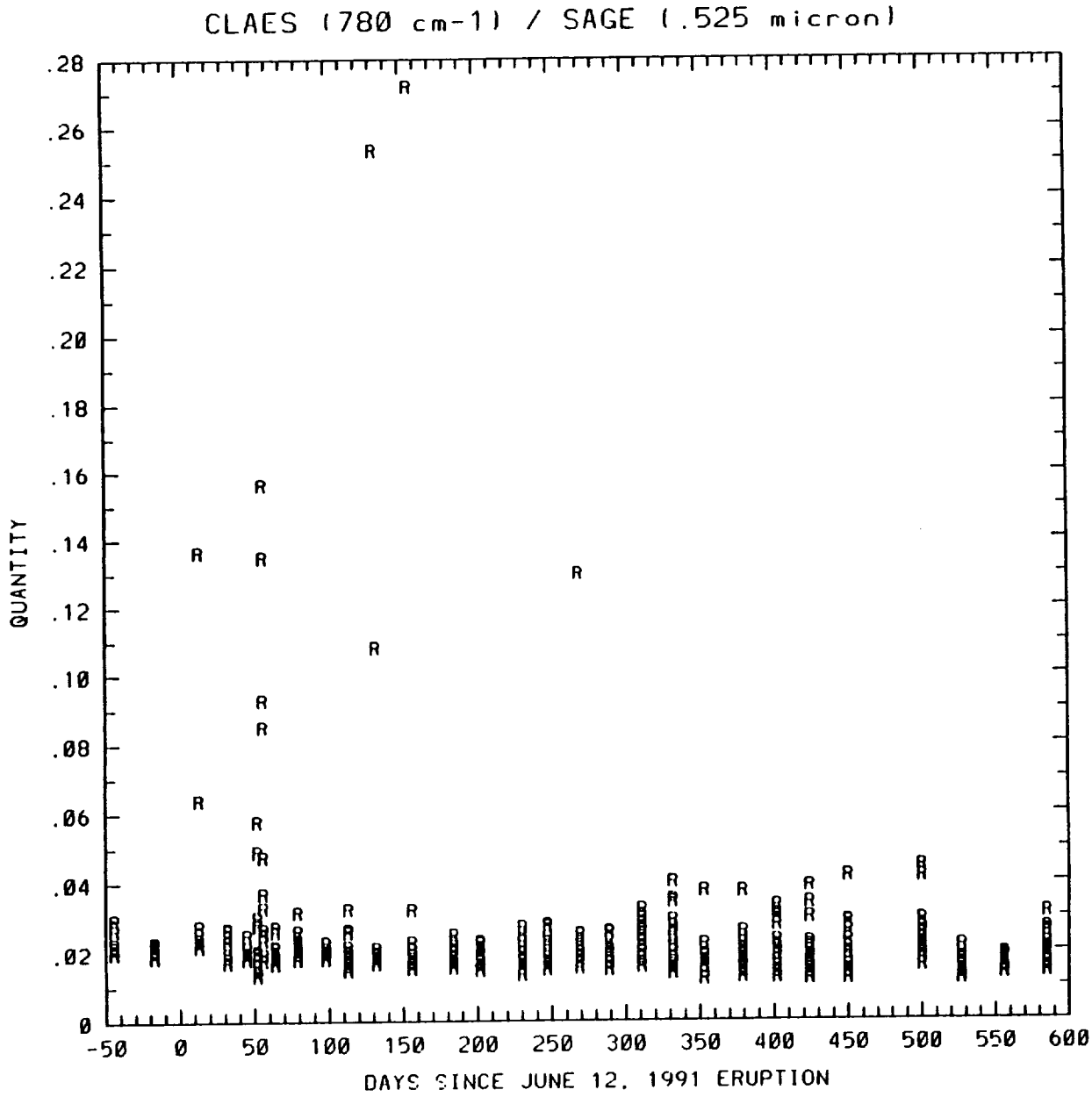

Figure 3.3-2 Theoretical ratios of extinction at 12.82 μ and 0.525 μ for altitudes from 18-24 km based upon Deshler particle size distribution.

780 cm^{-1}

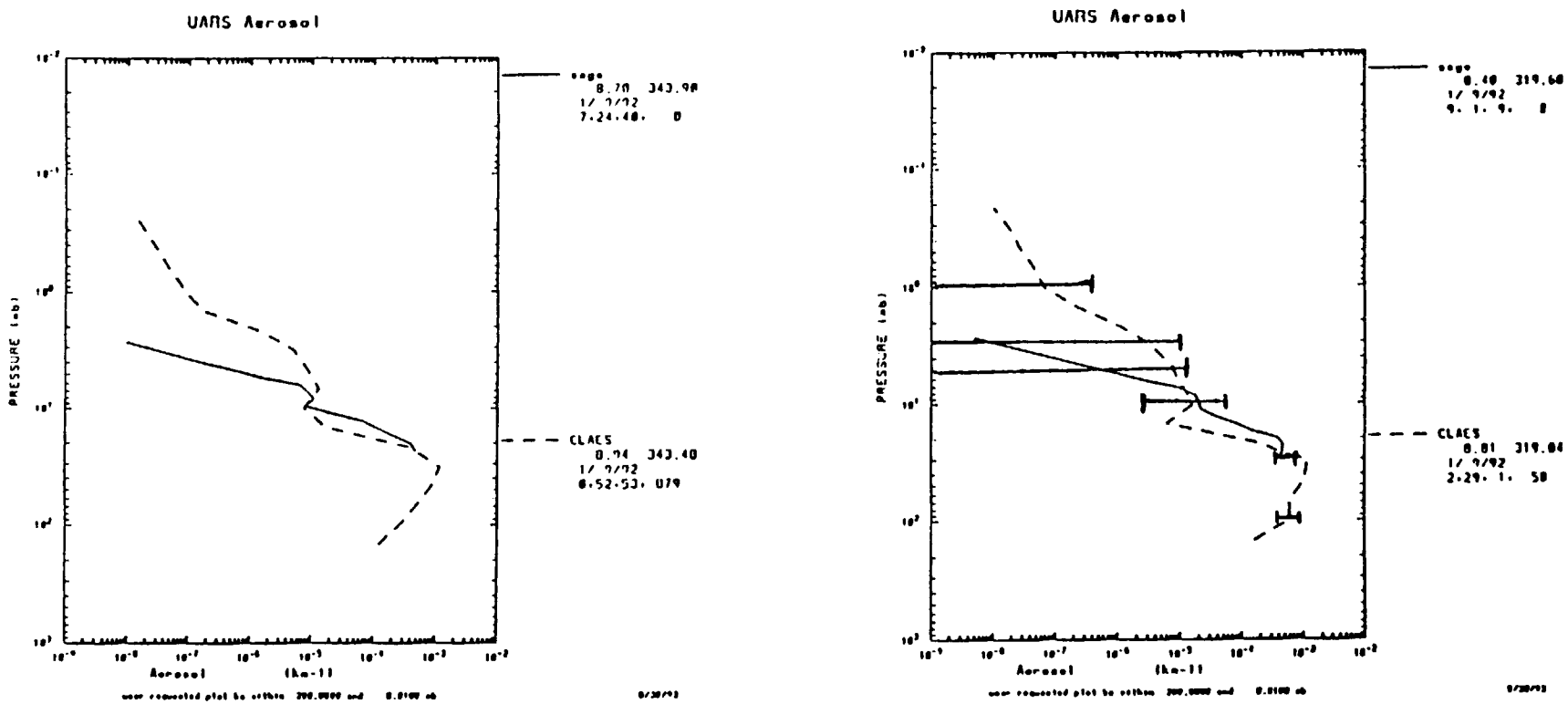

Figure 3.3-3 Comparison of CLAES (- - -) and ISAMS (——) extinction profiles on Jan. 9, 1992. Error bars are given for the CLAES data.

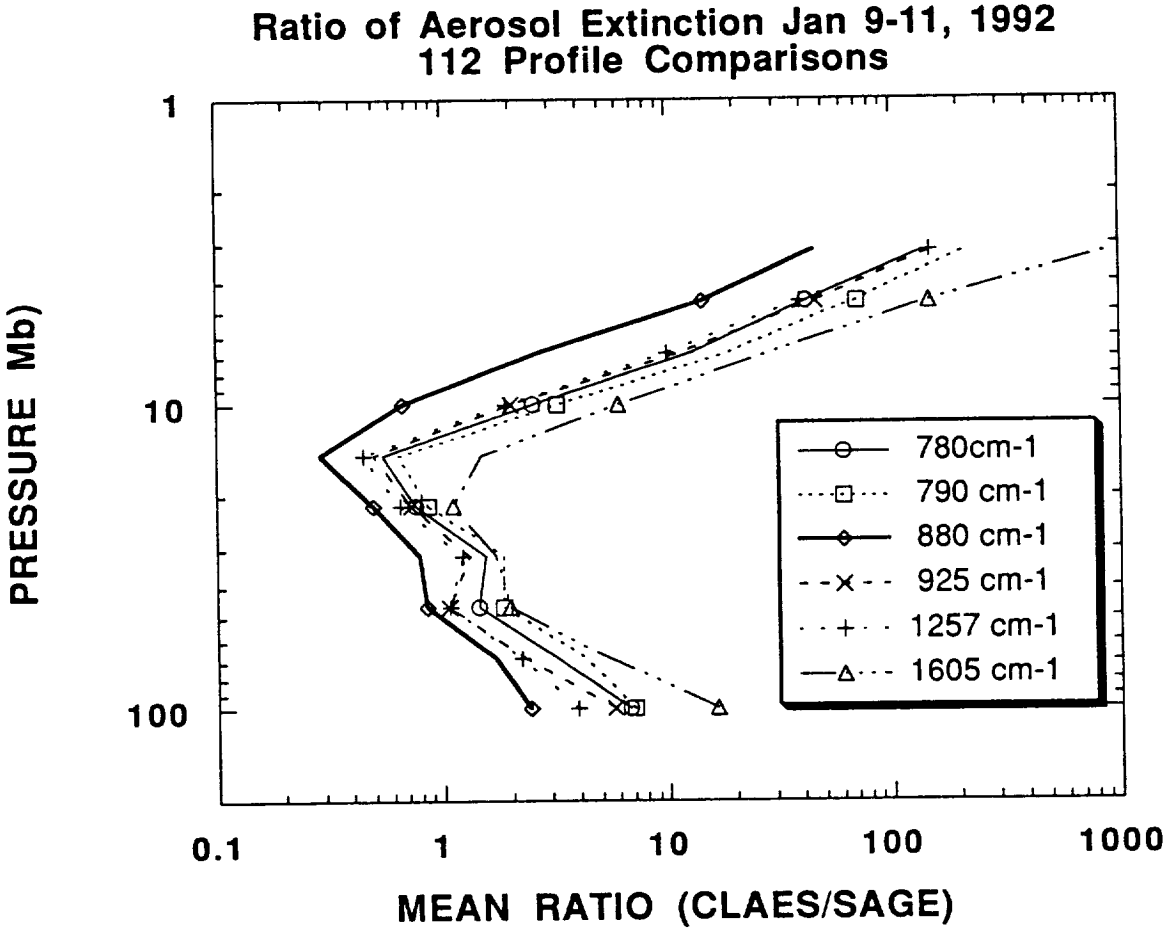

Figure 3.3-4 Mean ratios of aerosol extinction, CLAES/SAGE, for Jan. 9-11, 1992.

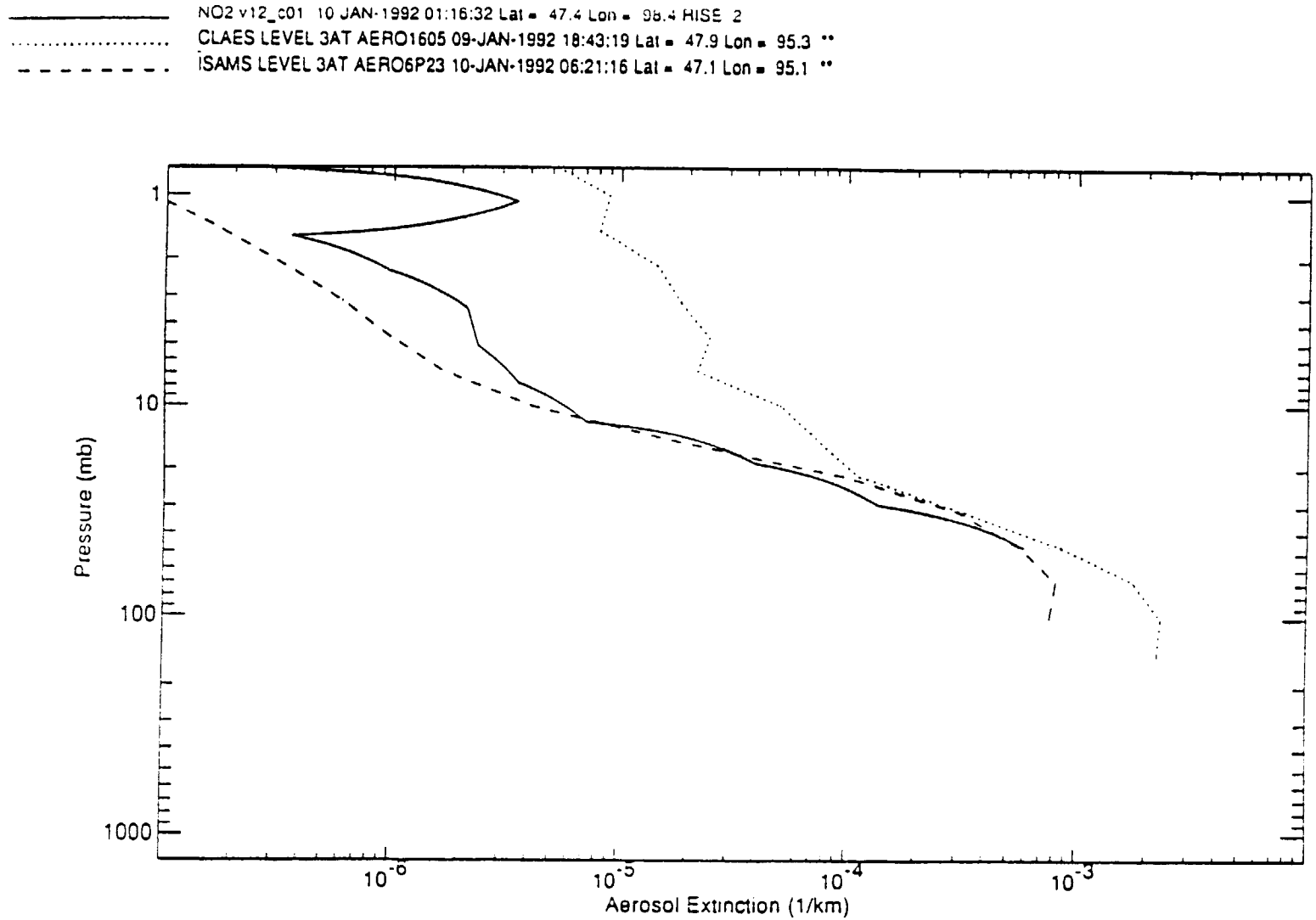

Figure 3.4-1 Comparison of HALOE, CLAES, and ISAMS aerosol extinction profiles at 6.23 μ for Jan. 9-10, 1992.

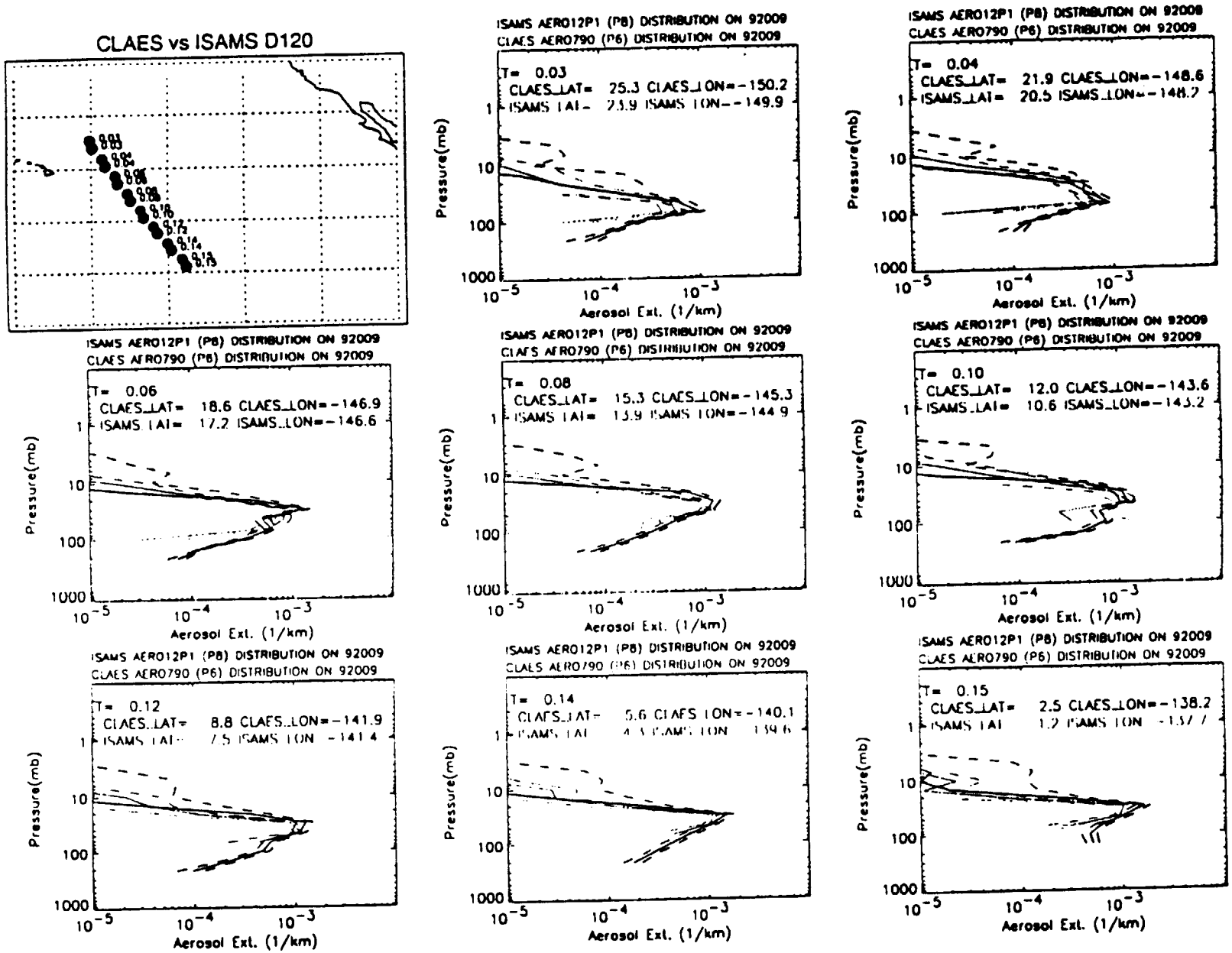

Figure 3.4-2 Comparison of CLAES and ISAMS aerosol extinction profiles on Jan. 9, 1992, over the Pacific Ocean.

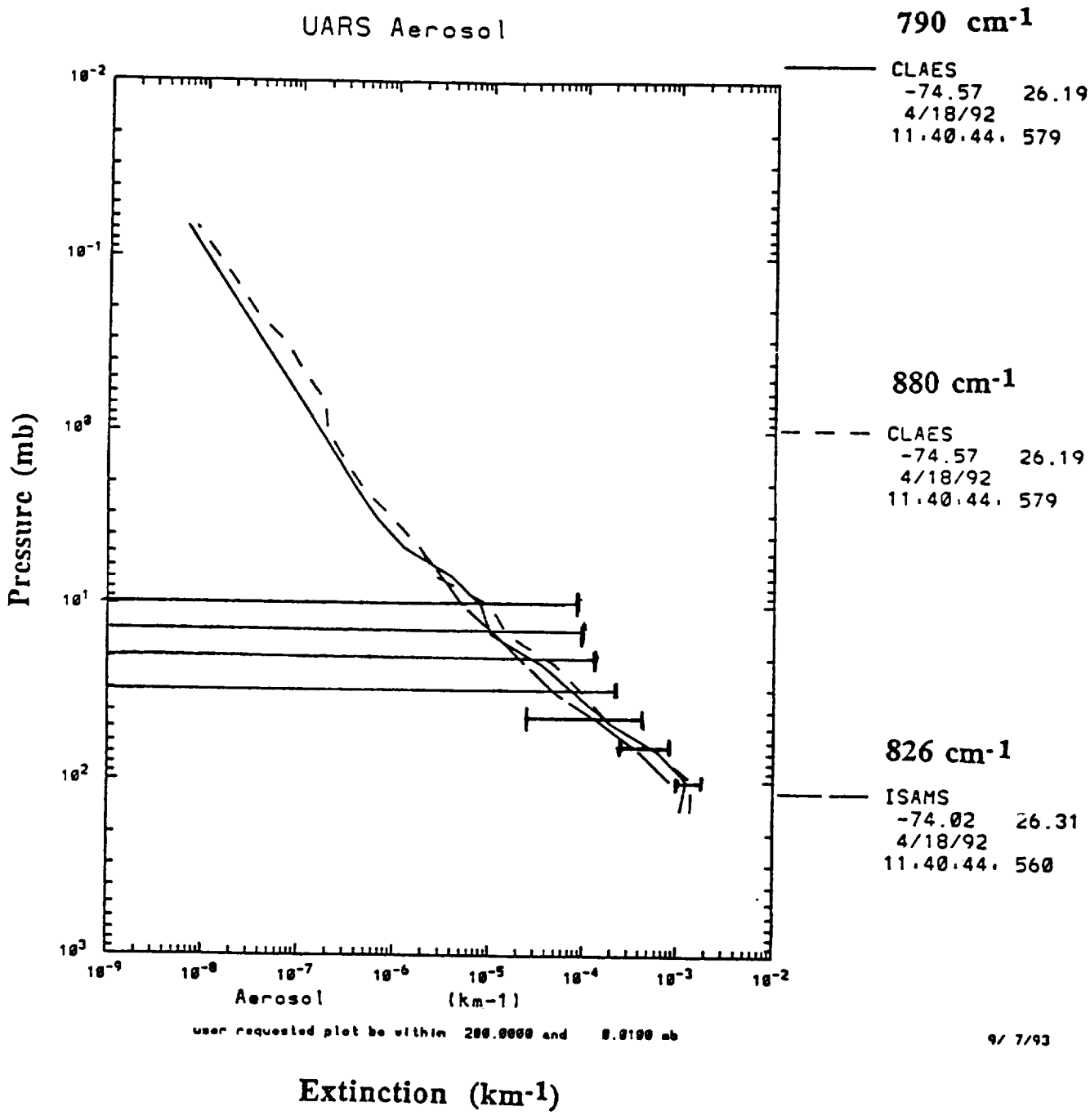

Figure 3.4-3 Comparison of CLAES and ISAMS aerosol extinction at 74S on April 18, 1992, for low aerosol loading. Error bars are given for the CLAES data.

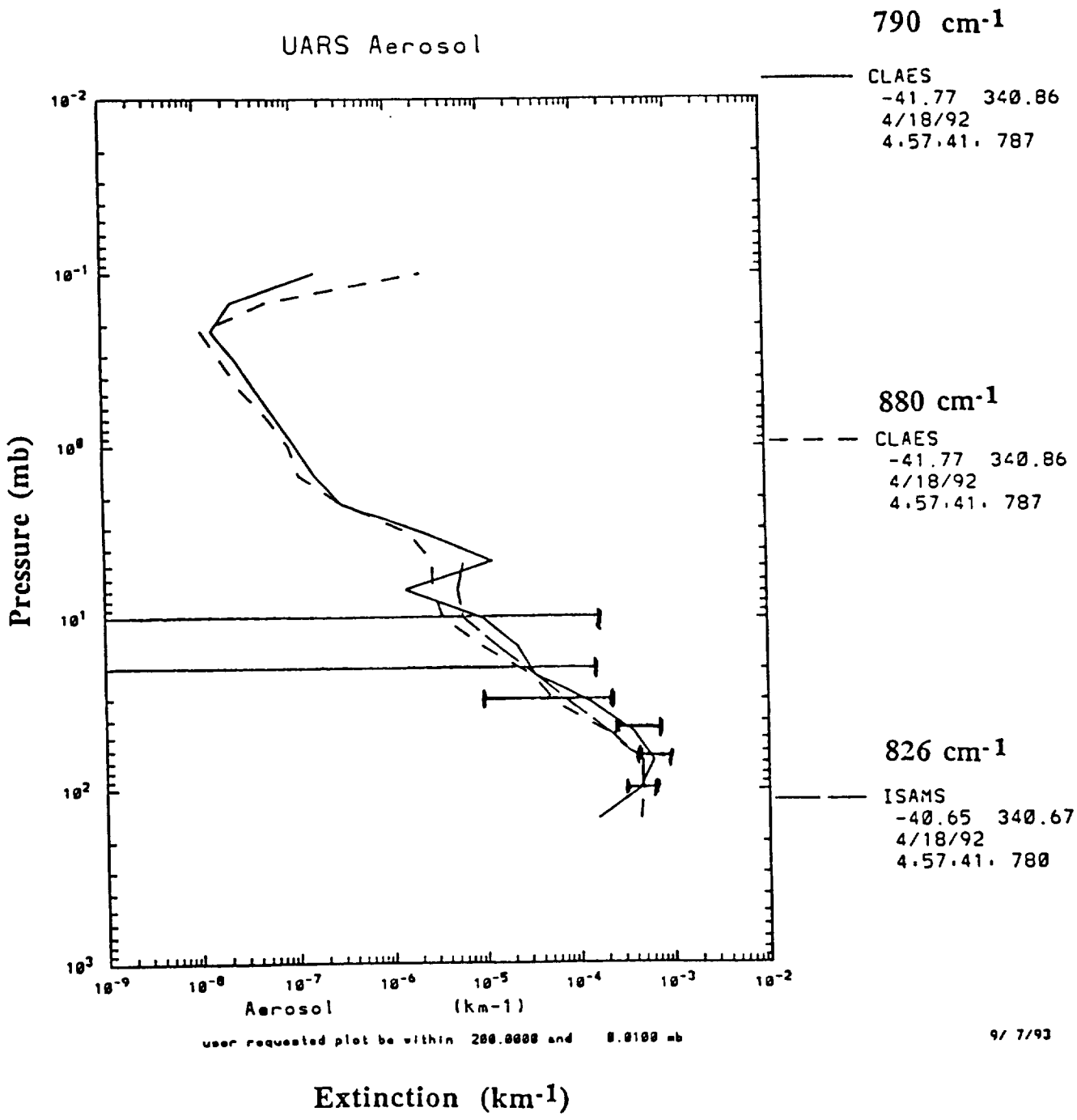

Figure 3.4-4 Comparison of CLAES and ISAMS aerosol extinction at 41S on April 18, 1992, for medium aerosol loading. Error bars are given for the CLAES data.

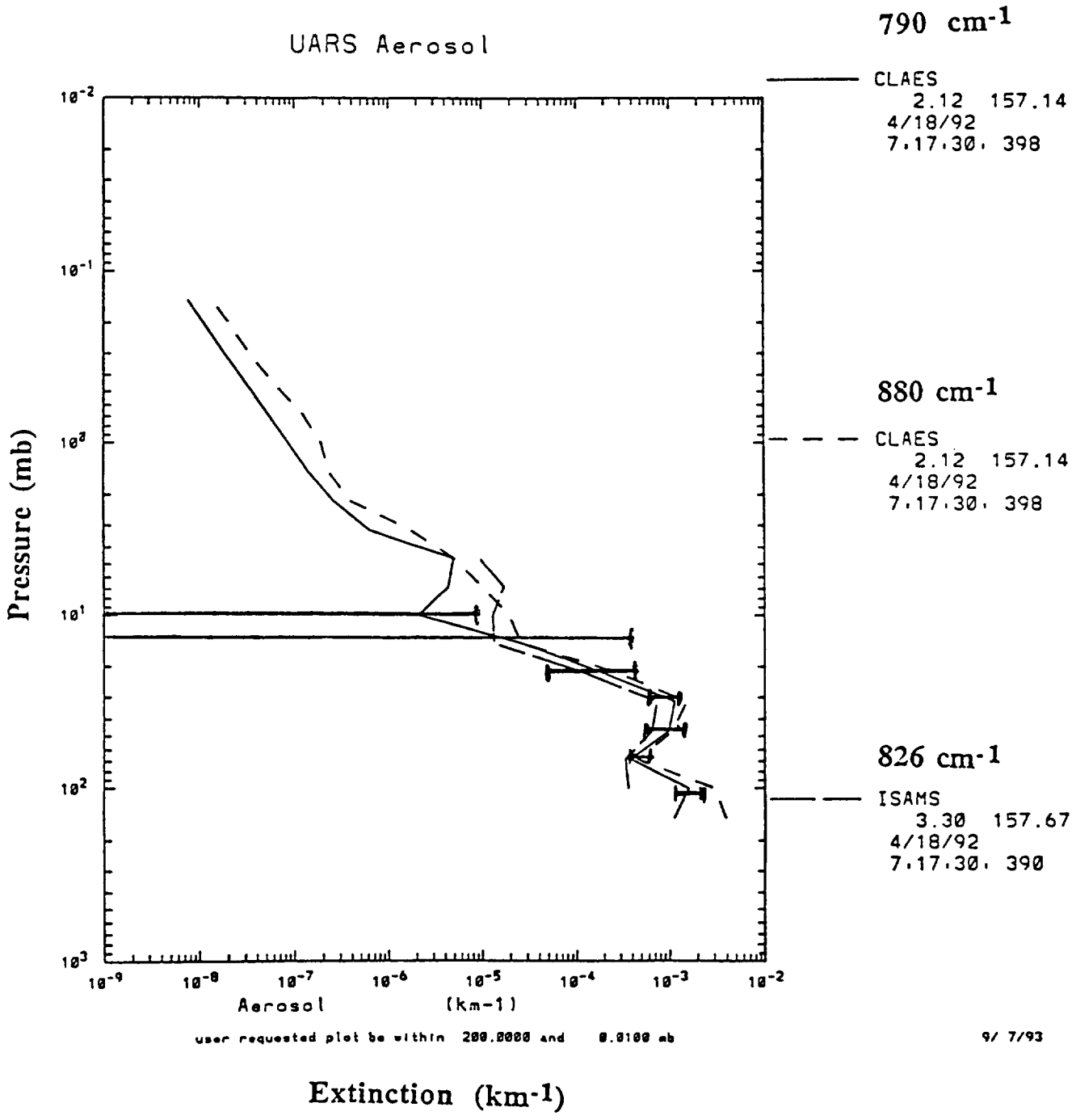

Figure 3.4-5 Comparison of CLAES and ISAMS aerosol extinction at 2N on April 18, 1992, for heavy aerosol loading. Error bars are given for the CLAES data.

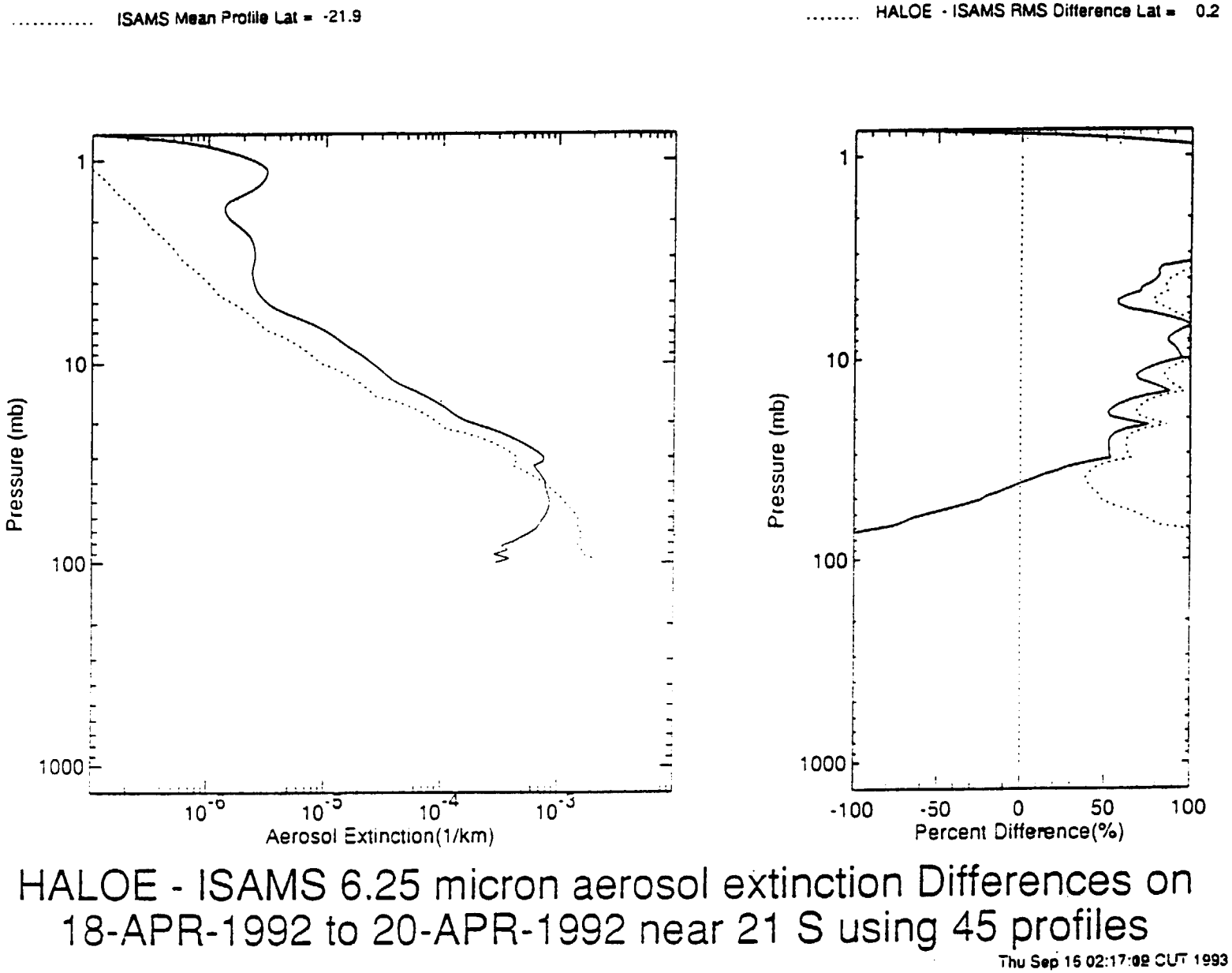

Figure 3.4-6 HALOE-ISAMS 6.25 μ profile differences, based upon 45 profiles for April 18-20, 1992.

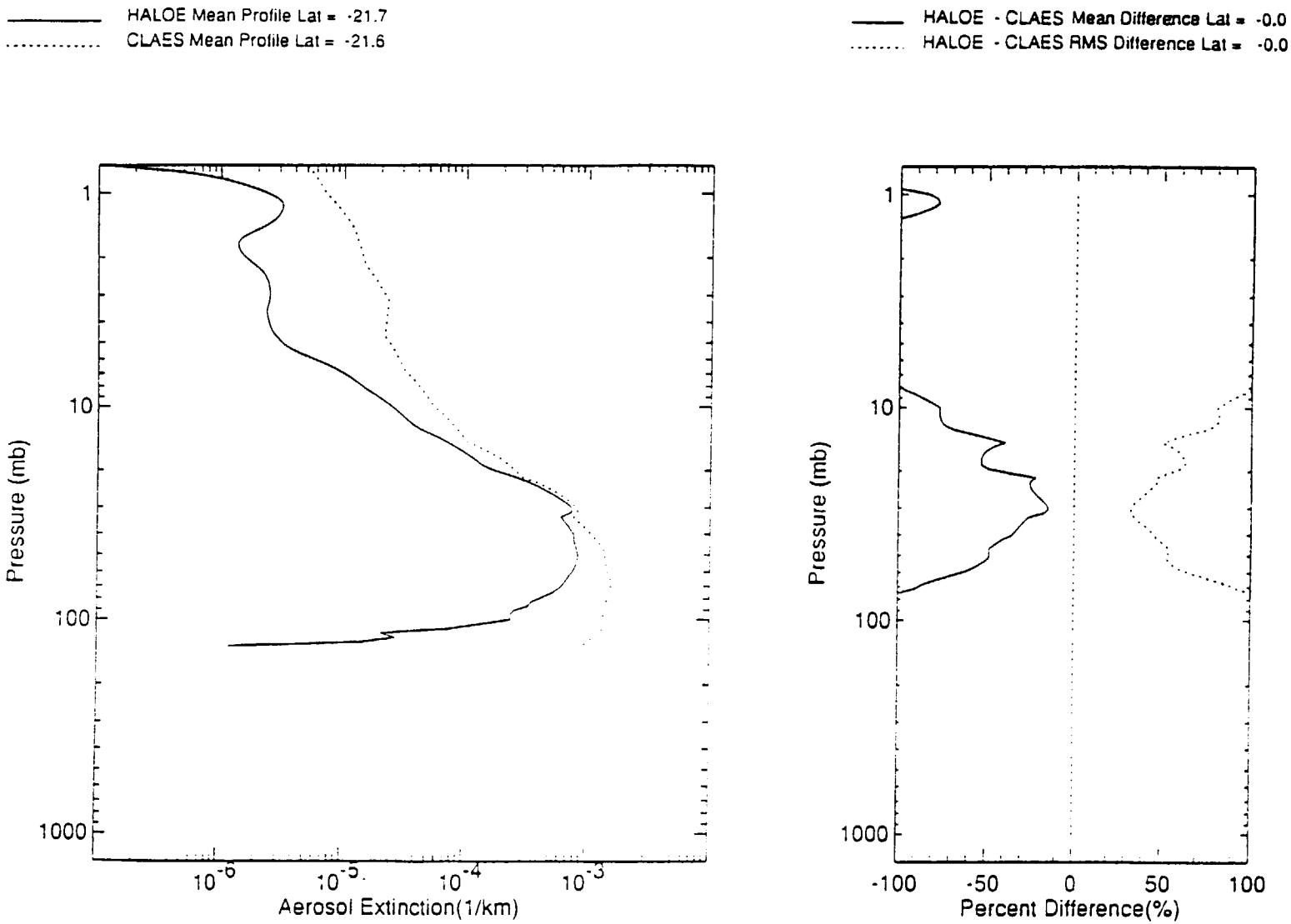

Figure 3.4-7 HALOE-CLAES 6.25 μ profile differences, based upon 45 profiles for April 18-20, 1992.

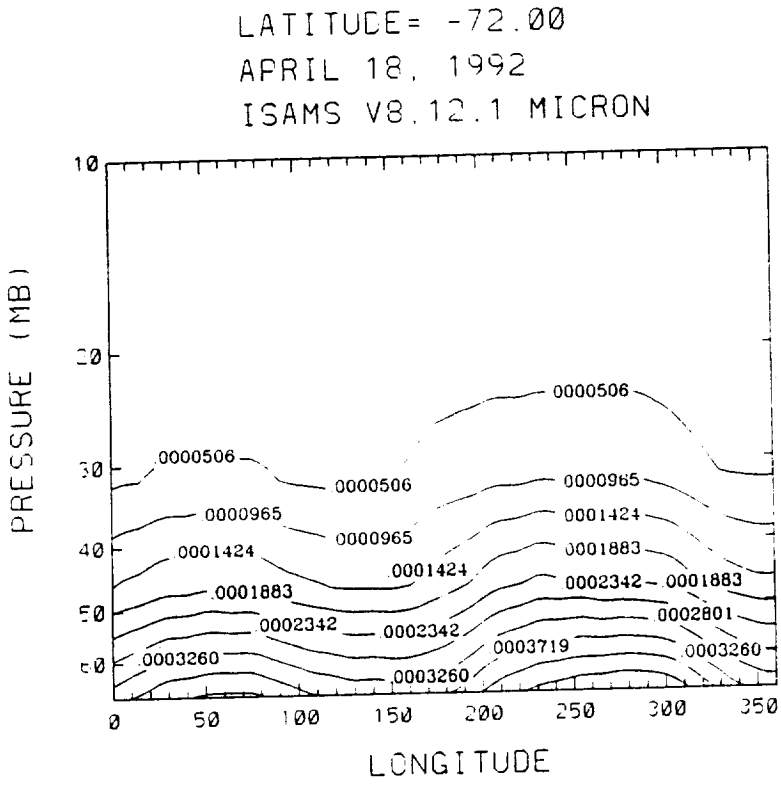

Figure 3.5-1 ISAMS 12.1 μ extinction at 72S on April 18, 1992.

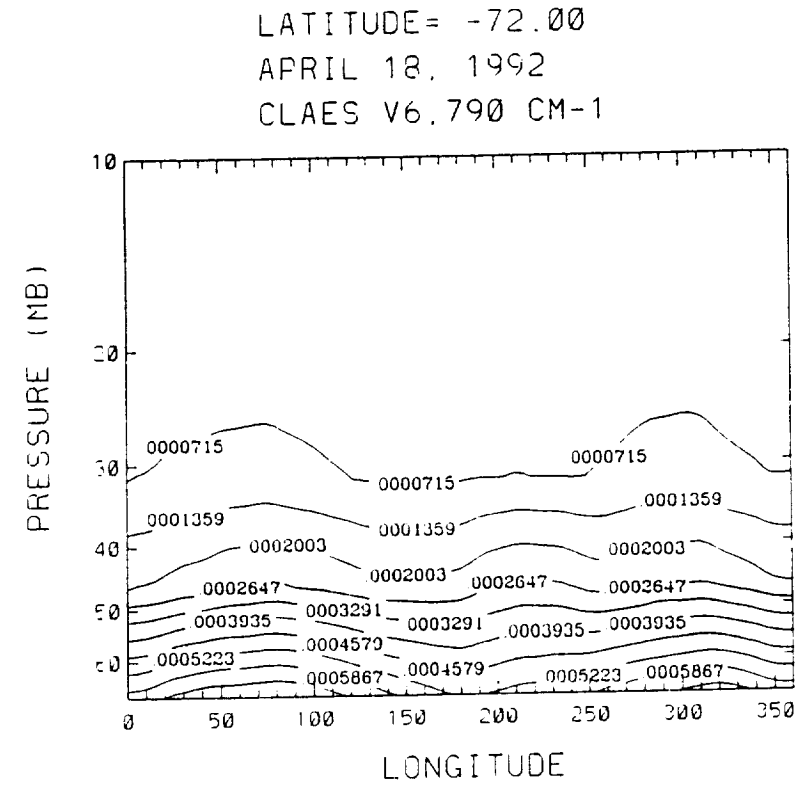

Figure 3.5-2 CLAES 12.65 μ extinction at 72S on April 18, 1992.

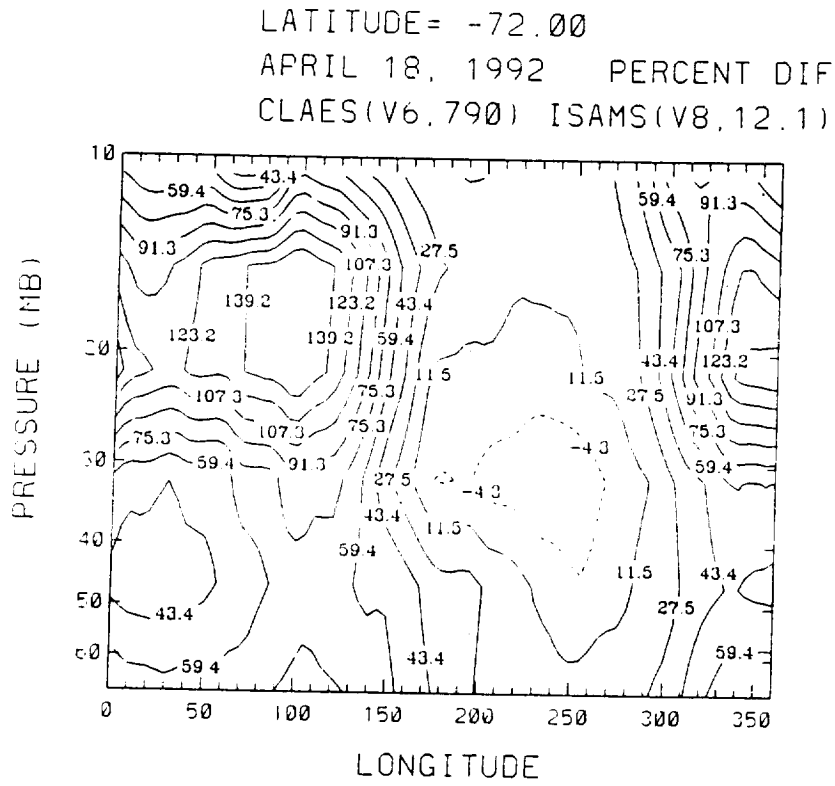

Figure 3.5-3 Percent difference map for the data presented in Figures 3.5-1 and 3.5-2.

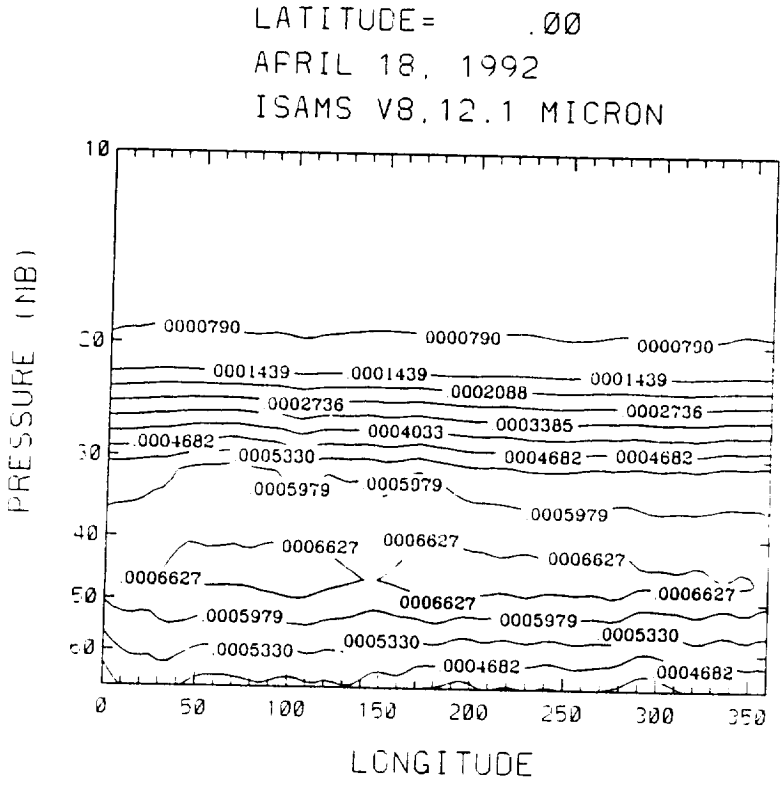

Figure 3.5-4 ISAMS 12.1 μ extinction at the Equator on April 18, 1992.

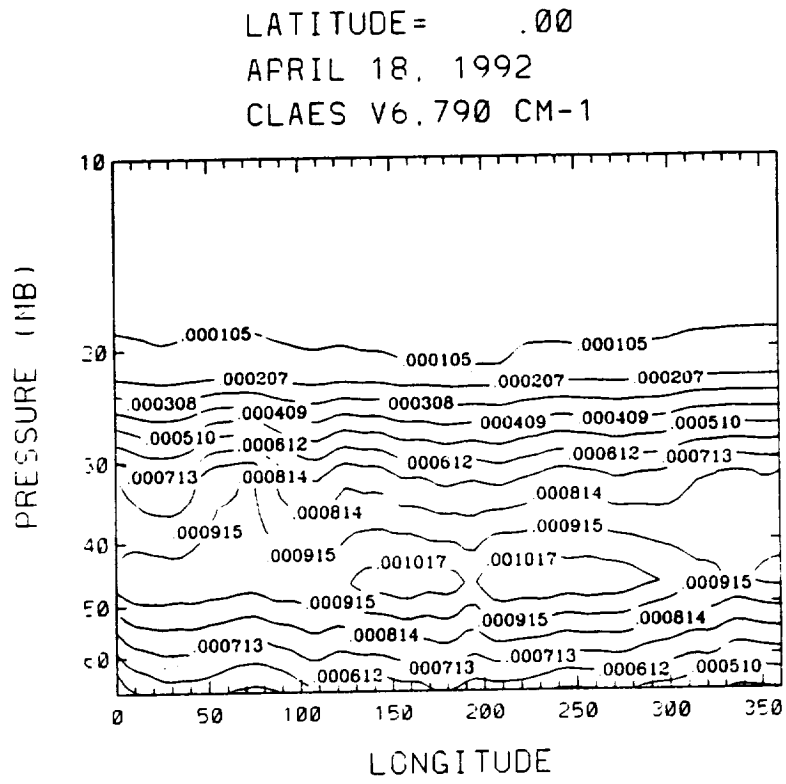

Figure 3.5-5 CLAES 12.65 μ extinction at the Equator on April 18, 1992.

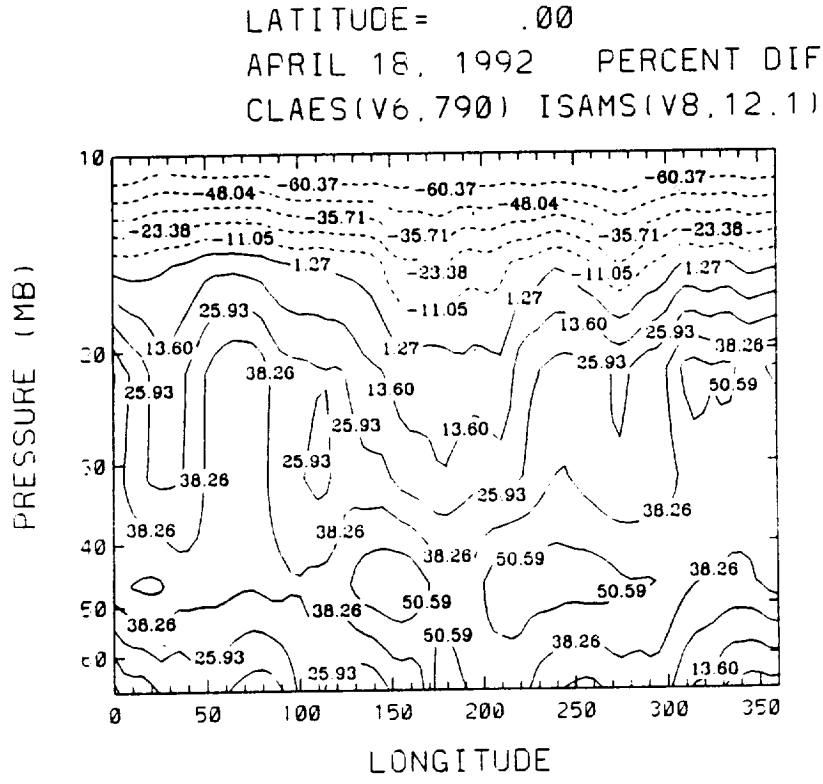

Figure 3.5-6 Percent difference map for the data presented in Figures 3.5-4 and 3.5-5.

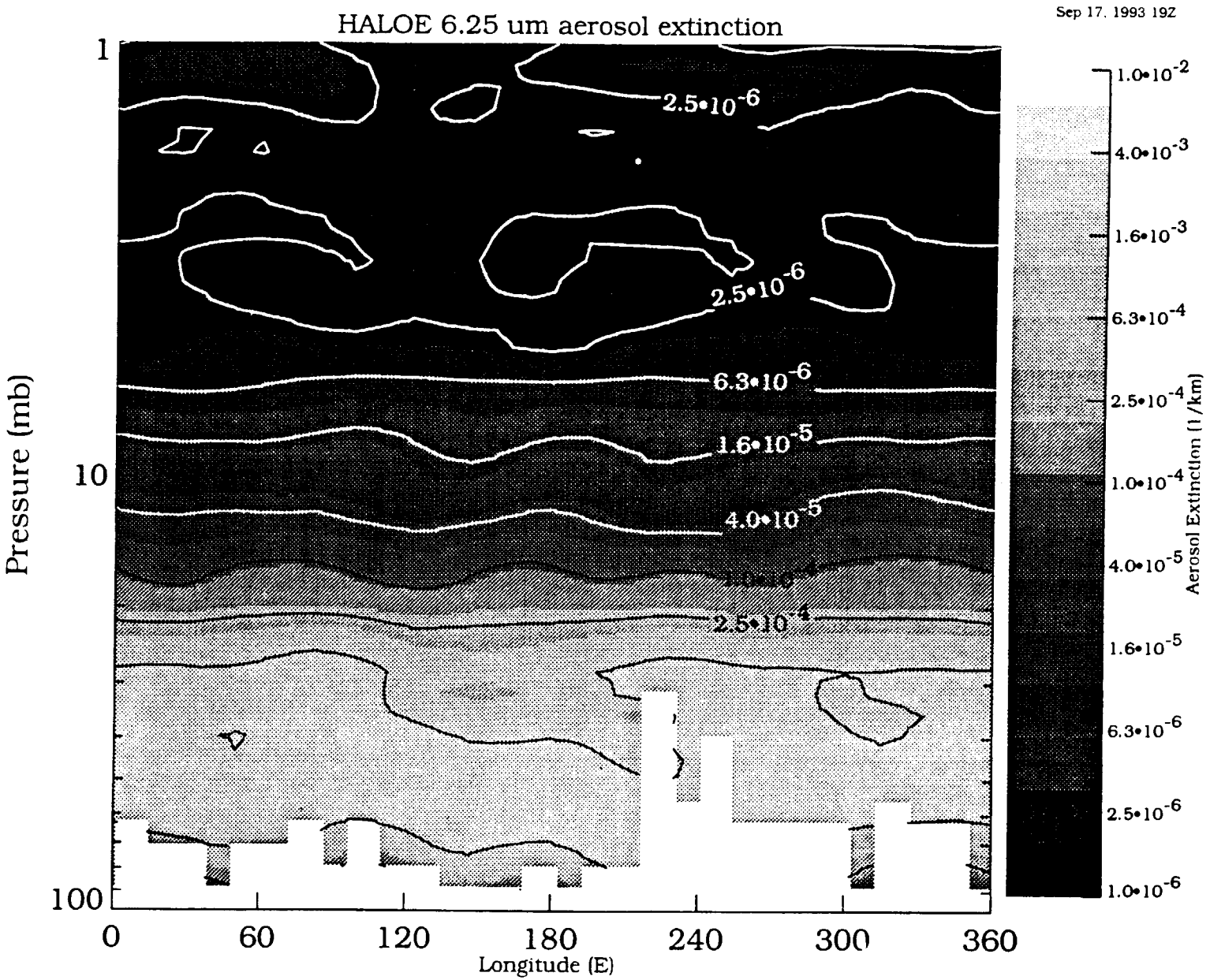

HALOE Aerosol Pressure vs Longitude Cross Section, Sunrise on 18-APR to 20-APR-1992 at 21 S

Figure 3.5-7 HALOE aerosol extinction at 6.25 μ for April 18-20, 1992, at 21S as a function of pressure and longitude.

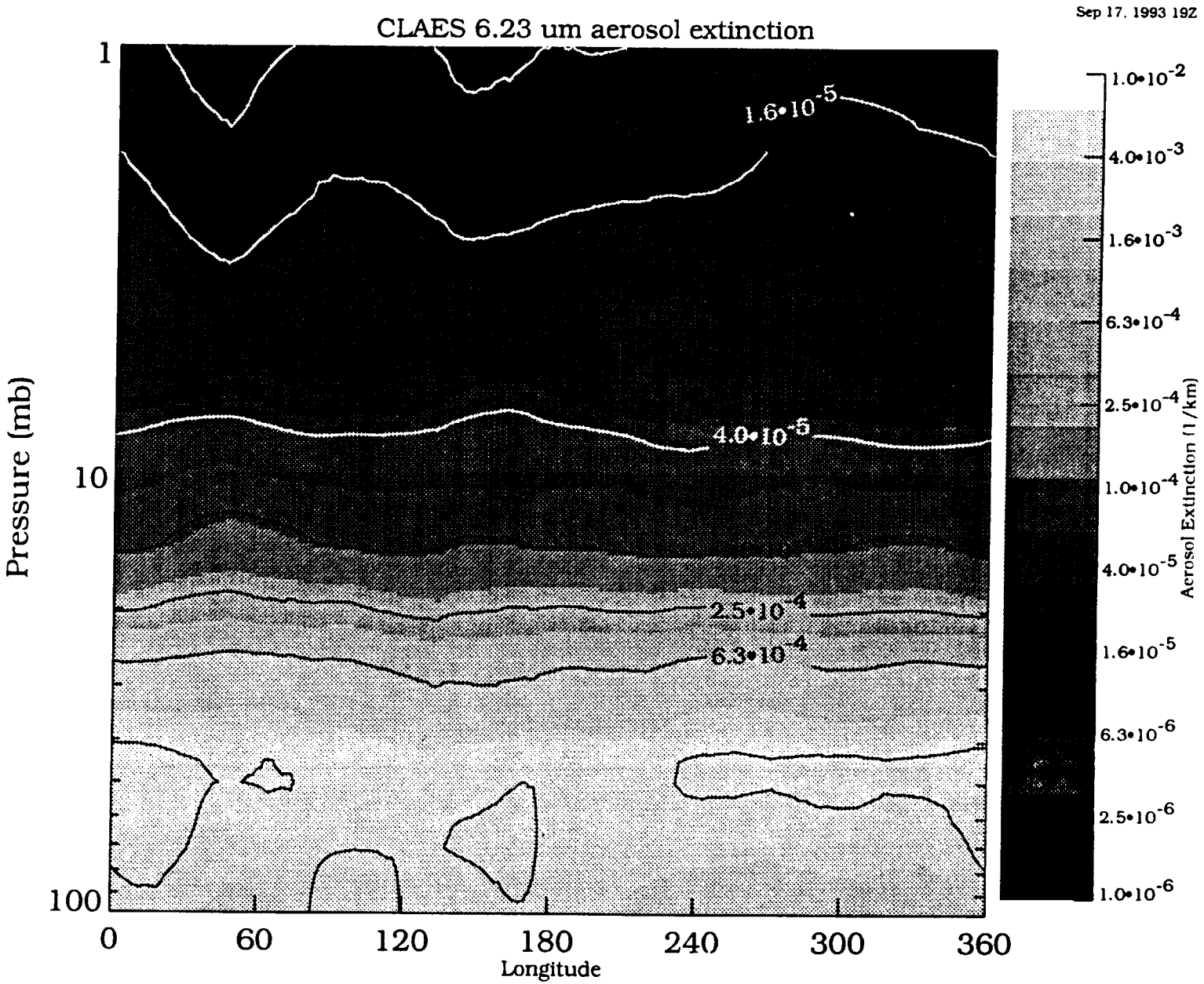

Aerosol Pressure vs Longitude Cross Section, on 18-APR to 20-APR-1992 at 21 S

Figure 3.5-8 CLAES aerosol extinction at 6.23 μ for April 18-20, 1992, at 21S as a function of pressure and longitude.

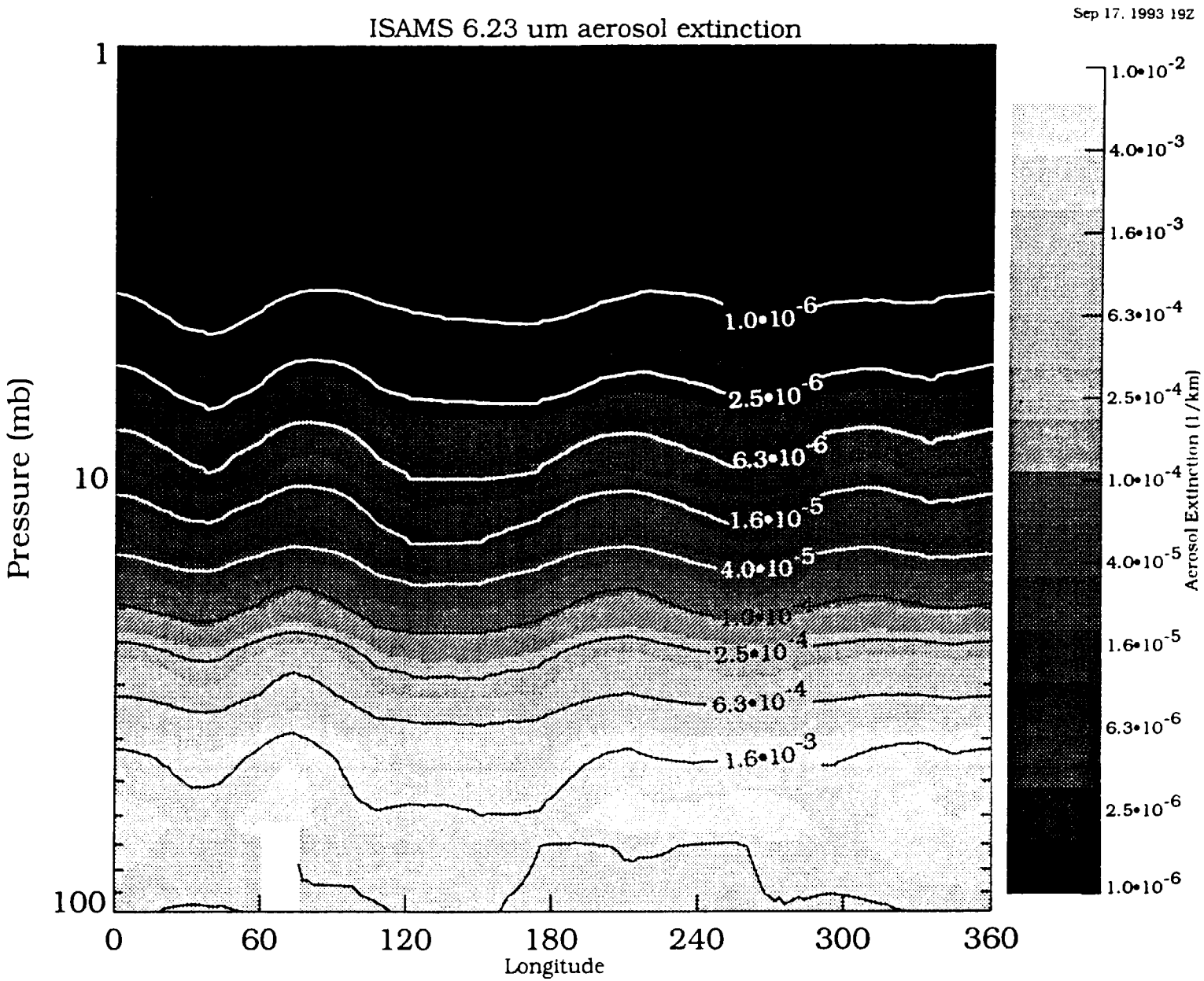

Figure 3.5-9 ISAMS aerosol extinction at 6.23 μ for April 18-20, 1992, at 21S as a function of pressure and longitude.

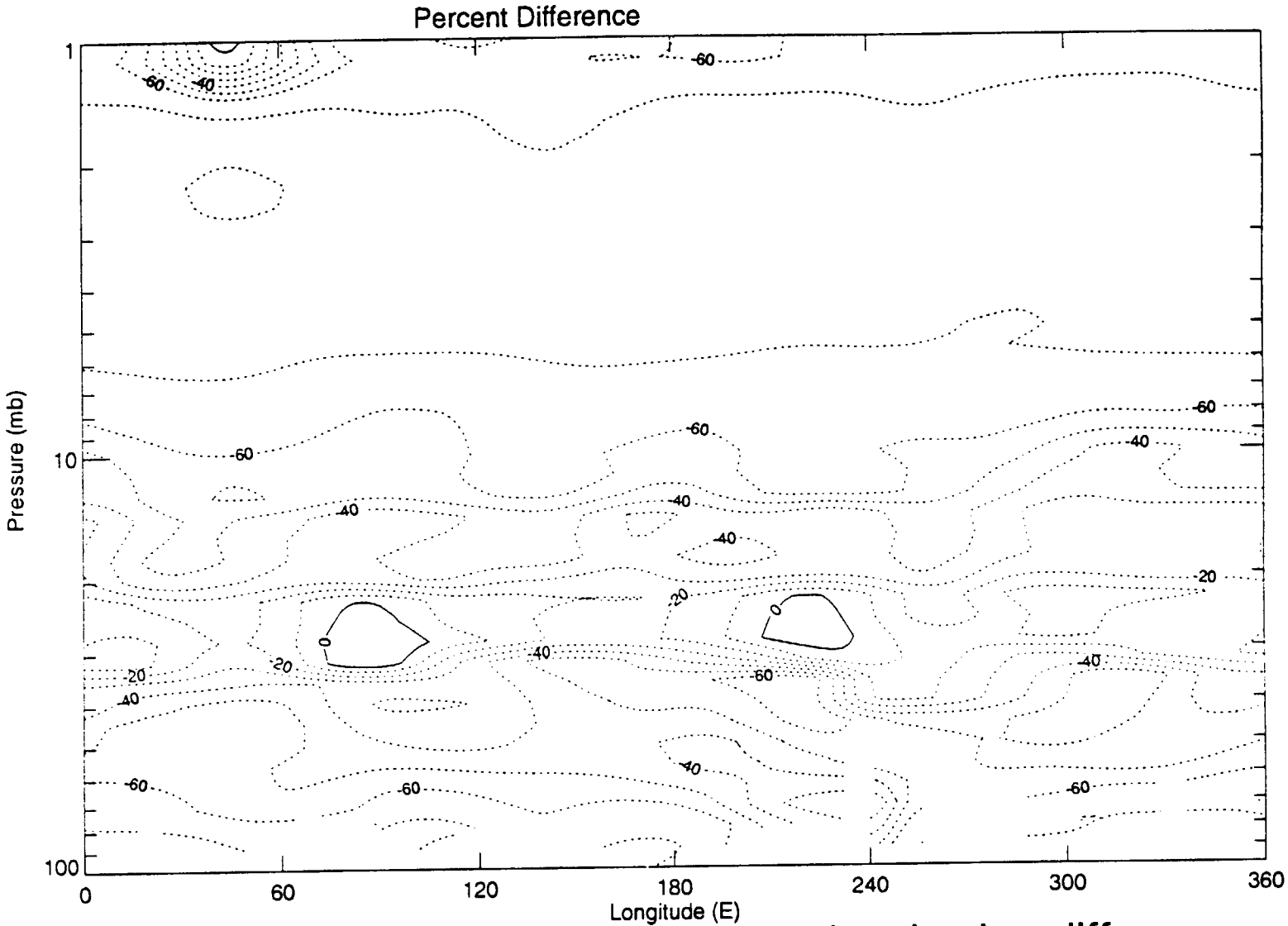

Figure 3.5-10 Percent difference map for the data presented in Figures 3.5-7 and 3.5-8.

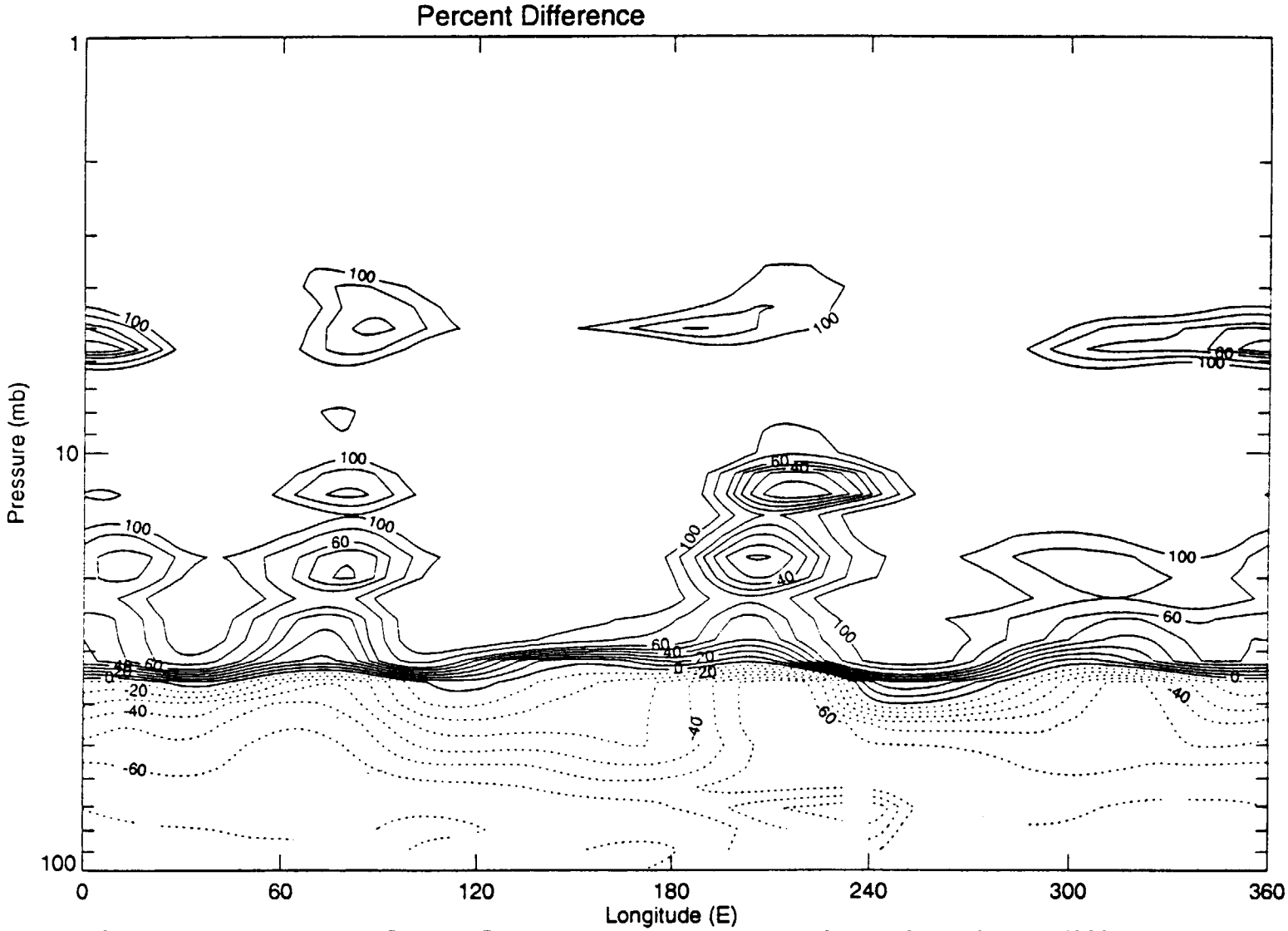

Figure 3.5-11 Percent difference map for the data presented in Figures 3.5-7 and 3.5-9.

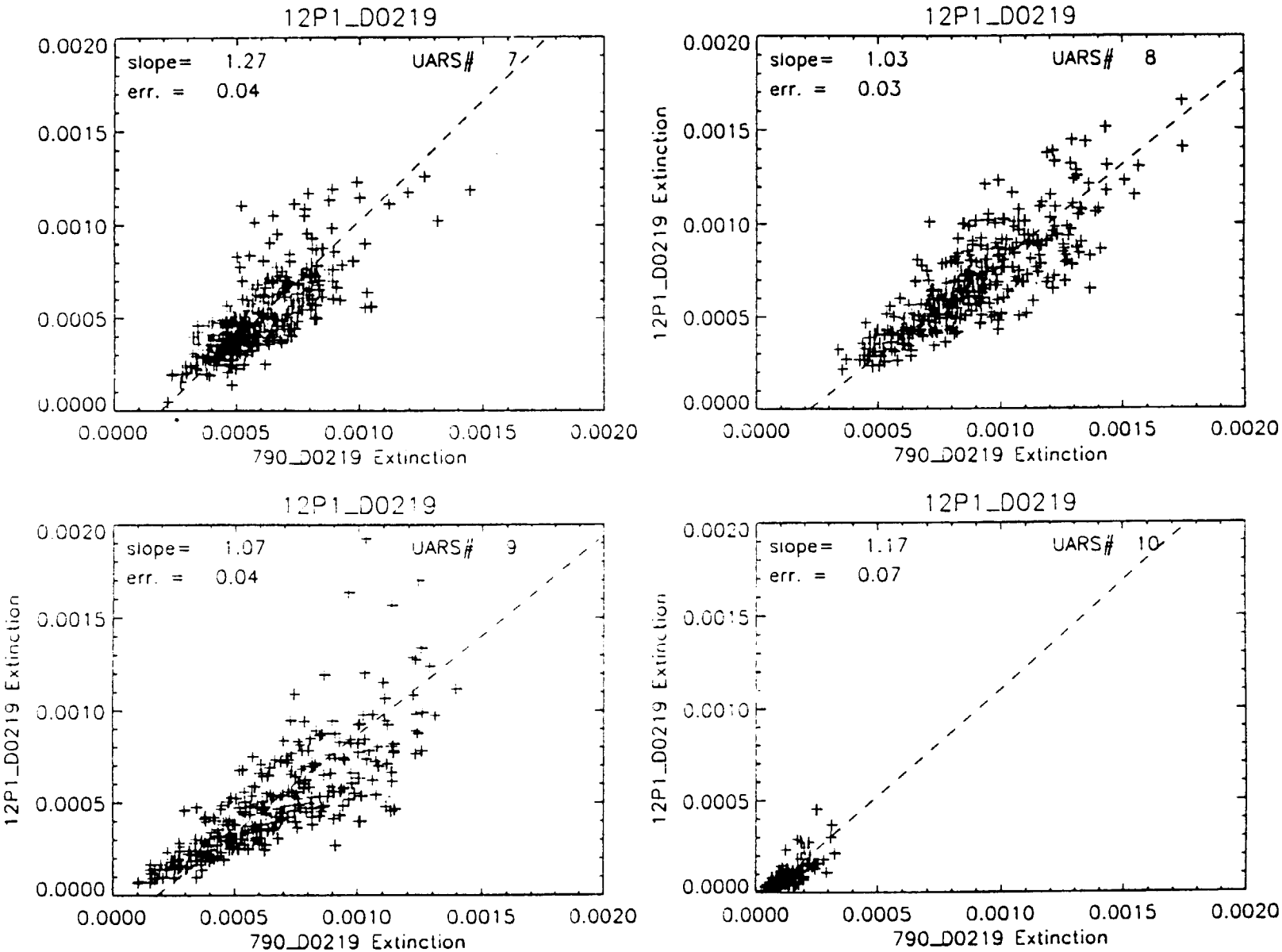

Figure3.6-1 Scatter diagrams of ISAMS (12.1 μ) and CLAES (12.65 μ) extinction on April 17, 1992.

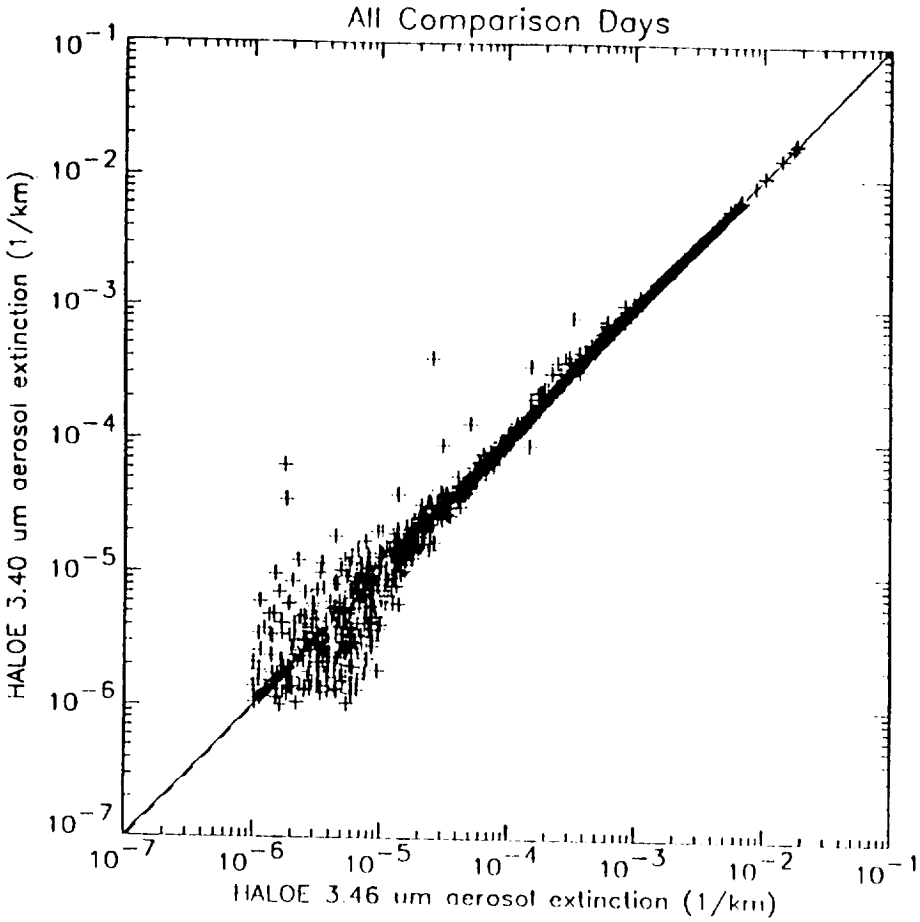

linear fit to log(extinction) ->

Y = 10 ^(0.0151504) * X ^(1.00543)

ratio from fit at X= 10e-5 : 0.972698

ratio from fit at X= 10e-3 : 0.997348

average ratio : 1.07028

extinction cutoff value = 1.00000e-06 (1/km)

244 profiles and 1611 points

Figure3.6-2 Scatter diagrams of HALOE 3.46 μ and 3.40 μ extinction.

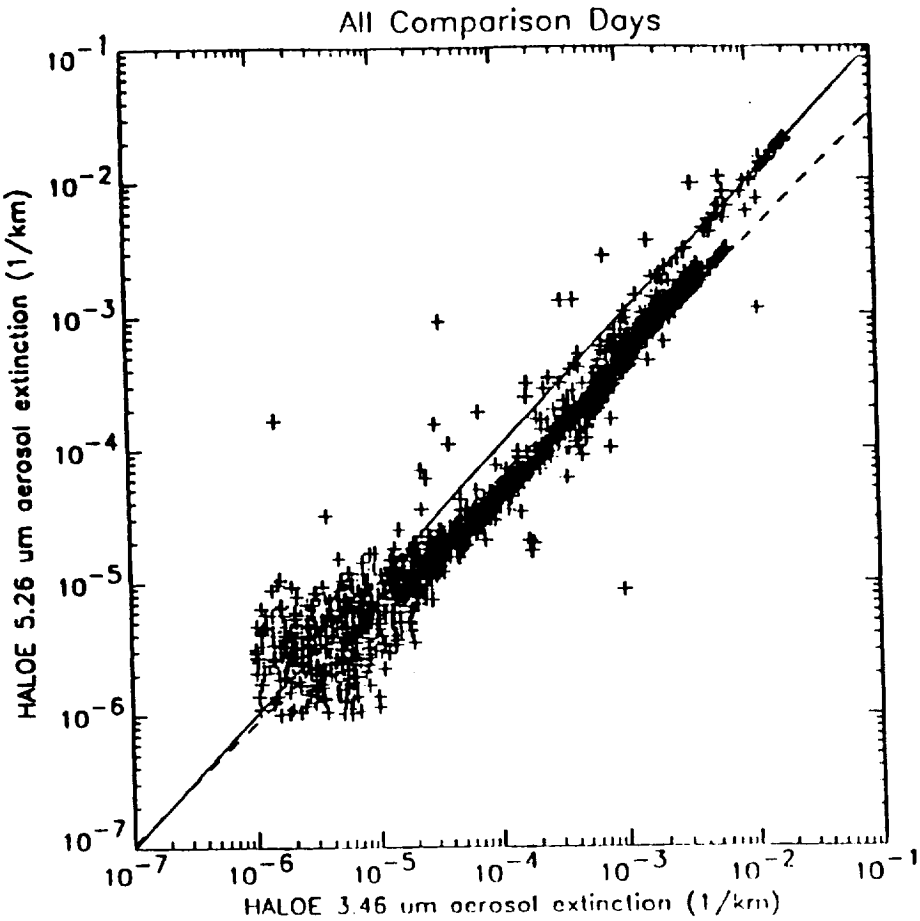

linear fit to log(extinction) ->
Y = 10 ^(−0.576369) * X ^(0.913617)
ratio from fit at X= 10e−5 : 0.717048
ratio from fit at X= 10e−3 : 0.481706
average ratio : 0.769434
extinction cutoff value = 1.00000e−06 (1/km)
288 profiles and 2003 points

Figure3.6-3 Scatter diagrams of HALOE 3.46 μ and 5.26 μ extinction.

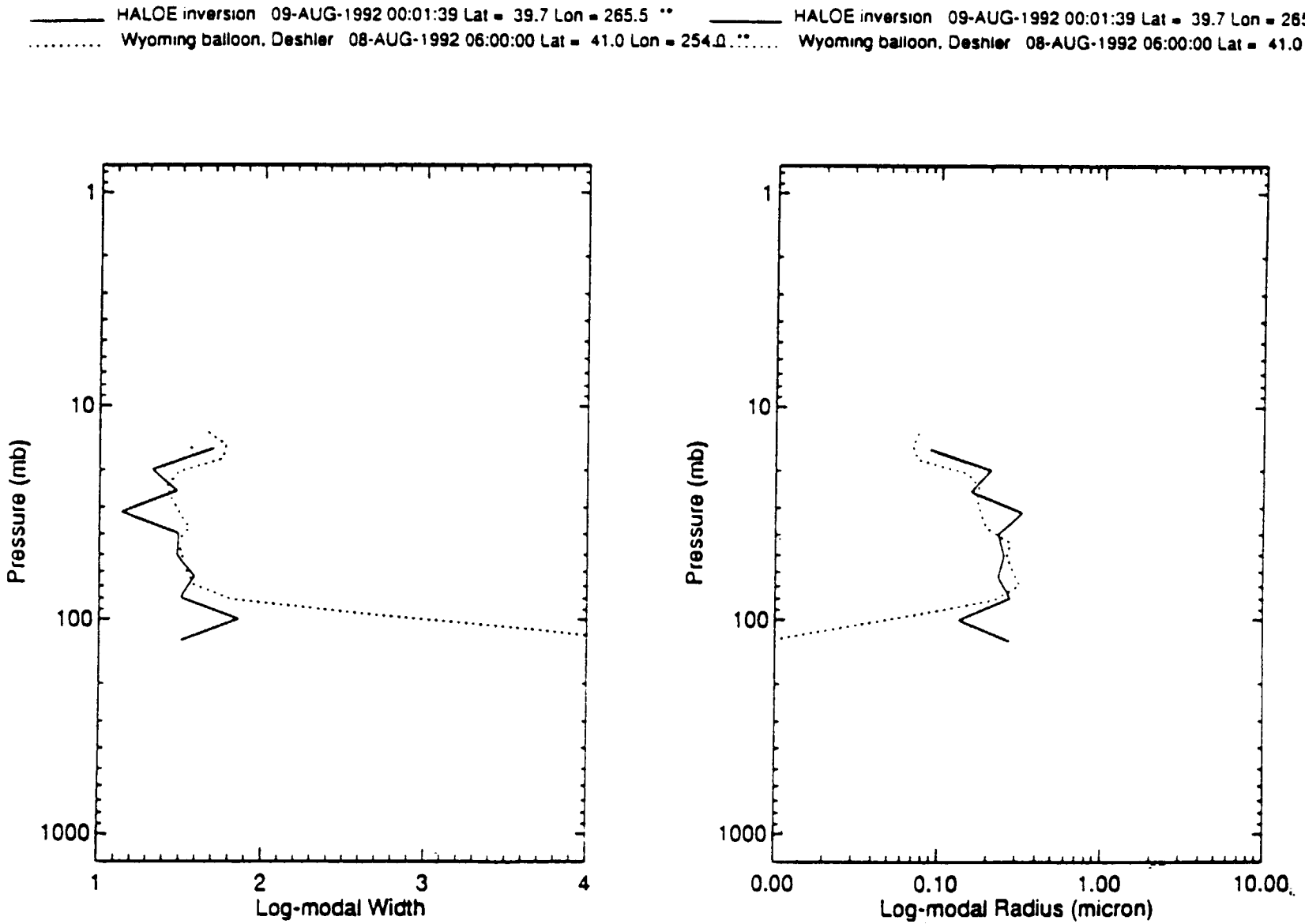

Figure 3.7-1 Comparison of HALOE and Deshler particle size parameters of modal width and modal radius.

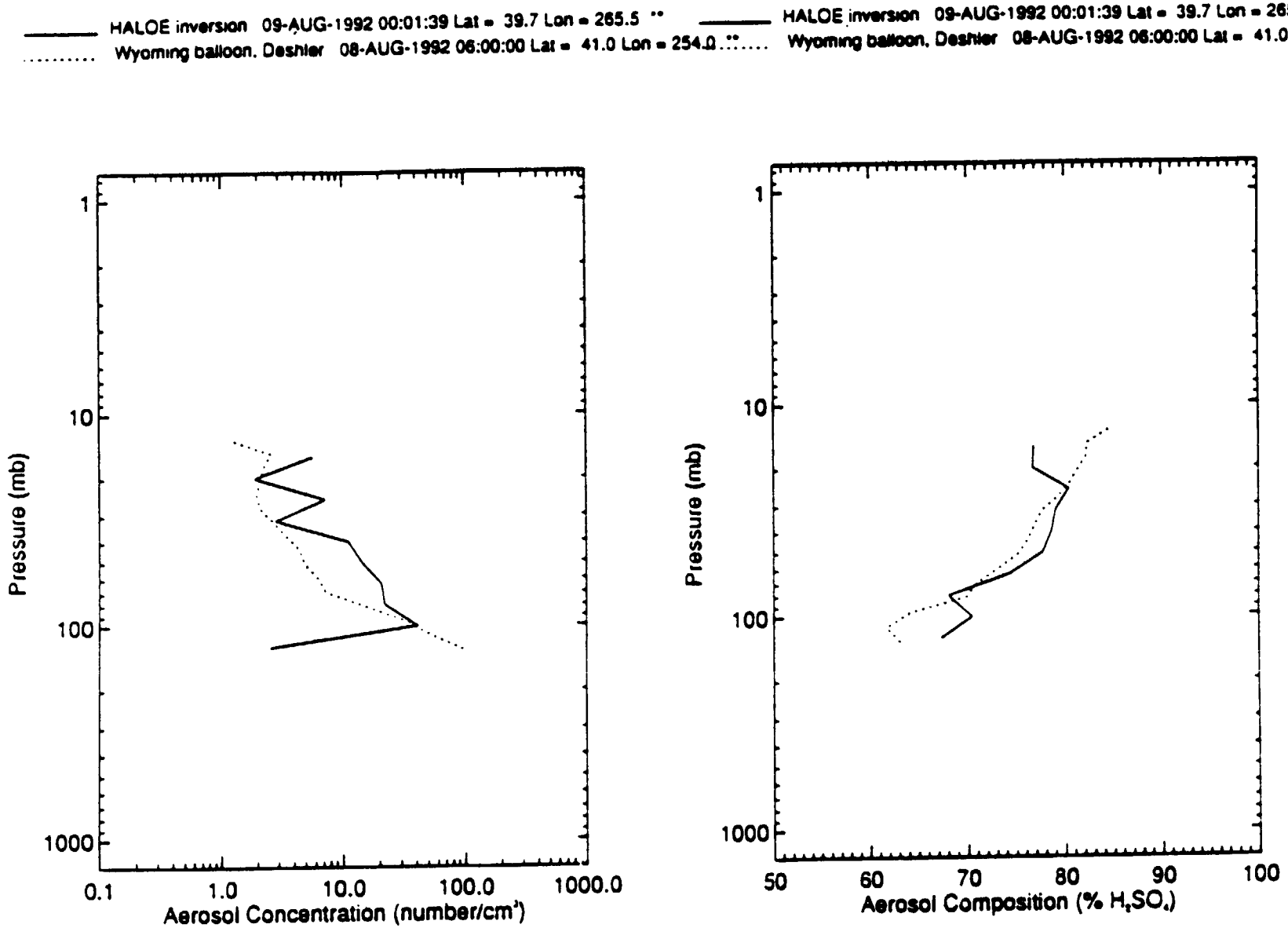

Figure 3.7-2 Comparison of HALOE and Deshler particle size parameters of aerosol concentration and composition.

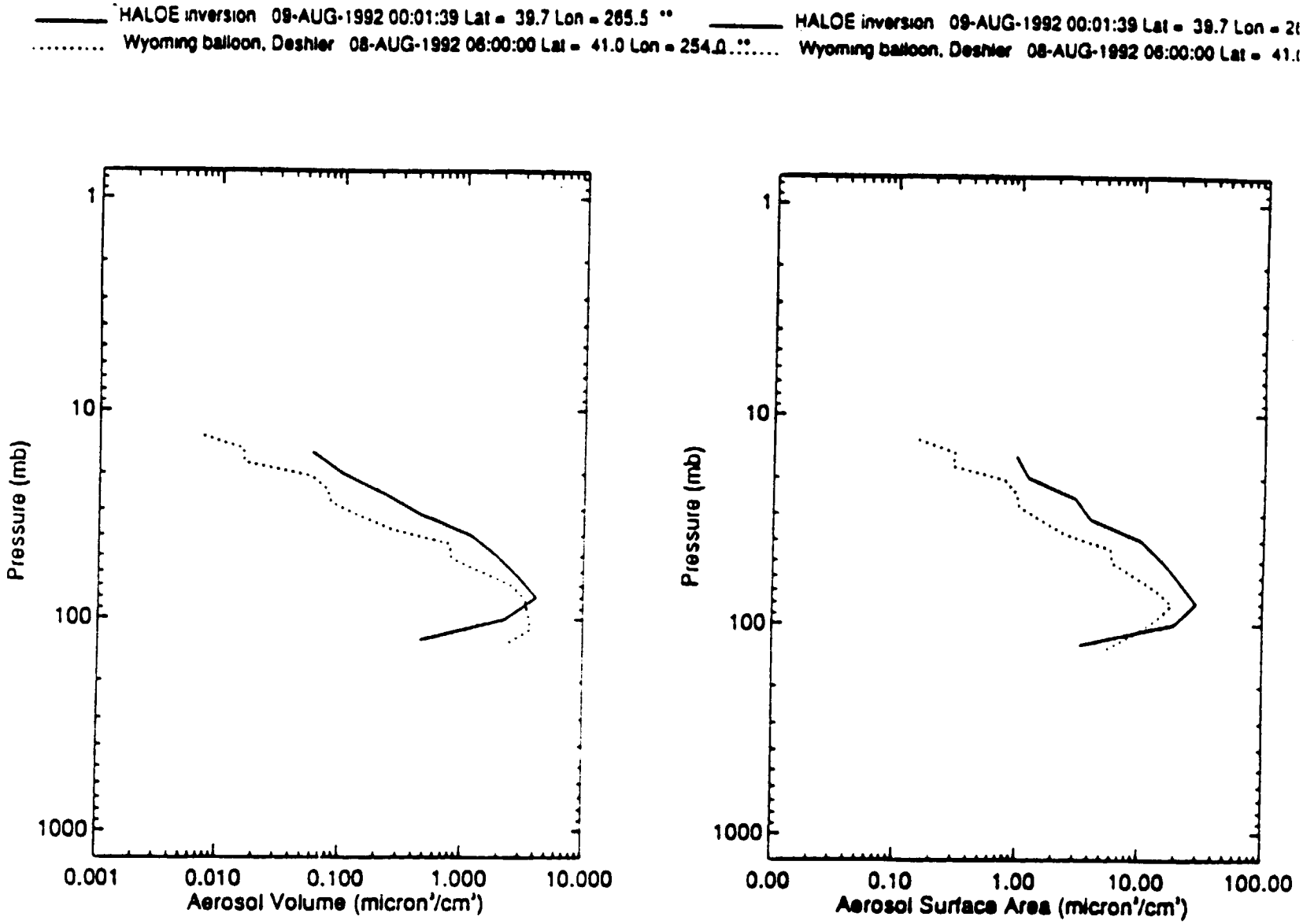

Figure 3.7-3 Comparison of HALOE and Deshler particle size parameters of aerosol volume and surface area.

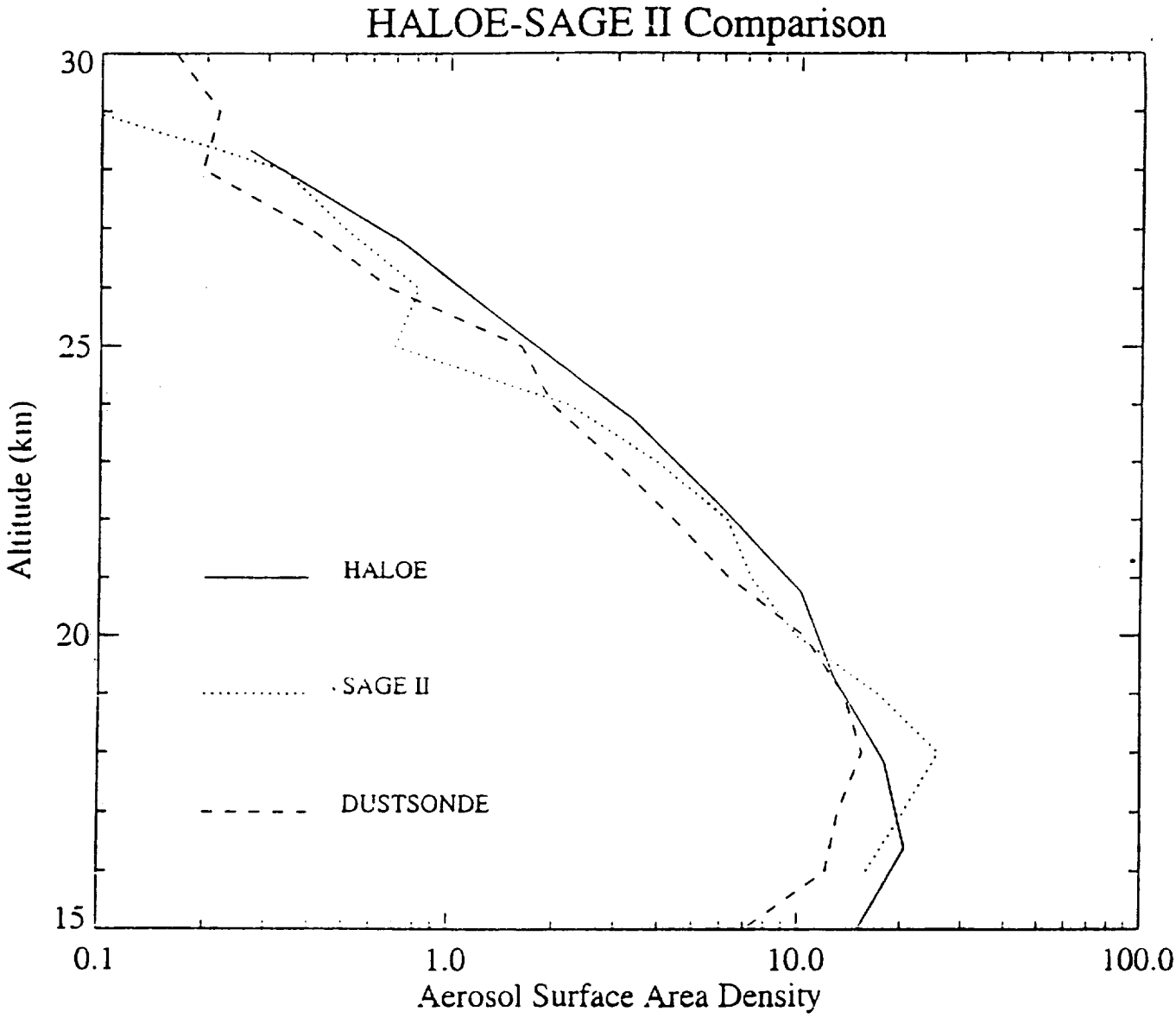

Figure 3.7-4 HALOE - SAGE II - Deshler comparison of the profile of aerosol surface area for April 3, 1992.

4. TEMPERATURE

4.1 Temperature Data and Validation Activities

Development and refinement of the UARS data processing algorithms has been going on continuously since the processing of the first data in September 1991. As a consequence, production algorithms at the CDHF have been replaced with better versions as the new codes were developed and shown to produce improved results. This validation deals with the following data versions:

CLAES	V6
ISAMS	V8
HALOE	V12
MLS	V3

Because of these algorithm upgrades, data processed with the most recent algorithms were not available for all instruments for the entire data period. In order to have a common set of days on which to compare UARS instrument results, the following set of standard periods was agreed upon:

Period 1	09–11 January, 1992	UARS Days 120–122	North-Looking
Period 2	15–20 April, 1992	UARS Days 217–222	South-Looking
Period 3	08–11 August, 1992	UARS Days 332–335	North-Looking
Period 4	25–30 August, 1992	UARS Days 349–354	South-Looking
Period 5	03–05 January, 1993	UARS Days 480–482	North-Looking
Period 6	01–03 April, 1993	UARS Days 568–570	South-Looking

These days were selected in part for the following reasons:

- Period 1 is the period upon which the first workshop at Oxford University in March, 1992 concentrated; it provides comparability to those first results.
- Period 2 is south-looking, and one for which ISAMS was operating.
- Period 3 is during a comparison period at the Observatoire de Haute Province and a time when HALOE data could be easily compared with other sounders.
- Period 4 is a longer south-looking period and one expected to show interesting features related to the Antarctic ozone hole.
- Period 5 is a year later than the first north-looking period and provides an test of long-term changes in the results.
- Period 6 is about a year later than the first south-looking period and tests for end-of-life effects on the CLAES data.

Data for these periods were processed with the most current algorithms and placed in the CDHF for general use.

These data then allowed UARS results to be easily compared with each other and with correlative data from radiosondes. Rocketsonde, lidar, and large balloon data are less frequent, and in general only a small fraction will fall within the selected days. In that case, such comparisons as were possible were carried out, as described below.

UARS data were compared with correlative profile data, in order to identify systematic biases between different techniques. Cross-sections and maps of UARS and analyzed meteorological data were intercompared to find systematic differences between results from the different instruments. Finally, time tracks were intercompared to show the

extent to which observed small-scale features were coherent from one instrument to another.

4.2 Profile Comparisons

4.2.1.1 Computational Approach to Statistical Comparisons

The mean differences between temperatures determined by the UARS instruments and correlative systems have been calculated. In order to make the results comparable between UARS instruments, the time period was limited to the interval between January 1, 1992 and July 7, 1993 in the case of lidar and rocket intercomparisons. Radiosonde comparisons were performed during each of the six special campaign periods. Level 3AT temperature profiles from CLAES, ISAMS and MLS were collected in the vicinity of the correlative measurements. The differences between each of the UARS instruments and the correlative sensors were computed at the standard UARS pressure grid points.

In the case of lidar systems which reported on altitude grids, the NMC temperature and height data for the particular day were used to transfer the ground based measurement to the proper pressure scale for comparison. The mean differences and standard deviations of differences were calculated at each pressure level for each instrument for coincidences of UARS measurements which fell within specified latitude, longitude, and time windows. The size of the windows depended on the number of correlative measurements of a particular type available for the comparison. Windows for radiosonde comparisons were therefore considerably more constrained than for rockets, which were quite sparsely scattered in space and time. It should be noted that for the large windows, the standard deviations may reflect a large component of atmospheric variability in addition to instrumental uncertainty.

4.2.1.2 Results: Comparisons to Radiosondes

Comparisons were made against uncorrected standard meteorological radiosondes in each of the six comparison periods. NMC and other weather services correct the raw observations for radiation and other effects, which differ for each type of radiosonde. Attempts to obtain or calculate corrected radiosonde data were unsuccessful. Thus, there may be differences between the radiosonde comparisons and the fields analyzed from those data by the weather services.

The coincidence criteria used for the radiosonde comparisons were 1 degree in latitude, 4 degrees in latitude equivalent longitude, and 3 hours. The mean differences and standard deviations of differences were computed globally and in various latitude bands for each UARS instrument and are shown in Figures 4.2.1.2–1 to 4.2.1.2–19.

GLOBAL COMPARISONS

Mean differences (biases) are of order 1–2 K for CLAES, ISAMS and MLS over the altitude range 100–10 mb. Somewhat larger biases (near 4 K) are found at the uppermost radiosonde levels (10–7 mb) in January 1992. CLAES shows a negative bias near –4 K at 46 mb in January 1992, but this is not seen in January 1993. RMS differences are typically of order 2 K up to 7 K for the altitude range 100–15 mb for all three nstruments, with differences generally larger in winter, and smaller in summer. Larger RMS differences are seen at and above 10 mb for most comparison periods, and some profiles show isolated maxima at individual pressure levels (notably 22 mb in August 1992 and in

January 1993). CLAES exhibits very large RMS differences (> 10 K) in January 1992, but this is not repeated in any other month.

REGIONAL COMPARISONS

The January 1992, August 1992, and January 1993 comparison periods are separated into polar, midlatitude, and tropical region comparisons (Figures 4.2.1.2–11 through 4.2.1.2–19). There is not a strong dependence of the bias structures on latitude, aside from the observation that the January 1992 bias at the uppermost levels (10–7 mb) occurs primarily in Northern Hemisphere polar regions (with local biases of 5–12 K).

4.2.2 UARS Profile Comparisons with Lidar and Rockets

4.2.2.1 Comparisons of NMC temperatures with Lidar

It is important to compare lidar data measured with different instruments to evaluate the ability of lidars to measure temperature consistently. However, since the instruments are not collocated, and do not necessarily take measurements on the same days, they do not measure the same atmosphere, and it is difficult to compare these measurements directly. Here the NMC temperature analyses are used to assist in the lidar temperature comparison. By assuming that NMC analyses represent the atmosphere consistently around the globe, lidar / NMC comparisons can be used at each site to study the consistency of the various lidar instruments.

To accomplish this the NMC temperature analyses were interpolated to the site of interest, and the lidar values as a function of altitude were interpolated to the NMC pressure levels using the NMC heights for the altitude-pressure relationship.

The lidar temperature data cataloged in CDHF consists of the following:

Table 4.2-1 Lidar Sites

Site	Latitude, Longitude	Time of Measurement	Investigator(s)	No. of Points in the Comparison
OHP	44N, 6E	10/91–9/92	Chanin, Hauchecorne	115
CEL	41N, 1W	10/91–9/92	Chanin, Hauchecorne	70
TMO	34N, 118W	9/91–2/93	McDermid	123
Hanscom	42N, 71W	9/91–7/93	Meriwether, Dao, Farley	26
Frascati	42N, 13E	9/91–11/92	Adriani, Congeduti, Gobbi	34
GSFC	39N, 87W	9/91–1/92	McGee	16
TMO	34N, 118W	2/92–3/92	McGee	19
OHP	44N, 6E	7/92–8/92	McGee	22

Most of these are long term investigations. The short term measurements by McGee at OHP and TMO are designed specifically for intercomparison with other lidars at these sites. For the purposes of this study, only the long term investigations are used. The study is further restricted to the first year of data for each station. This eliminates any possible seasonal dependence in the comparison. Note that all of these stations are northern mid-latitude stations. This is consistent with the assumption that NMC measures temperatures in the same way at all of the stations.

Figure 4.2.2.1–1 shows the average difference between the NMC temperature and the

lidar temperature for each site at the various pressure levels. Twice the standard estimate of error (95% confidence limit) for each of these points is 1 – 2 degrees. The ideal result would have been that all the points from different stations lie on top of each other. Then any global non-zero bias would have indicated differences between the lidar and NMC measurement techniques. Unfortunately, this is not the case; there is a spread in the points of up to 8 degrees.

The Frascati team is preparing a reprocessed data set, and their data have been excluded. Also, since time series graphs show a seasonal dependence in the NMC-lidar difference, it is unfair to compare the GSFC data set, since it spans a half year instead of the full year represented by the other sets. Even with the elimination of these data sets, the spread of the NMC – lidar differences is 4 K to 8 K, increasing with altitude.

The previous analysis does not include any consideration of the time of day at which the data are taken. The NOAA satellite, from which NMC stratospheric analyses are derived, crosses the equator at approximately 3 AM or 3 PM local time. The NMC analysis procedure uses data that come from 6 UT to 18 UT which produces a "12 UT" temperature map. Over Europe the 3 PM data are used; over the US the 3 AM data are used, with actual times for each site depending on the distance from the equator. Thus global comparisons of NMC – lidar data may be affected by significant diurnal and semidiurnal effects. In addition, though lidar data are generally taken at night, the measurements occur anytime between sunset and sunrise causing further, though somewhat smaller, diurnal/semidiurnal contamination.

UARS data may be used to estimate the variation of the temperature with the time of day. While the NOAA satellite is sun-synchronous, the UARS satellite is not. This means that profiles taken at a site are not taken at the same time each day. For UARS, the data span a full 24 hours in several weeks. This allows the use of UARS data to model the time of day dependence of stratospheric temperatures. The following analysis uses MLS data.

Figure 4.2.2.1–2 shows NMC – MLS temperature difference at Table Mountain for each day at 1 mb as a function of time of day of the MLS measurement for several seasons. Using NMC – MLS instead of just the MLS temperatures eliminates the day-to-day temperature variation. Also shown on Figure 4.2.2.1–2 is a fit to the data with a constant term, a trend term, and sine and cosine terms with 24 and 12 hour periods. Since the signal is expected to be seasonally dependent, each season and year is fitted separately. This fit gives a representation of the diurnal and semidiurnal variations of the stratosphere. To make the diurnal adjustment in the NMC/lidar comparisons for each lidar measurement, the value of the fitted curve at the time of the lidar measurement is subtracted from the value of the curve at the NMC time. This difference is used to adjust the lidar measurement to the NMC time prior to calculating the average NMC – lidar difference for each pressure level. In Figure 4.2.2.1–2 the NMC time is at 12 UT, and the bulk of McDermid's measurements range from 4 to 9 UT. This results in a correction of less than 5 degrees at 5 mbar. Note that a unique fit is obtained for each site, each pressure level, and each season.

Figure 4.2.2.1–3 shows the adjusted average temperature differences for all of the long term data stations in the same format as Figure 4.2.2.1–1. GSFC and Frascati data are not shown for the reasons given above. There is improvement in the inter-station

agreement at all levels (summarized in the table below). As expected the greatest improvement is at the highest altitude where diurnal effects are large.

Table 4.2-2 Spread in average NMC – lidar differences from 4 sites

Pressure level	No correction	Diurnal correction
1 mb	8 K	4 K
2 mb	4 K	2 K
5 mb	4 K	3 K
10 mb	4 K	3 K

Next, consider the inter-comparison data from OHP and TMO. Figures 4.2.2.1–4a and b show the McGee and McDermid data from Table Mountain (2/19/92–3/19/92) as compared to NMC. Figure 4.2.2.1–4a contains no diurnal correction, 4.2.2.1–4b does. Except at 5 mb, there is statistically significant disagreement between the two lidar data sets when no diurnal adjustment is made. When the data are adjusted to compensate for the time of day of the measurement, there is considerable improvement. Only at 10 mb do the lidar data sets continue to significantly disagree.

Figure 4.2.2.1–5a and b show a similar comparison between McGee and Chanin temperatures at OHP during 7/13/92–8/17/92. In this case the agreement before the diurnal correction (Figure 4.2.2.1–5a) is very good—within 1 degree from 5 to 1 mb. When the diurnal correction is applied (Figure 4.2.2.1–5b) this agreement is diminished somewhat for these levels; however, the average NMC – lidar differences still agree well within the error bars. For 10 mb the agreement is substantially improved after the correction.

In conclusion, we see that in comparing stratospheric temperature profiles, diurnal and semidiurnal effects must be considered. However, even though the removal of these effects improves the agreement among lidars from different stations, there is still a spread in the data that must be explained.

4.2.2.2 UARS Comparisons with Lidar Temperatures

Statistical comparisons were made against ground based lidars for the period January 1, 1992 through September 15, 1992. In order to obtain a large statistical sample, the coincidence criteria were set at 4 degrees latitude, 12 degrees latitude equivalent longitude, and 24 hours.

Comparisons with OHP, Table Mountain, GSFC, and Hanscom lidars are shown in Figures 4.2.2.2–1 to 4.2.2.2–4. As noted above, there are differences among the lidar sites that have not been corrected here. ISAMS is 5 K to 10 K too cold over 1–0.02 mb at each site, and overall, about 4 K too warm near 10 mb. CLAES biases vary strongly between the different sites, although most exhibit a cold bias of 2–5 K over 5–1 mb and warm biases of order 5 K at 20–10 mb and near 0.1 mb. MLS shows the best comparison with the lidars, with small biases of order 2 K over 20–0.46 mb.

4.2.2.3 Time Series Comparisons between UARS Instruments and Table Mtn Lidar

Time series of temperature and temperature differences show the quality with which

atmospheric trends are represented in the data sets. A more detailed study of the comparisons with the Table Mountain Lidar was carried out.

During the period from September 14, 1992 through February 11, 1993, the Table Mountain Lidar Station (TMO) provided 159 temperature profiles. Time series were generated from smoothed TMO profiles which possessed the same vertical resolution as the CLAES and MLS retrieval grids (evenly spaced in $\log_{10}$ (P/mb) with grid spacings of 1/6 or 1/3).

Profiles were selected from the UARS instrument's L3AT data files within 25 degrees longitude and 12 degrees latitude, during the UDT day of the TMO profile. For the profiles satisfying these constraints, a latitude-weighted distance (sum of geodetic and meridional distances) to TMO was evaluated, and the closest and next closest profiles compared to the TMO profile. Without the latitude weighting, it was found that profiles at similar latitudes to TMO, and having similar profiles, were not selected for comparison. For CLAES and MLS, 62 and 146 pairs of profiles were coincident; the root mean square (RMS) distance to the closest and next closest profiles were approximately 370 km and 480 km.

To test whether proximity of the UARS profiles to the TMO profiles was a significant component of the differences, Figures 4.2.2.3–1 and 4.2.2.3–2 show profiles of the RMS temperature differences between the TMO profiles, and CLAES and MLS closest and next closest profiles. RMS differences using the next closest profiles are typically within 0.5 K of those using the closest profiles. Furthermore, the RMS differences are not systematically smaller for the closest profiles, suggesting that the differences between the TMO and CLAES and MLS are not attributable to poor coincidences.

Figures 4.2.2.3–3 and 4.2.2.3–4 show time series of the smoothed TMO temperature and the closest and next closest CLAES and MLS temperatures for fixed pressure (the grid points of the retrieval grids for CLAES and MLS. In general, both MLS and CLAES temperatures tend to be colder than TMO temperatures. Although systematic differences are seen between data sets, all data sets show the annual cycle of cooling during the autumn, followed by warming during the spring. Also seen are a sequence of warmings in February, March, and April 1992 between 4.6 and 1 mb.

Time series of differences between CLAES and TMO and between MLS and TMO (Figures 4.2.2.3–5 and 4.2.2.3–6) show that the biases and scatter are not correlated with season or time within the mission. In summary, with only 62 or 146 coincident measurements, it is difficult to arrive at robust conclusions. However, based on these data sets, there is no evidence to believe that the systematic errors and precisions in the TMO, CLAES, or MLS data sets are time or seasonally dependent.

4.2.2.4 UARS Comparisons with Rockets

Statistical comparisons were made against 156 temperature rocketsondes for the period January 1, 1992 through September 15, 1992. Both thermistor sensor and falling sphere sondes launched from Antigua, Ascension Island, Cape Canaveral, Kwajalein, Point Mugu, Ryori, and Wallops Island were included in the comparisons. Due to the sparcity of rockets, the coincidence criteria were set at 4 degrees latitude, 12 degrees latitude equivalent longitude, and 24 hours. Summary statistics are shown in Figure 4.2.2.4–1.

ISAMS shows a cold bias of 5–10 K over the range 1–0.15 mb (similar to the bias inferred from the lidar comparisons), and warm biases of order 10 K above 0.07 mb (opposite to the lidar structure). CLAES shows a small cold bias of 2 K over the range 10 – 0.2 mb, unlike the larger positive and negative biases seen in the lidar comparisons. MLS also shows small, altitude-dependent biases of order 2 K over the range 20–0.46 mb.

4.2.2.5 Summary of Profile Comparisons

- Radiosondes (100–7 mb): CLAES, ISAMS and MLS show biases of order 1–2 K over this region, with RMS differences of 2–5 K over 100–30 mb and 5–10 K over 20–7 mb. Larger differences were calculated in January 1992, but these were not repeated in any other month (including January 1993).
- Lidars/Rockets (100–0.01 mb): MLS has the smallest biases of order 2 K over 20–0.46 mb. CLAES shows biases of order 5 K compared with lidars, but much smaller values (2 K) compared with rockets. ISAMS shows warm biases near 4 K over 10–7 mb and cold biases near 10 K over 1–0.1 mb in both comparisons. At the uppermost levels (0.07–0.02 mb), the lidar and rocket comparisons show opposite warm and cold biases near 10 K.

4.2.3 Estimates of UARS Temperature Precision

The accuracy, A, and precision, P, associated with a retrieved temperature R are defined by:

$$R = T + A \pm P$$

where T is the true temperature. Precision may be defined in two ways:

(1) Local Precision: the repeatability of the retrieval error given the same atmospheric profile and instrument characteristics and is thus largely determined by the noise of the measurement;

(2) Global Precision: the repeatability of the retrieval error over a range of profiles and instrument characteristics, which thus incorporates both the local precision and the global variation of the local accuracy. In the limit of the accuracy becoming constant (not necessarily zero) over a wide range of measurements, the two definitions converge.

LOCAL PRECISION

The UARS limb-viewing track intersects itself so that in each orbit there are measurements close to those made in the previous orbit. Restricting comparisons to pairs of profiles within ± 1 degrees latitude, ± 2 degrees longitude from successive orbits usually yields one or two matches per orbit close to the 34N/34S limit. Assuming the atmosphere and instrument characteristics remain unchanged (i.e. T and A are constant) over such a short spatial and temporal scale (1 orbit = ≈ 96.4 minutes), the RMS difference between these pairs of retrievals gives a measure of the local precision:

$$\left\langle \left| R_i - R_j \right|^2 \right\rangle = 2P^2$$

or

$$P = \sqrt{\left\langle \left| R_i - R_j \right|^2 \right\rangle / 2}$$

where brackets indicate an average over the number of comparison pairs.

Figure 4.2.3–1 shows average values of precision calculated in this way for the UARS instruments during each of the validation periods. Note that the improving repeatability indicated at the ends of the ISAMS and MLS profiles reflect the increasing constraints imposed by NMC data or climatology, and does not imply improving accuracy.

GLOBAL PRECISION

The UARS limb-viewing instruments (CLAES, ISAMS, MLS) nominally observe the same tangent track for much of the time. The mean-square difference between a pair of collocated retrievals R_a, R_b from different instruments is given by:

$$\left\langle \left| R_a - R_b \right|^2 \right\rangle = \left\langle \left| A_a - A_b \right|^2 \right\rangle + P_a^2 + P_b^2$$

where $A_a - A_b$ represents the average bias between the two instruments for the set of profiles compared, and $P_a^2 + P_b^2$ represents the variance, σ^2. Thus for 3 instruments, the variances of the comparisons contain enough information to identify the 3 individual values of precision:

$$\sigma_{ab}^2 = P_a^2 + P_b^2$$

$$\sigma_{bc}^2 = P_b^2 + P_c^2$$

$$\sigma_{ca}^2 = P_c^2 + P_a^2$$

Solving these equations for the SD values (i.e. σ) listed in Table 4.3–1, the calculated precisions are plotted in Figure 4.2.3–2 for the three latitude bands (i.e. not strictly "global"). These values are more "approximate" than the local precision and in two cases (indicated by the two points on the y-axis in each plot) yielded negative solutions for P^2 for one of the instruments. However, the general pattern is that the global precision is larger than the local precision, as expected, and also larger for high latitudes than low latitudes, probably reflecting the wider range of atmospheric profiles and variations in bias differences at higher latitudes.

4.3 Zonal Mean Cross-Sections

One of the goals of intercomparisons is to determine whether there are systematic differences between different instruments or techniques. Random variations, or variations within the precision, can mask the systematic differences. By taking averages around latitude circles, i.e. calculating zonal means, the random variations can be reduced and more stable quantities formed for comparison.

4.3.1 Cross-sections

4.3.1.1 UARS differences from NMC and UKMO analyses

The stratospheric data from the NMC have been used for many years as a standard for stratospheric temperatures and for stratospheric research. It is natural that the UARS temperatures should be compared against them. Recently the UKMO has also produced stratospheric temperature analyses through assimilation of the same satellite-observed radiances that go into the NMC analyses. The UARS results will also be compared against these analyses. Here, the UARS results have all been analyzed in the same way, in that a Kalman filter mapping of the Level 3AT data has been carried out. Note that while comparisons with MLS are shown down to 100 mb for uniformity, MLS values reported below 22 mb are essentially NMC values. Some differences between results obtained on the ascending and descending parts of the orbit, which correspond to different local times, led to the use of ascending orbit data only in the comparisons. Differences for descending orbit data would be very similar. It should be clear that the UARS data are all obtained at the same local time, but this will differ in general from the times of the NMC and UKMO data, which is 1200 UT.

All temperature data show the same gross features and are distinguished by relatively small differences. For this reason, for the comparison dates discussed below, only one zonal mean cross-section will be shown to indicate the large-scale temperature structure of the atmosphere. Figure 4.3.1–1 shows the UKMO temperature distribution for January 10, which shows the cold polar lower-stratosphere and latitudinal structure in the middle and upper stratosphere. Figures 4.3.1–2 shows that the three UARS sounders are cooler than NMC by a few degrees at most latitudes and altitudes, especially between 30–1 mb, with largest differences ($\approx$ 7 K) in the polar winter and in the upper tropical stratosphere, but UARS temperatures are up to 10 degrees warmer in the tropical lower mesosphere. ISAMS results also show warmer temperatures in the tropics below 20–30 mb, which may be due to the incomplete removal of aerosol effects. The similarity of the pattern of the differences is striking.

Patterns of difference between the UARS and UKMO temperatures are presented in Figure 4.3.1.3. They are seen to be broadly similar to differences from the NMC analysis, but the large differences in the polar regions are not present, and the differences are generally smaller.

The zonal mean cross-section for April 17, during a south-looking period is displayed in Figures 4.3.1–4. Although it is early austral autumn, a cold pool is already present over the polar region. Figures 4.3.1–5 and 6 present the corresponding UARS - NMC and UARS - UKMO differences. For this south-looking period, the UARS sounder results again are lower than NMC, though apparently by smaller amounts. The UARS results again show difference features that are similar to one another, notably being several degrees cooler in the high-latitude upper stratosphere region. The differences from the UKMO show similar patterns, although smaller. A tendency for the UARS sounders to be warmer in the low-altitude tropics can also be seen.

The zonal mean cross-sections for August 10, which views the northern hemisphere summer, and the UARS – NMC and UARS – UKMO differences are shown in Figures 4.3.1–7, 8 and 9, respectively. There is an indication of a wave-like structure in the tropics. Again, the UARS instruments show similar patterns versus the UKMO data, being generally cooler from 20–1 mb, with larger oscillatory differences in the tropics. The same differences are seen with the NMC data, although they are larger.

The same quantities for August 27, when the UARS sounders were viewing the end of the southern winter. are shown in Figures 4.3.1–10 to 12. The differences in the tropics are similar to those seen in the previous period, indicating no large view-direction dependent differences, and supports the idea that there are systematic effects. MLS and CLAES are generally cooler than the NMC and UKMO analyses, with large areas of UARS being cooler in the cold polar region. Again, differences are smaller with UKMO.

Results for the second year, for January 4, 1993, a northern winter day, one year after the first one, are presented in Figure 4.3.1–13 to -15. The patterns and magnitudes of the differences with the UKMO are generally similar to those of a year earlier. The differences with NMC are rather larger and higher in altitude in the polar regions.

Finally, results are shown in Figure 4.3.1–16 to –18 for the south-looking April 2, 1993. The differences with NMC are similar to those in Figure 4.3.1–5, again evidencing lower UARS temperatures in the high-latitude stratopause region. Similar patterns are also seen in Figures 4.3.1–18, showing continuity and stability of the characteristic differences.

The differences probably arise for the most part from the much higher vertical resolution of the UARS sounders than the operational TOVS sounder ($\approx$ 3 km versus $\approx$ 10 km). Differences from NMC are also influenced by the way in which the TOVS radiances are inverted and by the simple nature of the corrections which are applied. Differences from the UKMO are more difficult to discuss, given the more complex nature of the data processing. The consistency of the pattern of the differences suggests that all systems are performing in stable and repeatable ways.

Tabulated values of the mean differences between UARS and NMC temperatures for the first two comparison periods are contained in Table 4.3–1. Results are summarized in Table 4.3–2. Both tables are located in the first part of section 4.3.1.3.

4.3.1.2 Intercomparison of UARS Temperature Results

CLAES – MLS

The differences among the UARS instruments are smaller than those between UARS and NMC. Figure 4.3.1–19 shows that the CLAES – MLS differences have a consistent pattern during the north-looking periods, with CLAES being warmer from 22 to about 5 mb, and cooler above. The differences are usually less than 2 K, but locally may reach 4 K. There is also a hint that CLAES is slightly warmer at the stratopause in the northern tropics, which could show up as a difference in stratopause altitude.

The same general features for south-looking periods are shown in Figure 4.3.1–20, which again shows CLAES warmer by 2–4 K below 5 mb, and cooler above. In this case there are larger differences in the upper stratopause, with CLAES cooler near 60 degrees on the April days by 5 or 6 K and by as much as 8 K in the winter polar period. Again, CLAES appears to be very slightly warmer at the tropical stratopause.

ISAMS – CLAES AND ISAMS – MLS

Differences between ISAMS and CLAES and MLS for January 10, 1992, a north-looking day, are contained in Figure 4.3.1–21. Again, differences tend to show bands in

altitude, with ISAMS 4–5 K warmer than CLAES and MLS from about 10–1 mb and cooler by several degrees above 1 mb. Below 10 mb, ISAMS is slightly warmer in the tropics and cooler at higher latitudes. This is an altitude range where ISAMS temperatures are strongly affected by aerosols.

Figure 4.3.1–22 displays the same differences for April 17, 1992, a south-looking day. A distinct banded pattern is seen which indicates ISAMS warmer by up to 4 K than CLAES and MLS in the upper stratosphere , with the lower stratosphere tropics and extratropical region again warmer and cooler, respectively, than the other two sounders. ISAMS temperatures are several degrees cooler than MLS or CLAES at the tropopause. ISAMS becomes cooler than MLS at a lower altitude in April than in January. These comparisons indicate that the differences between the UARS sensors tend to be fairly small, and primarily a function of altitude rather than latitude. The exceptions are the polar regions, especially the winter polar regions, where differences can be larger and a function of latitude.

4.3.1.3 Tabulated Differences of Zonal Means for Comparison Periods 1 and 2

1. UARS COMPARISONS WITH NMC DATA

Table 4.3–1 presents results of intercomparisons between the 3AT profiles from all the UARS sounders (CLAES, HALOE, ISAMS, and MLS) and NMC for days when the three emission instruments were viewing the same tangent track: January 9-11, 1992 and April 16-20, 1992 (ISAMS was viewing both sides on April 15, 1992 and was not functioning during the subsequent intercomparison periods). The NMC data were interpolated to the UARS measurement locations, and the recommended corrections were applied. Table 4.3–1 lists the aggregate Bias, SD, and RMS difference between temperatures from a UARS instrument and NMC. The comparisons are split into low (35S–35N), medium (60S–35S, 35N–60N), and high (80S–60S, 60N–80N) latitude bands and presented at alternate UARS surfaces to match the MLS retrieval surfaces. Table 4.3–2 summarizes the information from Table 4.3–1.

Table 4.3–1 UARS – NMC Temperature Comparisons

(CLAES - NMC)

		Low Latitudes (0–35°)			Middle Latitudes (35–60°)			High Latitudes (60–80°)			
Srfc. No.	*p*	Bias	SD	RMS Diff.	Bias	SD	RMS Diff.	Bias	SD	RMS Diff.	Notes
20	0.46	2.70	5.61	6.23	–4.17	7.84	8.88	3.01	9.04	9.53	
18	1.0	–2.53	4.13	4.84	–3.80	5.64	6.80	–5.94	7.68	9.71	
16	2.2	–3.43	4.30	5.50	–4.38	6.36	7.72	–7.48	6.82	10.12	
14	4.6	–2.80	3.54	4.51	–2.57	5.38	5.96	–4.65	6.33	7.85	
12	10	–1.19	2.70	2.95	–1.84	3.70	4.13	–3.41	6.94	7.73	
10	22	–0.27	2.31	2.33	–1.21	2.92	3.16	–4.04	6.45	7.61	
8	46	0.44	1.84	1.89	–0.50	2.23	2.28	–1.47	5.08	5.29	

ISAMS – NMC

		Low Latitudes (0–35°)			Middle Latitudes (35–60°)			High Latitudes (60–80°)			
Srfc. No.	*p*	Bias	SD	RMS Diff.	Bias	SD	RMS Diff.	Bias	SD	RMS Diff.	Notes
20	0.46	–3.93	5.09	6.43	–8.11	6.52	10.40	–3.51	9.56	10.19	
18	1.0	–3.78	3.75	5.32	–5.41	4.53	7.05	–8.02	5.00	9.45	
16	2.2	0.11	3.35	3.36	–2.17	4.28	4.80	–6.09	4.86	7.79	
14	4.6	0.89	2.53	2.68	–0.46	3.32	3.36	–1.29	4.98	5.15	
12	10	–0.26	2.38	2.40	–0.80	3.32	3.42	–1.87	4.88	5.22	
10	22	–0.25	2.71	2.72	–2.73	2.69	3.83	–3.79	3.21	4.96	
8	46	0.07	1.80	1.80	–1.81	2.09	2.77	–2.53	2.31	3.42	

MLS – NMC

		Low Latitudes (0–35°)			Middle Latitudes (35–60°)			High Latitudes (60–80°)			
Srfc. No.	*p*	Bias	SD	RMS Diff.	Bias	SD	RMS Diff.	Bias	SD	RMS Diff.	Notes
20	0.46	1.89	5.11	5.45	–3.43	8.04	8.74	4.11	9.04	9.93	
18	1.0	–0.48	4.15	4.18	–1.81	5.48	5.77	–3.76	7.58	8.46	
16	2.2	–0.92	3.26	3.39	–1.09	5.10	5.22	–3.99	6.37	7.51	
14	4.6	–2.45	2.72	3.66	–0.94	4.45	4.54	–2.49	6.17	6.65	
12	10	–2.82	2.15	3.54	–2.33	2.99	3.79	–2.98	4.71	5.57	
10	22	–1.85	2.05	2.76	–1.98	3.71	4.20	–4.19	6.86	8.04	
8	46	–0.01	0.19	0.19	0.05	0.28	0.28	0.13	0.48	0.50	(1)

HALOE – NMC

Srfc. No.	p	Low Latitudes (0–35°) Bias	SD	RMS Diff.	Middle Latitudes (35–60°) Bias	SD	RMS Diff.	High Latitudes (60–80°) Bias	SD	RMS Diff.	Notes
20	0.46	–1.29	4.62	4.80	–7.49	8.08	11.02	3.78	2.58	4.58	
18	1.0	–5.45	3.51	6.48	–6.86	5.72	8.93	–1.89	2.10	2.83	
16	2.2	–4.13	2.22	4.69	–2.19	3.18	3.86	–4.29	1.66	4.60	
14	4.6	–0.39	0.54	0.67	0.61	1.03	1.20	0.07	0.51	0.52	
12	10	0.13	0.18	0.22	0.24	0.48	0.54	0.14	0.18	0.23	(2)
10	22	–0.17	0.15	0.22	–0.03	0.26	0.26	–0.09	0.16	0.18	(2)
8	46	–0.21	0.21	0.30	0.04	0.27	0.27	–0.08	0.18	0.20	(2)

Notes. (1) MLS data are taken directly from NMC data at this level
(2) HALOE data are taken directly from NMC data at these levels

Table 4.3–2—Summary of UARS – NMC Temperature Comparisons

SRFC #	PRES S	Hottest l	m	h	Coldest l	m	h	Minimum SD l	m	h	Maximum SD l	m	h	Minimum RMS Diff. l	m	h	Maximum RMS Diff. l	m	h	NOTES
20	0.46	C	M	M	I	I	I	H	I	H	C	H	I	H	M	H	I	H	I	
18	1.0	M	M	H	H	H	I	H	I	H	M	H	C	M	M	H	H	H	C	
16	2.2	I	M	M	H	C	C	H	H	H	C	C	C	I	H	H	C	C	C	
14	4.6	I	H	H	C	C	C	H	H	H	C	C	C	H	H	H	C	C	C	
12	10	I	I	I	M	M	C	M	M	M	C	C	C	I	I	I	M	C	C	(3)
10	22	I	C	I	M	I	M	M	I	I	I	M	M	C	C	I	M	M	M	(3)
8	46	C	C	C	I	I	I	I	I	I	C	C	C	I	C	I	C	I	C	(4)

Outline type indicates NMC data is warmer than all UARS instruments at these points.
Notes (3) HALOE data excluded from summary at these levels
(4) MLS and HALOE data excluded from the summary at this level.
Abbreviations: l=low latitudes (0–35°), m=middle latitudes (35–60°), h=high latitudes (60–80°), C=CLAES, I=ISAMS, M=MLS, H=HALOE.

2. INTERCOMPARISONS AMONG UARS TEMPERATURES

Table 4.3–3 shows temperature intercomparisons between the three UARS limb sounders (CLAES, ISAMS, MLS) based on the days when all 3 instruments were viewing the same tangent track: January 9–11, 1992 and April 16–20, 1992. These comparisons are based on the Level 3AT profiles. The table lists the aggregate Bias, SD, and RMS Difference between each pair of instruments. Table 4.3–4 summarizes the information from Table 4.3–3.

Table 4.3-3—Limb Sounder Intercomparisons

CLAES – ISAMS

		Low Latitudes (0–35°)			Middle Latitudes (35–60°)			High Latitudes (60–80°)			
Srfc. No.	*p*	Bias	SD	RMS Diff.	Bias	SD	RMS Diff.	Bias	SD	RMS Diff.	Notes
22	0.22	10.31	4.25	11.16	9.33	5.42	10.79	7.59	6.68	10.11	
20	0.46	7.12	3.65	8.00	6.64	4.31	7.92	4.79	5.04	6.96	
18	1.0	1.15	3.17	3.37	1.86	4.46	4.83	–0.20	5.08	5.09	
16	2.2	–2.89	2.78	4.01	–3.09	4.62	5.56	–1.63	4.69	4.96	
14	4.6	–3.56	2.41	4.30	–2.83	4.25	5.11	–2.09	3.99	4.51	
12	10	–0.49	2.37	2.42	–0.69	3.03	3.11	–1.39	7.04	7.17	
10	22	–0.30	3.46	3.47	1.95	3.18	3.73	1.34	6.76	6.89	
8	46	0.22	2.02	2.03	1.48	3.39	3.70	1.38	7.38	7.51	

CLAES – MLS

		Low Latitudes (0–35°)			Middle Latitudes (35–60°)			High Latitudes (60–80°)			
Srfc. No.	*p*	Bias	SD	RMS Diff.	Bias	SD	RMS Diff.	Bias	SD	RMS Diff.	Notes
22	0.22	14.69	5.37	15.64	14.97	8.17	17.05	11.79	11.54	16.50	(1)
20	0.46	0.46	3.50	3.53	–0.86	3.50	3.60	–0.58	4.80	4.83	
18	1.0	–2.35	2.79	3.65	–2.19	3.41	4.05	–1.15	4.49	4.64	
16	2.2	–2.10	2.92	3.60	–2.95	3.99	4.96	–1.73	4.98	5.28	
14	4.6	–0.17	2.66	2.67	–1.27	3.92	4.12	–0.47	5.15	5.17	
12	10	2.12	2.44	3.23	0.51	3.04	3.08	0.12	6.96	6.96	
10	22	1.49	2.85	3.22	0.85	3.41	3.52	0.46	7.87	7.89	
8	46	0.54	1.89	1.97	–0.60	2.82	2.89	–1.09	6.94	7.02	(2)

ISAMS – MLS

Srfc. No.	p	Low Latitudes (0–35°) Bias	SD	RMS Diff.	Middle Latitudes (35–60°) Bias	SD	RMS Diff.	High Latitudes (60–80°) Bias	SD	RMS Diff.	Notes
22	0.22	4.05	5.38	6.74	5.61	6.41	8.52	4.12	8.66	9.59	(1)
20	0.46	–6.55	3.13	7.26	–7.51	3.90	8.46	–5.32	4.96	7.27	
18	1.0	–3.50	3.22	4.76	–3.97	4.29	5.85	–0.87	5.33	5.40	
16	2.2	0.74	2.59	2.70	0.12	3.45	3.45	–0.11	4.62	4.62	
14	4.6	3.37	2.15	4.00	1.55	3.76	4.07	1.59	5.38	5.61	
12	10	2.62	2.18	3.41	1.24	2.67	2.94	1.43	3.70	3.96	
10	22	1.76	2.80	3.31	–1.04	4.32	4.45	–0.94	6.55	6.62	
8	46	0.14	1.85	1.86	–2.11	2.13	3.00	–2.50	2.36	3.43	(2)

Notes. (1) It is recommended that MLS data be ignored at this level
(2) MLS data are taken directly from NMC data at this level

Table 4.3–4—Summary of Limb Sounder Intercomparisons

SRFC #	PRES S	Hottest l	m	h	Coldest l	m	h	Minimum SD l	m	h	Maximum SD l	m	h	Minimum RMS Diff. l	m	h	Maximum RMS Diff. l	m	h	NOTES
22	0.22	C	C	C	M	M	M	C	I	I	M	M	M	I	I	I	C	C	C	(1)
20	0.46	C	M	M	I	I	I	M	M	M	C	I	I	M	C	C	I	I	I	
18	1.0	M	M	M	I	I	C	C	M	C	I	I	I	C	C	C	M	I	I	
16	2.2	I	I	M	C	C	C	I	M	I	C	C	C	M	M	I	C	C	C	
14	4.6	I	I	I	C	C	C	I	M	C	C	C	M	M	M	C	I	C	M	
12	10	I	I	I	M	M	M	I	I	M	C	C	C	C	M	M	M	C	C	
10	22	I	C	C	M	I	I	M	C	I	C	M	C	C	C	I	I	I	C	
8	46	C	M	M	M	I	I	M	M	M	C	C	C	M	M	M	C	I	C	(2)

Notes. (1) It is recommended that MLS data be ignored at this level
(2) MLS data are taken directly from NMC data at this level
Abbreviations: l=low latitudes (0–35°), m=middle latitudes (35–60°), h=high latitudes (60–80°), C=CLAES, I=ISAMS, M=MLS.
Max/Min columns: e.g. the "C" (CLAES) entry at 0.22 mb in the Min SD, low latitude column implies that the highest SD is observed between the other two instruments (ISAMS and MLS).

4.3.2 Latitudinal Variations of Zonal Means on Pressure Surfaces

Comparison plots of the latitudinal variations of the zonal mean temperatures on pressure surfaces aid in bringing out some of the differences and characteristics of the different data sets. This is illustrated by Figure 4.3.2–1, which displays the variations averaged over the January 9–11 period on the 1 mb surface. The three UARS instruments display the same variations with latitude, which NMC only roughly follows. MLS generally finds the highest temperature among the UARS instruments, with a total spread of 3–5 K. Figure 4.3.2–2 compares zonal means at 10 mb derived from ascending and descending parts of the orbit, demonstrating that there are differences, but that they are usually small. It also illustrates that the UARS temperatures are usually cooler than NMC and still show more latitudinal structure, probably due to their higher vertical resolution. The total spread in the UARS temperatures is similar to that at the higher altitudes. The UARS temperatures are all several degrees cooler than NMC at high northern latitudes, at this level and at 21 mb. MLS temperatures are lower and don't show the increase at 65 N, although showing more structure at 15 S.

The same features shown in Figure 4.3.2–1 are seen in reverse at 1 mb in the south-looking fourth period. At 4.6 mb (Figure 4.3.2–3) and 10 mb, CLAES and MLS temperatures again show more structure and lower temperatures than NMC, but are in reasonable agreement with each other. At 21.5 mb, shown in Figure 4.3.2–4, CLAES and MLS are considerably lower than NMC in the polar region, in agreement with other information. This fact is important because of the implications for the retrievals of constituent concentrations in the Antarctic polar vortex in the spring.

4.3.3 Time Series of Zonal Mean Daily Temperatures for 1992

In this section, daily zonal mean temperatures from the NMC fields are compared with MLS, CLAES, and ISAMS temperatures at the same latitudes and pressure levels. The purpose of this comparison is to inspect the temperature record over the course of a full year to determine the extent of agreement among the various data sets in depictions of temperature changes during 1992.

UARS data were taken from the 3AT archive for each instrument. CLAES data were available for a limited number of days during 1992, while ISAMS data were available for most days until failure of the instrument in July 1992. For each latitude shown, an average was taken of all ascending orbital data for the day within plus and minus 2.5 degrees latitude. Checks were made for data quality flags and to assure that sufficient numbers and quality of data for each day are given for deriving a representative zonal mean temperature.

NMC zonal mean temperatures were derived from the daily hemispheric fields by interpolating from the 65 by 65 fields to each given latitude, every 10 degrees longitude, and then averaging over all longitudes. A temperature adjustment was applied, making all 1 mb NMC temperatures higher by 6.2°C degrees, as recommended by Finger et al, 1993. No adjustment is applied at 10 mb. The NMC temperatures were available continuously for all latitudes, thus providing a convenient reference to compare to the UARS data.

Results are shown for 1 and 10 mb, each for the five latitudes, 60N, 30N, equator, 30S, and 60S. All figures have a common format. Temperature, on the vertical scale, is

plotted for each day of 1992 on the horizontal scale. In each figure plotting symbols are shown, one for each of the three UARS data sets and one for NMC temperatures. In addition, a fifth curve depicts the 36-day cycle of alternate UARS instrument viewing of the northern and southern hemispheres (poleward of approximately 39 degrees latitude).

The figure for 1 mb at the equator (Figure 4.3.3–1) shows that the MLS and NMC temperatures usually depict similar variations throughout the year, but the MLS variations have substantially greater amplitude. This behavior is especially apparent around days 10, 61, 230, and 350. Only the 5K variations in the MLS data about days 160 to 180, also supported by the limited amount of CLAES data, have no apparent counterpart in the NMC data. On the other hand, the CLAES data appear to agree more with the NMC data around days 320 to 340.

Figures 4.3.3–2 and 3, for 1 mb, 30N and 30S, show similar characteristics as for the equator. However, in addition, it is apparent from the continuous record of MLS versus NMC data that there are sometimes jumps in the MLS temperatures at the time of UARS turnaround. This problem has been mentioned by the MLS team in the discussion of MLS data. Temperature jumps are especially apparent at 30S around the turnaround days 45, 122, 226, 265, 305, and 334. For some of these days, temperature jumps in the MLS data are also shown by the CLAES or ISAMS data. It is unclear whether this agreement indicates the reality of these temperature variations in the atmosphere, or if it suggests a common registration or platform pointing error for the UARS instruments. As more data become available from all instruments for the entire first year and beyond, these matters will be investigated.

Figures 4.3.3–4 and 5, for 1 mb at 60N and 60S show that the large annual variation in temperature at these latitudes are usually outlined similarly by all systems. However, disagreement at 60S is especially apparent between NMC and the three UARS measurements around days 100 to 120. On the other hand, during days 121 to 151 the MLS and NMC temperatures agree and are somewhat different from the CLAES and ISAMS temperatures. Throughout the year it is possible to find periods when all systems agree and also periods when all disagree (and various combinations in between).

The same level of agreement and disagreement among measurements is also seen at 10 mb (Figures 4.3.3–6 to 10). Best agreement appears on the 10 mb figures for 60N and 60S. For 30N there is more agreement among NMC, ISAMS and CLAES, with MLS somewhat lower than the others throughout most of the year. The same appears true at 30S for the first few months of 1992, but there is much more diversity during the rest of the year. At the equator, all measurements agree well for the first few months, but diverge by up to 5K thereafter.

In summary, the zonal mean comparisons show a mixture of agreements and disagreements between instruments and NMC data. For the most part, the UARS data are in good agreement and they track each other within 5K.

4.4 Temperature Comparisons with HALOE

4.4.1 Introduction

A series of temperature profile comparisons was performed between HALOE and CLAES, MLS and ISAMS, for five comparison periods. Profiles were compared when their respective locations fell within the coincidence criteria of 2 degrees latitude x 10 degrees longitude x 12 hours. The mean and RMS differences between HALOE and other UARS instruments were computed on a high resolution grid. Along with the differences, a mean temperature profile for each instrument was computed at every point a comparison was made. Table 4.4–1 shows a summary of the time periods that were used in the comparisons.

Table 4.4-1 Time Periods for HALOE Coincidences with MLS, CLAES, ISAMS

Period	Dates	Number of days	HALOE Latitude Range.	SR/SS
1	9–11 Jan. 1992	3	46N – 49N	SR
2	15–20 Apr. 1992	6	23N – 31S	SR
2a	15–17 Apr. 1992	3	23N – 10S	SR
2b	18–20 Apr. 1992	3	10S – 31S	SR
3	8–10 Aug. 1992	3	34N – 48N	SR
4	25–30 Aug. 1992	6	30S – 19N	SS
4a	25–27 Aug. 1992	3	30S – 9S	SS
4b	28–30 Aug. 1992	3	9S – 19N	SS
5	1–3 Apr.1993	3	36N – 40N	SR

From the collection of coincident profiles, longitude versus pressure cross-sections of temperature (and temperature differences) were constructed for each period in an attempt to better characterize differences indicated by the profile comparisons. Only 3 day periods were used to create longitude versus pressure cross sections.

Features common to all intercomparisons are described in section 4.4.2 with the aid of one period, namely April 1992 (period 2). In section 4.4.3 the period of January 9–11, 1992 is discussed. During this period large differences are seen throughout the longitude range where a large temperature gradient exists.

4.4.2 Summary of Coincident Profile Comparisons

The mean profiles and their respective mean and RMS differences are shown for HALOE versus MLS, CLAES, and ISAMS, respectively, for the April 15–20, 1992 period in Figures 4.4.2–1 to –3. The differences seen during this period are fairly representative of all the periods used in the comparison. The following is a summary of the major characteristics found in the differences. It is noted that HALOE, at present, does not retrieve temperatures below about 10 mb. The temperatures shown below 10 mb are NMC values merged with the retrievals above.

UPPER STRATOSPHERE (10 –1 MB)

HALOE mean temperatures in this region agree with other UARS results to within ± 1 K to 6 K. The RMS difference is about 5 K. The mean profiles usually come into agreement at 4 mb.

STRATOPAUSE TEMPERATURE

HALOE underestimates the stratopause temperature generally by 2–8 K in comparison with MLS, CLAES and ISAMS. During April 1–3, 1993, however, CLAES and HALOE show close agreement (< 1 K) at the stratopause (see Figure 4.4.2–4).

STRATOPAUSE HEIGHT

HALOE and ISAMS agree on the stratopause height location, while CLAES and MLS agree with each other, but show a slightly higher location than the other two experiments.

LOWER MESOSPHERE

CLAES tends to be warmer than HALOE by a few degrees from the stratopause upward. At 0.2 mb MLS shows a large low temperature feature, and ISAMS is also colder than HALOE (<5 K) throughout the region. RMS differences are in the range 5 to 10 K.

HALOE shows a "kink" at 0.4 mb and again at a lower level apparently where NMC is "tied on" at the 8–10 mb level. The persistent "kink" in the HALOE temperature profile at 0.4 mb occurs where the HALOE retrieval vertical resolution becomes more coarse in order to compensate for decreased signal-to-noise.

4.4.3 Longitude Versus Pressure Cross-Sections

These cross-sections were produced using the profiles obtained from the coincidence criteria discussed earlier. Typically the cross sections did not indicate any longitude trends which were different from the characteristics shown by the profile statistics. Two periods are discussed that show best and worst agreement. The first is April 1–3, 1992, which tends to show the best agreement between HALOE and other UARS instruments. The second period is January 9–11, 1992, which tends to show the worst agreement, apparently due to a large temperature gradient which the retrievals from the four experiments handle differently.

APRIL 1–3, 1993

It is not clear why CLAES and HALOE agree on stratopause temperature during this period and not during the other time periods. Inspection of longitude versus pressure cross sections in Figures 4.4.3–1 (HALOE) and 4.4.3–2 (CLAES) show that the atmosphere is relatively quiescent. Differences shown in Figure 4.4.3–3 (CLAES – HALOE) and other plots not shown for the remaining comparison periods, tend to substantiate the characteristic difference features noted in the profile plots.

JANUARY 9–11, 1992

This period shows a great deal of longitudinal and vertical variation in the temperature fields. Figure 4.4.3–4 shows a longitude versus pressure cross-section of temperature for HALOE. There is a large area of cold air from 240 to 360 E which extends up through the stratosphere which is well represented by all instruments. Nevertheless, fairly large

differences are still seen in this region as displayed in Figure 4.4.3–5 which shows a comparison of HALOE with ISAMS. Large differences of up to 10 K are seen in the stratopause region from 240 to 360 E. Relatively small differences (2 K to 6 K) occur in other regions of the upper stratosphere. Like the profile differences, ISAMS is colder than HALOE in the lower mesosphere. Although not shown, mostly similar, but in some cases, even larger differences were computed between MLS versus HALOE and CLAES versus HALOE.

4.4.4 HALOE Versus Correlative Data

Comparison of HALOE temperature profiles with those obtained from all available lidar profiles (125 comparisons) shows good agreement throughout the stratosphere. In Figure 4.4.4–1, it can be seen that from 30 km to just above 70 km mean differences do not exceed 5K. As before, HALOE tends to underestimate the temperature of the stratopause. The RMS difference is nearly flat at 8 K from 30 km to 60 km, and from 60–80 km the RMS slowly increases to values greater than 20 K.

4.4.5 Summary of Temperature Comparisons with HALOE

All coincident profile comparisons show agreement in the ± 8 K range throughout the upper stratosphere. Lidar comparisons with HALOE show differences which are within ± 6 K throughout the stratosphere (above about 35 km where HALOE retrievals begin) and the lower mesosphere. HALOE nearly always measures a lower stratopause temperature than CLAES, MLS and ISAMS.

There is general agreement on the stratopause height location with HALOE/ISAMS and CLAES/MLS agreeing best with each other, but with the two pairs slightly offset from one another.

MLS shows a consistently low temperature feature in the vertical profile at about the 0.2 mb level and HALOE shows a 0.4 mb "kink" in all temperature retrievals. ISAMS and MLS tend to give colder temperatures than HALOE in the lower mesosphere while CLAES results are warmer.

The pressure versus longitude comparisons show features which are similar to those indicated by the profiles. The notable exception occurs during the period, January 9–11, 1992, where sharp temperature gradients exist longitudinally and vertically in the 240 E to 330 E region. Under these circumstances, larger differences with HALOE exist than are observed in other periods, and the comparisons suggest that the differences are due to the way the algorithms for each experiment deal with these gradients. This is a time period and location which warrants further study.

4.5 Temperature Map Comparisons of UARS and NMC Data

Temperature maps were constructed from UARS data and NMC maps for January 9–11, 1992. Results for other periods are expected to have similar results, as was seen from comparisons of earlier versions of UARS data, so they will not be presented here. The NMC maps at 10 mb are a combination of radiosonde and a first guess using NOAA-11 TOVS satellite data. The NMC map at 1 mb is TOVS data only.

UARS gridded maps were made from 24 hours of Level 3AT ascending node data only,

for each day, using the successive iteration technique used in the NMC/CAC stratospheric temperature maps. Ascending node only data were used to eliminate expected differences between ascending and descending data from UARS instruments. Maps were constructed for only the 10 and 1 mb levels.

Figures 4.5–1 to –4 show the MLS, CLAES, ISAMS, and NMC maps in that order for January 9–11, 1992. Figures 4.5–1a to c are the MLS 10 mb maps for January 9–11 in order and Figures 4.5–1d to f are the 1 mb maps for January 9–11. Similarly, the order is the same in Figures 4.5–2 to 4 for CLAES, ISAMS, and NMC, respectively.

Overall, the temperature comparisons are quite good, with all maps showing similar large-scale features in addition to many of the small-scale features. Many of these can be followed from one map time to another. The maps are also meteorologically consistent on a day-to-day basis at both levels for all the maps shown. There are no apparent discrepancies between any of the maps. The largest difference occurs at 1 mb in the tropical region south and east of Florida, where the north-south gradient in the temperatures seems to build from January 9 to 11 in MLS and CLAES. ISAMS builds the gradient a little slower and does not quite achieve the gradient of MLS and CLAES, although showing a definite gradient. NMC shows weak or no gradients in the region for the period. One of the possible explanations might be the ability of the UARS instruments to pick up features that have shallow vertical resolution. This behavior is seen quite well in the weaker-amplitude systems over Asia at 1 mb. The UARS instruments pick up the systems in a similar fashion, while the NMC maps show similar features, but at a weaker amplitude, probably because of the broad vertical resolution of the TOVS data used for the NMC analyses.

The differences between the maps in their high and low temperature regions can be seen by comparing the January 9 maps for 10 mb. In Figure 4.5–1a MLS shows a high temperature of –26.2C and a low temperature of –72.3C at high latitudes. For the same regions, CLAES shows –20.3C and –73.3C, ISAMS shows –18.9C and –70.5C, while NMC shows –17.7C and –77.3C, respectively.

Summarizing, all instruments show similar features with no apparent discrepancies. The data all seem to be quite consistent, with day-to-day changes that are quite believable. The largest differences occur between the UARS instruments and the NMC data, but the difference is probably caused by the higher vertical resolution of the UARS data versus the broader vertical resolution of the NMC data.

4.6 Temperature Time Series

Time track plots are used to compare retrievals along the level 3AT tangent point measurement track of the CLAES and MLS instruments, which look perpendicular to the orbit track from the cold side of the spacecraft, and ISAMS for those times when it is looking out the cold side. The data are obtained at 65 second resolution on standard UARS pressure surfaces. The time tracks are useful for establishing consistency of structure observed from one orbit to the next and for a top level view as to whether instruments are observing similar structure as a function of position on the orbit.

One must be careful in examining the instrument data because the plotting routine connects points with a straight line. If one is not cognizant of this, data gaps that occur

on one orbit but not the next, may erroneously be interpreted to be showing a difference in structure. The orbital structure of the temperature data is generally dominated by latitudinal variation, but over the course of a day the longitudinal variation can also play a large role.

For the temperature intercomparison, time track plots for CLAES, ISAMS, MLS, and NMC (by interpolating the CDHF NMC product to the L3AT grid) were generated and examined. These were generated for a subset of the intercomparison days, including January 9 and 10, a north looking period when a minor warming event was in progress, April 16 and 17 looking into the autumn southern hemisphere, August 9 looking into the bland northern hemispheric summer, and finally August 28 and 29 looking into the southern hemisphere winter ozone hole precursor conditions.

Time track comparisons on the 10 mb level for January 9 and 10 are shown on Figures 4.6–1 and 4.6–2. These tracks cover the entire 24 hour span of each day. The tracks clearly show the presence of a localized "hot spot" at high latitude for these days (this "hot spot" has been referred to in the section above on mapping). The time tracks clearly indicate that the instruments are "seeing the hot spot". They show that the event is intensifying from 9 to 10 January. From viewing the time tracks one sees that the NMC peak temperatures are not in phase with the instrument-measured temperature peaks, suggesting an effect of the time difference of the rawinsonde and NMC mapping times from the UARS instrument sampling times. These figures also show that the amplitude (from cold minimum to hot maximum) of the NMC is less than that of the instruments. This effect is to be expected since the NMC temperatures are an analysis product, and additional interpolation was required to move them to the L3AT grid. Figure 4.6–3 shows the latitude, longitude, and solar zenith angle of the tangent point as a function of time for 10 January corresponding with the Figure 4.6–2.

Inspection of the time tracks over the four subsets of intercomparison days lead to some general conclusions. Figures illustrating these will be kept to a minimum. Comparisons for January 10 for the 10 and 4.64 mb levels for a shorter segment of track (in order to more easily see comparison details) are shown on Figure 4.6–4. The top panel shows the latitude for the tangent points along the track as a function of time (UT). The middle panel shows the comparison at 10 mb and the bottom panel at 4.64 mb. The instruments appear to correlate with one another better than with NMC. This conclusion is especially true in the equatorial regions on the 4.64 mb surface. This characteristic is especially evident in the "quiet case" August 9 data (ISAMS not included) as shown by Figure 4.6–5. These data show remarkable correlation of the CLAES and MLS data over scales of several EMAFs.

Comparisons for January 10 for the 2.15 and 0.46 mb levels are shown on Figure 4.6–6. The largest temperature variations along the track that were observed in any of the data studied occur here over about 12 minutes. For example, for the spike beginning at approximately 7.58 hours the maximum observed variation (for MLS) is approximately 118 K and the smallest (for NMC) is approximately 70 K.

The "quiet case" August 9 data for the 2.15 and 0.464 mb levels are shown on Figure 4.6–7. Again these data show remarkable correlation of the CLAES and MLS data on very short scales (approaching 65 seconds).

The data are compared by a different format time track on Figure 4.6–8. The top panel shows the latitude tangent point track for August 28. The middle and bottom panels show

the difference between CLAES and MLS for points for which both instruments reported data. The error bars for each instrument are also shown for reference. The daily mean of the CLAES data, the mean difference of the CLAES – MLS data, the standard deviation of the CLAES – MLS data, and the correlation coefficient for the CLAES and MLS data are given on each panel. The data on Figure 4.6–8 illustrate events of relatively large disagreement between CLAES and MLS in the cold south winter polar vortex region at 4.64 mb.

A summary of the mean difference (MD), standard deviation (STDV) and correlation coefficient (CORR) for various instrument comparisons and representative days is given in Table 4.6–1 below.

Table 4.6-1 Mean Differences, Standard Deviations, and Correlation Coefficient

			Day			
p (mb)	Case	Parameter	9 Jan. (north)	16 Apr. (south)	9 Aug. (north)	28 Aug. (south)
10.0	CLAES – MLS	MD	1.42K	1.52K	1.17K	0.42K
10.0	CLAES – MLS	STDV	3.29K	2.64K	1.92K	3.21K
10.0	CLAES – MLS	CORR	0.96	0.96	0.91	0.95
4.64	CLAES – MLS	MD	–0.86K	–0.40K	–0.67K	–1.58K
4.64	CLAES – MLS	STDV	4.19K	2.61K	2.46K	3.64K
4.64	CLAES – MLS	CORR	0.96	0.97	0.92	0.87
2.15	CLAES – MLS	MD	–1.74K	–2.27K	–2.32K	–3.88K
2.15	CLAES – MLS	STDV	4.22K	2.89K	2.70K	4.06K
2.15	CLAES – MLS	CORR	0.96	0.98	0.93	0.81
0.46	CLAES – MLS	MD	–0.17K	–0.03K	0.20K	0.29K
0.46	CLAES – MLS	STDV	4.52K	3.18K	3.23K	4.07K
0.46	CLAES – MLS	CORR	0.92	0.86	0.93	0.92
10.0	CLAES – ISAMS	MD	–1.02K	0.15K	—	—
10.0	CLAES – ISAMS	STDV	2.79K	3.02K	—	—
10.0	CLAES – ISAMS	CORR	0.97	0.94	—	—
4.64	CLAES – ISAMS	MD	–3.41K	–2.65K	—	—
4.64	CLAES – ISAMS	STDV	3.54K	3.49K	—	—
4.64	CLAES – ISAMS	CORR	0.97	0.95	—	—
2.15	CLAES – ISAMS	MD	–2.41K	–2.18K	—	—
2.15	CLAES – ISAMS	STDV	4.29K	3.83K	—	—
2.15	CLAES – ISAMS	CORR	0.97	0.96	—	—
0.46	CLAES – ISAMS	MD	6.65K	5.91K	—	—
0.46	CLAES – ISAMS	STDV	4.39K	4.66K	—	—
0.46	CLAES – ISAMS	CORR	0.92	0.68	—	—

Some major conclusions of the time track comparisons are:

- The instruments clearly see the January 9 and 10 high latitude "hot spot" for all pressure levels, with greatest amplitude on the 2.15 mbar level.

- The amplitude of the temperature variation over the "hot spot" is greater for the UARS instruments than for NMC.
- At 2.15 mb, for example, the instruments are phased such that the hot spot is initially largest as measured by MLS, with a gradual transition to CLAES showing the largest values, with a maximum of ≈ 331K in the hot spot near ≈ 9.10 hours on January 10, 1992.
- For all days and pressure levels the instruments generally track one another closer than they do NMC.
- The NMC is particularly high compared to the instruments in equatorial regions for the 10 and 4.64 mb cases for all days, most evident near 4.64 mb.
- CLAES mean temperatures are generally warmer than MLS near 10 mb, cooler near 4.64 and 2.15 mb, and similar (within tenths of a K) near 0.46 mb.
- CLAES mean temperatures are generally close to ISAMS at 10 mb, cooler at 4.64 and 2.15 mb, considerably warmer at 0.46 mb.
- Relatively cold CLAES temperatures are especially evident in cold polar winter vortex conditions at 4.64 and 2.15 mb.
- Cases can be found in the bland August 9 summer north viewing data where CLAES and MLS seem to be correlated on short scales along the track. These scales seem to approach the 65 second scale on the 0.46 mb track.

4.7 Conclusions on UARS Temperatures

The data used in these comparisons were the CLAES V6, ISAMS V8, HALOE V12, and MLS V3. A considerable effort is going into the improvement of the data, and new versions are taking the place of those reported on here, so these results, while indicative, are only a snapshot of the quality of evolving data.

TEMPERATURE PRECISION

By comparing pairs of temperature profiles taken at nearly the same place within one orbital period (≈ 96.4 minutes) of each other, the precision of the temperatures has been estimated. Because of the orbital and viewing geometry, these locations are located only at latitudes of 80 and 32 degrees, in both hemispheres. These results are shown in Figure 4.2.3-1. They indicate that over the altitude range from 22 to 0.2 mb, MLS precision ranges from about 0.5 to 2K. From 100 to 0.1 mb, CLAES and ISAMS precision varies from about 1 to 2.5K.

TEMPERATURE ACCURACY

The accuracy has been estimated here through comparison with results obtained by other techniques, including radiosondes, lidars, rockets, and analyses based on operational satellite observations.

COMPARISON OF INDIVIDUAL PROFILES

100 – 10 mb

Comparison with radiosondes indicates mean biases for CLAES, ISAMS, and MLS of 1–2K. Considering differences in time and space, as well as the sampled volumes, this is regarded as satisfactory. However, there are few radiosondes in polar latitudes, and thus it is not always easy to compare data under the most extreme conditions, which are also of great interest. In addition, these comparisons are made against uncorrected radiosonde values. It was not possible to obtain corrected radiosondes, such as are input to the mapped analyses, for these evaluations, and we do not know how large an effect they might have.

Above 10 mb

In this altitude range, profiles were compared with lidar soundings (L) and a small number of rocket soundings (R). Roughly stated, the results indicate:

CLAES	10–0.1 mbar	5K< L	2K < R
ISAMS	10–7 mbar	4K > L	4K > R
	1–0.1 mbar	10K < L	10K < R
	0.07–.02 mbar	> L	10K < R
HALOE	8–3 mbar	2K > L	
	3–.4 mbar	5K < L	
	0.4– 0.05 mbar	2K < L	
MLS	20–0.4 mbar	2K ± L	2K ± R

For these comparisons, the major issues are the variations among lidar stations, and how to account for diurnal and semidiurnal temperature variations in the UARS temperatures.

COMPARISONS OF ZONAL MEAN TEMPERATURES

The UARS sensors agree better among themselves than with NMC or the UKMO, which agree well with each other. The UARS sensors return cooler temperatures from 10–1 mba The differences can be up to 8K in high latitude polar regions, especially in the Southern Hemisphere. There are smaller differences with the UKMO analyses.
Differences among MLS, ISAMS, and CLAES temperatures are mainly a function of altitude. MLS – CLAES differences are generally less than 2K, with occasional differences of 4K. ISAMS differences with MLS and CLAES are slightly larger.

MAPS AND TIME SERIES

NMC and UARS see the same features, although the UARS features are generally stronger. It is believed that a major reason for the differences between the UARS and operational NMC and UKMO temperatures is the higher vertical resolution of the UARS temperatures.

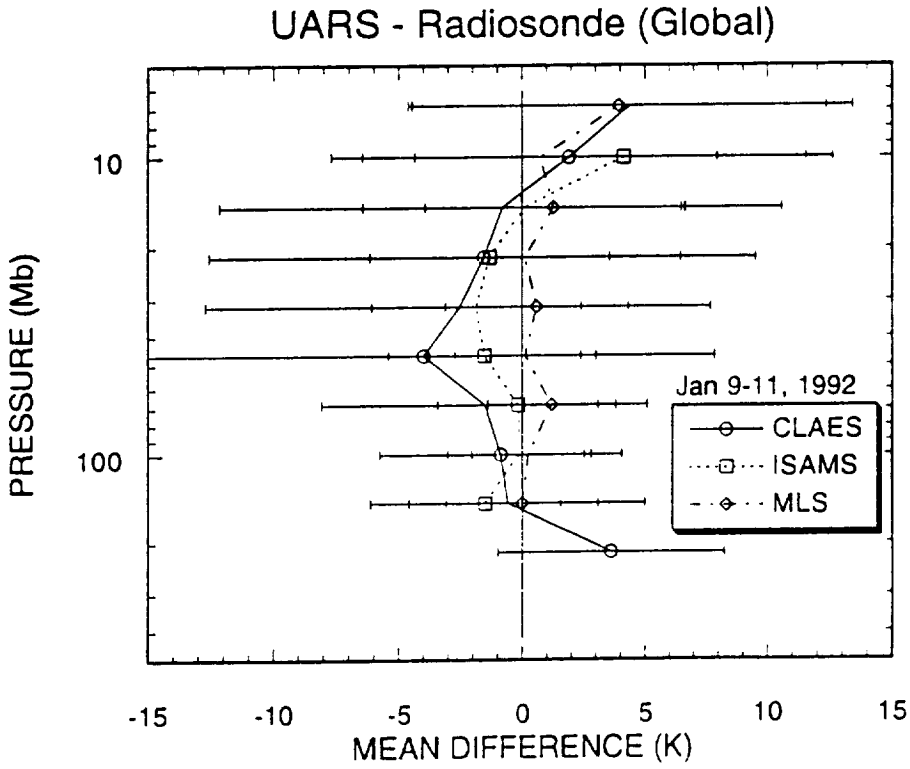

Figure 4.2.1.2–1

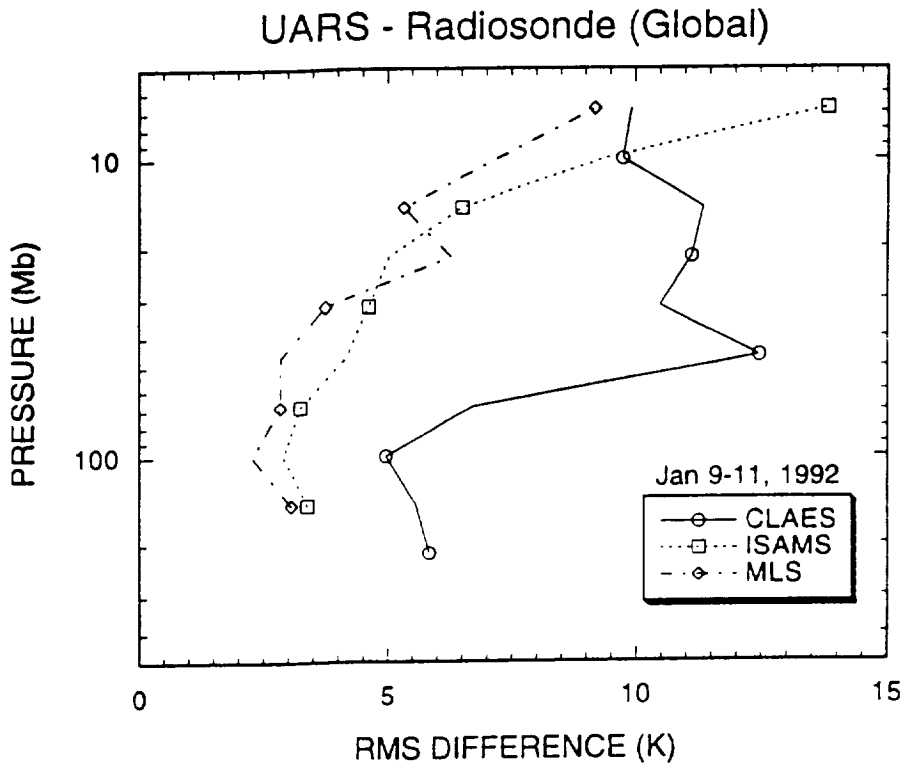

Figure 4.2.1.2–2

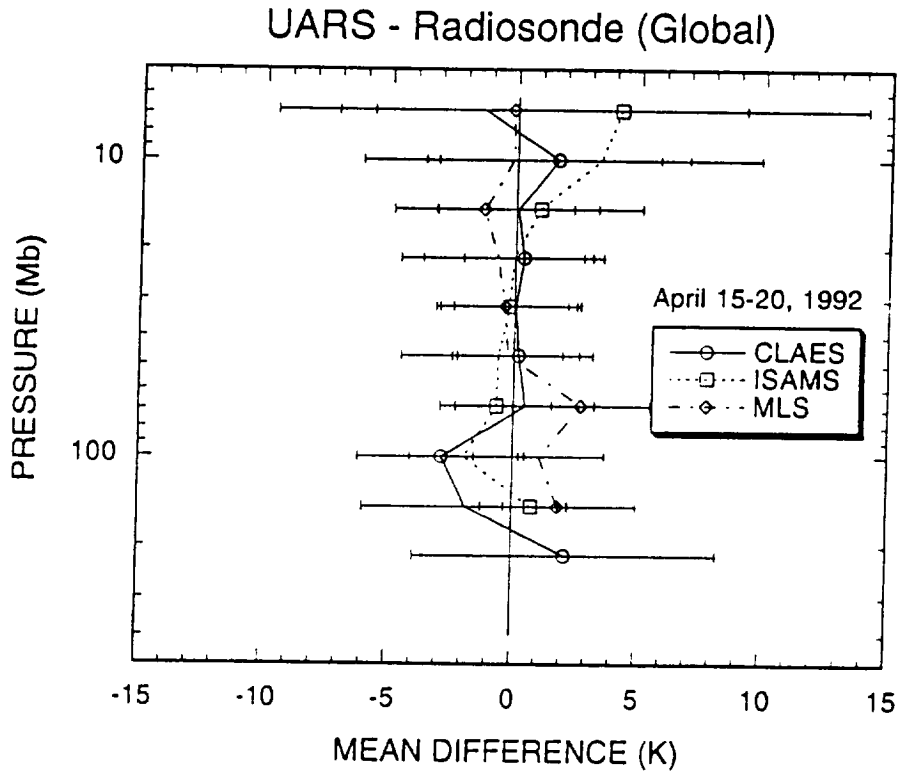

Figure 4.2.1.2–3

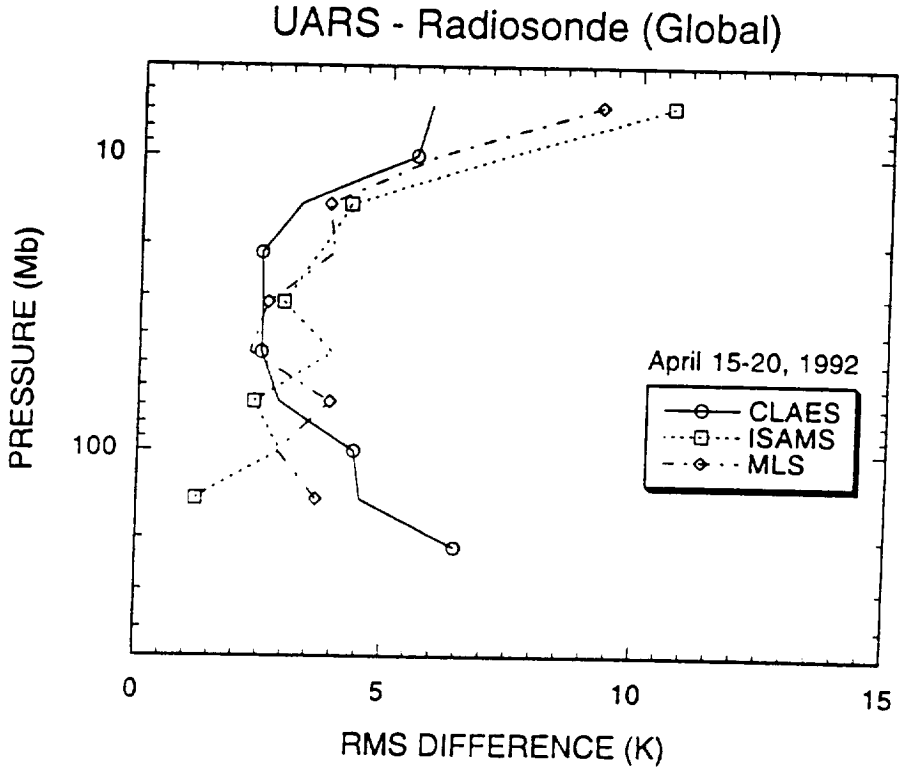

Figure 4.2.1.2–4

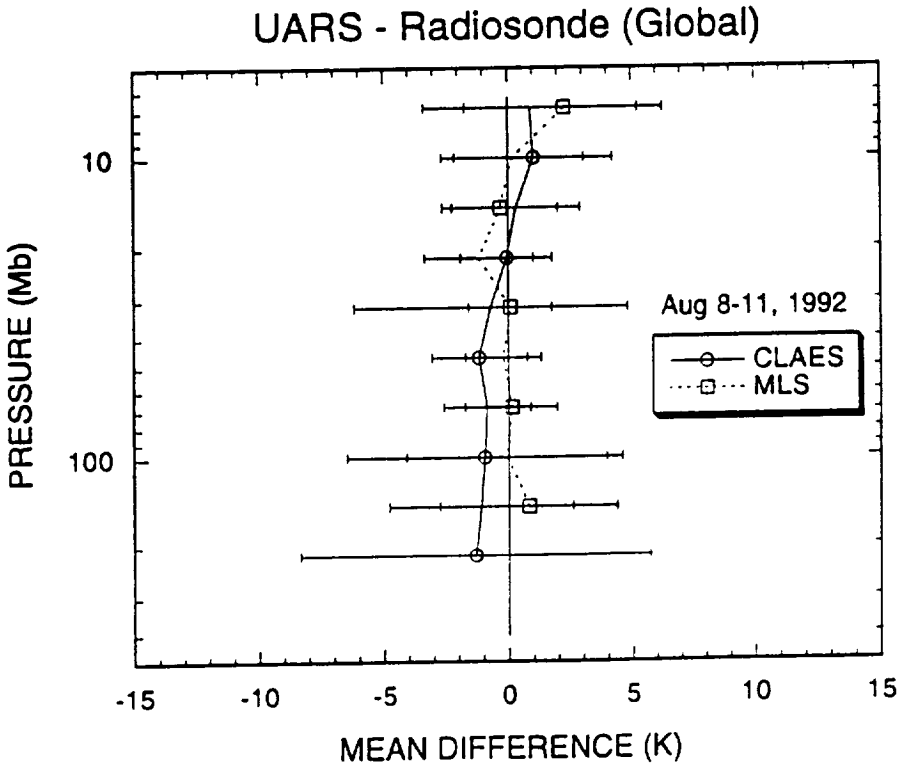

Figure 4.2.1.2–5

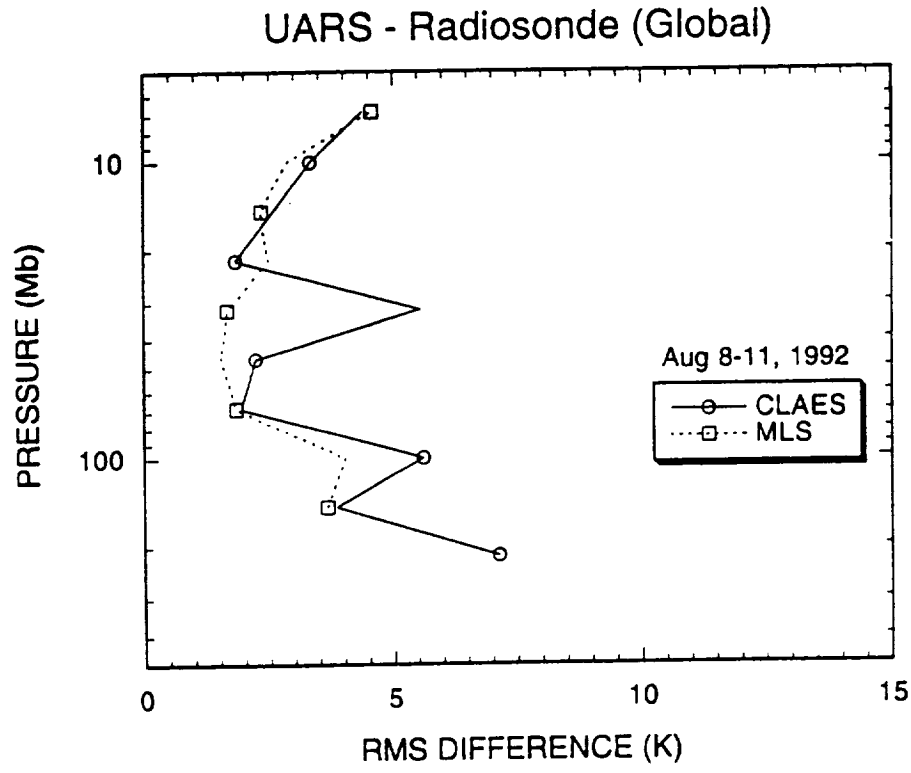

Figure 4.2.1.2–6

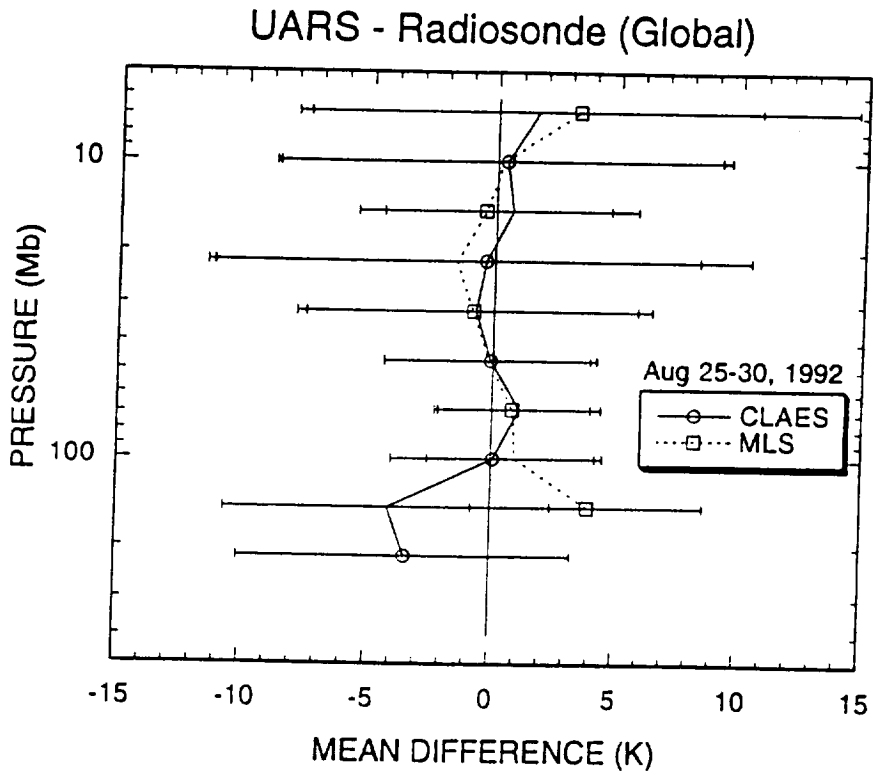

Figure 4.2.1.2–7

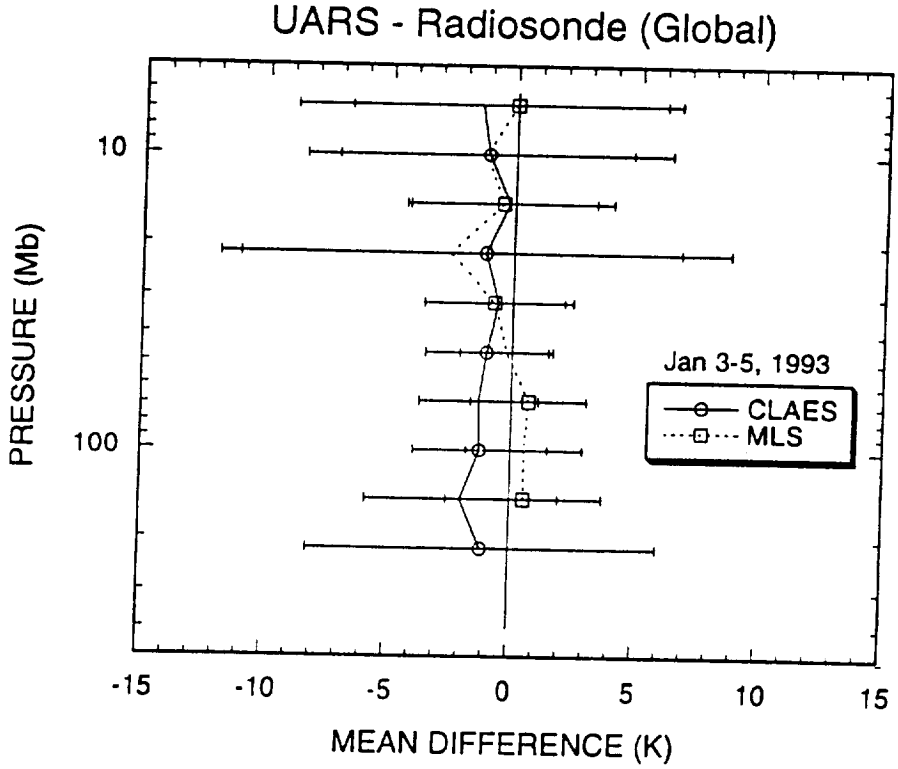

Figure 4.2.1.2–8

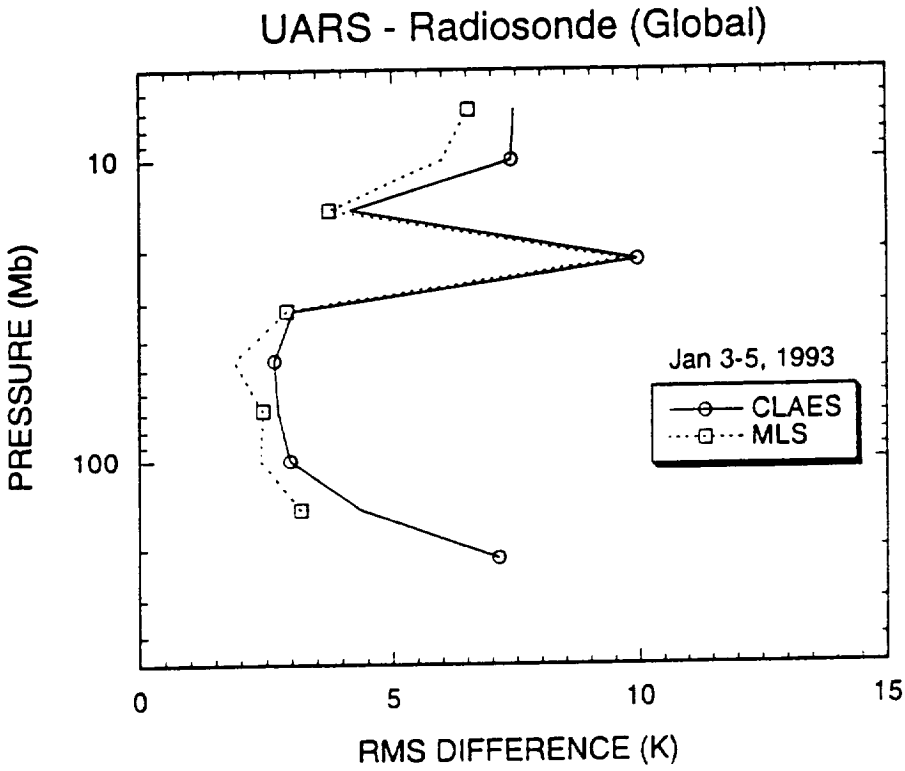

Figure 4.2.1.2-9

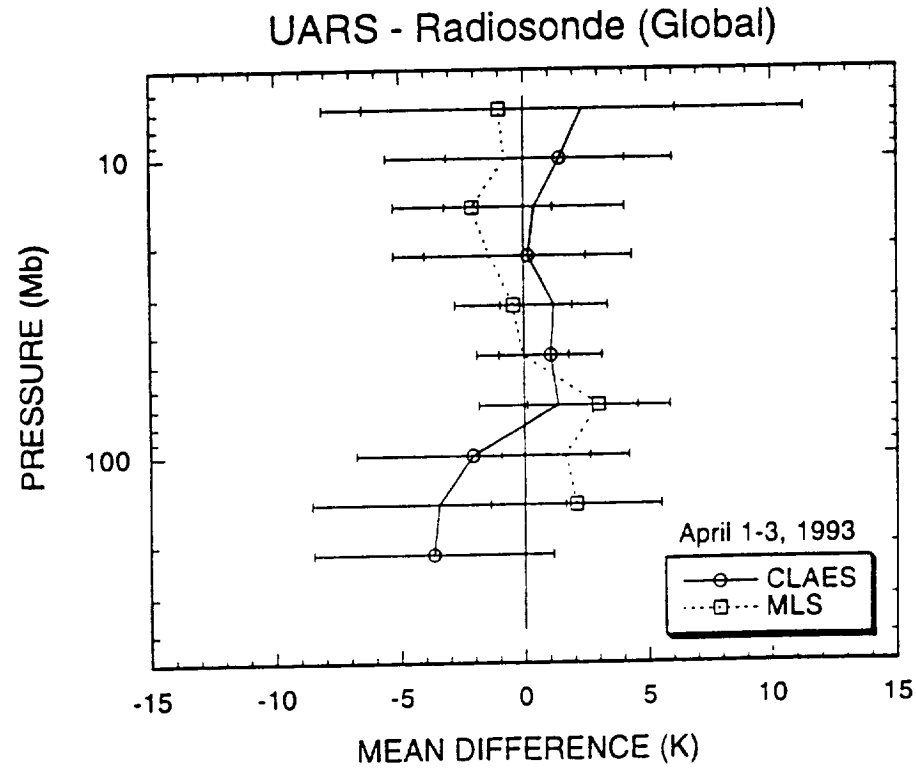

Figure 4.2.1.2–10

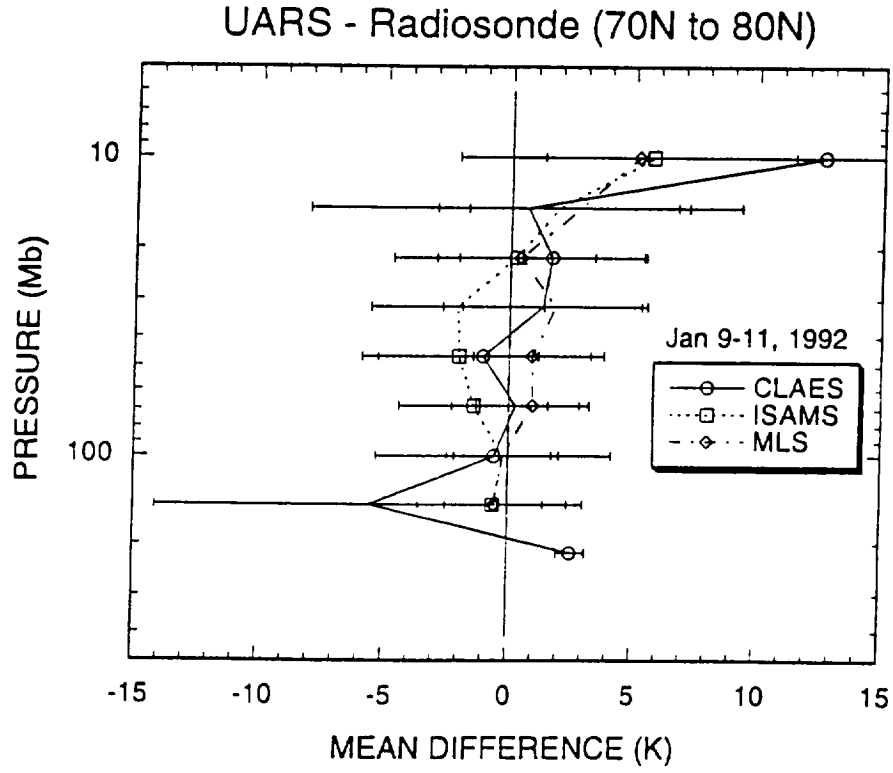

Figure 4.2.1.2–11

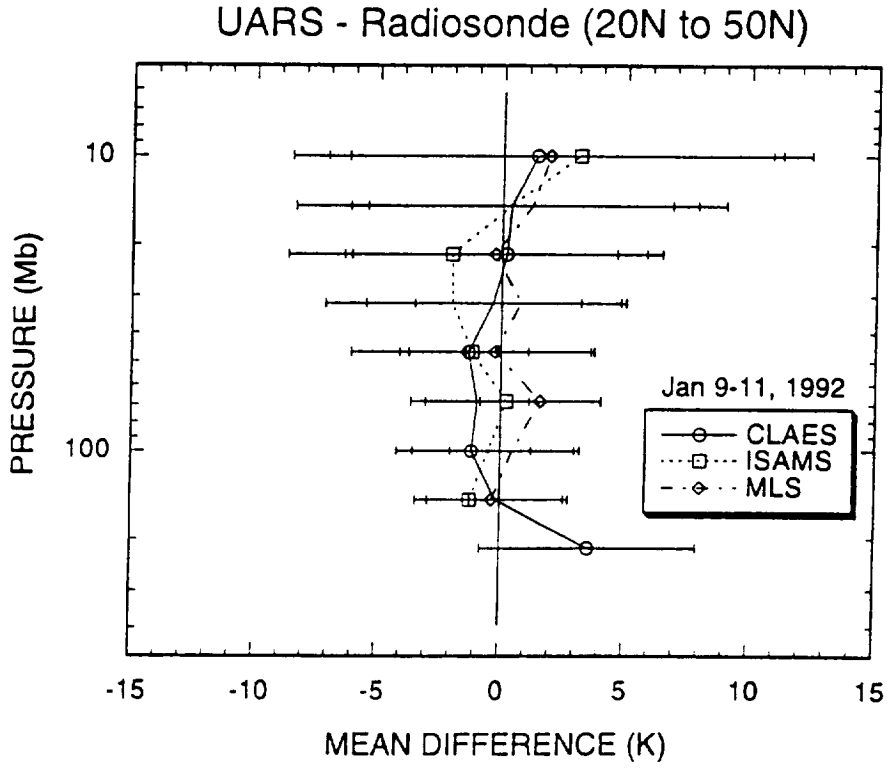

Figure 4.2.1.2–12

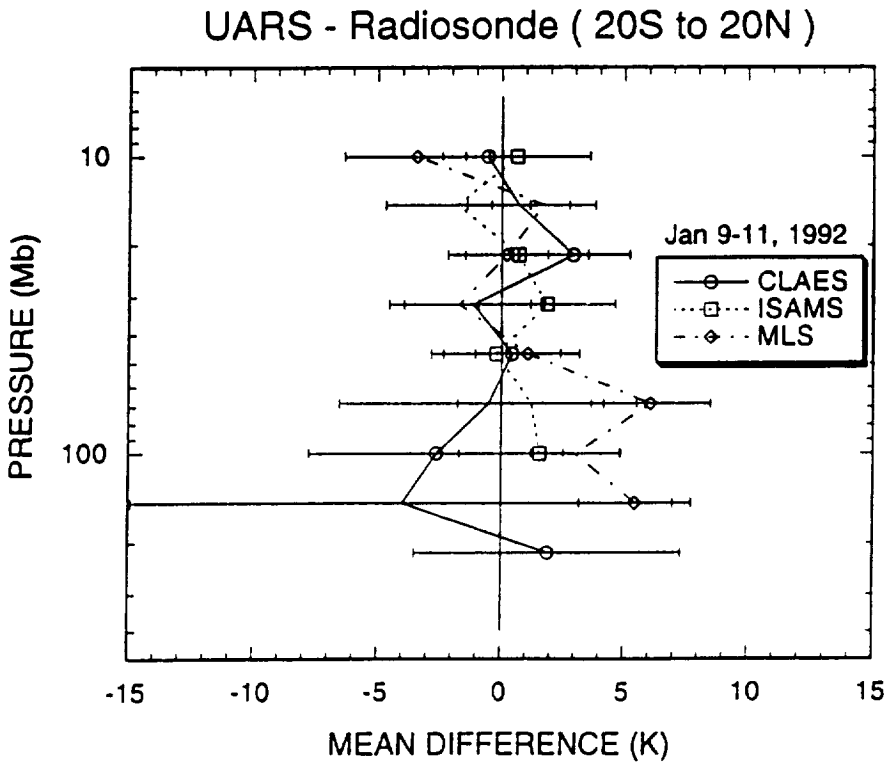

Figure 4.2.1.2–13

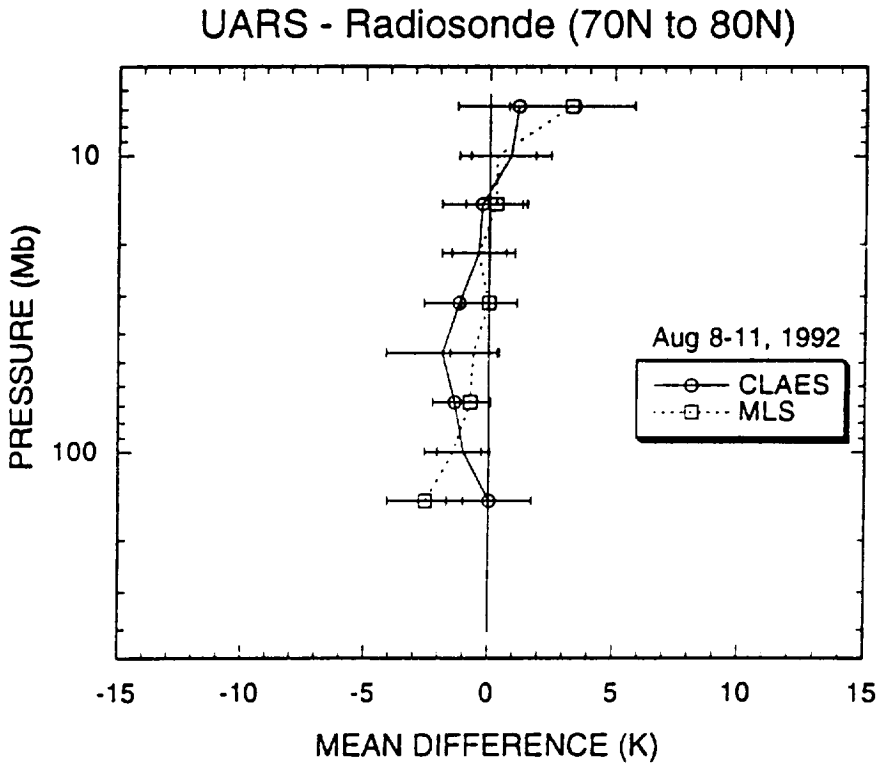

Figure 4.2.1.2–14

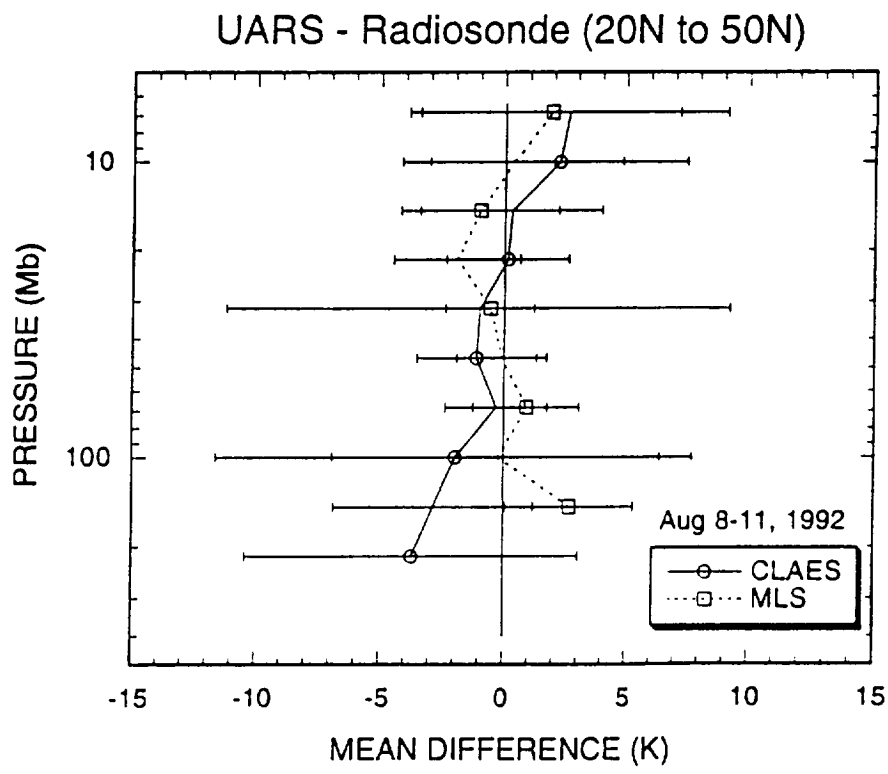

Figure 4.2.1.2–15

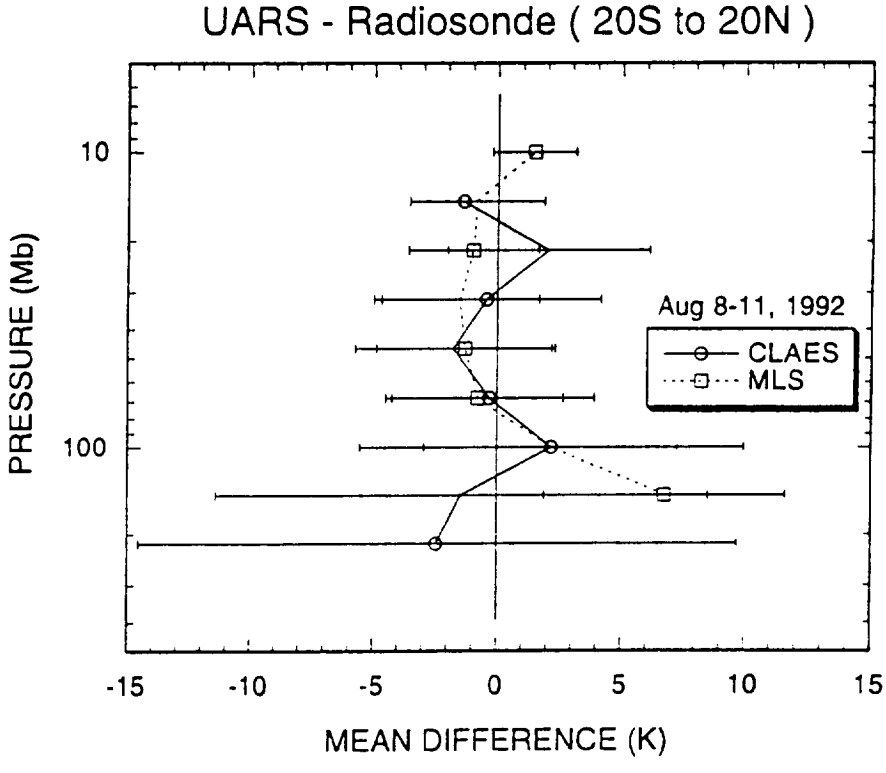

Figure 4.2.1.2–16

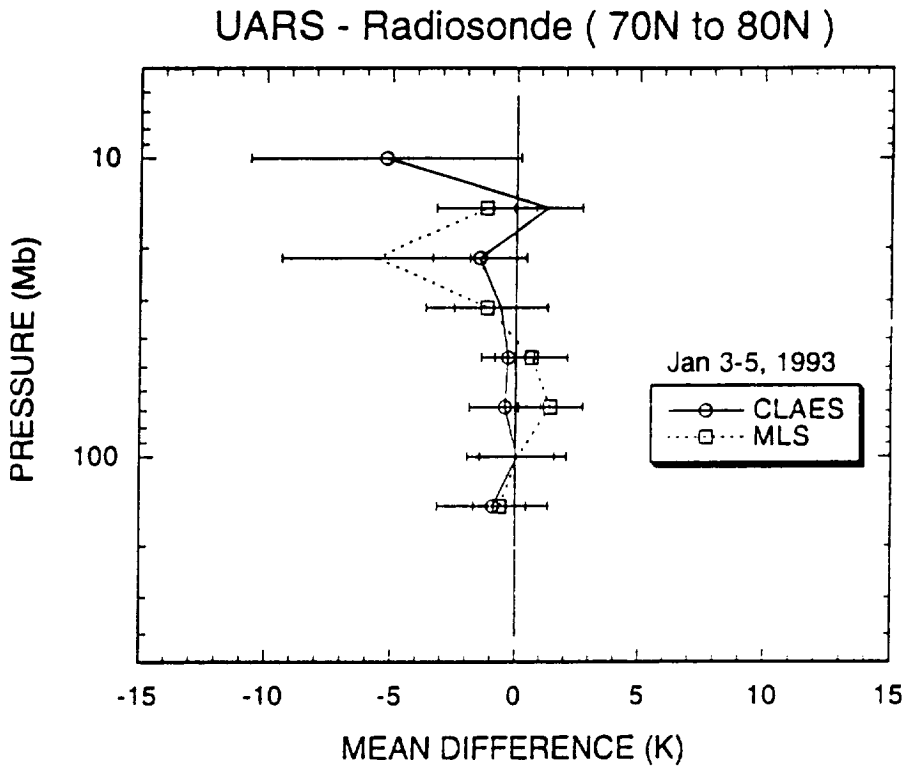

Figure 4.2.1.2–17

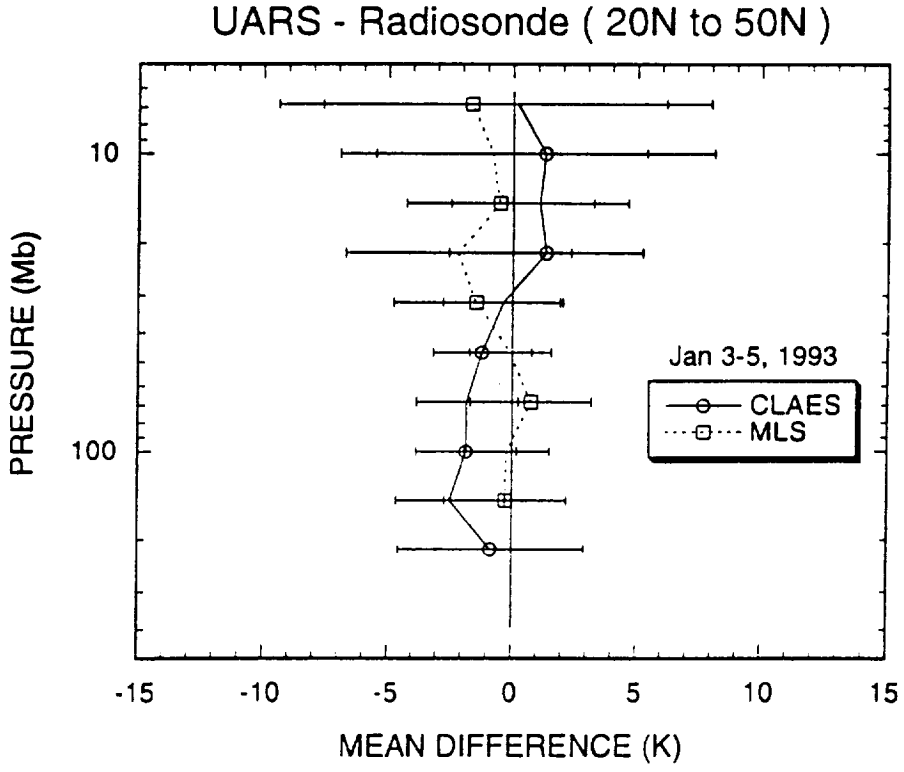

Figure 4.2.1.2–18

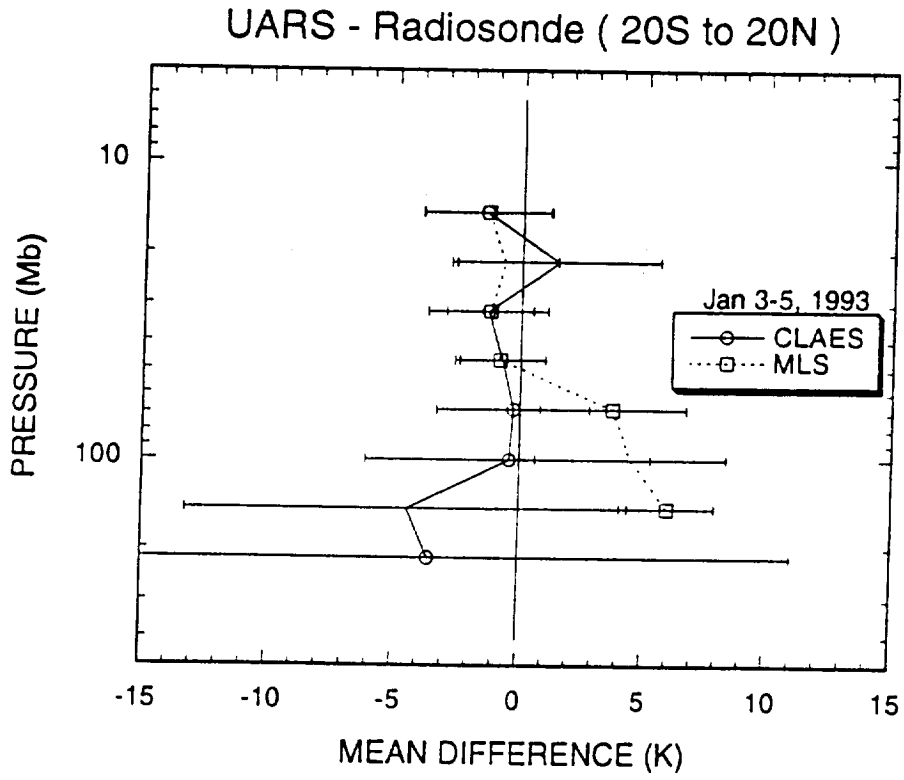

Figure 4.2.1.2–19

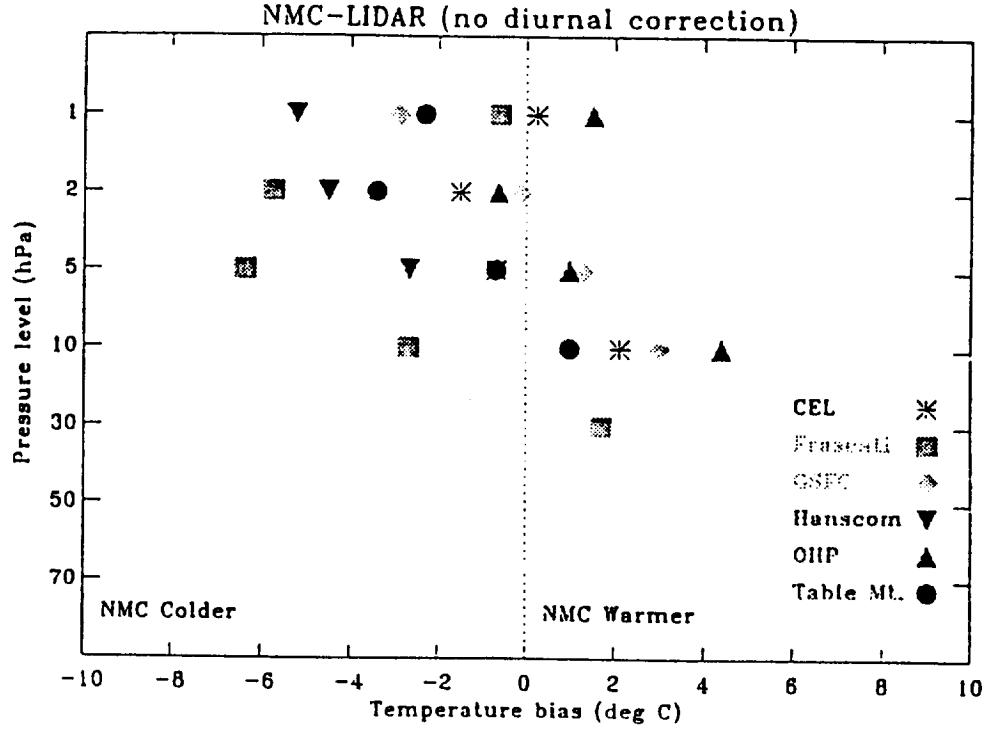

Figure 4.2.2.1–1

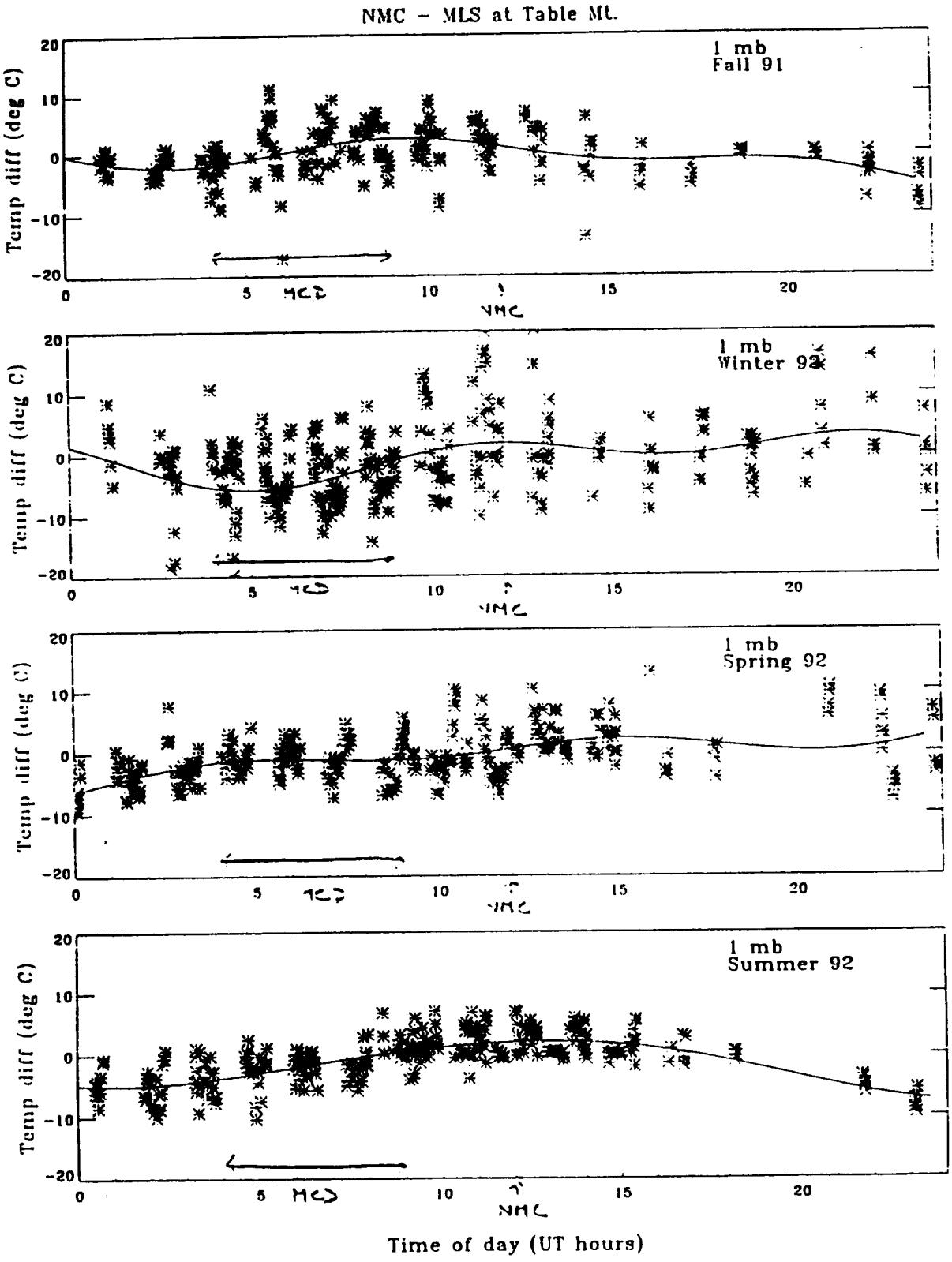

Figure 4.2.2.1–2

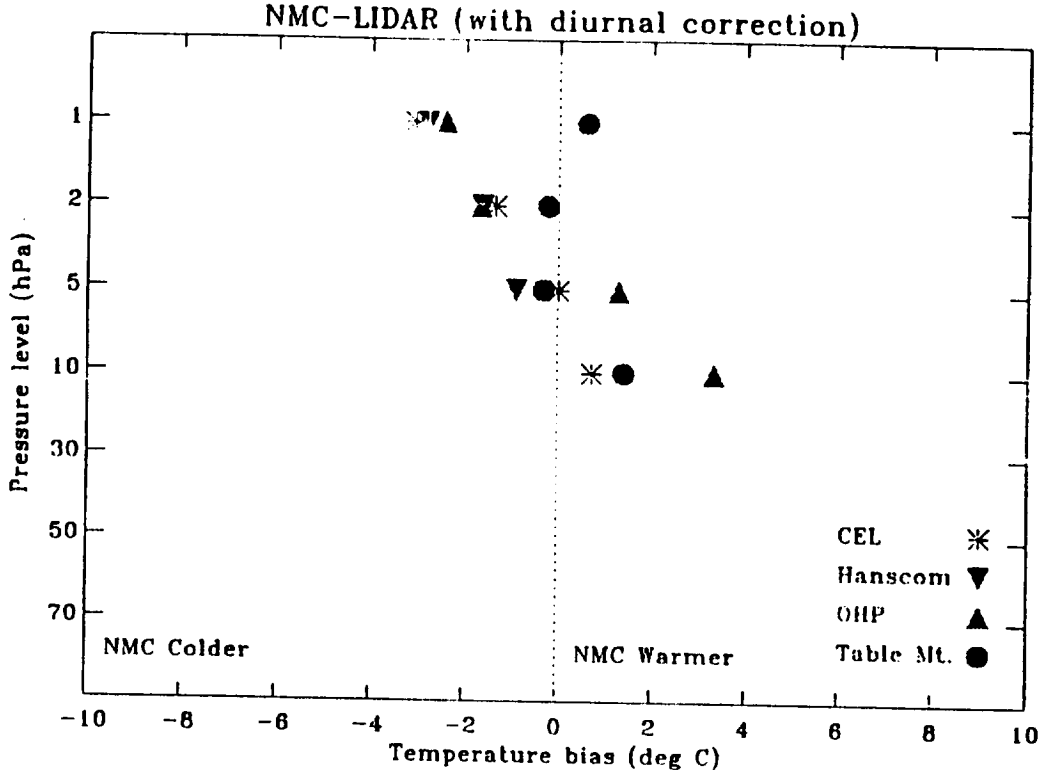

Figure 4.2.2.1–3

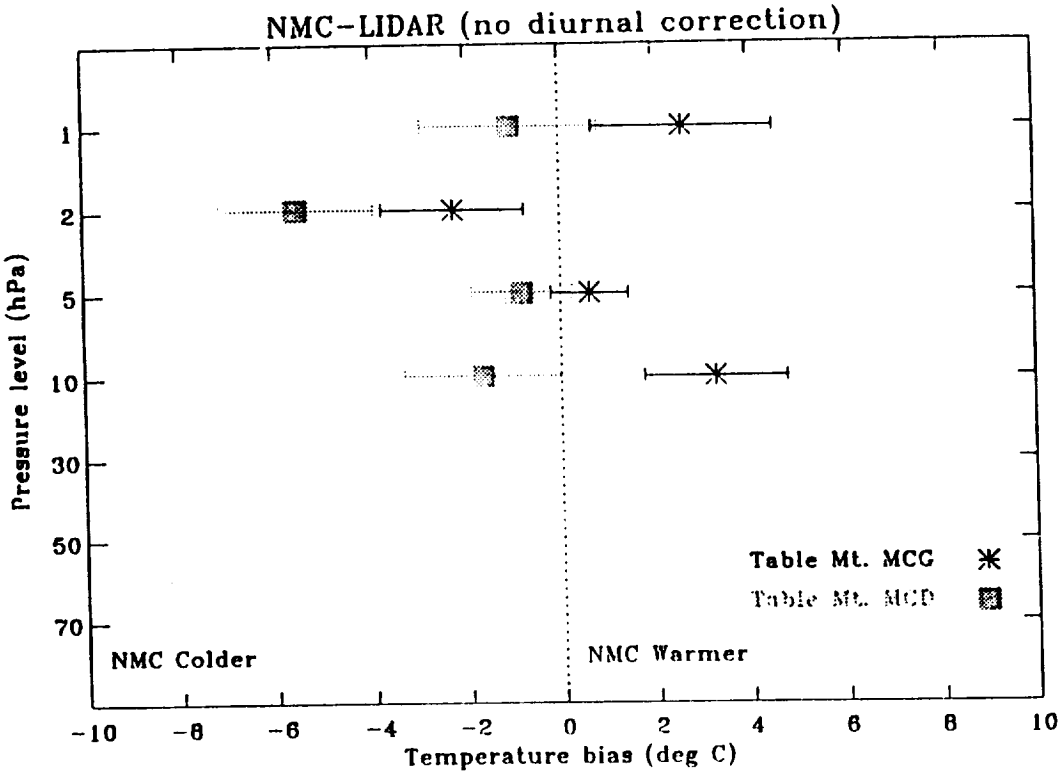

Figure 4.2.2.1- 4 (a)

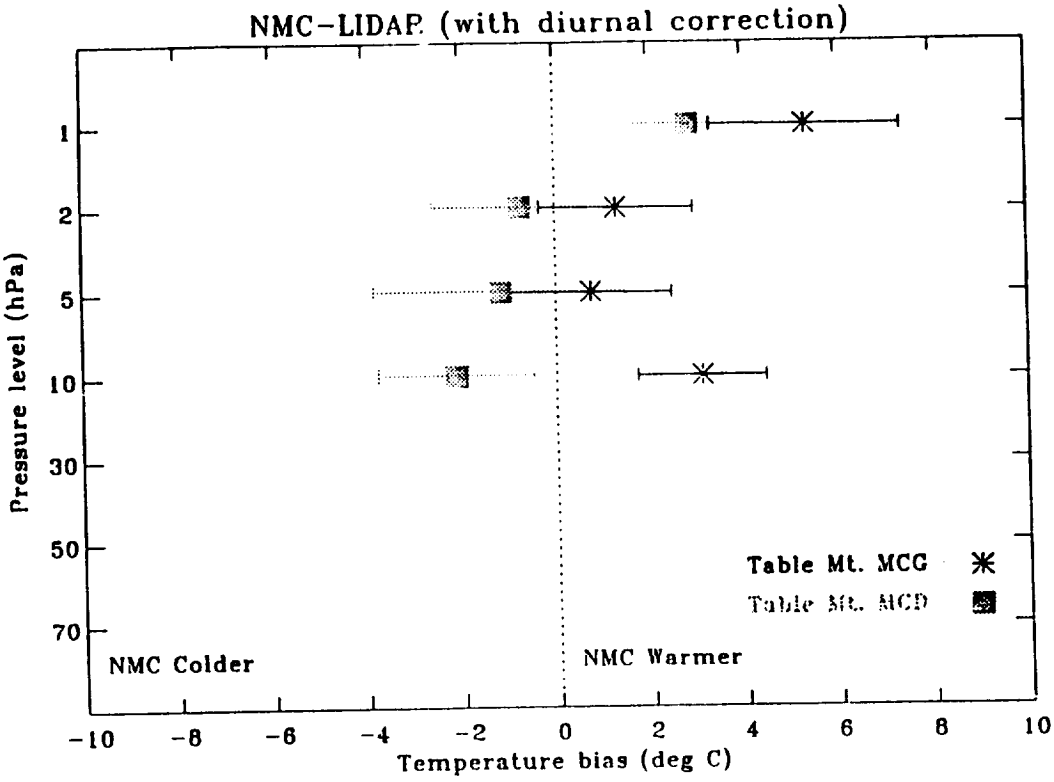

Figure 4.2.2.1- 4 (b)

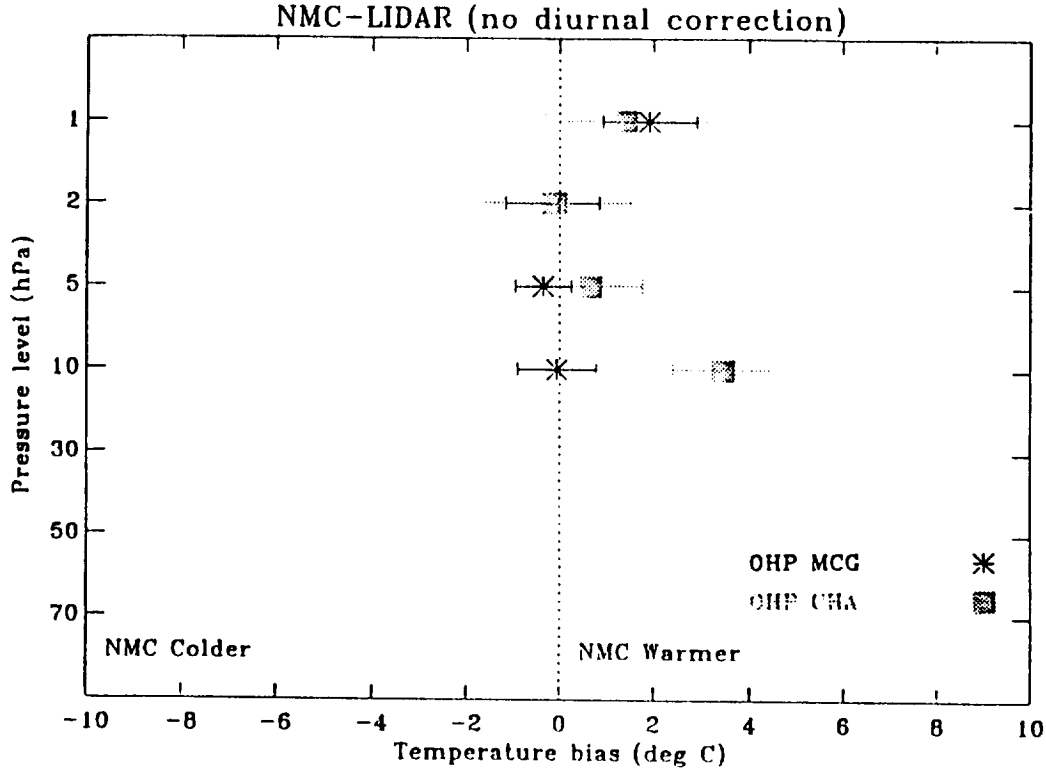

Figure 4.2.2.1- 5 (a)

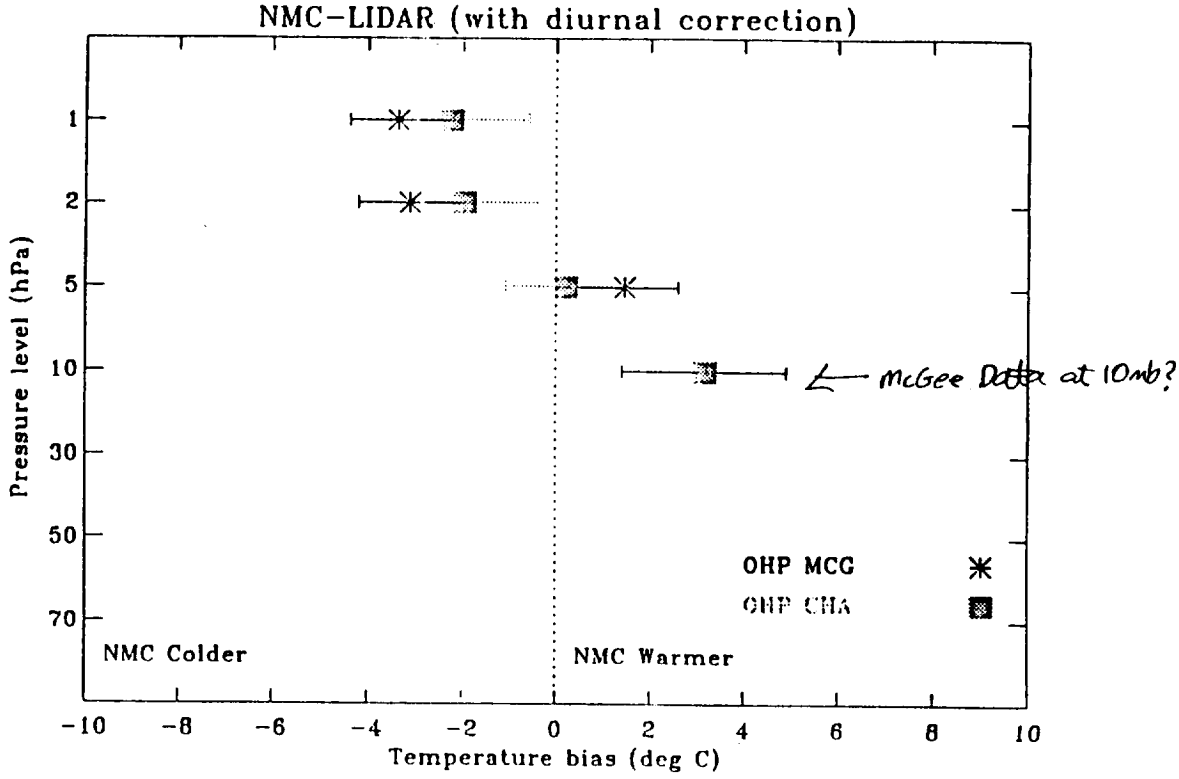

Figure 4.2.2.1- 5 (b)

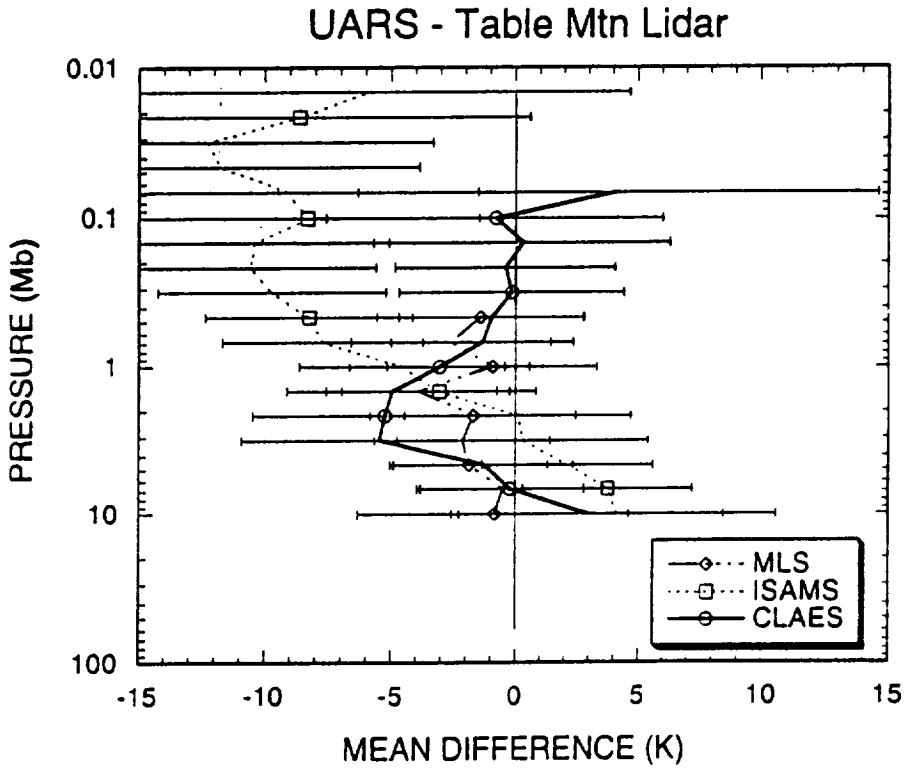

Figure 4.2.2.2–1

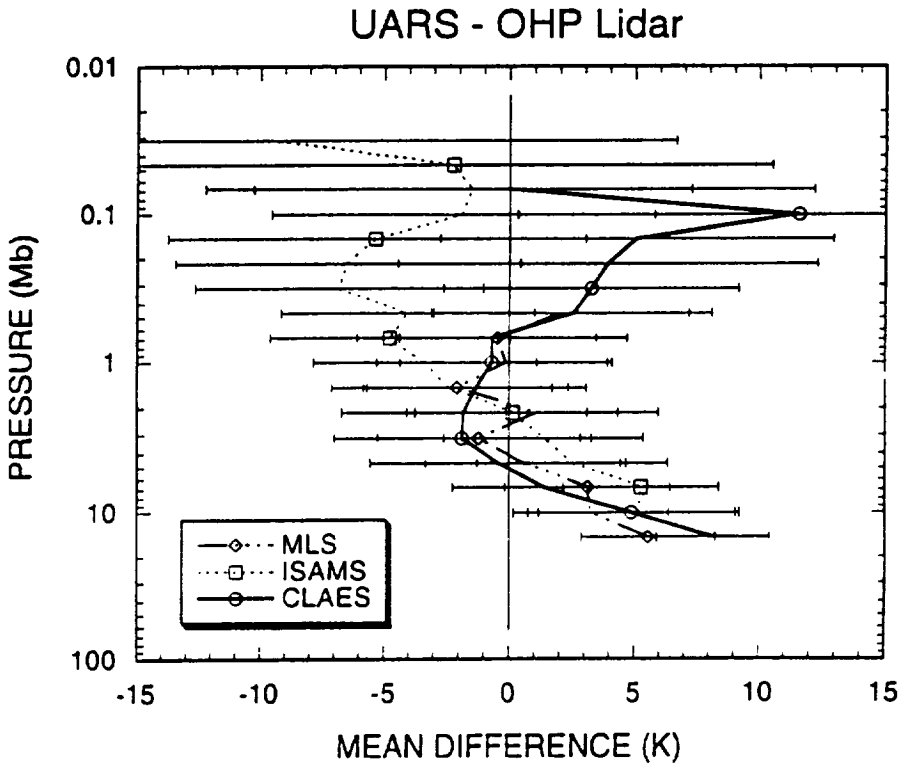

Figure 4.2.2.2–2

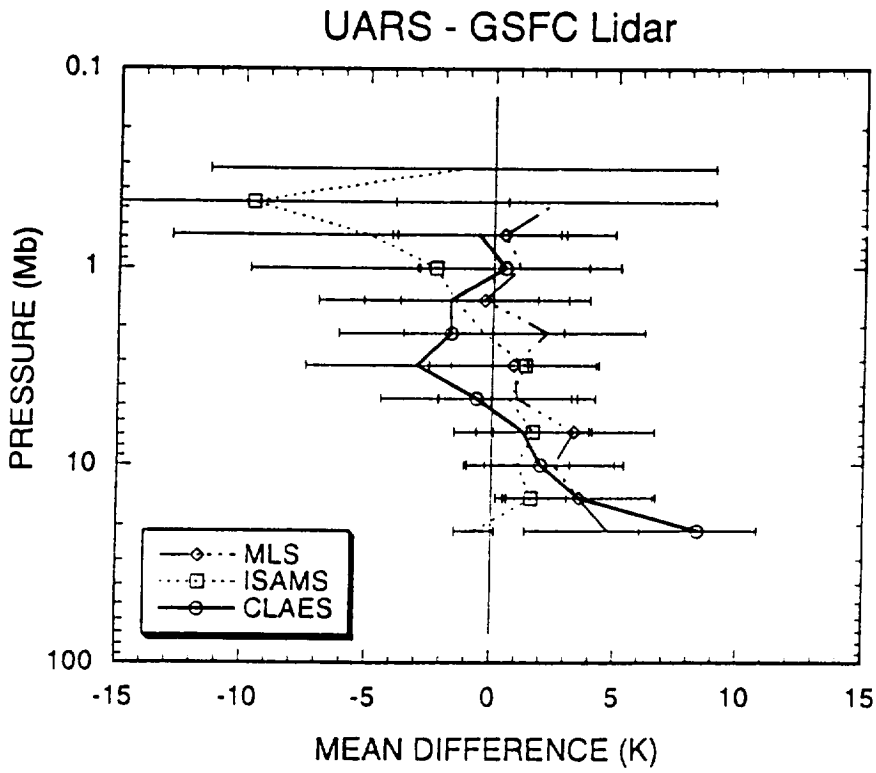

Figure 4.2.2.2–3

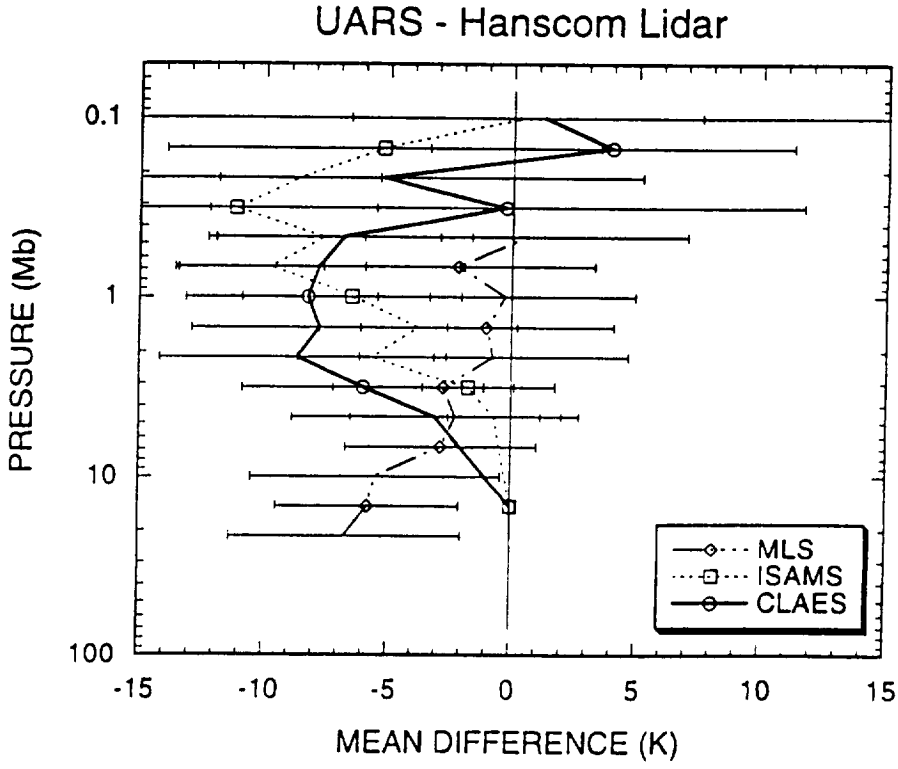

Figure 4.2.2.2-4

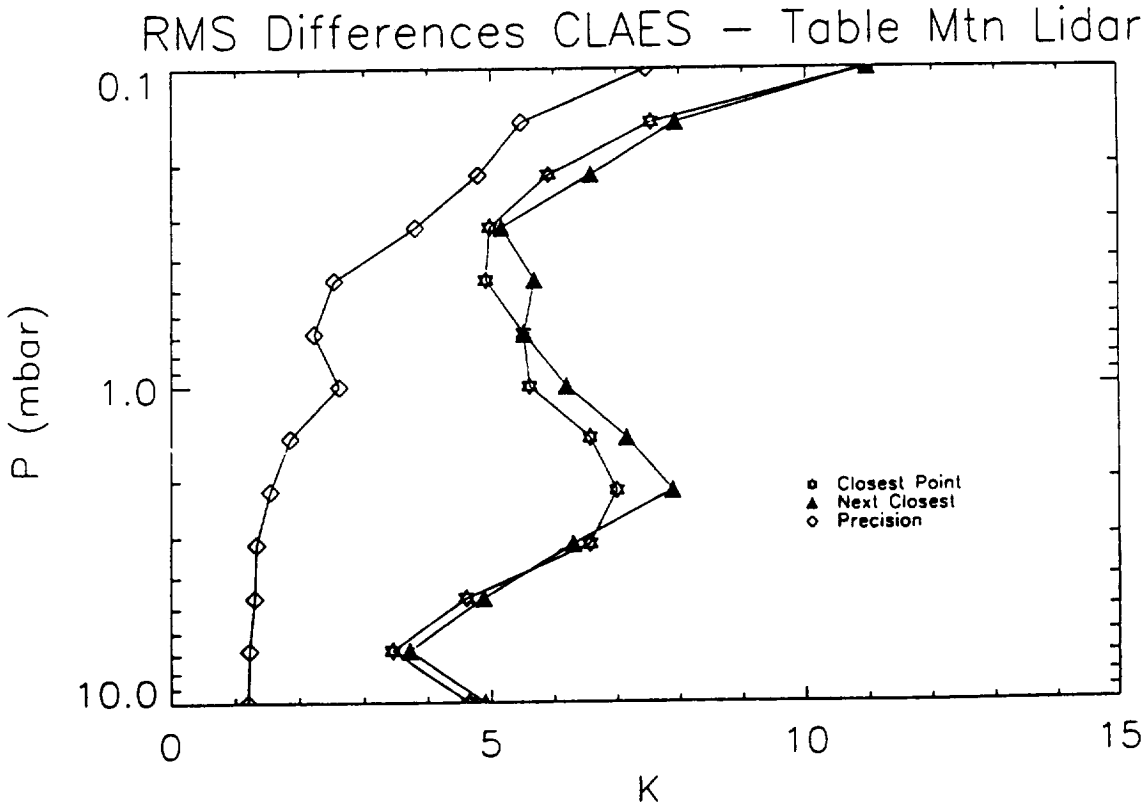

Figure 4.2.2.3–1

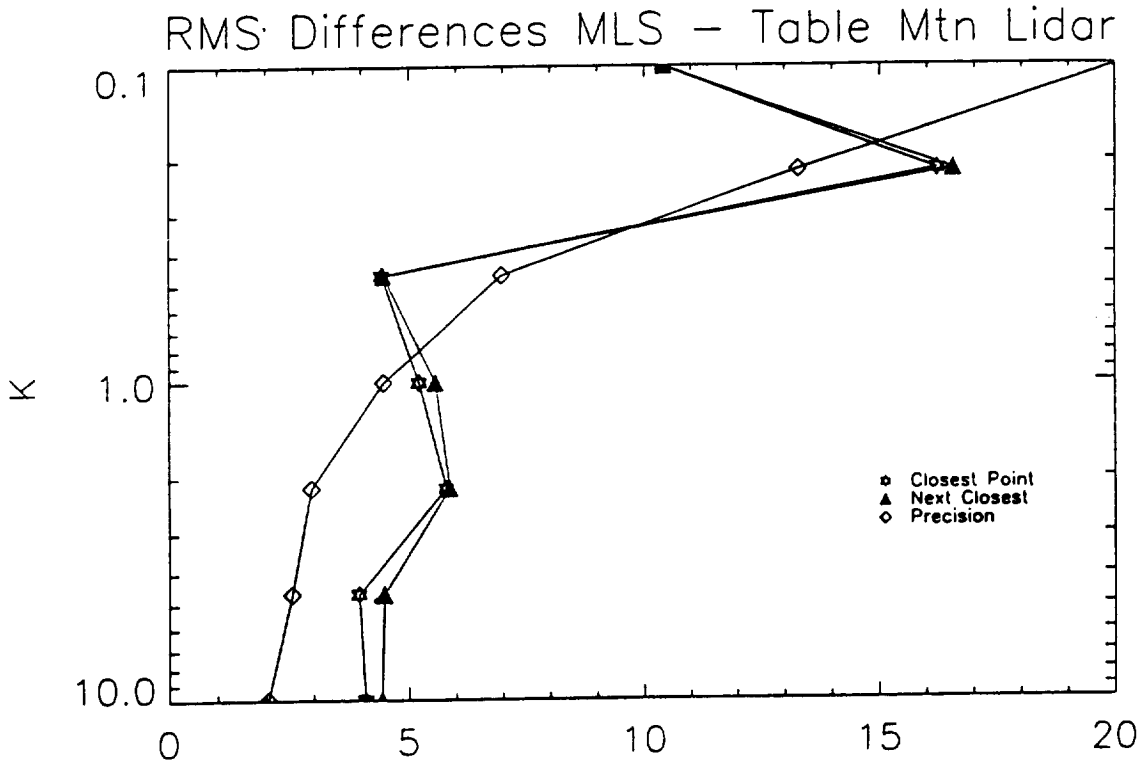

Figure 4.2.2.3–2

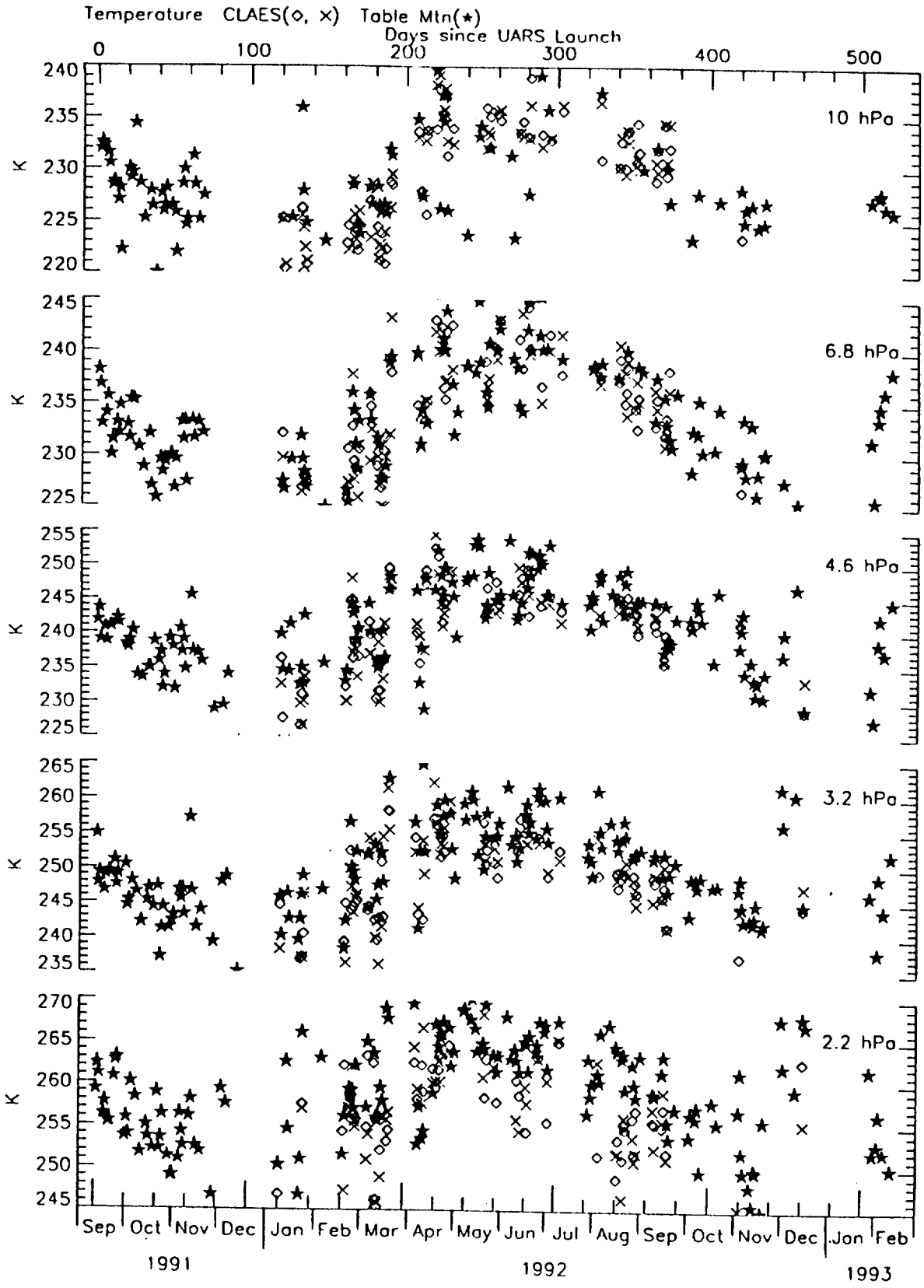

Figure 4.2.2.3–3

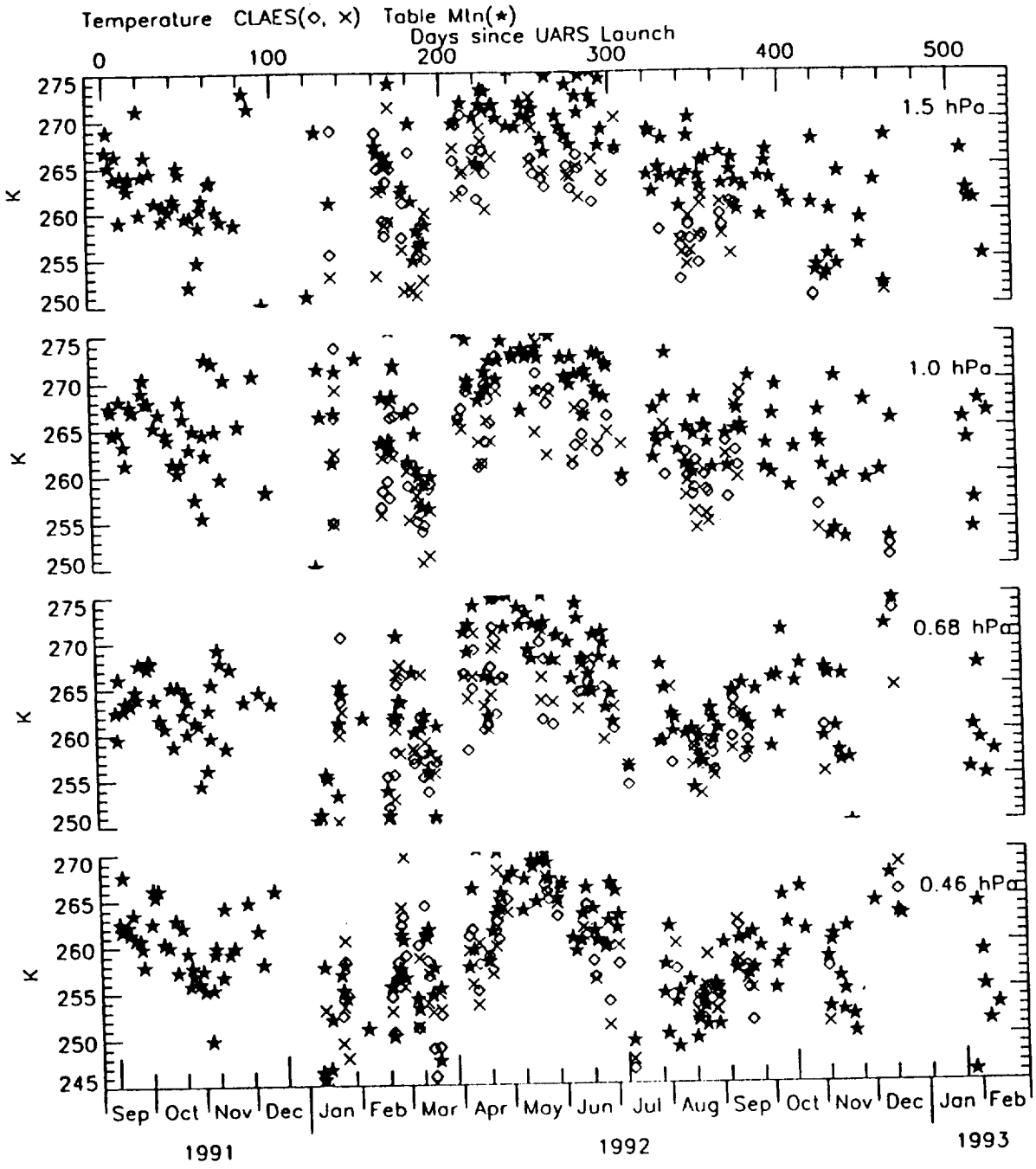

Figure 4.2.2.3-3 Concluded.

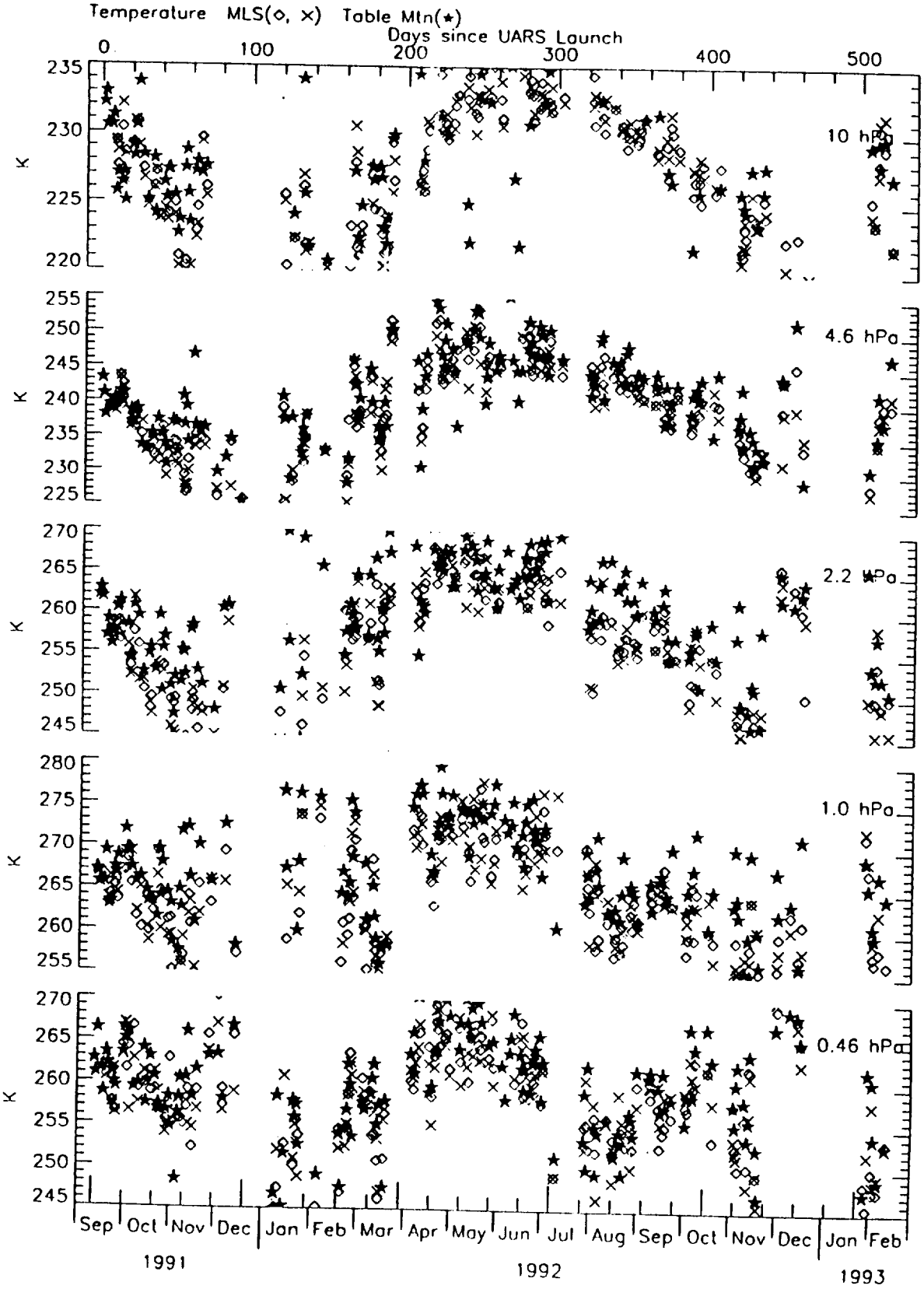

Figure 4.2.2.3–4

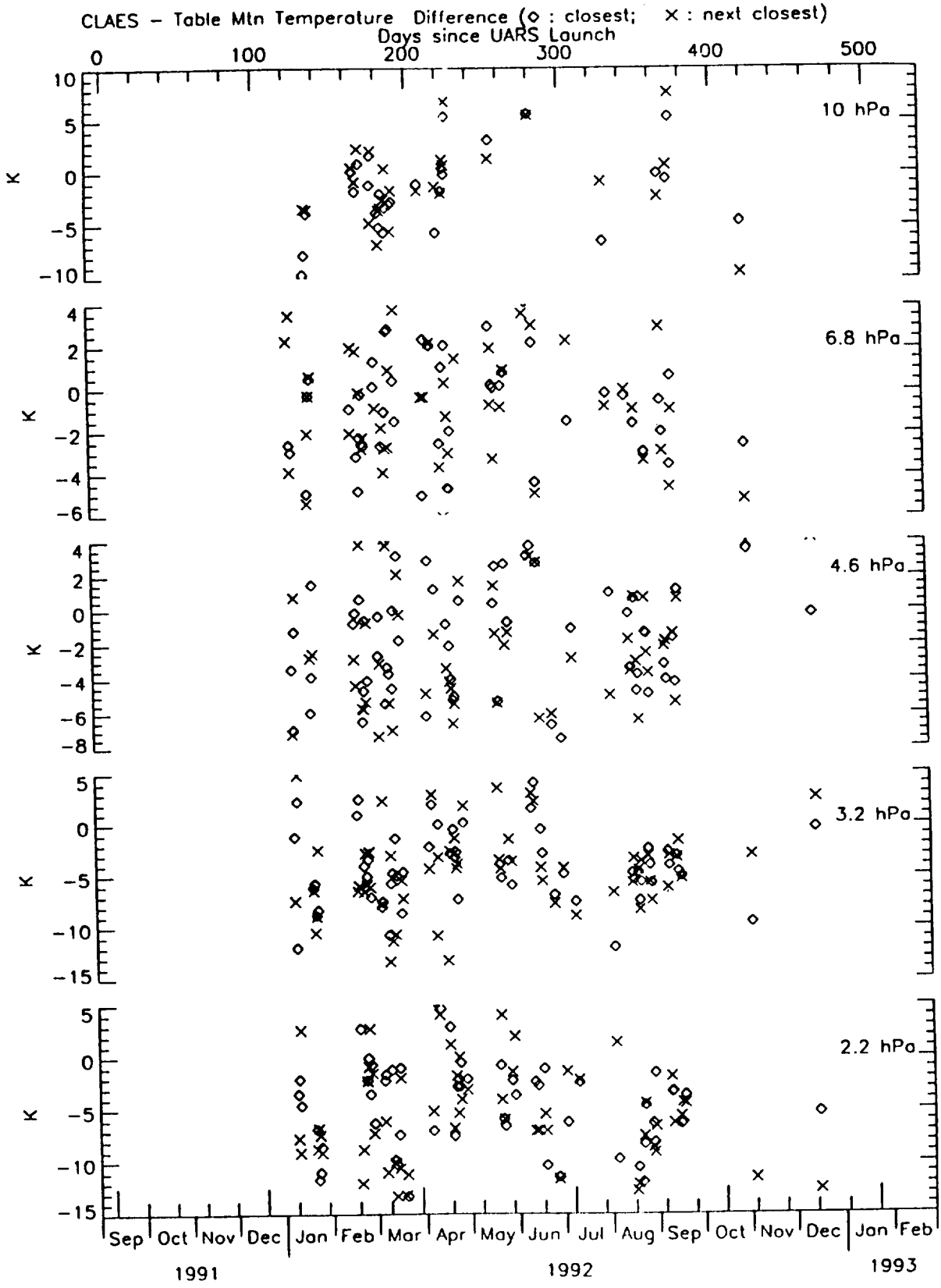

Figure 4.2.2.3–5

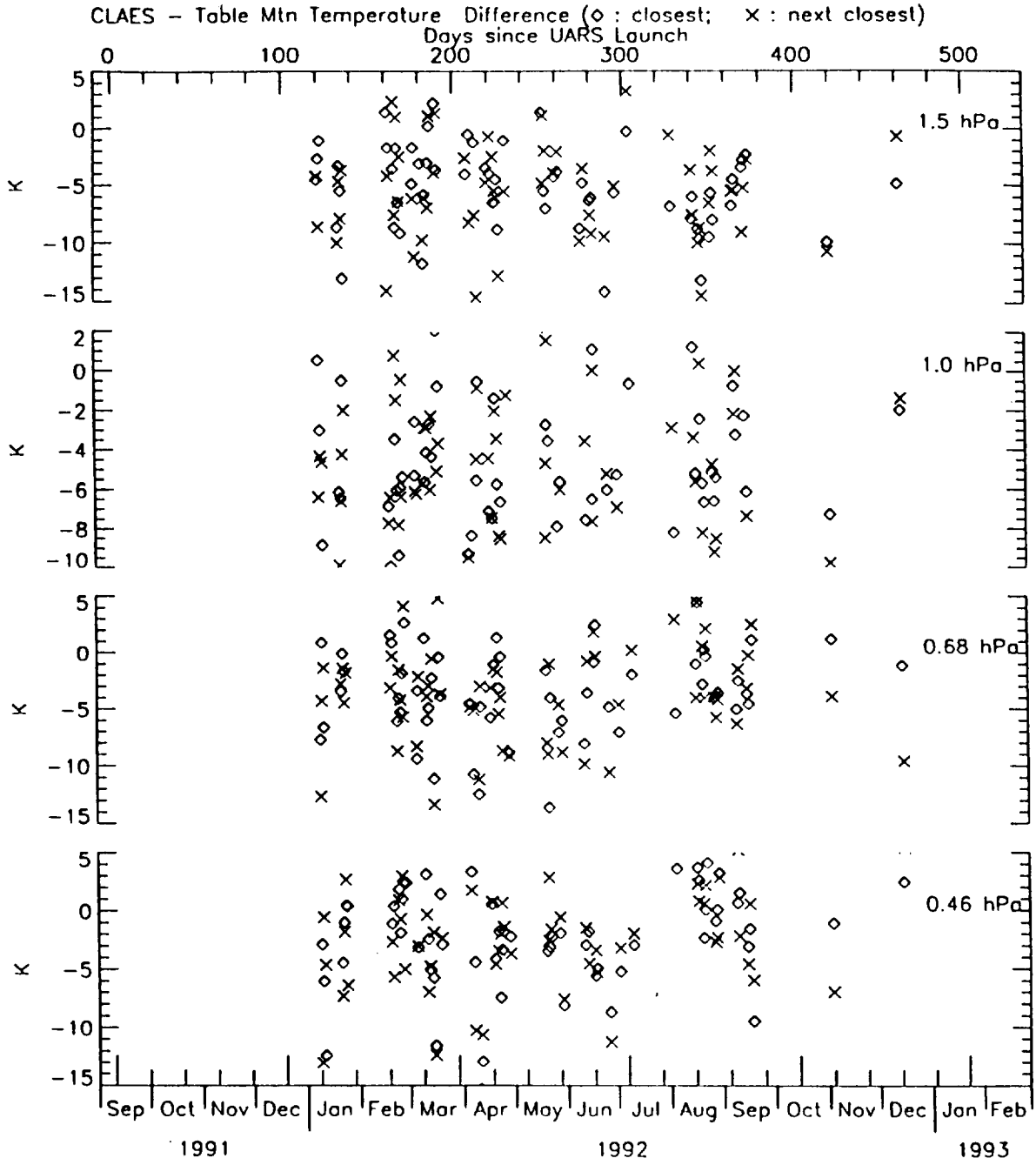

Figure 4.2.2.3-5 Concluded.

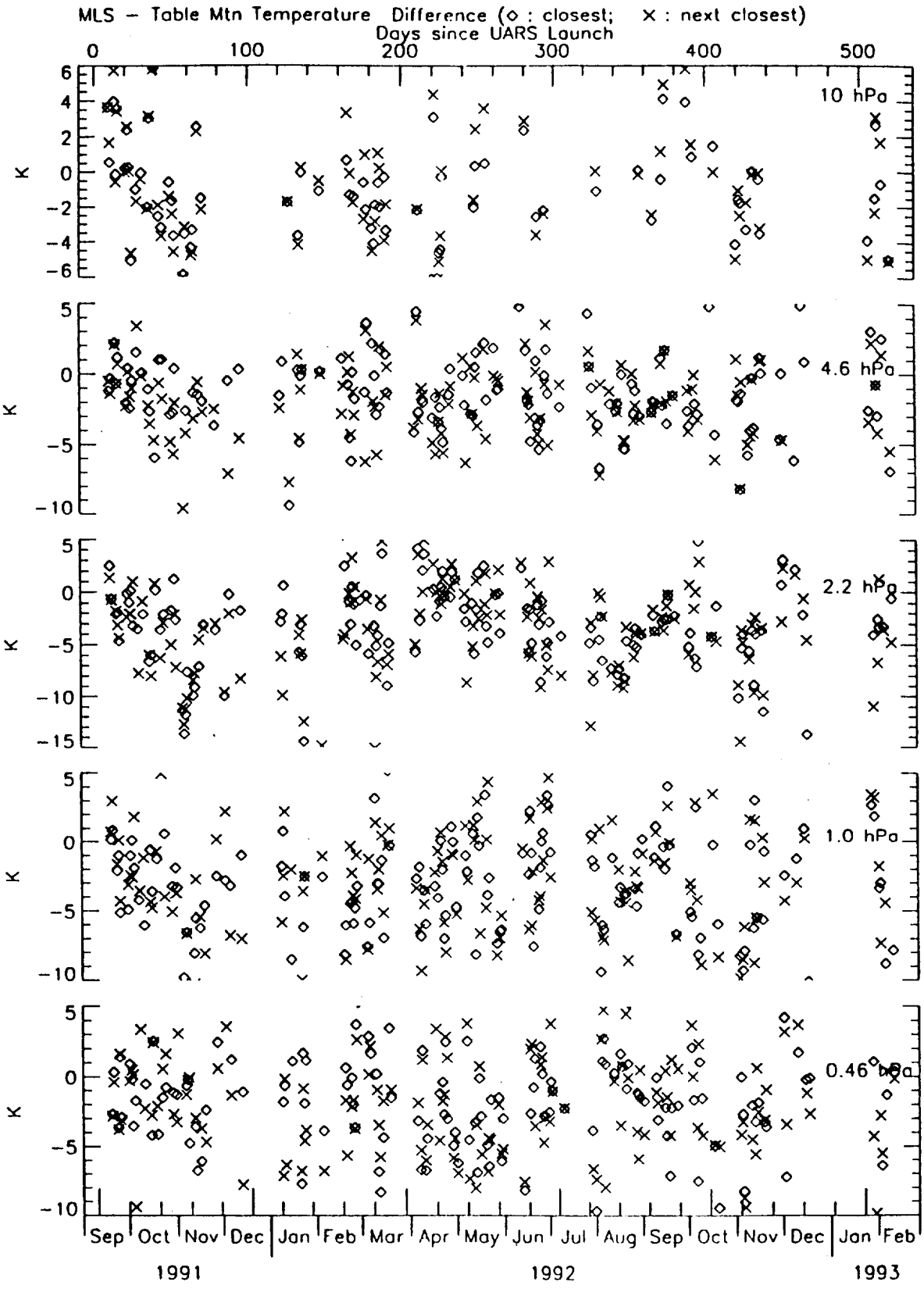

Figure 4.2.2.3–6

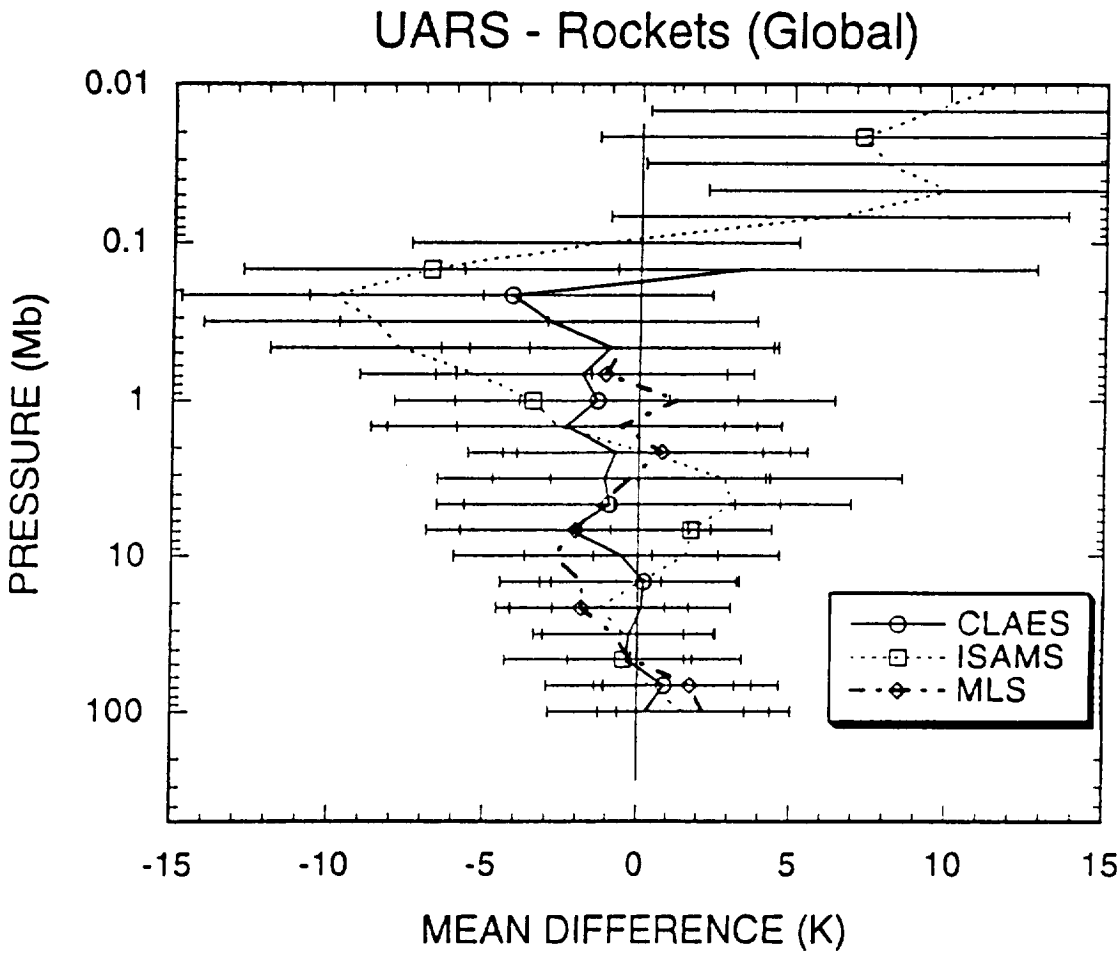

Figure 4.2.2.4–1

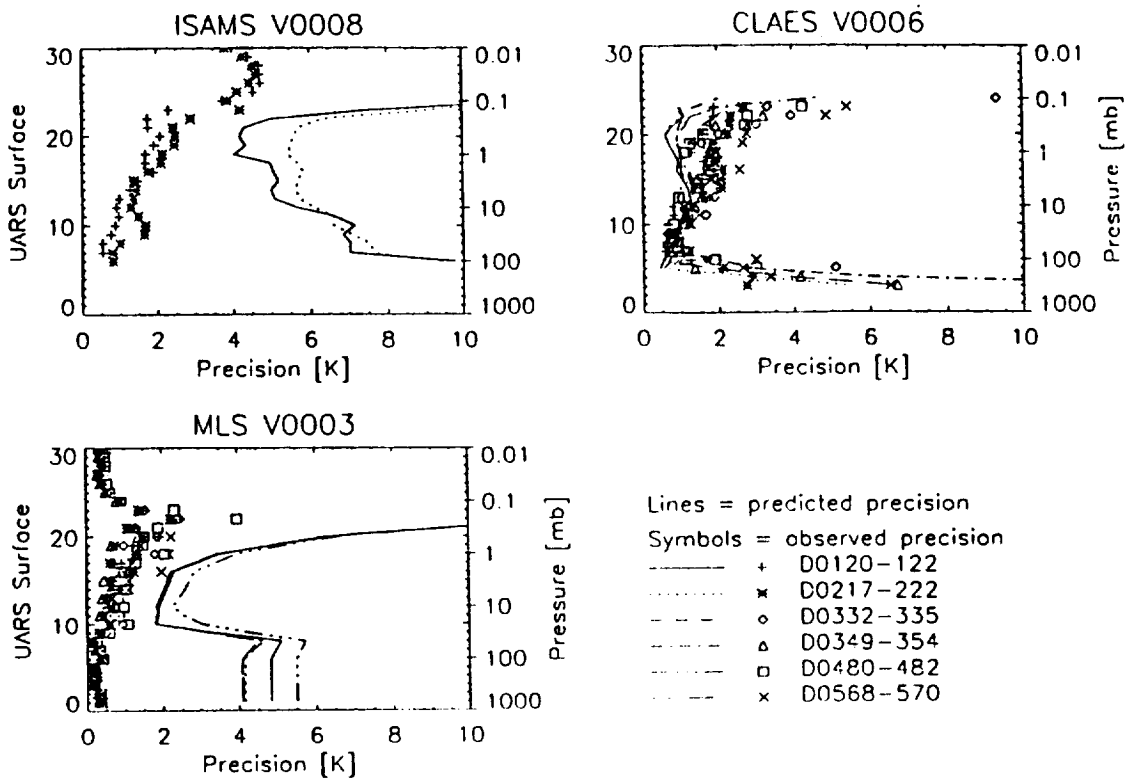

Figure 4.2.3–1

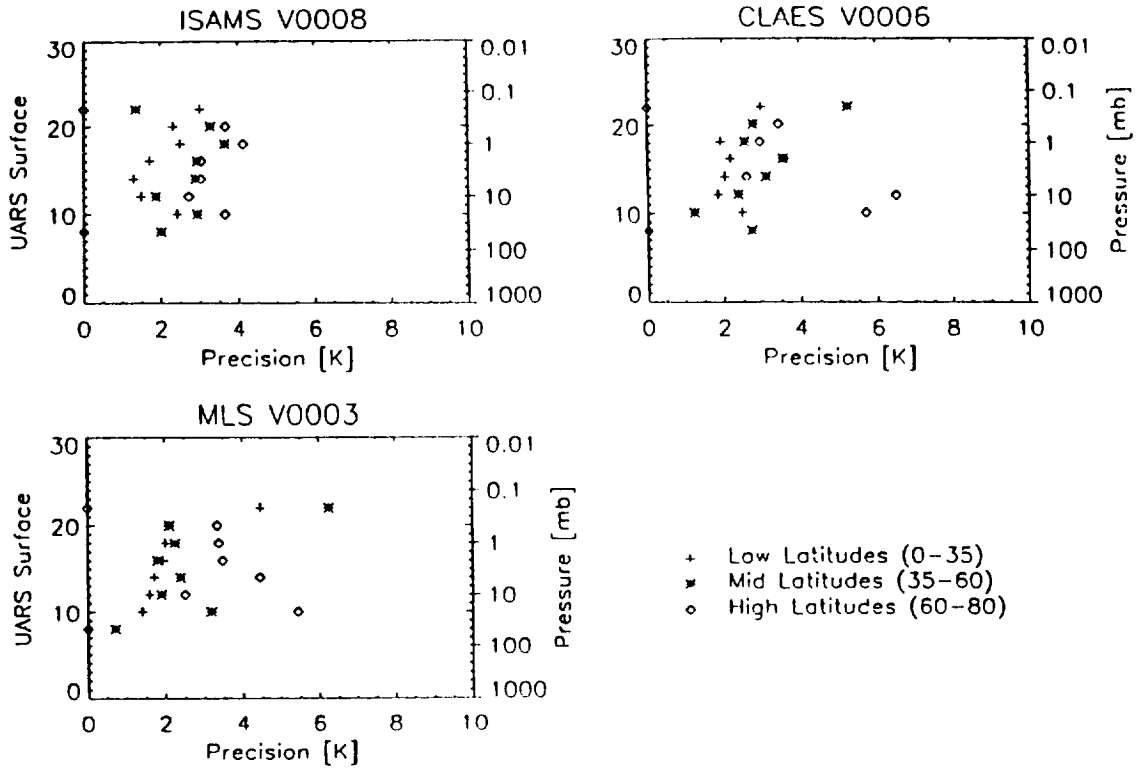

Figure 4.2.3–2

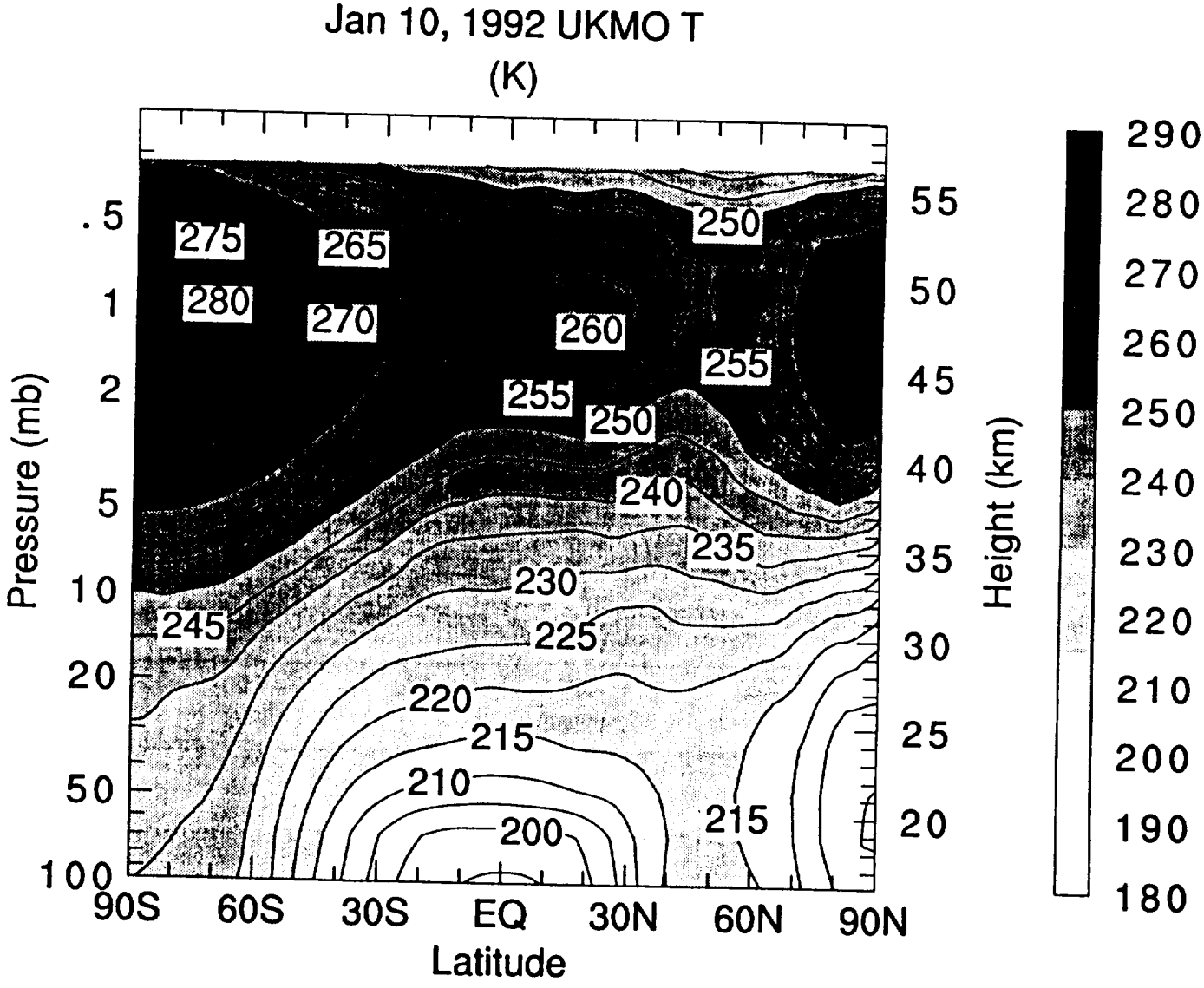
Jan 10, 1992 UKMO T
(K)
Pressure (mb)
.5
1
2
5
10
20
50
100
275
265
280
270
260
250
255
255
250
240
235
230
245
225
220
215
210
200
215
55
50
45
40
35
30
25
20
Height (km)
290
280
270
260
250
240
230
220
210
200
190
180
90S
60S
30S
EQ
30N
60N
90N
Latitude

Figure 4.3.1–1

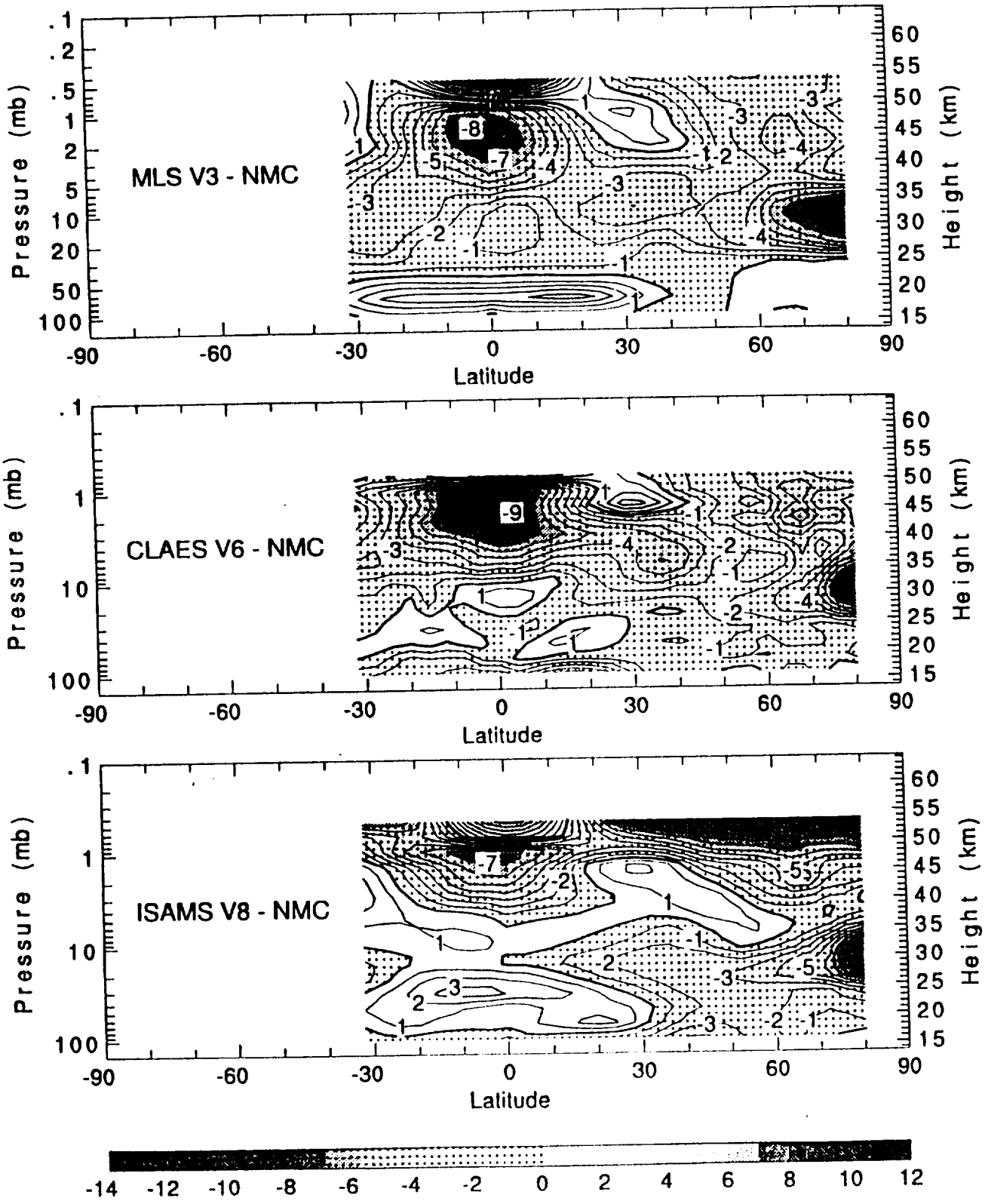
Jan 10, 1992 T Diff (K)
MLS V3 - NMC
CLAES V6 - NMC
ISAMS V8 - NMC
Pressure (mb)
Height (km)
Latitude
.1
.2
.5
1
2
5
10
20
50
100
60
55
50
45
40
35
30
25
20
15
-90
-60
-30
0
30
60
90
-14
-12
-10
-8
-6
-4
-2
0
2
4
6
8
10
12

Figure 4.3.1–2

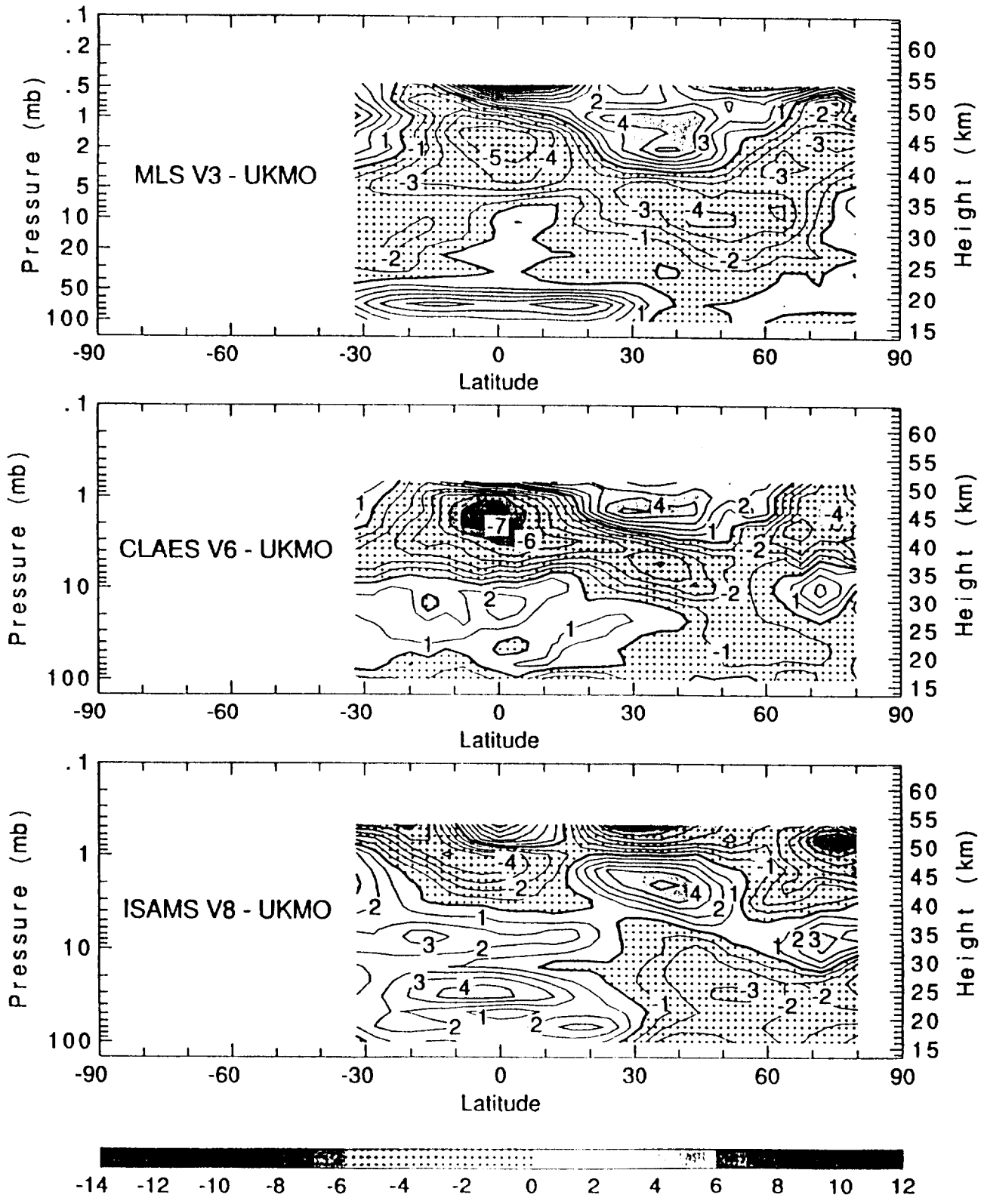
Jan 10, 1992 T Diff (K)
MLS V3 - UKMO
CLAES V6 - UKMO
ISAMS V8 - UKMO
Pressure (mb)
Height (km)
Latitude
.1
.2
.5
1
2
5
10
20
50
100
60
55
50
45
40
35
30
25
20
15
-90
-60
-30
0
30
60
90
-14
-12
-10
-8
-6
-4
-2
0
2
4
6
8
10
12

Figure 4.3.1–3

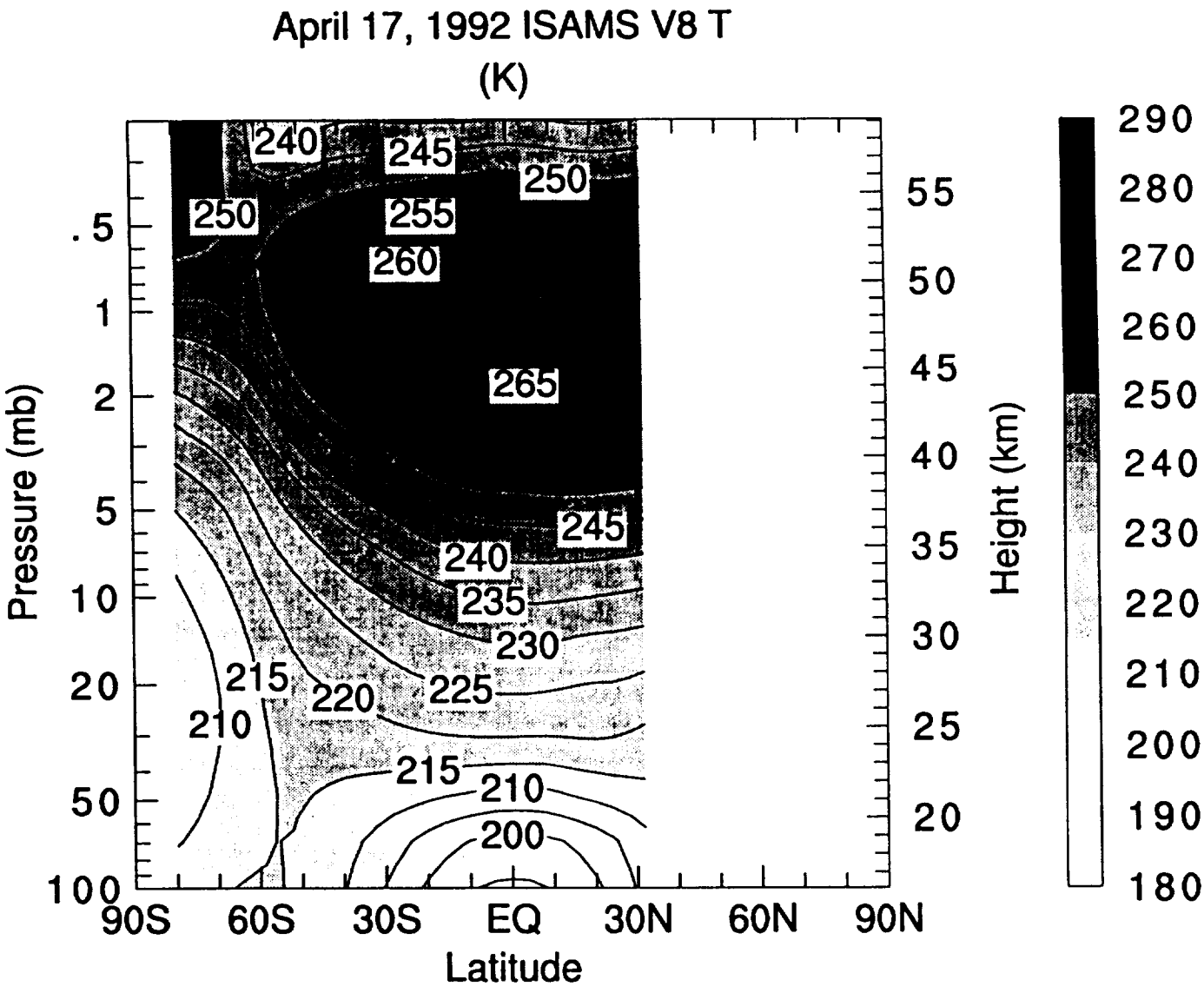
April 17, 1992 ISAMS V8 T
(K)
Pressure (mb)
.5
1
2
5
10
20
50
100
240
245
250
250
255
260
265
245
240
235
230
215
220
225
210
215
210
200
55
50
45
40
35
30
25
20
Height (km)
290
280
270
260
250
240
230
220
210
200
190
180
90S
60S
30S
EQ
30N
60N
90N
Latitude

Figure 4.3.1–4

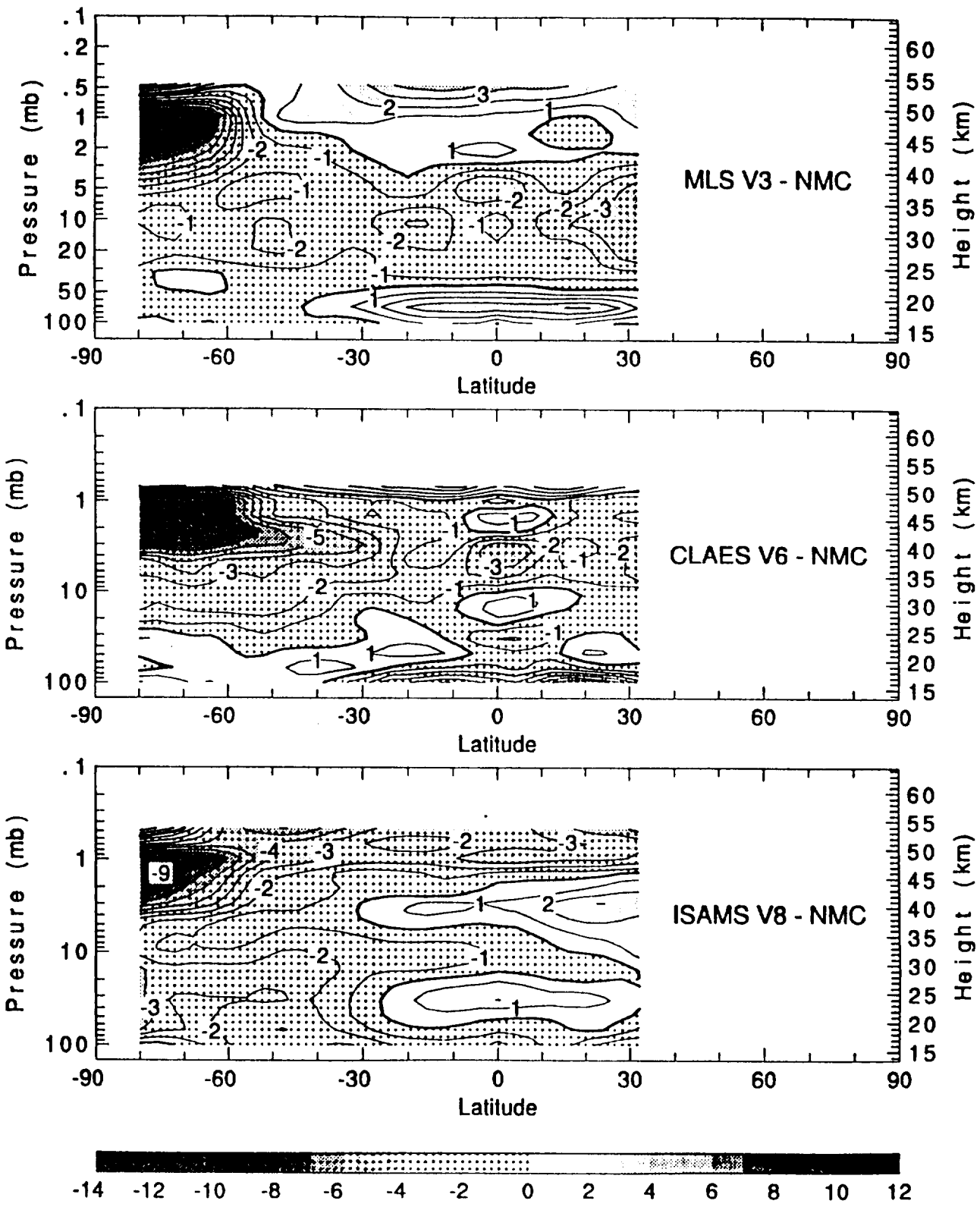
April 17, 1992 T Diff (K)
MLS V3 - NMC
CLAES V6 - NMC
ISAMS V8 - NMC
Pressure (mb)
Height (km)
Latitude
.1
.2
.5
1
2
5
10
20
50
100
60
55
50
45
40
35
30
25
20
15
-90
-60
-30
0
30
60
90
-14
-12
-10
-8
-6
-4
-2
0
2
4
6
8
10
12

Figure 4.3.1–5

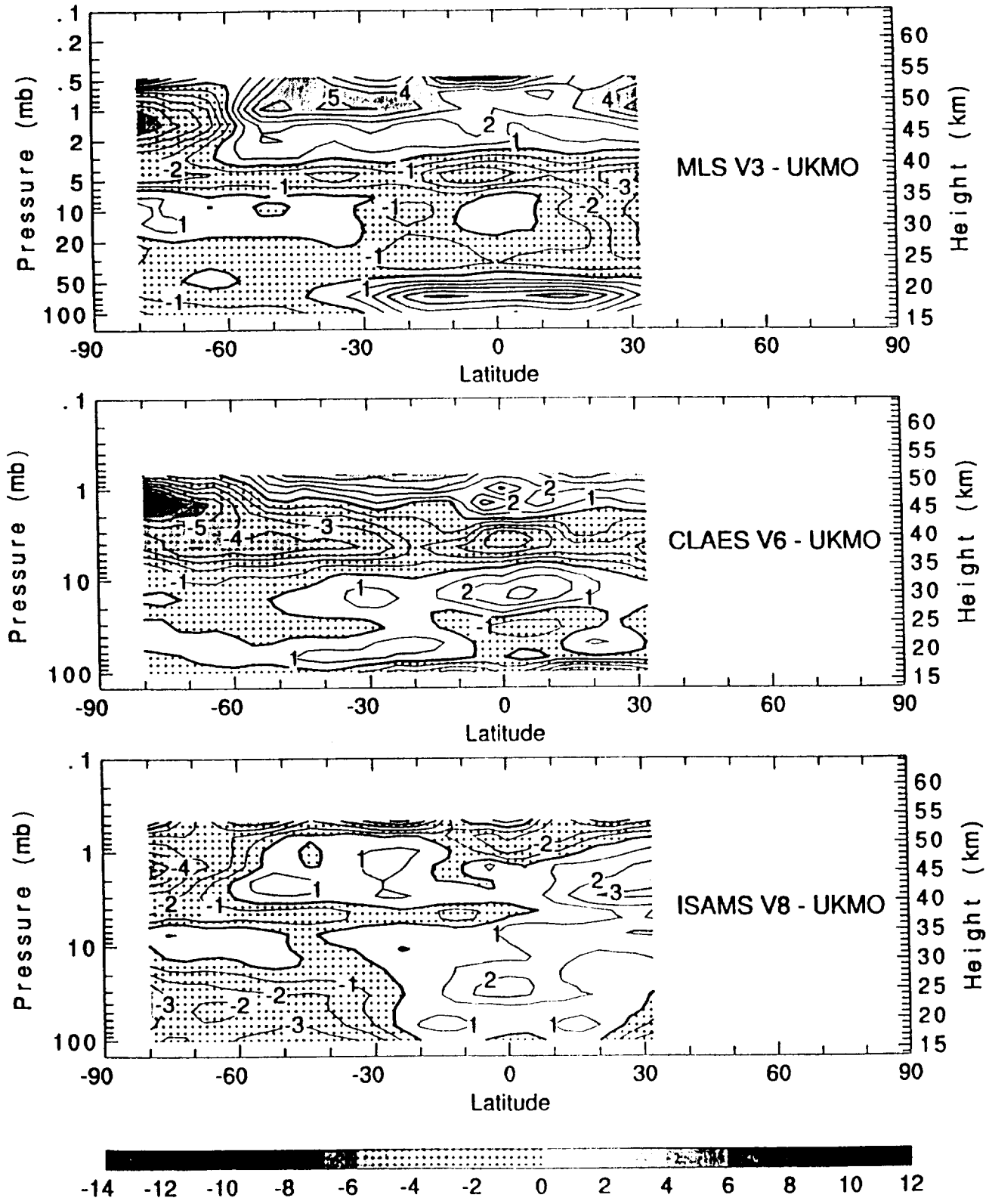
April 17, 1992 T Diff (K)
MLS V3 - UKMO
CLAES V6 - UKMO
ISAMS V8 - UKMO
Pressure (mb)
Height (km)
Latitude
.1
.2
.5
1
2
5
10
20
50
100
60
55
50
45
40
35
30
25
20
15
-90
-60
-30
0
30
60
90
-14
-12
-10
-8
-6
-4
-2
0
2
4
6
8
10
12

Figure 4.3.1–6

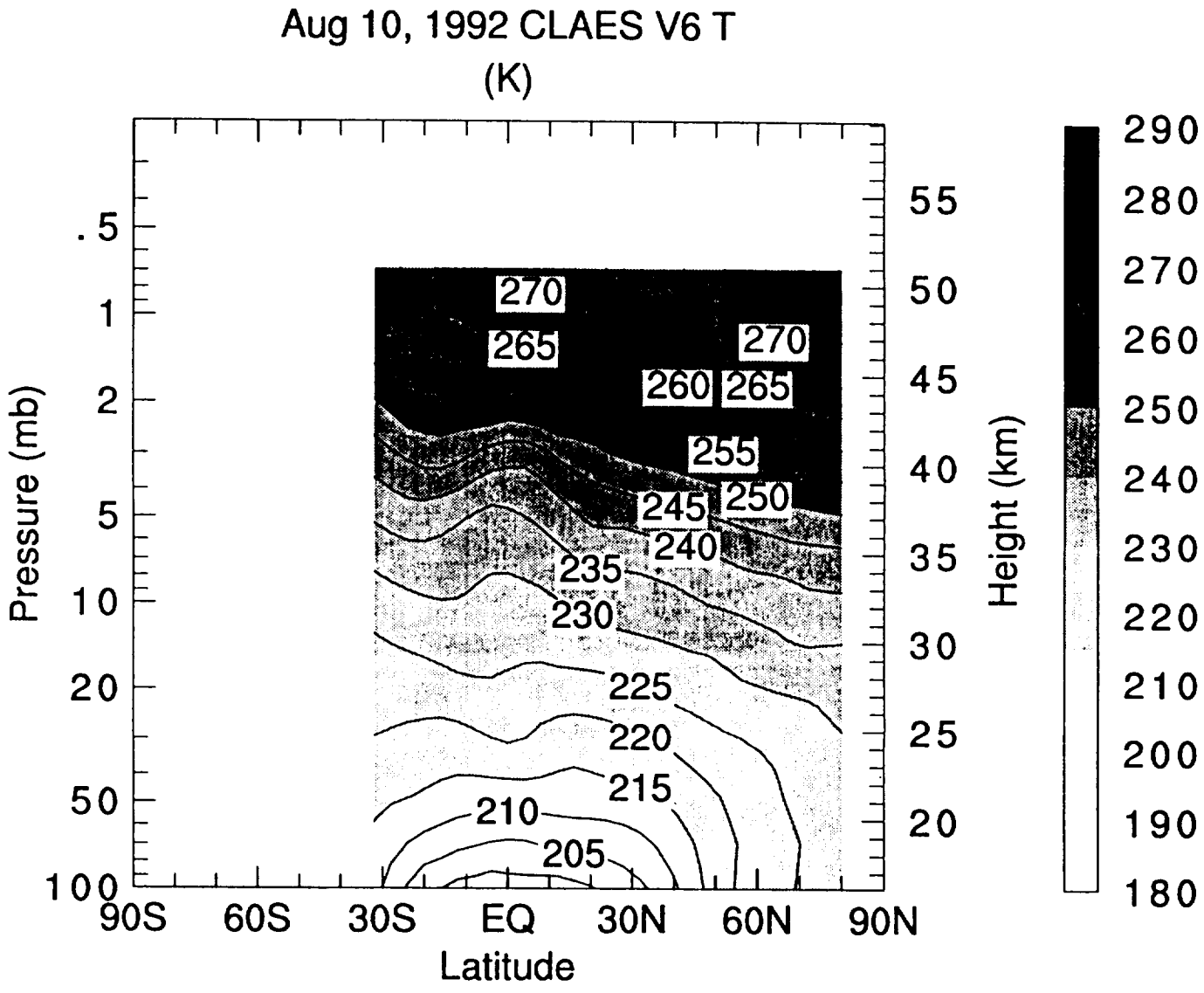
Aug 10, 1992 CLAES V6 T
(K)
Pressure (mb)
.5
1
2
5
10
20
50
100
90S
60S
30S
EQ
30N
60N
90N
Latitude
55
50
45
40
35
30
25
20
Height (km)
290
280
270
260
250
240
230
220
210
200
190
180
270
265
270
260
265
255
245
250
240
235
230
225
220
215
210
205

Figure 4.3.1–7

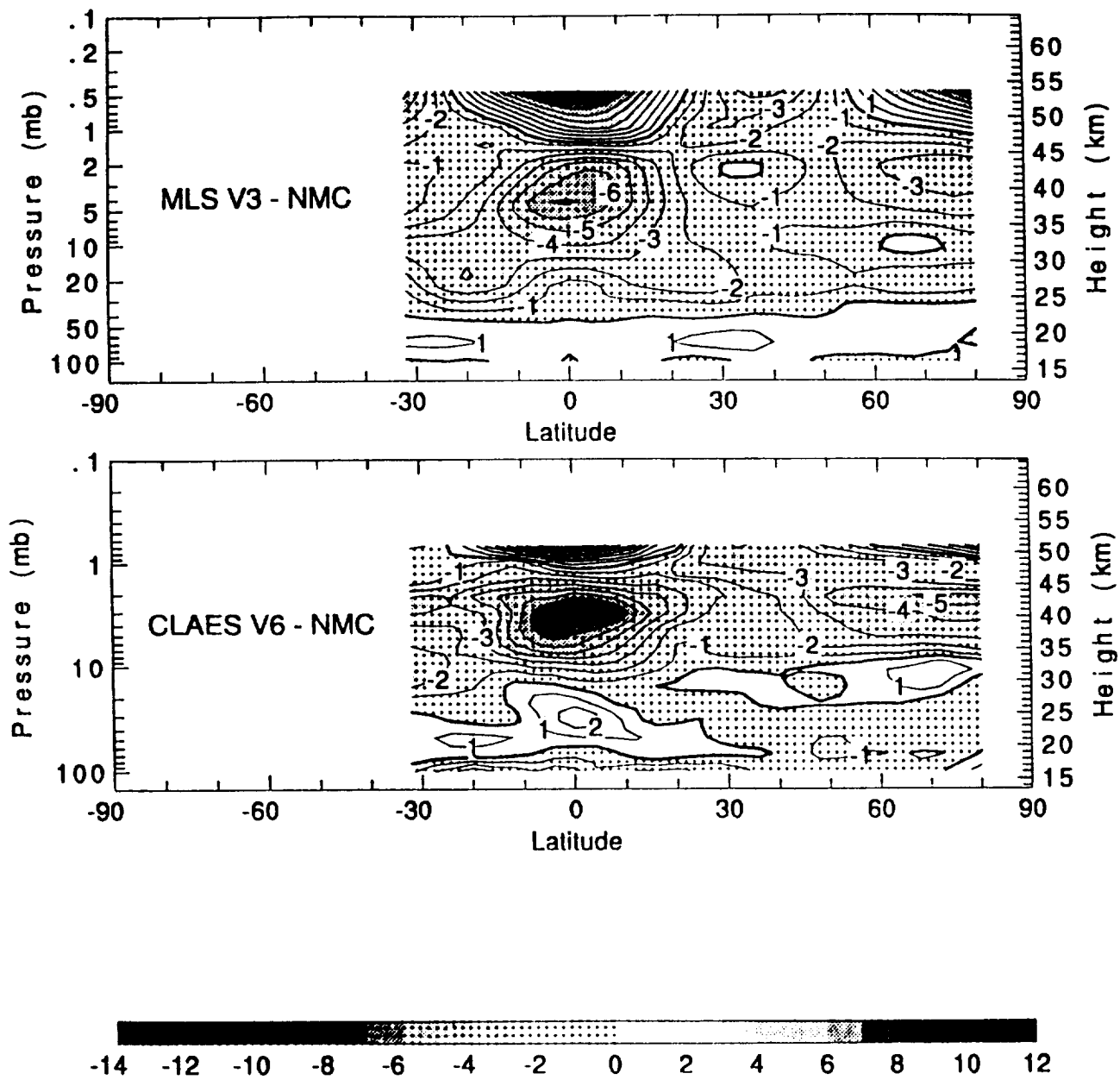
Aug 10, 1992 T Diff (K)
MLS V3 - NMC
CLAES V6 - NMC
Pressure (mb)
Height (km)
Latitude
-90
-60
-30
0
30
60
90
-14
-12
-10
-8
-6
-4
-2
0
2
4
6
8
10
12

Figure 4.3.1-8

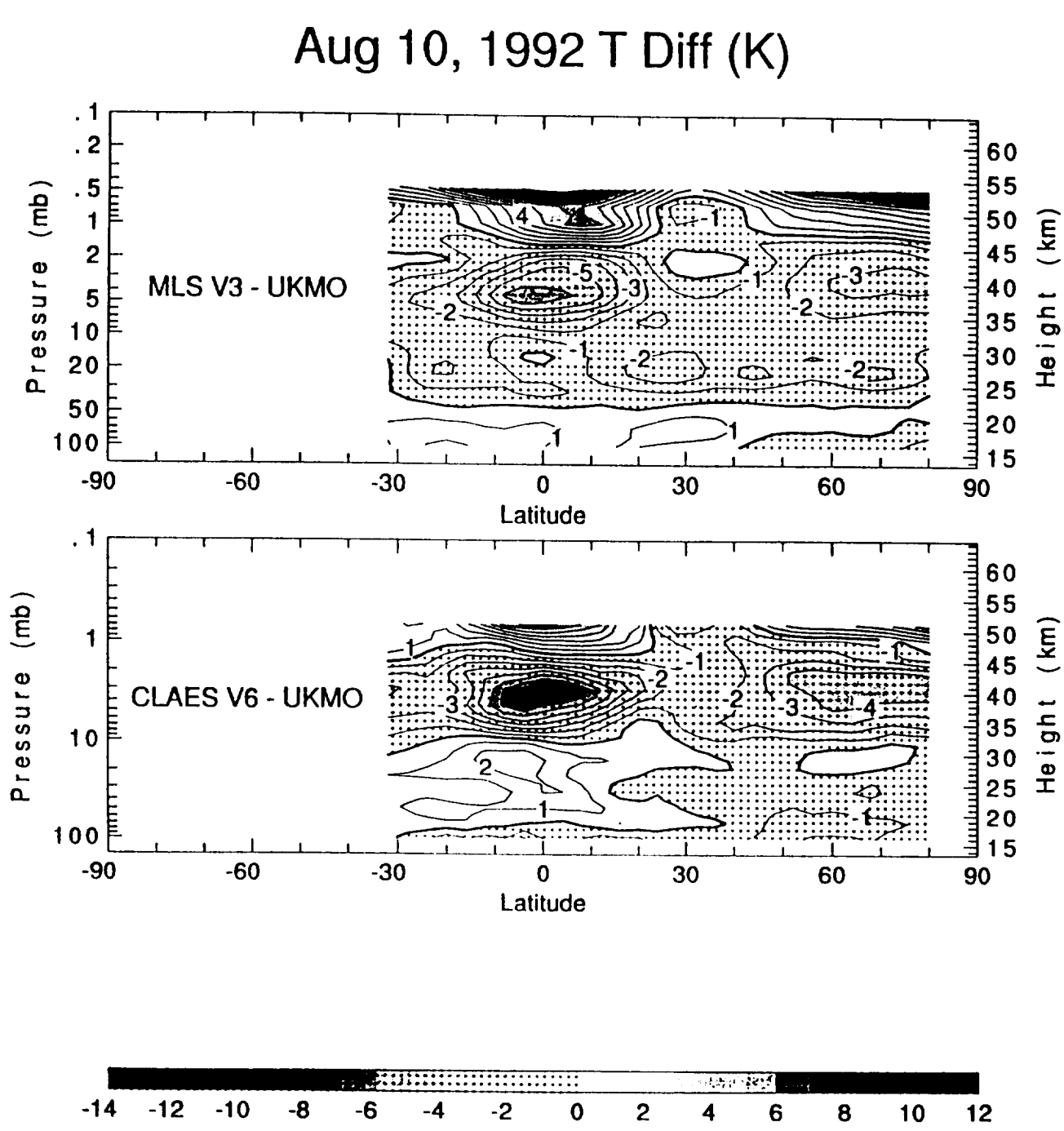
Aug 10, 1992 T Diff (K)
MLS V3 - UKMO
CLAES V6 - UKMO
Pressure (mb)
Height (km)
Latitude
.1
.2
.5
1
2
5
10
20
50
100
60
55
50
45
40
35
30
25
20
15
-90
-60
-30
0
30
60
90
-14
-12
-10
-8
-6
-4
-2
0
2
4
6
8
10
12

Figure 4.3.1–9

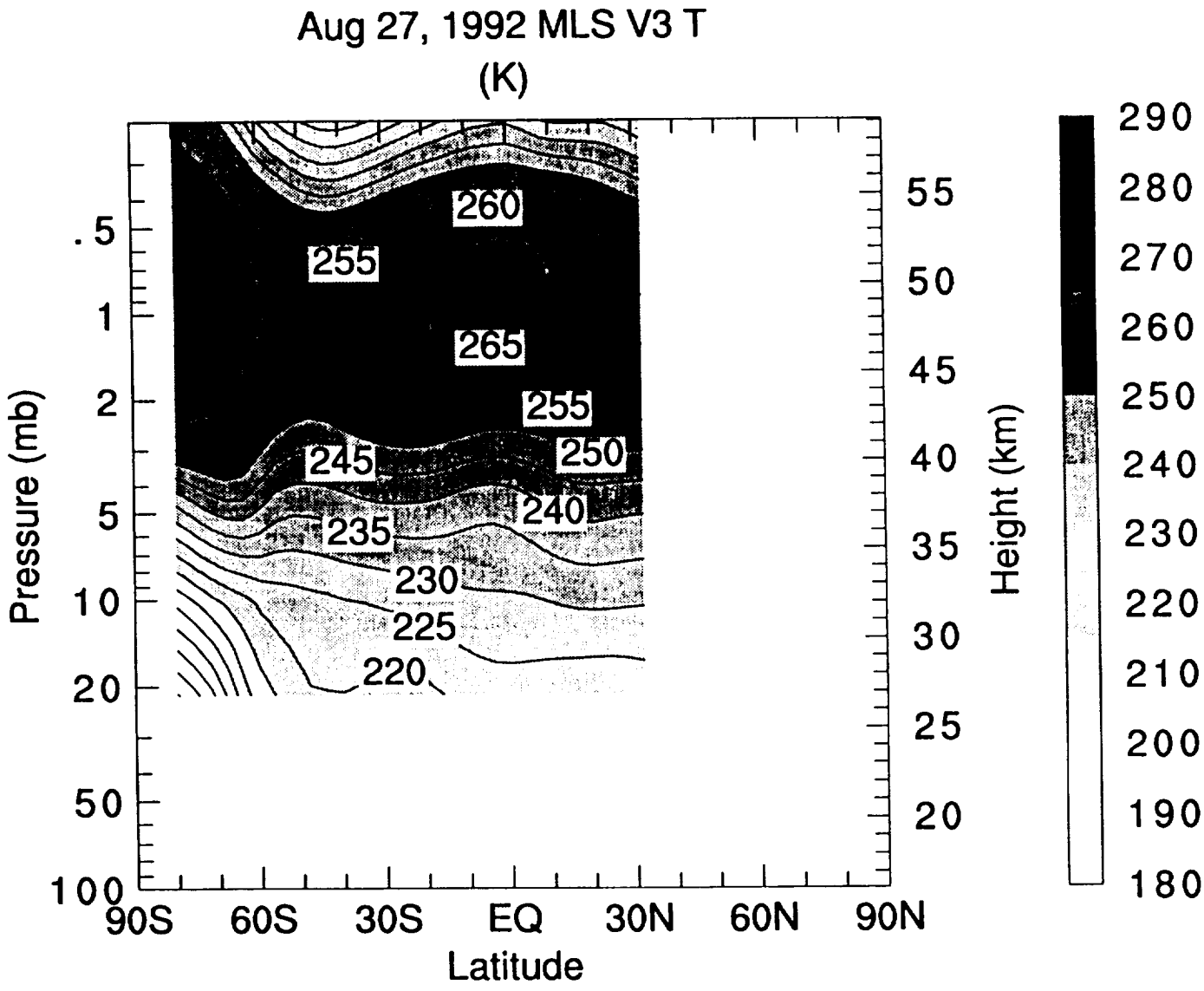

Figure 4.3.1–10

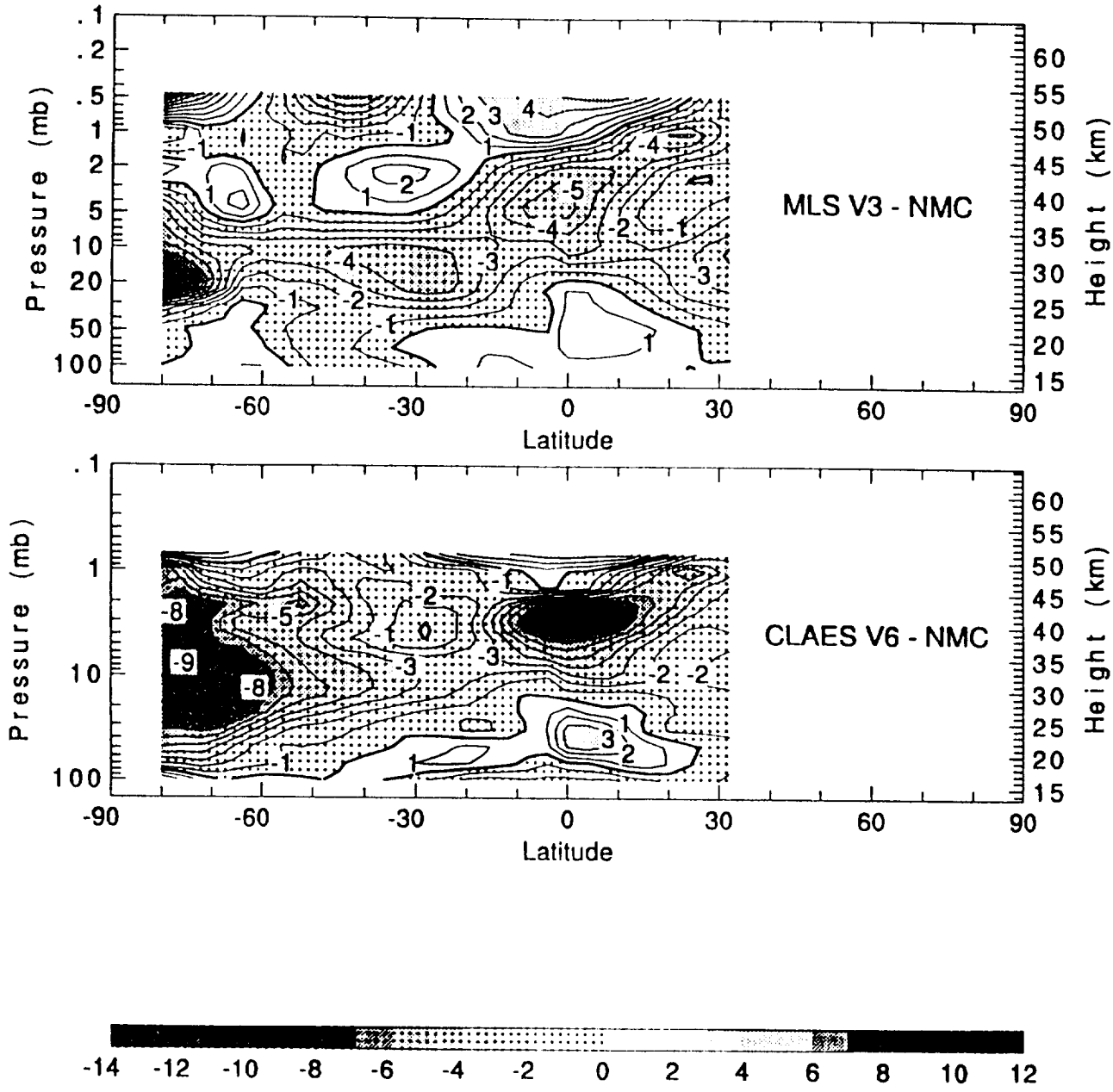

Figure 4.3.1–11

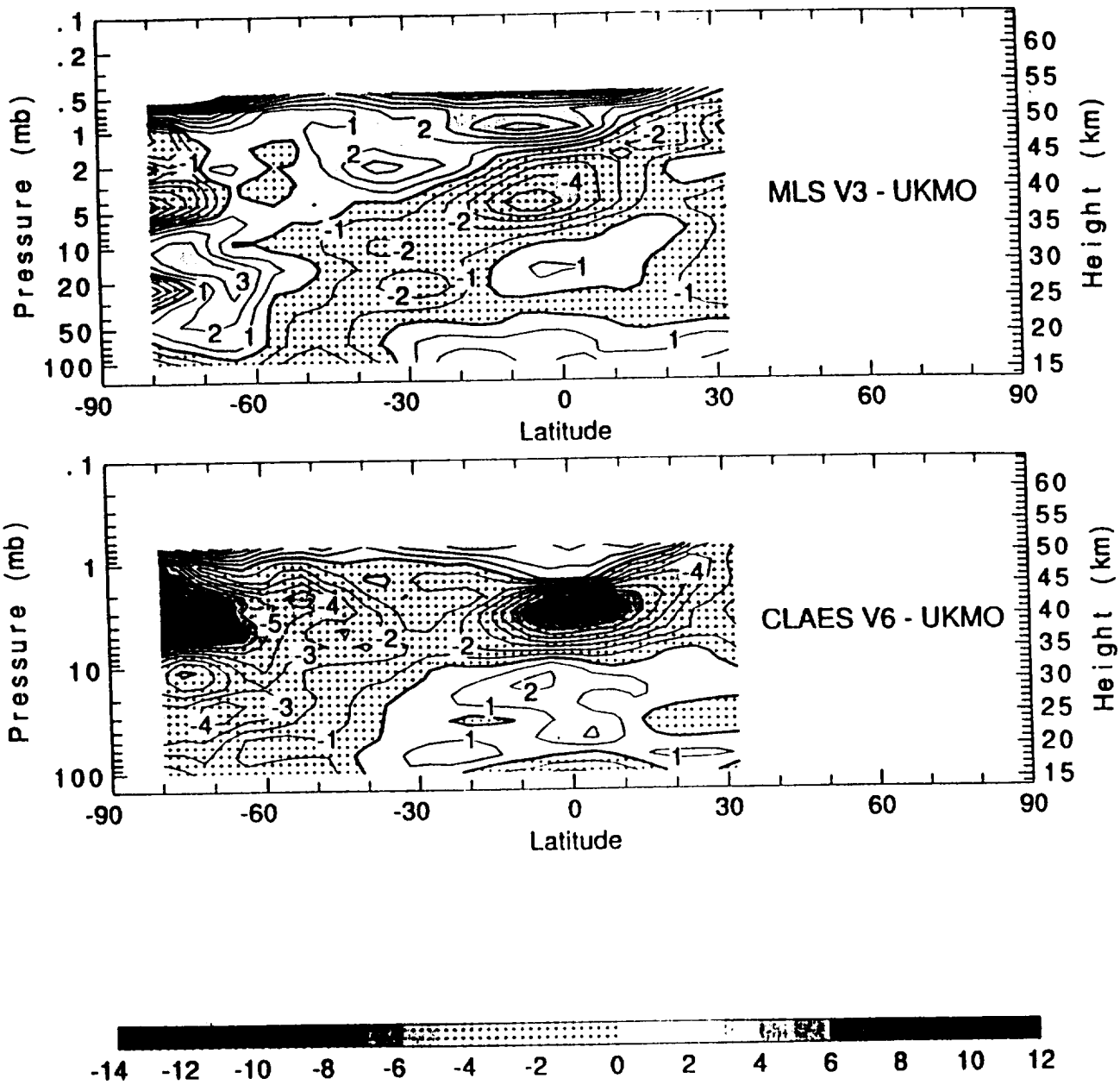

Figure 4.3.1–12

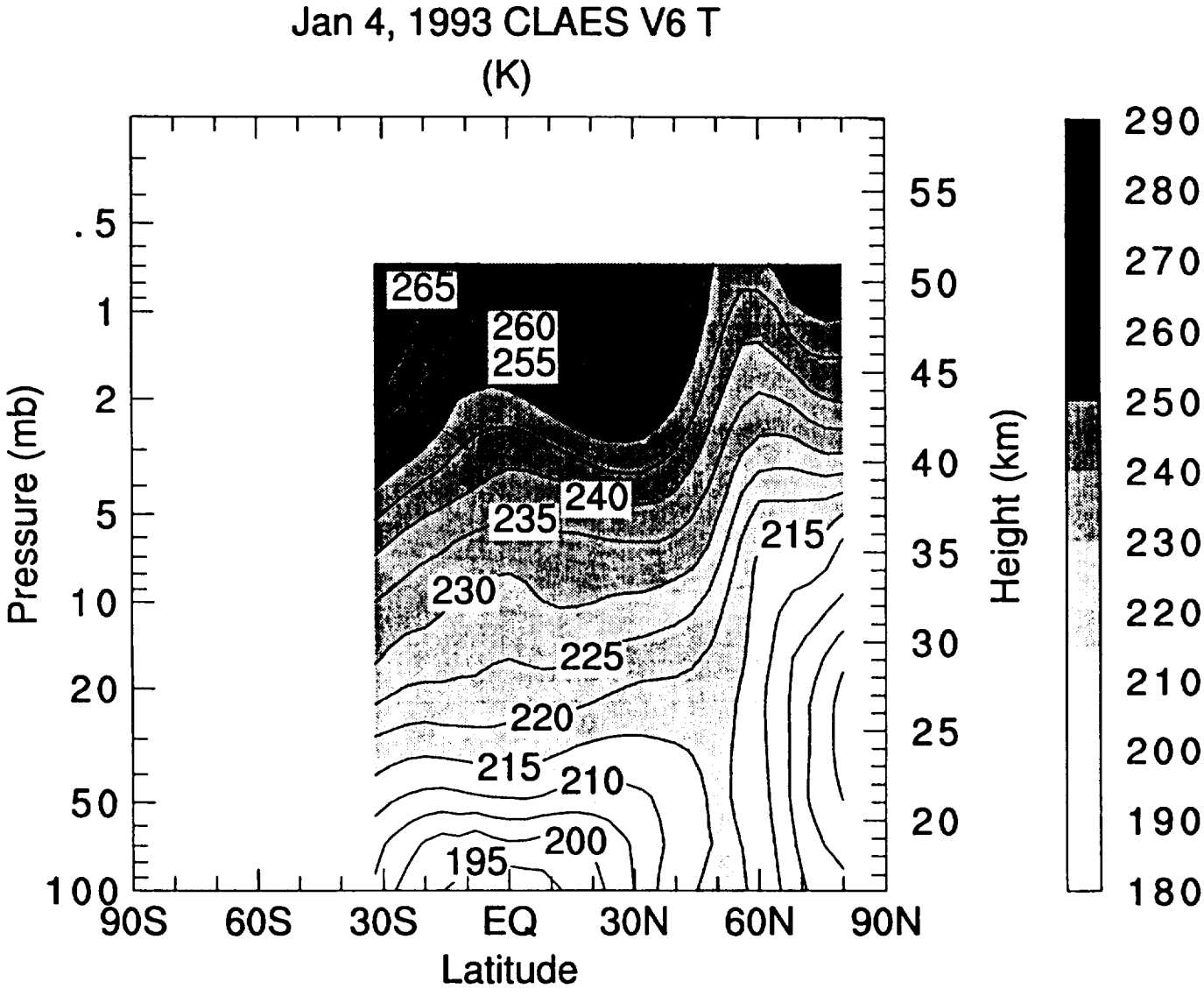

Figure 4.3.1–13

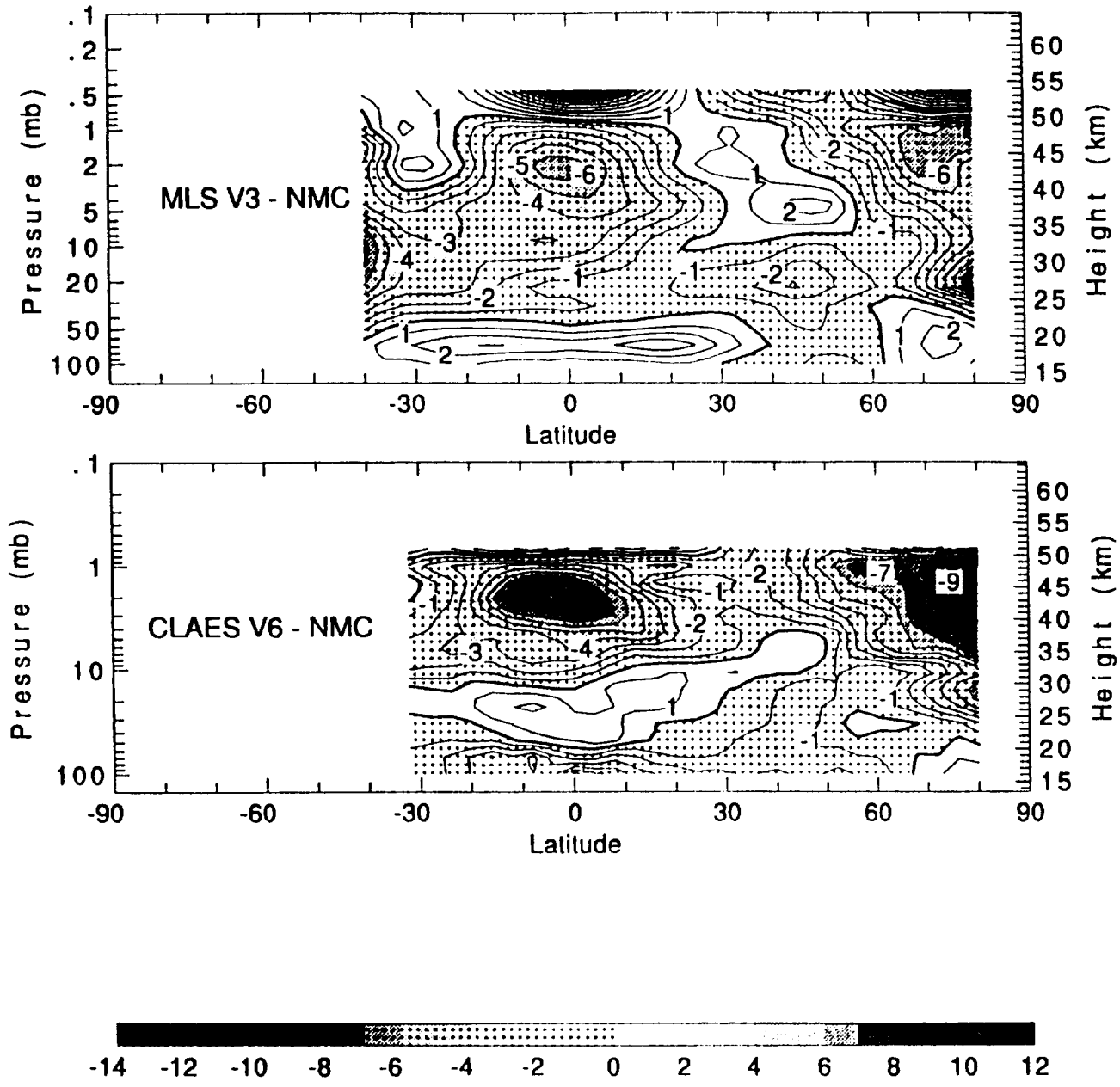

Figure 4.3.1–14

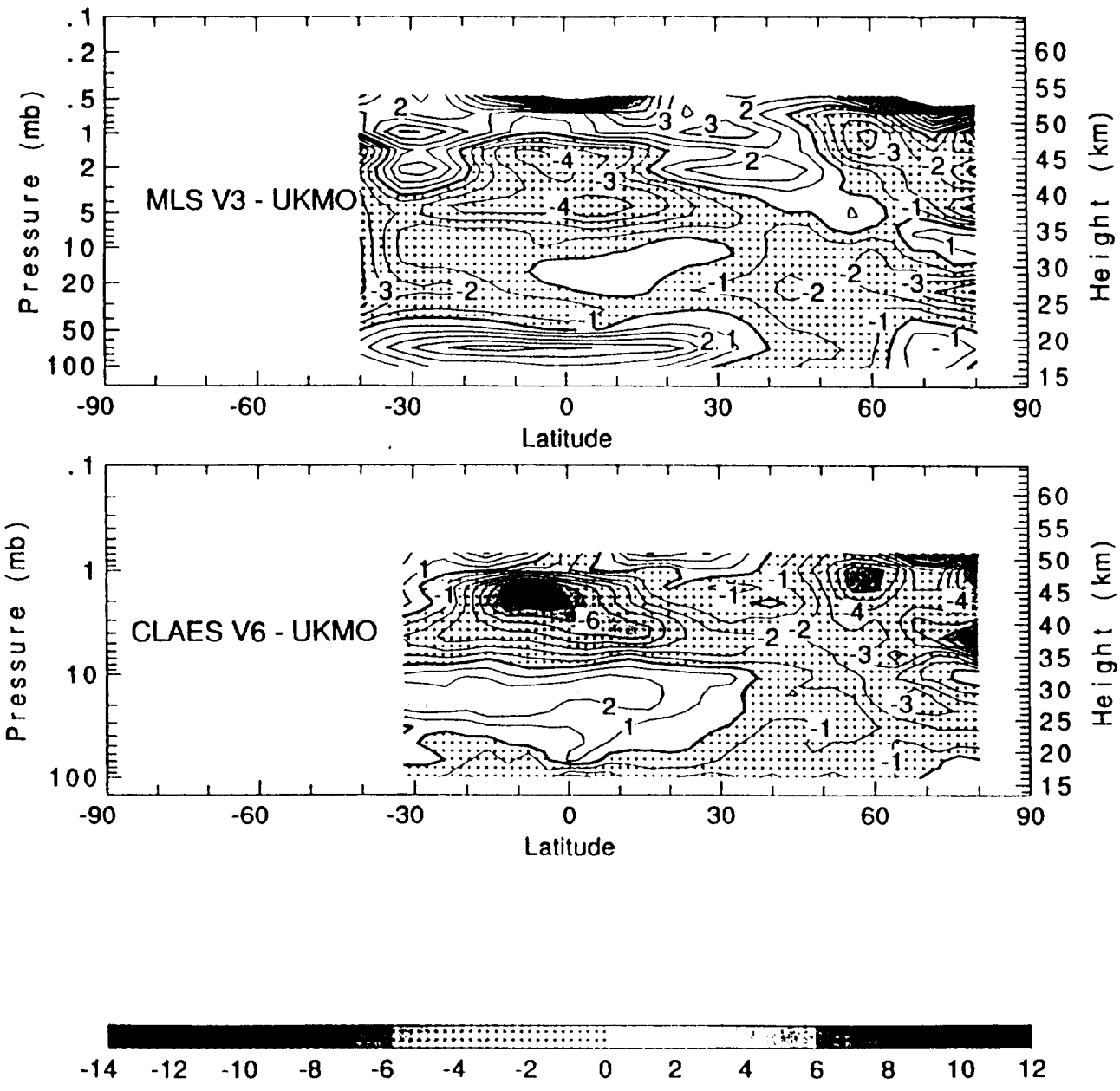

Figure 4.3.1–15

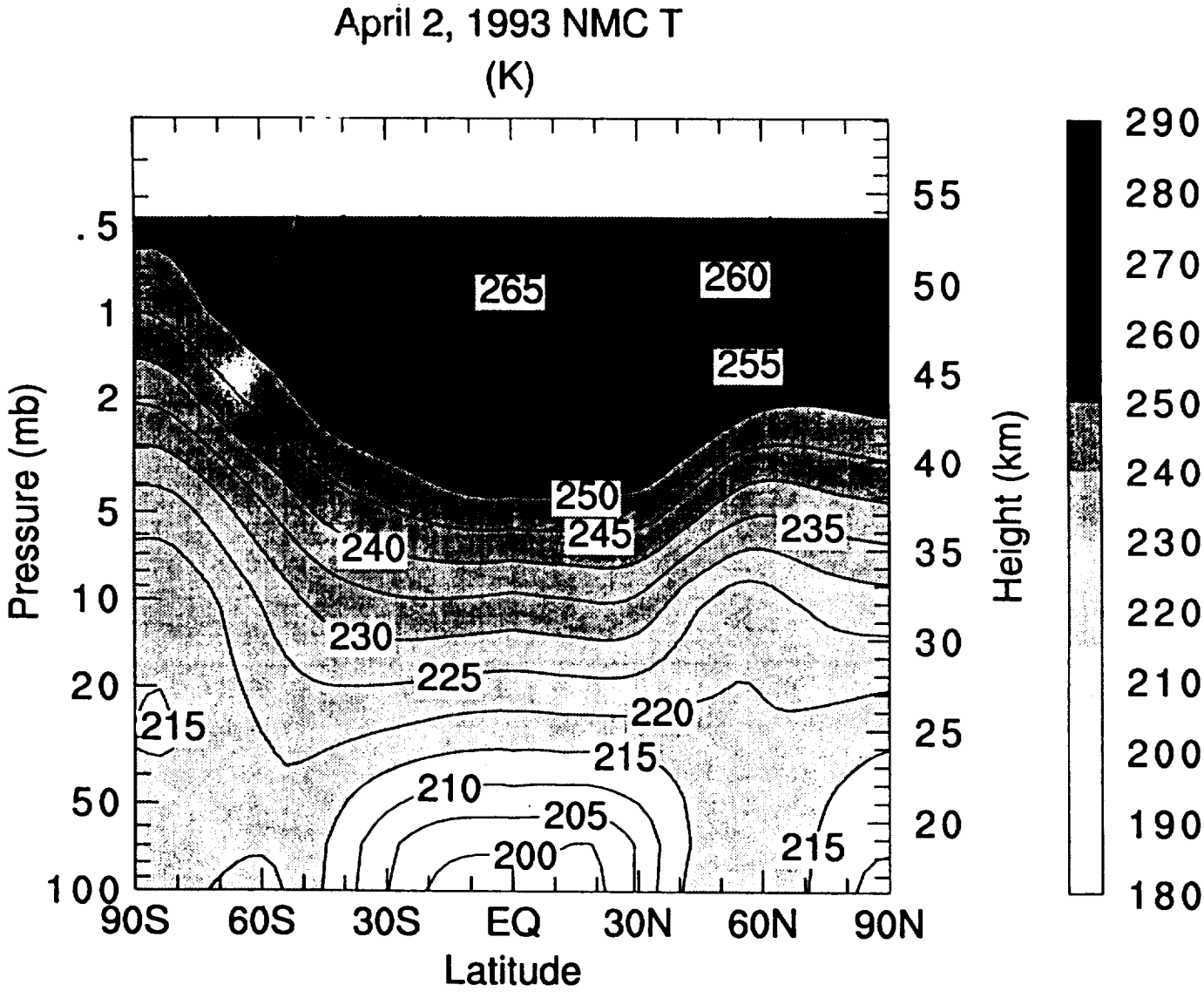

Figure 4.3.1–16

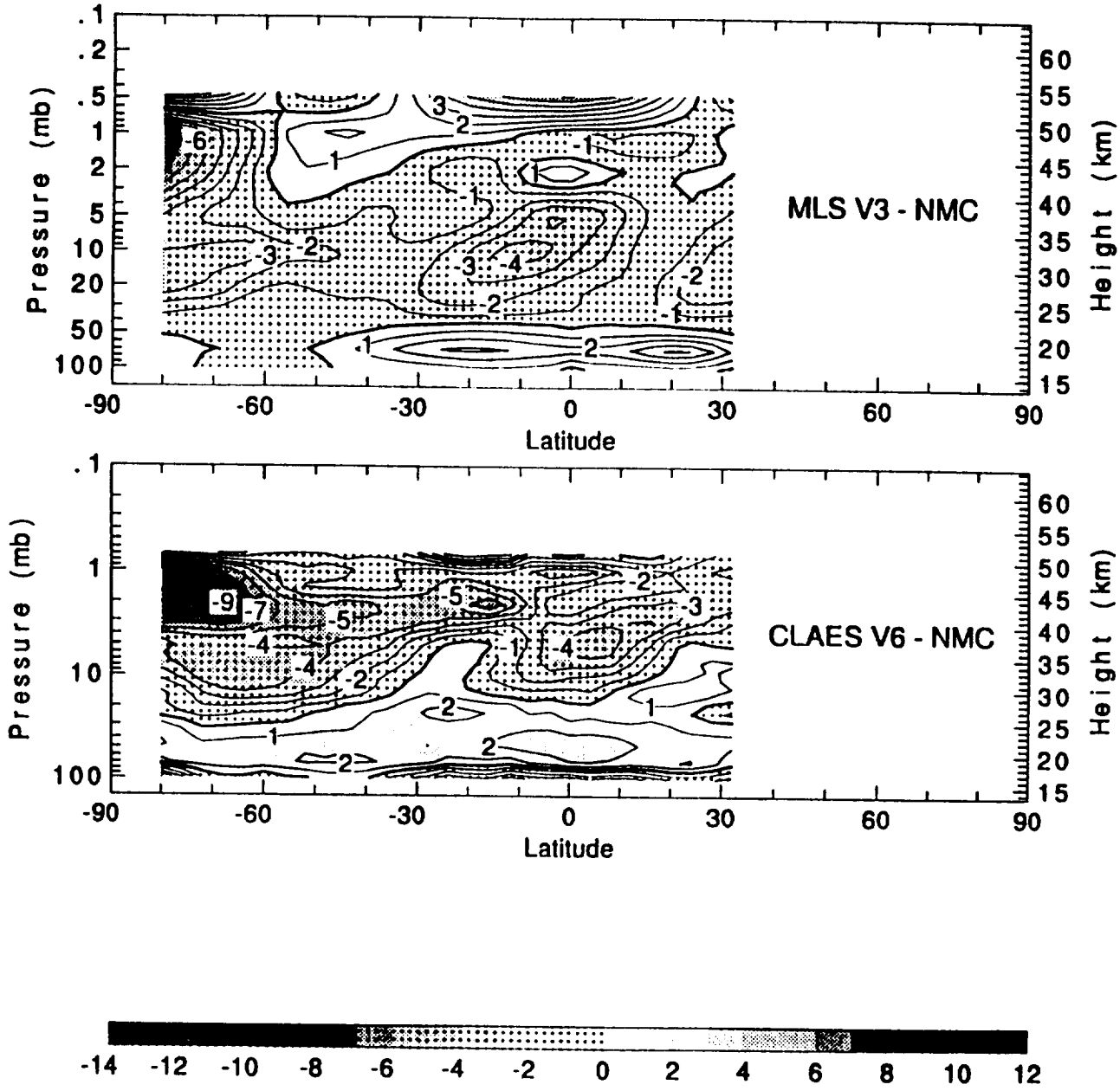

Figure 4.3.1–17

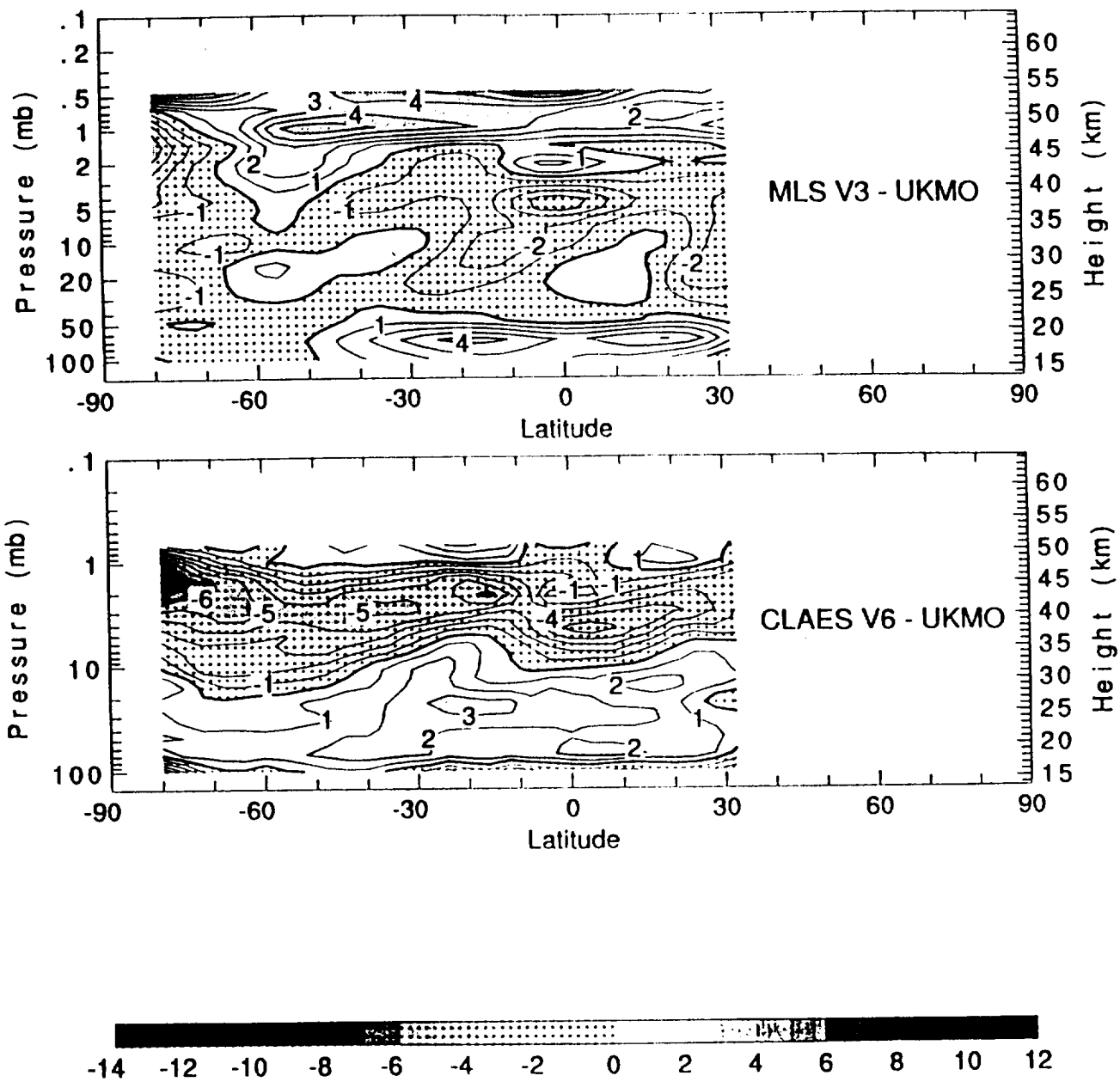

Figure 4.3.1–18

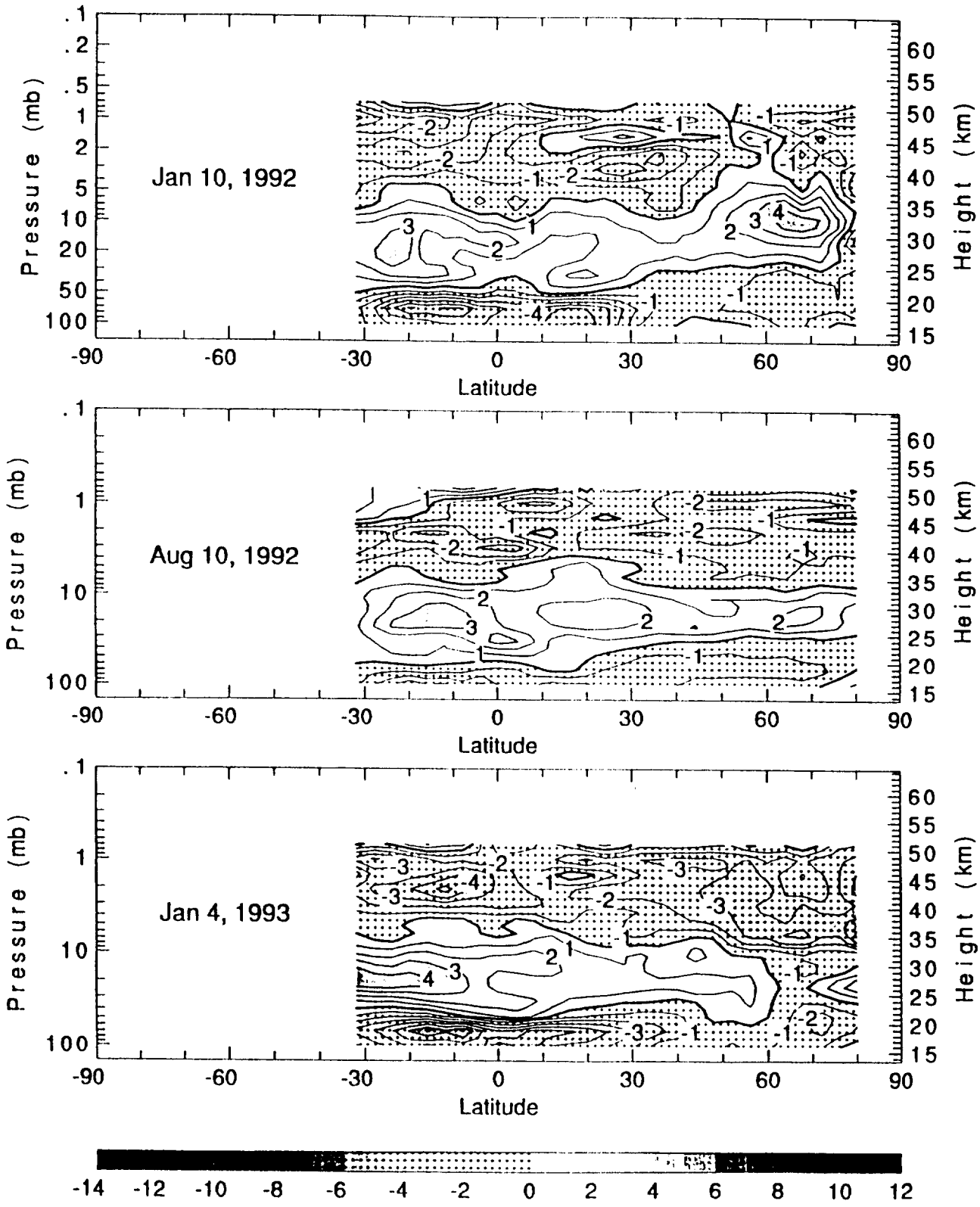

Figure 4.3.1–19

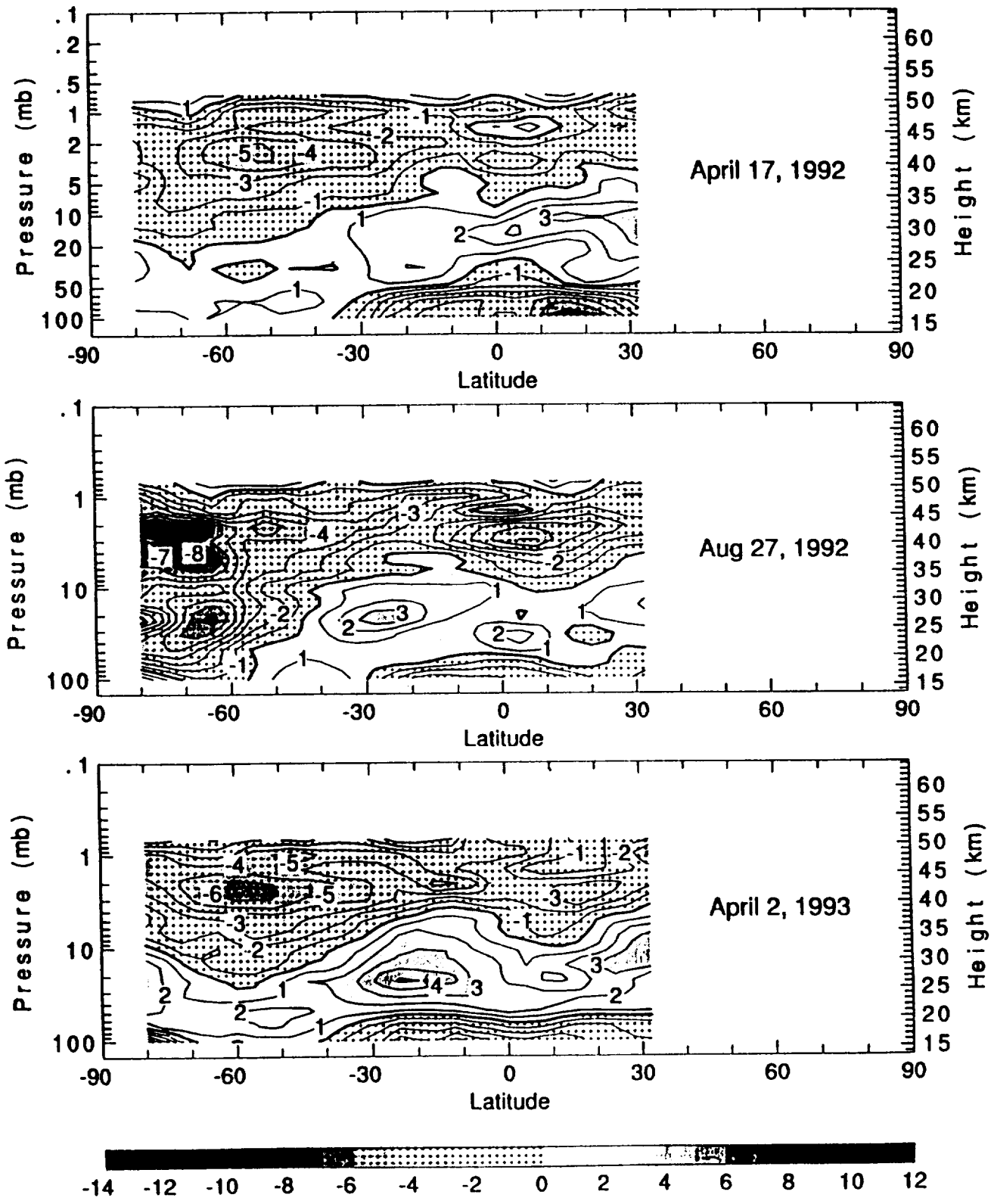

Figure 4.3.1–20

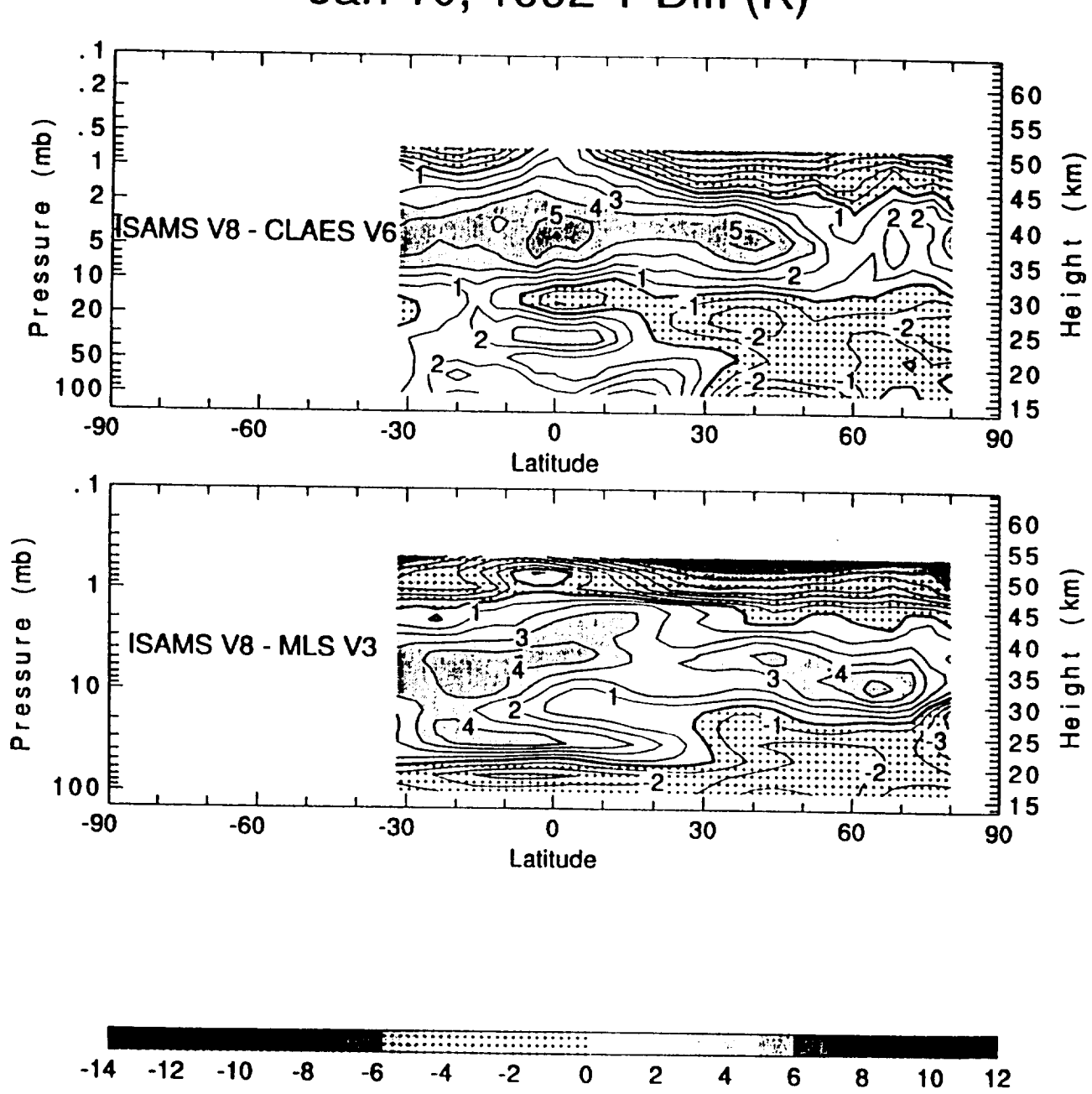

Figure 4.3.1–21

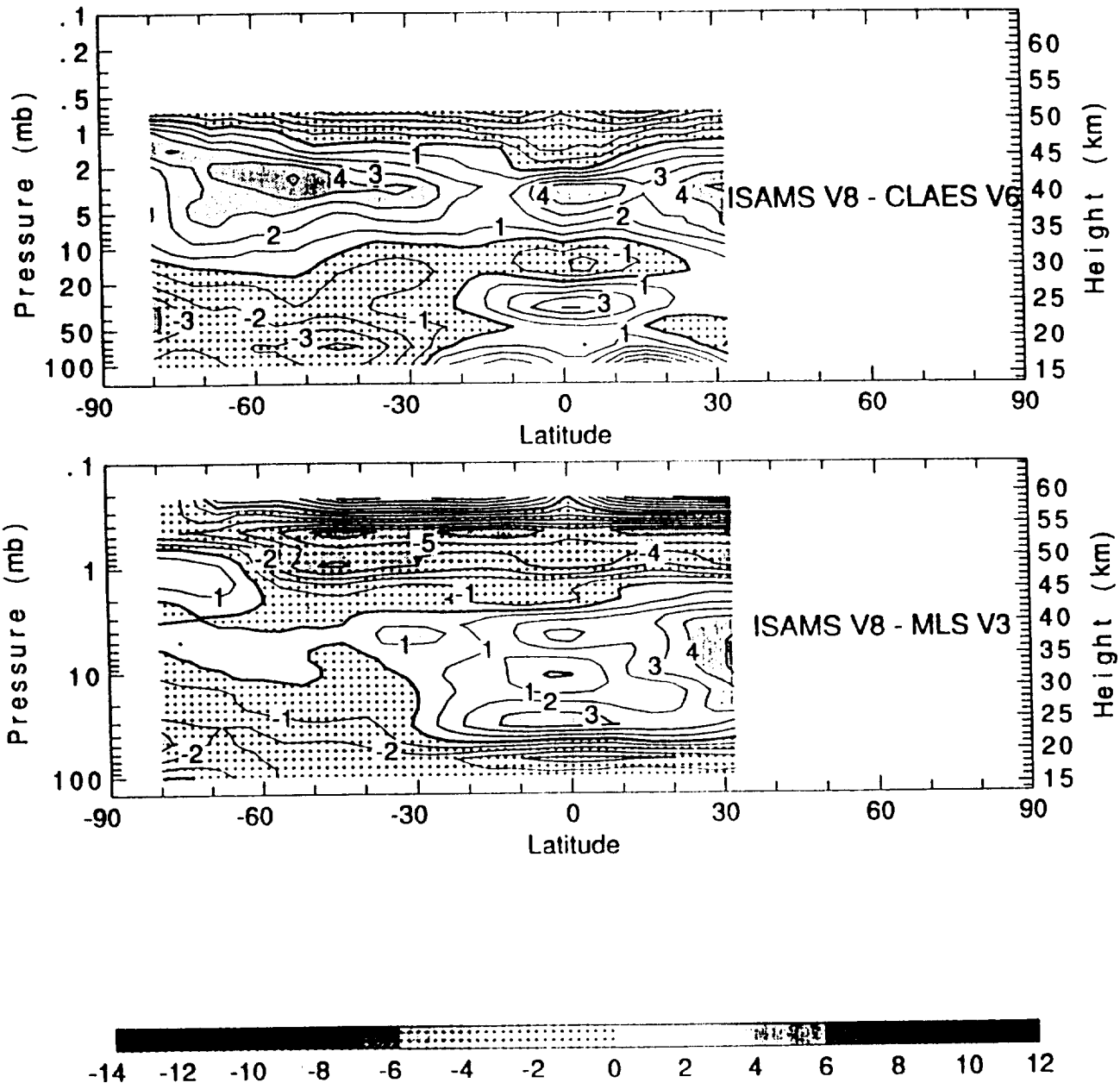

Figure 4.3.1–22

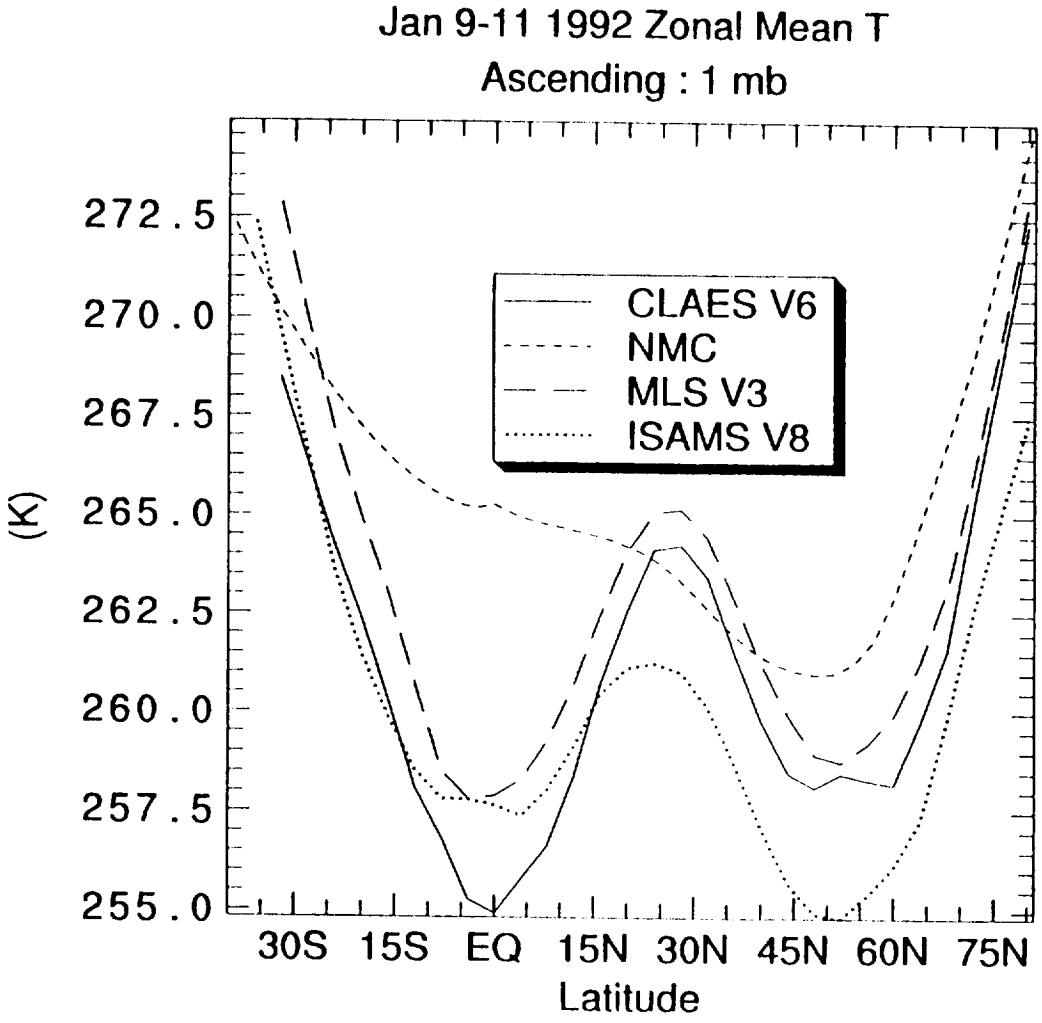
Jan 9-11 1992 Zonal Mean T
Ascending : 1 mb
272.5
270.0
267.5
265.0
262.5
260.0
257.5
255.0
(K)
CLAES V6
NMC
MLS V3
ISAMS V8
30S 15S EQ 15N 30N 45N 60N 75N
Latitude

Figure 4.3.2–1

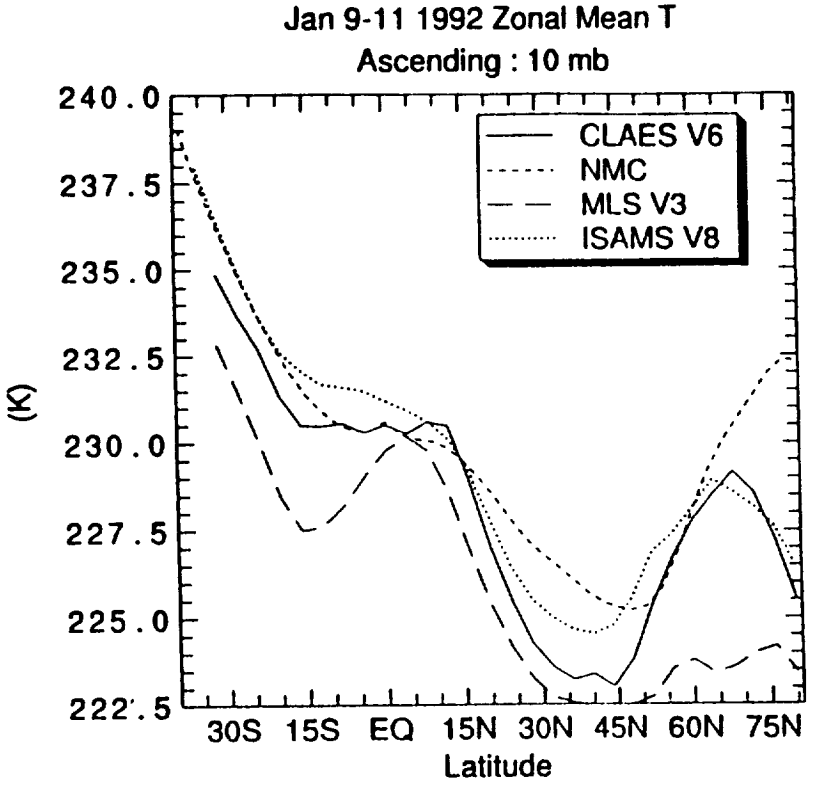
Jan 9-11 1992 Zonal Mean T
Ascending : 10 mb
240.0
237.5
235.0
232.5
230.0
227.5
225.0
222.5
(K)
CLAES V6
NMC
MLS V3
ISAMS V8
30S 15S EQ 15N 30N 45N 60N 75N
Latitude

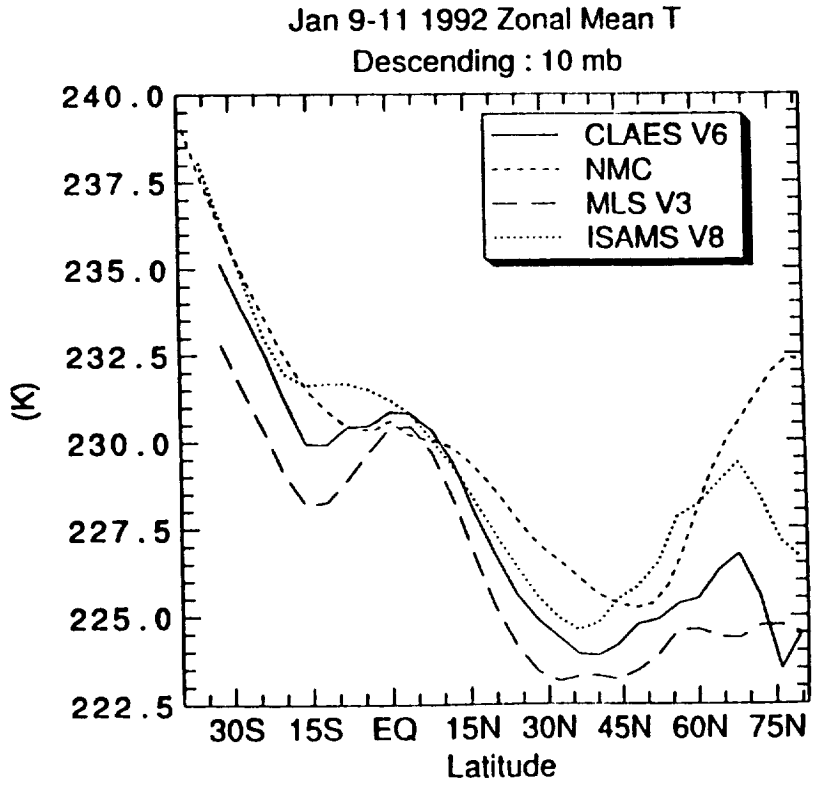
Jan 9-11 1992 Zonal Mean T
Descending : 10 mb
240.0
237.5
235.0
232.5
230.0
227.5
225.0
222.5
(K)
CLAES V6
NMC
MLS V3
ISAMS V8
30S 15S EQ 15N 30N 45N 60N 75N
Latitude

Figure 4.3.2–2

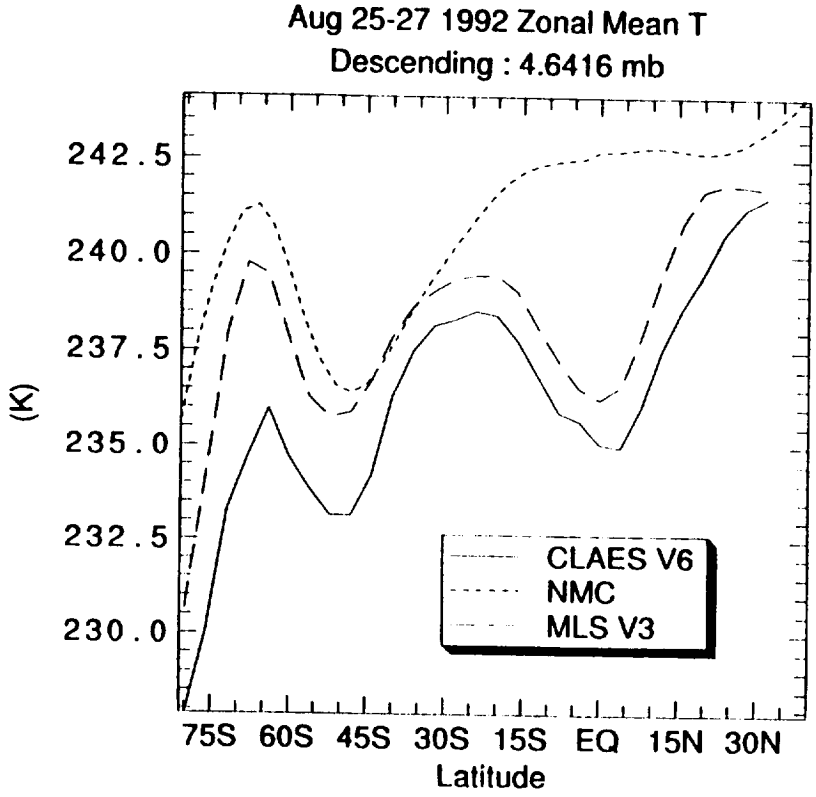

Figure 4.3.2–3

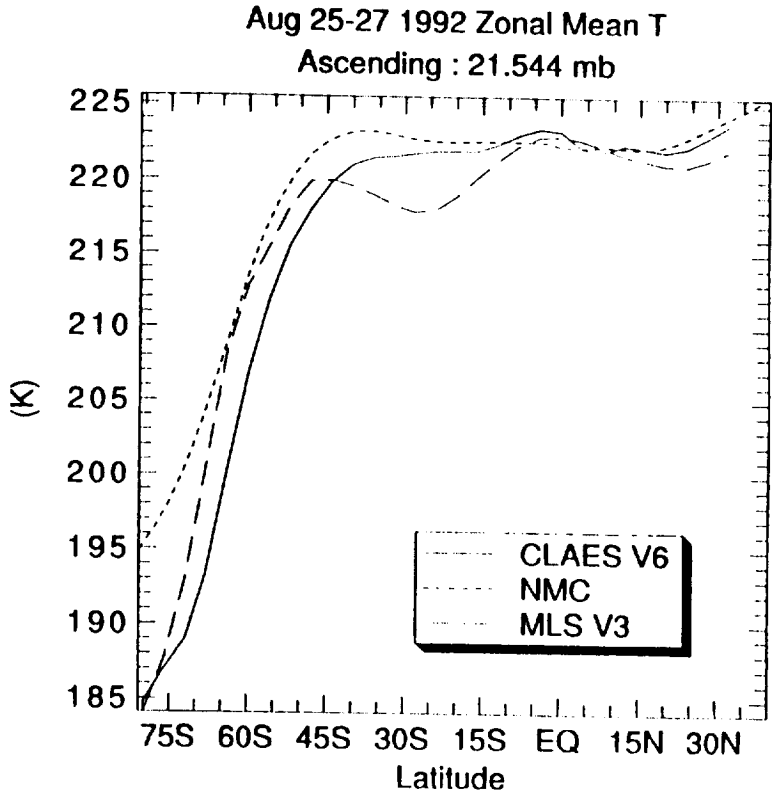

Figure 4.3.2–4

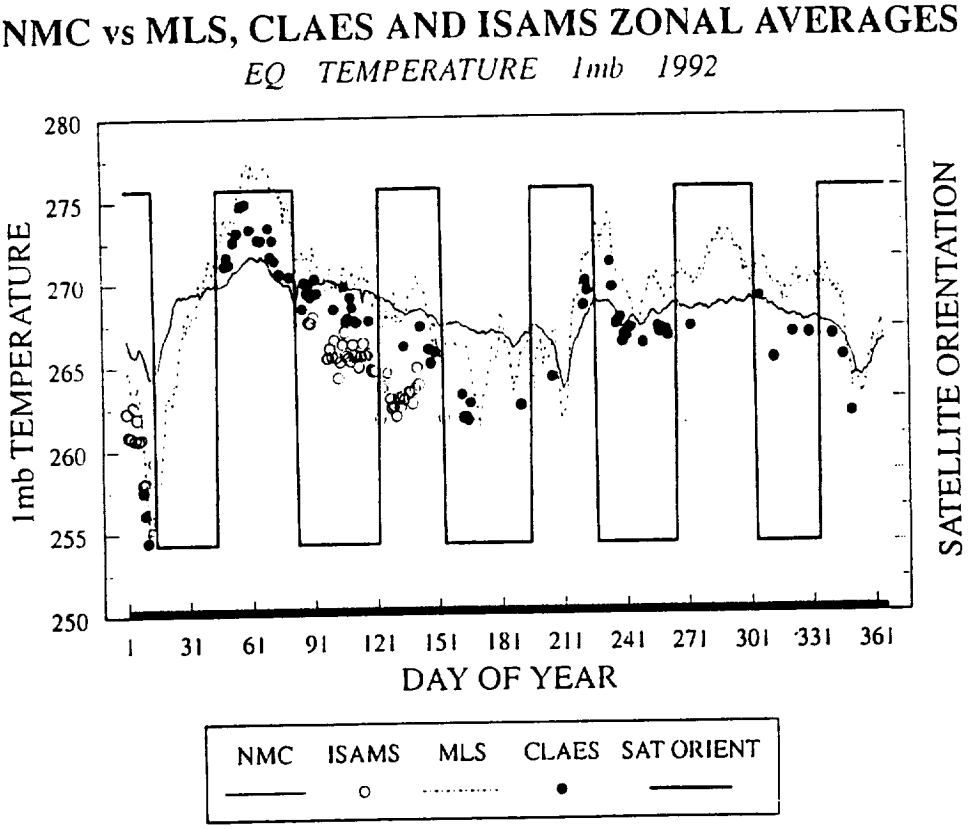

Figure 4.3.3–1

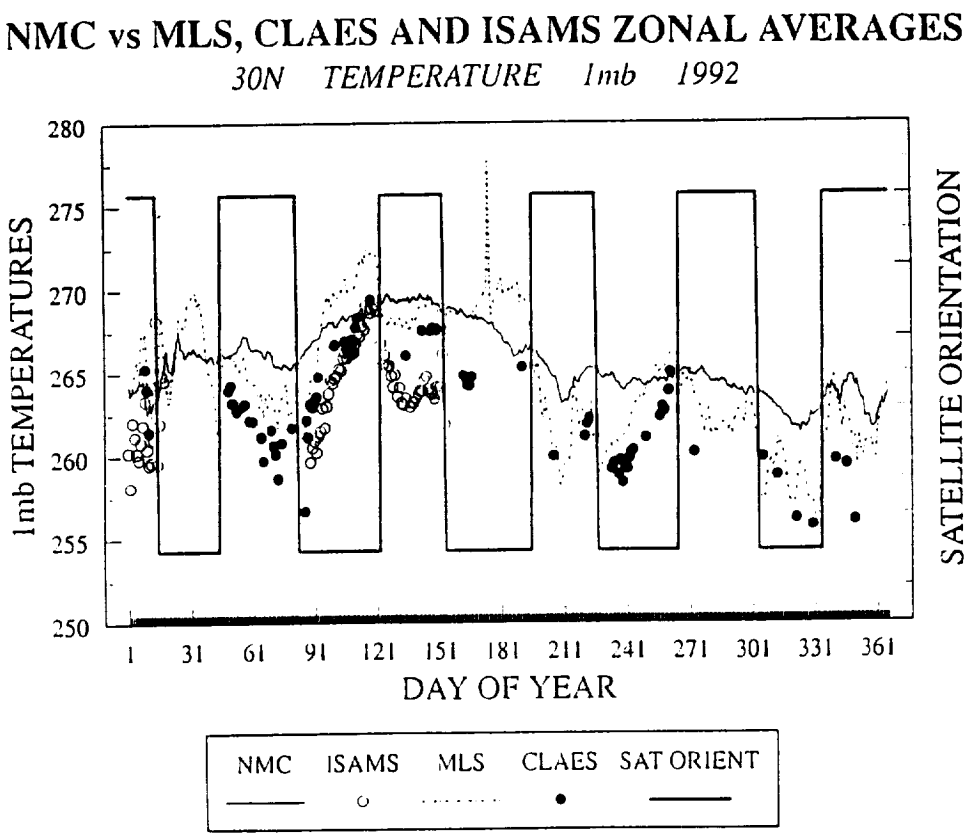

Figure 4.3.3–2

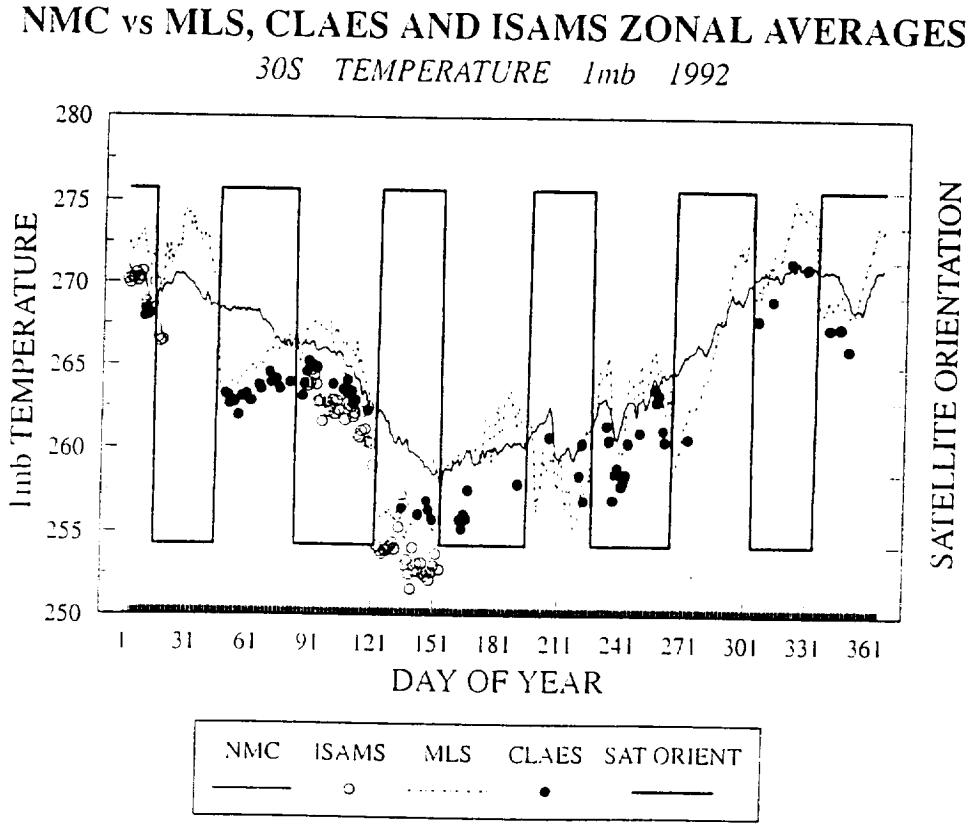

Figure 4.3.3–3

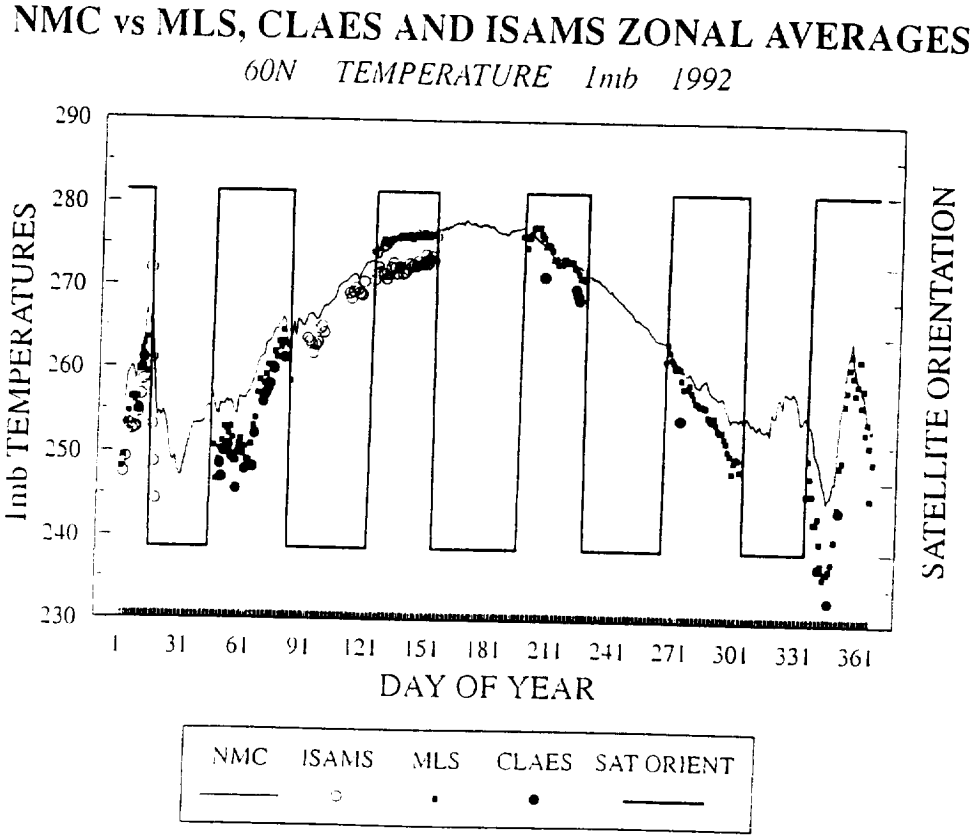

Figure 4.3.3–4

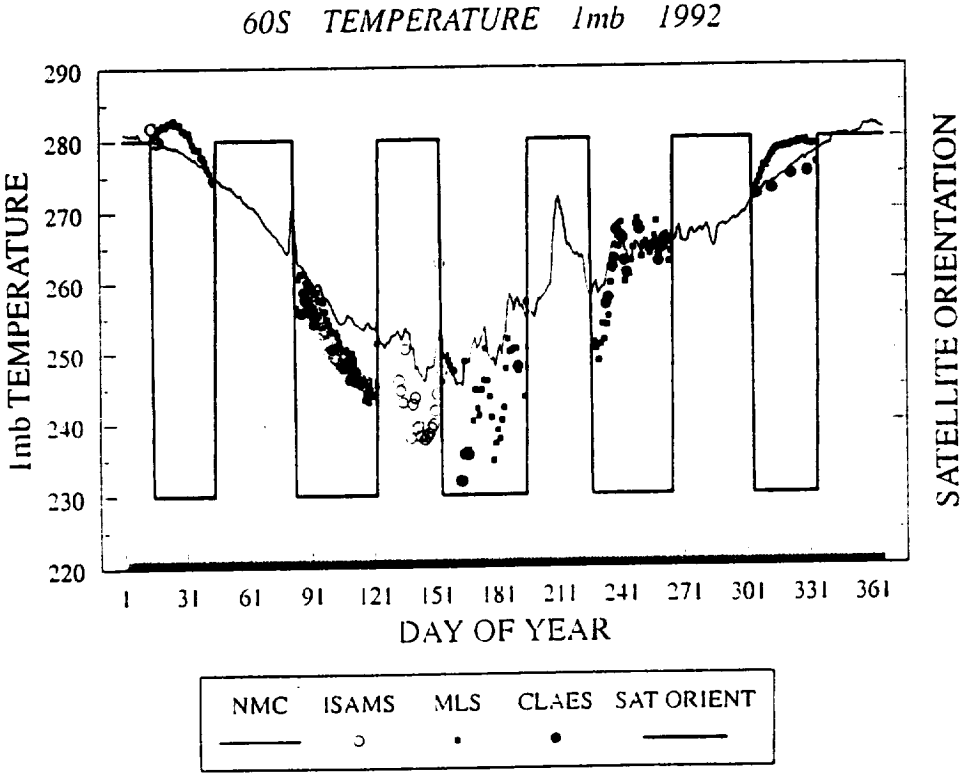

Figure 4.3.3–5

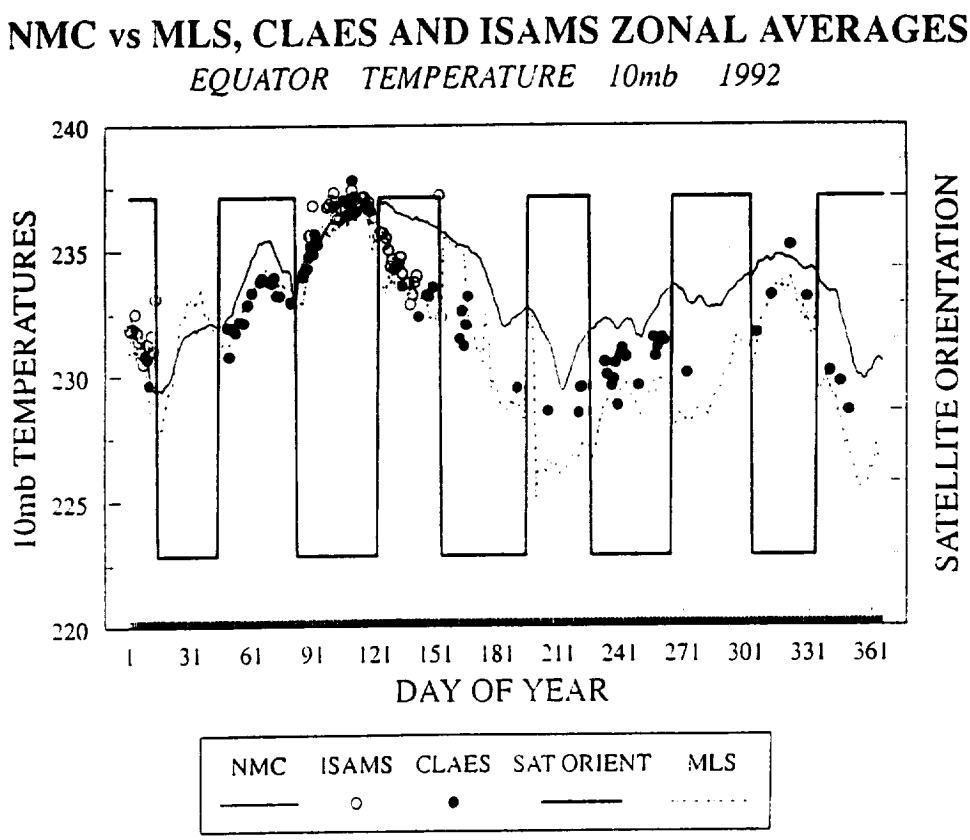

Figure 4.3.3–6

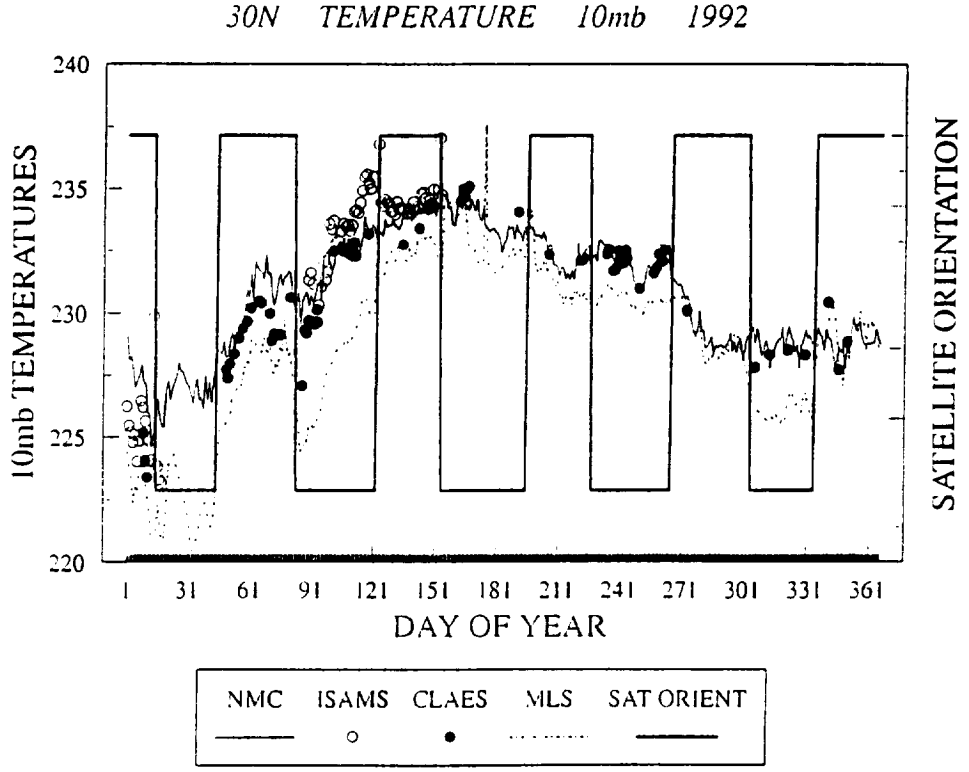

Figure 4.3.3–7

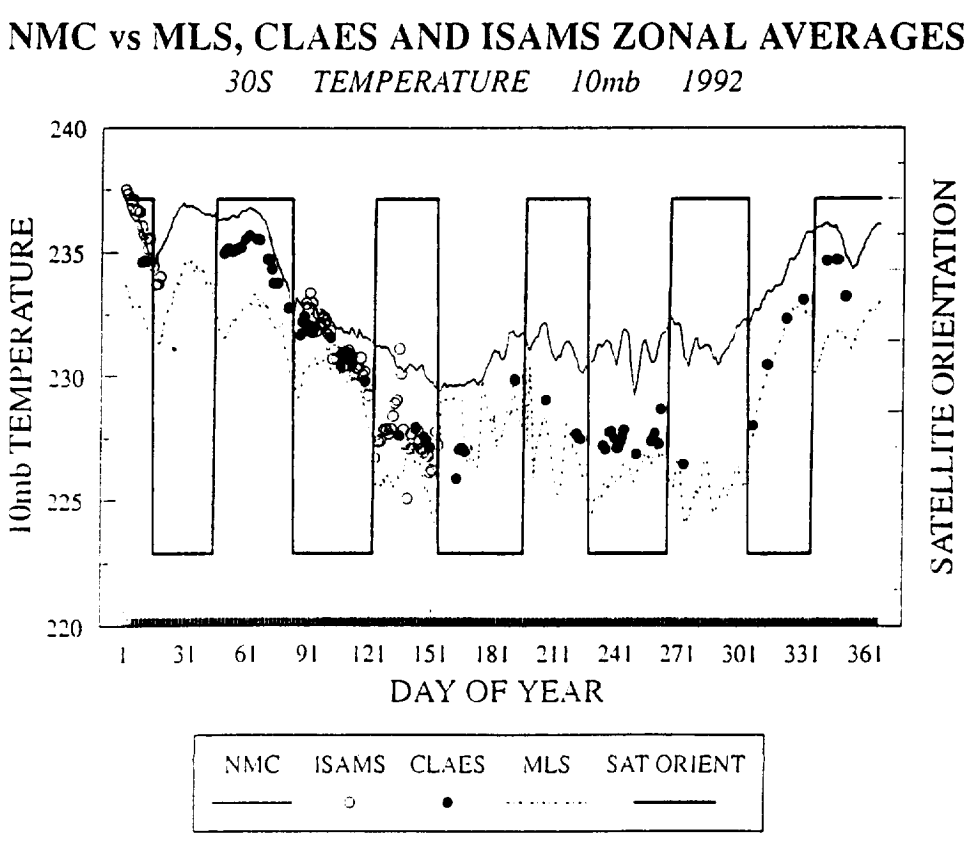

Figure 4.3.3–8

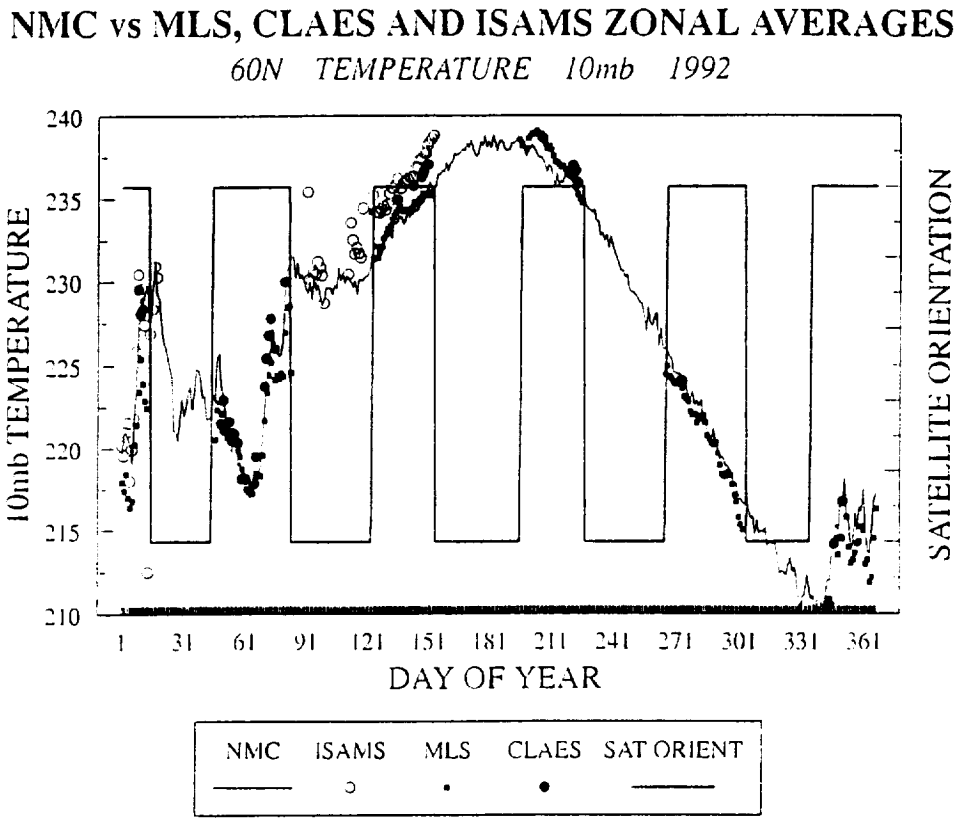

Figure 4.3.3–9

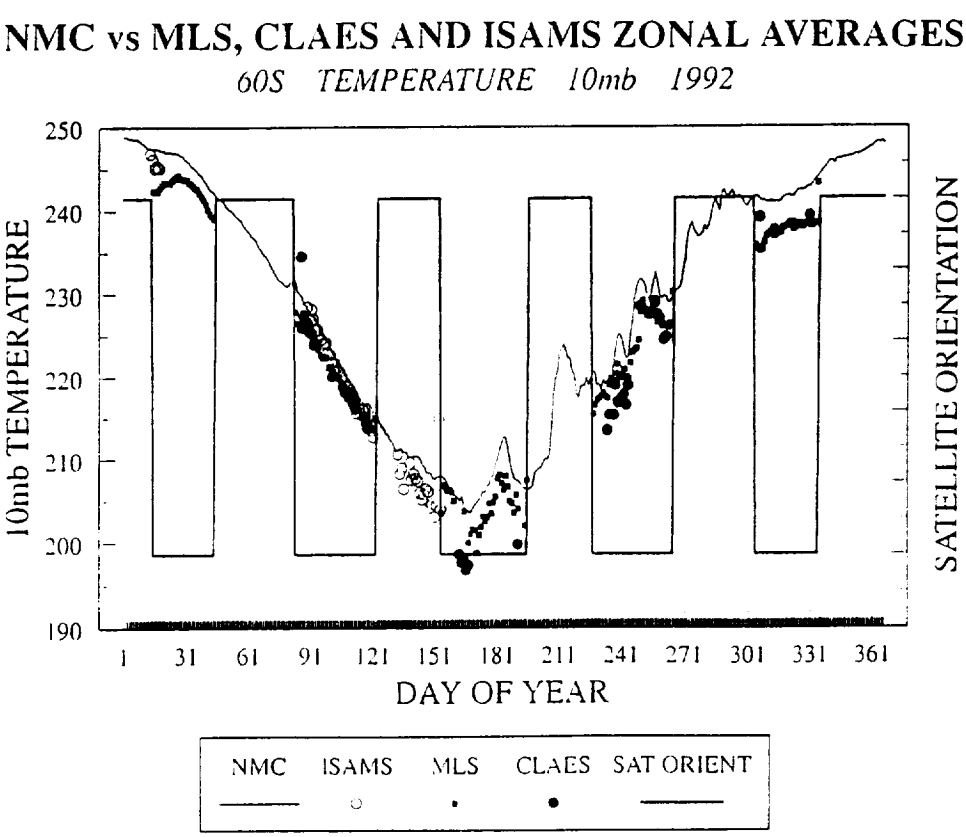

Figure 4.3.3–10

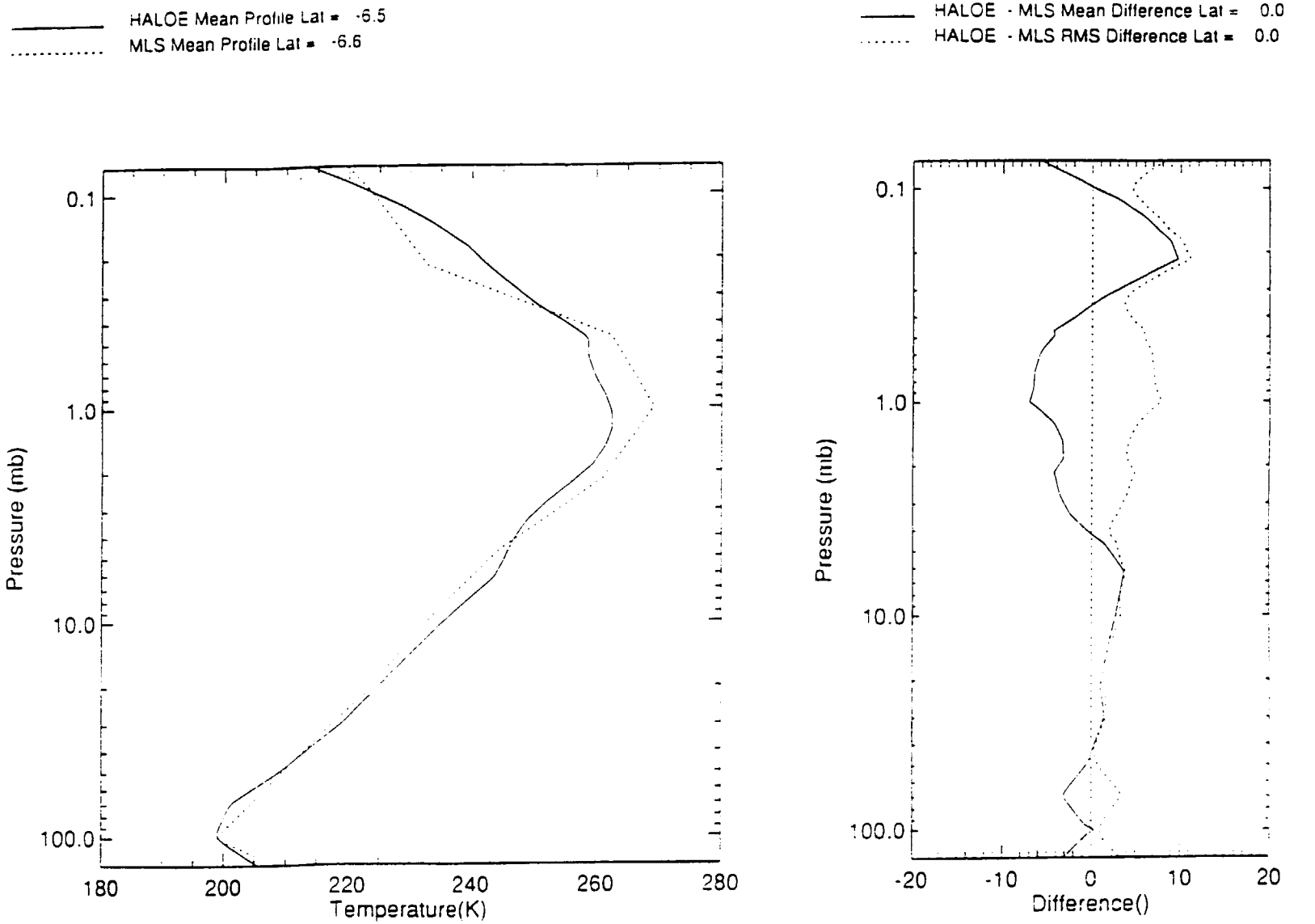
HALOE Mean Profile Lat = -6.5
MLS Mean Profile Lat = -6.6
HALOE - MLS Mean Difference Lat = 0.0
HALOE - MLS RMS Difference Lat = 0.0
Pressure (mb)
0.1
1.0
10.0
100.0
180
200
220
240
260
280
Temperature(K)
-20
-10
0
10
20
Difference()
HALOE - MLS Temperature (K) Differences on
15-APR-1992 to 20-APR-1992 near 6 S using 73 profiles

Figure 4.4.2–1

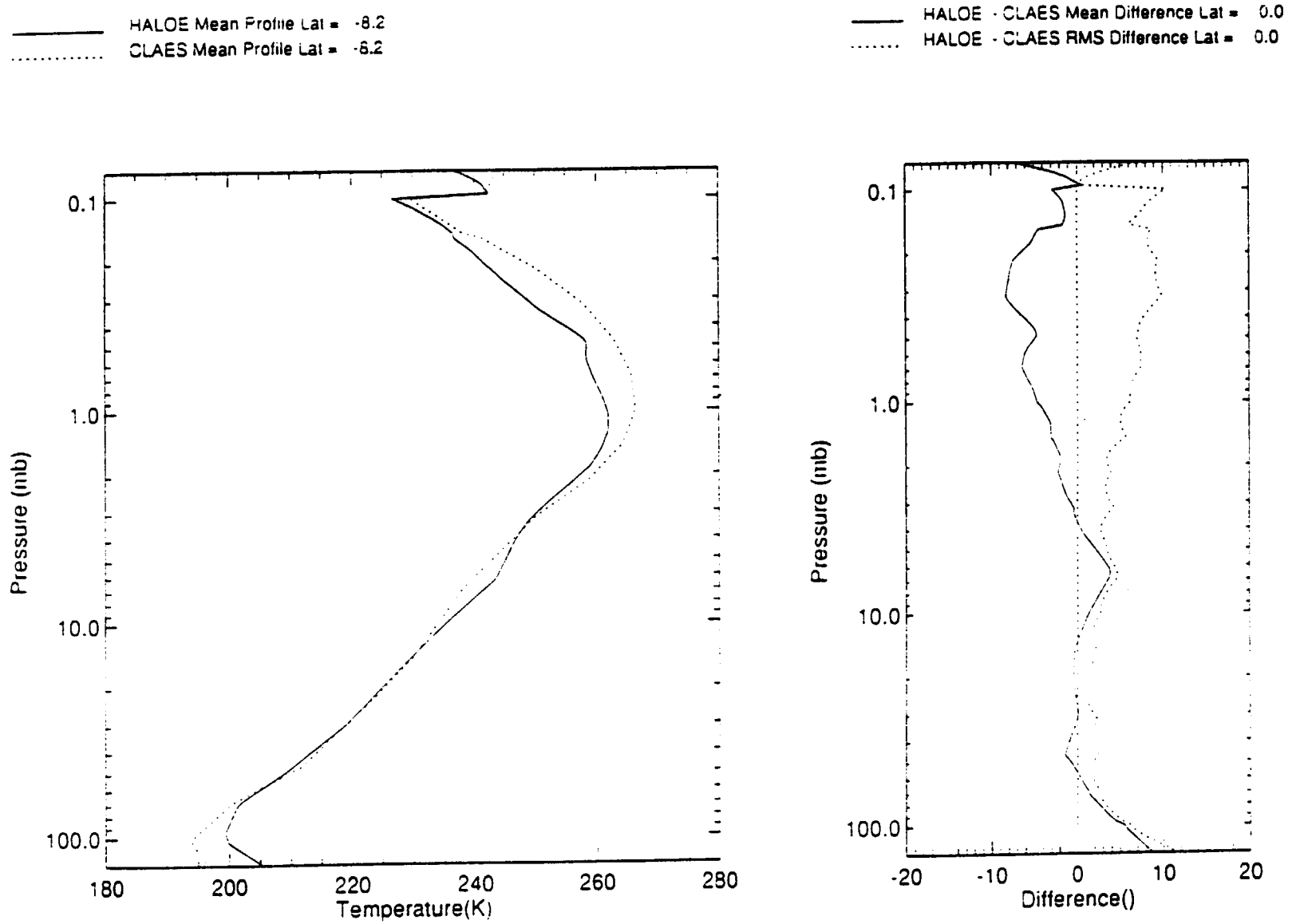
HALOE Mean Profile Lat = -8.2
CLAES Mean Profile Lat = -8.2
HALOE - CLAES Mean Difference Lat = 0.0
HALOE - CLAES RMS Difference Lat = 0.0
Pressure (mb)
0.1
1.0
10.0
100.0
180
200
220
240
260
280
Temperature(K)
-20
-10
0
10
20
Difference()
HALOE - CLAES Temperature (K) Differences on
15-APR-1992 to 20-APR-1992 near 8 S using 76 profiles

Figure 4.4.2–2

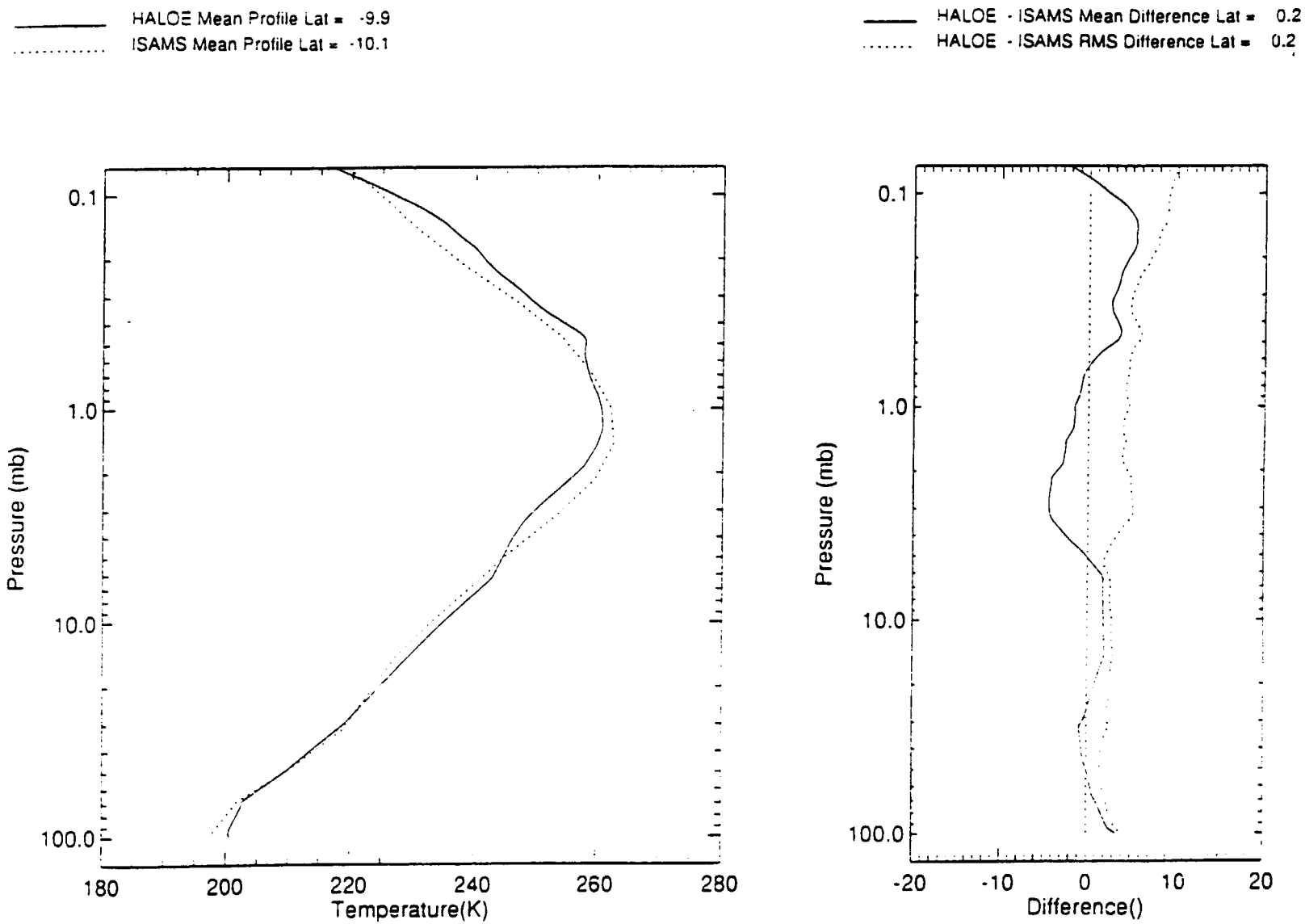
HALOE Mean Profile Lat = -9.9
ISAMS Mean Profile Lat = -10.1
HALOE - ISAMS Mean Difference Lat = 0.2
HALOE - ISAMS RMS Difference Lat = 0.2
Pressure (mb)
0.1
1.0
10.0
100.0
180
200
220
240
260
280
Temperature(K)
-20
-10
0
10
20
Difference()
HALOE - ISAMS Temperature (K) Differences on
15-APR-1992 to 20-APR-1992 near 9 S using 69 profiles

Figure 4.4.2–3

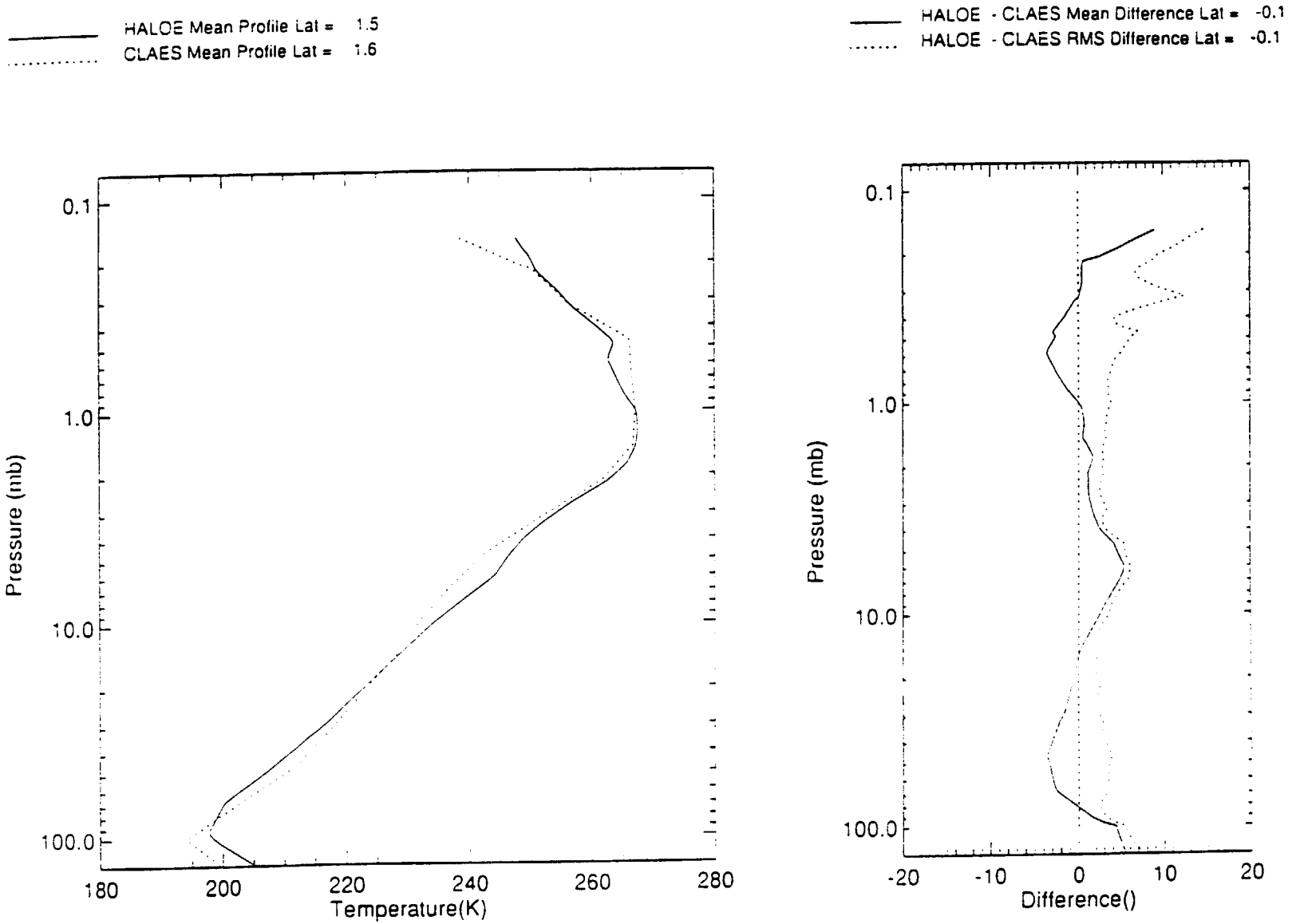
HALOE Mean Profile Lat = 1.5
CLAES Mean Profile Lat = 1.6
HALOE - CLAES Mean Difference Lat = -0.1
HALOE - CLAES RMS Difference Lat = -0.1
Pressure (mb)
0.1
1.0
10.0
100.0
180
200
220
240
260
280
Temperature(K)
-20
-10
0
10
20
Difference()
HALOE - CLAES Temperature (K) Differences on
1-APR-1993 to 3-APR-1993 near 1 N using 28 profiles
Thu Sep 9 10:59:08 CDT 1993

Figure 4.4.2–4

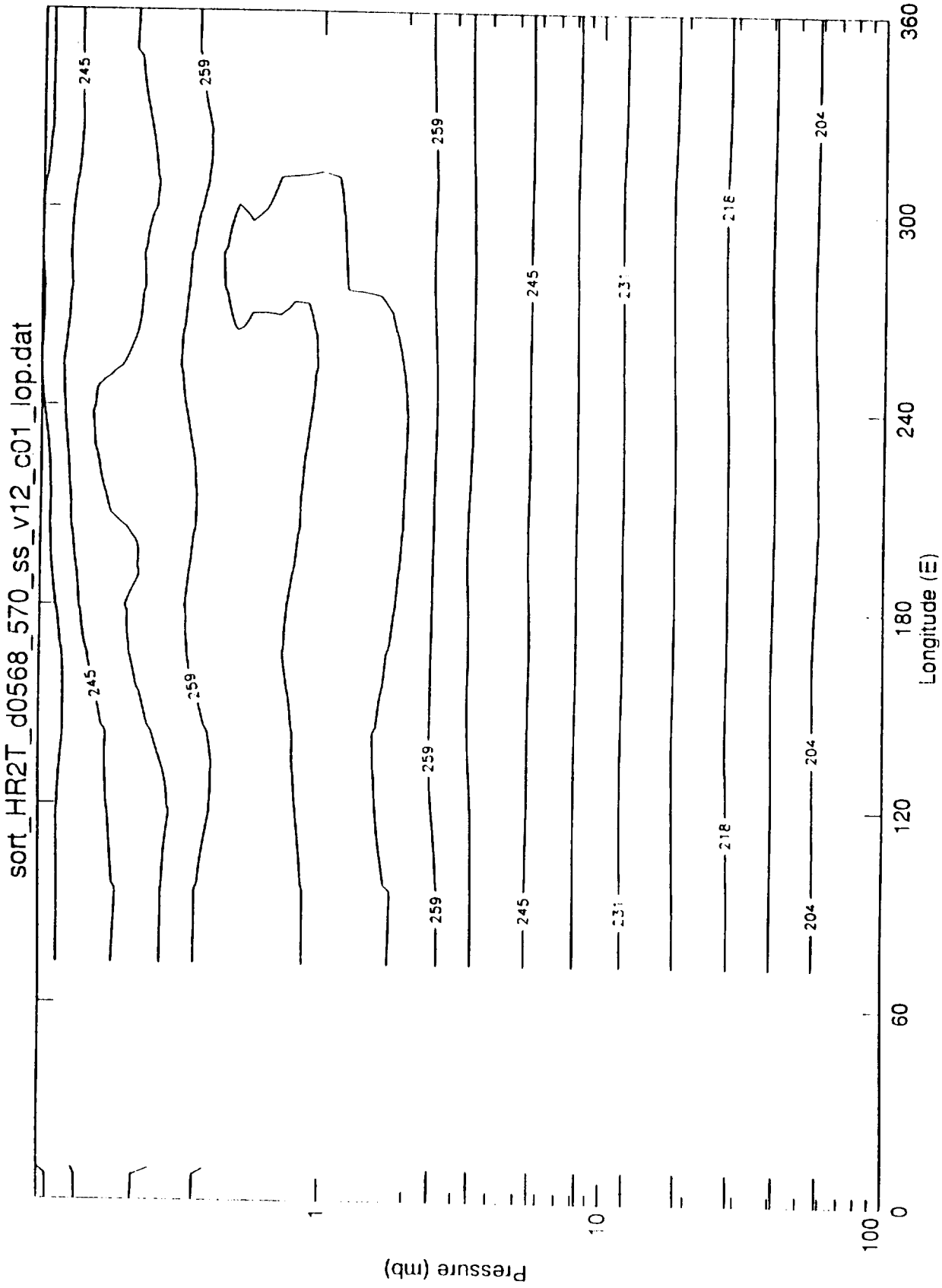
sort_HR2T_d0568_570_ss_v12_c01_lop.dat
Pressure (mb)
Longitude (E)
1
10
100
0
60
120
180
240
300
360
245
259
231
218
204

Figure 4.4.3-1

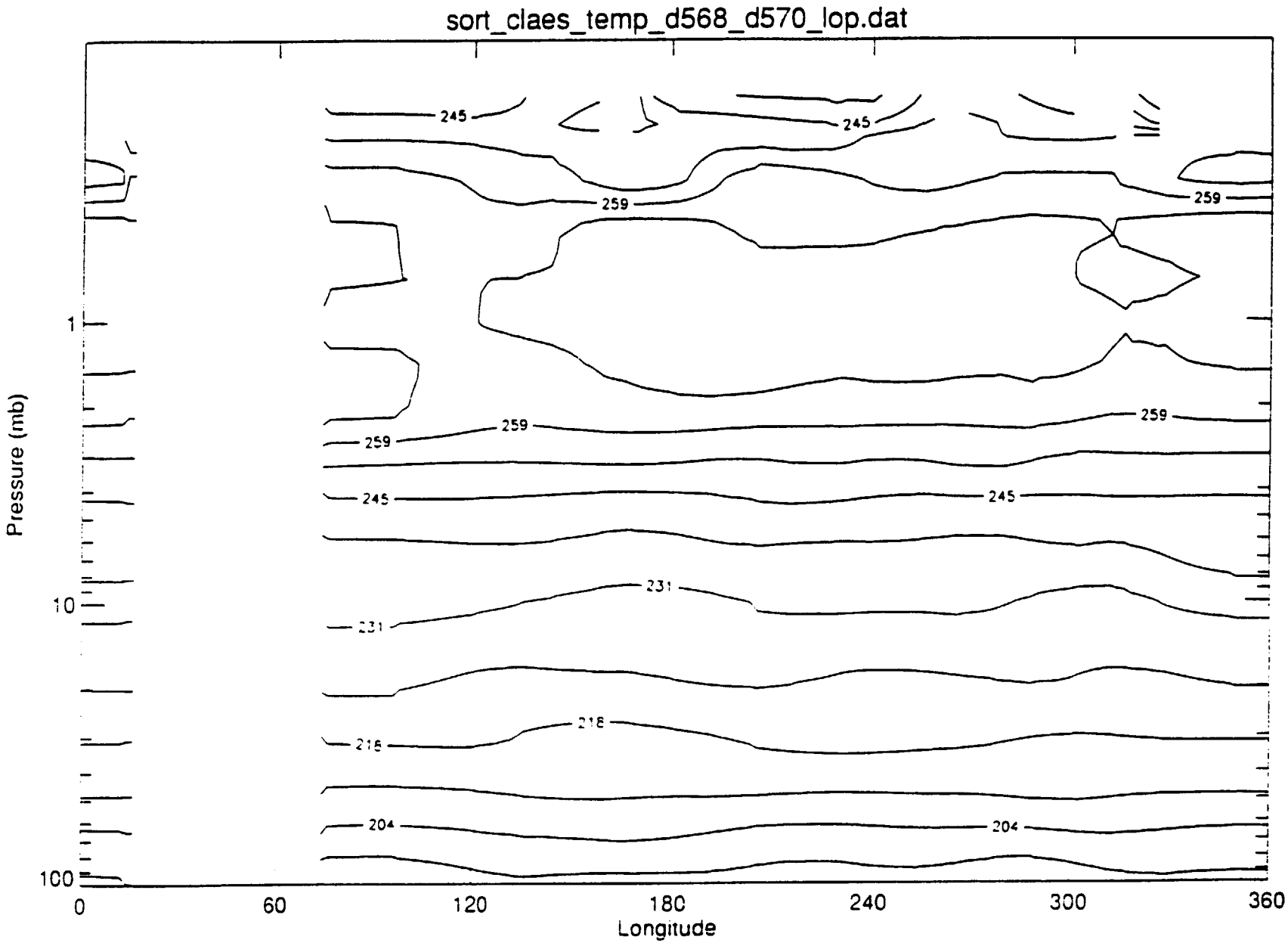
sort_claes_temp_d568_d570_lop.dat
245
245
259
259
259
259
259
245
245
231
231
218
218
204
204
Pressure (mb)
1
10
100
0
60
120
180
240
300
360
Longitude

Figure 4.4.3–2

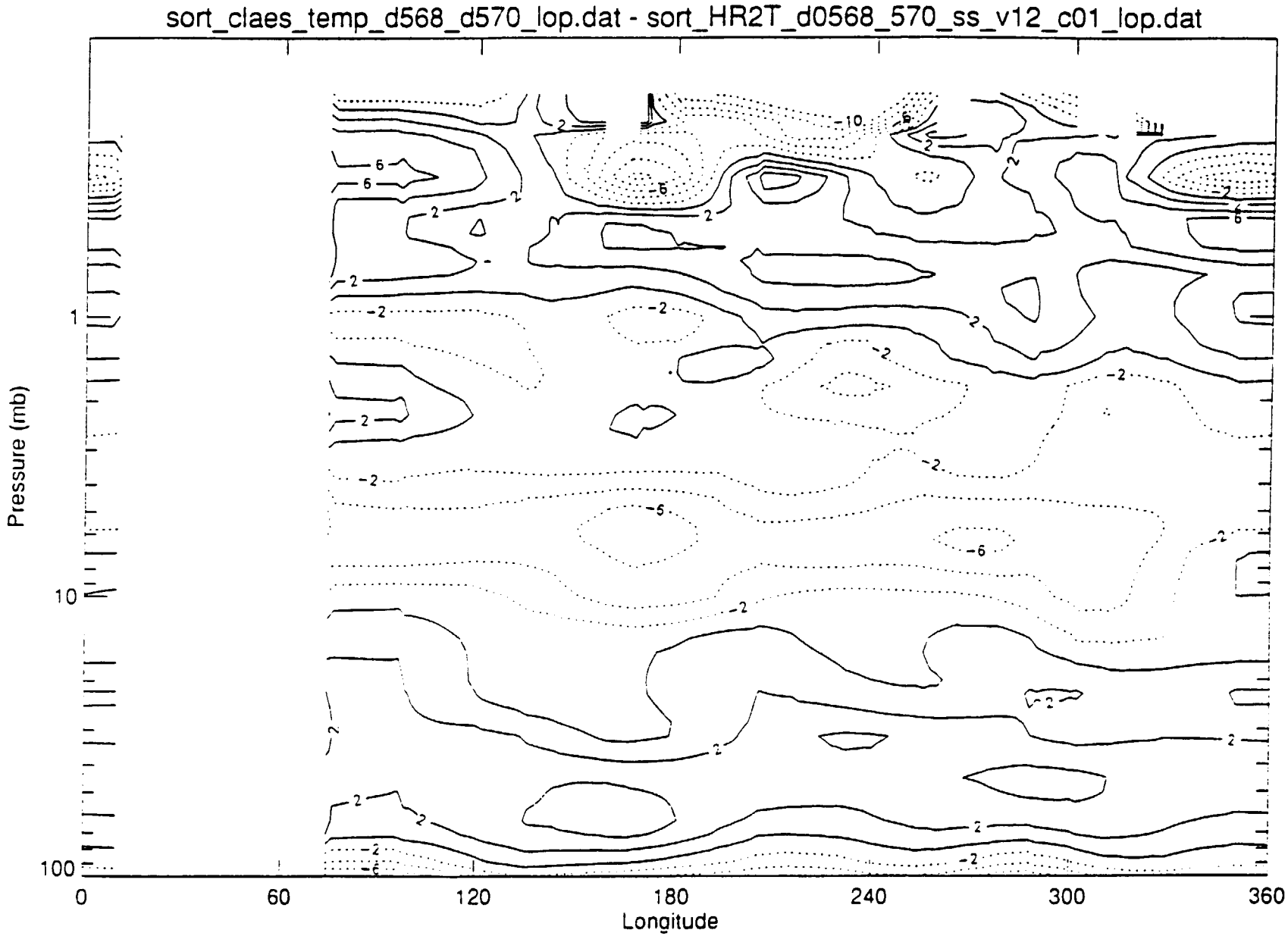
sort_claes_temp_d568_d570_lop.dat - sort_HR2T_d0568_570_ss_v12_c01_lop.dat
Pressure (mb)
1
10
100
0
60
120
180
240
300
360
Longitude

Figure 4.4.3–3

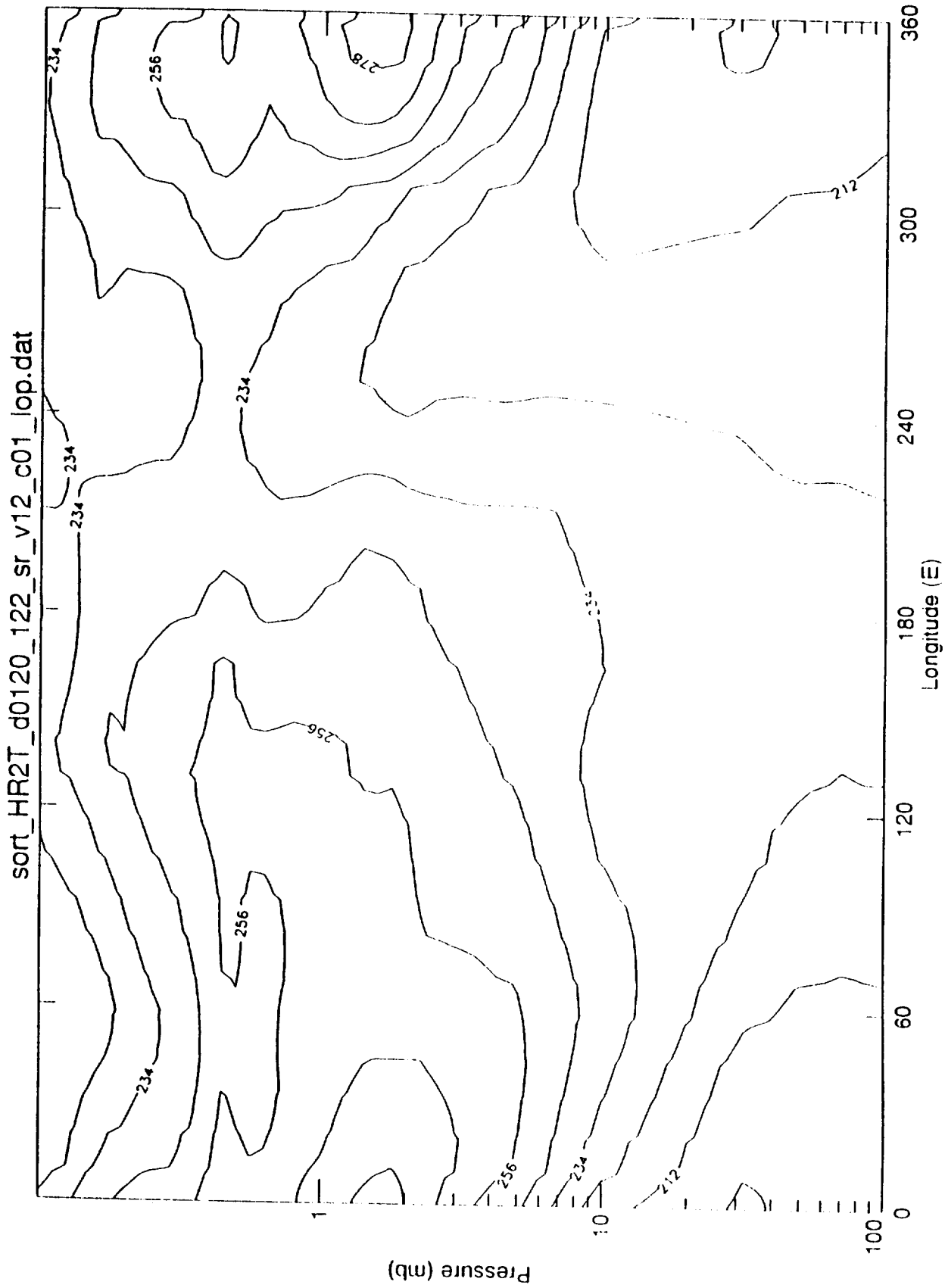
sort_HR2T_d0120_122_sr_v12_c01_lop.dat
Pressure (mb)
Longitude (E)
1
10
100
0
60
120
180
240
300
360
234
256
278
212

Figure 4.4.3–4

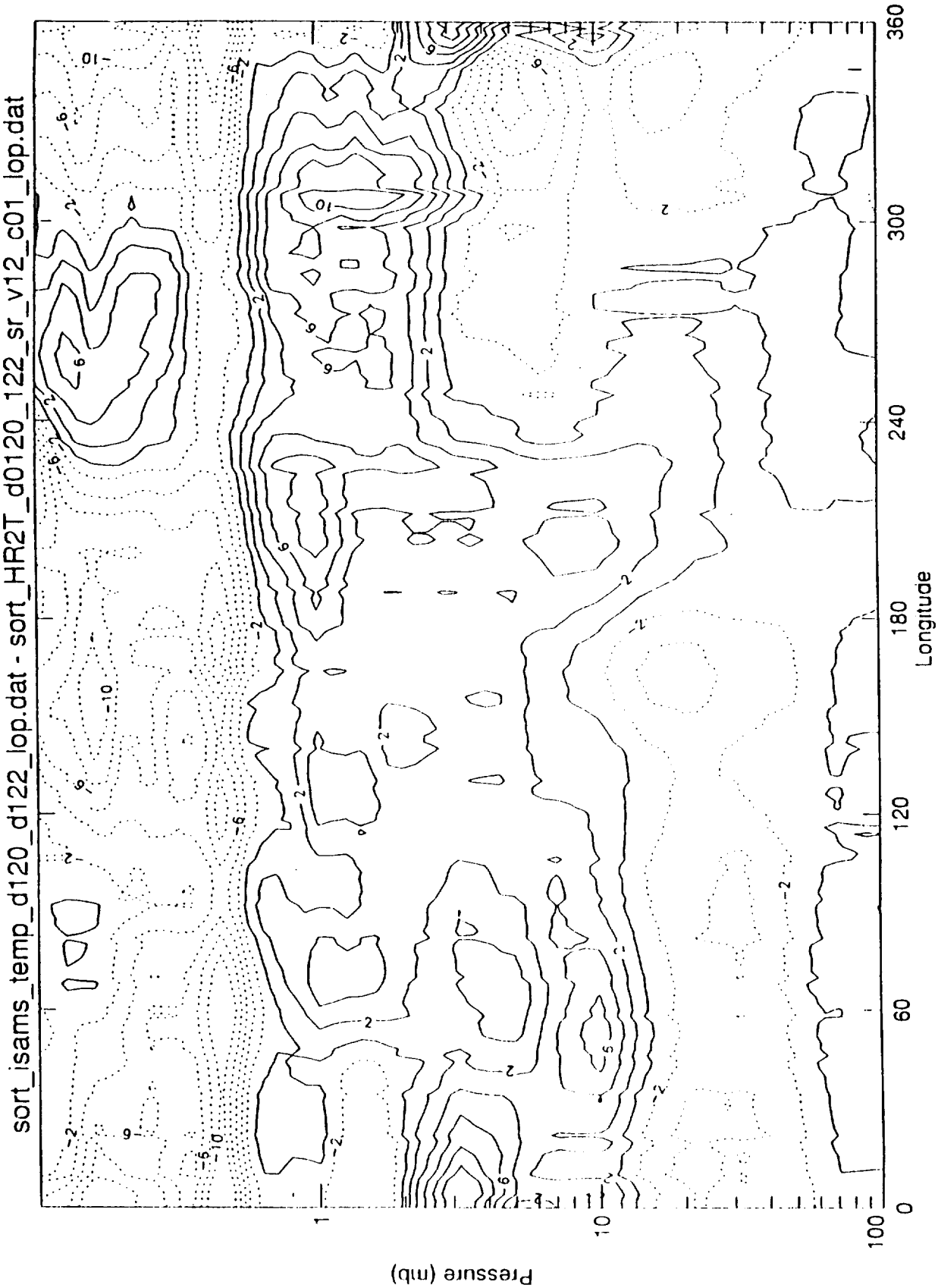
sort_isams_temp_d120_d122_lop.dat - sort_HR2T_d0120_122_sr_v12_c01_lop.dat
Pressure (mb)
1
10
100
0
60
120
180
240
300
360
Longitude

Figure 4.4.3–5

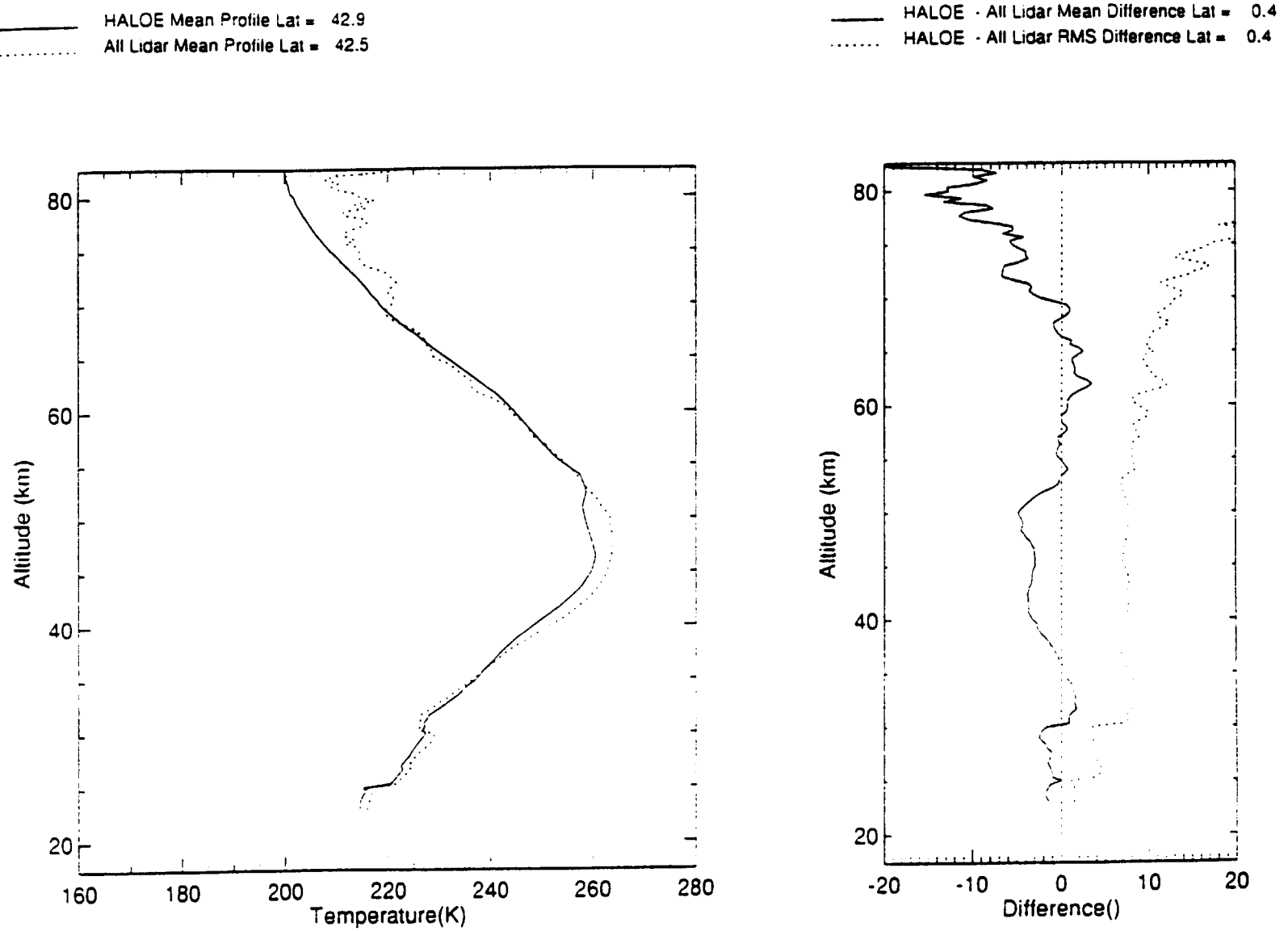
HALOE Mean Profile Lat = 42.9
All Lidar Mean Profile Lat = 42.5
HALOE - All Lidar Mean Difference Lat = 0.4
HALOE - All Lidar RMS Difference Lat = 0.4
Altitude (km)
Temperature(K)
Difference()
HALOE Temperature vs All LIDAR
(125 profiles)
Wed Sep 15 13:48:36 GMT 1993

Figure 4.4.4-1

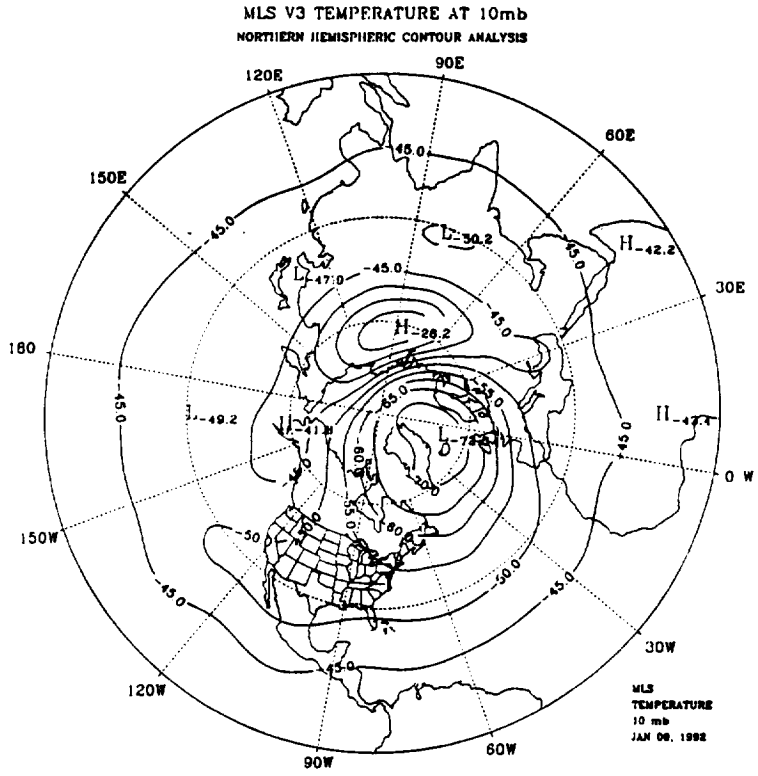

Figure 4.5–1 (a)

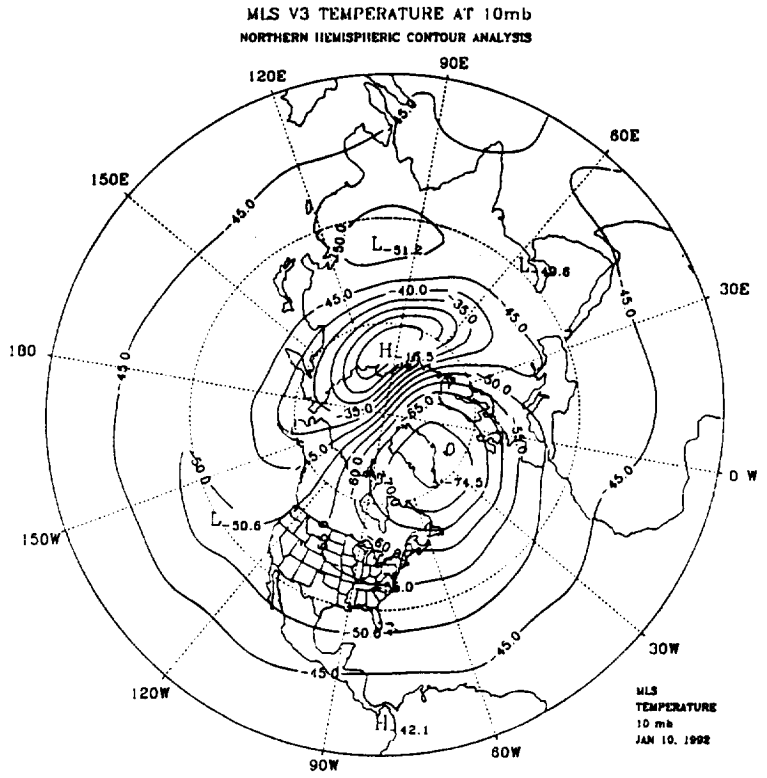

Figure 4.5–1 (b)

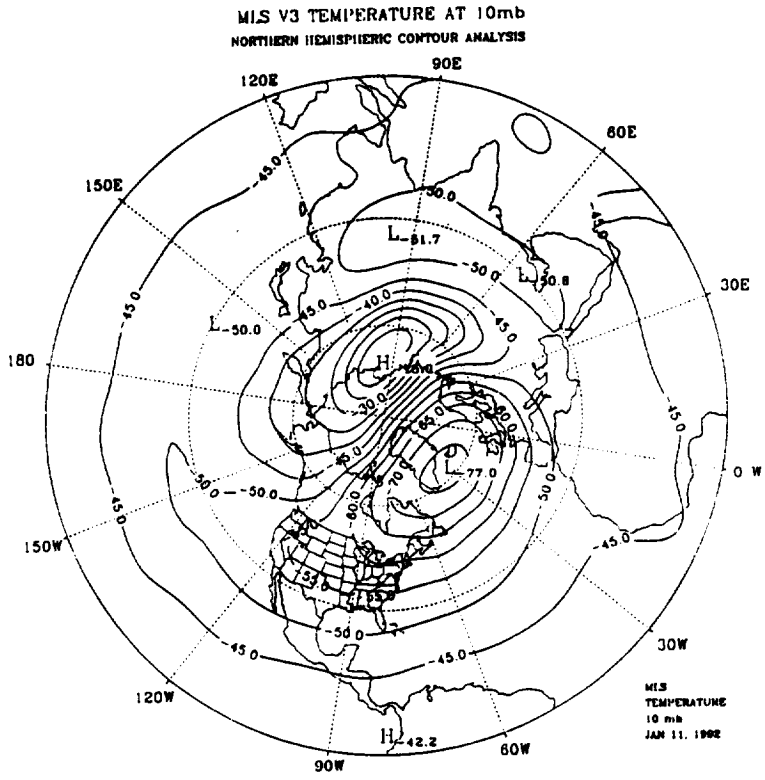

Figure 4.5–1 (c)

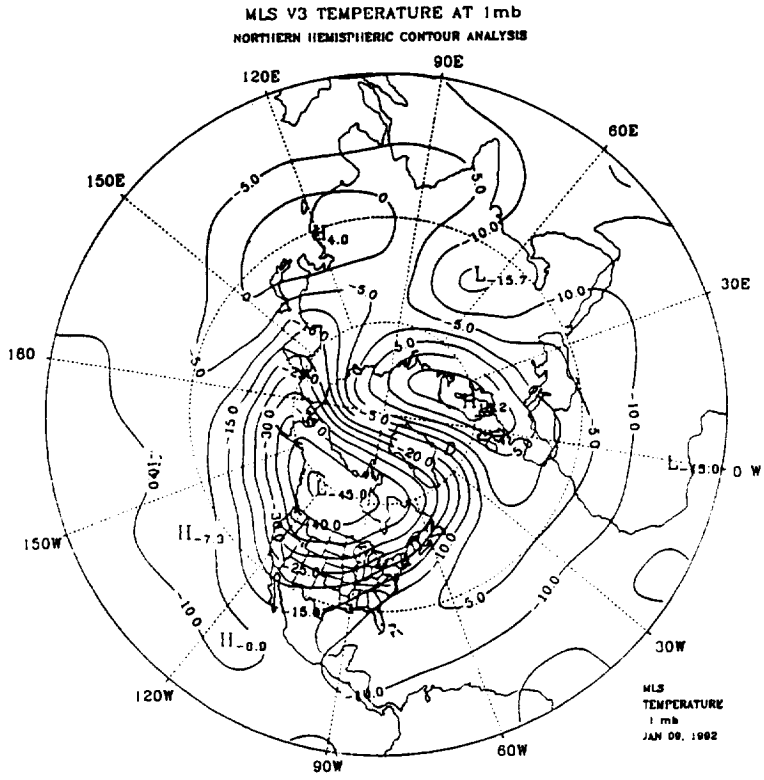

Figure 4.5–1 (d)

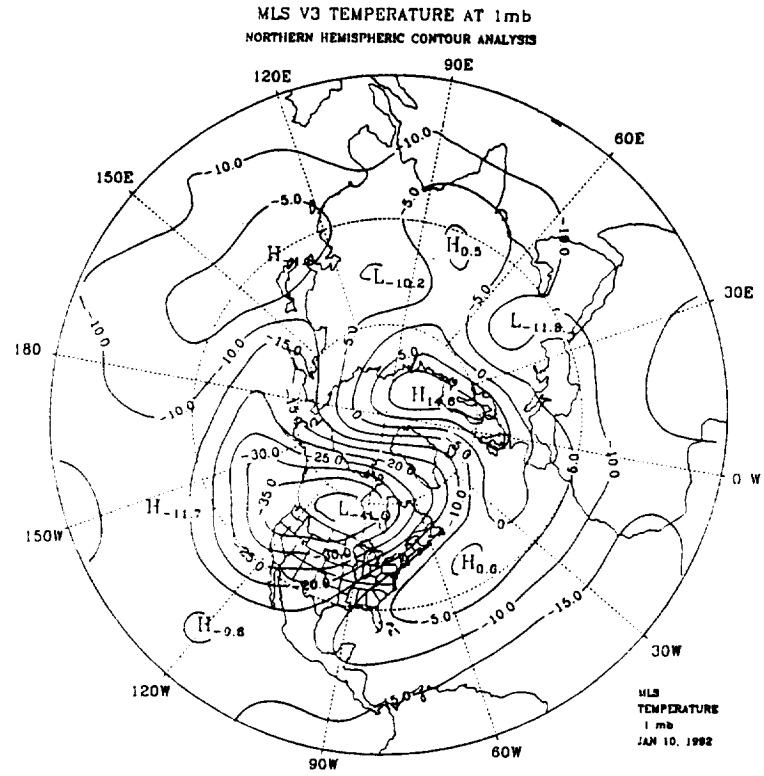

Figure 4.5–1 (e)

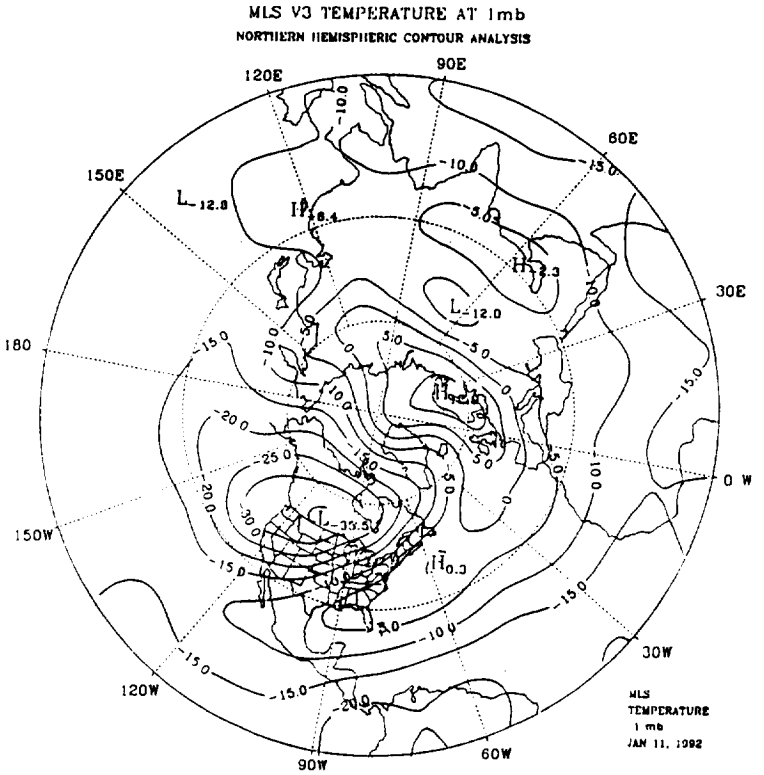

Figure 4.5–1 (f)

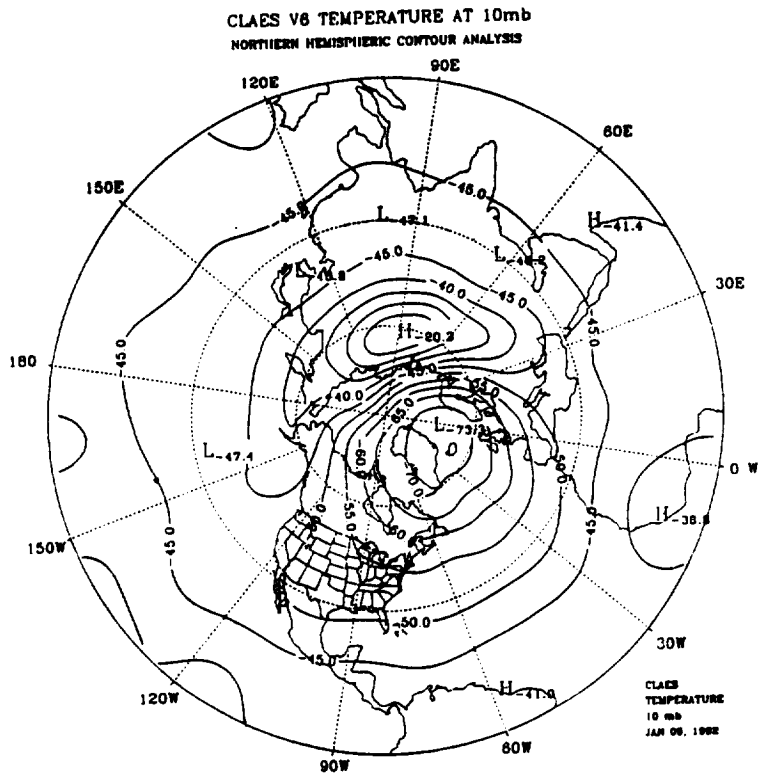

Figure 4.5-2 (a)

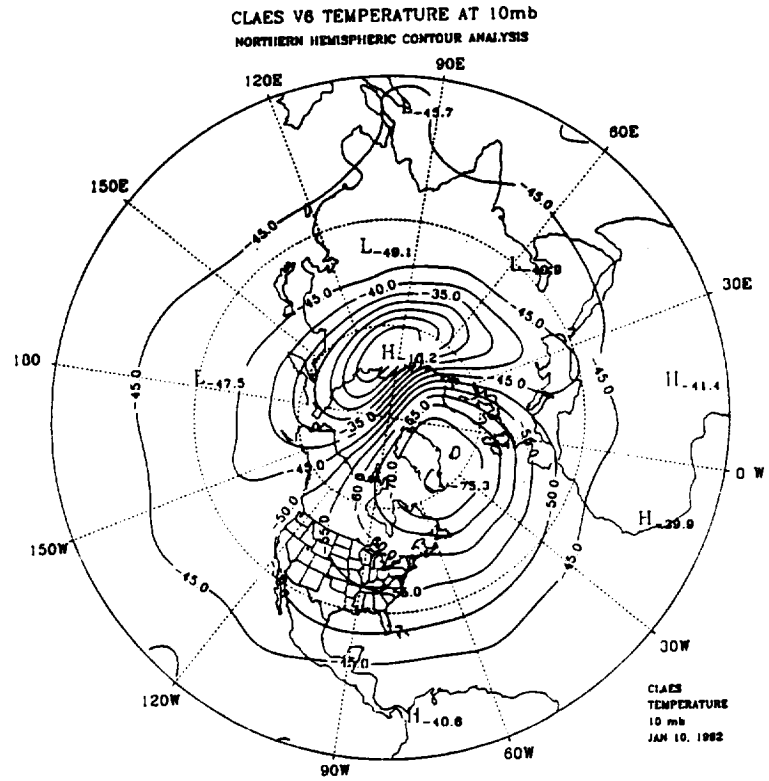

Figure 4.5-2 (b)

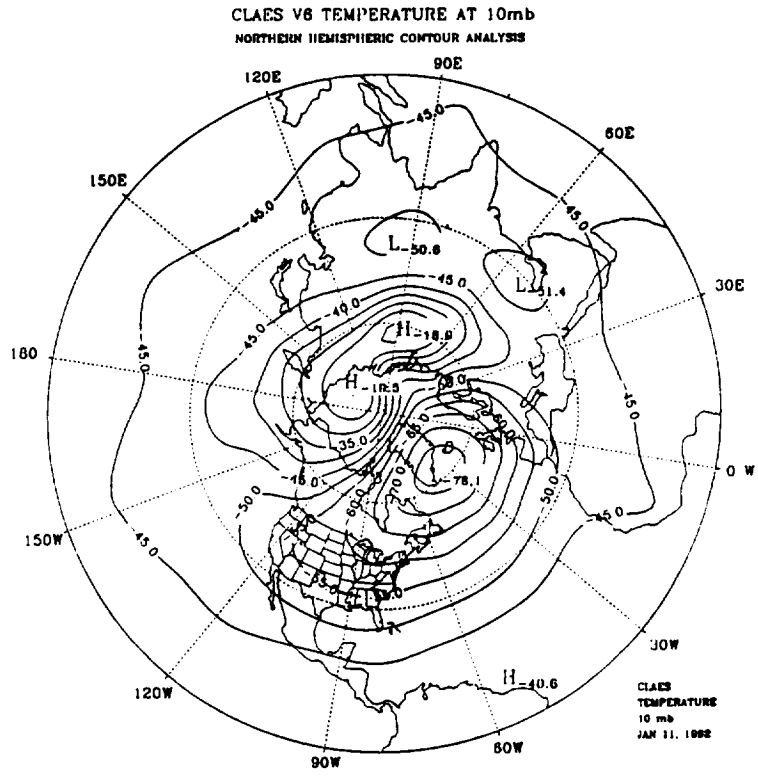

Figure 4.5-2 (c)

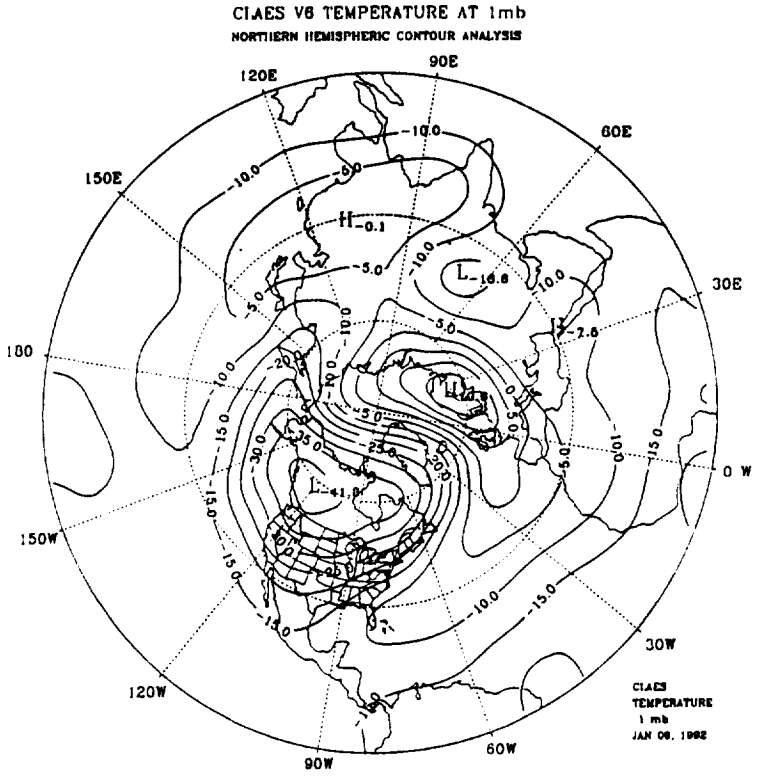

Figure 4.5-2 (d)

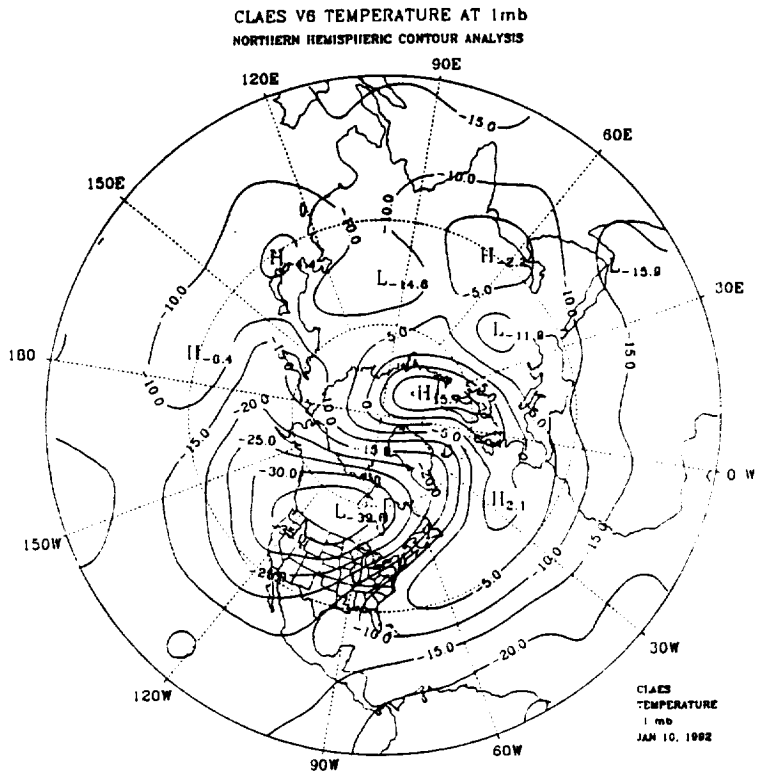

Figure 4.5-2 (e)

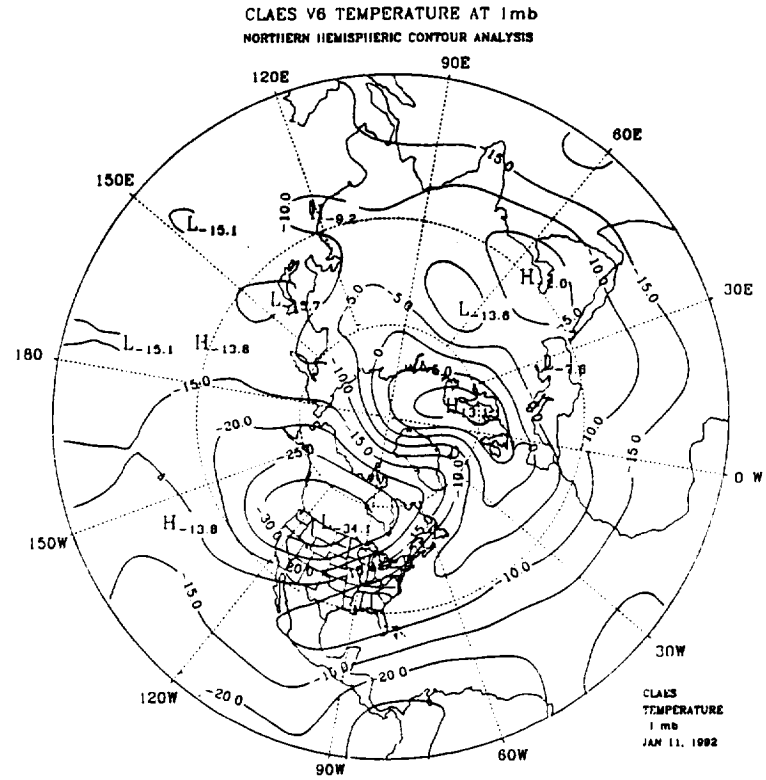

Figure 4.5-2 (f)

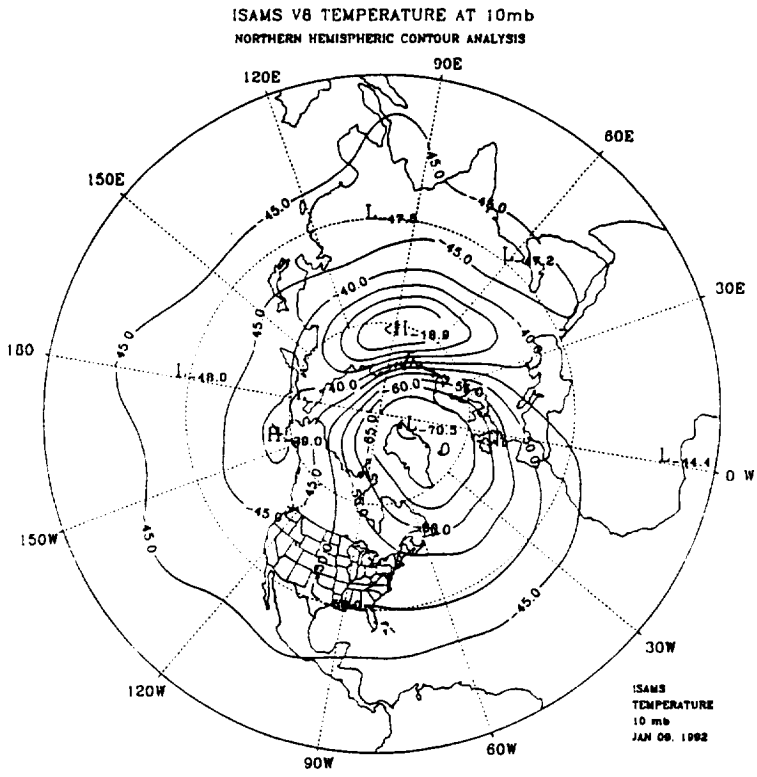

Figure 4.5-3 (a)

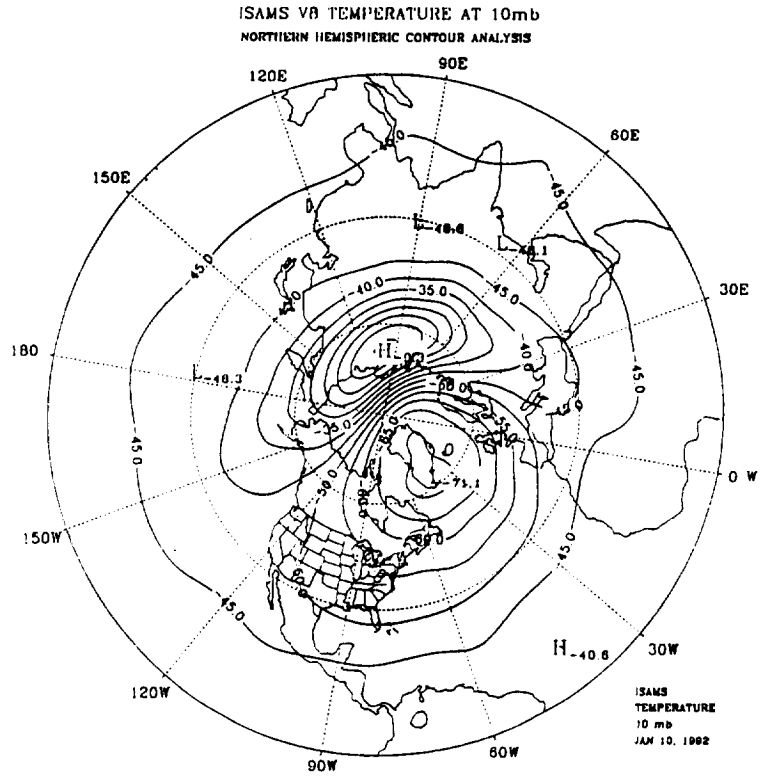

Figure 4.5-3 (b)

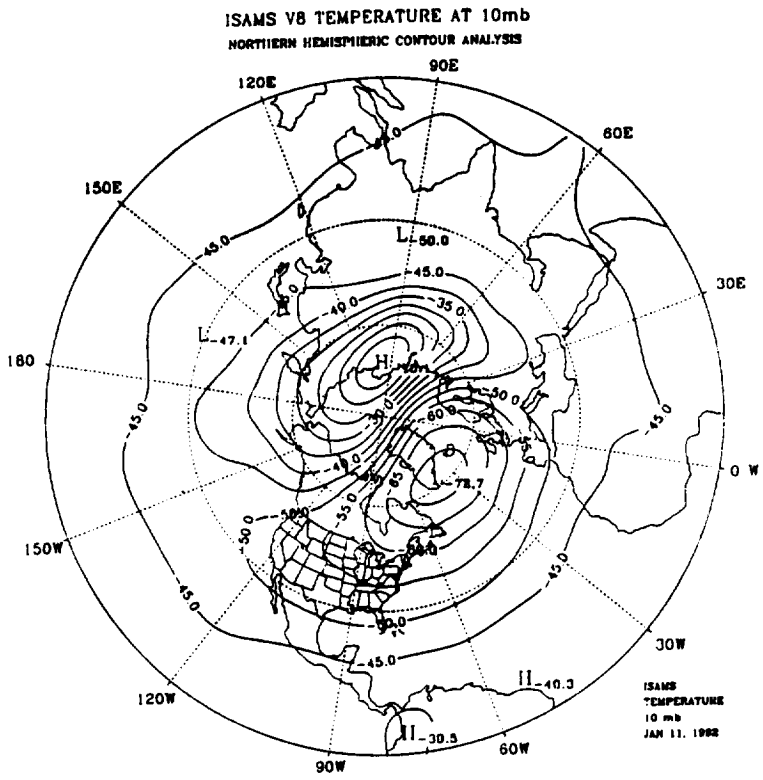

Figure 4.5-3 (c)

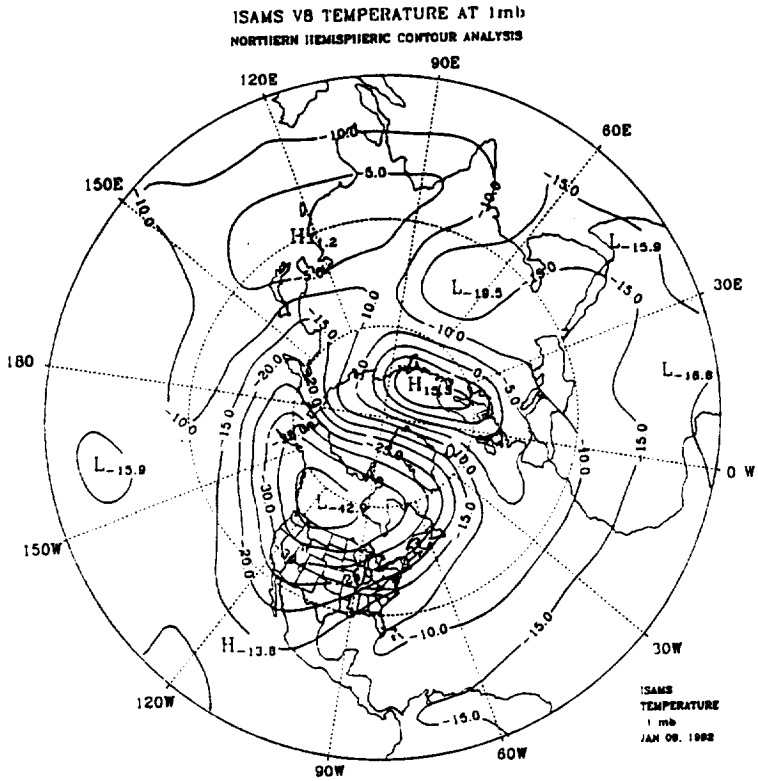

Figure 4.5-3 (d)

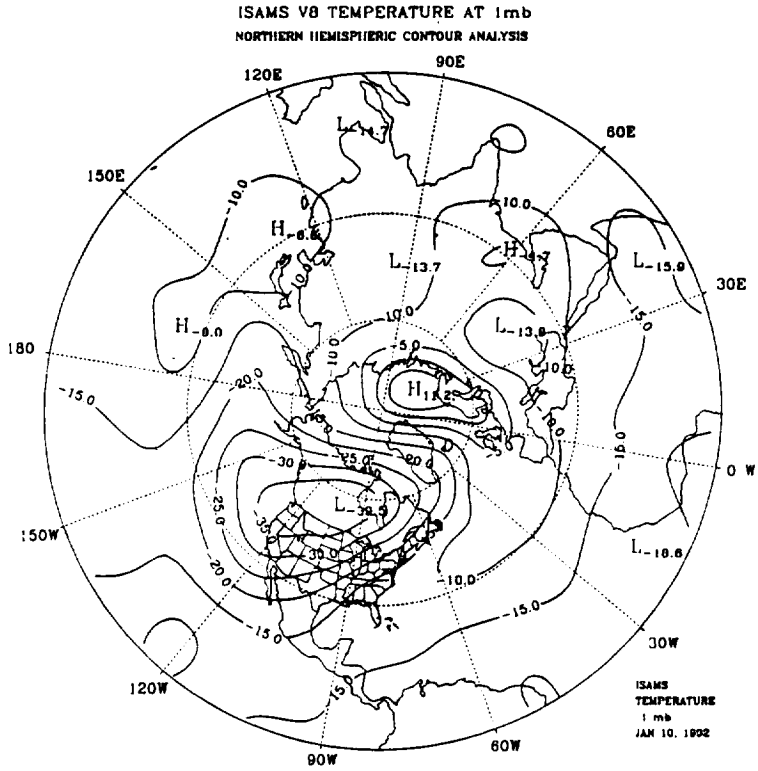

Figure 4.5-3 (e)

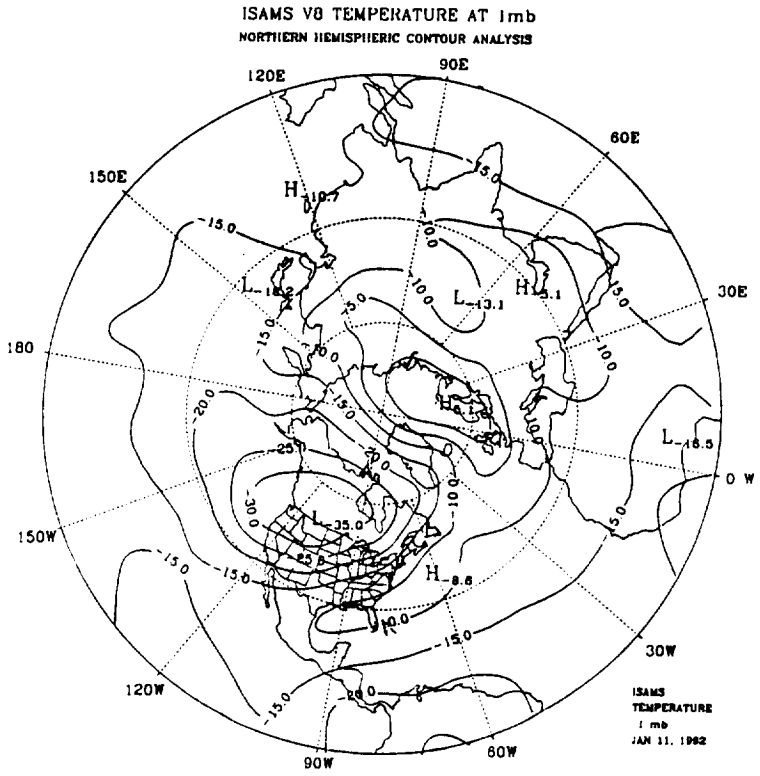

Figure 4.5-3 (f)

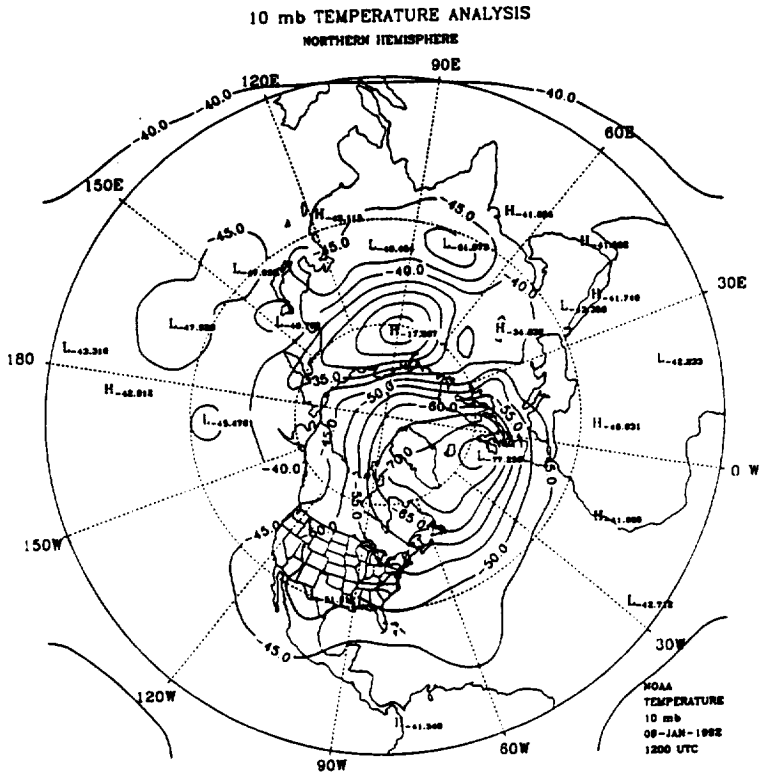

Figure 4.5-4 (a)

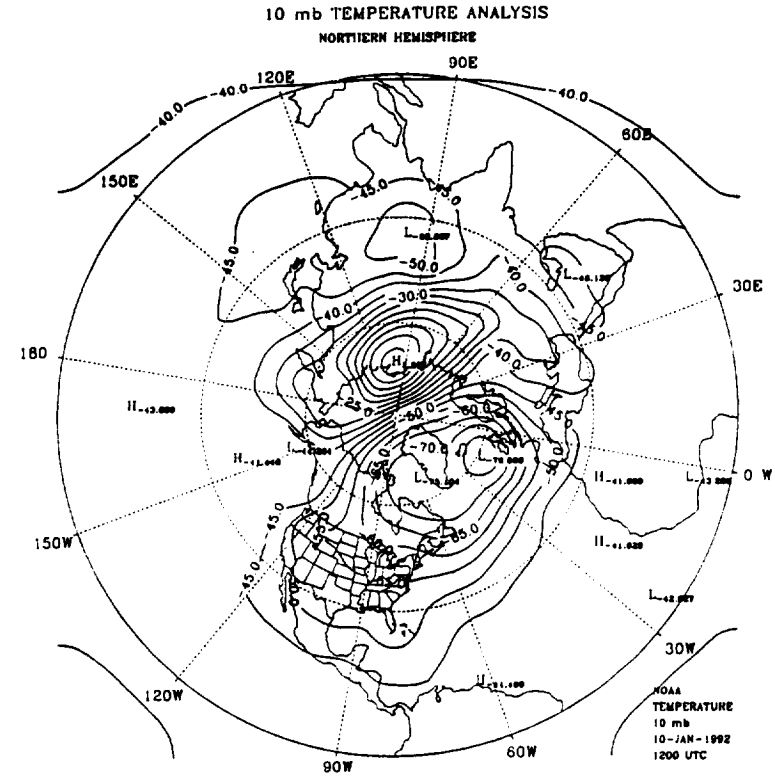

Figure 4.5-4 (b)

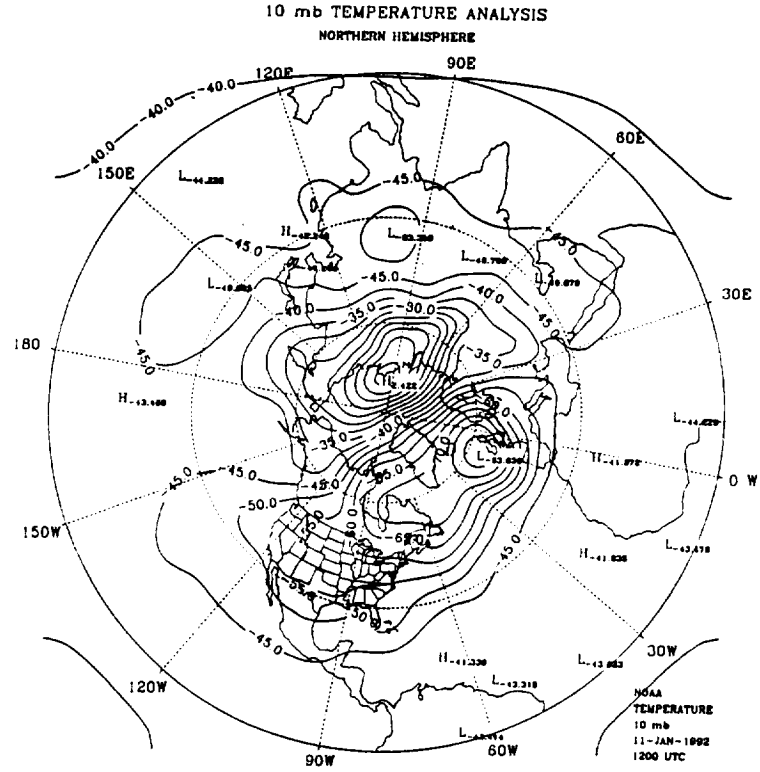

Figure 4.5-4 (c)

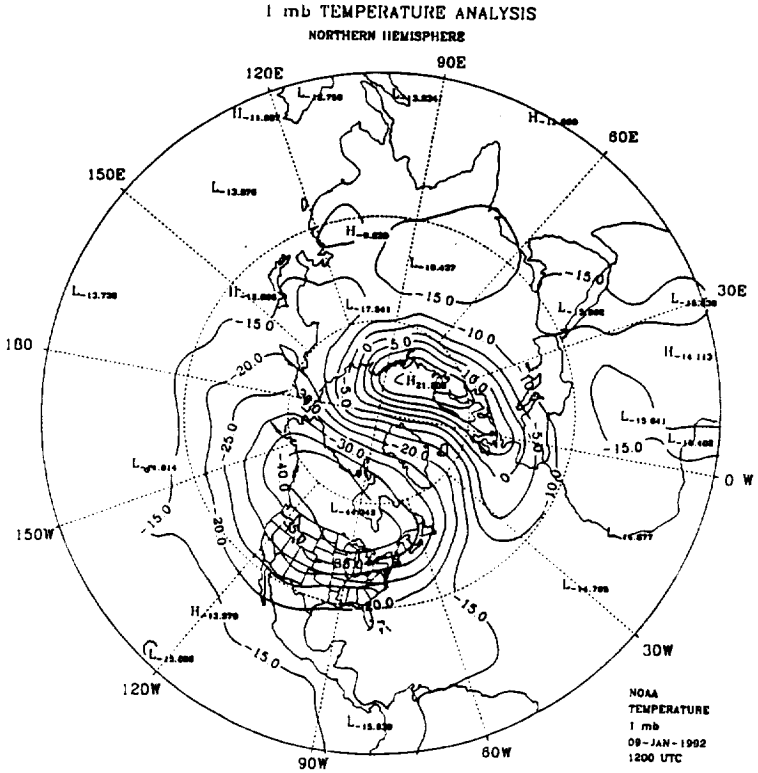

Figure 4.5-4 (d)

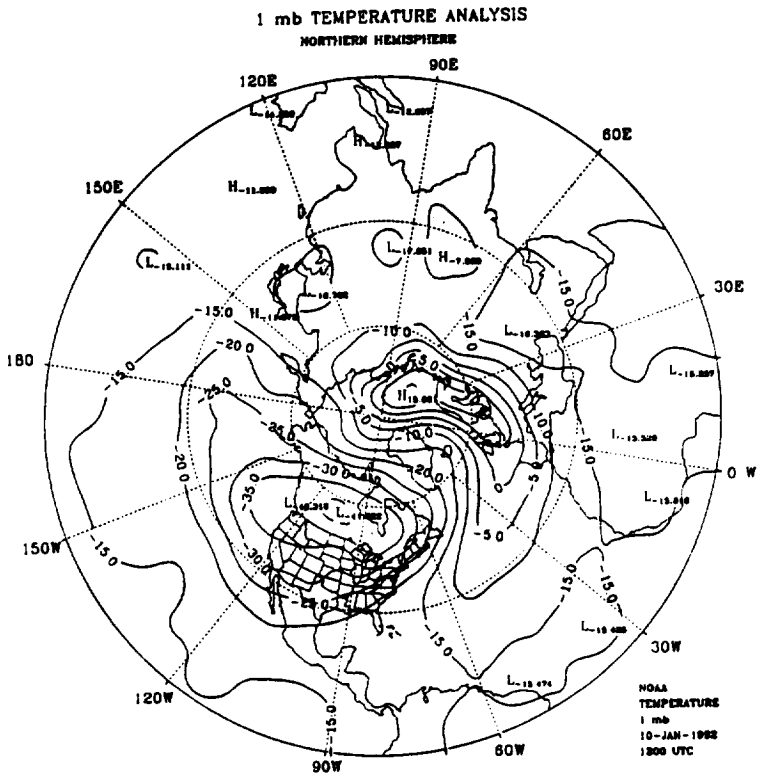

Figure 4.5-4 (e)

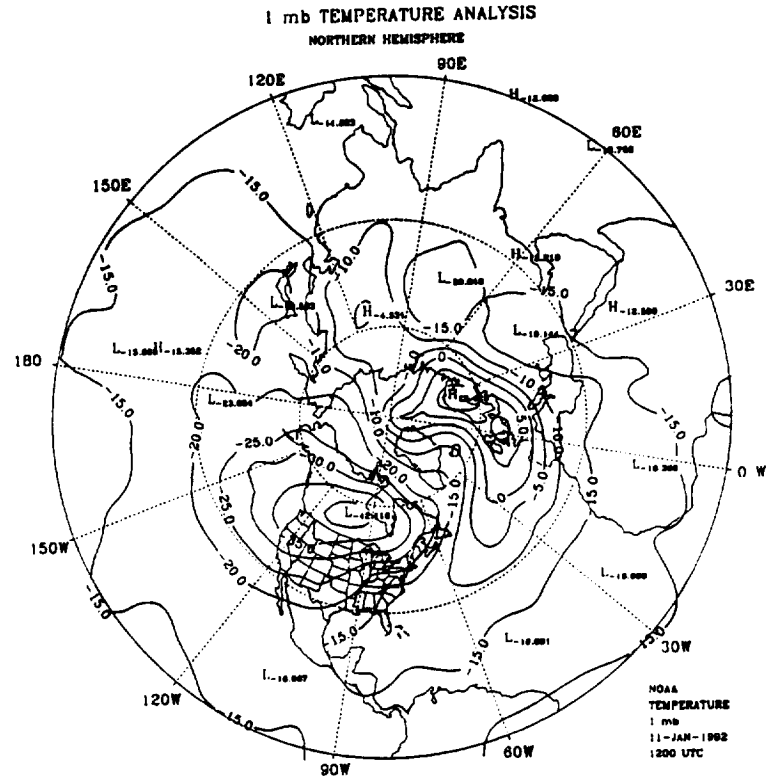

Figure 4.5-4 (f)

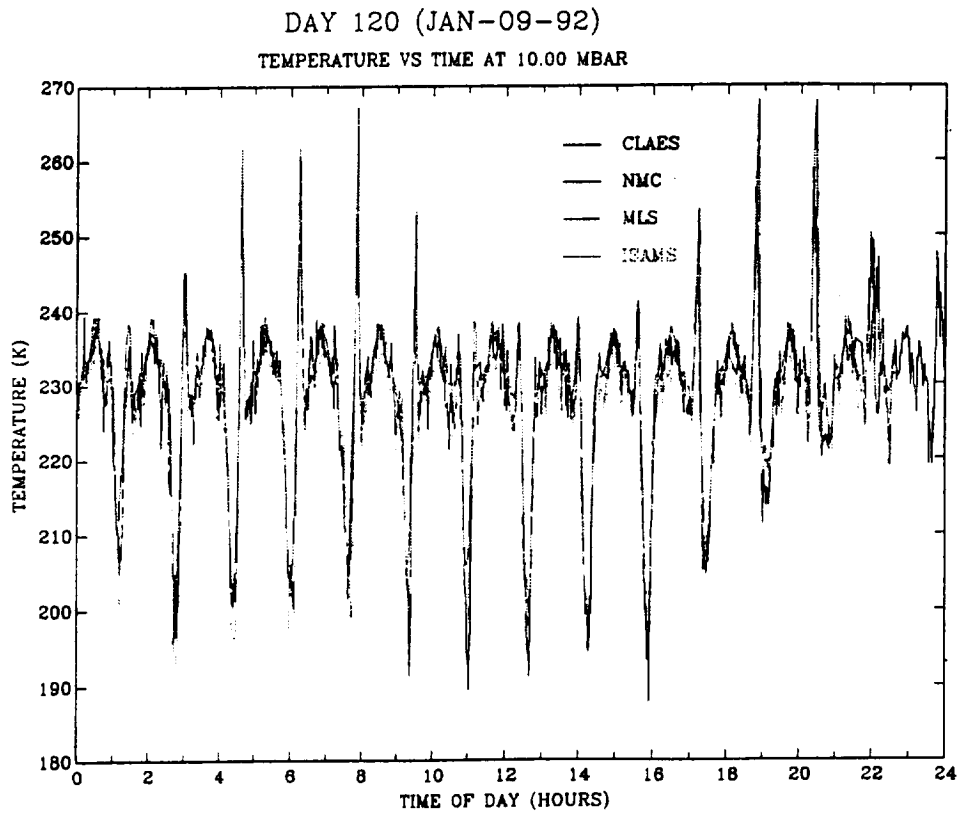

Figure 4.6–1

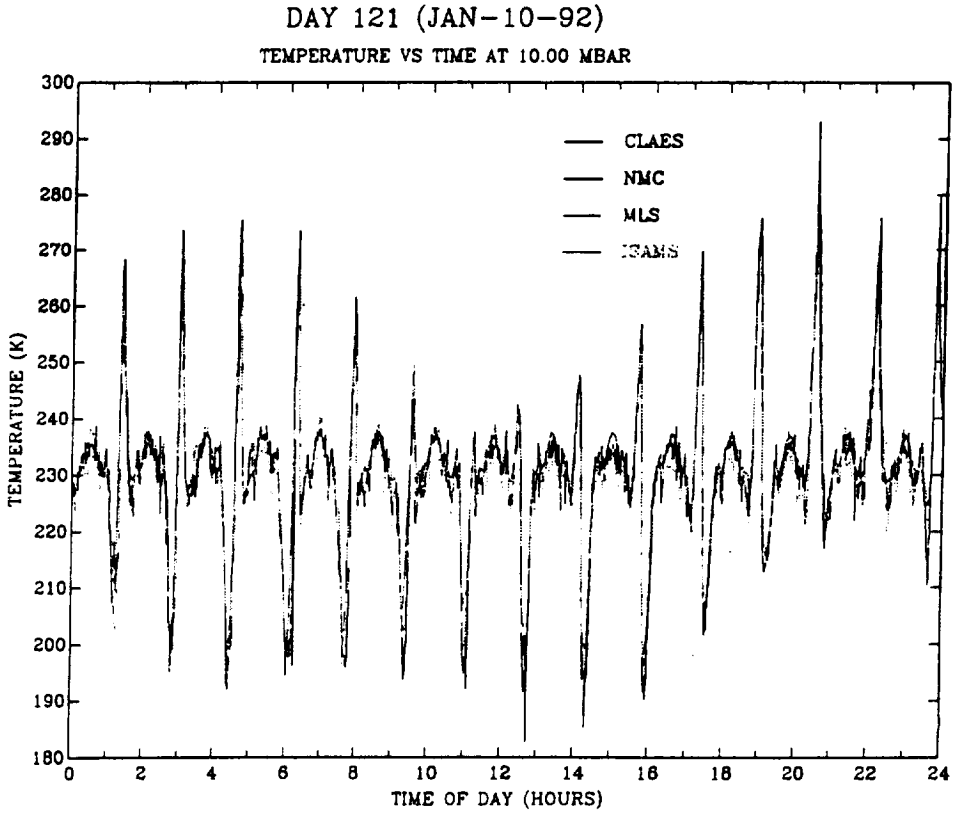

Figure 4.6–2

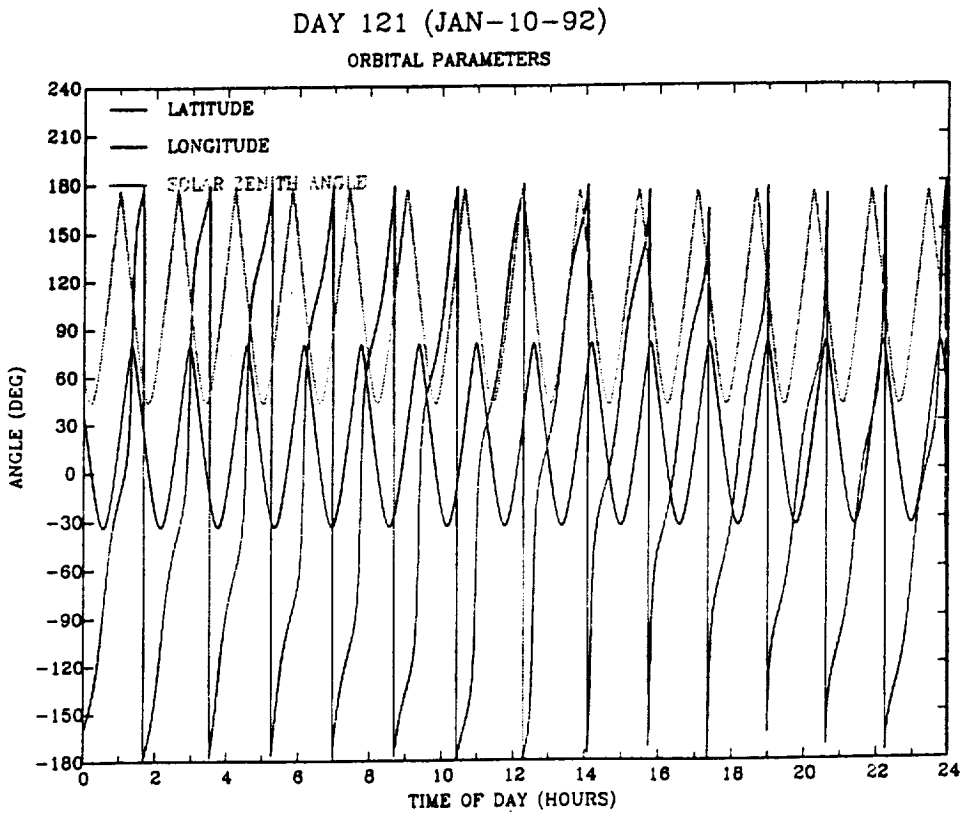
DAY 121 (JAN-10-92)
ORBITAL PARAMETERS
LATITUDE
LONGITUDE
SOLAR ZENITH ANGLE
ANGLE (DEG)
TIME OF DAY (HOURS)
240
210
180
150
120
90
60
30
0
-30
-60
-90
-120
-150
-180
0
2
4
6
8
10
12
14
16
18
20
22
24

Figure 4.6–3

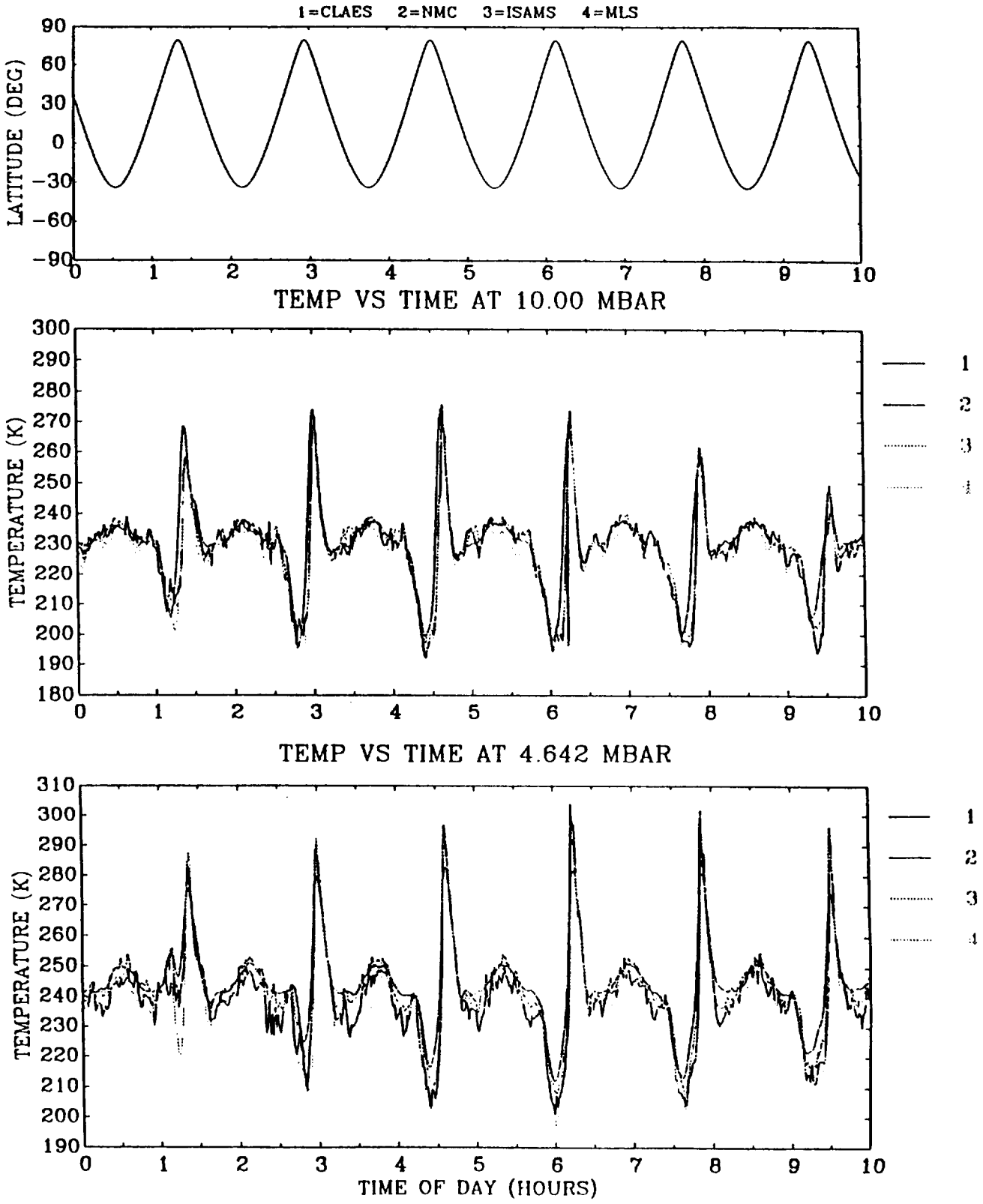
DAY 121 (JAN-10-92)
1=CLAES 2=NMC 3=ISAMS 4=MLS
LATITUDE (DEG)
TEMP VS TIME AT 10.00 MBAR
TEMPERATURE (K)
TEMP VS TIME AT 4.642 MBAR
TEMPERATURE (K)
TIME OF DAY (HOURS)

Figure 4.6–4

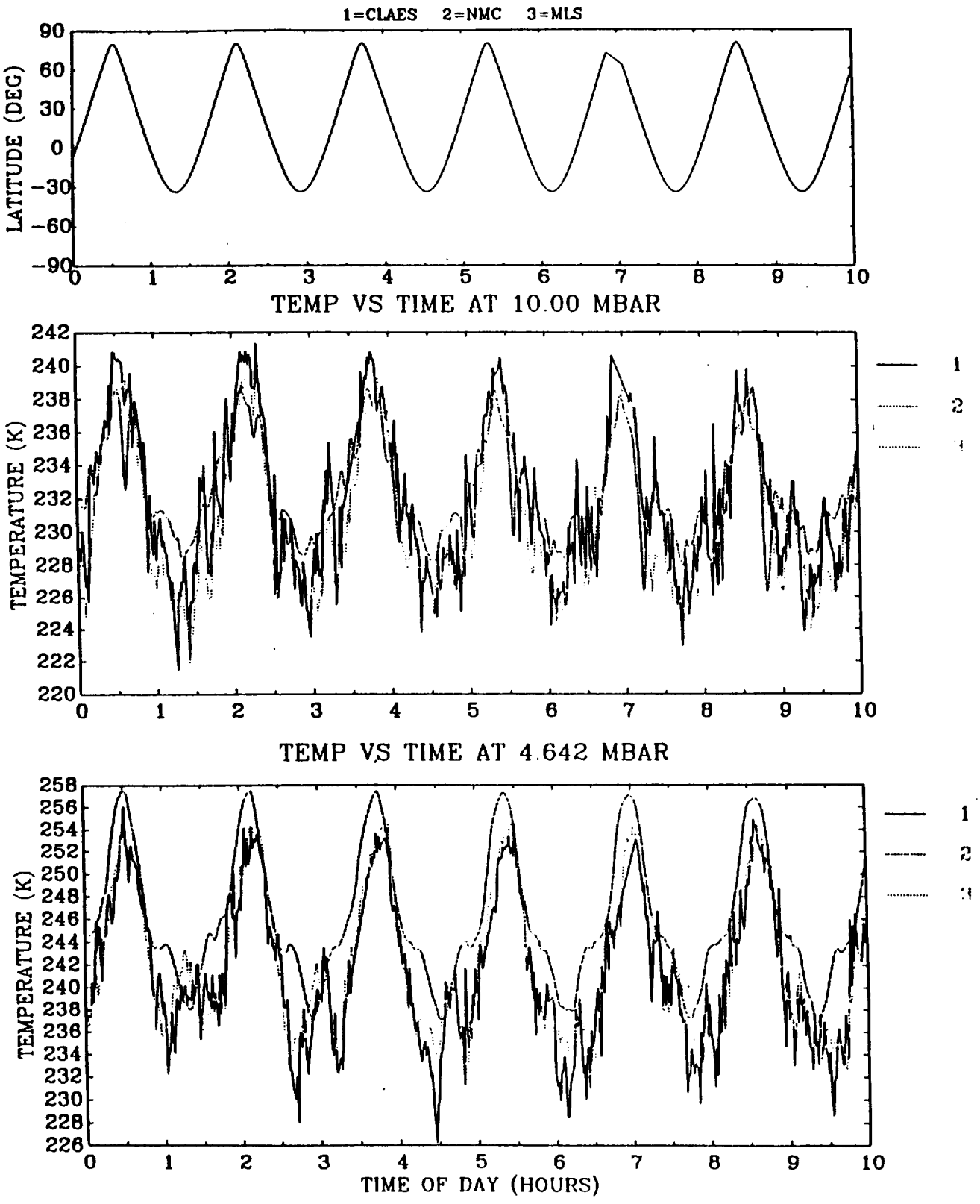
DAY 333 (AUG-09-92)
1=CLAES 2=NMC 3=MLS
LATITUDE (DEG)
TEMP VS TIME AT 10.00 MBAR
TEMPERATURE (K)
TEMP VS TIME AT 4.642 MBAR
TEMPERATURE (K)
TIME OF DAY (HOURS)

Figure 4.6–5

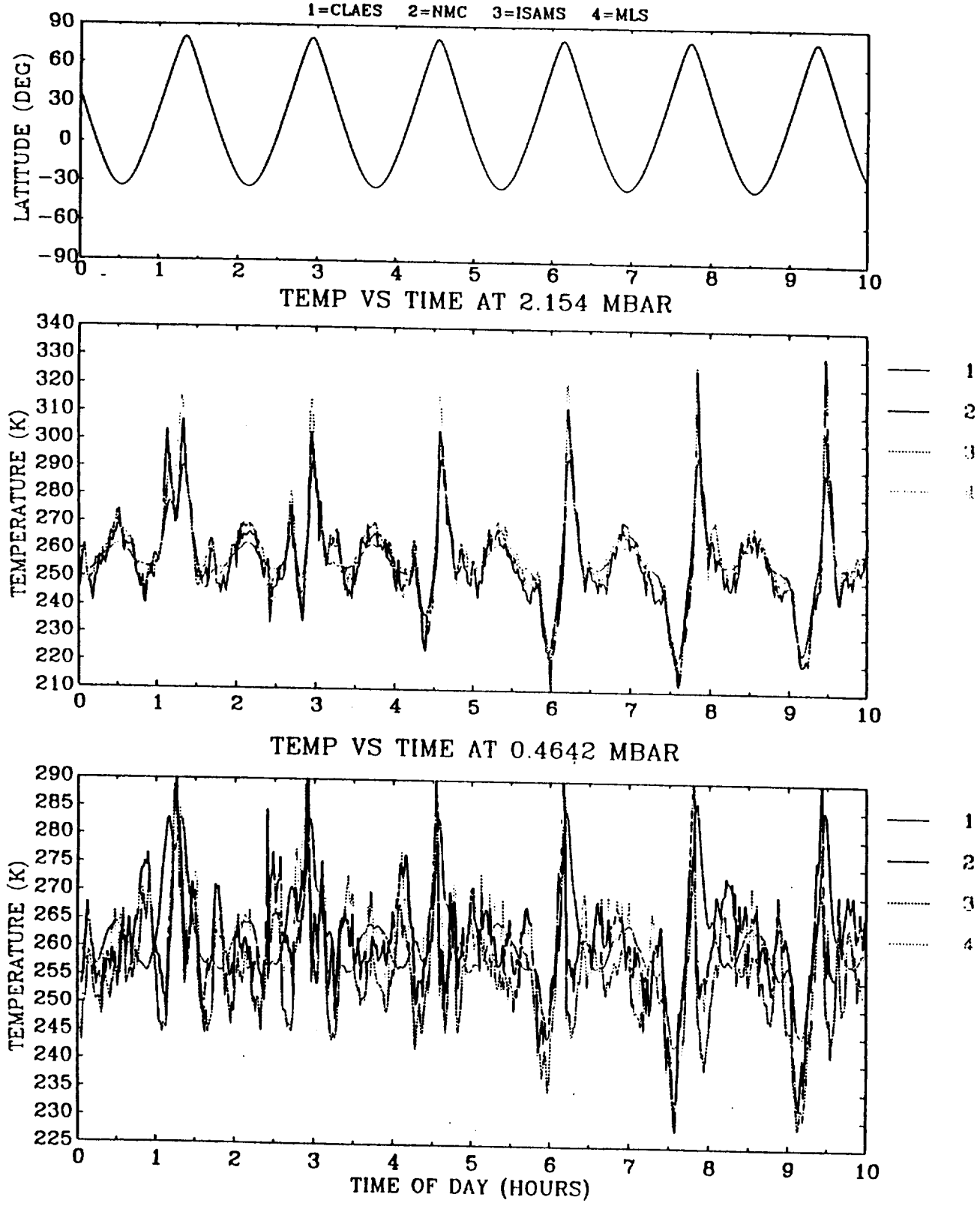
DAY 121 (JAN-10-92)
1=CLAES 2=NMC 3=ISAMS 4=MLS
LATITUDE (DEG)
TEMP VS TIME AT 2.154 MBAR
TEMPERATURE (K)
TEMP VS TIME AT 0.4642 MBAR
TEMPERATURE (K)
TIME OF DAY (HOURS)

Figure 4.6–6

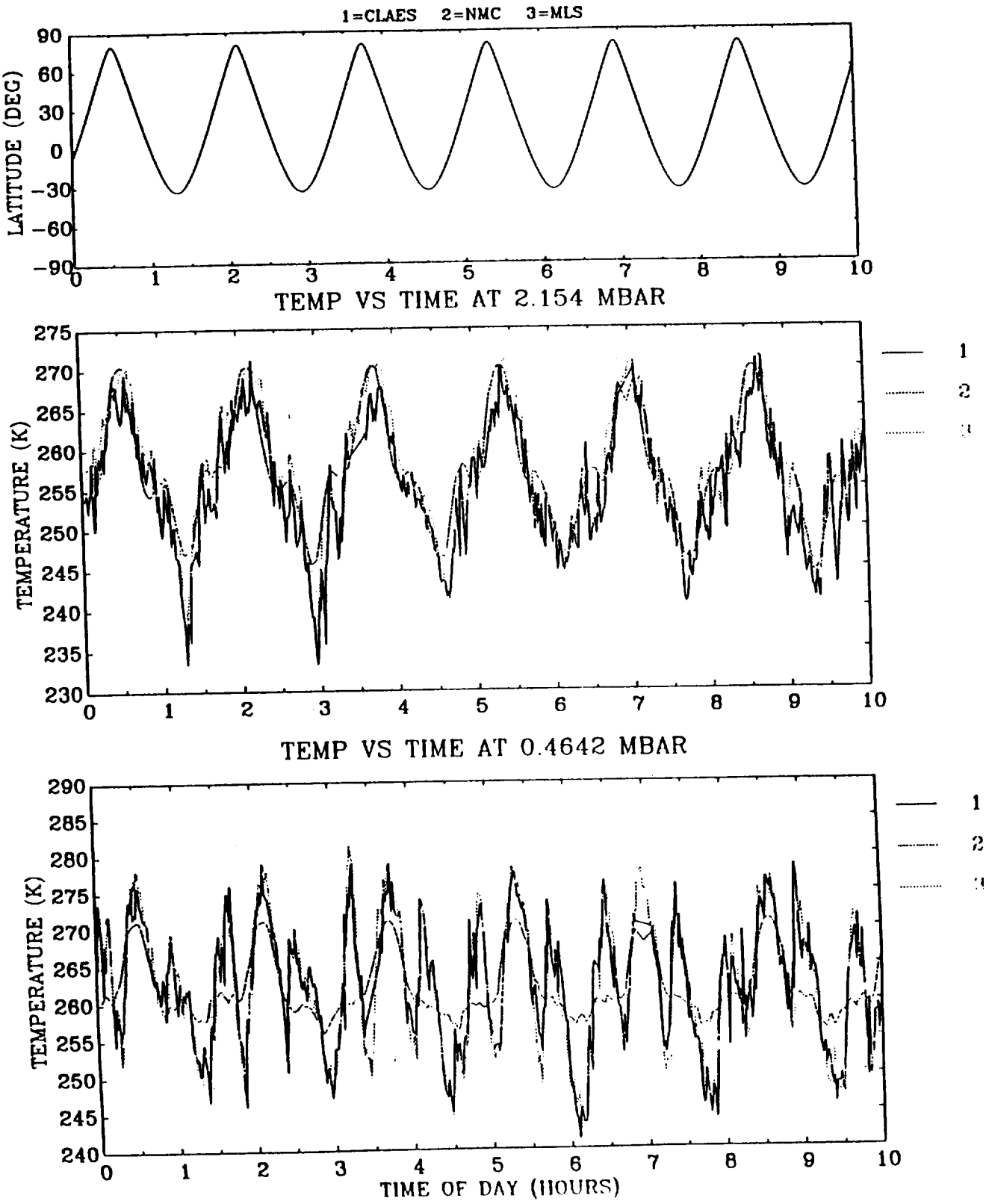
DAY 333 (AUG-09-92)
1=CLAES 2=NMC 3=MLS
LATITUDE (DEG)
TEMP VS TIME AT 2.154 MBAR
TEMPERATURE (K)
TEMP VS TIME AT 0.4642 MBAR
TEMPERATURE (K)
TIME OF DAY (HOURS)

Figure 4.6–7

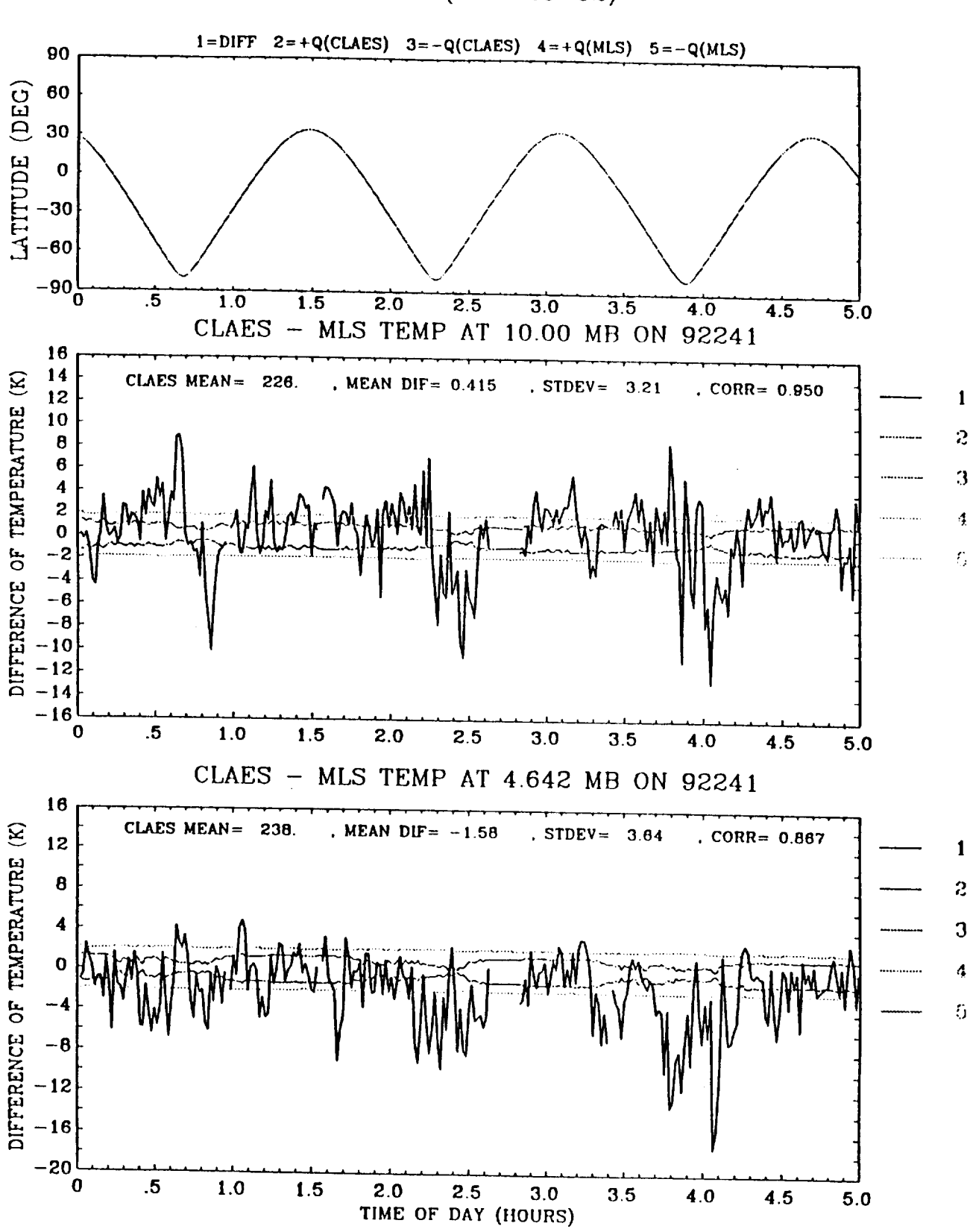
DAY 352 (AUG-28-92)
1=DIFF 2=+Q(CLAES) 3=-Q(CLAES) 4=+Q(MLS) 5=-Q(MLS)
LATITUDE (DEG)
CLAES - MLS TEMP AT 10.00 MB ON 92241
CLAES MEAN= 226. , MEAN DIF= 0.415 , STDEV= 3.21 , CORR= 0.950
DIFFERENCE OF TEMPERATURE (K)
CLAES - MLS TEMP AT 4.642 MB ON 92241
CLAES MEAN= 238. , MEAN DIF= -1.58 , STDEV= 3.64 , CORR= 0.867
DIFFERENCE OF TEMPERATURE (K)
TIME OF DAY (HOURS)

Figure 4.6-8

5. OZONE

5.1 CORRELATIVE DATA

5.1.1 SAGE II

SAGE II was launched at the end of 1984 and has been making measurements continuously since then. Sunrise and sunset observations of ozone mixing ratio and aerosol extinction at 1.02, 0.52, 0.45 and 0.38 nm for the month of October 1991 and for December 9-11, 1991 and January 9-11, February 18-21, April 15-20, and August 25-28, 1992 are available in the GA$DISK area on the CDHF. Sunset observations for NO_2 have also been included in that data set. The observations are retrieved at one km intervals in altitude and then converted to pressure levels using NMC temperatures. It should also be noted the NMC temperature profile is an integral part of the SAGE II retrieval procedure (it is used to obtain the molecular scattering contribution to the observed radiances).

In mid-1989, minor deterioration of the SAGE II scan mirror mechanism was noted with a resultant increase in SAGE II noise levels affecting the profile retrievals at low signal-to-noise levels (e.g., ozone above 50 km altitude). Following the eruption of the Pinatubo volcano, aerosol optical depths at SAGE II wavelengths in the direction of the Earth's limb became greater than unity in the tropics below 26 km altitude and sometimes elsewhere in the atmosphere at slightly lower altitudes. As a result, SAGE II gas retrievals have been substantially affected (or sometimes rendered impossible) below 30 km altitude. These uncertainties are reflected in the SAGE II profile error bars. SAGE II also measures water vapor and has yielded an interesting climatology up to mid-1989. Because of the effects noted above, the water vapor retrievals are of lesser quality since that time.

5.1.2 SBUV/2

Since 1985, NOAA has included an ozone sensing instrument on board the afternoon satellite of the NOAA operational satellite series. This instrument, the Solar Backscatter Ultraviolet Ozone Sensor /2 (SBUV/2), is based on the design of the SBUV flown on the NASA Nimbus 7 satellite. This sensor, which provides both total column ozone and ozone vertical profiles between 25-55 km, depends on measurements of the UV albedo in the sunlit portion of the globe. Thus, during winter, these measurements are unavailable in the polar night. Also, over the course of time, questions have been raised as to the relative drift of the ozone measurements due to possible degradation of the diffuser plate and/or changes in the orbit with time. Consequently, we regard the SBUV/2 data, at this time, as a relative rather than an absolute standard for comparison. Thus, we can compare relative map values for a single day, but should not regard the SBUV/2 values as an exact standard. An additional point for consideration is that the SBUV/2 ozone retrieval is independent of the NOAA temperature retrievals.

5.1.3 Lidar

Data on ozone with the DIAL technique are obtained by comparing a strongly absorbed laser wavelength (on) with a weakly absorbed wavelength (off). In most cases the "on" wavelength is 308 nm and the "off" is 351 nm. The algorithm to obtain ozone number density is based on the lidar equation which gives the power of the receiver as a function of optical thickness and backscattering coefficient. A logarithmic derivative of this equation, written for the "on" and "off" wavelengths, will give ozone density as a function of altitude.

The presence of the aerosol from the Pinatubo eruption will change both the optical depth and the backscattering coefficient. In particular, this coefficient can be written as a function of the backscattering ratio between that due to aerosols and that due to Rayleigh scattering. In recent times, backscattering ratios of 10-15 have been observed in the 15-25 km region of the stratosphere. To recover ozone profiles, the terms containing the backscattering ratio in the lidar equation must be extracted. The backscattering ratio at 351 nm is obtained by fitting a simulated signal to the observed one. The simulated signal is obtained from the atmosphere observed by an ozonesonde, and the fitting is made in a self-consistent way so that optical thickness from aerosols is taken into account. Once this is obtained, it is scaled down to the 308 nm line by an empirically derived relationship. This reduction technique gives reasonable results when compared to ozonesonde data. However, for large optical thickness and/or large backscattering ratios in the aerosol region there is a systematic underestimation of the ozone density. This is true in particular when there are very thin layers with large backscattering ratio. Because the ozone retrieval algorithm is sensitive to derivation of the signal with altitude, even a small error will introduce a large uncertainty in the ozone profile.

Some of the lidar are taking data on visible wavelengths together with the DIAL lines, and this may give further information. Comparisons have been made against the McDermid lidar at Table Mountain Observatory (TMO; 34N, 118W), the McGee transportable lidar which has been operated at GSFC, TMO and Observatorie Haute Provence (OHP) and the Visconti lidar at L'Aquila (42N, 13E).

5.1.4 Ground-based Microwave

Ozone has been observed with a microwave radiometer at Table Mountain, California (34.4 N, 117.7 W), from July 1989 to June 1992, and then with the same instrument at OHP (43.9N, 5.7E) from July 15 - August 15, 1992. Brian Connor, of NASA Langley, and Alan Parrish, University of Massachusetts, are Co-principal investigators. The instrument operates at a frequency of 110.8 GHz with a bandwidth of 630 MHz. Profiles are retrieved from 20-70 km. The estimated precision is 4-8 %, accuracy 4-10 %, and resolution 8 km below 40 km and 15 km above 60 km. A measurement is recorded every 20 minutes, 24 hours a day, weather permitting. These data are normally averaged into 5-6 hour blocks (2 daytime and 2 nighttime per day) for intercomparison with other experiments. Retrieved profiles from 56 mb to 0.04 mb are available on the CDHF.

5.1.5 Ozonesondes

Ozonesondes provide a very important continuous (weekly to bi-weekly launches typically) source of information for the lower stratosphere (up to ~ 10 mb), with accuracies generally quoted in the 5 % range. Moreover, these measurements are not believed to be adversely affected by aerosols.

The measurements from Ascension Island and Brazzaville, Congo (kindly provided by J. Fishman) represent essentially the only source of continuous data in the tropical lower stratosphere, and those observations are not currently scheduled to continue past the summer of 1993. Given the apparent effects of Mt. Pinatubo on UARS measurements (in the infrared) and differences between the ozone profiles measured by the UARS sensors in the tropical lower stratosphere, comparisons with ozonesonde data are critical for an evaluation of the attempts to remove such effects from the UARS retrievals.

5.1.6 UARS Data - CLAES

The CLAES data processing software (Versions 6 and 5) retrieves ozone in two blocker filter regions. Blocker 8 is centered at about 792 cm^{-1} and includes emission features from both ozone and carbon dioxide. Blocker 9 is spectrally located near 840 cm^{-1} and includes emission from ozone, CO_2 and $CLONO_2$. At the present time, the ozone profiles derived from the radiance measurements in the two blockers show relatively large systematic differences. Possible causes for these discrepancies are currently being investigated. The CLAES team recommends use of profiles obtained from blocker 9 for use in the current validation exercise.

However, blocker 9 ozone profile retrievals exhibit a quasi-systematic pattern of relative minima and maxima in the vertical as can be seen in Figure 5.1.6-1. These artifacts are present in the statistical comparisons with correlative measurements and can also be seen in comparisons with the other UARS instruments which measure ozone. While the exact cause is yet to be verified, it is thought that they result from difficulties in establishing the radiometric calibration curves for each detector at low radiance levels in this long wavelength region. It is anticipated that these problems will be corrected in the next version of the software.

Under the current data release plan, it is possible that not all of the CLAES data will be processed with the Version 6 algorithm by the time the first year of UARS data are available to the public. If some of the data released are Version 5, it may be useful to know how Version 5 and Version 6 differ. Figure 5.1.6-2 shows the altitude profile of the mean difference between Versions 6 and 5 ozone profiles for all observations made between 20 degrees North and 50 degrees North on January 9, 1992. The horizontal bars represent standard deviations. For altitudes above 30 mb, the newer version predicts 10-15 percent more ozone than the Version 5. For altitudes below 30 mb, the ozone mixing ratio in the newer version has decreased by 10 to 15 percent.

5.2 COMPARISON RESULTS

5.2.1 Profiles

5.2.1.1. UARS Limb Sounders /HALOE Intercomparisons

UARS Limb Sounders (MLS, CLAES, and ISAMS) and HALOE vertical profile mean differences were compared for the four main intercomparison periods: January 9-11, April 15-20, August 8-10, and August 25-30, 1992. Approximately 90 HALOE / emission sounder coincidences were found in each period using criteria of 1000 km miss distance and 6 hours miss time. Mean and RMS profiles were determined from individual profiles of differences. MLS and CLAES were operating during all four periods and ISAMS was taking data during January and April. The January data are typical of the kinds of variations observed, and these are plotted in Figures 5.2.1-1 through 5.2.1-3.

For the April 15-17 period at $10^{o}S$ (Figure 5.2.1.1-1), MLS and HALOE show mean differences ranging as high as 25% above the 3 mb level with MLS ozone consistently higher. Between 3 and 10 mb, MLS still shows 10% higher ozone than HALOE and a

higher altitude level for the ozone mixing ratio maximum. Between 10 and 20 mb, the two datasets agree to within ~10%. This pattern is representative of MLS-HALOE comparisons for the other periods (at 17°S and 39°N) with the exception of the January (47°N) period which shows better agreement throughout the entire profile (less than 15% above 50 mb).

ISAMS and HALOE data for April (Figure 5.2.1.1-2) indicate as much as a 25% mean difference above 12 mb. HALOE data is consistently higher than ISAMS through most periods, especially at the peak ozone level. The January period (mid-latitude) shows the best agreement between HALOE and ISAMS (within 10% at all altitudes), while the period shown (15-17 April) and 18-20 April (tropical latitudes) show differences on the order of 25%.

CLAES and HALOE differences in April vary greatly with pressure level. Above 10 mb, CLAES is generally higher with differences ranging from 0 to just over 1 ppmv (~20%). CLAES, like MLS, also shows a higher altitude level for the ozone peak than does HALOE, whereas HALOE and ISAMS show the peak at the same altitude. This pattern is similar in all other comparison periods. CLAES and MLS show maximum ozone mixing ratios at the same or higher altitudes than HALOE for the April and August periods, but all four experiments show almost the same altitude for the peak in the January 9-11 period. The difference in peak location may be due to slight altitude registration differences and to different vertical resolutions of the experiments.

5.2.1.2 Lidar and Microwave Comparisons

For the comparison period of the UARS data, the available ground-based stratospheric ozone profile information is as follows:

LIDAR	TIME	INVESTIGATOR
TMO	9/91 - 12/92	McDermid
TMO	2/92 - 3/92	McGee
GSFC	9/91 - 1/92	McGee
L'Aquila	9/91 - 12/92	Visconti
MICROWAVE		
TMO	9/92 - 4/92	Connor/Parrish

There are, then, more than a year of data from the McDermid lidar at Table Mountain Observatory (TMO) and the Visconti lidar data at L'Aquila. The McGee lidar observations were split between his home site at Goddard Space Flight Center (GSFC) and TMO where he was assigned as part of an overall comparison with the McDermid lidar and the Connor/Parrish microwave instruments. The following comparisons also include data from the NOAA Solar Backscatter Ultraviolet Ozone Sensor (SBUV/2) satellite, with coincidence criteria of the same day and 5 degree latitude and longitude 5 or 10 degree differences.

With respect to the time phasing of the comparisons, the SBUV/2 data are sun synchronous

and during the comparison period were available at about 3:30 p.m. local time. Thus, while the lidar data tend to be taken in the early evening, the diurnal phase relationship to the SBUV/2 should be similar at all sites. The microwave instrument, on the other hand, is capable of full day operation and during its stay at TMO reported 4 times per day; 2-daytime and 2-nighttime (0500, 1100, 1700 and 2300 local time).

Figures 5.2.1.2-1 and 5.2.1.2-2 show mean profiles at TMO for the two validation periods, January 9-11, 1992 and April 15-20, 1992 when MLS, ISAMS and CLAES were all operating. The profile shapes and heights of the maxima are in good agreement, except for CLAES which has oscillations between about 2 and 46 mb. These characteristic oscillations are believed to the an artifact of the radiance calibration process. The agreement is better for the January period and all measurements (except CLAES) are mostly within 0.5 ppmv or better between 2 and 10 m. At altitudes below 10 mb the agreement is poorer as ISAMS and CLAES begin to be influenced by stratospheric aerosol. In the April period, MLS values are highest between 2 and 10 mb except for the lidar near 2 mb, while ISAMS values are the lowest down to 10 mb. Below 10 mb, CLAES values become the highest, followed by MLS. The good agreement between ISAMS and microwave below 10 mb is of questionable significance because this version of the ISAMS retrievals are weighted towards climatology below 10 mb due to temperature problems in the aerosol layer.

HALOE ozone data have also been compared to the McDermid lidar results and to the Connor microwave measurements at Table Mountain Observatory (Figure 5.2.1.2-3). Some significant differences exist in these measurements. On three days, Febr. 25,1992, March 15,1992, and March 18,1992, all three measurements were made at Table Mountain. The mean of the differences between HALOE and each measurement type is shown in Figure 5.2.1.2-3a. These differences show that McDermid lidar data are systematically higher than HALOE at most altitudes, while McGee lidar data and Connor microwave results tend to show differences which alternate in sign in a quasi-systematic way. The McGee lidar data tend to be lower than HALOE at the lowest and highest altitudes and the microwave tends to be higher at the highest altitudes (a diurnal effect). In general, HALOE and correlative ozone measurements agree as well or better than the agreement between the three correlative data sets.

Figure 5.2.1.2-3b shows a scatter plot of three profile pair differences (Correlative-HALOE) for three days February 22-24, 1992 at Table Mountain Observatory. These profile differences show similar characteristics to those in Figure 5.2.1.2-3a with the McDermid lidar measurements showing larger ozone differences than the McGee lidar and Connor microwave.

Comparisons against the McGee lidar at OHP and zonal mean UARS profiles (Figure 5.2.1.2-4 to 5.2.1.2-5) show overall lower ozone values measured by the lidar at all altitudes. Differences are approximately 10% at the 10 mb ozone peak and are as high as 30-40% at the highest and lowest altitudes. HALOE data was used for August 10 instead of August 8 to improve the latitude difference of the coincidence from 8 degrees to 1 degree.

Although 10-30% differences appear when comparing zonal means to one McGee lidar profile, two individual profile comparisons of HALOE versus McGee lidar at OHP (Figure 5.2.1.2-5a and b) give better results. The latitude differences are within 2 degrees and the days are within 2 days. The agreement is excellent (less than 0.5 ppmv differences) and the profiles shapes are virtually identical. This suggests that the effect of comparing a single lidar profile to a zonally averaged measurements UARS can lead to erroneous conclusions.

The mean differences between MLS and the McDermid lidar are shown in Figure 5.2.1.2-6. The mean relative differences between the UARS instruments and the GSFC, Table Mountain and Frascati lidars beginning January 1, 1992 have also been calculated (Figure 5.2.1.2-7). The differences between MLS and the lidars are 5-10% (MLS lowest near 1 mb). The larger MLS differences at altitudes lower than 50 mb are in the region where the lidar measurements are less reliable. For pressures between 20 and 0.6 mb, CLAES is about 10 to 30 percent lower than the lidar measurements. Below 20 mb, the CLAES observations are greater than the lidars by 20-30 percent. The horizonal bars show the standard deviations of the differences. The lidar measurements are about 30% larger than ISAMS for altitudes above 10 mb.

The means of the comparisons of UARS observations against the microwave measurements are shown in the next series of figures. Figure 5.2.1.2-8 shows MLS to be systematically higher than the microwave measurements, particularly near 5 mb. Figure 5.2.1.2-9 shows the ISAMS measurements to be systematically lower than the microwave between 2 and 10 mb with the largest differences (0.5 ppmv) near 7 mb. Below 10 mb, ISAMS values are higher than the microwave (although this is probably not significant because of relaxation to climatology).

A simultaneous comparison of the mean difference of CLAES, ISAMS, and MLS with the microwave measurements taken after January 1, 1992 was also made. The sampling window used was within 4 degrees of latitude, 12 degrees of latitude equivalent longitude, and 12 hours of the microwave measurements. The mean differences and standard deviations of differences were computed as a function of pressure at each of the standard UARS pressure levels. Because of the large sampling window, the standard deviations reflect a large component of atmospheric variability in addition to instrumental uncertainty. The mean differences (Figure 5.2.1.2-10) for CLAES oscillate between ± 25% from 50 to 0.6 mb. The effects of the artifacts in the blocker 9 retrievals are responsible for the oscillatory nature of the differences. The ISAMS measurements in the mean are about 15% lower than the microwave measurements over the 0.21 to 10 mb pressure range. The MLS measurements in these comparisons are about 10 percent greater than the microwave and are consistent with the results cited earlier.

A comparison of HALOE and microwave mean profiles is shown in Figure 5.2.1.2-11. Between 0.46 and 15 mb, the differences are less than approximately 5%, and the rms differences are approximately 10%. HALOE values below 15 mb are generally larger by 10-20%. The large differences above 0.46 mb might be associated with diurnal variations of ozone in the upper stratosphere and lower mesosphere (a mean night-to-day ozone ratio of 3 has been observed at 0.1 mb by Connor and Parrish , personal communication, 1993).

Figure 5.2.1.2-12 shows that the McDermid (TMO) lidar gives, on average, 3 to 8% larger values than the microwave between 1.5 and 10 mb, whereas SAGE II measurements (Figure 5.2.1.2-13) show excellent agreement (better than 3% mean and 10% rms) over the same pressure range.

Figure 5.2.1.2-12 has shown that the McDermid lidar often gives larger ozone concentrations than the microwave, but Figure 5.2.1.2-3 suggests that this lidar may give larger ozone concentrations (±10%) than the McGee lidar. These lidars and the microwave instrument have been compared to SBUV/2 in an attempt to further elucidate these differences. Figures 5.2.1.2-14a and b show the microwave minus SBUV/2 results, day and night respectively with 133 matchups included in the former and 121 in the latter. The horizontal bars denote the 95% confidence limits on the mean. We see that for the daytime

case, the values are within a few percent of zero from 30 to 1 mb and increase significantly above and below. The nighttime values indicate a somewhat similar pattern, but above 5mb indicate an increasing difference caused by the diurnal variation of ozone. Figure 5.2.1.2-14c shows the SBUV/2 results versus the McDermid (nighttime) lidar over the somewhat longer time period. We see that at 2 mb, the lidar and nighttime microwave comparisons overlap, but at 5 and 10 mb the lidar data are higher. The lidar results at 1 mb are significantly more positive than the microwave data, but this is about the top level of the lidar data and is probably not significant.

In Figure 5.2.1.2-15a and b we present similar comparisons against McDermid and the microwave instrument, but for the more limited period of February to March when McGee participated in the comparisons. We see that the results show larger error bars, in line with the smaller data sets of 5 and 18 respectively, but that the pattern is quite similar. At 10 mb, the two again overlap, but at 5 mb a bias is again noted. In the McGee comparisons, Figure 5.2.1.2-15c, with 7 matchups, we see that at 1 mb the lidar results are considerably lower than the others (but we do not regard this as significant as stated above). At the lower levels we see that all three observations agree at 2 mb, the two lidars agree at 5 mb, McGee is slightly low at 10 mb (but within error bars) and McGee and the microwave agree at 30 mb.

These results therefore suggest that the lidars give 5-10% larger ozone values at 5 mb with the SBUV/2 agreeing better with the microwave values. On further inspection, however, this difference also seems to be time dependent. For example, the McGee observations at GSFC prior to February, 1992 give better agreement with SBUV/2 (and by implication with the microwave) (Figure 5.2.1.2-16). Here, there is a difference at 10 mb which is absent in McGee's later measurements because of the use of Raman scattering techniques which improved the signal/noise ratio in the aerosol layer when this lidar was operated at TMO.

Figure 5.2.1.2-17 shows SBUV/2 comparisons at L'Aquila for the extended period of September 1991-December 1992 with 25 matchups. At L'Aquila the lidar has somewhat less power than the McGee or McDermid lidars, and as a result increased error bars are found at 5-mb rather than at 1-mb for the other systems. At 10 and 30 mb, the results are well within the error bars and it is not until 50 mb that we see a significant difference with the microwave observations. For this period the lidar results are greatly influenced by the Pinatubo aerosols at and below 10 mb and the agreement with the microwave at 10 and 30 mb should be interpreted as indicating that they have, effectively, taken this into consideration. This lidar is not, however, able to shed any light on the 5 mb discrepancy.

In Figure 5.2.1.2-18a we present time series, at 5 mb, of the SBUV/2 data, both version 6 and an earlier version 5.5, the McDermid lidar observations and the MLS data. Also included in this diagram is the sawtooth pattern showing the times UARS looked north and south. In the early part of January, the lidar, MLS and SBUV/2 observations seem to agree, but in late January the lidar and MLS observations show a substantial high-bias (roughly 10%) with respect to SBUV/2. Figure 5.2.1.2-18b contains a similar diagram for the Connor/Parrish microwave observations and we see that beyond the January period the microwave observations are significantly lower than the lidar and in agreement with the SBUV/2 data.

Time series of average daily values for ISAMS, MLS, and microwave at 10, 4.6, and 2.2 mb are shown in Figures 5.2.1.2-15a-c. The straight section of the ISAMS curves between 1992.05 and 1992.25 indicates missing data during the first ISAMS chopper

failure. The values show similar seasonal variations and small timescale features; for example, the wave structure at 2.2 mb from 1991.9 to 1992.05 may be noted. The absolute values differ systematically, with MLS higher than microwave, which in turn is higher than ISAMS. Figures 5.2.1.2-20a to c shows the fractional differences between the microwave and MLS (Figure 5.2.1.2-20a) and microwave and ISAMS (Figure 5.2.1.2-20b is pre-chopper failure, Figure 5.2.1.2-20c is after chopper restart). MLS is higher than microwave throughout the period by 5-15%, and it may be noted that at 5 mb MLS/microwave differences increase approximately 10% at the end of January. ISAMS values are generally 5-15% lower than microwave between 2 and 10 mb, and at 5mb the differences appear to be at the high end following the chopper restart. Below 10 mb ISAMS tends to be 10-20% higher than microwave early on, with better agreement later (although as stated previously, ISAMS retrievals below 10 mb are dubious).

In summary, the MLS and HALOE measurements have typically shown agreement with the lidar and microwave measurements within approximately 10% between 0.46 and 15 mb, with the MLS and the McDermid lidar giving the largest values, followed by HALOE and the McGee lidar, and then the microwave. The ISAMS measurements are typically 10% smaller than the microwave values, and the CLAES mean values are similar to the microwave values, but give a vertically oscillating structure in the differences of magnitude 10-15%. On average, SAGE II and SBUV/2 also give good agreement with the microwave measurements. However, there are some indications of temporal changes in some of the differences, the most curious of which is a discontinuity in January, 1992 at 4.6 mb which results in an apparent decrease (± 10%) in the microwave and SBUV/2 results relative to the MLS and McDermid lidar results. There is also a suggestion that ISAMS gives lower concentrations at this level following the chopper restart.

5.2.1.3 Ozonesonde Comparisons

More comparisons between UARS sensors and ozonesondes were made than for the previous validation report and some statistical comparisons exist as well, for MLS (time and data availability constraints precluded such a study for other UARS sensors). We provide some sample comparisons for various sites, and some average comparisons for MLS.

Table 5.1 gives a list of investigators who kindly provided data sets for the ozonesondes at the indicated site locations. Although not all comparison plots are shown here, two or more comparisons were generally made for each site; the dates used were chosen to be close to or on the same days as the January (9-11), April (15-20), or August (8-11; 25-30) 1992 "validation days" for UARS studies.

Table 5.1 Ozonesonde Data

Ozonesonde Site (Latitude, Longitude)	Investigator(s)
Boulder, Colorado (40.0N, 254.7E)	D. Hofmann/S. Oltmans
Hilo, Hawaii (19.4N, 205.0E)	D. Hofmann/S. Oltmans
Ascension Island (8.0S, 345.7E)	J. Fishman
Brazzaville, Congo (4.3S, 15.0E)	J. Fishman
Gardermoen (60.1N, 11.0E)	G. Braathen
Bear Island (74.5N, 19.0E)	G. Braathen
McMurdo (77.5S, 166.4E)	T. Deshler
Hohenpeissenberg (47N, 11E)	Claude
Neumayer (71S, 352E)	Gernandt

Figures 5.2.1.3-1 through 5.2.1.3-5 show sample comparisons for Boulder, Hilo, Ascension Island, Bear Island, and McMurdo, respectively. Comparisons for the other two stations listed above are not shown, for brevity, and because no significantly different conclusions can be drawn from these additional profiles. Note that although ISAMS data are shown below 10 mb in these plots, the intent is to mainly draw conclusions on ISAMS data near the peak (10 mb) of the ozone profile (as desired by the ISAMS team). The HALOE profiles shown are plotted on a vertical grid with significantly finer resolution than the actual HALOE retrievals (which are close to 3 km in spacing).

The plots above cover a range of latitudes from the Antarctic to the Arctic. A few general conclusions can be reached, and we will not attempt here to track down the reason for every discrepancy between sonde data and UARS data. For MLS, the conclusions can be strengthened somewhat, based on statistical companions for longer time periods at various sites (not all of which will be shown below). Plots of average comparisons for Boulder ozonesonde measurements versus MLS coincident profiles taken during 1992 (42 profiles total) are given in Figure 5.2.1.3-6. Similar plots for Ascension Island (in the tropics) for

the period October 1991 through October 1992 are given in Figure 5.2.1.3-7 (average of 26 profiles). The last average comparison versus MLS is for the high southern latitudes (McMurdo) during the development of the 1992 ozone hole (16 profiles during August/September), shown in Figure 5.2.1.3-8.

Based on the overall picture obtained from the above comparisons, and others not shown, which tend to support the following conclusions, some statements can be made about each of the instruments:

The CLAES ozone values (from blocker 9) are often on the high side of the ozonesonde data in the lower stratosphere (for pressures greater than 20 mb). CLAES ozone values near 10 to 20 mb are often lower than the sonde data (by more than 10%). Despite general agreement at the 10-20% level, more meaningful comparisons will probably have to wait for possible removal of the systematic oscillation in CLAES ozone discussed elsewhere in this report.

For ISAMS comparisons versus the ozonesondes, only data within a few km of the 10 mb level were considered. The ISAMS ozone values are generally lower than the sonde values, for tropical and mid-latitude comparisons (there is not an obvious systematic difference at high latitudes). Conclusions in terms of the altitude of the peak ozone will have to wait for a future version of the ISAMS retrievals.

Some HALOE comparisons appear to give slightly lower values than ozonesondes near the peak and slightly higher values below the peak, but these are not trends which can be generalized without more comparisons. Figure 5.2.1.3-9 shows mean HALOE differences for eight profiles from Hohenpeissenberg. These eight profile comparisons were all within one day (six on the same day), and no more than 2 degrees in latitude and 20 degrees in longitude apart. The HALOE measurements possess a small subsidiary maximum at an altitude below 46 mb, and the HALOE team is currently uncertain about the validity of ozone retrievals below approximately 46 mb. Figure 5.2.1.3-10 shows a series of HALOE comparisons at Neumayer in the Antarctic. The agreement with the ozonesondes is generally within 0.5 ppmv (~10%).

For MLS comparisons, agreement with the ozonesonde data is also generally within 0.5 ppmv, based on the more extensive set of comparisons performed so far. The average trends versus latitude are very similar in both the MLS and ozonesonde data. However, some systematic differences emerge. There is a tendency for MLS to overestimate (by roughly 5%) the sonde data in the 10 and 22 mb region. At 46 mb, the MLS values are generally lower than the sonde values by about 0.4 ppmv (15 to 25%). Based on the limited sonde data sets in the tropics, it appears that the latitudinal gradients observed by MLS at 46 mb are somewhat overestimated (too steep) but that the actual gradients are steeper than implied by CLAES data (see section on the zonal mean comparisons). At 100 mb, MLS values are generally higher than the sonde data by 0.1 to 0.2 ppmv, which can amount to a large percentage difference. The 100 mb difference is more pronounced for the McMurdo comparisons (1.5 ppmv for MLS versus 0.7 ppmv for the sonde data in August/September 1992). Further refinements in the MLS retrievals and the use of a finer vertical retrieval grid will hopefully lead to better comparisons in the lowermost stratosphere. The current differences are probably largely responsible for the apparent overestimate of column ozone by MLS (based on comparisons with TOMS and other data not shown here).

Some of the differences mentioned above may change if the fine resolution sonde data were to be mapped onto the coarser resolution satellite sensors' retrieval grid, although the trends will probably remain qualitatively similar.

5.2.1.4 SAGE II Comparisons

(a) Systematic comparisons against MLS

MLS ozone measurements (at 205 GHz) have been compared against colocated SAGE II ozone profiles. The colocation criteria were ~ 12 hours in time, ~ 2^{o} in latitude and ~ 14^{o} in longitude. At altitudes below 55 km (approximately 0.3 mb), SAGE II sunrise and sunset ozone measurements should represent nighttime concentrations. Therefore, only MLS nighttime measurements have been used in this comparison. Moreover, because differences between SAGE II sunrise and sunset measurements have been noted from time to time near 1 mb (the origin of these differences is currently under investigation), the sunrise and sunset measurements have been treated separately.

Fig. 5.2.1.4-1 shows that the differences between MLS and SAGE II ozone are essentially independent of latitude, and fig. 5.2.1.4.2 shows that these differences are approximately independent of time (although an approximately 5% increase in the differences in January at 4.6 mb is evident which serves to further confuse the microwave, lidar, MLS, SBUV/2 differences at this time; this difference is typically not as evident in the other latitude belts). Actually, the lack of temporal dependency in the differences only applies above an altitude corresponding to approximately 14 mb. Below that altitude, there is evidence that the current SAGE II ozone retrievals are influenced by the high aerosol concentrations resulting from the Pinatubo eruption (which possess a time-dependent behavior). Above an altitude corresponding to 14 mb, the SAGE II - MLS differences may be effectively summarized by fig. 5.2.1.4-3 as a function of pressure only. In fact, between 14 and 1.4 mb, it is seen that MLS ozone concentrations are systematically larger than SAGE II concentrations by approximately 5%. An independent comparisons of SAGE II and SBUV version 6 measurements for 1984-1986 shows close agreement between 10 and 1.5 mb; moreover, Fishman's analyses have shown that differences between TOMS-derived columnar ozone and SAGE II-derived stratospheric column ozone yield reasonable values of tropospheric ozone. It is therefore concluded that MLS (205 GHz) ozone values are approximately 5% too large.

Above 1.5 mb, there is a curious oscillation in the SAGE II/MLS differences (although typically it only has an amplitude of approximately 5%). Here it should be noted that MLS ozone is currently only being retrieved in 2 layer increments and the SAGE II retrievals contain 5 km smoothing above approximately this altitude. It is interesting to note that in several of the ozonesonde comparisons of the previous section, irregular structure is seen in the MLS profiles above 1.5 mb. It has been stated that the 185 GHz ozone values are more precise than the 205 GHz values above 1 mb; it is therefore planned that this analysis be extended to include the 185 GHz values above 1 mb. Below 15 mb, preliminary indications are that SAGE II and MLS ozone concentrations agree (within 5%) when the SAGE II aerosol extinction at 1.0 μm is less than approximately 10^{-3}/km.

(b) UARS/SAGE II comparisons during validation periods

SAGE II ozone profiles were compared against MLS, CLAES (blocker 9) and ISAMS

measurements over the periods: January 9-11 (45 UARS nighttime profiles between 5S and 10N, and 45 UARS daytime profiles at 21-34N), and April 15-17 (42 nighttime profiles at 22-36N). Comparisons were also made for August 25-28 (56 UARS daytime profiles at 44-53S) with CLAES data being unavailable for August 27 and ISAMS not operating throughout the period, for April 18-20 (45 UARS nighttime profiles at 5-22N, and 44 UARS nighttime profiles at 3-29N). The time differences between the SAGE II and the UARS measurements varied between 0 and 7 hours (averaging 3 hours) and the spatial colocation differences varied within each comparison period over the range 0 to 14 degrees longitude (averaging ~7 degrees) and 0 to 2 degrees in latitude (average ~1 degree). Data was only utilized if the error bars for the two instruments being compared were less than 50% of the measured ozone mixing ratios. The SAGE II profiles were all smoothed over the altitude range of ~2.5 km between UARS pressure levels.

Figure 5.2.1.4-4 shows the mean differences of the UARS ozone measurements from the SAGE II measurements over the period January 9-11 between 21 and 34N. The standard errors in the differences are seen to be small (typically < 0.2 ppmv). MLS and ISAMS show differences of less than ~0.5 ppm except at 10 and 15 mb where the ISAMS retrievals are known to be affected by the high concentrations of Pinatubo aerosols (which affect ozone via incorrect temperature retrievals) and below 32 mb where the SAGE II ozone retrievals are also affected by the high aerosol concentrations. The CLAES differences possess a characteristic, strongly varying vertical structure with minima at approximately 0.68, 3.2 and 14.7 hPa.

Figure 5.2.1.4-5 compares standard deviations of the UARS-SAGE II differences over the January 9-11 period to the means of the error bars provided with each profile. Of the intercomparison periods analyzed, only this period (at these latitudes) and the August 25-28 period showed covariances (i.e. stratospheric variability) exceeding 1% of the product of the ozone mean values, and even then only near 1 and 10 mb. The vertical structure of the MLS/SAGE II correlation reflects this with a minimum being exhibited near 3 mb. This result is consistent with the expected behavior of the variability of atmospheric ozone and results from a change of phase of the response of ozone to dynamical variations near 3 mb. If the error bars provided with each measurement are realistic, the standard deviations of the UARS-SAGE II differences should be equal, in a statistical sense, to the square root of the sum of the square of the errors. First, however, the SAGE II error bars should be reduced by a factor of approximately 1.2 to account for the smoothing of SAGE II profiles to the UARS levels.

Standard deviations of the MLS/SAGE II differences are consistent with predicted error bars over the range 0.46 to 10 mb. Below this altitude the SAGE II error estimates appear to be somewhat high, perhaps because they are including systematic errors due to probable aerosol effects. Above 1.5 mb, the MLS error estimates increase rapidly and it is interesting that the standard deviations of the differences have local maxima at 1.0 and 0.46 mb, which are exactly the altitudes at which the SAGE II/MLS mean differences (Figure 5.2.1.4-3) are different from those at the other altitudes.

Figure 5.2.1.4-5 also shows that for ISAMS there is good correlation with the SAGE II measurements between 2.2 and 0.32 mb and also at 10 mb. The ISAMS error bars are clearly too large at all altitudes, and this figure suggests that the error bars might be 10% (or better) over most of this altitude range. The CLAES results show that the altitudes where the CLAES ozone values are small are associated with large error bars. The CLAES error bars are in fact approximately a factor of 2 too large (corresponding in part to the inclusion of some systematic errors). Note, however, that there are encouragingly large

correlations with SAGE at 1 and 10 mb and that the standard deviation of the SAGE II CLAES differences possess a vertical structure which is unrelated to the structure of the CLAES error bars. For CLAES (blocker 8), the standard deviations of the CLAES (blocker 8)/SAGE II differences (not shown) are no worse than for blocker 9, suggesting that the differences between CLAES (blocker 8) and SAGE II are dominated by systematic errors.

The results shown in Figures 5.2.1.4-4 and 5.2.1.4-5 are typical of the MLS and CLAES comparisons. Figure 5.2.1.4-6 shows the means and standard deviations of all the validation period differences. Here also, MLS measurements are approximately 5% larger than SAGE II from 1.5 to 10 mb. For MLS, the standard deviations support the 5% error bars for MLS from 1.5 to 10 mb. Note, however, the large standard deviations at 1 and 0.46 mb. The ISAMS measurements are biased approximately 10% low relative to SAGE below 0.46 mb and the standard deviation of the differences suggest approximately 10% precision for ISAMS from 0.46 to 4.6 mb. Below that altitude, the differences are more variable because of the aerosol effects on ISAMS temperatures. The vertical structure in the mean CLAES/SAGE II differences is evident in fig. 5.2.1.4-6. The precision of the CLAES measurements appears to be approximately 15% with the smallest values (~10%) being at 1 mb.

Comparing the standard deviations shown in Figure 5.2.1.4-6 with the "typical" random errors inferred from the standard deviations of the differences given in Figure 5.2.1.4-5, a self-consistent set of approximate profile repeatability values for each instrument are shown in Table 5.2. This table also shows biases with respect to SAGE II obtained by taking means and standard deviations of the latitudinal differences shown in Figure 5.2.1.4-6. We conclude that the accuracy and precisions are approximately 5% for MLS, 10% for ISAMS (where aerosol effects are small) and 15% for CLAES (B9) based on these few comparison periods and latitudes. The accuracies and precisions listed may extend to altitudes below 21 hPa, for MLS in particular, but it is not possible to conclude this from these intercomparisons because of potentially significant aerosol-related errors in the SAGE II profiles at low altitudes during this intercomparison period.

Table 1.
Estimated repeatability and systematic differences of UARS ozone measurements inferred from differences with SAGE II measurements between 0 and 55 latitude over data intercomparison periods between January and August 1992.

Instrument	Repeatability	Pressure Range	Bias with respect to SAGE II	Pressure Range
MLS	5%	1.5 - 15 mb	+ 5%	1.5 - 10 mb
ISAMS	10%	0.46 - 3.2 mb	- 10%	0.32 - 15 mb
CLAES	15%	0.68 - 21 mb	_ 10%	0.46 - 21 mb
SAGE II	5%	0.46 - 10 mb	accuracy ~ 5%	0.32 - 10 mb

One set of comparisons has been made between HALOE and SAGE II consisting of 15 profiles on May 6 at 50S (Figure 5.2.1.5-7). HALOE mixing ratios are a few percent larger than SAGE II values between 0.46 and 32 mb. At latitudes above 0.46 mb, where

SAGE is beginning to lose its sensitivity to ozone, the HALOE and SAGE II profiles begin to diverge. More comparisons at these altitudes are needed. Rms differences (which include the mean differences) are 5-10% between 0.46 and 3.2 mb (see also Figure 5.2.1.5-8). These increase to approximately 15% at 32 mb, possibly because of some residual aerosol effects on the retrievals.

5.2.1.5 Balloon Flights

The UARS correlative program includes periodic flights from large balloons, generally at northern mid-latitudes. Each balloon often carries several instruments (in situ or remote sensors). Sample comparisons are given here for brevity, along with some average comparisons with UV in situ measurements, a reliable technique with the most correlative profiles. A table of the balloon flight instruments and investigators is given in Table 5.3, followed by Table 5.4, which describes what instrument comparisons were performed (most but not all of the potentially available UARS data had been processed with the desired software version). Some non-balloon correlative data were also included (lidar, ground-based microwave data from Table Mountain).

Table 5.3.
List of instruments and investigators for which comparisons with UARS ozone data were made, in conjunction with balloon flights between Oct. 1991 and May 1993. Abbreviations for instruments are given for use in Table 5.2.1.5b.

Instrument	Investigator(s)	Abbreviation
UV in situ	J. Margitan	UVJM
SLS	R. Stachnik	SLS
MARK IV	G. Toon	MkIV
FIRS-2	W. Traub	FIRS
IBEX	I. Nolt /B. Carli	IBEX
UV (laser)	G. Moreau	UVGM
ECC sonde	S. Oltmans	ECC
TMF lidar	S. McDermid	TMFL
TMO Microwave	B. Connor /J.J. Tsou	GdMM

Table 5.4

List of data available for each balloon flight comparison (not all of which are shown in this report).

	INSTRUMENT											
DATE/ PLACE	UVJM	SLS	MkIV	FIRS	IBEX	UVGM	ECC	TMFL	GdMM	CLAES	ISAMS	HALOE	MLS
911001 Fort Sumner USA	X	X				X	X				X		X
920220 Daggett USA	X	X					X	X	X	X			X
920504 Fort Sumner USA					X						X		X
920514 Aire/ l'Adour FRANCE						X				X	X		X
920529 Fort Sumner USA	X			X						X	X	X	X
920915 Fort Sumner USA			X							X			X
920929 Fort Sumner USA	X	X		X						X		X	X
930324 Daggett USA				X						X			X
903403 Daggett USA	X	X		X						X		X	X
930531 Fort Sumner USA	X				X							X	X

Figure 5.2.1.5-1 shows profiles from all UARS instruments (CLAES, ISAMS, HALOE and MLS) above (or nearly above) Ft. Sumner, New Mexico, on May 29, 1992. Although the ISAMS points are shown below 10 mb, the focus here as elsewhere in this report should be on the higher altitudes. The characteristic oscillation in CLAES ozone profiles is another caveat to keep in mind; this shows up in all balloon flight comparisons (not all of which are displayed here). Also note that the HALOE profile (which has been interpolated to a finer resolution than the HALOE retrieval grid) is not as close in time and space to the balloon flight as the other UARS sensors (see the figure legend for time, latitude, longitude differences from the nominal UV in situ measurements of J. Margitan). The other balloon-borne instrument data plotted is from the Far Infrared Spectrometer (FIRS-2) of W. Traub (showing good agreement with the UV data). Other features in this figure are some evidence for a slight overestimate by MLS near and above the peak, and a slight underestimate by ISAMS in that region (compared to the UV data).

Two more sample balloon flight comparisons are given in Figures 5.2.1.5-2 and 5.2.1.5-3 (above Daggett, California, in 1992 and 1993). Balloon data include the UV in situ data (J. Margitan), SLS data (sub-millimeter emission measurements; R. Stachnik), ECC sonde data (S. Oltmans), as well as the infrared interferometer (Mark IV) data (G. Toon); non-balloon data from the Table Mountain Facility (TMF) lidar (S. McDermid), and the ground-based microwave instrument (B. Connor and J.J. Tsou) at Table Mountain are also shown. Differences between UARS and correlative profiles are generally less than 10%, with the exception of CLAES values, which can show larger excursions.

More statistics are needed, however, in order to classify a difference as a systematic offset (note that error bars were omitted in the above figures for legibility). The next set of figures give comparisons between UARS sensors and the average of UV in situ flight data available at the time of the Workshop; this includes 6 data sets from J. Margitan over Daggett and Ft. Sumner (U.S.A.) and one from G. Moreau over Aire sur l'Adour (France). The number of available comparisons is 5 for CLAES (Figure 5.2.1.5-4), 3 for ISAMS (Figure 5.2.1.5-5), 4 for HALOE (Figure 5.2.1.5-6), and 7 for MLS (Figure 5.2.1.5-7). Based on these comparisons and bearing in mind the small number of profiles of latitudes at which the comparisons were made, the following conclusions are made:

ISAMS comparisons show generally lower ozone values than the correlative data near and above the ozone peak. The systematic difference with respect to the average of 3 uv in situ balloon measurements is about 10 percent.

CLAES ozone values (from blocker 9) are more than 20% high, compared to the average of 5 uv in situ balloon measurements, in the 30 to 100 mb region. In the region near the ozone peak, CLAES ozone oscillates around the balloon data, with higher values from CLAES at the peak, and lower values just below the peak. The oscillation amplitude is of order 20%.

HALOE comparisons with balloon correlative data give good agreement (within 5%) from 5 to 50 mb, with HALOE values being slightly lower near the ozone peak. In comparison to the 4 uv in situ balloon measurements used here, HALOE data are somewhat higher than the average in the lowermost stratosphere, but the HALOE team have expressed reservations about the retrievals below 46 mb.

MLS comparisons provide the largest number of coincidences with the balloon data. Good agreement is found overall, although MLS values are 5 to 7% higher than the average of 7 uv in situ balloon measurements near the ozone peak. At 100 mb, a slight overestimate

exists as well (less than 0.1 ppmv in absolute value, but almost 20% as a relative value).

The UV in situ balloon data provide the best comparison in a statistical sense (using the same instrument or technique). Other balloon data sets (not all of which were shown here) do not lead to significantly different conclusions.

5.2.2 Cross-Sections

Figure 5.2.2-1 shows zonal mean cross-sections of ozone mixing ratio versus latitude and pressure (on a log scale), for the average of January 9-11, 1992 (one of the validation time periods used in previous workshops). Since ISAMS retrievals for Version 8 have a recommended vertical range which starts at 10 mb, extending upwards (to lower pressures), the plot is only shown down to 10 mb for this instrument. These UARS fields are generally similar, but we will focus on the main systematic differences, which can be significant in places, as displayed in Figure 5.2.2-2 for percent differences.

The differences between MLS and CLAES ozone exhibit the same general pattern as in the previous Workshop Report, i.e. an oscillatory pattern produced by the artifacts still present in CLAES ozone vertical profiles (at the 10-20% level). In the tropical lower stratosphere, large differences (in percent) exist between MLS and CLAES fields, with MLS values significantly lower than CLAES values.

At low latitudes in the mid-stratosphere (2 to 10 mb), the MLS ozone field is generally higher than the ISAMS ozone field by about 20%. This result is caused by a decrease in ISAMS values from the previous Workshop Report, where better agreement was found (tendency is towards an increase in the next Version of ISAMS retrievals); the strong sensitivity of ozone to temperature retrieval errors is the main cause for the change in the ISAMS field. MLS fields have only changed by a few percent in the mean from previous versions of the retrievals. At mid-to-high latitudes, as well as in the upper stratosphere at low latitudes, the differences between MLS and ISAMS fields are smaller, i.e. of order 5 to 10%.

The differences between ISAMS and CLAES fields can be inferred from the comparisons mentioned above; as can be seen in the bottom panel of Figure 5.2.2-2, ISAMS values are also generally lower than CLAES values.

The nature of the differences in ozone zonal mean fields is very similar during the other validation time periods studied (i.e. April 15-20, 1992; August 8-10, 1992; August 25-30, 1992), although the August time period shows somewhat smaller differences between MLS and CLAES (ISAMS was no longer operational then).

A significant discrepancy exists in the tropical lower stratosphere, and in the latitudinal gradients at certain pressure levels (46 mb in particular). This discrepancy is illustrated in Figure 5.2.2-3, where latitudinal variations are plotted at 46 mb (bottom panel) and at 10 mb (top panel). ISAMS data are only shown at 10 mb. Estimated error bars are intentionally left out so that the plots remain fairly legible. The MLS tropical values of ozone at 46 mb are significantly lower (by 0.5 to almost 2 ppmv) than the CLAES values, but become closer to the CLAES values at high latitudes (which implies differences in the latitudinal gradients). These differences, however, vary with height and for example the MLS values at 10 mb are higher than both CLAES and ISAMS values. At 4.6 and 2.2 mb (see Figure 5.2.2-4), systematic differences are evident as well, with ISAMS values and

latitudinal gradients being the smallest. Differences between MLS and CLAES latitudinal gradients and tropical values are reduced in the later validation periods, perhaps indicating a lesser aerosol-related influence on CLAES data (see Figure 5.2.2-5 for plots of averages for August 25-30, 1992).

In summary, the main differences between MLS and CLAES have not changed from the previous report, although slightly smaller differences are observed now. The ISAMS fields appear to be on the low side, compared to MLS and CLAES data in the mid-to-upper stratosphere (see also comparisons with other data sets). The MLS data are the highest at 10 mb. Best agreement between instruments is obtained at the higher (altitude) levels.

Figures 5.2.2-6 - 5.2.2-8 are pressure versus latitude cross-sections for the differences between ISAMS, MLS, CLAES, and HALOE in the April 15-20 time period. ISAMS is lower than HALOE (by 20-30%) below 10 mb. From 2 to 20 mb, ISAMS is 10% lower, while above 2 mb, ISAMS is 10-30% higher. The mean differences for approximately this same period were summarized in Figures 5.2.1.1-1 to 5.2.1.1-3.

CLAES data runs from 0 to 30% higher than HALOE above ~8 mb. These differences may be caused by altitude registration differences as suggested by the vertical profile statistics (Figure 5.2.1.1-2). From 8-11 mb, HALOE tends to be higher by 10-15%. This pattern is typical of all the intercomparison periods.

MLS also shows higher values than HALOE by 10-20% at altitudes above the 11 mb level.

This series of HALOE comparisons against the other UARS instruments seems to be giving somewhat different results from the comparisons in the rest of this report where, in particular, MLS was ~ 10% larger than HALOE above 11 mb. Comparisons with several other reliable data sets are needed, in order to decide where the "true" profiles are in relation to the various UARS measurements. Given some of the large discrepancies which still exist between UARS instruments, it should be possible with enough comparisons of reliable "ground-truth" data, such as ozonesondes or lidar, to ascertain where a particular instrument is biased low or high. Some feeling for this is given in other sections of this ozone chapter. Other problems, such as the CLAES oscillatory pattern, do not require a multitude of comparisons. Further research into the initial data quality and retrieval algorithms is needed for cases like this (this is a continuing activity for all the instrument teams).

5.2.3 Ozone Map Comparisons of UARS and SBUV/2 Data

Ozone maps were constructed from UARS data and SBUV/2 data for January 10-11, 1992. SBUV/2 data were used as an independent comparison to the UARS instruments, making it a mutually beneficial comparison of the datasets. Results for other periods are expected to have similar results, as was seen from comparisons of earlier versions of UARS data, so they will not be presented here. The data used are Version 3 from MLS, Version 6 from CLAES, Version 8 from ISAMS, and Version 6 from SBUV/2. SBUV/2 data for January 9 were not available, hence the two days of comparisons.

Gridded maps were made from Level 3AT data from the UARS instruments and level 2 type data from the SBUV/2 instrument using a successive iteration technique similarly used in the NMC/CAC stratospheric temperature maps. Maps were constructed for only the 10 mb and 1 mb levels.

Figures 5.2.3-1 to -5 show the MLS, CLAES, ISAMS, and SBUV/2 maps in that order for January 10-11, 1992. Figure 5.2.3-2a is the MLS 10 mb map for January 10, Figure 5.2.3-2b is the 10 mb map for January 11, Figure 5.2.3.2c is the 1 mb map for January 10, and Figure 5.2.3-2d is the 1 mb map for January 11. Similarly, the order is the same for Figure 5.2.3-3 for CLAES, Figure 5.2.3-4 for ISAMS, and Figure 5.2.3-5 for SBUV/2.

Overall, all maps show similar large-scale patterns, but for the most part the differences overshadow the similarities. We shall highlight some of the differences that seem to come up regularly, as seen from many maps for the present versions and earlier versions of UARS and SBUV/2 data. In Figures 5.2.3-2a and b, the MLS maps show a strong gradient at 10 mb in the subtropical regions compared to other maps at 10 mb. In Figures 5.2.3-2c and d, at 1 mb, MLS shows a stronger amplitude, high ozone region over the Pacific Northwest, and in general, MLS shows stronger amplitude systems than either ISAMS or SBUV/2.

At 10 mb CLAES shows a highly structured tropical region and a strong region of high ozone amount at high latitudes in Figures 5.2.3-3a and b. Systems seem to pop up in a noisy bulls-eye fashion as in Figure 5.2.3-2b over South America. Similarly, at 1 mb, the low latitudes appear to be quite noisy, making it difficult to sort through the noise to follow the systems that appear from one day to the next. However, the large-scale patterns in MLS are also seen in the CLAES data.

For ISAMS the highs are not as high, and the lows are not as low as either MLS or CLAES. Figures 5.2.3-4a and b show rather flat features with gradients in subtropical regions less than either MLS or CLAES. The 1 mb high ozone amounts in the Pacific Northwest (Figures 5.2.3-4a and b) show up as the major feature in similar fashion as the other instruments.

The 10 mb map for SBUV/2 at high latitudes shows a strong gradient (Figures 5.2.3-5a and b). This effect is probably a solar zenith angle problem. At mid-latitudes, the low ozone amounts are in similar regions as in the MLS or CLAES data, but the structure of MLS or CLAES is not shown in the SBUV/2 data, probably because of the lack of vertical resolution in the SBUV/2 data. As was seen in the other instruments at 1 mb, the major feature is the high ozone amounts in the Pacific Northwest, and the SBUV/2 data also show this major feature in Figures 5.2.3-5b and -5c.

In summary, all instruments seem to show varying degrees of the same large-scale features, but major differences are apparent in all four instruments. MLS shows stronger subtropical gradients than any of the other instruments at 10 mb corresponding to higher ozone amounts in the tropical regions. The high ozone regions are higher, and the low ozone regions are lower in both MLS and CLAES, with CLAES appearing very noisy at both 10 mb and 1 mb. The noise seems to be especially prevalent in the tropical regions for CLAES. ISAMS and SBUV/2 do not have the amplitudes that MLS or CLAES have. For SBUV/2 the vertical resolution is less than any of the UARS instruments, so this was not unexpected. The strong gradients at 10 mb at high latitudes pfor SBUV/2 seems to suggest a solar zenith angle problem, since the gradients are not apparent for any of the other instruments. The maps point out some of the striking differences between datasets and corroborate in a different way, some of the differences that other comparisons have shown. For example, the characteristic vertical structure in the CLAES data are also shown as horizontally varying noise in the maps.

5.2.4 Time Series

Time-series ntercomparisons of UARS ozone data were made for four periods (January 9-11, April 15-20, August 8-11, and August 25-30) in 1992. The data were level 3AT ISAMS (version 8), MLS 205 GHz (version 3), and CLAES Blocker 9 (version 6). These data are along-track, nearly co-located, pressure- and time-interpolated profiles output at approximately one minute intervals(about 1300 profiles per instrument per day). Any single day provides almost complete coverage of one hemisphere (depending if UARS is flying forward or backward), so only a single day from each period will be discussed. UARS was flying backward (looking north) during the January and early August periods and forward (looking south) during the April and late August periods. The important features tend to repeat each orbit (about 90 minutes), so the results are illustrated for two hour periods. There were no ISAMS data for the August periods.

Values for January 9 at 46.4 mb are presented in Figure 5.2.4-1. At low latitudes MLS values are smallest, sometimes approaching zero. CLAES data show considerable scatter and a few spikes, but ISAMS data appear smooth. However, ISAMS values at 46.4 mb are heavily weighted towards climatology. MLS values for April 15 (not shown) are again sometimes very small at low latitudes, and CLAES values show less scatter than for January 9. CLAES and MLS values for August 9 at 46.4 mb are shown in Figure 5.2.4-2 and agree much better at low latitudes than in January or April.

Figure 5.2.4-3 indicates that the scatter for ISAMS and CLAES data on January 9 at 21.5 mb is larger than at 46.4 mb. On April 15 at 21.5 mb, a reduction in scatteris is seen in Figure 5.2.4-4 . The August 9 comparison in Figure 5.2.4-5 shows MLS and CLAES in very good agreement. CLAES exhibits some unrealistically large values at high southern latitudes on August 25 (Figure 5.2.4-6).

Values for January 9 and April 15 at 10 mb are shown in Figures 5.2.4-7 and 8. The agreement is generally better in April, with ISAMS and CLAES showing less scatter at low latitudes. MLS values are consistently larger than those of CLAES and ISAMS at low latitudes. The August 25 comparison in Figure 5.2.4-9 shows a few more unrealistically large CLAES values at high southern latitudes, and MLS values generally larger than CLAES values at low latitudes.

Figure 5.2.4-10 depicts reduced scatter in ISAMS data on January 9 at 4.6 mb (compare with Figure 5.2.4-7), while CLAES continues to show some scatter. CLAES and MLS values generally agree well at low latitudes for April 15 as shown in Figure 5.2.4-11. ISAMS values are noticeably smaller than those of MLS at low latitudes, while the mid- and high- latitude agreement is good for both periods.

Comparisons for January 9 at 2.2 mb shown in Figure 5.2.4-12 exhibit the largest scatter in CLAES data. This level is approximately one at which the CLAES team has diagnosed radiance calibration problems which result in low concentrations. ISAMS and MLS track each other quite well, although ISAMS values continue to be smaller at low latitudes. The same result is true for April 15 (not shown). Data for January 9 at 1 mb is shown in Figure 5.2.4-13. The increased scatter (compare Fig. 5.2.4-10) seen for all instruments is representative of all periods.

For pressures exceeding 10 mb, CLAES and ISAMS data appear to be affected by aerosols (especially at low latitudes in January) causing excessive variability in the two-track data, the scatter decreasing with height and time. CLAES data have some spikes (August 25),

and some MLS values appear to be particularly low in January and April at 46.4 mb. At pressures less than 10 mb, the instruments show similar latitudinal tendencies. However, the agreement at mid- and high latitudes is better than at low latitudes, where MLS values tend to be larger than CLAES values, which in turn are larger than those of ISAMS. The CLAES time tracks also contain some spikes at these heights.

Time series of UARS and SBUV/2 zonal-mean ozone at 10 and 1 mb were calculated for 1992 at 60N, 30N, 0, 30S, and 60S (5 degree bands centered at the latitude). SBUV/2 provided a continuous year of data for comparison (except at 60S because of orbit precession). Figures 5.2.4-14 and 5.2.4-15 present time series at 10 and 1 mb with rectangular solid lines depicting the UARS yaw maneuver. Between 30N and 30S, both MLS and SBUV/2 had a continuous year of data.

In Figure 5.2.4-14a it can be seen that the MLS annual cycle in ozone at 10 mb and 60N has a larger amplitude than does SBUV/2, with lower values in winter and higher values in summer. CLAES does not appear to have the same annual cycle as SBUV/2 or MLS, whereas ISAMS seems to have a similar cycle to MLS. Figure 5.2.4-14b shows MLS and SBUV/2 data for 10 mb at 30N. Again MLS has a larger amplitude and a bias toward higher values than the other instruments. However, the bias changes with the gap larger during summer and smaller during winter. CLAES shows higher variability than the other instruments. Even during a single period when UARS is looking north or south, this variability is as large or larger than the annual variability in either MLS or SBUV/2 data. In the equatorial regions, a large bias exists between MLS and the other instruments (Figure 5.2.4-14c). Figure 5.2.4-14a shows CLAES data at one level for the period centered around day 61. After the yaw maneuver, the data seems to have jumped to another level for the next period, then fall back to the previous level after the next yaw maneuver. The summer and winter differences between MLS and SBUV/2 show up again at 30S. Figure 5.2.4-14e is for 60S, with SBUV/2 in darkness during winter, thus providing no data.

Figures 5.2.4-15a-b show SBUV/2 data at 1 mb lower than any of the UARS instruments except for a brief period during winter. Figures 5.2.4-15c-d show MLS and SBUV/2 with almost no systematic differences in some periods and MLS and ISAMS with no systematic differences in other periods. CLAES, in almost all of the figures, shows a bias on the high side at this level compared to the other instruments. If the biases are taken out, the instruments seem to track each other better than at 10 mb, where the scatter is much greater.

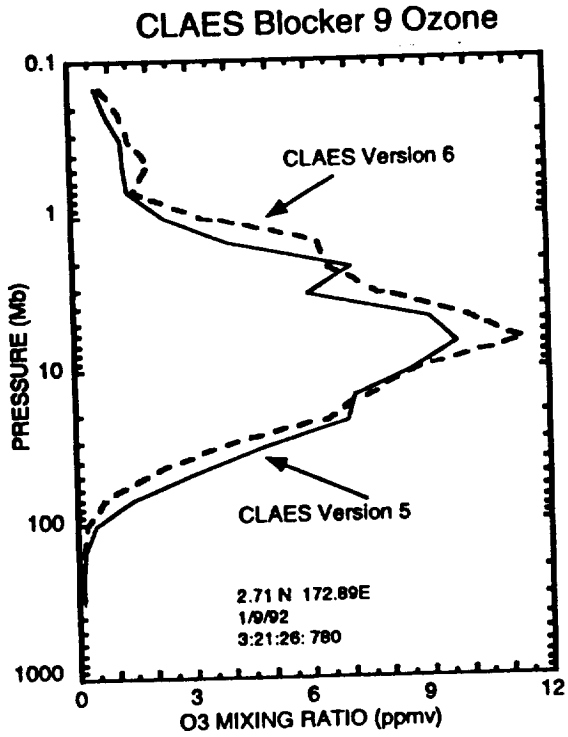

Figure 5.1.6-1 Comparison of CLAES ozone (blocker 9) retrieval versions 6 and 5 for Jan. 9, 1992.

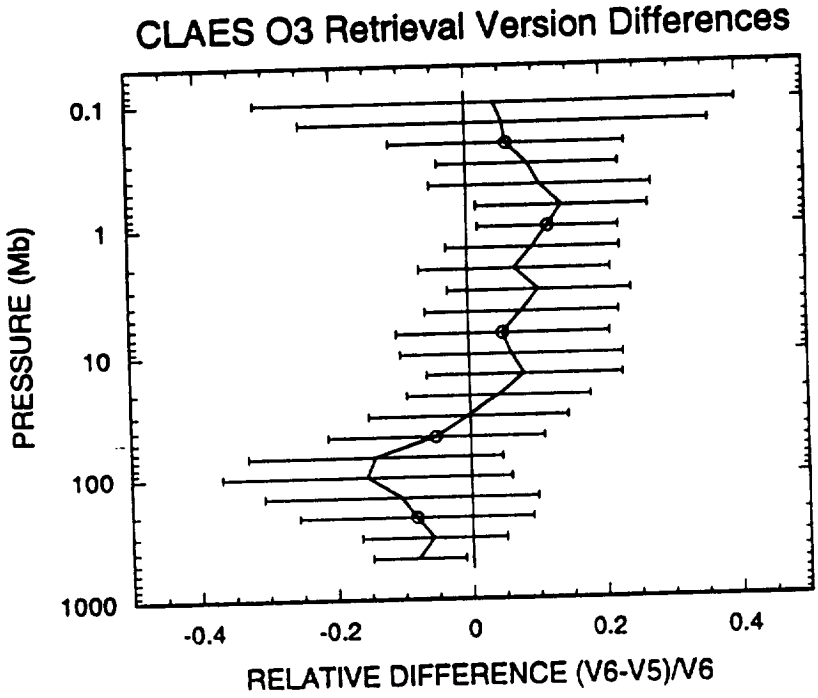

Figure 5.1.6-2 Mean relative difference between the CLAES profiles in Figure 5.1.6-1 (Version 4.10 - Version 4) for 20-50N on Jan. 9, 1992.

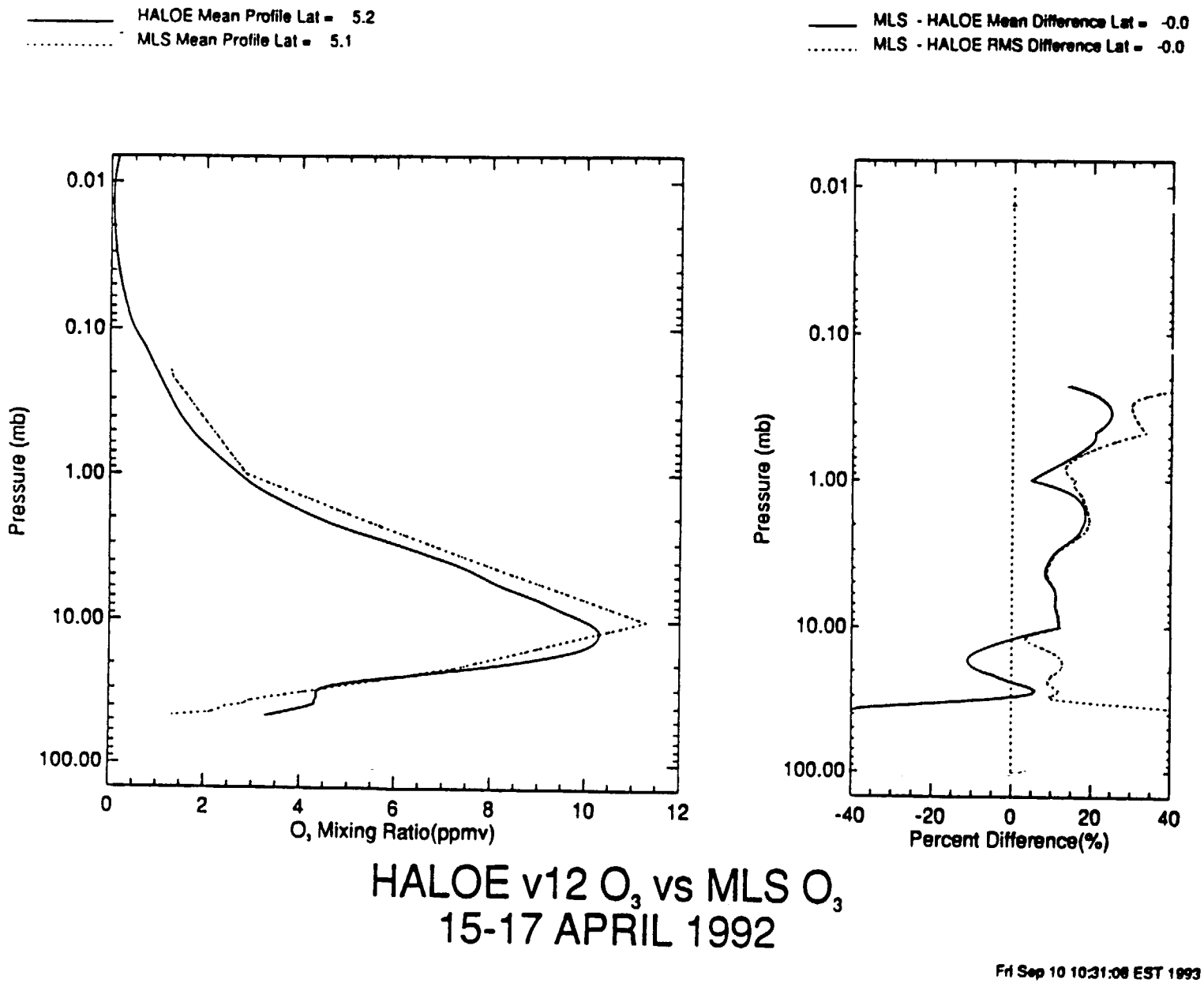

Figure 5.2.1.1-1 Mean profiles and differences (HALOE-MLS) for 45 coincident profiles at 5°N latitude for April 15-17, 1992.

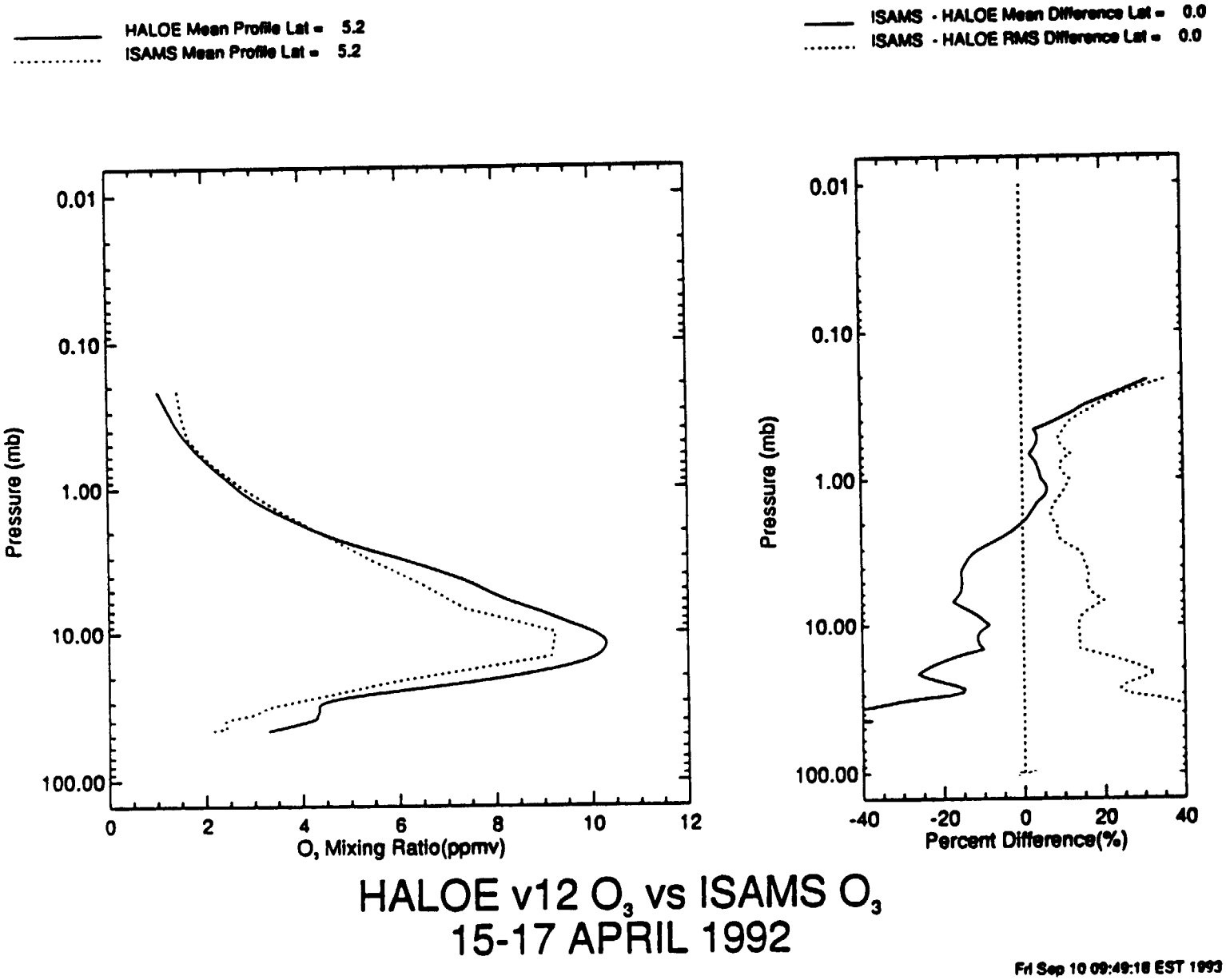

Figure 5.2.1.1-2 Mean profiles and differences (HALOE-ISAMS) for 45 coincident profiles at 5^{O}N latitude for April 15-17, 1992.

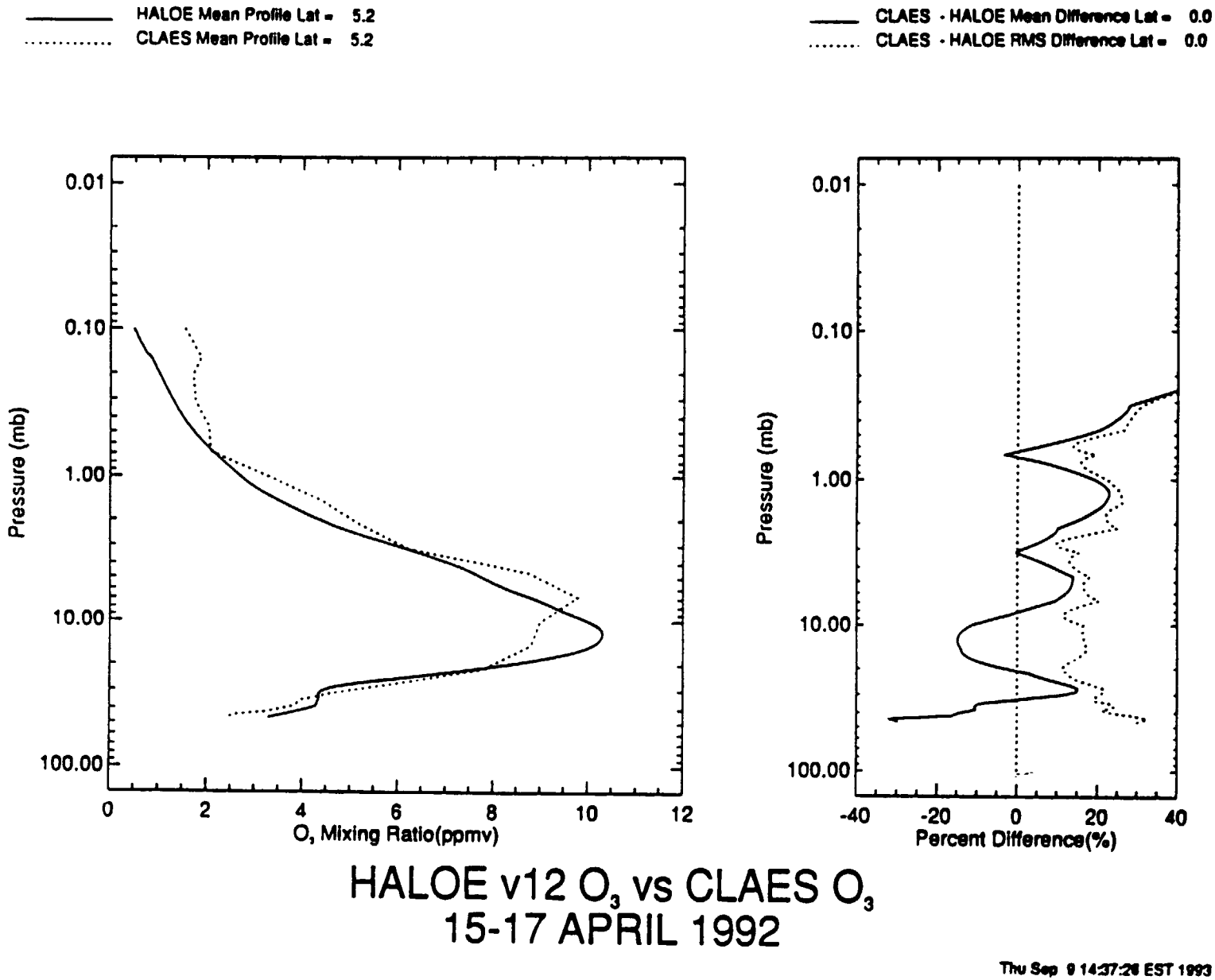

Figure 5.2.1.1-3 Mean profiles and differences (HALOE-CLAES) for 45 coincident profiles at 5°N latitude for April 15-17, 1992.

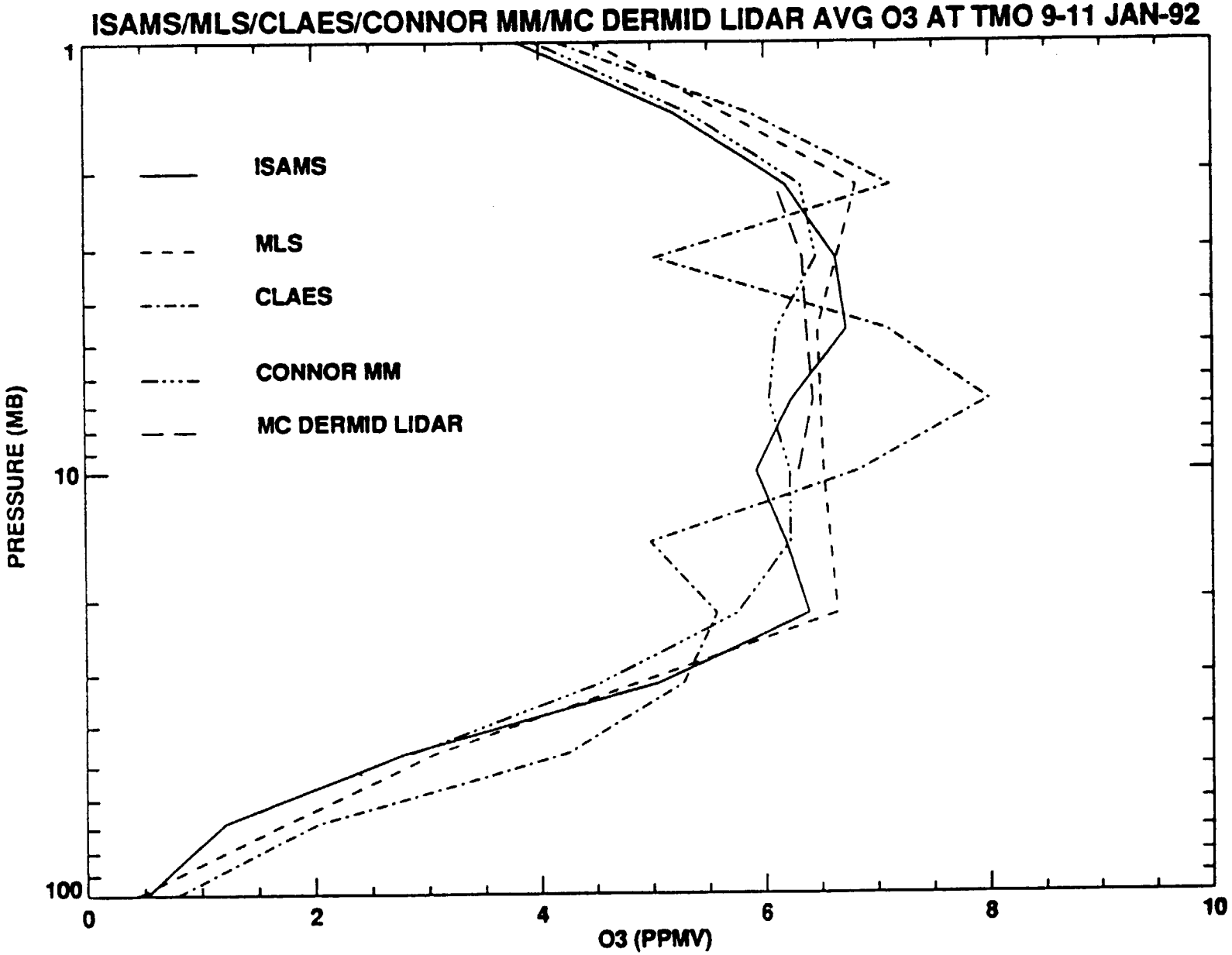

Figure 5.2.1.2-1 UARS comparisons against the McDermid lidar and the Connor/ Parrish microwave measurements at TMO on Jan. 9-11, 1992.

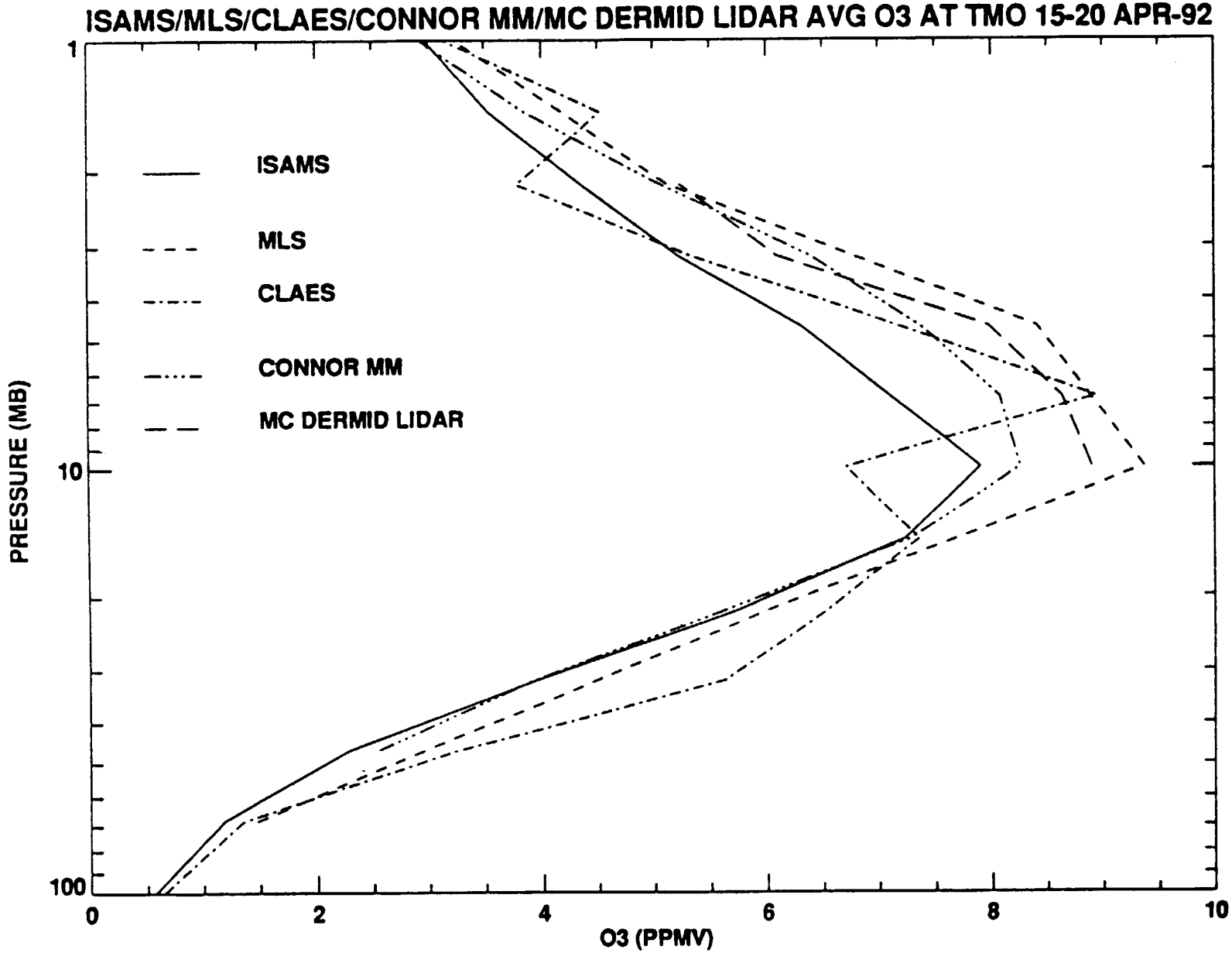

Figure 5.2.1.2-2 UARS comparisons against the McDermid lidar and the Connor/ Parrish microwave measurements at TMO on April 15-30, 1992.

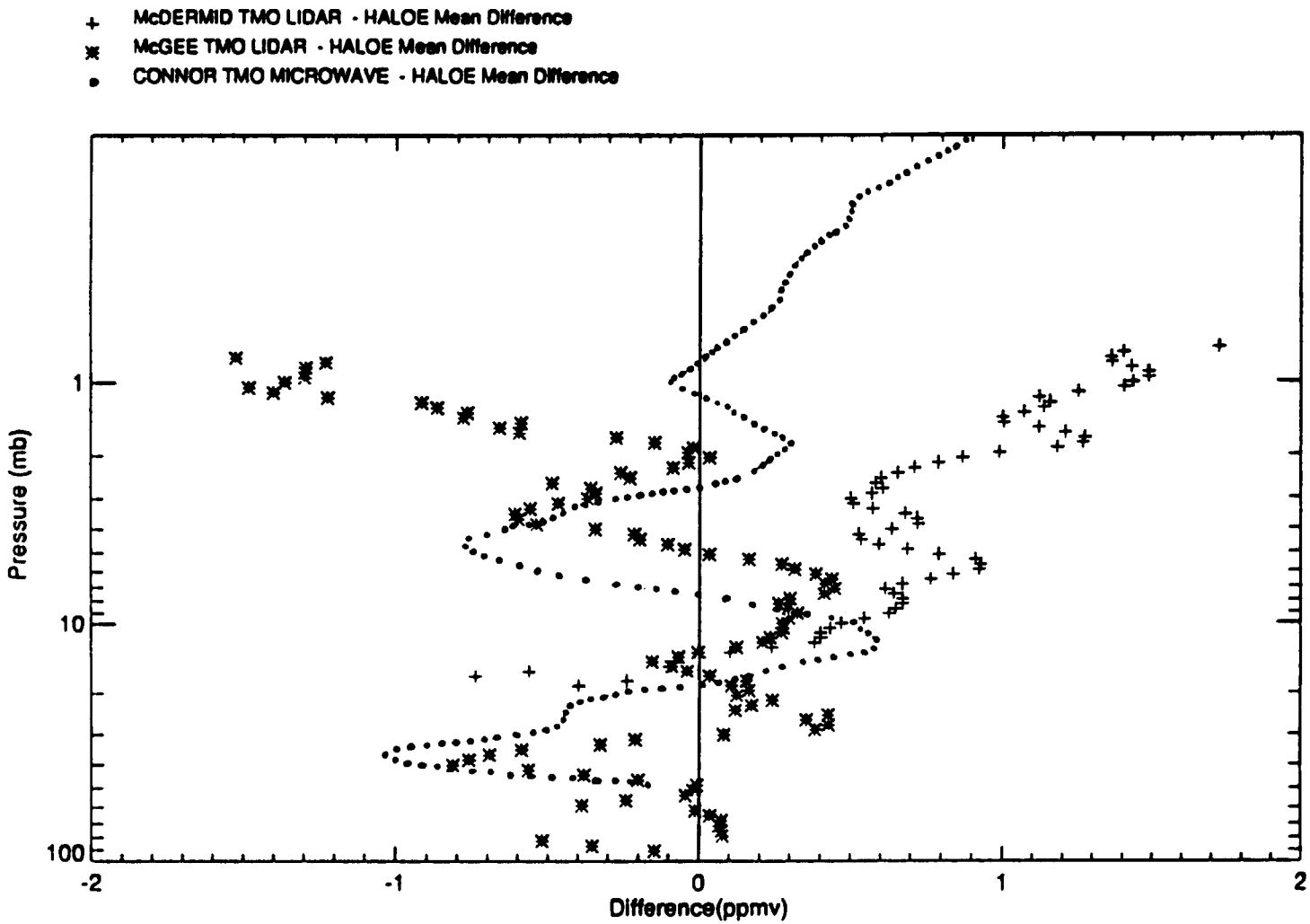

Figure 5.2.1.2-3a HALOE comparisons against the McDermid lidar and the Connor/Parrish microwave measurements at TMO on Feb. 22-25, 1992.

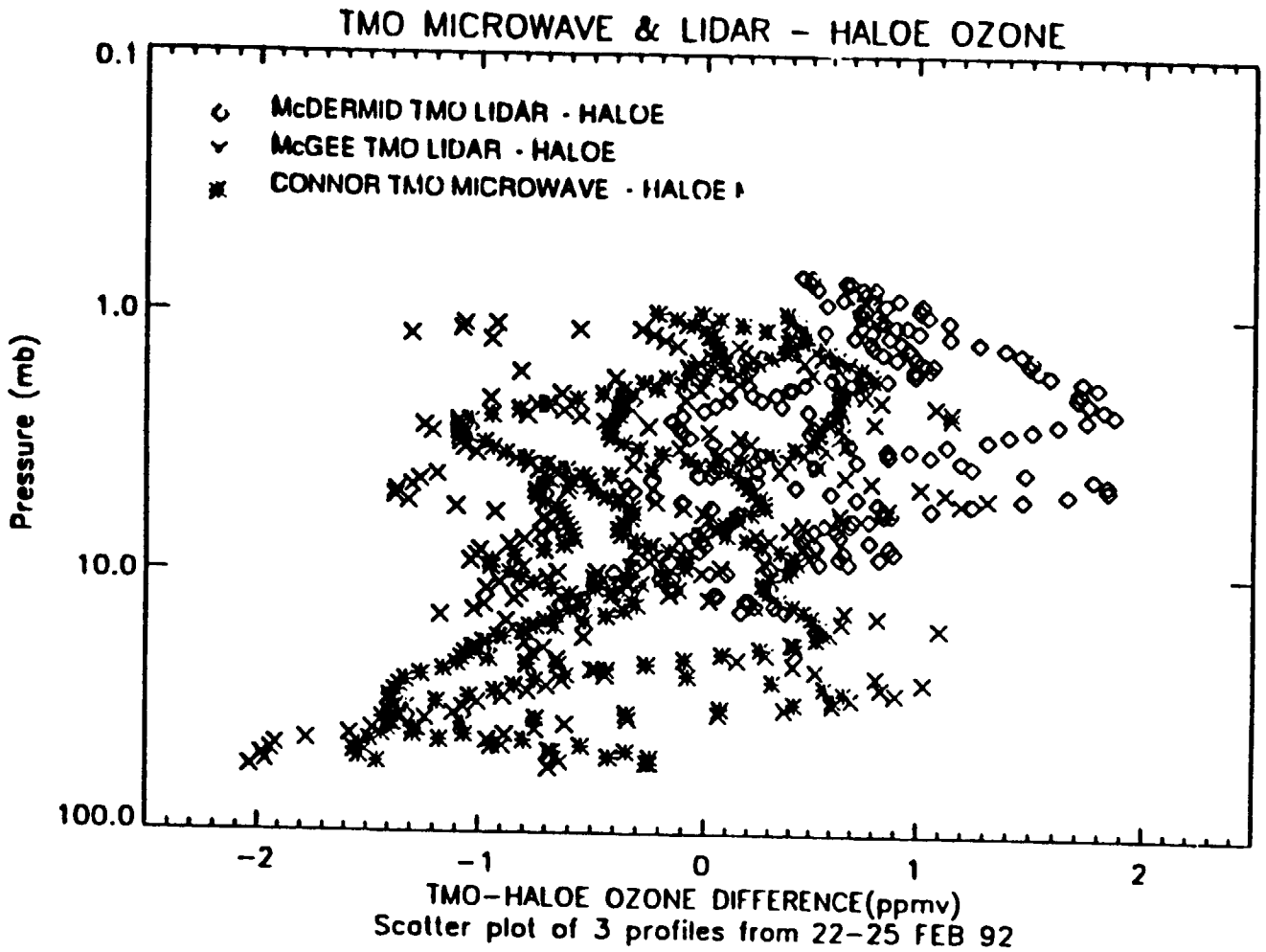

Figure 5.2.1.2-3b Scatter plot of McDermid lidar, McGee lidar and Connor/ Parrish microwave measurements at TMO on Feb. 22-25, 1992.

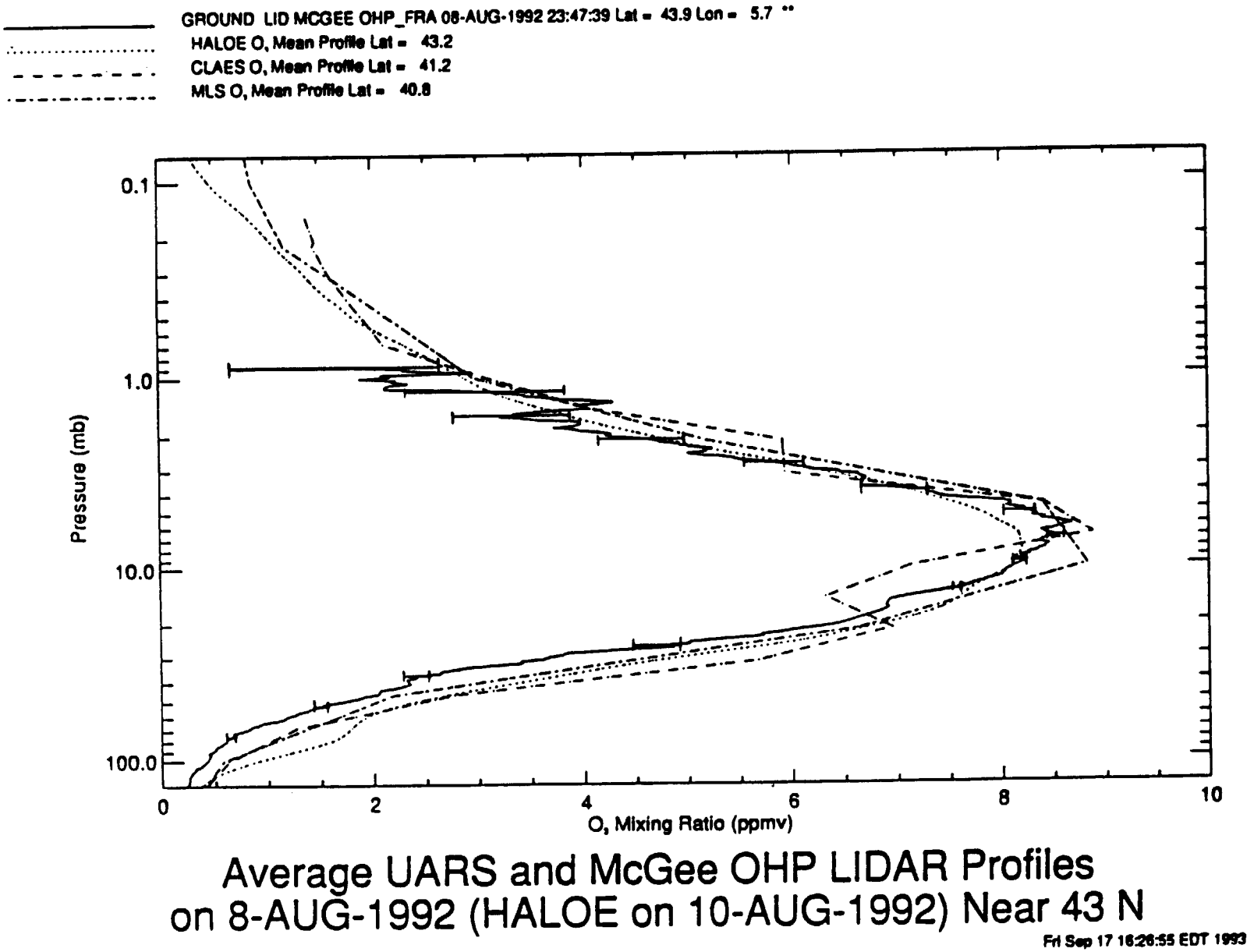

Figure 5.2.1.2-4a UARS comparisons against McGee lidar at OHP on Aug. 8, 1992.

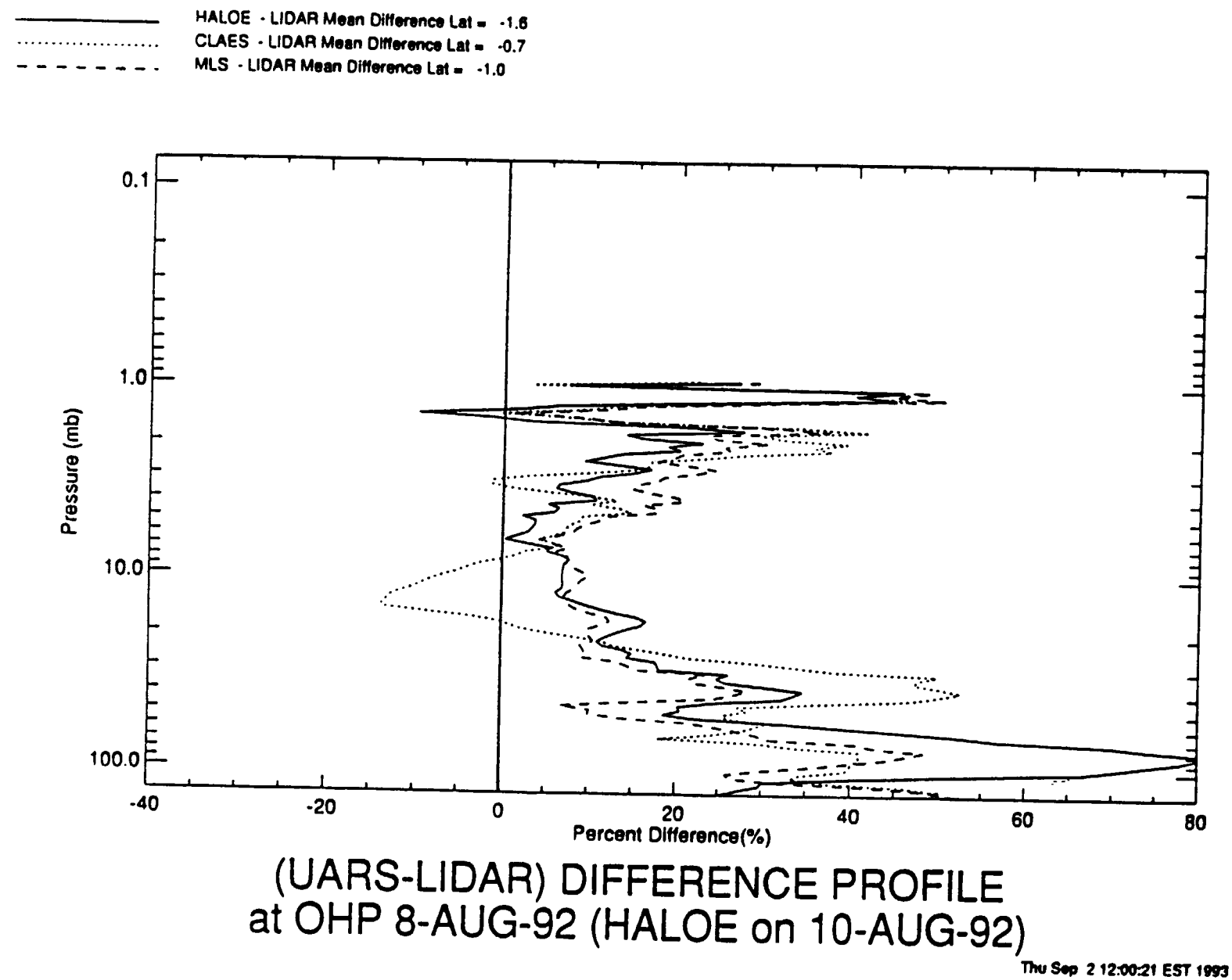

Figure 5.2.1.2-4b

Fig. 5.2.1.2-4 measurements expressed as differences (UARS-lidar).

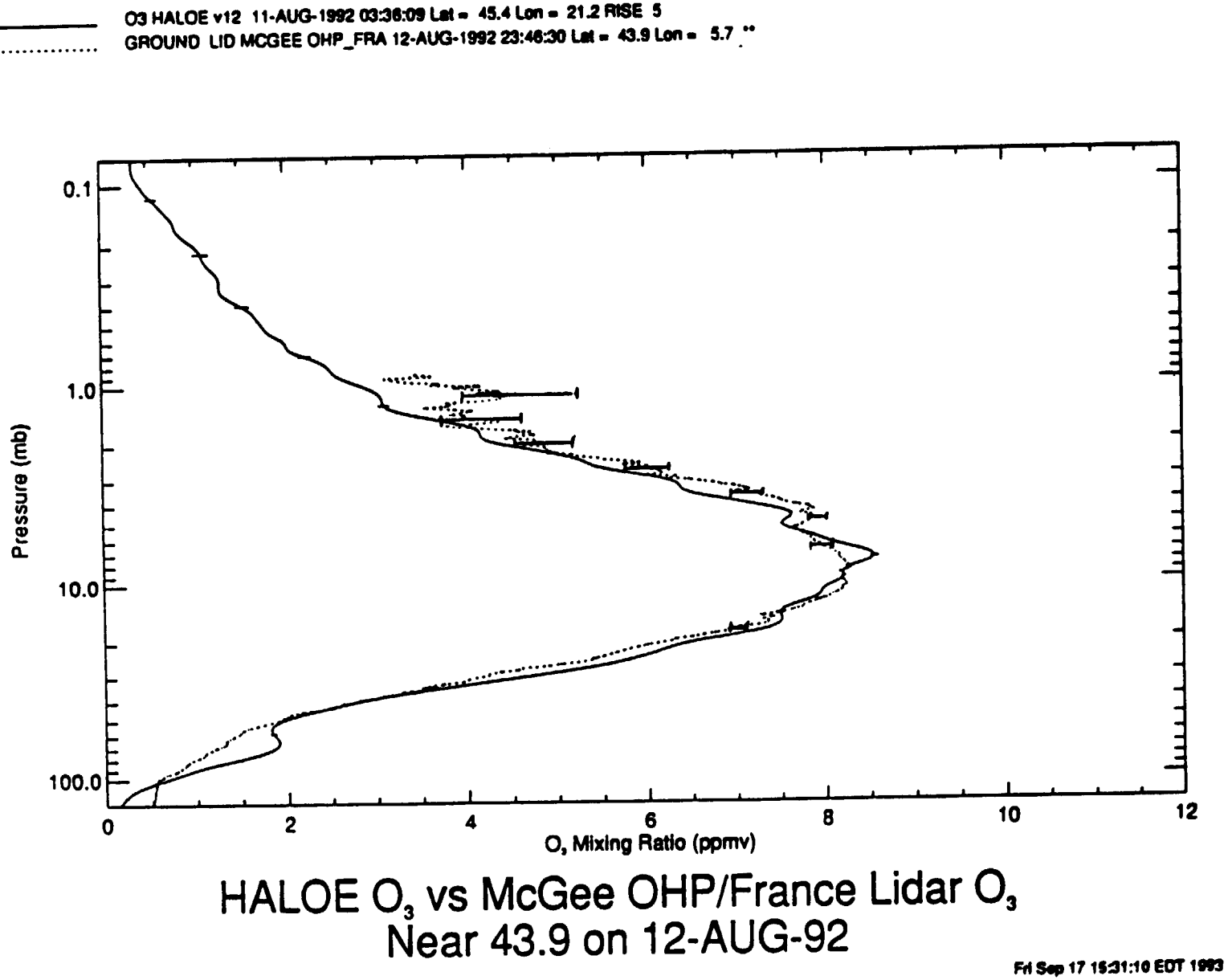

Figure 5.2.1.2-5a HALOE comparison against McGee lidar at OHP on Aug. 12, 1992.

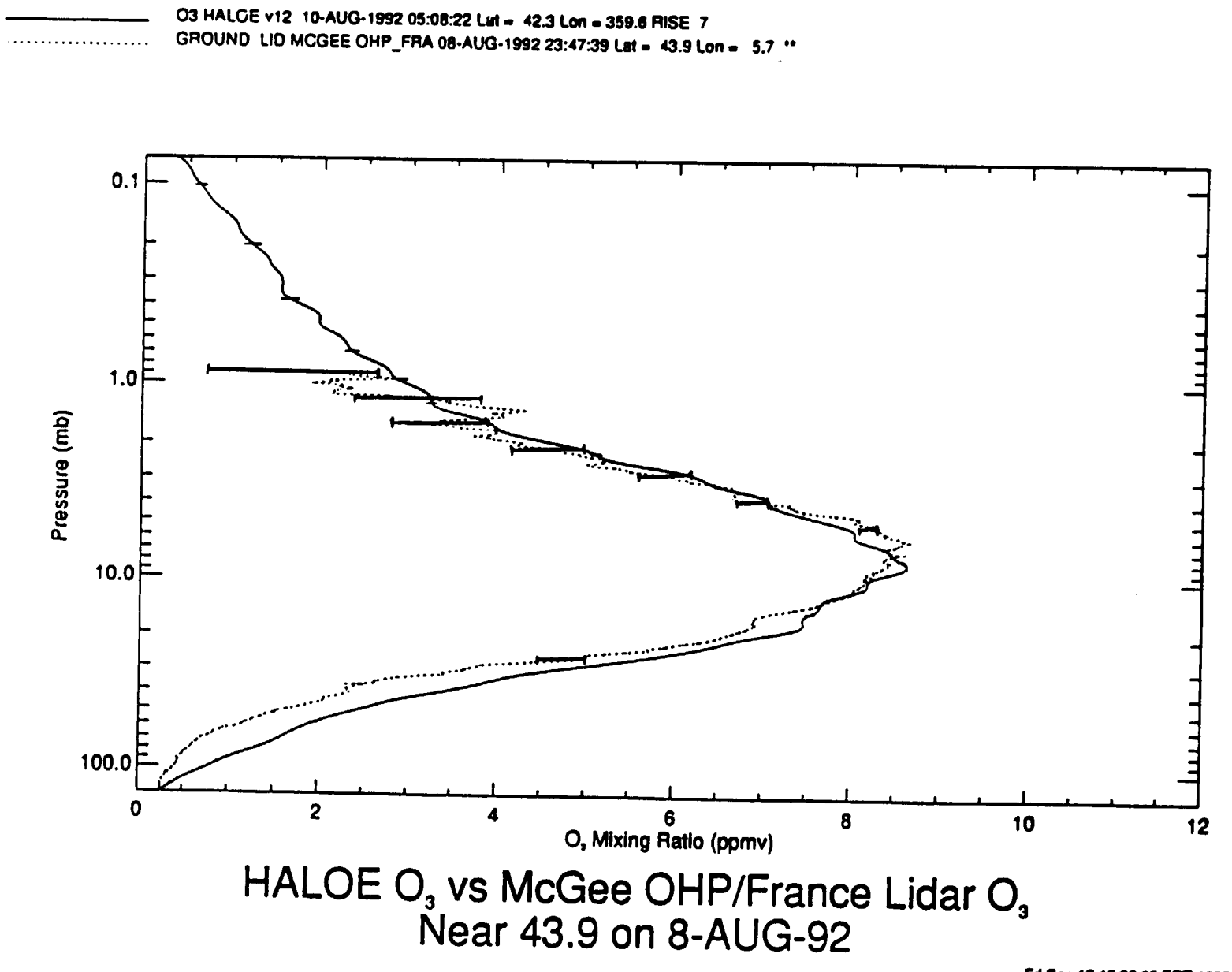

Figure 5.2.1.2-5b HALOE comparison against McGee lidar at OHP on Aug. 8, 1992.

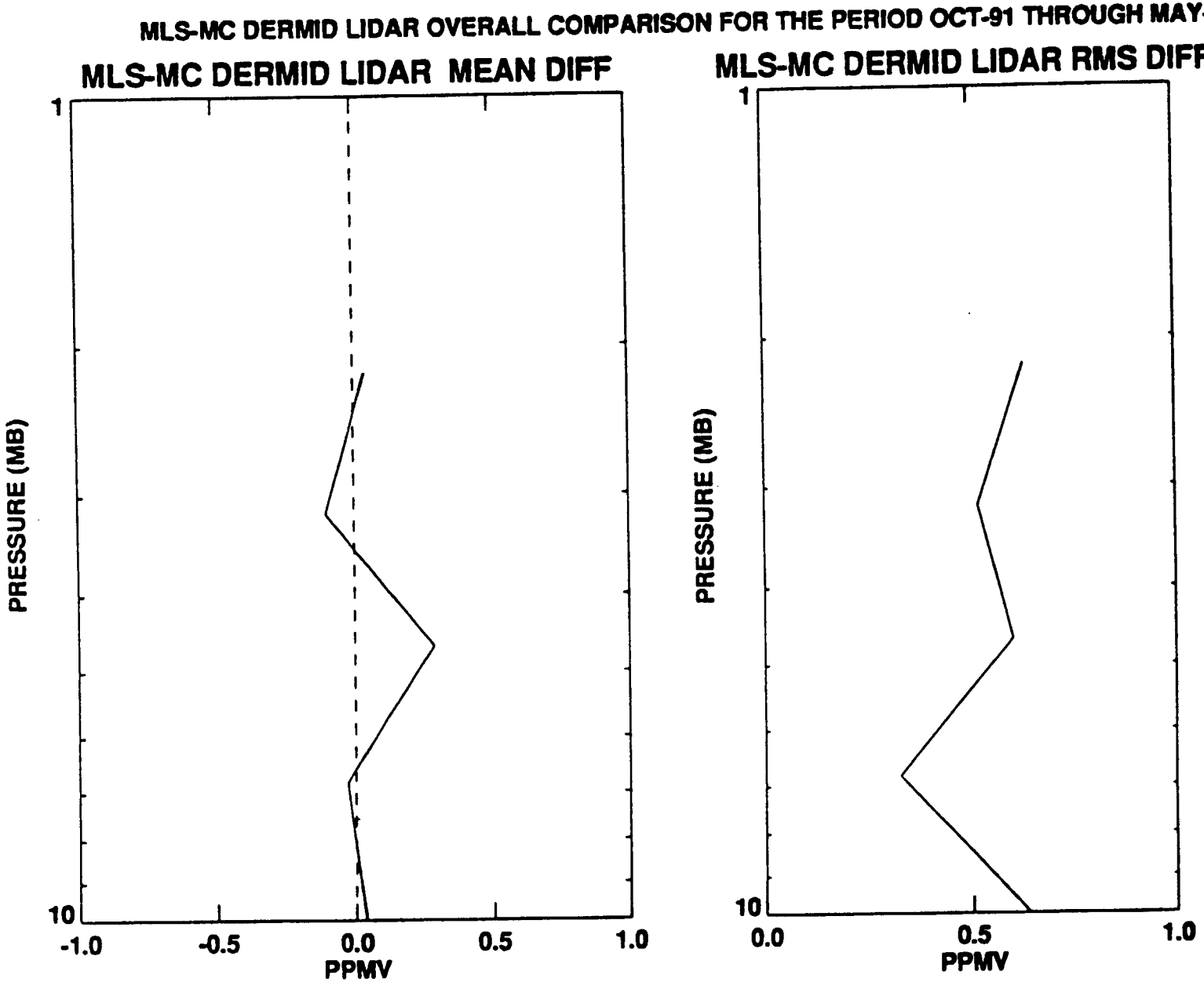

Figure 5.2.1.2-6 Mean differences between MLS and McDermid lidar at TMO for Oct. 1991-May 1992.

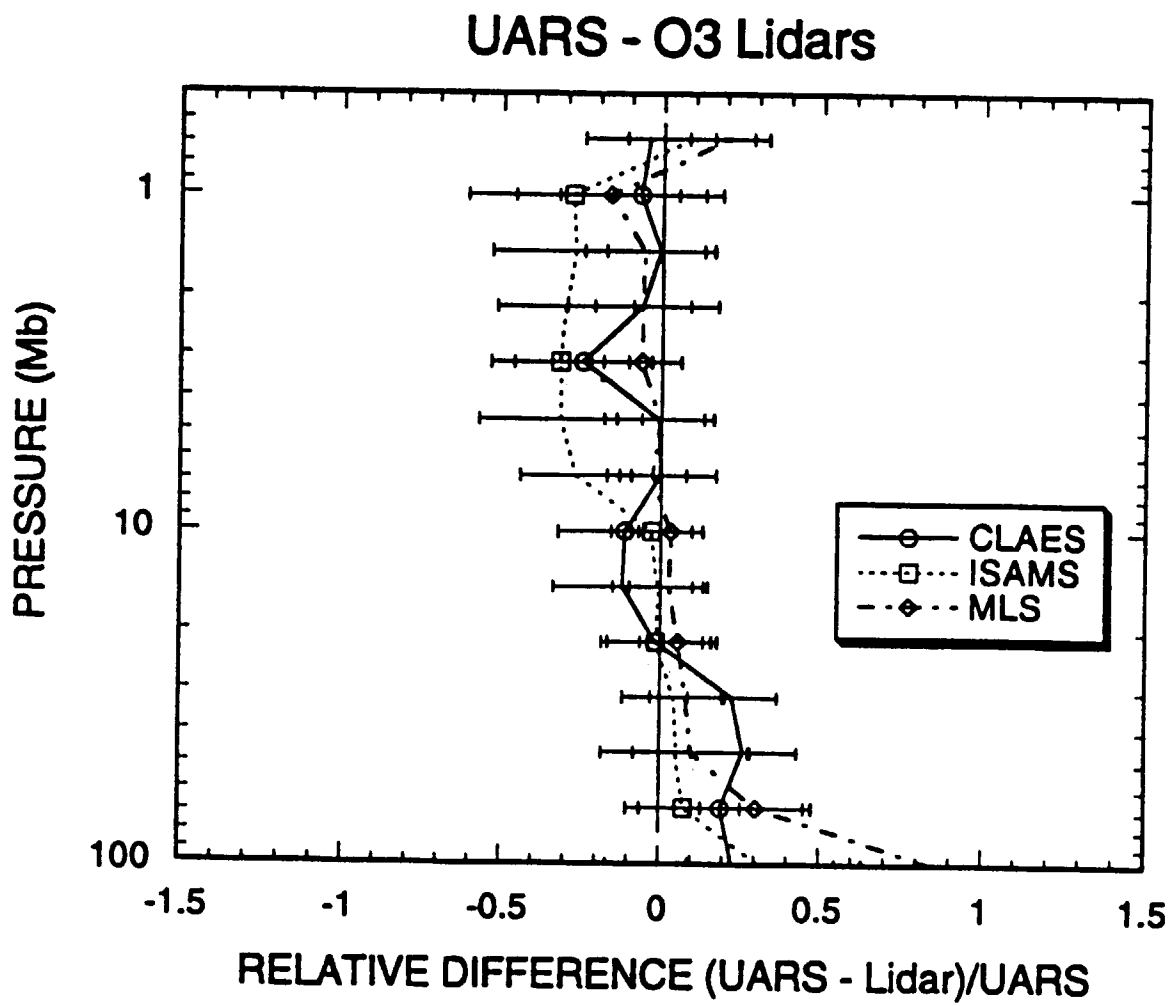

Figure 5.2.1.2-7 Mean relative differences between MLS, ISAMS and CLAES and all the coincident lidar profiles after Jan. 1, 1992. Coincident criteria are 4^{o} latitude, 12^{o} longitude and 12 hours.

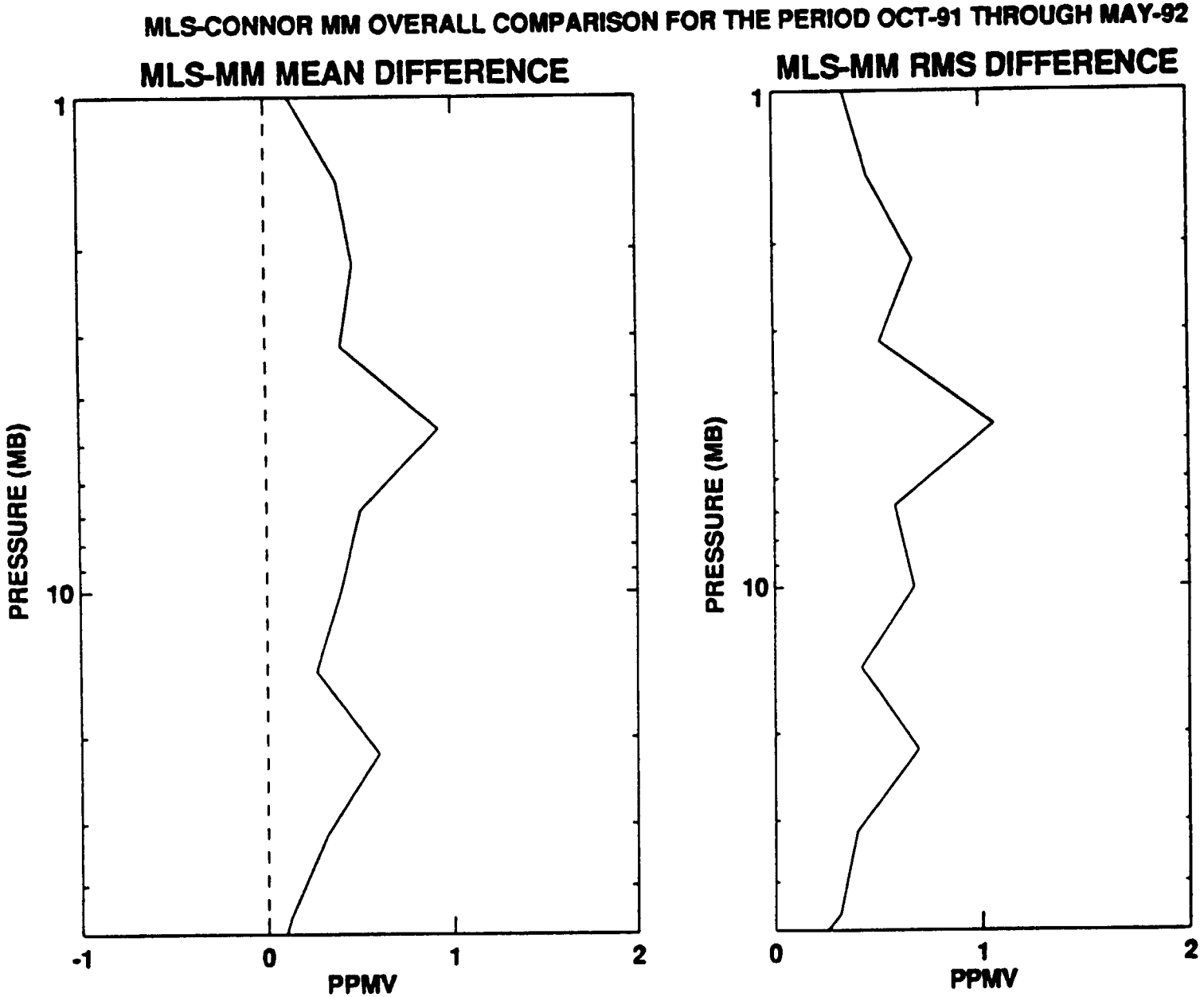

Figure 5.2.1.2-8 Mean differences between MLS and the Connor/Parrish microwave measurements between Oct. 1991 and May 1992.

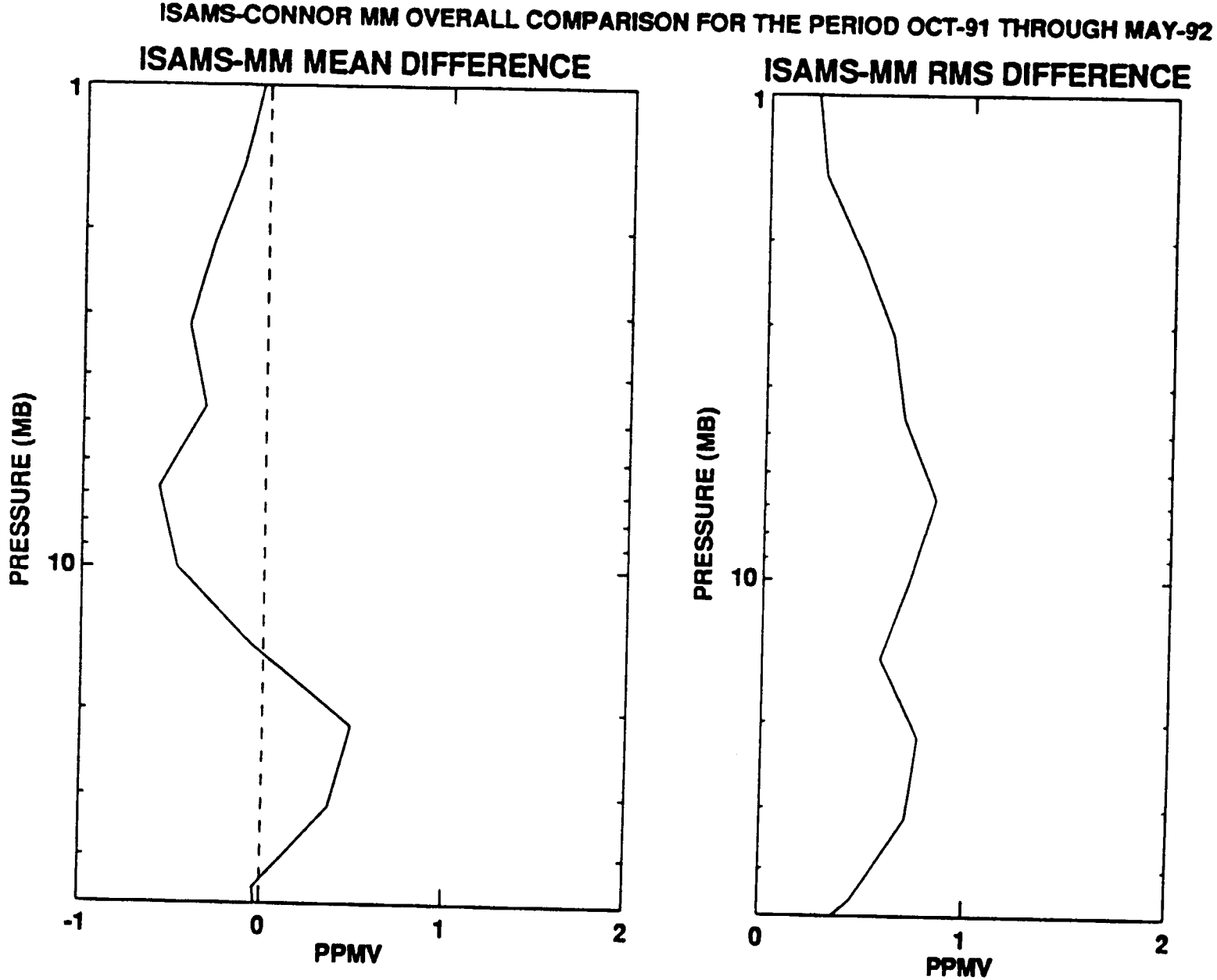

Figure 5.2.1.2-9 Mean differences between ISAMS and the Connor/Parrish microwave measurements between Oct. 1991 and May 1992.

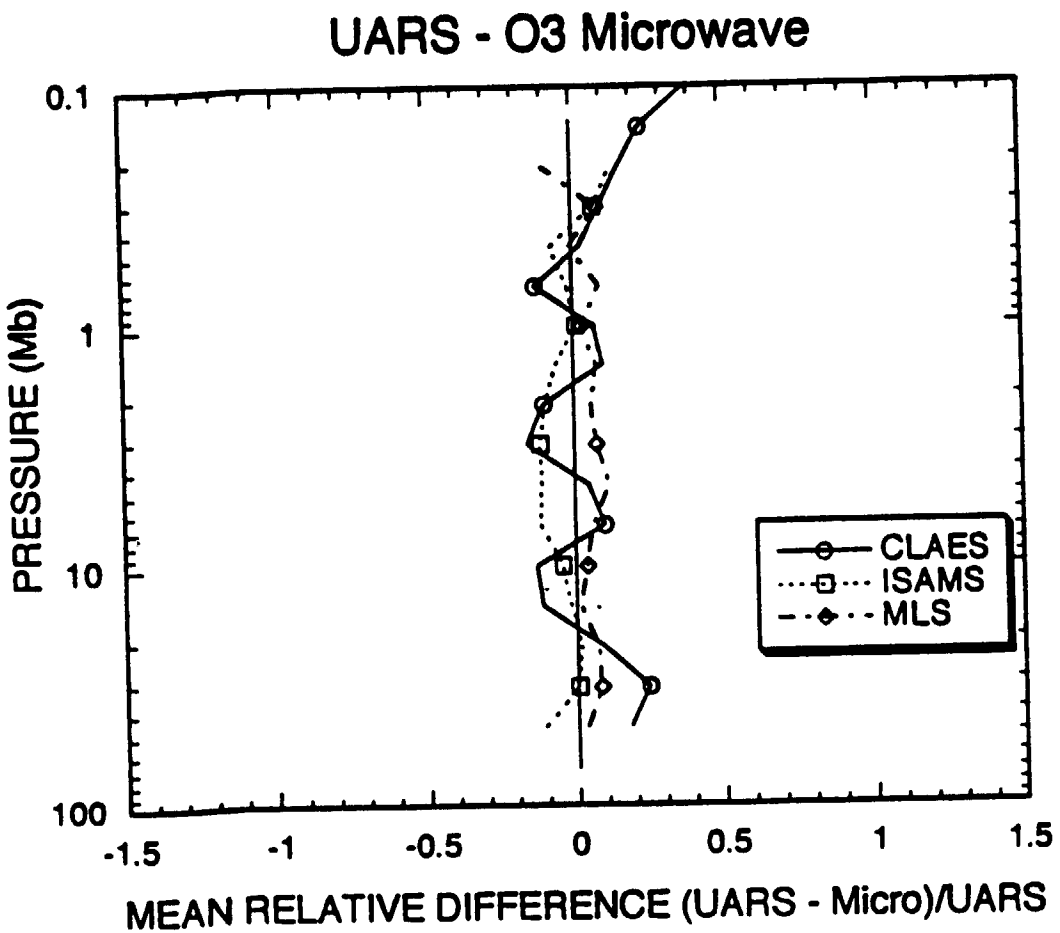

Figure 5.2.1.2-10 Mean relative ozone profile differences between the ozone microwave soundings taken as a group and coincident MLS, ISAMS and CLAES after Jan. 1, 1992. Coincidence criteria are 4^{o} latitude, 12^{o} longitude and 12 hours.

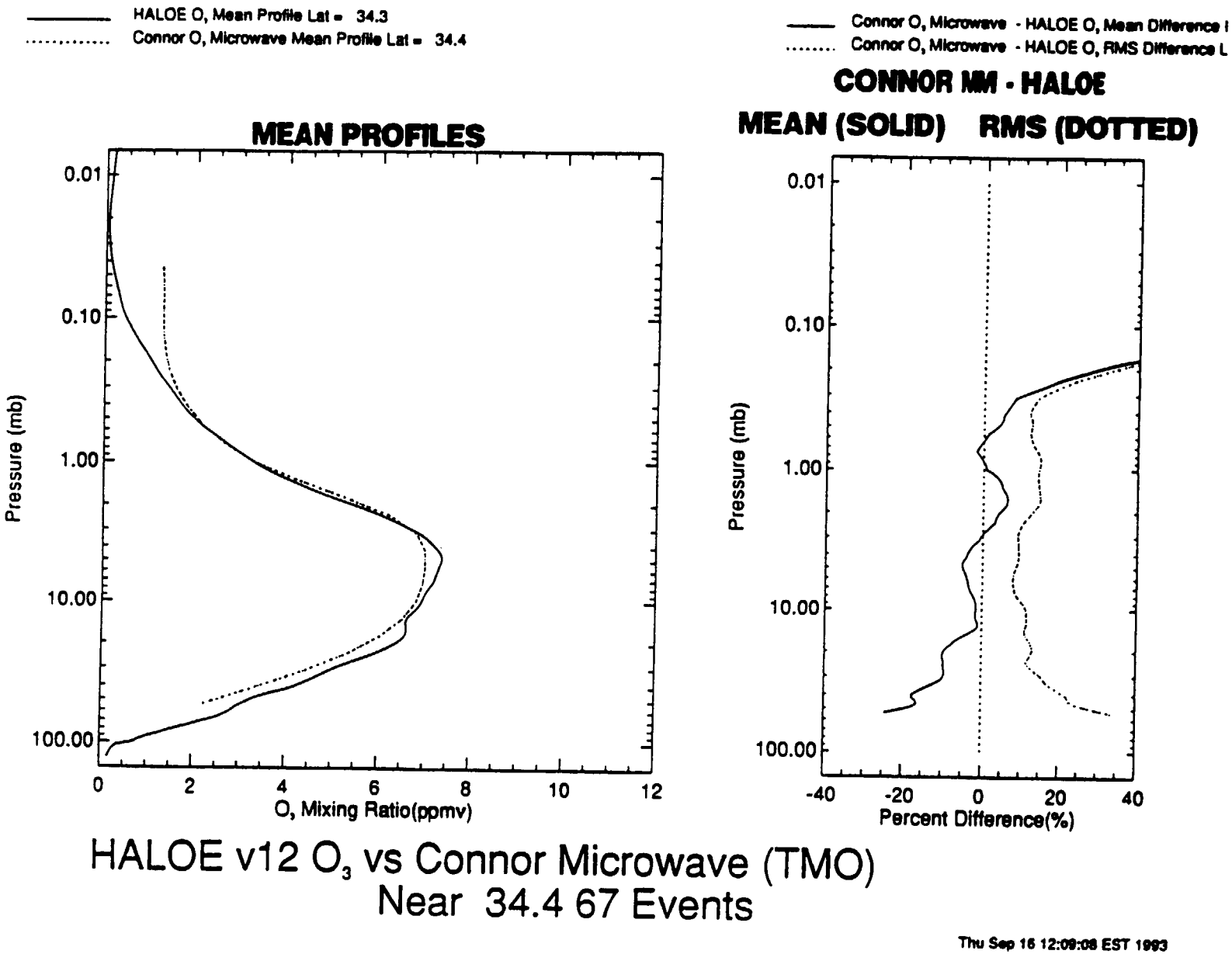

Figure 5.2.1.2-11 Mean differences between the HALOE and the Connor/ Parrish microwave measurements (67 events).

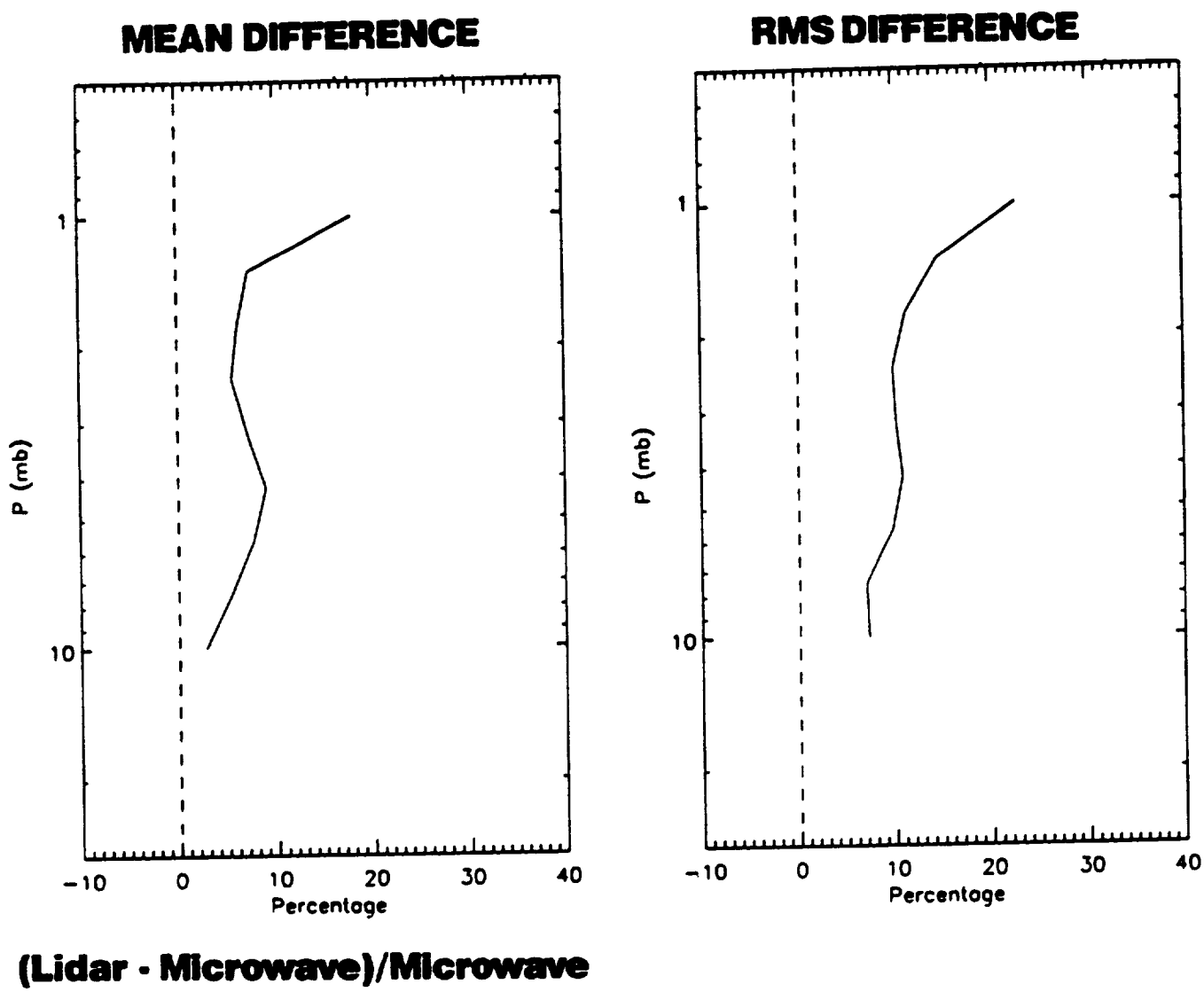

Figure 5.2.1.2-12 Mean differences between the HALOE and McDermid lidar microwave measurements for Oct. 1991-June 1992.

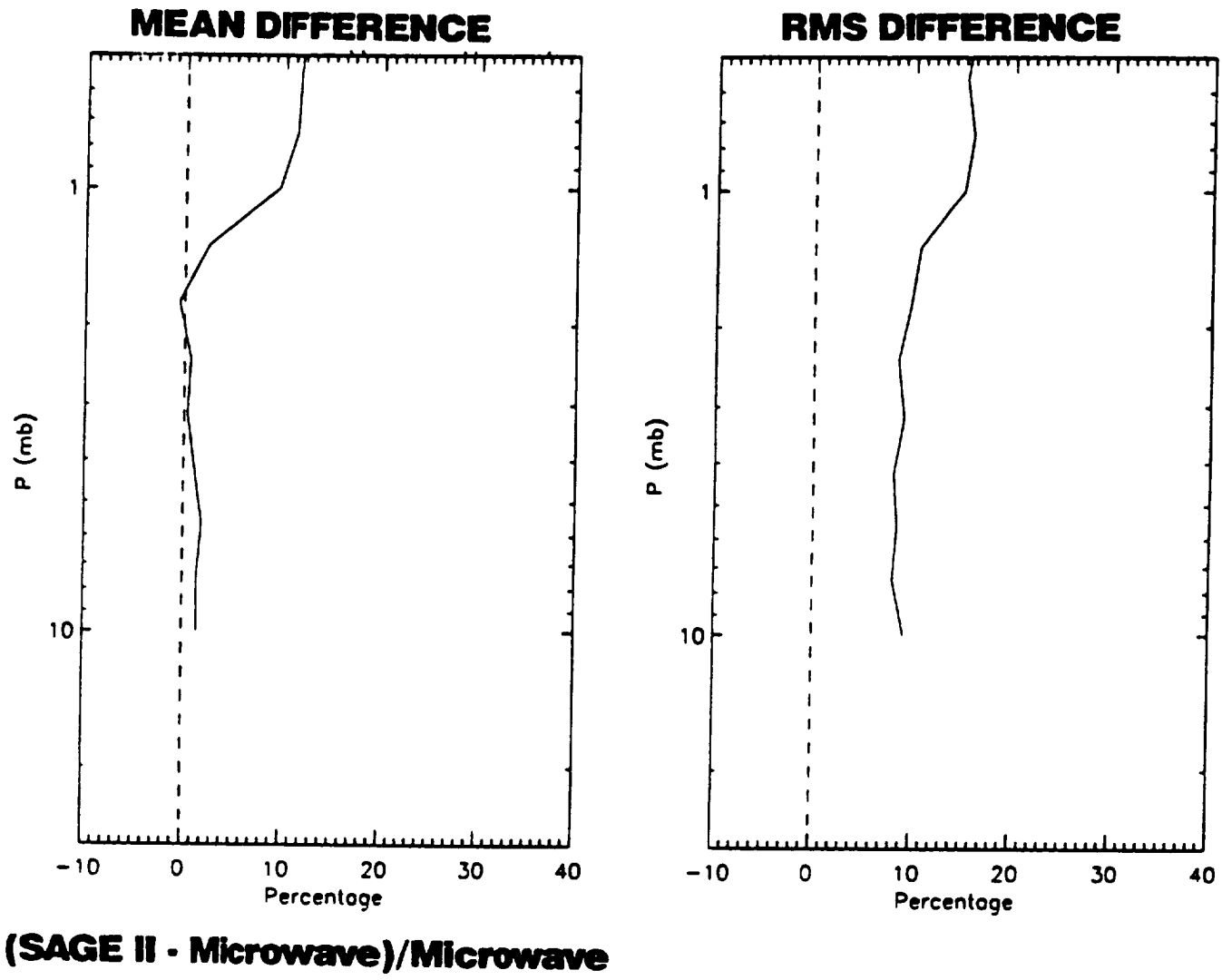

Figure 5.2.1.2-13 Mean differences between the HALOE and SAGE II microwave measurements for Oct. 1991-June 1992.

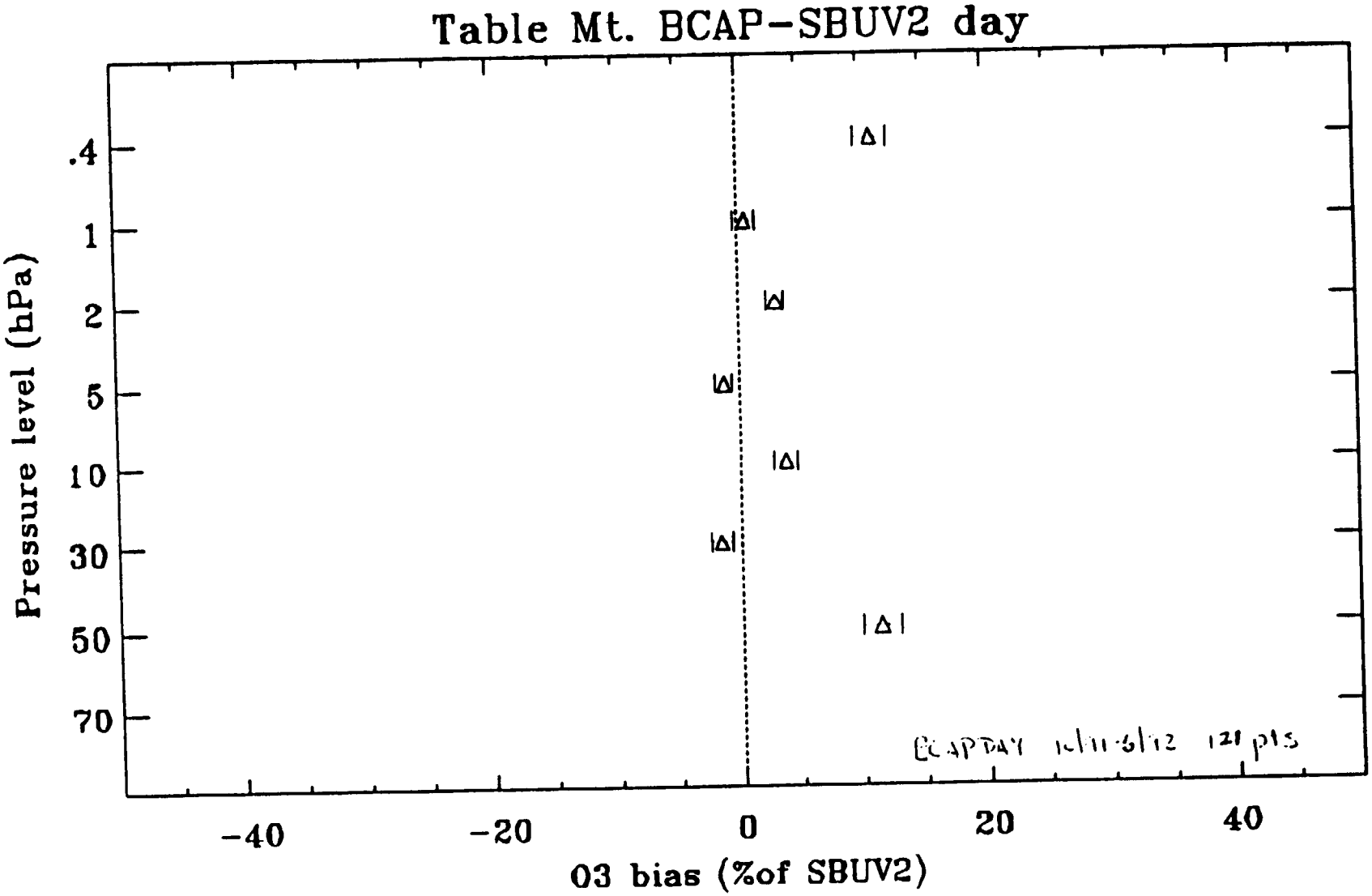

(a)

Figure 5.2.1.2-14 Average difference in ozone profiles from ground instruments and SBUV/2 version 6 at Table Mountain Observatory; error bars are twice the standard estimate of error; a) Connor/Parrish version 2 microwave daytime points, 10/92-6/92; b) Connor/ Parrish version 2 microwave nighttime points 10/91-6/92; c) McDermid lidar, 9/91-12/92.

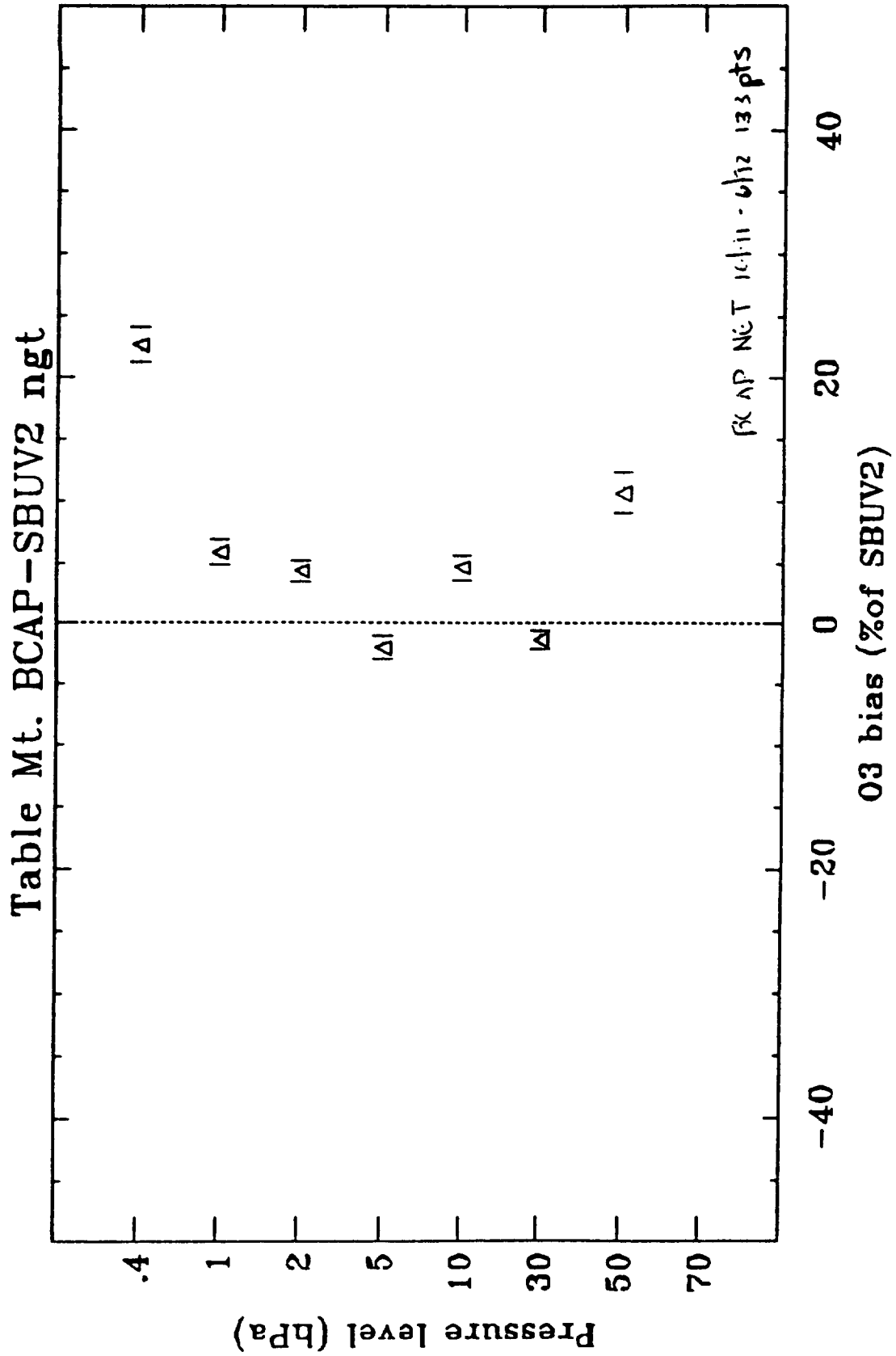

(b)

Figure 5.2.1.2-14 Continued.

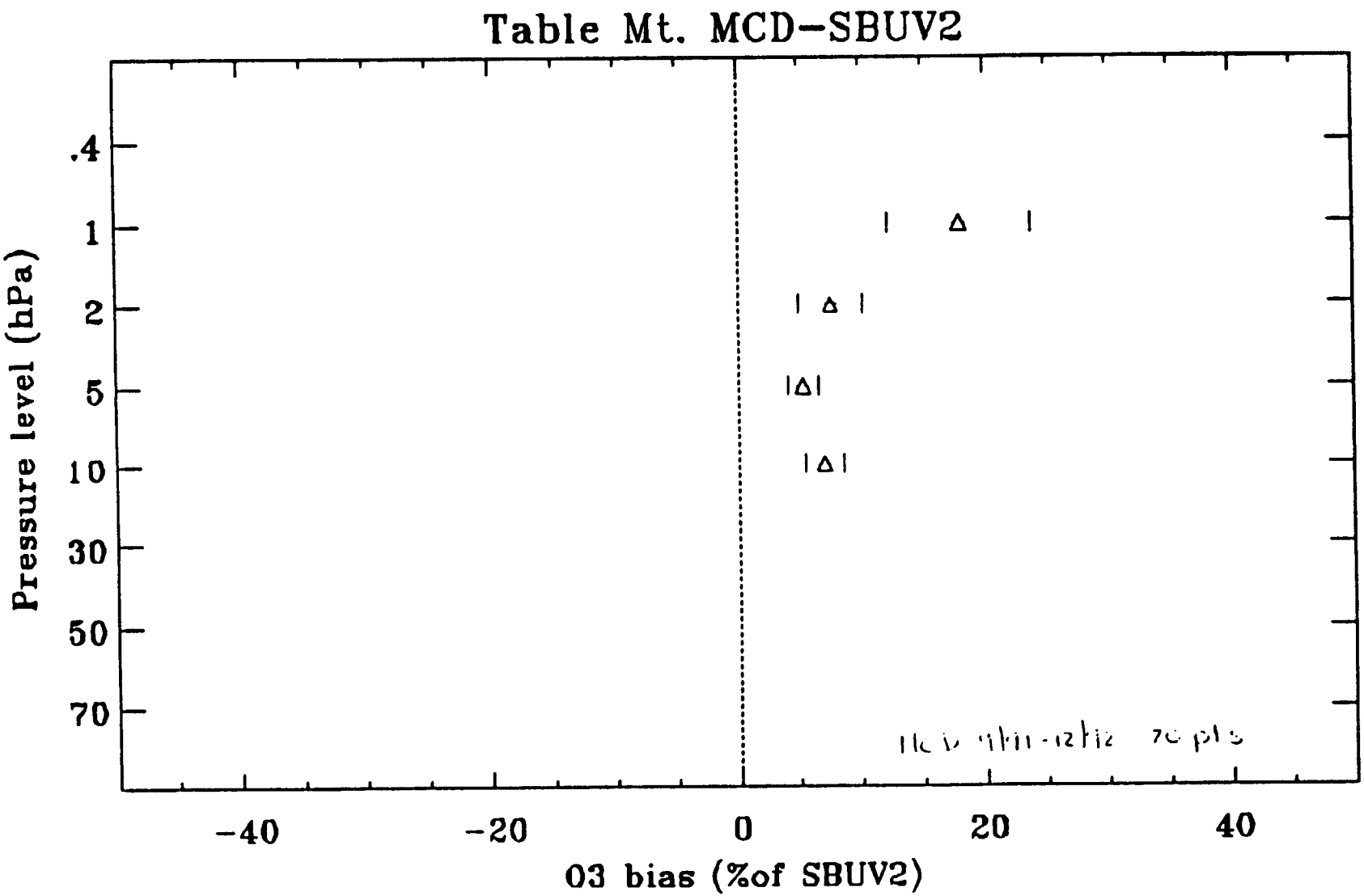

(c)

Figure 5.2.1.2-14 Concluded.

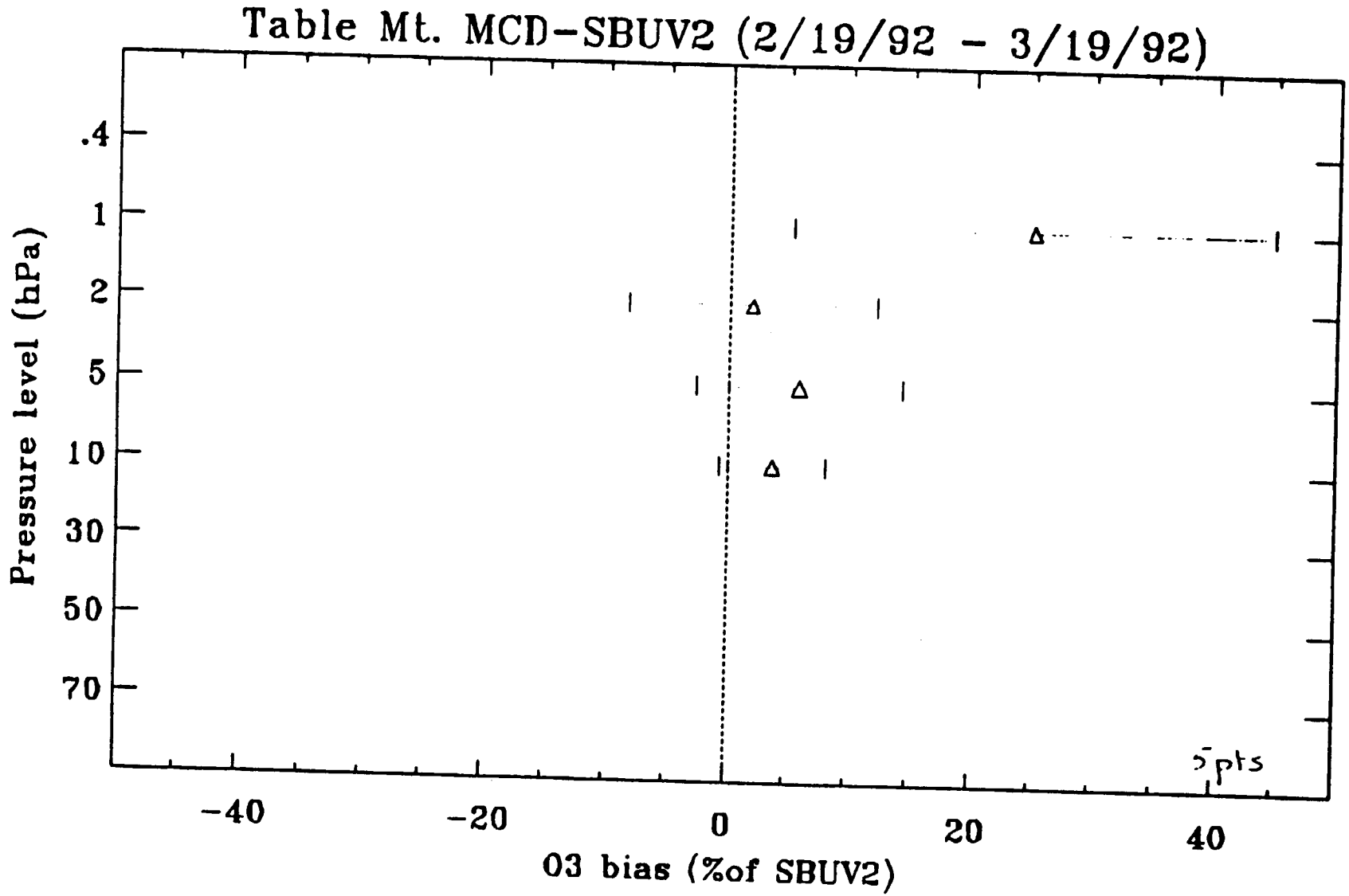

(a)

Figure 5.2.1.2-15 Average difference in ozone profiles from ground instruments and SBUV/2 version 6 at Table Mountain Observatory; data from 2/19/91-3/19/92; a) McDermid lidar; b) Connor/Parrish version 2 microwave nighttime points; c) McGee lidar.

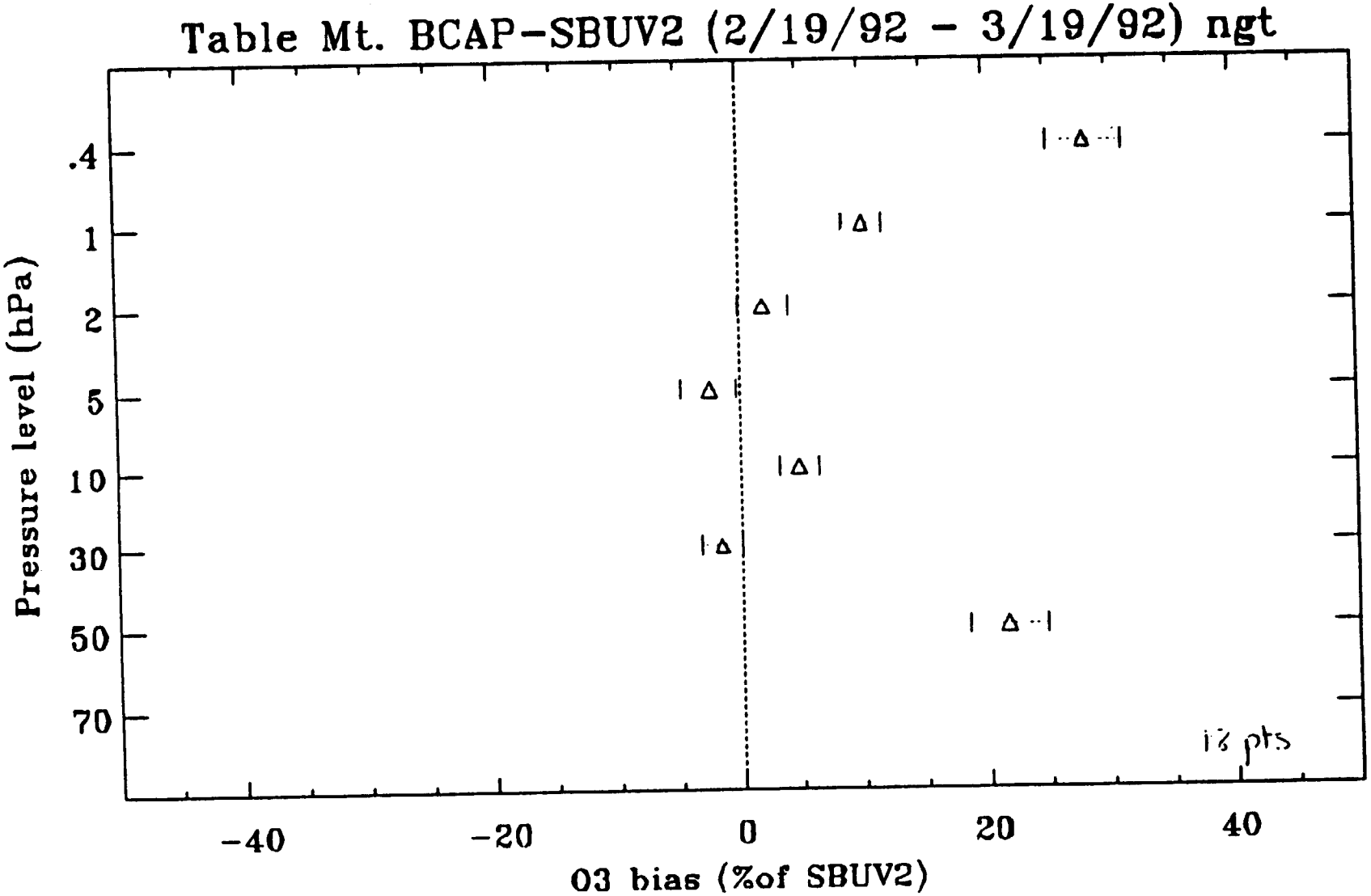

(b)

Figure 5.2.1.2-15 Continued.

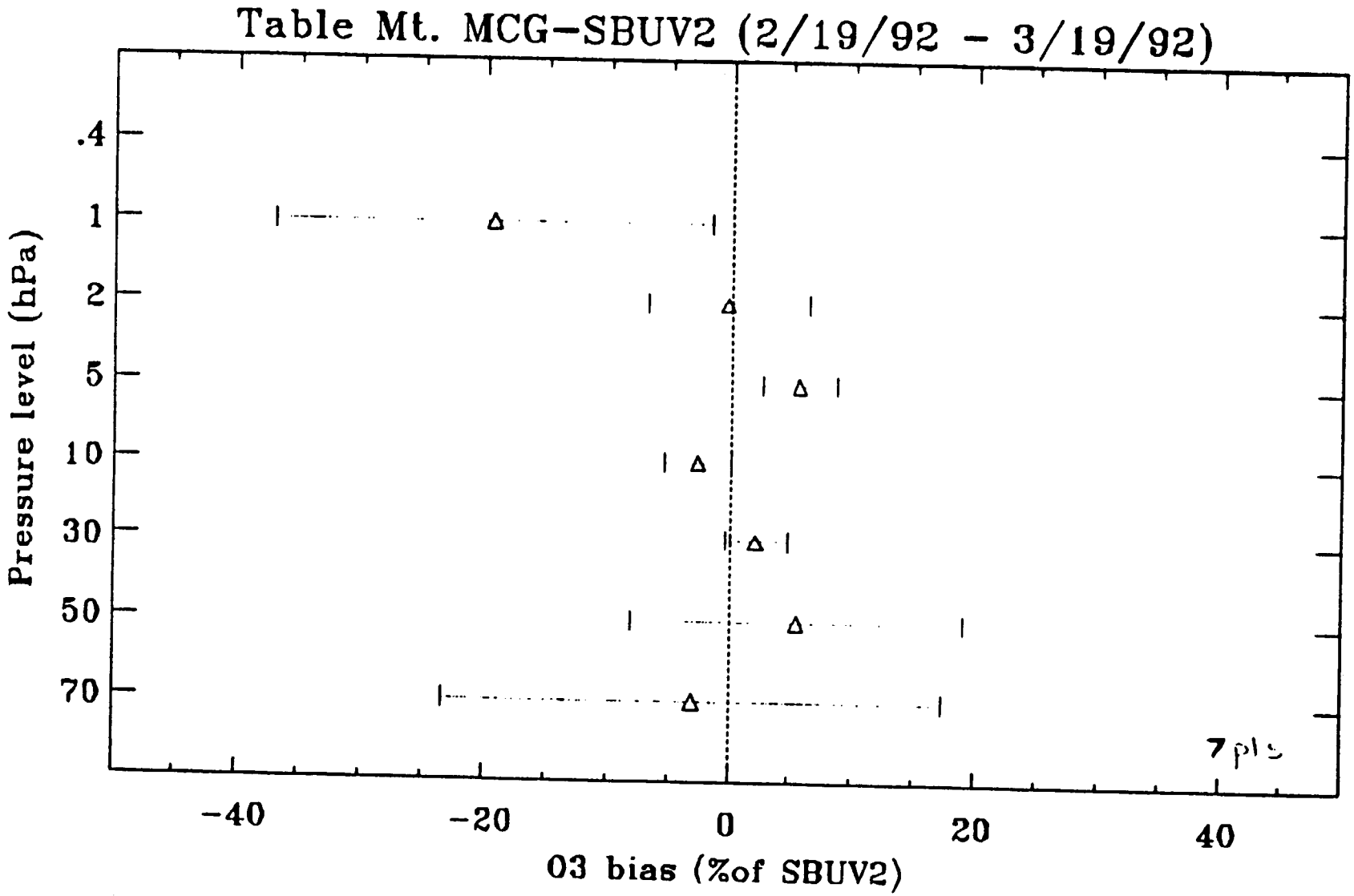

(c)

Figure 5.2.1.2-15 Concluded.

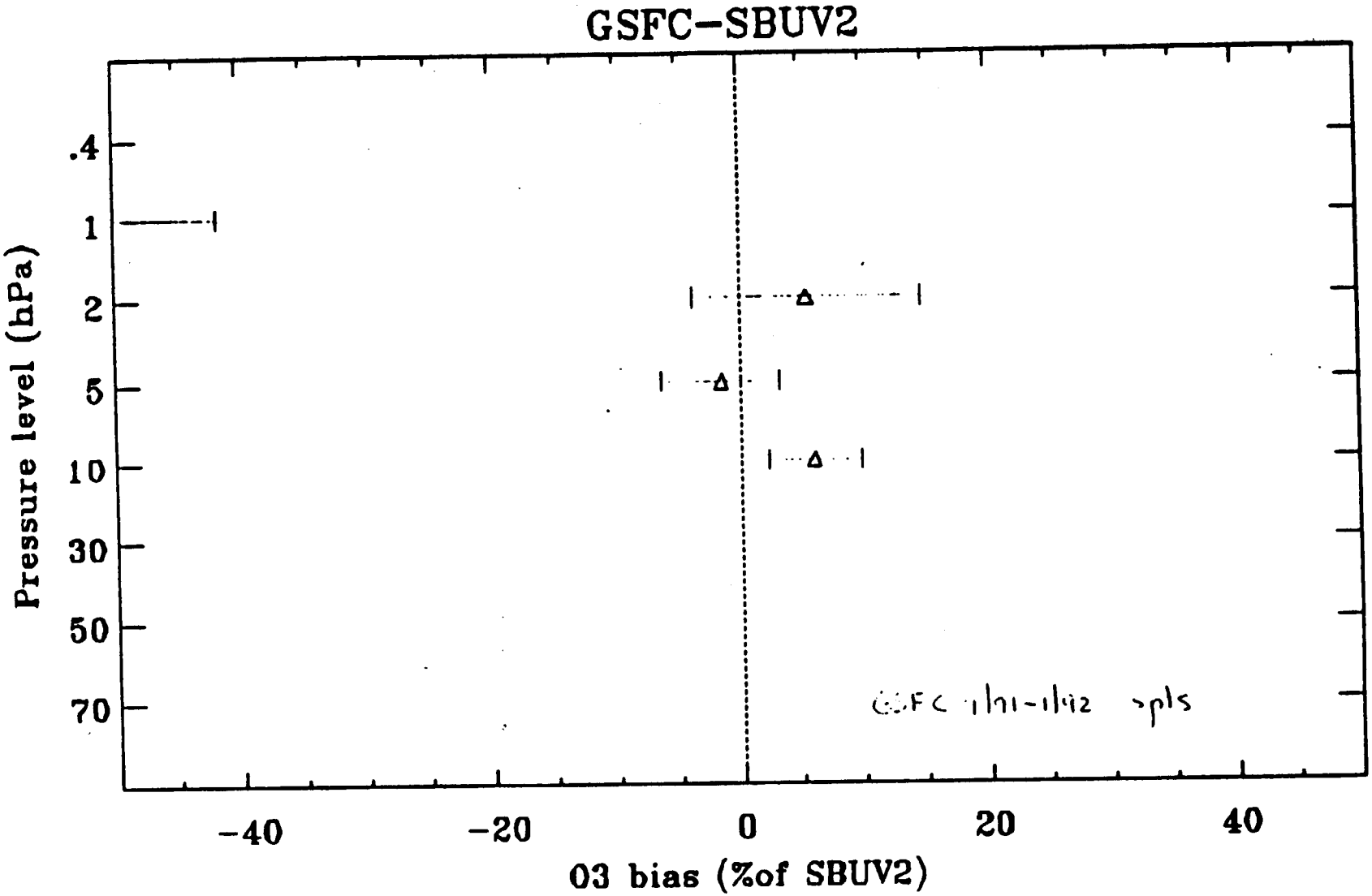

Figure 5.2.1.2-16 Average difference in ozone profiles from McGee lidar and SBUV/2 version 6 at GSFC; data from 9/91-1/92.

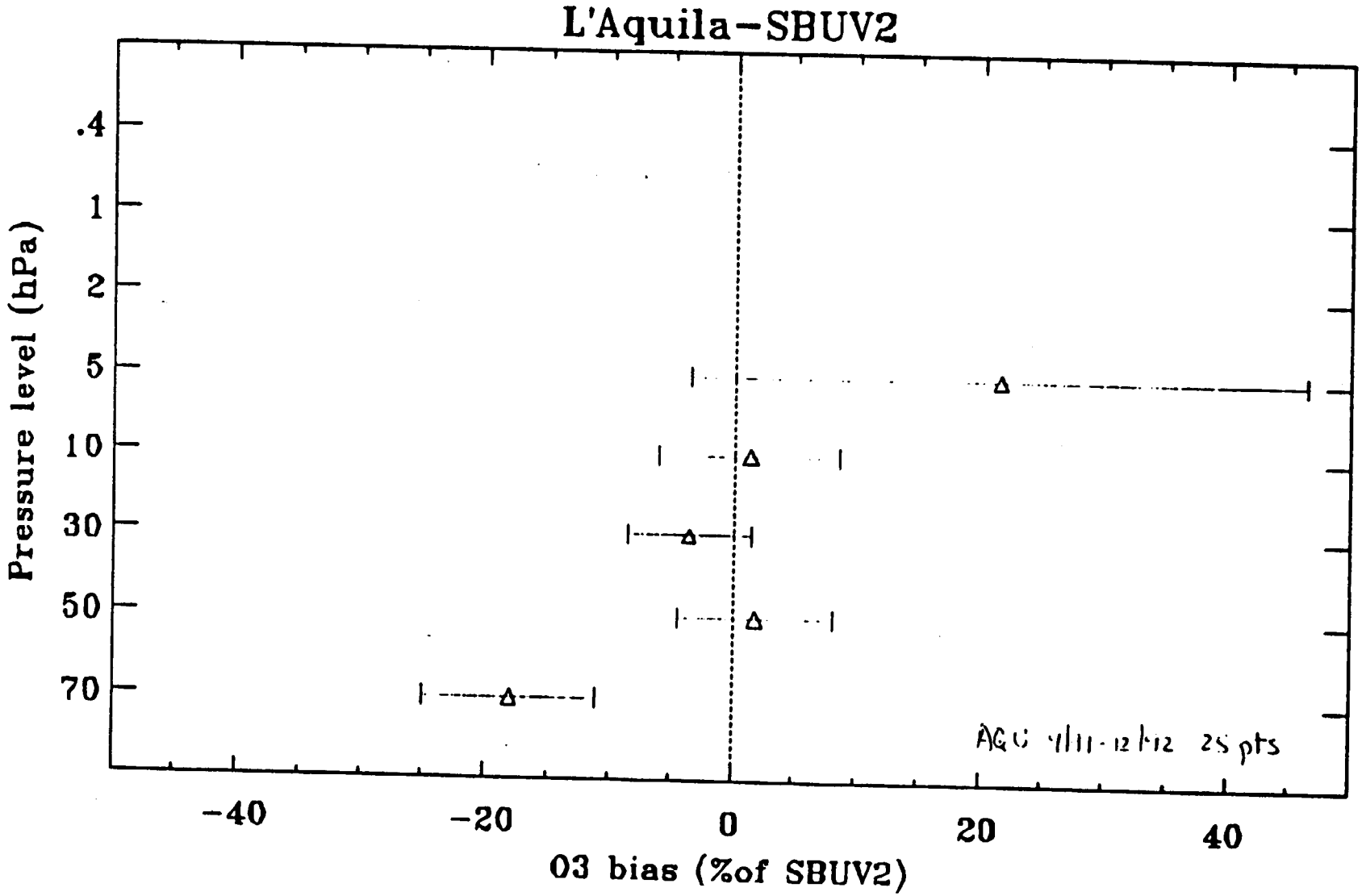

Figure 5.2.1.2-17 Average difference in ozone profiles from Visconti lidar and SBUV/2 version 6 at L'Aquila; data from 9/91-12/92.

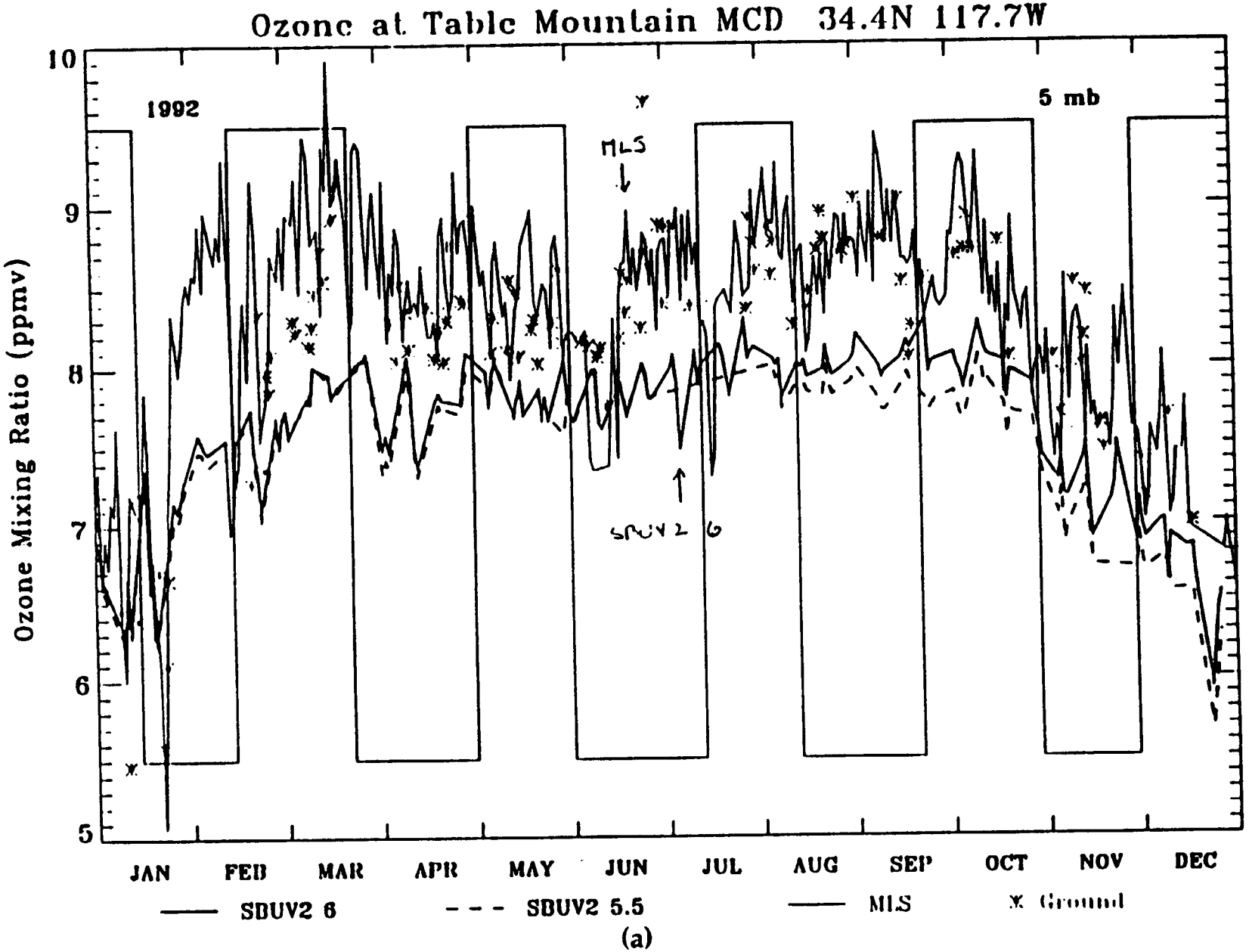

Figure 5.2.1.2-18 Ozone 1992 time series at 5 mb for SBUV/2 versions 5.5 and 6, MLS version 3, and ground instruments at Table Mountain Observatory; a) McDermid lidar; b) Connor/Parrish version 2 microwave.

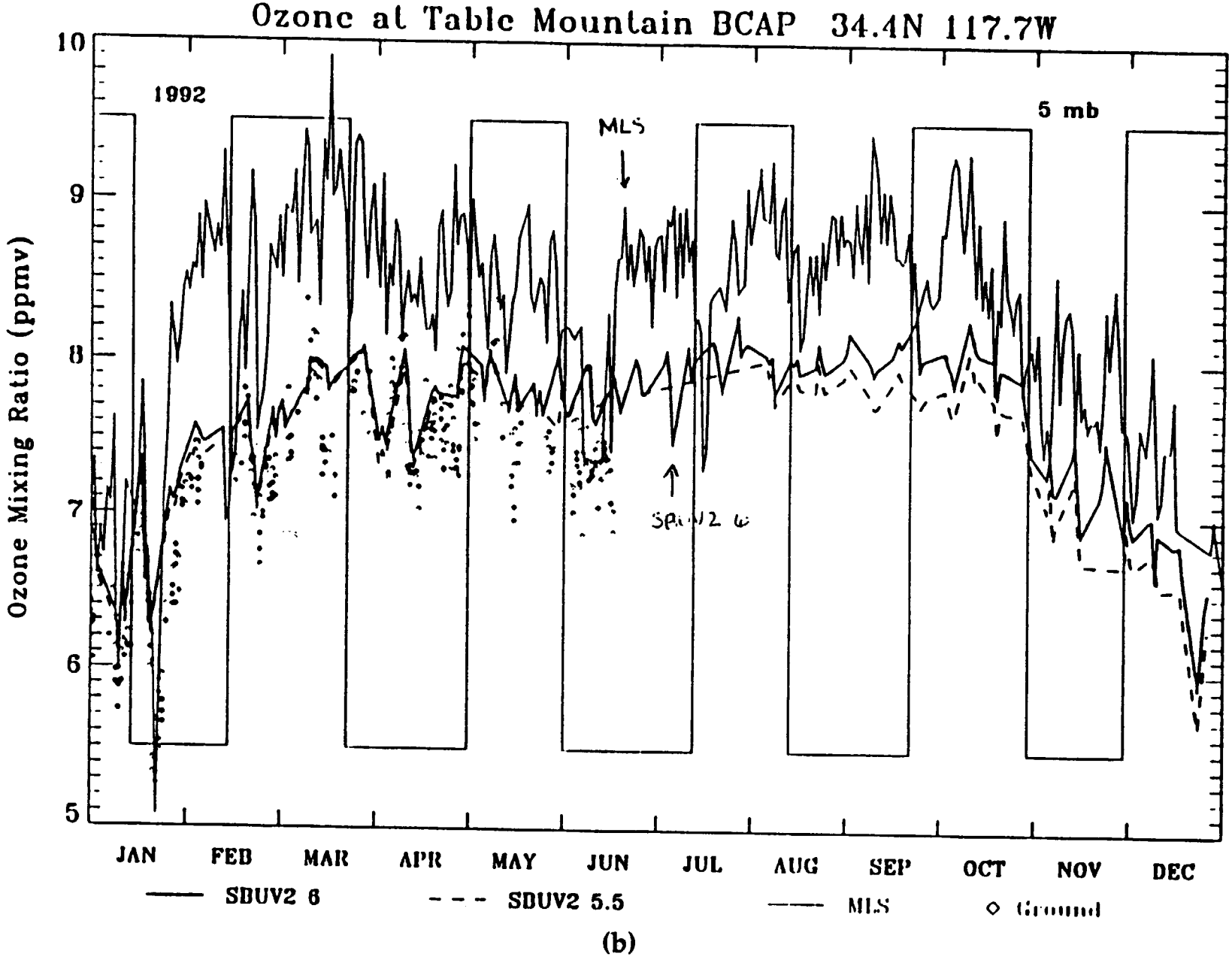

(b)

Figure 5.2.1.2-18 Concluded.

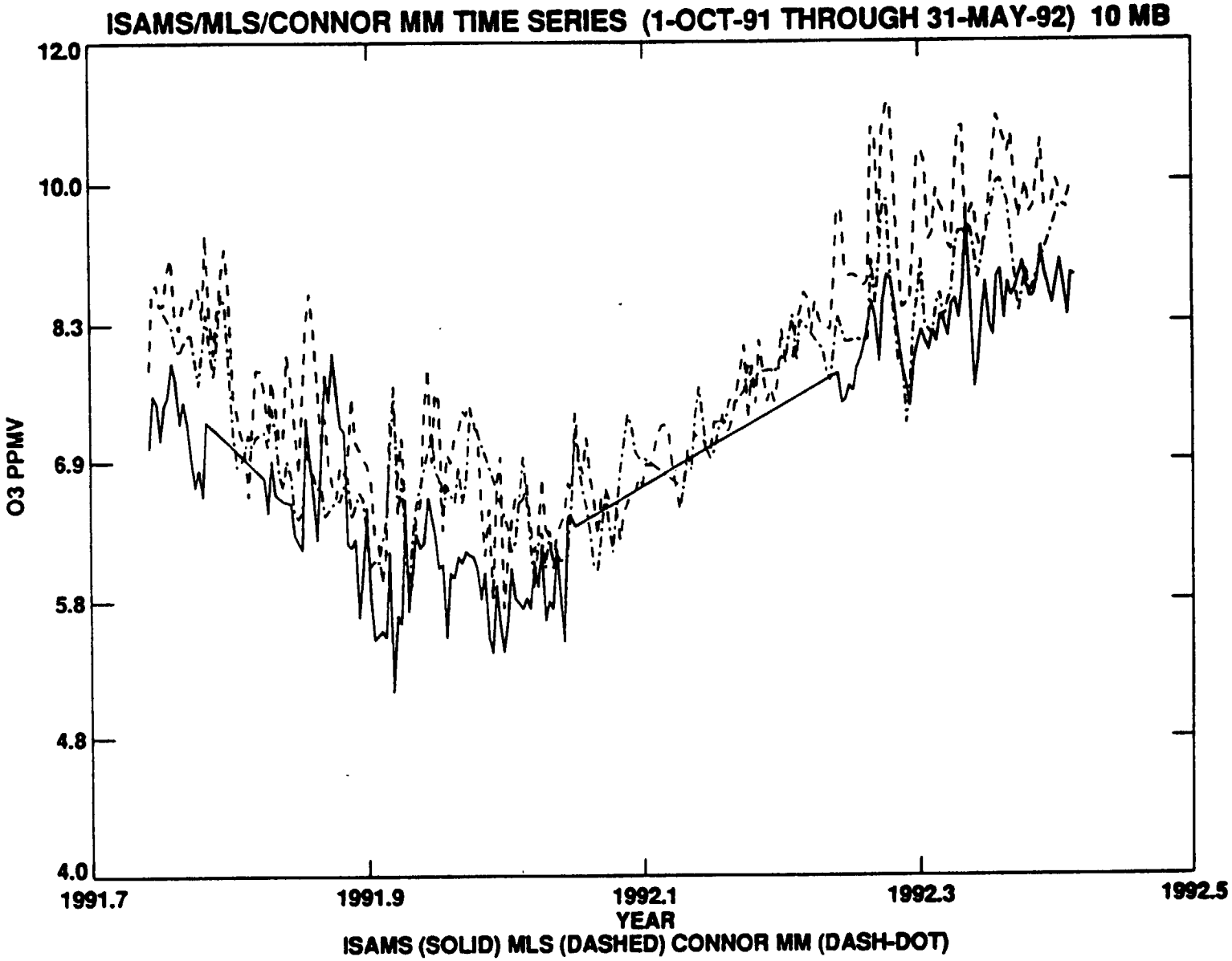

(a)

Figure 5.2.1.2-19 Time series comparison between ISAMS, MLS, and Connor/ Parrish microwave measurements for Oct. 1, 1991 to May 31, 1992, a) at 10 hPa, b) at 4.6 hPa and c) at 2.2 hPa.

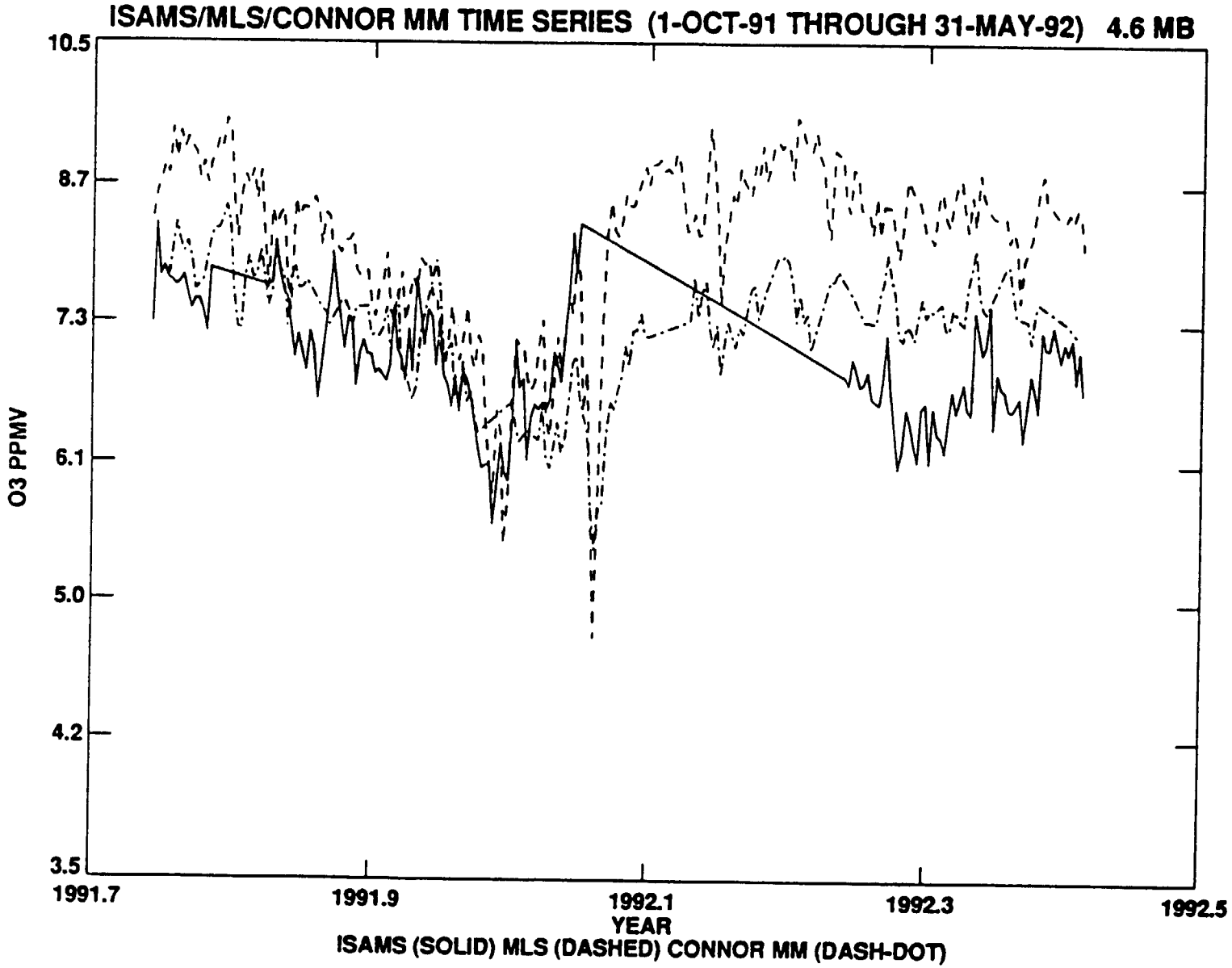

(b)

Figure 5.2.1.2-19 Continued.

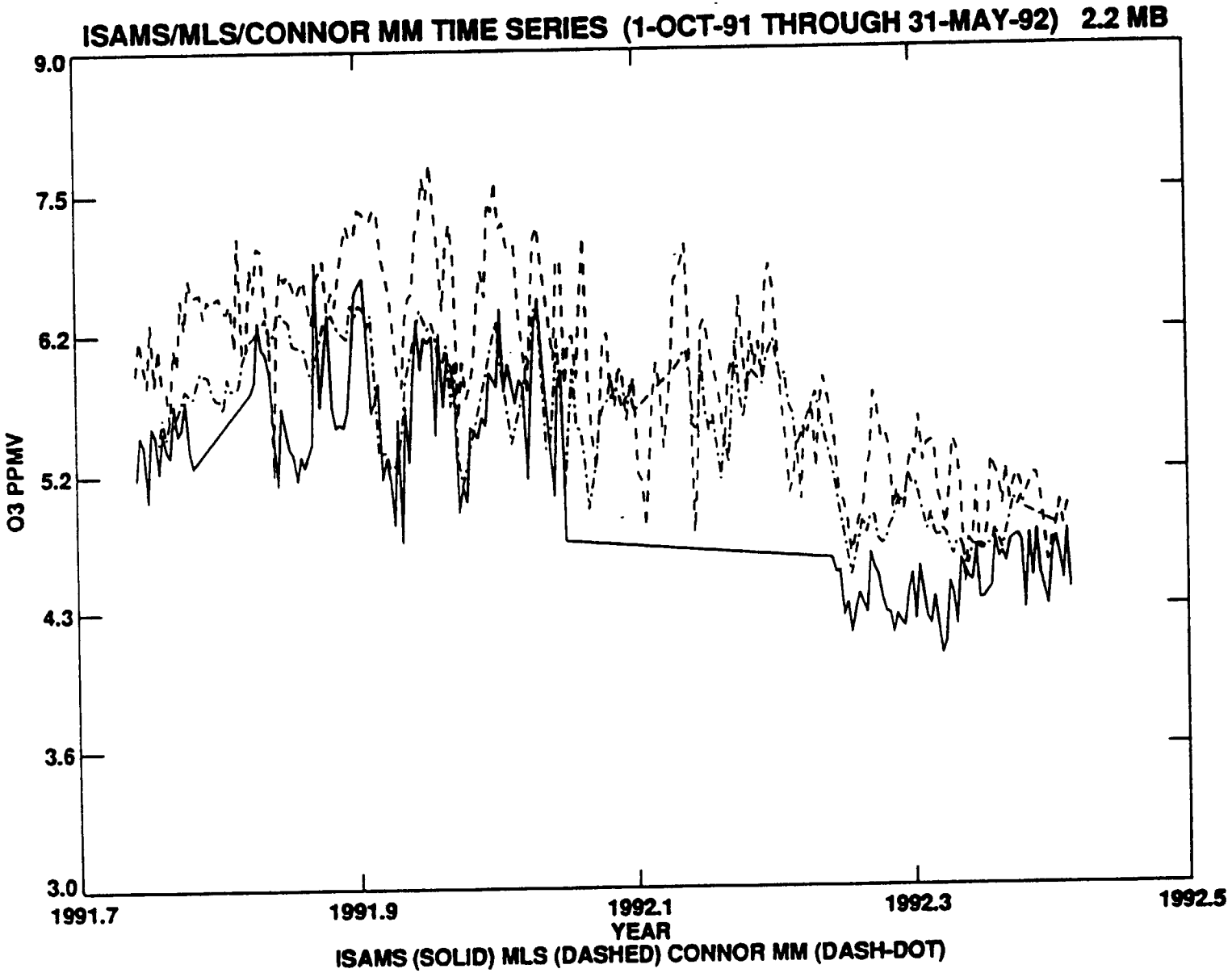

(c)

Figure 5.2.1.2-19 Concluded.

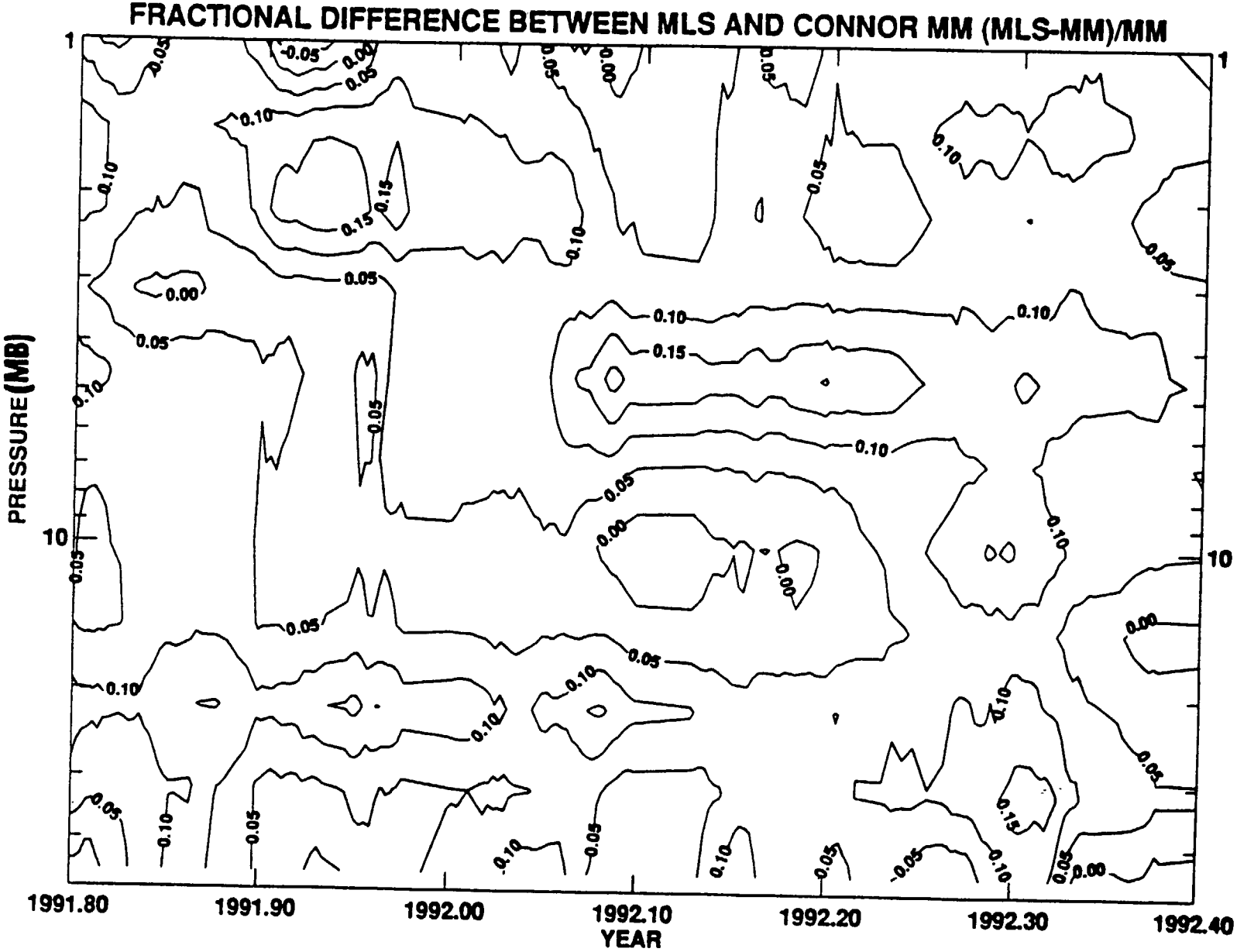

(a)

Figure 5.2.1.2-20 Fractional differences of UARS from the microwave measurements shown in Figure 5.2.1.2-19. a) MLS, b) ISAMS (before the first chopper motor failure) and c) ISAMS (after the first chopper motor failure).

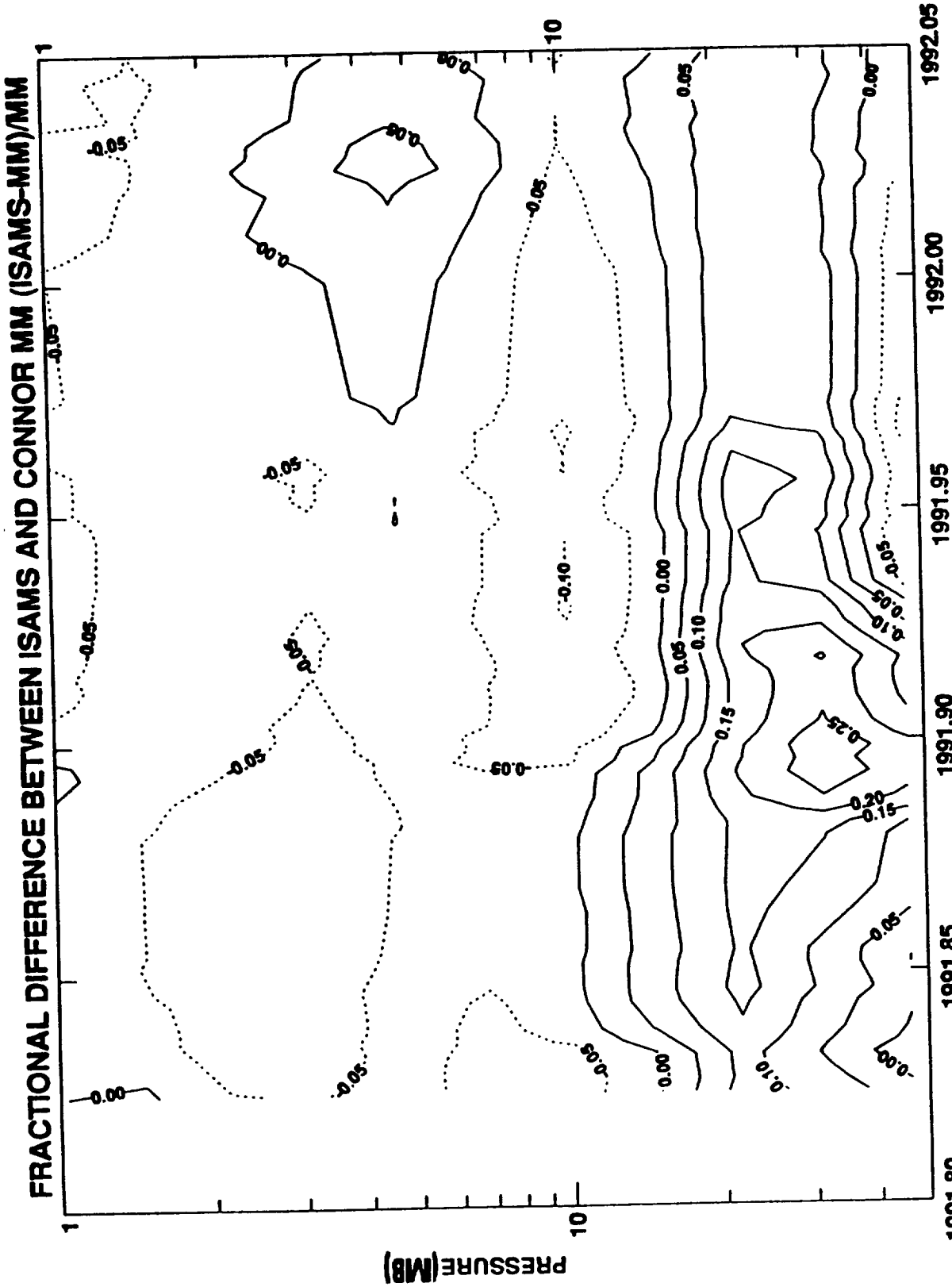

(b)

Figure 5.2.1.2-20 Continued.

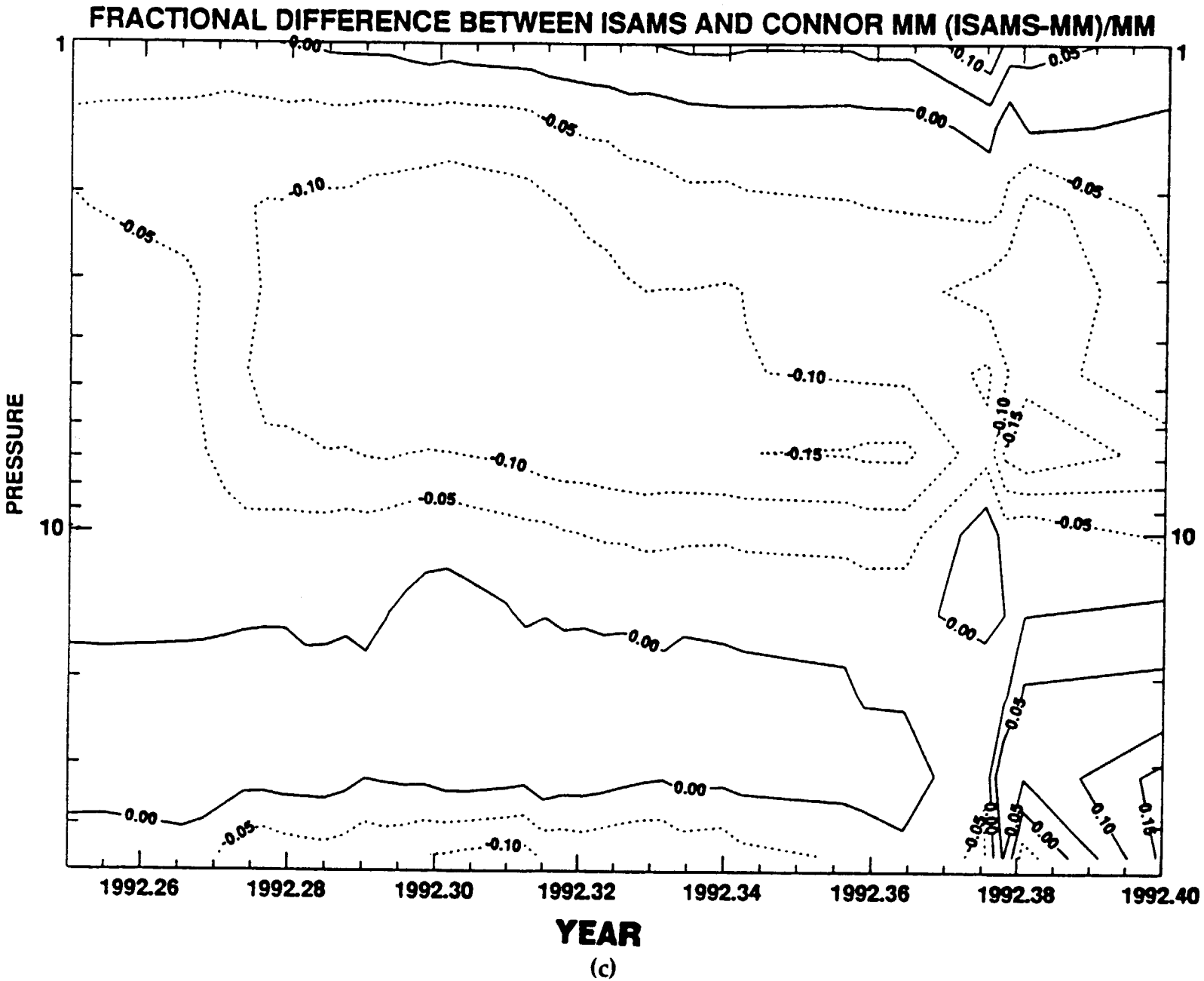

(c)

Figure 5.2.1.2-20 Concluded.

FIGURE UNAVAILABLE

Figure 5.2.1.3-1 Comparisons of Boulder ozonesonde data on Jan. 10, 1992 (top panel) and April 17, 1992 (bottom panel) with near-coincident UARS profiles. Sonde profile is the solid line with 5% "nominal" error bar indicated (dark shading). Error bars are generally omitted from the UARS profiles for clarity (except bottom panel of this figure). Legend at right of plot gives symbol meaning and distance (km) and time difference (hr) for UARS minus sonde. For HALOE (if plotted), latitude and longitude difference (HALOE minus sonde) are given in brackets in the plot title.

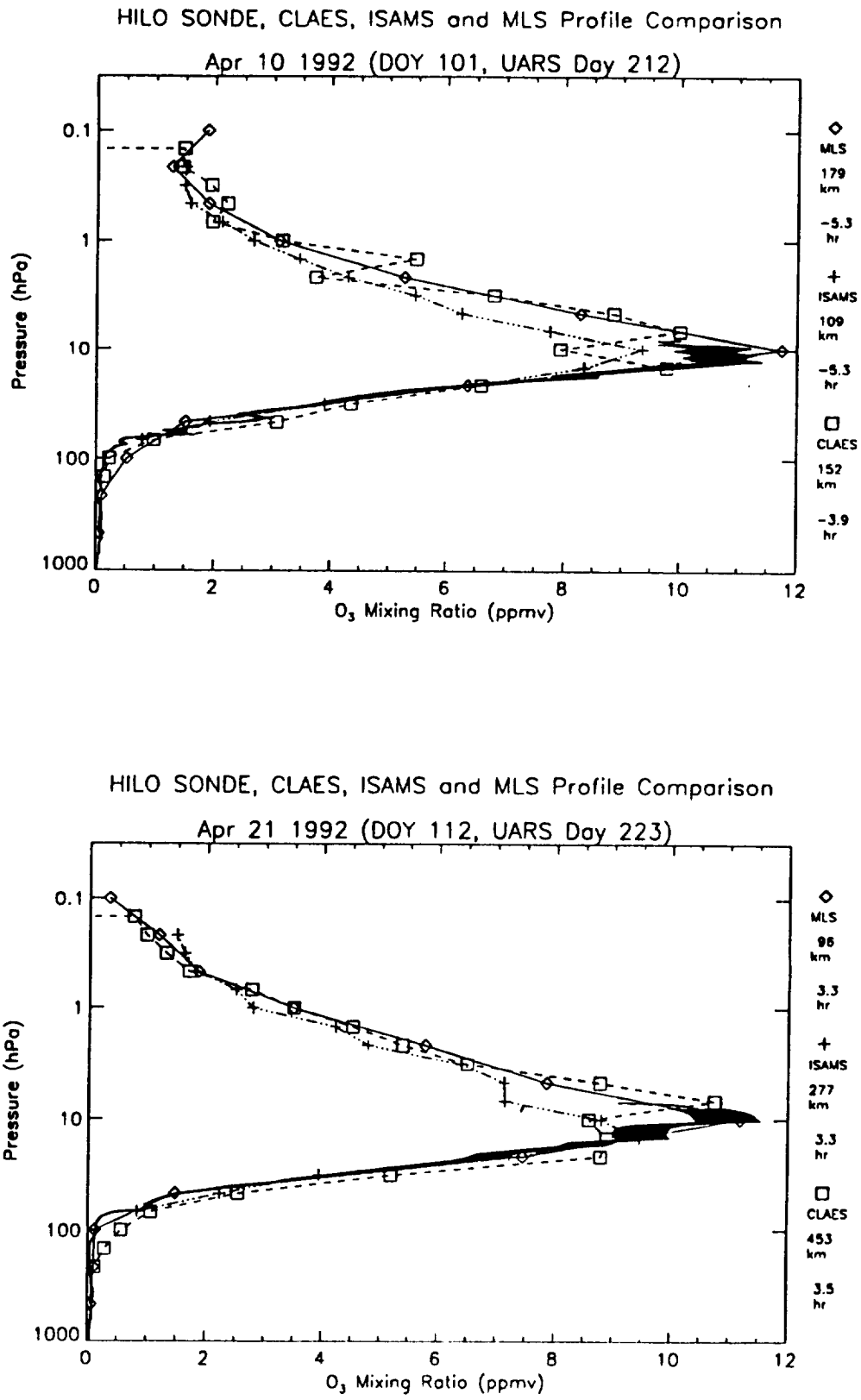

Figure 5.2.1.3-2 Same as Figure 5.2.1.3-1, but for April 1992 coincidences between UARS and Hilo ozonesondes.

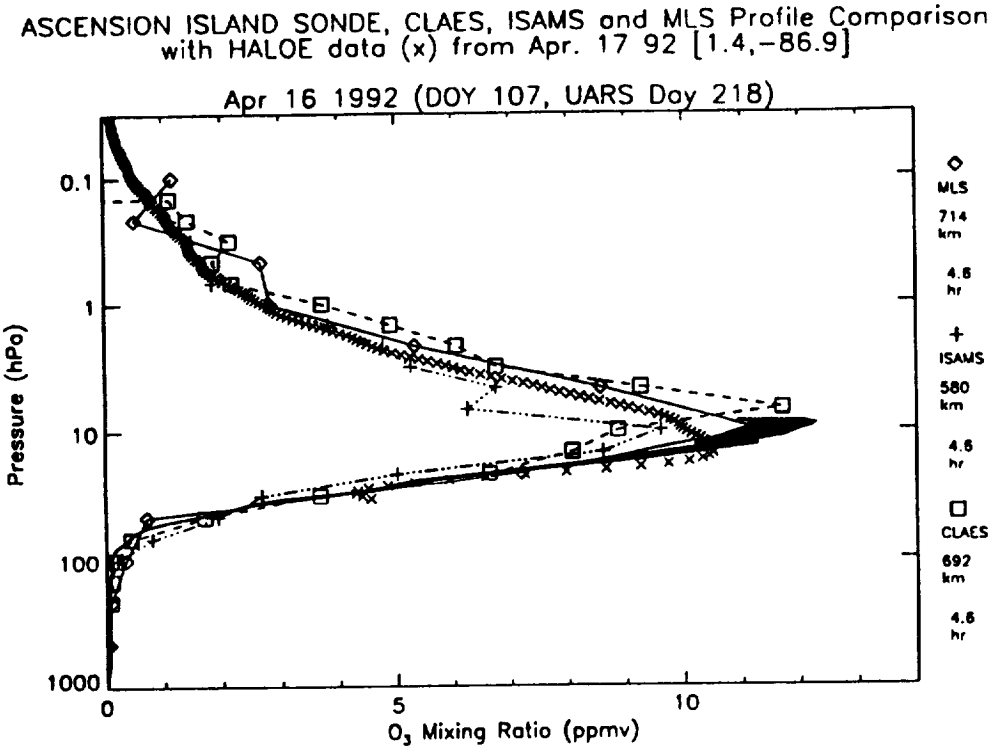

Figure 5.2.1.3-3

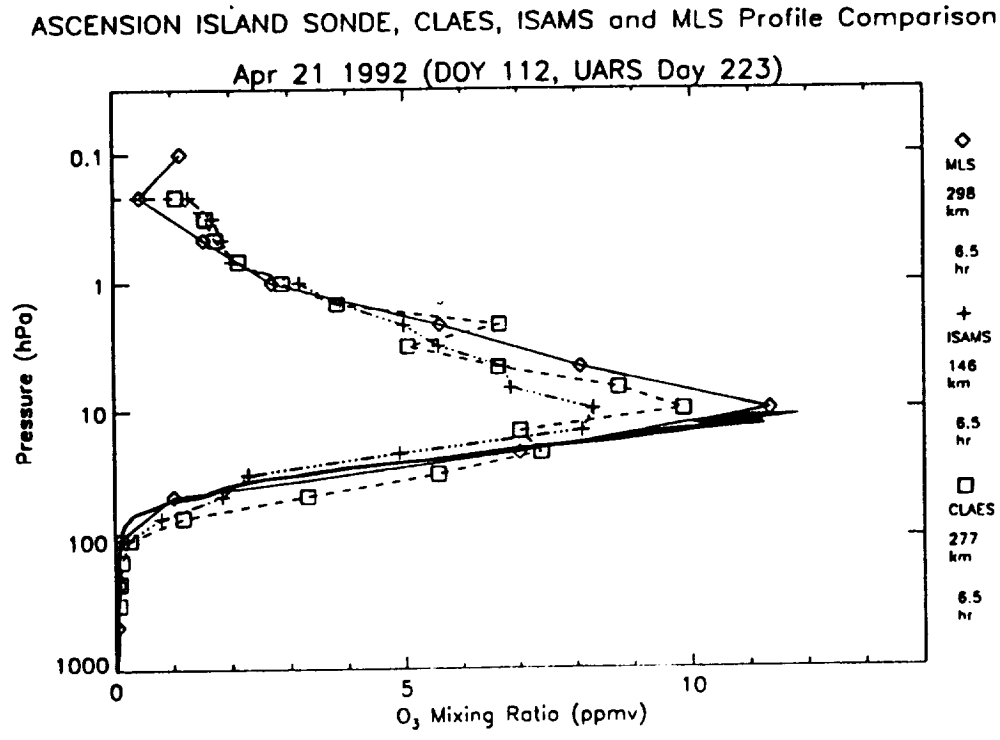

Figure 5.2.1.3-3 Same as Figure 5.2.1.3-1, but for April 1992 coincidences between UARS and Ascension Island ozonesondes.

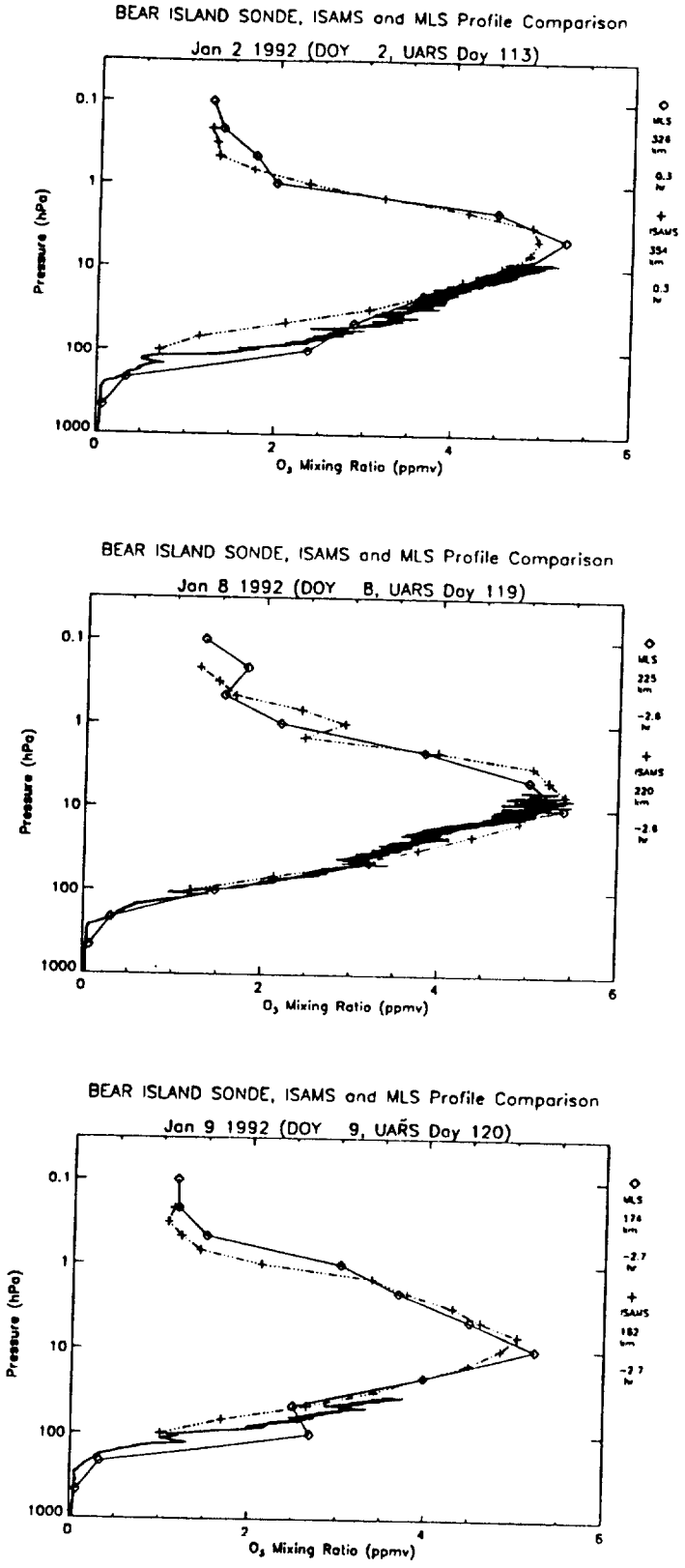

Figure 5.2.1.3-4 Same as Figure 5.2.1.3-1, but for Jan. 1992 coincidences between UARS and Bear Island ozonesondes.

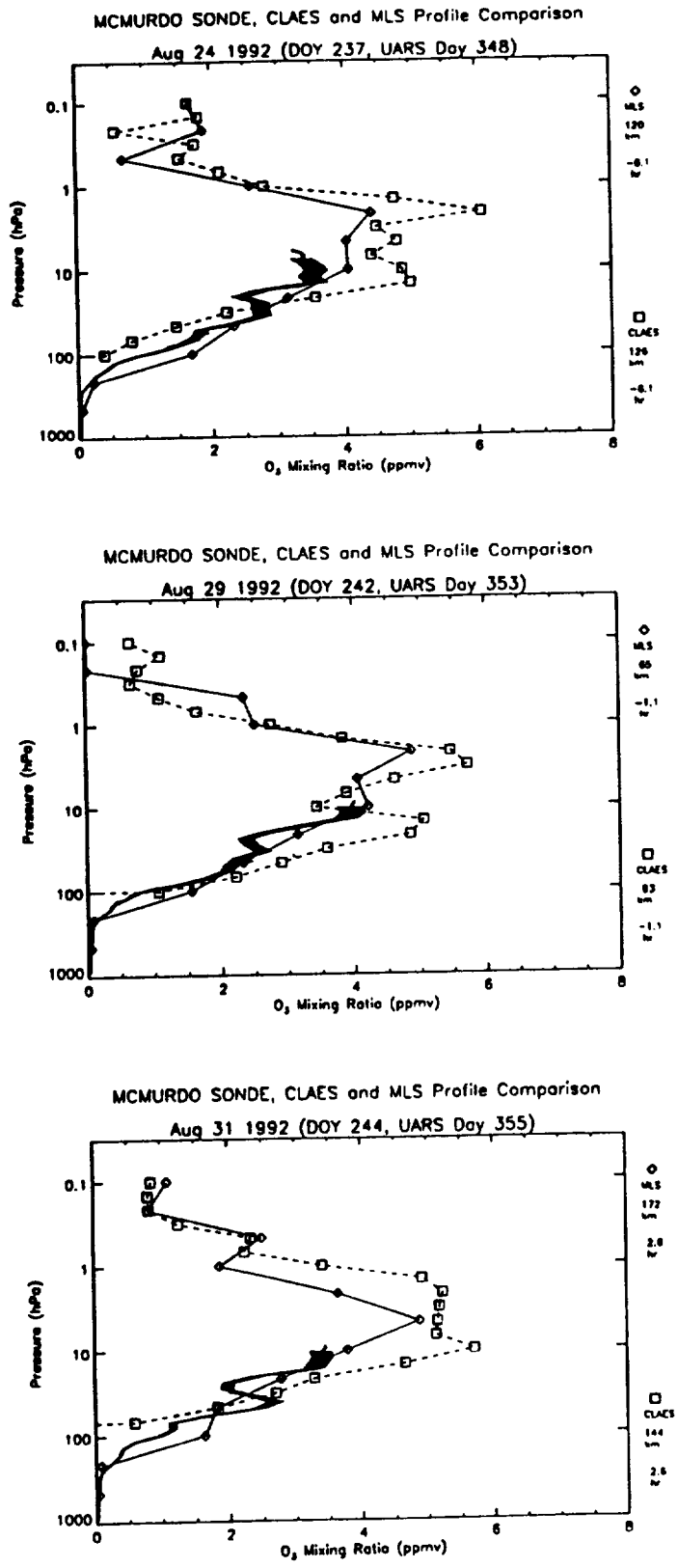

Figure 5.2.1.3-5 Same as Figure 5.2.1.3-1, but for Aug. 1992 coincidences between UARS and McMurdo ozonesondes.

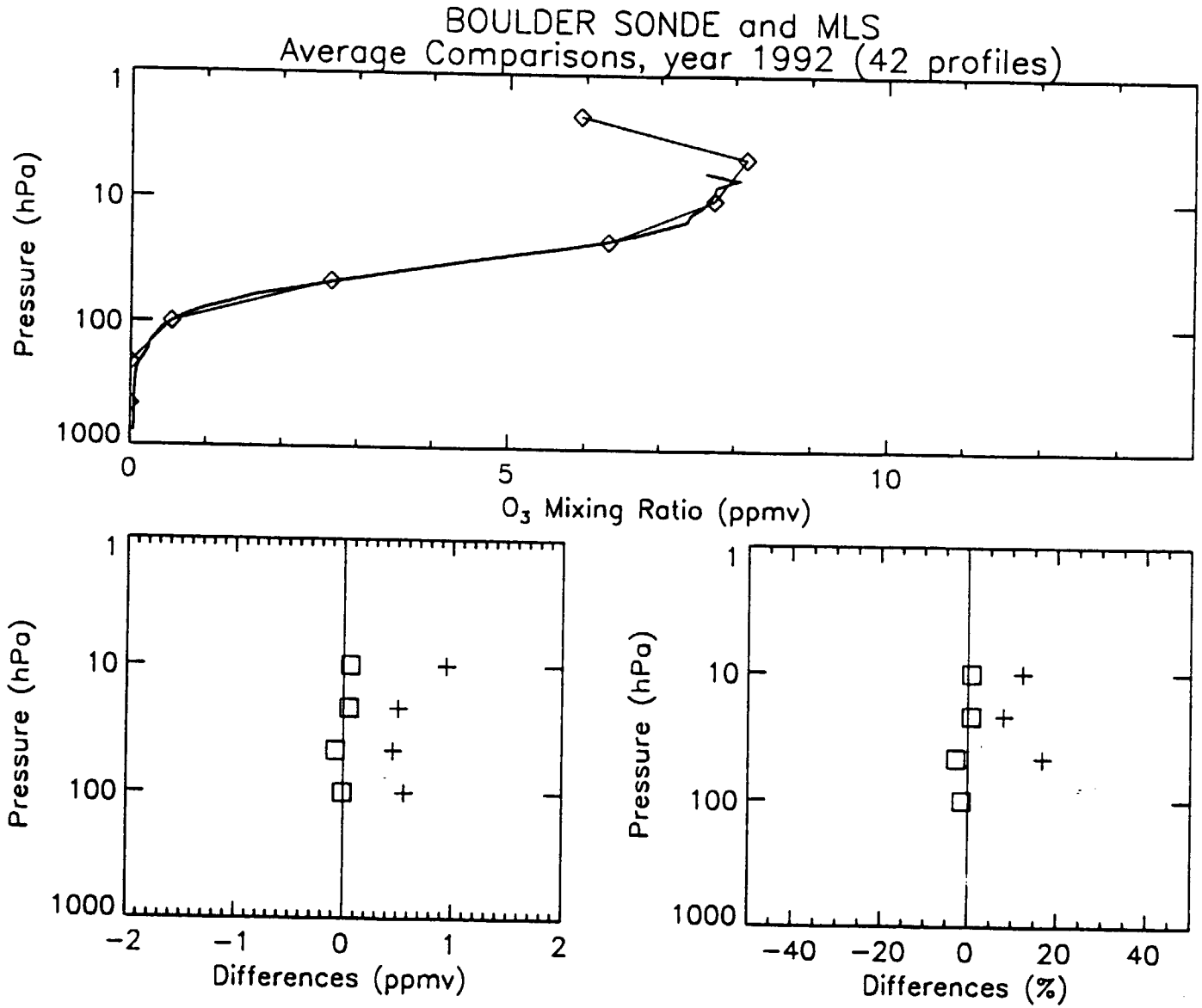

Figure 5.2.1.3-6 Top panel shows a comparison of the average profile from Boulder ozonesonde data (solid line) and the average of coincident MLS profiles for the year 1992 (42 profiles in all). Bottom panels give average differences (box symbols) and rms differences (plus symbols) in ppmv (left panel) and percent (right panel).

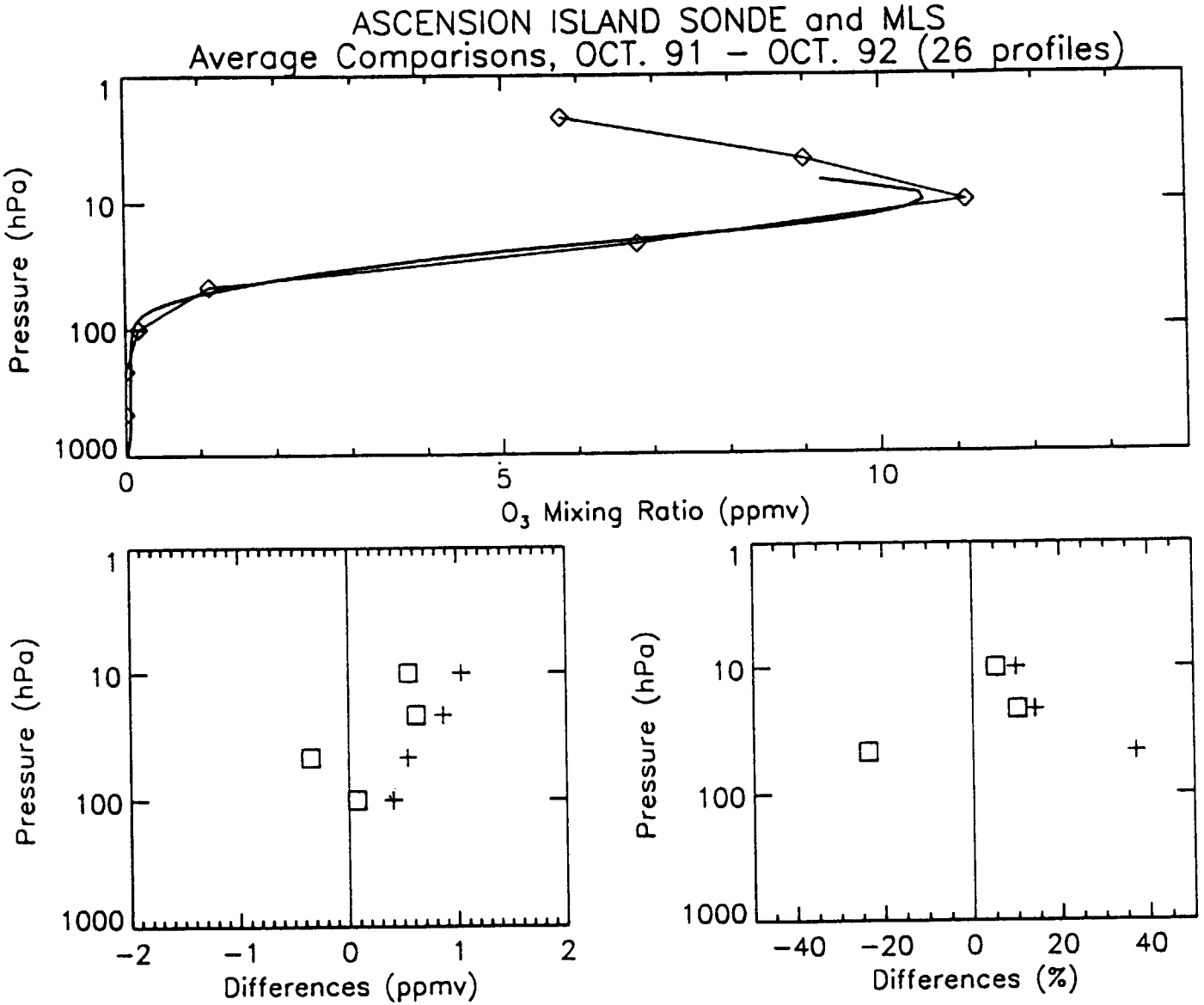

Figure 5.2.1.3-7 Same as Figure 5.2.1.3-6, but for Ascension Island (tropics), and for the time period Oct. 1991 to Oct. 1992 (26 profiles in all).

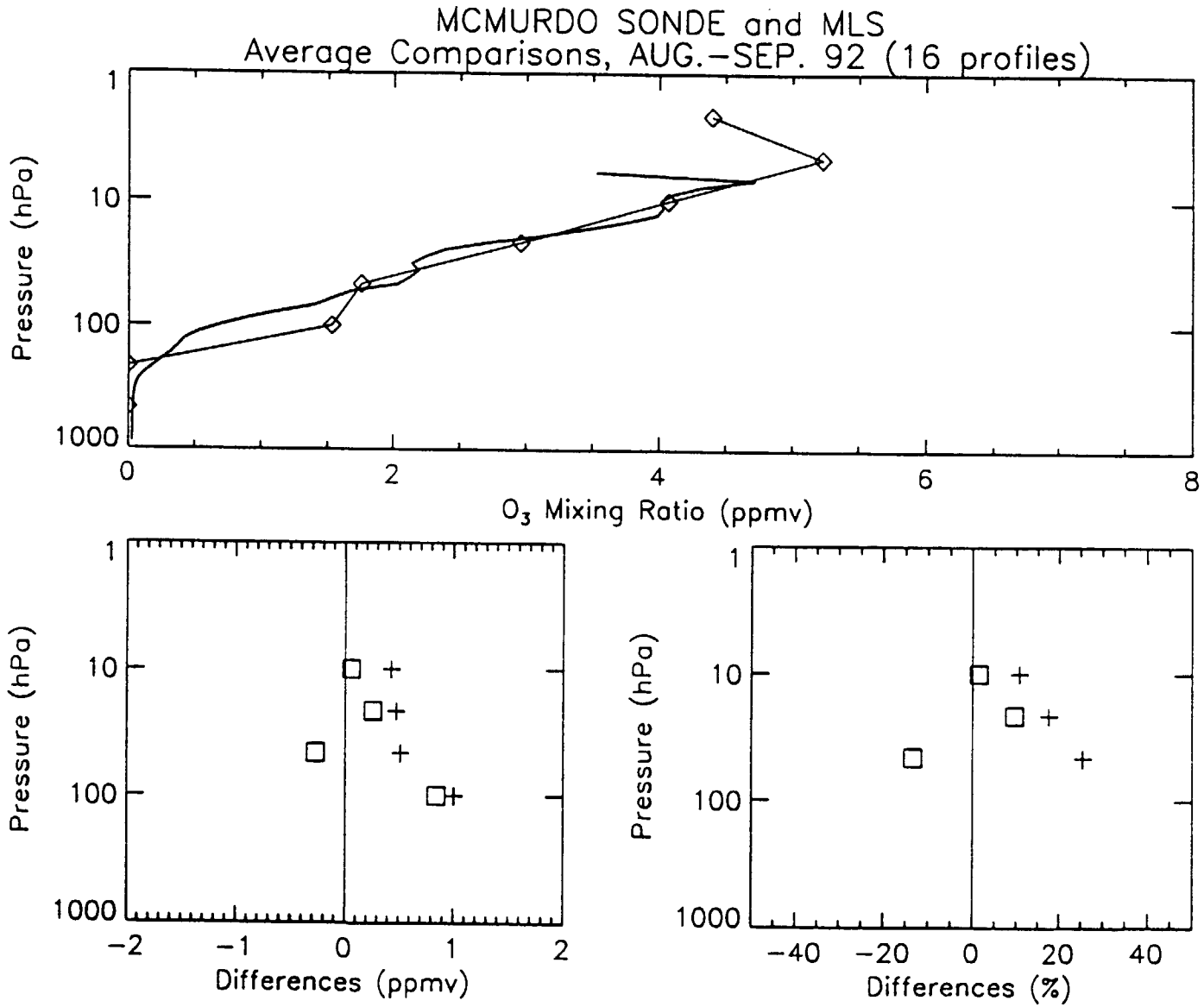

Figure 5.2.1.3-8 Same as Figure 5.2.1.3-6, but for McMurdo, and for the time period mid-Aug. to mid-Sept. 1992 (16 profiles in all).

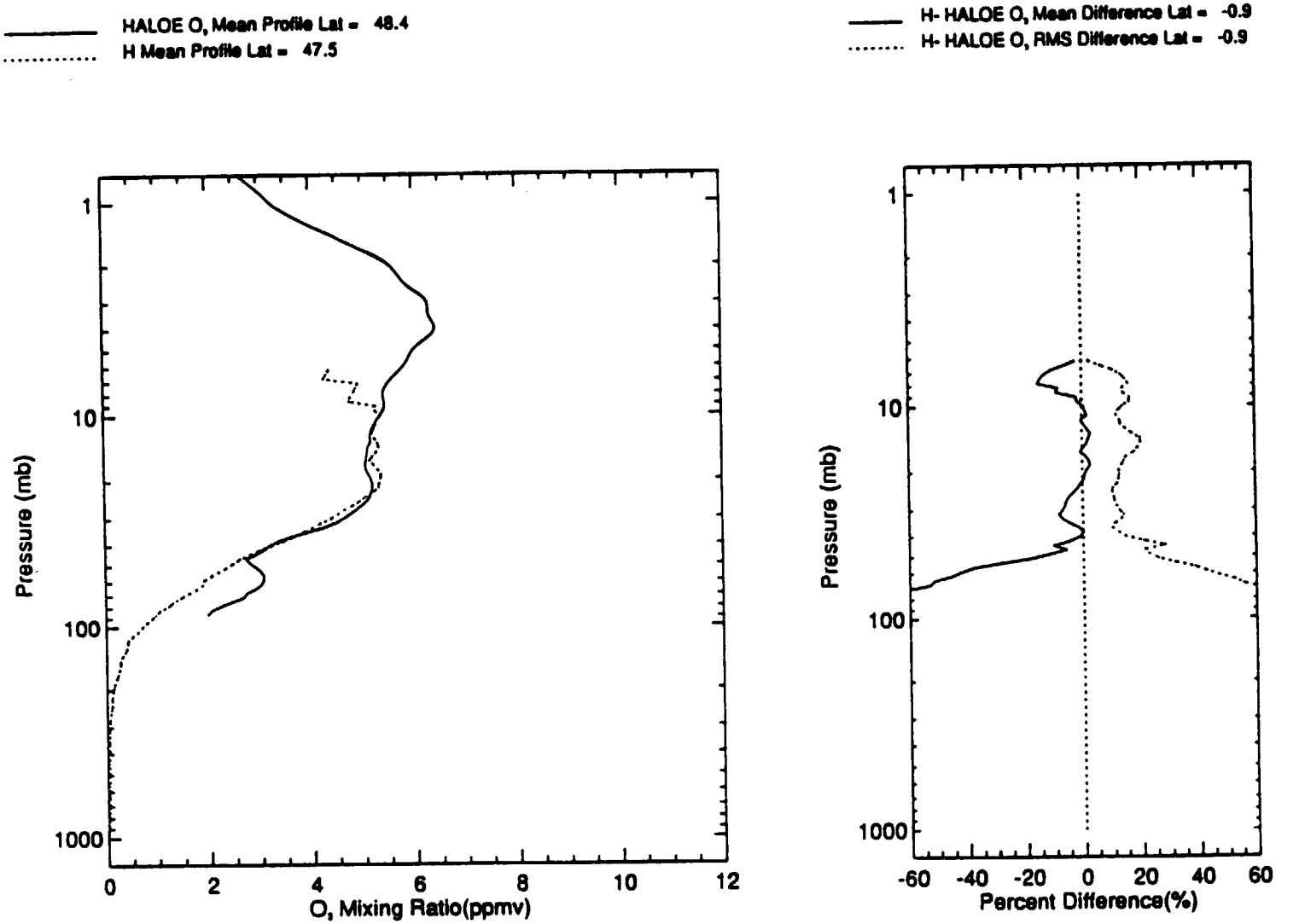

Figure 5.2.1.3-9 Comparisons of 8 Hohenpeissenberg ozonesondes (dashed line) in 1992 against nearly coincident HALOE profiles (solid line) at 47.5°N. Mean and rms percentage differences are also shown.

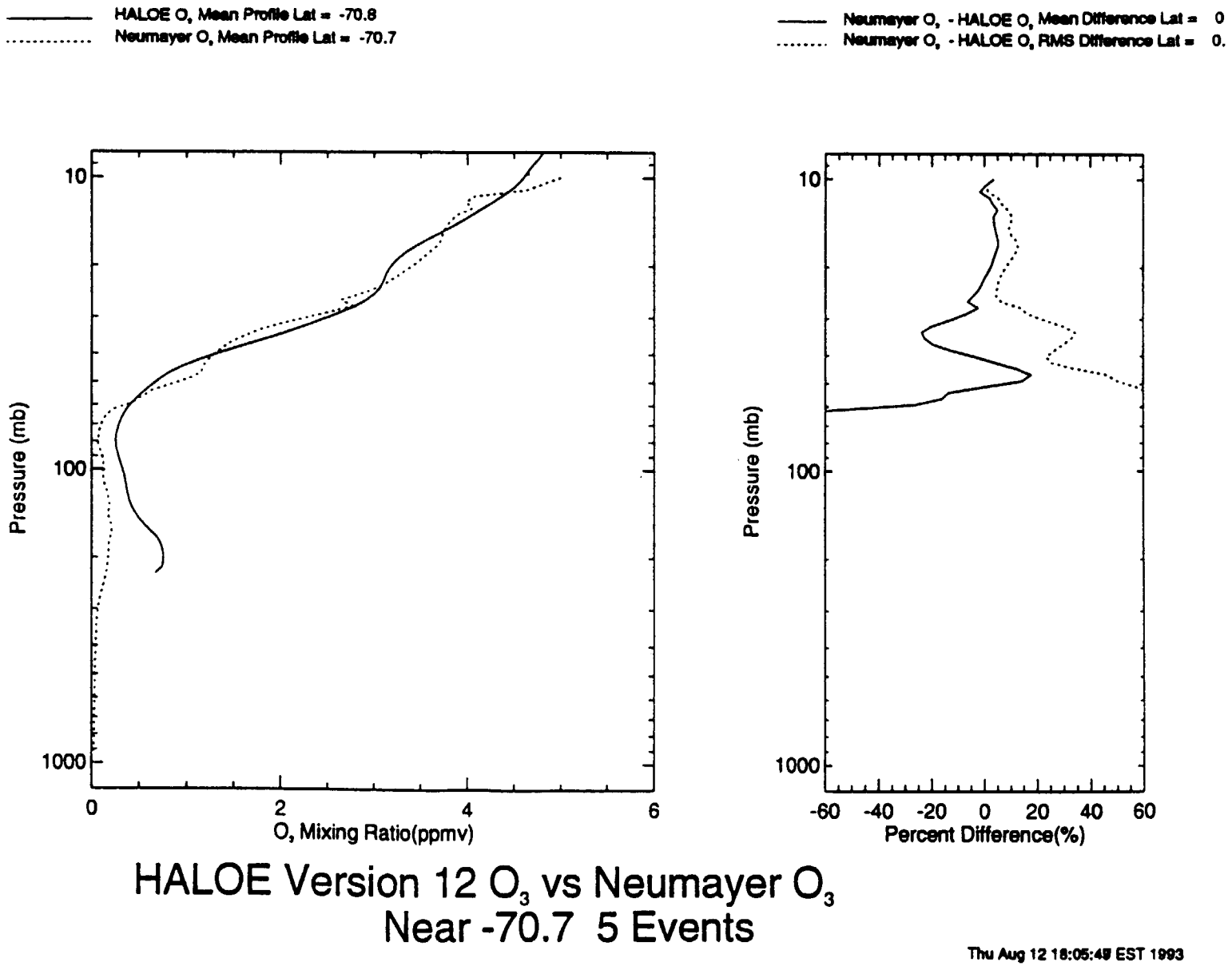

Figure 5.2.1.3-10 Comparisons of 7 Antarctic ozonesondes (dashed line) in 1992 against nearly coincident HALOE profiles (solid line) at 70.7°S. Mean and rms percentage differences are also shown.

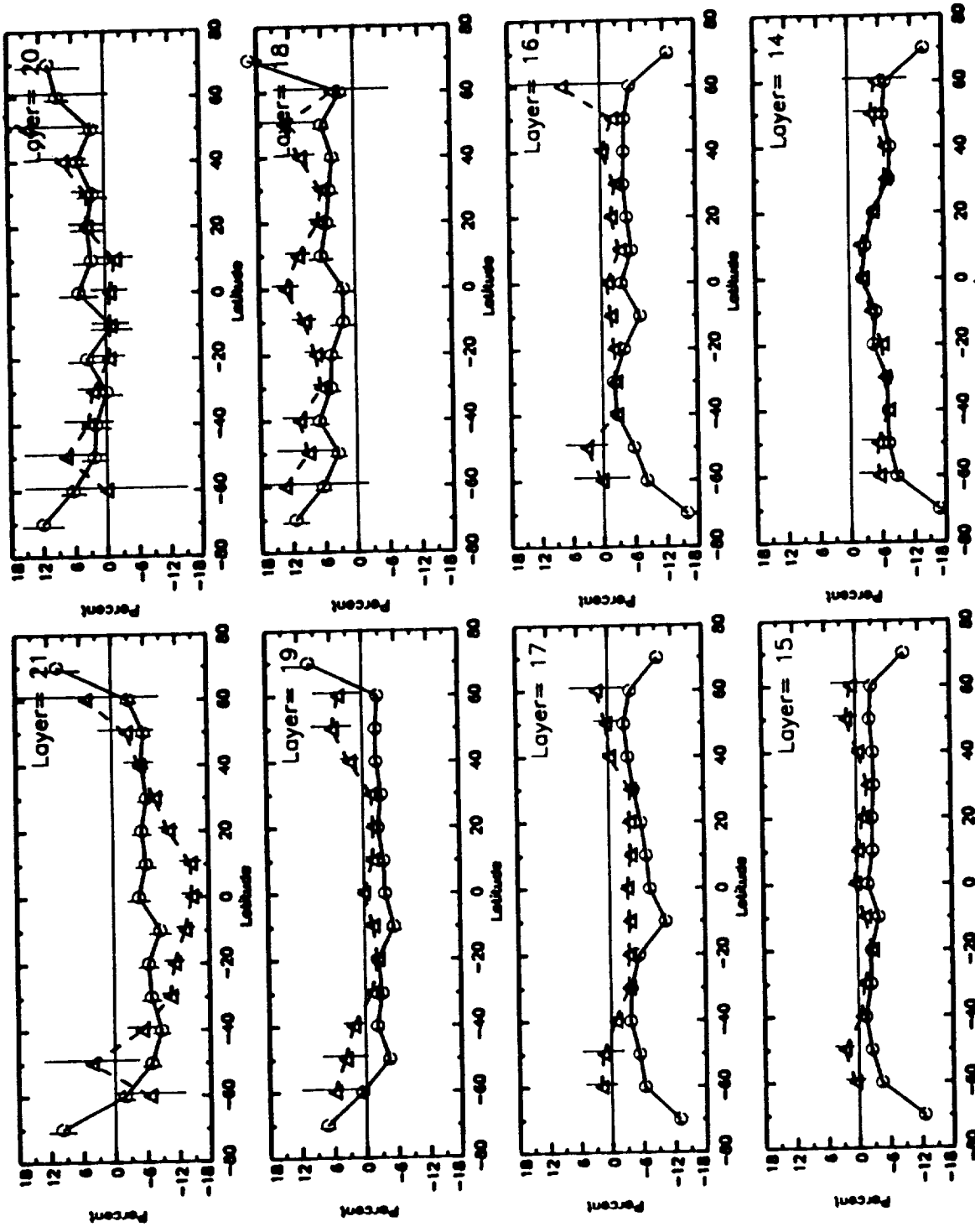

Figure 5.2.1.4-1 Comparisons of the means of coincident MLS and SAGE II events from Oct. 1991 to March 1993. Results are given as 100*(SAGE II-MLS)/MLS and are binned into 10^{o} latitude intervals. Full lines are sunset and dashed lines are for sunrise.

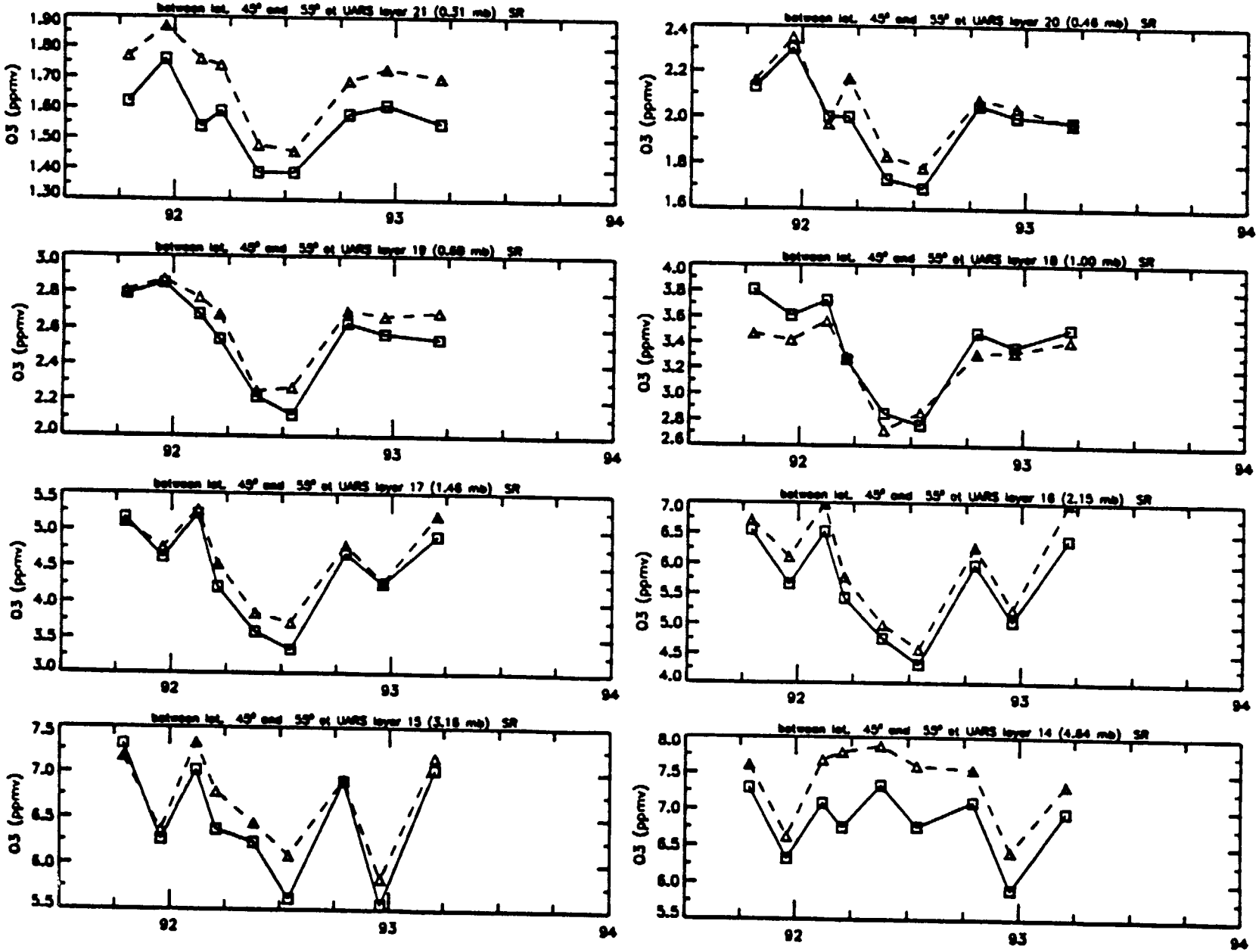

Figure 5.2.1.4-2 Comparisons of the monthly means of coincident MLS (dashed lines) and SAGE II (full lines) sunrise events from Oct. 1991 to March 1993 between 45^{O} and 55^{O}N and at each UARS level.

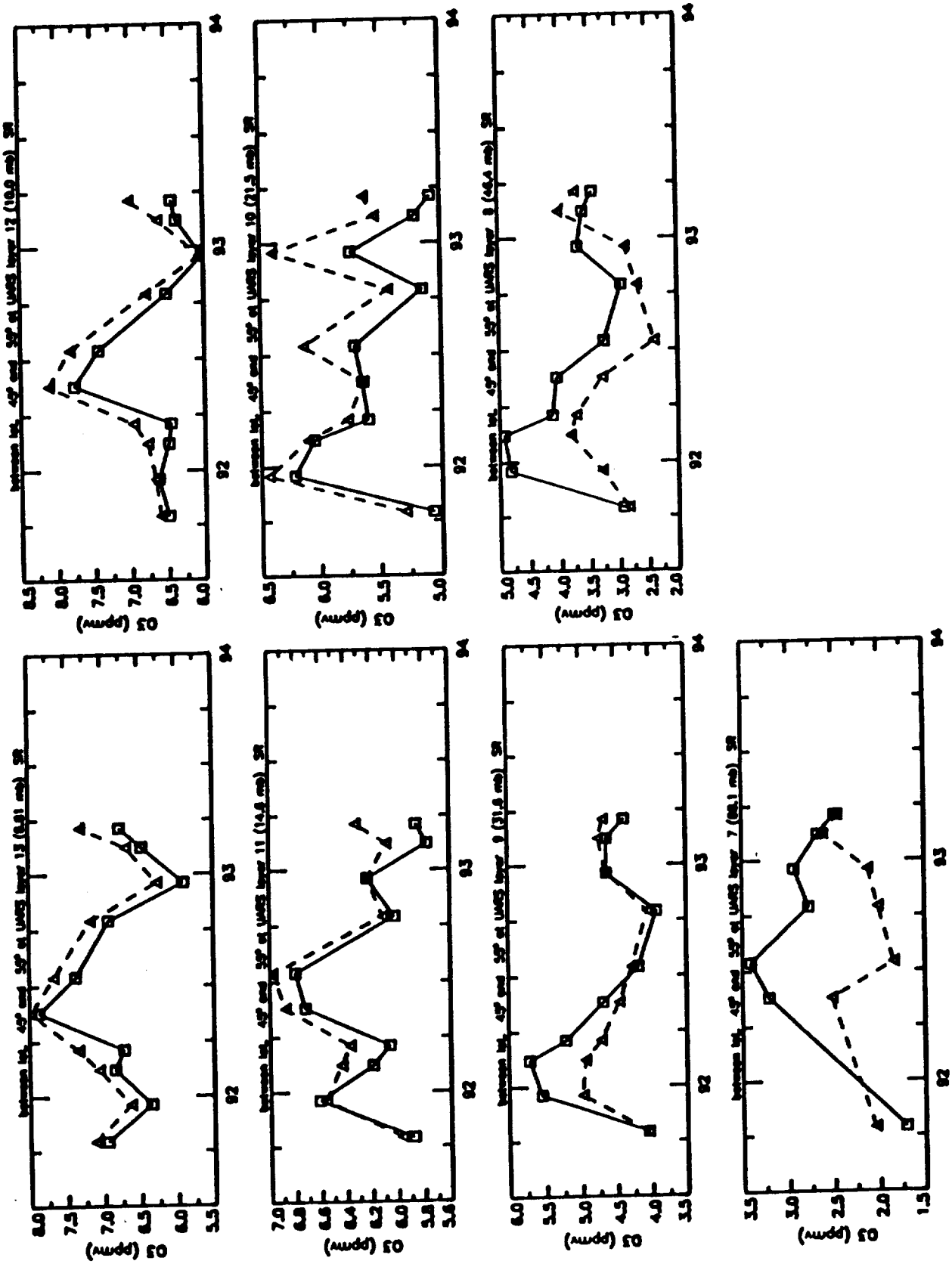

Figure 5.2.1.4-2 Concluded.

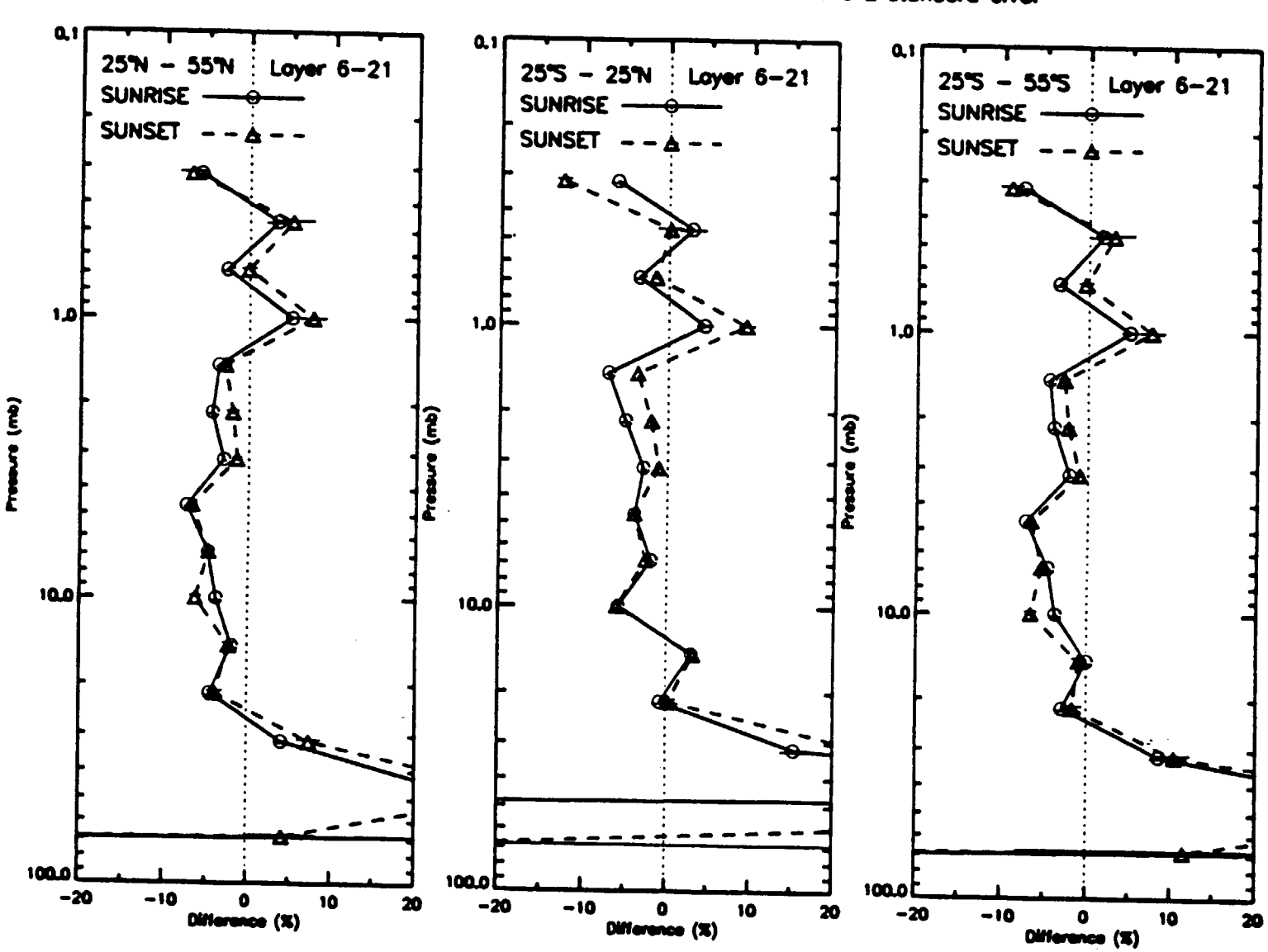

Figure 5.2.1.4-3

Comparisons of the means of coincident MLS and SAGE II events from Oct. 1991 to March 1993. Results are given as 100*(SAGE II-MLS)/MLS and are binned into just 3 latitude ranges. Full lines are sunrise, dashed lines are for sunset.

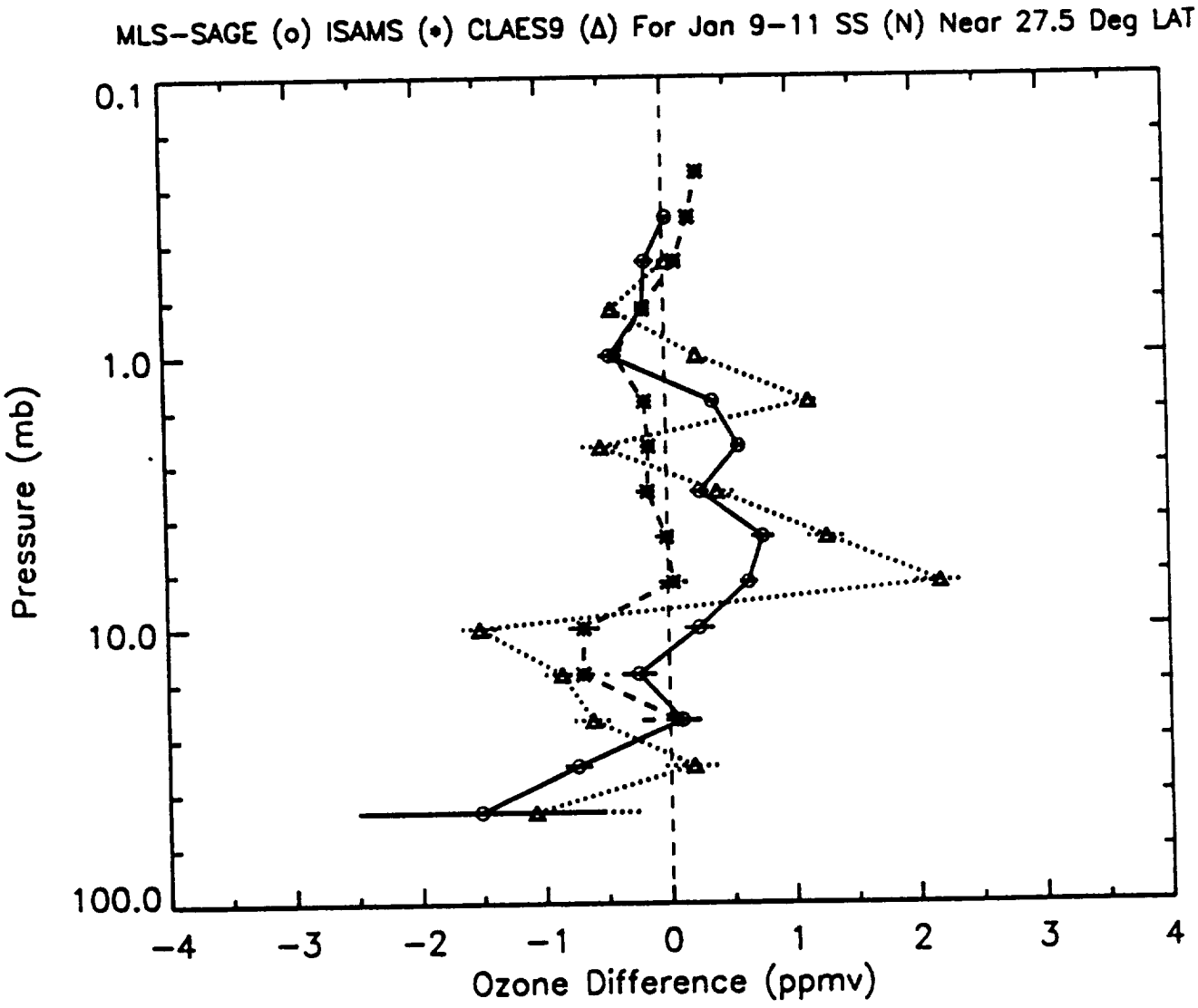

Figure 5.2.1.4-4 Ozone measurement differences between the UARS instruments and SAGE II (expressed relative to SAGE II) for 45 daytime profiles between 21 and 34N for Jan. 9-11, 1992. Coincidence differences were approximately 4 hours in time, 5 degrees in longitude and 1 degree in latitude. The error bars are standard errors of the mean differences.

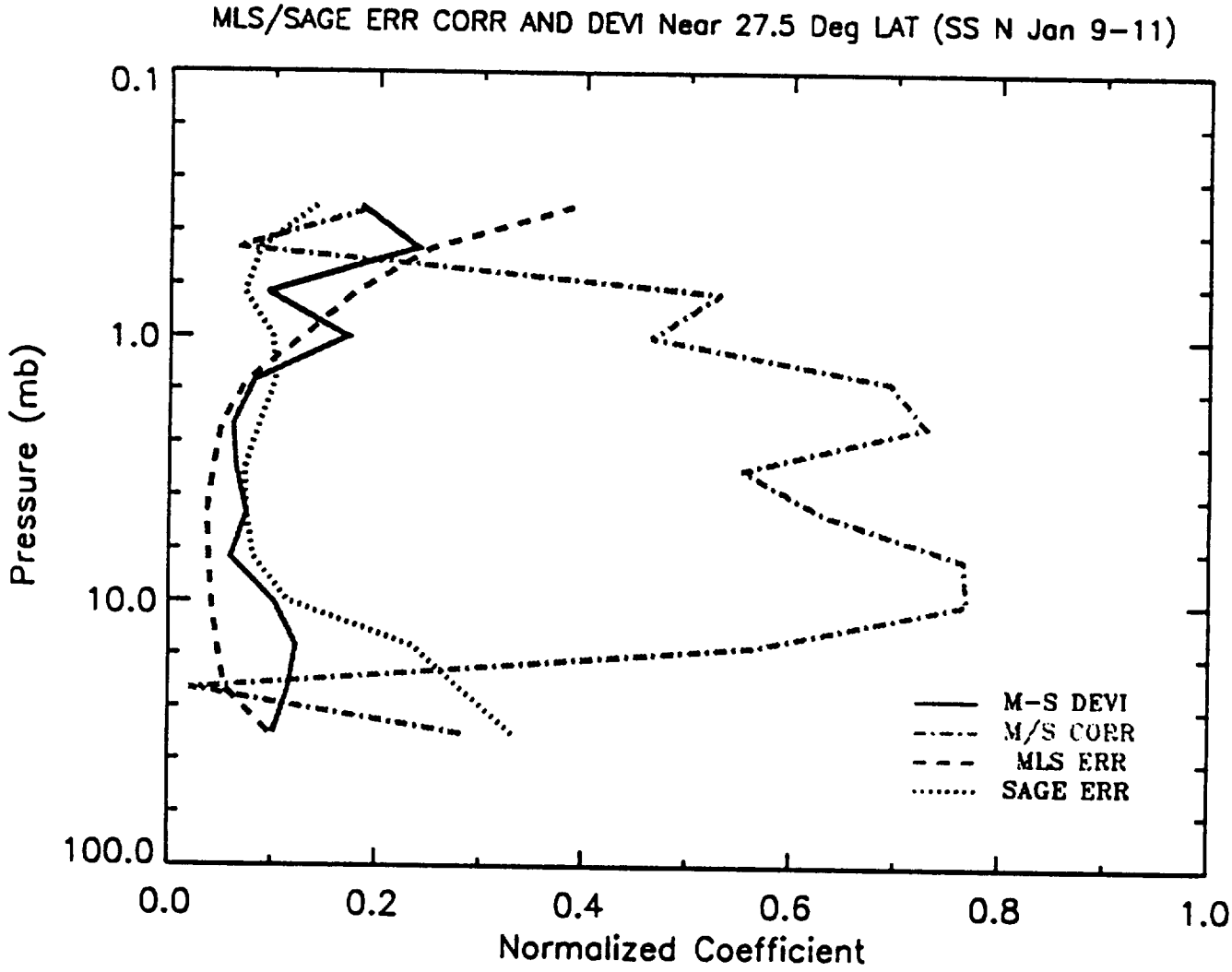

Figure 5.2.1.4-5 Standard deviations of the UARS/SAGE II measured ozone differences expressed as a ratio of the SAGE measurements, 21-23N for Jan. 9-11, 1992. Also shown are the correlations due to atmospheric variations between the SAGE II and the UARS measurements (the standard deviations due to atmospheric variations are estimated to have maximized at ~ 0.1 near 1 and 10 mb), and the means of the error bars supplied with each profile. The SAGE II error bars apply to the nominal 1 km resolution of the SAGE II measurements and because of vertical smoothing, should be reduced by a factor of ~ 1.2 for this comparison.

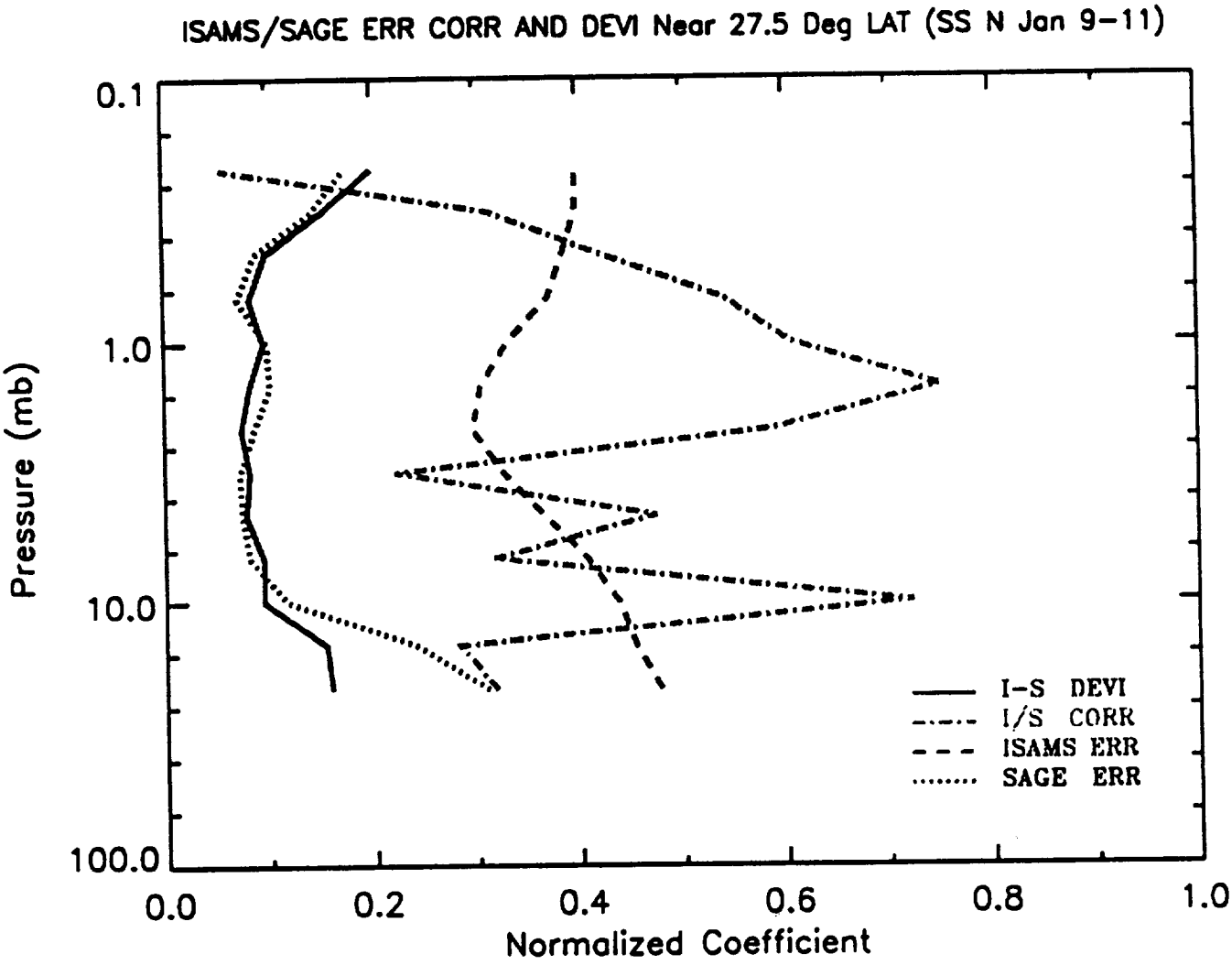

Figure 5.2.1.4-5 Continued.

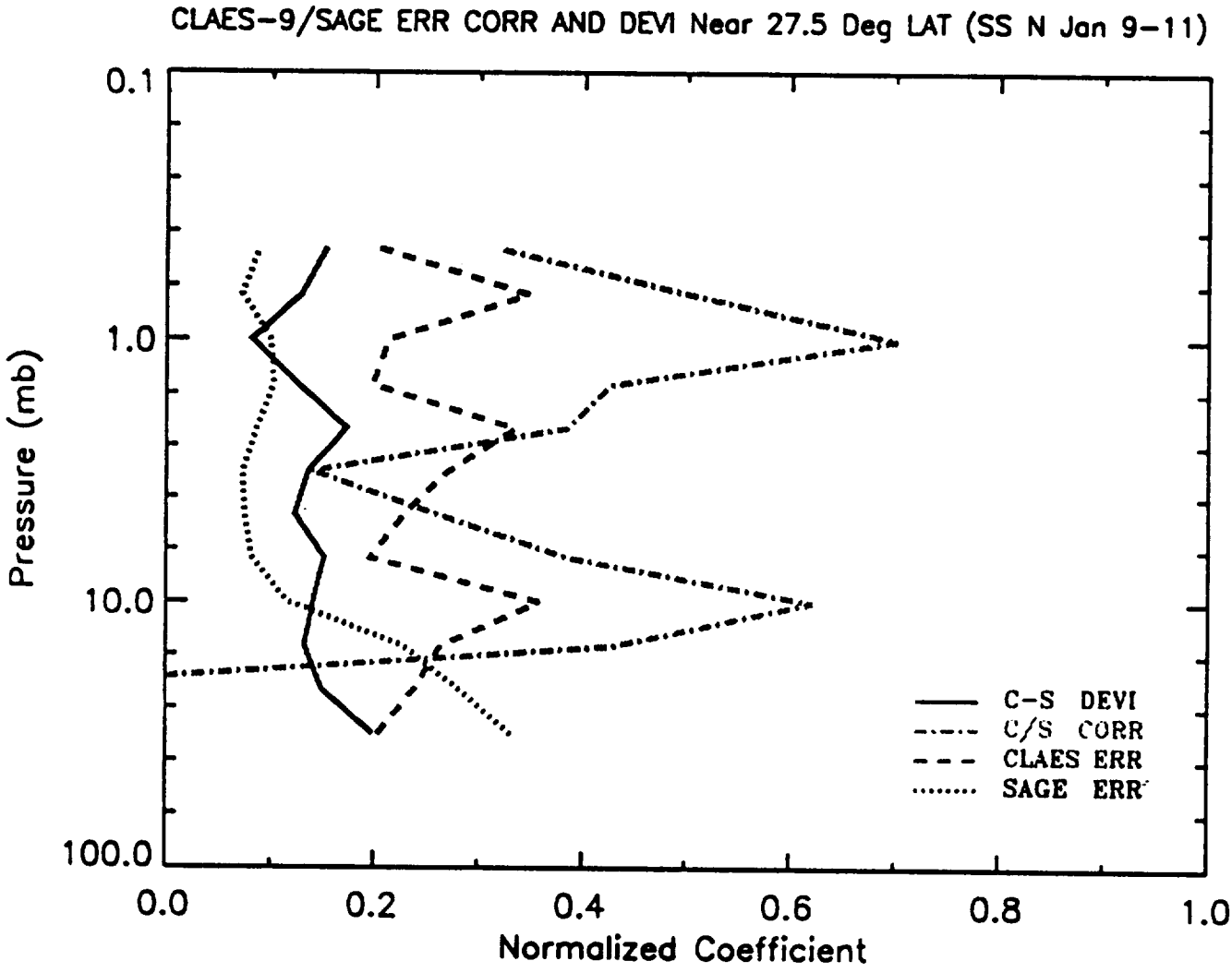

Figure 5.2.1.4-5 Concluded.

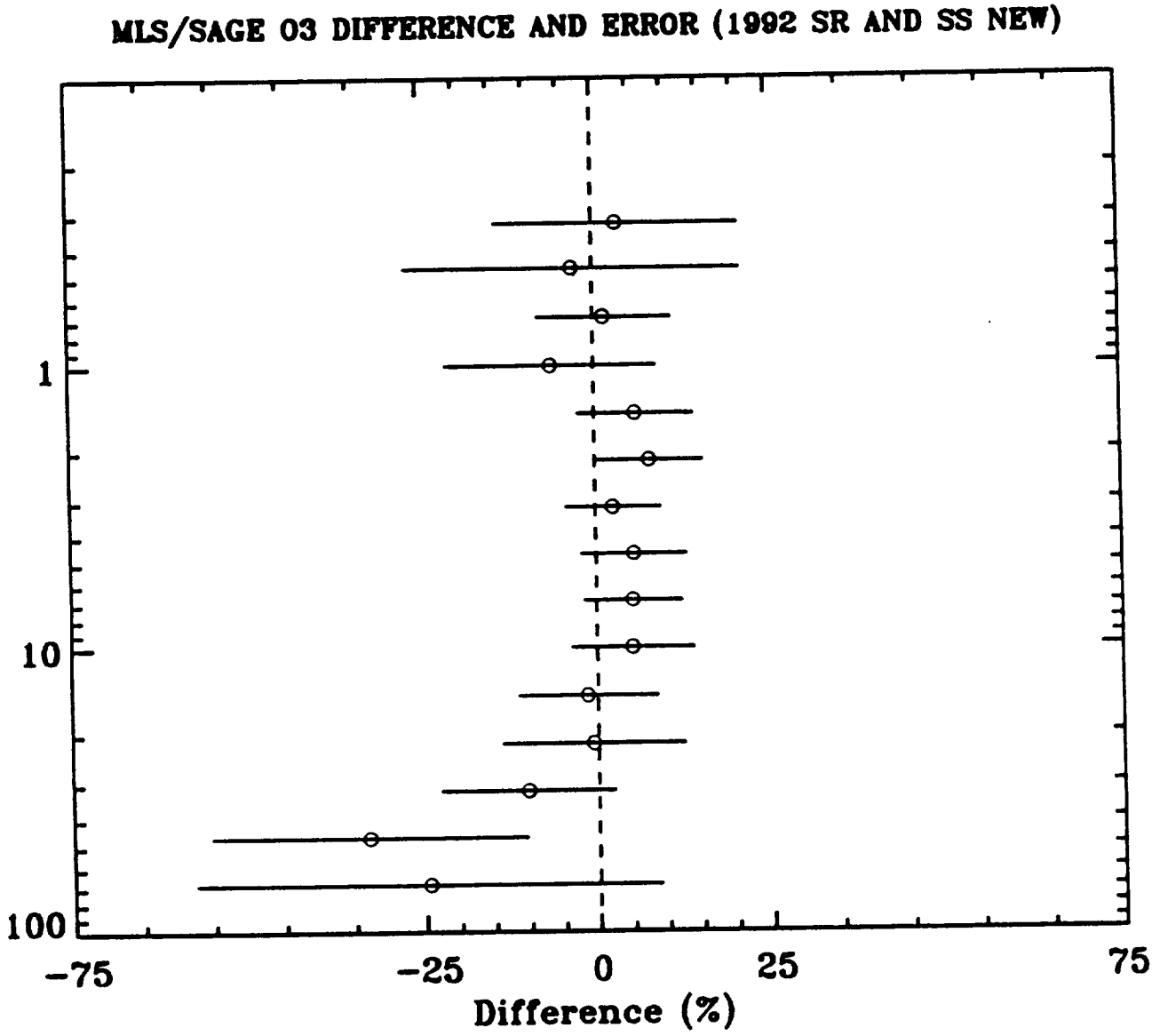

Figure 5.2.1.4-6 The means and standard deviations of 100*(MLS-SAGE II)/SAGE II ozone measurements and the similar products for ISAMS and CLAES over the intercomparison periods of Jan. and Aug. 1992 and 0 to 55 degrees latitude.

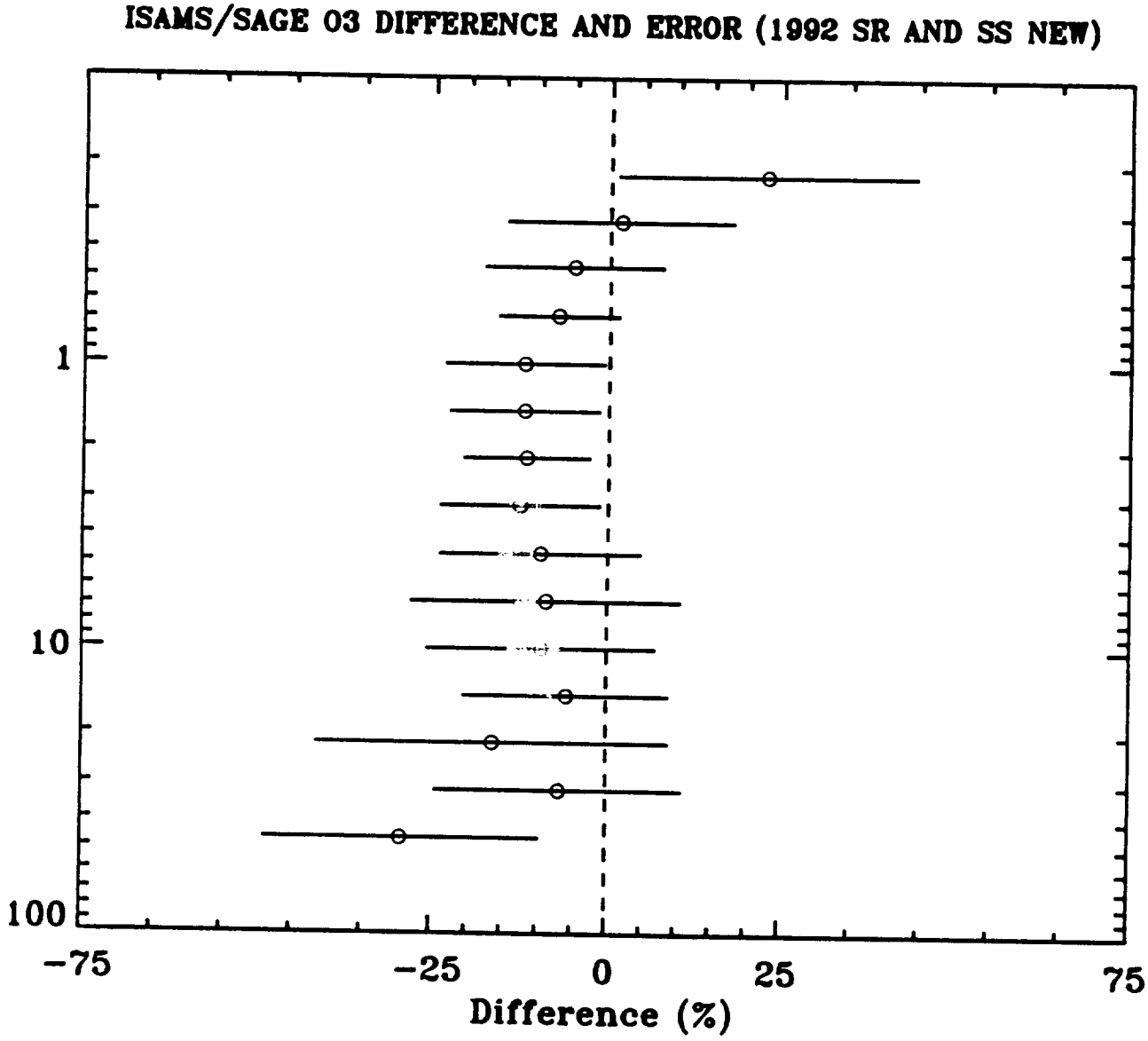

Figure 5.2.1.4-6 Continued.

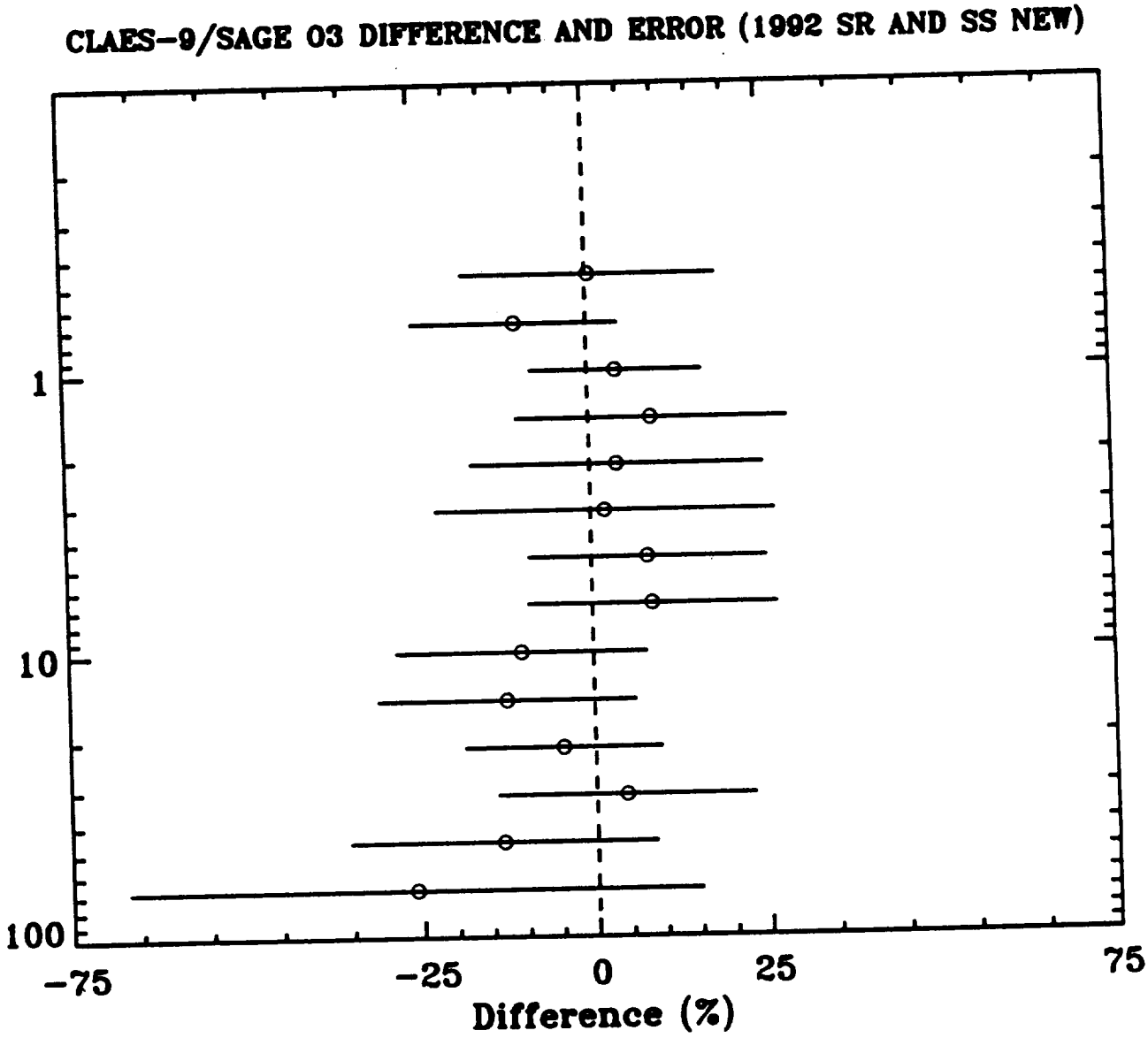

Figure 5.2.1.4-6 Concluded.

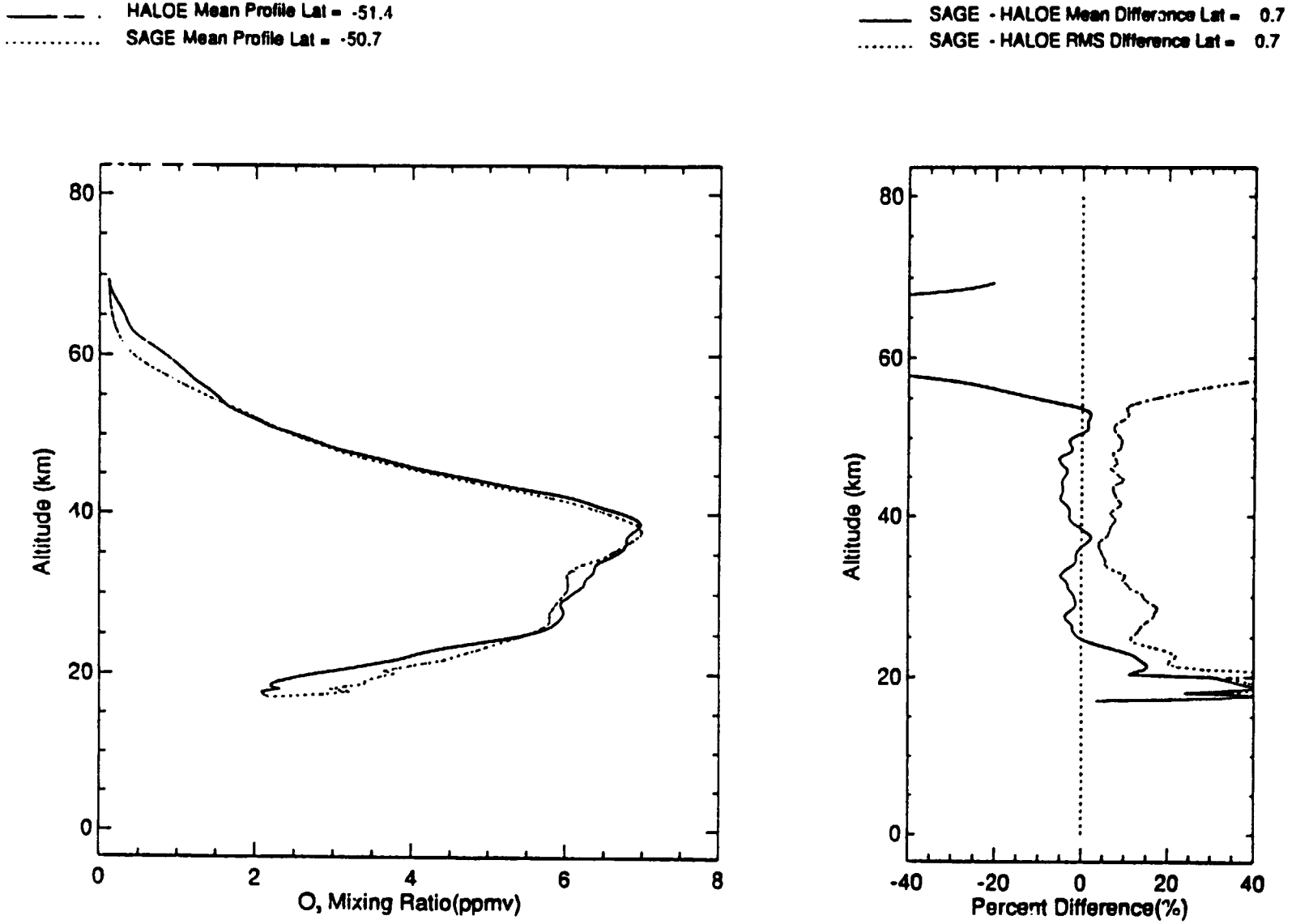

Figure 5.2.1.4-7 Comparison of HALOE and SAGE II ozone mixing ratios on May 6, 1992 at 50S.

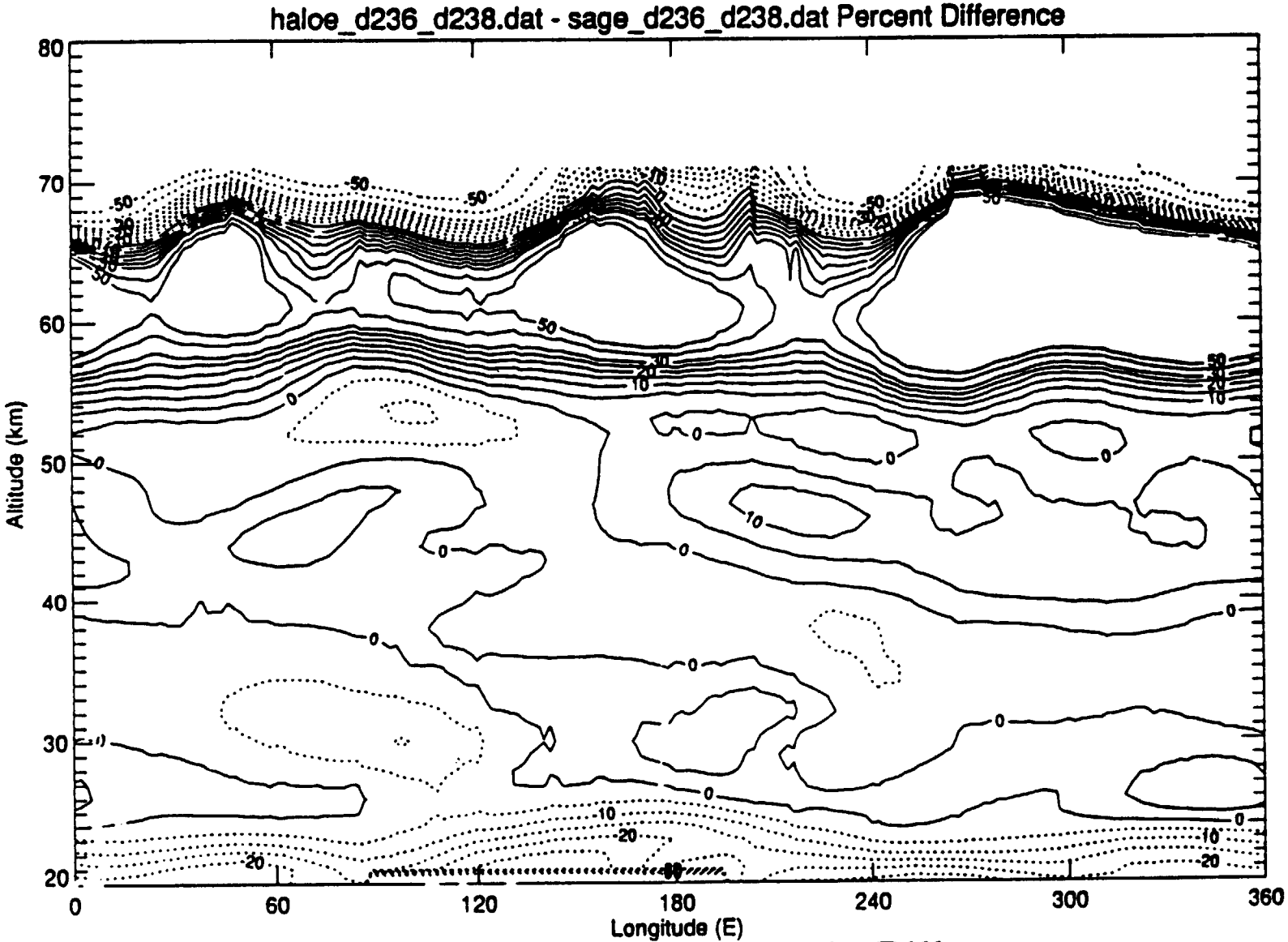

HALOE - SAGE II O_3 Mixing Ratio Difference
on 4-6 MAY 1992 near 50 S

Figure 5.2.1.4-8 Difference of SAGE II and HALOE ozone mixing ratios as a function of longitude for May 4-6, 1992 near 50S.

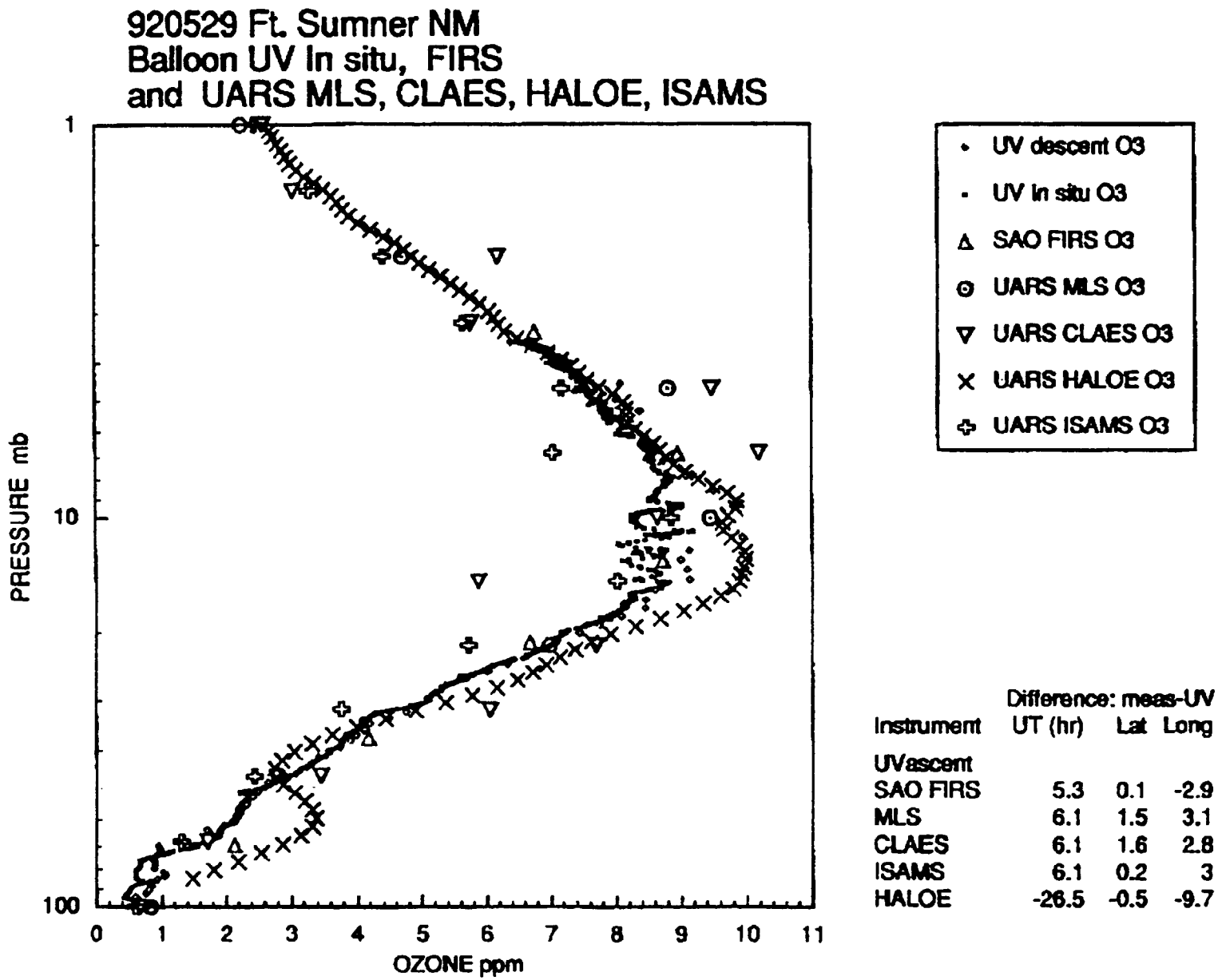

Instrument	Difference: meas-UV UT (hr)	Lat	Long
UVascent			
SAO FIRS	5.3	0.1	-2.9
MLS	6.1	1.5	3.1
CLAES	6.1	1.6	2.8
ISAMS	6.1	0.2	3
HALOE	-26.5	-0.5	-9.7

Figure 5.2.1.5-1 Ozone profile comparison (UARS and correlative data) for Fort Sumner (New Mexico) balloon flight on May 29, 1992. Error bars are omitted for clarity of plots.

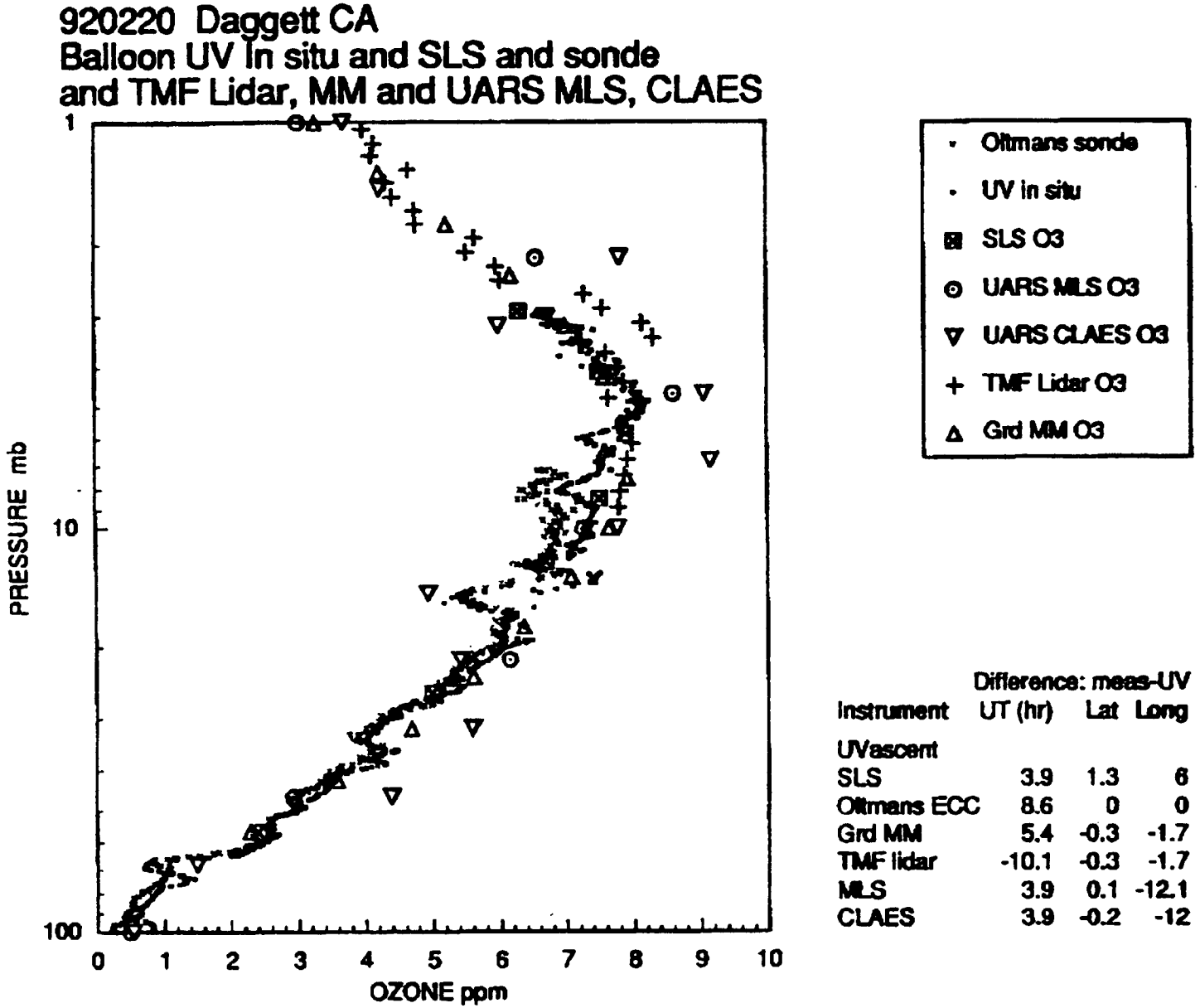

Instrument	Difference: meas-UV UT (hr)	Lat	Long
UVascent			
SLS	3.9	1.3	6
Oltmans ECC	8.6	0	0
Grd MM	5.4	-0.3	-1.7
TMF lidar	-10.1	-0.3	-1.7
MLS	3.9	0.1	-12.1
CLAES	3.9	-0.2	-12

Figure 5.2.1.5-2 Ozone profile comparison (UARS and correlative data) for Daggett (California) balloon flight on Feb. 20, 1992. Error bars are omitted for clarity of plots.

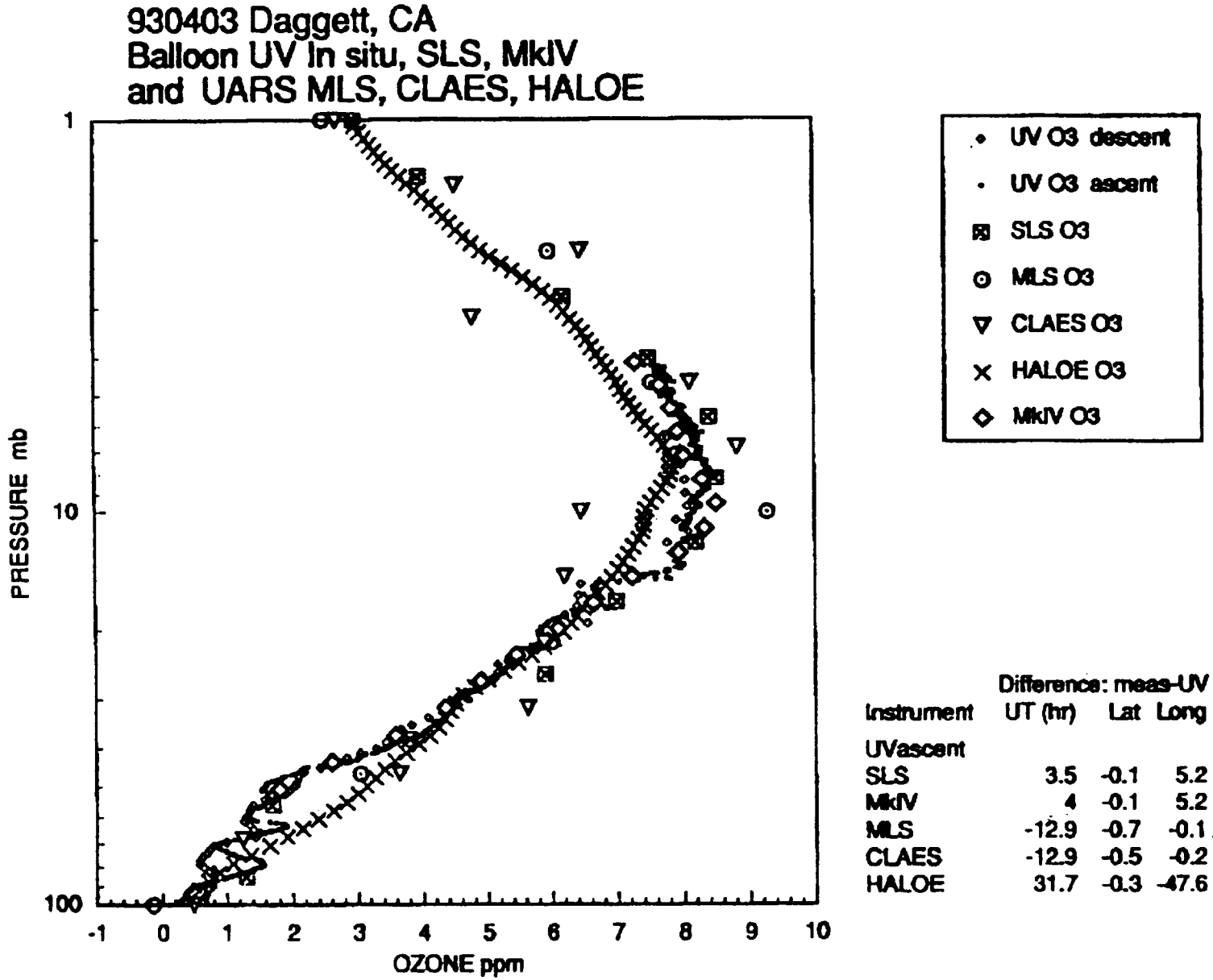

Instrument	Difference: meas-UV UT (hr)	Lat	Long
UVascent			
SLS	3.5	-0.1	5.2
MkIV	4	-0.1	5.2
MLS	-12.9	-0.7	-0.1
CLAES	-12.9	-0.5	-0.2
HALOE	31.7	-0.3	-47.6

Figure 5.2.1.5-3 Ozone profile comparison (UARS and correlative data) for Daggett (California) balloon flight on April 3, 1993. Error bars are omitted for clarity of plots.

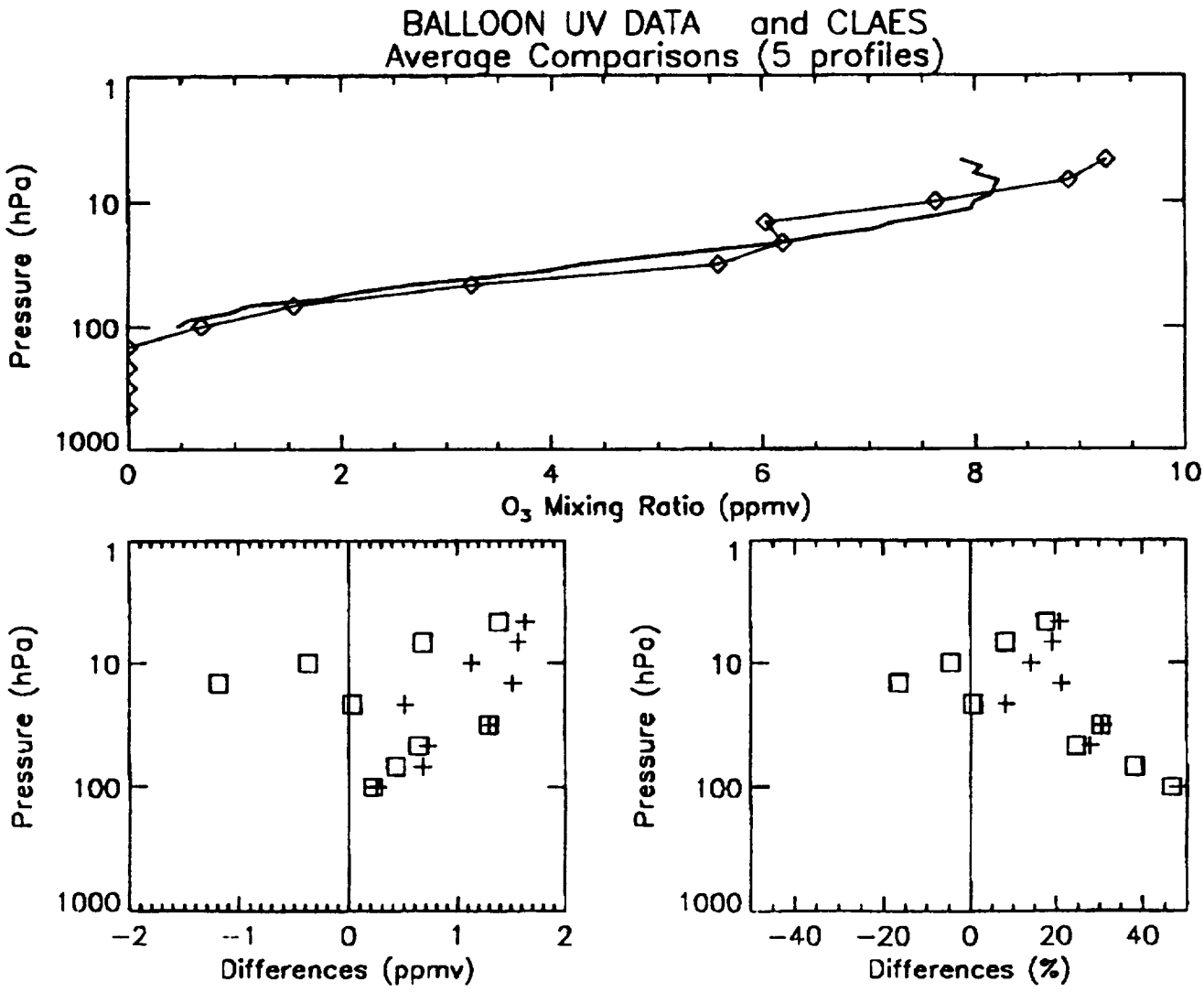

Figure 5.2.1.5-4 Average of 5 UV in situ balloon measurements of ozone (solid line, top panel) compared with the average of 5 coincident CLAES ozone profiles (diamonds). Bottom left panel shows differences (ppmv) for UARS minus balloon data and bottom right panel shows percent differences; box symbols are average differences, while plus symbols are rms differences.

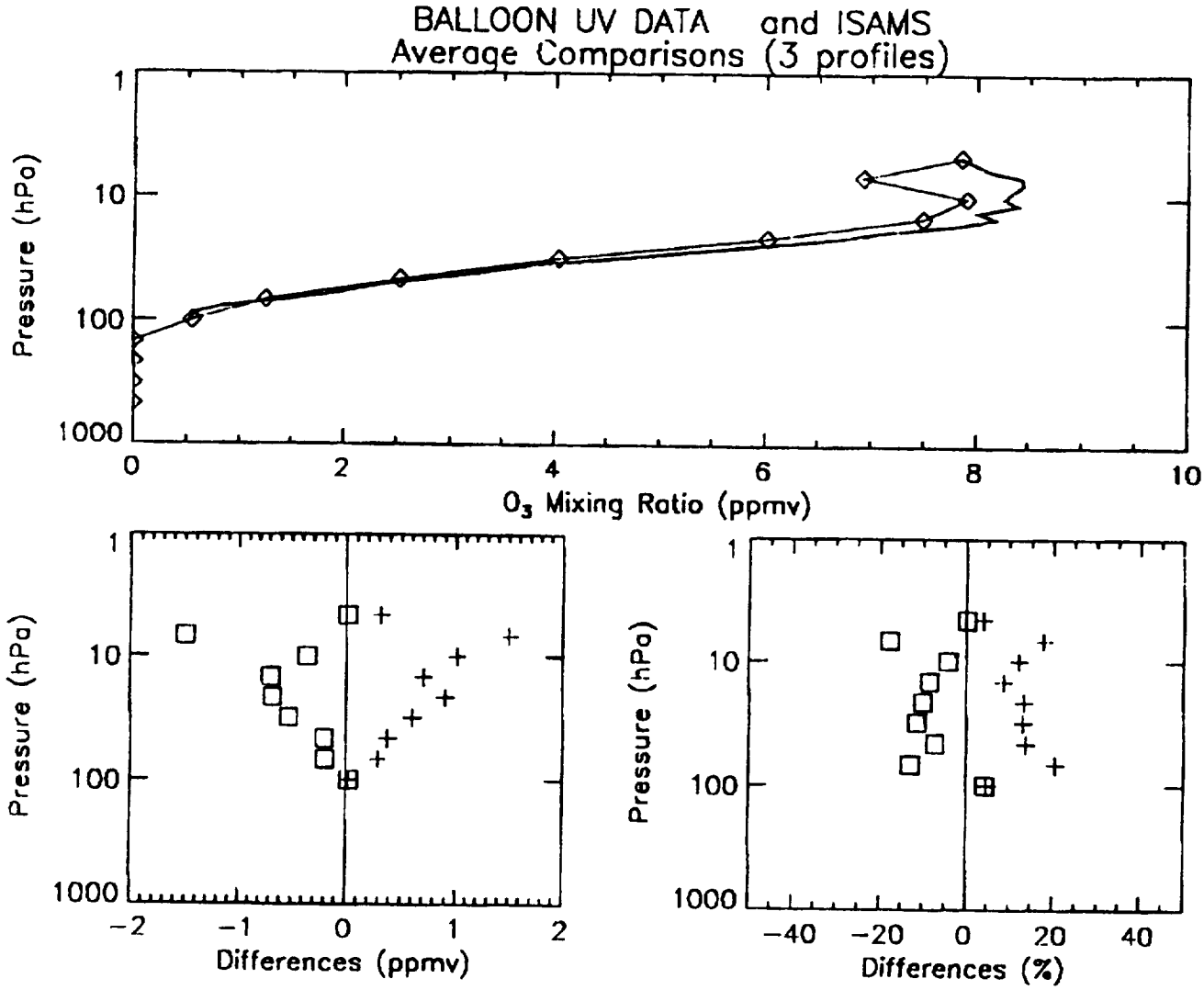

Figure 5.2.1.5-5 Average of 3 UV in situ balloon measurements of ozone (solid line, top panel) compared with the average of 3 coincident ISAMS ozone profiles (diamonds). Bottom left panel shows differences (ppmv) for UARS minus balloon data and bottom right panel shows percent differences; box symbols are average differences, while plus symbols are rms differences.

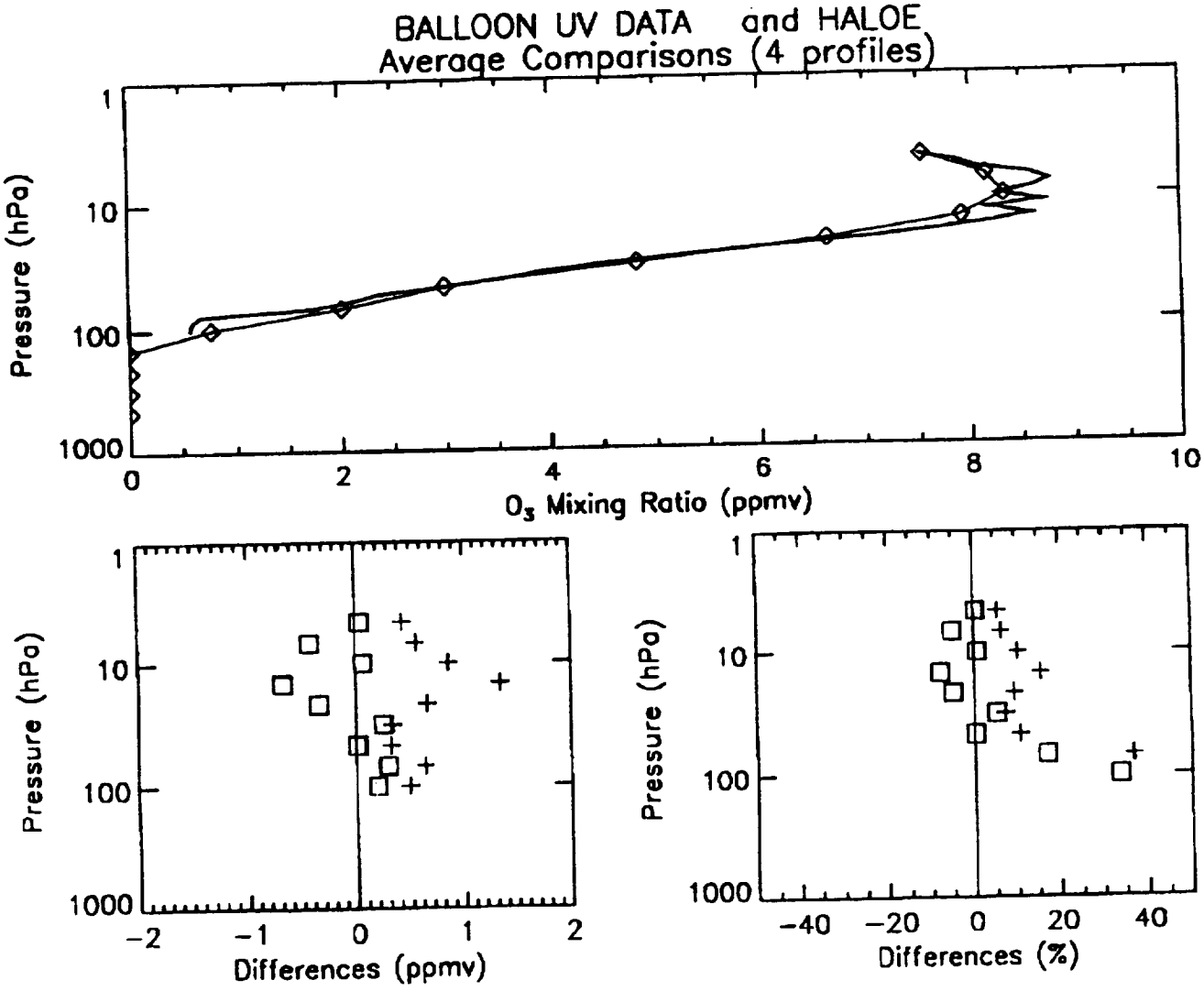

Figure 5.2.1.5-6 Average of 4 UV in situ balloon measurements of ozone (solid line, top panel) compared with the average of 4 coincident HALOE ozone profiles (diamonds). Bottom left panel shows differences (ppmv) for UARS minus balloon data and bottom right panel shows percent differences; box symbols are average differences, while plus symbols are rms differences.

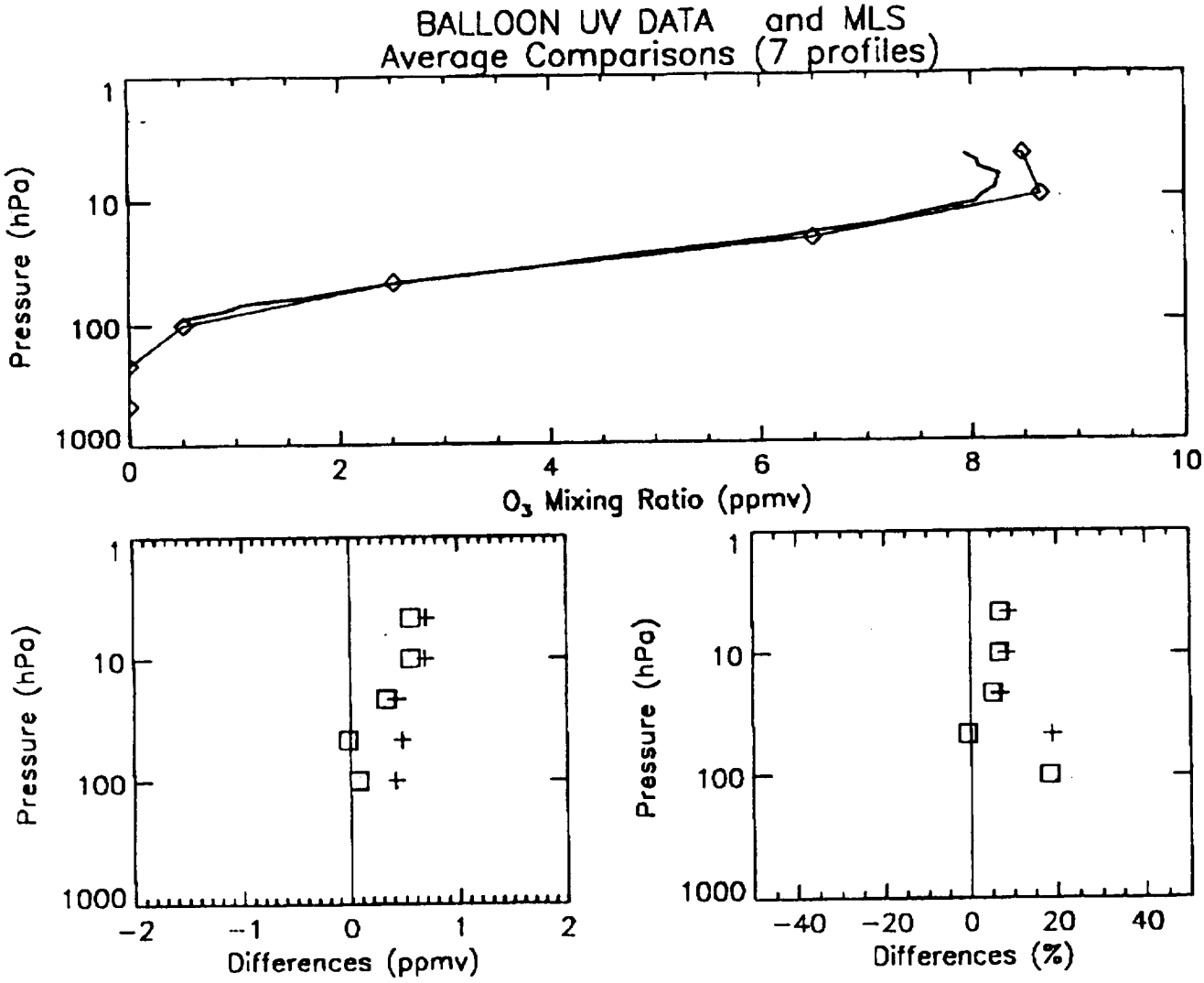

Figure 5.2.1.5-7 Average of 7 UV in situ balloon measurements of ozone (solid line, top panel) compared with the average of 7 coincident MLS ozone profiles (diamonds). Bottom left panel shows differences (ppmv) for UARS minus balloon data and bottom right panel shows percent differences; box symbols are average differences, while plus symbols are rms differences.

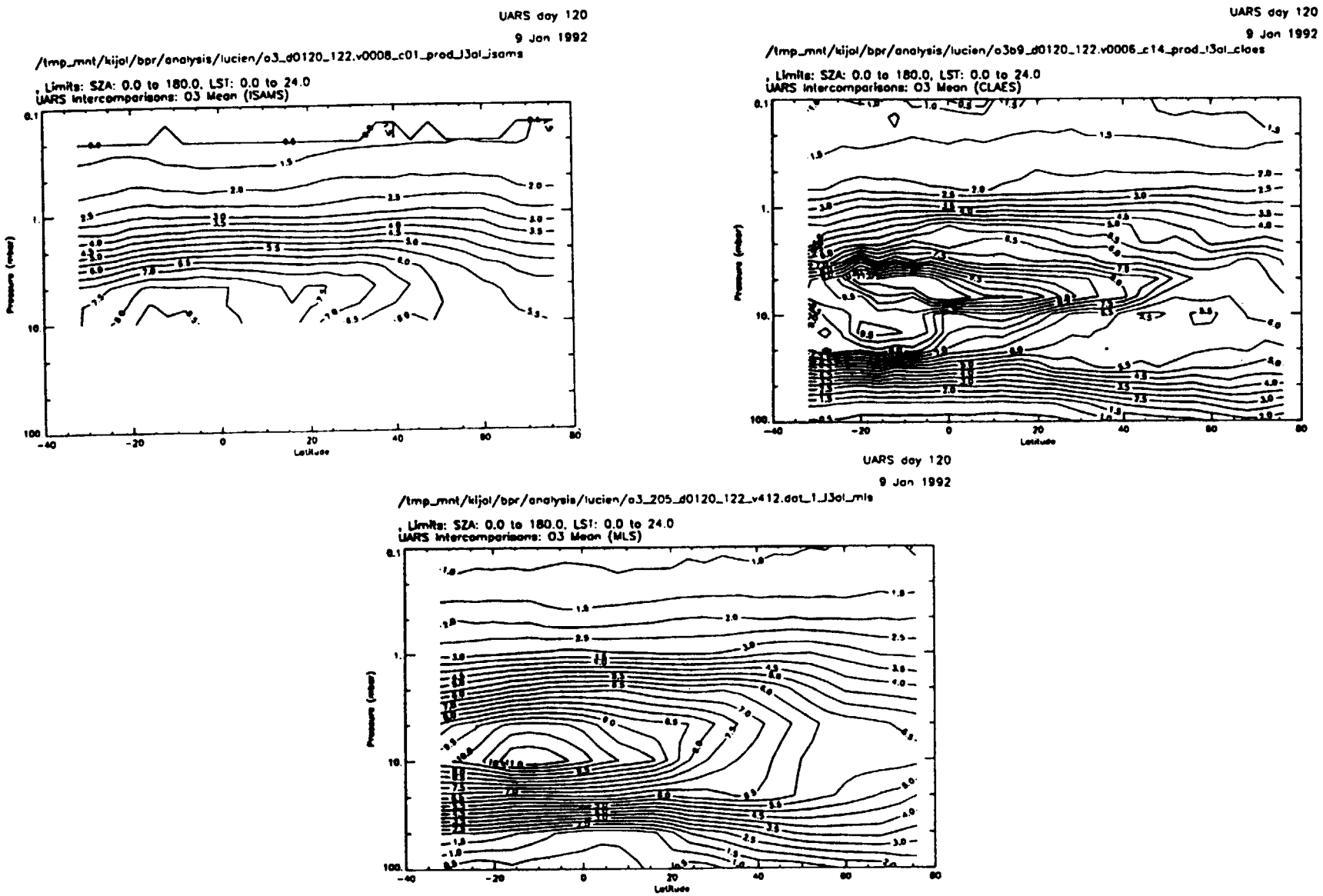

Figure 5.2.2-1 Cross section of zonal mean ozone fields from UARS, MLS, CLAES, and ISAMS experiments, for an average of three days (Jan. 9-11, 1992). Contours are labeled in ppmv, with a spacing of 0.5 ppmv. During this north-looking time period, only latitudes from 34S to 80N were observed simultaneously by all three instruments. ISAMS data are intentionally shown only down to 10 mb.

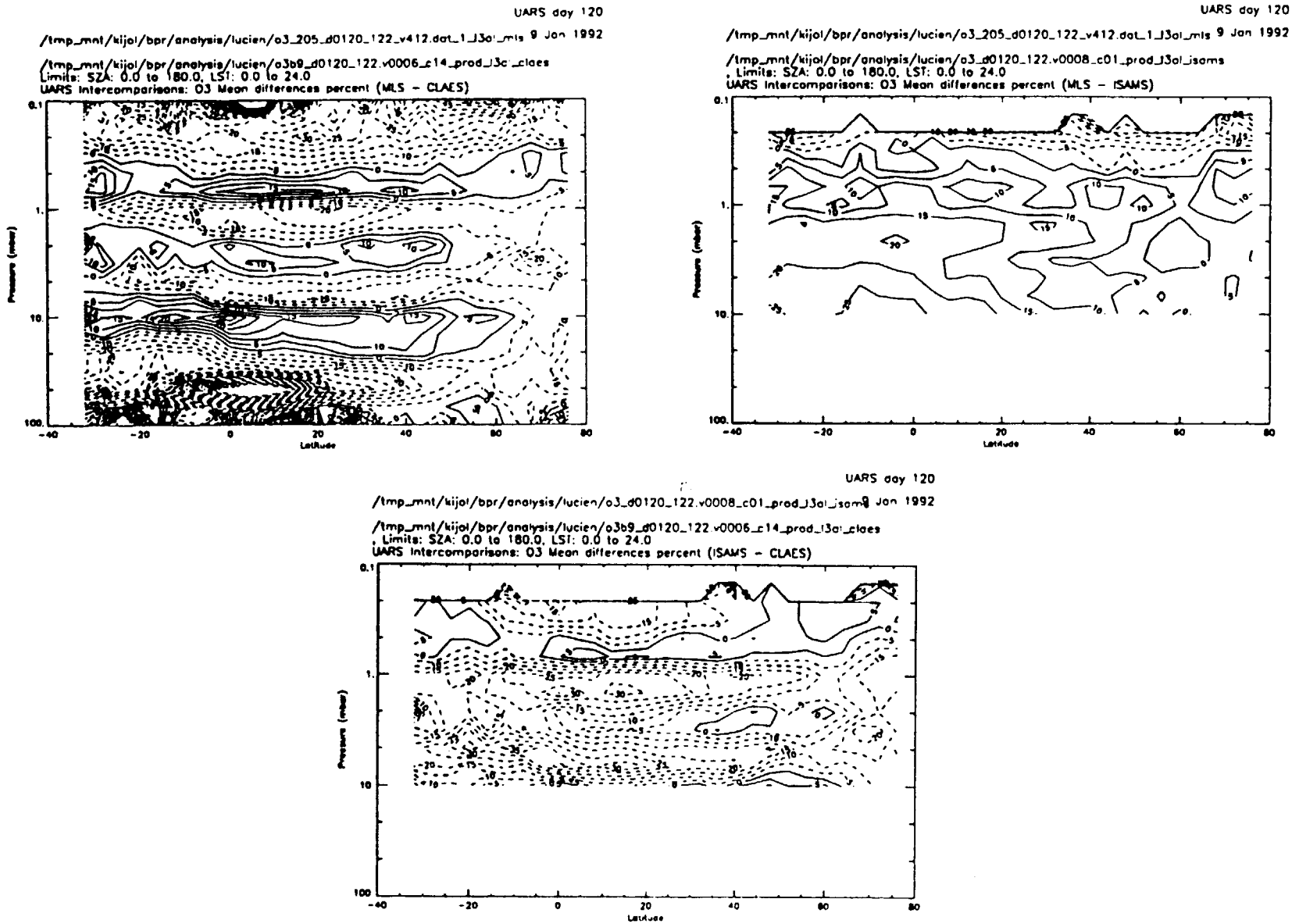

Figure 5.2.2-2 Percent differences between the mean ozone fields from Figure 5.2.2-1 (from top to bottom, MLS-CLAES, MLS-ISAMS, and ISAMS-CLAES). Contours are given every 5%, and negative contours are dashed.

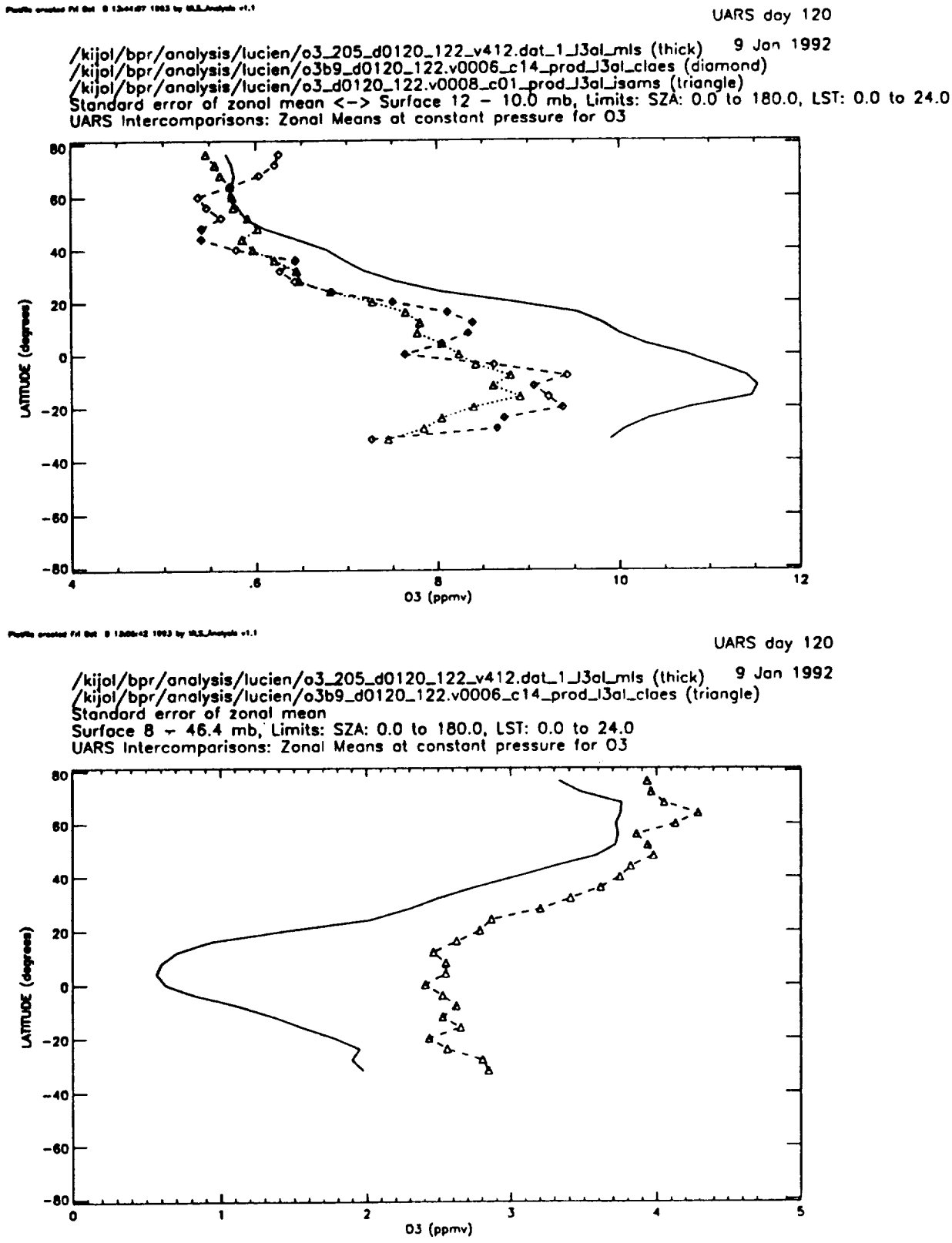

Figure 5.2.2-3 Latitudinal variation in ozone (ppmv) from UARS MLS (solid line), CLAES (diamonds), and ISAMS (triangles) zonal mean fields at 46 mb (bottom panel) and 10 mb (top panel). The same time period as in Figures 5.2.2-1 and -2 is used.

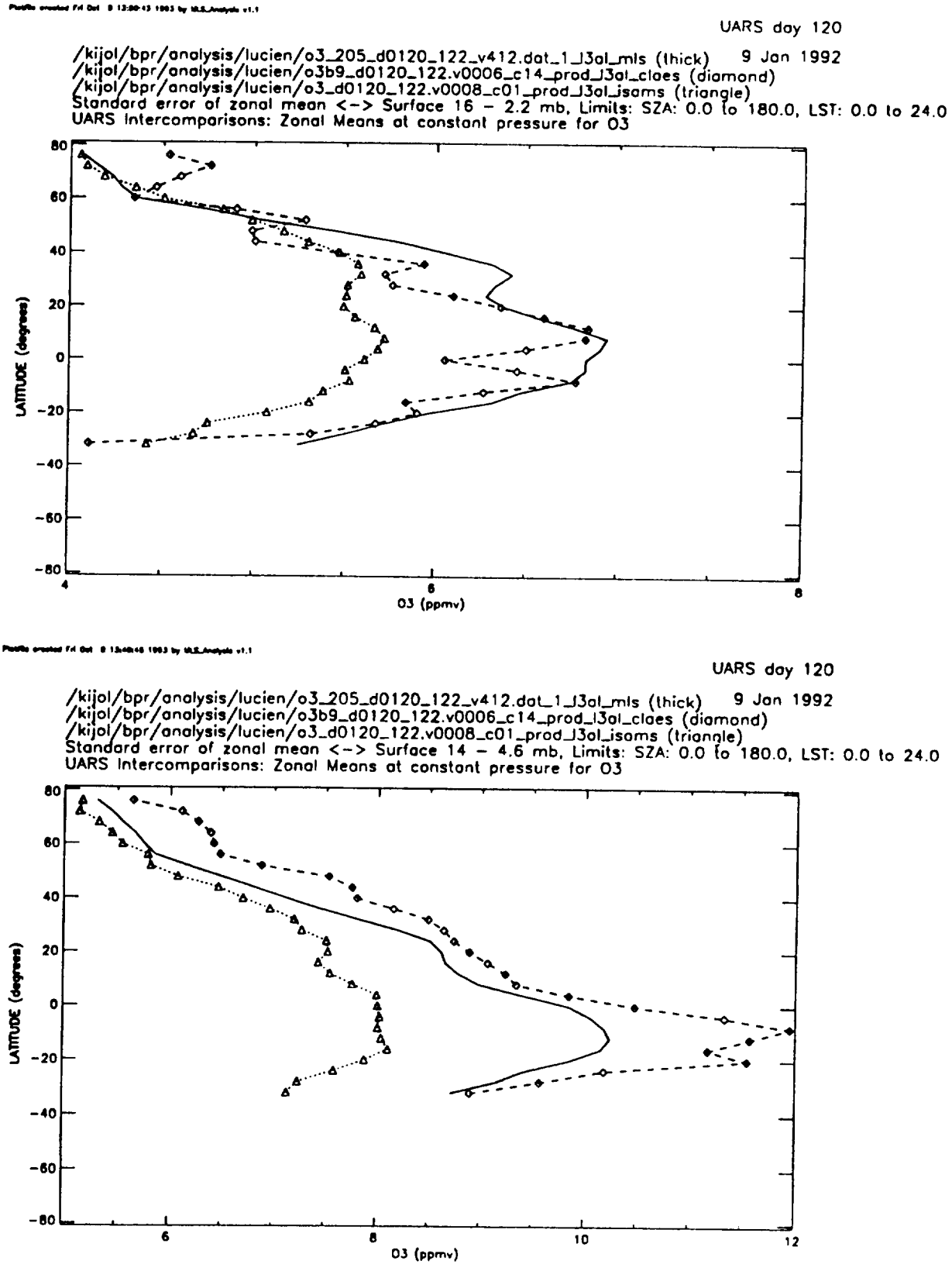

Figure 5.2.2-4 Same as Figure 5.2.2-3, but for 4.6 mb (bottom panel) and 2.2 mb (top panel).

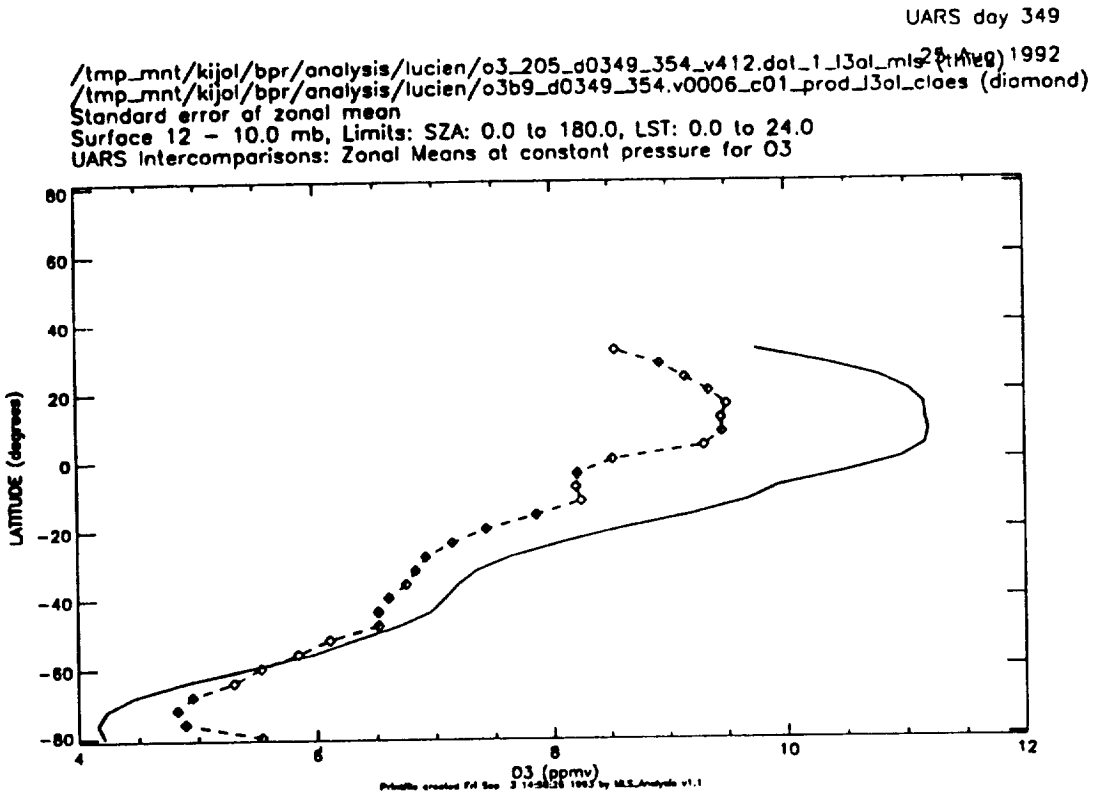

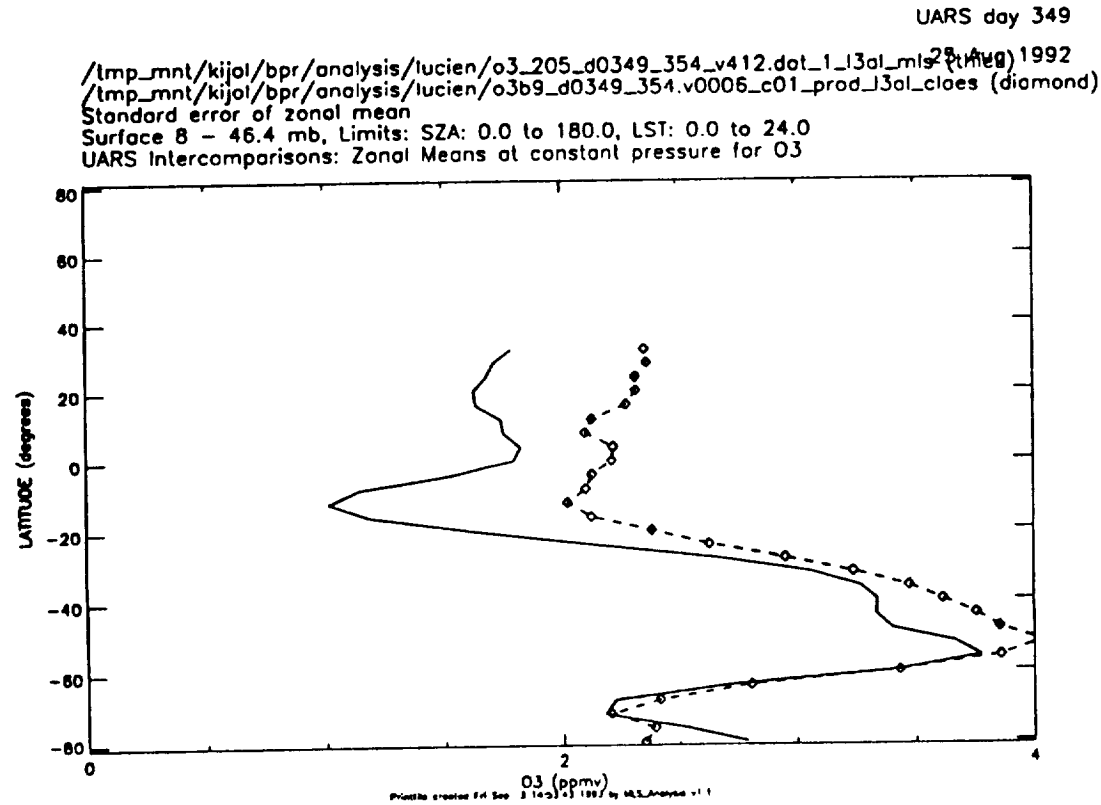

Figure 5.2.2-5 Same as Figure 5.2.2-3, but for Aug. 25-30, 1992 time period, and just for MLS (solid line) and CLAES (diamonds) data.

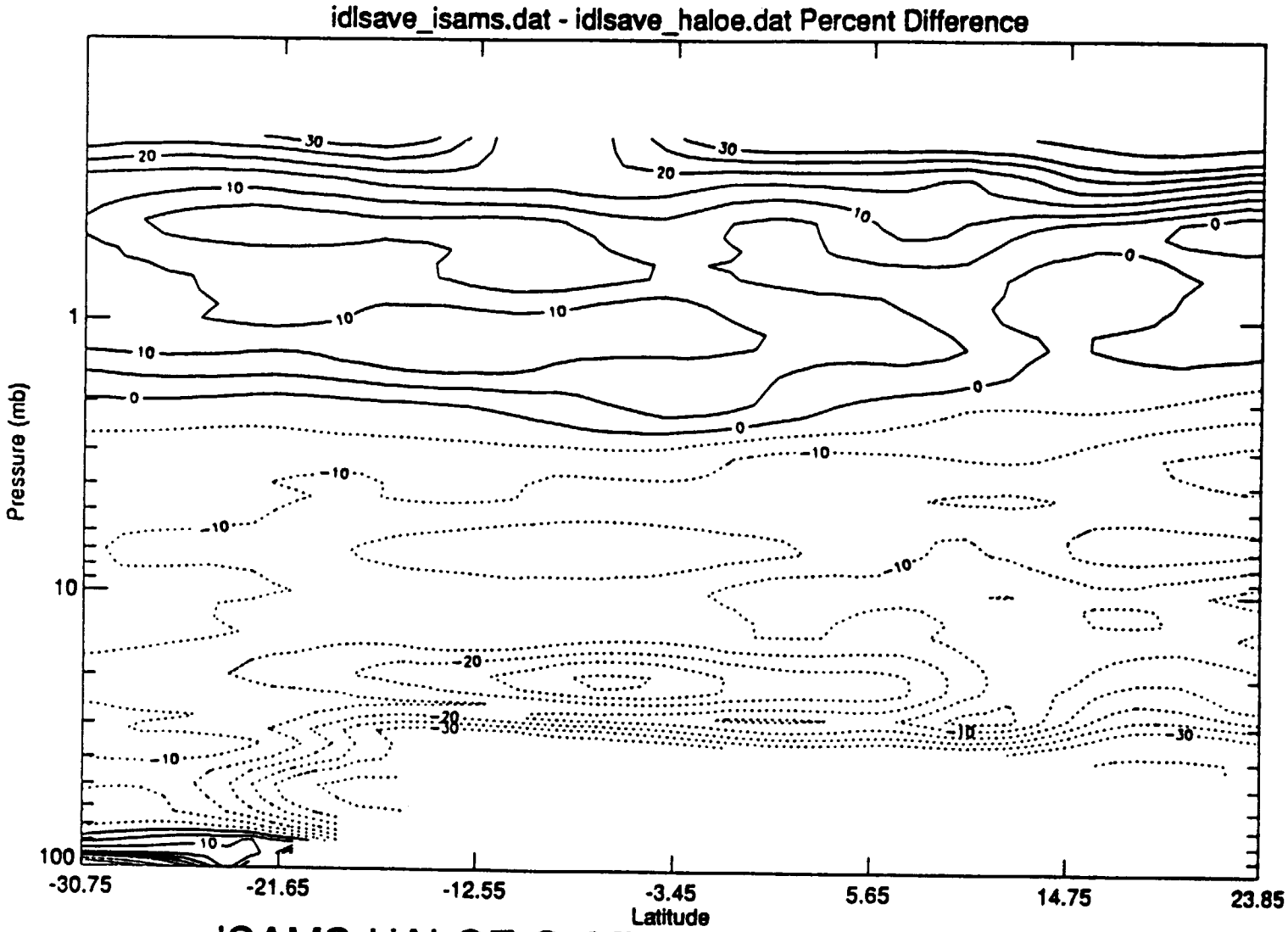

Figure 5.2.2-6 Percentage differences between ISAMS and HALOE ozone retrievals (ISAMS-HALOE) for April 15-20, 1992 near 5°N.

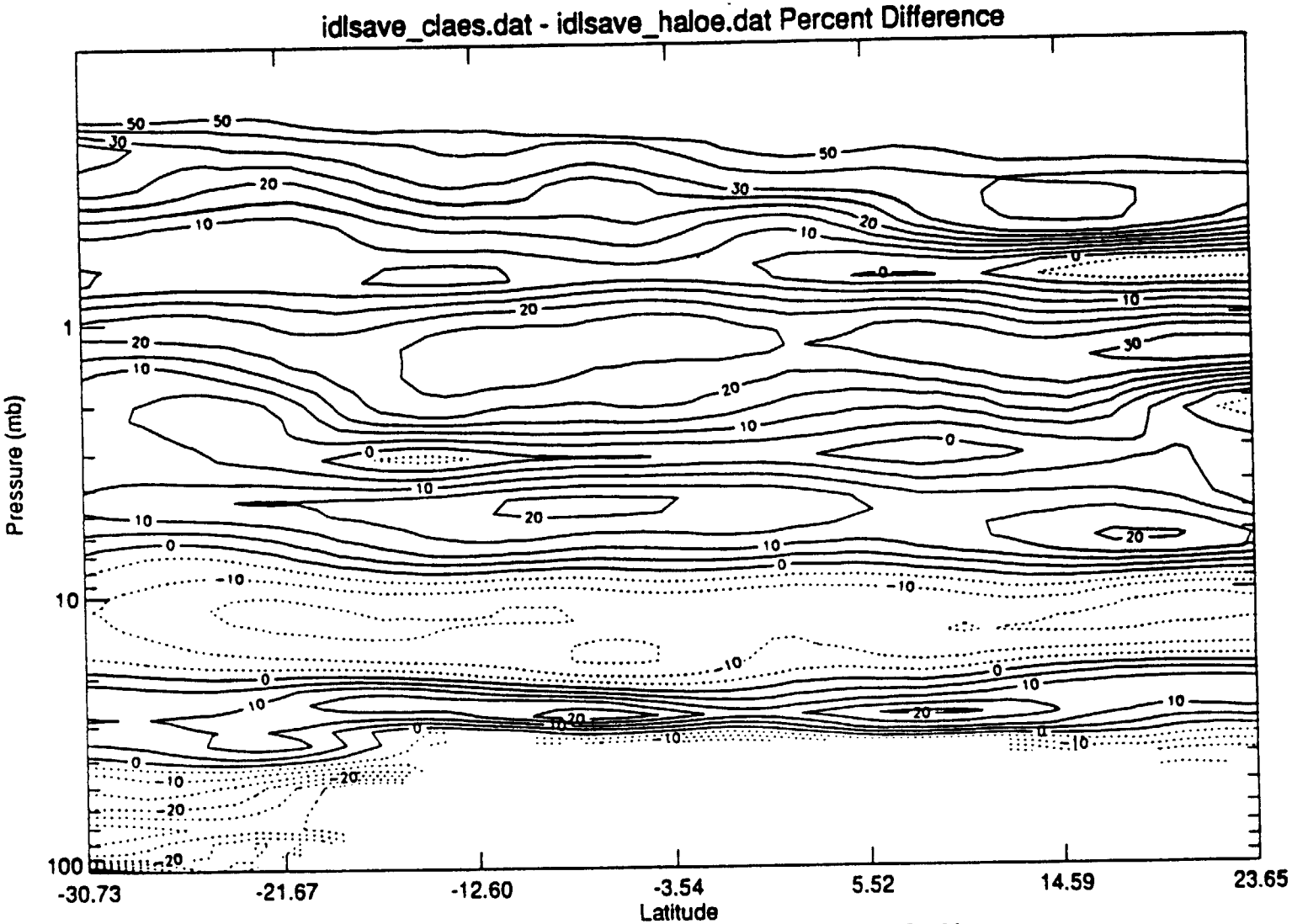

Figure 5.2.2-7 Percentage differences between CLAES and HALOE ozone retrievals (CLAES-HALOE) for April 15-20, 1992 near 5^{O}N.

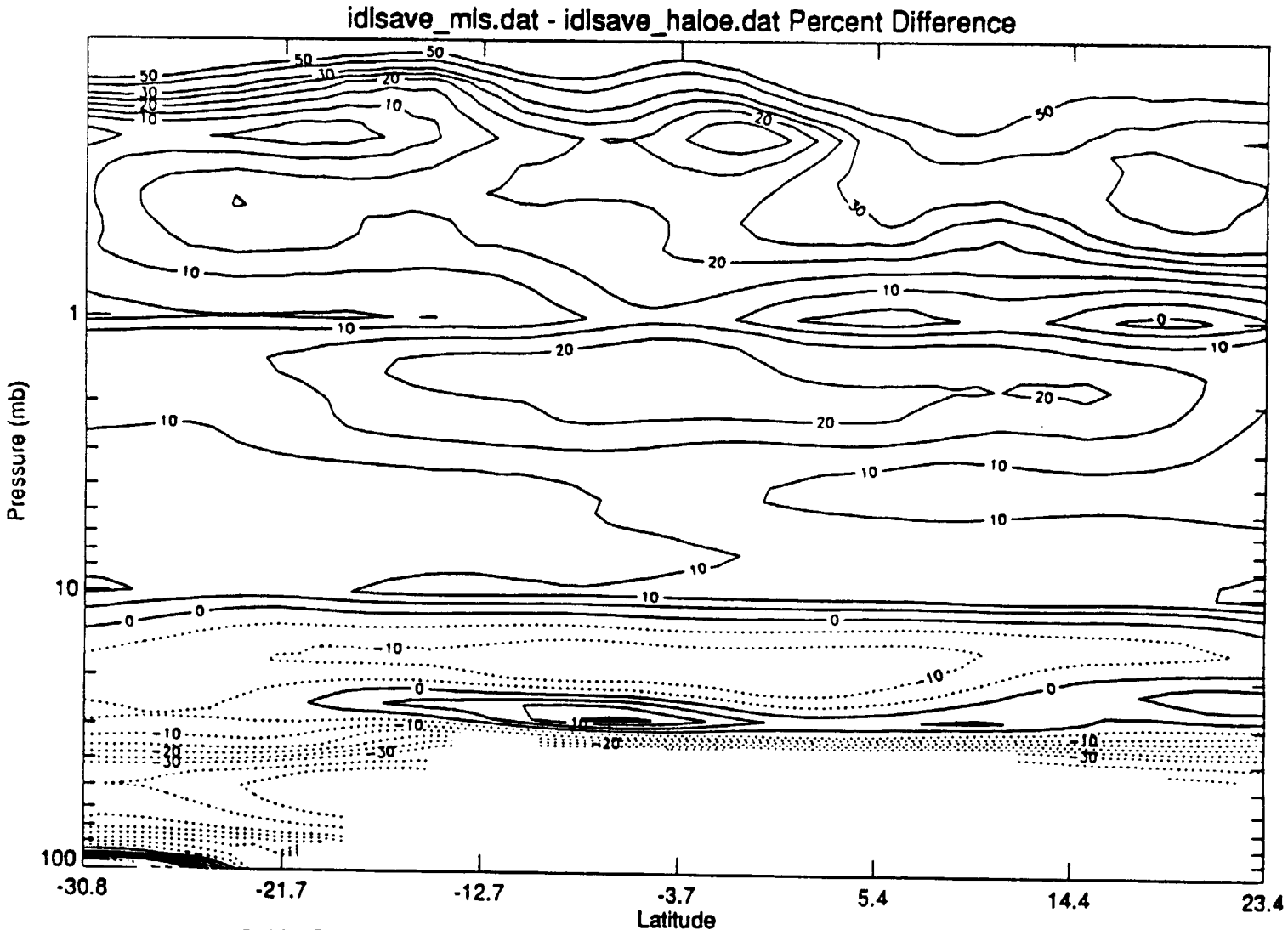

Figure 5.2.2-8 Percentage differences between MLS and HALOE ozone retrievals (MLS-HALOE) for April 15-20, 1992 near 5°N.

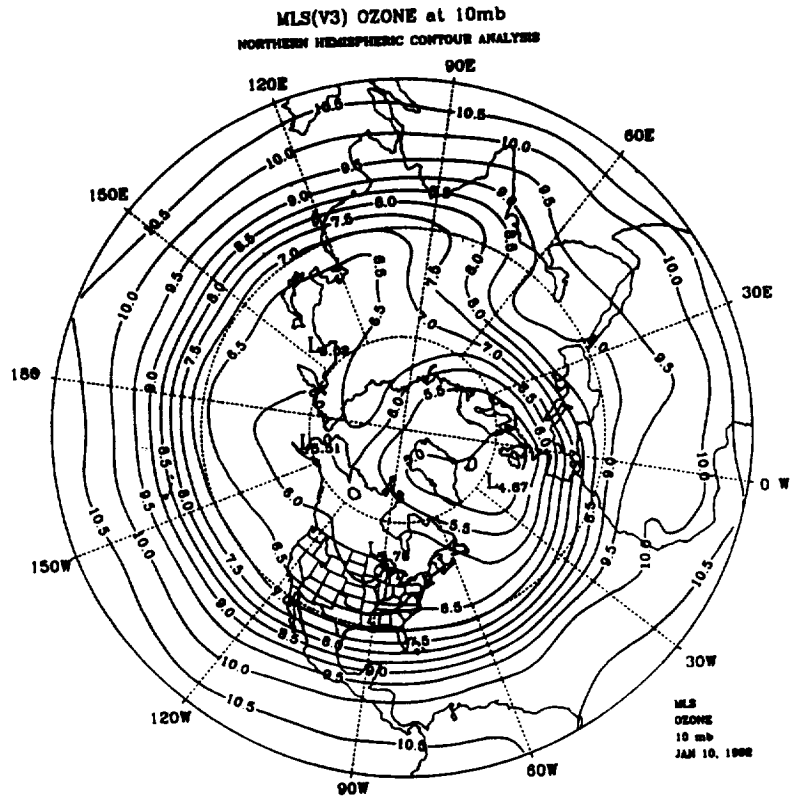

(a)

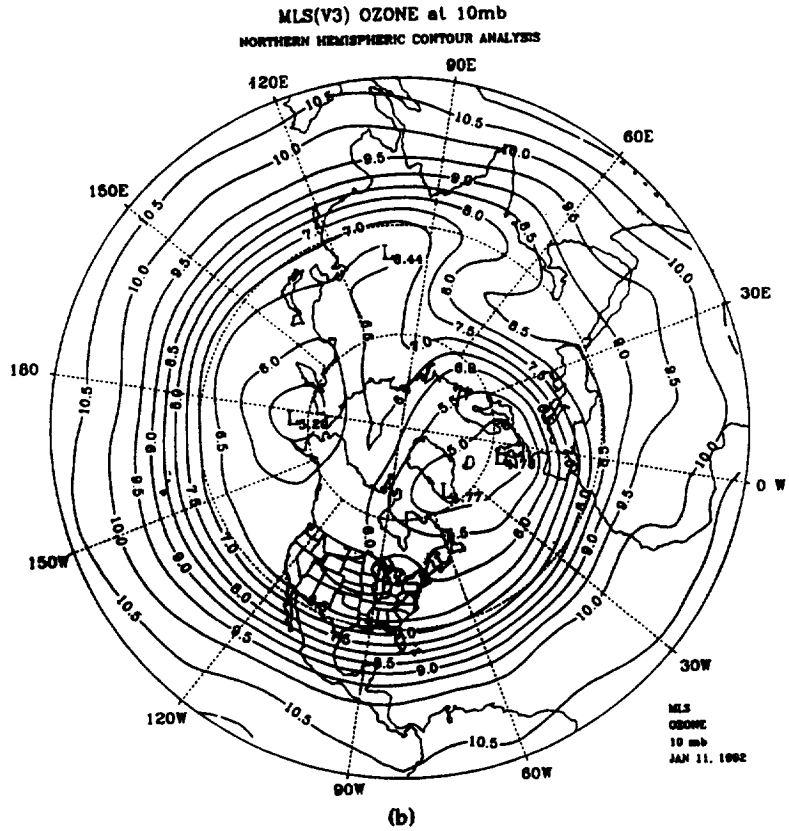

(b)

Figure 5.2.3-1 (a,b) MLS ozone map at 10 mb for Jan. 10-11, 1993. (c,d) MLS ozone map at 1 mb for Jan. 10-11, 1993.

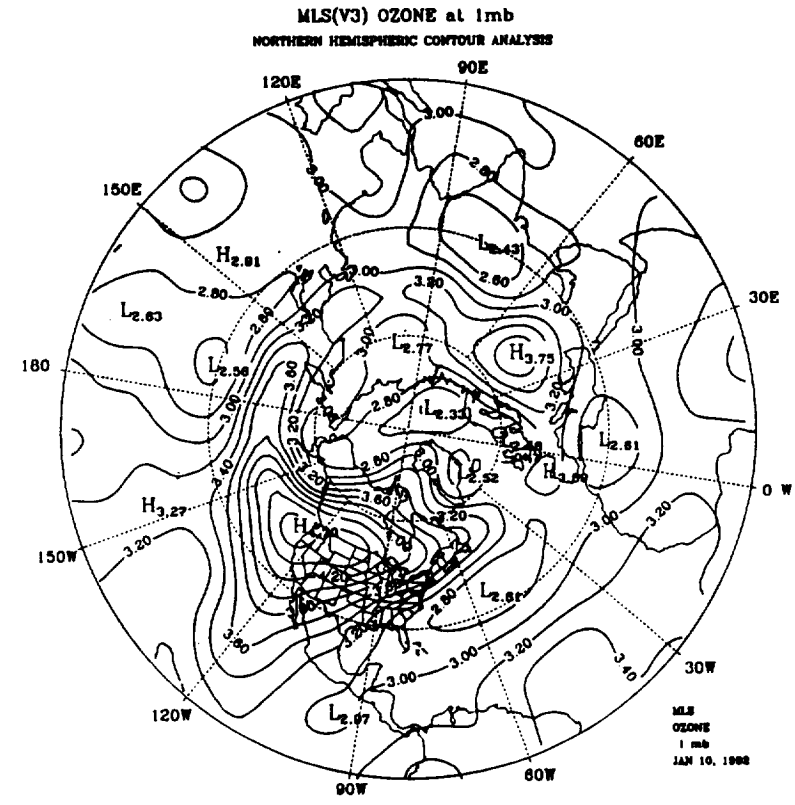

(c)

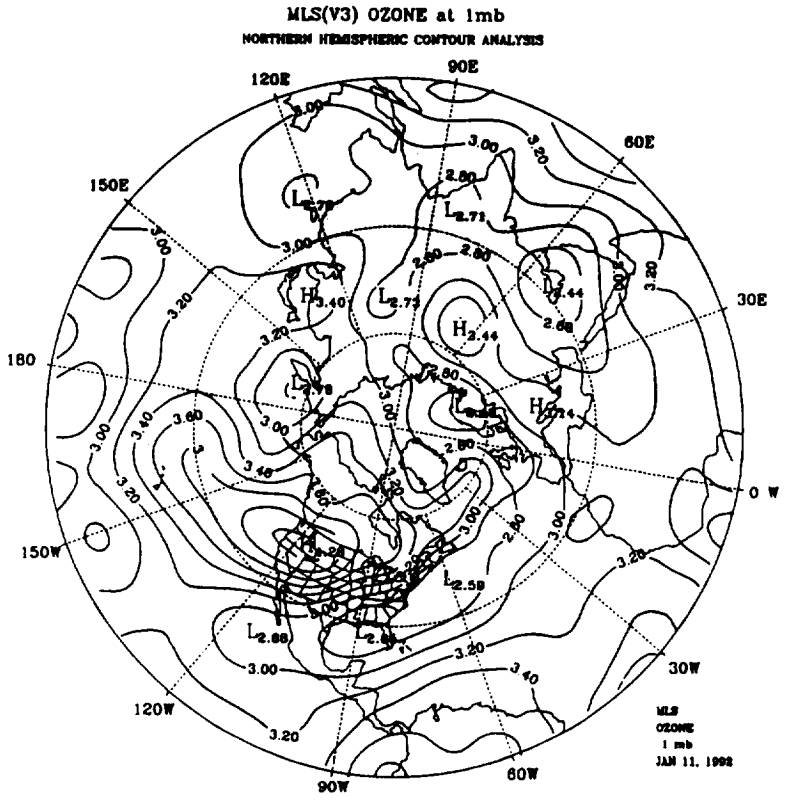

(d)

Figure 5.2.3-1 Concluded.

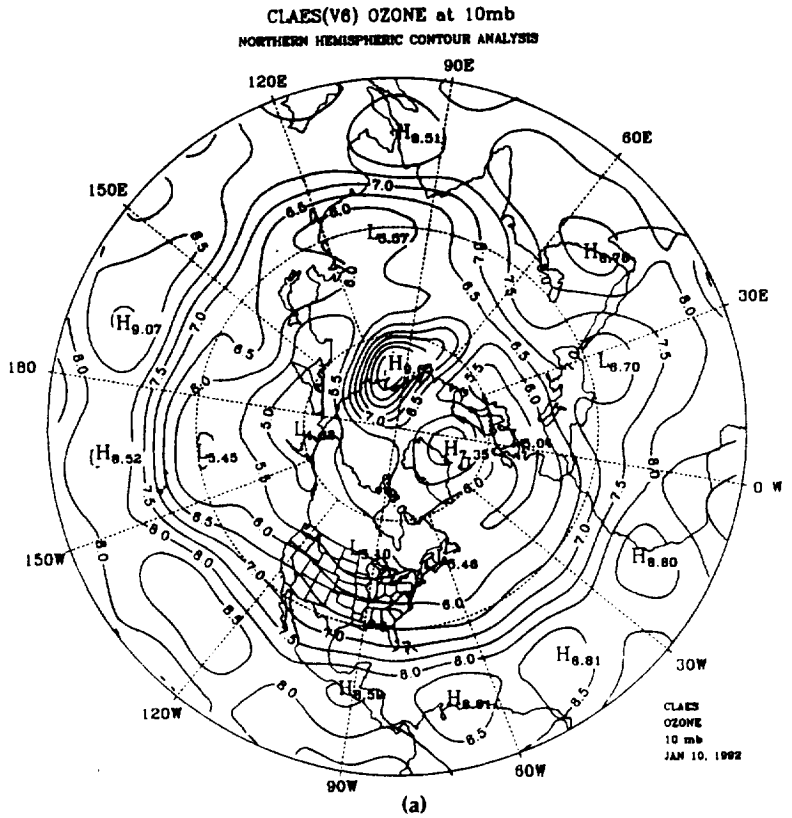

(a)

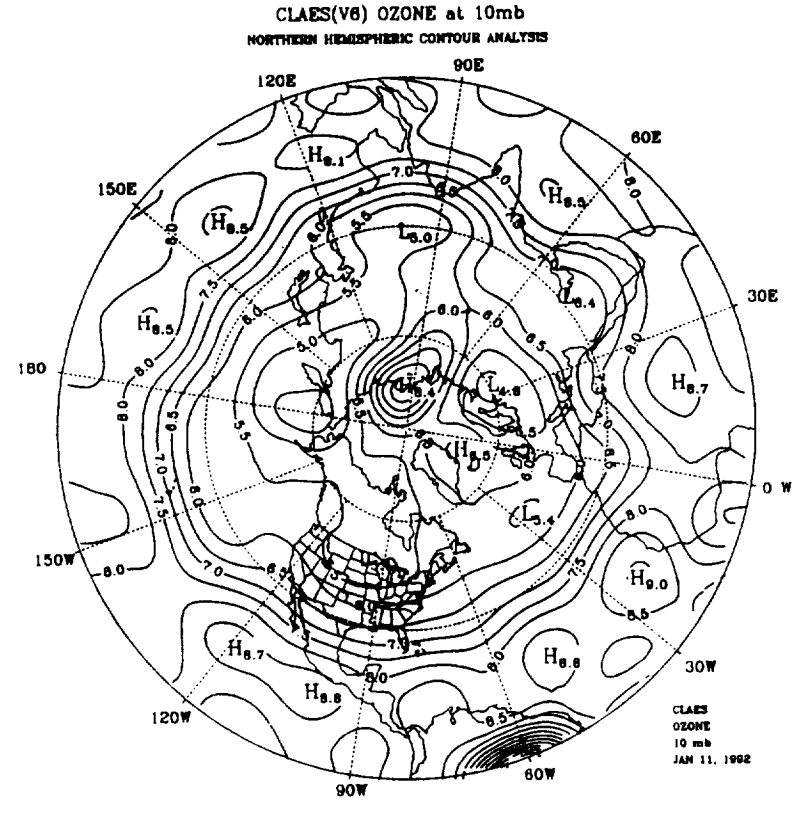

(b)

Figure 5.2.3-2 (a,b) CLAES ozone map at 10 mb for Jan. 10-11, 1993. (c,d) CLAES ozone map at 1 mb for Jan. 10-11, 1993.

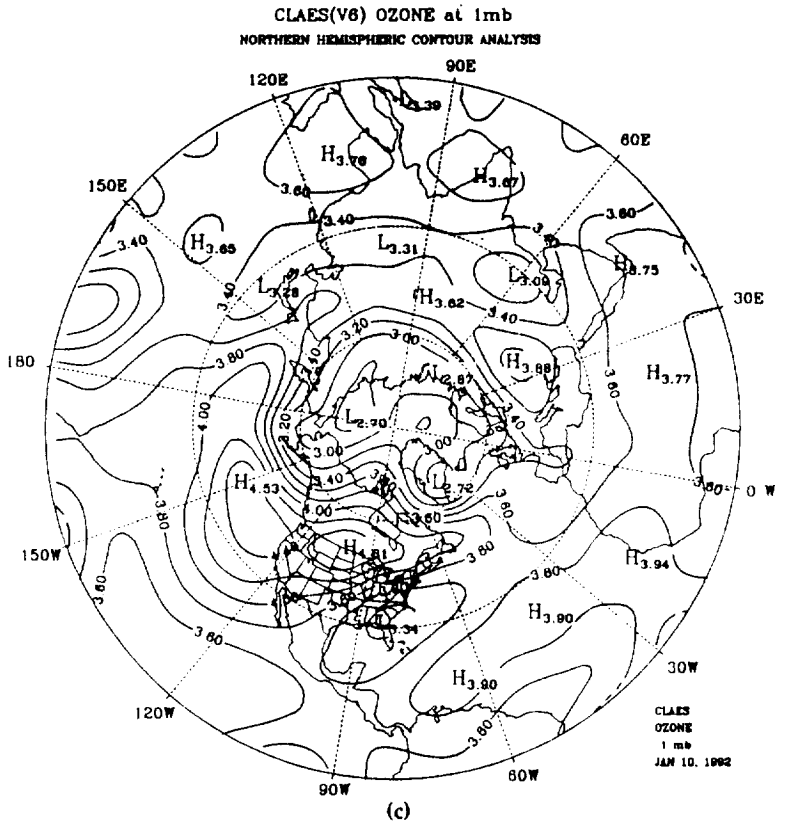

(c)

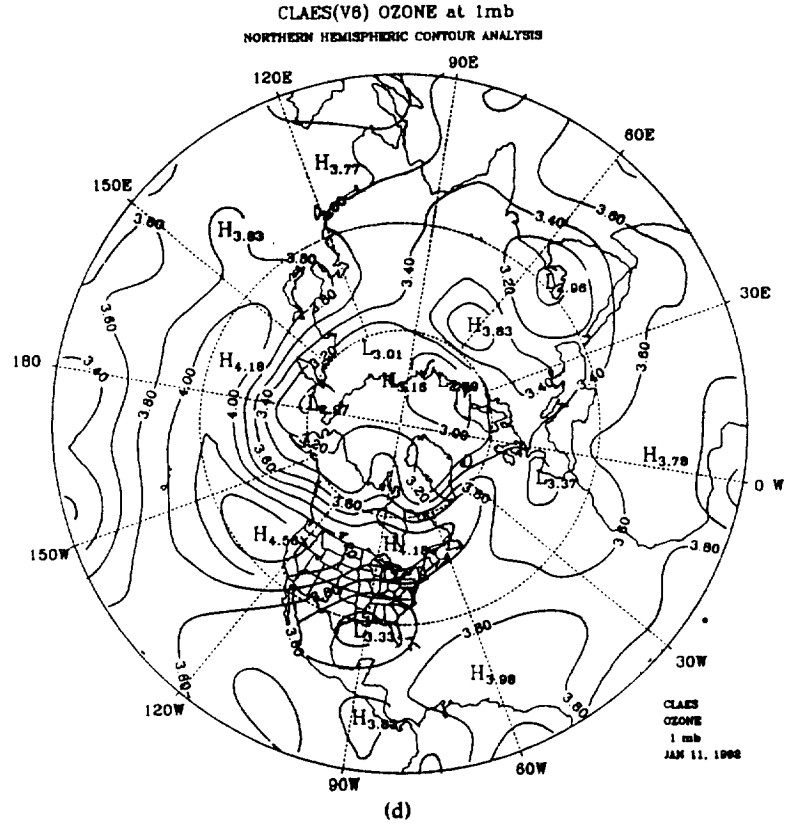

(d)

Figure 5.2.3-2 Concluded.

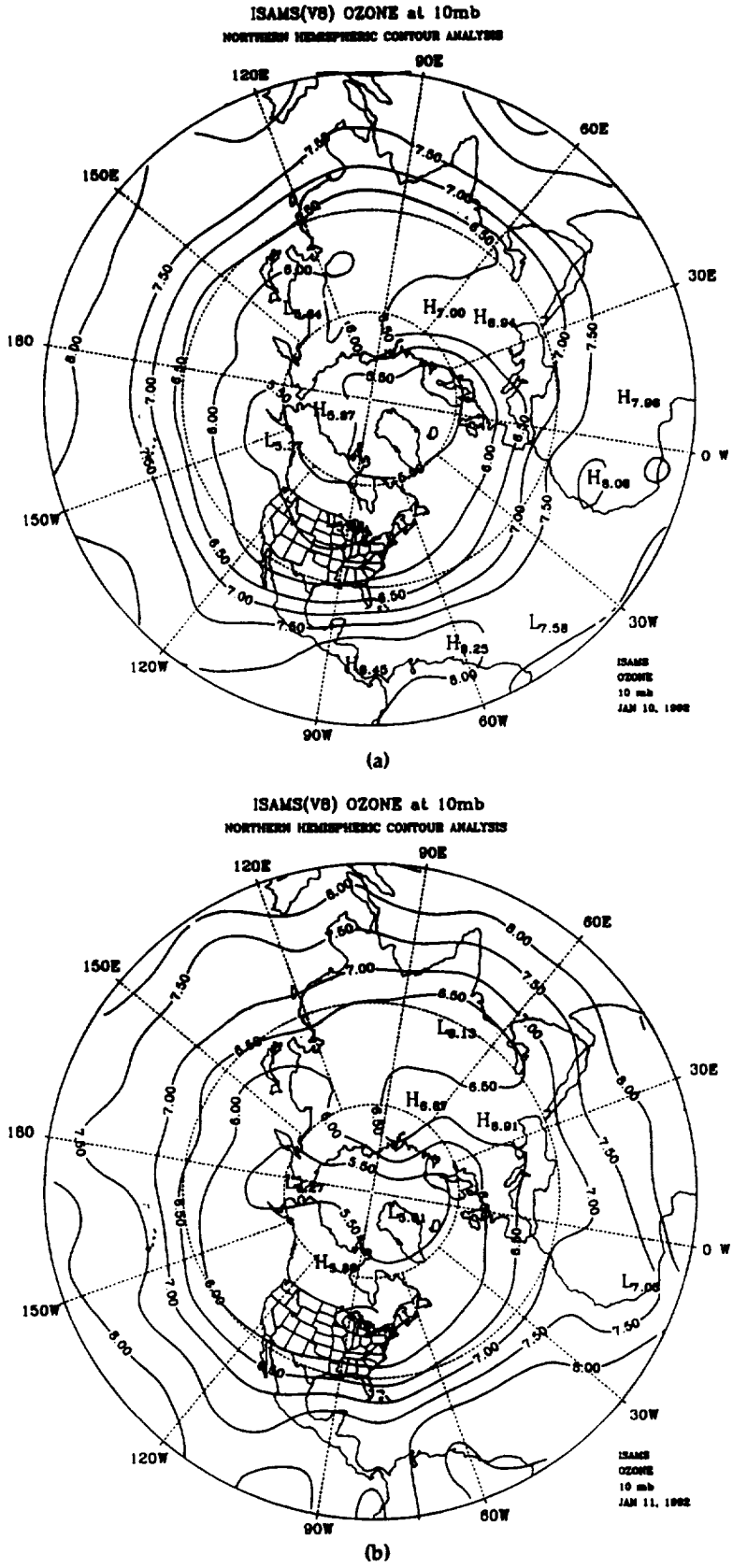

Figure 5.2.3-3 (a,b) ISAMS ozone map at 10 mb for Jan. 10-11, 1993. (c,d) ISAMS ozone map at 1 mb for Jan. 10-11, 1993.

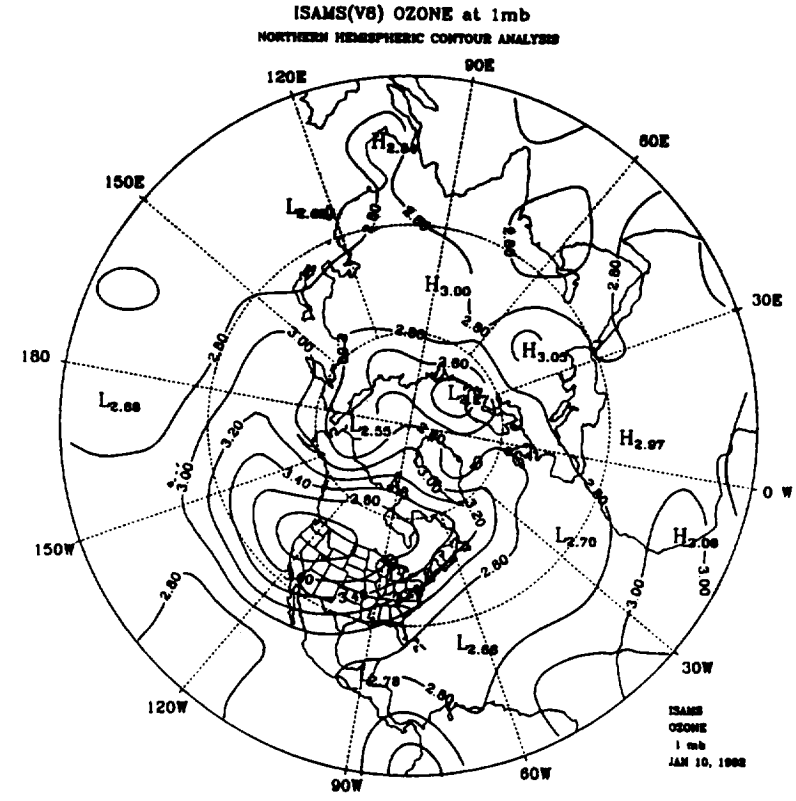

(c)

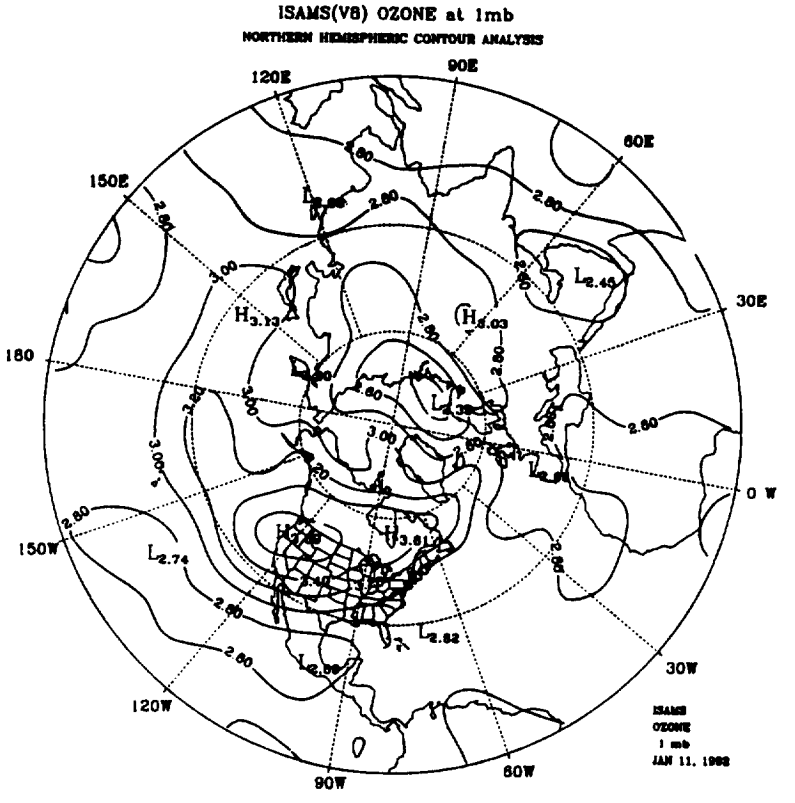

(d)

Figure 5.2.3-3 Concluded.

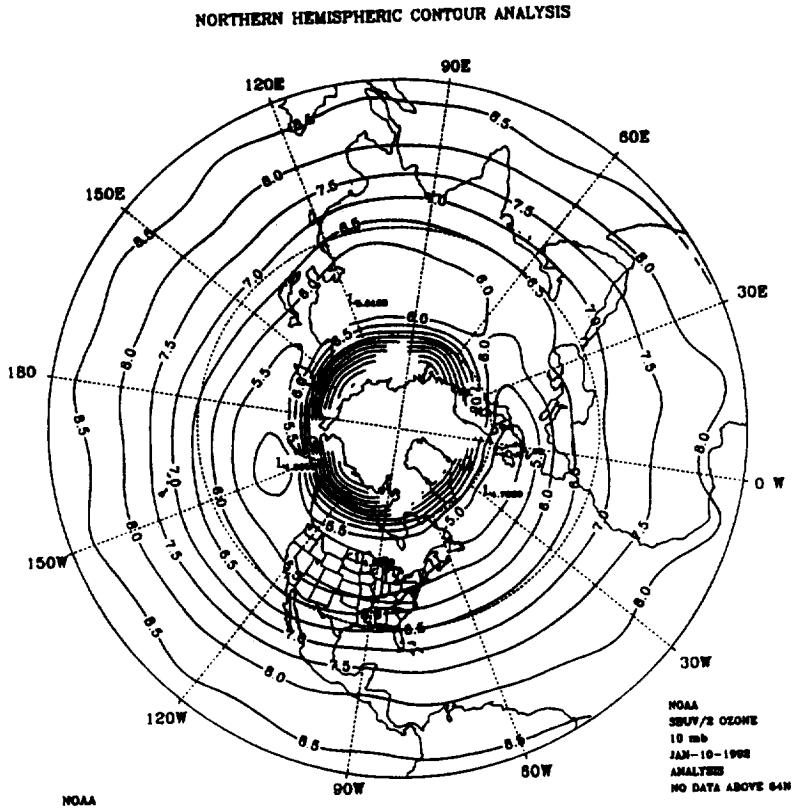

(a)

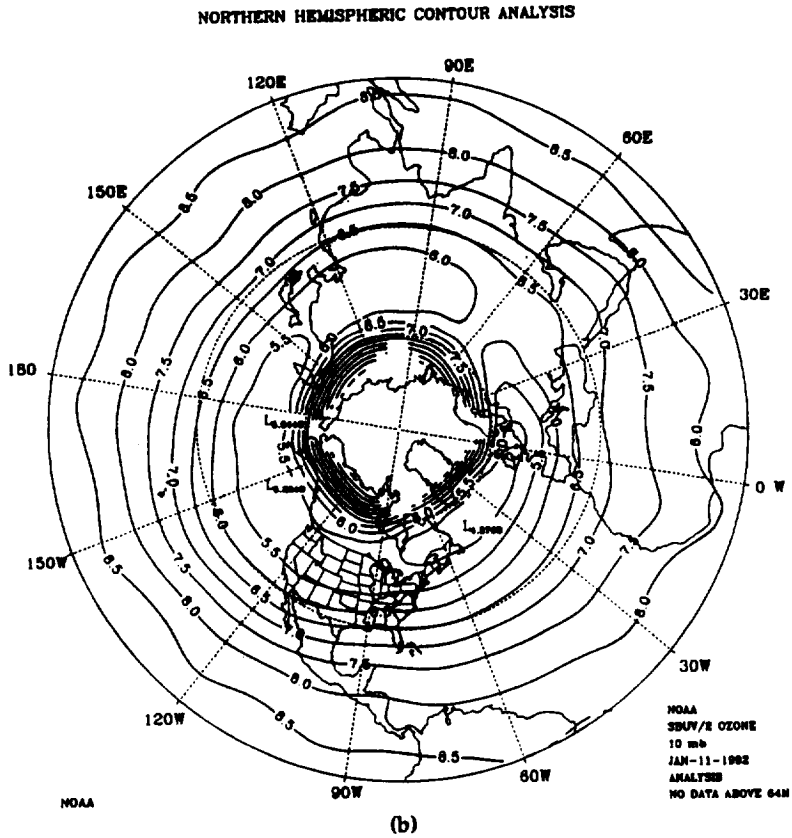

(b)

Figure 5.2.3-4 (a,b) SBUV/2 ozone map at 10 mb for Jan. 10-11, 1993. (c,d) SBUV/2 ozone map at 1 mb for Jan. 10-11, 1993.

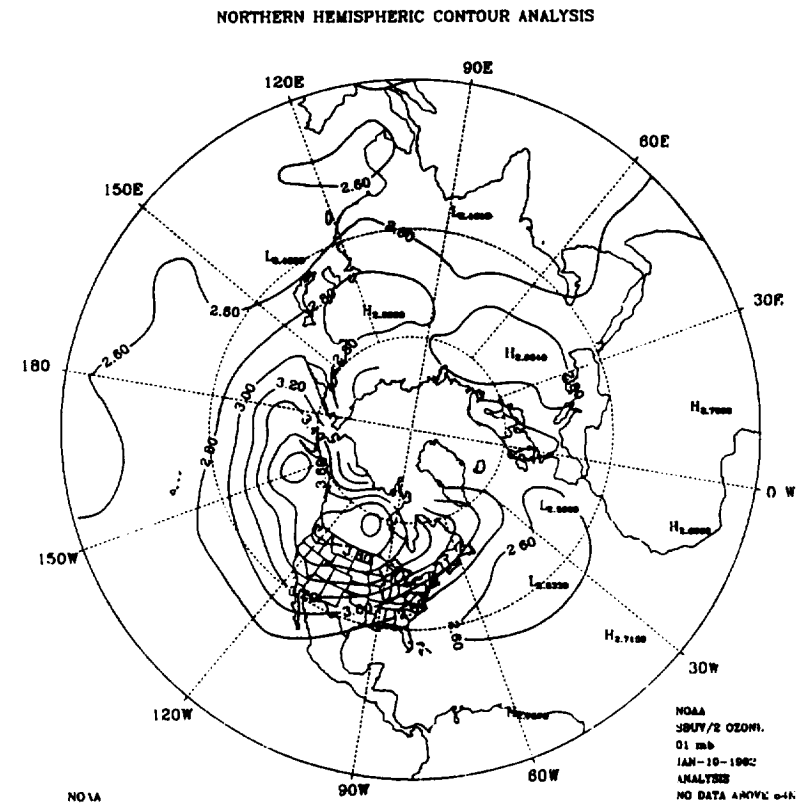

(c)

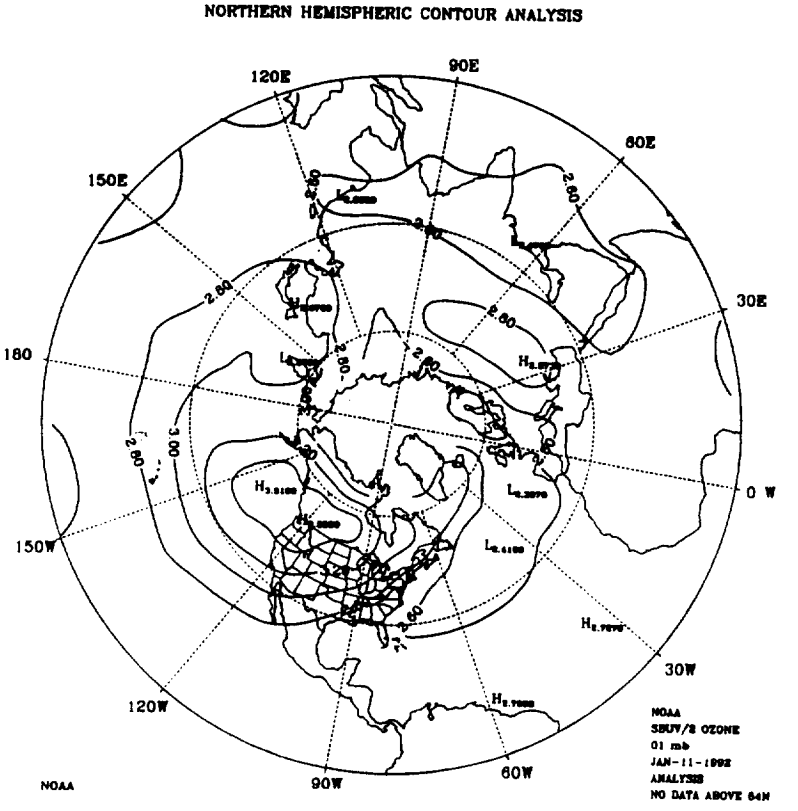

(d)

Figure 5.2.3-4 Concluded.

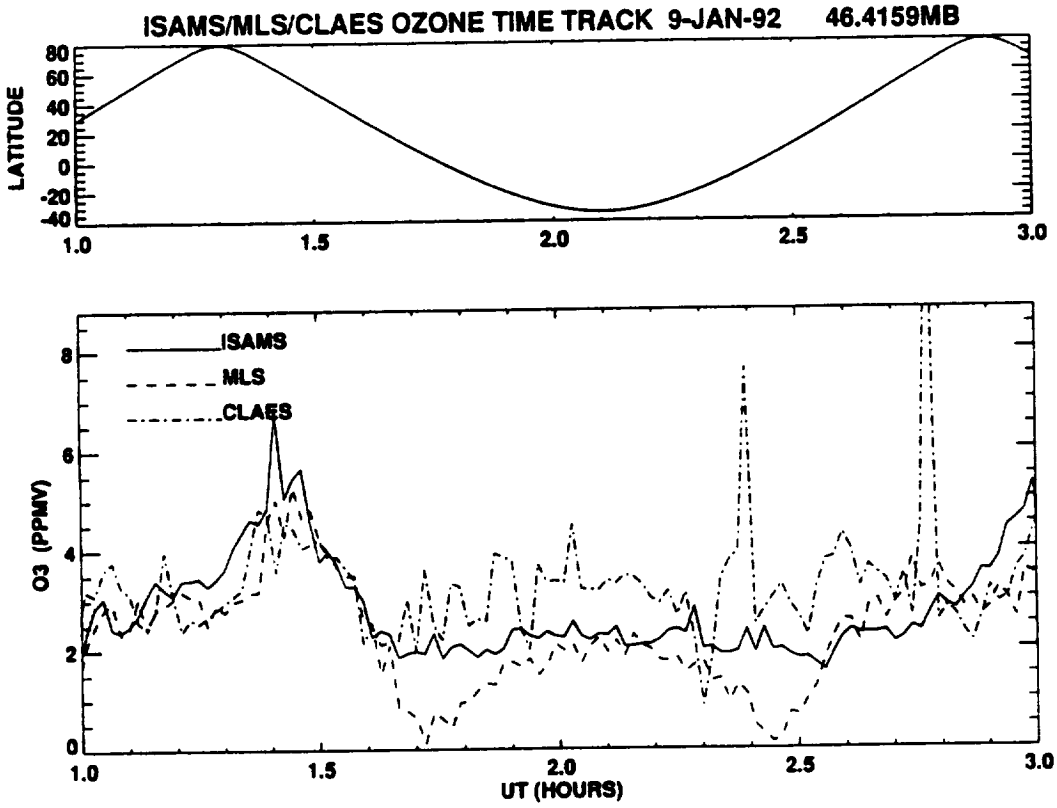

Figure 5.2.4-1 ISAMS/MLS/CLAES time tracks for Jan. 9, 1992 at 46.4 mb.

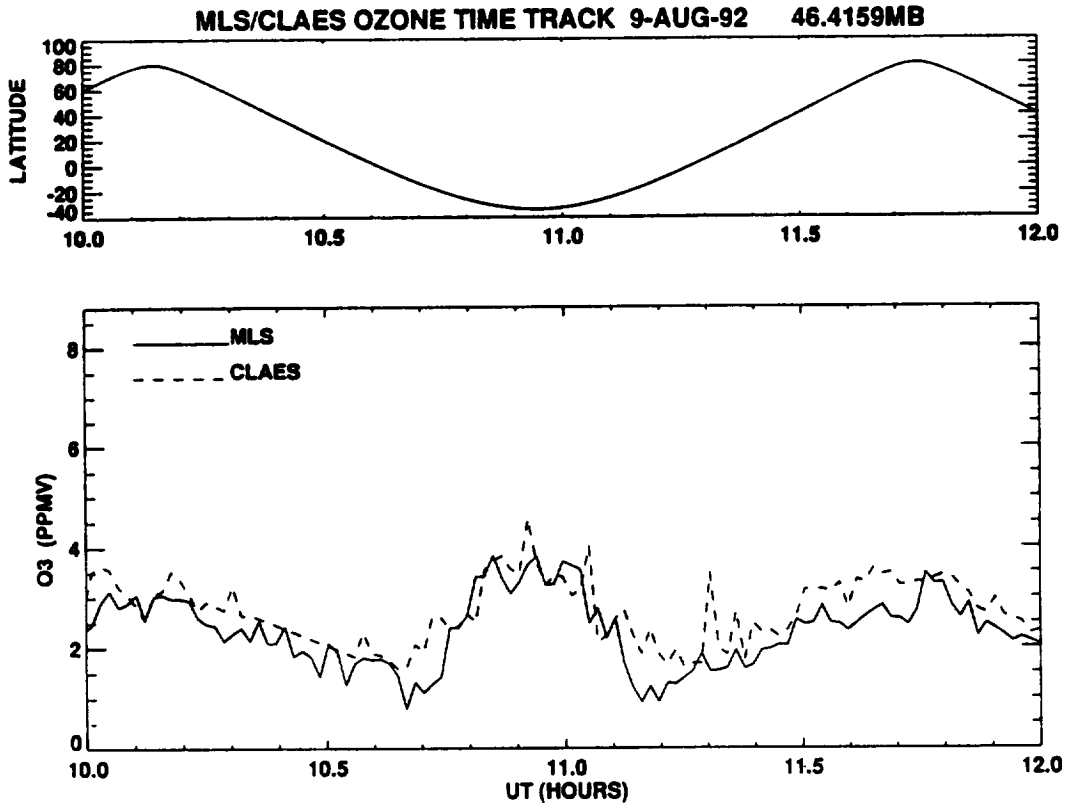

Figure 5.2.4-2 MLS/CLAES time tracks for Aug. 9, 1992 at 46.4 mb.

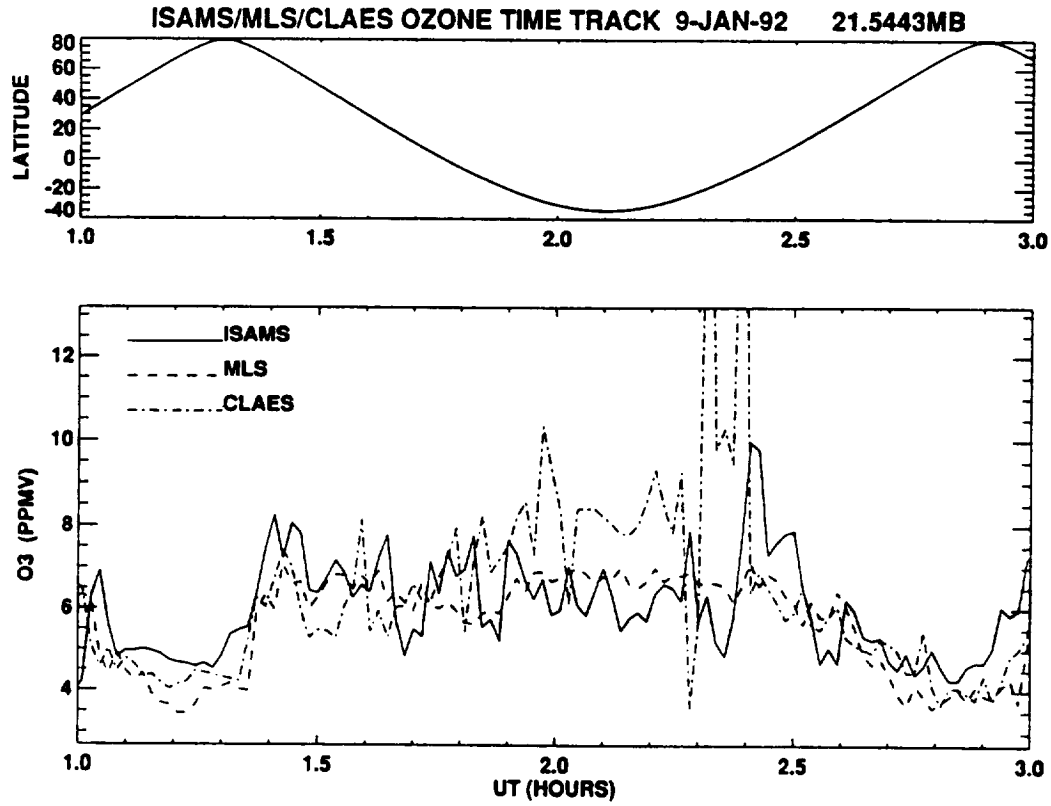

Figure 5.2.4-3 ISAMS/MLS/CLAES time tracks for Jan. 9, 1992 at 21.5 mb.

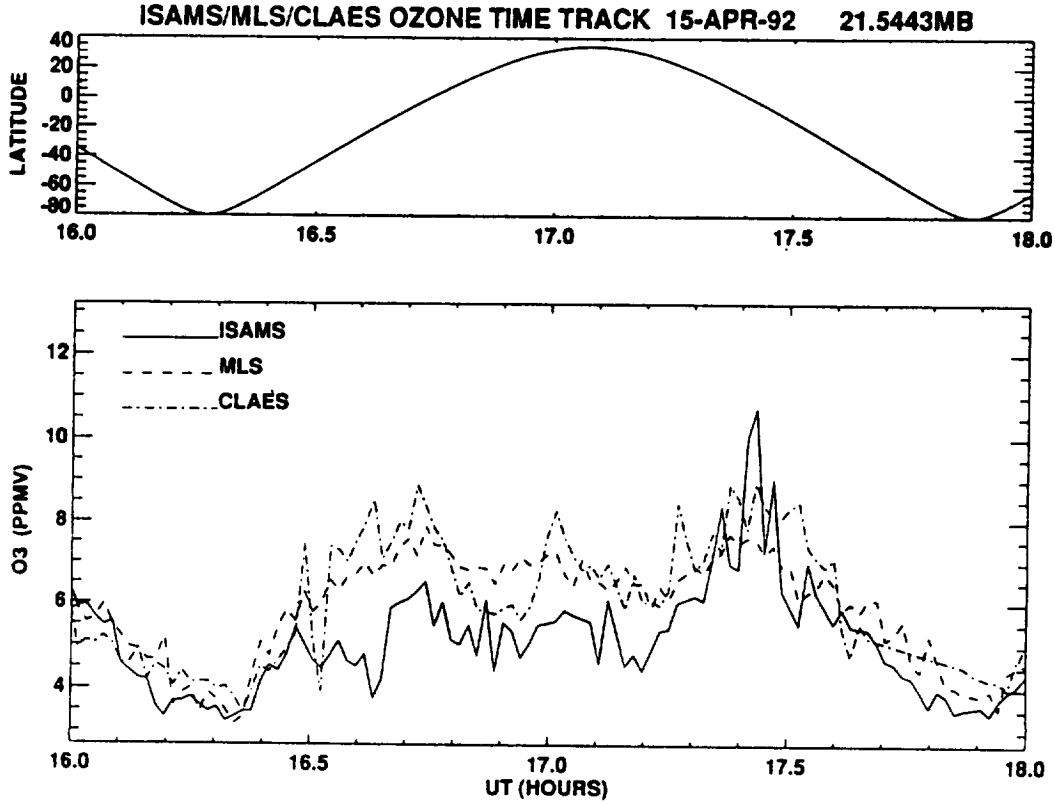

Figure 5.2.4-4 ISAMS/MLS/CLAES time tracks for April 15, 1992 at 21.5 mb.

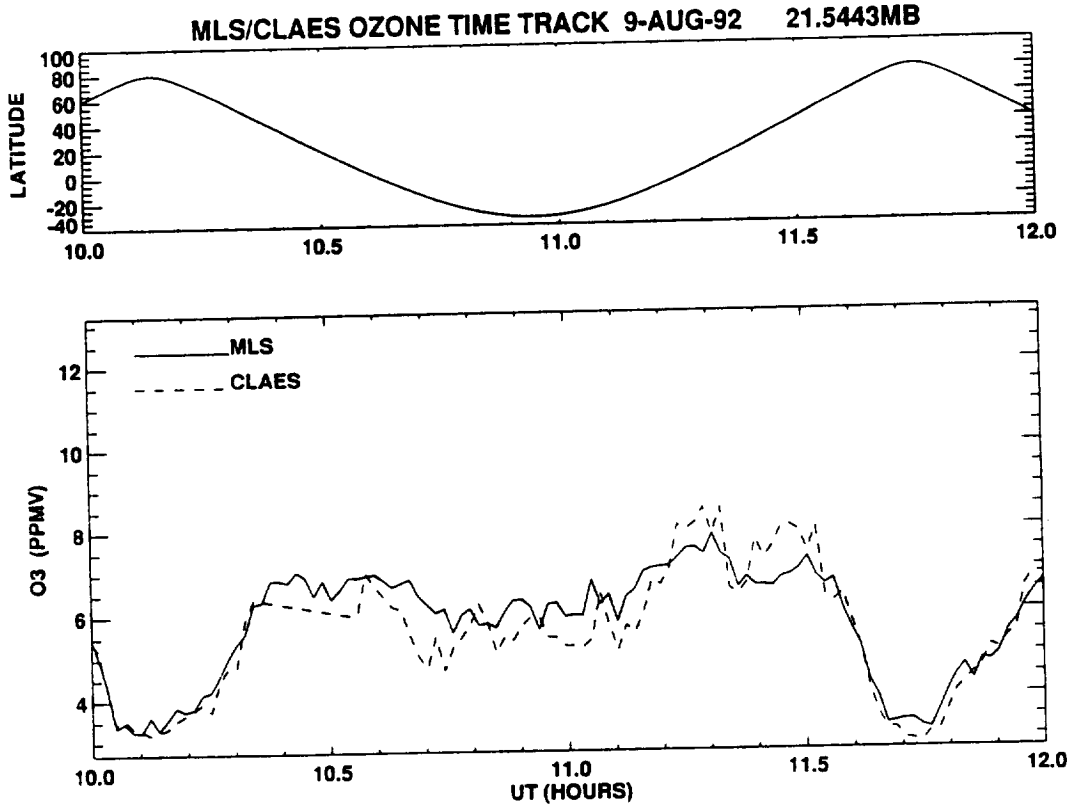

Figure 5.2.4-5 MLS/CLAES time tracks for Aug. 9, 1992 at 21.5 mb.

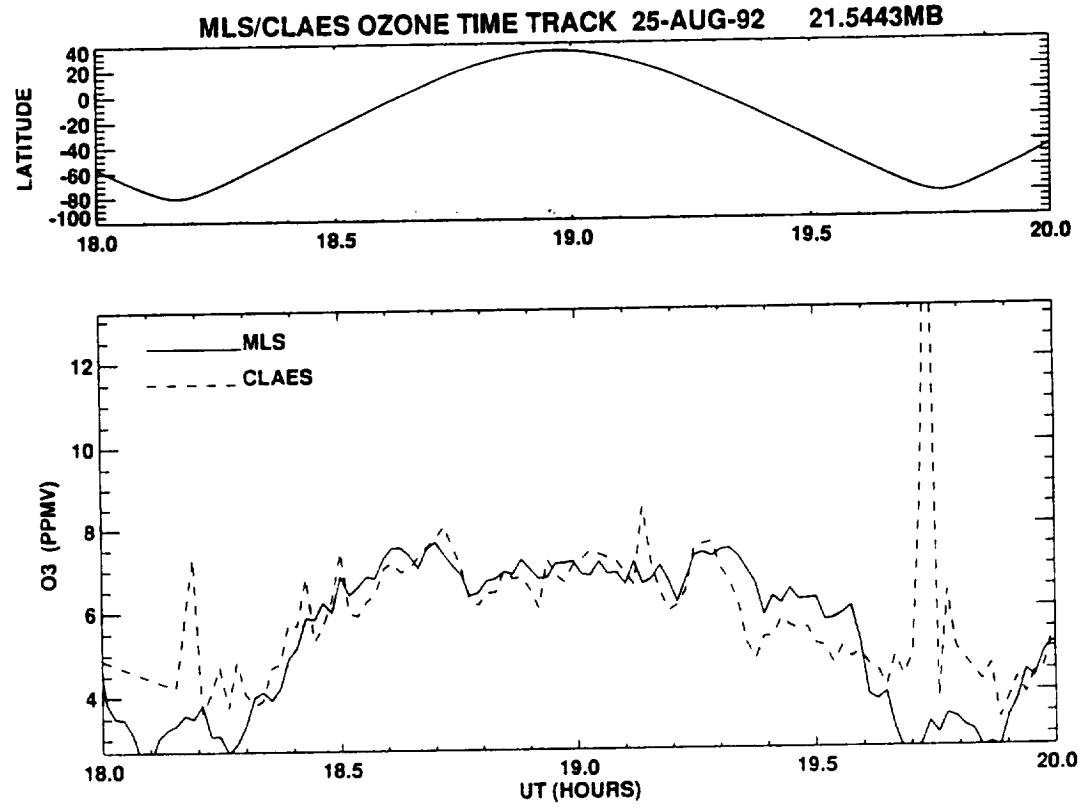

Figure 5.2.4-6 MLS/CLAES time tracks for Aug. 25, 1992 at 21.5 mb.

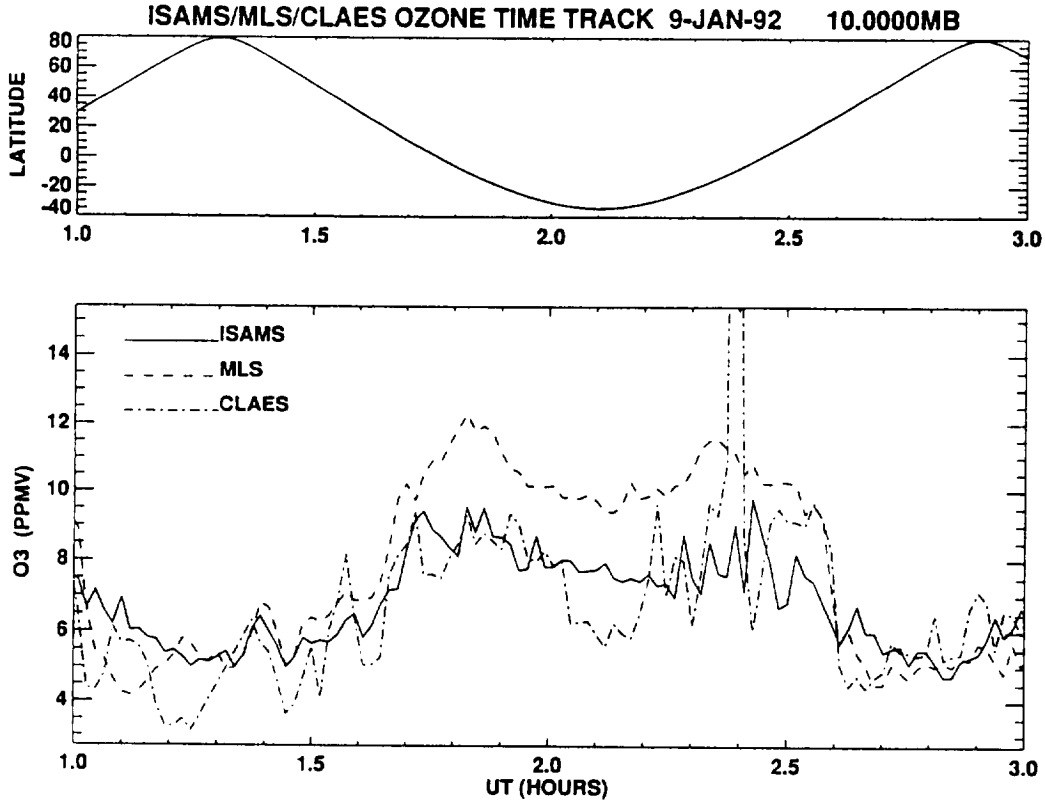

Figure 5.2.4-7 ISAMS/MLS/CLAES time tracks for Jan. 9, 1992 at 10 mb.

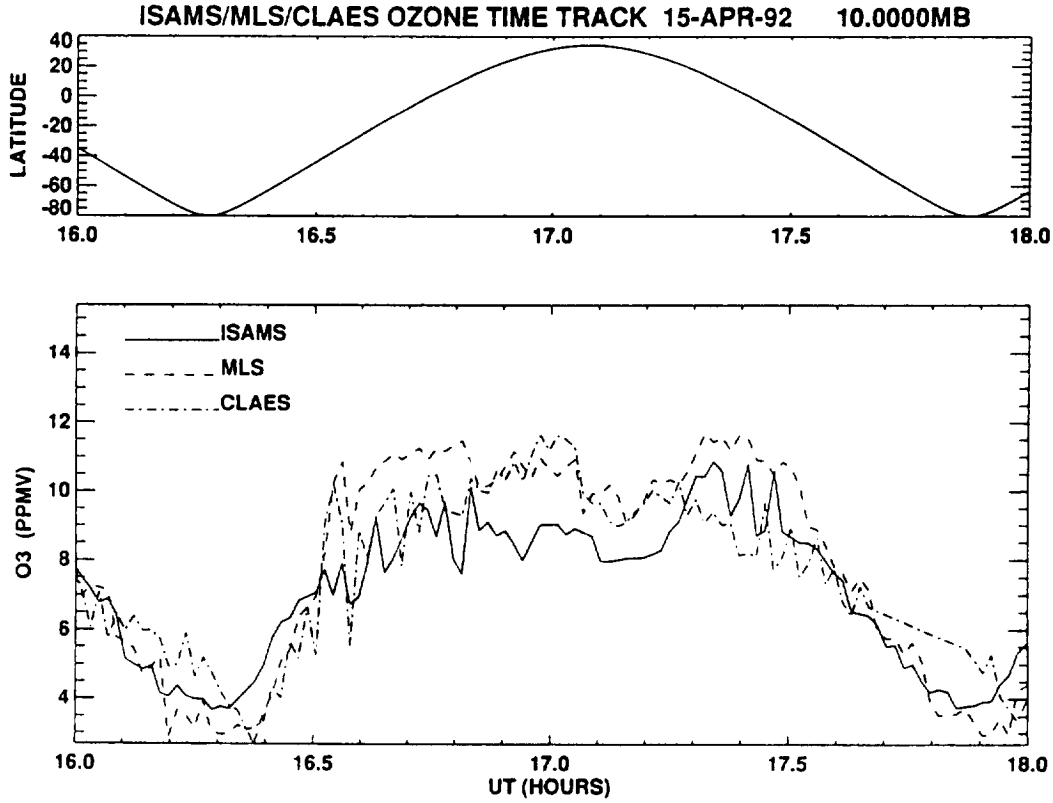

Figure 5.2.4-8 ISAMS/MLS/CLAES time tracks for April 15, 1992 at 10 mb.

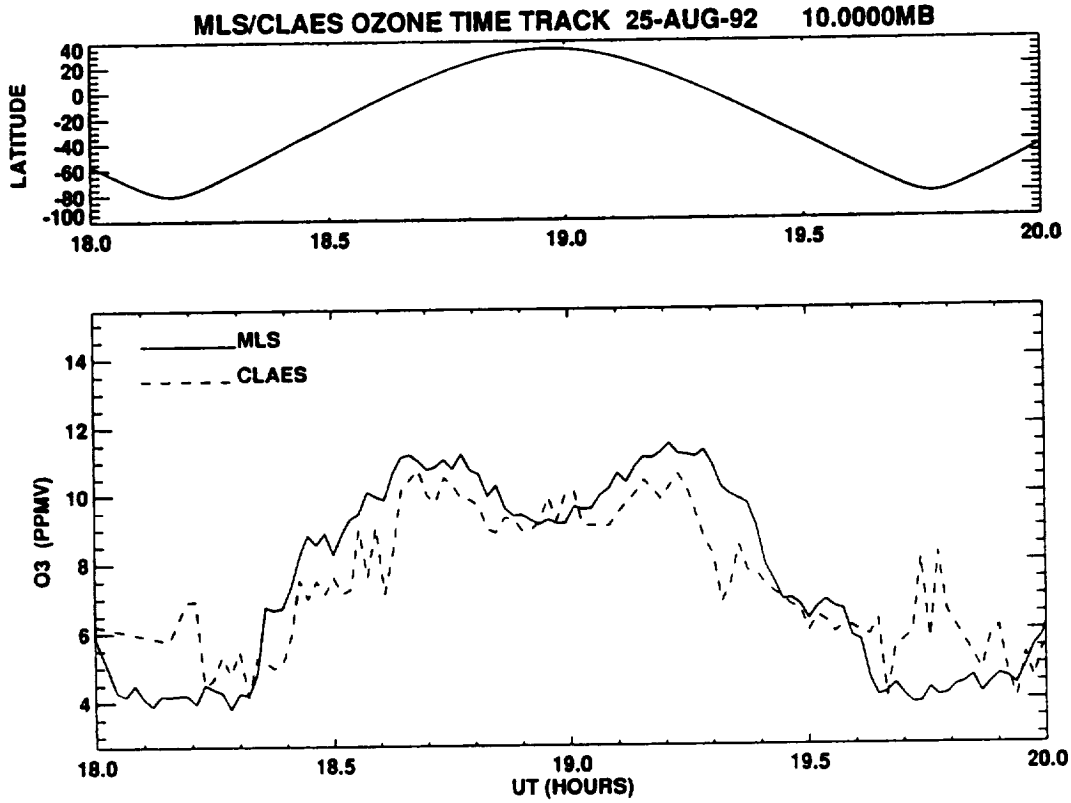

Figure 5.2.4-9 MLS/CLAES time tracks for Aug. 25, 1992 at 10 mb.

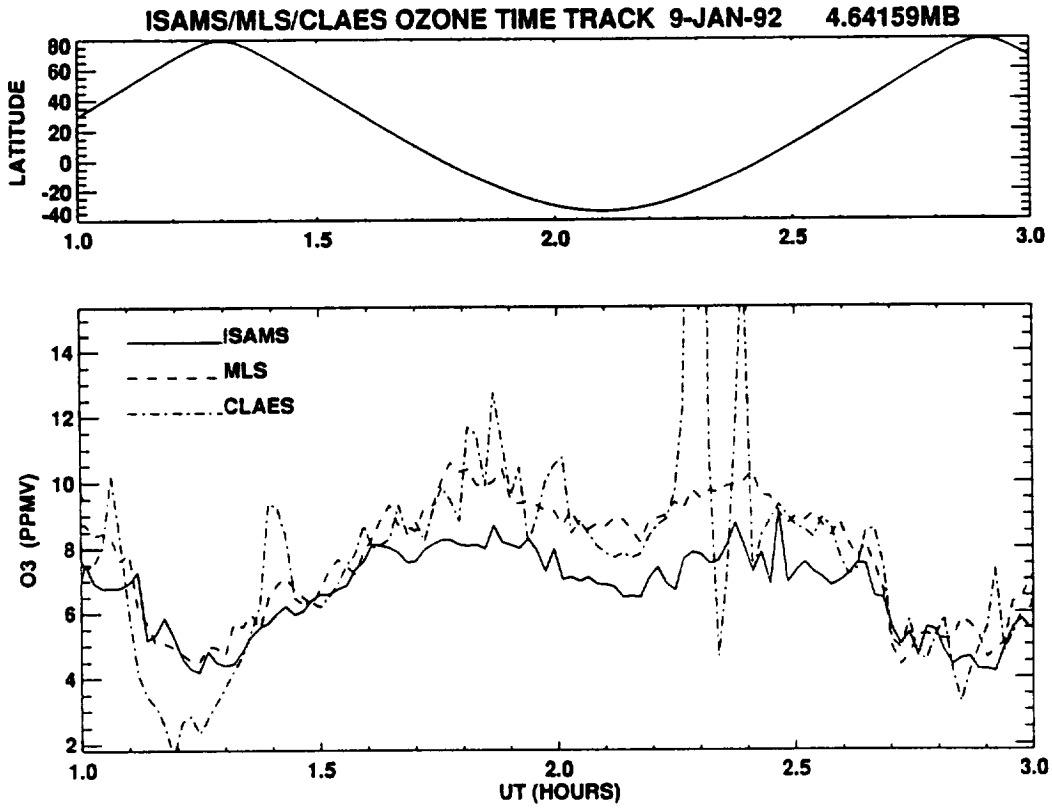

Figure 5.2.4-10 ISAMS/MLS/CLAES time tracks for Jan. 9, 1992 at 4.6 mb.

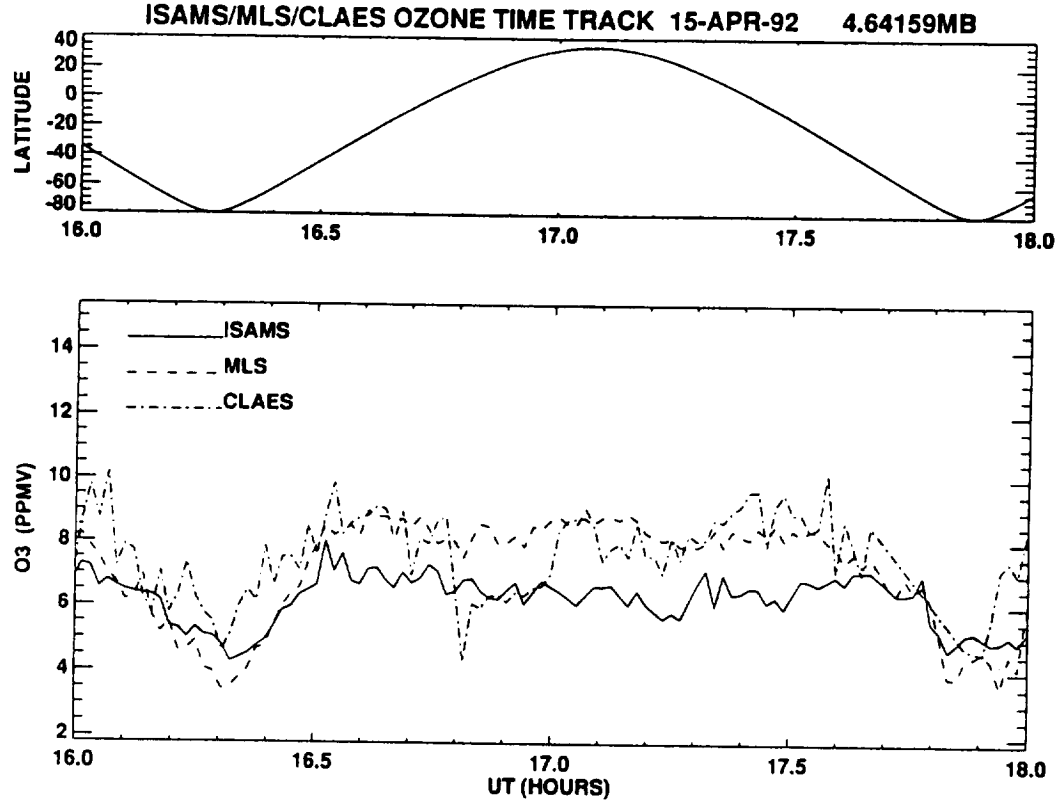

Figure 5.2.4-11 ISAMS/MLS/CLAES time tracks for April 15, 1992 at 4.6 mb.

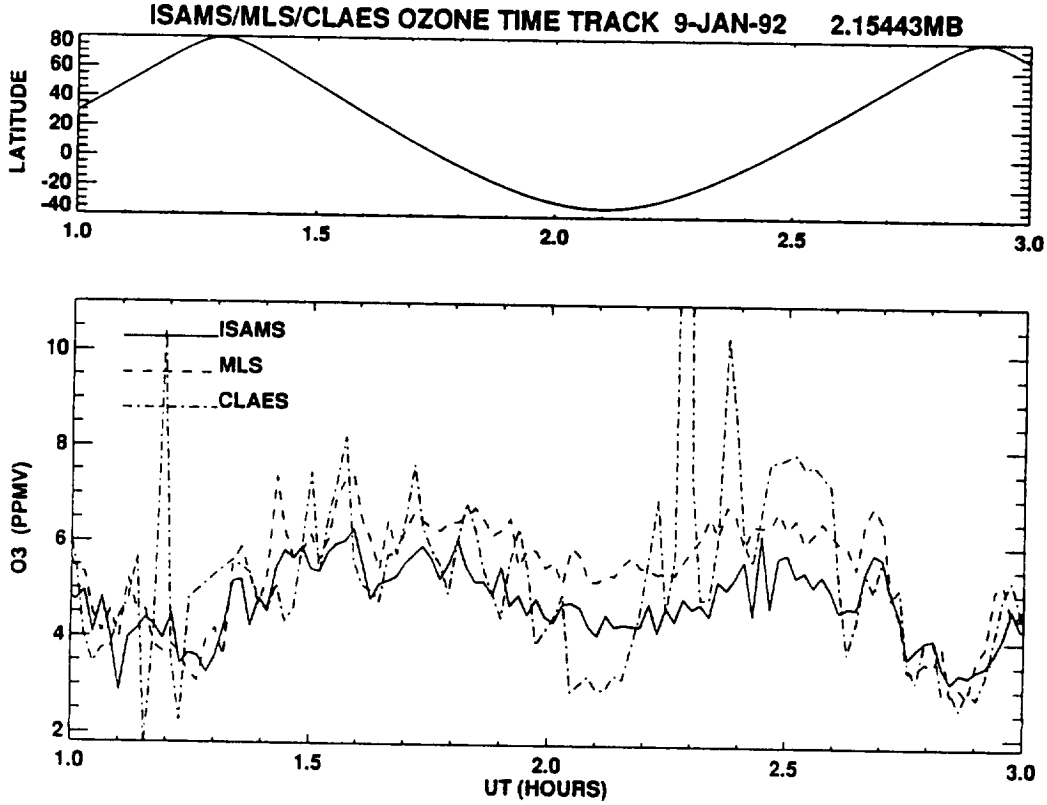

Figure 5.2.4-12 ISAMS/MLS/CLAES time tracks for Jan. 9, 1992 at 2.2 mb.

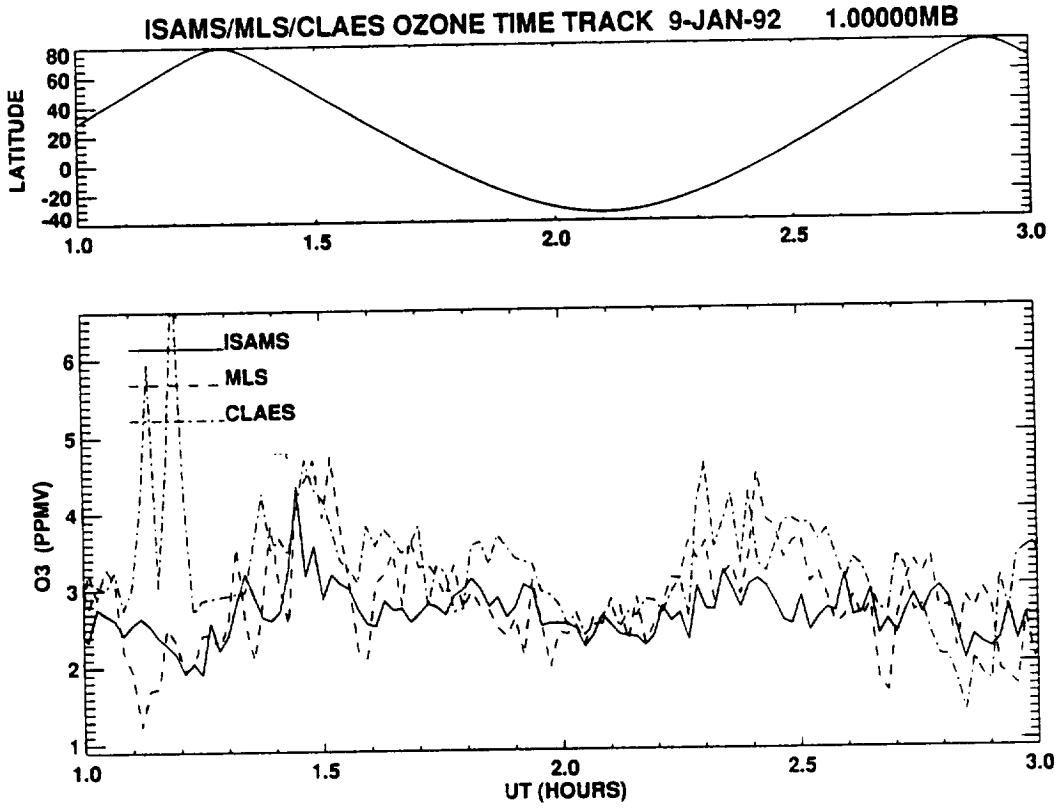

Figure 5.2.4-13 ISAMS/MLS/CLAES time tracks for Jan. 9, 1992 at 1.0 mb.

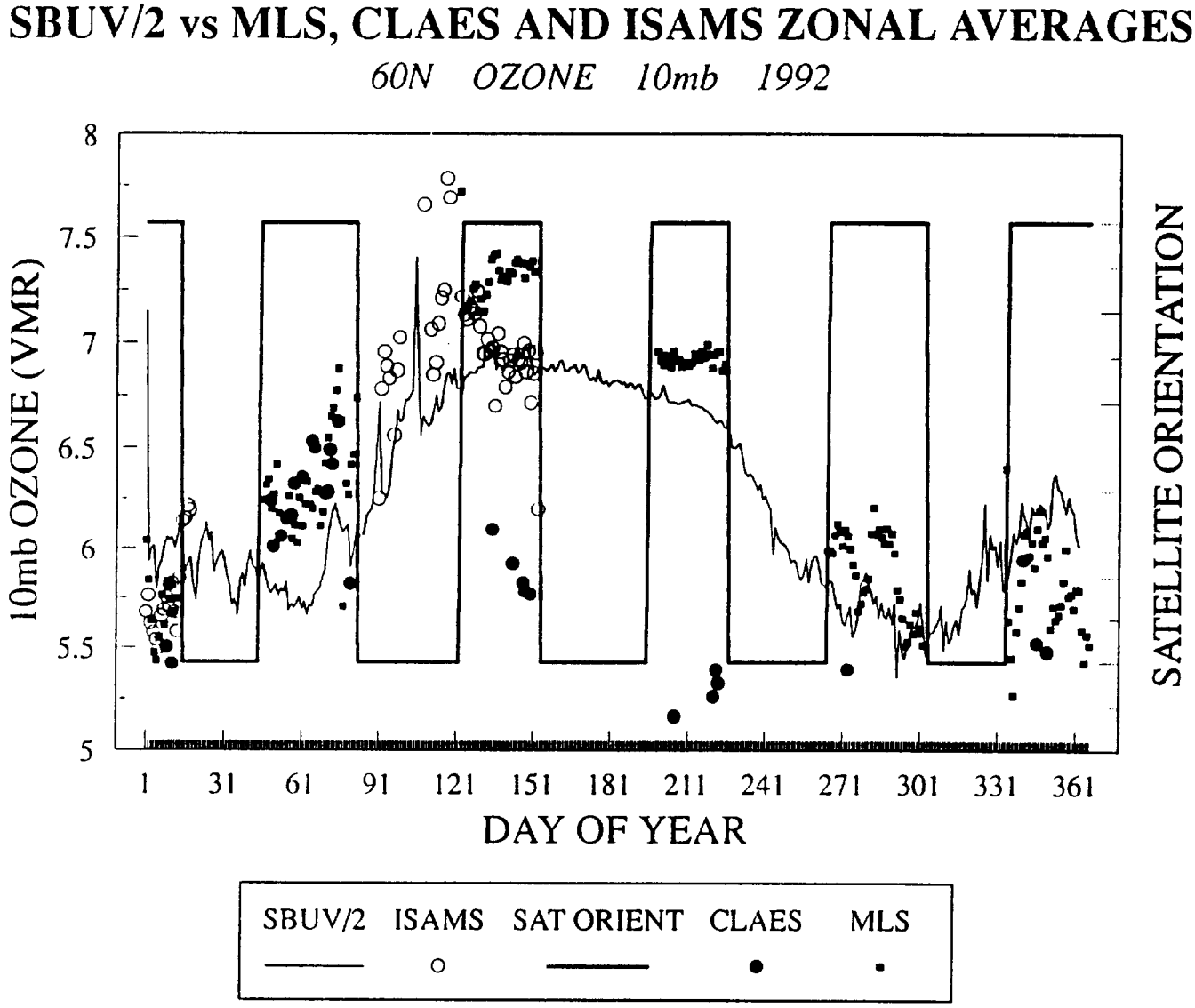

Figure 5.2.4-14 Time series of zonal mean ozone data at 10 mb for SBUV/2, MLS, CLAES, and ISAMS for 1992 at (a) 60N, (b) 30N, (c) Equator, (d) 30S, and (e) 60S.

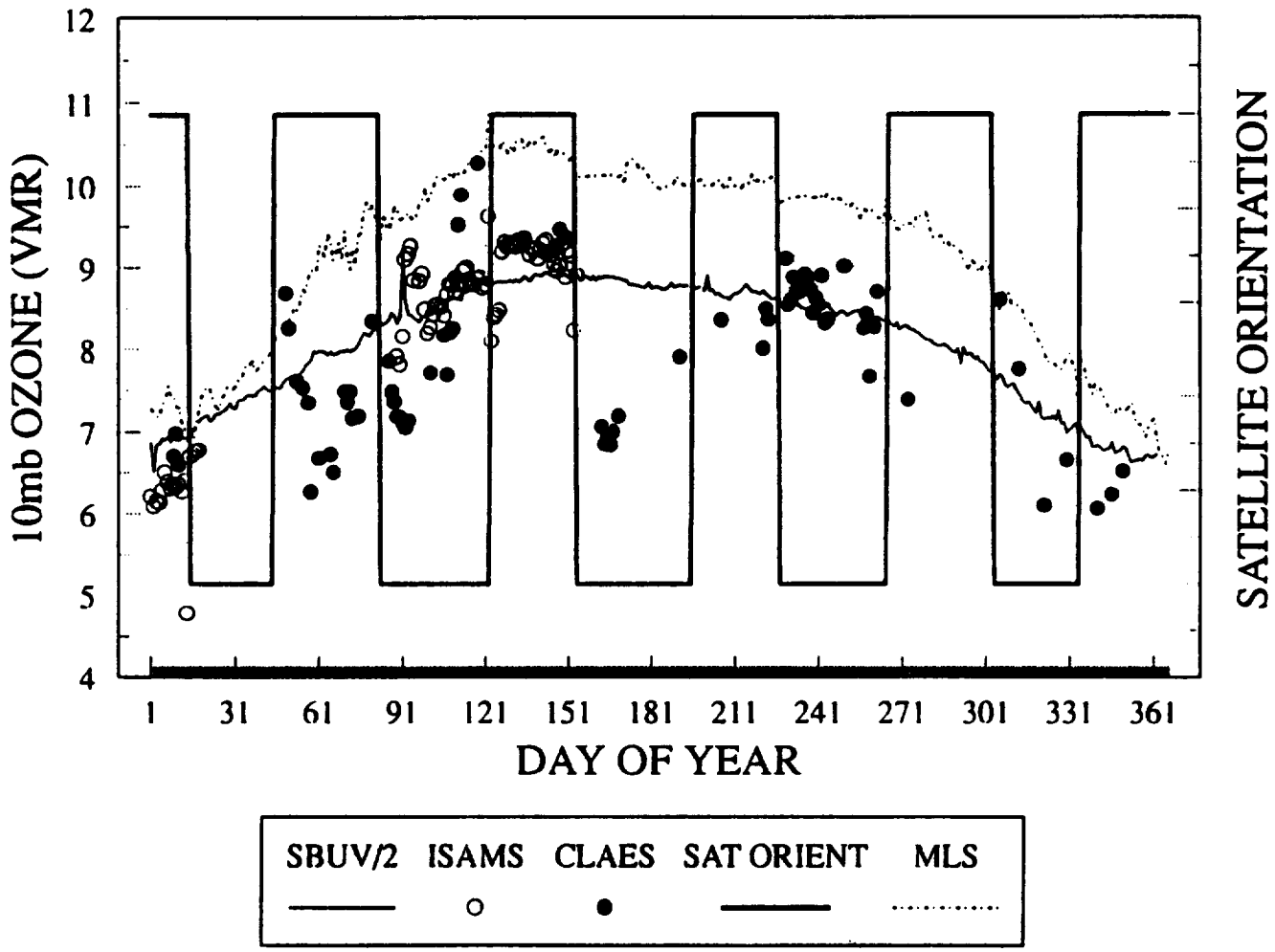

(b)

Figure 5.2.4-14 Continued.

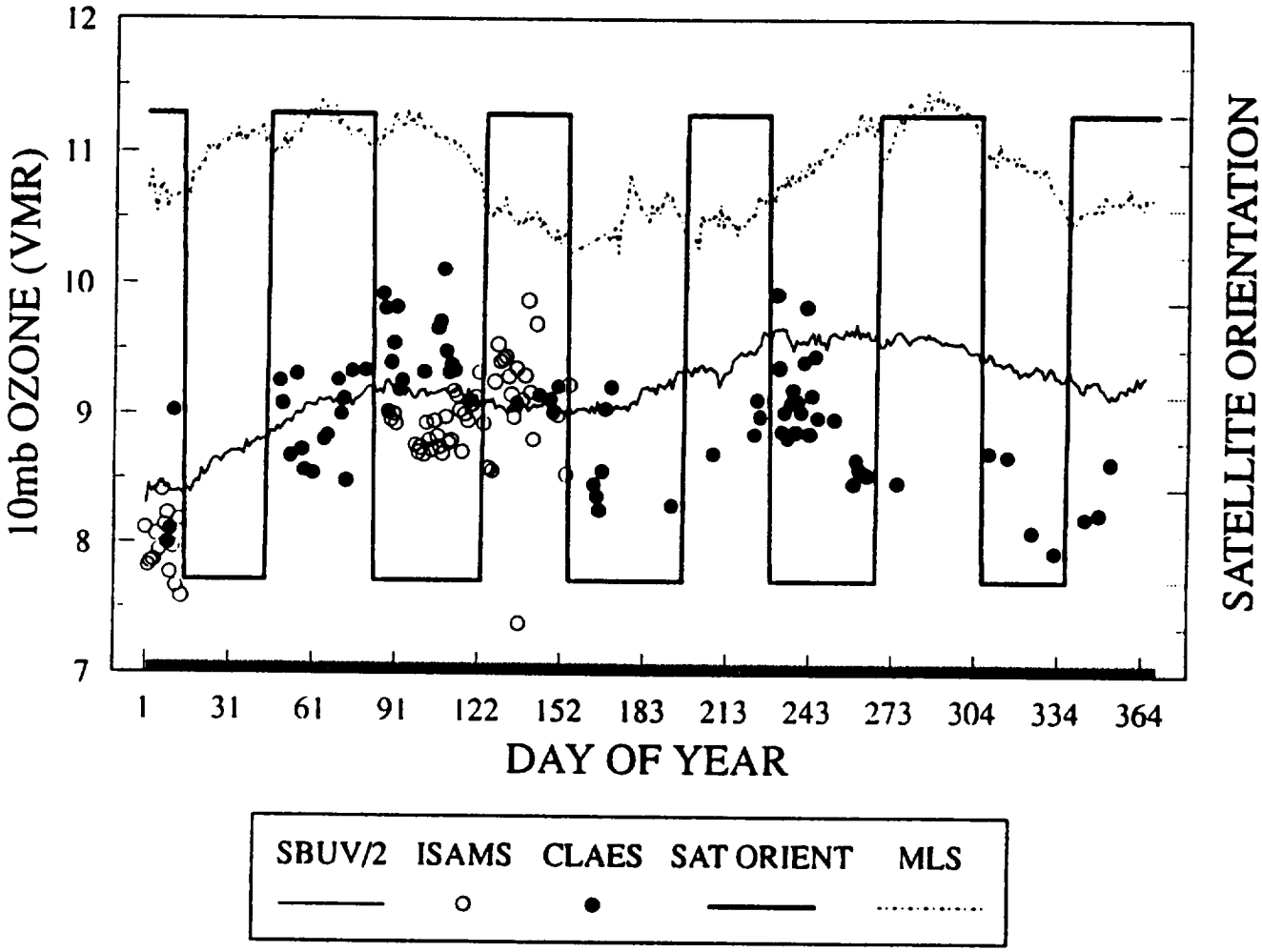

(c)

Figure 5.2.4-14 Continued.

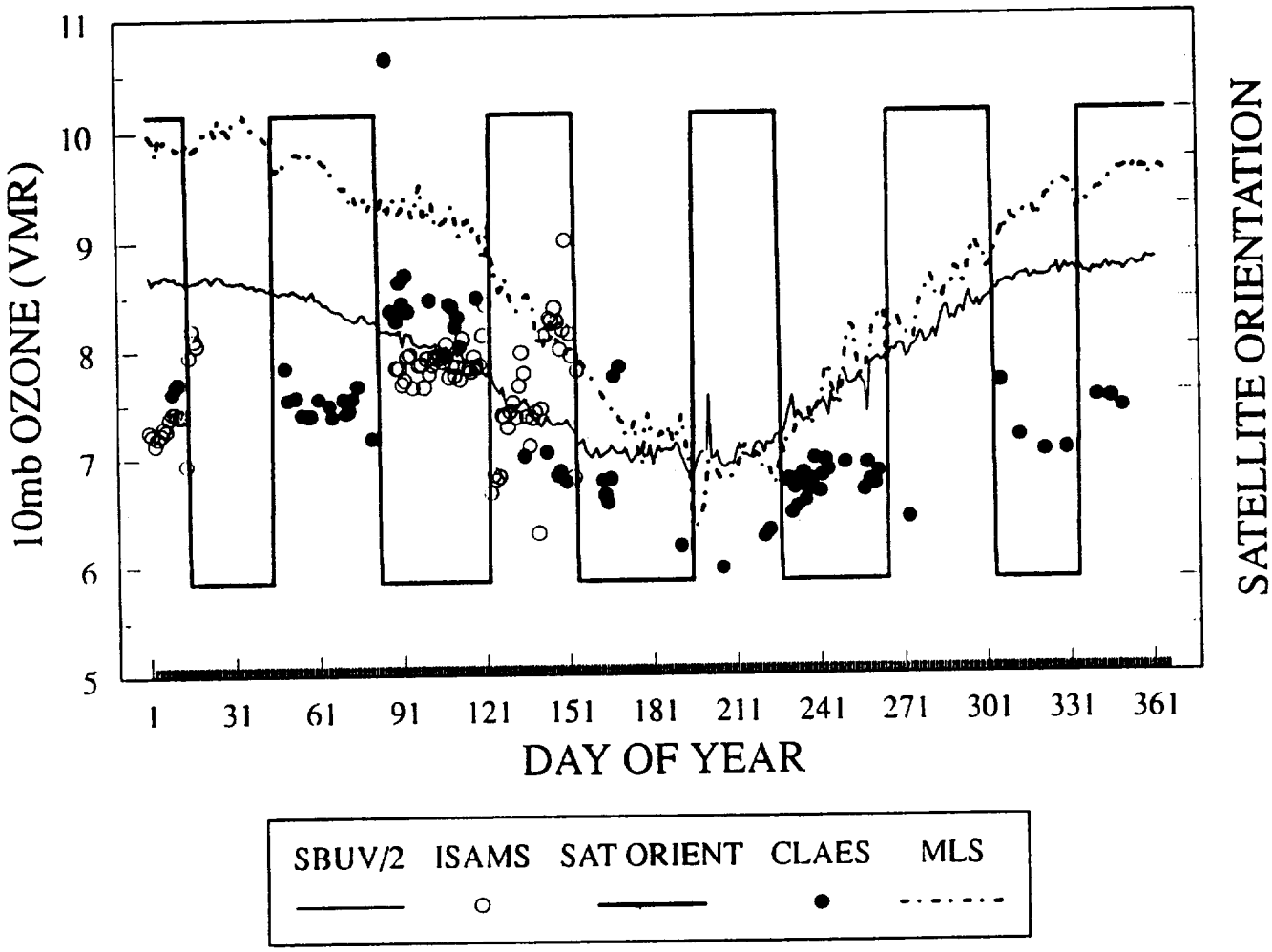

(d)

Figure 5.2.4-14 Continued.

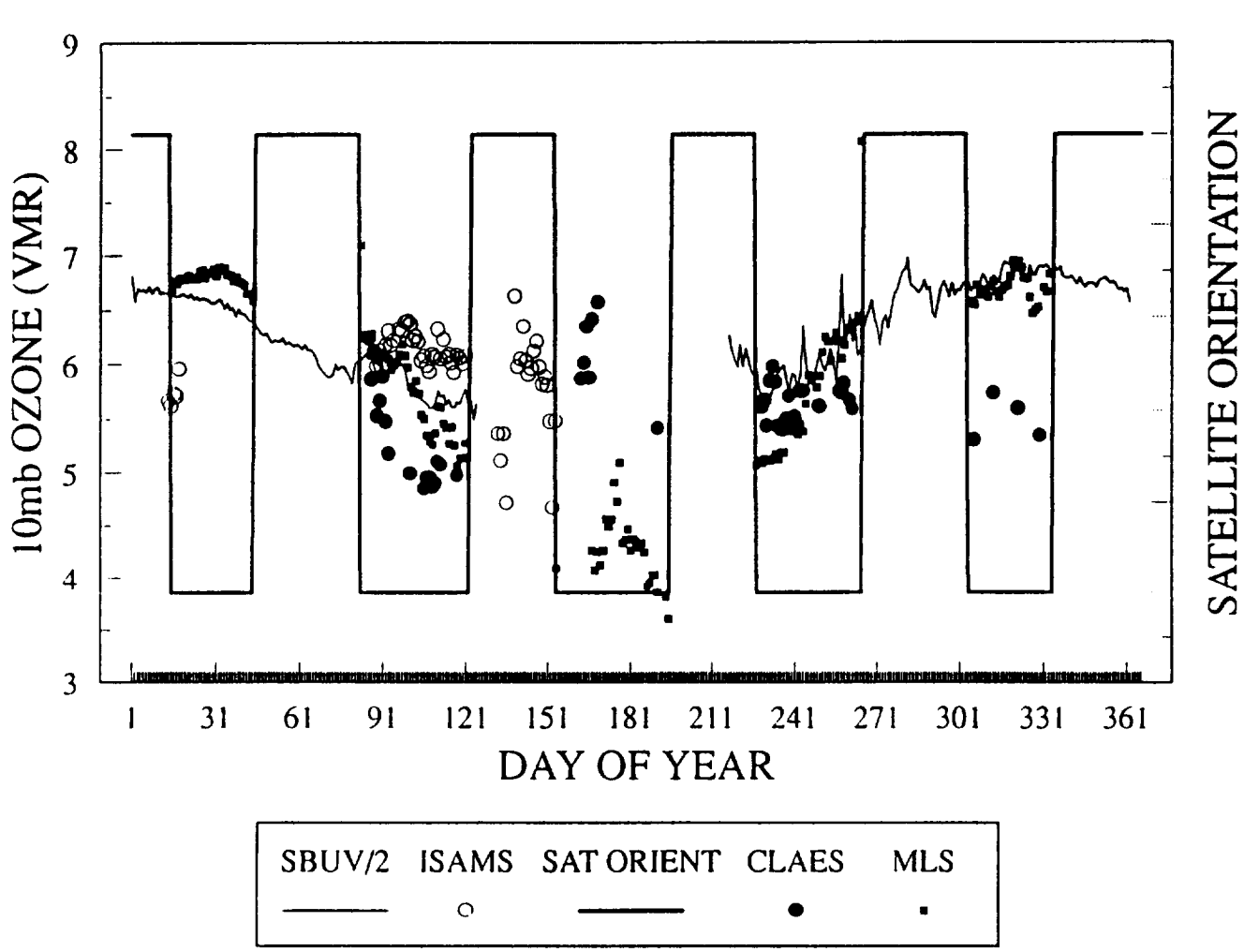

(e)

Figure 5.2.4-14 Concluded.

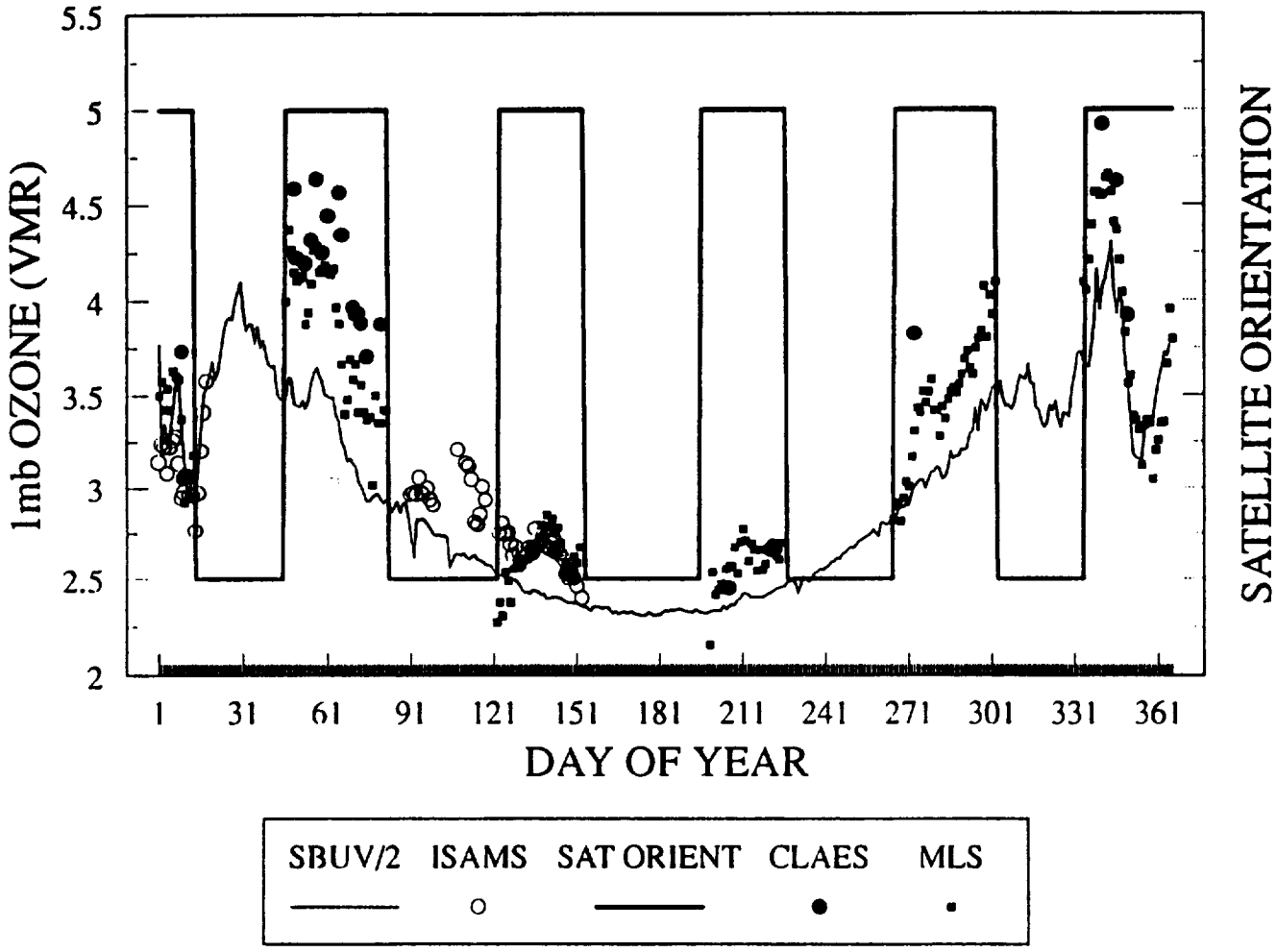

Figure 5.2.4-15 Time series of zonal mean ozone data at 1 mb for SBUV/2, MLS, CLAES, and ISAMS for 1992 at (a) 60N, (b) 30N, (c) Equator, (d) 30S, and (e) 60S.

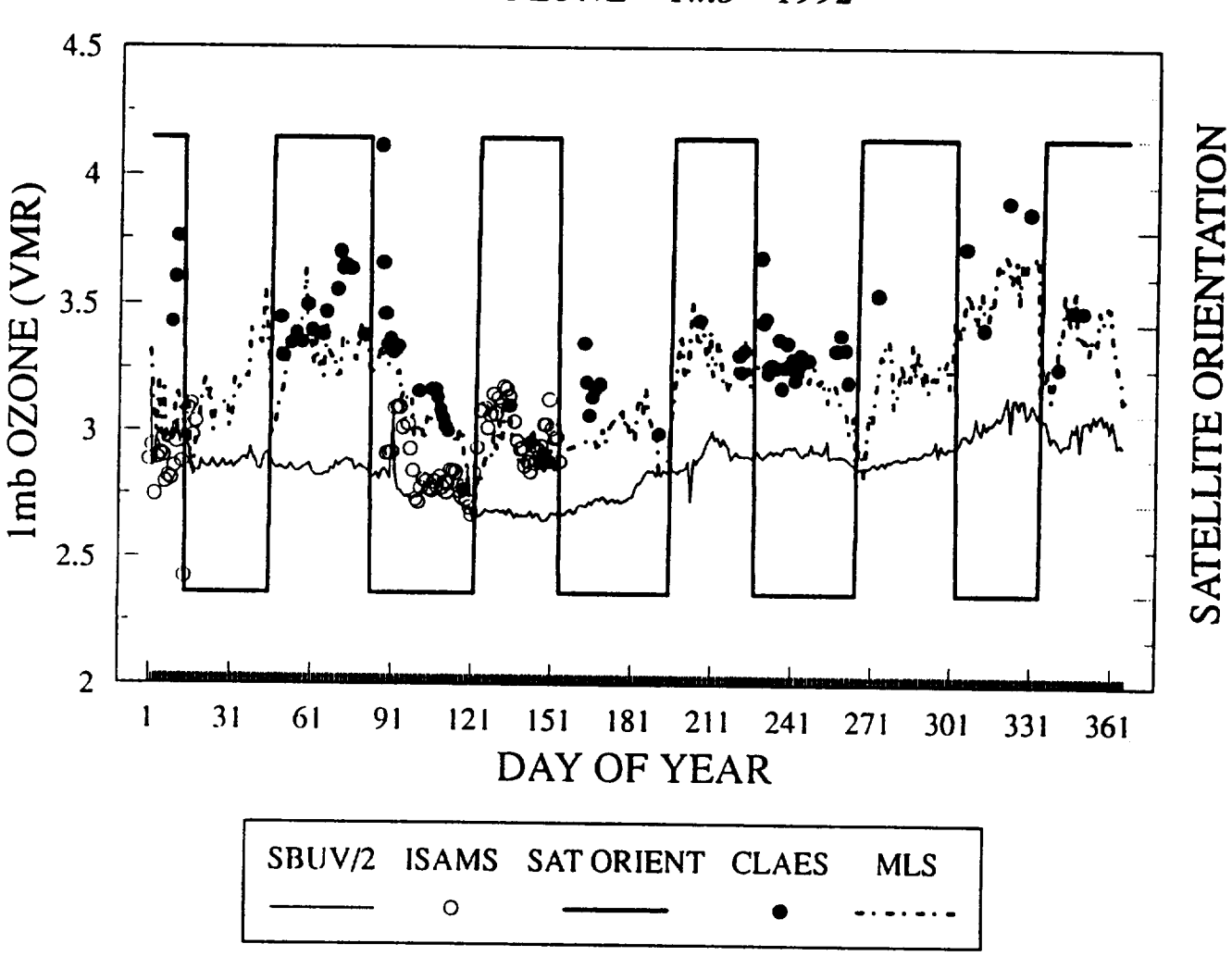

(b)

Figure 5.2.4-15 Continued.

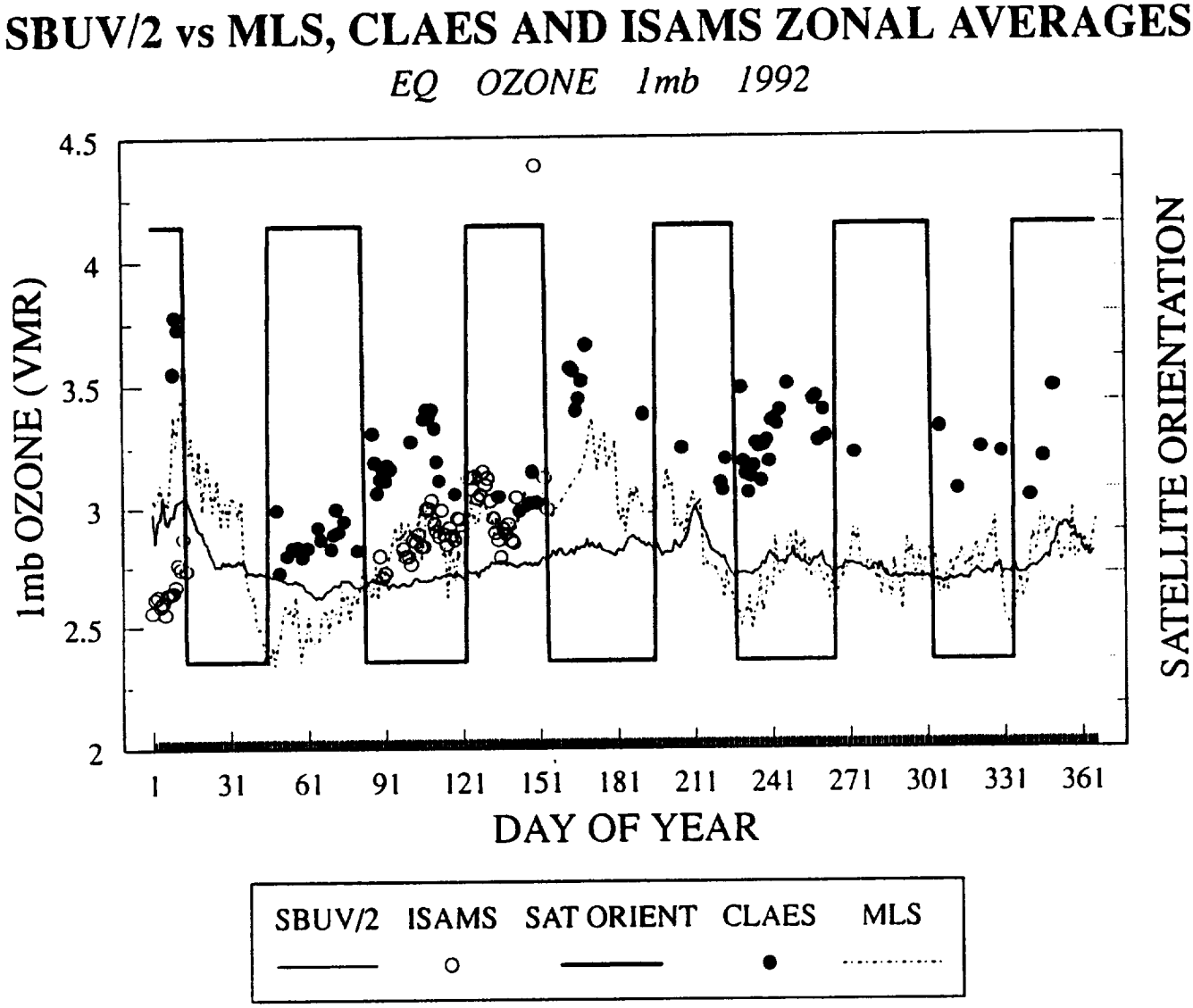

(c)

Figure 5.2.4-15 Continued.

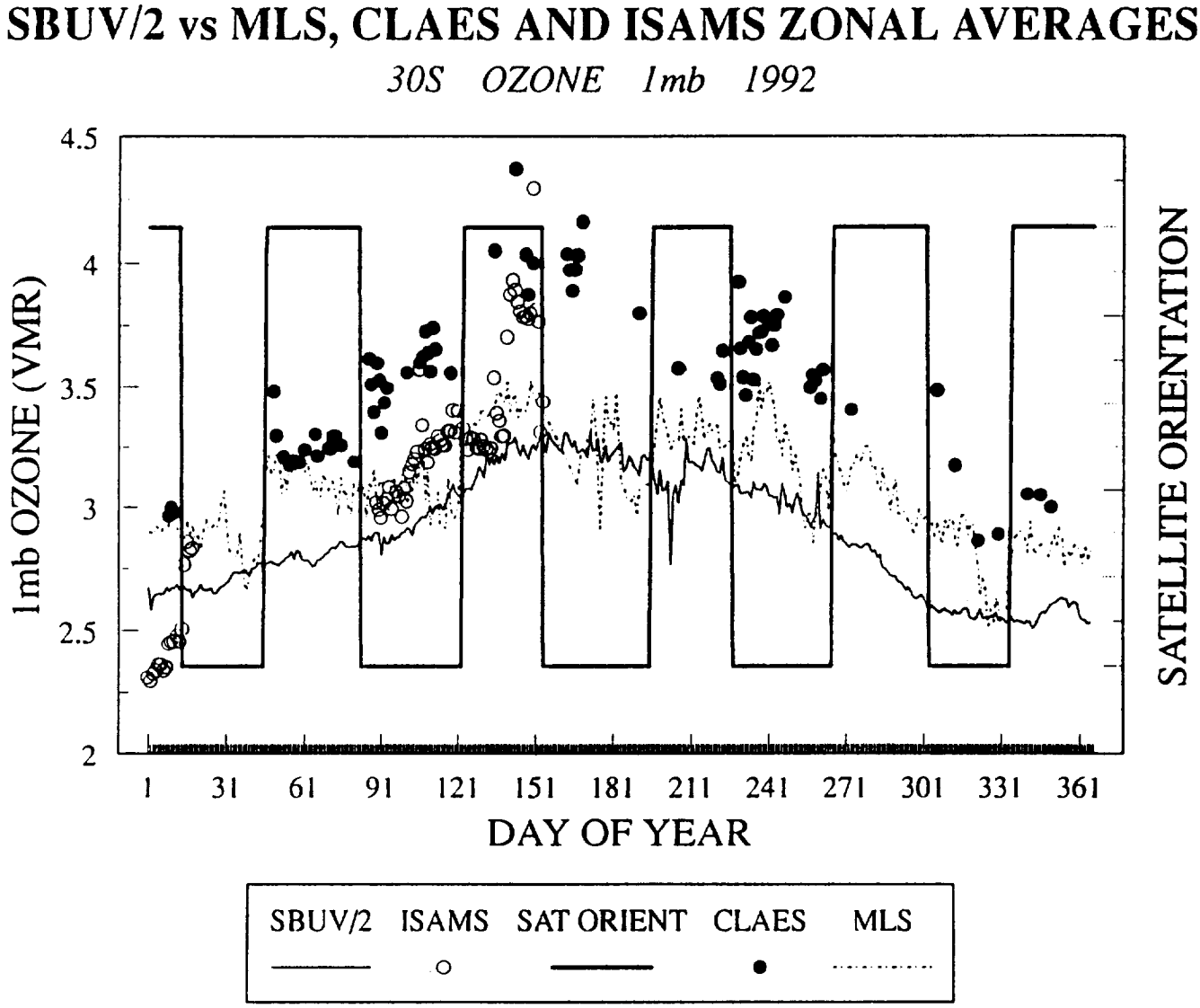

(d)

Figure 5.2.4-15 Continued.

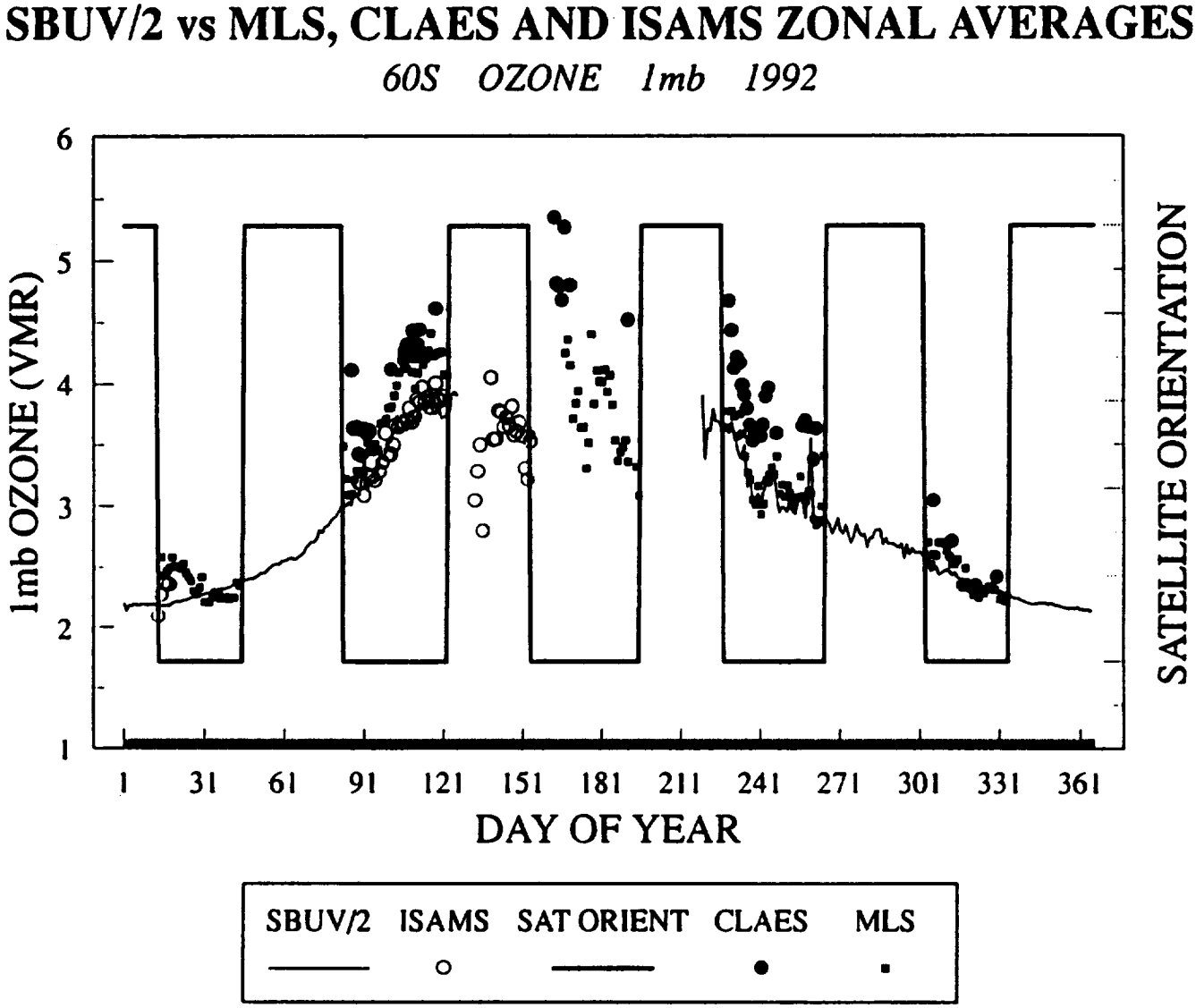

(e)

Figure 5.2.4-15 Concluded.

6. WATER VAPOR

6.1 Data Used in the Comparisons

6.1.1 Correlative Data

At the time of the Validation Workshop held in Atlanta, Georgia in September 1993, there were a series of water vapor correlative measurements data sets in the CDHF. The data sets which were used in these comparisons were those of Samuel Oltmans and David Hofmann of NOAA/Boulder, Richard Bevilacqua of the Naval Research Laboratory, Ira Nolt of NASA Langley, and Wesley Traub of the Smithsonian Astrophysical Observatory.

Oltmans' instrument is a frost point hygrometer carried on a balloon platform. For H_2O measurements, the instrument has an altitude range from the ground to ~28 km with a vertical resolution of 250 m. The accuracy of these measurements is 10%; their precision is 10% in the stratosphere. The Oltmans measurement sites which have been used in this UARS-correlative comparison are: Boulder (40.0N, 255.0E), Daggett (34.4N, 243.0E), Hilo (19.7N, 204.9E), Lauder, New Zealand (45.7S, 168.8E) and McMurdo, Australia (77.5S, 166.4E).

Bevilacqua's instrument is a ground-based water vapor millimeter wave spectrometer. The measurements made by Bevilacqua with this instrument have two altitude ranges: ~55 - ~75 km or ~35 - ~75km. This instrument has a vertical resolution of ~10 km. The total absolute error of these measurements is 15-18% (40-50 km); their precision is 9-10% (40-50 km). The Bevilacqua measurement site is TMO (Table Mountain Observatory), situated at 34.4N, 243.)E. The Bevilacqua data is a daily average. The correlative data provided by Bevilacqua was on a height grid rather than on a pressure grid. Bevilacqua has provided suitable atmospheric profiles to enable one to make the transformation from a height grid to a pressure grid or vice-versa. In future comparisons, it would be useful to take into account the different vertical resolutions of the instruments whose data sets are being compared. For example, the MLS field of view (FOV) is ~4 km, whereas the instrument with which Bevilacqua makes his measurements has a FOV of ~10 km.

The comparison between MLS, ISAMS and CLAES and the correlative data sets from Oltmans' and Bevilacqua's measurements did not concentrate on any particular UARS period due to the irregularity in the days for which correlative data was available. For each comparison day, the UARS instrument profile chosen was the nearest in space to the correlative site. In a few days, data was available from all three UARS instruments.

The Nolt and Traub measurements are from far-infrared spectrometers on balloons launched from Fort Sumner, New Mexico (34.5N, 255.7E). The measurements covered an altitude range from ~20 to 40 km with a vertical resolution of 2-3 km.

6.1.2 UARS Data

The instrument teams estimate that the quality of the UARS H_2O data used in the Atlanta Validation Workshop is as follows. At 46 mb CLAES (version V0006) has a precision of 0.5 ppmv and an accuracy of 30%, MLS (version V0003) has a precision of 0.8--1 ppmv (the higher values being prevalent at high latitudes) and an accuracy of ~15%. At 4.6 mb CLAES has a precision of 0.5 ppmv and an accuracy of 20%. MLS has a precision of 0.4 ppmv and an accuracy of ~ 20%. For an indication of the height range over which the

MLS team recommends its H_2O retrievals, see the section on MLS algorithm status. For ISAMS V0008, the estimated precision is ~20% and the accuracy is ~20% for pressures between 10 and 1 mb. HALOE software version V12 has been used at this Workshop. The total precision and accuracy of this HALOE data set is 5-10% over the pressure range 0.1-100 mb.

For the Atlanta Validation Workshop, ISAMS V0008 nighttime profiles only were used as the ISAMS team believes its daytime H_2O values suffer from non-LTE effects. The MLS H_2O retrieved using version V0003 tends to be ~ 5-10% lower in the stratosphere than that retrieved using versions V0001 and V0002 which were used in the previous validation workshops which were held in 1992 (see the MLS algorithm status section). Because the MLS team feels that its retrieved H_2O data for pressures $p > 46$ mb contains less information than that at pressures $\sim 46 > p > \sim 1$ mb, no MLS H_2O data will be discussed for pressures $p > \sim 46$ mb.

6.1.3 CLAES and ISAMS Day-Night Differences

A difference between the values of water vapor mixing ratio retrieved by CLAES under daylight and nighttime conditions has been observed. It is suspected that this is a result of a solar radiation induced non-LTE emission. A similar situation has been seen by ISAMS, and it is for this reason that only nighttime ISAMS profiles are included in the Level-3 data for this version (V0008). The magnitude of the effect has been characterized by zonally averaging CLAES Level-3AT data for nighttime and daytime conditions. Figure 6.1.3-1 compares mean profiles taken between latitudes 5S and 5N for the period January 9-11, 1992. During this time, the UARS orbit was such that daytime solar zenith angles ranged between 36 and 48 degrees at the CLAES observation points. The daytime mean profile shows enhancements of around 2 ppmv over the nighttime profile in the upper stratosphere. Below 10 mb the differences are much smaller and fall within the variability of the data. Figure 6.1.3-2 shows a similar display for a situation where the UARS orbit allowed CLAES observations to be made at large daytime solar zenith angles. In this case, the daytime and nighttime mean profiles are much closer together and resemble the nighttime mean in Figure 6.1.3-1. Calculations carried out for a range of daytime solar zenith angle conditions are summarized in Figure 6.1.3-3. Here the difference between the daytime and nighttime profiles at the 1.5 mb level are plotted against daytime solar zenith angle. The largest day/night water vapor differences are seen to be correlated with the greatest solar illumination as would be expected from a non-LTE emission. Future versions of the CLAES retrieval software may attempt to correct for this effect. However, users of Version V0006 CLAES water vapor data should not mix daytime and nighttime profiles in data applications at altitudes above 10 mb. At these higher altitudes, the nighttime profiles are expected to be a more reliable indicator of temporal and spatial variability in water vapor.

6.1.4 CLAES Version V0006/Version V0005 Differences

Under the current data release plan, it may be possible that not all of the CLAES data will be processed with the Version V0006 algorithm by the time the data are available to the public. If some of the data released are Version V0005, it may be useful to know how Version V0005 and Version V0006 differ. Figure 6.1.4-1 shows the altitude profile of the mean difference between Versions V0006 and V0005 H_2O profiles for all observations

made between 20N and 50N on January 9, 1992. The horizontal bars represent standard deviations. For altitudes above 100 mb, the newer version predicts about 5% more water vapor than the Version V0005. For altitudes below 100 mb, the H_2O mixing ratio in the newer version has increased by as much as 30%.

6.2 Comparison Results

6.2.1 Profiles

6.2.1.1 UARS Instruments

Vertical profile comparisons were carried out between the UARS instruments MLS, HALOE, ISAMS and CLAES for the UARS day periods: 120-122 (January 9-11); 217-219 (April 15-17); 220-222 (April 18-20); 332-335 (August 8-11); 349-351 (August 25-27); and 352-354 (August 28-30). Approximately 45 HALOE emission sounder coincidences were found in each of the 6 periods using coincidence criteria of 2 degrees in latitude, 10 degrees in longitude, and 12 hours time difference. Mean profiles were calculated for each UARS day period for each instrument and the mean difference and root mean squares (rms) difference profiles were computed. These computations show the following:

- In general, CLAES (which here include both daytime and nighttime measurements) and HALOE agree to within 5% from 68 mb up to the 10 mb level. Above 1 mb, CLAES values are lower than those of HALOE by ~0-15% (see Figure 6.2.1-1). This pattern holds true for the January 9-11 period as well. For the April and August 8-11 periods, CLAES values are even lower than HALOE values below the 2 mb level (as much as 25%, but typically 5-15%).

- MLS tends to overestimate HALOE by 10-25% (0.5 to slightly more than 1 ppmv) over the 46 mb to ~0.2 mb range, with the better agreement occurring in the 50 to 10 mb region (see Figure 6.2.1-2). This behavior is true of all three August periods and for the January period as well. The April periods show greater differences which reach 20% difference around 25 mb (MLS higher).

- The April comparison shows that ISAMS measurements tend to be larger than those of HALOE by 18-35% (0.8 to 2 ppmv) over the 0.1 to 10 mb range of the profiles, with the better agreement occurring from ~3-8 mb (see Figure 6.2.1-3). The January differences possess similar profile shapes with ISAMS values higher than those of HALOE by 5% at 10 mb increasing to 40% at 0.1 mb.

In summary, between 10 and 46 mb MLS, CLAES and HALOE sensors all show agreement within approximately 10% with MLS values being the largest, and ISAMS values still suffer from aerosol contamination which is preventing retrievals near 10 mb in the tropics. Above 10 mb, the differences between the UARS water vapor retrievals widen with ISAMS giving the largest values followed in order by MLS, HALOE and CLAES.

6.2.1.2 Comparisons against Bevilacqua

A sample profile comparison is shown for April 18, 1992 in Figure 6.2.1-4. On this day, MLS agrees well with Bevilacqua (both ascending and descending orbit modes), ISAMS

tends to overestimate the Bevilacqua data, and CLAES retrievals underestimates the Bevilacqua measurements. While the CLAES differences shown in this comparison seem to be typical of CLAES nighttime retrievals, the agreement for MLS seems to be unusually good in this case.

Time series of MLS and Bevilacqua data close to the stratopause (0.46 mb), together with some CLAES and ISAMS measurements are shown in Figure 6.2.1-6 (Figure 6.2.1-5 contains coincidence information for these comparisons). The MLS and Bevilacqua data seem to track each other well, and the differences at this level are often roughly within the MLS error bars (the precision at the one sigma level), which are ~10%. These differences are also roughly within the standard deviation of the MLS data at this site which suggests that the differences might be mostly explained by atmospheric variability. However on the average, the MLS values exceed the Bevilacqua values by approximately 9% at this level. For pressures > 0.5 mb (the lower end of the range of Bevilacqua's measurements), where it is understood that Bevilacqua's data have higher absolute errors, the agreement is less good, with MLS values exceeding those of Bevilacqua by -1 ppmv (~15%). From 2 to 0.5 mb, the MLS time series at the TMO correlative site does not exhibit any significant ascending/descending mode differences, indicating that, as expected, MLS H_2O is showing little diurnal variation at these levels.

Throughout the upper stratosphere and lower mesosphere (2-0.5 mb), ISAMS tends to overestimate the Bevilacqua data set by approximately 1.5 ppmv (approximately 25%).

The mean difference between CLAES (v0006) and Bevilacqua data after January 9, 1992, has also been calculated. In this statistical comparison, level 3AT H_2O profiles were identified in the vicinity of the ground based sounder, and differences between the measurements from CLAES and the microwave were computed at the standard UARS pressure grid points. The mean differences and standard deviation of differences were computed as a function of pressure for coincidences of CLAES which were within 4 degrees of latitude, 20 degrees of longitude and 12 hours of the ground based measurements. These large windows were required to obtain a sufficient number of coincidences. Daytime and nighttime CLAES profiles were considered separately. The mean differences for CLAES compared to Bevilacqua's measurements are shown in Figure 6.2.1-8. The CLAES nighttime profiles very between 10 to 30% lower than the microwave measurements at all altitudes. The daytime profiles are ~20% higher below 1 mb and as much as 15% lower above 1 mb. The horizontal bars indicate the standard deviation of the differences. With such large windows, the standard deviations reflect a large component at atmospheric variability in addition to instrumental uncertainty.

Comparisons between HALOE and ground based microwave data from Bevilacqua were performed for a set of 18 profile pairs. The mean profiles, the mean difference profiles, and the RMS difference profiles were calculated (Figure 6.2.1-8). Excellent agreement in the mean profiles is obtained over the entire range from 5 mb to 0.03 mb. The largest negative mean difference of 12% (microwave smaller) occurred at 3 mb, and the largest positive difference (microwave 3% greater) occurred at 0.2 mb. This comparison is a considerable improvement over the comparison shown in the previous workshop report, and the differences are now well within estimated error limits.

6.2.1.3 Comparisons against Oltmans

MLS, HALOE and CLAES measurements all show excellent agreement (within 10% in the

mean) with Oltmans' frost point hygrometer measurements. A sample comparison is shown in Figure 6.2.1-9. Time series of MLS H_2O data and Oltmans' data at Boulder, Colorado, show very good agreement at 22 mb (within the MLS error bars, which are ~10% ; see Figures 6.2.1-10 to 6.2.1-12) and at 46 mb (within the MLS error bars, which are ~15-20%). The differences between the MLS H_2O and Oltmans data tend to be less than the standard deviation of the MLS H_2O data, indicating that these differences can be ascribed to atmospheric variability. The MLS H_2O Boulder time series exhibits little difference between its ascending and descending orbit modes, indicating that, as expected, MLS H_2O is showing little diurnal variation. Similar time series for MLS H_2O at Mauna Loa (Hawaii) provide evidence that there is little seasonal and diurnal variation in the tropical lower stratosphere (not shown). The differences between retrieved CLAES H_2O and Oltmans' data (see Figure 6.2.1-11 to 6.2.1-12) also are in general within the CLAES error bars, which are ~15% in the lower stratosphere.

The HALOE comparisons against Oltmans' data are based on 13 events which were used to calculate mean profiles and statistics (Figure 6.2.1-13). These 13 profiles were from various measurement sites including Boulder, Colorado, Lauder, New Zealand, Daggett, California and McMurdo, Antarctica. Agreement is very good from 15 mb down to about 120 mb with differences less than 10%. Below ~120 mb, differences increase to 40%. The profile shapes agree well. RMS differences are less than 20% from 15 mb to 80 mb.

6.2.1.4 Comparisons against Balloon Measurements

Figure 6.2.1-14 shows a single profile comparison from Traub's measurements compared to the 4 UARS instruments. The balloon measurement gives slightly larger values than all the UARS measurements above 40 mb. Two other FIRS balloon measurements for September 29, 1992 and March 24, 1993 also indicate higher H_2O values than HALOE measurements. The reasons for these discrepancies are not known.

A HALOE comparison profile on May 7, 1992 against the far infrared measurement made by Nolt et al. on May 4, 1992 (Figure 6.2.1-15), shows remarkable agreement over the full altitude range of the comparison. The maximum difference over the entire profile is less than 0.5 ppmv.

6.2.2 UARS Cross-Section Comparisons

Water vapor pressure versus longitude cross-sections were compared for CLAES, MLS and HALOE for the January and April periods. Differences between paired observations were plotted and analyzed on a pressure versus longitude grid. We include here examples at ~39N for CLAES, MLS and HALOE for the early August period; and ~47N for ISAMS in the January period. The patterns showed virtually identical differences as those indicated by the profile comparisons for these same periods (section 6.2.1-1). The HALOE, CLAES (Figure 6.2.2-1) and MLS (Figure 6.2.2-2) differences are seen to be relatively independent of longitude, but the ISAMS (Figure 6.2.2-3) differences show more longitudinal variability, particularly at 10 mb.

A comparison of zonal mean cross-sections for MLS, ISAMS and CLAES for January 9, 1992, is shown in Figure 6.2.2-4 to -6 with percentage differences relative to MLS being shown in Figure 6.2.2-7 and -8. The general impressions/conclusions are as follows:

- Both MLS and CLAES show minimum concentrations in the expected location, i.e. the cold region above the tropical tropopause. However, MLS concentrations are 30-50% larger than CLAES values there.

- Both MLS and CLAES tropical values increase with height from this level up to above the 1 mb level, but with MLS values being approximately 20% larger than CLAES values.

- ISAMS tropical values at 10 mb, on the other hand, seem obviously contaminated by aerosol effects. Above 4.6 mb, they increase with altitude to 10% larger values than those of MLS at 0.32 mb. Above that altitude, ISAMS and CLAES values tend to decrease, but MLS values continue to increase (in the tropics).

- The latitudinal structure of all three sets of measurements is relatively similar and is basically consistent with upwelling in the tropics and photochemical production of H_2O from CH_4 and downwelling at high latitudes, except for CLAES values poleward of 60^oN at altitudes below approximately 10 mb. The CLAES retrievals there may be affected by the cold temperatures in that region at this time of year. As a result, the CLAES H_2O latitudinal gradient in the lower stratosphere is much steeper than the MLS gradient there (a similar result was found in the August comparison), and the apparent agreement between MLS and CLAES and the frost point hygrometer measurements seems to be coincidental in that these Oltmans' comparisons were made at mid-latitudes, where MLS and CLAES give similar values.

- In general, MLS and ISAMS zonal means are within ~10-20% in the range 5-0.5 mb. Differences between MLS and CLAES zonal means can be as high as ~50% in the tropics (CLAES lower) and ~50-100% at high latitudes (CLAES higher) (see Figure 6.2.2-7 and 6.2.2-8).

A comparison between MLS, the Limb Infrared Monitor of the Stratosphere (LIMS) and the Stratospheric Aerosol and Gas Experiment (SAGE) II monthly zonal means for the month of May (MLS: 1992; LIMS: 1979; SAGE II: 1988) reveals than, in general, the MLS and SAGE II values are higher than those from LIMS (not shown). However, the fields show similar features such as a hygropause and the "expected" transport circulation involving the injection of freeze-dried air into the stratosphere through the tropical tropopause and transport from the tropics to the poles, although LIMS shows a dry "tongue" extending to the winter pole which is not seen by MLS or SAGE II. Such a discrepancy may be due to the phase of the quasi-biennial oscillation (QBO) being different in 1979 from that in 1988 or 1992.

6.2.3 H_2O Maps

In general, water vapor maps for ISAMS and MLS from 46 to 1 mb show the feature associated with the just discussed zonal mean transport circulation. For example, the maps show an increase of H_2O in going from the tropics toward the poles (Figure 6.2.3-1 and -2). Furthermore, the MLS map at 46 mb for UARS day 350 (August 26, 1992), which is representative of the SH winter, shows evidence of dehydration (values < 2.5 ppmv) likely to be associated with the low temperatures prevalent (not shown). However, one must stress that at this pressure level and these high latitudes, the MLS H_2O retrieval does have a substantial contribution from the "a priori" input. The ISAMS fields, however, exhibit

what appear to be unrealistically high data spikes (values > 8 ppmv at 10 mb in January, compared to MLS values ~6.5 ppmv) at high latitudes (see Figure 6.2.3-1). The ISAMS maps also show evidence of aerosol contamination at 10 mb where, at the tropics, ISAMS H_2O mixing ratios can exceed 6 ppmv (compared to ~4.5 ppmv for MLS) (see Figure 6.2.3-1).

The morphology of the CLAES maps at the same pressure levels appears to be less consistent with such a transport picture (see Figures 6.2.3-1 and 6.2.3-2), although one must remember that these CLAES maps are a daily average and hence mix daytime and nighttime values which are known to differ significantly in the upper stratosphere (see prior comments on day-night differences for CLAES V0006 H_2O). CLAES H_2O values tend to underestimate MLS and ISAMS in the tropics, with the CLAES H_2O values perhaps being unrealistically low at 10 mb (values less than 3.5 ppmv in January, compared to MLS values ~4.5 ppmv) (see Figure 6.2.3-1). At high latitudes, CLAES overestimates MLS and ISAMS and, especially in wintertime, the CLAES H_2O values appear to be unphysically high (values > 8 ppmv at 22 mb in January, compared to MLS values ~6.5 ppmv).

A comparison between the MLS H_2O fields for January 9, 1992 (NH winter) at 22 and 10 mb with fields of CLAES N_2O and isentropic potential vorticity (PV), derived from UK Meteorological Office (UKMO) temperature and winds, shows that the MLS H_2O distribution is consistent with the dynamical features associated with the stratospheric polar vortex. Similar consistency is found in the MLS H_2O fields for August 26, 1992 (SH winter). The ISAMS fields on January 9, 1992 are less consistent with this dynamical picture; in particular, the above-mentioned high data spikes must be ignored in order to get qualitative agreement with the N_2O and isentropic PV fields. The CLAES H_2O fields do not appear to show much consistency with this dynamical picture.

6.2.4 Time Tracks

Examination of time tracks for CLAES, ISAMS and MLS at Level 3AT at constant pressure levels support conclusions regarding differences between the instruments seen in zonal mean cross-section comparisons. Examples shown are CLAES, ISAMS and MLS at 10 mb for January 9 and April 16, 1992, in Figure 6.2.4-1. The differences between CLAES and ISAMS, along with estimated errors for the instruments, are shown in Figure 6.2.4-2. The straight line segments in the ISAMS curves span daytime parts of the orbit where no ISAMS data are reported. All instruments show a latitudinal gradient with CLAES showing the greatest contrast between the tropical and the polar conditions. CLAES shows unrealistically large mixing ratios in winter polar situations corresponding to cold temperatures (however, some improvement in this behavior has been made over CLAES Version V0005). The large mixing ratio values in cold polar regions are accompanied by large uncertainty estimates as shown in curves 2 and 3 in Figure 6.2.4-2. Users of the water vapor data from UARS instruments are reminded that data quality values for a particular measurement should always be checked to determine if the measurement is appropriate for a particular application. Figure 6.2.4-2 also shows the differences between CLAES and ISAMS are fairly consistent with the quality or error estimates. This situation represents an improvement over earlier versions of the retrievals.

The CLAES/MLS time tracks in Figure 6.2.4-3 show reasonably good correlation of major

features. Again, the CLAES data show some spikes in the cold polar regions which probably indicates that further refinement of the calibration/retrieval software is necessary. Figure 6.2.4-4 indicates that CLAES-MLS differences are generally largest where the CLAES data are shown to have the largest uncertainties as represented by the quality indicators.

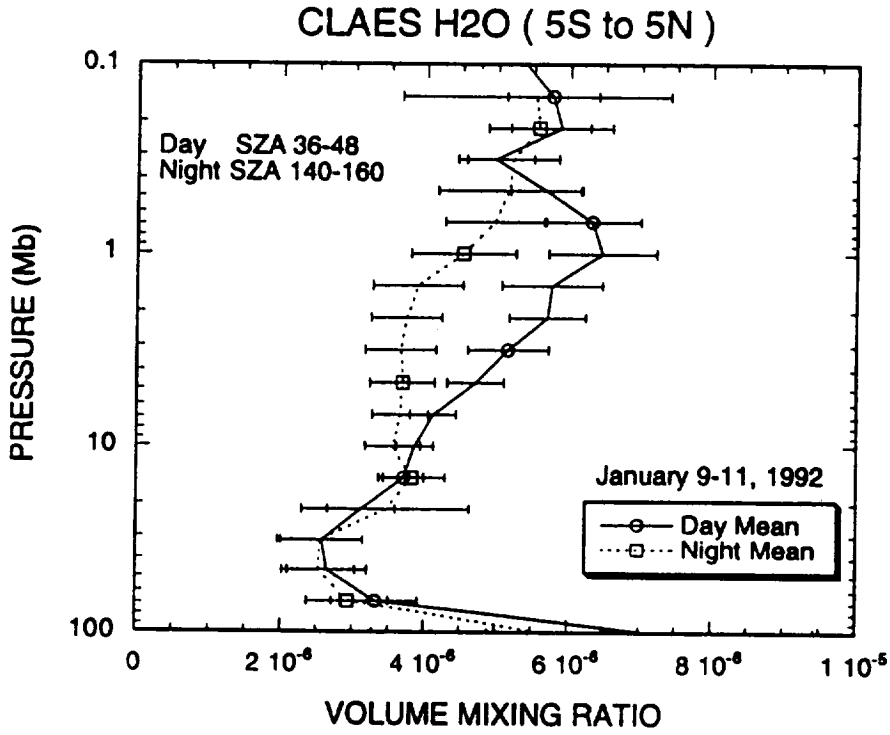

Figure 6.1.3-1 Mean nighttime and daytime CLAES level 3AT profiles data for Jan. 9-11, 1992, showing day-night differences in the retrieved water mixing ratio for high sun conditions.

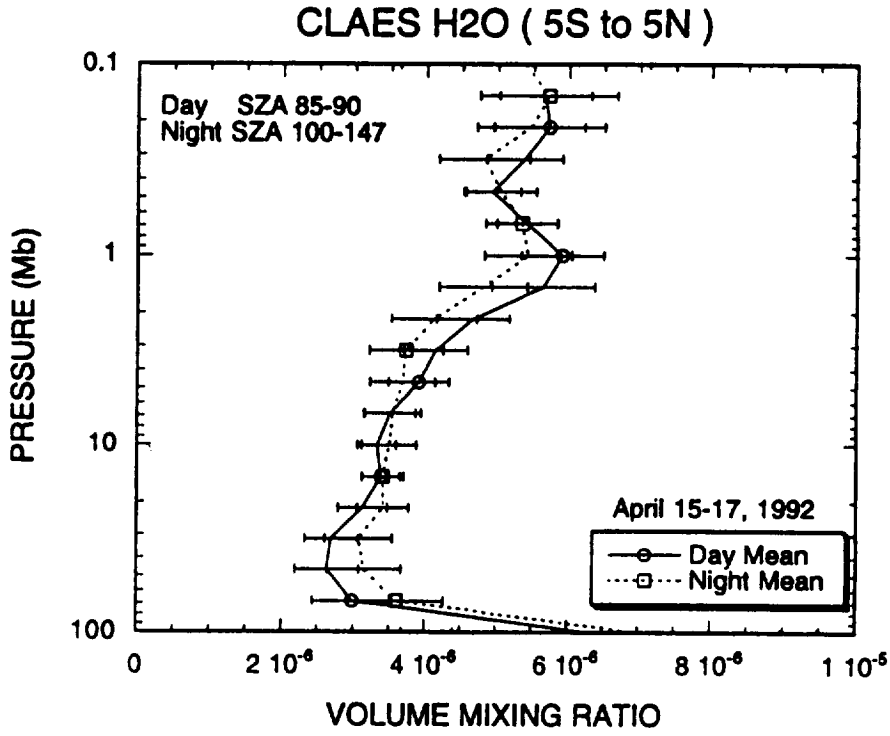

Figure 6.1.3-2 Mean nighttime and daytime CLAES level 3AT profiles data for April 15-17, 1992, showing day-night differences in the retrieved water mixing ratio for low sun conditions.

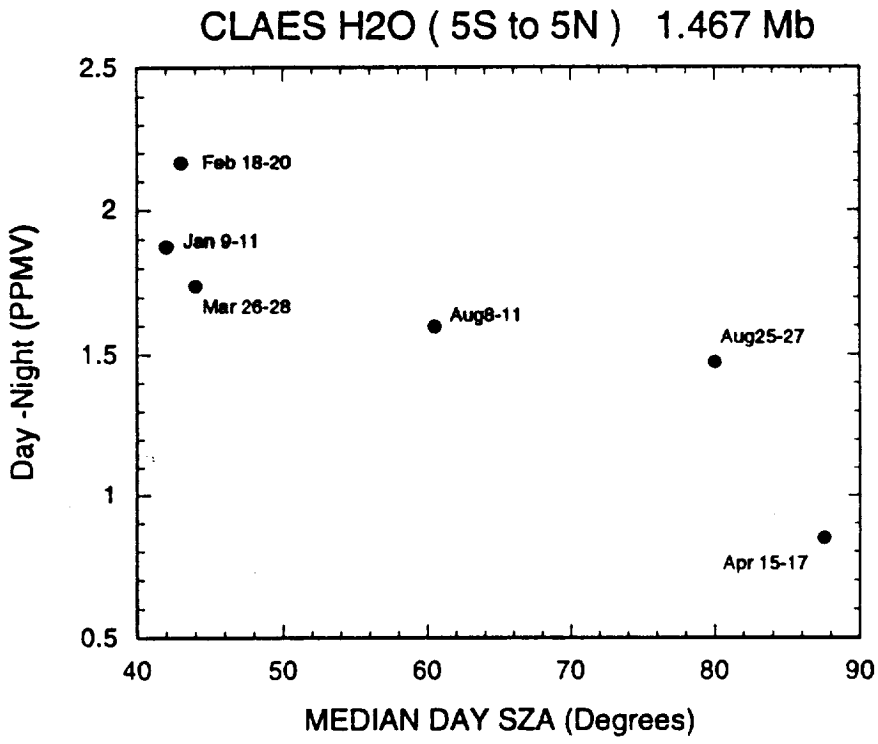

Figure 6.1.3-3 Mean day-night differences in CLAES retrieved water mixing ratio at 1.467 mb as a function of daytime solar zenith angle.

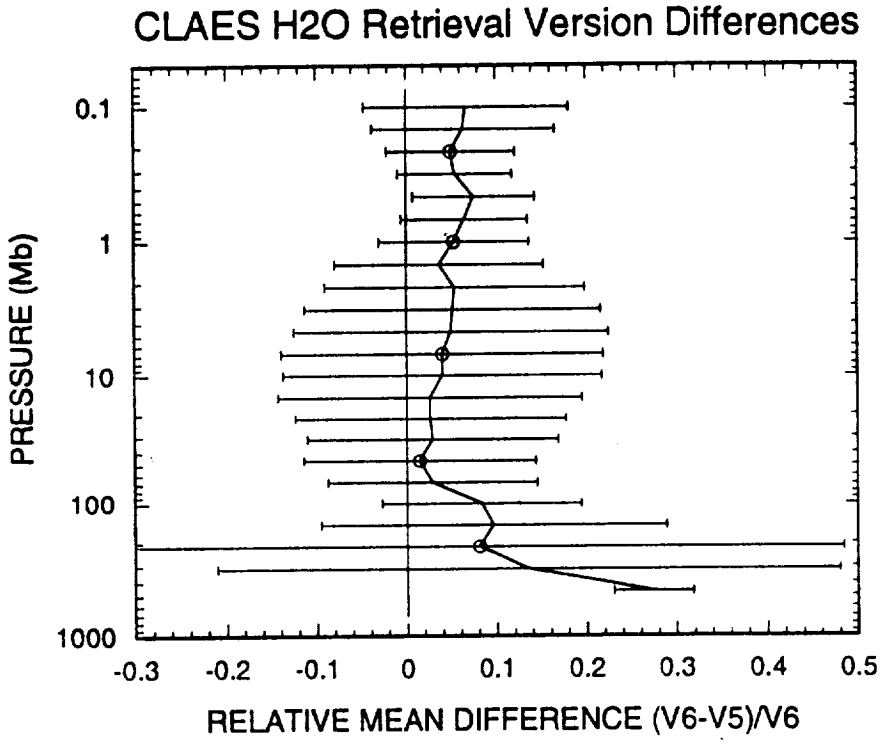

Figure 6.1.4-1 Differences between CLAES water vapor retrievals (Version V0006 - Version V0005) averaged over latitudes 20-50 degrees for Jan. 9-11, 1992. Differences have been expressed as a ratio of the Version V0005 mixing ratios.

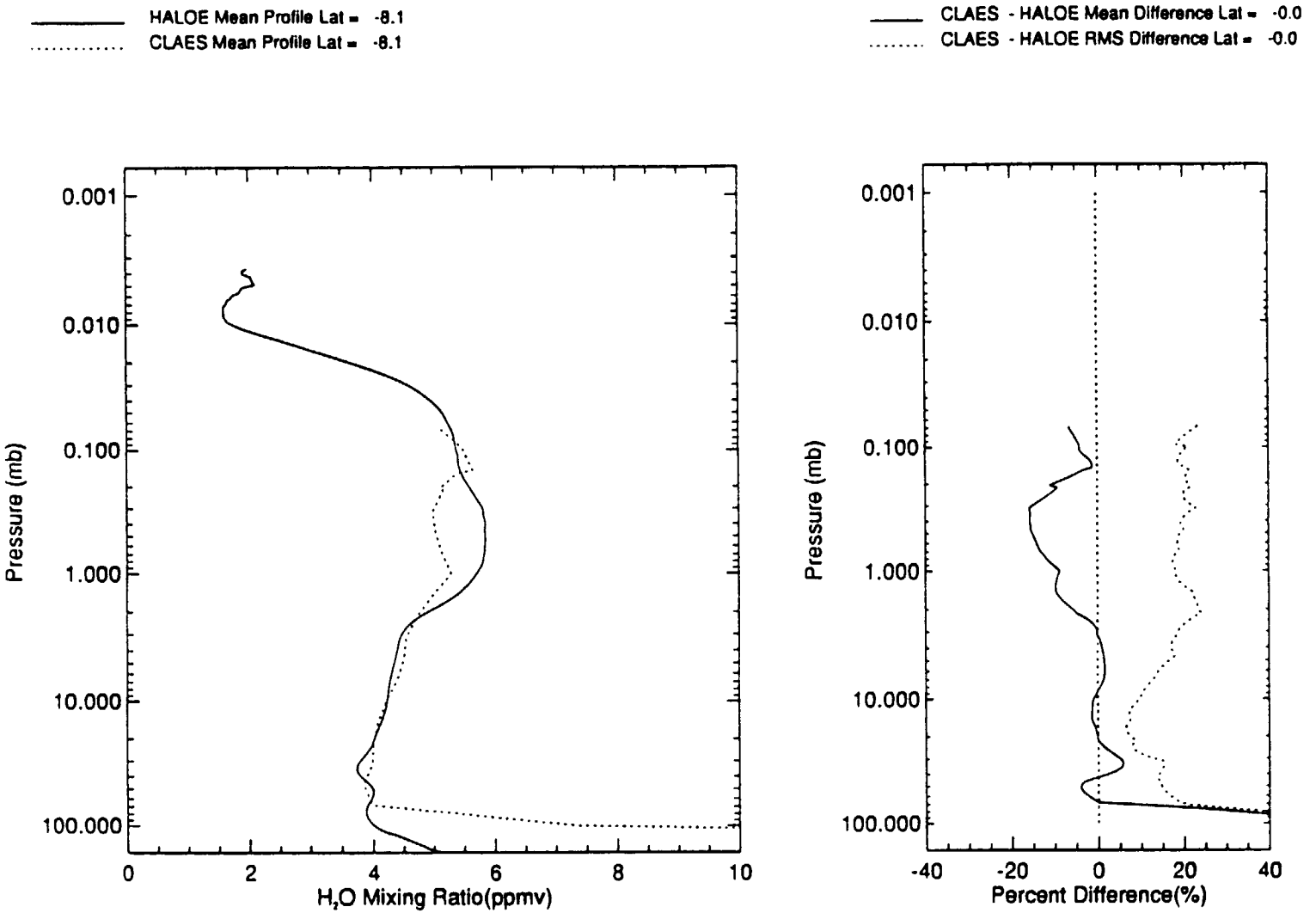

Figure 6.2.1-1 Profile comparison between HALOE and CLAES H_2O for the period Aug. 25-30. The left hand panel shows the average profiles for the period. The right panel shows the mean and rms differences between the profiles.

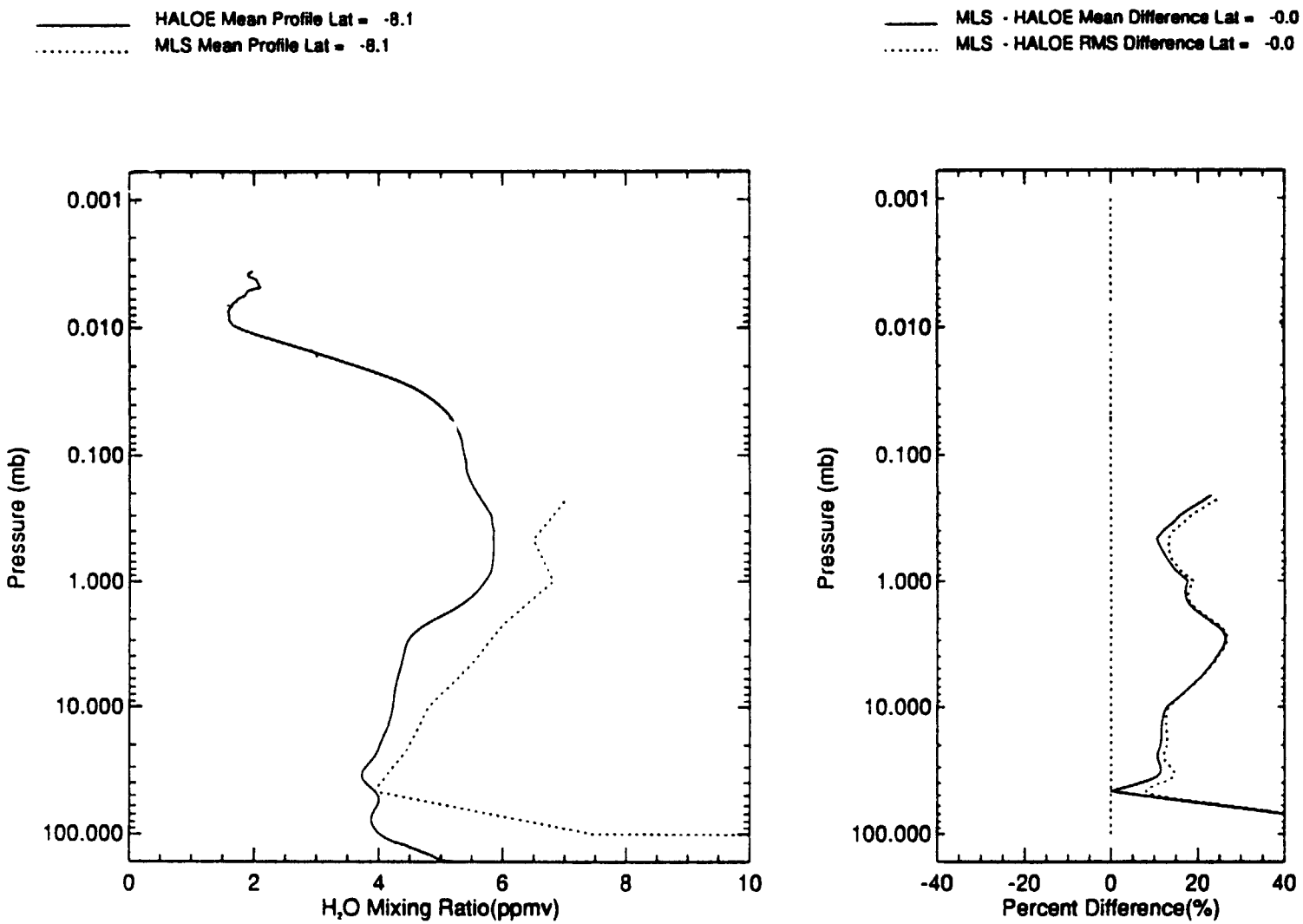

Figure 6.2.1-2 Profile comparison between HALOE and MLS H_2O for the period Aug. 25-30. The left hand panel shows the average profiles for the period. The right panel shows the mean and rms differences between the profiles.

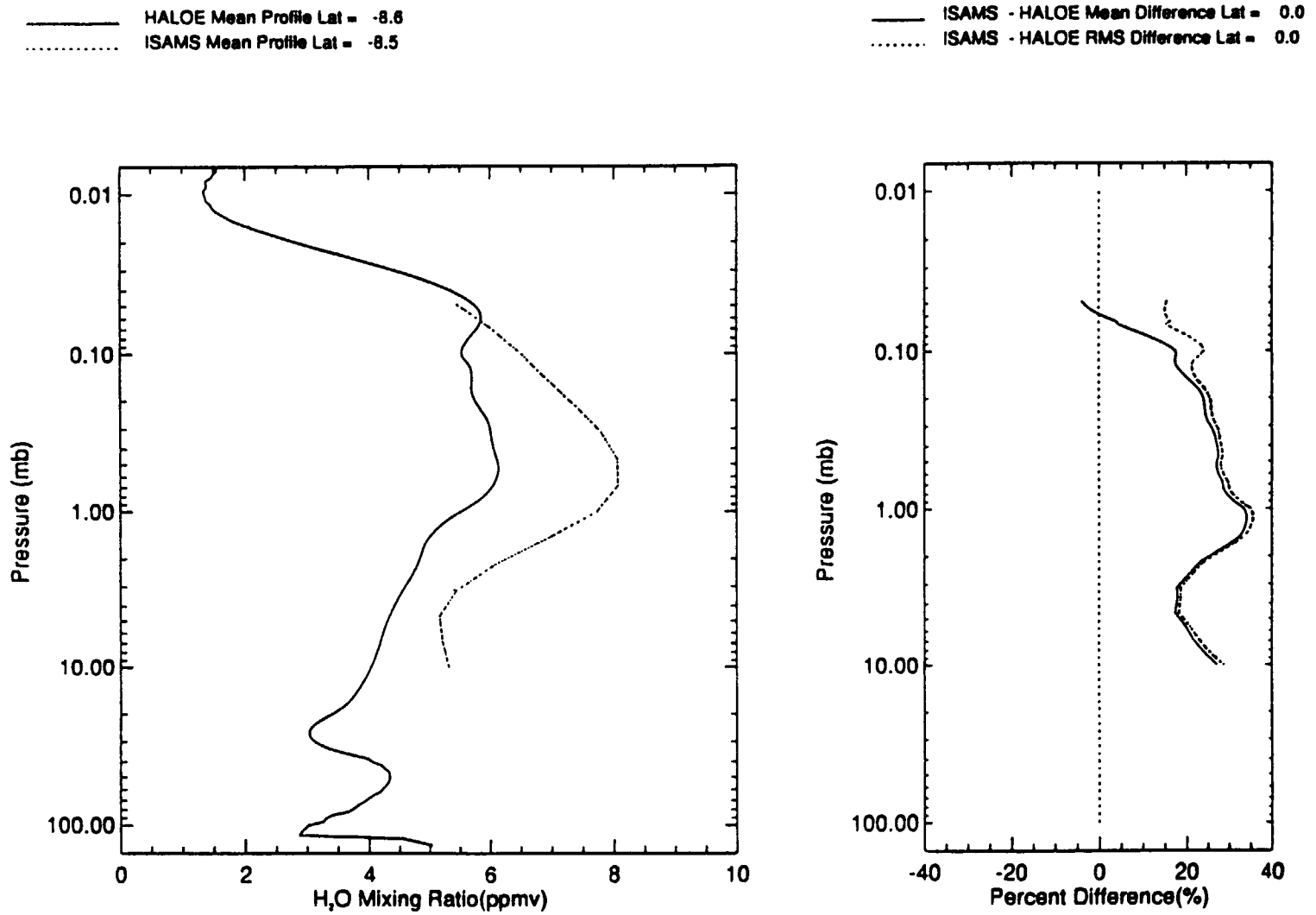

Figure 6.2.1-3 Profile comparison between HALOE and ISAMS H_2O for the period April 15-20. The left hand panel shows the average profiles for the period. The right panel shows the mean and rms differences between the profiles.

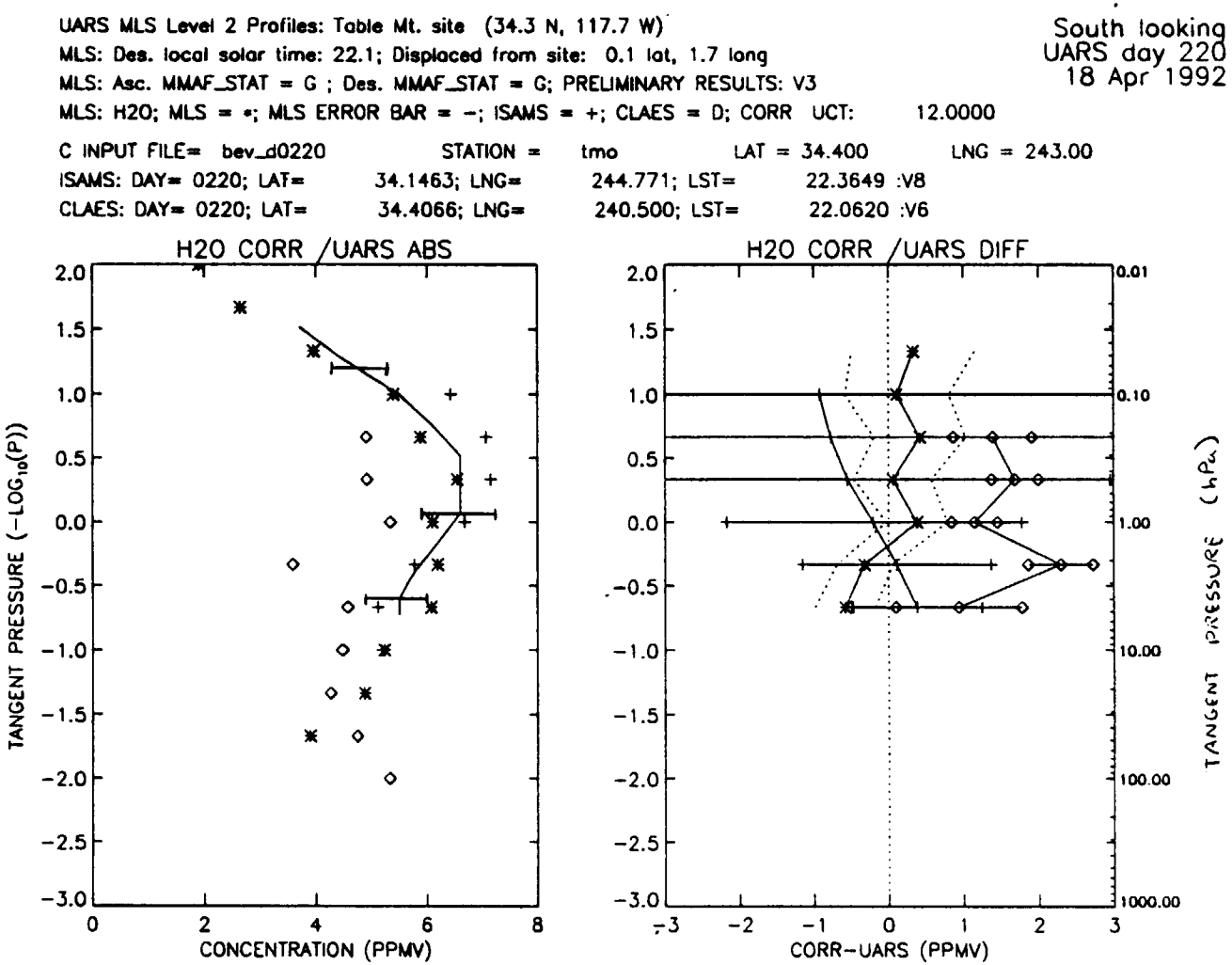

Figure 6.2.1-4 Profile comparisons between MLS, ISAMS and CLAES H_2O and Bevilacqua's data for UARS day 220 (April 18, 1992). The left panel shows profile values (horizontal bars are typical precision values for the Bevilacqua data); the solid line Bevilacqua's data, the asterisks MLS, the plus ISAMS, and the diamonds CLAES. The right panel shows the differences between the Bevilacqua data and each of the UARS instruments. The dashed lines are the MLS error bars; the horizontal bars are the ISAMS error bars (plus) and the CLAES error bars (diamonds).

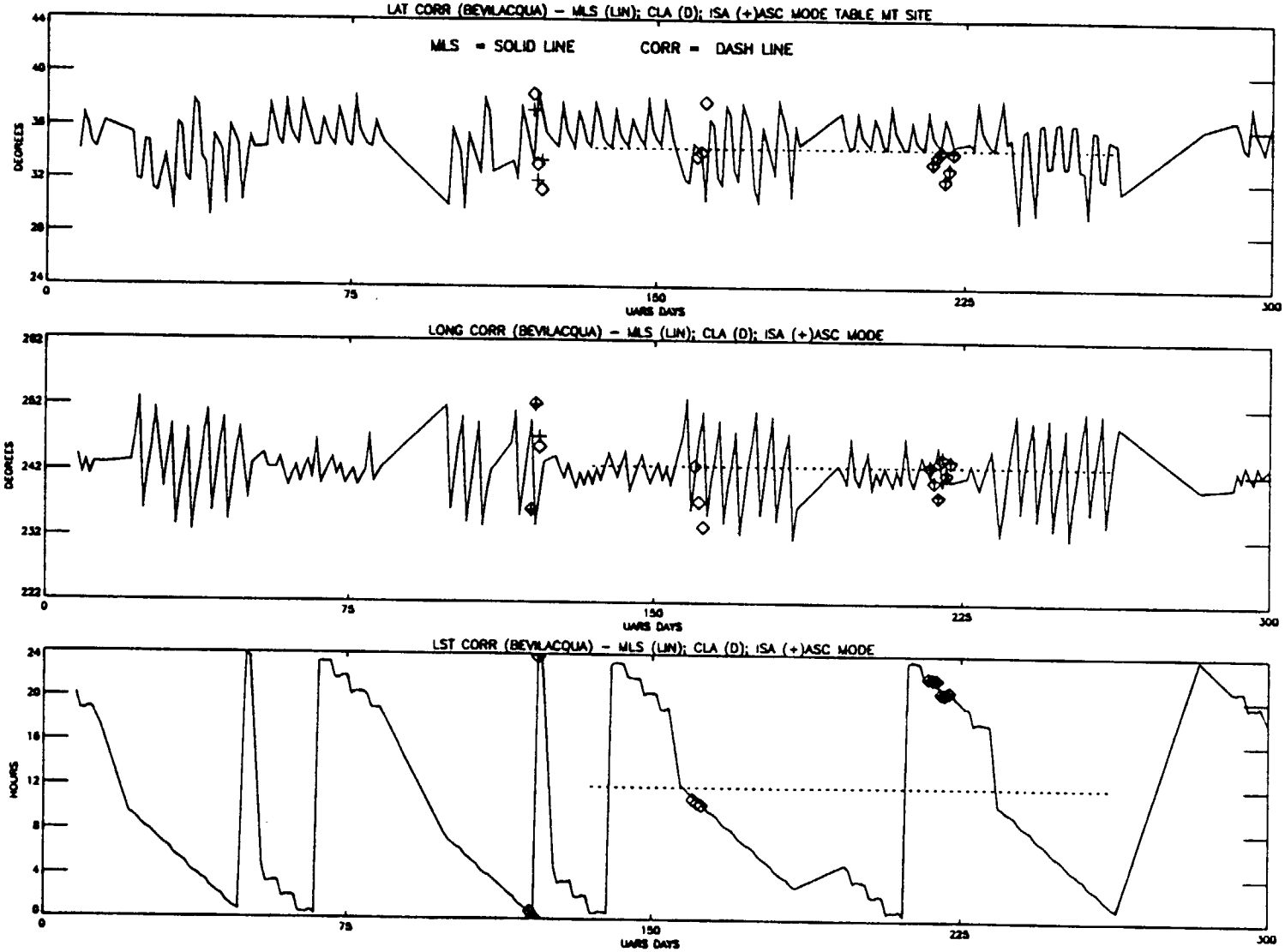

Figure 6.2.1-5 Plot representing the latitude (top panel), longitude (middle panel), and local solar time (bottom panel) for the UARS/Bevilacqua coincidences used to obtain a time series. The solid line represents MLS coincidences, the plus and diamonds represent ISAMS and CLAES coincidences respectively. The dashed line represents the Bevilacqua coincidences. The abscissa is the date in UARS days.

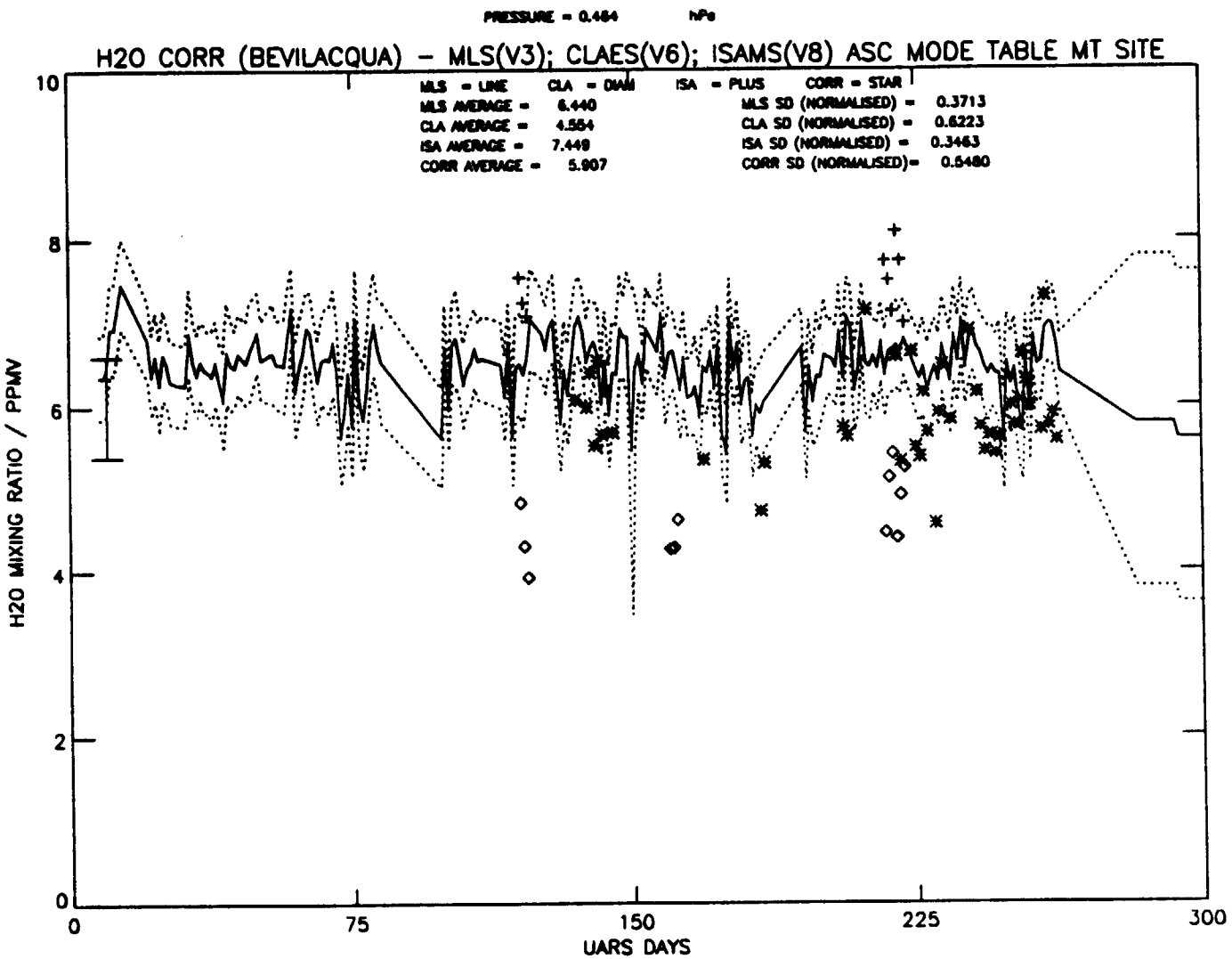

Figure 6.2.1-6 Time series of MLS H_2O data (solid line) against Bevilacqua's data (asterisks) at 0.46 mb. The dashed lines represent the MLS error bars. The plus and diamonds represent ISAMS and CLAES data, respectively, for the days in the UARS intercomparison periods. The abscissa is the date in UARS days. The vertical line is the typical precision (10%) for Bevilacqua's data corresponding to a mixing ratio of 6 ppmv.

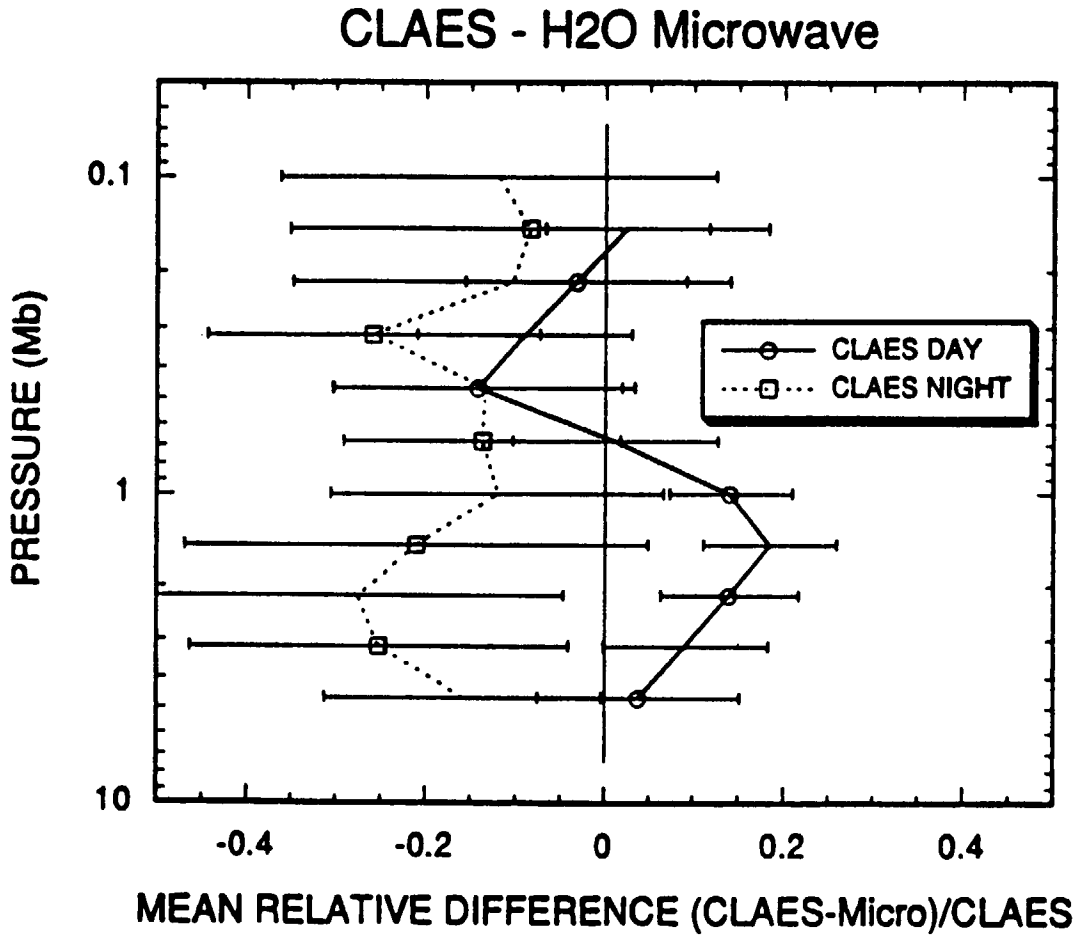

Figure 6.2.1-7 Differences between CLAES water vapor measurements and microwave measurements at TMO by Bevilacqua (103 nighttime and 38 daytime coincidences were identified since January, 1992). The differences have been expressed as a ratio of the microwave measurements and the error bars serve to indicate the standard deviations of the differences.

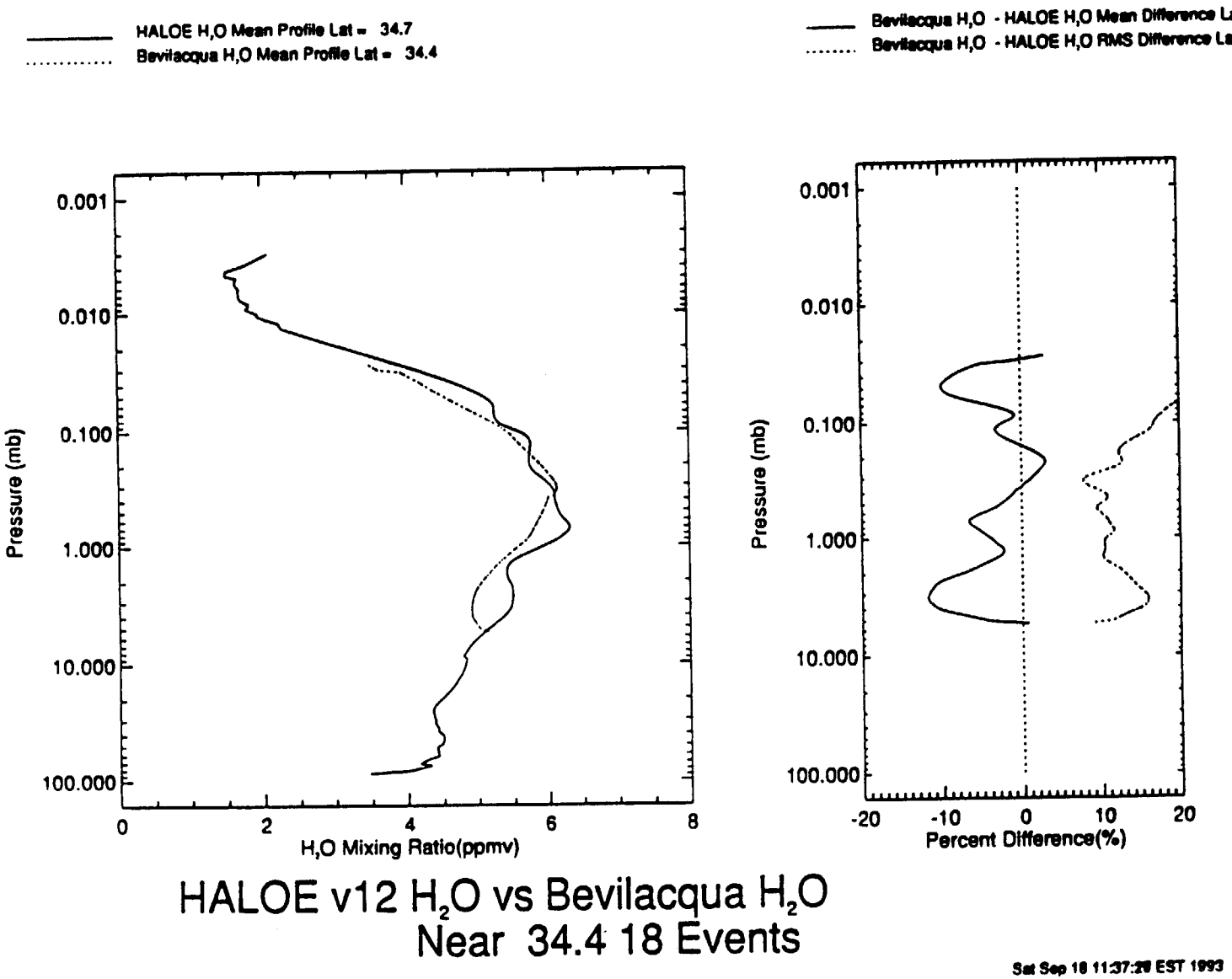

Figure 6.2.1-8 Profile comparison between HALOE H_2O data and Bevilacqua's data. The left panel shows the average profiles for the period. The right panel shows the mean and rms differences between the profiles.

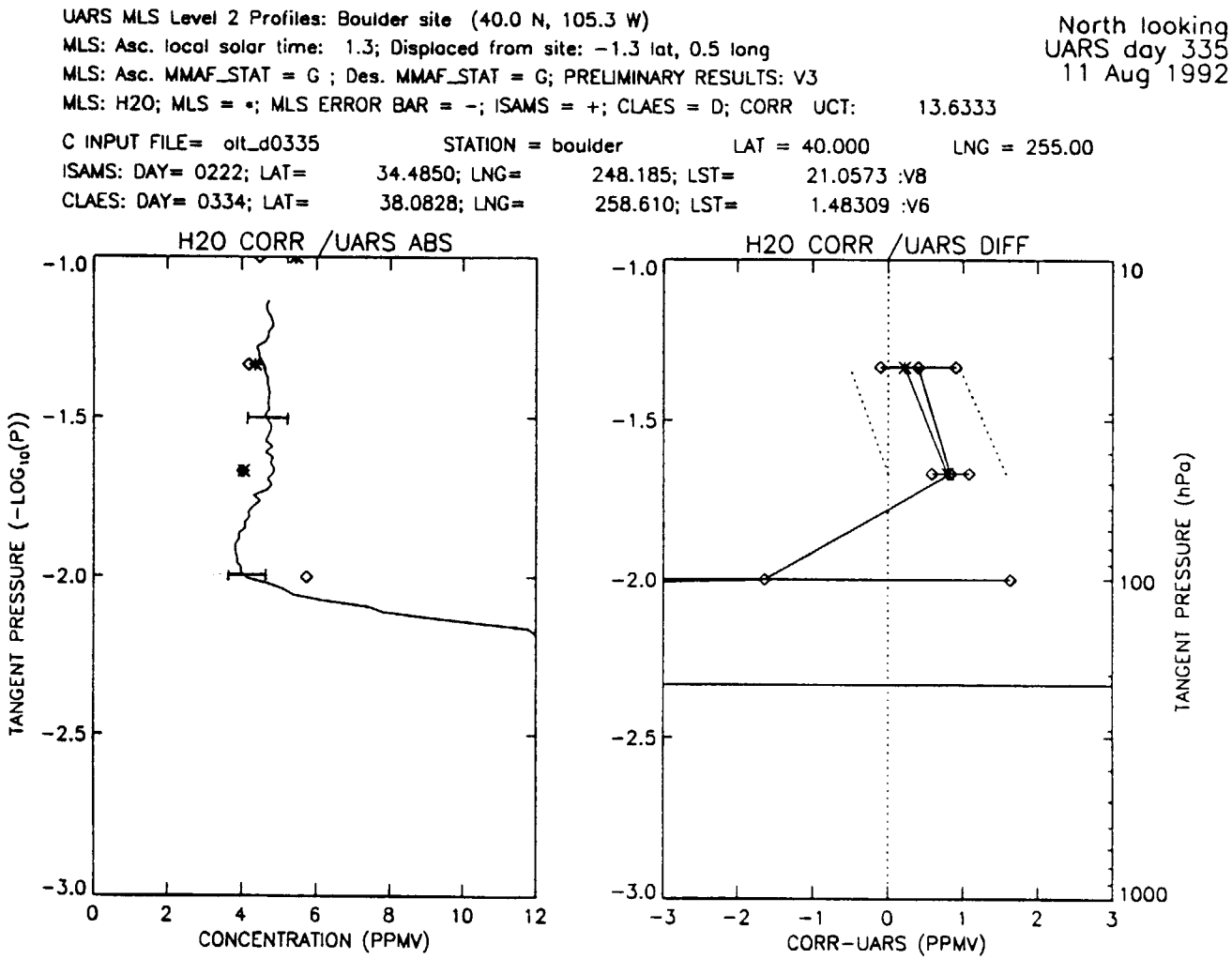

Figure 6.2.1-9 Profile comparison between MLS H_2O data against Oltmans' data for UARS day 335 (Aug. 11, 1992) and CLAES H_2O data for UARS day 334 (Aug. 10, 1992). The left hand panel shows the profile values (the horizontal bars are typical precision values for the Oltmans' data). The solid line is Oltmans' data, the asterisks MLS, and the diamonds CLAES. The right panel shows the differences between the Oltmans' data and the MLS and CLAES data. The dashed lines are the MLS error bars, and the horizontal lines are the CLAES error bars.

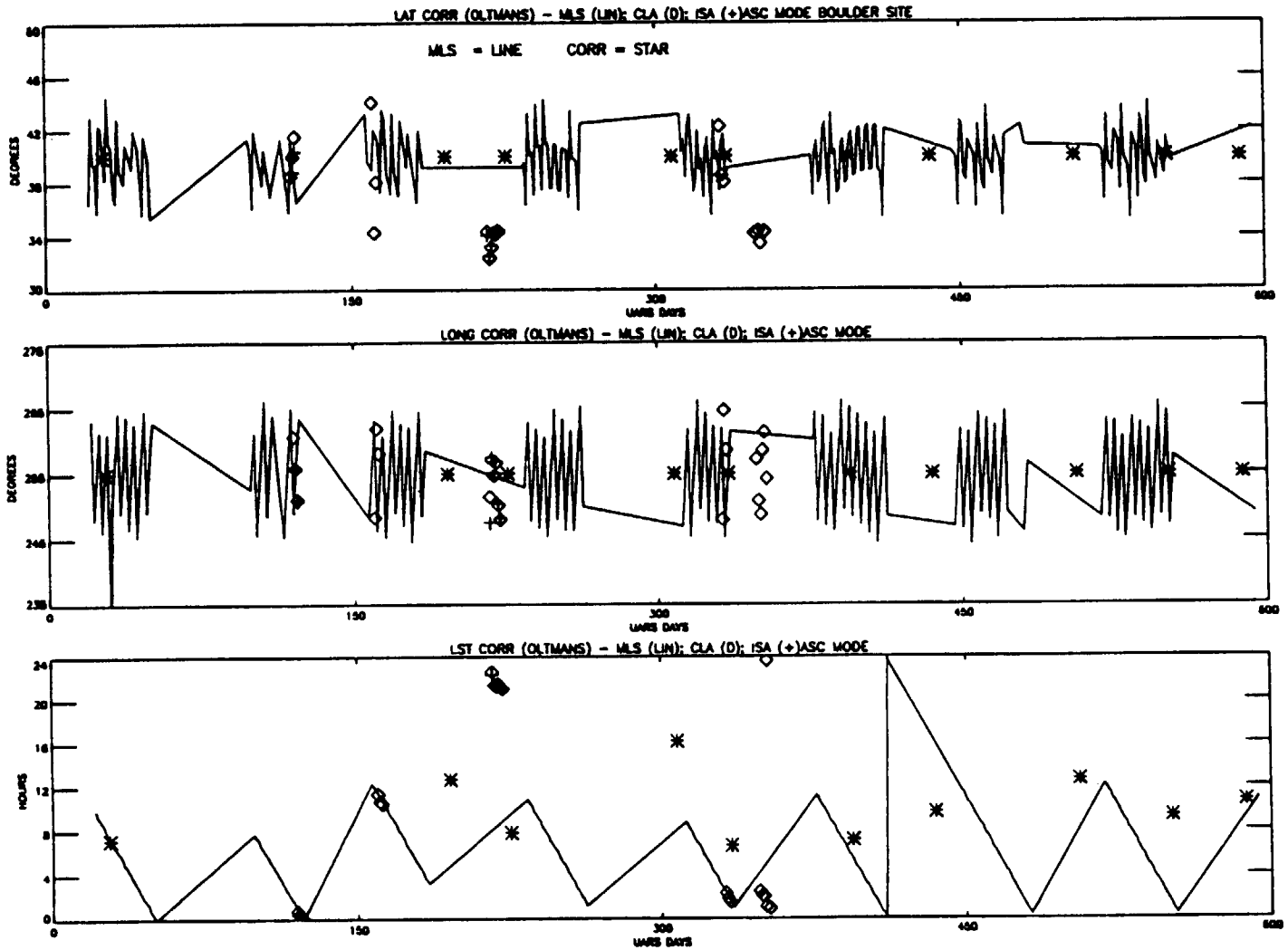

Figure 6.2.1-10 Plot representing latitude (top panel), longitude (middle panel), and local solar time (bottom panel) for the UARS/Oltmans coincidences used to obtain a time series. The solid line represents MLS coincidences, while asterisks, pluses, and diamonds represent Oltman's, ISAMS and CLAES coincidences, respectively, for the days used in the UARS intercomparison periods. The abscissa is the date in UARS days.

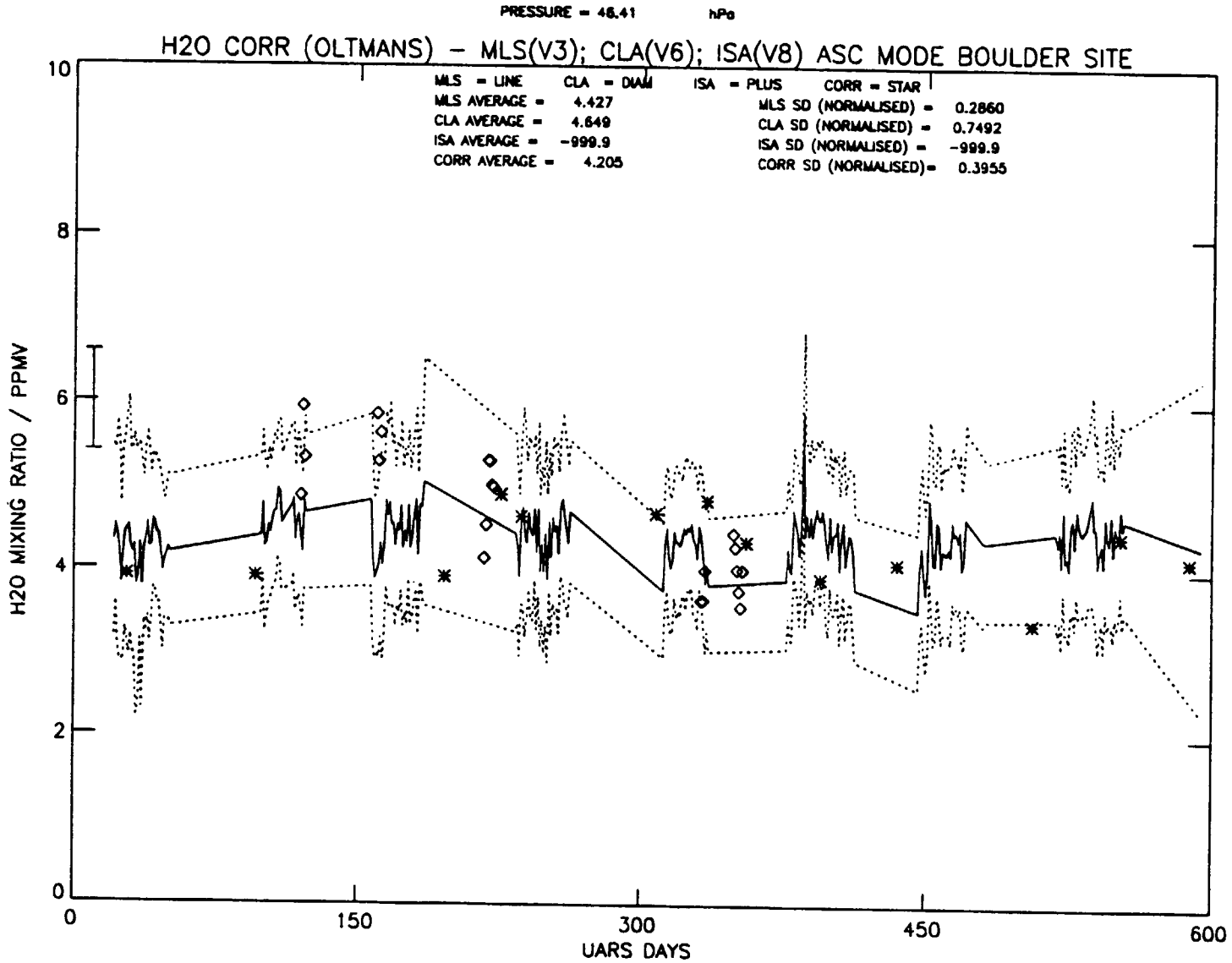

Figure 6.2.1-11 Time series of MLS data (solid line) against Oltmans' data (asterisks) at 46 mb. The dashed lines represent the MLS error bars, the diamonds represent CLAES data for the days in the UARS intercomparison periods. The abscissa is the date in UARS days. The vertical line represents typical precision (10%) for Oltmans data corresponding to a mixing ratio of 6 ppmv.

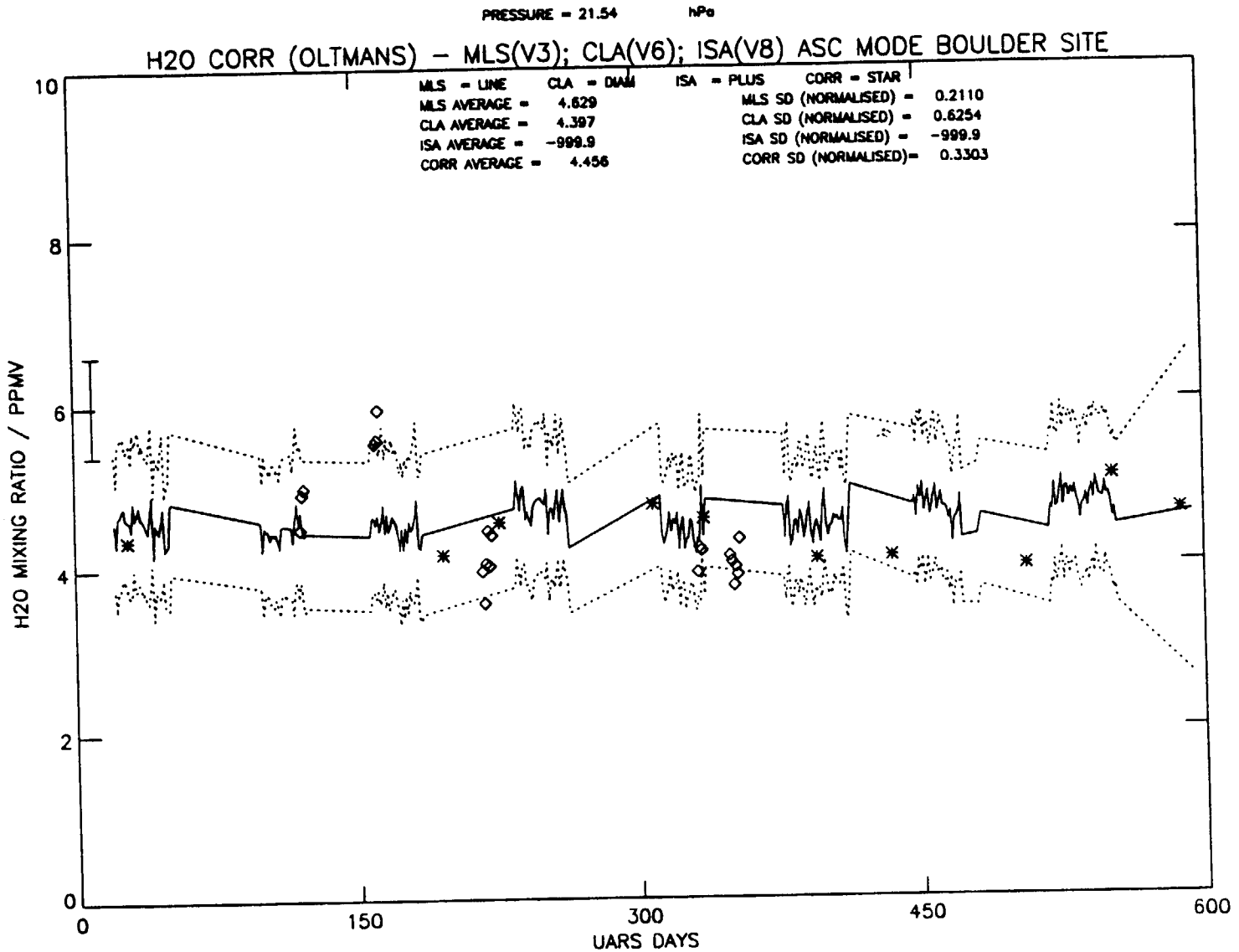

Figure 6.2.1-12 Same as Figure 6.2.1-11, but at 22 mb.

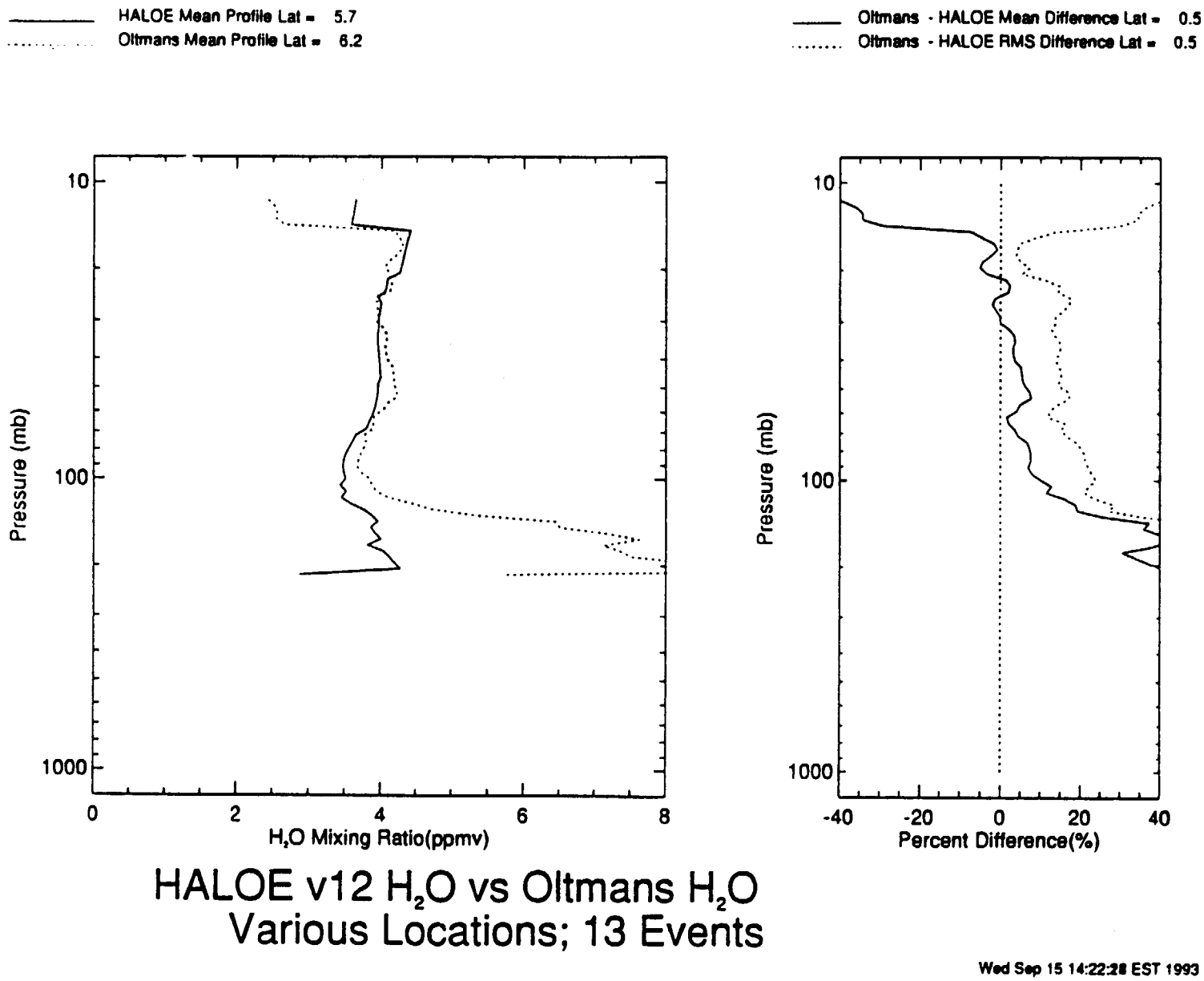

Figure 6.2.1-13 Profile comparison between HALOE H_2O data and Oltmans' data. The left panel shows the average profiles for the period. The right panel shows the mean and rms differences between the profiles.

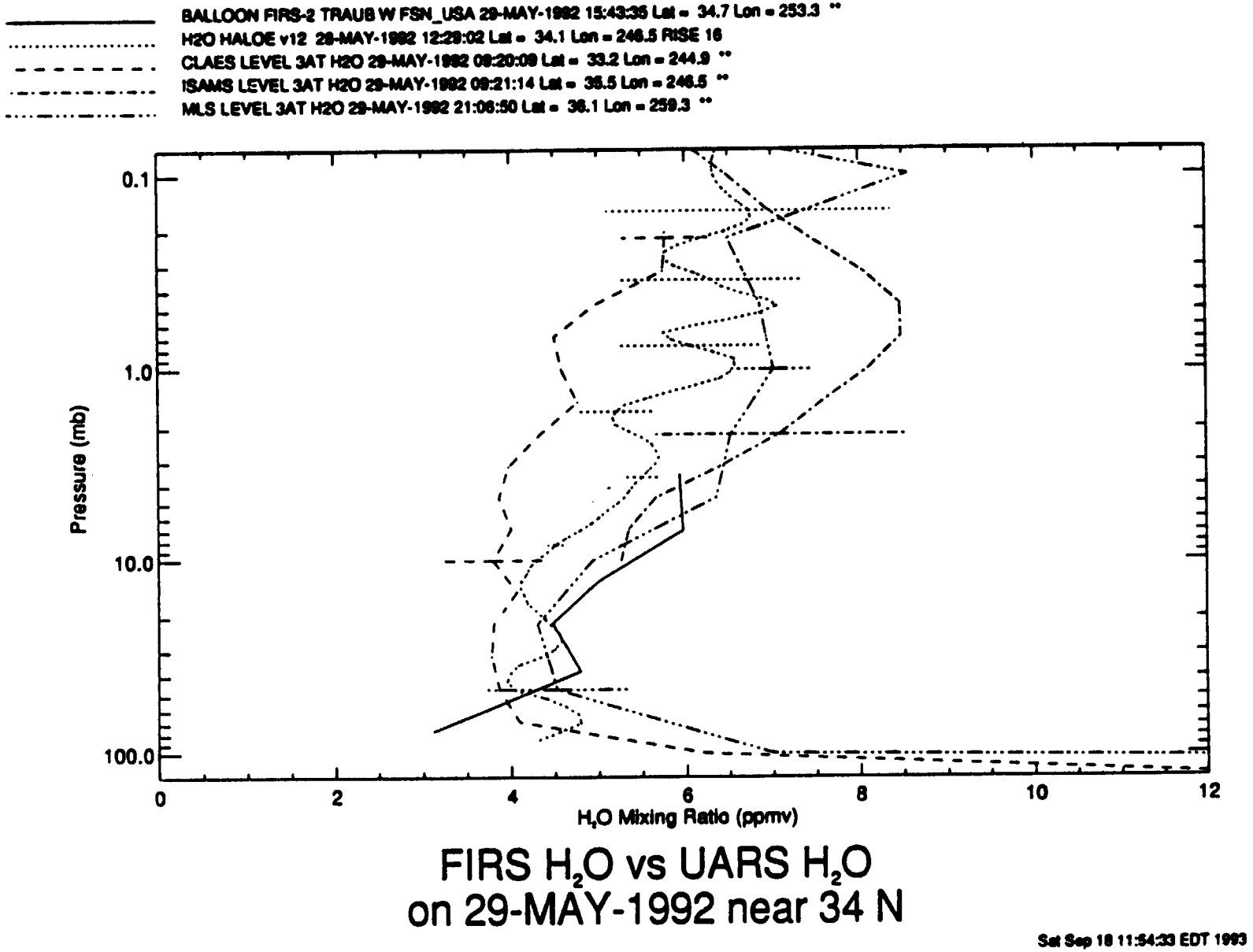

Figure 6.2.1-14 Profile comparison between FIRS H_2O data and HALOE, CLAES, ISAMS, and MLS data on May 29, 1992. The HALOE profile is for May 28, 1992 for closer latitude coincidence.

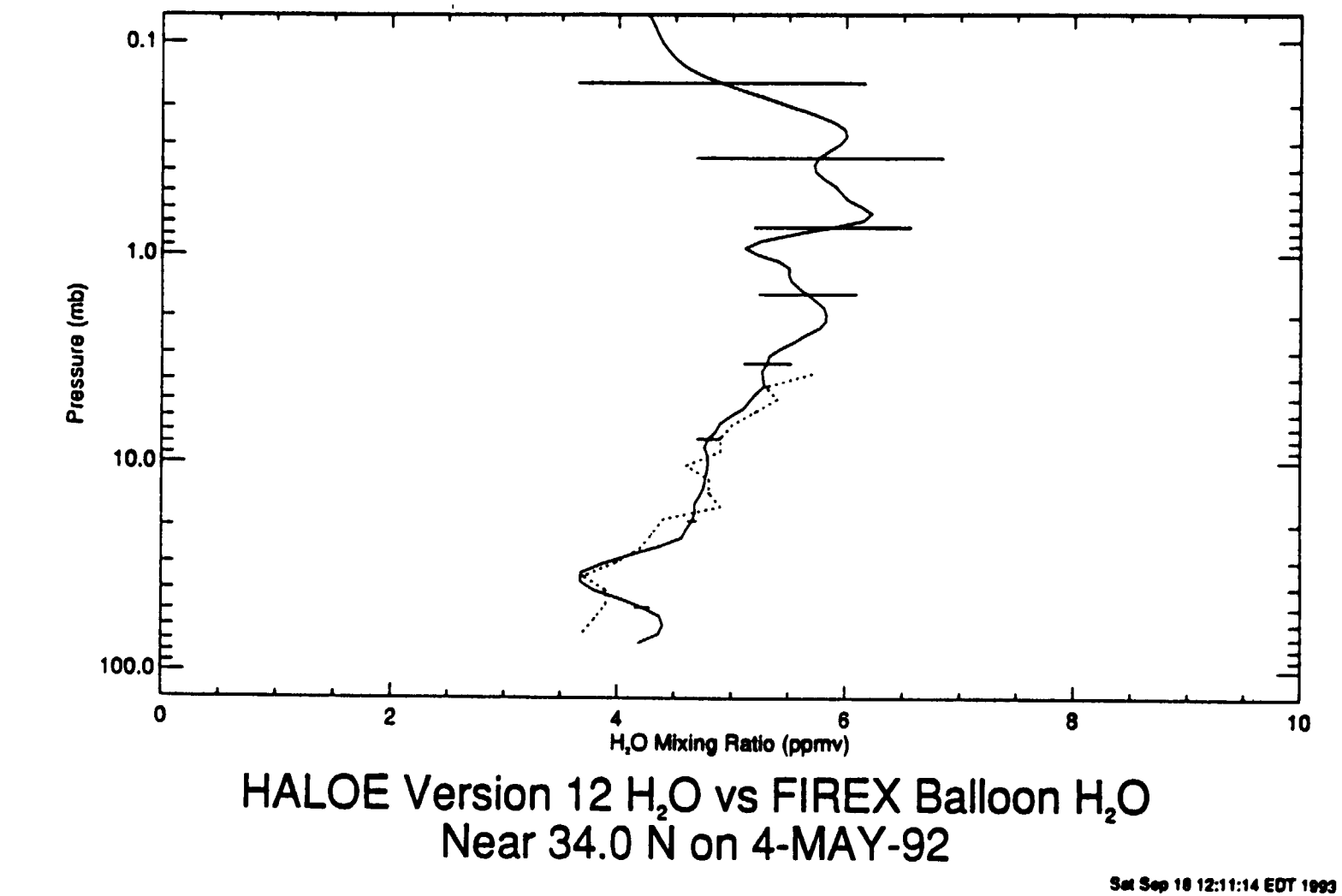

Figure 6.2.1-15 HALOE water vapor measurements on May 7, 1992 compared against FIREX balloon measurements on May 4, 1992.

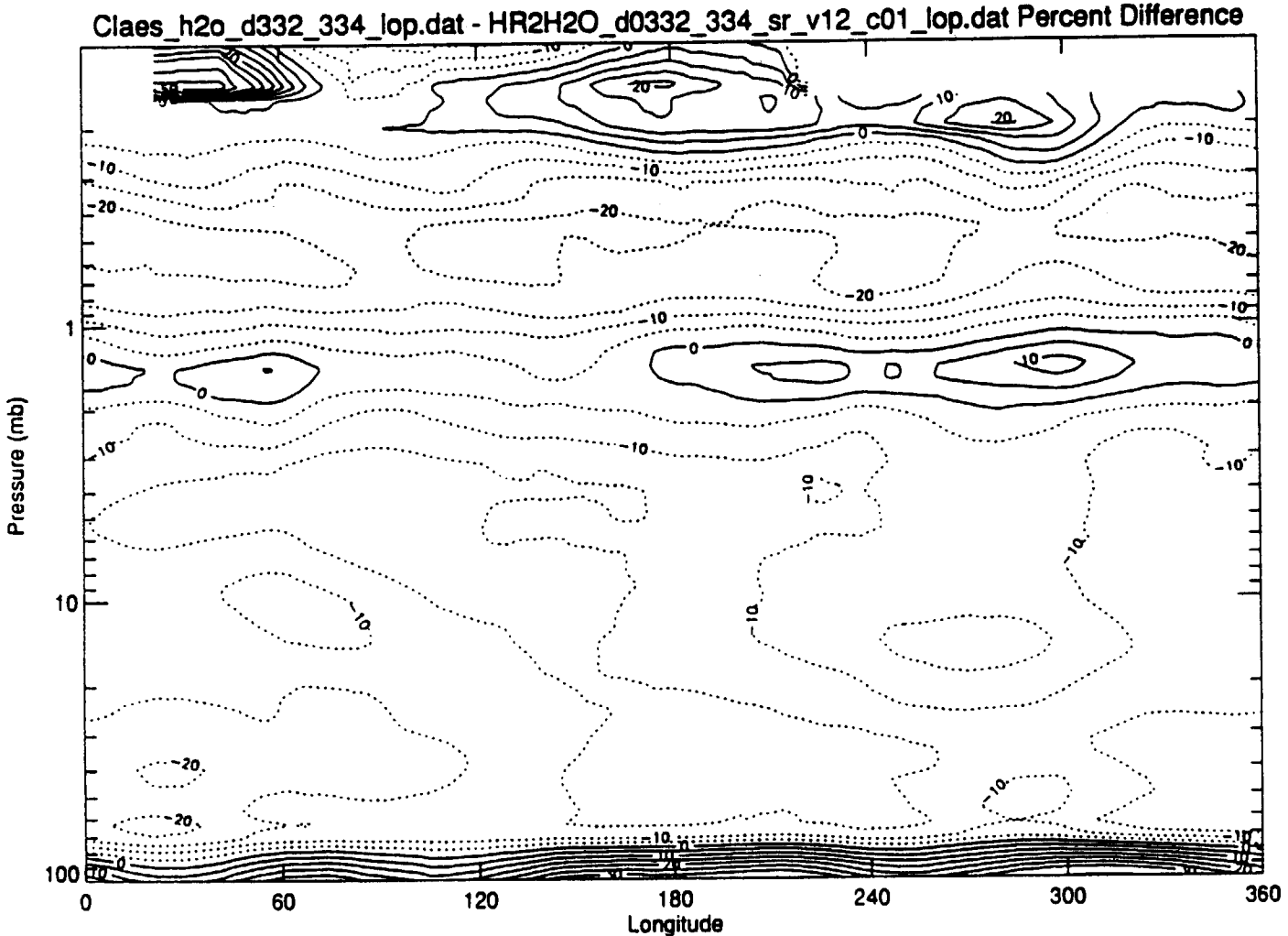

Figure 6.2.2-1 Difference plot of the pressure versus longitude cross-sections between CLAES and HALOE H_2O for the period Aug. 8-10, 1992 at a latitude near 39 N.

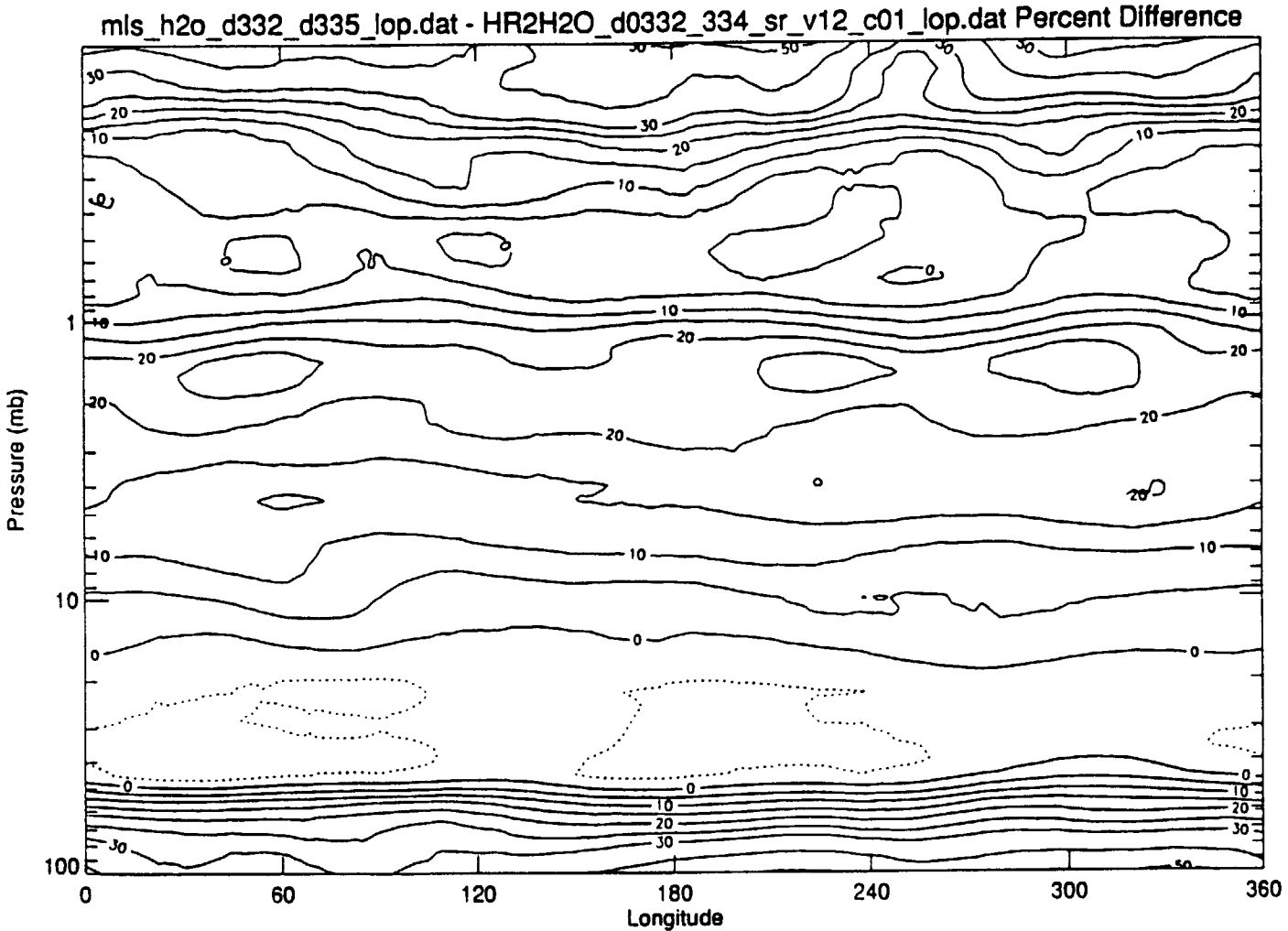

Figure 6.2.2-2 Difference plot of the pressure versus longitude cross-sections between MLS and HALOE H_2O for the period Aug. 8-10, 1992 at a latitude near 39 N. Differences are expressed as a percentage of the HALOE values.

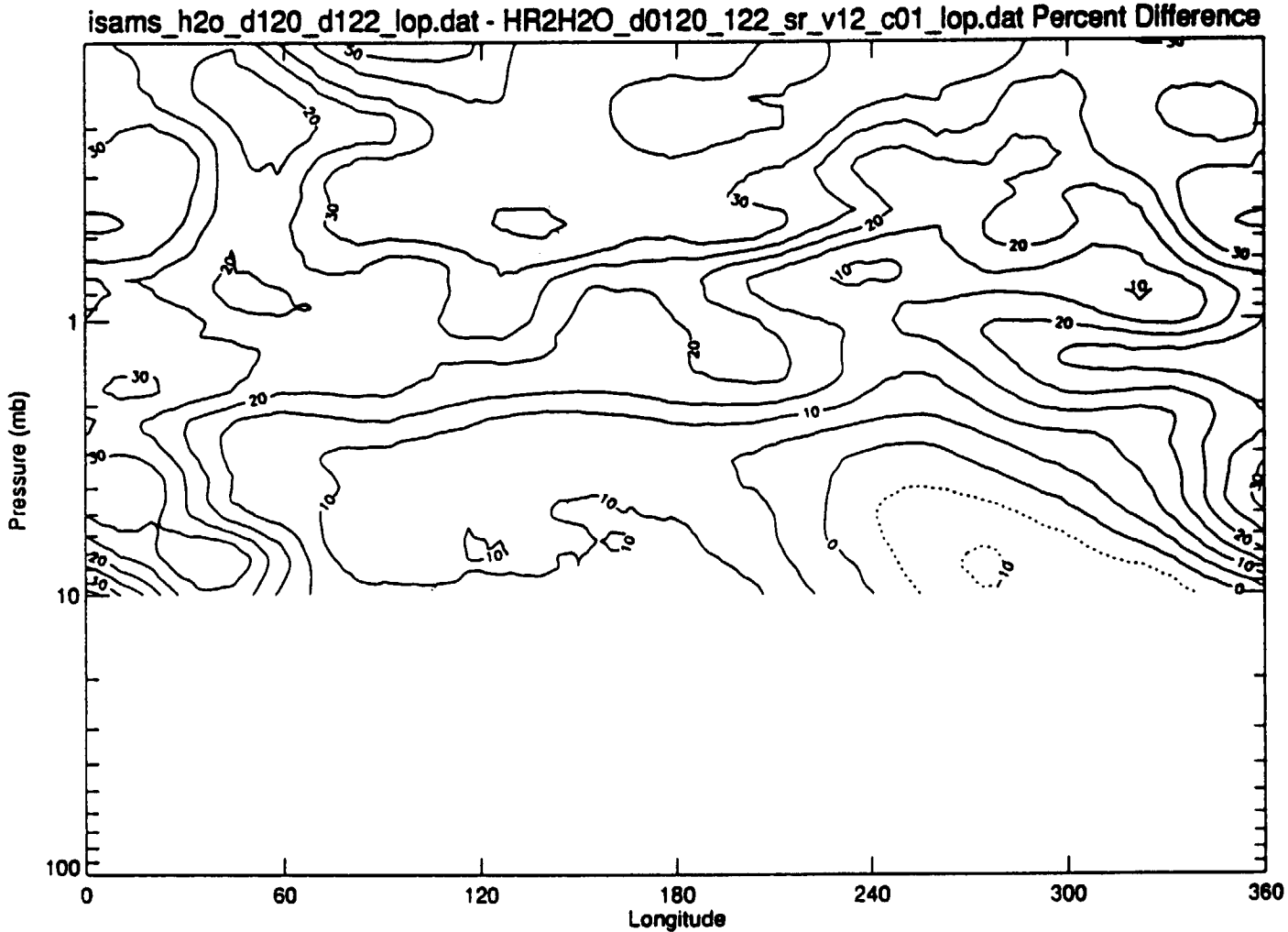

Figure 6.2.2-3 Difference plot of the pressure versus longitude cross-sections between ISAMS and HALOE for the period Jan. 9-11, 1992 at a latitude near 47 N. Differences are expressed as a percentage of the HALOE values.

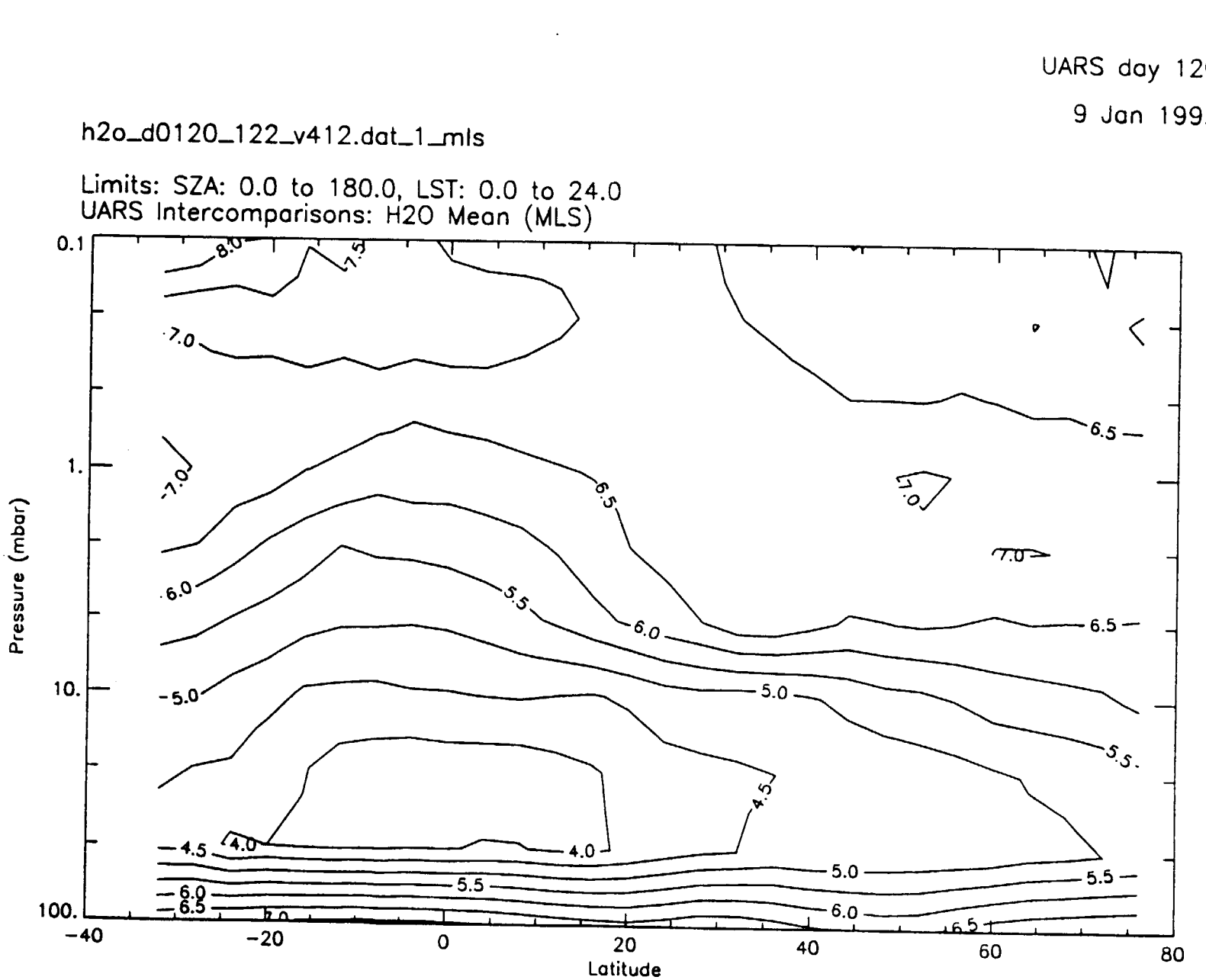

Figure 6.2.2-4 H_2O mean on a latitude-pressure grid for MLS for the three day period Jan. 9-11, 1992. The contour step is 0.5 ppmv.

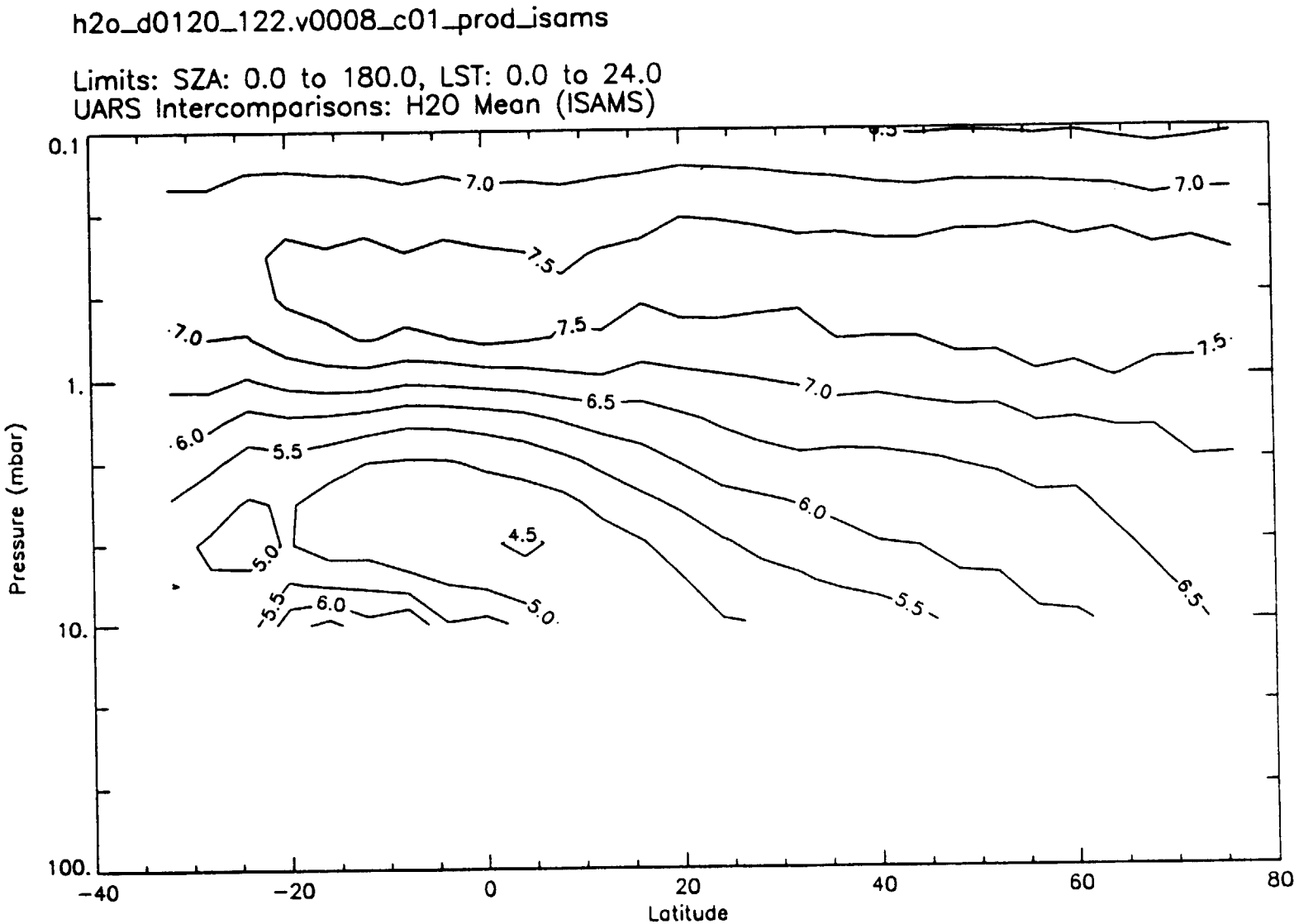

Figure 6.2.2-5 H_2O mean on a latitude-pressure grid for ISAMS for the three day period Jan. 9-11, 1992. The contour step is 0.5 ppmv.

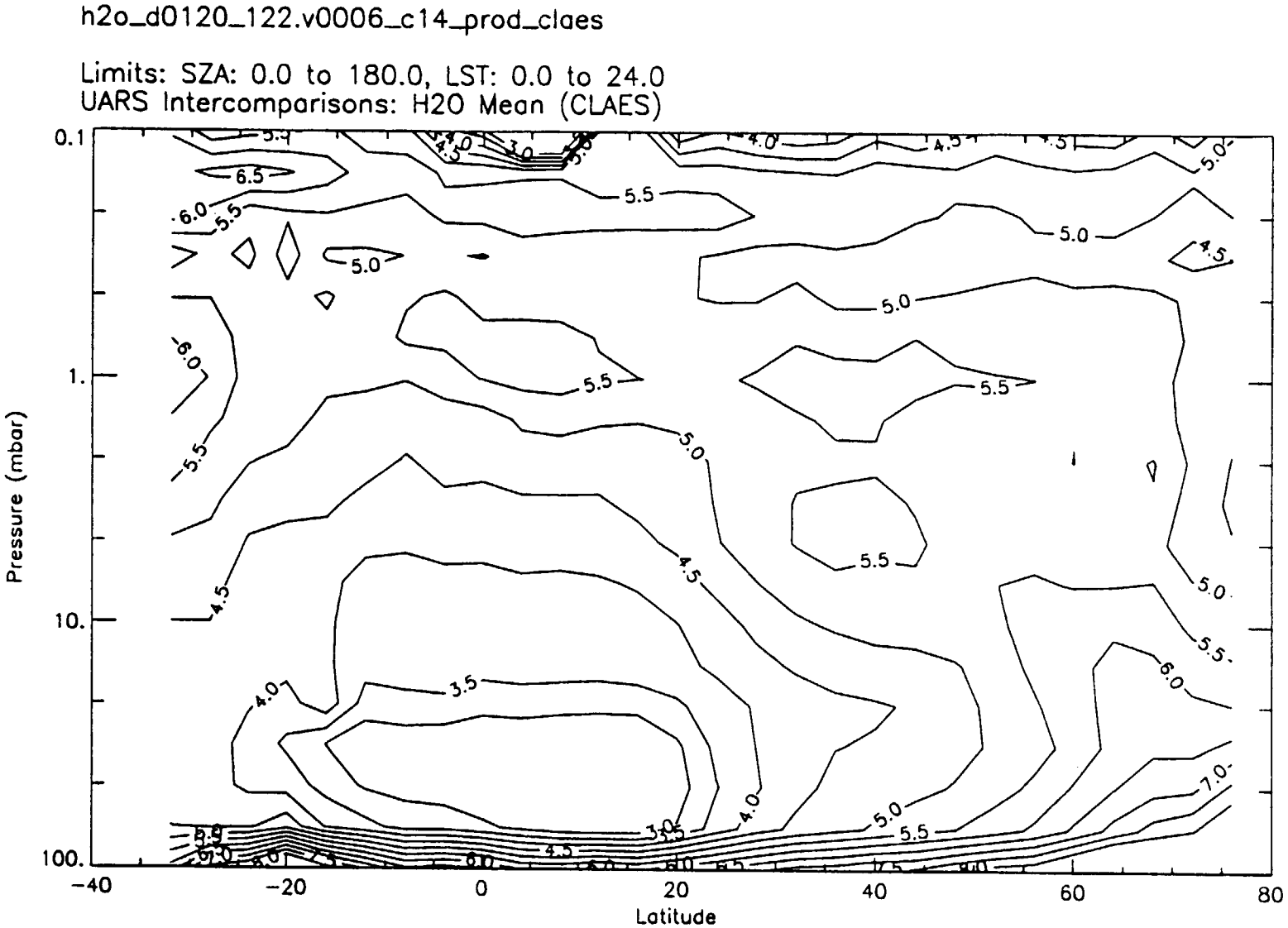

Figure 6.2.2-6 H_2O mean on a latitude-pressure grid for CLAES for the three day period Jan. 9-11, 1992. The contour step is 0.5 ppmv.

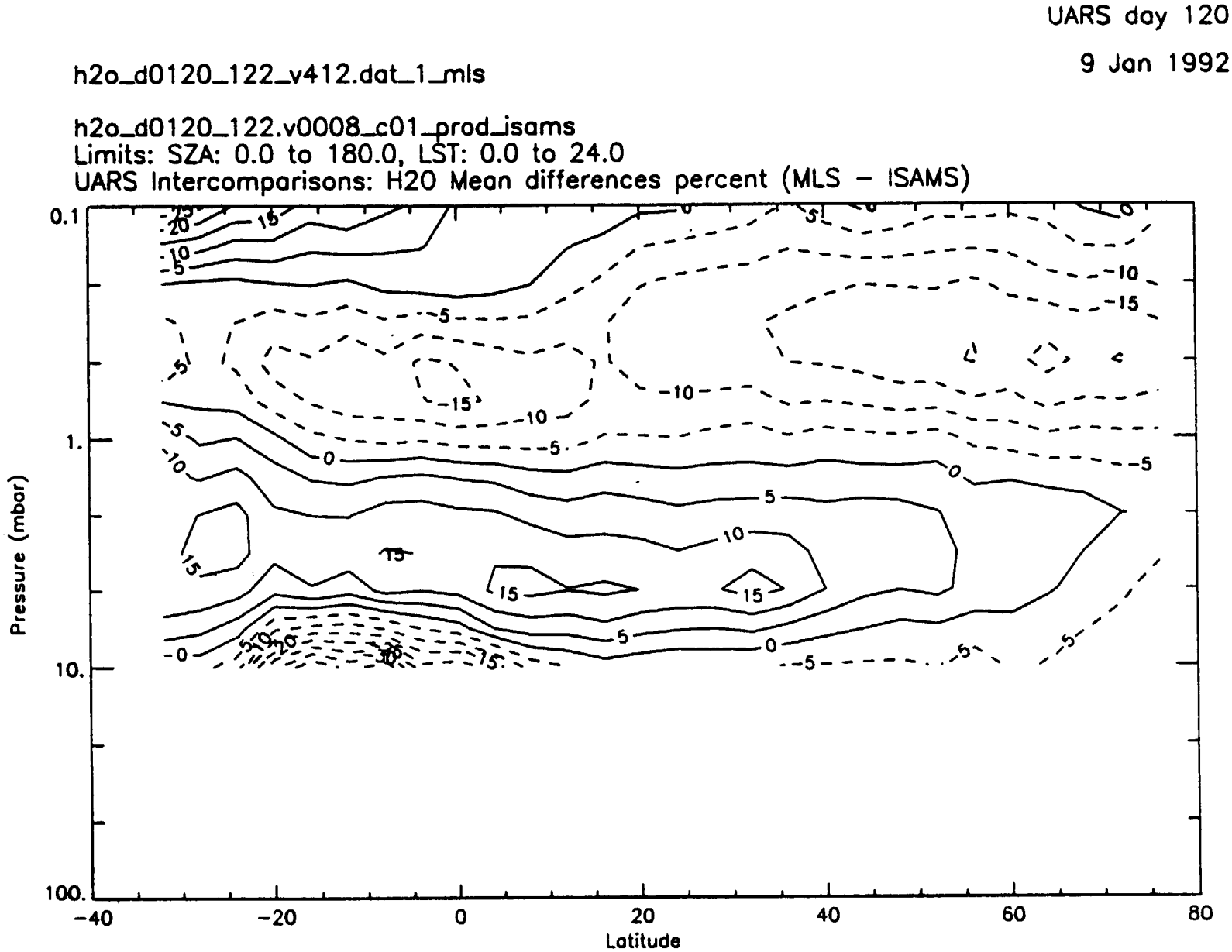

Figure 6.2.2-7 H_2O mean percent differences on a latitude-pressure grid between MLS and ISAMS for the three day period Jan. 9-11, 1992. The contour step is 5 %. Differences are expressed relative to MLS.

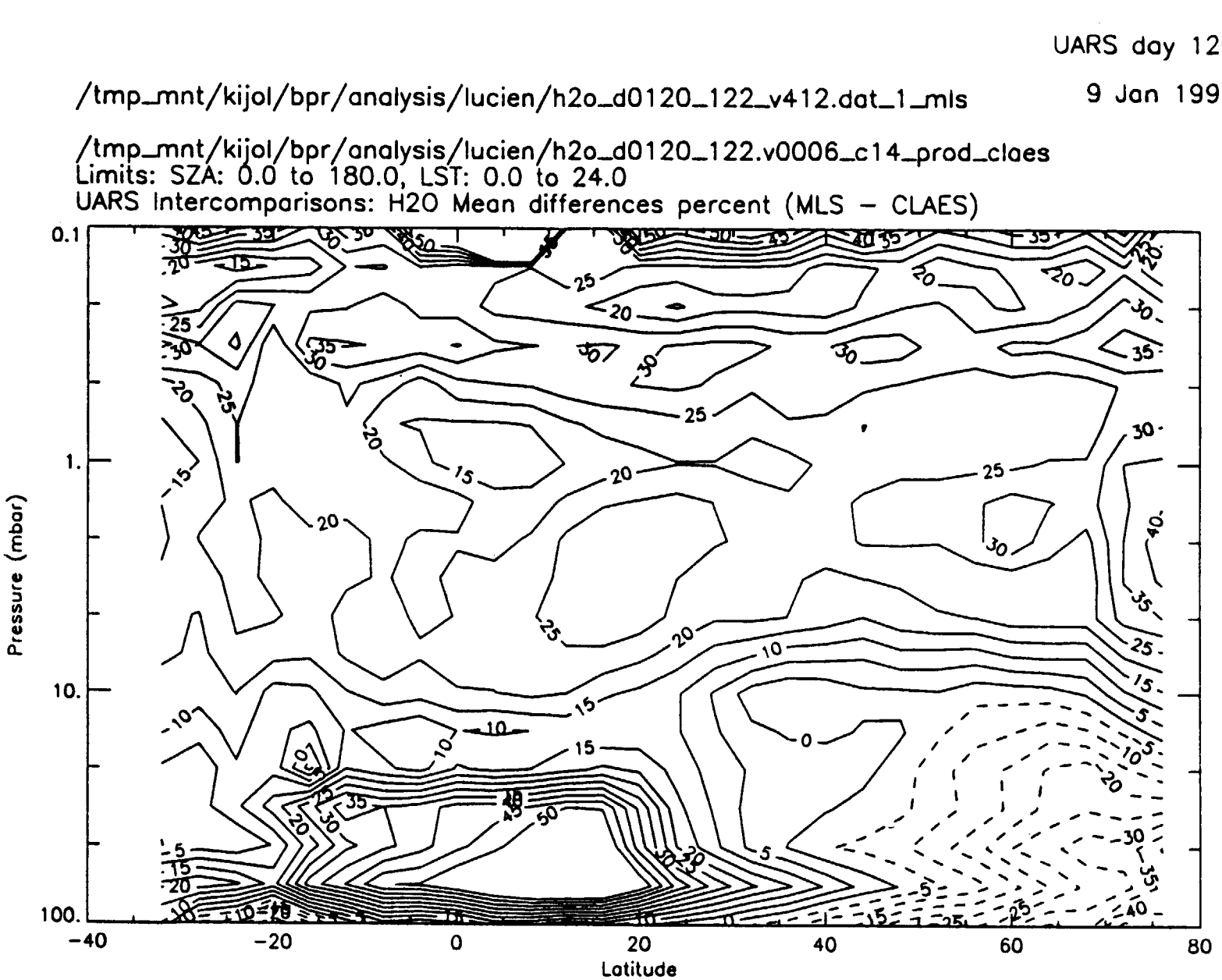

Figure 6.2.2-8 H_2O mean percent differences on a latitude-pressure grid between MLS and CLAES for the three day period Jan. 9-11, 1992. The contour step is 5 %. Differences are expressed relative to MLS.

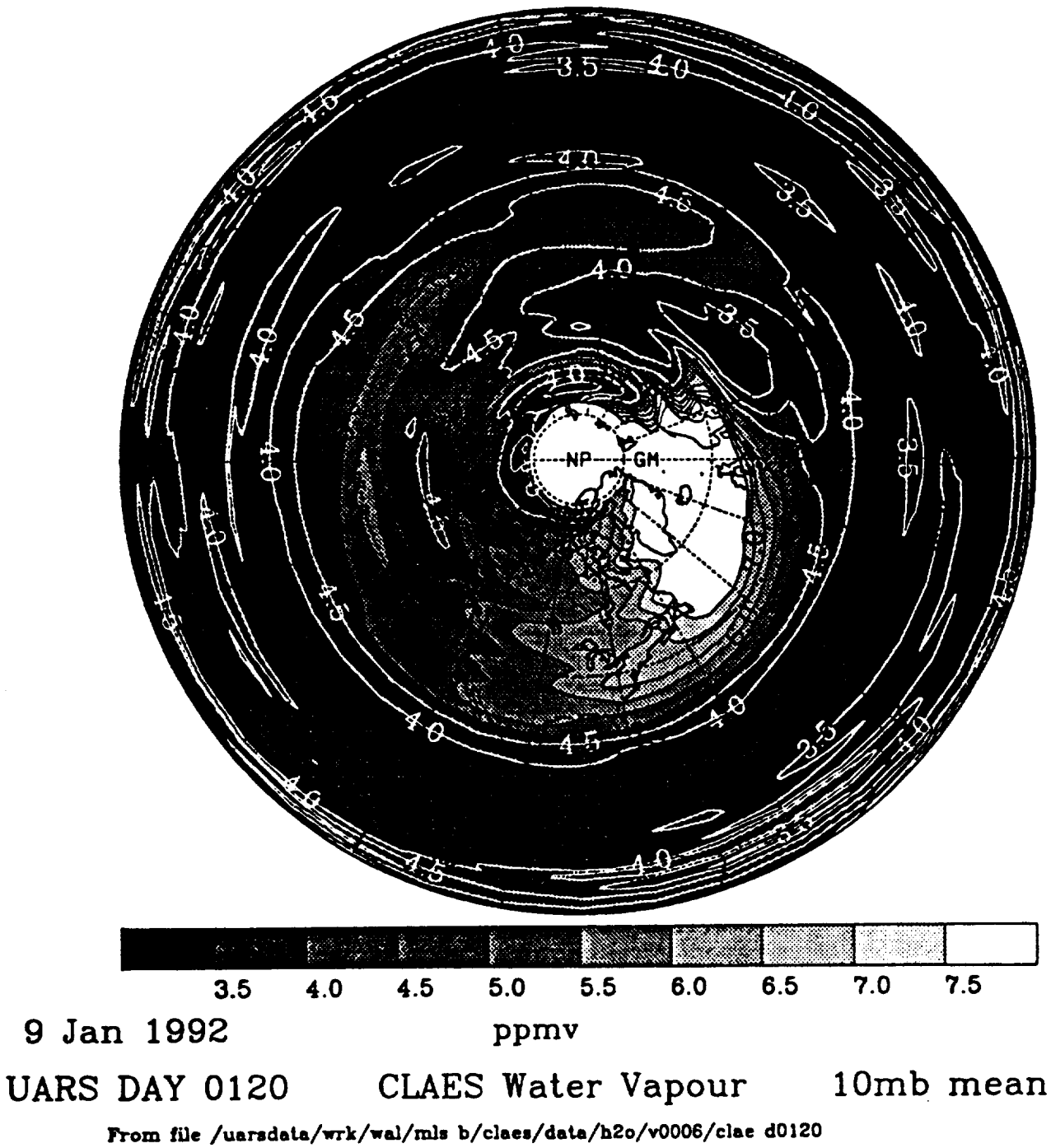

(a)

Figure 6.2.3-1 A comparison of (a) CLAES, (b) MLS and (c) ISAMS water vapor maps at 10.2 mb on Jan. 9, 1992. The latitude range is 30S-80N. The Greenwich meridian is marked GM.

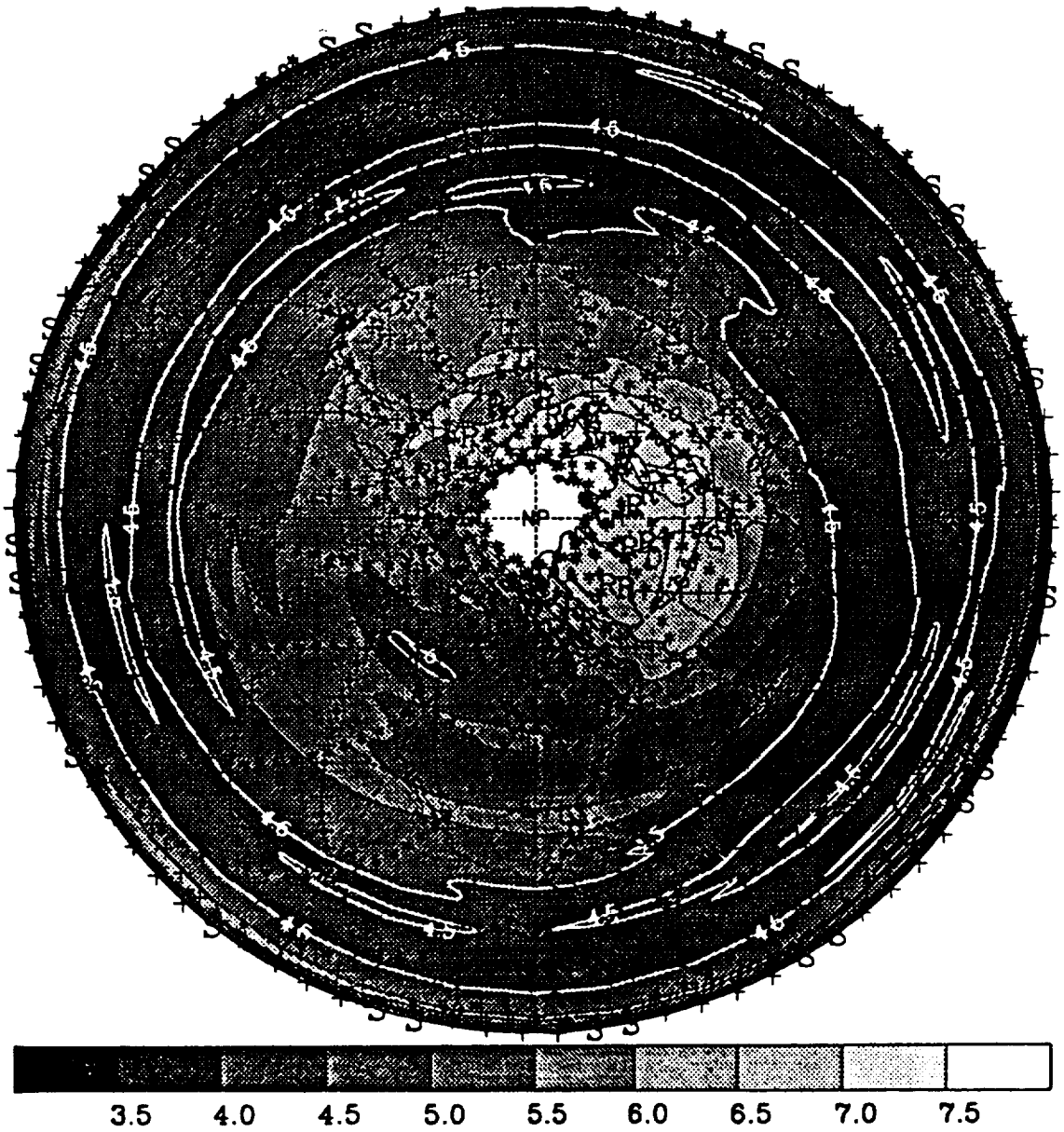

(b)

Figure 6.2.3-1 Continued.

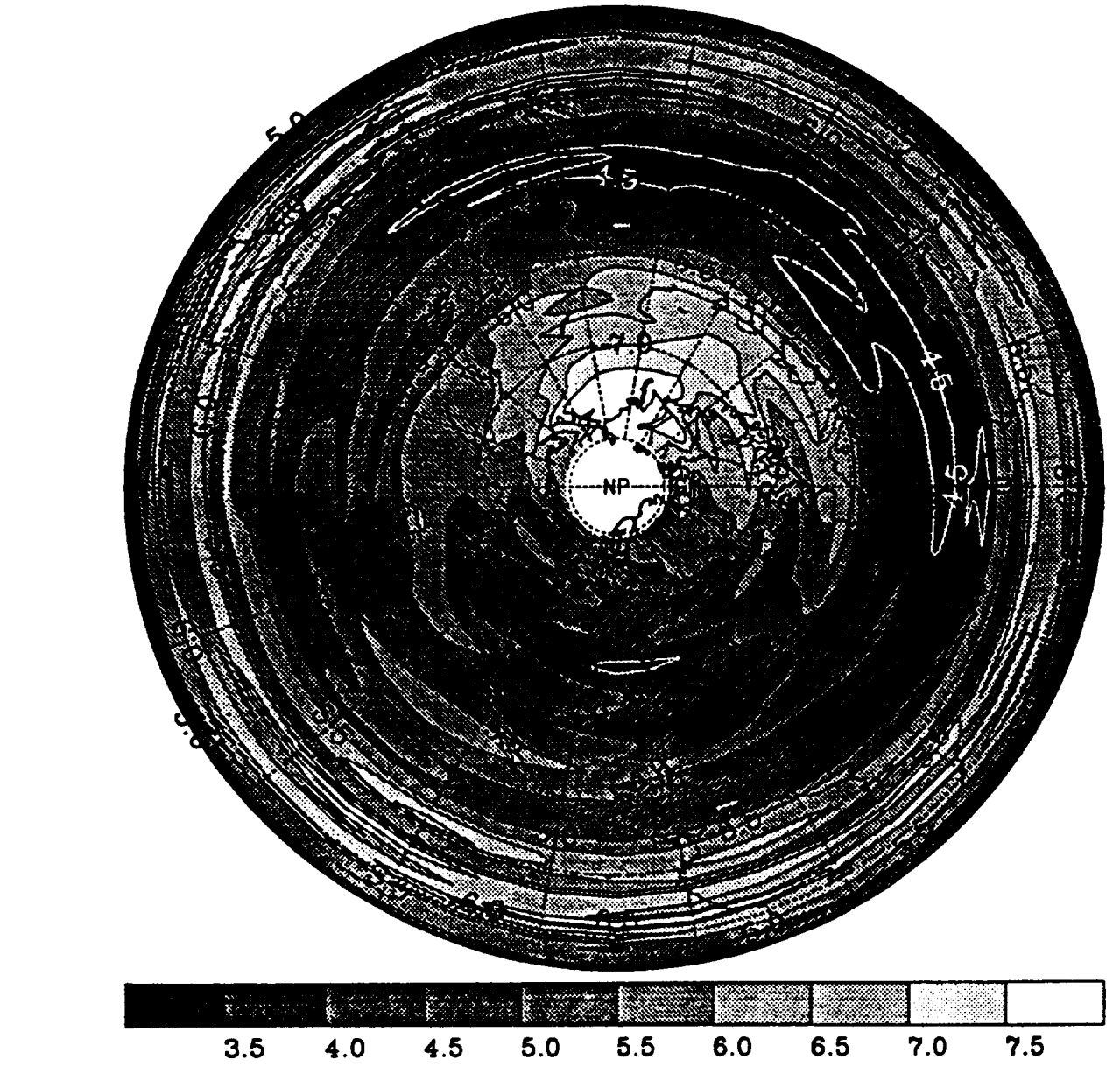

(c)

Figure 6.2.3-1 Concluded.

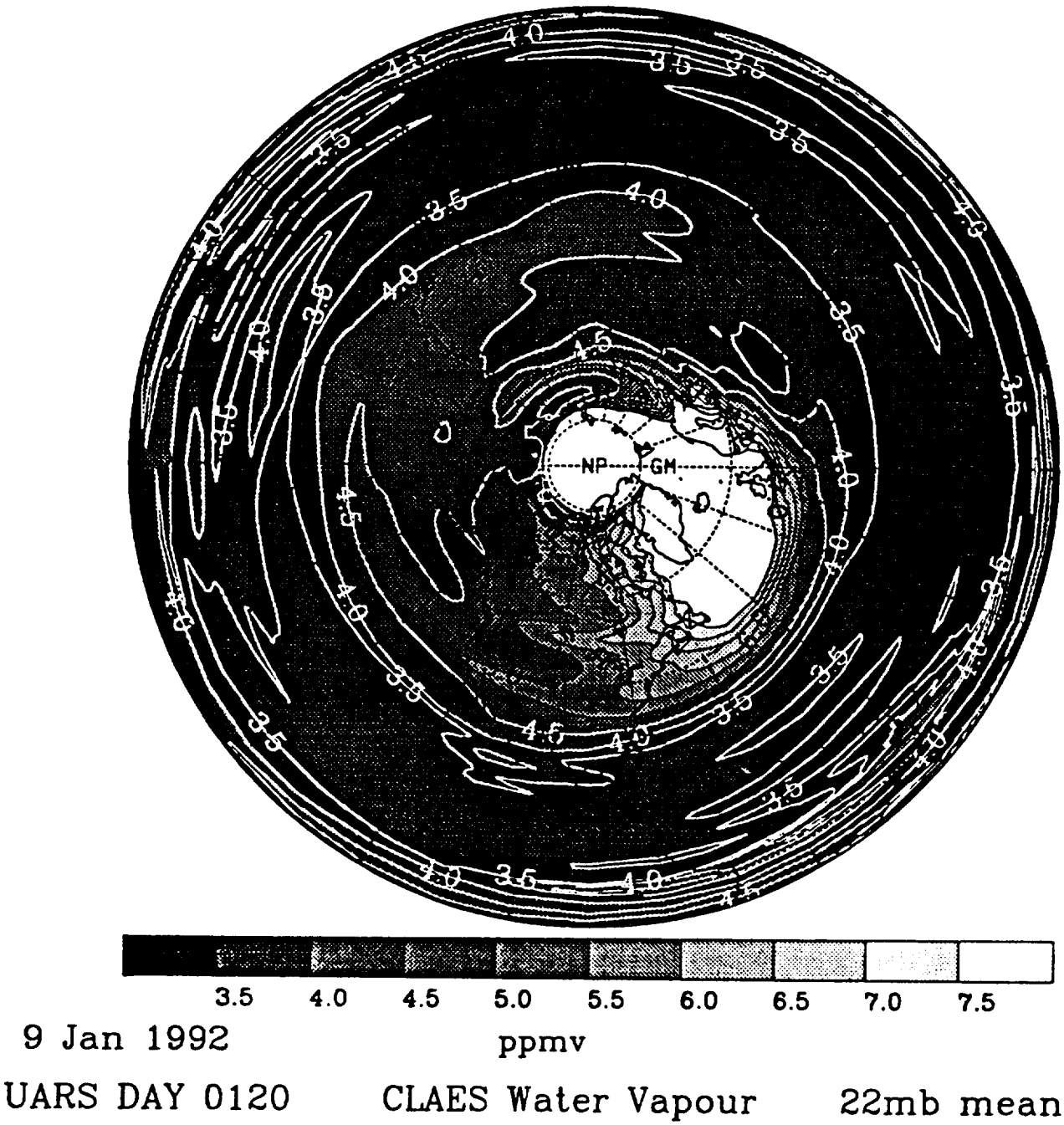

(a)

Figure 6.2.3-2 A comparison of CLAES and MLS water vapor maps at 22 mb on Jan. 9, 1992 (a-b) and April 18, 1992 (c-d). The latitude range is 30S-80N (January) or 30N-80S (April). The Greenwich meridian is marked GM.

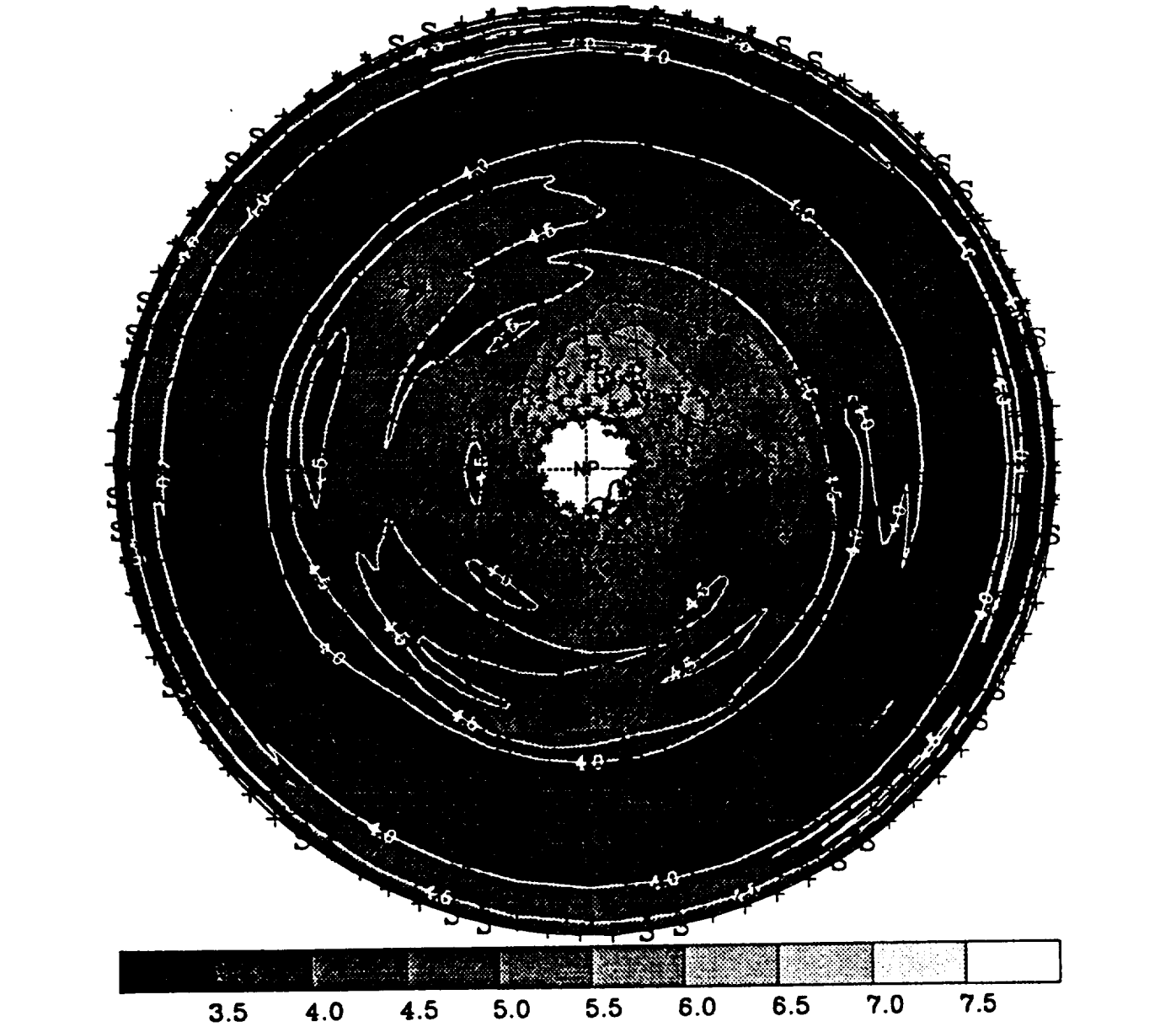

(b)

Figure 6.2.3-2 Continued.

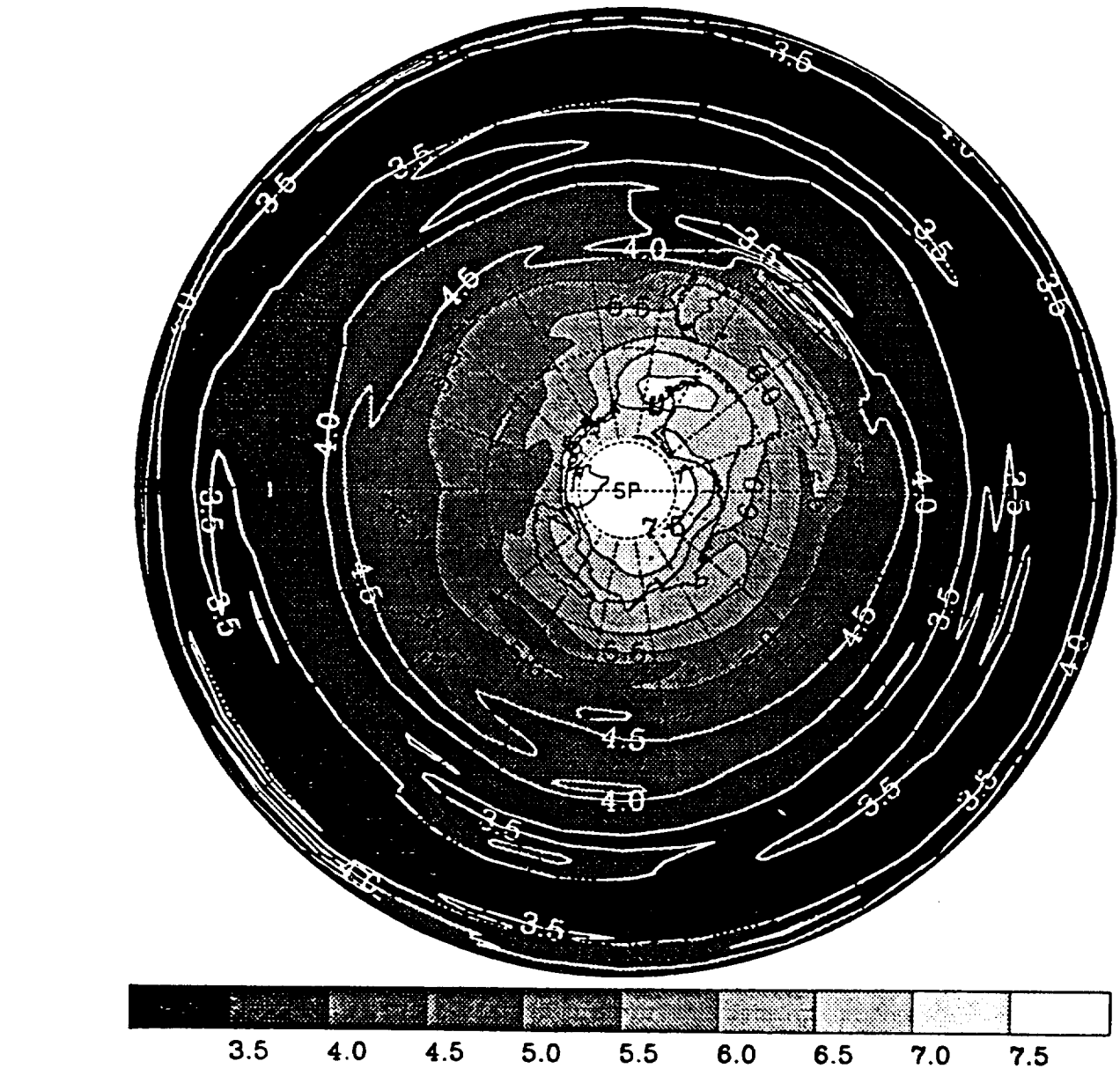

(c)

Figure 6.2.3-2 Continued.

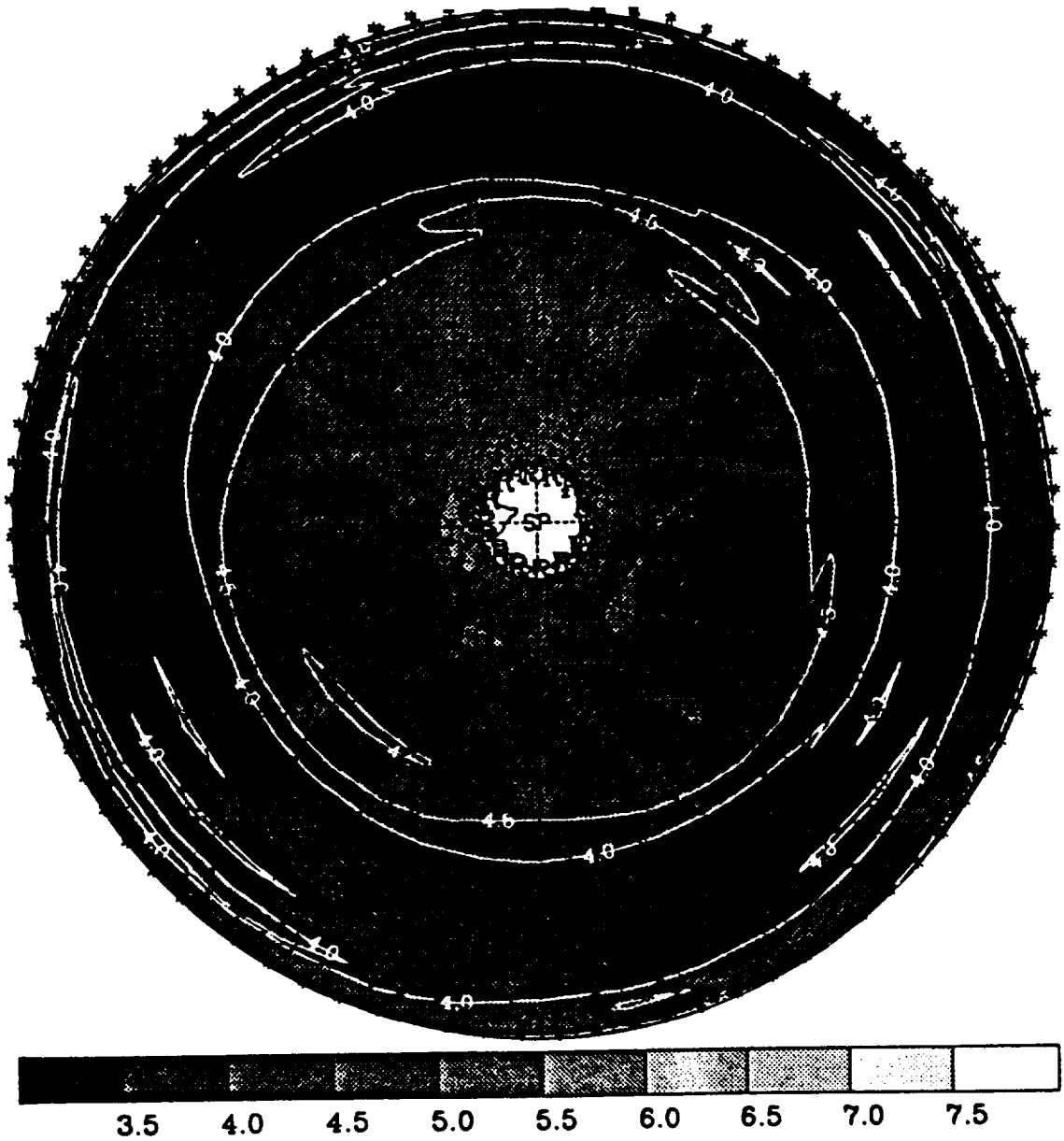

(d)

Figure 6.2.3-2 Concluded.

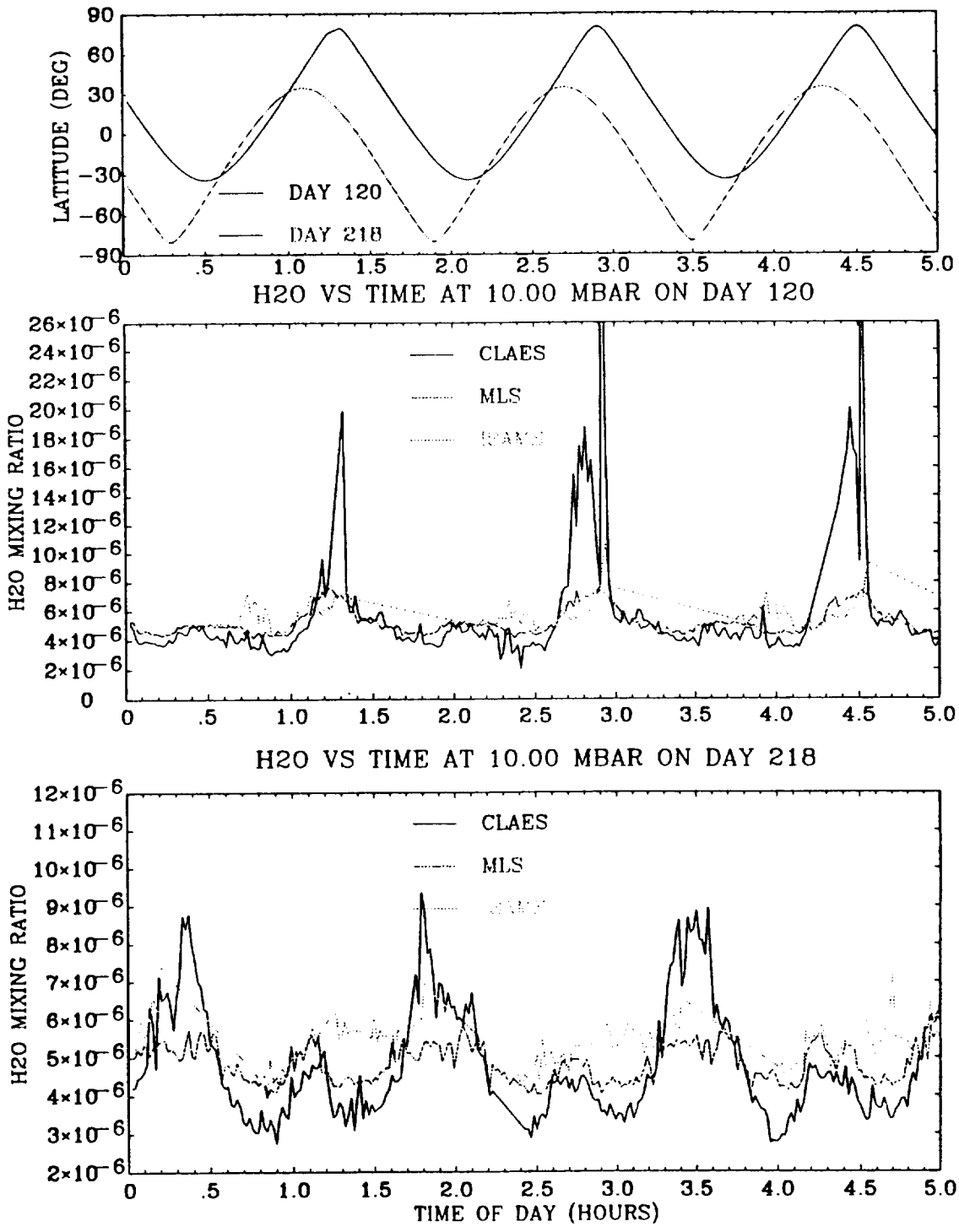

Figure 6.2.4-1 Time tracks of the CLAES, MLS and ISAMS water vapor mixing ratio at 10 mb on Jan. 9, 1992 and April 16, 1992. The top panel shows the latitudinal variation of the time track, the bottom two panels show mixing ratios on the two days.

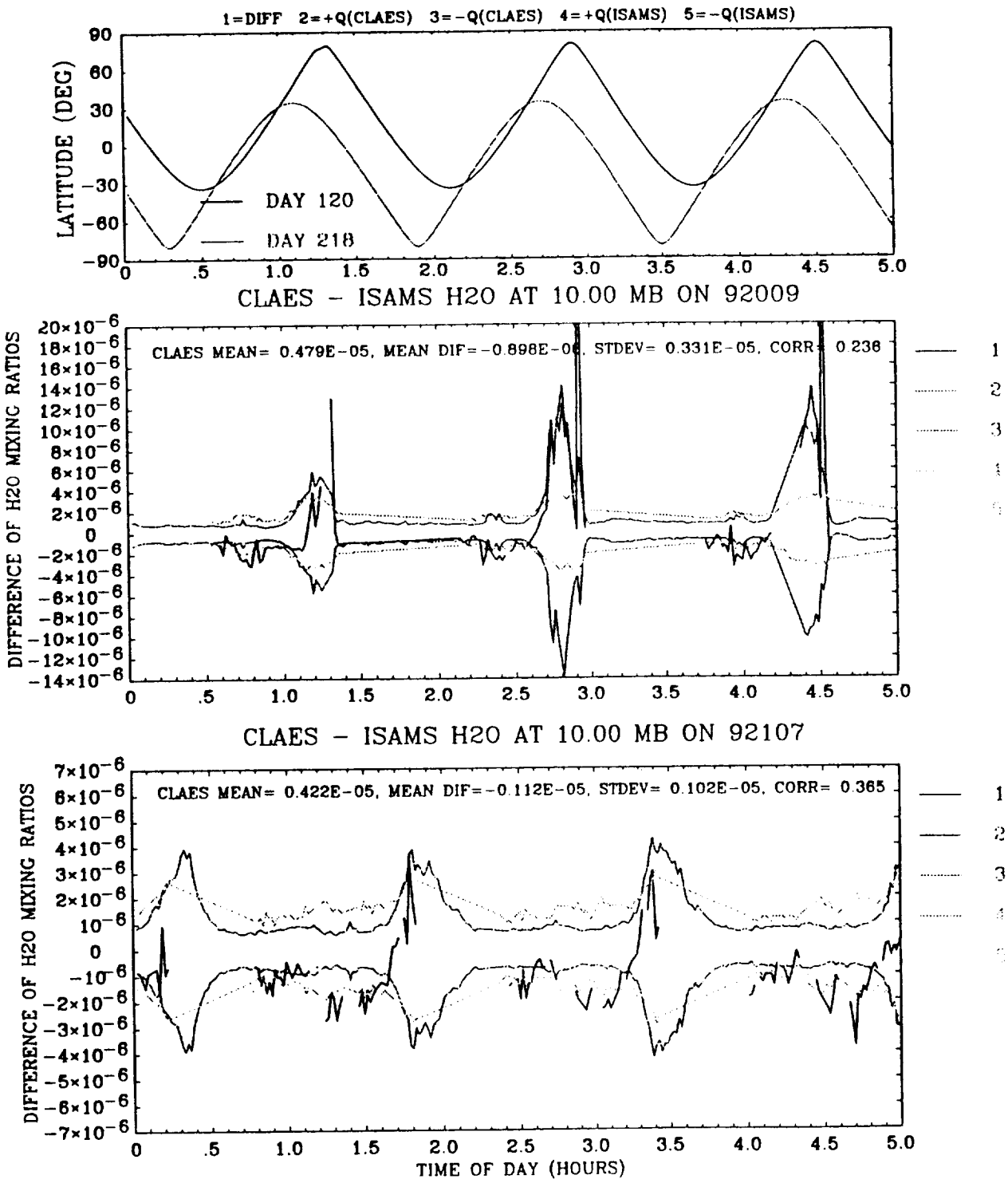

Figure 6.2.4-2 Analysis of the CLAES-ISAMS H_2O distribution at 10 mb on Jan. 9, 1992 and April 16, 1992. The top panel shows the latitudinal variation of the time track. The bottom two panels show the differences and CLAES and ISAMS quality indicators.

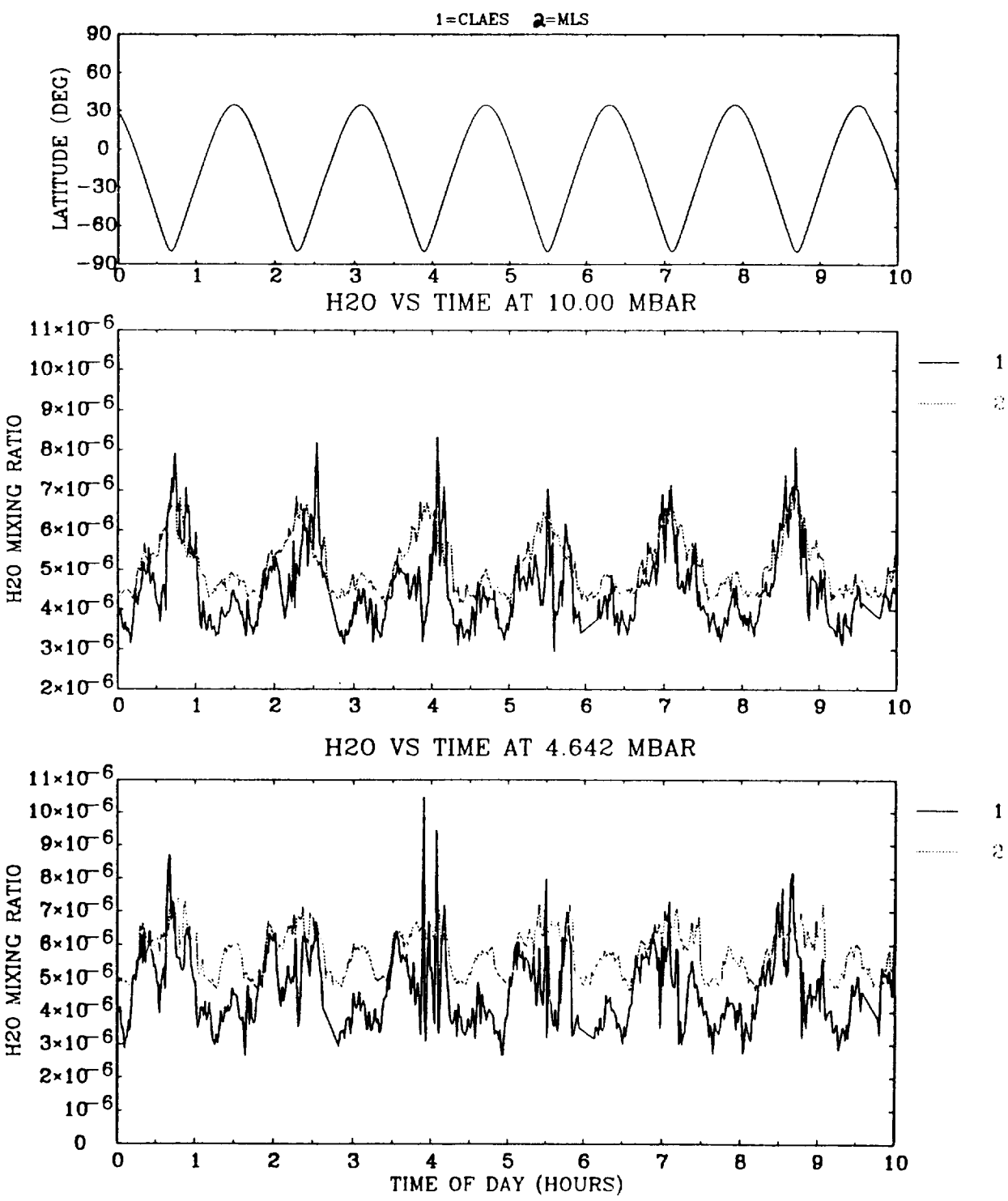

Figure 6.2.4-3 Time tracks of the CLAES and MLS water vapor mixing ratio at 10 mb and 4.6 mb on Aug. 28, 1992. The top panel shows the latitudinal variation of the time track. The bottom two panels show mixing ratios at the two pressure levels.

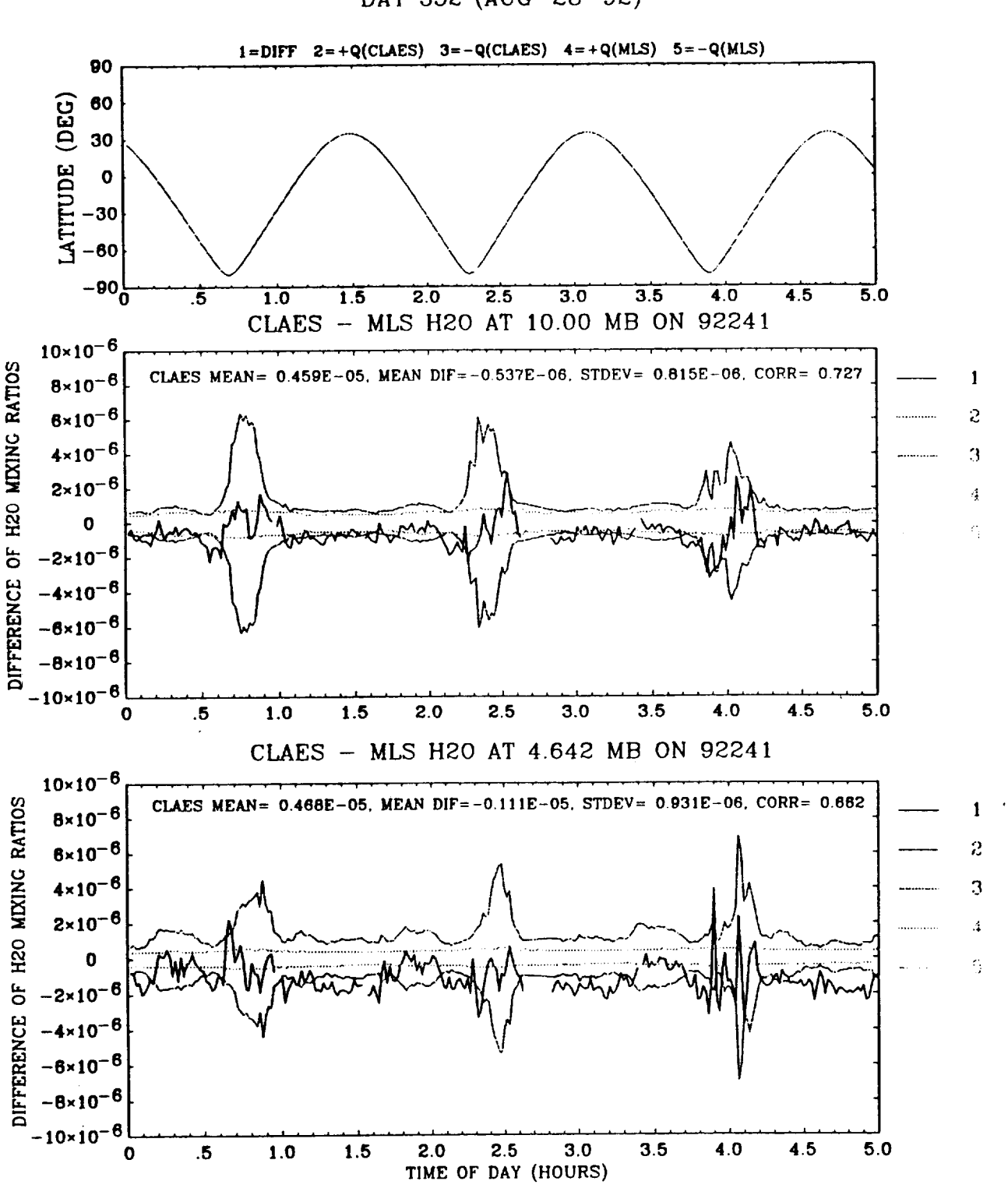

Figure 6.2.4-4 Analysis of the CLAES-MLS H_2O distribution at 10 and 4.6 mb on Aug. 28, 1992. The top panel shows the latitudinal variation of the time track. The bottom two panels show the differences and the CLAES and ISAMS quality indicators.

7. LONG-LIVED TRACERS (CH_4, N_2O, CO, CF_2CL_2)

7.1 Correlative Data

Correlative data were available from a number of different Correlative Measurement Investigator (CMI) instruments for validation of the long-lived tracer data. The principal correlative instruments for the long-lived tracers are briefly described in this section. In all cases comparisons are made with CLAES Version V0006, ISAMS Version V0008, and HALOE Version V0012.

7.1.1 Cryogenic Whole Air Sampler (Ed Zipf)

Mixing ratio data was available for methane (CH_4), nitrous oxide (N_2O), and carbon monoxide (CO) for six flights of the cryogenic whole air sampler launched from the White Sands Missile Range (32.4N, 253.7E) as part of the CMI program. Samples were recovered in the altitude range 30 - 60 km. Flights were conducted in 5 series of 2 flights each. Only one-half of the altitude range was sampled in any single flight, so data from both flights in a series must be used to produce vertical profiles over the whole range of altitudes sampled. Results from these flights are shown as vertical profiles (Fig. 7.2.1-2, Fig. 7.3.1-2, and Fig. 7.4-5).

7.1.2 Far-Infrared Fourier Transform Spectrometer (Wes Traub)

Data on N_2O was available from a single balloon flight of this instrument launched from Fort Sumner, New Mexico (34.7N, 253.3E) on May 29, 1992, covering the altitude range 18-50 km. A comparison with CLAES and ISAMS profiles within ~600 km of the balloon is shown in Fig. 7.3.1-4.

7.1.3 Mk IV Interferometer (G. C. Toon)

The MK IV instrument is a high resolution infrared solar absorption interferometer capable of obtaining vertical profiles of volume mixing ratio for a number of species, including $CFCl_3$, CF_2Cl_2, and N_2O between about 17 - 37 km and can also obtain total column measurements above balloon float altitude. One flight of this instrument on September 15, 1992 (35N, 255E) was available for this validation.

7.2 Methane Results

7.2.1 Vertical Profiles

Mixing ratio profile comparisons for the January and April validation periods were carried out for CLAES, ISAMS, and HALOE. Similar comparisons were made between CLAES and HALOE for the August validation dates. All profiles cover the pressure range from 0.2 - 10 mb for ISAMS with HALOE and CLAES extending down below the 10 mb level in most cases. The general shape of the individual and mean profiles is similar down to the 10 mb level for all instruments. The profile slope is steeper for HALOE in the January period and somewhat steeper for CLAES and HALOE than for ISAMS in the April period. Figure 7.2.1-1 shows the mean for 28 coincident profiles for each instrument from the January intercomparison period. These data are representative of all the intercomparison periods down to the 10 mb level. The exception is ISAMS, which appears 10-20% higher than CLAES and HALOE in the April period. The ISAMS and CLAES mixing ratios are generally about 20% higher than the HALOE values above the 1 mb level with closer agreement at the top of the profiles. The HALOE mixing ratios values are lower than those of CLAES and ISAMS by up to 40% between 1-10 mb for this

January period, but HALOE is 30% lower, at most, than CLAES on the April and August dates. Below the 10 mb level the January means in figure 7.2.1-1 indicate that HALOE is lower than CLAES except around the 30 mb level where there is a dip in the CLAES mean profile. In the other three intercomparison periods, this dip around the 30 mb level is larger with resulting 20-40% differences between CLAES and HALOE. In the January period there is a considerable longitude dependence in the CLAES-HALOE profile differences around 10 mb. The differences are similar to those of the other periods between 20 to 100 degrees and 150 to 250 degrees east longitude, but this is not the case for the other longitudes where a large temperature gradient may influence the inversions in this period. These regions with large temperature gradients are addressed further in the longitude cross-sections discussion. Below the 30 mb level, CLAES and HALOE differ by up to 20%. Below the 50-mb level the CLAES data is preliminary.

Five sets of correlative measurements for UARS methane profiles from the Cryogenic Whole Air Sampler rocket flights and a single balloon flight were available for comparison. Figure 7.2.1-2 shows comparisons between the five rocket flights and CLAES, HALOE, and ISAMS data (ISAMS for May 1992 flights only). On average, HALOE and CLAES appear to be within 20% of the rocket measurement at all levels , with HALOE low and CLAES high. ISAMS is within 20% of the May 22, 1992 rocket flight (low altitude sampling), but ISAMS is higher than the May 27, 1992 rocket flight (high altitude sampling).

Figure 7.2.1-6 compares CLAES and HALOE profiles to a balloon occultation measurement on September 15, 1992. CLAES and the balloon measurement are within the error bars down to the 3 mb level, as well as from the 7 mb level down to 20 mb. CLAES is higher than the balloon measurement by up to 20% in the 3-7 mb range and lower by up to 40% below the 20 mb level.. HALOE and the balloon measurement are within the error bars down to the 2 mb level and below the 10 mb level. In the 2-10 mb range, HALOE is lower by up to 30%. It should be noted that the HALOE measurement was taken 14 days after the balloon flight.

Finally, Figure 7.2.1-7 shows the relative difference between the UARS emission measurements of methane during March 25 - April 2, 1992 and the ATMOS data obtained during a shuttle flight in the same period during 1985. Overall, both individual and zonal mean profiles are similar for all three instruments. The ISAMS and CLAES mixing ratios are consistently higher than HALOE, with correlative data between the three in most cases. CLAES and HALOE values agree reasonably well above the 1 mb level, with ISAMS higher than both. HALOE values are nearly always lower than CLAES and ISAMS from the 1 mb level down to about the 10 mb level. The magnitude of the discrepancy is not the same during the different intercomparison periods and even shows a longitude dependence in the January period. Between about 10 and 50 mb when there is HALOE data, the HALOE values are greater than those of CLAES. At the 50 mb level the two instruments have good agreement. It should be noted that the latest HALOE results indicate there may be a low bias in HALOE methane on the order of 10% from 5 - 100 mb and possibly an even larger bias around the 1 mb region. This bias estimate is based on comparisons of data from HALOE retrievals of methane mixing ratio using three field-of-view convolutions with data from the present retrieval which has one convolution. The HALOE group is currently testing this new retrieval, and if this bias is present for the intercomparison dates, the agreement of HALOE with CLAES and ISAMS would be improved. In addition, methane profiles produced from future HALOE retrievals using the HCI channel (radiometer) V signals can be compared with the current methane profiles from all three instruments.

7.2.2 Zonal Mean Latitude-Height Cross -Sections

Zonal mean cross-sections for ISAMS and CLAES methane are presented in Figure 7.2.2.1 (January 9, 1992) and Figure 7.2.2.2 (April 16, 1992). Also shown are ratios of the zonal mean

data from the UARS instruments (ISAMS - CLAES/ ISAMS), and a 2-D model simulation (Edinburgh/Cambridge model). The model is a transformed Eulerian mean model including photochemistry and an equatorial zonal wind quasi-biennial oscillation in which the modeled equatorial wind is relaxed to observed values. It does not contain an explicit parameterisation of the semi-annual oscillation. The ISAMS CH_4 data are contaminated by aerosol at pressures of 10 to 5 mb and latitudes of -30S to 20N with the effect varying through the data set. CLAES data tend to exhibit a maximum near the Equator, but the effect varies with season and may well represent a problem with aerosol correction of the CLAES data. The ratio plots show that the zonal mean difference between ISAMS and CLAES is of the order of 10% in January, but closer to 20% in April with more structure to the difference.

The CH4 distributions measured by ISAMS and CLAES are consistent with the mean meridional circulation simulated by 2-D models (i.e. regions of higher mixing ratios at equatorial latitudes and regions of lower mixing ratios at higher latitudes). The ISAMS data suggest a particularly strong cross-equatorial flow from south to north in January (Fig. 7.2.2-1). This flow may be distorted by residual aerosol effects, but is also evident in the CLAES data. The ISAMS data also show steeper poleward gradients in the mid-latitudes (30-5ON) than does CLAES in January. Data from both instruments show a pronounced "double peak'" structure at higher altitudes for April (Fig. 7.2.2-2), confirming earlier observations by the SAMS instrument. The double peak is thought to be related to the circulation pattern associated with the equatorial semi-annual oscillation, and this would explain why it is not well represented in this particular 2-D model. The UARS CH_4 data therefore confirm the expected circulation patterns and have some interesting features which need to be investigated.

7.2.3 Longitude-Height Cross-Sections

Longitudinal cross-section comparisons for the January and April validation periods were carried out for CLAES, ISAMS, and HALOE. Similar comparisons were made between CLAES and HALOE for the August validation dates. The general features compare fairly well in the January period and better in the other three periods, although the magnitudes of the mixing ratio values can be quite different for the different instruments.

Longitudinal cross-sections for the January 9-11 period are given in Figures 7.2.3-1 and 7.2.3-2 for CLAES, ISAMS, and HALOE, along with the HALOE temperature cross-section for January 9. The percent difference cross-sections are given in Figure 7.2.3-3. From 0.1 to 1 mb, ISAMS values are 10-30% higher than those of HALOE. Between 1-10 mb, the difference is also 10-30% from 20 to 250 degrees east longitude. Outside this longitude range the difference is 50% or larger. From 0.1-0.2 mb there is a large percent difference, with CLAES higher than HALOE by up to 50%. From 0.2-2 mb CLAES is higher than HALOE by 10-20%, with a small area reaching 30% (note however, some regions with HALOE 10% higher than CLAES). Between 2 -20 mb there are large longitudinally dependent differences between CLAES and HALOE (see subsequent discussion). In the 20-30 mb range, CLAES and HALOE differ by 20-30%.

The large 50% or greater differences observed between the three instruments, corresponding to large temperature gradients in the 2-20 mb region, are also coincident with a region of strong vertical descent observed by HALOE (Fig 7.2.3-2). This strong descent also appears in the longitudinal cross-sections of HALOE HF and 5.26 micron aerosol (Figure 7.2.3-4) in the same region for January 9. The three HALOE tracers show consistent dynamical patterns. This type of strong vertical descent is also reported for the 1991 Antarctic vortex region (see Russell et al. 1993). The CLAES and ISAMS methane cross-sections (Figure 7.2.3-1) also show some sign of

this descent, but not as strong as seen in the HALOE data, resulting in the large percent differences seen in Figure 7.2.3-3. The previously mentioned sizable temperature gradients observed by the three instruments (Fig 7.2.3-2 for HALOE) may be one important source of the large differences in this region, since the CLAES and ISAMS measurements could be sensitive to horizontal and vertical temperature gradients. This temperature effect warrants further investigation.

Longitudinal cross-sections for the April 15-17 period are shown in Figure 7.2.3-5, and the percent differences are shown in Figure 7.2.3-6. For this period ISAMS is higher than HALOE by 20-50% above the 3 mb level, and the two are within 10% below the 3 mb level. Above the 0.2 mb level, CLAES and HALOE differ by as much as 50%. From the 0.2 mb level down to the 10 mb level, the difference is 10-30% with CLAES generally higher than HALOE. Below 10 mb HALOE is higher than CLAES by 10-30%. The results in the two August intercomparison periods are similar to those of April for CLAES and HALOE.

7.2.4 TimeSeries

Comparisons of CLAES and ISAMS were made along the orbital track for January 9-10, 1992 (UARS days 120 and 121) and April 16, 17, and 18, 1992 (UARS days 218, 219, and 220) for UARS pressure surfaces 10, 4.64, 2.15, and 0.46 mb. Direct comparisons and difference plots were made with computed 24-hour mean differences, standard deviations of the differences, and correlation coefficients. There are no ISAMS CH_4 data for the later comparison days in early and late August 1992.

COMPARISON RESULTS: 10 and 4.6 MB

Direct comparisons and selected difference plots are shown in Figures 7.2.4-1 through 7.2.4-4 for January 9 and April 17, 1992. Table 7.2.1 summarizes differences and correlations for the whole set of 5 days and 4 pressure levels examined. At the 10 mb level, there is good overall agreement in absolute magnitude between the two instruments, with 24-hour mean difference between -5.3% and -11% (ISAMS greater) and the standard deviation between 25 and 34% ,for the 5 days examined. Examination of the comparison and difference plots for January 9 and April 17 show that most of the contribution to the mean difference occurs near tropical latitudes. ISAMS exceeds CLAES by as much as 65%, for example on April 17 in the region 0 to 25S, but agrees within a few percent for latitudes outside this range. For all latitudes the differences between the instruments are contained within their estimated errors, except for the large CLAES "spike" at high latitude on January 9.

At the 4.6 mb level the instruments also agree well in magnitude (24-hour mean difference lies between 11.3 and 21.2 % and standard deviations between 19 and 22% for the 5 days examined) with the April days showing the better agreement. The large tropical difference signature seen at the 10 mb level is much less evident, with the difference between the data sets much more constant with latitude. The January 9 and April 17 figures also show that the instruments track one another better around the orbits at 4.6 mb than at 10 mb, as evidenced by the smaller standard deviations and higher correlation coefficients for the 4.6 mb cases. Again the differences are contained within the instrument error estimates, although there are occasional "spikes" in the January 9 CLAES data which exceed the ISAMS error estimates. The large CLAES spike seen in the January 9 data at 10 mb is also evident at 4.6 mb. There is no equivalent spiking in the April data. The source of these spikes is under investigation with the intention of eliminating them in future software versions.

COMPARISON RESULTS: 2.2 and 0.46 MB

At the 2.2 mb level the 24-hour mean difference between the instruments lies between -5.5 and -8.7 % and standard deviations between 25 and 29% for the days examined (Table 7.2.1). The data sets track one another well around the orbits, as evidenced by correlation coefficients in the 0.82 range. The largest differences tend to occur between 30N and 30 S where ISAMS can exceed CLAES by the order of 60%, and there are occasional situations where spikes in the CLAES data can cause differences well in excess of the error estimates. At the 0.46 mb level, the 24-hour mean differences between the data sets are also small (1 to 5%), and the instruments track the major features well around the orbits, although at this altitude noise in the retrieved data plays a bigger role and contributes to the lower correlation coefficients. We have also observed some negative values in the April ISAMS tracks, confined to a few degrees of latitude near 25N on the descending node that are not seen by CLAES. These features are being investigated.

SUMMARY

The instruments are in overall good agreement in absolute magnitude for all days and pressure levels examined. The 24-hour mean differences (with the exception of the 21% seen for 4.6 mb on January 9) are all less than 15% for all days and pressure surfaces, and standard deviations about the mean are less than 34%. The main contribution to the standard deviation usually comes from tropical latitudes where the ISAMS mixing ratios can exceed CLAES by as much as 60%, especially at 10 mb. Differences are typically contained within the listed instrument error estimates except for occasional spikes seen in the CLAES data which can induce large differences. The instruments track one another reasonably well around the orbits, especially at the 4.6 and 2.2 mb levels, where correlation coefficients are typically in the 0.8 range. Tracking is somewhat poorer at the 10 mb level (correlation coefficients in the 0.7 range in January, 0.5 in April), and poorest at 0.46 mb (correlation coefficients from 0.54 to 0.58).

Table 7.2.1- CH4: CLAES Versus ISAMS Differences				
Date	Pressure	Mean Diff. (ppmv)	Standard Dev. (ppmv)	Correl. Coef
	10 mb	0.088 (8.9%)	0.24 (24.7%)	0.68
Jan 9	4.6 mb	0.19 (21.2%)	0.20 (21.6%)	0.8
	2.2 mb	-0.035 (5.6%)	0.16 (25.4%)	0.82
	10 mb	- 0.11 (11%)	0.31 (31.3%)	0.67
Jan 10	4.6 mb	0.13 (14%)	0.18 (19.4%)	0.84
	2.2 mb	-0.024 (3.8%)	0.16 (25.0%)	0.8
	0.46 mb	0.0026 (1 %)	0.041 (16.4%)	0.54
	10 mb	0.13 (13.2%)	0.26 (26.3%)	0.54
April 16	4.6 mb	0.13 (15.4%)	0.18 (21.4%)	0.81
	2.2 mb	0.057 (9.1%)	0.18 (28.6%)	0.83
	0.46 mb	-0.015 (4.9%)	0.077 (25.7%)	0.55
	10 mb	-0.05 (5.3%)	0.34 (34.3%)	0.51
	4.6 mb	0.1 (11.8%)	0.18 (21.2%)	0.78
April 17	2.2 mb	-0.046 (7.3%)	0.18 (28.6%)	0.82
	0.46 mb	-0.014 (4.7%)	0.073 (24.5%)	0.58
	10 mb	-0.056 (5.7%)	0.34 (34.3%)	0.52
April 18	4.6 mb	0.096(11.3%)	0.17(20%)	0.81
	2.2 mb	-0.054 (8.7%)	0.18 (29%)	0.83
	0.46 mb	-0.0094 (3.1 %)	0.074 (24.7%)	0.58

7.3 Nitrous Oxide Results

7.3.1 Vertical Profiles

A number of correlative comparisons have been made for nitrous qxide. Figures 7.3.1-1 and 7.3.1- 2 compare UARS measurements with the Cryogenic Whole Air Sampler (CWAS) rocket data from Ed Zipf. All the CWAS flights considered here could be compared with co-located CLAES data. A summary of the mean differences between CWAS and CLAES is therefore provided (Fig. 7.3.1-2, right panel). On average, CLAES data are lower than CWAS data in the 30 km to 45 km region by up to 30%, but there are considerable differences from flight to flight as indicated by the standard deviation curve. At higher altitudes, there is less evidence of any

systematic disagreement. The large average fractional difference above 55 km is caused by the poor comparison for March 10, with other days showing better results. ISAMS recorded data at the same time as two of the CWAS flights, and the results are presented in Figure 7.3.1-l (middle). The ISAMS data are higher than the CWAS data at all heights, but agree best with the CWAS data between 35 km and 40 km.

It was also possible to compare UARS N_2O measurements with data from two balloon flights. A comparison of ISAMS and CLAES data with that from Wes Traub's flight of May 29, 1992 is shown in Figure 7.3.1.3. The CLAES data agree much better with the Traub data than do the ISAMS data, but below 10 mb there is considerable difference between the CLAES and Traub data. Figure 7.3.1.4 shows a comparison with Toon data on September 15, 1992 and CLAES data. The agreement is reasonably good except in the 10 to 40 mb region where the CLAES profile shows a distinct kink which is not reflected in the Toon data.

It was also possible to compare CLAES data with ground-based microwave measurements by De Zafra on four days in February 1992 and five days in March 1992. Figure 7.3.1.5 shows the average difference between the CLAES and De Zafra data, the error bars being the standard deviations of the differences. On average, CLAES data are larger than the microwave data by about 20%, but there is a large scatter in the differences as indicated by the error bars.

Finally, the CLAES and ISAMS N_2O are compared with data from the 1985 ATMOS shuttle observations in Figure 7.3.1-6.

7.3.2 Zonal Mean Latitude-Height Cross -Sections

Zonal mean cross-sections for ISAMS and CLAES N_2O data are presented in Figures 7.3.2.1 (January 9, 1992) and 7.3.2.2 (April 16, 1992). Also shown are ratios of the zonal mean data from the UARS instruments (ISAMS - CLAES/ISAMS), and results from a 2- D model simulation (Edinburgh/Cambridge model). The model is a transformed Eulerian mean model with photochemistry. It includes an equatorial zonal wind quasi-biennial oscillation in which the modeled equatorial wind is relaxed to observed values, but it does not contain an explicit parameterisation of the semi-annual oscillation. The results may also be compared with the zonal mean CH_4 plots of Figures 7.2.2.1 and 7.2.2.2 and show excellent agreement in the gross features. The major difference between the two UARS measurements of N_2O is the large systematic offset between them (which on average is about a factor of two), but can be as high as a factor of three (at 2 mb on January 9). Smaller features which are problematic include the small maximum in the CLAES data at 15 mb on January 9 (not obviously present in the CLAES data for April) which may indicate a small problem with aerosol correction as noted for the CLAES CH_4 data. Calculations show that the ISAMS N_2O data are also contaminated by aerosol at pressures between 10-5 mb and latitudes of -30S to 20N as was noted for ISAMS CH_4 data. The N_2O distributions measured by ISAMS and CLAES agree well with the mean meridional circulation predicted by the 2-D model and with the CH_4 distributions measured by the same instruments (see section 7.2.2). CLAES data showed different gradients in CH_4 and N_2O at certain times (e.g. August in the southern hemisplIere), but it was not clear that the same effect could be seen in ISAMS data (which does not cover the same vertical range). The UARS N_2O data, as for the UARS CH4 data, are therefore consistent with the gross features of the expected circulation, but the details require some investigation.

7.3.3 Time Series Comparisons

Comparisons between CLAES and ISAMS data were made along the orbital track for January 9

and 10, 1992 (UARS days 120 and 121) and for April 16-18, 1992 (UARS days 218, 219, and 220) for UARS pressure surfaces 10, 4.64, and 2.15 mb. Both direct comparisons and difference plots were made with computed 24-hour mean differences, standard deviations of the differences, and correlation coefficients. There are no ISAMS N_2O data for the later comparison days in early and late August.

COMPARISON RESULTS: 10, 4.6, and 2.2 MB

Direct comparisons and selected difference plots for 10 and 4.6 mb levels are shown in Figures 7.3.3-1 through 7.3.3-4 for January 9 and April 17, 1992. Table 7.3.1 summarizes differences and correlations for the whole set of 5 days and three pressure levels examined.

At 10 mb, Figures 7.3.3-1 and 7.3.3-3 show that the instruments track one another reasonably well around orbits, especially in January, where a correlation coefficient of 0.75 is calculated. However, there are systematic differences between the data sets, especially at tropical latitudes, where ISAMS can exceed CLAES by 60% or more. This effect is more evident in the difference plots (Figures 7.3.3-2 and 7.3.3-4). These tropical differences are the main contributors to the overall 24-hour mean differences of about 26% for the 5 days examined , with standard deviation of about 44%. In general, the differences between the instruments are within the combined error estimates, except for occasional spikes where CLAES exceeds ISAMS by significant factors.

Similar behavior is seen at 4.6 mb (i.e. the instruments track well around the orbits as evidenced from correlation coefficients in the 0.82 to 0.88 range) and the data sets show systematic differences, most noticeably in the tropics. The 24-hour mean difference for all the days examined is approximately 48%, with standard deviation of about 48%. The April days tend to show larger differences. Unlike the results for the 10 mb level, the differences in the tropics are not generally within the combined error estimates.

At the 2.2 mb level (Table 7.3.1), the instruments were observed to continue to track well with similar correlation coefficients to those at other levels. However, the systematic differences are considerably larger, reaching as much as a factor of 10 near tropical latitudes, with resultant mean difference and standard deviation exceeding a factor of 2, well in excess of the combined error estimates

SUMMARY

For all of the days and pressure levels examined, CLAES and ISAMS show reasonably good correlation along time tracks. However, ISAMS is systematically larger than CLAES, mostly in the tropics and most noticeably at 2.2 mb. Tropical differences are between 60-100% at 10 and 4.6 mb and as much as a factor of 10 at 2.2 mb. The 24-hour mean differences average approximately 26 % at 10 mb, 48% at 4.6 mb, and 116% at 2.2 mb. Apart from the 10 mb level, the systematic difference between the data sets are well in excess of the combined error estimates.

Table 7.3.1 N_2O: CLAES versus ISAMS Differences				
Date	Pressure	Mean Diff. (ppbv)	Standard Dev. (ppbv)	Correl. Coef
	10 mb	-3.9 (4%)	39.2 (41.0%)	0.7S
Jan 9	4.6 mb	-11.9 (24%)	21.3 (43%)	0.88
	2.2 mb	-26.6 (123~)	27.9 (129%)	0.872
	10 mb	- 40.4 (41%)	37.1 (38%)	0.8
Jan 10	4.6mb	-29.7 (58%)	21.2 (41%)	0.82
	2.2 mb	-27.9 (123%)	27.8 (122%)	0.88
	10 mb	11.3 (11%)	42.2 (41%)	0.61
April 16	4.6 mb	-14.9 (37%)	20.8 (52%)	0.83
	2.2 mb	-22 (105%)	21.1 (101%)	0.79
	10 mb	-37.3 (37%)	52.2 (51%)	0.6
April 17	4.6 mb	-24.4 (59%)	21.3 (51%)	0.85
	2.2 mb	-24 (116%)	21.7 (105%)	0.82
	10 mb	-36 (35%)	51.6 (51%)	0.63
April 18	4.6 mb	-24.7 (63%)	20 (51%)	0.88
	2.2 mb	-23.2 (115%)	21.1 (104%)	0.83

7.4 ISAMS Carbon Monoxide Data

Zonal mean ISAMS CO data for January 9, 1992 are compared in Figure 7.4.1. to results from the GSFC 2-D model. In ISAMS Version 8 data, the errors are much higher in the nighttime data than in the daytime, implying that the tie to climatology is much greater in the nighttime data . Nevertheless, the structure in the zonal mean cross-sections for day and night is similar, although there is a bias between the two. Since the daytime data is of better signal-to-noise and smaller bias towards climatology, it is more usefully compared to the 2-D model simulations. Apart from the much larger values of CO retrieved by ISAMS, there is also a difference between ISAMS and the model results in the gradients of mixing ratio toward the winter pole. This difference gives rise to the big feature in the difference plot, centered at 40N and 0.35 mb. The difference might be expected, given the dynamical situation on January 9. It is encouraging that both model results and data show strong downward movement of the isopleths near the winter pole.

ISAMS is the only UARS instrument that measures CO, and correlative measurements are therefore of great importance. So far, it has only been possible to compare CO data with Ed Zipf's Cryogenic Whole Air Sampler (CWAS) rocket data during May 1992. The comparisons are shown in Figure 7.4.2. The two data sets give reasonably good agreement at low altitudes, but differ considerably at the upper altitudes in the data of day 259 (May 27, 1992). It is hoped that data from the ATLAS mission in April 1992 will be soon be available for comparison with

the ISAMS data and should be very useful in understanding the differences with the Zipf data.

7.5 CF_2Cl_2 Data

CLAES is the only UARS instrument that measured CF_2Cl_2 (CFC12). At the time of this validation workshop, the only correlative data available for comparison was that from the balloon-borne MKIV interferometer (Toon, 1993) for September 15, 1992 at 34.9N, -105.8E. This comparison is shown in Figure 7.5.1-1. We also made a comparison with an ATMOS 1985 profile, but with the ATMOS tropopause mixing ratio scaled to match the most recent tropospheric measurements of CFC12 (Elkins et al., 1993). This comparison is shown in Figure 7.5.1-2. There were no correlative cross-section data for comparison, and we used the Lawrence Livermor National Laboratory (LLNL) 2-D model for comparison purposes.

7.5.1 Allitude Profiles

Figure 7.5.1-1 shows good agreement in the vertical profile shape of the CLAES and balloon data over the 5-40 mb range of overlap. The absolute values of the balloon data are within the CLAES error estimates. However, the CLAES mixing ratios are systematically higher than the balloon data, especially at altitudes below 10 mb (by about 30% for averaged sunset/sunrise data or about 20% for the sunrise data). Given the size of the error estimates for the balloon data, this comparison would also suggest that the CLAES errors are overestimated. Comparisons with the scaled 1985 ATMOS data (Fig. 7.5.1-2) is mainly of interest for qualitative assessment of profile shapes, since it might be expected that both interannual variability and different meteorological conditions, would make absolute comparisons between data sets separated by 7 years of limited value. Considerable variability is seen in the three CLAES profiles shown in Figure 7.5.1-2 over the six-week period March 15 to April 27, especially above 24 km. Nevertheless, quite good agreement is seen between the CLAES data and the scaled ATMOS profiles. All 4 profiles are within about 10% of one another from 15 to 25 km. The most divergent profile above 24 km is that for April 27, 1992.

7.5.2 Zonal Mean Latitude-Height Cross-Sections

Comparisons between CLAES zonal mean cross-sections and the LLNL 2-D model simulations are shown for January 10, April 16, August 9, and August 25, 1992, in Figures 7.5.2- 1 and 7.5.2-2. These comparisons include winter high latitudes for both hemispheres and a northern hemisphere spring. For January 10, 1992 (Figure 7.5.2-1, left panels), reasonable agreement is seen in the overall structure, especially above 20 mb. The data show a much more pronounced bulge between 15S and 15N and in general shows steeper latitudinal gradients and more large-scale structure. In absolute values, the data show higher values near the tropics, especially below about 20 mb and better agreement with the model poleward of about 30N.

For April 16, 1992 (Figure 7.5.2-1 right panels), the equatorial bulge in the CLAES mixing ratios is not as pronounced, and better agreement is seen both in structure and absolute value for all altitudes, especially between 60S and 32N. The data show an apparent maximum near the south pole that is not seen in the northern polar data, nor reproduced by the model. This feature is not consistent with the expectation of down-welling of air near the cooling pole. This feature is discussed further below in relation to the August 26 comparison.

For August 9, 1992 (Figure 7.5.2-2, left panels), agreement between the data and model are much improved in the equatorial region. As with the January 10 data, there is little evidence of a

northern polar maxinlum as seen in the April south pole data.

For August 26. 1992 (Figure 7.5.2-2, right panels), there is generally reasonable agreement in structure and absolute value between the data and the model, except in the south polar region, poleward of about 50S, where a very distinct apparent upwelling is seen.

7.5.3 Summary and conclusions for CF_2Cl_2

Altitude Profiles: Comparison with 32N correlative balloon data for September 1992 shows good profile shape agreement and absolute value differences varying be~ween about 10% and 30% from 10-40 mb with CLAES being higher. Comparison with the 1985 scaled ATMOS profile at 32N for the April-May period shows good agreement in shape and absolute value for a series of CLAES profiles, especially between 16 and 24 km.

Zonal Mean Cross-Sections: There is reasonable structural agreement with the 2-D model for all periods, except for the southern winter polar latitudes. Overall, the data tends to show steeper latitudinal gradients poleward of 30S and 30N. Above 20 mb the mixing ratios are in fair agreement. At lower altitudes in the tropics, CLAES starts off significantly higher than the model values in January 1992, with better agreement as we progress into the later months This behavior might suggest incomplete removal of the effects of interference from the Pinatubo aerosol cloud in the CFC12 retrieval. The cloud would be most intense in the tropics at altitudes below 30 mb, dissipating significantly between January and August 1992. Additional correlative data will be important in investigating this issue and will guide the possible need for improved aerosol handling in future software versions.

The most noticeable difference between the data and the model results occurs for the southern winter polar comparison of August 26, 1992, where an apparent upwelling is seen in the CFC12 mixing ratio cross-sections. A possible explanation for this feature is incomplete removal of nitric acid interference from the measured spectra. Only weak HNO_3 lines are normally present in the CFC12 spectra. The current algorithm (producing version 0006 data) uses climatological values of the HNO_3 mixing ratio to remove these weak contributions. In the southern winter polar stratosphere however, there is a large build-up of HNO_3 in a collar region near 60S, then a band of very low values poleward of this collar inside the polar vortex (Roche et al, 1993). The high collar values are much higher and the low values are much smaller than the climatological values, so that the use of climatology may be inadequate for removal of HNO_3 effects in this region of the atmosphere for winter conditions. The fact that the effect is not as evident in the northern hemisphere winter may be due to the much less pronounced HNO_3 collar structure. If HNO3 interference is indeed the problem, use of retrieved (rather than climatological) mixing ratios of HNO_3 in the retrieval of CFC12 should greatly improve the situation. This approach will be incorporated in future software versions. Improved HNO_3 spectral parameters are now available for this region and will be incorporated in the future retrieval software versions. We also note that PSC's are very evident in the August south pole data, although at much lower altitudes (under 20 km) than the region where the CFC12 shows the upwelling feature, but they may be a contributing factor. Again, correlative data for the southern winter pole will be very valuable in investigating these features.

7.6 Correlation Diagrams for Long-lived Tracers

Correlation of long-lived trace species is a powerful tool for understanding atmospheric behavior (e. g. Plumb and Ko, 1992 and references therein). Figure 7.6-1 shows the observed CH_4 versus N_20 scatter plot from balloon observations, AAOE and AASE aircraft, and ATMOS (from

theModels and Measurement Report, Prather and Remsberg, 1993; hereinafter M&M). The aircraft data include the whole-air samples from the ER-2, and hence, explicitly have both CH_4 and N_2O dats in the Southern Hemisphere. The aircraft data provide high horizontal resolution, and the balloon data provide high vertical resolution. The balloons reach sufficient altitude that the turnover at small tracer values is observed.

The plot does not include tropical data. The CH_4-N_2O plot is both compact and linear for N_2O values greater than 30 ppbv. The signal is robust at extratropical latitudes for all times of the observation. The robustness of the signal is consistent with both constituents being "long-lived." Long- lived means a year or more in winter latitudes where mixing is strong and much longer in the summer hemisphere. The persistence of the relationship for all observations shows that it is not necessary to have data from specific time periods, and hence, the value of the correlative data is expanded in both space and time.

Figure 7.6-2 shows that CLAES scatter plots for August 1992 at 60 - 70 S and for February 1992 at 60-70 N are very similar. All UARS data shown are from the CDHF and are Version 6 and ISAMS version 8. The data have been checked to assure that the data value is greater than the quality parameter value. For the observations below 10 mb the slope is similar to the M&M line (the dashed line on the figure). However, the scatter is much larger. ISAMS data for January 1992 at 60-70 N is shown in figure 7.6-3. ISAMS data is not retrieved at altitudes below 10 mb, hence, the range of the data is limited. Comparing to data at similar altitudes, the ISAMS N_2O is consistently higher than that of CLAES. The ISAMS data is in closer agreement with the M&M curve, but it must be emphasized there is only limited data in the M&M curve from high altitude balloons. The scatter in the ISAMS data is similar to that of the CLAES data. The CLAES N_2O at high altitudes does not turn over in the same way as the M&M curve, and there are high values of methane for very low values of N_2O.

CLAES data from summer high latitudes are shown in figure 7.6-4. In August 1992 at 60-70 N the correlations are much more compact than in the winter. The slope is slightly steeper than the M&M curve. This difference is driven by the bulge of relatively high methane for N_2O between 170 and 240 ppbv. The summer data from the southern hemisphere show the compact relationship only at the higher altitudes, with tremendous scatter below 10 mb. There are also periods when the data are out of range of possibility, with $N2O > 400$ ppbv and $CH4 > 2000$ ppbv.

Figure 7.6-5 shows both CLAES and ISAMS scatter plots. The CLAES plots at 30 - 40 S from August of 1992 show that the slope of the scatter within the data from different altitudes is not continuous. Often there are also distinct offsets between different altitudes. Similar characteristics are seen in the ISAMS data. This characteristic in CLAES is most prevalent at altitudes below 10 mb and increases at lower latitudes.

Figure 7.6-6 shows CLAES and ISAMS data from the tropics. There is tropical data in the M&M curve, but the balloon data presented in Goldan et al. (1980) show the tropical profiles to be very smooth for all measured long-lived tracers. The CLAES data show many characteristics described above. At altitudes below 46 mb, N_2O can take on almost any value for tropospheric values of CH4. The ISAMS data, though scattered, follows the M&M curve much more closely. The smooth nature of the profile data suggest, however, that the tropical lower stratosphere is well behaved and that the constituents will be highly correlated.

Figure 7.6-7 shows a set of ISAMS correlations for different latitude bands and time periods . In the tropics (not shown), the ISAMS data tend to follow the M&M curve with the exception of

observations from the lowest altitudes. The northern hemisphere plots are similar to the southern hemisphere plots shown here. At middle latitudes the scatter is large, but with the exception of summer, loosely approximates the M&M curve (the solid line on these graphs). In summer, the CH_4 is distinctly lower than M&M curve for a given value of N_2O. At high latitudes the CH_4 is distinctly below the M&M curve for a given value of N_2O at all times.

Tlle correlation plots reveal significant scatter in the long-lived tracers from both CLAES and ISAMS. There are significant disagreements with what would be expected from the correlative data and analyses of aircraft observations. To sort out the causes of the differences will require further study.

7.7 SUMMARY

Methane (CLAES, HALOE, and ISAMS)

Profile comparisons show good overall agreement. In general ISAMS is higher than CLAES and HALOE is close to CLAES above 1 mb, and somewhat lower than CLAES between 2 mb and 10 mb. Correlative data tend to be consistent with the three UARS measurements. Between 10 mb and 50 mb HALOE is greater than CLAES. The CLAES vs. ISAMS along-orbit time series generally track each other very well. At levels from 0.46 to 10 mb the mean differences are 1-21%. Correlation coefficients between the two series are generally about 80%, except at the 10 mb level where the correlation coefficients are 0.68 in January and 0.54 in April. Zonal mean sections show the expected pattern of elevated mixing ratio surfaces in the tropics, and depressed surfaces at high latitudes, particularly in winter. Longitude-height sections are generally consistent with profile results except in January when large differences between HALOE and the other two instruments occur in a longitude range where there are very large temperature gradients.

Nitrous Oxide (CLAES and ISAMS)

Profile comparisons. The profile shapes for CLAES and ISAMS are generally in agreement with correlative data and with each other. CLAES values tend to be somewhat lower than correlative data, ISAMS somewhat higher. Time tracks show reasonably good correlation, but ISAMS is systematically higher than CLAES, particularly in the tropics. Mean differences are as high as 115% (April 18 at 2.2 mb). The systematic difference is generally well in excess of combined error estimates.

Carbon Monoxide (ISAMS)

ISAMS provides CO fields between 10 and 0.05 mb. There is a bias between day and night data, with much larger errors in the night. Zonal mean fields show good agreement with 2-D model simulations. The data agree reasonably well with a rocket observation at low altitudes, but differ by a large amount at higher altitudes. Comparison with the ATLAS data of April, 1992 may help to resolve this issue.

Chlorofluorocarbons (CLAES)

Freon 11 and 12 are both observed by CLAES, but the Freon 11 data was not ready for presentation. A vertical profile of Freon 12 compared well with correlative balloon data in the 5mb to 50 mb altitude range. Zonal mean sections have the shape and seasonal dependence expected for a long-lived tracer of tropospheric origin, although some departures are apparent in the Southern Polar region.

Methane – Nitrous Oxide Correlations

Scatter plots of methane versus nitrous oxide observations from ISAMS and CLAES reveal far more scatter than shown by equivalent plots from aircraft and balloon data. This suggests that there are problems remaining in the UARS data.

References

Goldan, P. D., W. C. Kuster, D. L. Albritton, and A, L. Schmeltekopf, Stratospheric $CFC1_3$, CF_2C1_2, and N_20 height profile measurements at several latitudes, J. *Geophys.Res.*, **85,** 413-423, 1980.

Plumb, R. A., and M. K. W. Ko, Interrelationships between mixing ratios of long-lived stratospheric constituents, *J. Geophys. Res.*, **97**, 10145-10156, 1992.

Prather, M. J., and E. E. Remsberg, The Atmospheric Effects of Stratospheric Aircraft: Report of the 1992 Models and Measurements Workshop (Volume III, Section H, Simultaneous observations of long-lived tracers), NASA Reference Publication 1292, 1993.

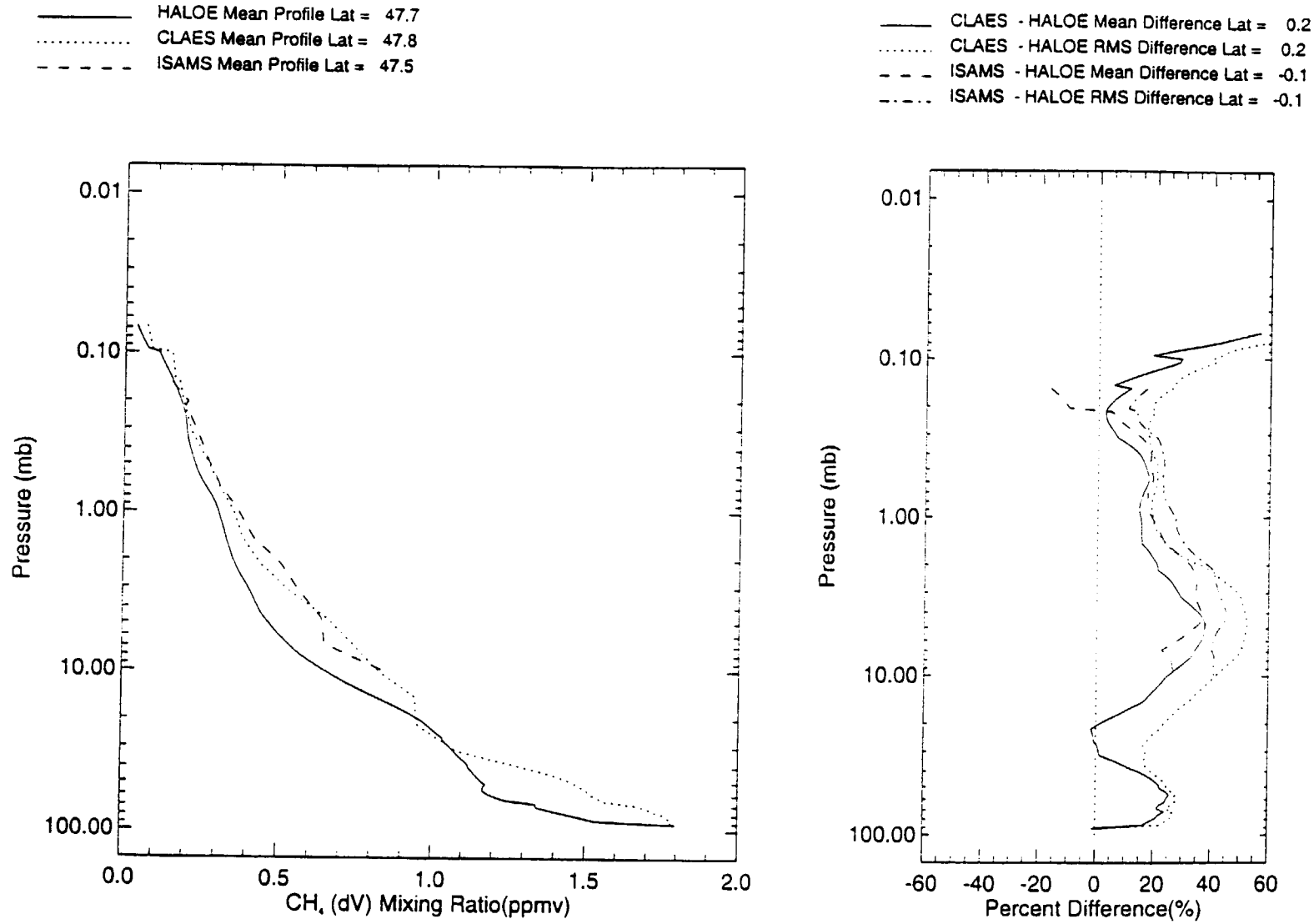

Figure 7.2.1-1. Mean of 28 coincident methane profiles for ISAMS, CLAES and HALOE.

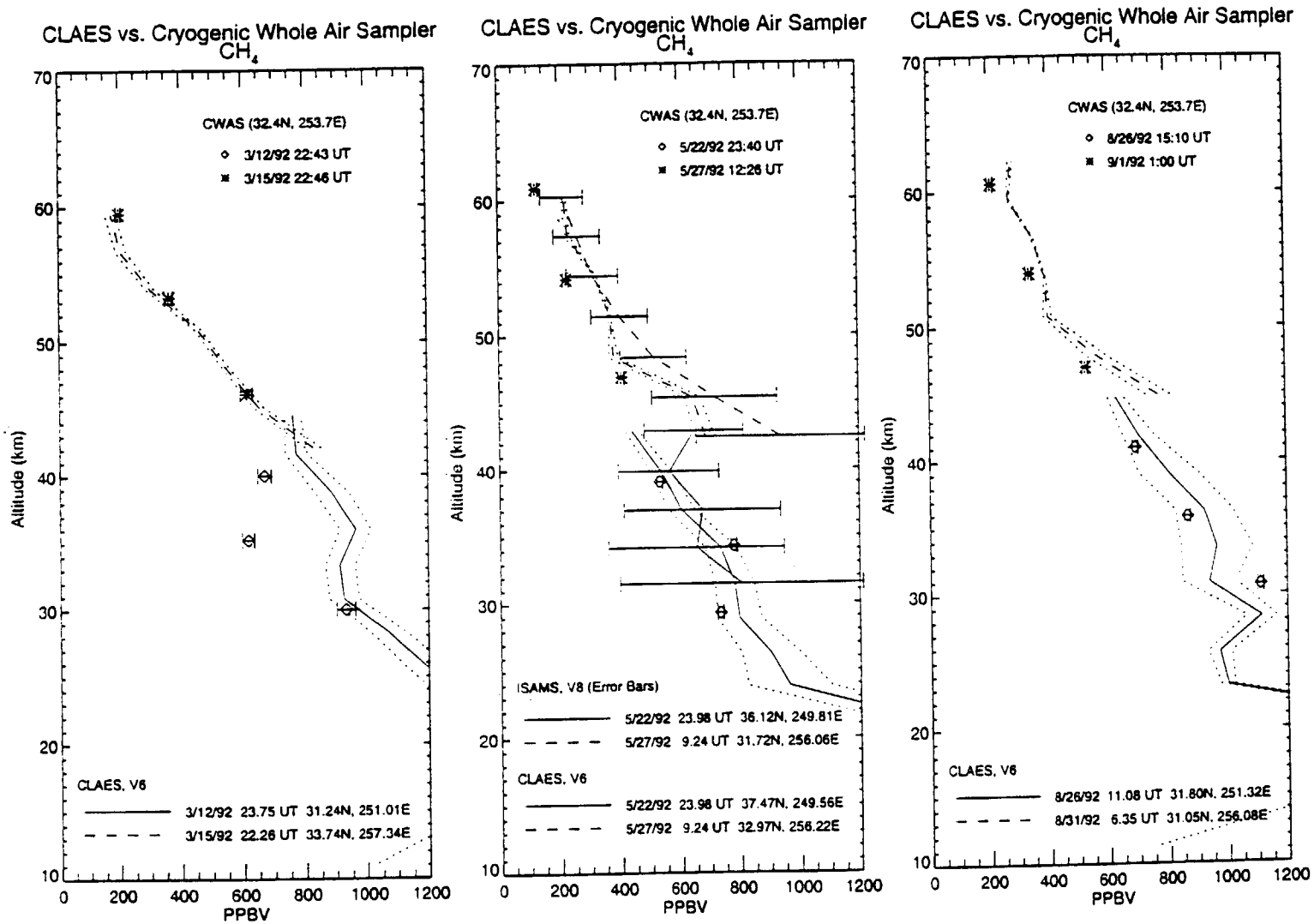

Figure 7.2.1-2. Comparison of CLAES methane with correlative data from 3 pairs of flights of the Cryogenic Whole Air Sampler. ISAMS error bars are also shown for the May flights (middle panel).

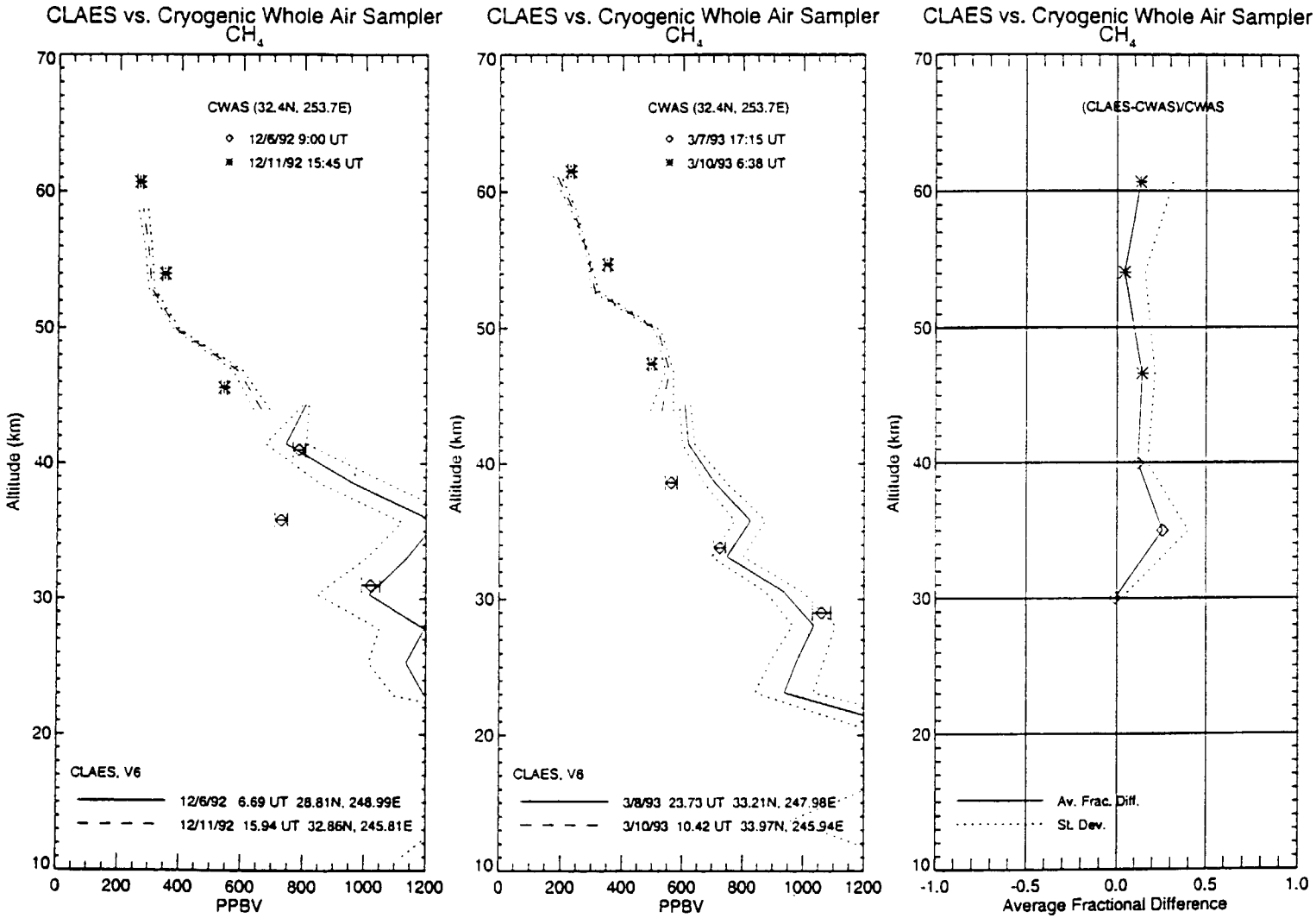

Figure 7.2.1-3. Same as Figure 7.2.1-2 but for 2 additional flight pairs. CLAES - CWAS fractional differences shown in right panel.

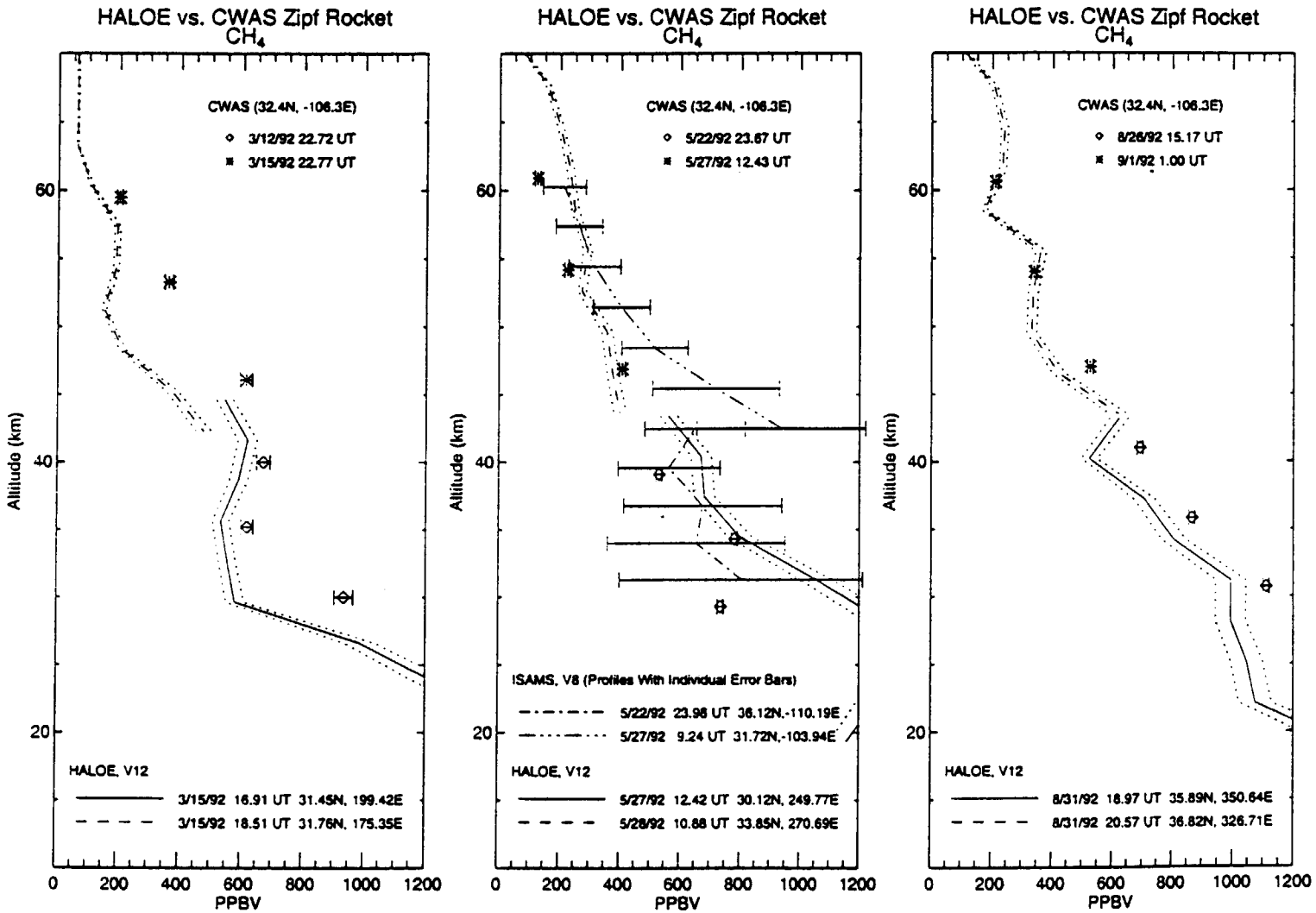

Figure 7.2.1-4. Comparison of HALOE methane with correlative data from 3 pairs of flights of the Cryogenic Whole Air Sampler. ISAMS error bars are also shown for the May flights (middle panel).

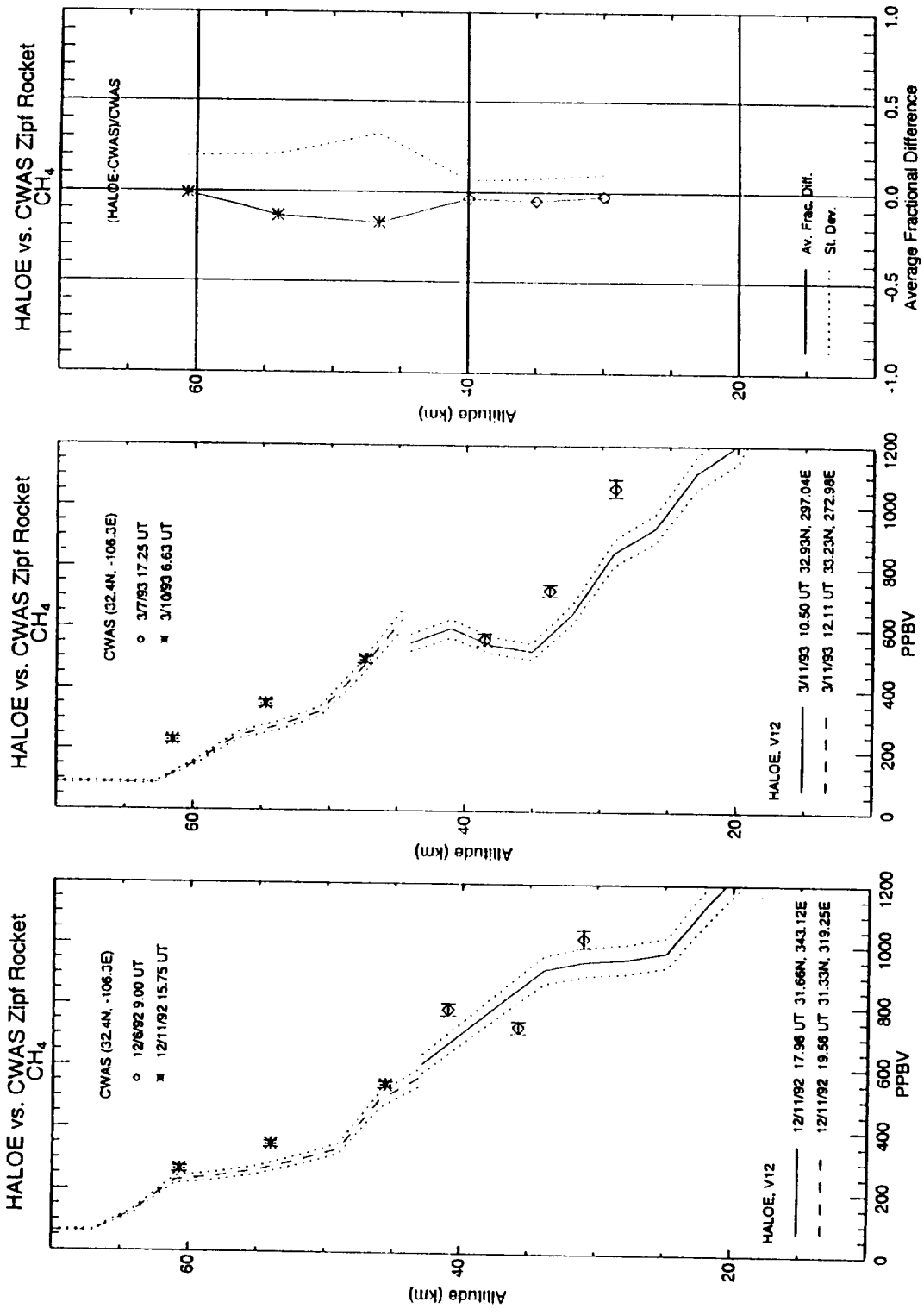

Figure 7.2.1-5. Same as Figure 7.2.1-4 but for 2 additional flight pairs. HALOE - CWAS fractional differences shown in right panel.

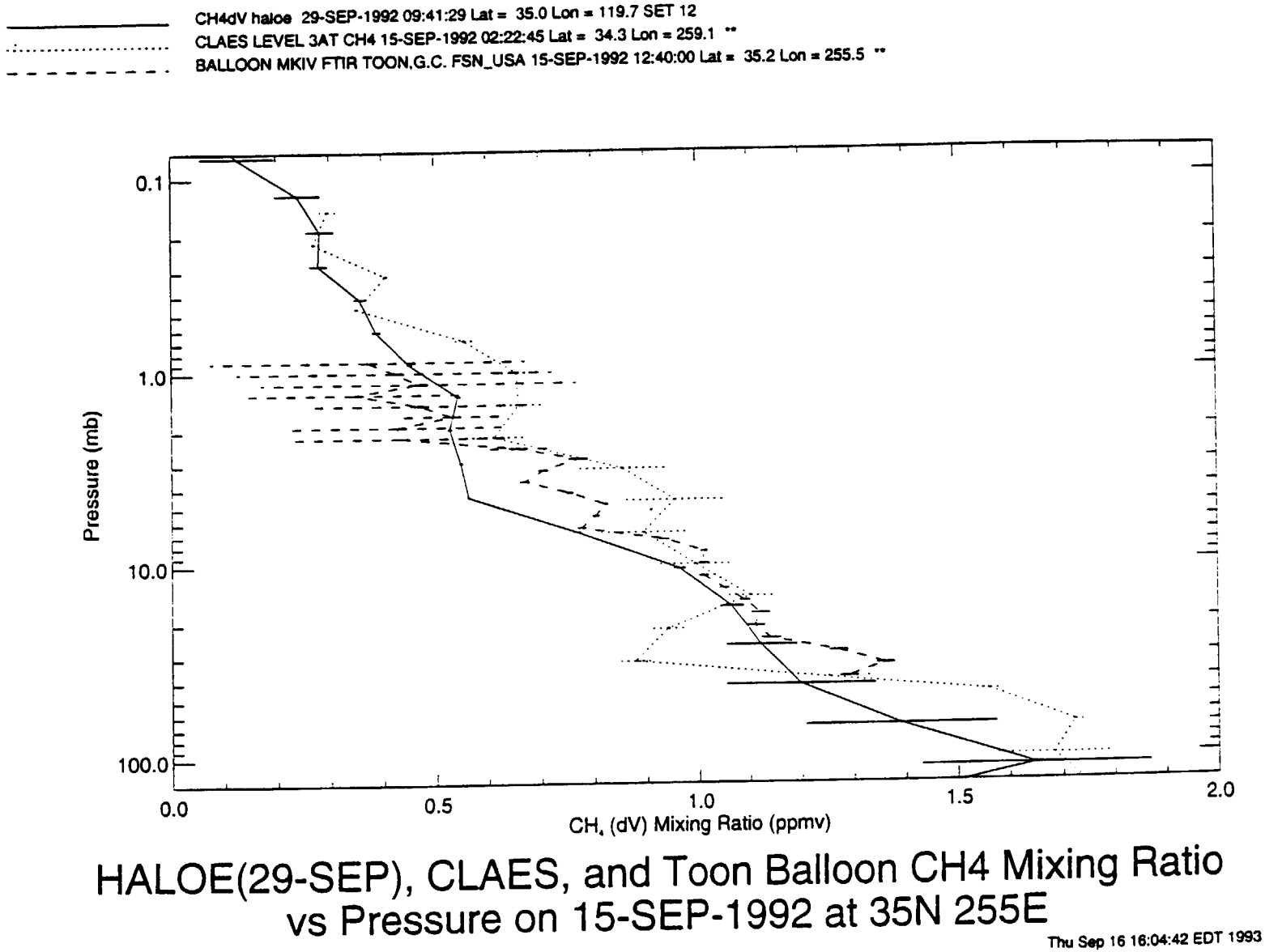

Figure 7.2.1-6. Profile comparison of CLAES and HALOE CH_4 with a MK IV balloon flight of Sept. 15, 1992. (Note HALOE data is for Sept. 29, 1992).

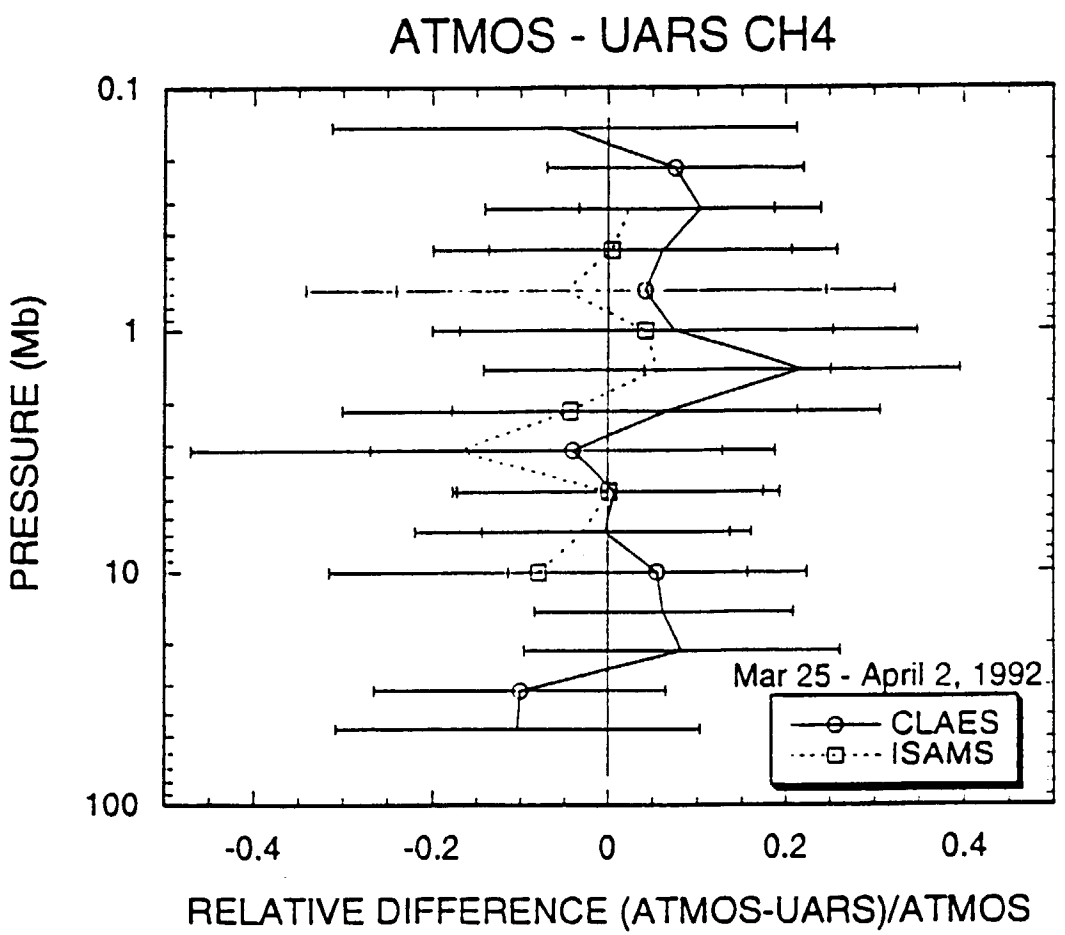

Figure 7.2.1-7. Relative difference between CLAES and ISAMS methane profiles for March 25-April 2, 1992, and data from an ATMOS flight in Spring 1985.

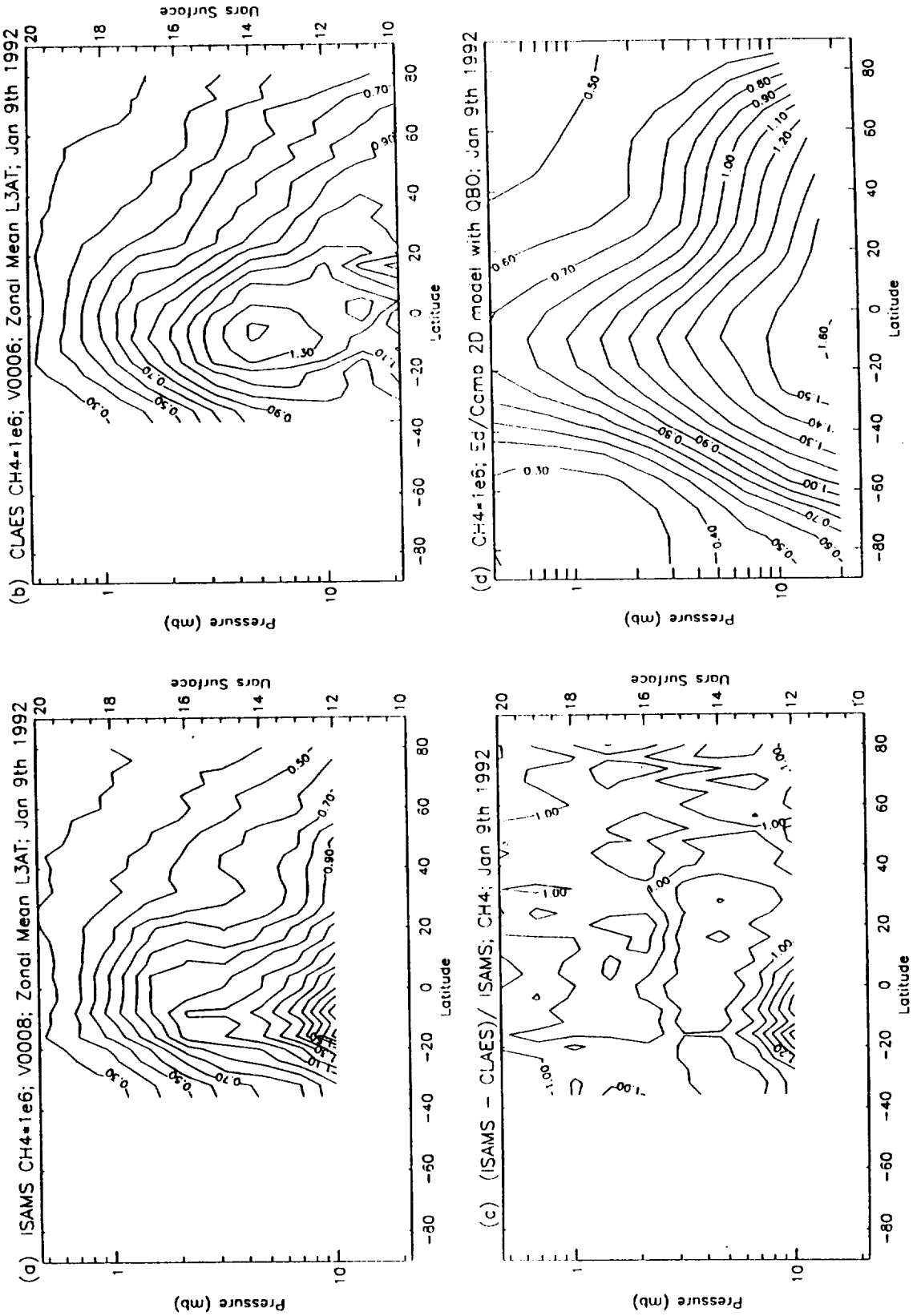

Figure 7.2.2-1. ISAMS CH4 and CLAES CH4 zonal mean mixing ratios for Jan. 9, 1992. Also shown is an (ISAMS - CLAES)/ISAMS difference plot and comparison with a 2-D model result.

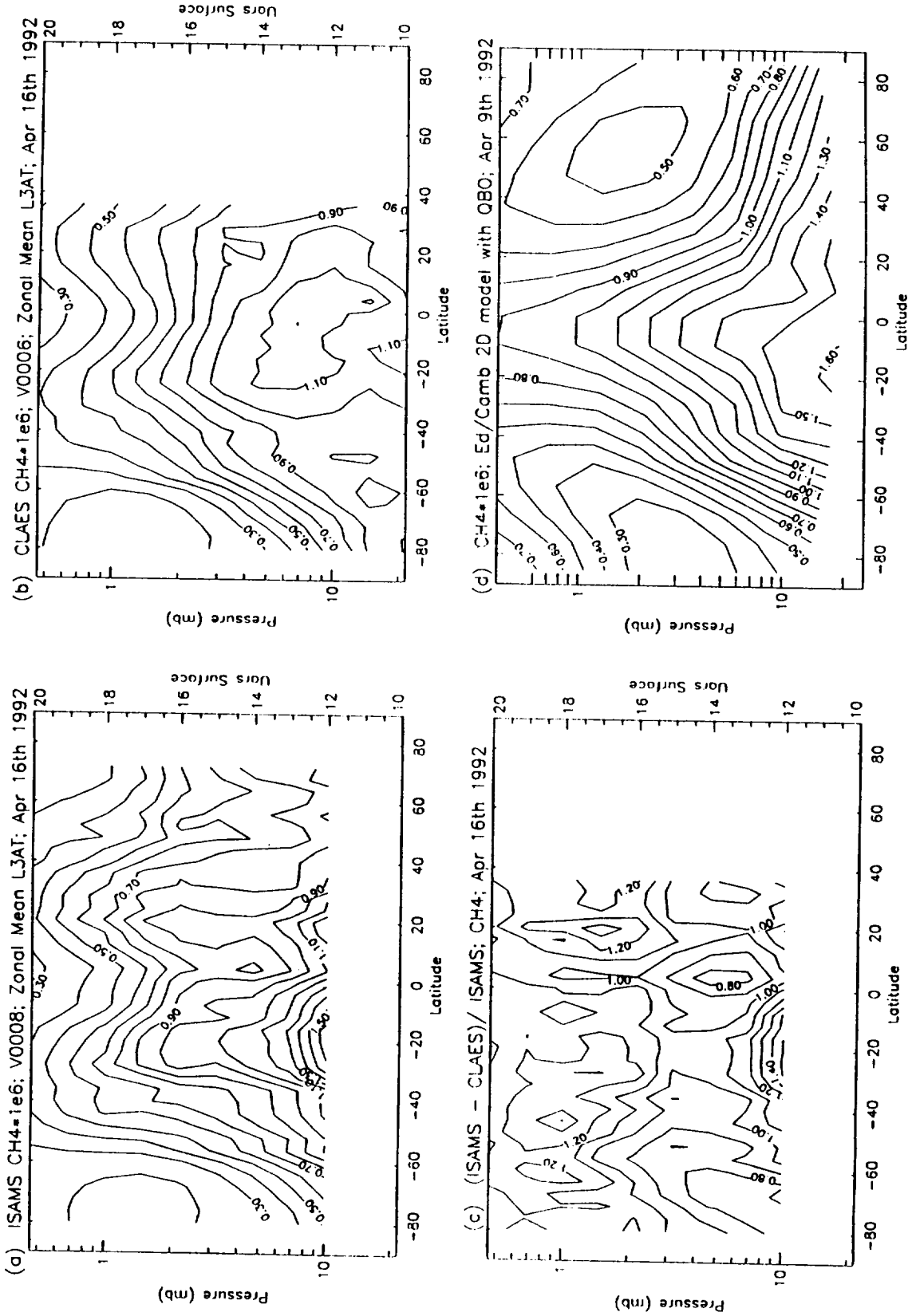

Figure 7.2.2-2. Same as Figure 7.2.2-1, but for Apr. 16, 1992.

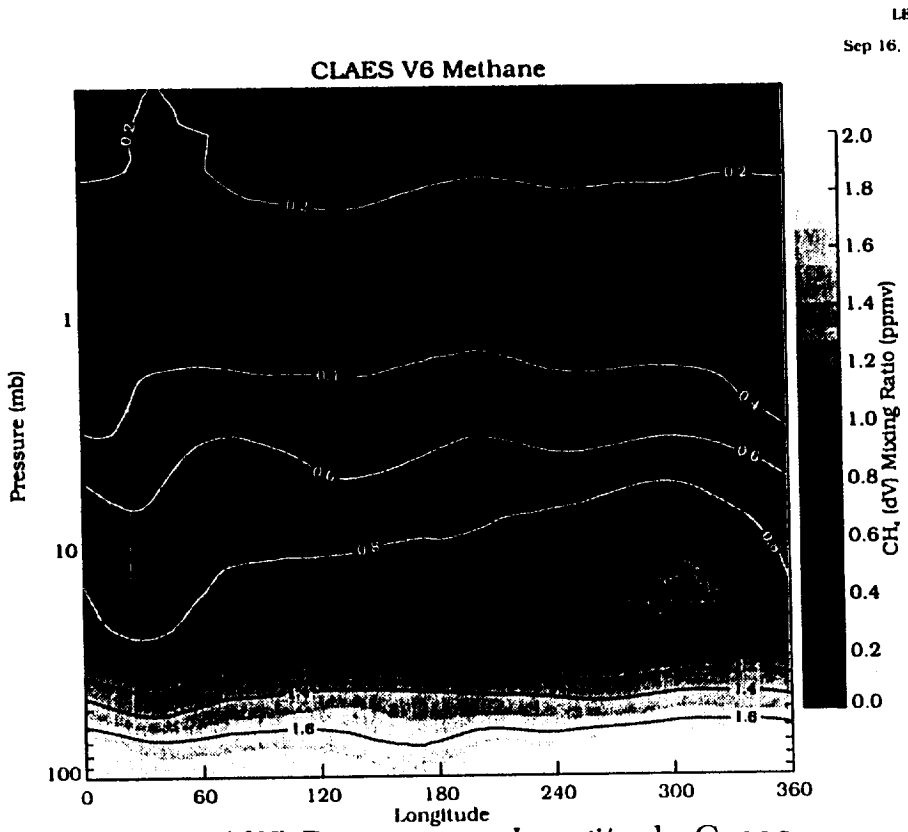

CH_4 (dV) Pressure vs Longitude Cross Section, on 09-JAN to 11-JAN-1992 at 47 N

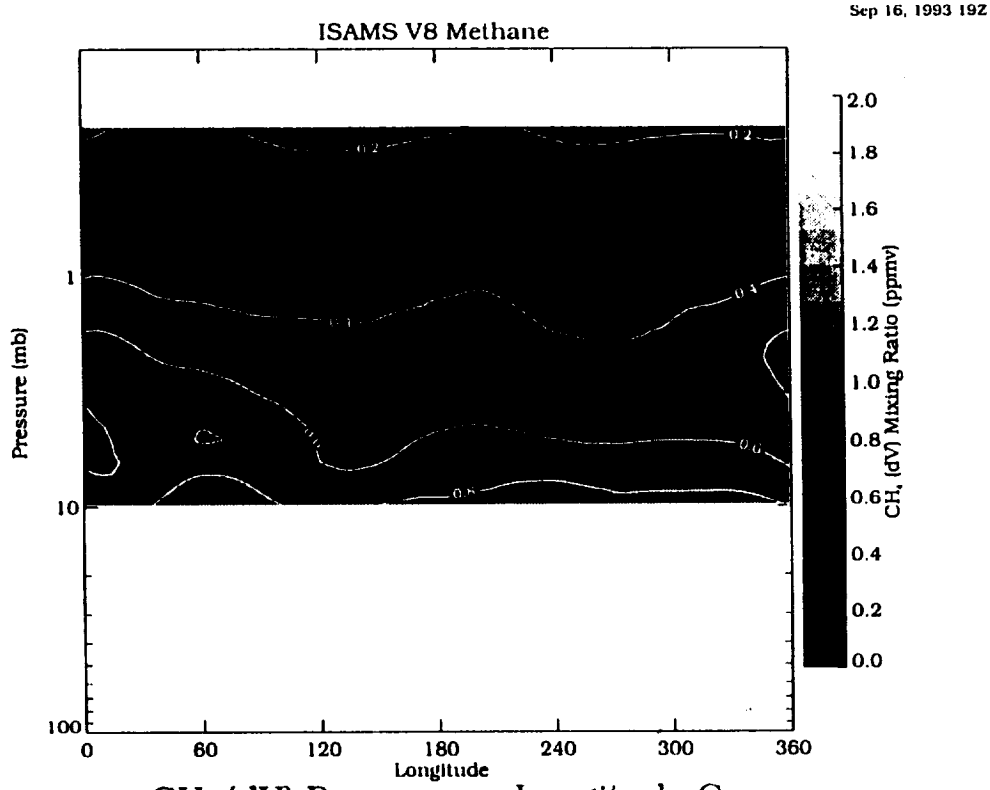

CH_4 (dV) Pressure vs Longitude Cross Section, on 09-JAN to 11-JAN-1992 at 47 N

Figure 7.2.3-1. Longitude-height cross-sections of CH4 volume mixing ratio at 47N for Jan. 9- 11, 1992 for CLAES and ISAMS.

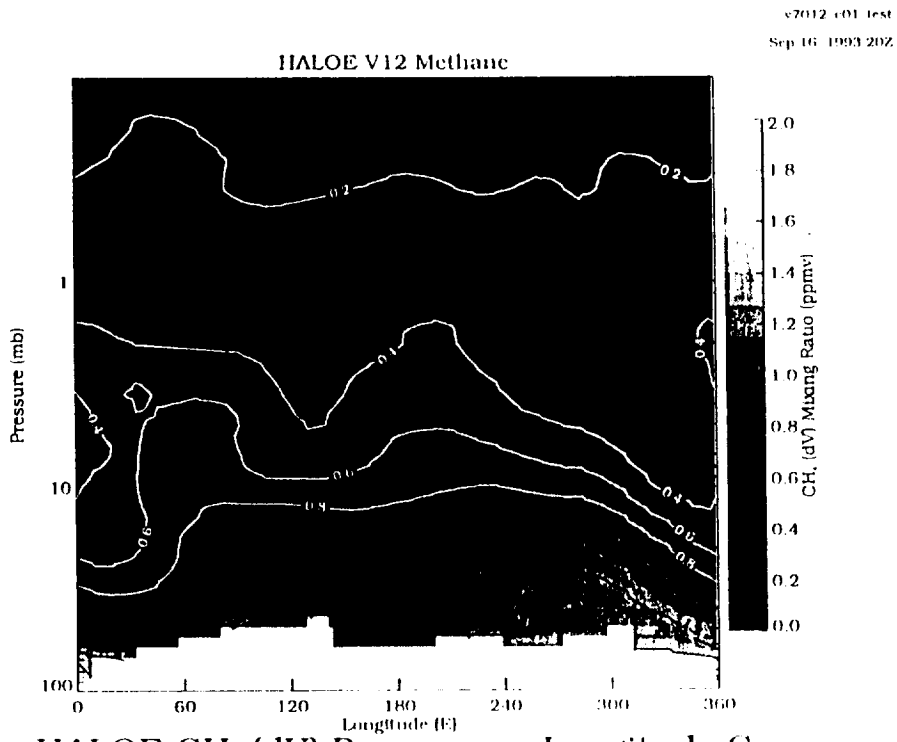

HALOE CH_4 (dV) Pressure vs Longitude Cross Section, Sunrise on 09-JAN to 11-JAN-1992 at 47 N

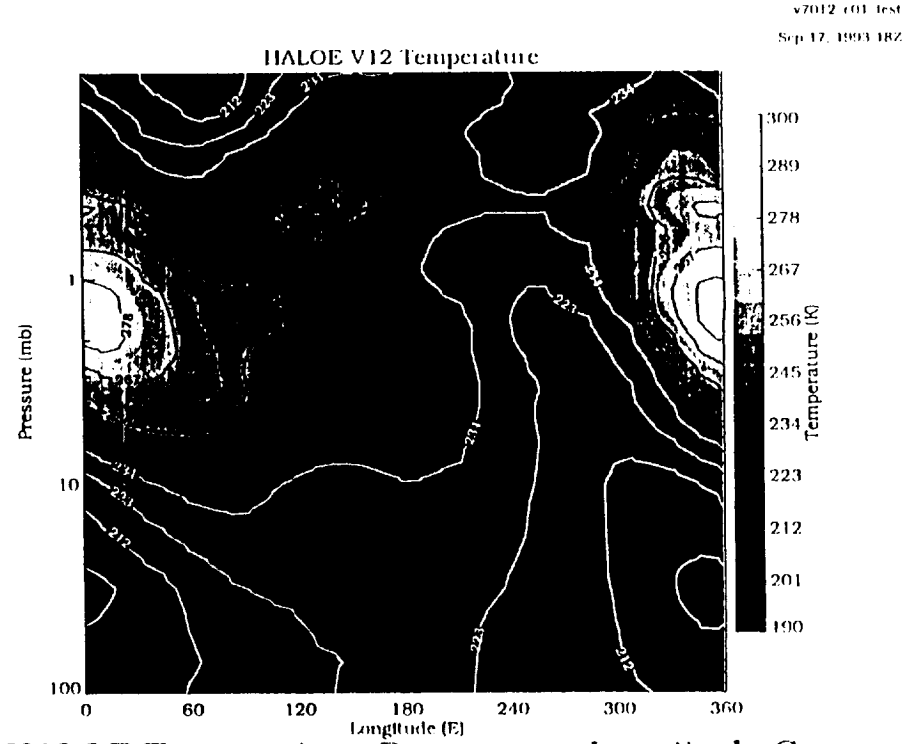

HALOE Temperature Pressure vs Longitude Cross Section, Sunrise on 09-JAN-1992 at 46 N

Figure 7.2.3-2. Longitude-height cross-section of temperature and CH4 volume mixing ratio at 47N for Jan. 9- 11, 1992 for HALOE observations.

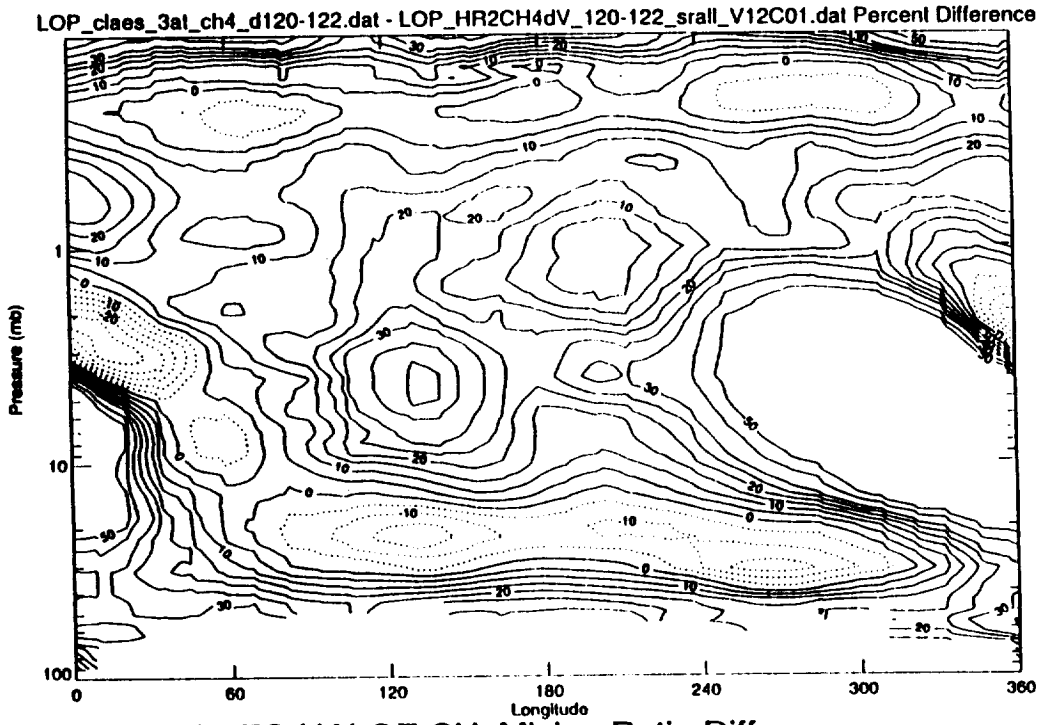

CLAES-HALOE CH_4 Mixing Ratio Difference
on 9-JAN-1992 to 11-JAN-1992

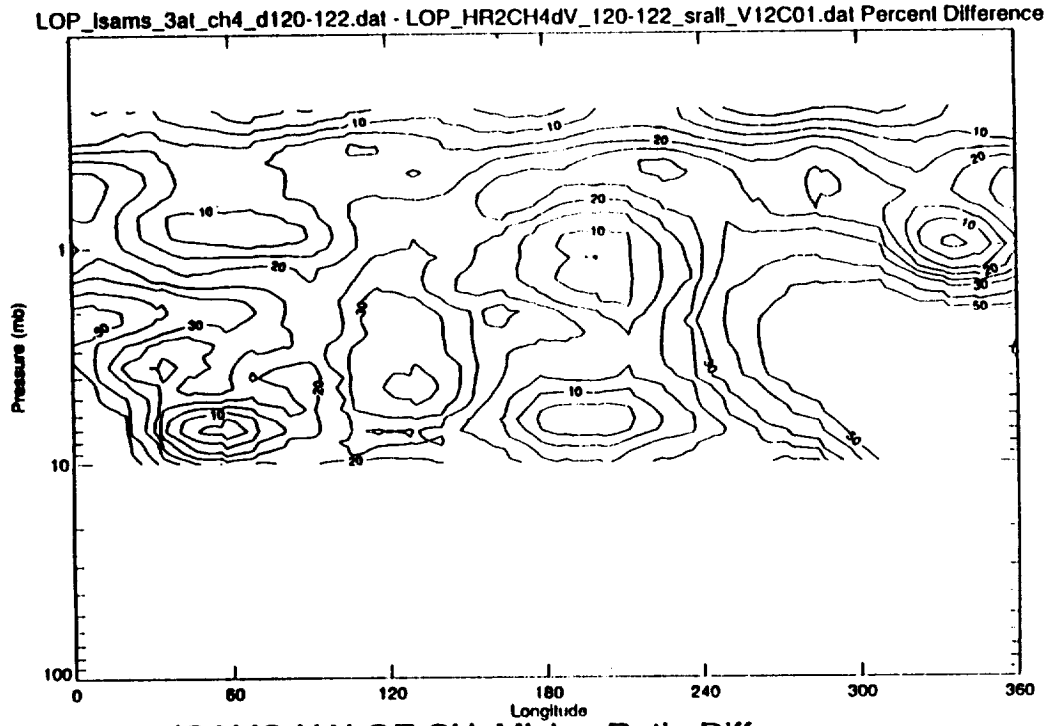

ISAMS-HALOE CH_4 Mixing Ratio Difference
on 9-JAN-1992 to 11-JAN-1992

Figure 7.2.3-3. Longitude-height sections of CLAES -HALOE mixing ratio percent differences (top) and ISAMS - HALOE differences (bottom) for data of Figures 7.2.3-1 and 7.2.3-2.

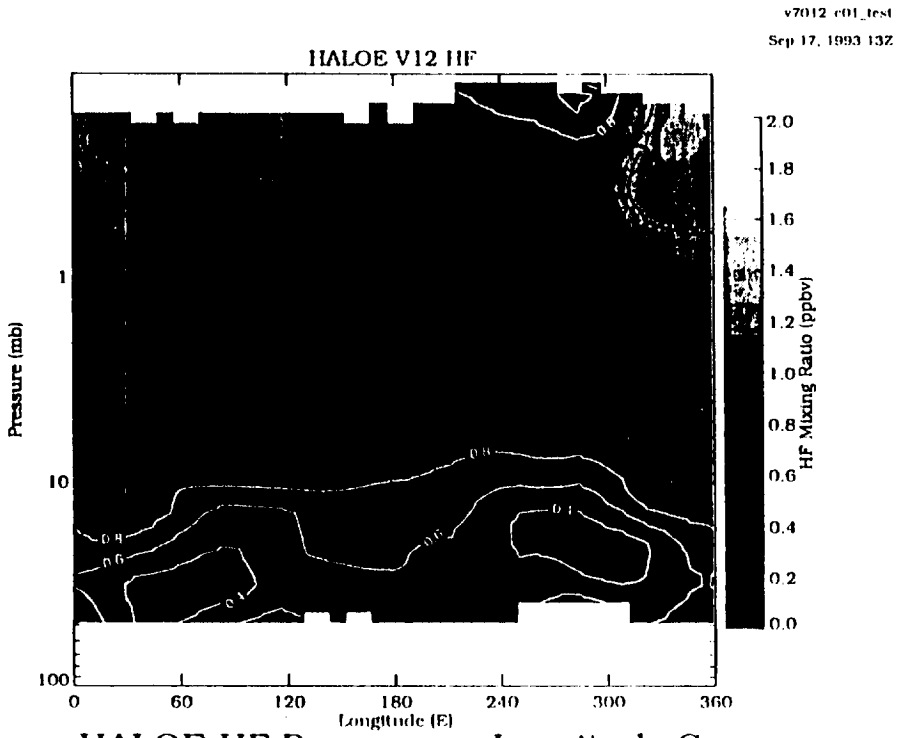

HALOE HF Pressure vs Longitude Cross Section, Sunrise on 09-JAN-1992 at 46 N

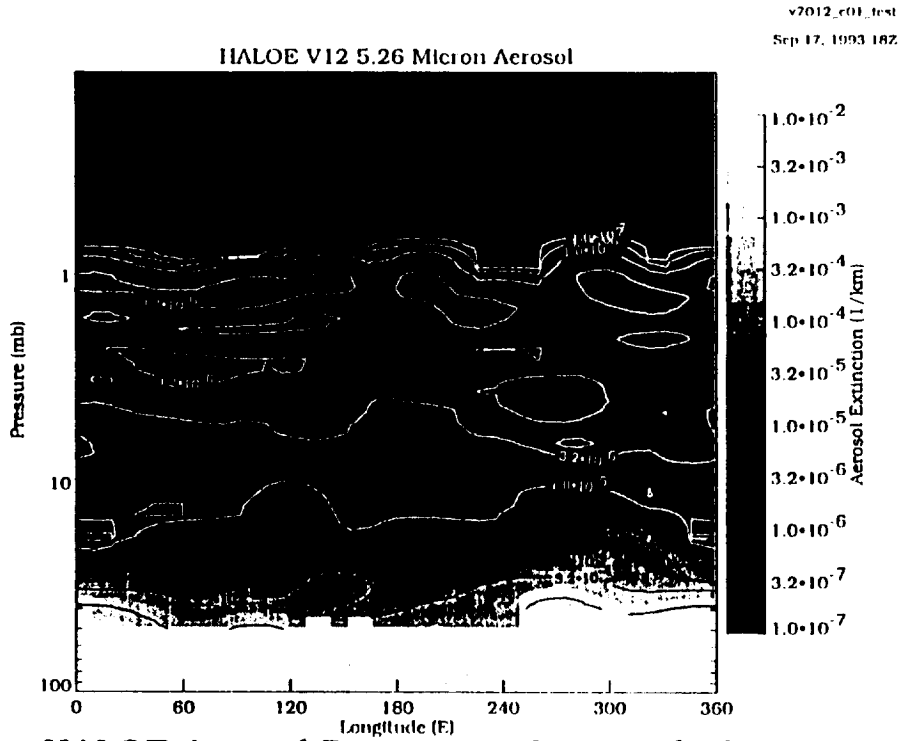

HALOE Aerosol Pressure vs Longitude Cross Section, Sunrise on 09-JAN-1992 at 46 N

Figure 7.2.3-4 Longitude-height sections of HALOE HF mixing ratio and aerosol extinction at 47N for Jan. 9-11, 1992.

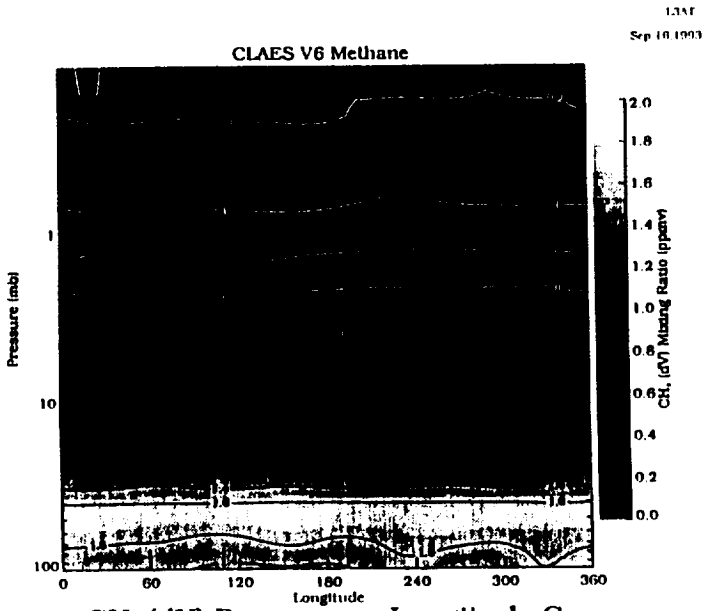

CH_4 (dV) Pressure vs Longitude Cross Section, on 15-APR to 17-APR-1992 at 8 N

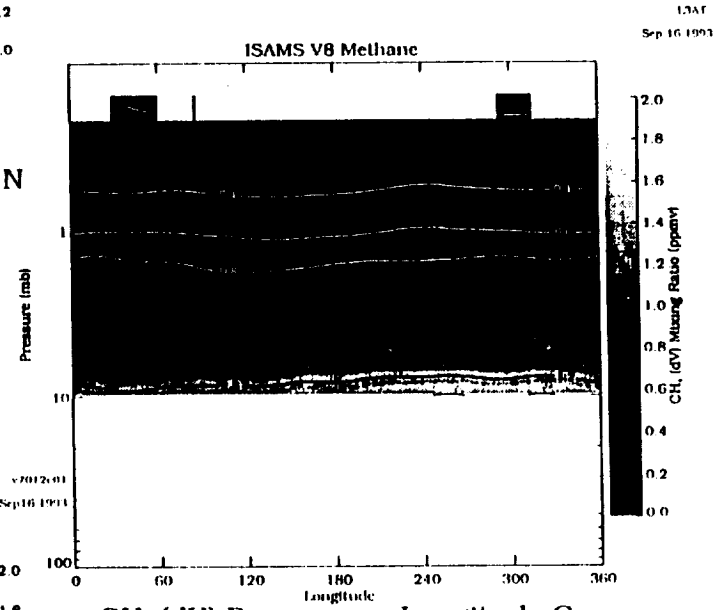

CH_4 (dV) Pressure vs Longitude Cross Section, on 15-APR to 17-APR-1992 at 8 N

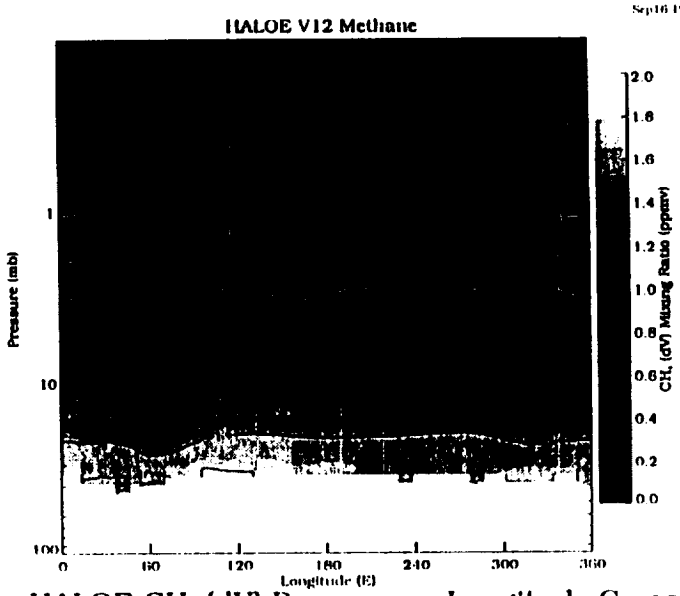

HALOE CH_4 (dV) Pressure vs Longitude Cross Section,Sunrise on 15-APR to 17-APR-1992 at 5 N

Figure 7.2.3-5. Longitude-height cross-sections for April 15-17, 1992 for CLAES at 8N (top), ISAMS at 8N (middle), and HALOE at 5N (bottom).

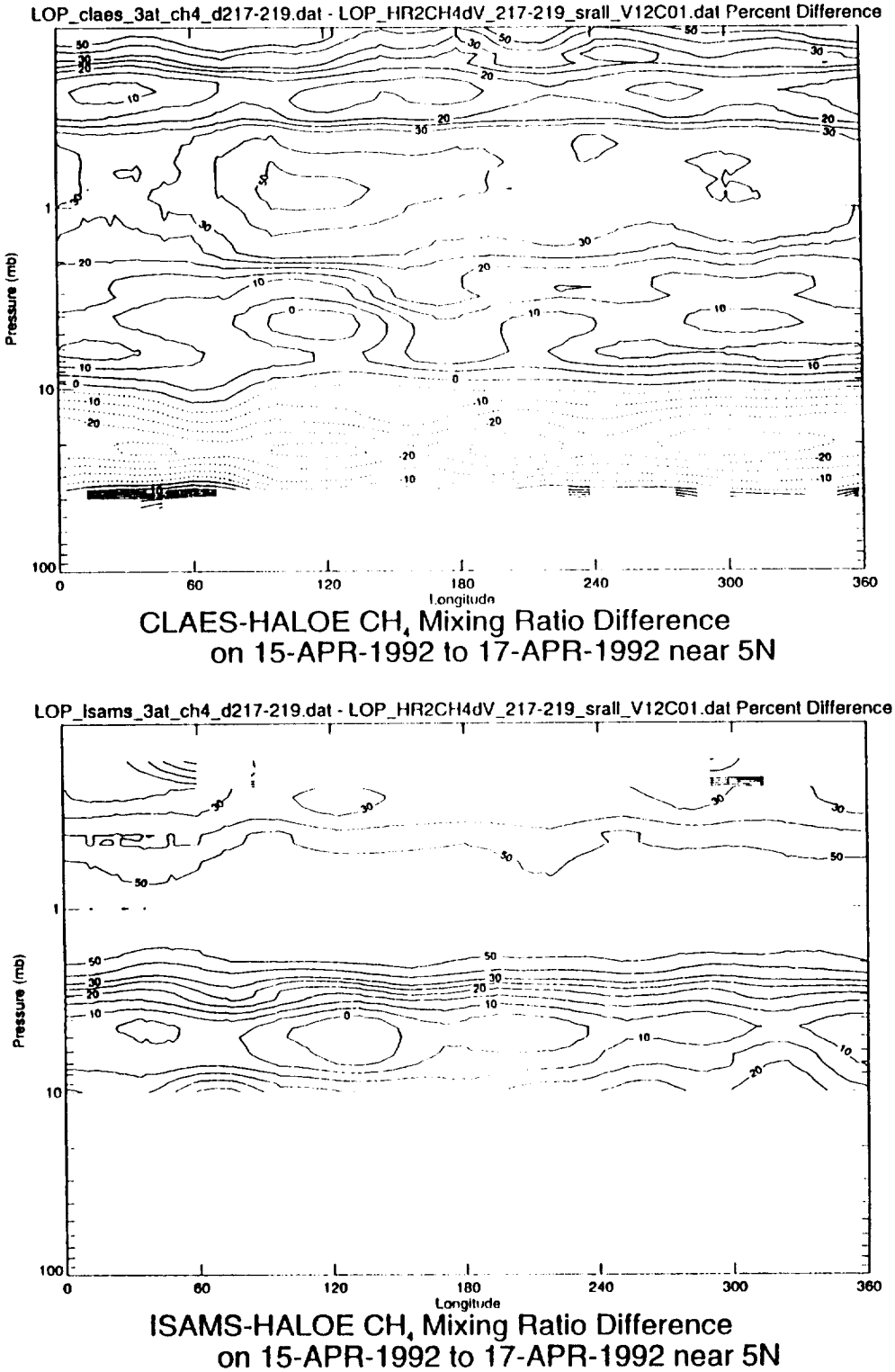

Figure 7.2.3-6. Longitude-height sections of CLAES - HALOE mixing ratio percent differences (top) and ISAMS - HALOE differences (bottom) for data of Figure 7.2.3-5.

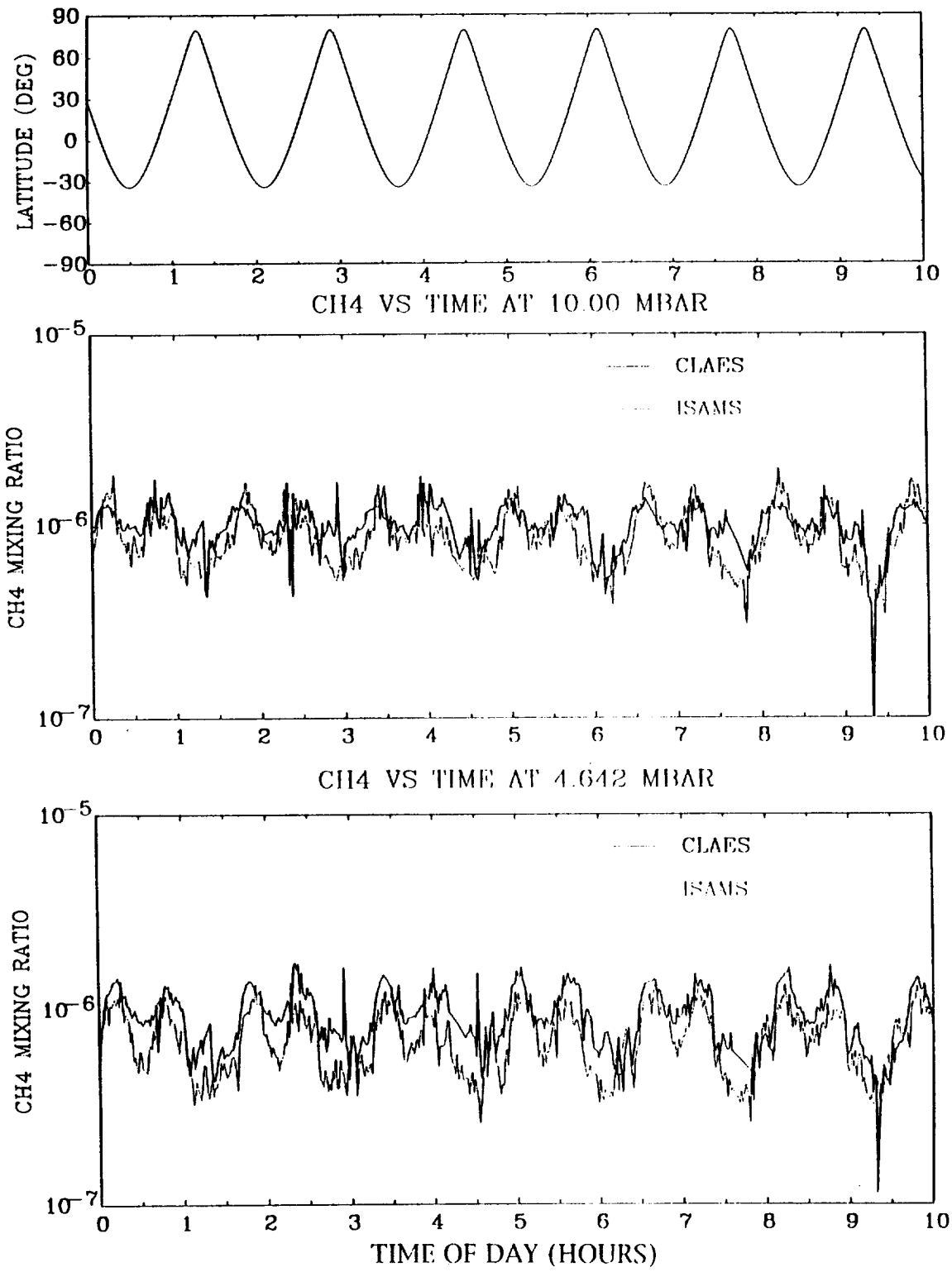

Figure 7.2.4-1. Direct comparison of CLAES and ISAMS tangent track CH4 series for Jan. 9 (day 120) at 10 and 4.6 mb.

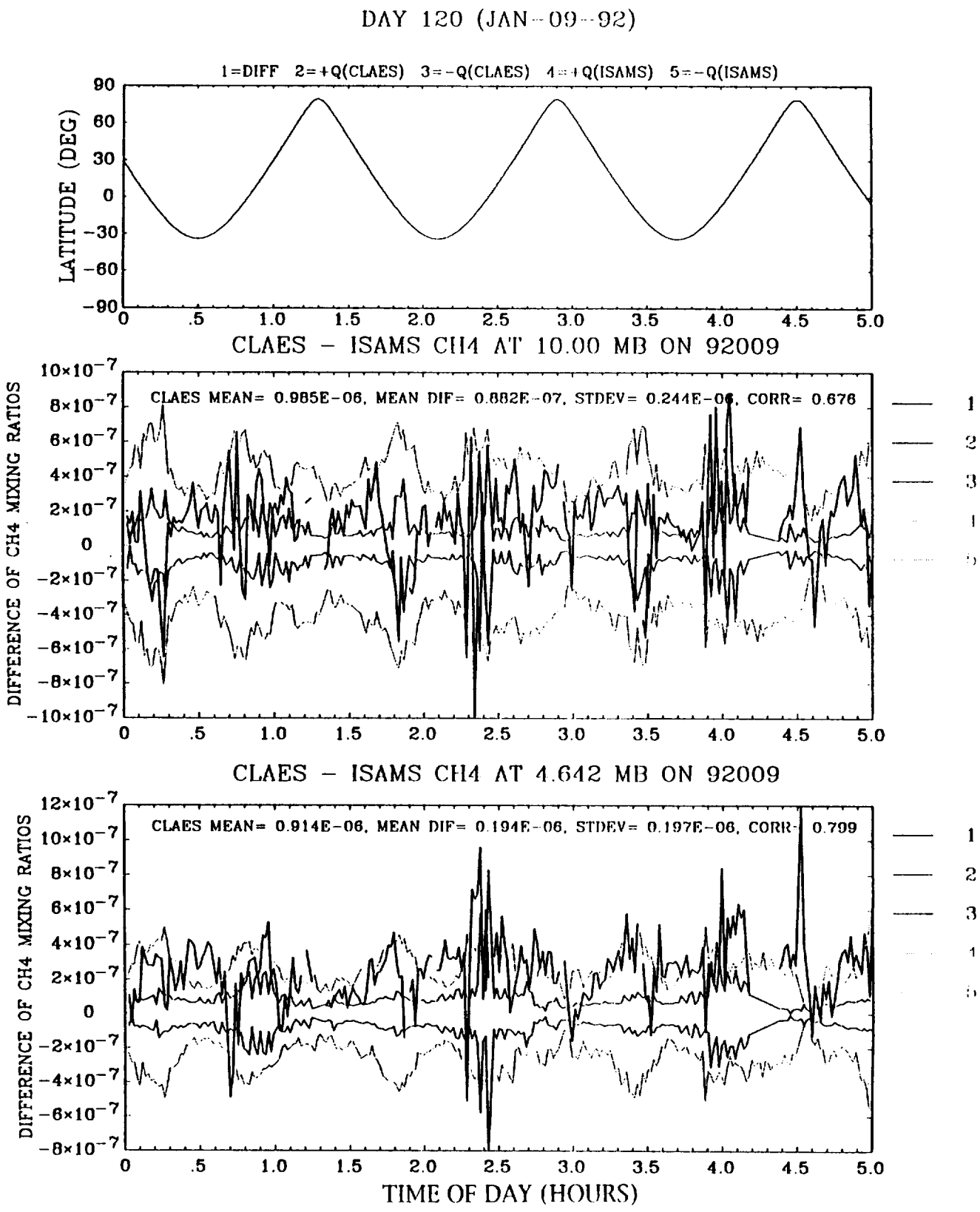

Figure 7.2.4-2. CLAES-ISAMS CH_4 differences for tangent tracks of Figure 7.2.4-1.

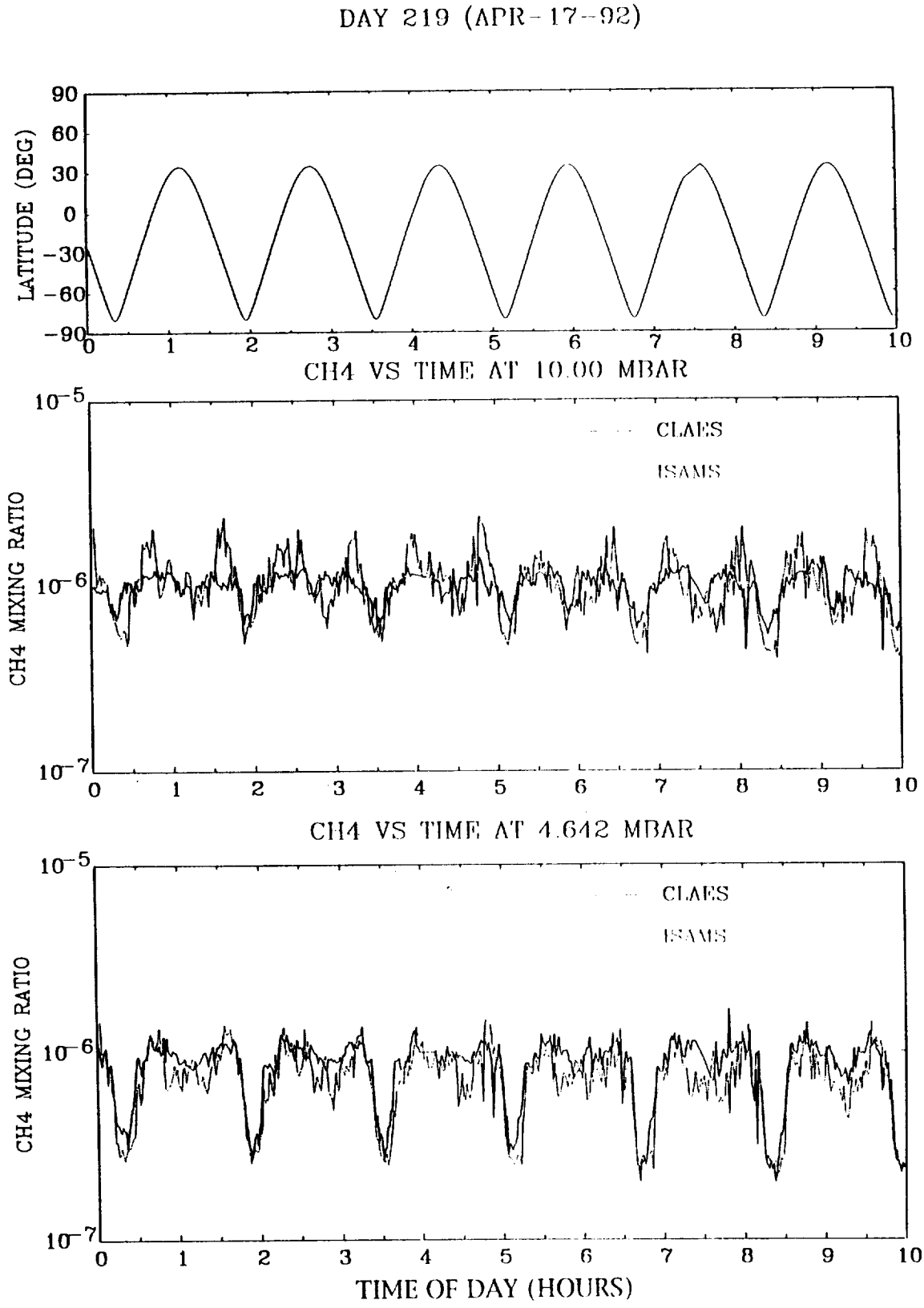

Figure 7.2.4-3 Direct comparison of CLAES and ISAMS tangent track CH_4 series for April 17 (day 219) at 10 and 4.6 mb.

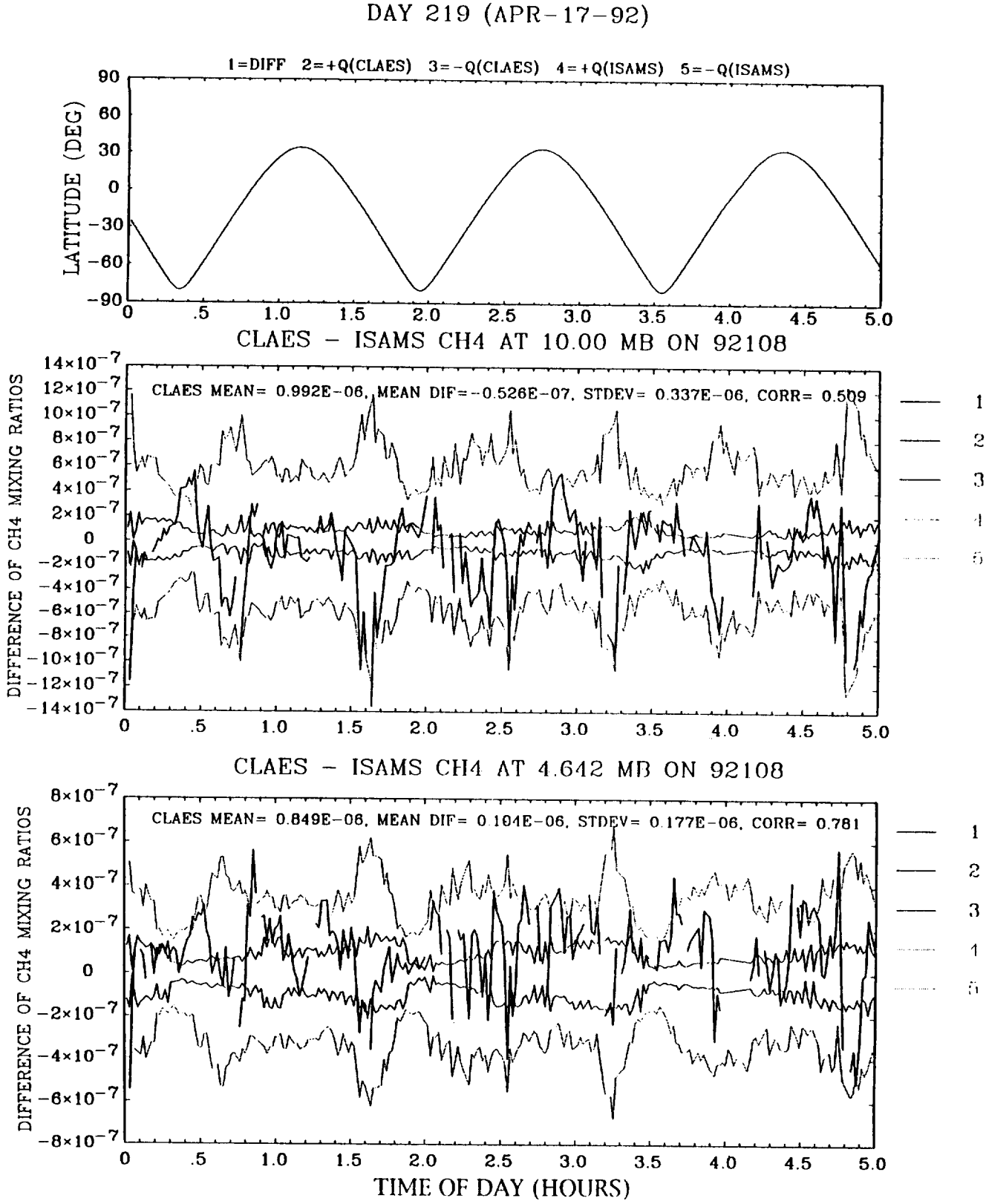

Figure 7.2.4-4 CLAES-ISAMS CH_4 differences for tangent tracks of Figure 7.2.4-3.

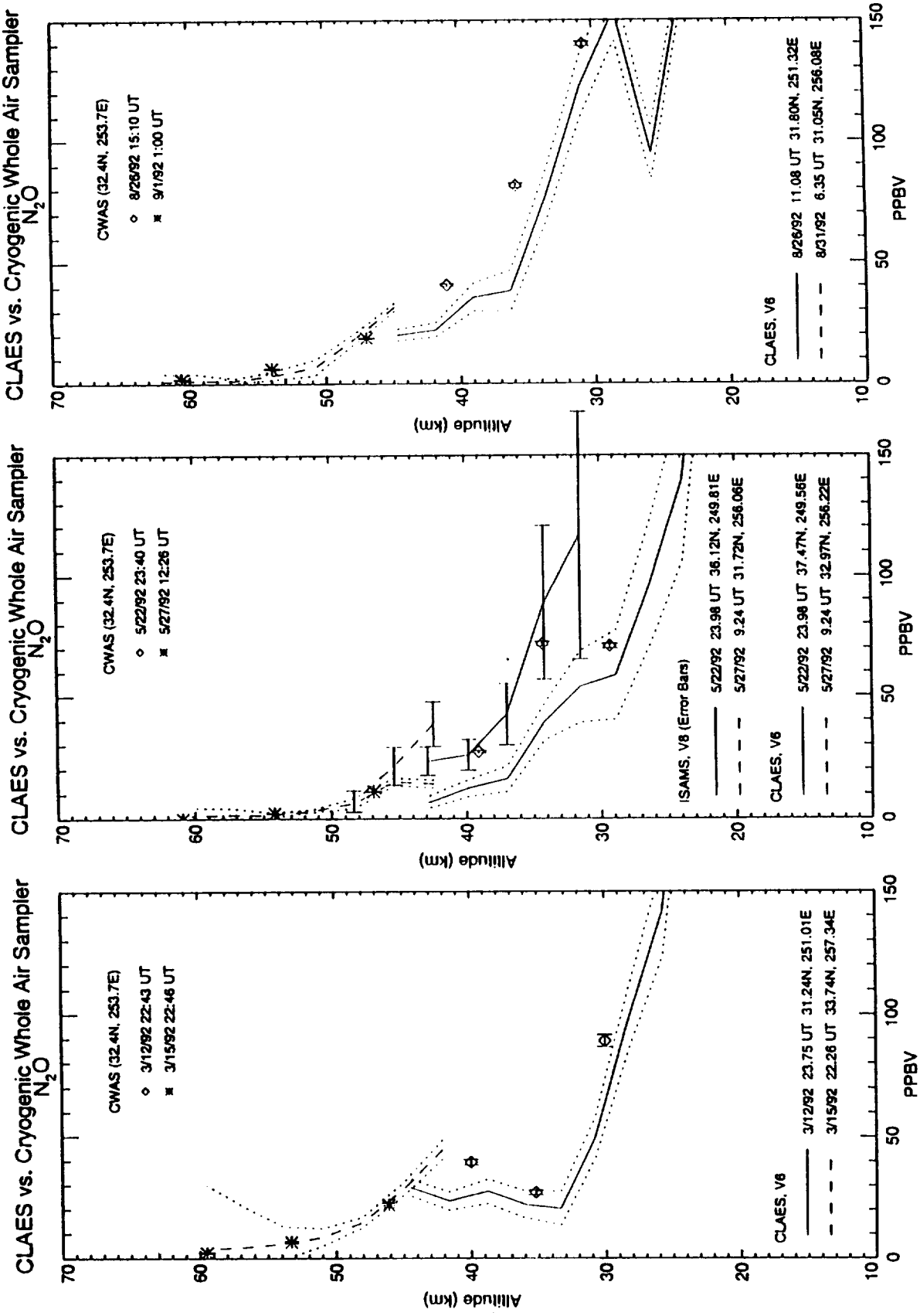

Figure 7.3.1-1. Comparison of CLAES N_2O with data from 3 pairs of flights of the CWAS. ISAMS error bars are shown for the May flights (middle panel).

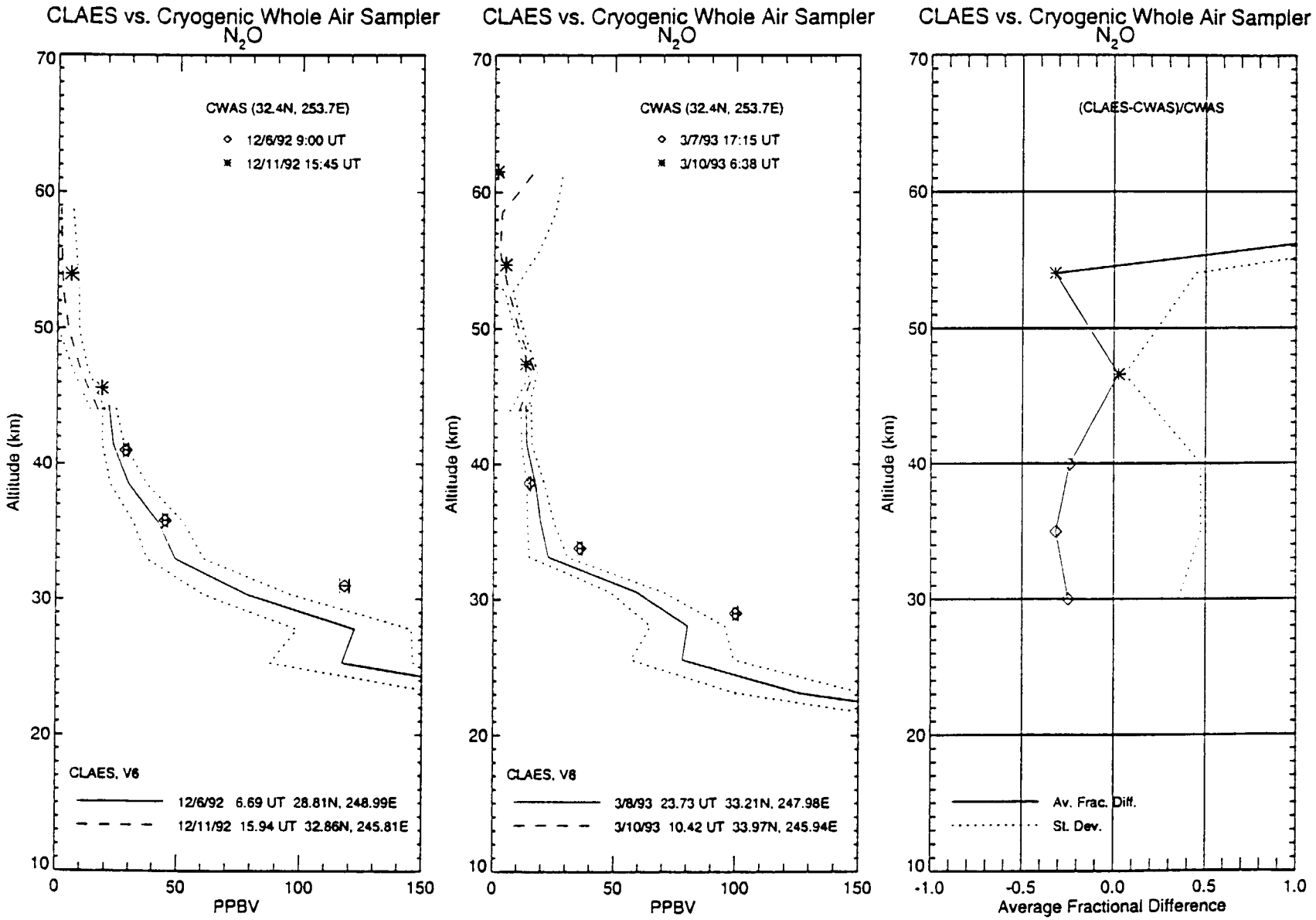

Figure 7.3.1-2. Same as Figure 7.3.1-1 but for 2 additional flight pairs. CLAES - CWAS fractional differences shown in right panel.

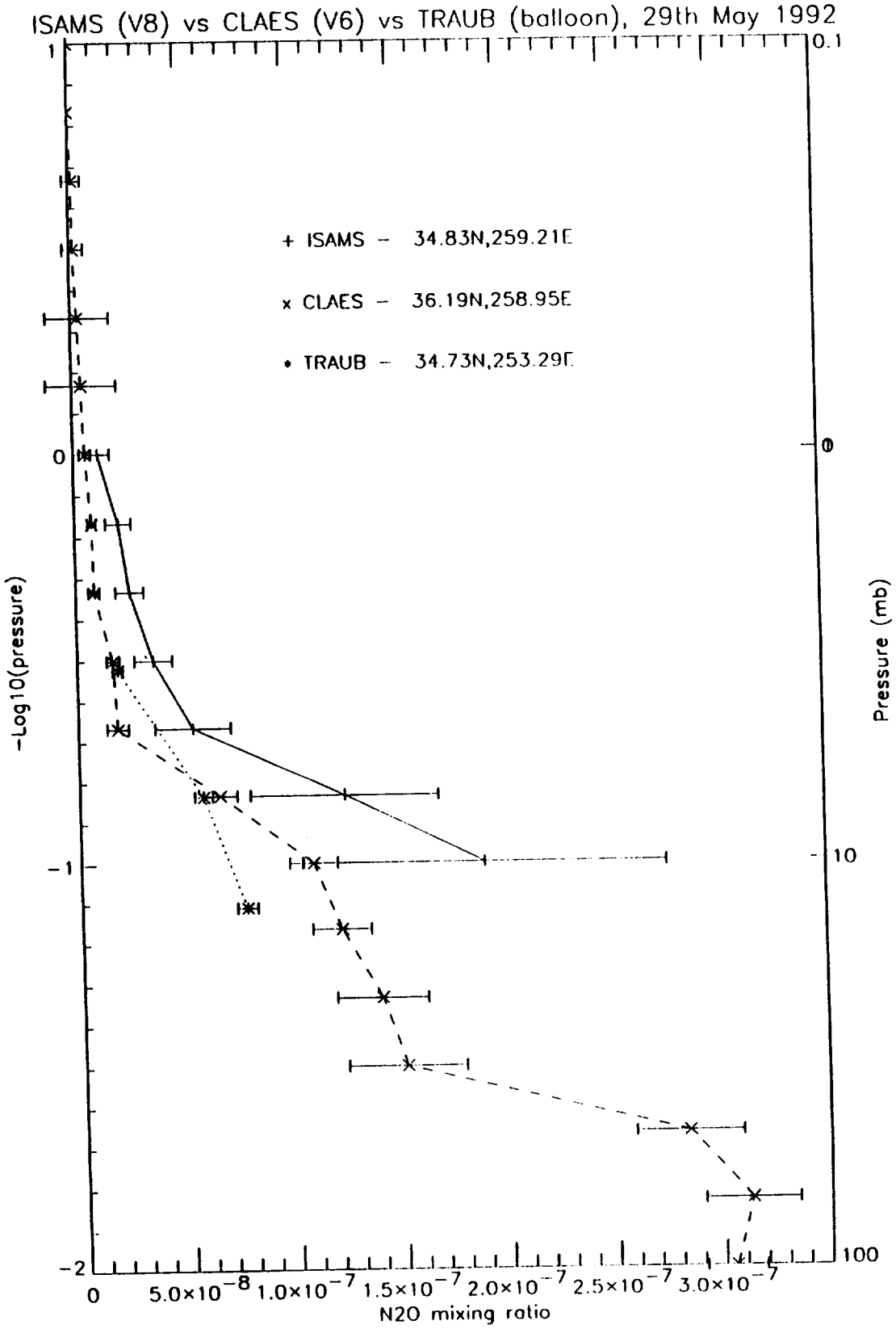

Figure 7.3.1-3. ISAMS and CLAES N_2O profiles compared to measurements by the balloon-borne Far Infrared Fourier Transform Spectrometer.

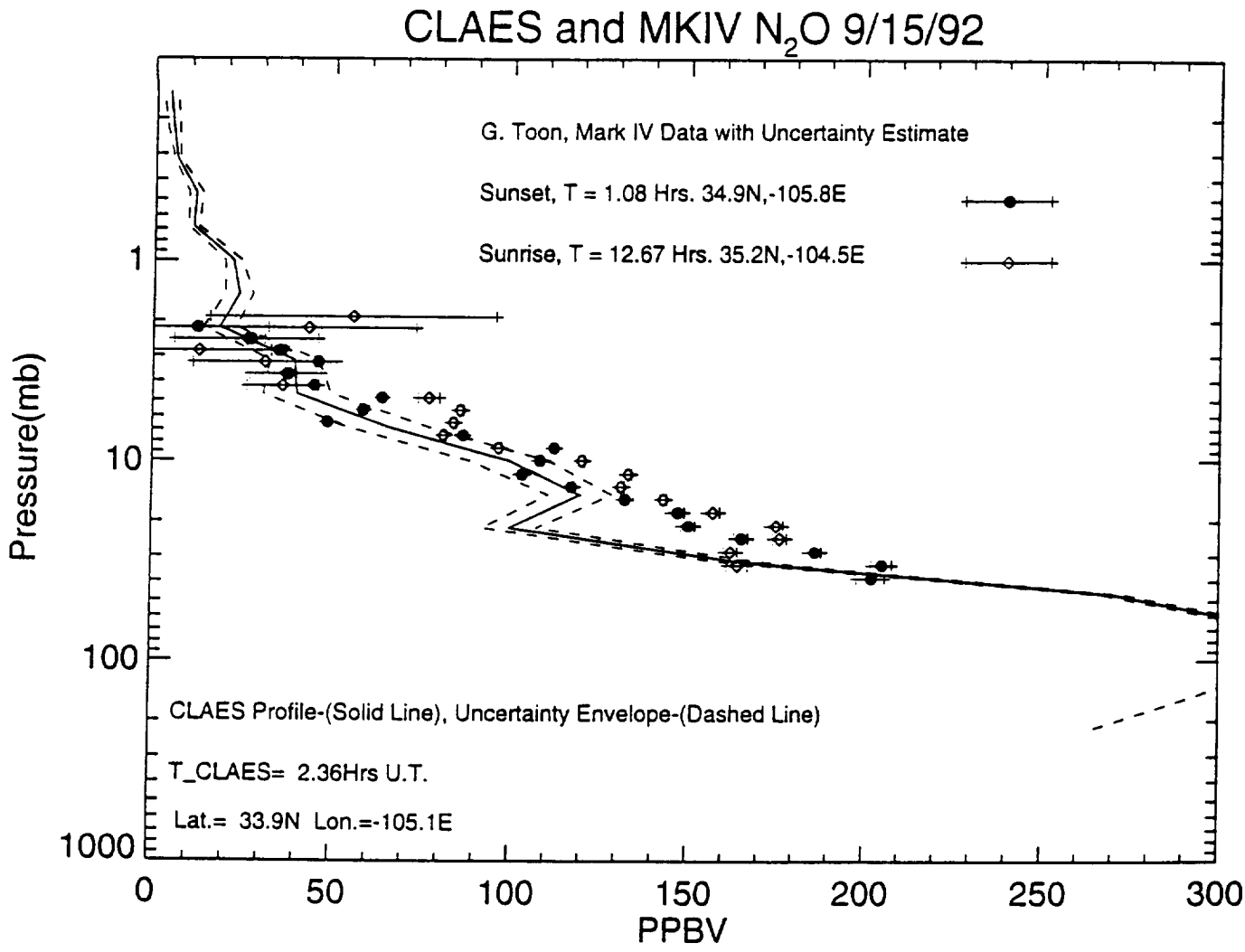

Figure 7.3.1-4. Profile comparison of CLAES N_2O with a balloon flight of the MK IV nstrument on September 15, 1992.

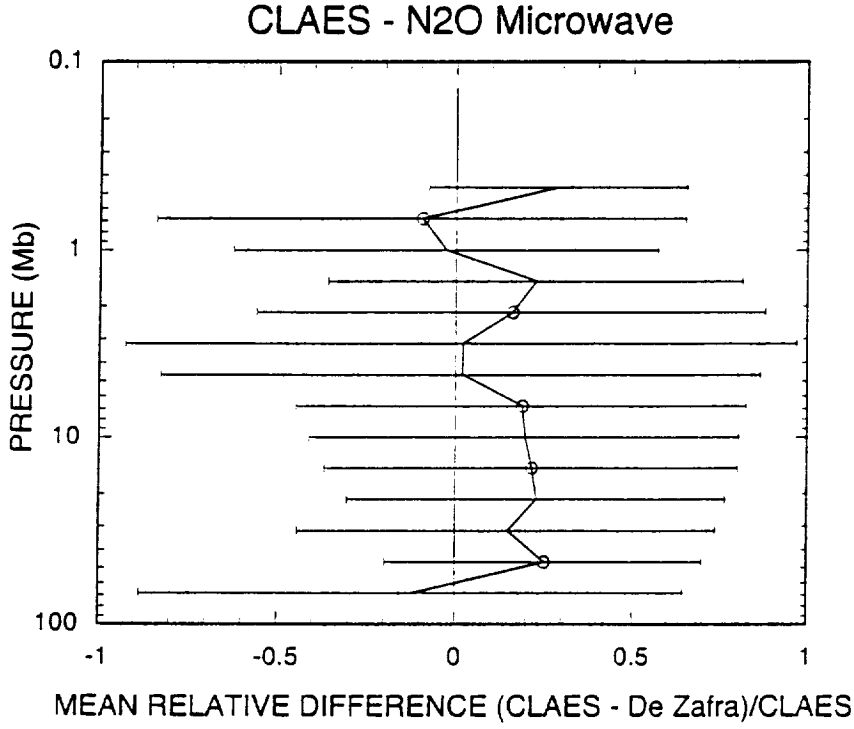

Figure 7.3.1-5. Mean relative difference profile for CLAES compared with the ground-based microwave instrument of De Zafra for 9 days in Feb. and Mar. 1992.

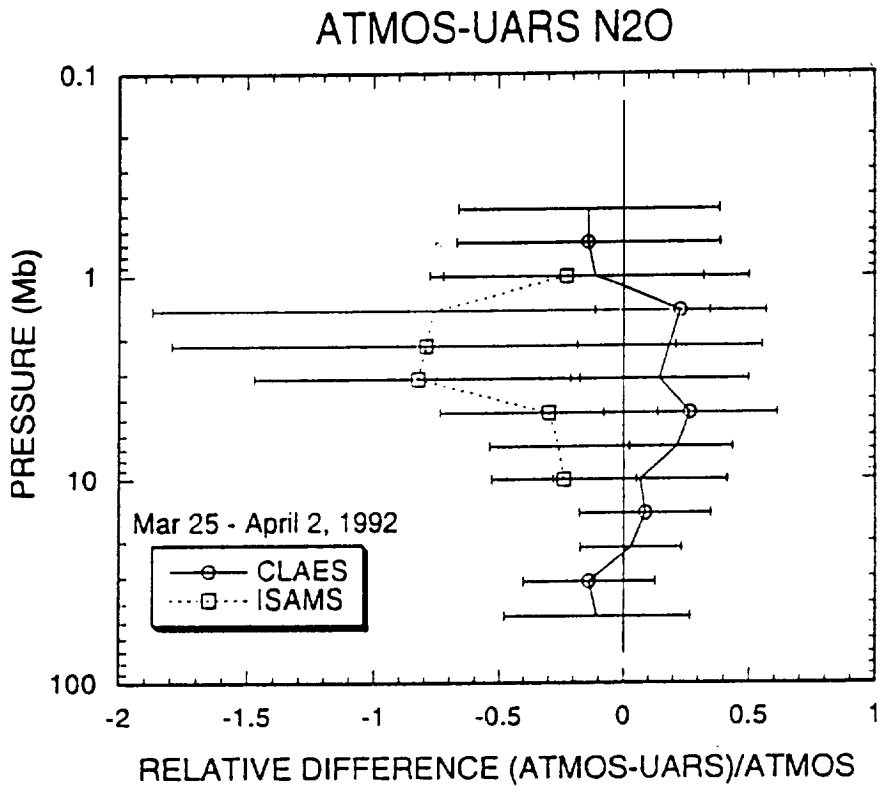

Figure 7.3.1-6. Relative difference between CLAES and ISAMS N_2O profiles for March 25-April 2, 1992, and data from an ATMOS shuttle flight in Spring 1985.

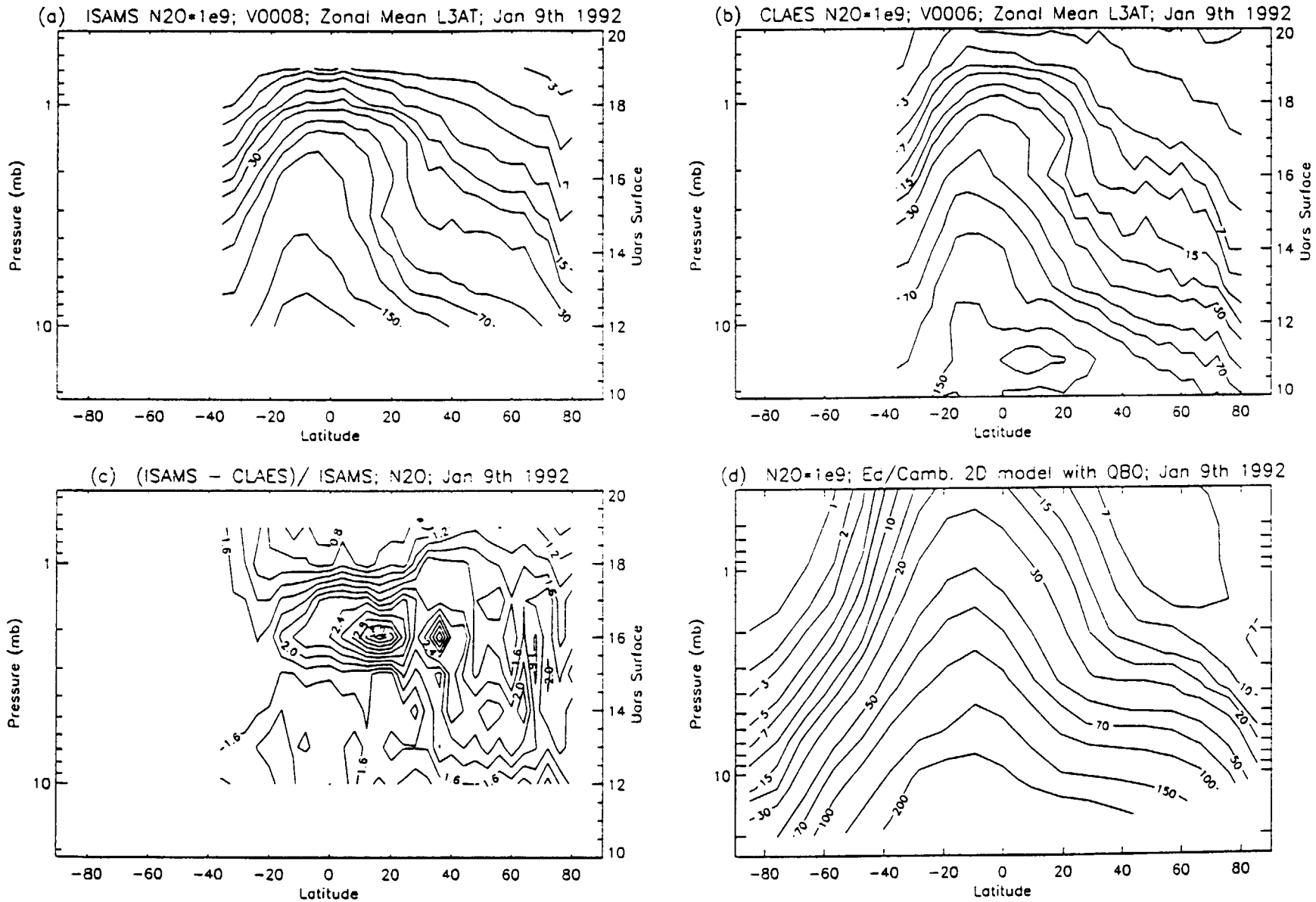

Figure 7.3.2-1. ISAMS N_2O and CLAES N_2O zonal mean mixing ratios for Jan. 9, 1992. Also shown are an (ISAMS - CLAES)/ISAMS difference plot and comparison with 2-D model results.

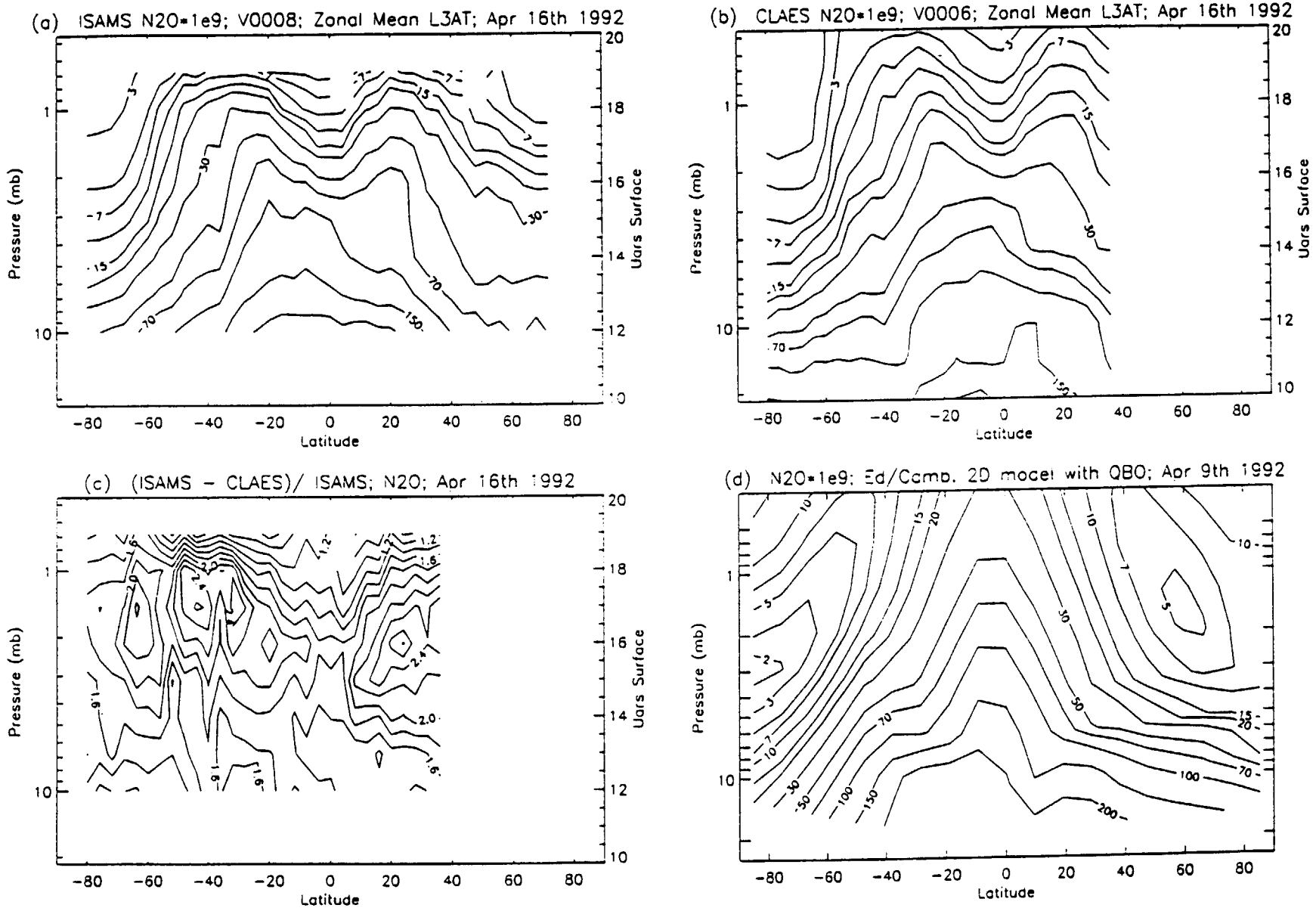

Figure 7.3.2-2. Same as Figure 7.3.2-1, but for April 16, 1992.

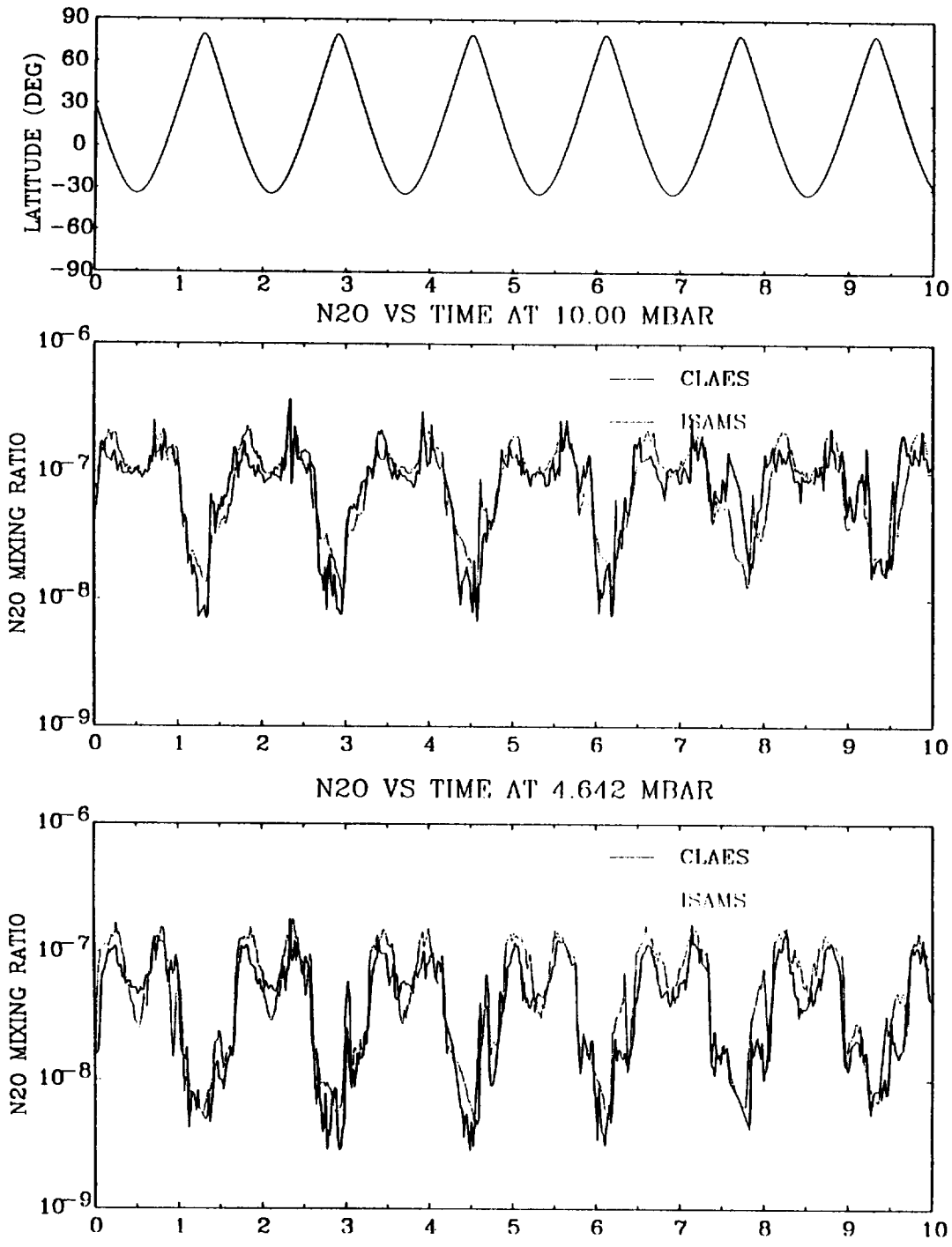

Figure 7.3.3-1. Direct comparison of CLAES and ISAMS tangent track N_2O series for Jan. 9 (day 120) at 10 and 4.6 mb.

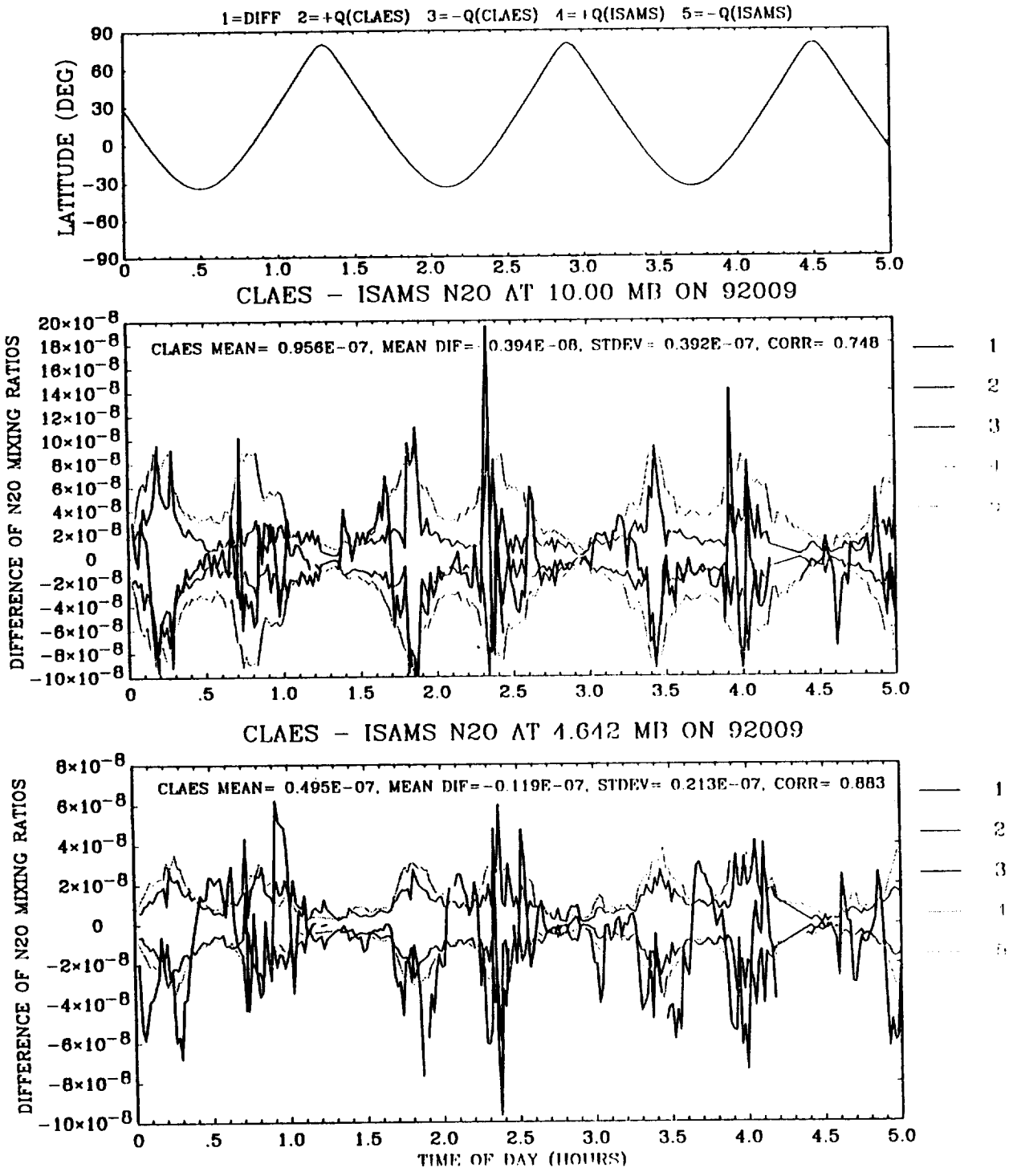

Figure 7.3.3-2. CLAES-ISAMS N_2O differences for tangent tracks of Figure 7.3.3-1.

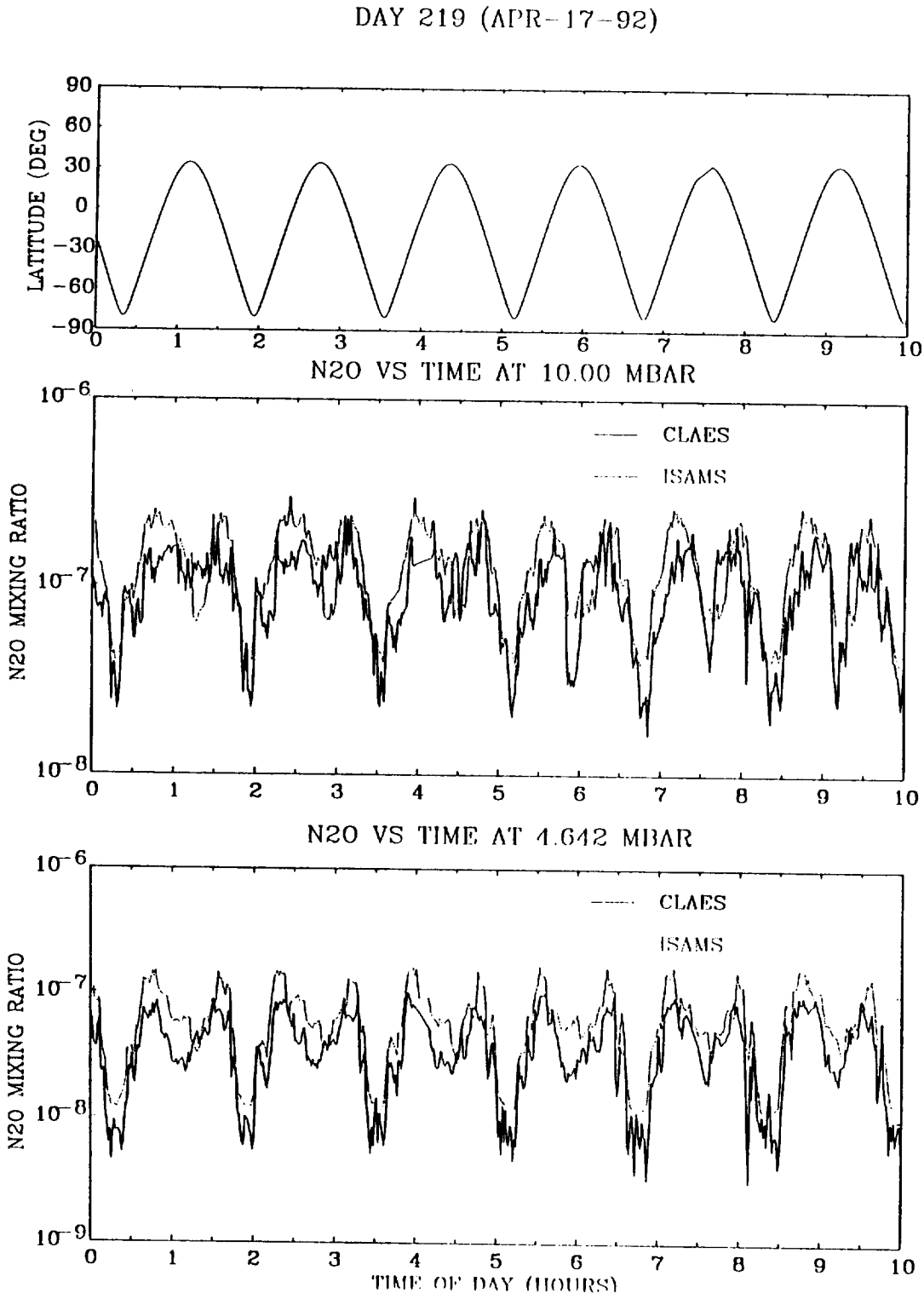

Figure 7.3.3-3. Direct comparison of CLAES and ISAMS tangent track N20 series for April 17 (day 219) at 10 and 4.6 mb.

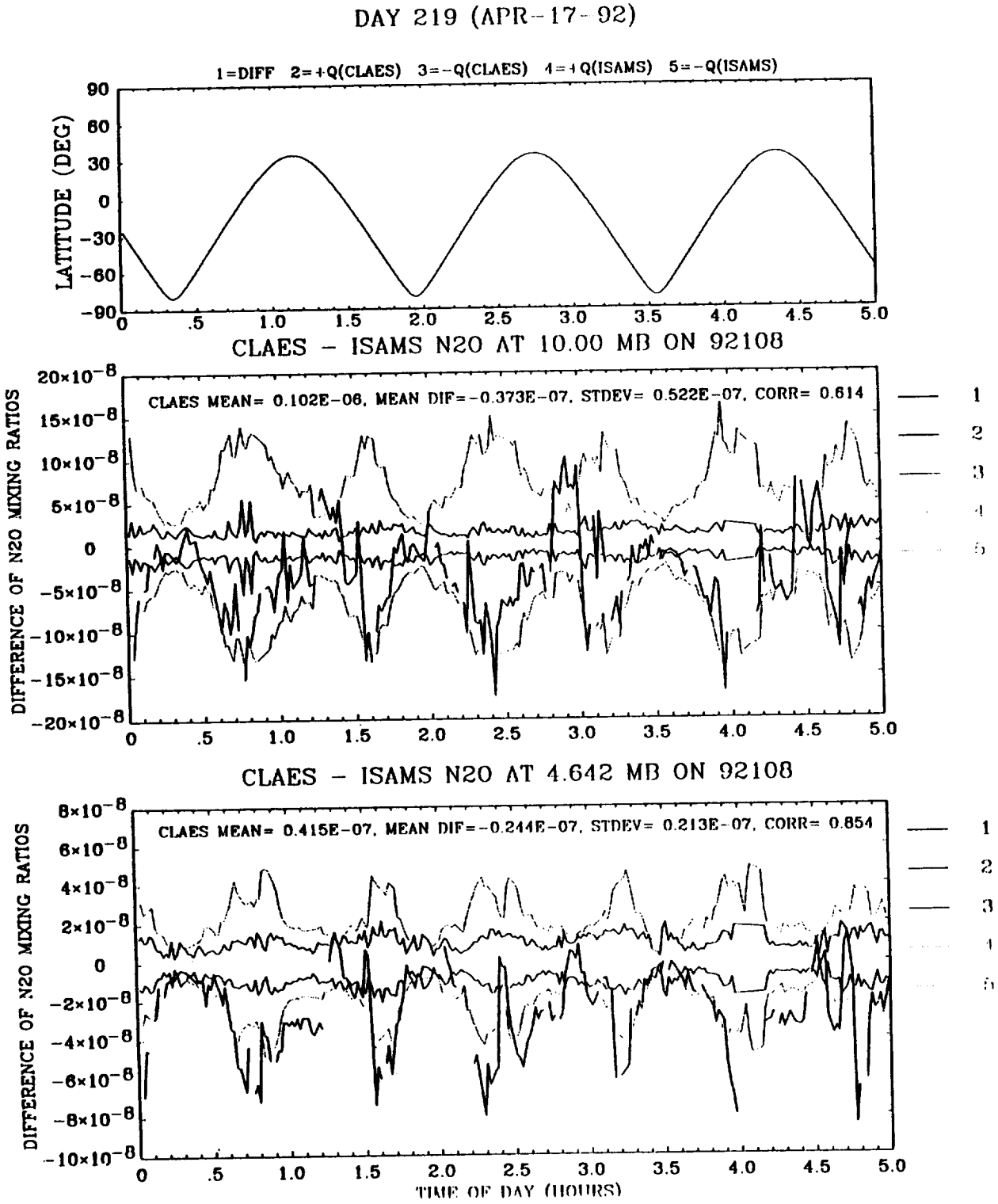

Figure 7.3.3-4. CLAES-ISAMS N20 differences for tangent tracks of Figure 7.3.3-3.

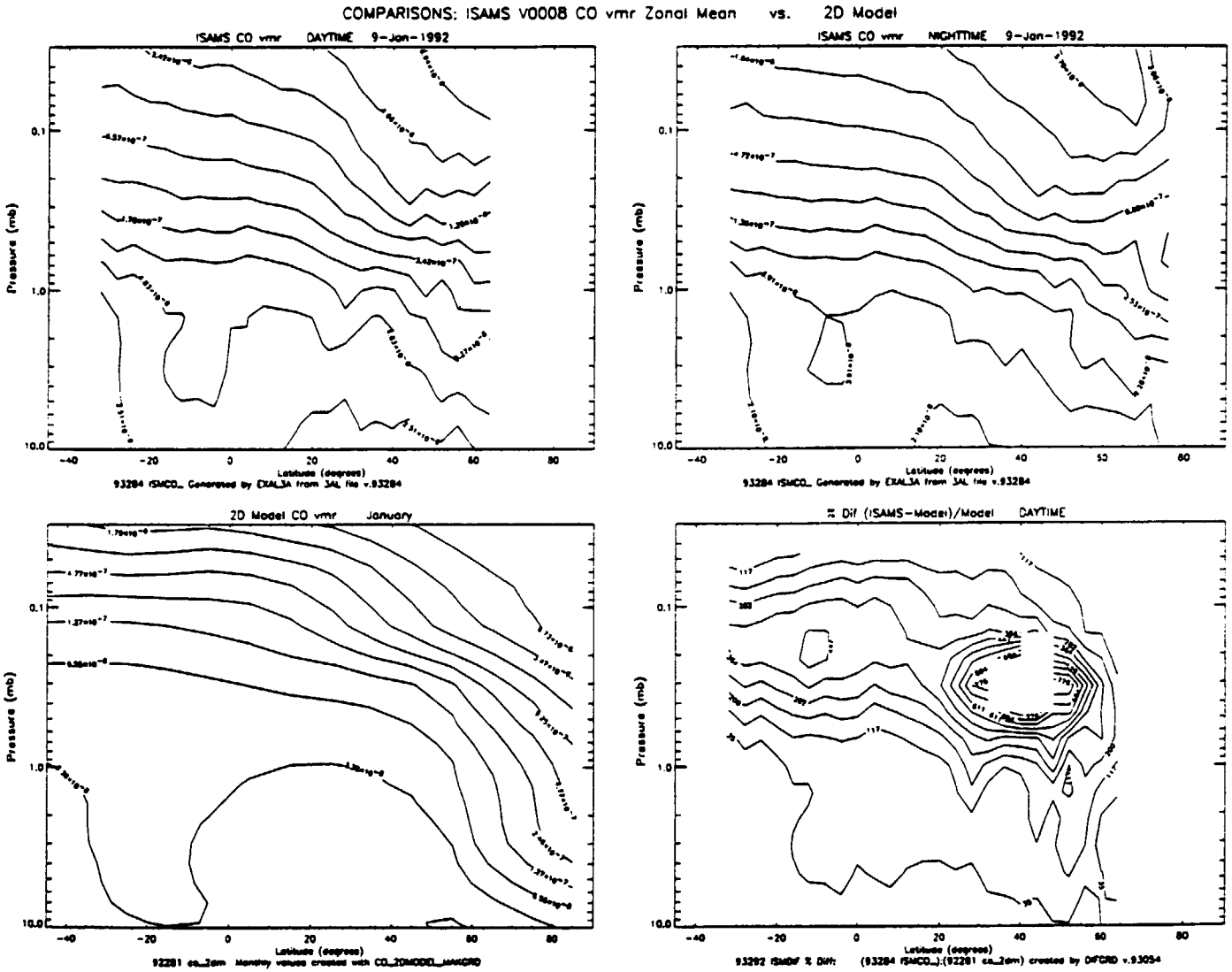

Figure 7.4-1. ISAMS zonal mean CO volume mixing ratio for Jan. 9, 1992. Upper left and right panels show daytime and nighttime retrievals, respectively. Lower left hand panel shows results from the GSFC 2-D model, and lower right panel shows the relative difference between daytime ISAMS and the model results.

Comparison colocated ISAMS and Rocket measurements

Zipf Rocket: Lat=32.4°N, Lon=253.7°E

D0254 ISAMS Prof 2637: Lat=33.64°N, Lon=251.0°E, SZA=64°

D0259 ISAMS Prof 1016: Lat=32.48°N, Lon=256.4°E, SZA=116°

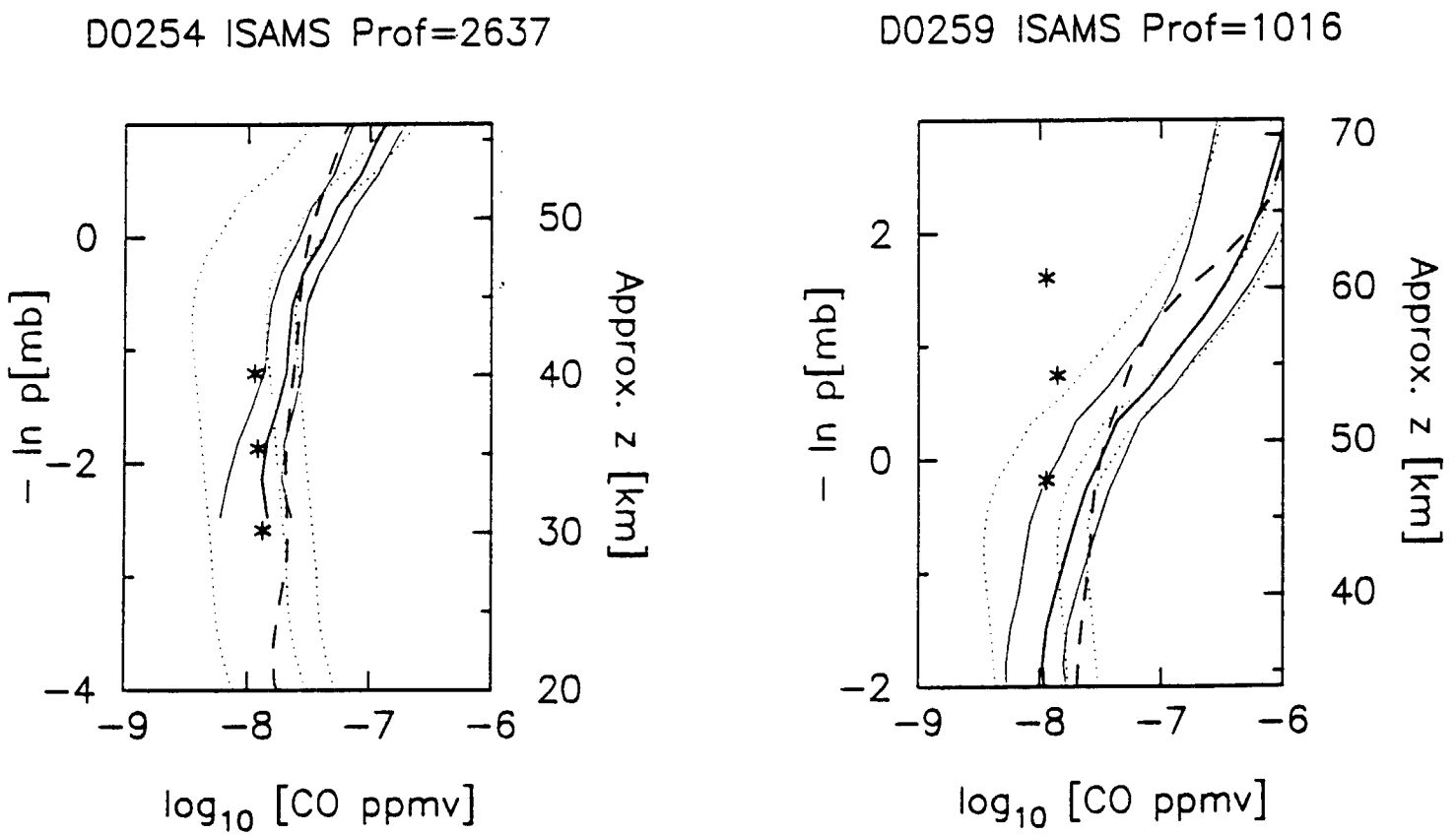

Figure 7.4-2. Comparison between ISAMS CO profiles and the CWAS correlative data for May 22, 1992 (left) and May 29, 1992 (right).

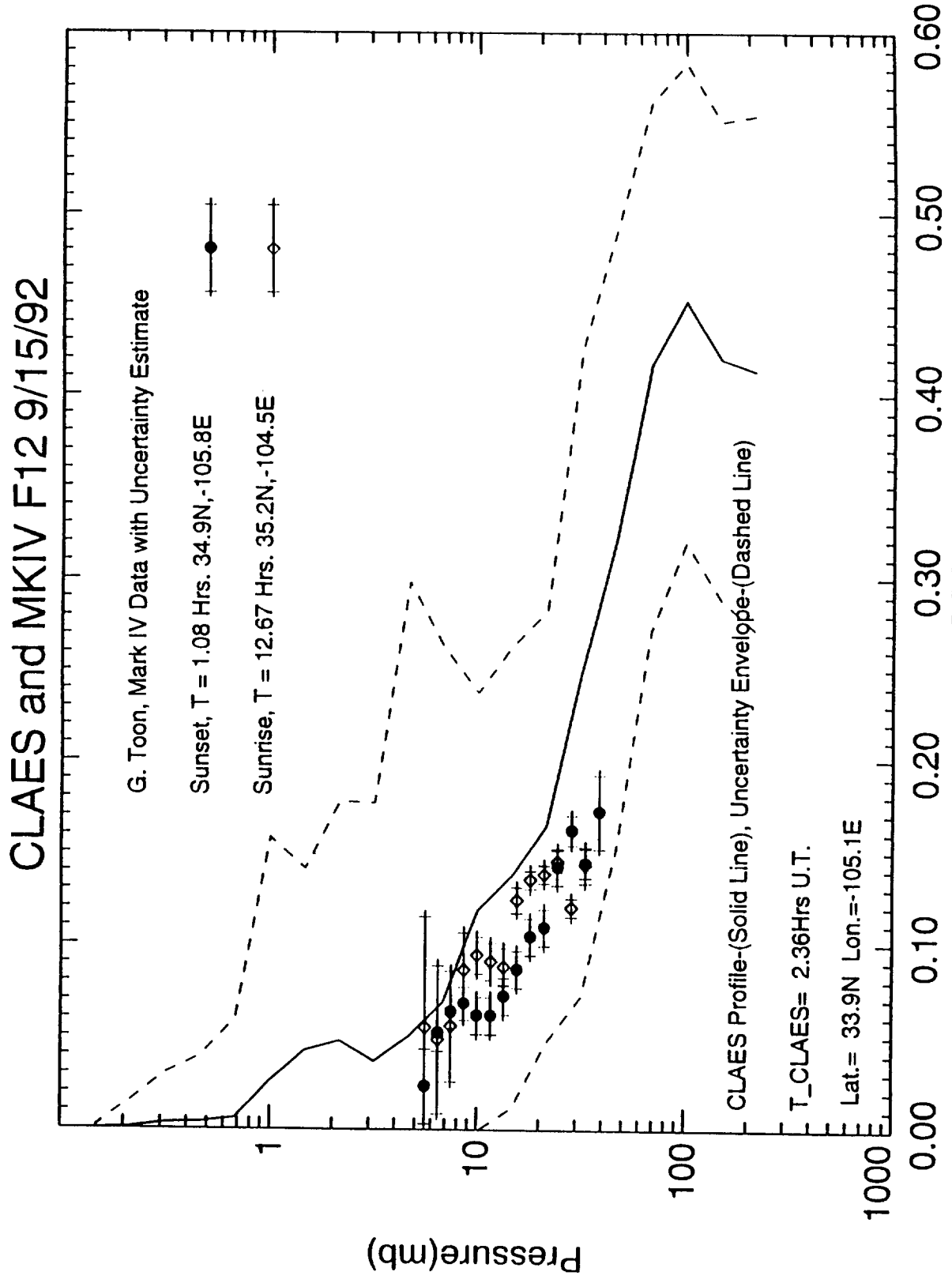

Figure 7.5.1-1. Comparison between CLAES CF_2Cl_2 altitude profile and data from the MKIV balloon instrument for Sept. 15, 1992 at 34.4N.

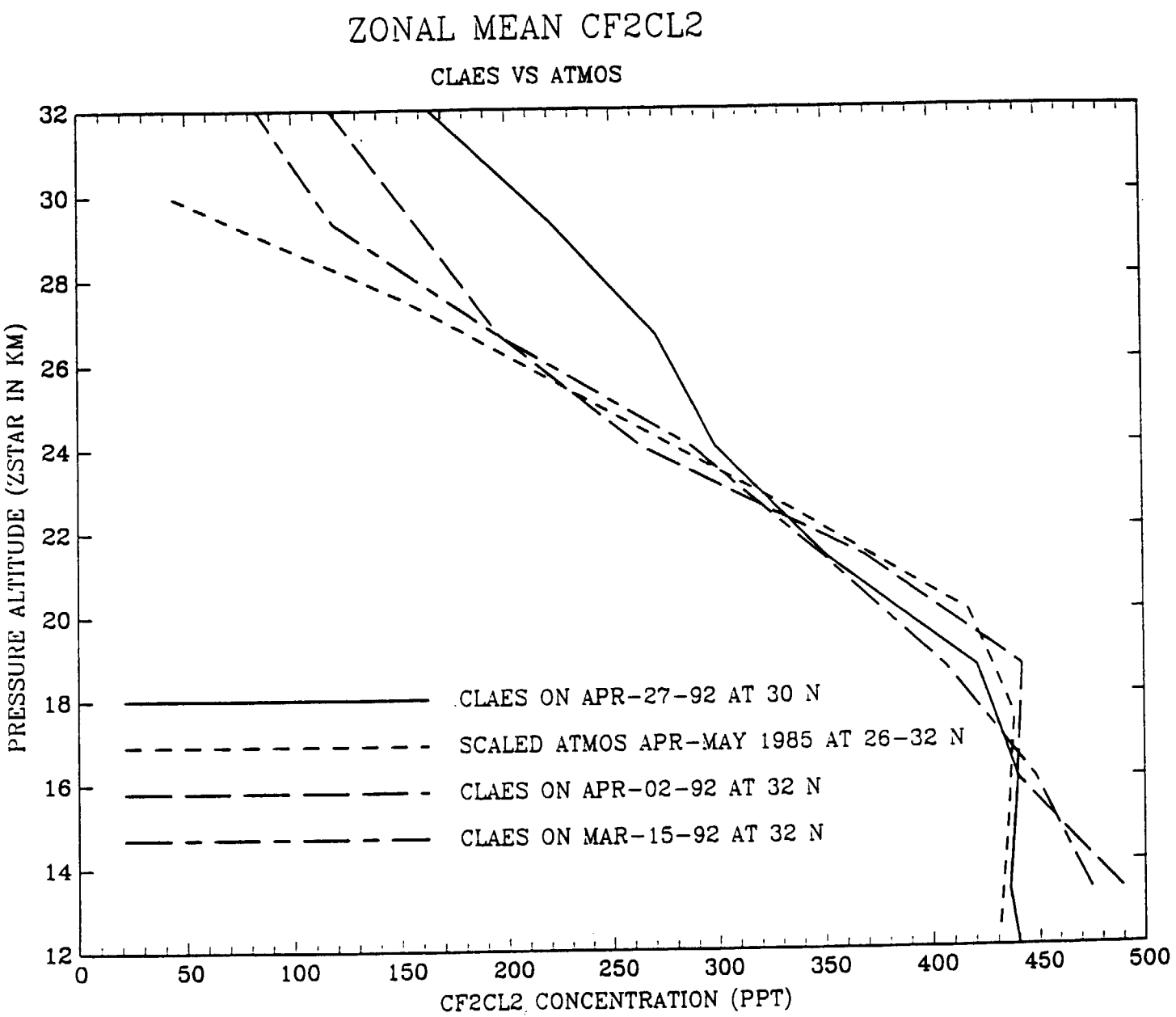

Figure 7.5.1-2. Comparison between CLAES CF_2C1_2 altitude profiles for March-April 1992 and a scaled ATMOS 1985 profile at 30N.

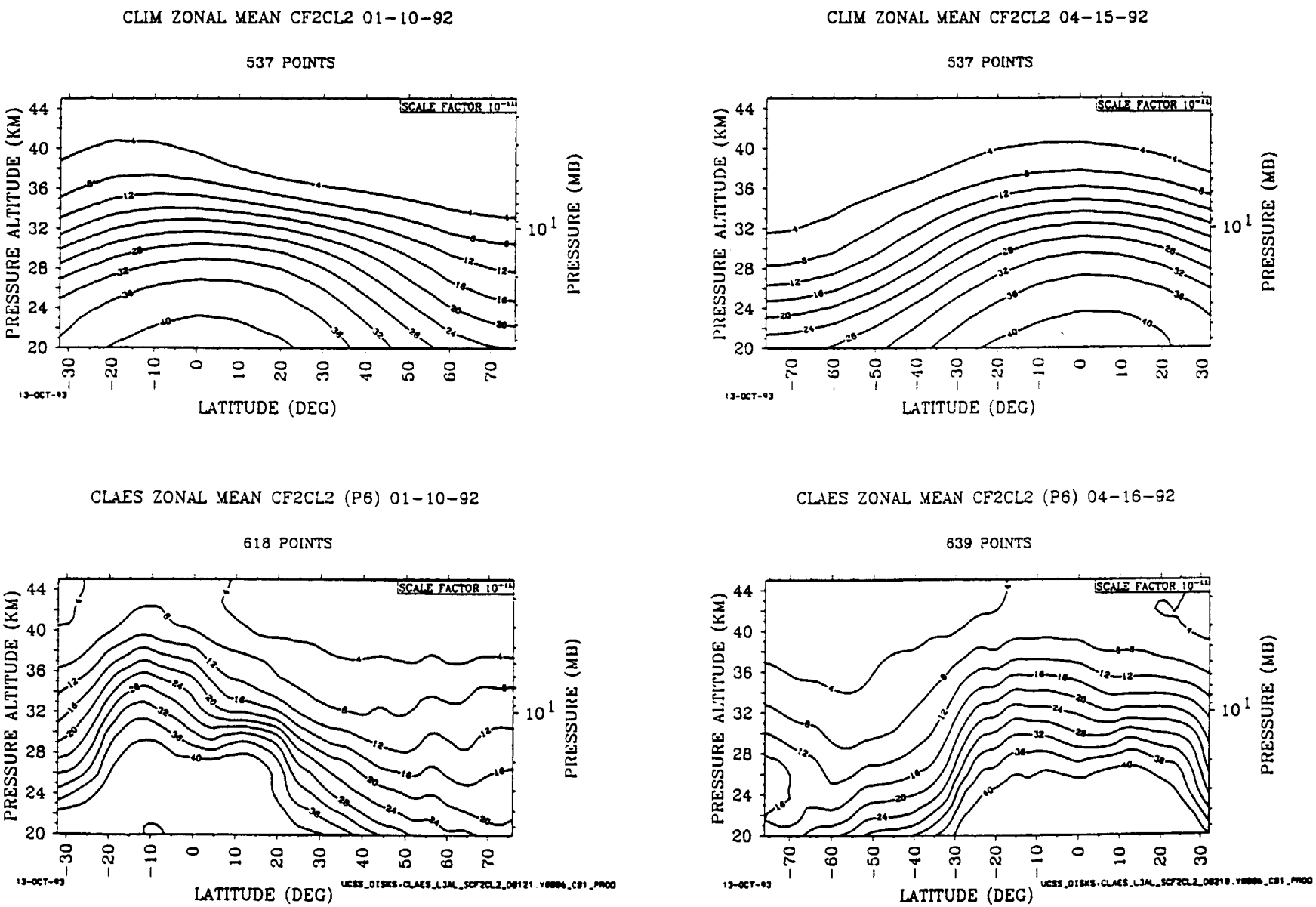

Figure 7.5.2-1. Comparison between CLAES CF_2C1_2 zonal mean latitude-height cross-sections and LLNL 2-D model results for Jan. 10 and April 16, 1992.

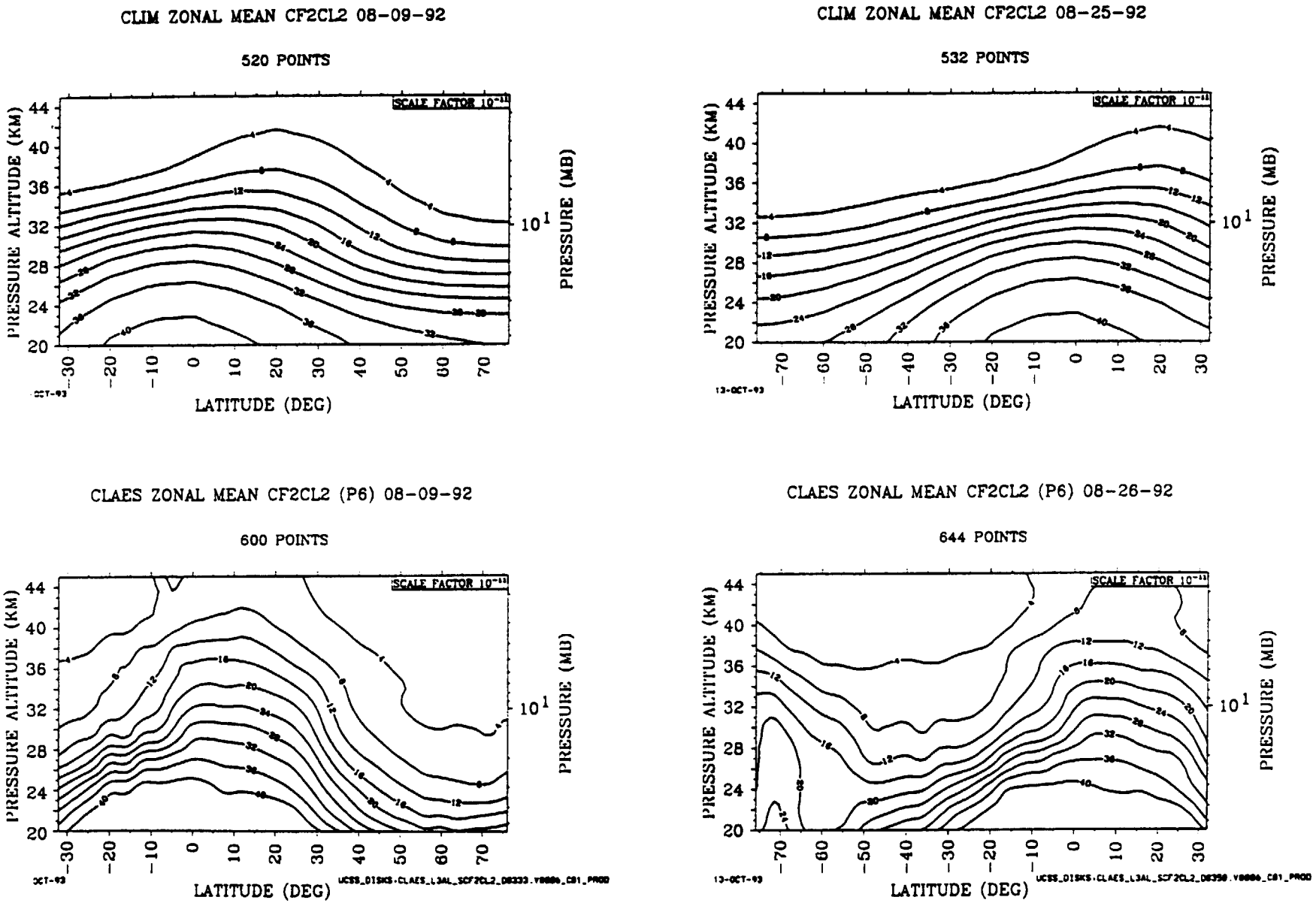

Figure 7.5.2-2. Comparison between CLAES CF_2Cl_2 zonal mean latitude-height cross-sections and LLNL 2-D model results for Aug. 9 and Aug. 26, 1992.

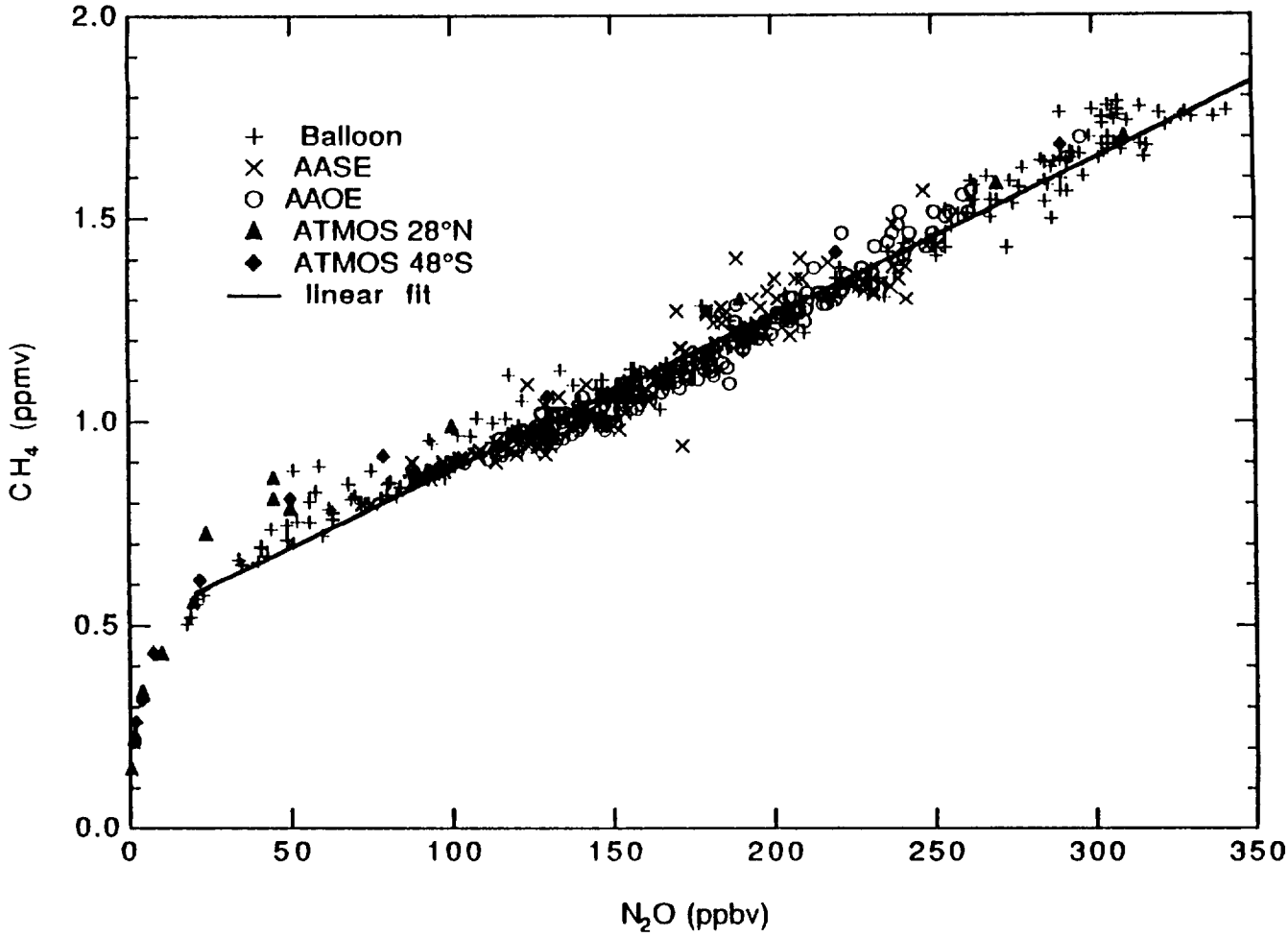

Figure 7.6-1. Observed CH_4 versus N_2O scatter plot from balloon observations, AAOE and AASE aircraft, and ATMOS (from Models and Measurement Report, Prather and Remsberg, 1993).

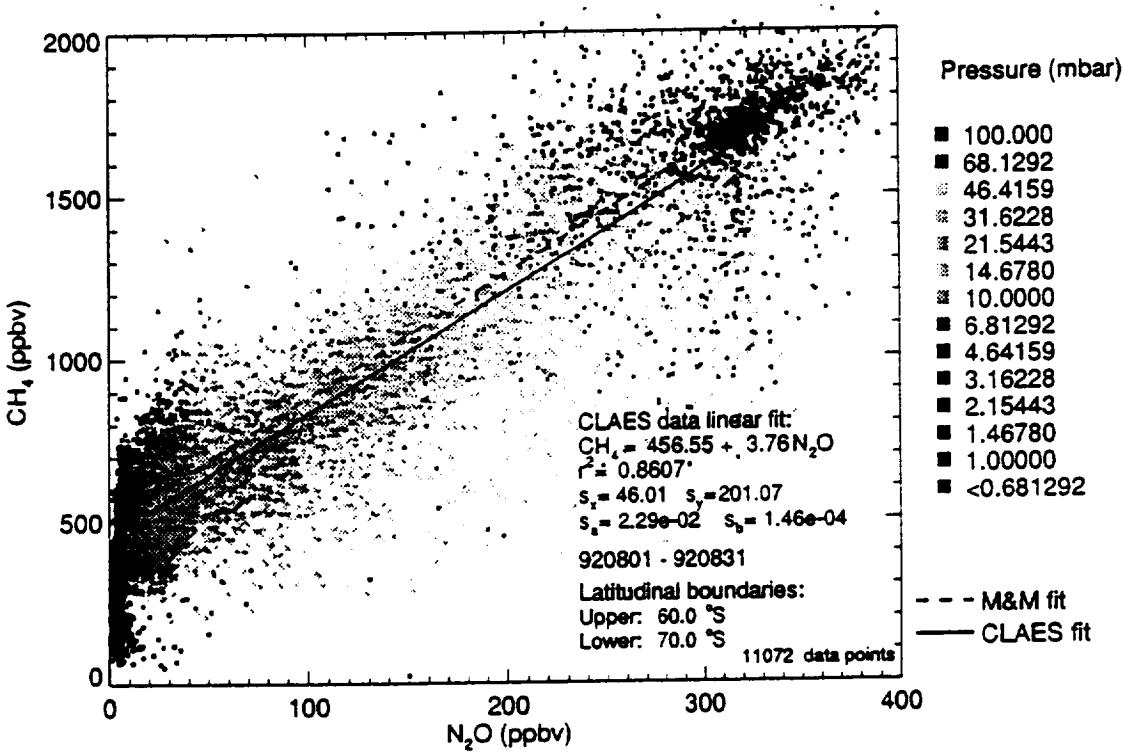

(a)

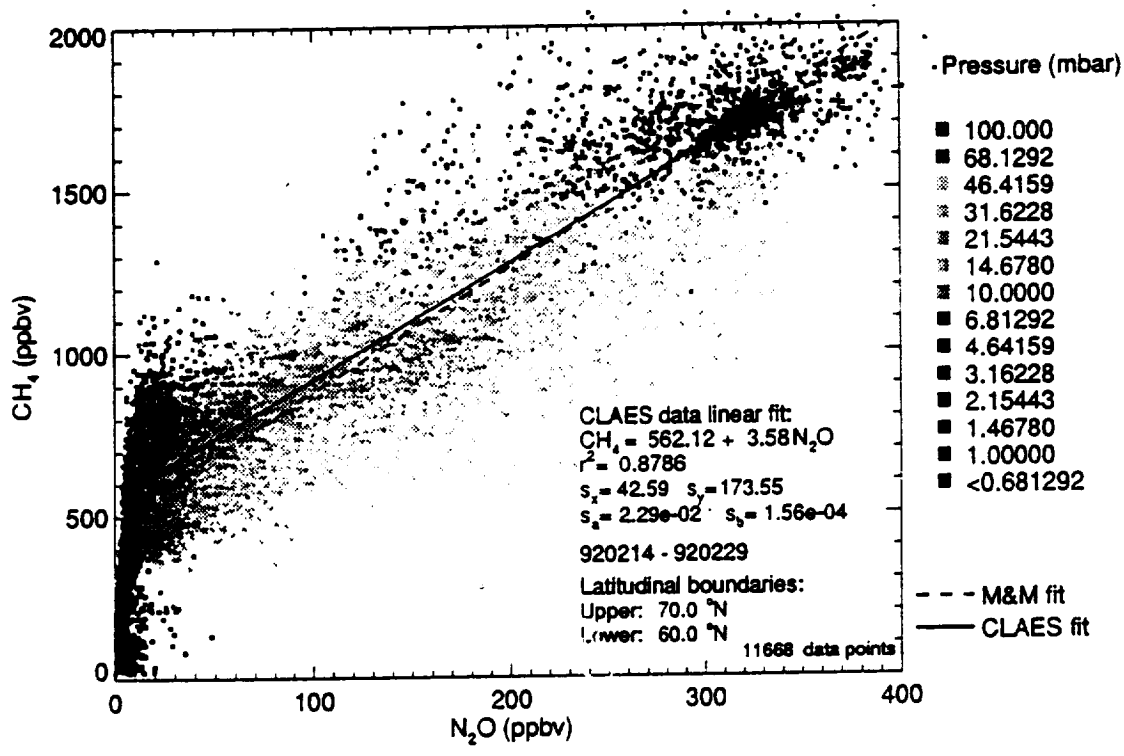

(b)

Figure 7.6-2. CLAES CH_4 versus N_2O scatter plots for (a) Aug. 1992 at 60-70 S and (b) Feb. 1992 at 60-70 N.

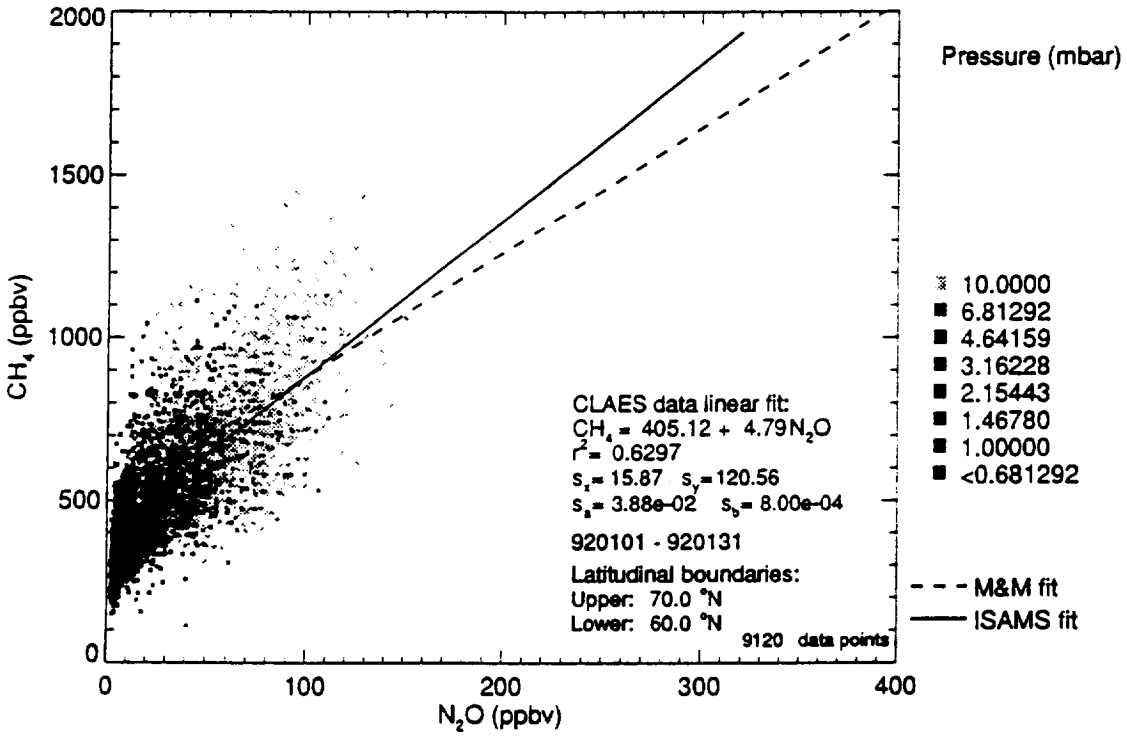

Figure 7.6-3. ISAMS CH_4 versus N_2O scatter plot for Jan. 1992 at 60-70 N.

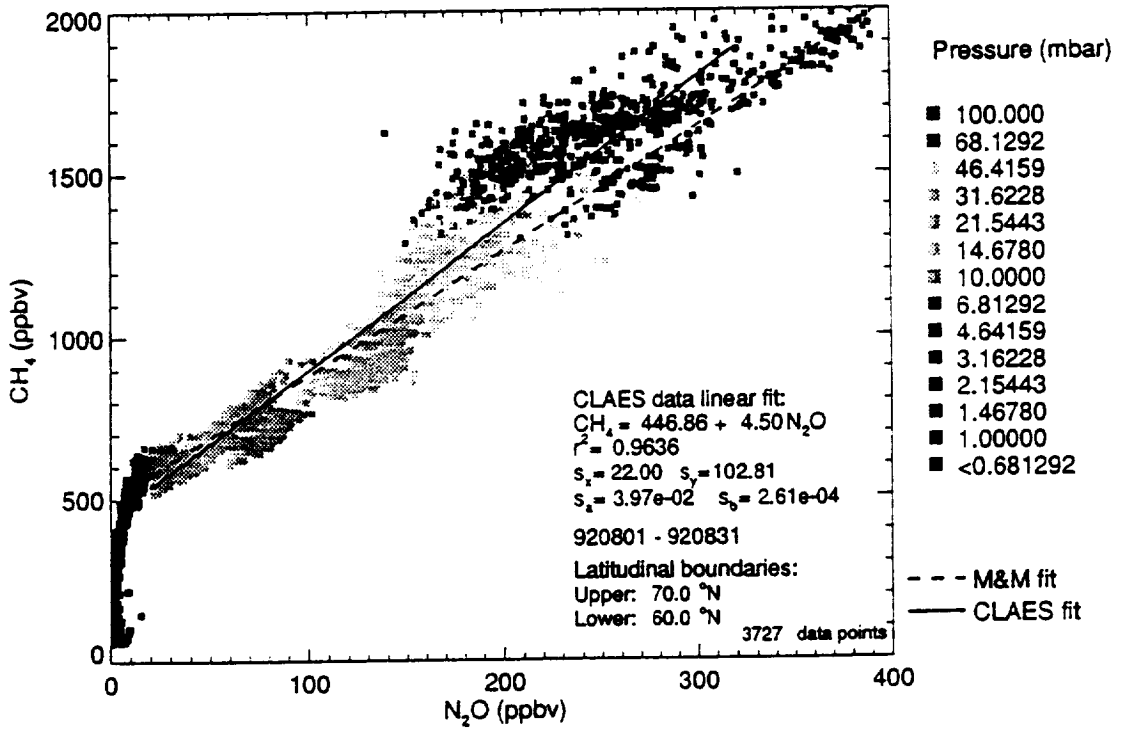

(a)

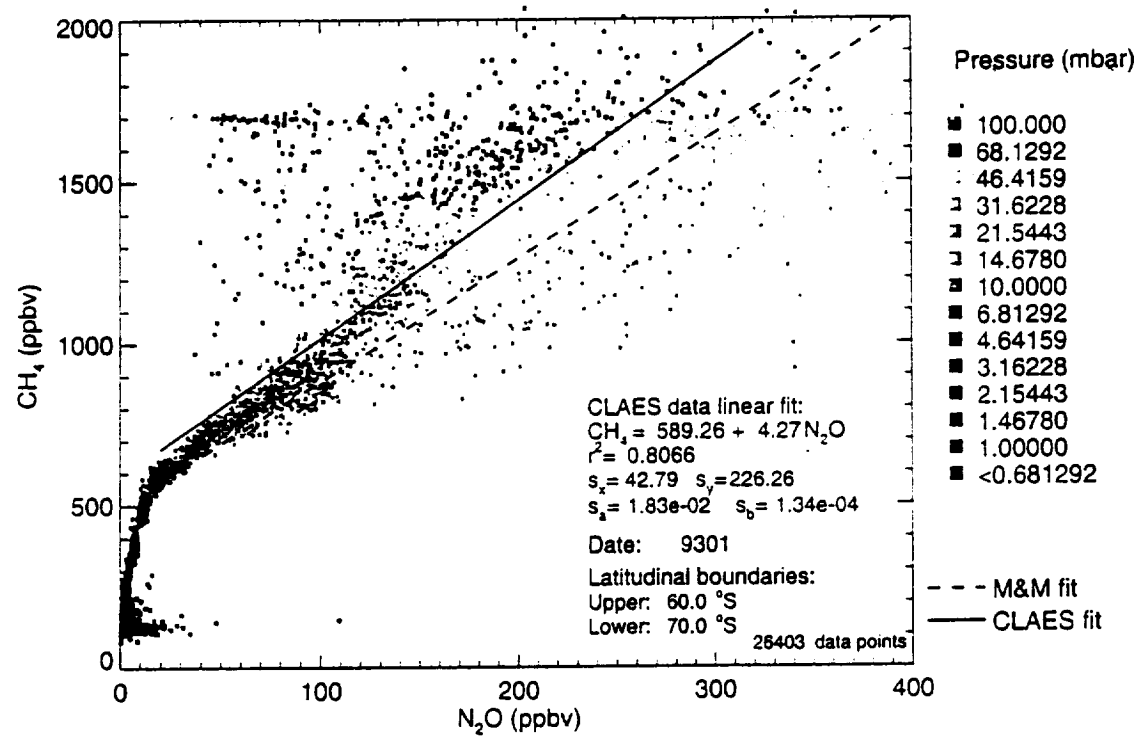

(b)

Figure 7.6-4. CLAES CH4 vs. N20 data from summer high latitudes: (a) north and (b) south.

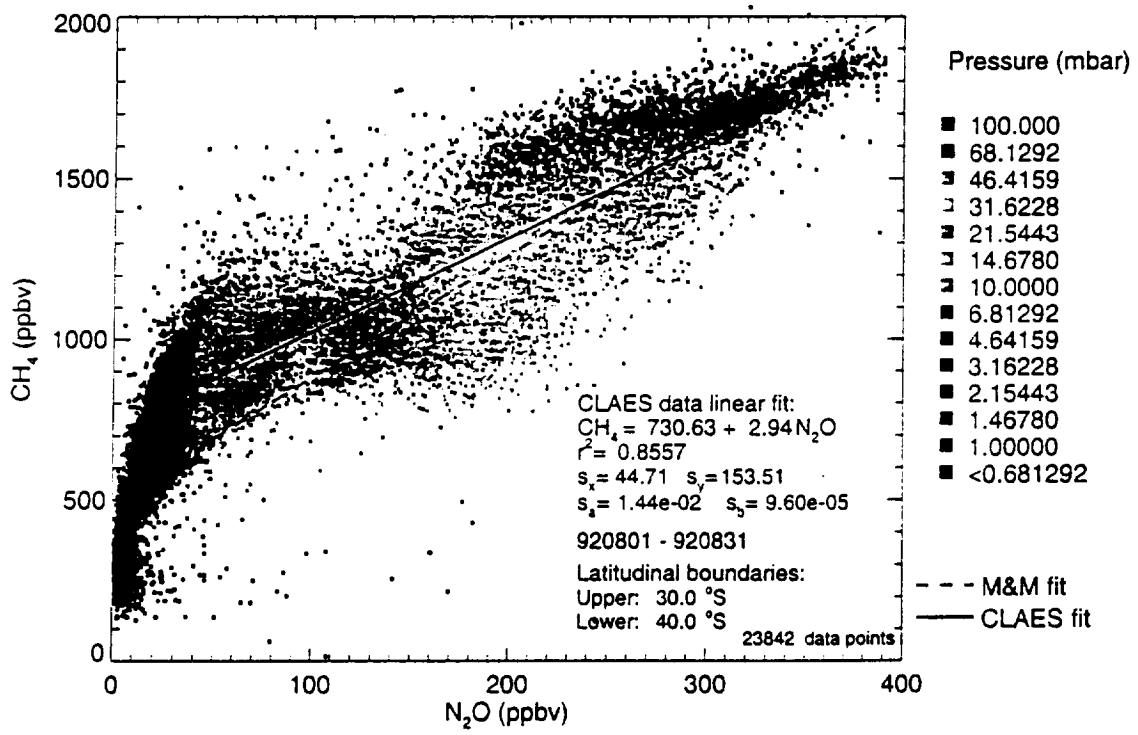

(a)

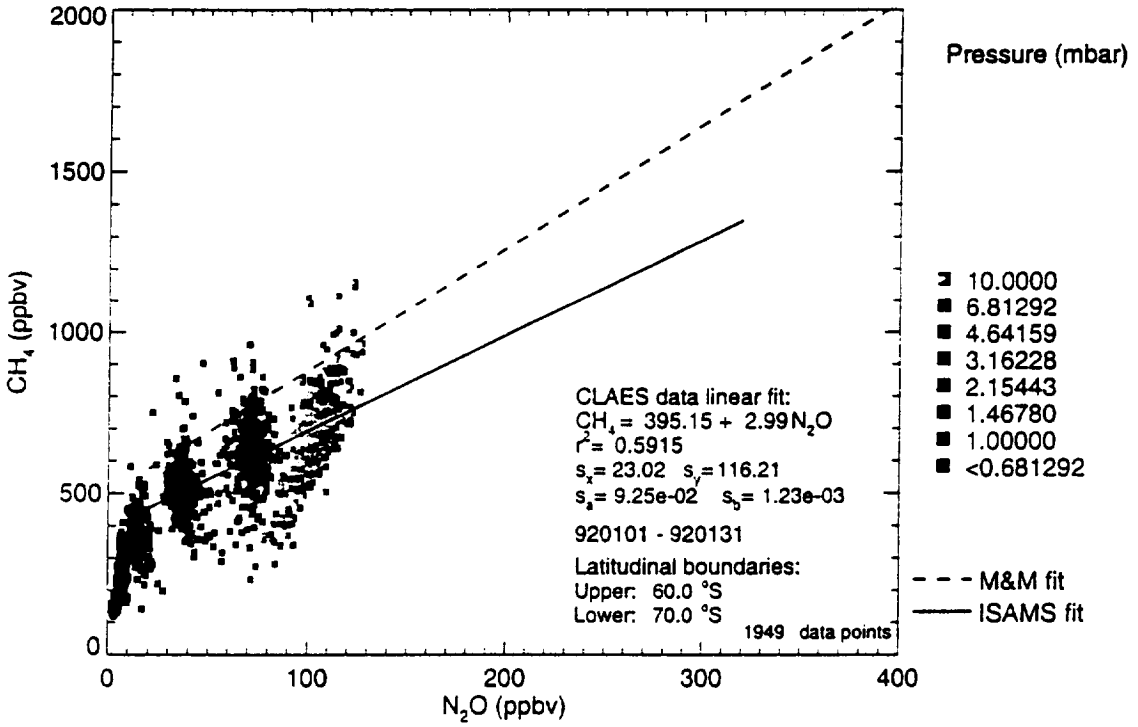

(b)

Figure 7.6-5. CLAES (a) and ISAMS (b) CH_4 versus N_2O scatter plots.

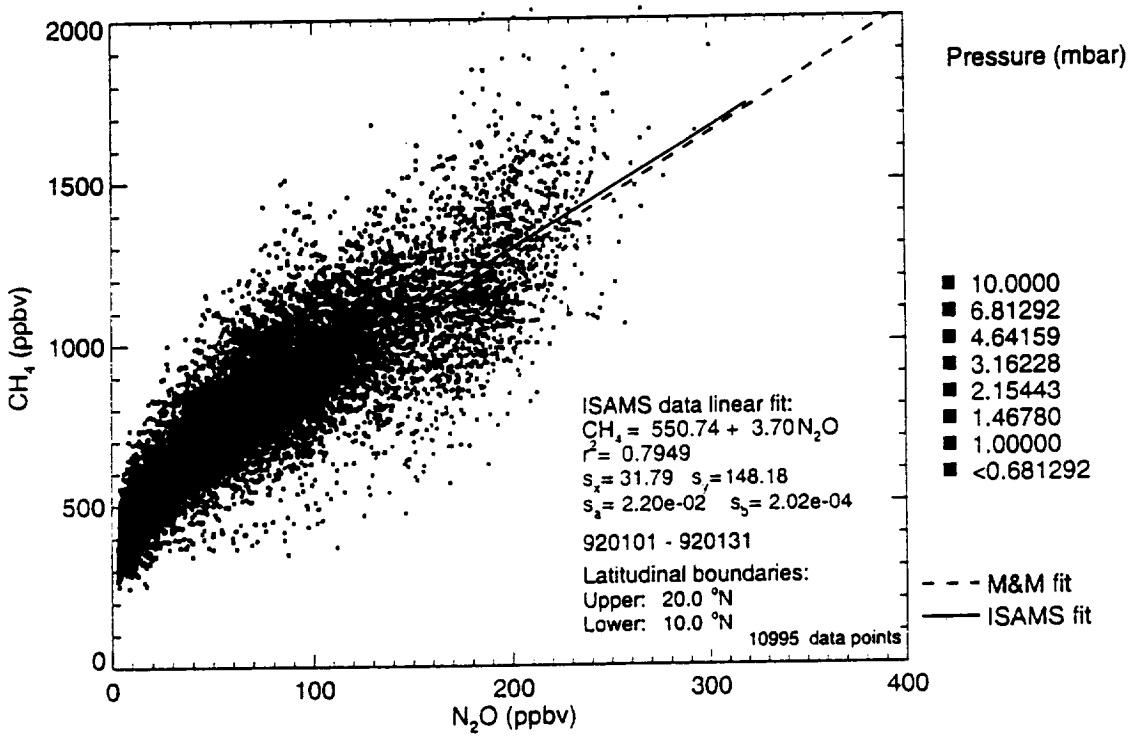

(a)

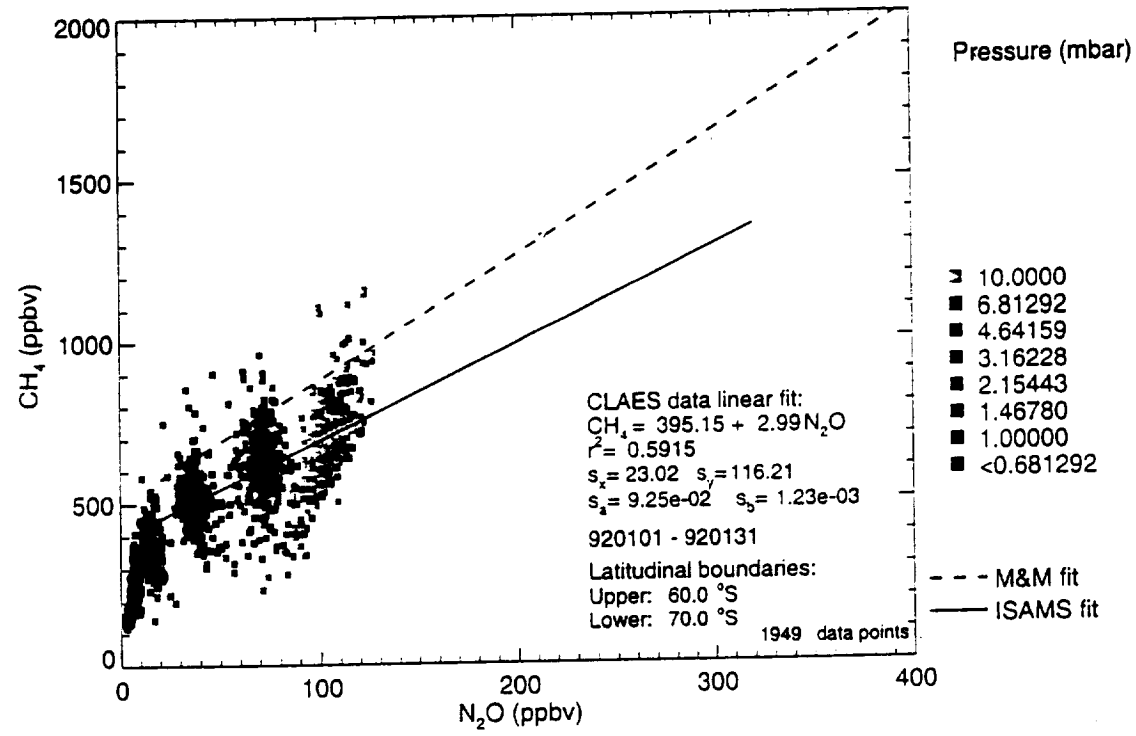

(b)

Figure 7.6-6. CLAES (a) and ISAMS (b) CH4 versus N20 scatter plots for the tropics.

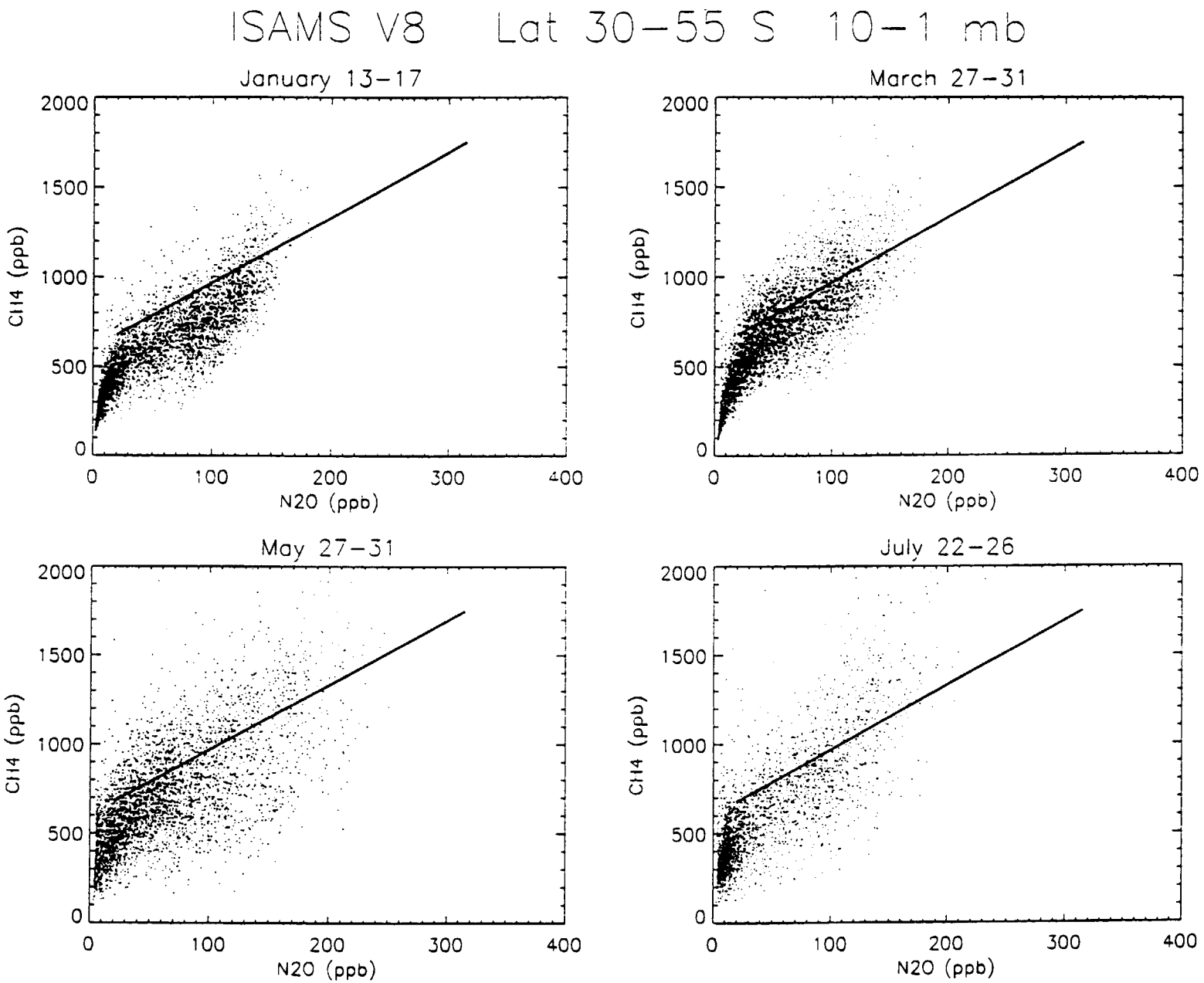

Figure 7.6-7. ISAMS CH_4 versus N_2O scatter plots for different time periods in different latitude bands.

8 HALOGENS AND SULFUR DIOXIDE

8.1 Chlorine Monoxide (ClO)

8.1.1 Correlative Data

8.1.1.1 Historical (Pre-UARS) Data

A collection of prior ground based, balloon, and aircraft measurements are available having limited spatial coverage..

8.1.1.2 Correlative Balloon Measurements

ClO profiles were measured by the balloon-borne Submillimeter Limb Sounder of Stachnik, et al., as part of the UARS correlative measurements program. SLS measurements at the same time as MLS were obtained on October 1, 1991 (launched from Ft. Sumner, New Mexico), February 20, 1992 (launched from Daggett, CA), September 29, 1992 (launched from Ft. Sumner, New Mexico) and April 3, 1993 (launched from Daggett, CA). The estimated accuracy is 0.1 ppbv or better over a vertical range between 50 and 1 hPa.

8.1.1.3 Correlative Ground-based Measurements

Ground-based measurements have been made by deZafra, et al., as part of the UARS correlative measurements program. Column measurements over Thule, Greenland, at the same time as MLS measurements are available for February and March 1992 with estimated accuracy of approximately 1.0×10^{16} molecules per square meter. Profile measurements over McMurdo Station, Antarctica, are available for mid-September 1992 with an estimated accuracy of 0.1--0.3 ppbv over a vertical range between 100 and 1 hPa.

8.1.1.4 Coincident Aircraft Measurements

Several in situ measurements of lower stratospheric ClO were made by Toohey, et al., from the ER-2 aircraft during measurement campaigns during 1991 and 1992. These measurements have excellent precision (better than 0.01 ppbv) and cover pressure altitudes between about 50 and 65 hPa.

Remote submillimeter measurements of ClO have also been made by Crewell, et al., from a German aircraft operating in the Arctic in 1992 and 1993.

8.1.2 ClO Comparison Results

8.1.2.1 Comparison with Pre-UARS Data

8.1.2.1.1 Upper Stratospheric ClO

Many pre-UARS measurements of upper stratospheric ClO were made at 20-40° N latitudes. Figure 8.1.2.1.1-1 shows 20-40° N monthly zonal mean mid-day profiles from MLS for every north-looking UARS month up to, and including, July-August 1993. The variation in these monthly zonal means is seen to be small (approximately 0.1 ppbv) indicating that useful comparisons can be made without regards to the particular season of the measurements. Figure 8.1.2.1.1-2 compares the MLS monthly zonal means with the summary of mid-latitude upper stratospheric ClO measurements given in Waters et al.

(1988). There is general agreement to approximately 0.1 ppbv below 35 km. Above 35 km, some of the earlier measurements give 0.2-0.4 ppbv more ClO than observed in the MLS monthly zonal means.

Ground-based measurements of the variation in upper stratospheric ClO over a complete diurnal cycle have been reported by Solomon, et al. [1984]. These were made in October and December 1982 from Hawaii (19° N), and have been compared with model predictions (Ko and Sze, 1984). Figure 8.1.2.1.1-3 compares these results with the 10-30° N zonal mean diurnal variation observed by MLS during the UARS north-looking months of October 1992 and December 1991. Both the measurements and the theory have been normalized in the same manner. There is generally good agreement, with the MLS measurements fitting more closely the model predictions of a steeper morning rise than is evident in the ground-based measurements. The mid-day column (above 30 km) inferred from the ground-based measurements is $0.7\text{-}0.8 \times 10^{18}$ molecules/m^2, whereas that inferred from MLS is $1.0\text{-}1.2 \times 10^{18}$ molecules/m^2. The difference of approximately 50% between the times of the measurements is consistent with the approximately 5% per year increase expected in stratospheric chlorine.

8.1.2.1.2 Enhanced Lower Stratospheric ClO

Enhanced ClO levels in the lower stratosphere over Antarctica were obtained prior to UARS by ground-based microwave measurements obtained at McMurdo Station (78°S). Figure 8.1.2.1.2-1 shows the ground-based measurements made between Sept. 20-24, 1987 reported in Barrett, et al. [1988], and compares them with MLS 75-81° S zonal means for Sept. 16-20, 1992 (the last 5 days before UARS yaw to the north). Both measurements show the 'double-peaked' ClO profile which results from separate regimes of gas-phase chemistry in the upper stratosphere and heterogeneous chemistry in the lower stratosphere. The location of the peaks are in acceptable agreement. Agreement in abundances are generally within the error bars, except for the lower stratospheric peak where MLS is approximately 0.5 ppbv higher (after day-night differences in the MLS data have been taken). MLS also gives approximately 0.5 ppbv lower abundances in the upper stratosphere.

Enhanced lower stratospheric ClO was observed from the ER-2 aircraft during the 1987 Antarctic campaign. Figure 8.1.2.1.2-2 compares the 1987 recalibrated ER-2 measurements [D. Toohey, private communication] with averages from MLS data made during the same time of year. The MLS measurements are averages of data taken between September 7-17, 1992, equatorwards of 72°S, but only where greater than 1 ppbv ClO was observed at 46 hPa. This is similar to the location of the ER-2 measurements: inside the "chemically-perturbed region", but only to 71°S. The MLS value at 46 hPa appears in acceptable agreement with the upward extrapolated ER-2 measurements, especially when the expected increase of approximately 25% in stratospheric chlorine between 1987 and 1992 is accounted. The 100 hPa ClO value from MLS is lower than expected from the ER-2 measurements which, again, suggests problems with the MLS 100 hPa values.

8.1.2.2 Comparison with Balloon Data

Figures 8.1.2.2-1 to 8.1.2.2-3 compare MLS 30-40° N zonal mean ClO profiles with those measured on individual balloon flights of the Submillimeter Limb Sounder (SLS) [R.A. Stachnik, private communication]. The daily zonal means from MLS agree, to

within that expected from the estimated error bars, to the SLS profiles over the full vertical range. The MLS monthly zonal means agree to within 0.1 ppbv or better with SLS over the full vertical range. The April 3, 1993 SLS flight occurred when MLS was looking south, so that MLS profiles are not available on that date for comparison (measurements at the northern extreme of the south-looking orbit were in darkness); data from that flight are compared later (Figure 8.1.2.4-5) in a time series of MLS data.

8.1.2.3 Comparison with Ground-Based Data

Figure 8.1.2.3-1 shows column measurements of ClO over Thule, Greenland during February and March of 1992 [R. deZafra, private communication] compared with MLS. The ground-based measurements were taken during mid-day and are averages over periods of 3-5 days. Column ClO computed from individual MLS measurements made nearest Thule on both the ascending and descending portions of the orbit are shown, and the MLS data have been smoothed with a 5-day running average. During the period of these comparisons, the `day' side of the orbit for MLS measurements switched from ascending to descending. The solar zenith angle and local solar time of the MLS measurements are shown in the two bottom panels. The agreement between the day MLS measurements and the ground-based measurements is comparable to the observed variations (about 10^{18} molecules per square meter), all that might be expected given the different horizontal and temporal samplings of the two techniques.

Figure 8.1.2.3-2 compares ClO profiles from ground-based measurements over McMurdo on September 15 and 19, 1992 [R. deZafra, private communication] with averages of MLS profiles taken near McMurdo during September 15-20, 1992. The profile from the ground-based measurements has been converted (using a least-squares best fit) to the profile representation basis (piece-wise linear in logP) used by MLS. The MLS averages are measurements made within 500 km longitude and 2^{o} latitude of McMurdo and include approximately 20 individual profiles. When day-night differences of MLS profiles are taken below 10 hPa (as is effectively done for the ground-based profiles) there is agreement to within approximately 0.1 ppbv between MLS and ground-based measurements of the peak abundance in the lower stratosphere. However, there appears to be a discrepancy in the profile shape and, perhaps, the peak values in the upper stratosphere. MLS shows a local minimum near 22 hPa, whereas the ground-based profile has a minimum mear 10 hPa. Upper atmospheric ClO abundances from the MLS and ground-based measurements differ up to 0.4 ppbv between 2 and 22 hPa, and appear larger than would be expected from the error bars. Note that the 'night' ClO profile from MLS more closely matches the ground-based profile at 22 hPa and above. More investigations of this apparent discrepancy are needed.

8.1.2.4 Comparison with Aircraft Data

Figures 8.1.2.4-1 to 8.1.2.4-5 compare ClO measurements from the ER-2 aircraft reported by Fahey, et al. (1993), with averages of profiles from MLS. Monthly zonal means of MLS data are required to reduce the noise to a level at which comparisons are meaningful. The ER-2 measurements were made during two mid-latitude northern hemisphere flights in September 1991 and March 1992. Figures 8.1.2.4-1 and 8.1.2.4-2 compare the nearest monthly zonal mean vertical profiles from MLS with the ER-2 values. Figure 8.1.2.4-3 shows height-latitude cross-sections of the MLS monthly zonal means and indicates the locations of the ER-2 measurements. It is clear from this figure that MLS observed an increase in lower stratospheric ClO at middle and high northern latitudes between October 1991 and March 1992, with increasing ClO to the north in

March 1992 and little variation with latitude in October 1991. Figure 8.1.2.4-4 compares the MLS and ER-2 measurements as a function of latitude, and the MLS data agree with the ER-2 to within the estimated MLS error bars of about 0.04 ppbv for the monthly zonal mean. MLS appears to be tracking the ER-2 measurements and both show more ClO in March 1992, with a significant increase towards the north in March 1992. Figure 8.1.2.4-5 shows a time-series of all MLS 30-50° N monthly zonal mean lower stratospheric ClO, compared with the ER-2 and SLS measurements. This figure illustrates that, at least according to MLS, the variation between September 1991 and March 1992 appear to be part of a slowly varying seasonal cycle, and that a comparison of the two measurements - made with vastly different temporal and spatial average - is meaningful. The MLS seasonal and longer-term time series of lower stratospheric measurements are extremely important for understanding the extent to which Pinatubo contributed to the enhanced ClO being observed in the mid-latitude lower stratosphere, or whether these enhanced values are mainly caused by background sulfate aerosols. More comparisons with the very precise ER-2 measurements will be extremely valuable.

Comparisons have also been made with ER-2 measurements of enhanced ClO in the 1992 winter arctic vortex, and with German aircraft measurements in the 1992 and 1993 arctic winters. All comparisons done to date have shown agreement in the location of the enhanced ClO.

8.1.2.5 Model Validation Studies

The high ClO values routinely seen by MLS within the polar vortex are rarely co-located with temperatures cold enough to suport polar stratospheric clouds (PSCs) and the heterogeneous chemistry which produces reactive chlorine from reservoir species. Three-dimensional model calculations, which are based on independent meteorological fields, show the importance of mixing and transport processes to qualitative and quantitative explanations of ClO observations. During December, temperatures cold enough for PSC processing occur mostly poleward of 70 N. The air which has experienced PSC processing is transported towards middle latitudes, where ClO is produced by rapid photolysis of the products of heterogeneous reactions (Cl2 and HOCl). High ClO thus appears sporadically south of 60 N (Douglass et al., 1993).

Schoeberl et al. (1993) used an isentropic trajectory model to characterize the early January 1992 ClO observed by MLS for the 465 K potential temperature surface between 40 and 80 N. This includes some high values seen at middle latitudes. A histogram of nighttime values (not shown), when ClO is expected to have very low values, is well represented by a Gaussian of width 0.4 ppbv centered near zero. A histogram of daytime values is given in Figure 8.1.2.5-1. The solid line is a Gaussian of width 0.4 ppbv centered at 0.06 ppbv (the average of middle latitude aircraft observations). The high values outside the Gaussian distribution is clearly apparent. Back trajectory analyses determine the minimum temperatures encountered by the parcels. Using T<197K as a criterion for PSC formation, it is possible to separate two components of the ClO distribution. A histogram of ClO values greater than 0.4 ppbv is given in Figure 8.1.2.5-2. The shaded area, parcels whose minimum temperature is greater than 197 K, is represented by the Gaussian distribution appropriate for middle latitudes. The parcels which comprise the remainder of the distribution have encountered cold temperatures within the polar vortex. This distribution has greater variance, which results from differing rates of photochemical reactions following the PSC encounters. Outside the

polar vortex, the occasional occurrence of ClO amounts greater than 0.4 ppbv appear statistically consistent with MLS instrument noise.

8.2 Chlorine Nitrate ($ClONO_2$)

8.2.1 Correlative Data

Correlative data on chlorine nitrate is very limited. The comparison data gathered for this report comes from three balloon-borne FTS instruments. The first discussed here is an emission measurement from a MIPAS-B flight from Kiruna, Sweden on the night of March 14-15, 1992 (Oelhaf et al.,1993) inside the Arctic polar vortex. The second is a near-sunset July 24, 1992 balloon-borne FTS solar occultation profile measurement from a Palestine, Texas launch by the Denver University (DU) CMI group. The third and final comparisons available for the UARS period are a pair of sunset and sunrise solar occultation measurements by CMI G. Toon from Ft. Sumner, N. Mexico on September 15, 1992 with the JPL Mark IV Instrument.

8.2.2 Comparison Results

8.2.2.1 Profiles

The uncertainty indicated by the error bars is lgenerally less than about 30% for the highest quality retrievals. The error bars on the CLAES retrieved mixing ratios are a good indicator of whether the particular datum is truly retrieved or is closely related to the UARS climatology. If the error bars are large, as one frequently finds at pressures typically below 6 mb, the profile is dominated by climatology. At high pressures, approximately above 68 mb, the profile also may be influenced heavily by climatology, again this is indicated by large error bars which show an uncertainty of 100% or more. Frequently the relaxation to climatology results in local maximum in the profile at 4-6 mb. When compared with several mid-latitude measurements, the climatology used in the CLAES retrieval is an overestimate of the $ClONO_2$ mixing ratio above 10mb. Therefore, it is likely that the tangent point mixing ratio retrieved by CLAES just below the region dominated by this climatoloy is suppressed as the algorithm compensates for the increased $ClONO_2$ in limb path at higher altitudes.

Figure 8.2.2.1-1 shows a comparison of the MIPAS-B data with a CLAES near-coincidence measurement. The air volume sampled by MIPAS-B data was located at (67N, 30E). The measurement was within the polar vortex during a period the temperatures were above PSC formation temperature. The time of the measurement was between 19:51 U.T. on March 14 and 3:37 U.T. on March 15, 1992. The CLAES measurement was taken at (69.5N, 32.7E) at 2.65 U.T. on March 15, 1992. The MIPAS-B and CLAES error bars overlap in the region of the CLAES mixing ratio peak. This is the only correlative profile measurement in an area of high (near 3 ppbv) $ClONO_2$ as seen in high latitude winters outside the region of PSC processing The agreement is good above 100 mb.

Figure 8.2.2.1-2 shows a CLAES comparison with Denver University data provided by D. Murcray, F. Murcray, and A. Goldman. The DU data was taken over Texas near 1:00 U. T. on July 24, 1992 at (31.6 N, -101E). The nearest time/space CLAES measurement was (29.4N, -104.5E) at 3:15 U. T. on July 24, 1992 when the SZA was -102 degrees. While the peak mixing ratios are similar, the DU data shows a peak at approximately 13

mb while the CLAES peak is located at about 20 mb. The DU uncertainty estimate is 25% in mixing ratio at the peak. While one could argue that the DU and CLAES error bars overlap except perhaps at 30 mb, the comparison suggests a disagreement in altitude registration between the two instruments, although comparison of HNO_3 (another gas whose mixing ration is peaked sharply in the stratosphere) from the same times show excellent altitude agreement. Some altitude differences are observed for the $ClONO_2$ profile peak between adjacent CLAES measurements separated by about 400 km. Since the DU measurement is a little more than 200km from the nearest CLAES measurement on this day, a portion of the discrepancy could be geographical and temporal variability. Note that the CLAES profile shown here displays large error bars and the local maximum at pressures below 6 mb resulting from the use of UARS climatology as described above. Figure 8.2.2.1-3 shows a comparison of the Toon MarkIV data with a CLAES near-coincident over northern New Mexico on September 15, 1992. The only reasonable comparison was with the sunset data since the CLAES was south-looking during this period, and the only New Mexico over-flight was a few hours after sunset. In this comparison, the MarkIV data in the region of the CLAES mixing ratio peak agree well. This is the altitude regime where the error bars on both measurements are the smallest.

8.2.2.2 Comparison with Previous Measurements and Climatology

Figure 8.2.2.2-1 shows a comparison of a Denver University June 6,1988 sunset measurement from a Palestine, Texas launch and the same CLAES profile compared with DU data above. This comparison shows excellent profile agreement through the region where the error bars indicate a high degree of confidence in the CLAES data. The altitude of the peak in the $ClONO_2$ mixing ratio in the DU data agrees well with many adjacent post-sunset CLAES measurements on July 24, 1992.

Figure 8.2.2.2-2 shows the midday to midnight variations in the $ClONO_2$ profiles on February 18, 1992 at 30N. Nine locations were picked for this study which were observed by CLAES on descending and ascending portions of the UARS orbit on the same day. The local time difference helps emphasize the diurnal component in $ClONO_2$. This comparison shows in a qualitative fashion the nighttime increase expected in $ClONO_2$. in the 10 to 68 mb region. Figure 8.2.2.2-3 shows a comparison of sunrise and sunset $ClONO_2$ measurements taken by the Mark IV instrument at 12.67 U.T. on September 15, 1992 near 35.2N, -104.5E. Although CLAES did not gather near-sunrise data at this latitude on this day, the set of Mark IV sunrise and sunset measurements is interesting as it shows diurnal behavior of profile shapes similar to that shown by the ATMOS (Zander et al., 1986) in 1985. A comparison of the profile shapes in Figure 8.2.2.2-2 and Figure 8.2.2.2-3 suggests that CLAES $ClONO_2$ may be low in the 10-20 mb pressure regime where the Mark IV shows a maximum and CLAES does not. This effect could be the manifestation of the high climatological $ClONO_2$ at high altitudes discussed above. It could also be connected with he pattern noise seen in ozone profiles also retrieved in this spectral region.

Figure 8.2.2.2-4 shows a comparison of the CLAES zonal mean data with the LLNL 2-D model results for nights in the January and August periods. Inspection of this figure shows that the zonal mean structure of CLAES chlorine nitrate resembles the LLNL model results both in geographical and temporal variation. The biggest discrepancy is that the model tends to put the peak of the $ClONO_2$ at higher altitudes.

Another consistency check is a comparison of the CLAES mixing ratio profile with past

past measurements presented in Massie (1987). The historical data entirely from the mid-latitudes and sub-tropics indicates that the CLAES peak $ClONO_2$ around 1 ppbv is consistent with these measurements. The CLAES $ClONO_2$ mixing ratio peak is found at lower altitude than most other measurements.

Another comparison has been carried out against the JPL Mark IV column measurements taken in the Arctic in 1989 (G. Toon et al., 1992). This work showed column amounts of $2.2 \pm 0.1 \times 10^{15}$ molecules·cm^{-2} for a DC-8 flight leg at 66N on January 9. Comparing column amounts from a portion of a CLAES orbit shown in Figure 8.2.2.2-5 with the Toon numbers yields good agreement, although the variability of $ClONO_2$ makes this comparison little more than a rough check.

8.3 Hydrochloric Acid (HCl) and Hydrofluoric Acid (HF)

8.3.1 HALOE Data Processing and Error Estimates

The general description of the HALOE data processing version 12 algorithm is found in Chapter 2 of this report. Since the last UARS Validation Workshop, many algorithm improvements have made the HALOE data quality substantially better. Some of these improvements include: retrievals which extend to lower altitudes; sun spot detection; and the inclusion of other interfering spectra in the HCl channel. The quality of the HALOE data will further improve as new CH_4 spectral parameters, namely the air and self broadened half-widths in the 3.4 micron region, become available. The HALOE error bars plotted on comparison plots are precision. A more formal and rigorous error analysis to determine sytematic errors will be completed and documented at a later date.

8.3.1.1 Comparisons of HCl and HF with Other Reported Profiles

HALOE HF and HCl profiles are compared with measurements from balloon instruments and the Space Shuttle. These correlative measurements use spectrally resolved information to determine mixing ratio profiles and are compared to the HALOE profiles which have the best coincidences in time and space. Comparisons of HALOE pressure versus latitude cross-sections with those predicted from theoretical models are useful for qualitative comparisons. Measurements made prior to the launch of UARS are shown to examine not only the time variations of these species, but also to show the validity of all the measurements.

8.3.2 HCl and HF Comparison Results

8.3.2.1 Comparison with Pre-UARS Measurements

Figures 8.3.2.1-1 and 8.3.2.1-2 show HALOE zonal mean HF and HCl profiles compared with the zonal mean profiles measured from the ATMOS instrument in 1985. This comparison is worthwhile to examine the long term trend of these species and also to show the validity of all the comparisons. The amount of HF increase measured by HALOE since the 1985 ATMOS measurement is consistent with several model predictions and is also consistent with other measurements. The HCl increase is not consistent with some predictions over this same time period.

8.3.2.2 Comparison with Correlative Data

Since the launch of UARS, several correlative measurements have been made from

balloon platforms as part of the UARS Correlative Measurements Program. Other measurements include the Grille Spectrometer and the Atmospheric Trace Molecule Spectroscopy (ATMOS) Fourier transform spectrometer. Both instruments have collected data from the Space Shuttle and are occultation experiments. For this report, we only show comparisons with data that are available through the UARS Central Data Handling Facility (CDHF) database.

The HALOE profiles to compare with the balloon profiles are selected giving latitude coincidence the highest weighting, longitude coincidence the next highest, and finally time coincidence. Since HF and HCl are not diurnally variable, the local time of the measurement is not important. However, it is important that the measurements occur during the same season. If the difference in time between the two measurements is greater than a few weeks only a qualitative examination can be made. In the mid-latitude summer hemisphere, the distributions of these trace gases are usually near-zonal so that longitude coincidence i s less important.

The correlative HF profiles include: measurements from three balloon flights of the FIRS-2 experiment (Traub), the May 4, 1992 flight of the FIREX instrument (Nolt), and the sunrise occultation measurement from the JPL Mark IV Interferometer (Toon). Figure 8.3.2.2-1 shows the FIREX HF measurement from Ft. Sumner and the HALOE HF profile from the nearest HF event. The agreement is excellent below 10 mb and remains within the error bars for the entire profile.

Figure 8.3.2.2-2 compares a balloon profile by Traub on May 29, 1992 to a HALOE profile. The coincidence in time and longitude are excellent, but the difference in latitude (3 degrees) is probably enough to cause the noted disagreement between the two profiles. In this latitude region (35 degrees), there is a strong latitudinal gradient that is noted in all the tracer species measured by HALOE. Figure 8.3.2.2-3 shows a HALOE profile compared with another Traub measurement from Ft. Sumner in September 1992. This figure shows excellent agreement between the two profiles below 30 mb, but it is not understood why the profiles disagree above this pressure level. Figure 8.3.2.2-4 shows the March 1993 balloon measurement from Traub. Excellent agreement is noted below 8 mb even though the difference in time between these two measurements is almost two weeks. The profile obtained from the JPL Mark IV Interferometer is plotted in Figure 8.3.2.2-5 with the nearest HALOE profile. The time coincidence is on the order of two weeks, but the agreement between 10 and 2 mb is very good. Below this pressure range the two profiles differ by up to 0.25 ppbv, and above it, the interferometer retrieval becomes noisy.

Correlative HCl measurements include the same instruments and investigators who collected the HF data presented above. Additional profiles were obtained from the BLISS instrument (Webster), the Sub-millimeter wave Limb Sounder (SLS) from JPL (Stachnik), and the grating occultation instrument (Zander). Figure 8.3.2.2-6 shows the FIREX HCl profile and the HALOE HCl profile near the same location. The two profiles agree within the error bars on the FIREX measurement, however there is a hint that the HALOE profile may be slightly lower. Figures 8.3.2.2-7 through 8.3.2.2-9 show the three profiles obtained by Traub compared to the nearest HALOE profiles. The HALOE measurements are lower than the profiles obtained by Traub for all three measurements between 30 and 8 mb, but by only 15%. Also the profile shapes agree very well. The HCl measurement obtained by the JPL Mark IV Interferometer (Toon) is plotted with the nearest HALOE event in Figure 8.3.2.2-10. Considering the time difference between the two profiles, they agree reasonably well. The SLS measurement by Stachnik is plotted

with the nearest HALOE event in Figure 8.3.2.2-11. The profiles agree to within the error bars on both measurements, and again the slopes agree well. The Ft. Sumner balloon flight profile from Zander is plotted with the nearest HALOE HCl profile and is shown in Figure 8.3.2.2-12. This profile is within error bars when compared to the FIREX profile, however, above 10 mb it differs from the HALOE measurement by as much as 0.5 ppbv, again the HALOE profile being lower. The BLISS measurement (Webster) is shown with a coincident HALOE measurement in Figure 8.3.2.2-13. This plot shows differences by as much as 0.4 ppbv near 15 mb. The difference in time between these measurements is about three weeks, so it is possible that the disagreement could be caused by temporal variations.

Figures 8.3.2.2-14 and -15 show the mean difference and rms difference profiles in percentages between the HALOE measurements and the correlative measurements for HF and HCl, respectively. For HCl, the mean difference ranges between 5 and 15 % between 30 mb and 3 mb with the HALOE measurements being lower. The reason for this discrepancy is under investigation by the HALOE team. The shapes of the mean profiles agree well. Above and below this pressure range, the statistics are calculated on a smaller sample set since not every profile extended into these regions. The HF mean difference plot shows an alternating sign over the pressure range. Also, the statistics show a mean difference between 15 and 20 mb that is over 15% with HALOE being lower. There are two comparison plots which are causing this feature; the comparison with the JPL instrument and the September 1992 flight of the FIRS-2 instrument. Since such a limited number of profiles exist at less than perfect coincidences, the statistics are probably of limited value.

Figure 8.3.2.2-16 shows the mean HF/HCl value obtained from the HALOE data and the mean HF/HCl profile obtained from the balloon instruments which make simultaneous observations of HF and HCl. T he differences can be attributed to the usually lower HCl values measured by the HALOE instrument.

8.3.2.3 HALOE Sunset /Sunrise Latitude Coincident Comparisons

Approximately ten times per year, the HALOE sunrise and sunset events occur over the same latitude. Since HF and HCl are not diurnally variable, comparisons of the sunrise and sunset profiles can be used as a validation tool to determine if any biases may be occurring. Figure 8.3.2.3-1 shows the HF sunrise and sunset mean profile and statistics. The mean profiles differ on the order of 5 %, but profile shapes are almost identical. Figure 8.3.2.3-2 shows the same plot for the HALOE HCl channel. This profile does indicate a larger offset between sunrise and sunset. This reason for this offset is being investigated by the HALOE Team.

8.3.2.4 Model Comparison Studies

HALOE pressure versus latitude cross-sections for HF and HCl are compared to results from the NCAR 2-D Model with data provided by Drs. Mingzhao Luo at the University of California-Irvine. Figures 8.3.2.4-1 and 8.3.2.4-2 show the HALOE HF and HCl pressure versus latitude cross-sections for the August 25-30, 1992 intercomparison period. Figures 8.3.2.4-3 and 8.3.2.4-4 show the results produced by the model. Qualitatively and quantitatively the model data are very similar to the HALOE data. The HF cross-sections are different in the zonal distribution of HF, but this may be attributed to the differences between the atmospheric dynamics and that of the model. A similar

pattern is noted in the HALOE CH_4 pressure versus latitude cross-section for this same time period shown in Figure 8.3.2.4-5.

8.4 Sulfur Dioxide (SO_2)

8.4.1 SO_2 Correlative Data

8.4.1.1 TOMS Data

TOMS measured the SO_2 column and the cloud disbursement following the June 1991 Pinatubo Eruption for about two weeks until the SO_2 concentrations fell below its detection limit. The TOMS scientists inferred that 20 metric Mtonnes (MMT) of SO_2 had been injected into the stratosphere and decayed with a 35 day e-folding time constant (Bluth et al. 1992). TOMS also detected SO_2 from the April 1993 Lascar eruption [Lebow et al., private communication, 1993].

8.4.1.2 NOAA-11 SBUV/2 Data

The SBUV/2 instrument on the NOAA-11 satellite also detected SO_2 after the eruption of Mt. Pinatubo. On June 19, July 1, July 17, 1991, sufficiently strong SO_2 absorption features were observed near the equator to provide an estimate of the SO_2 budget. On the latter two days, SBUV/2 retrievals indicate there was 8.4 and 4.1 MMT of SO_2, respectively (McPeters, 1992).

8.4.1.1 Aircraft COSPEC Data

Aircraft flights over the Caribbean Sea made column SO_2 measurements using an infrared spectrometer (COSPEC) on July 12, 1991. When combined with SAGE II aerosol data, a total SO_2 burden of 6.2 MMT was inferred (Mankin et al. 1992).

8.4.2 SO_2 Comparison Results

UARS was launched 92 days after the Mt. Pinatubo eruption, and MLS began measurements 8 days later. The MLS, as a consequence of its vertical limb scanning capability, can determine the vertical structure of SO_2. At this time, however, there are no known profile measurements to allow a direct comparison. Comparisons thus rely on inferences of the initial loading and decay rates. Figure 8.4.2-1, from Read, et al. (1993), compares SO_2 budgets as determined from TOMS, SBUV/2, COSPEC and MLS. The MLS results have been corrected for biases by removing long term non-decaying SO_2 amounts as discussed in section 2.4.5. The MLS amounts are separated into layer contributions, which are summed together to obtain the column. The MLS column has been extrapolated backwards in time to infer a total initial loading. The time decay during the MLS measurements provides an e-folding time. We obtain 17 MMT initial loading and 33 day decay rate from MLS, which agrees very well with the TOMS values as indicated in the figure. TOMS measures 12 MMT and SBUV/2 estimates 8.4 MMT on 1 July 1992 compared to the MLS extrapolated value of 10.2 MMT, which is viewed as acceptable agreement. The aircraft measurement, although a highly-derived quantity appears consistent with these results. The individual layer concentrations at 46 and 22 hPa (which contain 90% of the SO_2) decay with e-folding times of 41 and 29 days respectively. The SO_2 decay occurs by catalytic destruction by OH. These layer decay rates have been used to infer an OH profile, and values are obtained which are approximately 50% higher than typical equinox models with only gas-phase chemistry, but the inferred OH vertical gradient appears to agree well with the models. See Read et al. (1993) for further discussion.

8.5 Ratios and Sums

8.5.1 Comparison Results for Chlorine Species

HALOE, CLAES, and MLS collectively measure the species that account for more than 90% of the chlorine released by chlorine-containing source gases through most of the stratosphere, given current understanding. Total abundance of inorganic Cl-containing species and their partitioning are both important quantities in determining stratospheric photochemistry. Beyond the direct validation of halogen species abundances by comparison to independent measurements, composites of the UARS-measured halogen-containing species can be compared to such constraints as the total available stratospheric Cl and F, and abundance ratios determined by fast, relatively simple photochemistry.

Global average surface values of the principal Cl and F source gas abundances, for mid-1992, sum to about 3.8 ppbv Cl and 2 ppbv F, although not all of either species is released within the stratosphere. Additionally, there is a lag in time between surface release of the source gas and halogen release in the stratosphere, so that current stratospheric air reflects the composition of older tropospheric air. This time lag varies from one to a few years depending on location and altitude.

While HCl and HF in the stratosphere should not vary diurnally, ClO and $ClONO_2$ are coupled in a diurnal cycle in which ClO is converted to $ClONO_2$ by reaction with NO_2 at and after sunset, and $ClONO_2$ releases Cl during the day when it is photolyzed. HALOE HCl and HF measurements are taken at sunrise and sunset. MLS ClO and CLAES $ClONO_2$ measurements may be taken at any local solar time, depending on the orientation of the satellite orbit. For sums and especially ratios of species abundances, it is useful to increase the precision of the ClO and $ClONO_2$ observations through zonal averaging of the individual profiles. Separating profiles from the ascending and descending portions of the orbit in zonal averaging, when forming ratios including ClO or $ClONO_2$, will allow more straightforward comparisons with expected behavior based on photochemical theory.

When the results of the May 1992 flight of the ATMOS and Grille instruments become available, they will provide an independent measurement of the Cl and F inventories in the stratosphere (cf Zander et al, 1992). There were no correlative measurements available for this report, made during the validation period, that would establish the sum of inorganic Cl species independent of the UARS instruments.

During the validation periods selected for this report, April 15-20, 1992 and August 25-30, 1992, HALOE sunrise and sunset events, respectively, sweep over the mid- and low-latitudes from roughly 30 S to 20 N. Figures 8.5-1 and 2 show the sum of the zonal averages over these ranges of latitude and time of HCl, $ClONO_2$, and ClO. The sums were constructed using the zonal average of the daytime ClO less the nighttime ClO below 10 hPa (effectively assuming complete nighttime conversion of ClO to $ClONO_2$ at those pressure levels) and the daytime zonal average $ClONO_2$. The value of the sum ranges from a few tenths of a part per billion near 100 mb, increasing with altitude to a maximum around 3.2 ppbv above 1 mb and fairly constant with latitude with a few spikes related to high HCl values. The maximum value of 3.2 ppbv is consistent with tropospheric values of the Cl sources. The broad smooth shape of the contours is also consistent with theoretical predictions.

The ratio of the MLS daytime zonal average ClO to HALOE HCl is shown in Figures 8.5-3 and 8.5-4 for the same validation time periods. The overall shape of the ratio is similar to expectations for daytime ClO, with a maximum of 10 to 14% between 10 and 3 mb. In both time periods because of orbital orientation, the ClO daytime profiles correspond to large solar zenith angles (near 90 degrees) at the low latitudes imaged, however the April profiles are near sunset and the August profiles near sunrise. The somewhat smaller values for the August time period reflect the substantially smaller ClO abundances expected near sunrise.

The ratios of $ClONO_2$ to HCl and ClO to $ClONO_2$ are also important indicators of photochemical behavior, controlling the partitioning of inorganic stratospheric Cl among active forms, temporary reservoirs and inactive forms. No close coincidence correlative data were available for this report for these species in combination. Nighttime $ClONO_2$ as a per cent of HCl is shown in Figure 8.5-5 for the August validation period. Figure 8.5-6 shows the mid-August diurnal average result from the LLNL 2-D model. The UARS data shows a maximum at about 40 mb with a $ClONO_2$ maximum close to the HCl abundance, while the model maximum is displaced upward to 20 mb with $ClONO_2$ and HCl again about equal. Figures 8.5-7 and 8.5-8 show ClO as a percentage of $ClONO_2$ for UARS daytime zonal averages and model diurnal and zonal average, respectively. The values of the distributions are similar between 10 and 60 mb, but the lack of overlap between the ClO peak and the ClONO2 peak makes this a difficult measurement.

For the sparse set of results on stratospheric inorganic chlorine inventory and partitioning that could be assembled for this report, there were no obvious large anomalies relative to our understanding of the photochemistry underlying inorganic Cl species abundances. Total inorganic Cl abundance and its distribution are consonant with the current levels of Cl-containing source species.

8.6 Summary

Chlorine Monoxide (MLS)

Intercomparisons between ClO from MLS and other measurements generally show agreement to within that expected for the estimated errors and different samplings of the techniques. The Version 3 ClO files are thought to be acceptable for use in scientific analyses, providing the following caveats are adequately accounted for:

1. Individual ClO retrievals generally have poor signal-to-noise (an exception is for enhanced lower stratospheric ClO in the polar winter vortices), and most scientific uses of these data will require averaging to reduce the noise. The rms noise value (for individual profiles) is a maximum value of approximately 1.5 ppbv at the extremes of the vertical range (100 and 0.46 hPa), and a minimum of approximately 0.3--0.5 ppbv between 46 and 4.6 hPa. In order to allow averaging of the retrieved `noisy' profiles, as opposed to requiring averaging of the radiance with separate retrievals needed for each average, no constraint has been applied to force the retrieved ClO values to be positive (since this would bias the average), and negative ClO values will appear in the data files. The MLS ClO noise distribution is demonstrated to be Gaussian, and Gaussian statistics can be used with confidence for estimating the effects of noise.

2. There is an expected `scaling uncertainty' (multiplicative term) of 10--15% at pressure surfaces between 46 and 2.2 hPa, which increases to 30--40% at 100, and 0.46 hPa.

3. There is an expected `bias uncertainty' (additive term) which varies from approximately 0.5 ppbv in the lower stratosphere under enhanced ClO conditions to approximately 0.1 ppbv in the upper stratosphere. Errors due to this uncertainty can be reduced by taking appropriate (day-night, for example) differences.

4. The 100 hPa ClO values have not been adequately validated for use in general scientific studies, and 100 hPa CLO values SHOULD NOT BE USED WITHOUT ENDORSEMENT BY THE MLS TEAM.

Additional ClO validation efforts should investigate the apparent discrepancy in upper stratospheric ClO measured over Antarctica in September 1992 by MLS and by ground-based techniques. Additional comparisons with aircraft measurements would be very helpful: (1) with mid and low latitude in situ lower stratospheric measurements to provide better validation of the MLS observed variations to a precision of better than 0.05 ppbv, and (2) with the planned future Antarctic campaigns to resolve discrepancies at 100 hPa. Planned improvements in future version of the MLS retrieval algorithms include the following:

- A full non-linear iterative retrieval scheme
- Using radiances obtained at tangent pressures greater than 100 hPa
- Better accounting for interference by HNO_3 and N_20, and possibly other gases
- Better accounting, in Level 1 software, for small (approximately 0.05 K) systematic spectral effects in the radiances.
- Investigating different vertical representation basis with (perhaps) better vertical resolution.

Chlorine Nitrate (CLAES)

The general seasonal and spatial variation are similar to climatology. The peak mixing ratio and column amount agrees well with limited correlative data.

The uncertainty indicated by the error bars is generally less than about 30% for the highest quality retrievals. The error bars on the CLAES retrieved mixing ratios are a good indicator of whether the particular data are truly retrieved or is closely related to the UARS climatology. If the error bars are large, as one frequently finds at pressures below 6 mb or so, the profile is dominated by climatology. At high pressures, approximately above 68 mb, the profile also may be influenced heavily by climatology, again this is indicated by large error bars which show an uncertainty of 100% or more.

The profile shape (V6) around 10 mb may be suppressed significantly by the use of UARS climatology at high altitudes. The profile shape may also be influenced by the calibration in the O_3 / $ClONO_2$ region, blocker 9, mentioned in Section 2.2.2.2 and also mentioned with respect to ozone retrieval, Chapter 5.

Future improvements will include an improved filter function, which may change the retrieved concentration by about 5%. The temperature dependent cross-sections for

$ClONO_2$ are being introduced to replace the current cross-sections representative of one temperature, 223K. A better upper boundary condition than provided by the current UARS climatology will be employed. An extensive improvement of use of calibration data is expected to eliminate the patterm noise problem in blocker 9.

Hydrogen Chloride and Hydrogen Fluoride (HALOE)

HF comparisons between HALOE and correlative data are very good between 15 mb and 4 mb considering the differences in time and space. The comparisons between HALOE sunrise and sunset coincident profiles show good agreement.

Comparisons of HALOE HCl measurements with correlative data show very similar profile shapes, however, the HALOE measurement is usually lower by values that can approach 15%. Some of these differences may be attributed to differences in the time and location of the measurements; but there is at least a part we believe to be caused by a systematic error in the HALOE HCl retrieval. The HALOE HCl retrievals appear to be very correlated with the UARS Beta angle. As the UARS Beta angle increases, the HALOE retrieved HCl VMR also increases. This error mechanism is probably a spectral effect and is also believed to cause the differences noted between the coincident sunrise and sunset HCl profiles. The HALOE Team is investigating this matter. Also, a multiple pass retrieval on the CH_4 channel is expected to increase the HALOE retrieved CH_4 about 5-10%. This will increase the retrieved HALOE HCl mixing ratio on the order of 3-5%.

The speedy analysis and validation of correlative measurements of HCl and CH_4 (where applicable) made by ATMOS, Grille, Zander, and Toon are highly recommended. Special attention should be given to the UARS CH_4 validation effort and assessment of accuracy.

The speedy analysis of CH_4 spectral line parameters in 3.4 micron region is very important to improve the accuracy of the HALOE CH_4 retrieval which will also improve the HALOE HCl retrieval.

Sulfur Dioxide (MLS)

At this time no direct profile comparisons have been made and are not known to be available. For MLS, SO_2 is a transient species which is detectable only during volcanic events. Currently there are no satellite measurements which can measure vertical profiles, making SO_2 a difficult species for correlative measurements. Direct profile measurements in the near future are unlikely. Inference of comparable quantities such as initial volcanic loading and e-folding decay times appear to be in good agreement with TOMS, SBUV/2, and aircraft results to the degree that these quantities are comparable. In terms of profile accuracy, the ClO discussion should apply generally. In summary, at 46 hPa and higher altitudes for the Version 3 files, the absolute error is expected to be the root sum square of 3ppbv, 15% of the retrieved value, and the uncertainties extimated by the retrieval algorithms (error quoted in the data files).

There may exist a possibility for a good time/space coincidence comparison between TOMS and MLS SO_2 for the Lascar eruption and initial MLS. results have been forwarded to the TOMS group for review. However, the coarse mapping capability of MLS and the fast decay of the weak (by TOMS detection standards) SO_2 concentrations caused by dynamical and chemical action may be limiting factors for obtaining a good

comparison. From the MLS measurements, the SO_2 vertical profile peak occurred at 46 hPa having 48 ppbv (column 2.6 Dobson units including 100 hPa and above) on 21 April 1993 5:05 GMT at 24.6°S and 68.6°W. The relatively poor MLS spatial mapping resolution precludes any determination of decay rates or initial loading.

REFERENCES

Barrett, J. W., P. M. Solomon, R. L. deZafra, M. Jaramillo, L. Emmons, and A. Parrish, Formation of the Antarctic ozone hole by the ClO dimer mechanism, *Nature*, 336, 455-458, 1988.

Bluth, G. J. S., S. D. Doiron, C. C. Schnetzler, A. J. Krueger, and L. S. Walter, Global tracking of the SO_2 clouds from the June 1991 Mount Pinatubo Eruptions, *Geophys. Res. Lett.*, 19, 151-154, 1992.

Douglass, A., R. Rood, J. Waters, L. Froidevaux, W. Read, L. Elson, M. Geller, Y. Chi, M. Cerniglia, S. Steenrod, A 3D simulation of the early winter distribution of reactive chlorine in the north polar vortex, *Geophys. Res. Lett.*, 20, 1271-1274, 1993.

Fahey, D. H., S. R. Kawa, E. L. Woodbridge, P. Tin, J. C. Wilson, H. H. Jonsson, J. E. Dye, D. Baumgardner, S. Borrmann, D. W. Toohey, L. M. Avallone, M. H. Proffitt, J. Margitan, M. Loewenstein, J. R. Podolske, R. J. Salawitch, S. C. Wofsy, M. K. W. Ko, D. E. Anderson, M. R. Schoeberl, and K. R. Chan, In situ measurements constraining the role of sulphate aerosols in mid-latitude ozone depletions, *Nature*, 363, 509-514, 1993.

Ko, M. K. W. and N. D. Sze, Diurnal variation of ClO: Implications for the stratospheric chemistries of ClONO2, HOCl, and HCl, *J. Geophys. Res.*, 89, 11619-11632, 1984.

Mankin, W. G., M. T. Coffey, and A. Goldman, Airborne observations of SO_2, HCl and O_3 in the stratospheric plume of the Pinatubo Volcano in July 1991, *Geophys. Res. Lett.*, 19, 179-182, 1992.

Massie, S. T., et al., *J. Geophys. Res.*, 92, 14 806, 1987.

McPeters, R. D., Global measurements of SO_2 from Pinatubo, presented at Dec. 1992 AGU meeting, .

Oelhaf, H., et al., Proc. of OSA Topical Meeting on Remote Sensing, Salt Lake City, Utah, Paper TuB5, Pg. 101, March 10-14, 1993.

Read, W. G., L. Froidevaux, and J. W. Waters, Microwave Limb Sounder (MLS) measurements of SO from Mt. Pinatubo volcano, *Geophys. Res. Lett.*, 20, 1299-1302, 1993.

Schoeberl, M., R. Stolarski, A. Douglass, P. Newman, L. Lait, J. Waters, L. Froidevaux, and W. Read, MLS ClO Observations and arctic polar vortex temperatures, submitted to *Geophys. Res. Lett.*, 1993.

Solomon, P. M., R. deZafra, A. Parrish, and J. W. Barrett, Diurnal variation of chlorine monoxide: a critical test of chlorine chemistry in the ozone layer, *Science,* 224, 1210-1214, 1984.

Toon, G. C., et al., *J. Geophys. Res.*, 97, 7939, 1992.

Waters, J. W., L. Froidevaux, G. L. Manney, W. G. Read, and L. S. Elson, Lower stratospheric ClO and O_3 in the 1992 southern hemisphere winter, *Geophys. Res. Lett.*, 20, 1219-1222, 1993.

Waters, J. W., L. Froidevaux, W. G. Read, G. L. Manney, L. S. Elson, D. A. Flower, R. F. Jarnot, and R. S. Harwood, Stratospheric ClO and ozone from the Microwave Limb Sounder on the Upper Atmosphere Research Satellite, *Nature*, 362, 597-602, 1993.

Waters, J. W., R. A. Stachnik, J. C. Hardy, and R. F. Jarnot, ClO and O_3 stratospheric profiles: balloon microwave measurements, *Geophys. Res. Lett.*, 15, 780-783, 1988.

Zander, R., et al., *J. Atmos. Chem.*, 171-186, 1992.

Zander, R., . et al., *Geophys. Res. Lett.*, 13, 757, 1986.

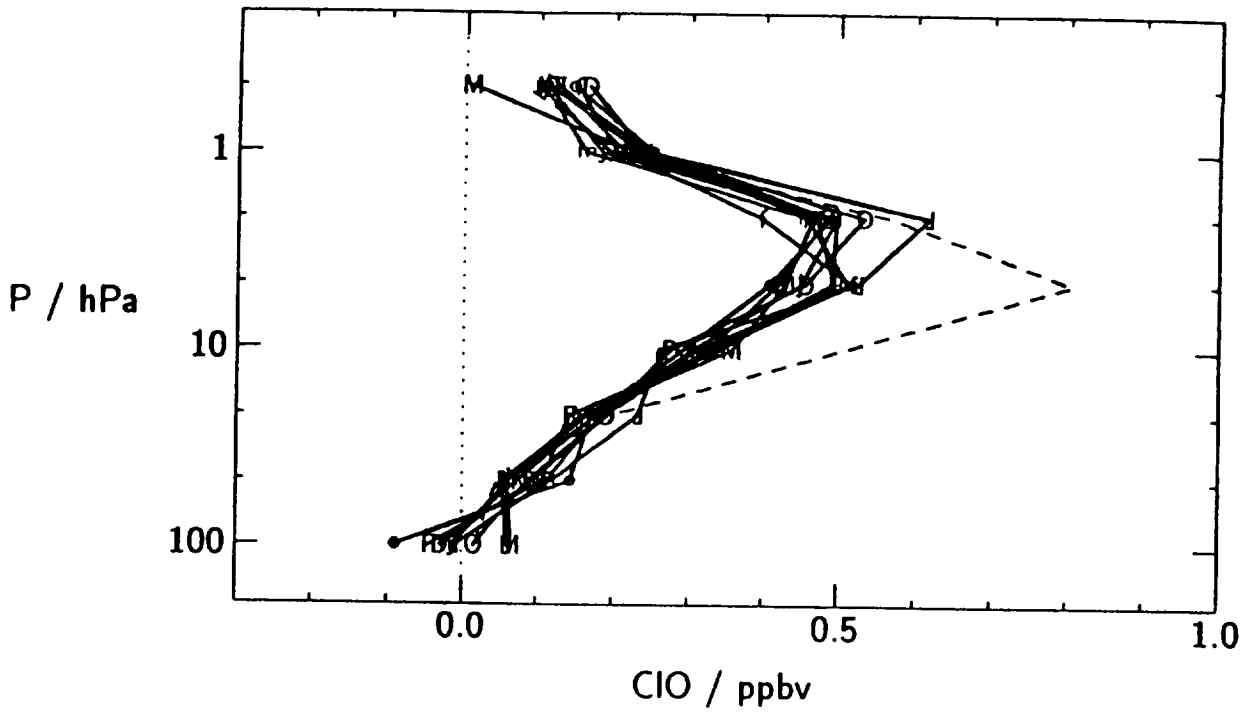

o:	27 Sep 1991 – 3 Nov 1992	UARS days 16–53, month 91.08
d:	5 Dec 1991 – 14 Jan 1992	UARS days 85–125, month 91.10
f:	15 Feb 1992 – 23 Mar 1992	UARS days 157–194, month 92.02
m:	2 May 1992 – 1 Jun 1992	UARS days 234–264, month 92.04
j:	18 Jul 1992 – 13 Aug 1992	UARS days 311–337, month 92.06
O:	22 Sep 1992 – 29 Oct 1992	UARS days 377–414, month 92.08
D:	30 Nov 1992 – 9 Jan 1993	UARS days 446–486, month 92.10
F:	10 Feb 1993 – 19 Mar 1993	UARS days 518-555, month 93.02
M:	27 Apr 1993 – 28 May 1993	UARS days 594-625, month 93.04
J:	9 Jul 1993 – 8 Aug 1993	UARS days 626–666, month 93.06

dashed: a priori profile

Figure 8.1.2.1.1-1. Monthly 20-40° N monthly zonal averages of ClO profiles from MLS. Only data taken at solar zenith angles less than 80° and with local solar times between 9 am and 3 pm were included in the average. ClO values from the 'night' side of the orbit (solar zenith angles greater than 95°) have been subtracted from the MLS data at 10 hPa and greater pressures to remove biases of approximately 0.2 ppbv or less at lower altitudes. Only data having ClO quality indicator of 4 (good radiances and fits) and MMAF_STAT=G (good) have been included in the zonal means.

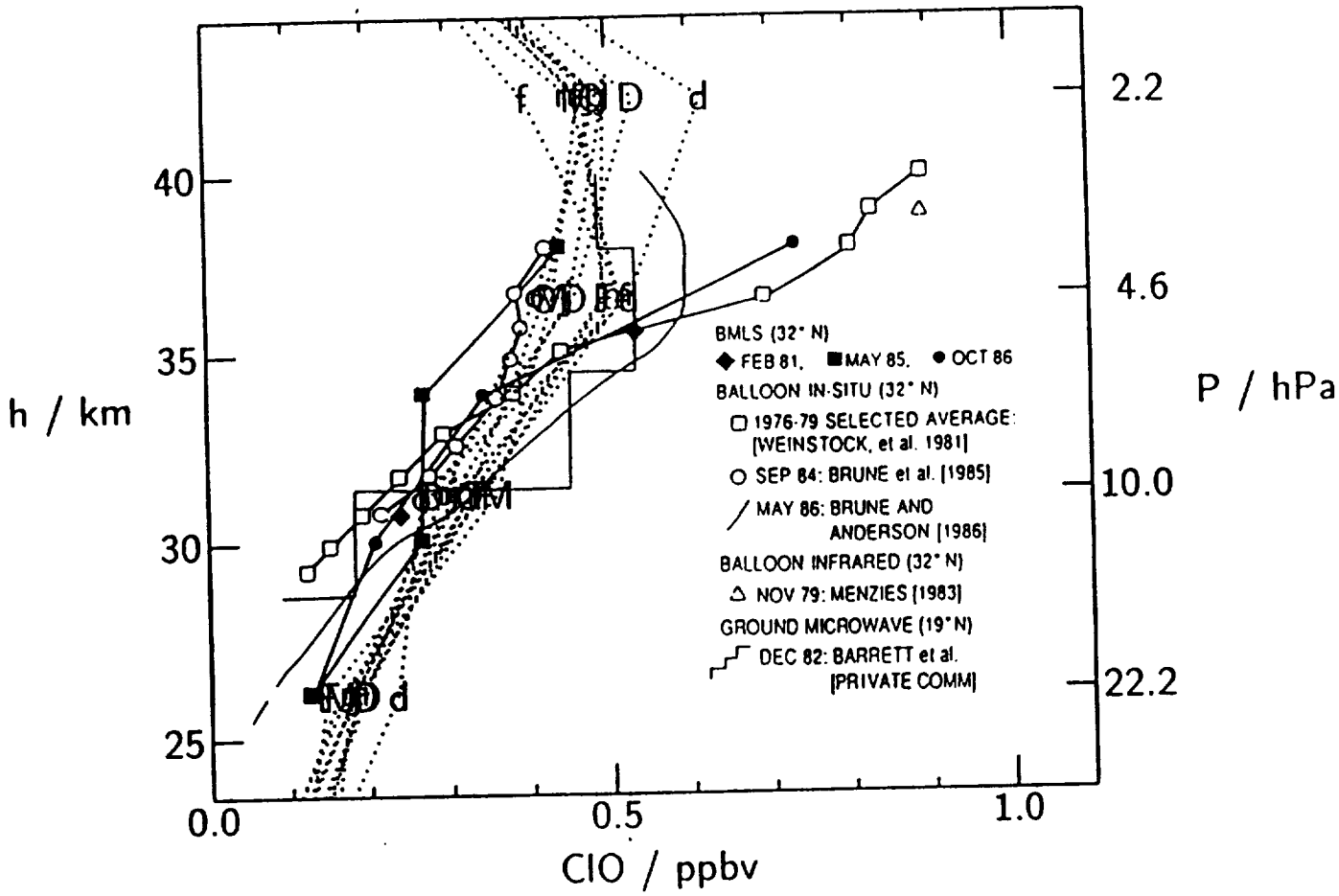

Figure 8.1.2.1.1-2. Comparison of MLS 20-40° N zonal mean ClO profiles with pre-UARS profiles measured at these latitudes as summarized in Figure 3 of Waters et al [1988]. The MLS profiles are dotted, and are the same as those given (over a larger vertical range) in Figure 8.1.2.1.1-1 (with the symbols indicating the same months).

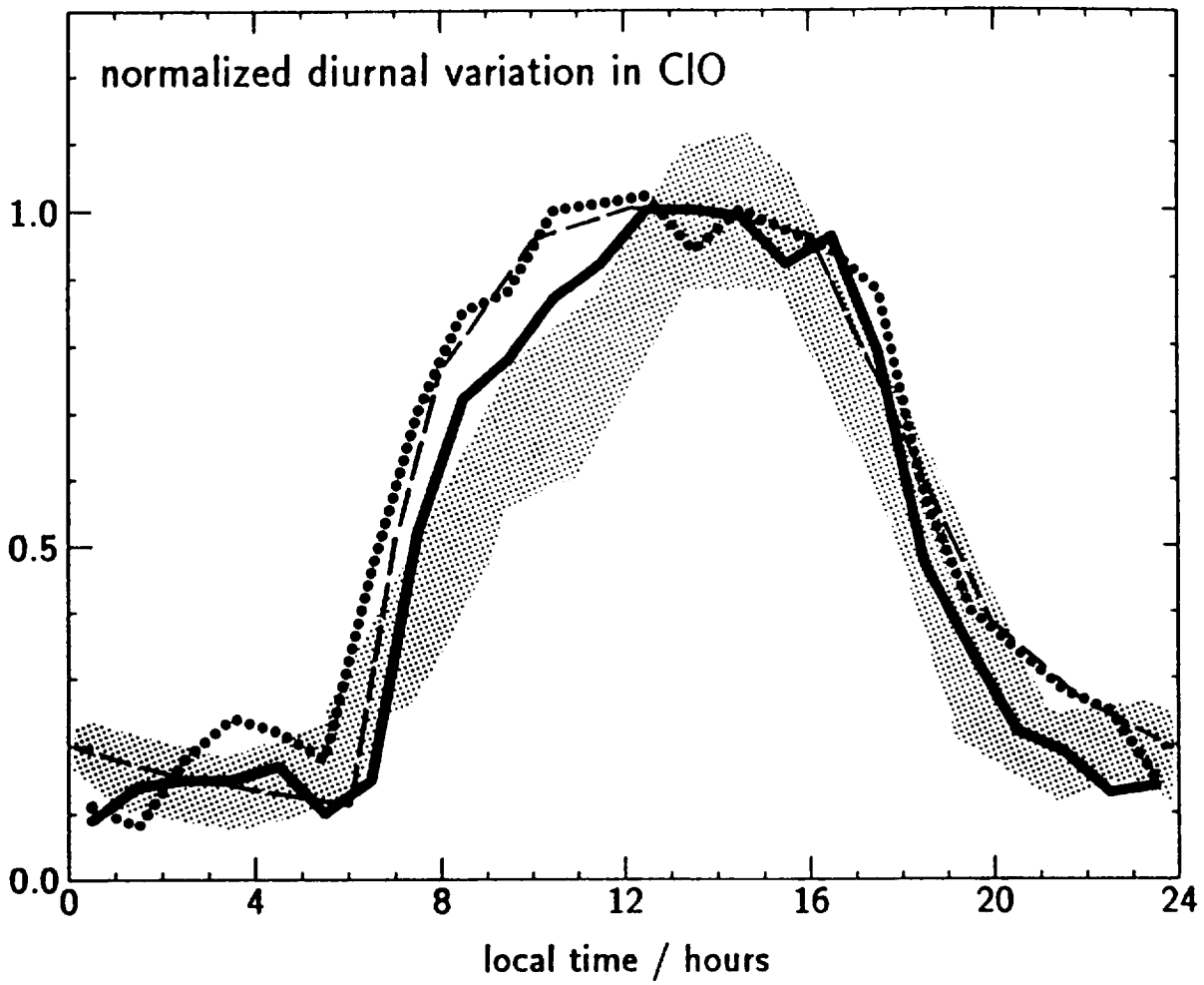

stippled	Ground-based 19° N measurements: Oct and Dec 1982 averages
solid	MLS 10–30° N monthly zonal mean for December 1991
dotted	MLS 10–30° N monthly zonal mean for October 1992
dashed	Model of Ko and Sze [1984]

Figure 8.1.2.1.1-3. Diurnal variation in upper stratospheric ClO. The measurements (MLS and P. Solomon, et al. [1984], ground-based) are for the column above 30 km, and have been normalized in the same manner. The inferred mid-day column above 30 km is 1.0-1.2x10^{18} molecules/m^2 for these MLS measurements, and 0.7-0.8x10^{18} molecules/m^2 from Solomon, et al. (1984). The approximately 50% increase in the inferred mid-day column between 1982 and 1992 is consistent with the approximately 5% per year expected increase in stratospheric chlorine. The MLS measurements have been binned in one-hour intervals. The horizontal axis gives the local solar time of the measurements . Between 100 and 500 individually-retrieved profiles were averaged for each local time bin. The ground-based measurements were binned in two-hour intervals, and the horizontal axis gives local time.

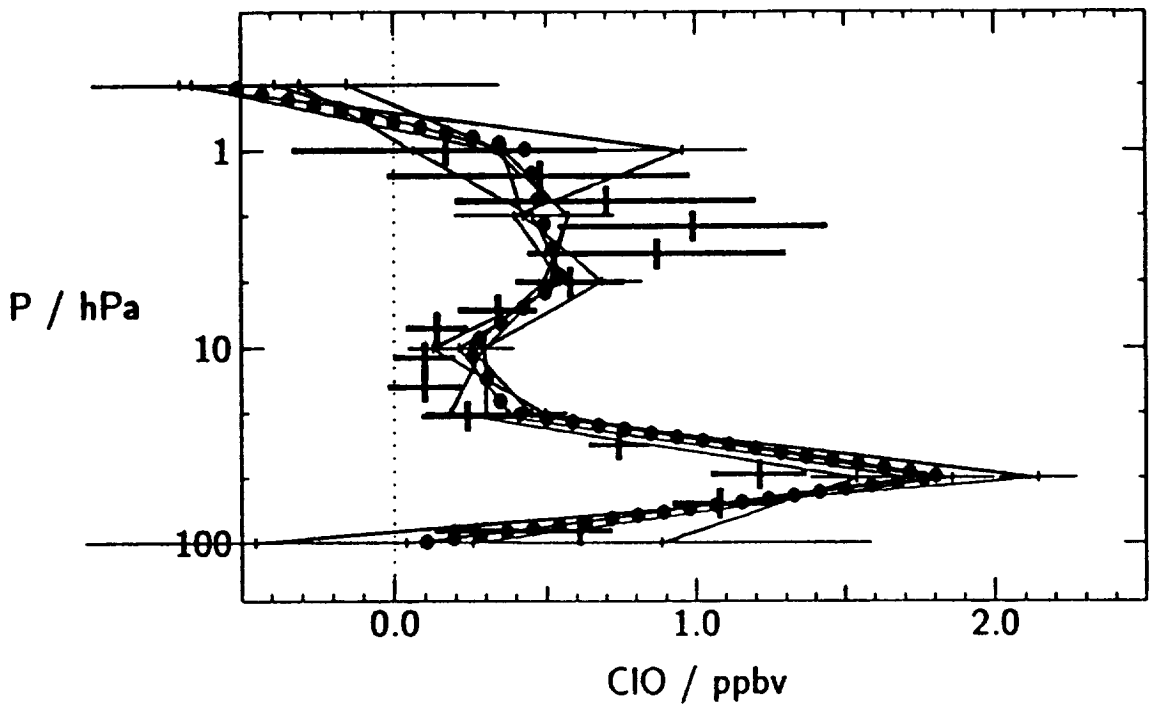

Figure 8.1.2.1.2-1. Comparison of ground-based ClO measurements made from Antarctica in September 1987 with zonal means from MLS in September 1992. The ground-based measurements are taken from Figure 1 of Barrett, et al., (1987) and are day-night differences of data taken over five days. A standard polar winter temperature-pressure profile has been used to convert the reported number densities as a function of altitude to mixing ratio as a function of pressure. The MLS zonal means are averages of measurements made at local solar times between 9 am and 3 pm all with local solar zenith angle >90°. ClO values from the 'night' side of the orbit (local times between midnight and 6 am) have been subtracted from the MLS data at 10 hPa and greater pressures to remove biases at lower altitudes. Each daily zonal mean is the average of 20-30 individually-retrieved profiles, and the average for all five days contains 130 individual profiles. Only data having ClO quality indicator of 4 (acceptable radiances and fits) and MMAF_STAT=G (good) have been included in the zonal means. The horizontal extent of the bars give the estimated +/-1 sigma uncertainty of the measurements.

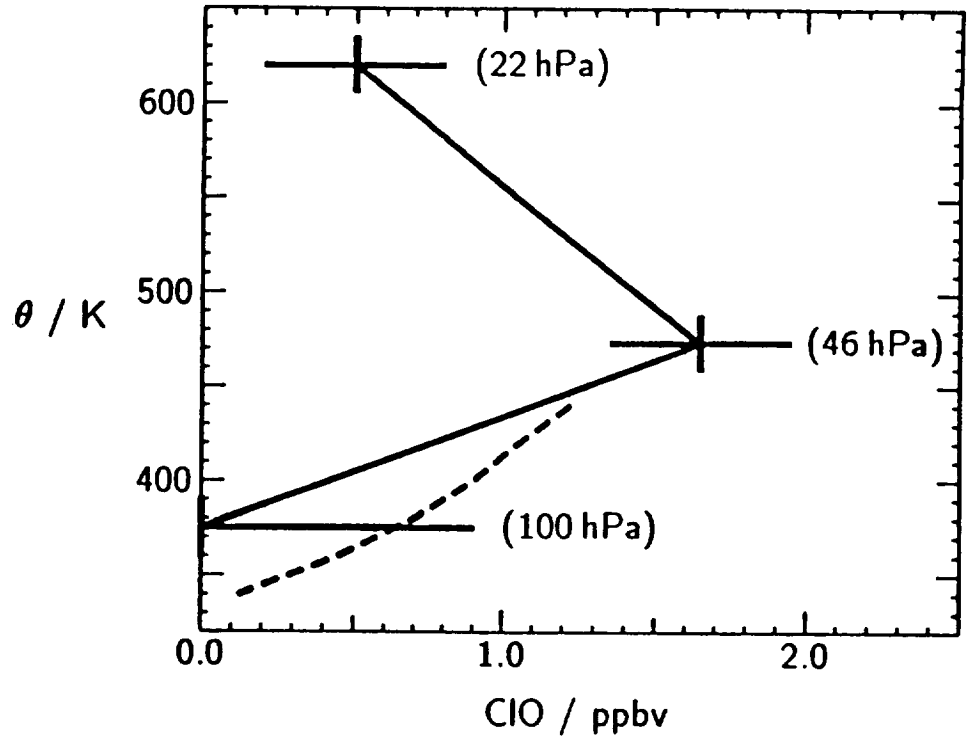

Figure 8.1.2.1.2-2. Comparisons of MLS September 1992 Antarctic ClO profiles (solid) with measurements made by the ER-2 aircraft in 1987 (dashed). The vertical coordinate is potential temperature. The ER-2 values are with latest calibration and were obtained from several flights covering the period 23 August to 22 September 1987, when essentially no variation was observed in ClO at a given potential temperature [D. Toohey, private communication]. The MLS values are 70-74° S zonal averages over the period 17 August to 20 September 1992.

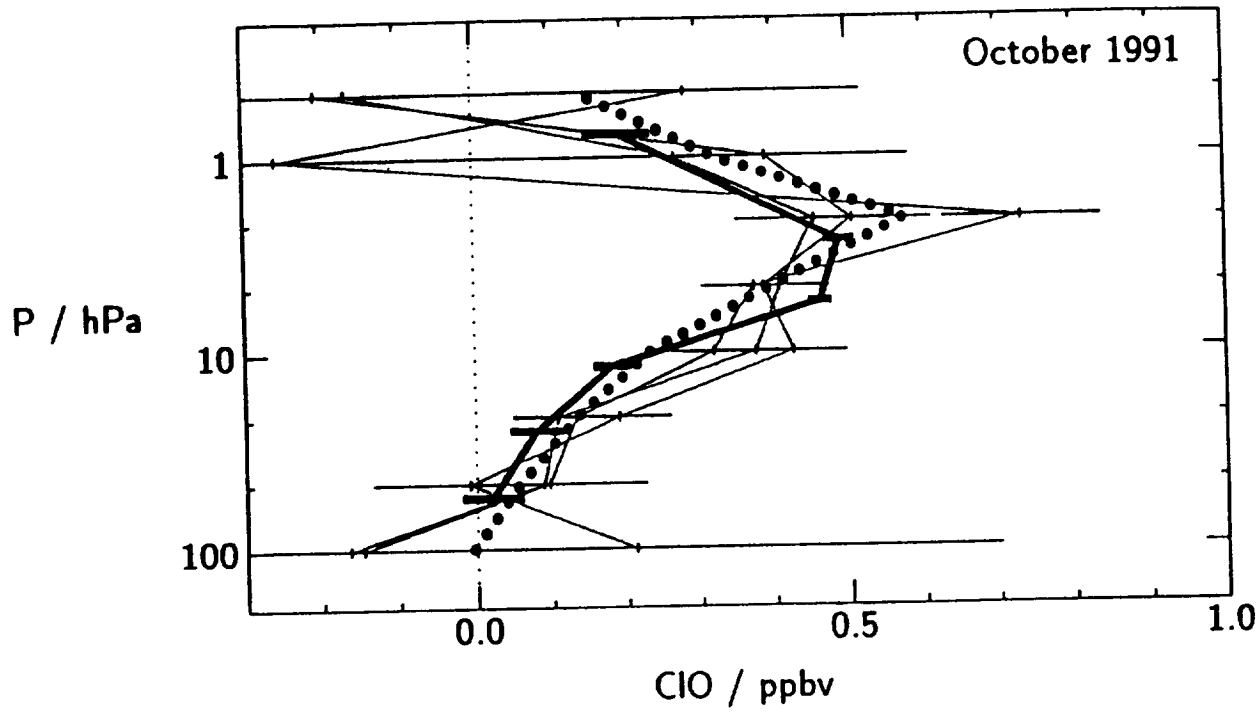

Figure 8.1.2.2-1. Comparison of Submillimeter Limb Sounder (SLS) ClO measurements on October 1, 1991 [R.A. Stachnik, private communication] with zonal mean ClO from MLS. The SLS measurements were made at local solar times between 11 am and 2 pm, and solar zenith angles between 40 and 45 degrees. The MLS daily zonal means are averages of approximately 40 individually-retrieved profiles having measurements made at local solar times between 9:30 and 10:30 am, and solar zenith angles between approximately 40 and 50 degrees. The MLS monthly zonal mean is an average of approximately 1100 individually-retrieved profiles having measurements made between 9 am and 3 pm local solar time. ClO values from the 'night' side of the orbit have been subtracted from the MLS data at 10 hPa and greater pressures to remove small biases at lower altitudes. Only data having ClO quality indicator of 4 (good radiances and fits) and MMAF_STAT=G (good) have been used. The horizontal extents of the bars give the estimated +/- 1 sigma uncertainty of the SLS measurements and the MLS daily zonal means.

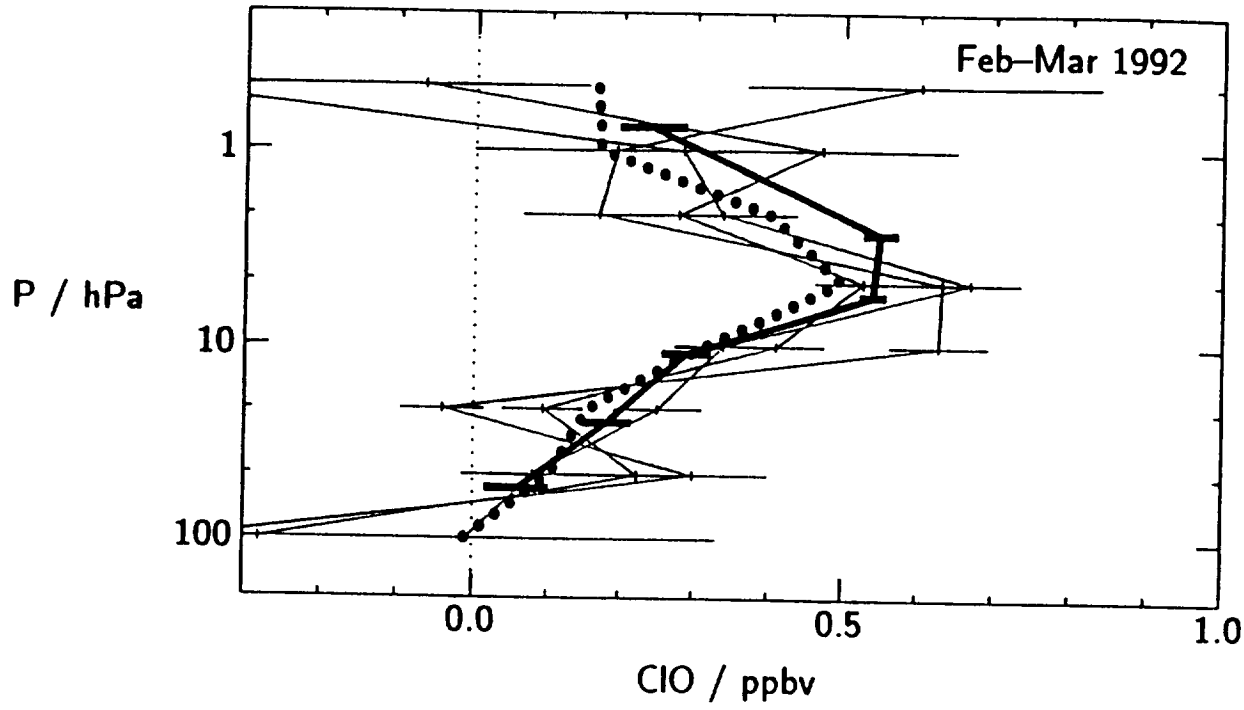

Figure 8.1.2.2-2. Comparison of Submillimeter Limb Sounder (SLS) ClO measurements on Feb. 20, 1992 [R.A. Stachnik, private communication] with ClO zonal means from MLS. The SLS measurements were made at local solar times between noon and 3 pm and solar zenith angles between 45 and 60 degrees. The MLS daily zonal means are averages of approximately 40 individually-retrieved profiles having measurements made at local solar times between 10 and 11 am, and solar zenith angles between approximately 45 and 55 degrees. The MLS monthly zonal mean is an average of approximately 1300 individually-retrieved profiles having measurements made between 9 am and 3 pm local solar time. ClO values from the 'night' side of the orbit (local times between 11 pm and midnight) have been subtracted from the MLS data at 10 hPa and greater pressures to remove small biases at lower altitudes. Only data having ClO quality indicator of 4 (good radiances and fits) and MMAF_STAT=G (good) have been included in the averages for the zonal means. The horizontal extent of the bars give the estimated +/- 1 sigma uncertainty of the SLS measurements and the MLS daily zonal means.

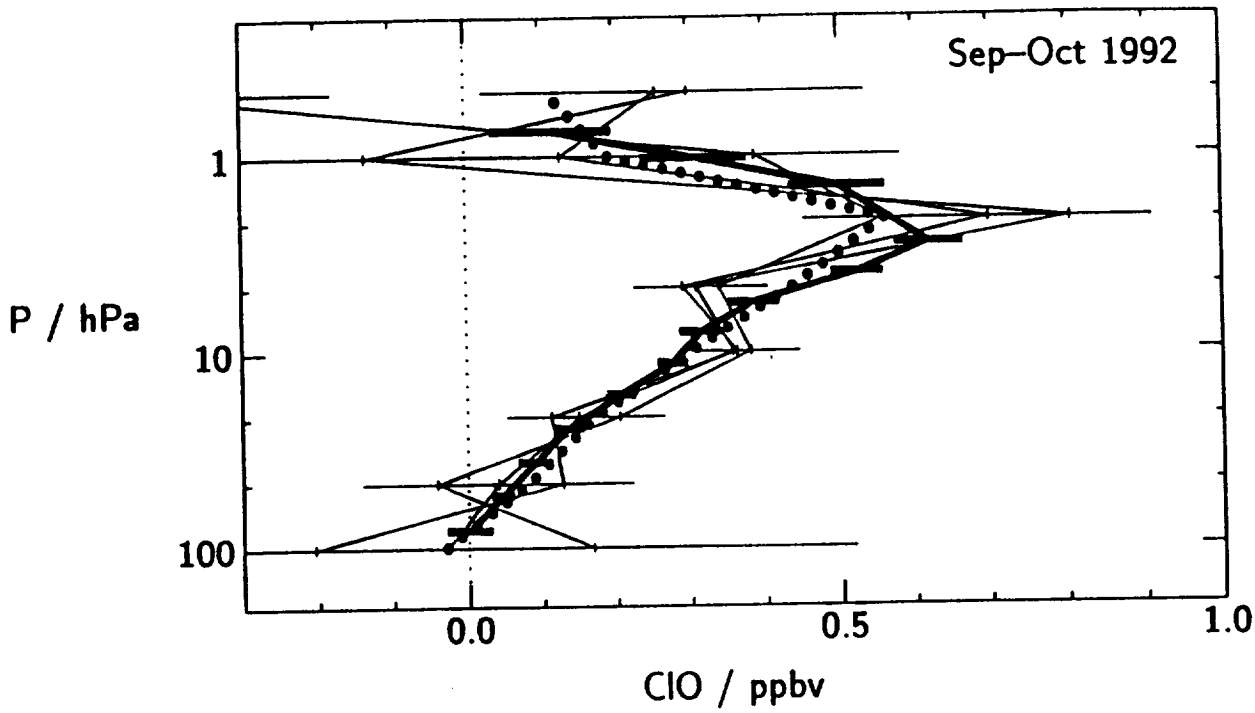

Figure 8.1.2.2-3. Comparison of Submillimeter Limb Sounder (SLS) ClO measurements on 29 September 1992 [R.A. Stachnik, private communication] with zonal mean ClO from MLS. The SLS measurements were made at local solar times between 1 and 3 pm, and solar zenith angles between 38 and 60 degrees. The MLS daily zonal means are averages of approximately 40 individually-retrieved profiles having measurements made at local solar times between 8 and 9 am, and solar zenith angles between approximately 55 and 65 degrees. The MLS monthly zonal mean is an average of approximately 1200 individually-retrieved profiles having measurements made between 9 am and 3 pm local solar time. ClO values from the 'night' side of the orbit (local times between 9:30 and 10:30 pm) have been subtracted from the MLS data at 10 hPa and greater pressures to remove small biases at lower altitudes. Only data having ClO quality indicator of 4 (good radiances and fits) and MMAF_STAT=G (good) have been included in the zonal means. The horizontal extent of the bars give the estimated +/- 1 sigma uncertainty of the SLS measurements and the MLS daily zonal means.

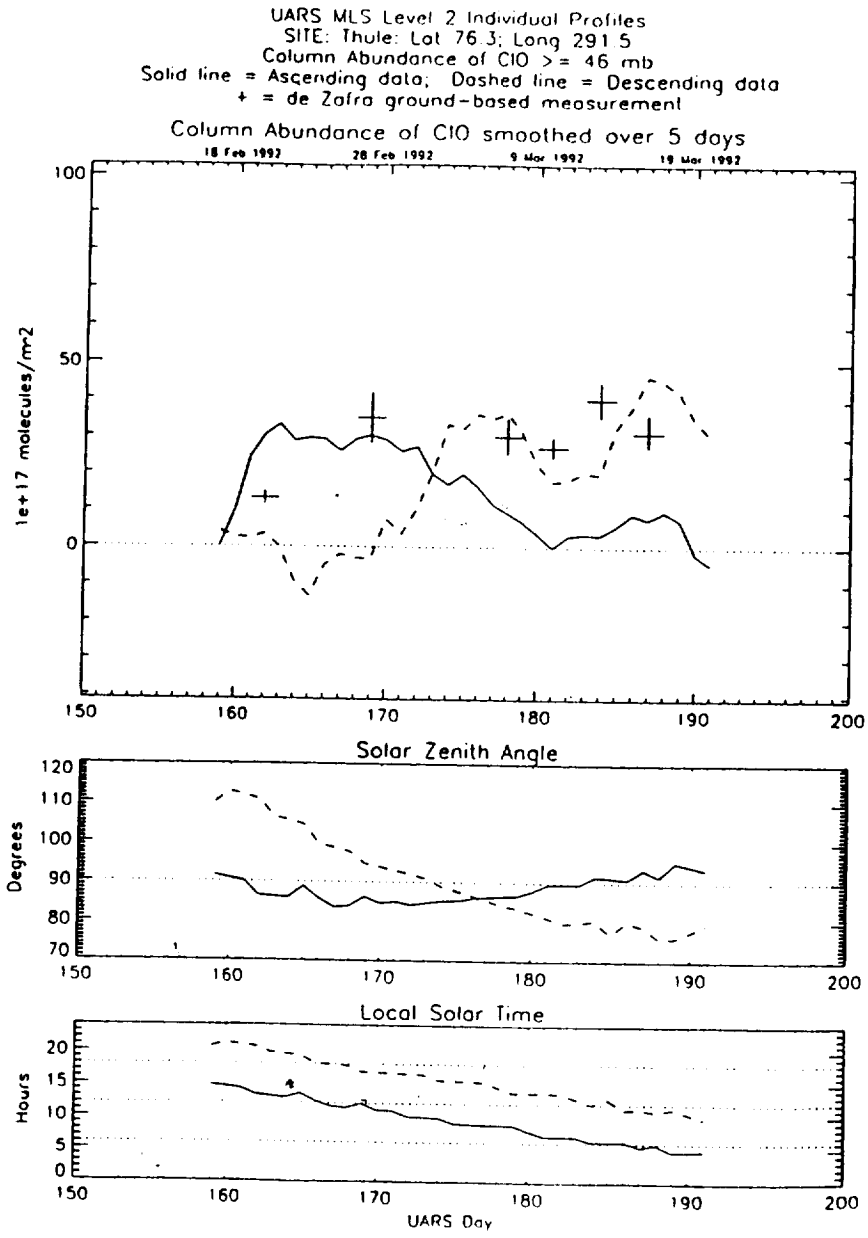

Figure 8.1.2.3-1. Comparisons of column ClO measurements over Thule, Greenland, in February and March 1992. The crosses are ground-based measurements [R. deZafra, private communication], and the lines are MLS. The ground-based measurements have been averaged over a period of 3-5 days, and the MLS measurements have been averaged by a running 5-day smoothing. The MLS measurements are each day's values measured nearest Thule; the solid line gives measurements on the ascending side of the orbit, and the dashed line gives measurements on the descending side of the orbit. The solar zenith angle and local solar time of the MLS measurements are shown in the two bottom panels. Prior to UARS day 175 the ascending side of the orbit gave measurements nearest mid-day (when the ground-based measurements were taken, and following day 175 the descending side of the orbit gave measurements nearest mid-day. Thus the solid curve should be used for comparisons before day 175 and the dashed curve following day 175.

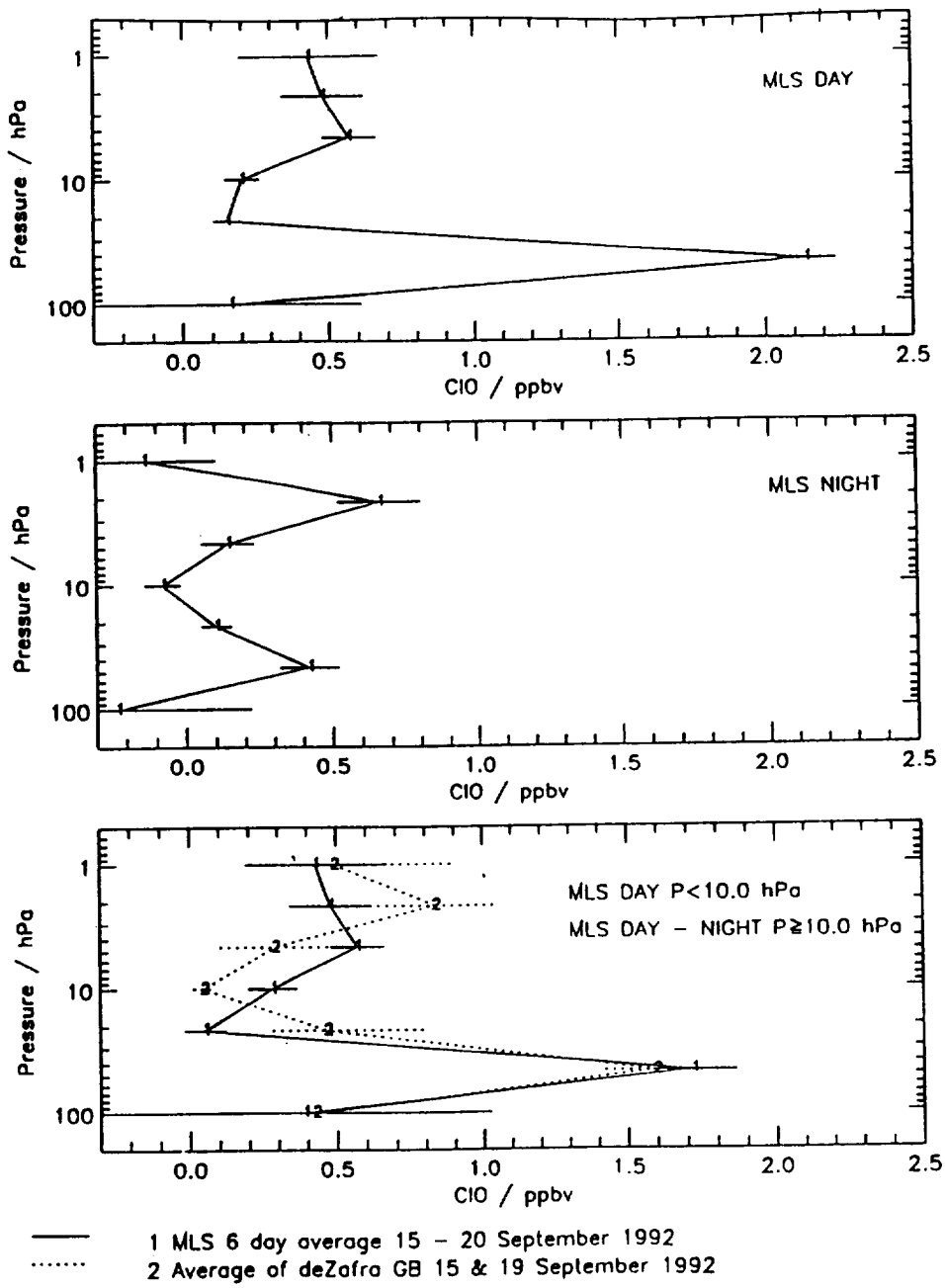

Figure 8.1.2.3-2. Comparison of ground-based [R. deZafra, private communication] and MLS measurements over Antarctica during September 1992. The ground-based (dotted) curve is the average of day-night measurements made September 15-19, 1992 from McMurdo Station, Antarctica (78° S), where the horizontal bars indicate the maximum variation among an ensemble of retrieved profiles. The MLS (solid) curves are averages of data taken over the period 15--20 September 1992 within 2 degrees latitude and 500 km longitude of McMurdo, where the horizontal bars indicate the expected 1 sigma precision of the profile. The ground-based profile has been converted to the MLS profile representation basis by a least-squares best fit.

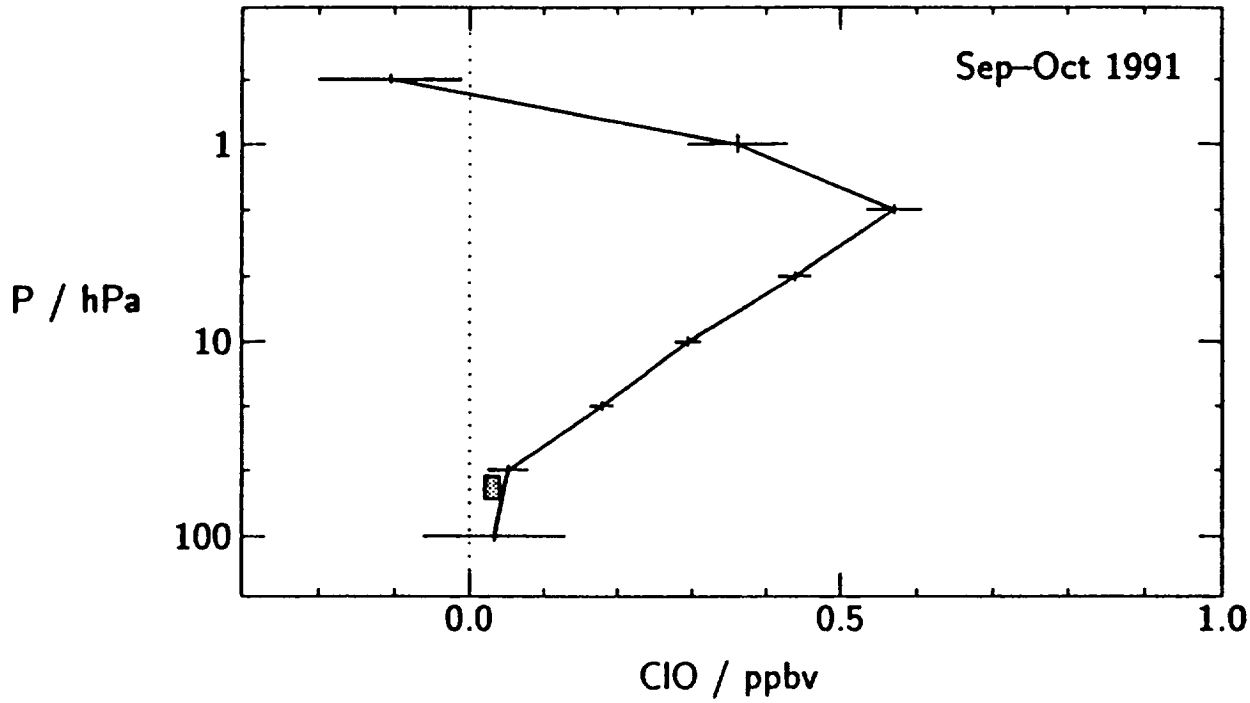

Figure 8.1.2.4-1. Comparison of in situ ER-2 ClO measurements on Sep 17, 1991 [Fahey, et al., 1993] with zonal mean ClO from MLS. The box shows the range of individual ER-2 measurements, all made after local solar noon within the solar zenith angle range of 35-40°, the pressure range of 50-65 hPa, and when N_2O was simultaneously measured to be in the range of 180-250 ppbv. The MLS zonal mean is an average of measurements made at local solar times between 9 am and 3 pm. ClO values from the 'night' side of the orbit (solar zenith angles greater than 100°) have been subtracted from the MLS data at 10 hPa and greater pressures to remove small biases at lower altitudes. Only data having ClO quality indicator of 4 (acceptable radiances and fits) and MMAF_STAT=G (good) have been included in the zonal means: 339 individually-retrieved profiles on the day side of the orbit, and 1157 on the night side of the orbit (which were subtracted from the day-side measurements for pressures of 10 hPa and greater. The horizontal extent of the bars give the +/- 1 sigma uncertainty of the MLS measurements as predicted by the retrieval algorithms.

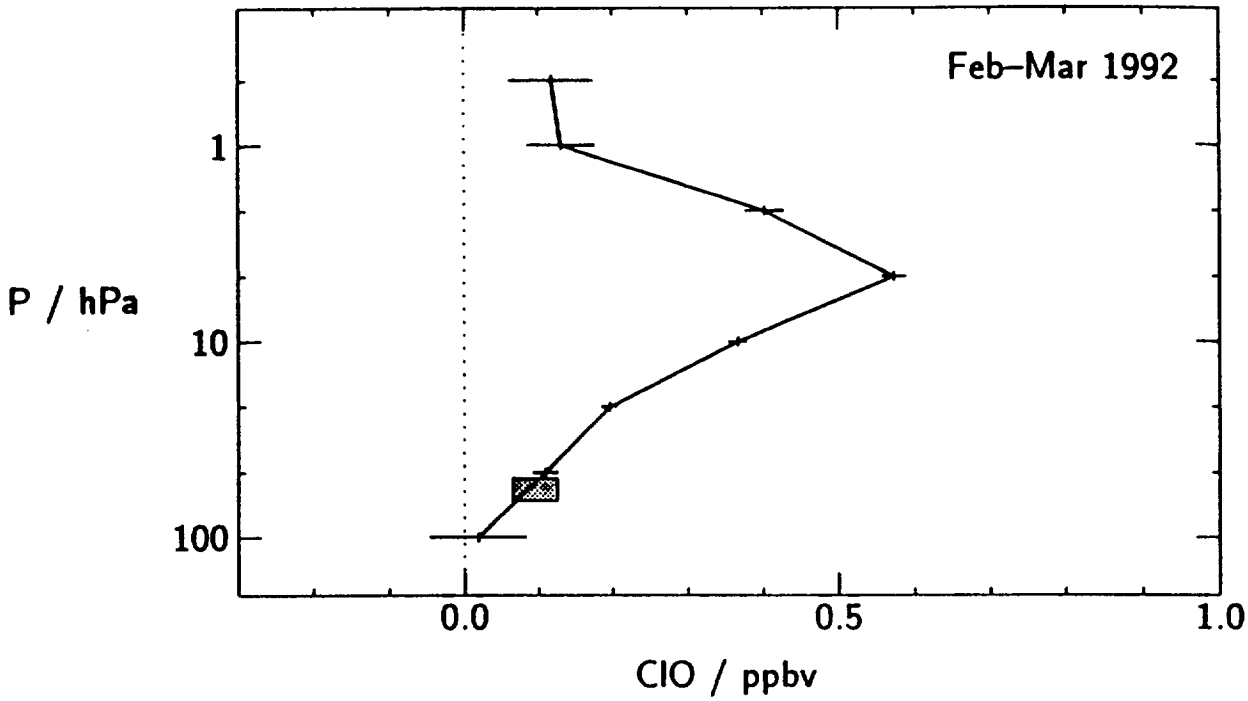

Figure 8.1.2.4-2. Comparison of in situ ER-2 ClO measurements on March 22, 1992 (Fahey, et al., 1993) with zonal mean ClO from MLS. The box shows the range of individual ER-2 measurements, all made after local solar noon within the solar zenith angle range of 35-40°, the pressure range of 50-65 hPa, and when N_2O was simultaneously measured to be in the range of 180-250 ppbv. The zonal mean is an average of measurements made at local solar times between 9 am and 3 pm. ClO values from the 'night' side of the orbit (local solar zenith angles greater than 100°) have been subtracted from the MLS data at 10 hPa and greater pressures to remove small biases at lower altitudes. Only data having ClO quality indicator of 4 (acceptable radiances and fits) and MMAF_STAT=G (good) have been included in the zonal means: 681 individually-retrieved profiles on the day side and 1553 on the night side of the orbits. The horizontal extent of the bars give the +/- 1 sigma precision of the MLS measurements predicted by the retrieval algorithms.

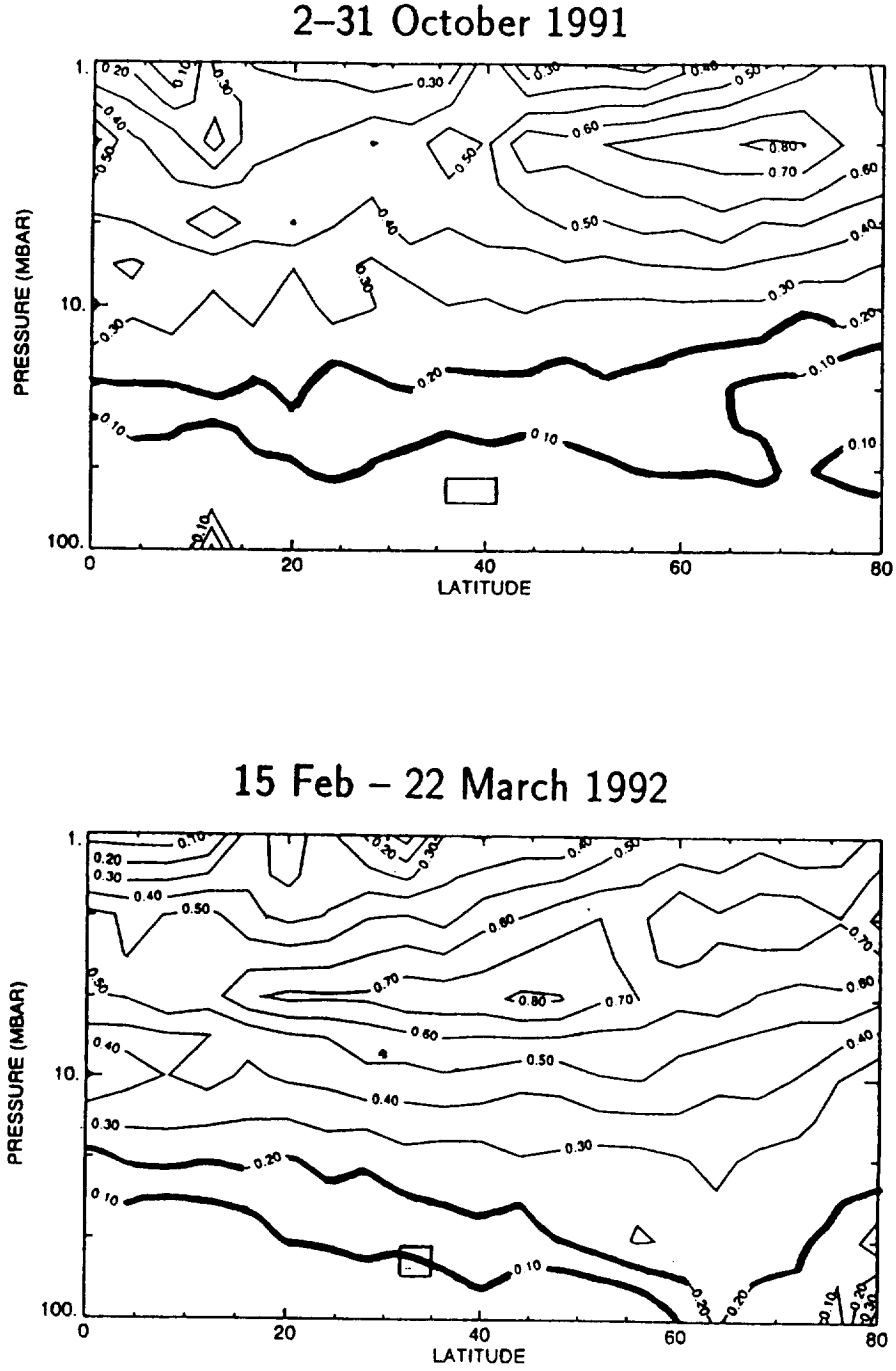

Figure 8.1.2.4-3. Zonal average height-latitude contours of ClO (in ppbv) measured by MLS during the north-looking periods of Oct. 2-31, 1991 (top) and Feb. 15 - Mar. 22, 1992 (bottom). There are independent measurements every 4° of latitude. Thick lines emphasize the 0.1 and 0.2 ppbv ClO contours. The zonal means are averages of MLS measurements made at local solar times between 9 am and 3 pm. ClO values from the 'night' side of the orbit (solar zenith angles greater than 100°) have been subtracted from the MLS data at 10 hPa and greater pressures to remove small biases at lower altitudes. Only data having ClO quality indicator of 4 (good radiances and fits) and MMAF_STAT=G (good) have been included in the zonal means. Boxes indicate locations of ClO measurements made by the NASA ER-2 aircraft which are compared with the MLS measurements in following figures.

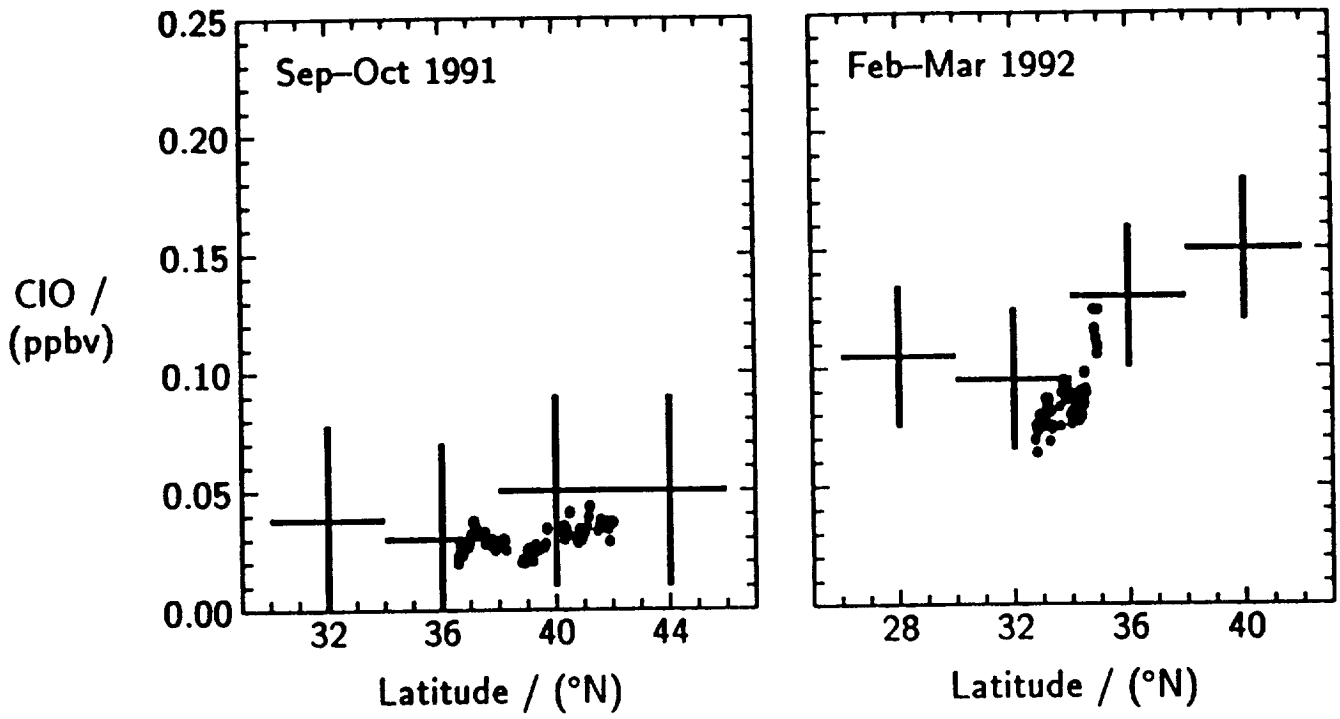

Figure 8.1.2.4-4. Comparison of in situ ER-2 lower stratospheric ClO measurements with zonal means from MLS. ER-2 values, from Figure 3a of Fahey, et al., (1993), are individual measurements made between 50 and 65 hPa on the indicated dates. MLS values, taken from higher-resolution versions of the contour plots in Figure 8.1.2.4-3, are day-night differences of zonal averages at the same altitudes as the ER-2 measurements.

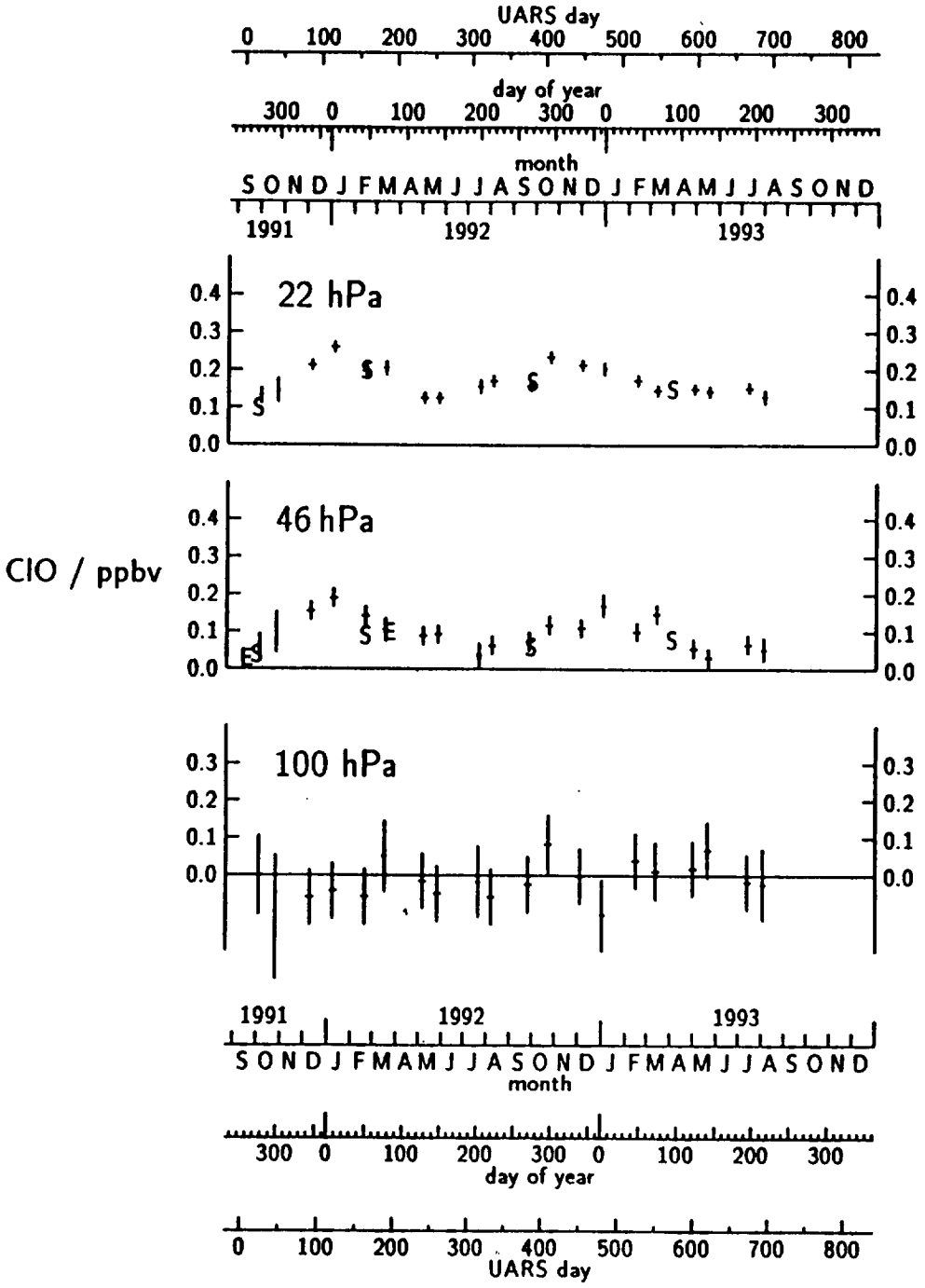

Figure 8.1.2.4-5. Time-series of 30-50° N monthly zonal means of MLS lower stratospheric ClO data (crosses) compared with ER-2 (E) and SLS (S) measurements. MLS data from the night side of the orbit have been subtracted to remove biases. The vertical extent of the crosses gives the estimated precision of the MLS means, and the horizontal extent gives the time period over which the data were taken. The ER-2 measurements (Fahey, et al., 1993) were made at 50-65 hPa, and the SLS measurements are from R.A. Stachnik [private communication].

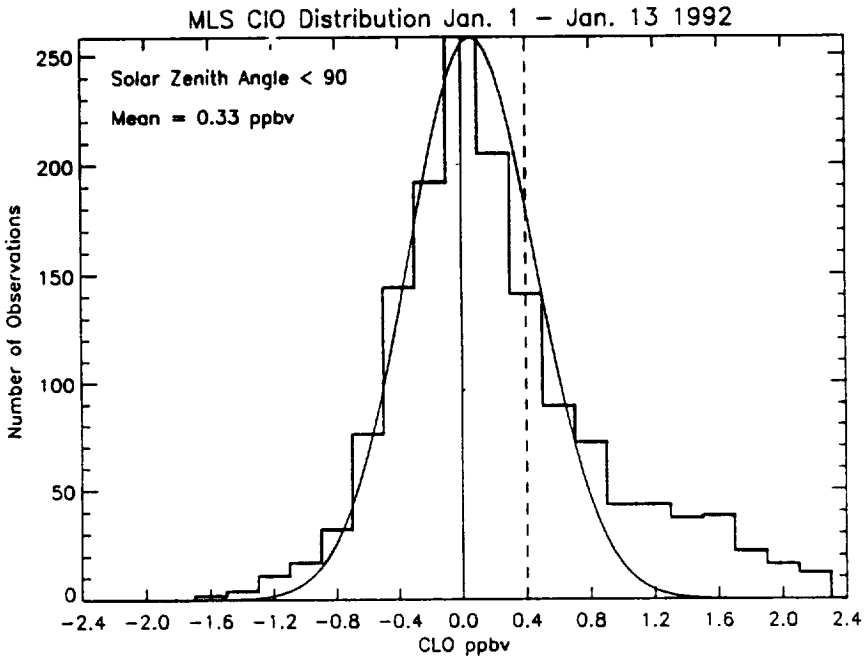

Figure 8.1.2.5-1. A histogram of the Jan 1-13 MLS Level 3at ClO data north of 40 N for solar zenith angles less than 90. The smooth curve is a Gaussian distribution with a 0.4 ppbv standard deviation centered at 0.06 ppbv.

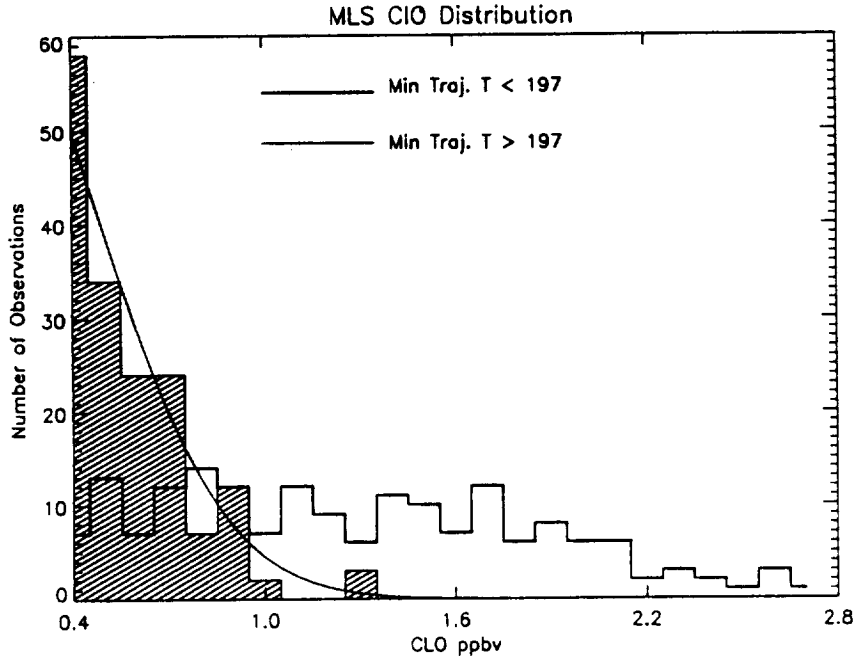

Figure 8.1.2.5-2. A histogram of the Jan 1-13 MLS Level 3at ClO data, greater than 0.4 ppbv, north of 40 N for solar zenith angles less than 90. Back trajectory calculations for 10 days show that most of the parcels with elevated ClO values have encountered PSC type temperatures. The distribution of parcels which have not encountered such cold temperatures (shaded) is consistent with a Gaussian (solid line) as in Figure 8.1.2.5-1.

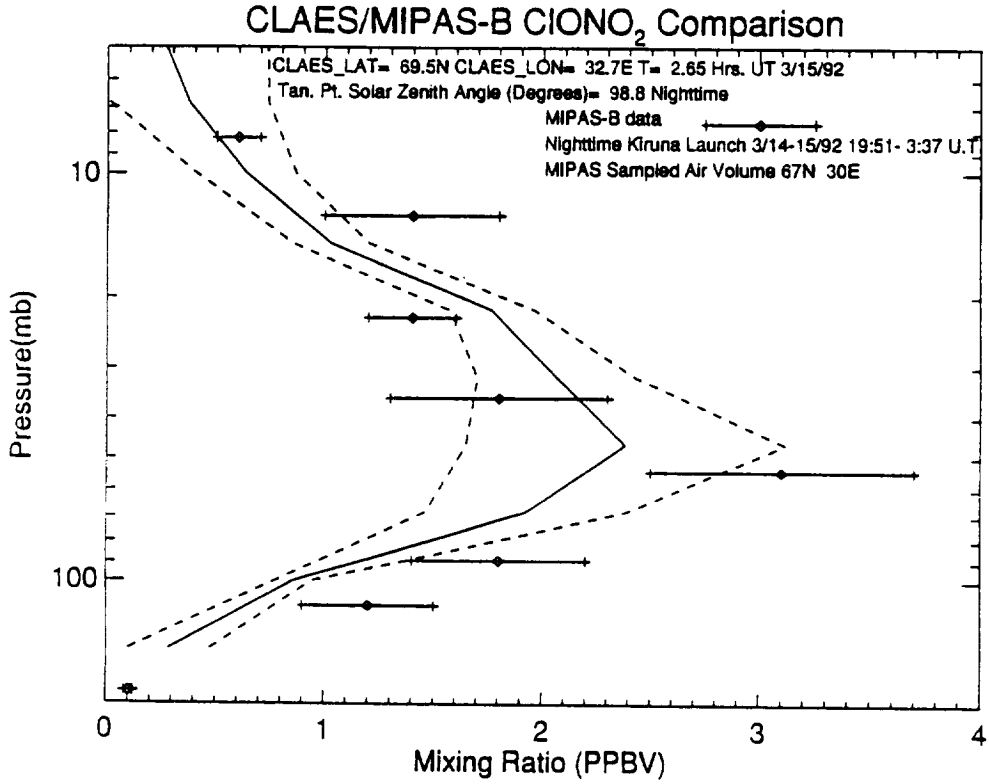

Figure 8.2.2.1-1 Comparison of a near-coincident CLAES $ClONO_2$ profile and a MIPAS-B FTIR balloon nighttime emission measurement launched from Kiruna, Sweden on March 4, 1992.

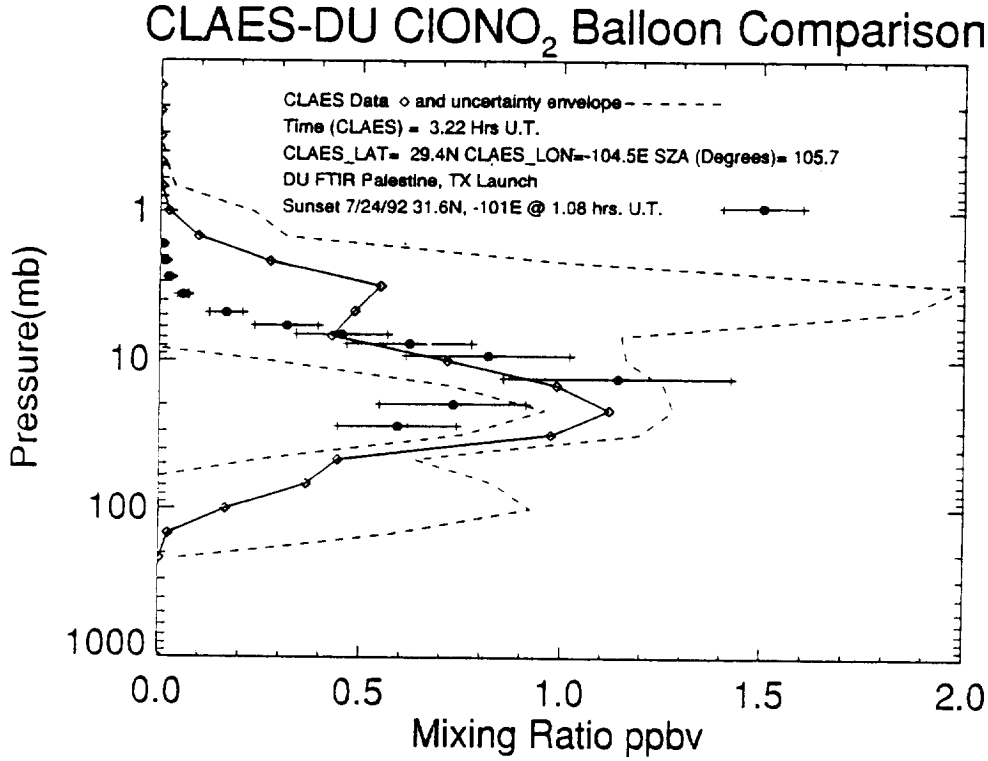

Figure 8.2.2.1-2 Comparison of a near-coincident CLAES $ClONO_2$ profile and a Denver University , FTIR balloon sunset occultation measurement launched from Palestine Texas on July 24, 1992.

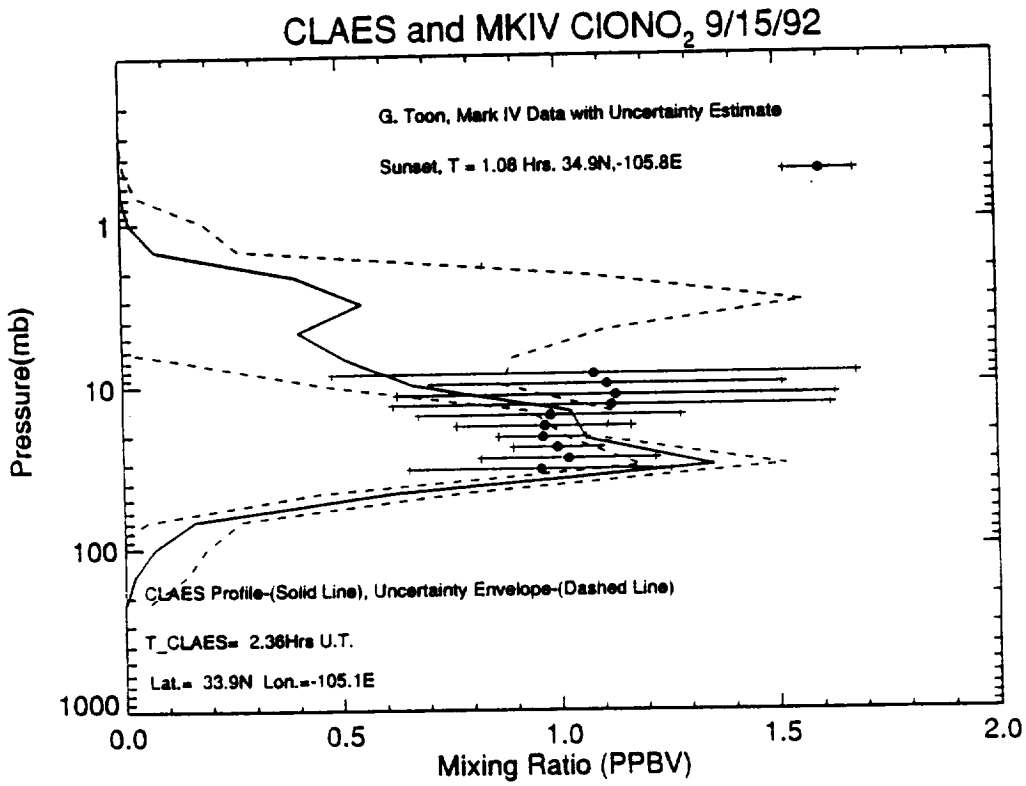

Figure 8.2.2.1-3 Comparison of a near-coincident CLAES $ClONO_2$ profile and a JPL Mark IV, FTIR balloon sunset occultation measurement launched from Ft. Sumner N. Mexico on Sept. 14, 1992.

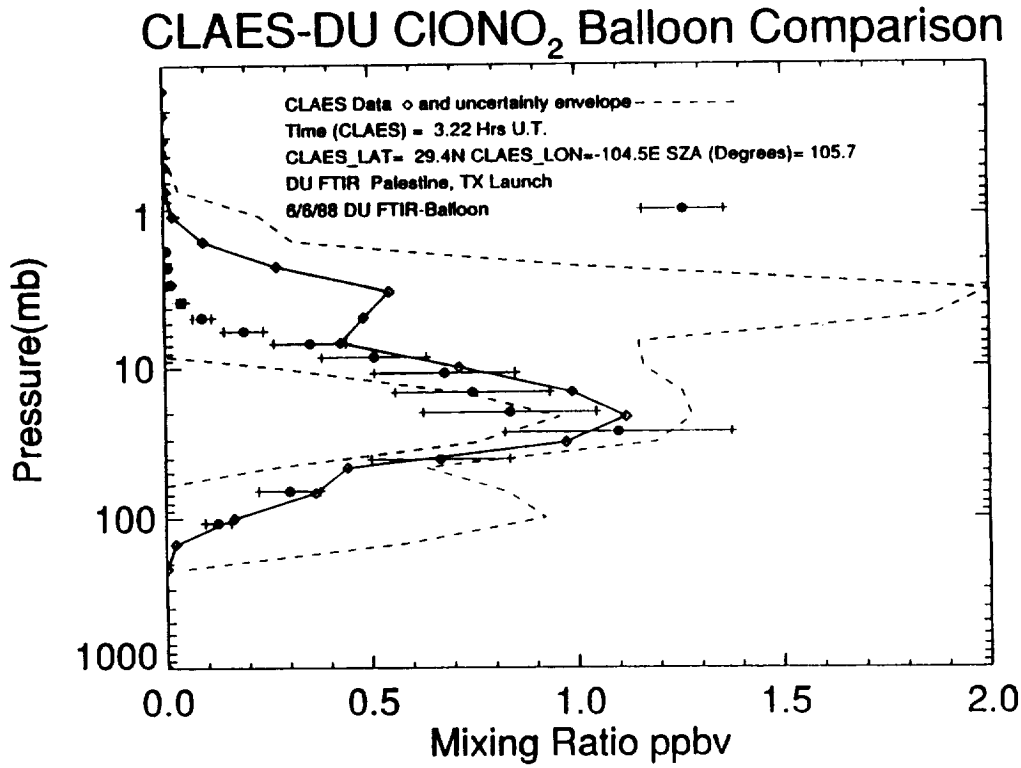

Figure 8.2.2.2-1 Comparison of a 7/24/92 CLAES $ClONO_2$ profile over southern Texas and a Denver University, FTIR balloon sunset occultation measurement launched from Palestine Texas on June 6, 1988.

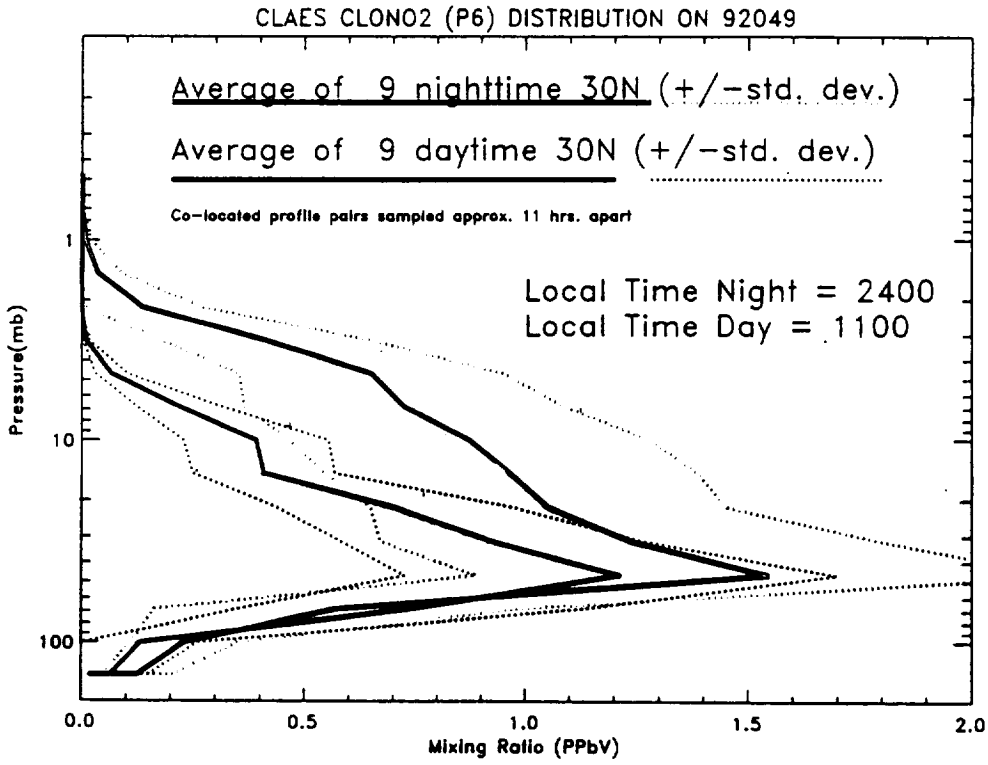

Figure 8.2.2.2-2. Average difference of 9 pairs of co-located midday/midnight $ClONO_2$ profiles at 30N on February 18, 1992.

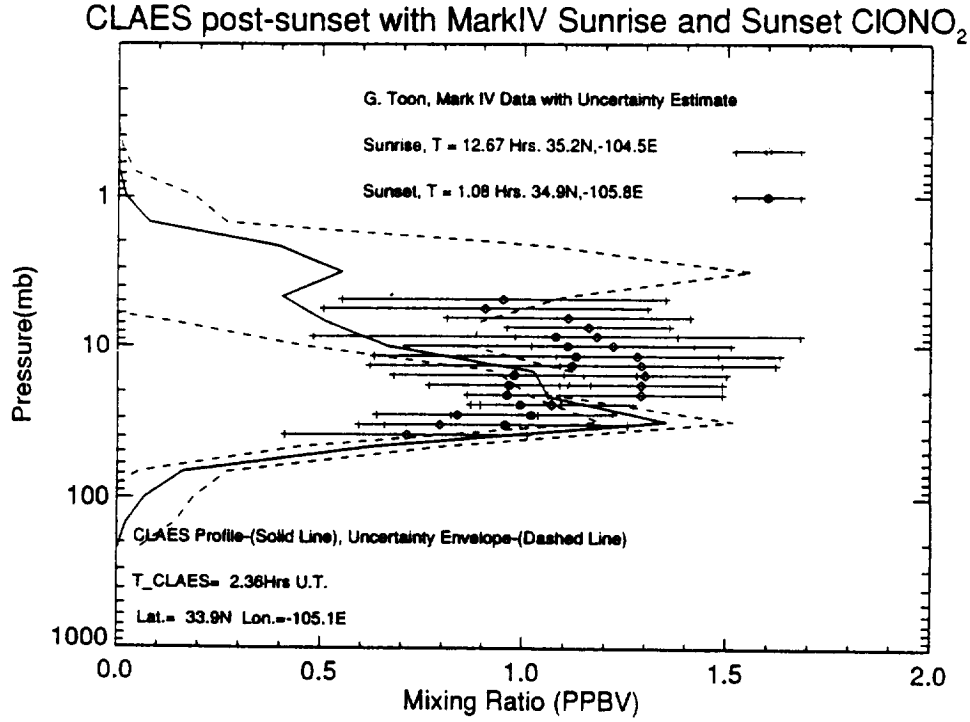

Figure 8.2.2.2-3 Comparison of a sunset and sunrise $ClONO_2$ profile measured by the JPL Mark IV, FTIR balloon launched from Ft. Sumner N. Mexico on Sept. 14, 1992.

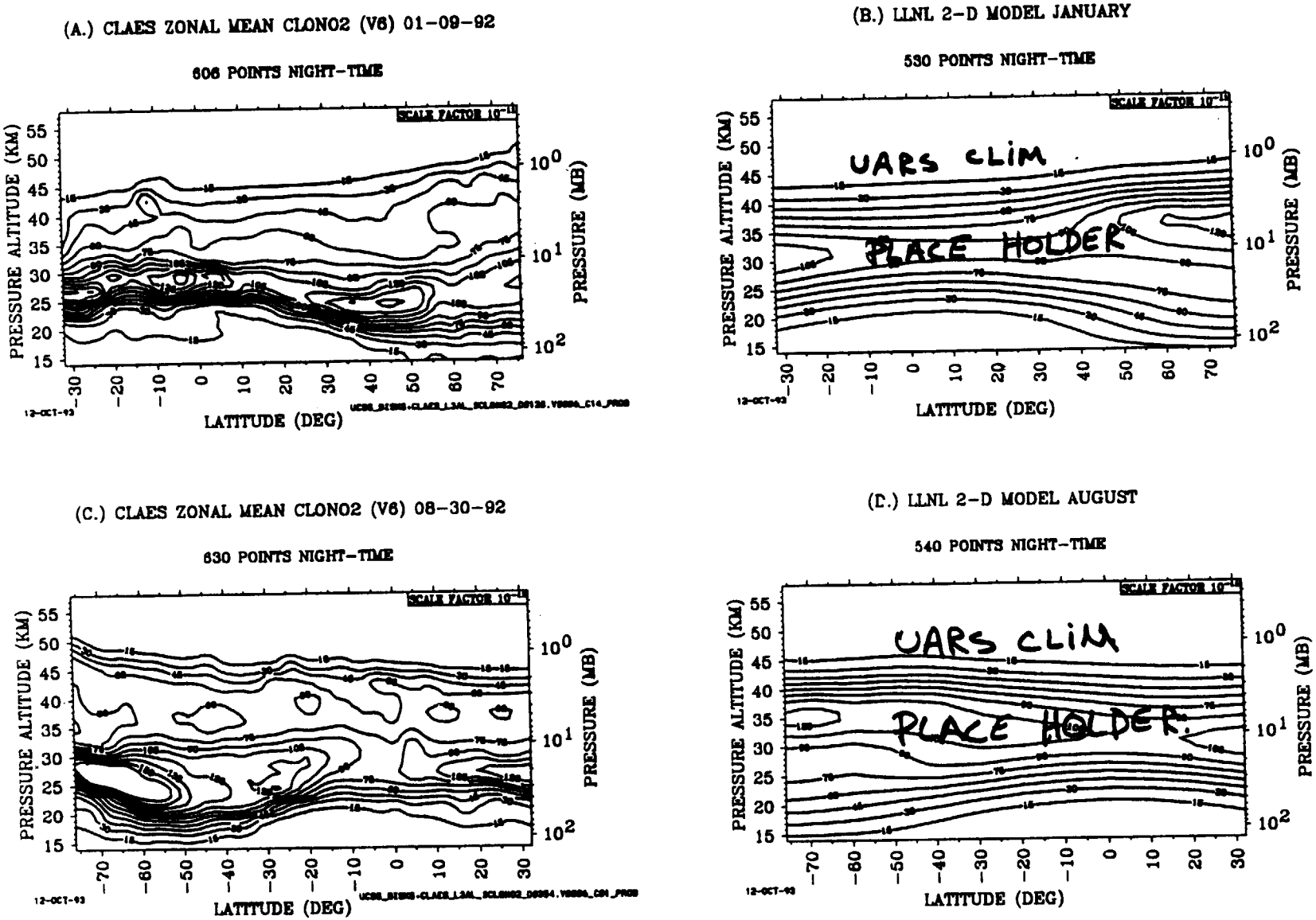

Figure 8.2.2.2-4a-d. Comparison of LLNL-2D model and CLAES zonal mean $ClONO_2$ nighttime data in Jan. and Aug. (a), CLAES zonal-mean nighttime $ClONO_2$ mixing ratio for Jan. 9, 1992. (b), 2-D model for Jan. (c), CLAES zonal-mean nighttime $ClONO_2$ mixing ratio for Aug. 30, 1992. (d), 2-D model for August.

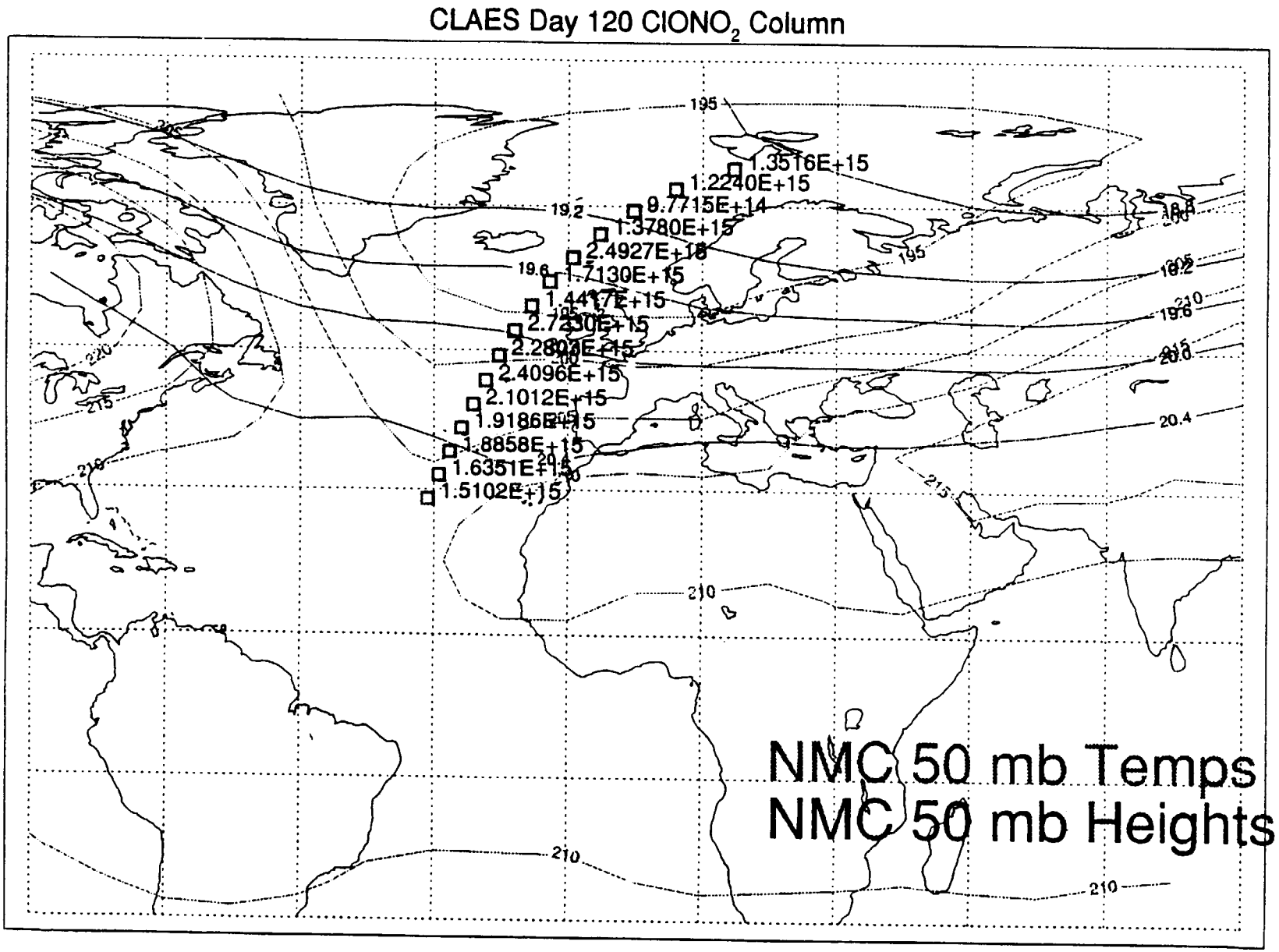

Figure 8.2.2.2-5. CLAES $ClONO_2$ column density for a portion of an orbit on Jan. 9, 1992.

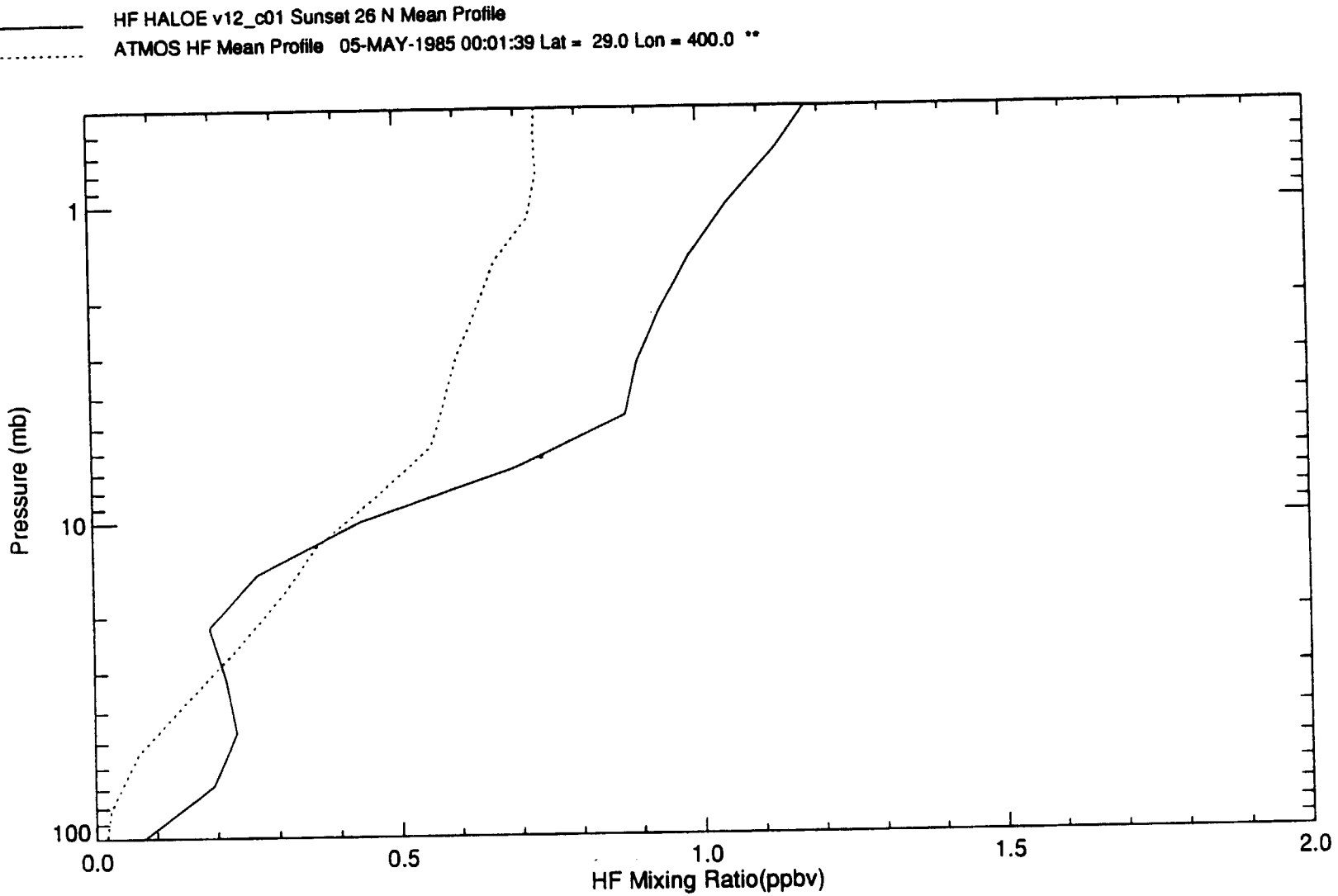

HALOE Zonal Mean HF Mixing Ratio 09-MAY-92 and ATMOS Mean HF Mixing Ratio 05-MAY-85

Figure 8.3.2.1-1. The mean ATMOS HF mixing ratio and the mean HALOE HF profile for similar latitude and season.

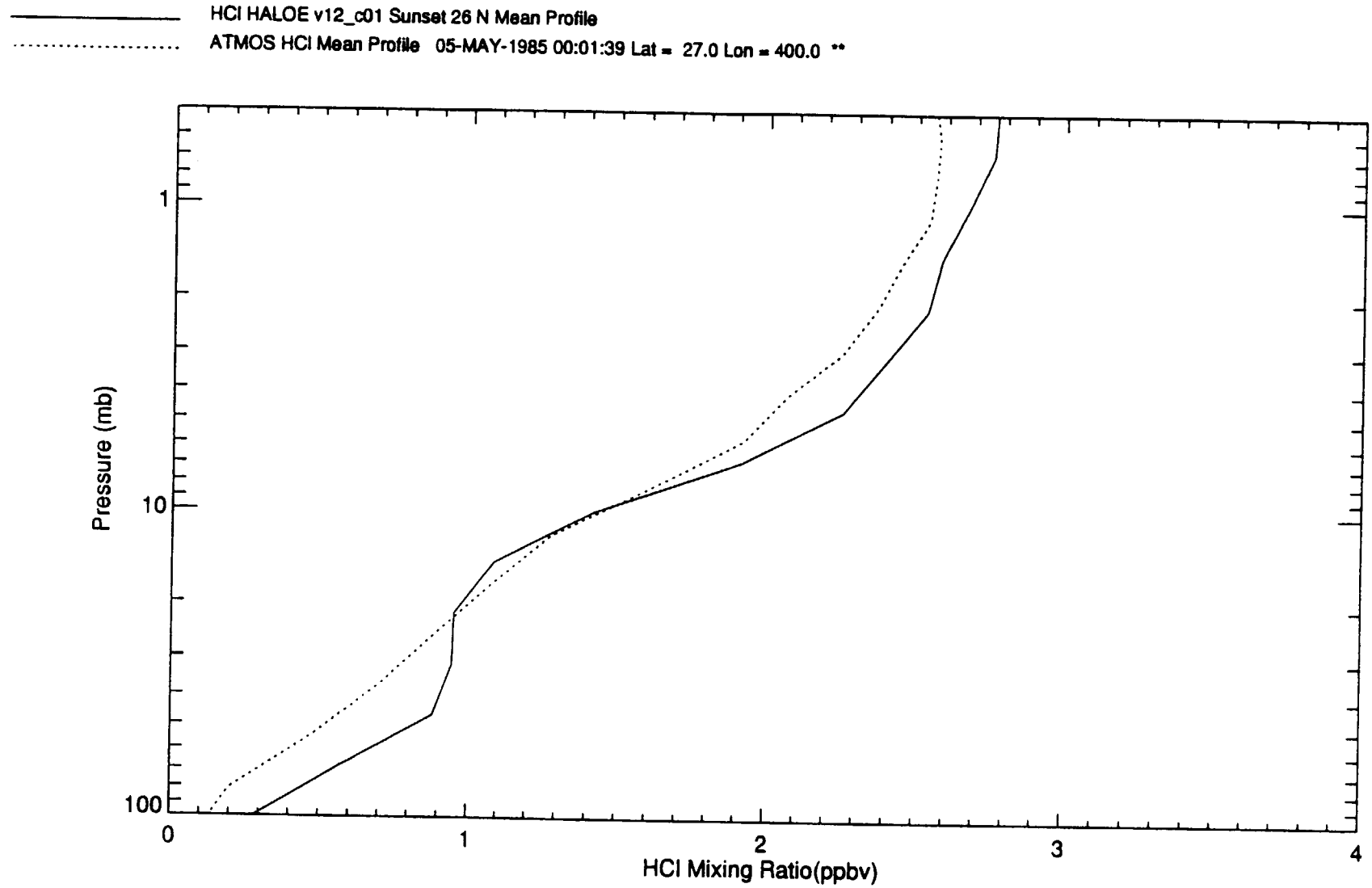

HALOE Zonal Mean HCl Mixing Ratio 09-MAY-92 and ATMOS Mean HCl Mixing Ratio 05-MAY-85

Figure 8.3.2.1-2. The mean ATMOS HCl mixing ratio and the mean HALOE HCl profile for similar latitude and season.

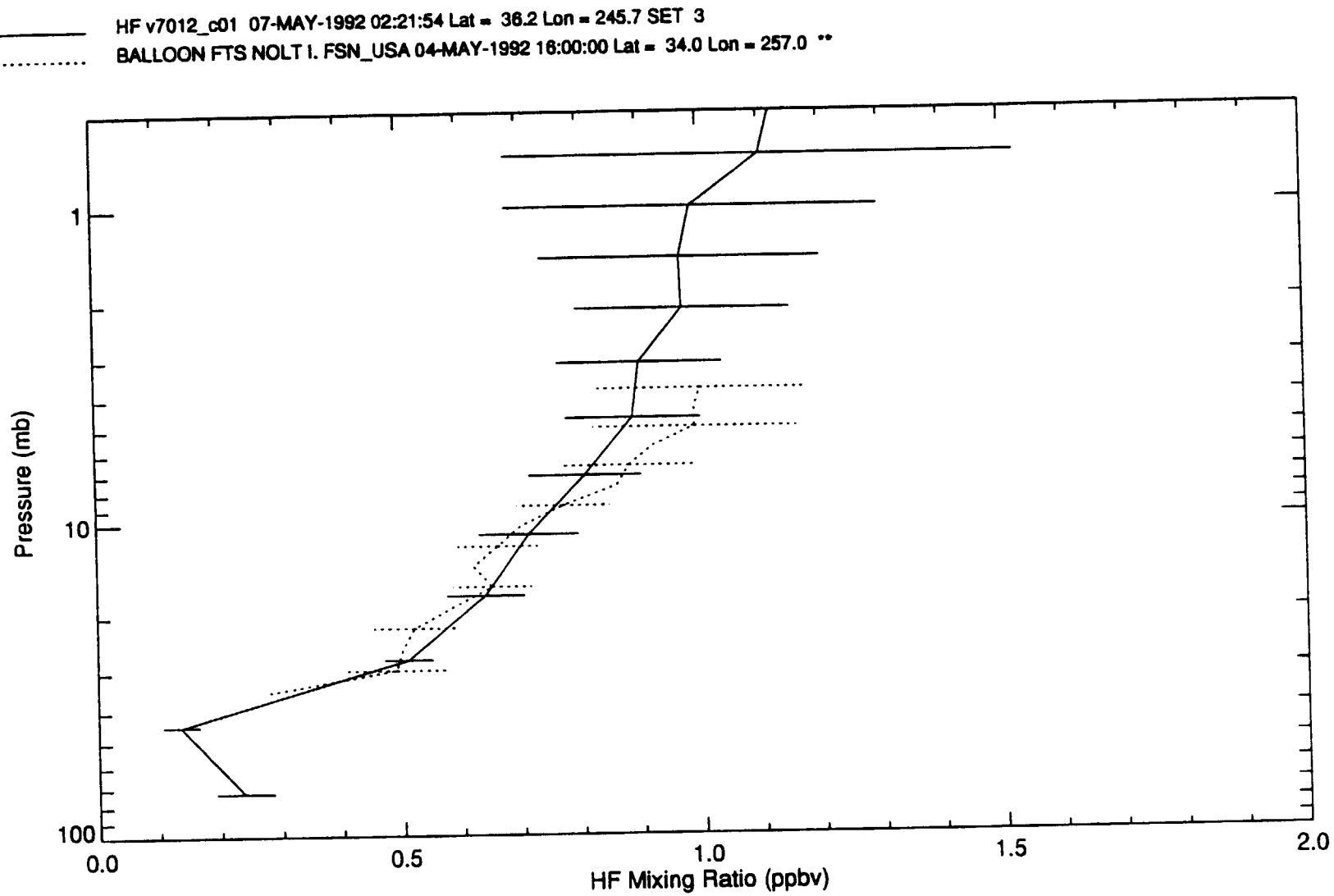

HALOE HF Mixing Ratio 07-MAY-92 and FIREX HF Mixing Ratio 04-MAY-92

Figure 8.3.2.2-1. The May 4, 1992 FIREX HF mixing ratio profile and the nearest HALOE HF profile.

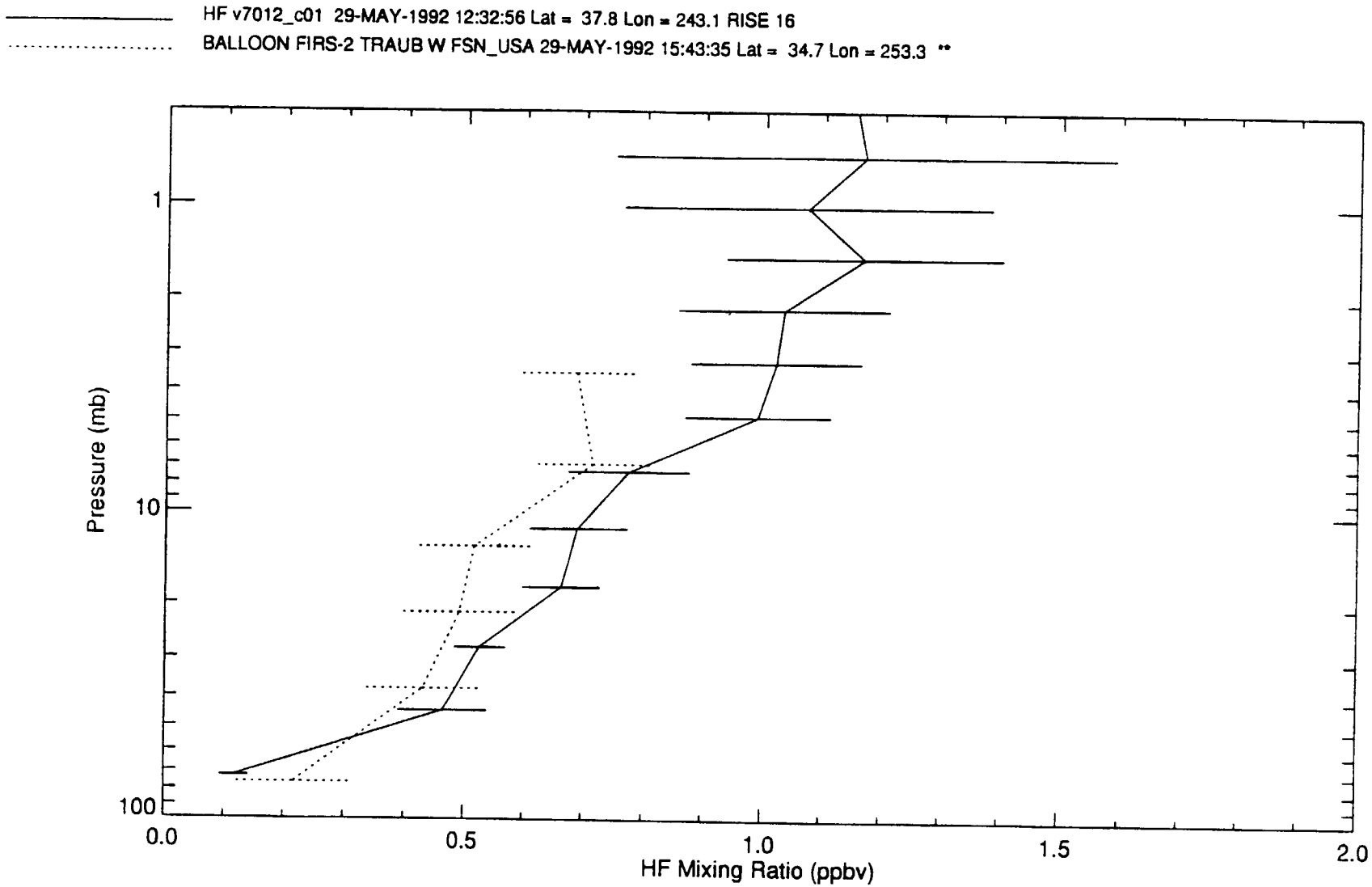

HALOE HF Mixing Ratio 29-MAY-92 and FIRS-2 HF Mixing Ratio 29-MAY-92

Figure 8.3.2.2-2. The May 29, 1992 FIRS-2 HF mixing ratio profile and the nearest HALOE HF profile.

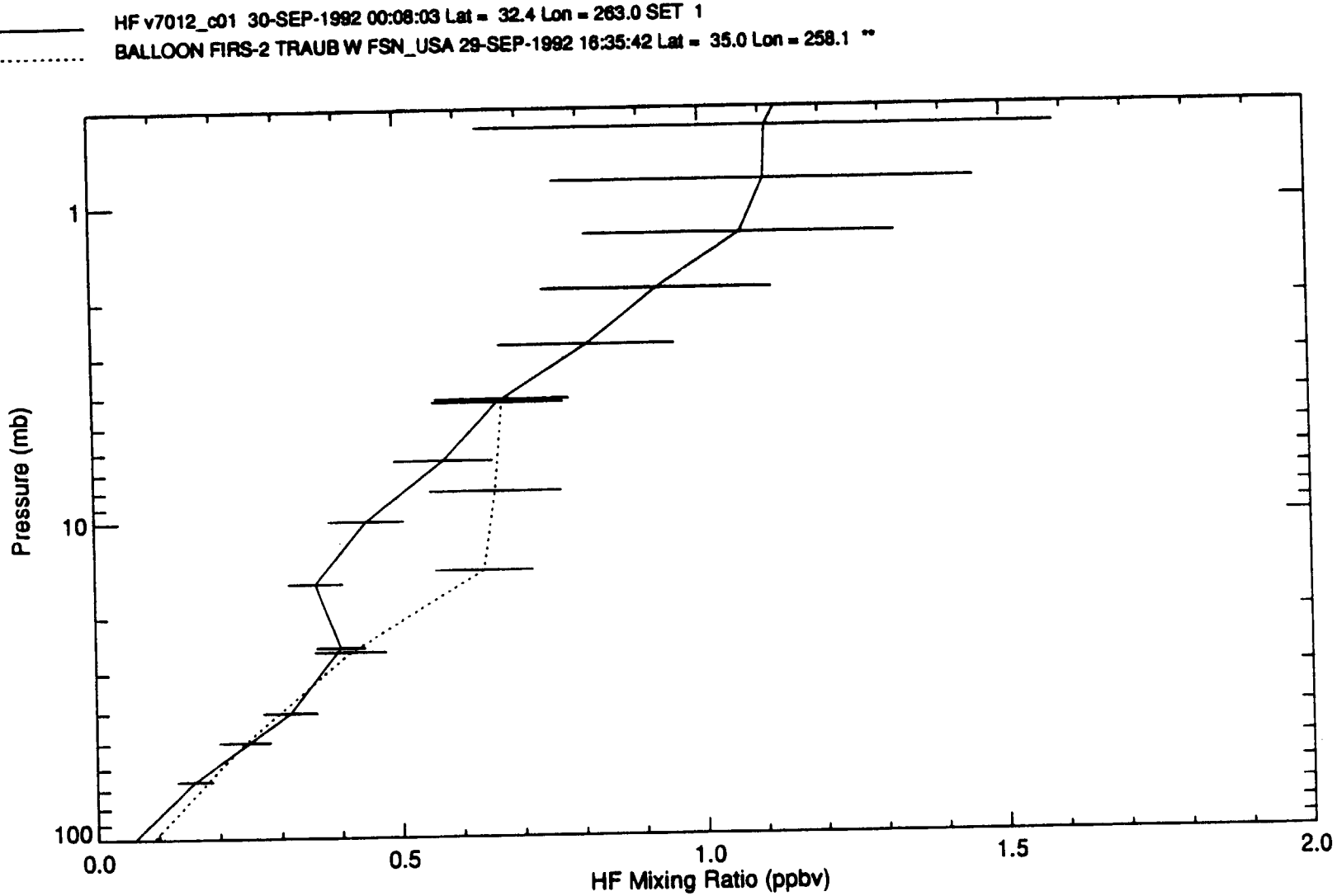

Figure 8.3.2.2-3. The Sept. 30, 1992 FIRS-2 HF mixing ratio profile and the nearest HALOE HF profile

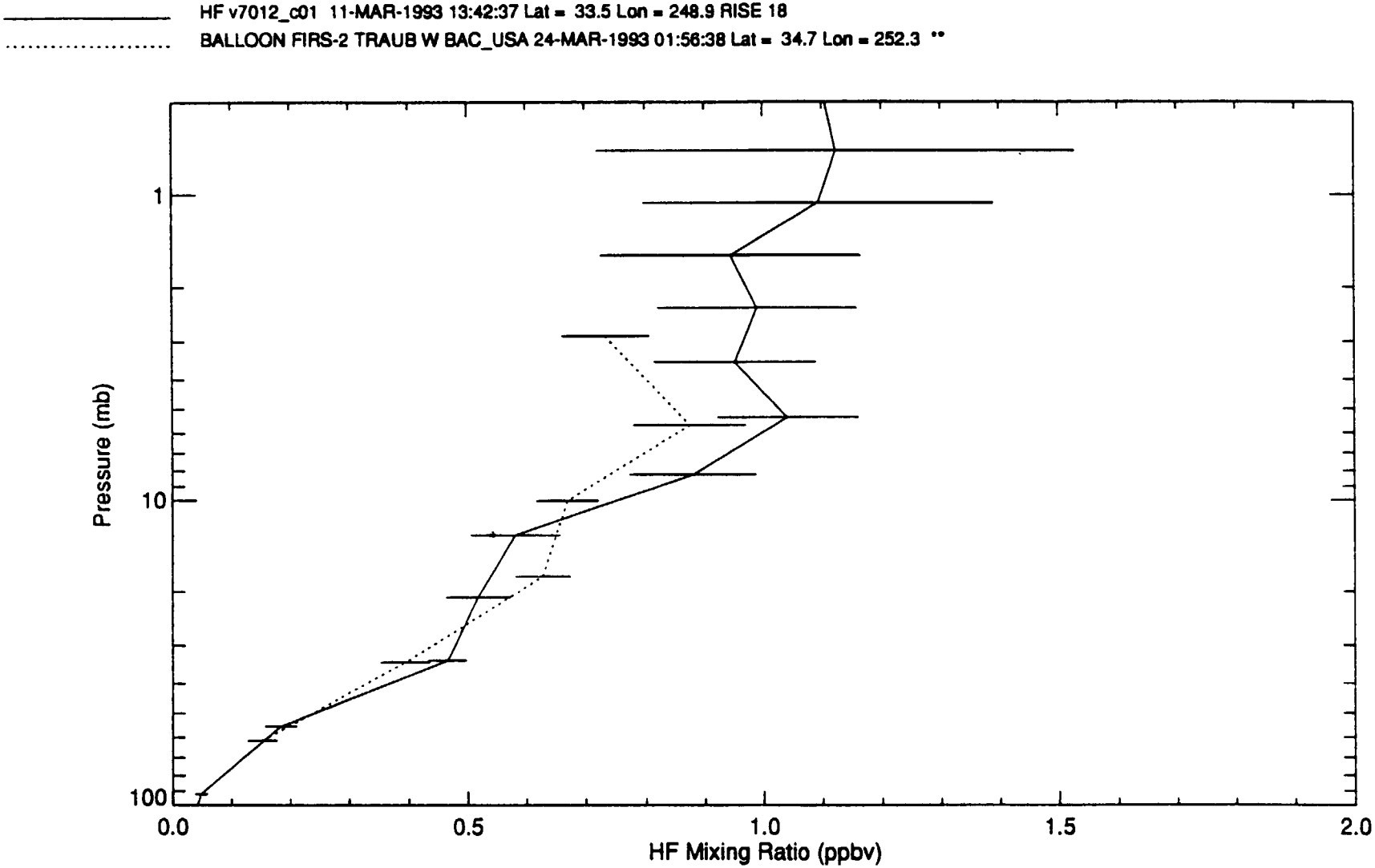

Figure 8.3.2.2-4. The March 24, 1993 FIRS-2 HF mixing ratio profile and the nearest HALOE HF profile

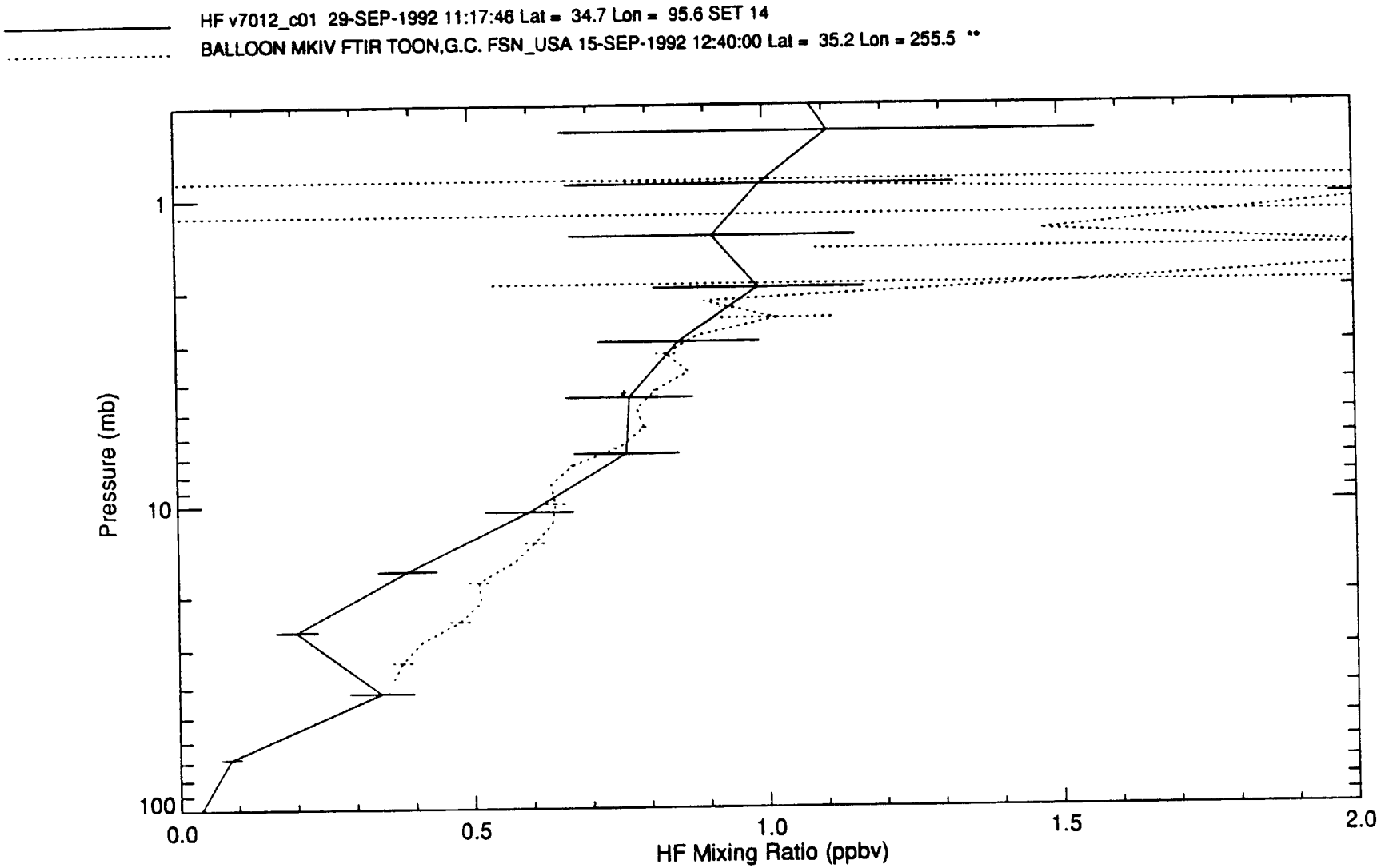

HALOE HF Mixing Ratio 29-SEP-92 and MKIV FTIR HF Mixing Ratio 15-SEP-92

Figure 8.3.2.2-5. The Sept. 15, 1992 JPL Interferometer HF mixing ratio profile and the nearest HALOE HF profile.

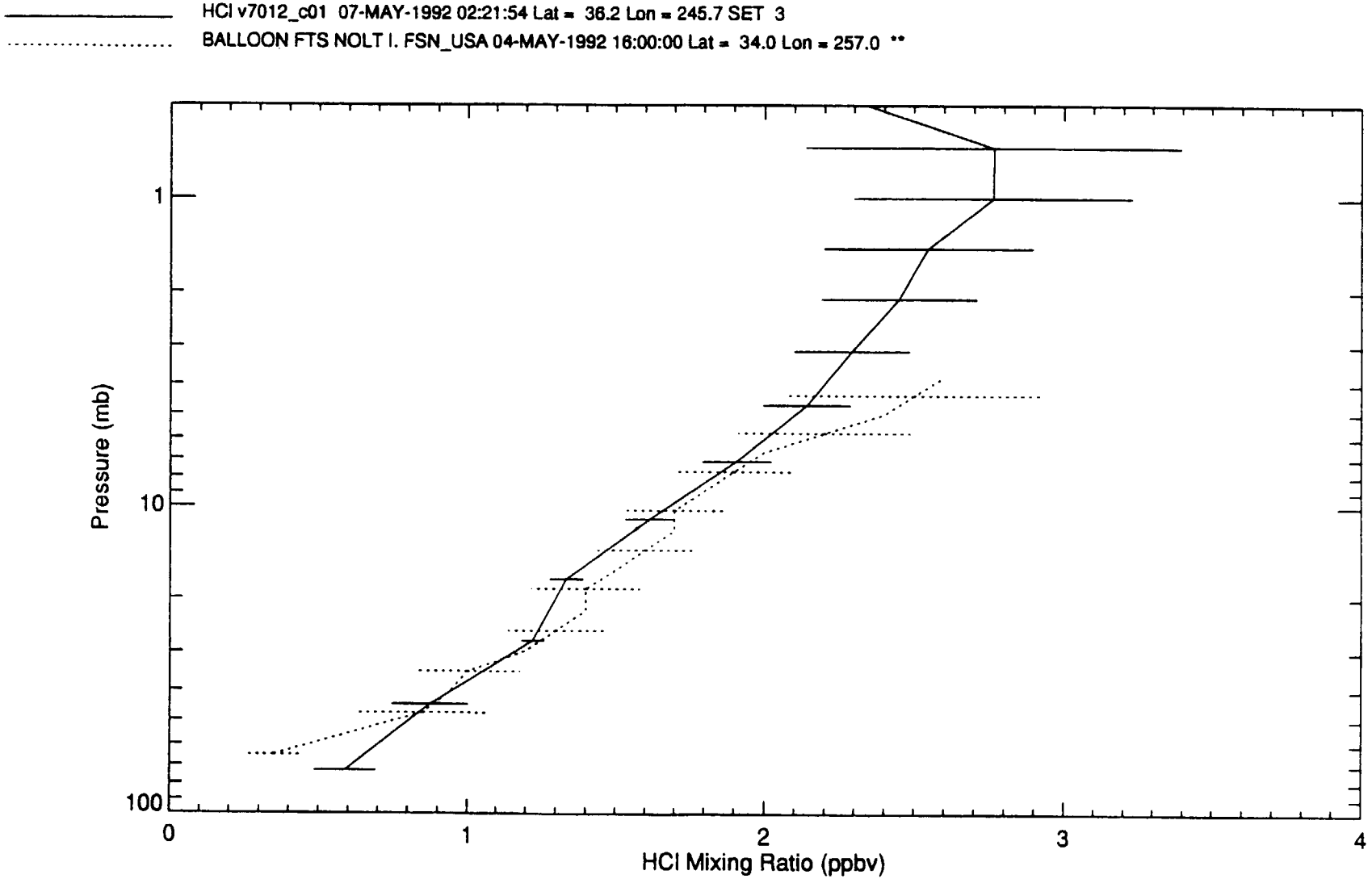

HALOE HCl Mixing Ratio 07-MAY-92 and FIREX HCl Mixing Ratio 04-MAY-92

Figure 8.3.2.2-6. The May 4, 1992 FIREX HCl mixing ratio profile and the nearest HALOE HCl profile.

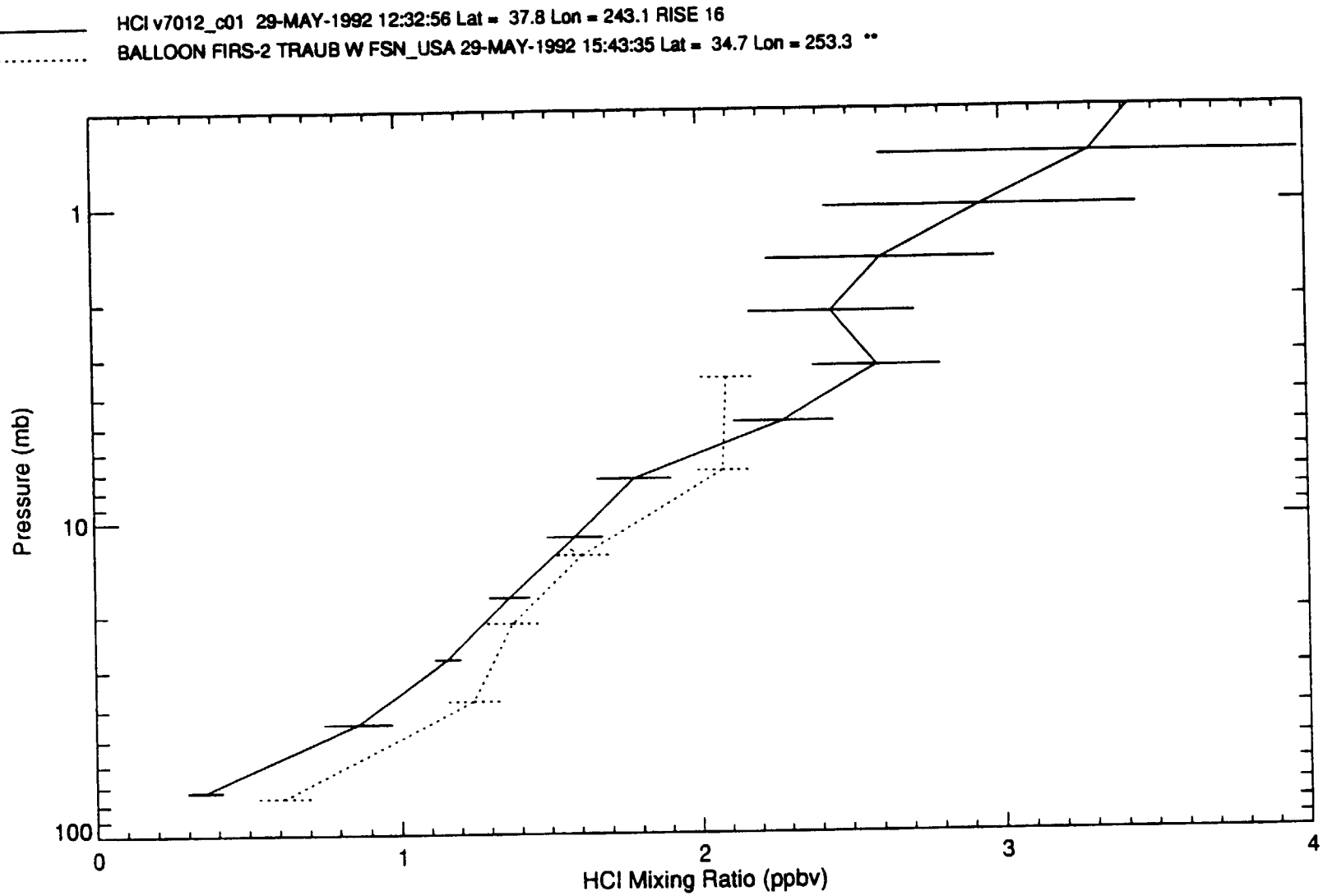

HALOE HCl Mixing Ratio 29-MAY-92 and FIRS-2 HCl Mixing Ratio 29-MAY-92

Figure 8.3.2.2-7. The May 29, 1992 FIRS-2 HCl mixing ratio profile and the nearest HALOE HCl profile.

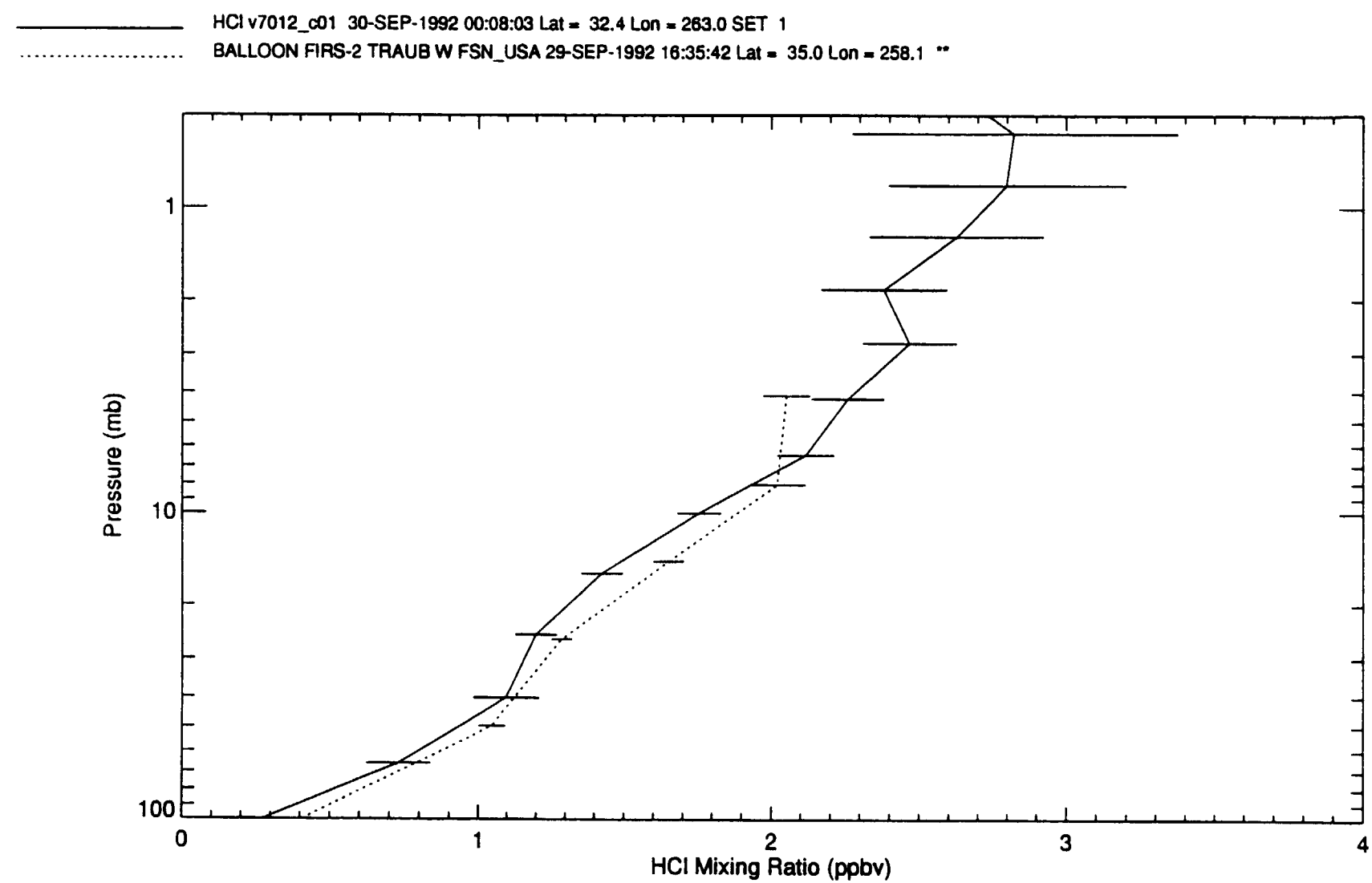

HALOE HCl Mixing Ratio 30-SEP-92 and FIRS-2 HCl Mixing Ratio 29-SEP-92

Figure 8.3.2.2-8. The Sept. 30, 1992 FIRS-2 HCl mixing ratio profile and the nearest HALOE HCl profile

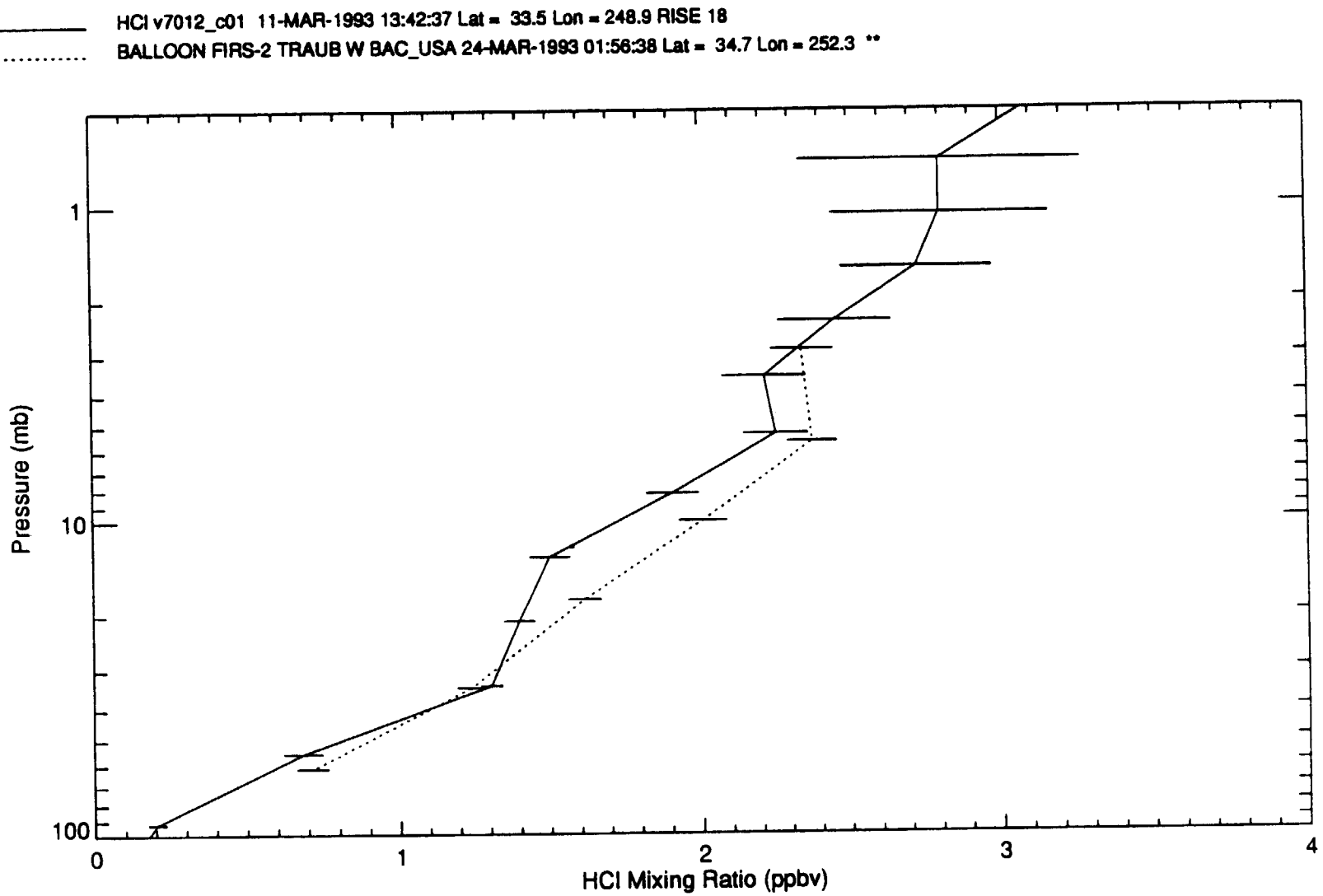

HALOE HCl Mixing Ratio 11-MAR-93 and FIRS-2 HCl Mixing Ratio 24-MAR-93

Figure 8.3.2.2-9. The March 24, 1993 FIRS-2 HCl mixing ratio profile and the nearest HALOE HCl profile

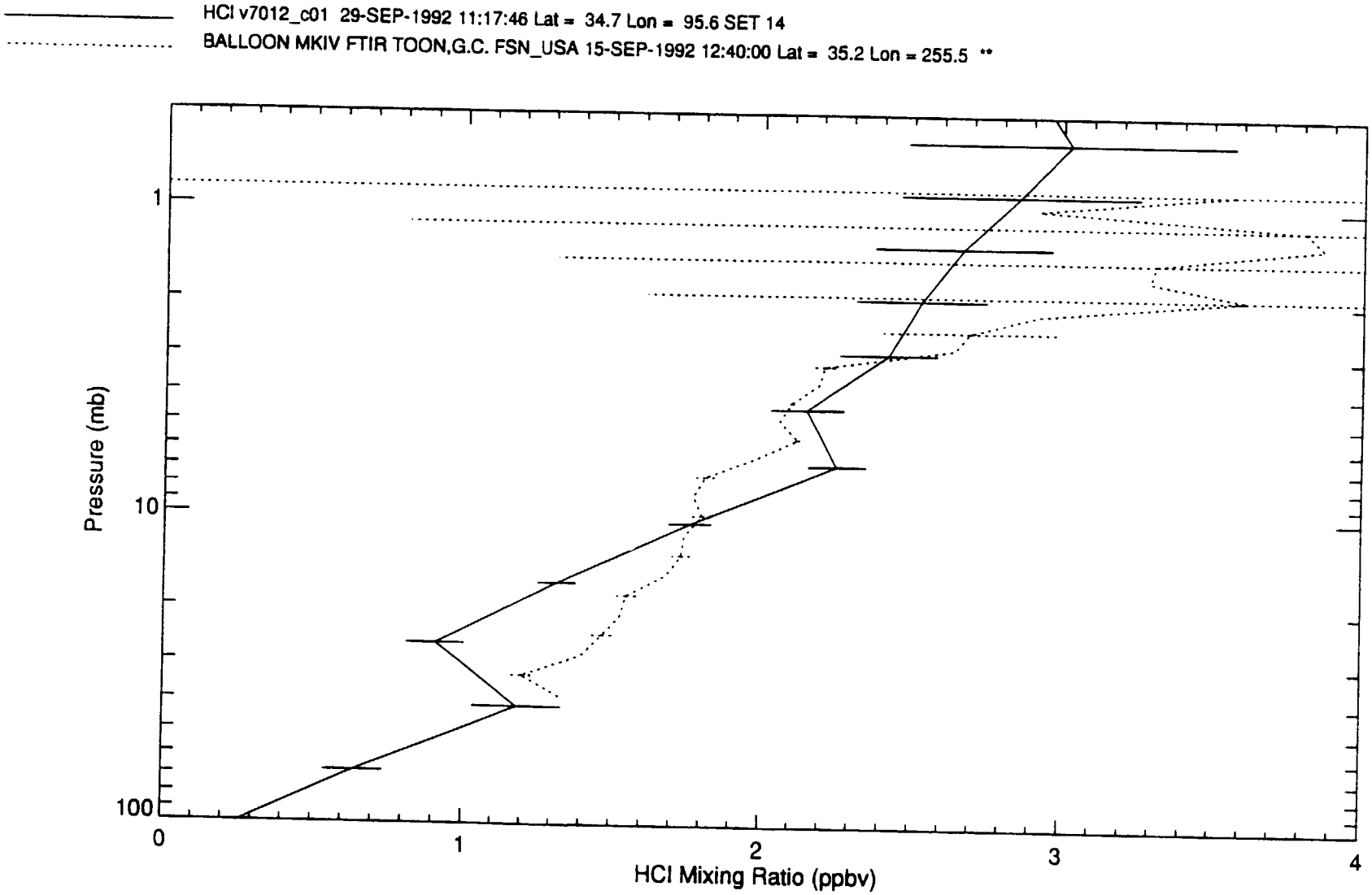

HALOE HCl Mixing Ratio 29-SEP-92 and MKIV FTIR HCl Mixing Ratio 15-SEP-92

Figure 8.3.2.2-10. The Sept. 15, 1992 JPL Interferometer HCl mixing ratio profile and the nearest HALOE HCl profile.

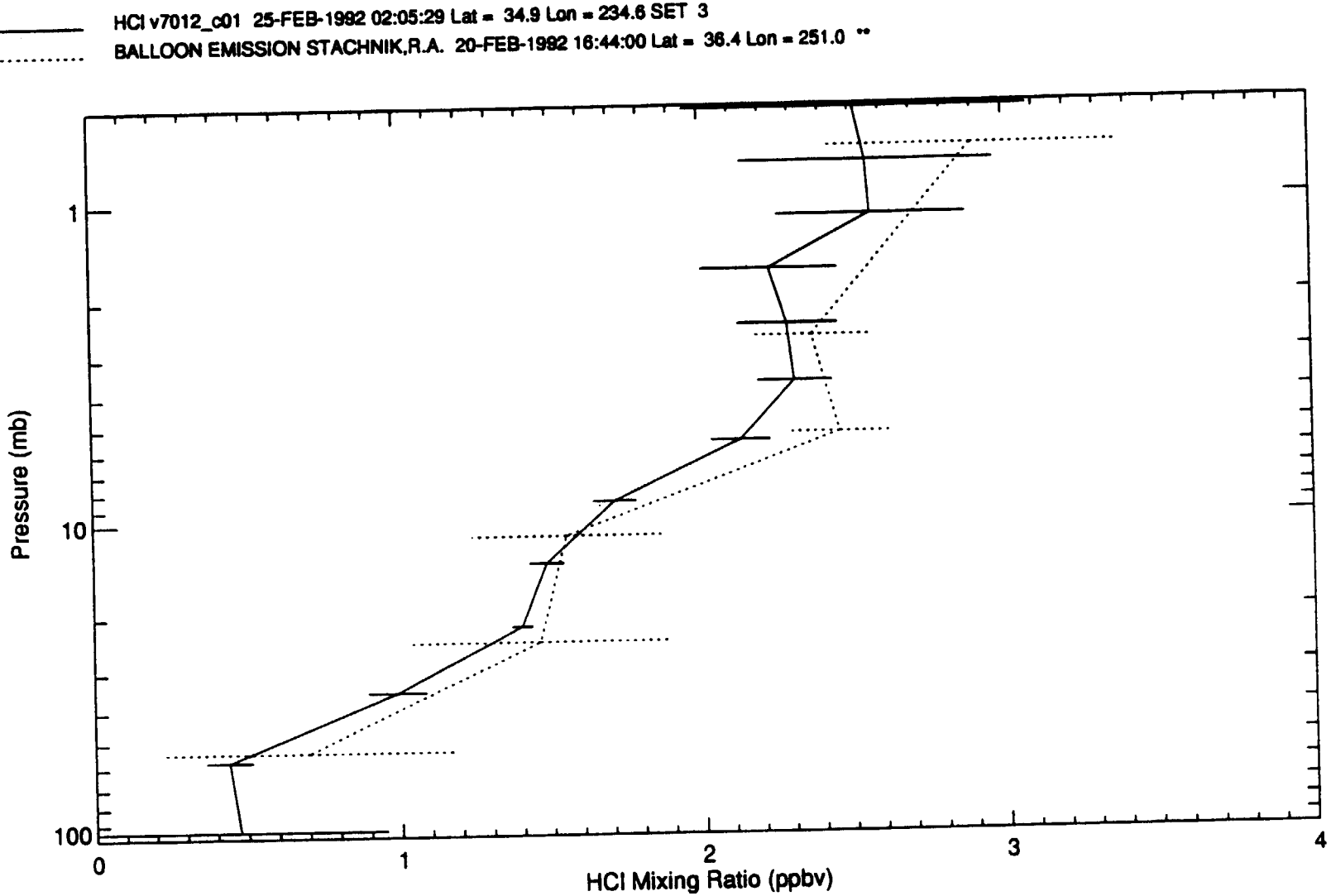

HALOE HCl Mixing Ratio 25-FEB-92 and SLS HCl Mixing Ratio 20-FEB-92

Figure 8.3.2.2-11. The Feb. 20, 1992 SLS HCl mixing ratio profile and the nearest HALOE HCl profile.

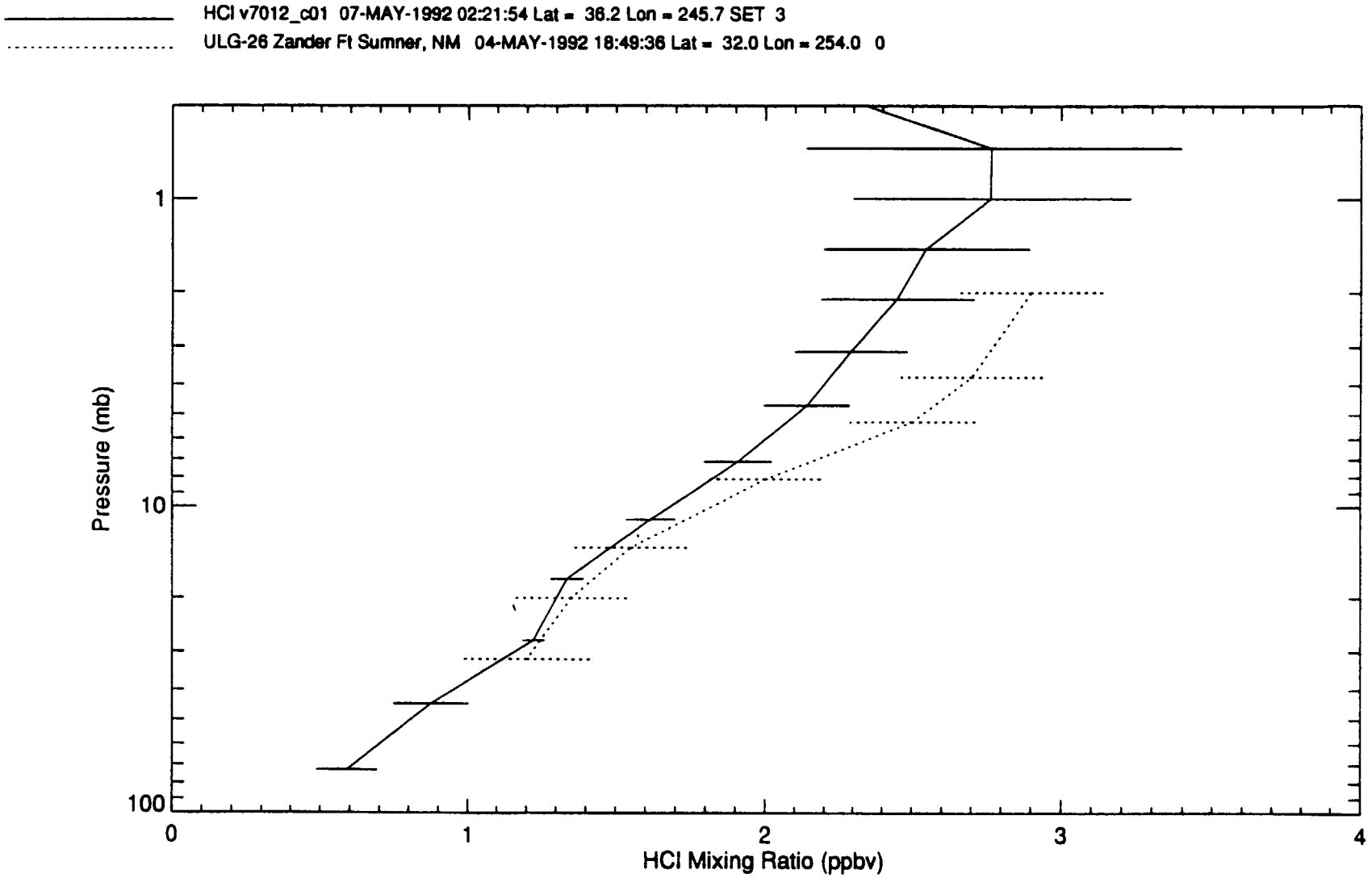

HALOE HCl Mixing Ratio 07-MAY-92 and ULG-26 HCl Mixing Ratio 04-MAY-92

Figure 8.3.2.2-12. The May 4, 1992 grating occultation instrument (Zander) HCl mixing ratio profile and the nearest HALOE HCl profile.

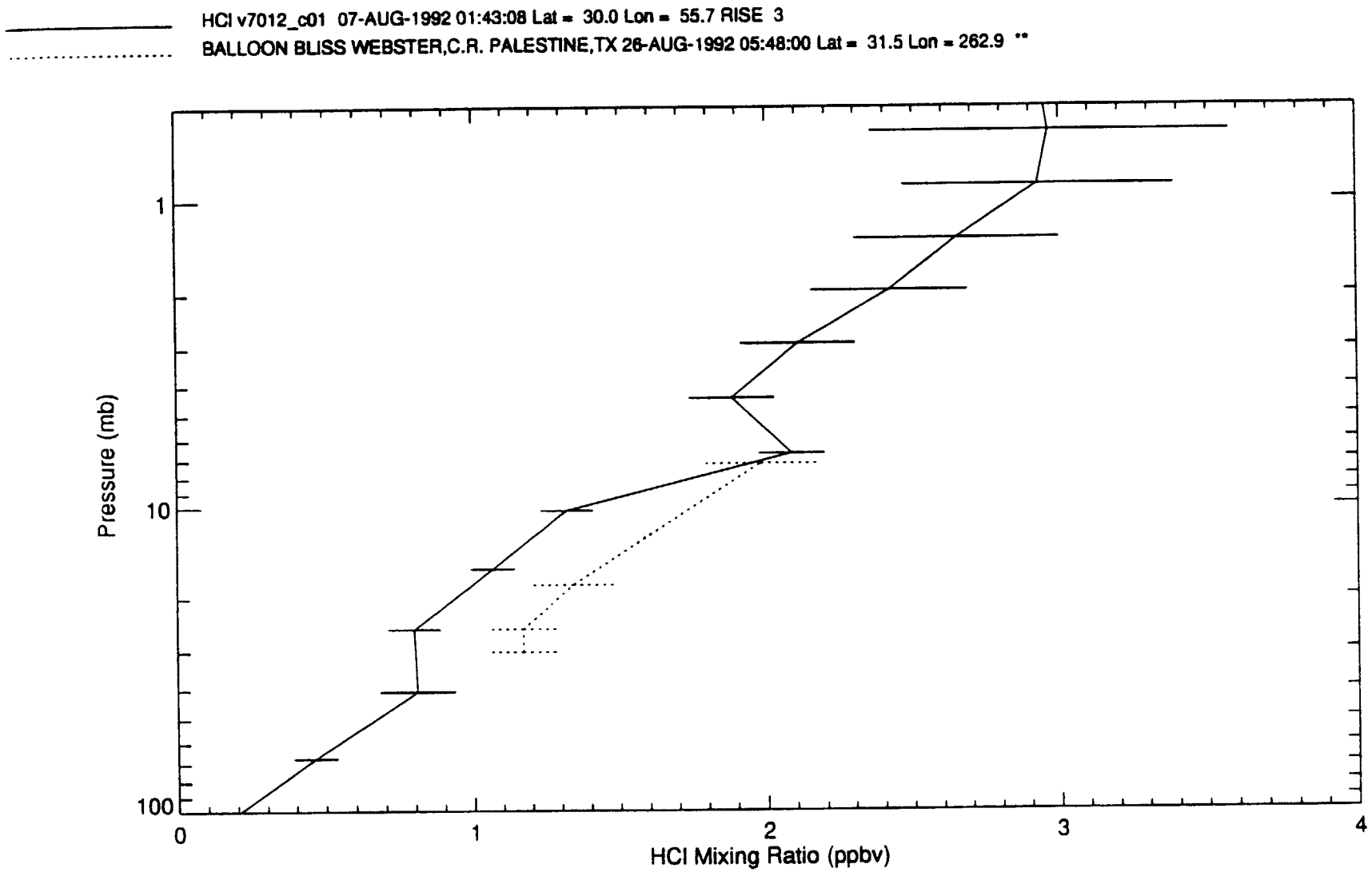

HALOE HCl Mixing Ratio 07-AUG-92 and BLISS HCl Mixing Ratio 26-AUG-92

Figure 8.3.2.2-13. The August 26, 1992 BLISS HCl mixing ratio profile and the nearest HALOE HCl profile.

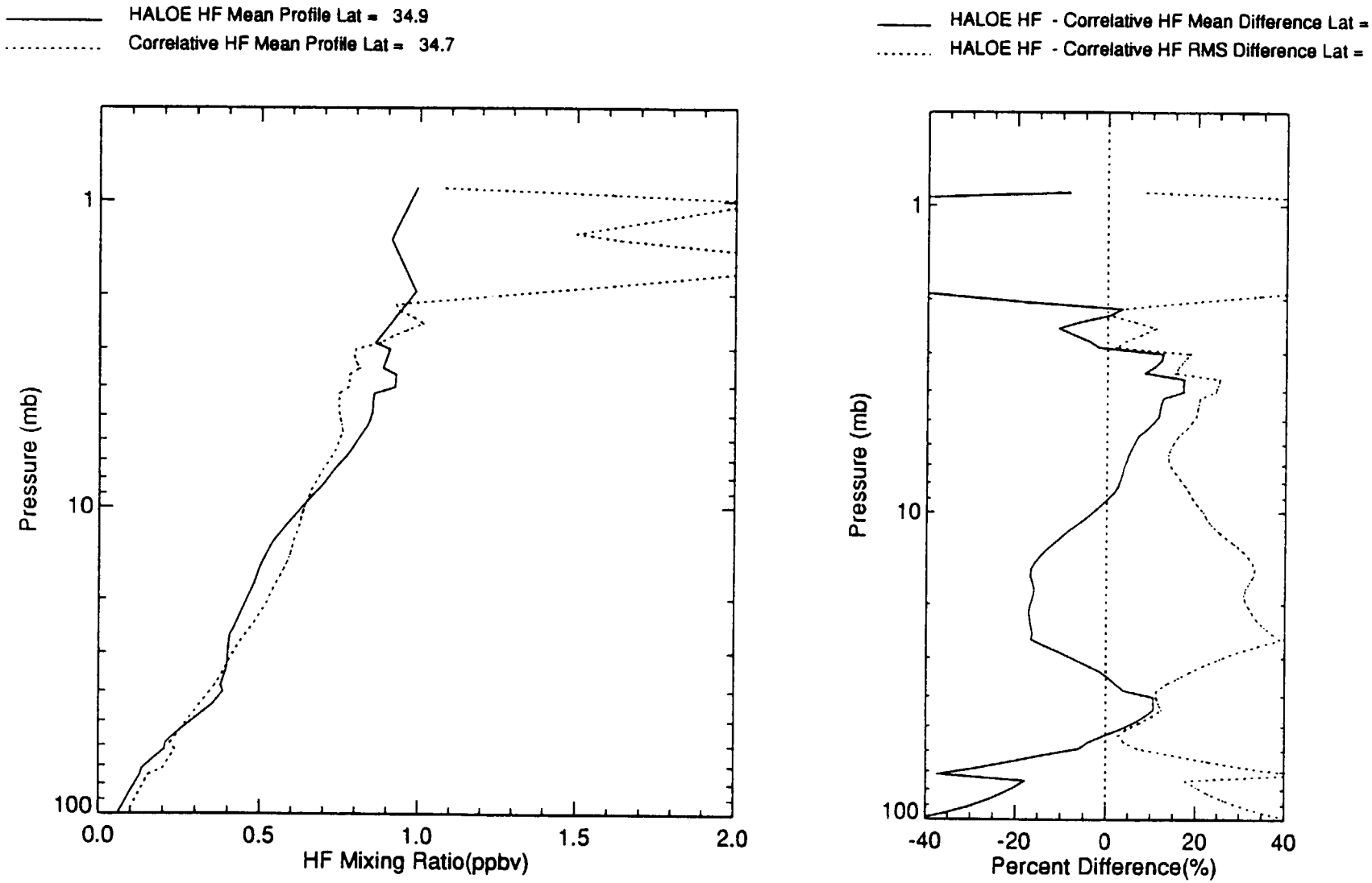

Figure 8.3.2.2-14. The HF mean profiles and statistics derived from the individual HALOE and correlative data comparisons.

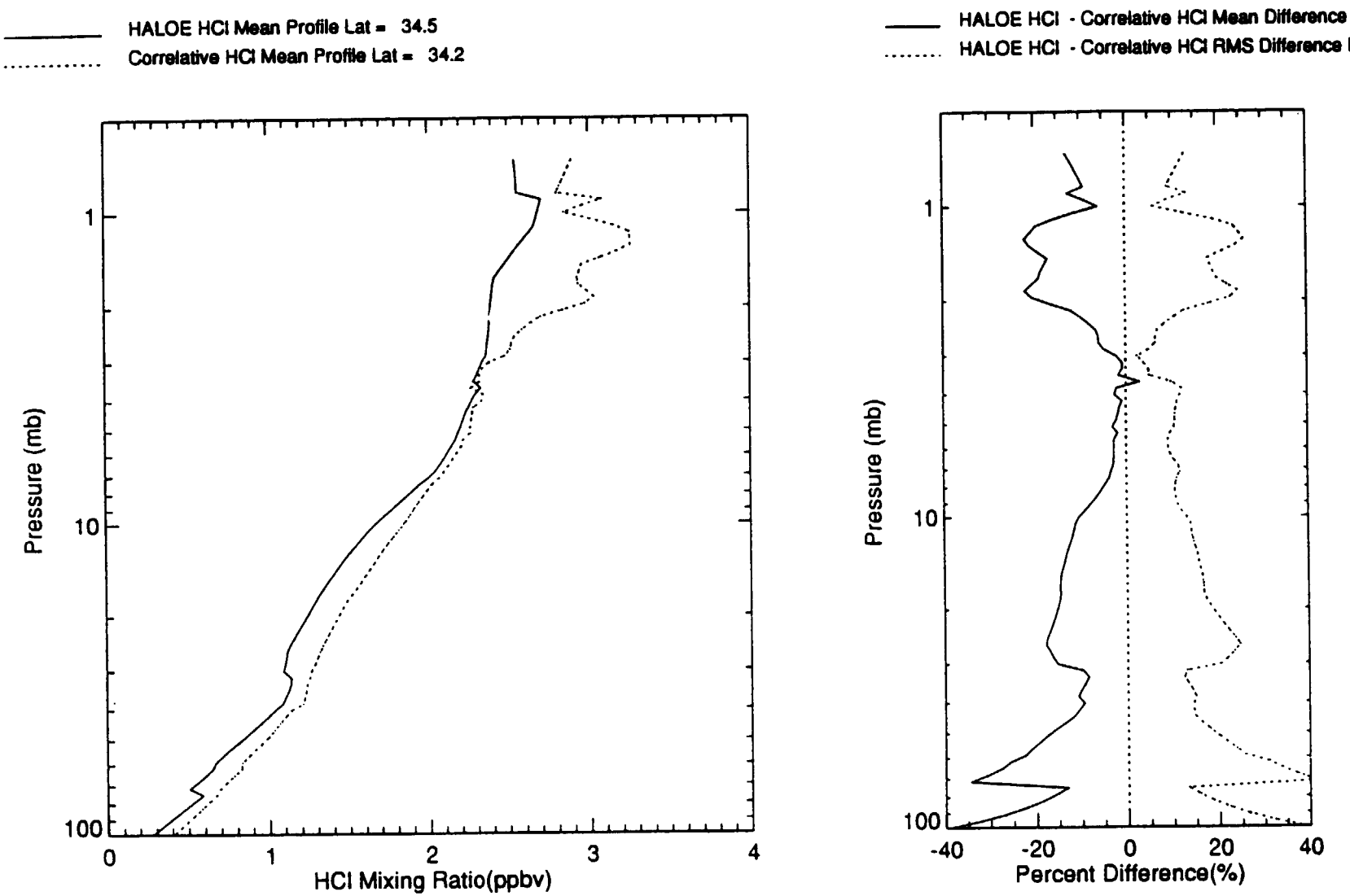

Figure 8.3.2.2-15. The HCl mean profiles and statistics derived from the individual HALOE and correlative data comparisons.

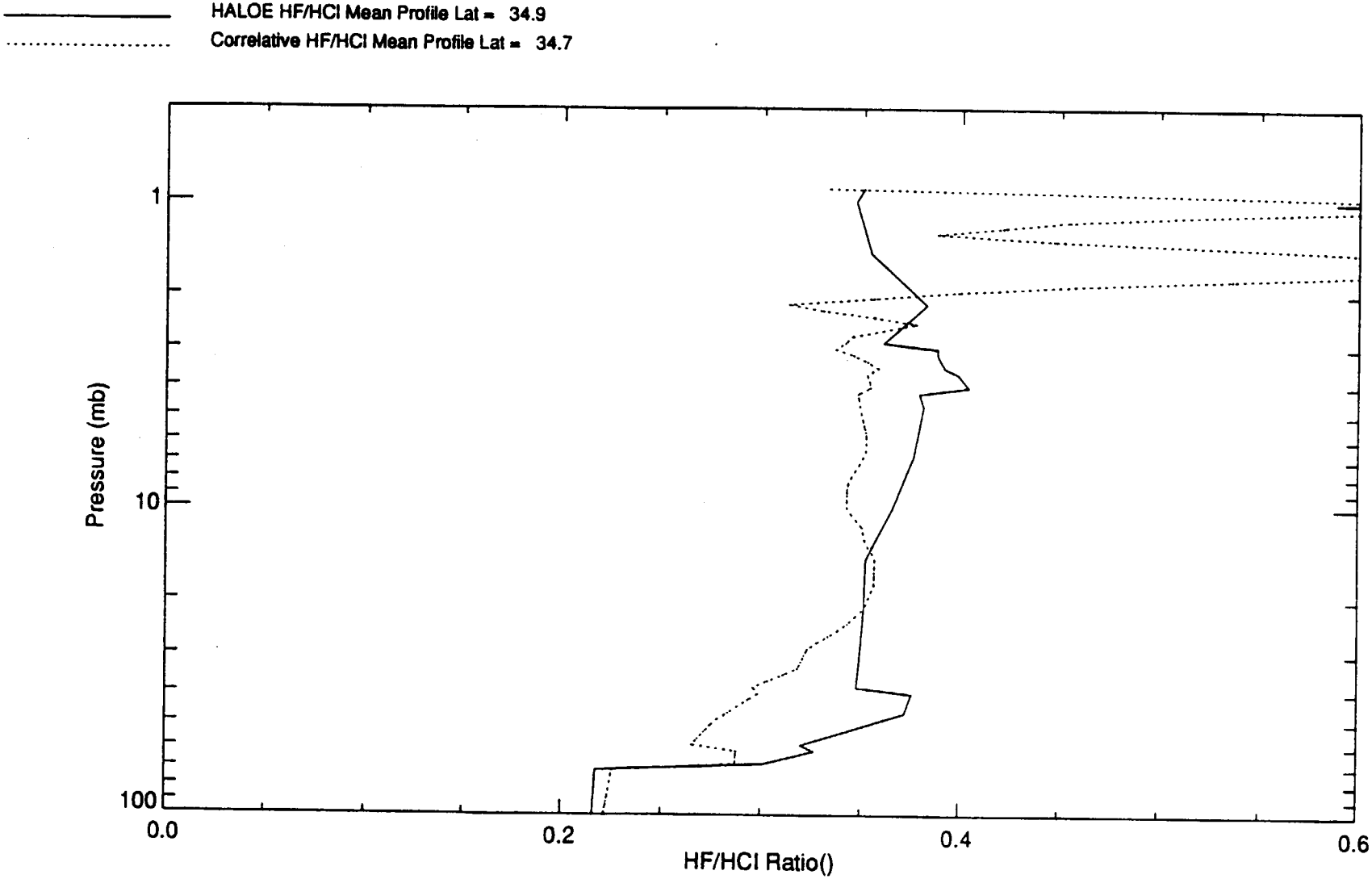

HALOE Mean HF/HCl and Mean Correlative HF/HCl from 5 Measurements

Figure 8.3.2.2-16. The HF /HCl mean profiles derived from the individual HALOE and correlative data comparison profiles.

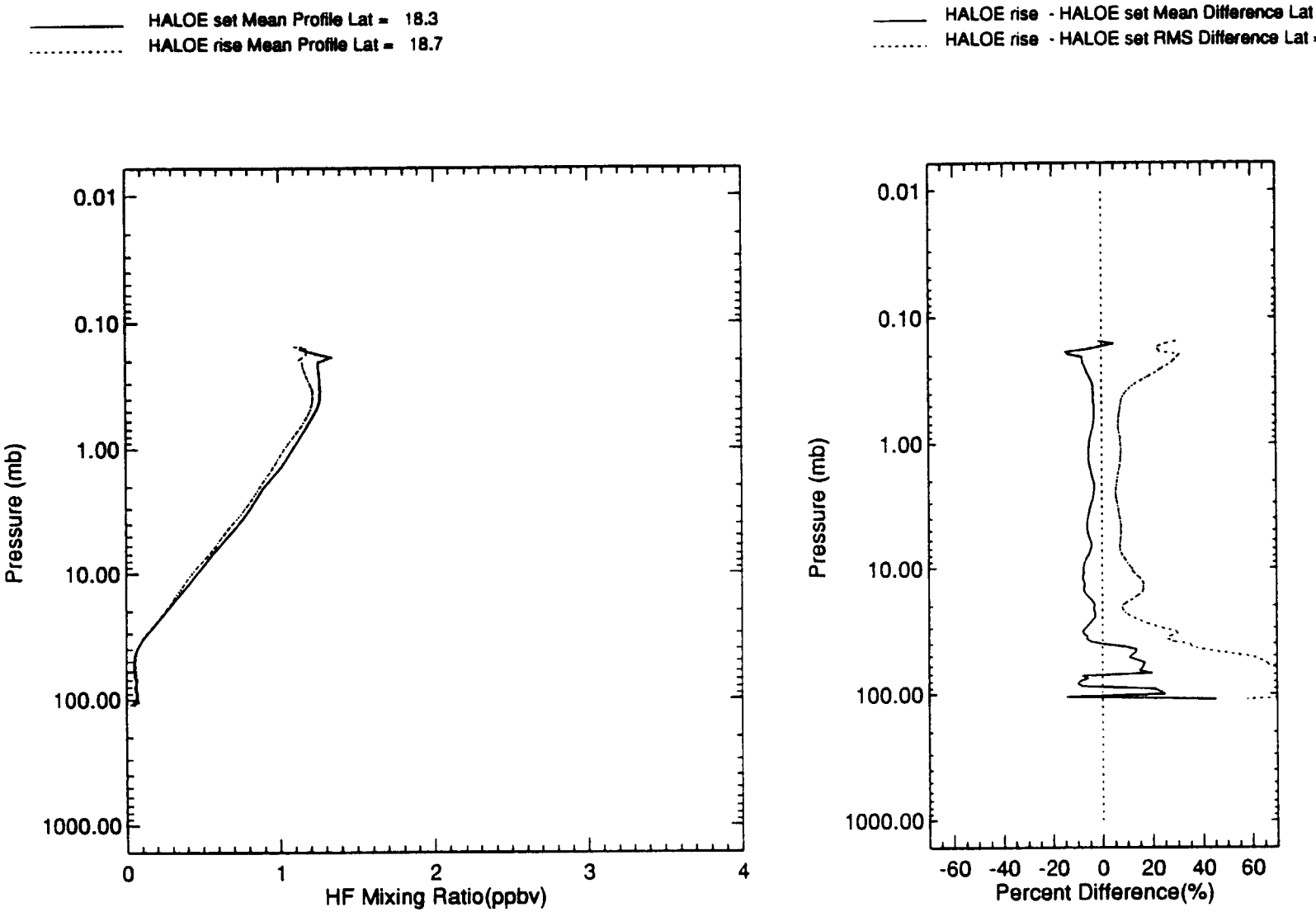

Figure 8.3.2.3-1. The mean HF mixing ratio profiles from a HALOE sunrise sunset coincident day and the mean and RMS. differences.

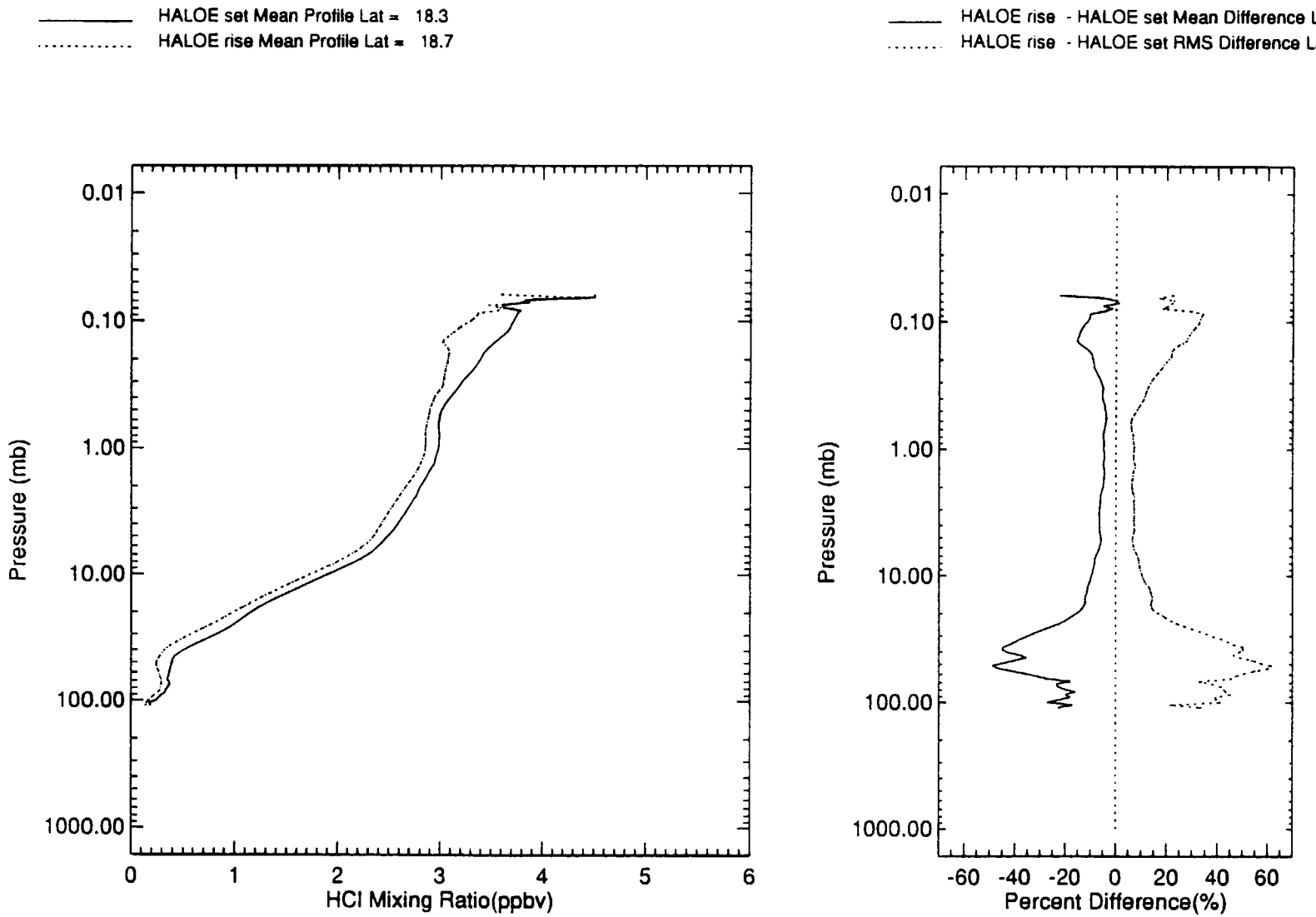

Figure 8.3.2.3-2. The mean HCl mixing ratio profiles from a HALOE sunrise sunset coincident day and the mean and RMS. differences.

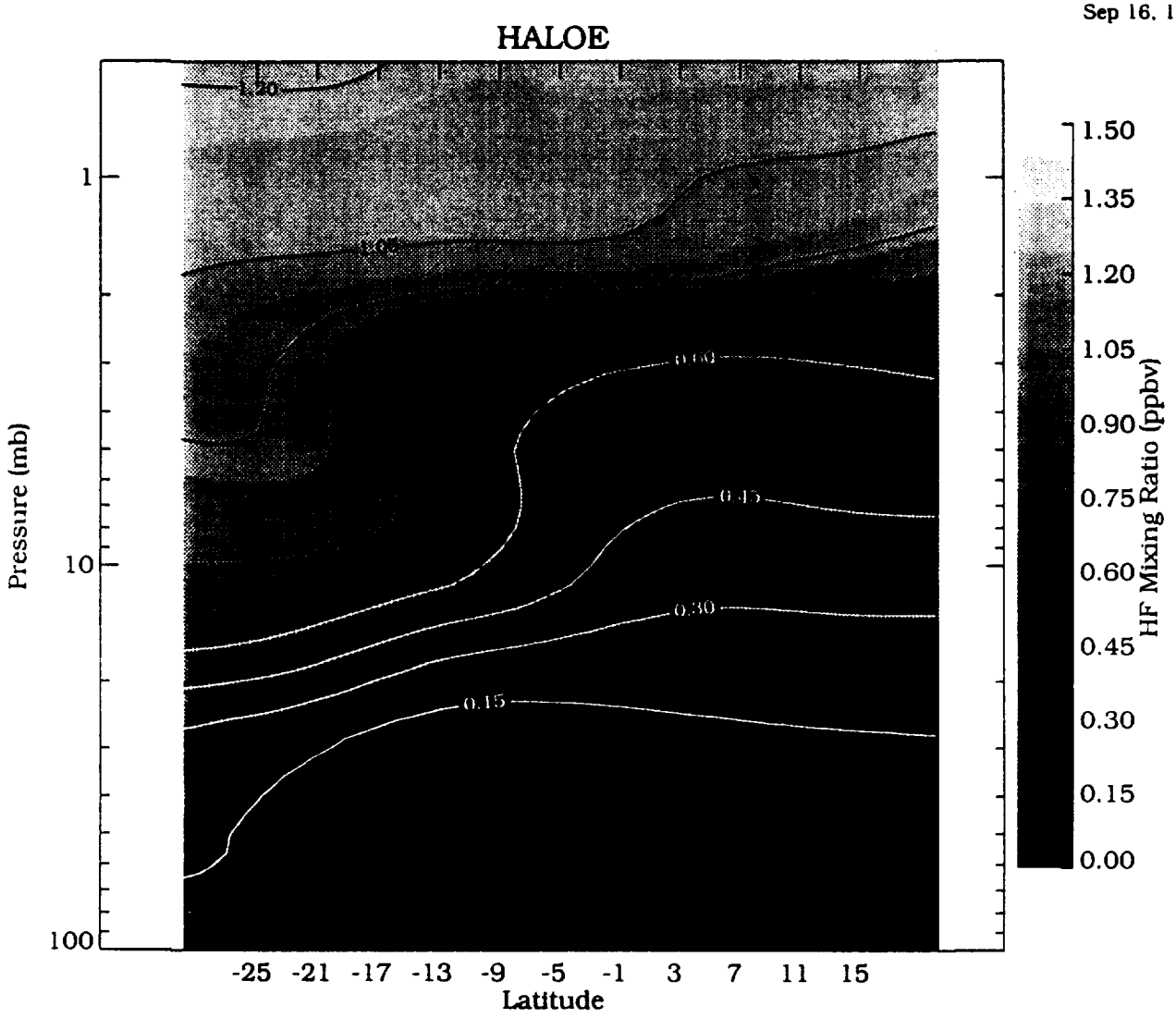

HALOE HF Pressure vs Latitude Cross Section, Sunset on 25-AUG to 30-AUG-1992

Figure 8.3.2.4-1. Pressure vs. latitude cross-section of zonally averaged HALOE HF mixing ratio for August 25-30, 1992.

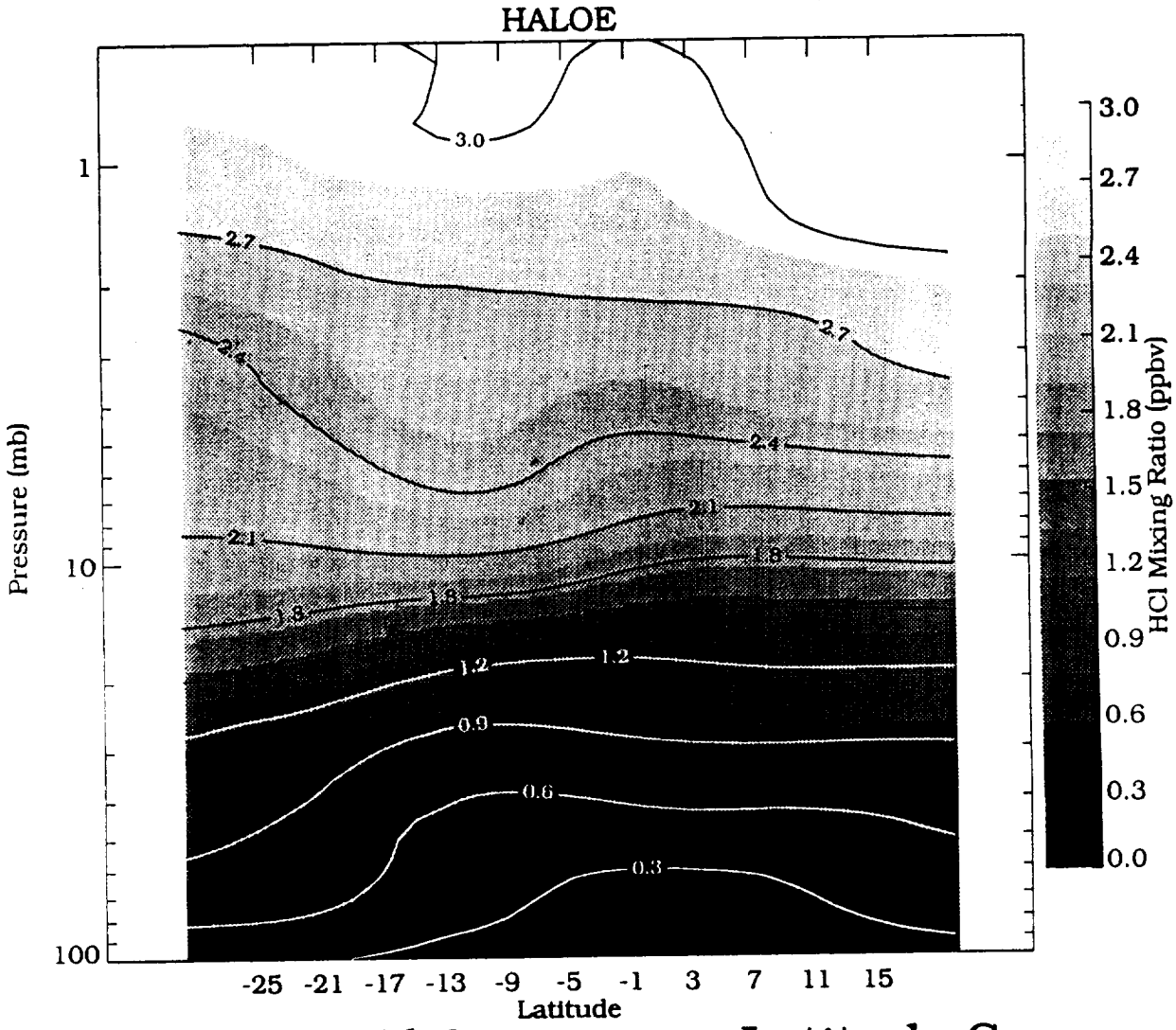

HALOE HCl Pressure vs Latitude Cross Section, Sunset on 25-AUG to 30-AUG-1992

Figure 8.3.2.4-2. Pressure vs. latitude cross-section of zonally averaged HALOE HCl mixing ratio for August 25-30, 1992.

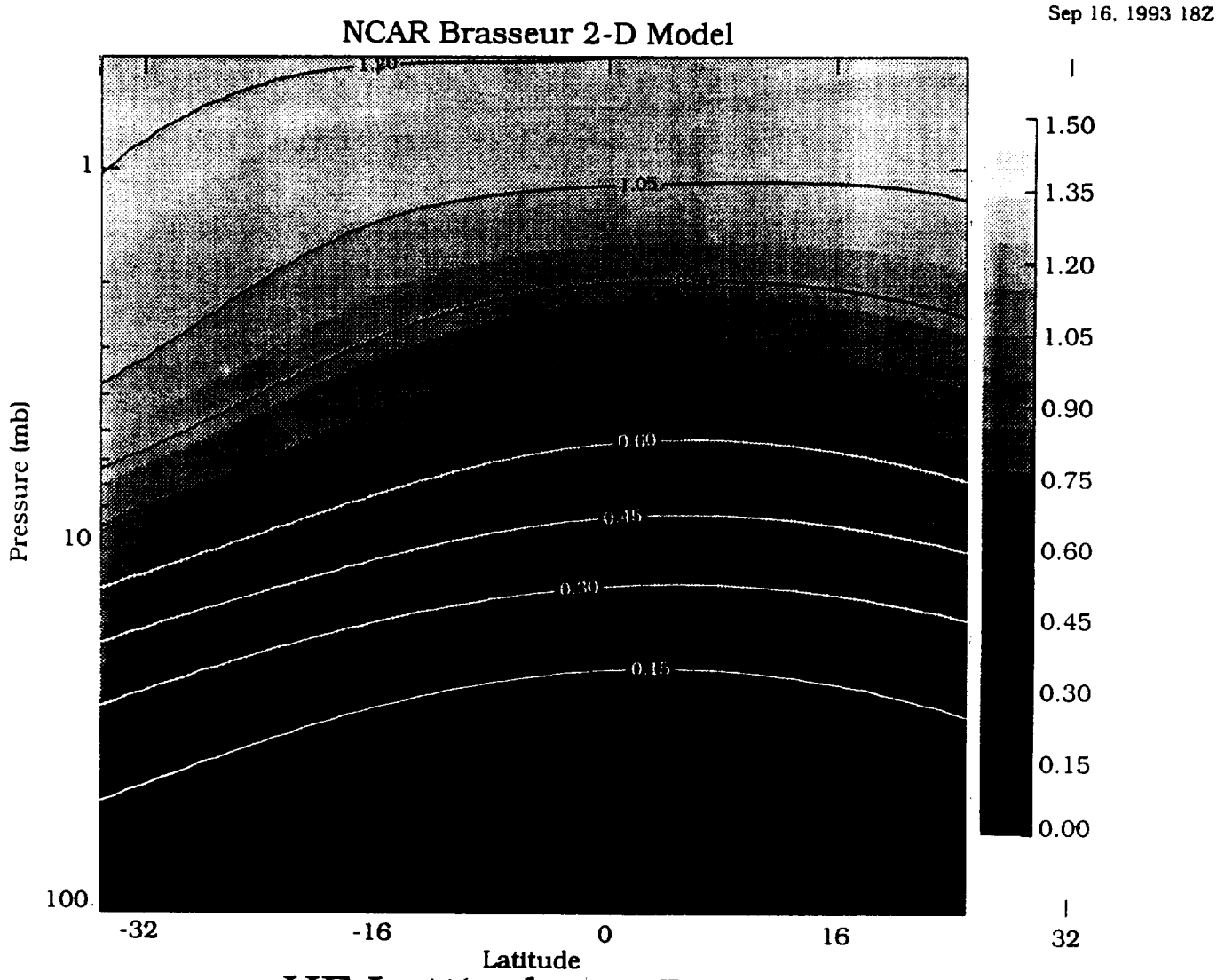

HF Latitude vs. Pressure Cross Section for August 15, 1992

Figure 8.3.2.4-3. NCAR model pressure vs. latitude cross-section of HF mixing ratio for August 15, 1992.

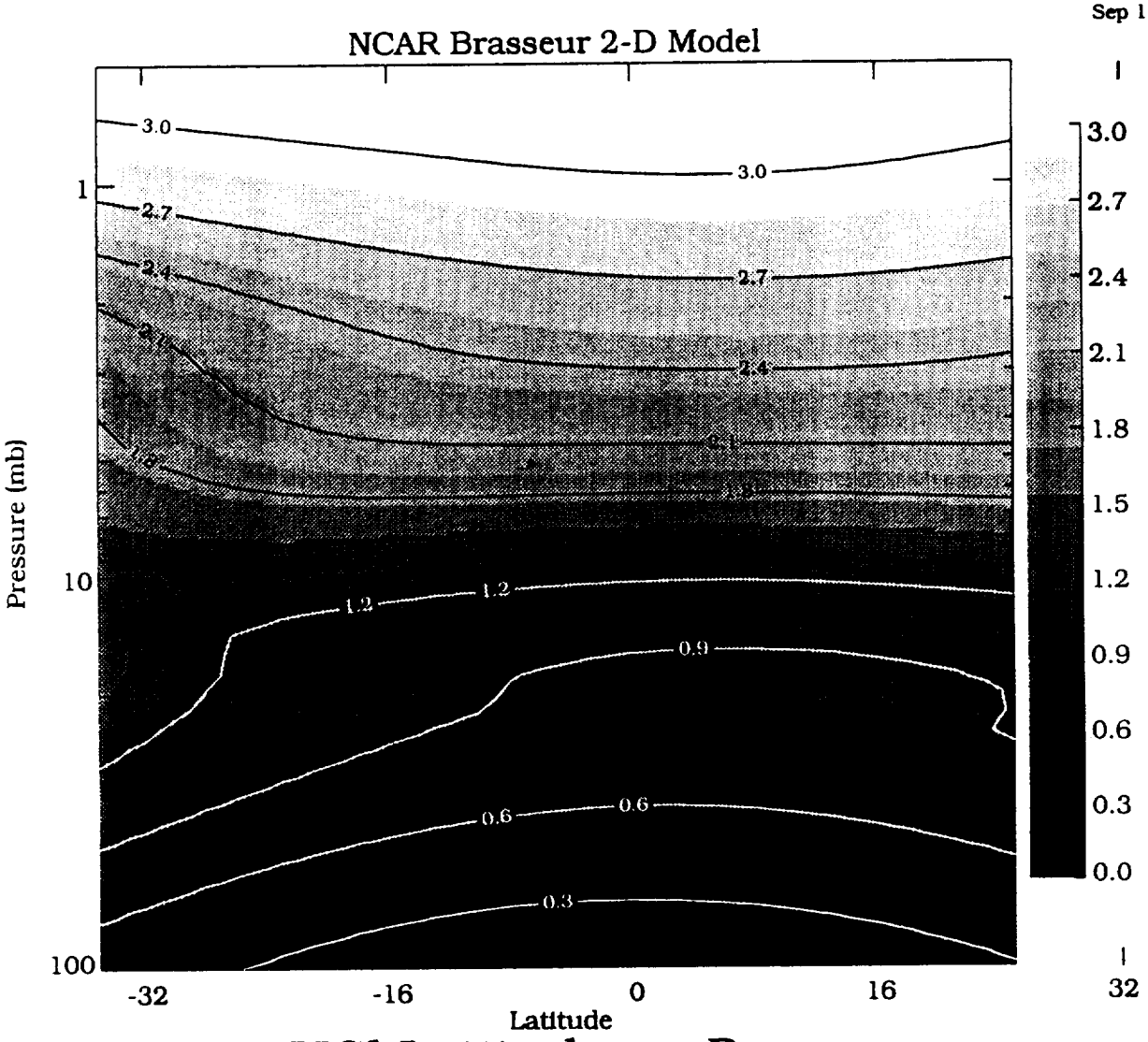

HCl Latitude vs. Pressure
Cross Section for August 15, 1992

Figure 8.3.2.4-4. NCAR model pressure vs. latitude cross-section of HCl mixing ratio for August 15, 1992.

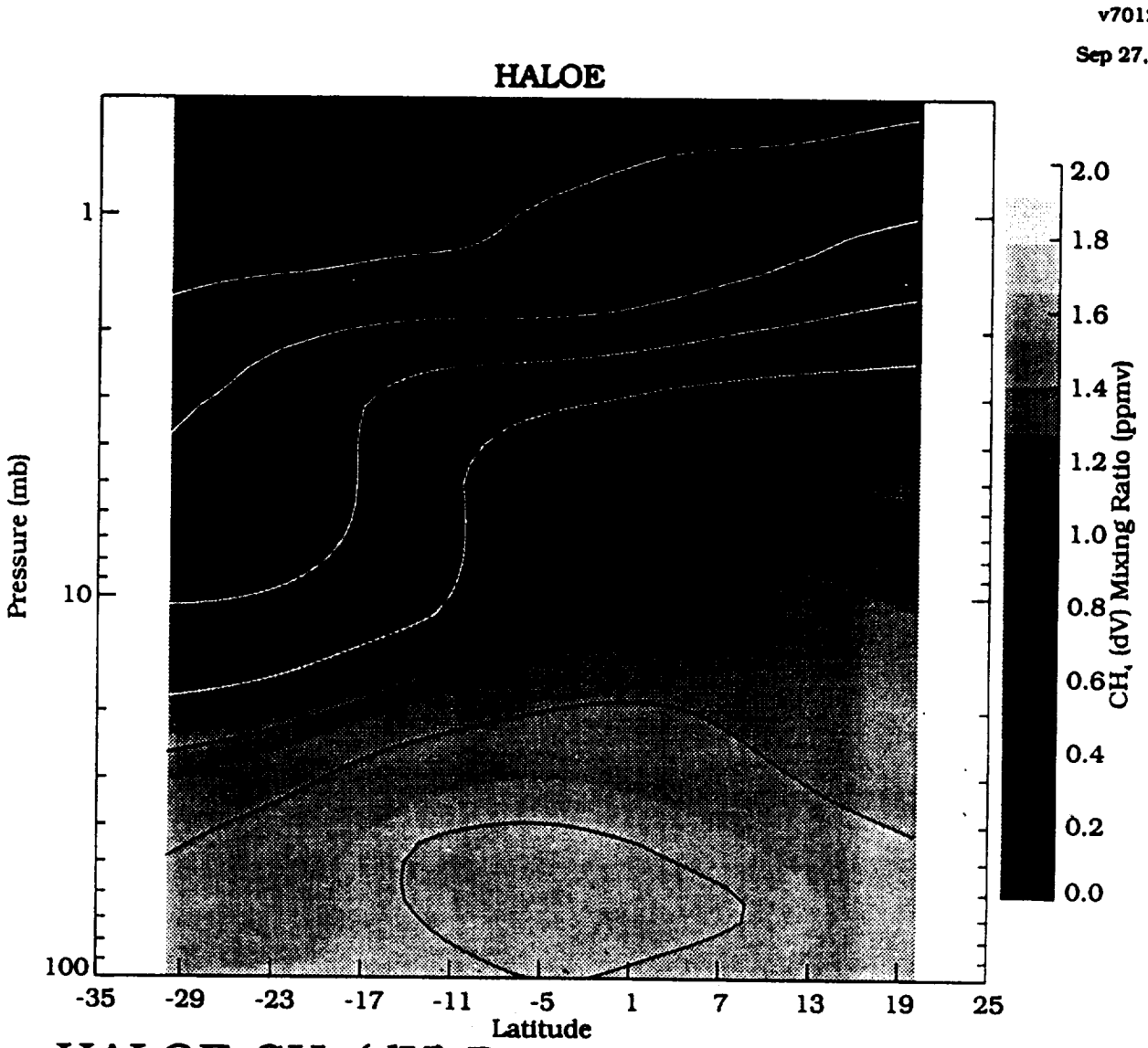

HALOE CH_4 (dV) Pressure vs Latitude Cross Section, Sunset on 25-AUG to 30-AUG-1992

Figure 8.3.2.4-5. Pressure vs. latitude cross-section of zonally averaged HALOE CH_4 mixing ratio for August 25-30, 1992.

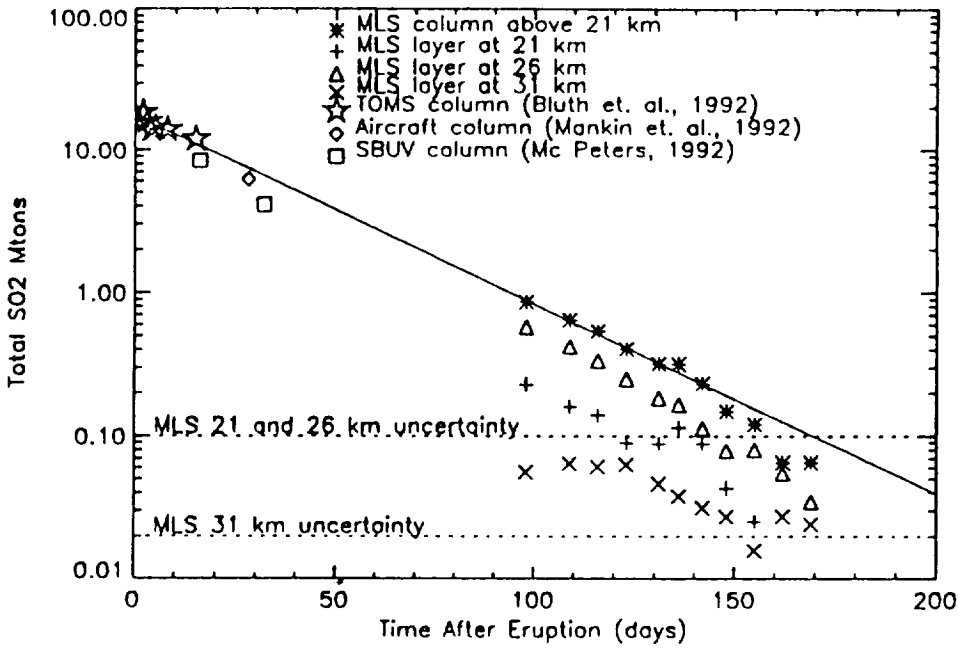

Figure 8.4.2-1. SO_2 budgets from TOMS, aircraft, SBUV, and MLS.

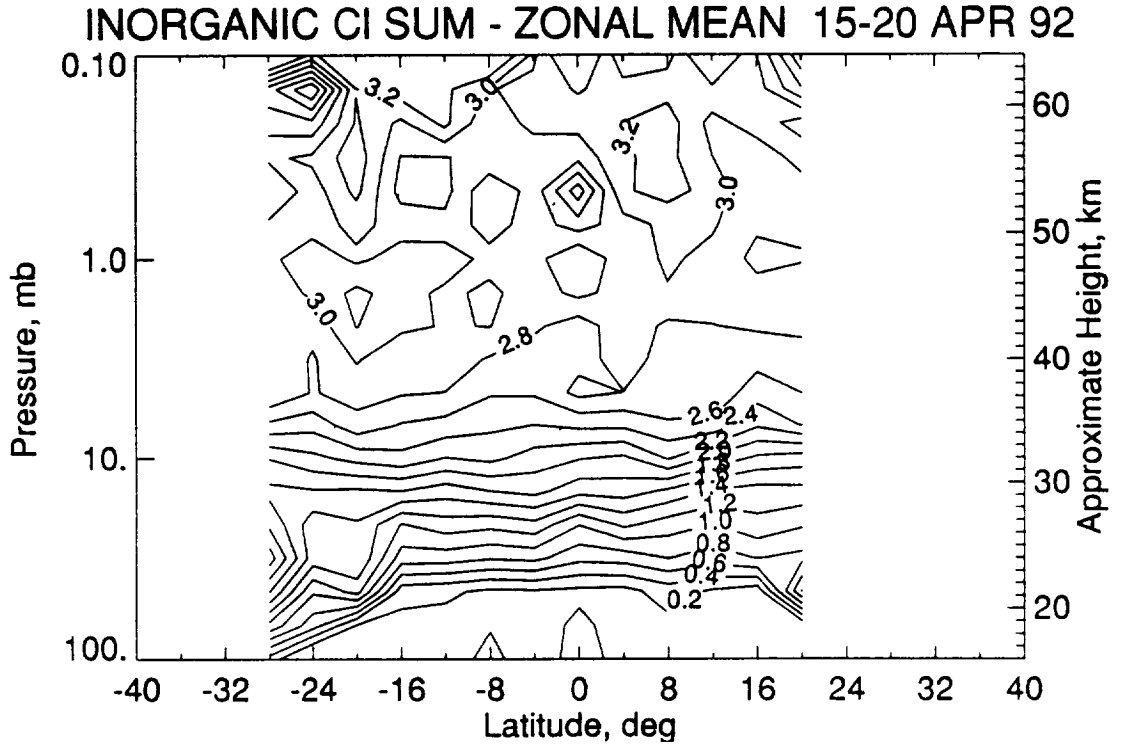

Figure 8.5.1-1. The sum of abundances of HALOE HCl, CLAES $ClONO_2$, and MLS ClO, zonally averaged over the period April 15-20, 1992 (UARS days 217-222). The ClO zonal average abundance is the difference of daytime and nighttime abundances at pressure surfaces greater than 10 hPa. For $ClONO_2$ abundance, only daytime profiles are included in the zonal average.

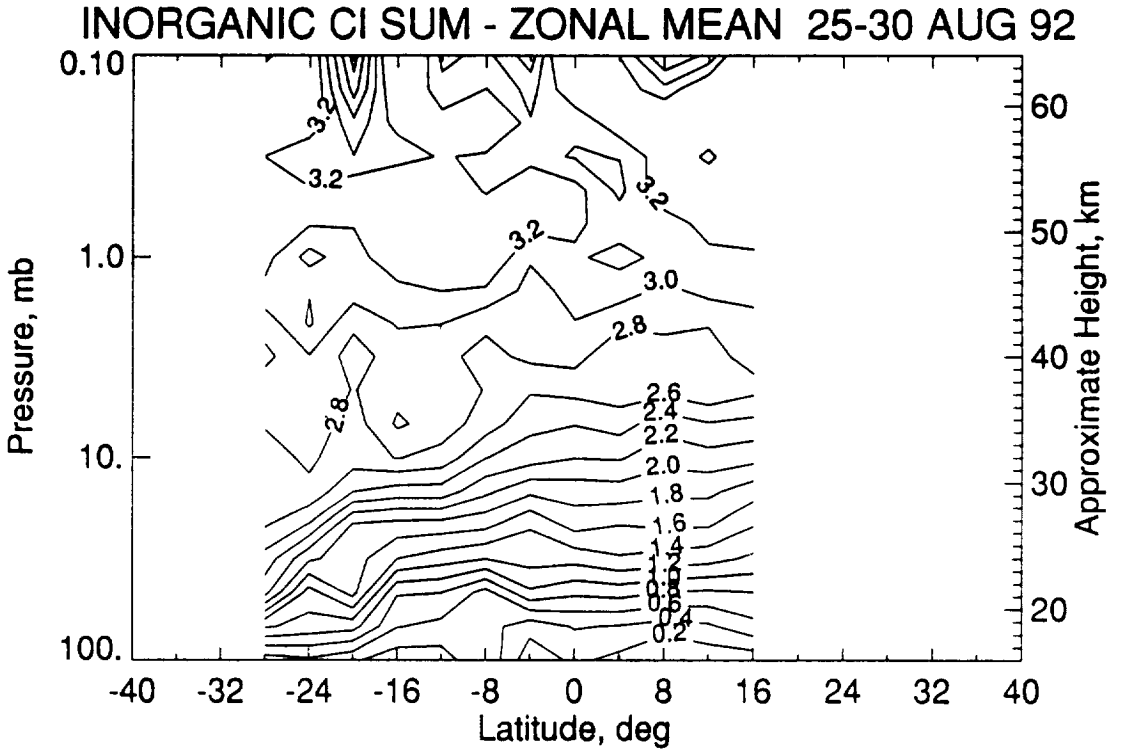

Figure 8.5.1-2. Same as Figure 8.5.1-1, but for the period August 25-30, 1992 (UARS days 349-354).

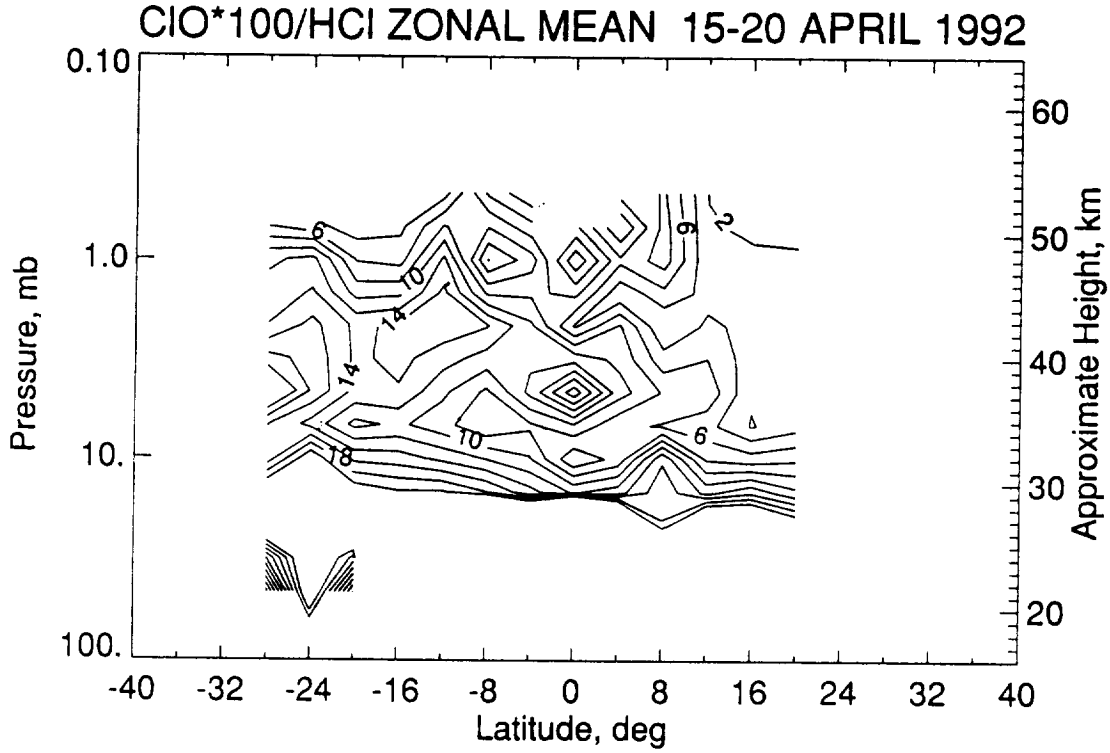

Figure 8.5.1-3. The ratio of zonal average MLS ClO abundance, evaluated as in Fig. 8.5.1-1, to zonal average HALOE HCl abundance, for April 15-20, 1992, presented as a percentage.

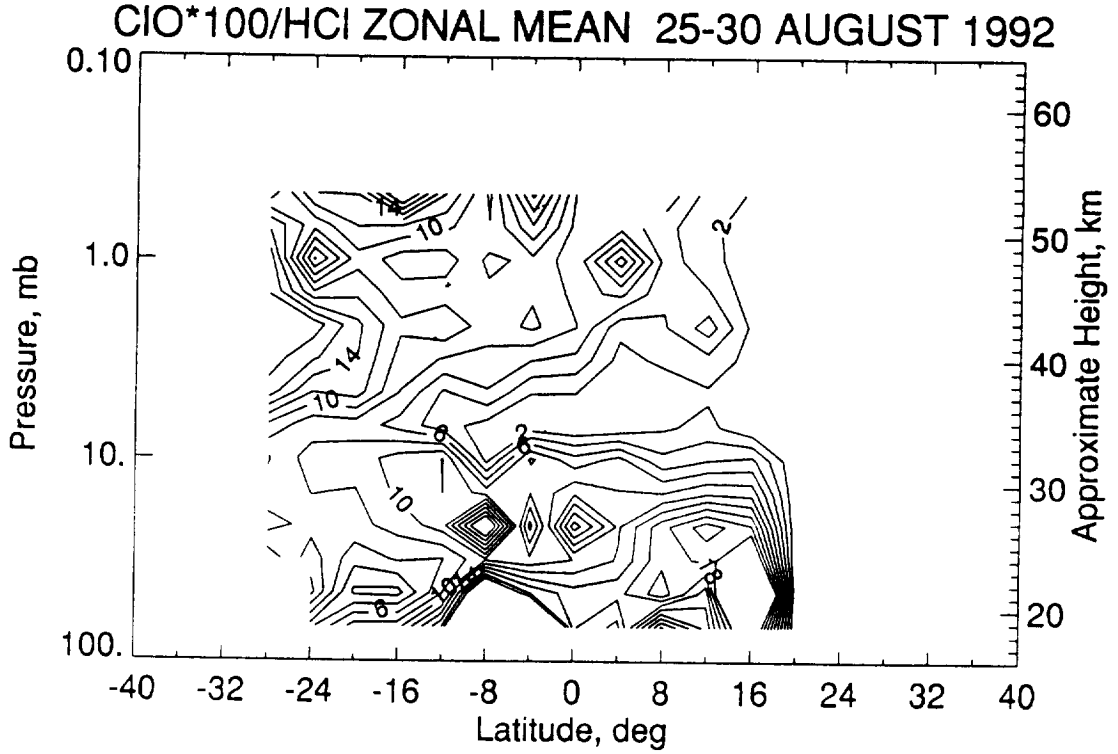

Figure 8.5.1-4. Same as Figure 8.5.1-3, but for the period August 25-30, 1992.

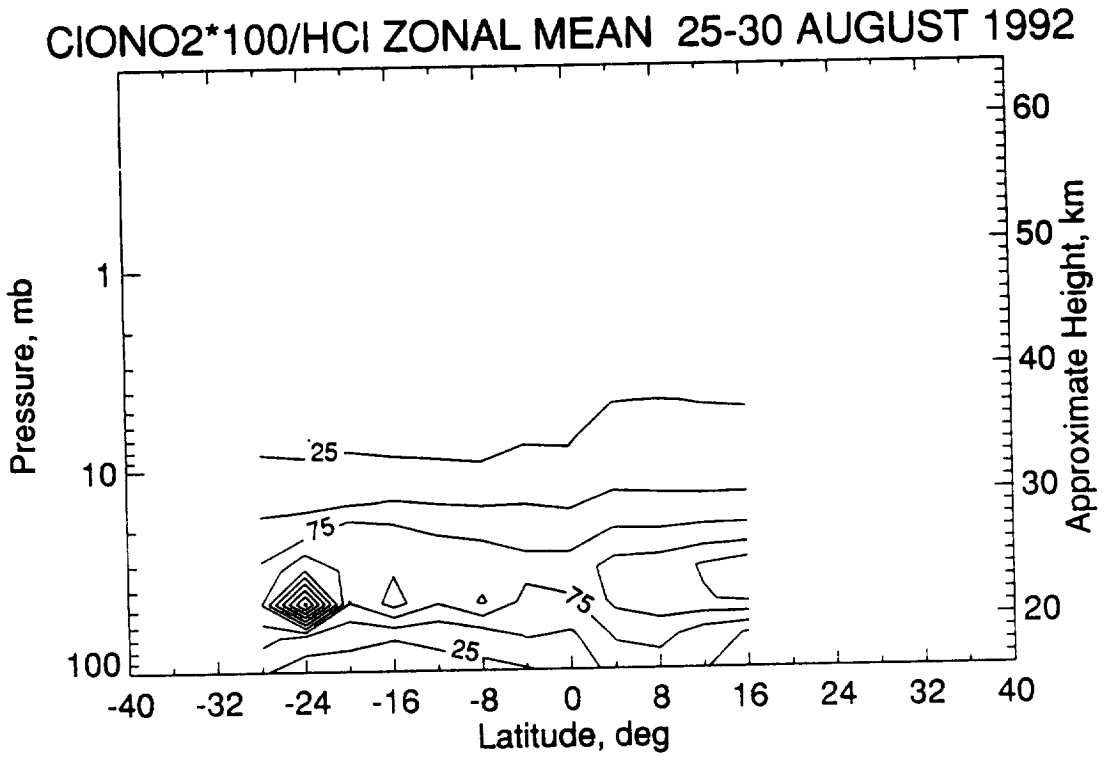

Figure 8.5.1-5. The ratio of zonal average nighttime CLAES $ClONO_2$ to HALOE HCl for the period August 25-30, 1992, expressed as a percentage.

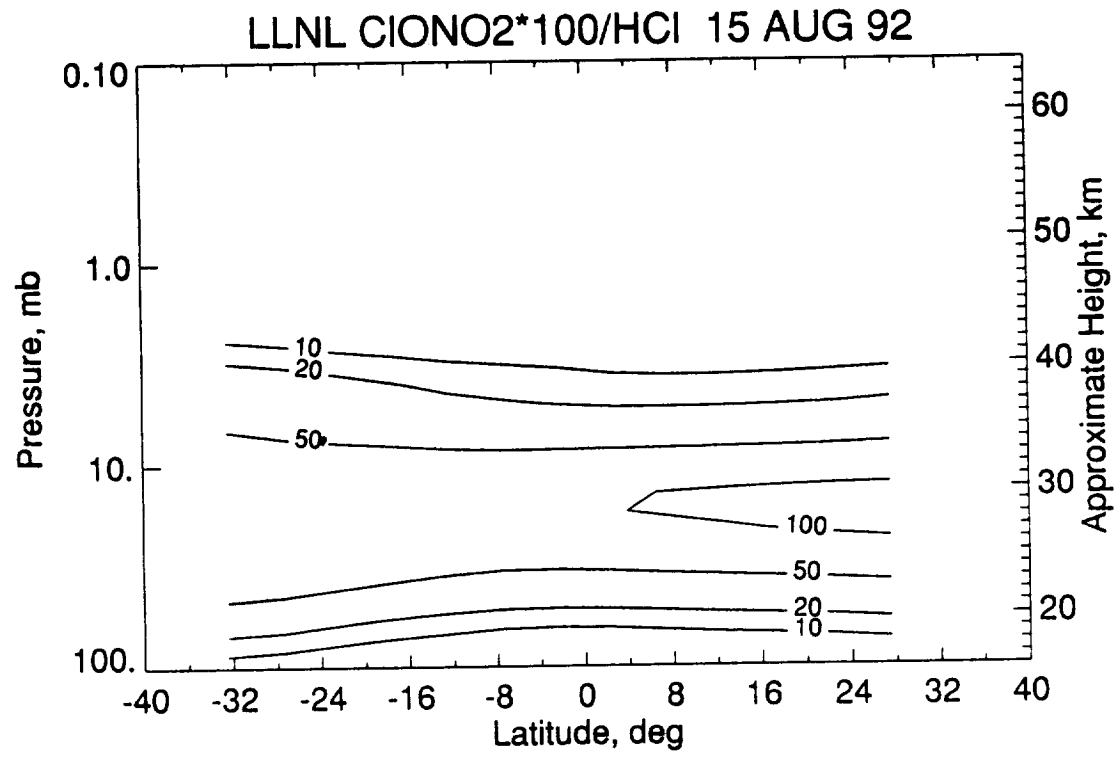

Figure 8.5.1-6. Ratio of diurnal averages of $ClONO_2$ and HCl from the LLNL 2-D model for mid August, expressed as a percentage.

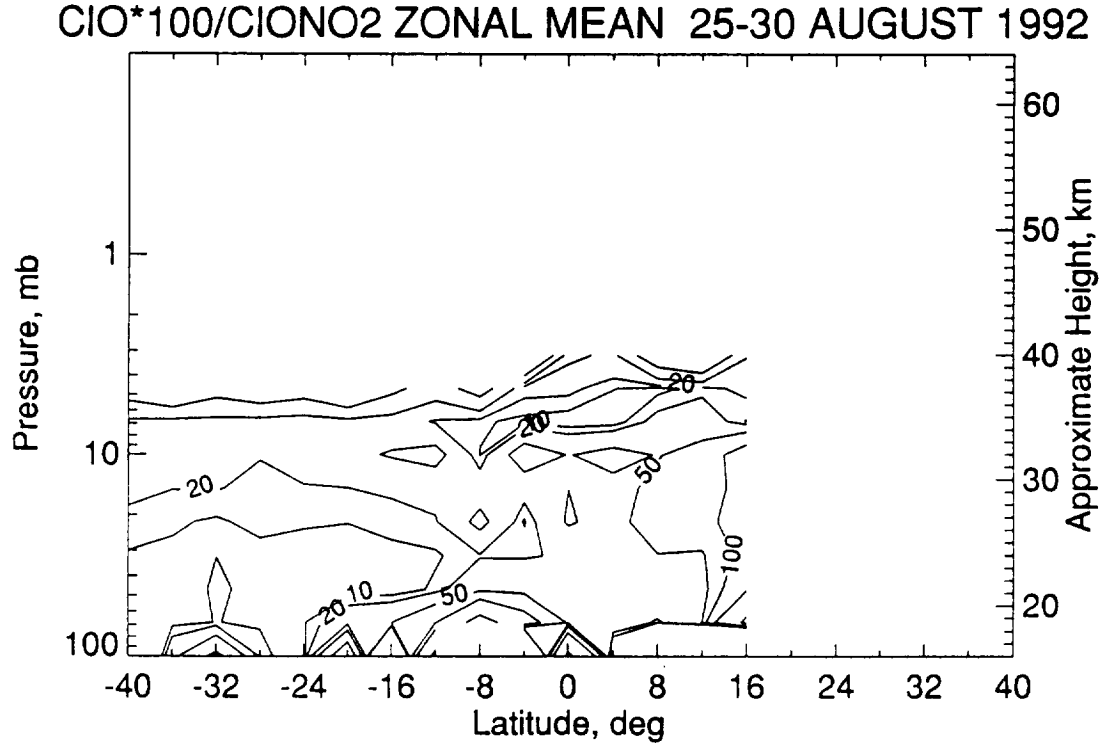

Figure 8.5.1-7. The ratio of zonal zverage MLS ClO abundance, evaluated as in Figure 8.5.1-2, to CLAES $ClONO_2$ daytime abundance for August 25-30, 1992, expressed as a percentage.

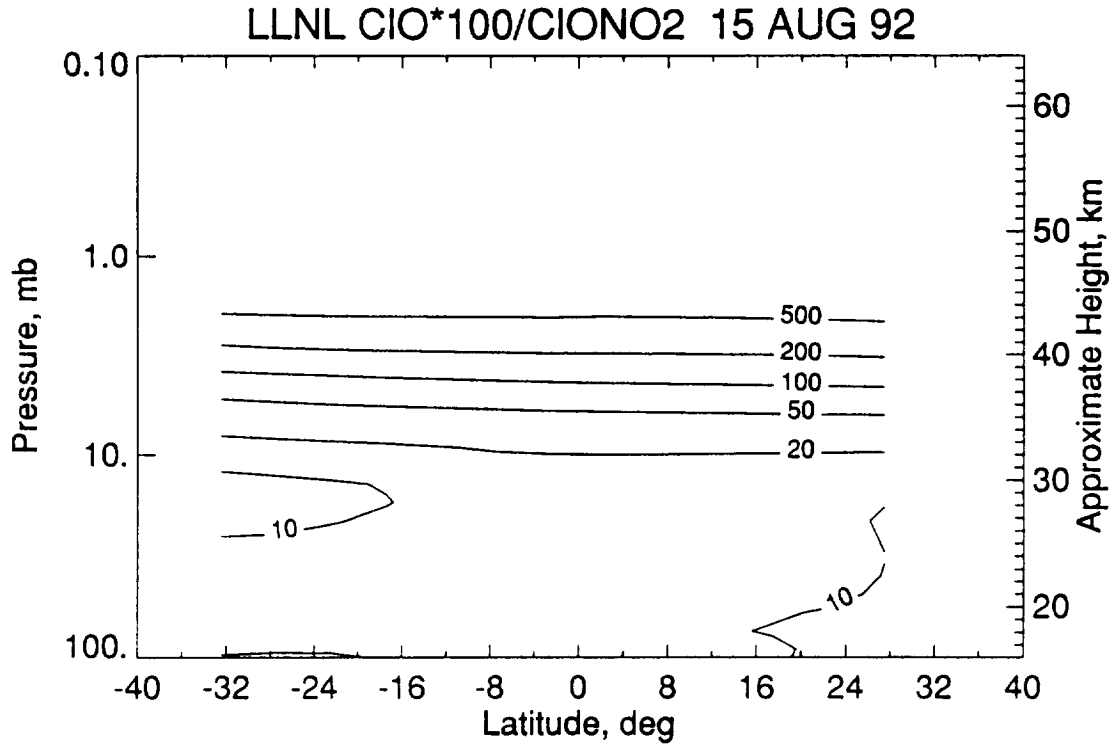

Figure 8.5.1-8. Ratio of diurnal averages of ClO and $ClONO_2$ from the LLNL 2-D model for mid August, expressed as a percentage.

9. REACTIVE NITROGEN SPECIES (NO, NO_2, HNO_3, N_2O_5)

9.1 Nitric Oxide (NO) Validation

9.1.1 Correlative Data

9.1.1.1 Coincident Measurements

There was only one coincident or near-coincident correlative data set available by the date of the workshop, September 1993. Several correlative data measurements were taken, but processed results haven't become available.

9.1.1.2 ATMOS - 1985

Nitrogen oxide profiles from the 1985 ATMOS (see description of ATMOS in previous section of this document) were compared with the UARS data. ATMOS is an interferometer used to infer transmission from orbital occultation measurements.

9.1.1.3 LIMS

LIMS was a broad-band radiometer aboard NIMBUS 7 that made limb emission measurements for inferring temperature, pressure, O_3, H_2O, HNO_3 and NO_2. NIMBUS 7 was inserted into a sun-synchronous polar orbit that resulted in LIMS equatorial measurements at local times of approximately 2:30 p.m. and 10:30 p.m. Night-time LIMS NO_2 was used as a proxy for total NO_X for comparison with HALOE NO_2 + NO. With NO_2 comparisons to ATMOS looking quite good, this might lend some confidence to NO results.

9.1.2 Comparison Results

The three UARS instruments with channels for NO inferrals are CLAES, HALOE and ISAMS. CLAES and ISAMS are limb emission sensors, and both experienced large NO channel signals from high altitudes due to non-LTE effects. Unfortunately, these altitudes are above the highest tangent altitudes viewed by either instrument. The inability to accurately correct for these signals has made retrieval results uncertain, especially at upper altitudes.

The ISAMS NO channel data has not been processed for the above reasons. However, signals look reasonable, and future releases will include an analysis to address the problems stated above.

The CLAES NO channel data are being processed with some encouraging results. Mid-stratosphere daytime results look reasonable with regard to expected climatology, expected diurnal dependence, and day-to-day consistency. There is no apparent contamination by aerosol. However, upper altitude results (above 1 mb) appear to be too large due to the high altitude radiance and a DC zero level offset problem that should be corrected in future releases.

The HALOE instrument does not have these difficulties, for several reasons. First, it is a transmission measurement of a fundamental vibrational band. Therefore, it is dependent only on ground state population densities which are relatively unaltered by non-LTE effects. Second, the atmospheric temperature uncertainty is a much smaller effect for transmission measurements. Third, the measurements are continuous from outside the atmosphere through occultation, allowing high altitude retrievals. The comparison difficulties encountered with HALOE data are primarily due to the natural limitation of occultation to only sunrise and sunset. Besides limited coincidence,

the diurnal variability of NO introduces additional difficulties. However, from all indications to date, the HALOE NO data look good with retrievals extending from 15 to 130 kilometers. Mixing ratio uncertainty at altitudes above 80 kilometers is largely due to temperature and pressure uncertainties, but implied densities should be reasonable. The data show expected seasonal, spatial and temporal (sunrise/sunset) variations with high altitude data correlated with aurora and solar flux levels (these studies are in progress). Upper mesospheric levels sometimes dip below instrument sensitivity, but stratospheric and thermospheric levels are always well above signal-to-noise (see Figures 9.1.2-1 and 9.1.2-2). Figure 9.1.2-2 shows a mean tropical profile with a precision estimate profile (dashed).

9.1.2.1 Profiles

Due to diurnal variability, only HALOE versus ATMOS profiles were compared, since they are both occultation experiments. A HALOE versus ATMOS profile is shown in Figure 9.1.2.1-1. There is very good agreement, but HALOE shows a lower altitude and lower value of the mixing ratio peak and falls off below the peak with nearly identical vertical slope and magnitude. The reader should see the NO_2 validation section and note that the 1985 ATMOS NO_2 shows similar differences with HALOE NO_2, yet the 1992 ATMOS comparisons show very good agreement. This behavior could arise from a temporal change in NO_X.

9.1.2.2 Cross-Sections

The CLAES and HALOE cross-sections for the January period are shown in Figures 9.1.2.2-1 and 9.1.2.2-2. The CLAES cross-sections show realistic values in the low- to mid-stratosphere, but increase to unrealistic values at high altitudes for reasons discussed above. The lower stratosphere, zonal features of the CLAES and HALOE data are similar, but the diurnal behavior of NO makes it difficult to come to any firm conclusions. HALOE sunrise NO would be expected to be lower than CLAES daytime NO, as observed. As expected for high-latitude, winter profiles, there is not a well defined mesospheric minimum.

Figures 9.2.2.2-8 and 9.2.2.2-9 present a LIMS night-time, zonal mean NO_2 cross-section for May 5, 1979 and a HALOE (NO_2 + NO) cross-section for April 21 through May 30. 1993, respectively. Even considering the expected asymmetries, the limited validity of comparing sunset (NO + NO_2) to 10:30 p.m. NO_2 (LIMS should be less), and the 13 year difference, the magnitudes and morphology appear very similar.

9.1.2.3 Time Series

Time-track plots are used to compare retrievals along the Level 3AT (L3AT) tangent point measurement track of the cold side, 90 degree looking CLAES and MLS instruments, and ISAMS for those times when it is pointed towards the cold side. These data are obtained with 65 second (1 EMAF) resolution on standard UARS pressure surfaces. The time-tracks are useful for establishing consistency of structure observed from one orbit to the next and for a top level view as to whether instruments are observing similar structure as a function of position on the orbit.

In subsequent figures, one must be careful in interpreting the instrument data because the plotting routine connects points with a straight line. If one is not cognizant of this fact, data gaps that occur on one orbit, but not the next, may erroneously be interpreted as showing a difference in structure. The orbital structure of the temperature data is generally dominated by latitudinal variation, but over the course of a day the longitudinal variation can play a large role.

For NO intercomparisons, only CLAES data were available at the time of the workshop. Several time-track plots were generated from CLAES data to support the intercomparison. CLAES data for January 9 on the 2.15 and 0.464 mb surfaces are shown in Figure 9.1.2.3-1. The top panel shows the latitude and the solar zenith angle for the tangent points along the track as a function of time (GMT). The middle panel shows the comparison with the UARS pre-launch climatology at 2.15 mb, and the bottom panel shows the comparison at 0.464 mb.

It is seen that there are large data gaps during night-time conditions. There is no apparent problem since no NO is expected to be present in the stratosphere during the night-time. During the day, the retrieved NO is noisy, but on average is in good agreement with climatology. Considering problems of single-profile signal-to-noise, the requirement to subtract high altitude contributions from the radiance data, and the possibility of non-LTE effects in the stratosphere, the agreement with climatology is remarkable.

9.1.3 Sensitivity to A Priori Assumptions

The HALOE processing uses no climatology. The onion peel retrieval procedure assumes a constant mixing ratio above the highest retrieved altitude. The effect of this assumption is small and confined to the uppermost 10 kilometers (>120 km). The CLAES retrievals were tested for a priori sensitivity by doubling the climatological profile, resulting in less than 10% change in NO results.

9.2 Nitrogen Dioxide (NO_2) Validation

9.2.1 Correlative Data

9.2.1.1 ATMOS - 1985 and 1992

ATMOS is an interferometer used to infer transmission from orbital occultation measurements. Nitrogen oxide profiles from the 1985 and 1992 ATMOS data were compared with the UARS data.

9.2.1.2 FIRS-2

The Smithsonian Astrophysical Observatory's Far-Infrared Spectrometer (FIRS-2) measures mixing ratio profiles of 13 constituents and 10 isotopomers, as well as pressure and temperature. The instrumentation comprises a collecting telescope with a field of view of about 0.3 scale height, a stabilized pointing platform, an emission Fourier transform spectrometer with an unapodized resolution of 0.004 cm^{-1}, and liquid helium cooled photoconductor detectors for the far-infrared (Ge:Ga, 80 to 210 cm^{-1}) and mid-infrared (Ge:Cu, 350 to 700 cm^{-1}), all mounted on a balloon-borne platform at about 39 km altitude. Stratospheric spectra are obtained sequentially at 7 discrete elevation angles corresponding to effective altitudes from approximately 16 to 44 km, or pressures from 100 to 3 mb, with a resolution of 0.5 scale height. For the UARS intercomparison, spectra from successive 50 minute limb-scan sequences are co-added and averaged, giving a typical sample window of 8 hours in time. Owing to the long slant path of the limb-scan method, as well as the drift of the balloon during the sample window, the effective sampling area is roughly 4° in latitude by 4° in longitude.

The following 21 quantities are measured, including isotopomers [-] and median uncertainties (-): temperature (0.3 % or 0.7 K), H_2O [18] (2%), H_2O [17] (3%), CO_2 (3%), pressure (3%),

O_3 (4%), HNO_3 (4%), HCl (4%), O_2 (5%), H_2O (6%), HDO (6%), N_2O (7%), O_2 [16,18] (8%), O_3 [16,16,18] (8%), OH (11%), HOCl (13%), HF (16%), O_3 [16,18,16] (18%), HO_2 (24%), H_2O_2 (28%), and NO_2 (35%). The indicated relative 1-sigma uncertainties include random systematic effects.

9.2.1.3 BLISS

The Balloon-borne Laser In Situ Sensor (BLISS) instrument is a high resolution (0.0001 cm^{-1}) absorption spectrometer operating in the mid-infrared wavelength region using tunable diode laser (TDL) sources. The instrument probes in situ a region of the stratosphere away from the gondola by sequentially transmitting TDL beams from each diode laser to a retroreflector suspended 200 m below the instrument gondola. The BLISS instrument measurement concept, operational details, and data reduction procedures have been described in the literature references (Webster and May, 1987; May and Webster, 1989; Webster et al., 1990).

Volume mixing ratios of NO_2, CH_4, HNO_3, and HCl have been determined for night-time conditions for August 26, 1992 following balloon deployment from Palestine, Texas. These data were obtained for the altitude range of 23 - 33 km. Three measurements for NO_2 were obtained at approximately 0.7, 0.9 and 3.0 mb. These measurements are compared to CLAES data in Figure 9.2.2.1-4 . Since only one species can be measured at any given time, the discrete measurements are obtained at altitude points that are considerably further apart than the intrinsic 0.2 km resolution of the instrument.

9.2.1.4 MKIV

The MKIV instrument is a high resolution infrared solar absorption interferometer that measures the spectrum from 650 cm^{-1} to 5500 cm^{-1}. The principle investigator is Dr. Geoffrey C. Toon of JPL. Several balloon flights in support of UARS were made. The instrument has the potential of measuring most of the species measured by UARS instruments.

9.2.1.5 SAGE II

SAGE II was launched at the end of 1984 and has been making measurements continuously since. SAGE II uses a limb viewing solar occultation technique similar to HALOE. Sunrise and sunset observations of ozone mixing ratio and aerosol extinction at 1.02, 0.52, 0.45 and 0.38 nm are available on the CDHF. Sunset observations for NO_2 are included in that data set. The observations are retrieved at one km intervals in altitude and then converted to pressure levels using NMC temperatures. It should also be noted that the NMC temperature profile is an integral part of the SAGE II retrieval procedure (it is used to obtain the molecular scattering contribution to the observed radiances).

In mid-1989, minor deterioration of the SAGE II scan mirror mechanism was noted with a resultant increase in SAGE II noise levels affecting the profile retrievals at low signal-to-noise levels (e.g., ozone above 50 km altitude). Following the eruption of the Pinatubo volcano, aerosol optical depths at SAGE II wavelengths in the direction of the Earth's limb became greater than unity in the tropics below 26 km altitude and sometimes elsewhere in the atmosphere at slightly lower altitudes. As a result SAGE II gas retrievals were substantially affected (or rendered impossible) below 30 km altitude. These uncertainties are reflected in the SAGE II profile error bars which are often greater than or equal to 100%. SAGE II also measures water vapor and has

yielded an interesting climatology up to mid-1989. Because of the effects noted above, the water vapor retrievals are of lesser quality since that time.

9.2.1.6 LIMS

LIMS, a broad-band radiometer, was launched aboard NIMBUS 7 in October 1988 and used emission measurements to infer temperature, pressure, ozone, water vapor, nitrogen dioxide, and nitric acid globally until late May of 1989 when cryogen depletion occurred on schedule. LIMS used a limb scanning technique to measure radiance profiles in each of six channels from -50 to 150 km every 12 seconds. The vertical resolution varied from 2.7 to 4.5 km depending on channel and processing technique. The NO_2 and H_2O data were processed at a 4.5 km vertical resolution, while temperature, pressure, O_3 and HNO_3 retrievals have about 2.7 km vertical resolution.

The experiment was very successful, achieving good quality with all products. The NO_2, H_2O and HNO_3 fields are still used as the primary source of global climatology for these species. However, it should be noted that recent analysis by Dr. Ellis Remsberg (private communication) have shown that improved spectroscopic parameters since LIMS processing imply some error in LIMS results. In particular, when the latest line parameters are used for reprocessing, the LIMS ozone results decrease in the lower stratosphere by as much as 30%, H_2O increases by about 10% at all altitudes and peak night-time NO_2 values are reduced by as much as 25% due to fine line splitting. Therefore, although the LIMS morphology is probably quite reasonable, it is difficult to use LIMS as an accuracy validation tool due to both time differences and spectroscopic limitations. The reader should keep this in mind when looking at all LIMS figures except for Figure 9.2.2.2-8. Figure 9.2.2.2-8 displays LIMS NO_2 data that has been reprocessed with the latest spectroscopic data.

NIMBUS 7 operated in a sun synchronous, polar orbit. The orbit, in combination with the fixed viewing geometry of the instrument, achieved local time measurements near 10:30 p.m. and 2:30 p.m. at low latitudes with transfer between the two at high latitudes. The resultant data are for middle day and middle night measurement conditions, nearly the extremes for the diurnally active NO_2.

LIMS measurements occurred under the fortunate condition of very low background aerosol, allowing uncontaminated retrievals throughout the stratosphere and often into the upper troposphere. The LIMS data should provide a valuable contrast to current conditions. For a detailed description of the LIMS instrument and data quality, see the LIMS validation papers in the Volume 89, 1984 issue of JGR.

9.2.2 Comparison Results

9.2.2.1 Profiles

CLAES versus FIRS-2

Profile comparisons of CLAES NO_2 versus the FIRS-2 data were obtained for two daytime cases, (May 29, 1992 and September 29, 1992) and are shown in Figures 9.2.2.1-1 and 9.2.2.1-2. A night-time case for March 24, 1993 is shown in Figure 9.2.2.1-3. The CLAES values are generally less in amount than those of FIRS-2, with overlap of error bars for three points for the May 29, 1992 data. For reference the UARS pre-launch climatology, which has been considerably influenced by the LIMS data, is also shown in these figures.

CLAES versus BLISS

Profile comparisons of CLAES NO_2 versus the BLISS data obtained in night-time conditions on August 26, 1992 is shown in Figure 9.2.2.1-4. For the three BLISS data points there is agreement within the overlap range of the error bars.

HALOE versus MKIV

Figure 9.2.2.1-5 shows a comparison of a HALOE sunset profile on September 29 versus a balloon measurement by G.C. Toon with the MKIV FTIR on September 15. There is fair agreement even though time (15 days) and space (3° latitude and 16° longitude) coincidence is not good. Both instruments use solar occultation, so diurnal photochemical adjustment is not needed.

HALOE versus ATMOS - 1985

Since both HALOE and ATMOS are occultation instruments, it is a useful comparison even with the time difference. Comparison of a daily mean HALOE profile with 1985 ATMOS data taken at 29° N latitude is shown in Figure 9.2.2.1-6. Considering the difference in time, the comparison is quite reasonable.

HALOE versus ATMOS - 1992

Figures 9.2.2.1-7 and 9.2.2.1-8 show the comparison of two nearly space coincident HALOE and ATMOS measurements. Although the time coincidence is only about two weeks, the agreement is quite good. The tropical and southern hemisphere time variations should be small during mid to late March, lending more credibility to the results.

Note the apparent waves in the HALOE profiles. HALOE NO_2 data is processed on an extremely fine vertical grid (0.3 km spacing) in an attempt to achieve the natural instrument resolution of 2 km. However, it is suspected that some of these apparent waves may be induced by solar tracking mechanisms. Processing methods to remove the tracking effects have been developed, but were not yet implemented at the time of the comparison.

Overall the ATMOS and HALOE agreement is very good in magnitude, vertical gradient and altitude registration.

HALOE versus SAGE II

Both SAGE II and HALOE are solar occultation instruments, allowing comparisons of data under similar conditions of zenith angle. However, SAGE II only processes NO_2 data for sunset events, which are more likely to have near-coincidence with HALOE sunrise events.

Three primary periods (see Figures 9.2.2.1-9, 9.2.2.1-10, and 9.2.2.1-11) were compared with latitude and longitude coincidence given higher priority than time. Latitude coincidence was within 1° , but time difference varied by as much as 4 days. The fourth period (see Figure 9.2.2.1-12) is a subset of the third period in which time coincidence was limited to one day. Each plot contains a comparison of mean profiles and a profile of mean difference and RMS difference. The first three periods contained roughly 60 profiles each with the last subset period containing 15 profiles.

In general HALOE NO_2 is larger than SAGE II, particularly above the peak mixing ratio value. Much of the difference is mean difference, greater than 25% above the peak. The RMS differences

are quite large, as high as 40%. Covariance and correlation studies are being done to further study the nature of these differences.

It should also be noted that the close time coincidence subset shows much better agreement in the mean, although HALOE is still larger at the peak by 20%, and the RMS differences are nearly as large as the other time periods.

The large differences in the lower stratosphere are primarily due to aerosol interference, which is a much bigger effect on SAGE II results.

ISAMS versus CLAES versus LIMS

Day and night zonal mean profiles for CLAES and ISAMS on January 10, 1992 and for LIMS on January 10, 1979 at 29° S are shown in Figures 9.2.2.1-13 and 9.2.2.1-14. These plots demonstrate the typical observed differences between CLAES and ISAMS NO_2. The ISAMS mixing ratios are nearly double those of CLAES for both day and night. Although the LIMS data more closely agree with ISAMS, it has recently been shown by E. Remsberg (personal communication) that the night peak mixing ratios are 25% to 30% too high, and the daytime mixing ratios are 10% to 15% too high. This result is due to spin splitting of the NO_2 emission lines, which was not included in the LIMS processing. This correction would result in LIMS data falling nearly midway between CLAES and ISAMS. Considering the time difference, it appears that the LIMS data are of little help in resolving the differences. However, the profile shapes and altitude of the peak seem to agree reasonably well. Structure observed near the peak of the CLAES profile is not observed in the ISAMS profile. It appears to be a systematic feature of the CLAES data.

CLAES versus HALOE

Two profile comparisons were performed in an attempt to evaluate agreement between CLAES and HALOE during sunrise conditions. Sunrise NO_2 profiles on HALOE were compared to mean profiles for zenith angles between 75° and 105° for CLAES. It was found that comparisons could range from that shown in Figure 9.2.2.1-15 to that shown in Figure 9.2.2.1-16, depending on zenith distribution. Although more rigorous study is needed, preliminary results imply good agreement below the peak (where it might be expected due to slower photochemistry) and fair agreement above the peak for distributions weighted toward daylight conditions (zenith angle < 90°). Statistical results for the January period are shown in Figure 9.2.2.1-17.

9.2.2.2 Cross-Sections

CLAES versus ISAMS versus LIMS: Latitude versus Pressure

Figures 9.2.2.2-1, 9.2.2.2-2, 9.2.2.2-3 and 9.2.2.2-4 show LIMS, ISAMS, and CLAES NO_2 cross-sections for day and night conditions in January and April. ISAMS and CLAES values are for January 10, 1992 and April 20, 1992, while LIMS values are monthly averages for January 1979 and April 1979. Again, LIMS is known to be 25% high at night and approximately 10% high during the day.

The NO_2 cross-sections reflect features seen in the profile comparisons. ISAMS values are typically double the CLAES results, but with similar features. LIMS tends to lie in between, but time difference minimizes the significance of LIMS data as a useful validation tool. However, LIMS and HALOE agreement (see section HALOE VERSUS LIMS) using the newly processed LIMS NO_2 tends to give increased value to the LIMS data for comparison with the UARS data.

ISAMS NO_2 measurements show increasing errors with decreasing altitude below 10 mb, so that by 46 mb there is a strong influence of the a priori on the retrieved values. Particularly near the winter pole, there is considerable structure in the error field at 46 mb, and the data should be used with caution. The error on the a priori is set to 75% in ISAMS Version 8 retrievals, and therefore, data with errors greater than 53% are weighted more towards climatology than towards the measurements. Also, the absolute values of the data should be considered with reference to the findings of this report on systematic uncertainties in UARS NO_2 measurements.

HALOE versus SAGE II: Longitude versus Pressure

Due to the difficulties of finding coincident local time and location, only one cross-section comparison between HALOE and SAGE II is shown. Figures 9.2.2.2-5, 9.2.2.2-6 and 9.2.2.2-7 display HALOE and SAGE II cross sections and differences for May 21-23, 1992 at 38° S.

In general, the agreement can be described as similar to the profiles. The maximum is narrower for HALOE, but at nearly identical altitude. The user should pay strict attention to the error bars and data flags contained in the SAGE II data files. Similar minimums and maximums can be observed in both data sets. Differences are generally the same as observed with the profiles.

In general, agreement is fair, but more careful and comprehensive comparisons are needed. Morphology appears to be the same, but magnitude differences are substantial relative to research requirements.

HALOE versus LIMS

A single day of LIMS nighttime (roughly 10:30 LST) NO_2 data, reprocessed by Dr. E. Remsberg (see Figure 9.2.2.2-8), is compared to HALOE sunset ($NO + NO_2$) data (see Figure 9.2.2.2-9) as an approximation of total active NO_X. The HALOE data is for April 21 through May 30 to get a complete latitude sweep about the May 5 LIMS data. The magnitudes and morphology are strikingly similar with HALOE slightly high 10 - 15%. However, given the time difference (both local and the 13 years), the neglect of N_2O_5 chemistry during the night, and the large aerosol content during the HALOE measurements, the comparisons are surprisingly good. Validation of accuracy must await further analysis and additional accurate correlative measurements.

9.2.2.3 Time Series

Time track plots are used to compare retrievals along the Level 3AT (L3AT) tangent point measurement track of the cold-side, 90 degree looking CLAES and MLS instruments, and ISAMS for those times when it is pointed towards the cold side. The data are obtained at a resolution of one EMAF (i.e., approximately 65 seconds) on standard UARS pressure surfaces. Only ISAMS and CLAES instruments obtain NO_2 data. For this validation exercise ISAMS and CLAES time track comparisons were generated for January 9-10, 1992 and April 16-17, 1992 on the 10.0, 4.642 and 2.154 mb surfaces.

The time tracks are useful for establishing consistency of structure observed from one orbit to the next and for a top level view as to whether instruments are observing similar structure as a function of position on the orbit. Several figures are included to illustrate what can be learned from the time track comparisons. Comparisons for January 9 are shown in Figure 9.2.2.3-1. The top panel shows the latitude and the solar zenith angle for the tangent points along the track as a function of time (GMT). The middle and bottom panels show comparisons at 10 and 4.642 mb, respectively.

The UARS day and night pre-launch climatologies are included for reference. Similar comparisons are shown for pressure levels 2.154 and 0.464 mb in Figure 9.2.2.3-2.

Caution is advised in interpreting these data, since the plotting routine connects points with a straight line. Data gaps, occurring on one orbit but not the next, might be erroneously interpreted as showing a difference in structure. The orbital structure of the NO_2 data is dominated by the diurnal variation. However, latitudinally dependent variations also play a strong role.

Figures 9.2.2.3-1 and 9.2.2.3-2 reveal that CLAES and ISAMS show reasonable diurnal variations . The CLAES and ISAMS orbital signatures are highly correlated, with best correlation occurring at 2.154 mb. There is some anti-correlation in the region of the sunlit equator at 10 mb where ISAMS shows an enhancement and CLAES shows a minimum. The enhancement in the ISAMS data at this point may be the result of aerosols. This feature is not present in the ISAMS data at 4.642 and 2.154 mb. Generally, the ISAMS data are a factor of 2 to 3 larger than the CLAES data, almost like a constant multiplicative factor that is independent of orbital position. The ISAMS values are larger and the CLAES values smaller than climatology.

Data are compared in a different format in Figure 9.2.2.3-3. The top panel shows the latitude tangent point track for January 9, 1992 and for April 16, 1992. Where both instruments reported data, CLAES and ISAMS differences are displayed in the middle and bottom panels for January 9 and April 16, respectively. Also, included on the difference plots are the error bars associated with the CLAES and ISAMS data sets. Other information printed on the difference plots includes the daily mean of the CLAES data, the mean difference, the standard deviation of the CLAES - ISAMS data, and the correlation coefficient for the CLAES and ISAMS data. Tabulated below are the correlation coefficients and best fit multiplicative factor, CLAES to ISAMS, as derived from the time tracks for 2 days and for 3 pressure levels, which gives a more quantified illustration of the increase in correlation with increasing altitude (perhaps a result of less aerosols in higher regions).

Pressure	Correlation Coefficient		Multiplicative Factor	
	1/9/92	4/16/92	1/9/92	4/16/92
10.0 mb	0.60	0.49	2.5	2.8
4.64 mb	0.83	0.79	2.2	2.2
2.15 mb	0.94	0.89	2.0	1.9

Some major conclusions of the time track comparisons follow:

- CLAES and ISAMS show expected diurnal dependence.
- Aerosols possibly influence the ISAMS data near the sunlit equator at 10 mb.
- CLAES and ISAMS are highly correlated, with correlation increasing as a function of altitude.
- ISAMS data are a factor of 2 to 3 greater than CLAES.
- ISAMS values are greater and CLAES values are less than climatology.

9.3 NITRIC ACID (HNO_3) VALIDATION

9.3.1 Correlative Data

Correlative data for HNO3 used in the validation studies are summarized in the table below.

Correlative Data Table (1)

CMI / CMA	DATE OF FLIGHT	LOCATION / TIME LAT x LONG / GMT (2)	INSTRUMENT(3) ACRONYM (4)	VERTICAL RANGE
D.G. Murcray	9 January 1992	67.5°N x 20.2°E/09:06 Launch: Kiruna, Sweden	CAESR Sonde with He- cooled grating spectrometer	15 to approx. 30 km with 500 m vertical resolution
	5 March 1992	67.5°N x 20.2°E/06:14 Launch: Kiruna, Sweden		
	12 March 1992	67.5°N x 20.2°E/10:38 Launch: Kiruna, Sweden		
	14 March 1992	67.5°N x 20.2°E/15:20 Launch: Kiruna, Sweden		
	24 July 1992	31.6°N x 100.5°W/01:36 Launch: Palestine,TX	Scanning Solar Fourier Transform Spectrometer (FTIR)	15 to approx. 40 km with several tangent point altitude line-of-sight measurements
H. Oelhaf (5)	14 March 1992	69.5°N x 32.7°E/23:37 Launch: Kiruna, Sweden	MIPAS-B Michelson Interferometer	Mid-troposphere to 38 km (float alt) with vertical resolution of less than 3 km
R.A. Stachnik	29 September 1992	35.5°N x 101°W/21:42 Launch: Ft. Sumner, NM	BMLS Submillimeter- wave heterod. radiometer	18 - 50 km with vertical resolution of approx. 3 km
G.C. Toon	14 September 1992	34.4°N x 104.9°W/14:35 Launch: Ft. Sumner, NM	MKIV Solar Absorption Interferometer	Vertically resolved volume mixing ratios from 17 - 37 km
	15 September 1992	34.9°N x 105.8°W/01:06 Launch: Ft. Sumner, NM		
		35.2°N x 104.5°W/12:42 Same Flight		
W. Traub	29 March 1992	34.4°N x 107.0°W/20:12 Launch: Ft. Sumner, NM	FIRS-2 Thermal Emission Fourier Transform Spectrometer	18 - 50+ km with 7 km vertical resolution above 38 km and 4 km vertical resolution below 38 km
	29 September 1992	35.0°N x 102.0°W/20:00 Launch: Ft. Sumner, NM		
	24 March 1993	34.7°N x 107.6°W/05:24 Launch: Daggett, CA		
C.R. Webster	26 August 1992	31.4°N x 98.8°W/07:30 Launch: Palestine, TX	BLISS, Laser Absorption Spectrometer	Single altitude in the 20 to 35 km region

Footnotes to Correlative Data Table:

(1) Significant portions of this table provided by Dr.Richard Nightingale of the CLAES team.
(2) Latitude, longitude, and time are from data file headers. Assumed to be an average position and time while data being taken.
(3) All instruments in the table operated from balloon platforms.
(4) Acronyms:
    CAESR - Cold Atmosphere Emission Spectral Radiometer
    MIPAS-B - Michelson Interferometer for Passive Atmospheric Sounding
    BMLS - Balloon Microwave Limb Sounder
    MKIV - Mark IV
    FIRS-2 - Far InfraRed Spectrometer
    BLISS - Balloon-borne Laser In-Situ Sensor
(5) Oelhaf is not a formal participant in the UARS correlative measurement program.

The Murcray HNO_3 sonde is a small grating spectrometer which operates at liquid helium μμtemperature in a small dewar. The unit obtains atmospheric emission spectra in the 8 to 13 μm wavelength region as the unit ascends on a balloon. The altitude profile for the constituent of interest is obtained by measuring the change in spectral radiance with altitude in the regions where the constituent has special features. The accuracy of the measurement is typically 5 - 10% and integration time is 2 minutes. Since the unit is small, lightweight, and has a low data rate, it is suitable for piggyback operation on larger gondolas. The HNO_3 sonde data listed in the table were collected in the piggyback mode on flights sponsored by the European Arctic Stratospheric Ozone Experiment (EASOE).

The Murcray solar instrument is a solar spectrometer scanning the spectral regions of 750 cm^{-1} to 1300 cm^{-1} at a spectral resolution of 0.003 cm^{-1}. Measurements of HNO_3 and other UARS validation and complementary constituents are made in the occultation mode while at balloon float altitude (approximately 37 - 40 km). Spectra can be obtained throughout the tangent point altitude range of 15 km to float altitude. Accuracy is 5 - 10% with each spectra requiring 2 minutes. The total time available for a sunrise or sunset transition is about 45 minutes.

The Oelhaf instrument is a scanning Michelson interferometer covering the spectral regions of 770 cm^{-1} to 970 cm^{-1} and 1170 cm^{-1} to 1400 cm^{-1} with a spectral resolution of 0.04 cm^{-1} unapodized. Measurements of HNO_3 and approximately twelve other trace gases are made by detecting thermal emissions of the gases at the Earth's limb at various elevation angles against cold space.

The Stachnik instrument is a submillimeter-wave radiometer simultaneously measuring thermal emission spectra from ClO, HCl, O_3, H_2O, and HNO_3 in the 600 GHz spectral region. Measurements provide stratospheric mixing ratio profiles for these constituents from 15 - 50 km with 3 - 5 km resolution from a balloon platform altitude, typically 38 km. Accuracy for the HNO_3 measurement is about 20% with an averaging time of 15 minutes as set by the duration of one limb scan sequence.

The Toon instrument is a high resolution solar absorption interferometer obtaining spectra with S/N ratios in excess of 500:1 throughout the entire 650 cm^{-1} to 5500 cm^{-1} spectral region at a resolution of 0.006 cm^{-1}. The Mark IV provides column abundances of stratospheric gases from ground, balloon, or aircraft platforms. From a balloon platform, the Mark IV can provide vertically resolved profiles of HNO_3 between approximately 17 and 37 km. Intercomparison accuracy is typically 5%

for the 25 minutes of observation provided by a sunrise or sunset limb scan. Overall, the Mark IV can provide measurements of most all UARS validation and complementary constituents. In addition, temperature and pressure can be retreived.

The Traub instrument is a Fourier transform spectrometer which operates as a limb sounder from a balloon platform at a nominal float altitude of 39 km. It operates in the far-infrared (80 - 250 cm^{-1}) and simultaneously in the mid-infrared (400 - 700 cm^{-1}) with an unapodized spectral resolution of 0.004 cm^{-1}. The FIRS-2 measures thermal emission spectrum of molecular rotational and vibrational transitions. Since it measures thermal emission, it can operate throughout the diurnal cycle. Accuracy of the HNO_3 measurement is 10% with an averaging time of 50 minutes set by the length of the limb-scan cycle. Overall the instrument measures vertical profiles of mixing ratios of up to fifteen UARS constituents and several isotopes, plus temperature and pressure.

The Webster instrument is a high resolution laser absorption specrometer using tunable diode lasers and a long pathlength established by lowering a corner cube reflector below the gondola. Typically for UARS, the instrument measures NO_2, O_3, HCl, CH_4, N_2O, and HNO_3 at a single altitude in the 20 - 35 km range. The predicted minimum detectable mixing ratio at 30 km is typically > 0.1 ppbv for many stratospheric constituents of interest and can be as low as 0.02 ppbv for HNO3 under ideal conditions. Accuracy of the HNO3 measurement is typically 10% with an averaging time of 32 seconds.

9.3.2 Comparison Results

Vertical profiles and latitude-pressure zonal mean cross-sections of the CLAES data were examined for the intercomparison periods January 9-11, 1992, April 15-20, 1992, and August 25-31, 1992. The CLAES data were compared with Nimbus 7 LIMS data for the January and April periods. Additional data were also selected for days corresponding to periods for which correlative data were available. ISAMS HNO_3 (Version 0006) data currently resident on the UARS CDHF are considered unusable and therefore are not presented in this report.

9.3.2.1 Profiles

CLAES and LIMS profiles were examined for the January and April comparison periods at 72° N, 0°, and 28° S when the CLAES instrument is northward looking and at 72° S, 0°, and 28° N when it was southward looking. The LIMS profiles were required to be within 2° in longitude.

Profiles for January 10 are presented in Figure 9.3.2.1-1. At 72° N the agreement between CLAES and LIMS is rather poor, CLAES being consistently lower (~ 50%) through much of the middle and lower stratosphere. Peak values of HNO_3 occur at approximately the same altitude (pressure), and the profile shapes are similar in the middle and lower stratosphere. The equatorial profiles agree somewhat better in magnitude, but there are significant differences. The LIMS profile has nearly constant mixing ratio values over the range 5 - 50 mb, while CLAES has a distinct maximum between 1 - 20 mb with mixing ratios decreasing above and below. The CLAES and LIMS profiles exhibit rather better agreement at 28° S, but peak mixing ratio occurs at a lower altitude for the LIMS data. Similar behavior is true for all days in the January comparison period.

Data for April 15 are shown in Figure 9.3.2.1-2. The equatorial profiles display the same features and differences as observed for January 10. The profiles at 28° N are in good agreement over the entire altitude (pressure) range, with LIMS mixing ratios smaller than those of CLAES below the 40 mb level and larger than those of CLAES above. These conclusions are representative of the entire April comparison period.

CLAES vertical profiles were also compared with correlative data supplied by Traub, Webster, Stachnik, Toon, Oelhaf, and Murcray (see table in Section 9.3.1).

Comparisons of CLAES data with the Traub FIRS-2 data are presented in Figure 9.3.2.1-3 for May 29, 1992, September 29, 1992, and March 24, 1993. In general, the three days show consistent levels of agreement, although somewhat better for September 29 and March 24. The CLAES profiles are within 2° latitude, 6° longitude, and within 6 hours of the mean time reported for the FIRS-2 data. For each of the three comparison days, CLAES mixing ratios exceed those of the FIRS-2 instrument at low levels and then are consistently lower over most of the altitude (pressure) range compared. For May 29 and September 29, peak mixing ratios for CLAES occur at a lower altitude (higher pressure). On March 24, 1993, the peak mixing ratio determined by both instruments occurs at approximately the same altitude (pressure).

A single comparison with the Webster BLISS data is shown for August 26, 1992 in Figure 9.3.2.1-4. The CLAES profile is within 1° latitude, 2° longitude and 1 hour of the mean time and position for the BLISS data. Peak mixing ratio values occur at approximately the same altitude (pressure), but the BLISS value is about 15% larger. The upper level BLISS data (~ 7 mb) agree with the CLAES values within the reported uncertainties.

Figure 9.3.2.1-5 shows a comparison with data from the Stachnik BMLS instrument for September 29, 1992. The CLAES profile is within 2° latitude, 2° longitude, and 6 hours of the mean time and position reported for the BMLS instrument. The general shape of the two profiles is much the same, but the BMLS peak mixing ratio occurs several kilometers higher than that of CLAES. At a number of levels, the two profiles agree within the reported uncertainties, but no consistent pattern is evident, and the reported uncertainties for the BMLS data become rather large at the lower altitudes (higher pressures).

Comparisons of CLAES profiles with data from the MKIV instrument for September 14-15, 1992 are shown in Figure 9.3.2.1-6. The CLAES profiles are within 2° latitude, 2° longitude, and 11 hours of the mean time and position reported for the MKIV instrument. The profile shapes for CLAES and MKIV are quite dissimilar for September 14. The MKIV profile exhibits a peak in mixing ratio in the lower stratosphere at a considerably higher altitude (lower pressure) than does CLAES. The MKIV profile also has a second peak in mixing ratio of even larger value in the upper stratosphere that is not apparent in the CLAES profile. The two profiles do agree within the reported uncertainties of the two instruments, but the MKIV uncertainties are very large (50% and greater). The magnitude of the MKIV uncertainties and the dissimilar profile shapes combine to prevent a meaningful comparison. For September 15, 1992 the agreement is somewhat better, but at present, it is unclear why the large disparity in the magnitude of the reported uncertainties exists between the September 14 and the September 15 data at levels below approximately 5 mb for MKIV.

Data from the MIPAS-B instrument are compared with that from CLAES for March 14, 1992 in Figure 9.3.2.1-7. The CLAES profile is within 2° latitude,10° longitude, and 12 hours of the mean time and position reported for the MIPAS-B instrument. The two profiles have similar shapes, but CLAES peak mixing ratio exceeds that of MIPAS-B by approximately 25%. Above the peak, MIPAS-B values are consistently lower than those of CLAES. Below the mixing ratio peak, the MIPAS-B values generally exceed those of CLAES. For the most part, the data from the two instruments do not agree within the reported uncertainties.

A series of sonde profiles obtained by the Murcray CAESR instrument near Kiruna, Sweden is shown in Figure 9.3.2.1-8. The profiles were obtained on January 9, 1992, March 5, 1992,

March 12, 1992, and March 14, 1992. The CLAES profiles shown for comparison are within 2° latitude, 1° - 40° longitude, and 8 hours of the sonde profiles. The comparison for January 9 is rather poor, both in terms of magnitude and the shape of the profiles. Better agreement is seen for March 5, but the sonde profile exhibits a much more distinct peak in mixing ratio value and is approximately 30% greater in magnitude. The profiles for March 12 show reasonably good agreement between 10 and 30 mb, but the sonde data values exceed those of CLAES by large margins at lower altitude (higher pressure). The comparison for March 14 displays better agreement similar to that seen for March 5.

A single profile for July 24, 1992 is shown for the CLAES and the Murcray FTIR instrument in Figure 9.3.2.1-9. In contrast to the sonde-CLAES comparisons shown in Figure 9.3.2.1-8, the agreement between CLAES and FTIR data is generally good, particularly above the 10 mb level. At lower altitudes (higher pressures), the FTIR data display larger values than does CLAES.

Figure 9.3.2.1-10 shows the relative mean differences between CLAES HNO_3 profiles and the Murcray data (balloon-borne IR limb emission sounders). These data were obtained by the Fourier Transform Interferometer (FTIR) on July 24, 1992 and the Cold Atmospheric Emission Spectral Radiometer (CAESR) on January 9, 1992, March 5, 1992, March 12, 1992, and March 14, 1992. Coincidence criteria for the comparisons were 2° latitude, 12° of latitude equivalent longitude, and 12 hours. For the 5 correlative data sets there were 19 such coincidences. Horizontal bars indicate the standard deviation of the differences.

In the pressure range 10 - 40 mb, the relative difference varies from +10% to -10%. At the lower altitudes (higher pressures), the relative difference is as large as -45%. The HNO_3 profile is falling off rapidly at these altitudes and the balloon data are relatively sparse. Also, with the relatively large coincidence windows, the standard deviations may reflect considerable atmospheric variability in addition to instrumental uncertainties.

9.3.2.2 Cross-Sections

CLAES daily zonal mean nitric acid distributions have been examined over the pressure range 100 mb to 1 mb and from 32° S to 80° N for the January period and from 80° S to 32° N for the April and August periods. The CLAES nitric acid data has structure that would be expected based upon models and the Nimbus 7 LIMS data.

CLAES zonal mean nitric acid on January 10, 1992 in Figure 9.3.2.2-1 displays a winter/summer asymmetry (about 2 to 1) which is typical of what was seen in the 1978/1979 LIMS data. Figure 9.3.2.2-2 shows LIMS zonal mean HNO_3 on January 10, 1979 which has characteristics very typical of early January. The CLAES peak mixing ratios occur at approximately 40 mb in the northern hemisphere and 25 mb in the southern hemisphere. In contrast, the LIMS distribution has peak values in both hemispheres at the same level. In general CLAES and LIMS zonal mean HNO_3 are very similar. However, one important difference is seen above 10 mb in the winter hemisphere where LIMS has a distinct horizontal gradient, and CLAES shows very little horizontal gradient. Similar conclusions hold for zonal mean HNO_3 on January 9 and 11.

CLAES zonal mean nitric acid from the April comparison period is represented in Figure 9.3.2.2-3 (15 April 1992). In contrast to the January period, there is a reversal in the peak values. That is, the southern hemisphere values are now larger than for the northern hemisphere, and again exhibit about a 2 to 1 asymmetry. Figure 9.3.2.2-4 displays LIMS zonal mean HNO_3 on April 15, 1979. The LIMS data show the same asymmetry in peak values as the CLAES data. CLAES HNO_3 is greater than LIMS HNO_3 in the southern hemisphere at 64° S. In the northern hemisphere, CLAES and LIMS zonal mean HNO_3 are approximately equal.

Figure 9.3.2.2-5 shows zonal mean nitric acid on August 25, 1992 for CLAES. In the southern hemisphere, the peak value has shifted to approximately 60° S and occurs at a much lower altitude between 40 - 50 mb. High latitudes exhibit very little HNO_3, and this is not too surprising since we might expect severe denitrification associated with polar stratospheric clouds (PSCs) during winter polar night.

9.4 DINITROGEN PENTOXIDE (N_2O_5) VALIDATION

At the time of this validation workshop neither of the UARS N_2O_5 products (CLAES V0006 and ISAMS V0008) is considered to be scientifically useful. However, these products have been catalogued to provide a baseline to measure progress in future versions. The current status of the UARS N_2O_5 products is given in the chapter that addresses algorithm status.

9.5 SUMMARY

Nitric Oxide (CLAES, ISAMS, HALOE)

The CLAES and ISAMS instruments experienced unusually large signals from high altitudes, apparently non-LTE effects. Because these altitudes are above the highest tangent altitudes viewed by these instruments, it has been impossible to correct for the non-LTE effects, thus introducing some uncertainty at the highest retrieved altitudes. For this reason the ISAMS NO data were not available for consideration at this time. HALOE does not suffer from this difficulty. The only other available data for comparison with the UARS instruments are the ATMOS and LIMS data sets. Because of the diurnal variability of NO, no direct comparisons of the limb emission data from CLAES were made with the occultation data from HALOE.

HALOE and ATMOS-1985 profiles showed very good agreement below the altitude of peak mixing ratio. Above that altitude, the ATMOS values are approximately 10% larger than the HALOE values. CLAES and HALOE pressure versus longitude cross-sections show some similarities, but because of the diurnal effects, it is difficult to make any firm conclusions.

Nitrogen Dioxide (CLAES, HALOE)

As for NO, the diurnal variation of NO_2 makes direct comparisons of CLAES and ISAMS with HALOE difficult to interpret. However, correlative NO_2 data were available from ATMOS, FIRS-2, BLISS, MK IV, SAGE II, and LIMS.

Comparisons of CLAES and FIRS-2 data show relatively poor agreement for three profiles (two in daytime and one in nighttime) . At this time, the reasons for the differences are not known. CLAES and BLISS profiles agree within the overlap range of error bars for a single nighttime comparison below 10 mb.

HALOE and MK IV (both solar occultation measurements) were compared for several days. One comparison gave fair agreement, but time coincidence was poor (15 days). The other comparisons showed poor agreement. The reasons for the disagreement are not known at this time. In contrast, HALOE profile comparisons with both ATMOS-1985 and ATMOS-1992 (also a solar occultation measurement) were quite good. HALOE and SAGE II are also both occultation instruments, but SAGE II NO_2 data is processed only for sunset events which are most likely to be near coincident with HALOE sunrise events. In general, the HALOE values are larger than the SAGE II values with mean differences about 25% above the altitude where the peak mixing ratio occurs. RMS

differences are as large as 40%. Large differences in the lower stratosphere result primarily from aerosol interference, which has a larger effect on SAGE II than on HALOE.

Zonal mean cross-section comparisons of CLAES and ISAMS with LIMS were conducted. ISAMS values are typically double those of CLAES for both day and night, but the cross-sections have somewhat similar features. LIMS values lie midway between those of CLAES and ISAMS. However, the substantial time difference between LIMS and UARS minimizes the utility of LIMS as a validation tool.

A single longitude vs. pressure cross-section of HALOE data was compared with an equivalent SAGE II cross-section. At best agreement was fair, with similar features, but substantial differences in magnitude.

A single day of LIMS nighttime NO_2 was compared with HALOE sunset $NO + NO_2$, as a measure of total diurnally active NO_x. The magnitudes and distributions are remarkably similar (particularly, considering the time difference of the two data sets) with HALOE values 10-15% higher.

Nitric Acid (CLAES, ISAMS)

A reasonable number of correlative data sets were available for the comparisons with the CLAES observations. The version 0006 ISAMS HNO_3 data were considered to be unusable and were not considered.

Profile comparisons of the CLAES and LIMS data for both the January and April intercomparison periods for various latitudes showed relatively poor agreement in most cases. At present the reasons for the differences have not been determined. Agreement of CLAES and FIRS-2 profiles is for the most part reasonable, although several of the comparisons indicate that peak mixing ratio occurs at a slightly higher altitude for the FIRS-2 data. The profiles generally differ by less than 25% over most of the common altitude range. A single CLAES/BLISS comparison agrees within the error estimates of the two instruments above 7 mb. CLAES and BMLS profiles display fair agreement in profile shape, and mixing ratio values agree within reported uncertainties at most levels (however, the BMLS uncertainties are very large at the lower end of the altitude range).

Three separate comparisons of CLAES profiles with MKIV profiles show a good deal of dissimilarity in shape with peak mixing ratio occurring at a higher altitude for MKIV. At the upper end of the altitude range the MKIV uncertainties also become rather large. These discrepancies prevent meaningful comparisons and conclusions at this time. A comparison of CLAES and MIPAS-B profile data reveals a somewhat similar shape, but the data do not agree within the reported uncertainties. Comparisons between CLAES and CAESR sonde profile data are mixed, with poor agreement during the January period, but somewhat better agreement during the March period. In addition to the CAESR data, Murcray provided data from an FTIR instrument. The agreement between CLAES and the FTIR is good above the 10 mb level. The mean relative difference between CLAES data and the Murcray CAESR and FTIR data varies from +10% to -10% in the 10-40 mb pressure range. At lower altitudes the relative difference is 45%.

Zonal mean cross-sections of CLAES data have been compared with LIMS data for the January and April time periods. In general the two data sets look quite similar with respect to both magnitude and structure. This is a surprising result considering the large time interval and the differences seen between CLAES and the current correlative data. Further study of both CLAES and correlative data will be required to resolve these differences.

REFERENCES

Traub, W.A., K.V. Chance, D.G. Johnson, and K.W. Jucks, "Stratospheric Spectroscopy with the Far-Infrared Spectrometer (FIRS-2): Overview and Recent Results", *SPIE*, 1491, **298**, 1991.

Johnson, D.G., K.W. Jucks, W.A. Traub, and K. Chance, "The Smithsonian Stratospheric Far-Infrared Spectrometer (FIRS-2) and Data Reduction System", in preparation.

May, R.D. and C.R. Webster,"In Situ Stratospheric Measurements of HNO_3 and HCl Near 30 km Using the BLISS Tunable Diode Laser Spectrometer", *J. Geophys.Res.*, **94**, 16343 - 16350, 1989.

Webster, C.R. and R.D. May, "Simultaneous In Situ Measurements and Diurnal Variations of NO, NO_2, O_3, JNO_2, CH_4, H_2O, and CO_2 in the 40 - 26 km Region Using an Open Path Tunable Diode Laser Spectrometer, *J. Geophys. Res.*, **92**, 11931-11950, 1987.

Webster, C.R. et al, "Active Nitrogen Partitioning and the Nighttime Formation of N_2O_5 in the Stratosphere: Simultaneous In Situ Measurements of NO, NO_2, HNO_3, O_3 and N_2O Using the BLISS Diode Laser Spectrometer, *J. Geophys. Res.*, **95**, 13851-13866, 1990.

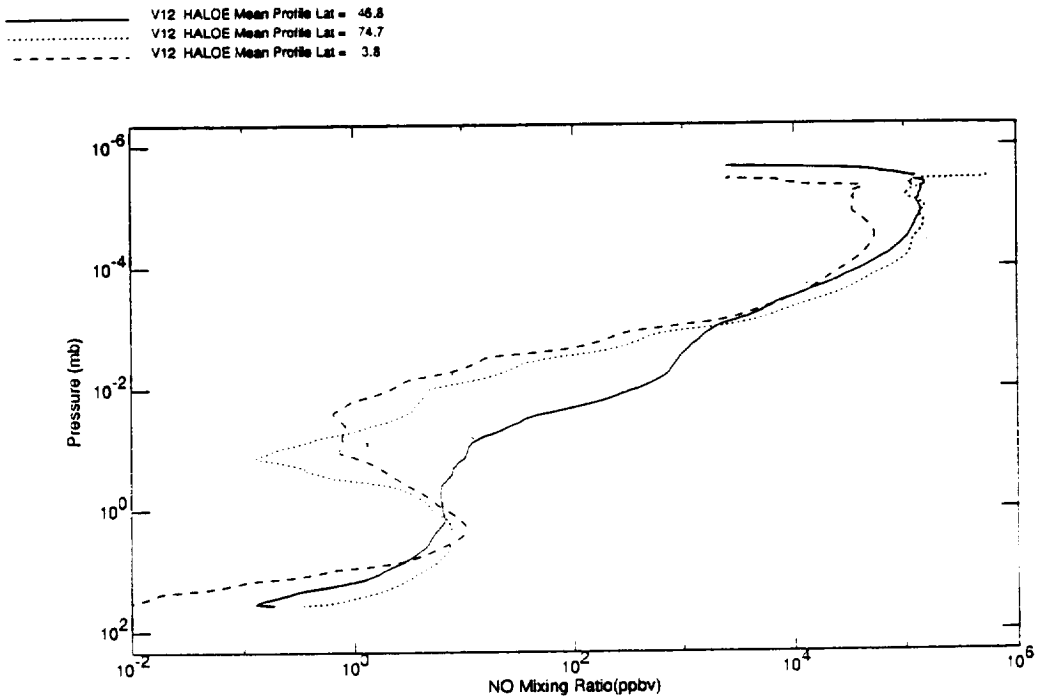

Figure 9.1.2-1. Mean Profiles of NO for HALOE at High Latitude in Winter, High Latitude in Summer, and Low Latitude in Spring.

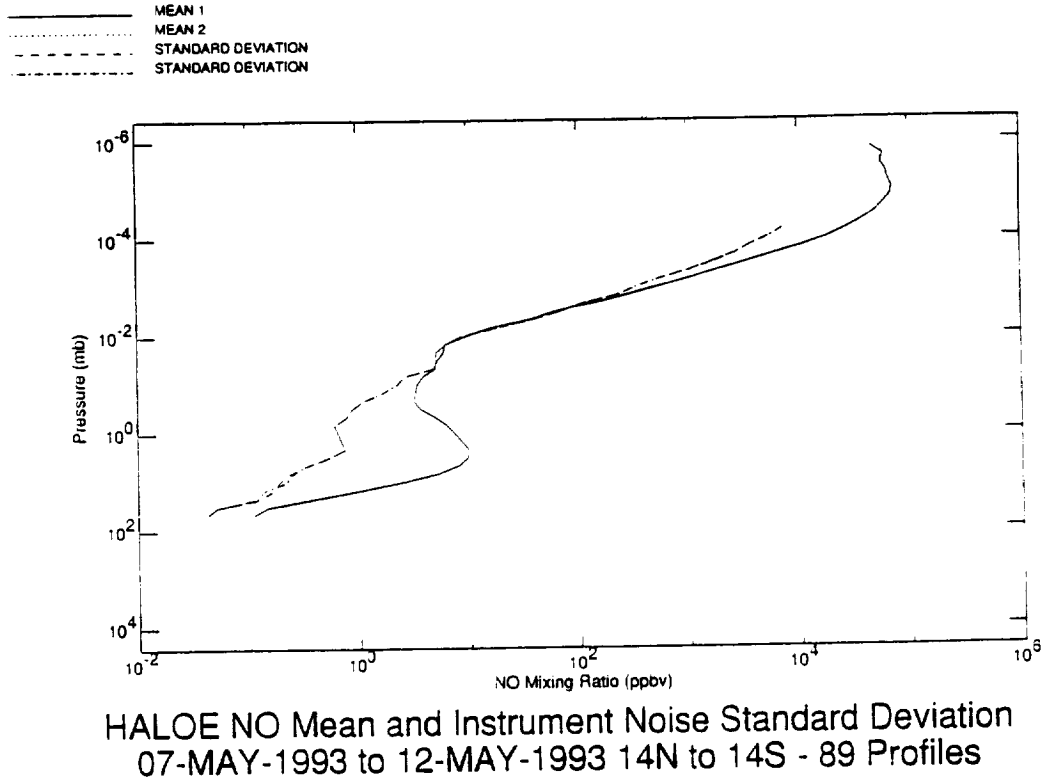

Figure 9.1.2-2. Profiles of HALOE NO Mean and Instrument Noise Standard Deviation for May 7-12, 1993, from 14° N to 14° S (89 Profiles).

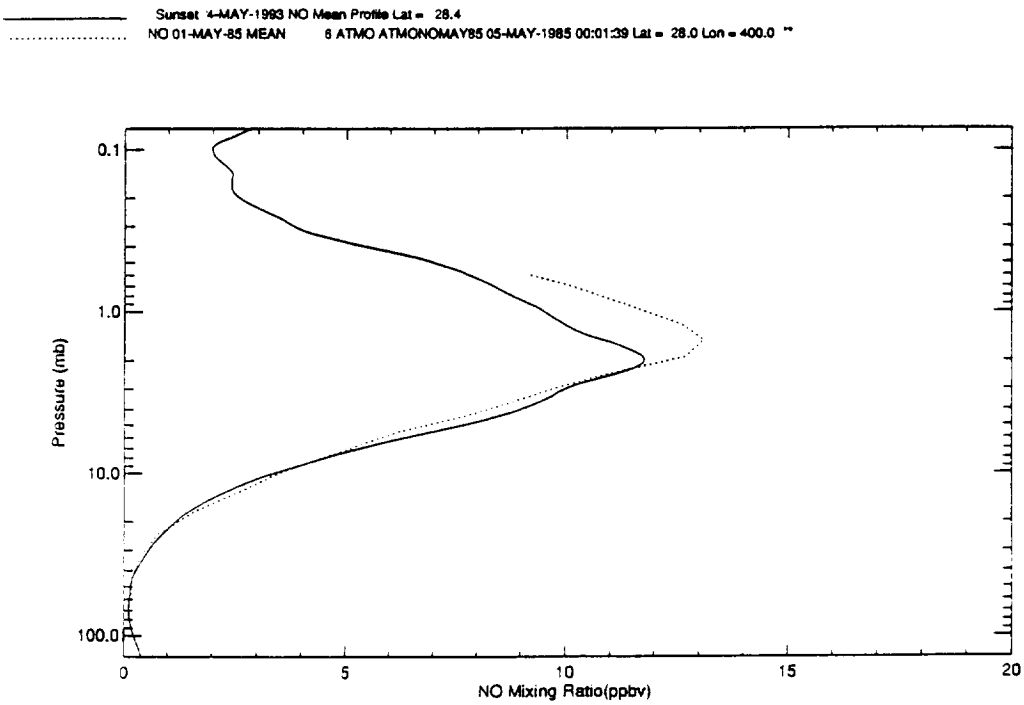

Figure 9.1.2.1-1. Profiles of NO for HALOE on May 4, 1993 and ATMOS on May 1, 1985, Near 28° N.

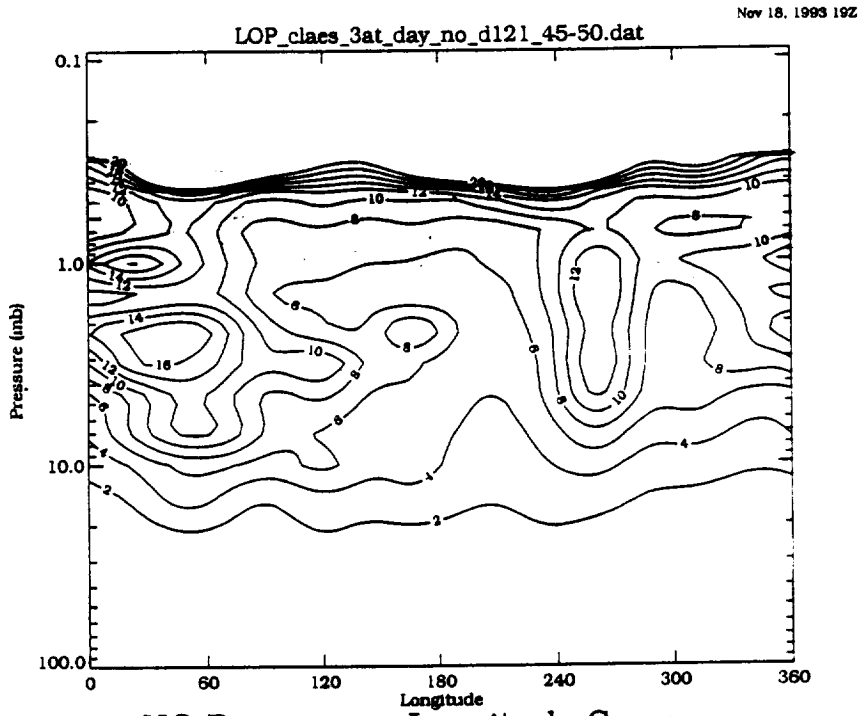

NO Pressure vs Longitude Cross Section, on 10-JAN-1992 at 47 N

Figure 9.1.2.2-1: CLAES NO Cross-Section for January 10, 1992, at 47° N.

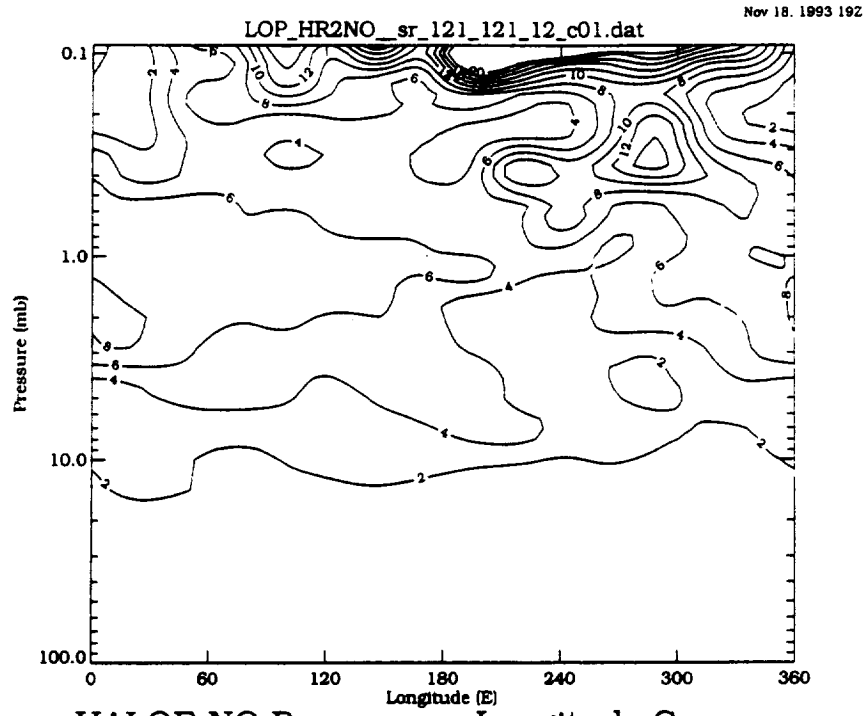

HALOE NO Pressure vs Longitude Cross Section, Sunrise on 10-JAN-1992 at 47 N

Figure 9.1.2.2-2. HALOE Sunrise NO Cross-Section for January 10, 1992, at 47° N.

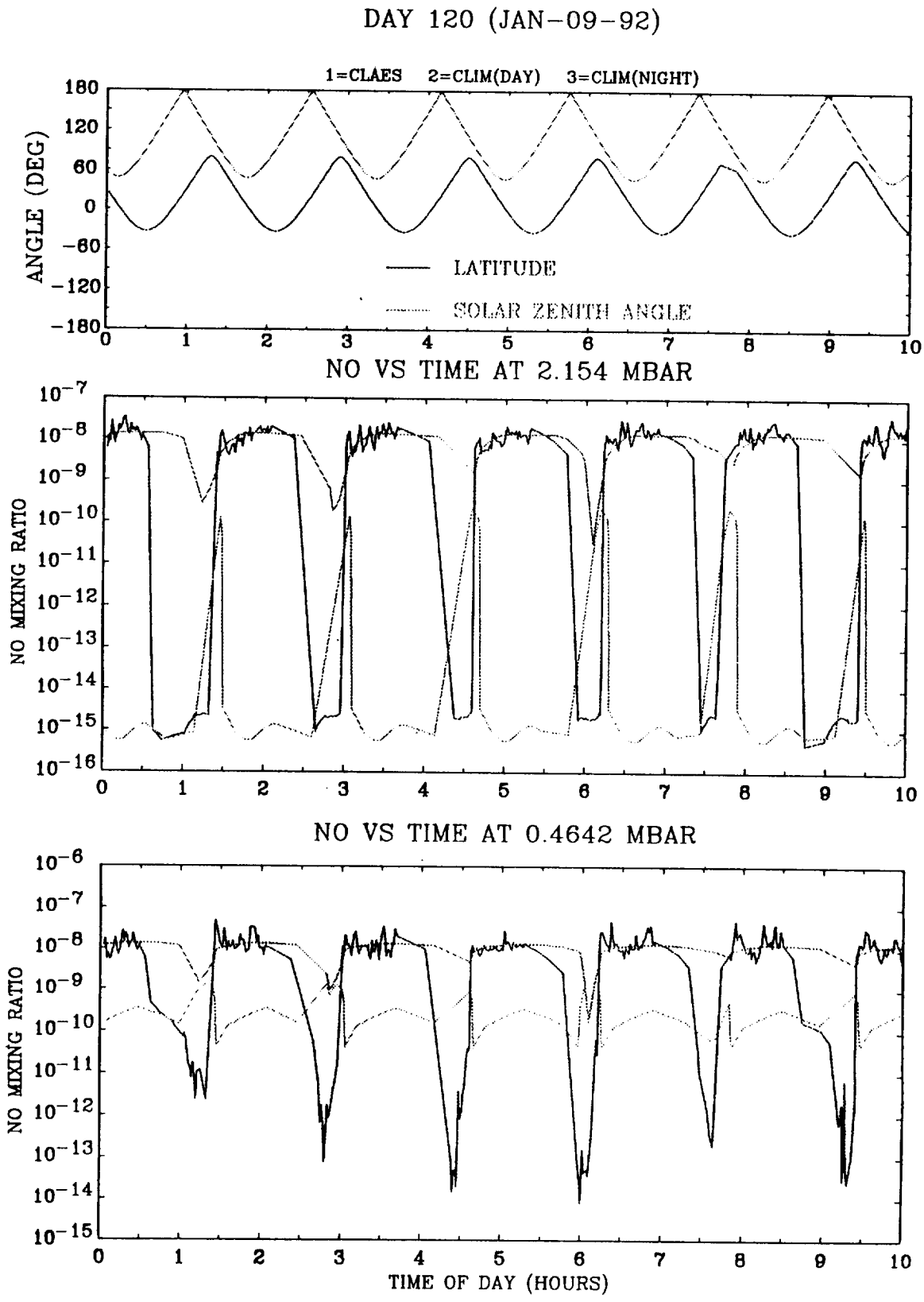

Figure 9.1.2.3-1. Time Series of CLAES NO for January 9, 1992 on the 2.154 and 0.464 mb Surfaces.

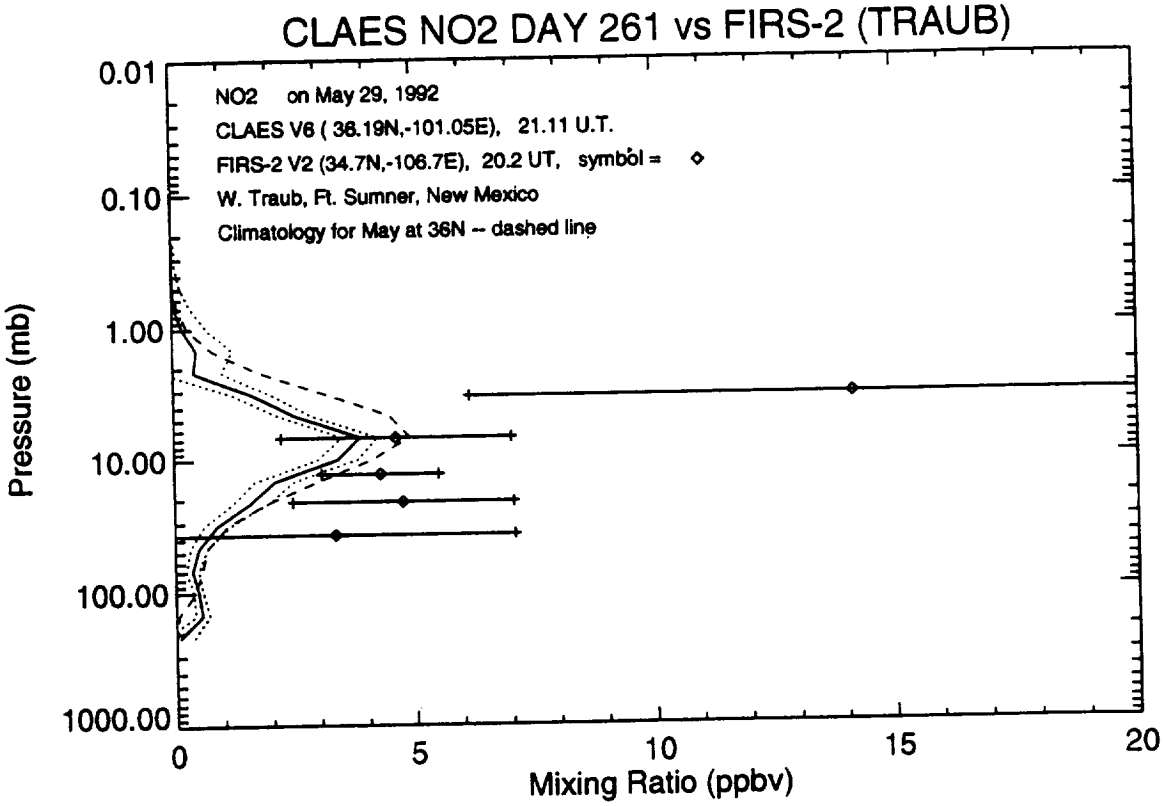

Figure 9.2.2.1-1. Profiles of Daytime NO_2 for CLAES and the Traub FIRS-2 Data on May 29, 1992.

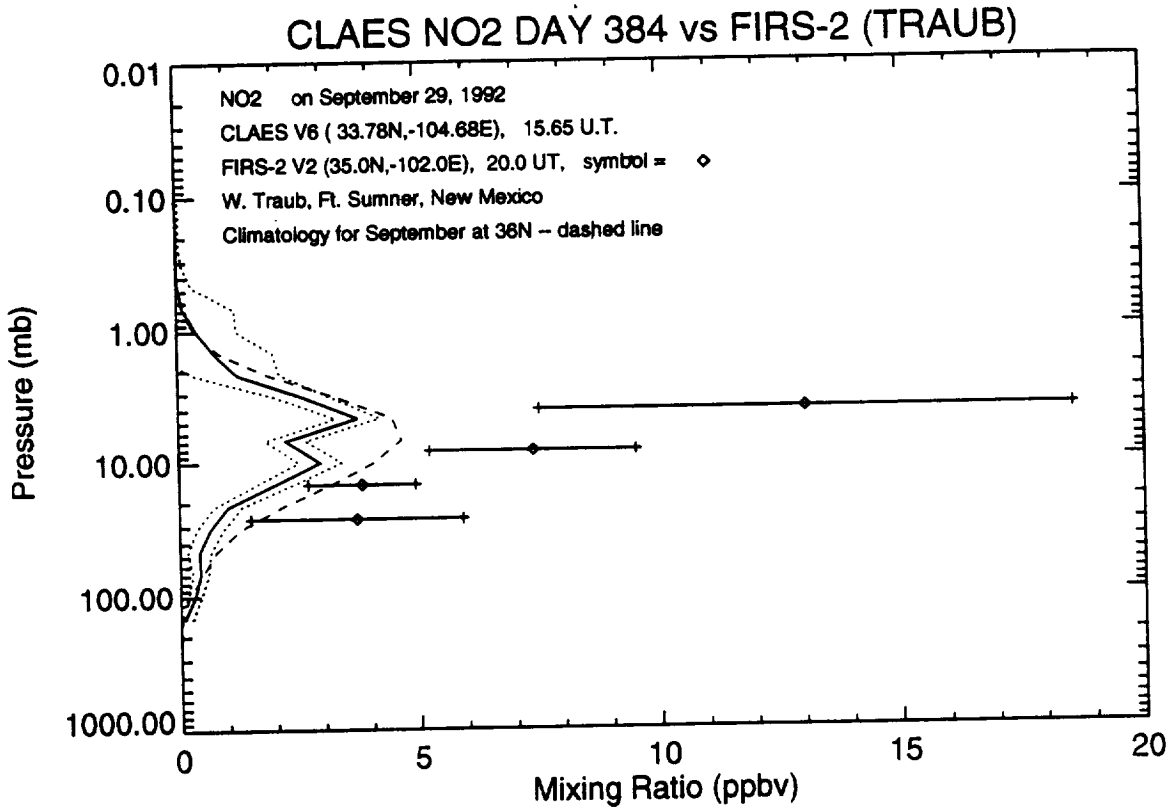

Figure 9.2.2.1-2. Profiles of Daytime NO_2 for CLAES and the Traub FIRS-2 Data on September 29, 1992.

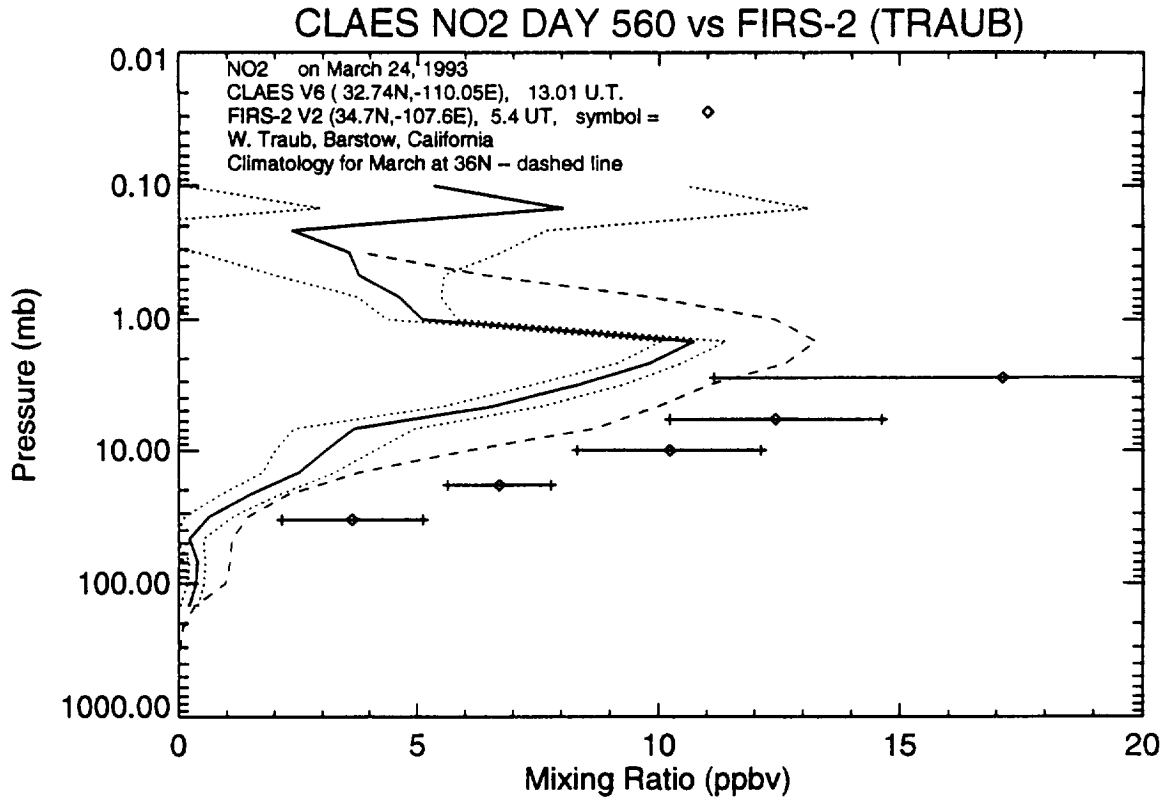

Figure 9.2.2.1-3. Profiles of Nighttime NO_2 for CLAES and the Traub FIRS-2 Data on March 24, 1993.

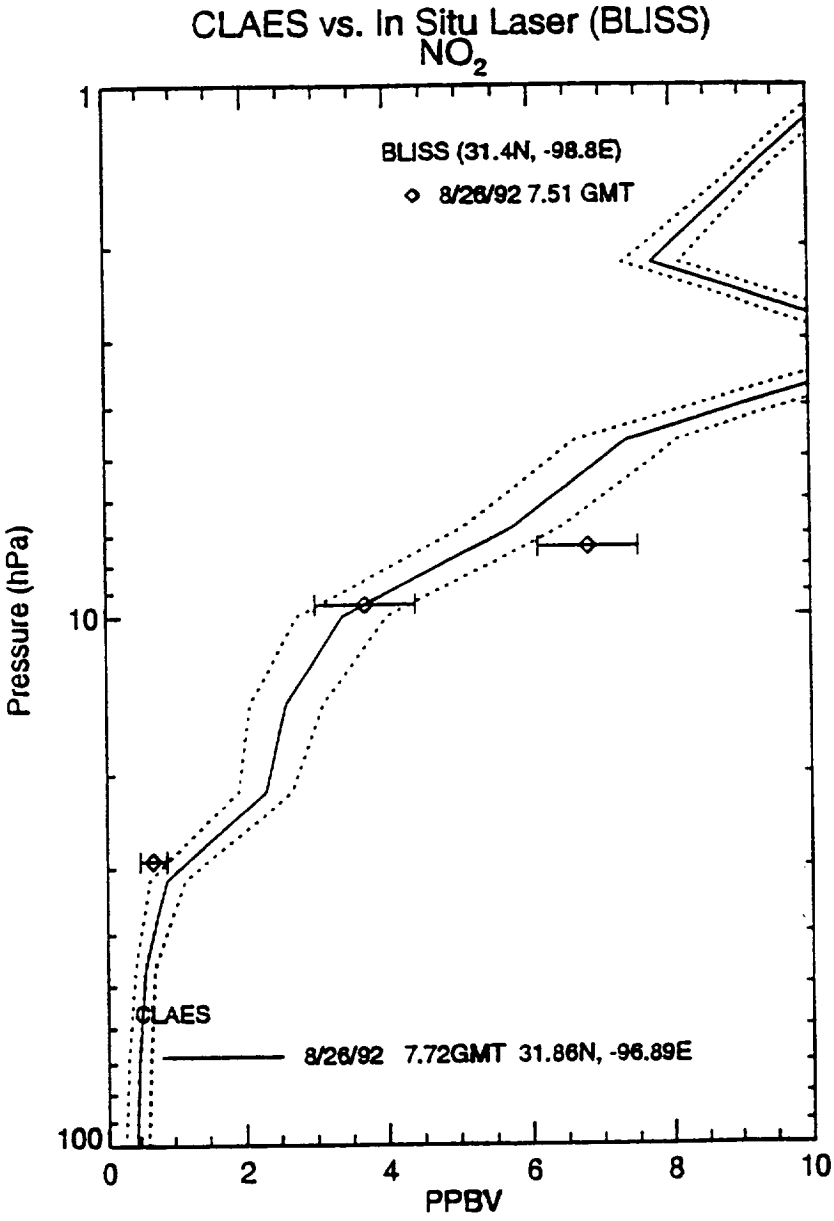

Figure 9.2.2.1-4. Profiles of Nighttime NO_2 for CLAES and BLISS Data on August 26, 1992.

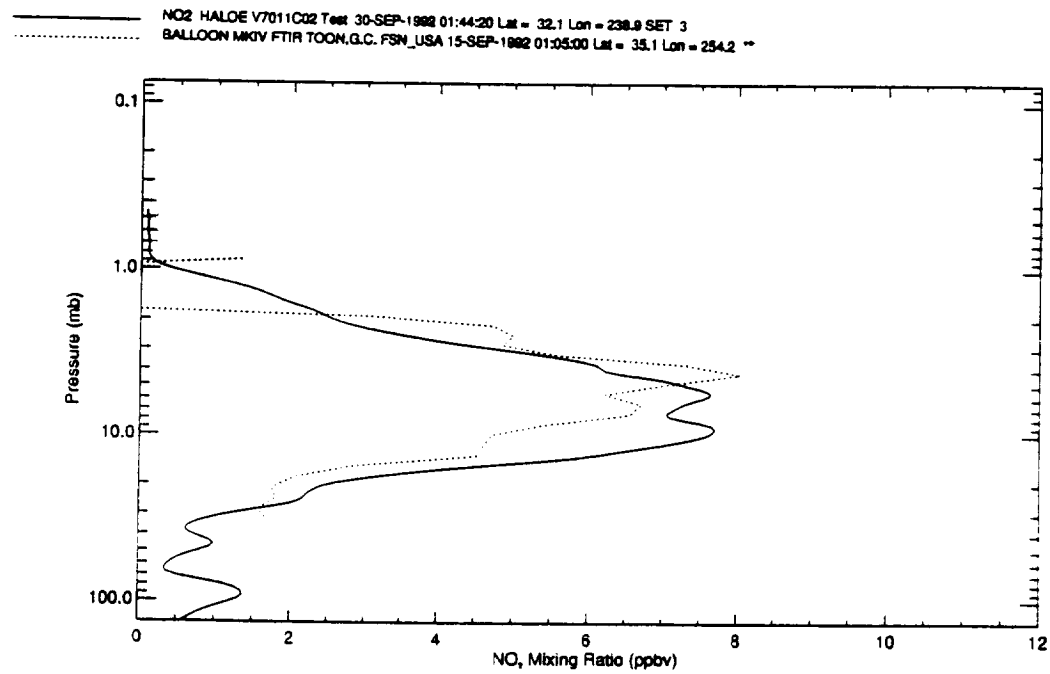

HALOE Version 9/11 and Balloon NO_2 Mixing Ratio
Near 35N on 29-SEP-1992

Figure 9.2.2.1-5. Profiles of NO_2 for HALOE on September 30, 1992 and the Toon MKIV (Balloon) Data on September 15, 1992.

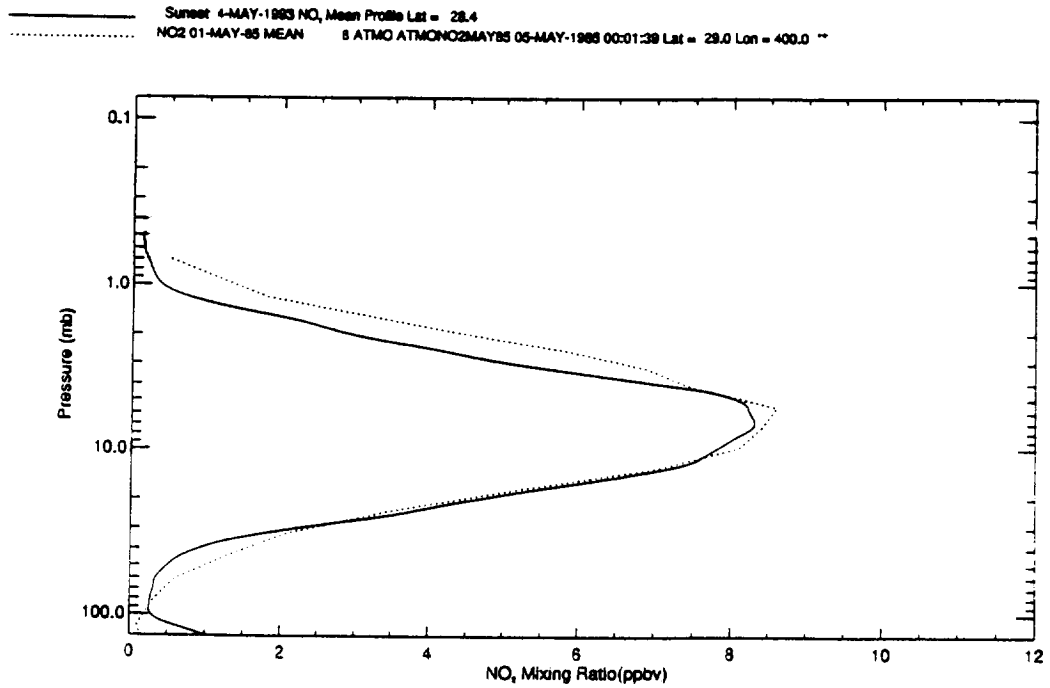

HALOE 04-MAY-1993 vs ATMOS 01-MAY-1985
Sunset NO_2 Mixing Ratio (ppbv) near 28N

Figure 9.2.2.1-6. Profiles of NO_2 for HALOE on May 4, 1993 and ATMOS on May 1, 1985.

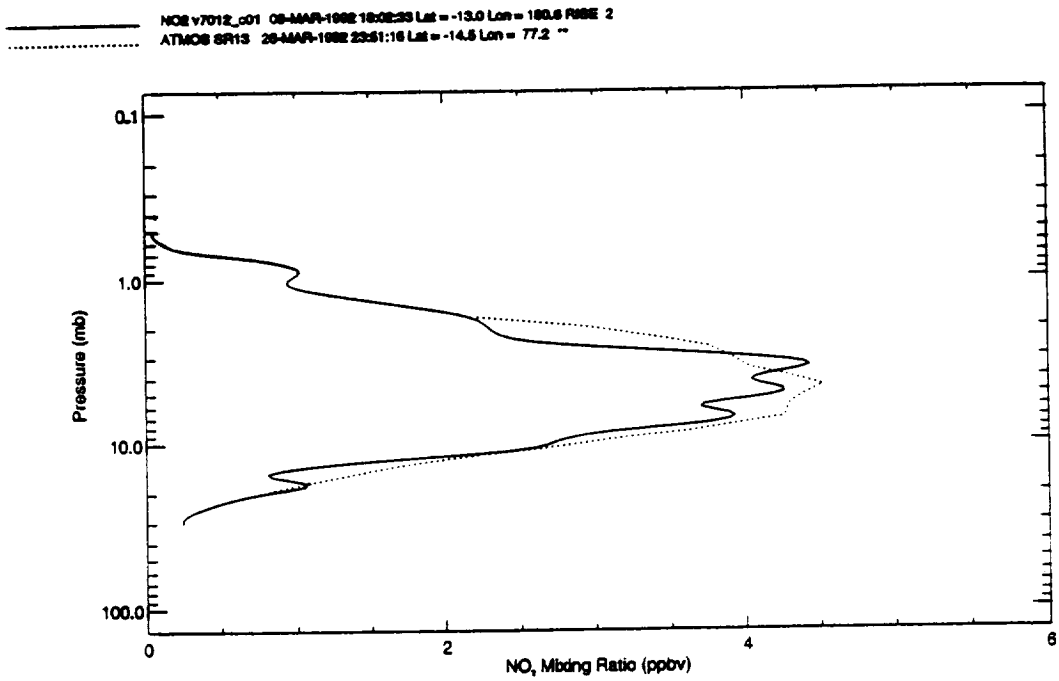

HALOE NO_2 Mixing Ratio 09-MAR-92 and
ATMOS NO_2 Mixing Ratio 26-MAR-92

Figure 9.2.2.1-7. Profiles of NO_2 for HALOE on March 9, 1992 and ATMOS on March 26, 1992.

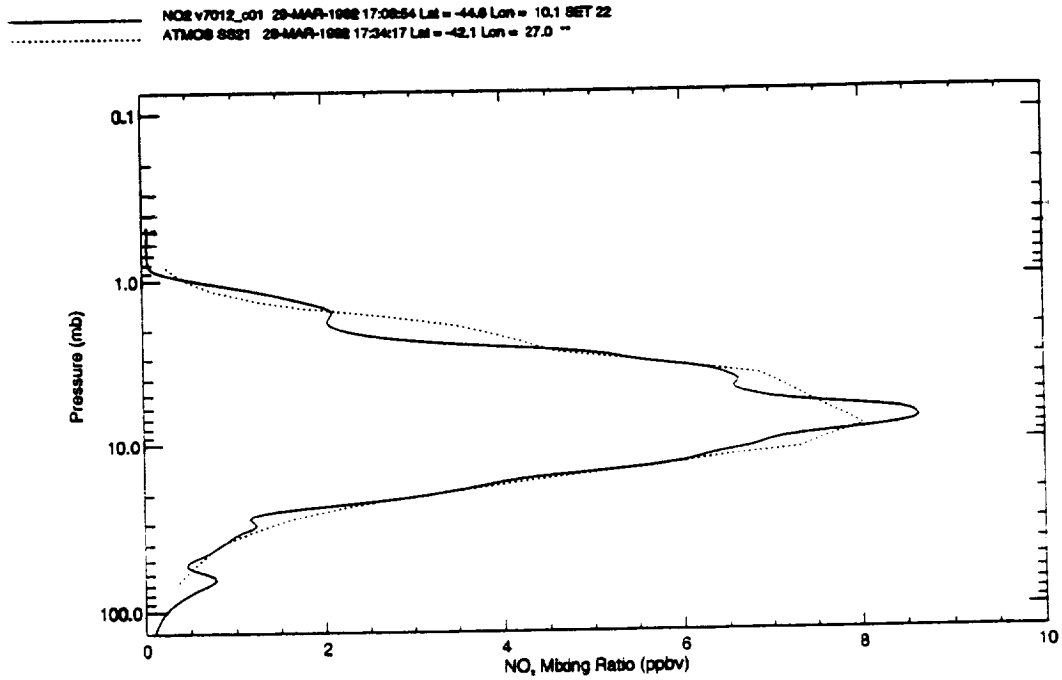

HALOE NO_2 Mixing Ratio 29-MAR-92 and
ATMOS NO_2 Mixing Ratio 28-MAR-92

Figure 9.2.2.1-8. Profiles of NO_2 for HALOE on March 29, 1992 and ATMOS on March 28, 1992.

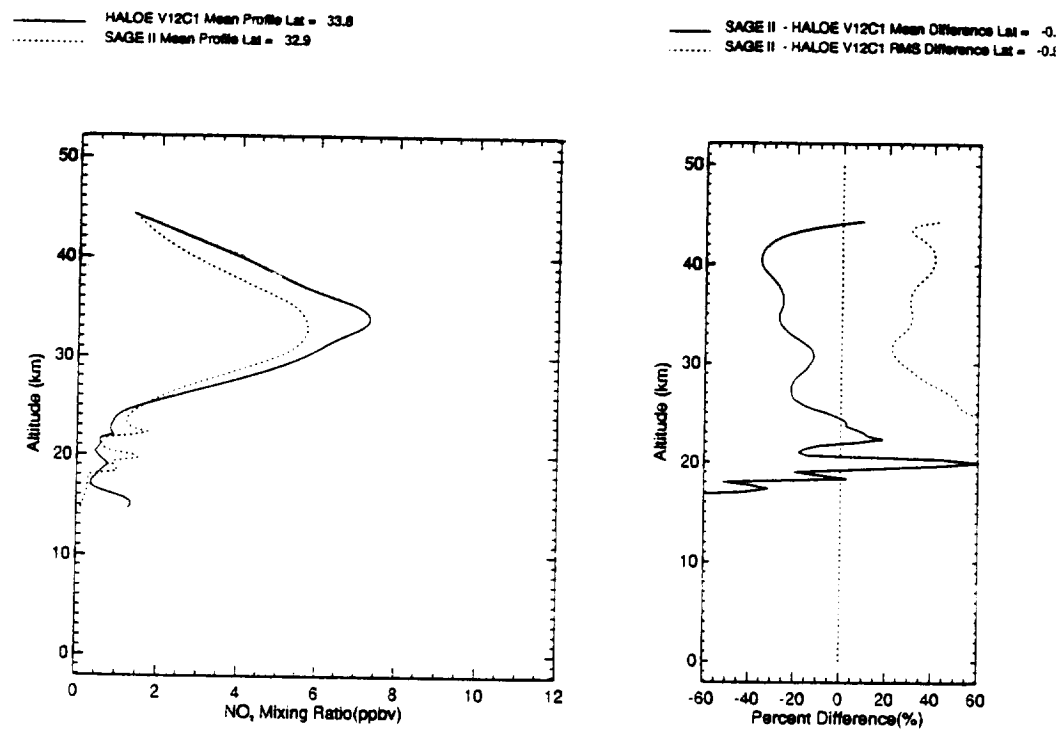

Figure 9.2.2.1-9. Mean Profiles of Sunset NO_2 for HALOE and SAGE II for November 23-25, 1991, Near 34° N.

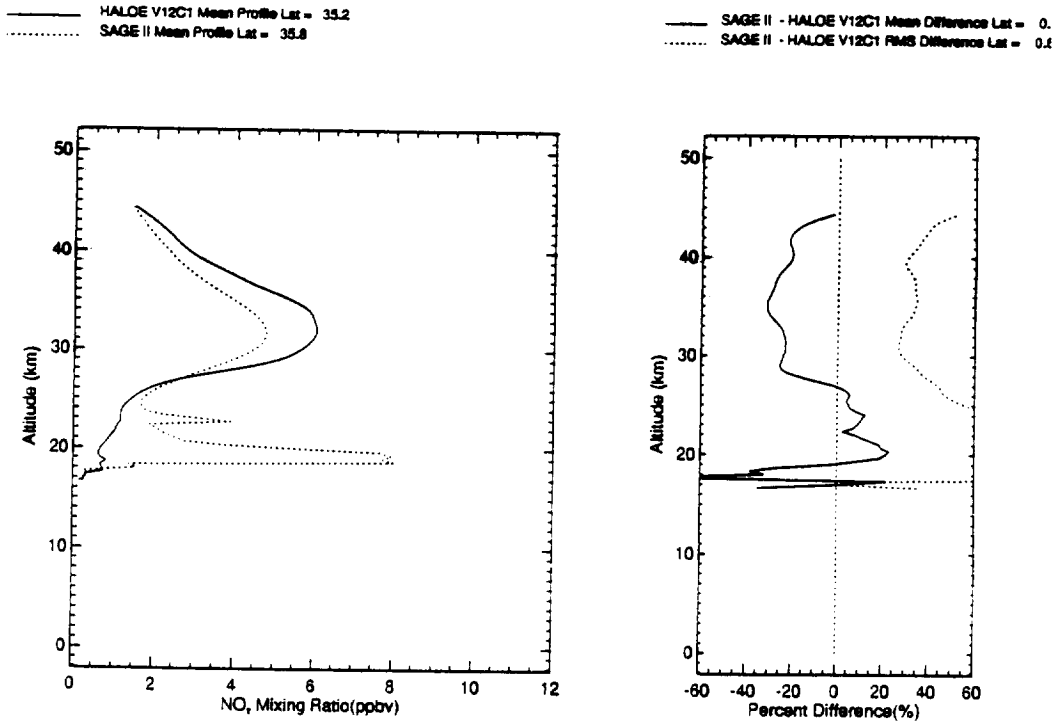

Figure 9.2.2.1-10. Mean Profiles of Sunset NO_2 for HALOE and SAGE II for February 1-4, 1992, Near 36° N.

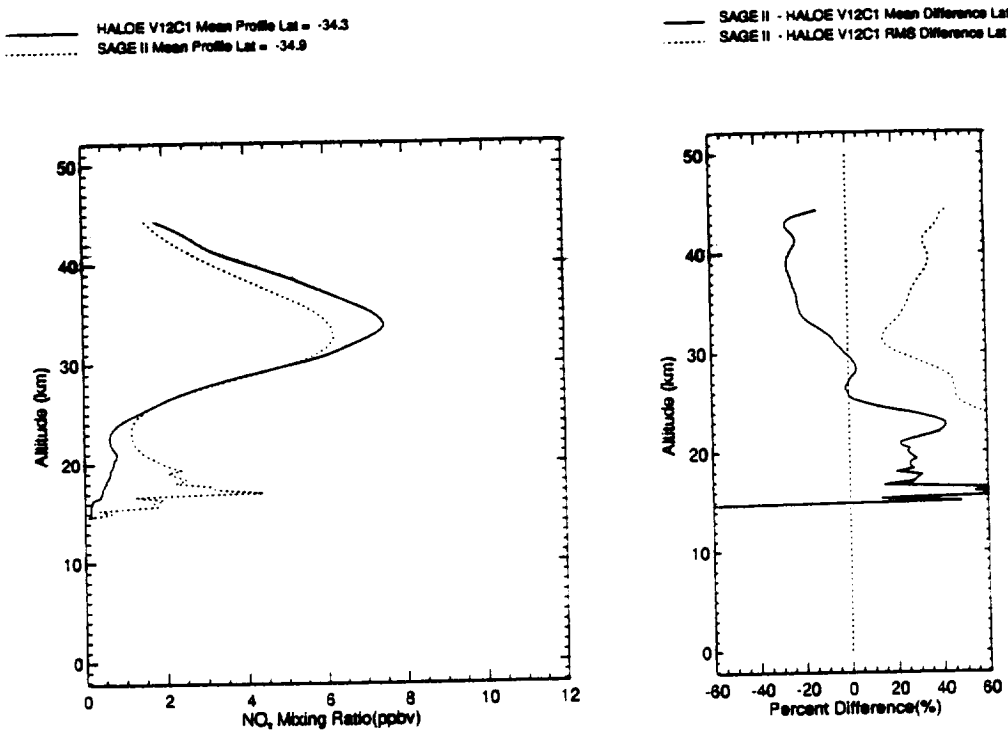

Figure 9.2.2.1-11. Mean Profiles of Sunset NO_2 for HALOE and SAGE II for May 20-24, 1992, Near 35° S.

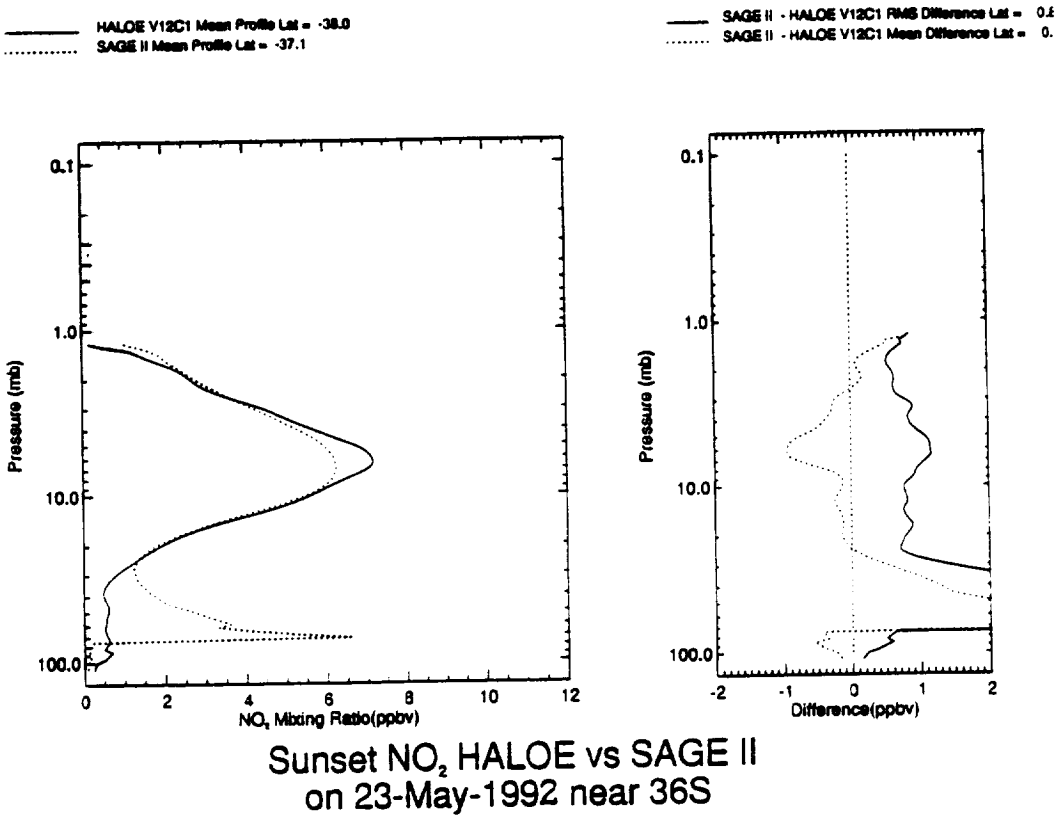

Figure 9.2.2.1-12. Mean Profiles of Sunset NO_2 for HALOE and SAGE II for May 23, 1992, Near 36° S.

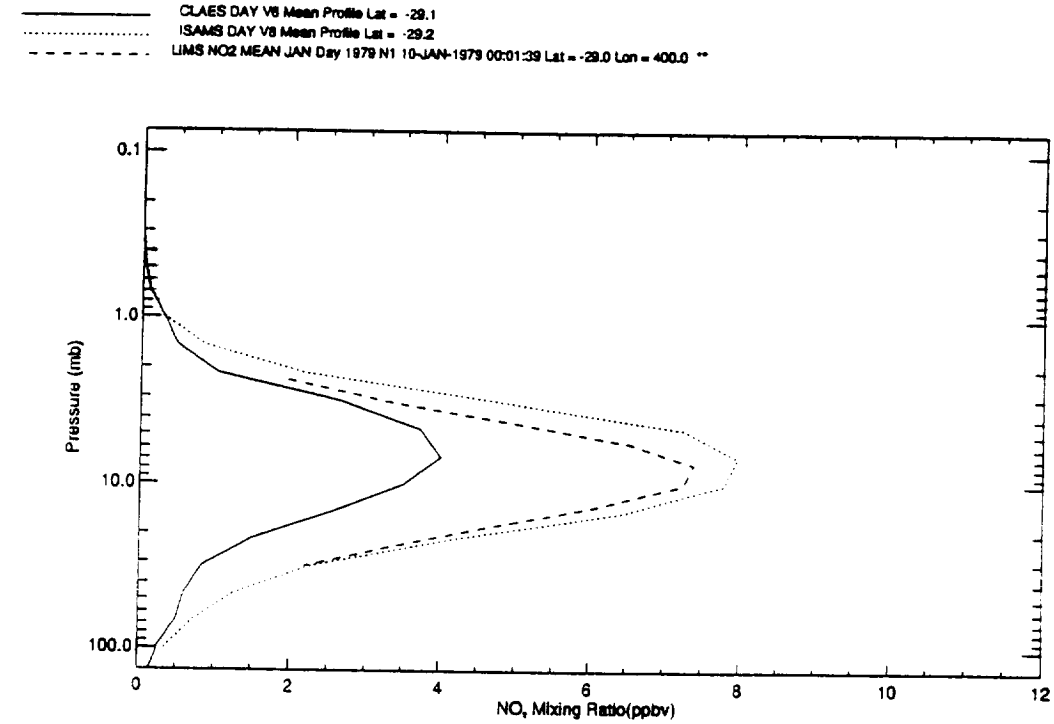

CLAES, ISAMS and LIMS Zonal Mean NO_2 Mixing Ratio Profiles, Daytime from January near 29 S

Figure 9.2.2.1-13. Zonal Mean Profiles of Daytime NO_2 for CLAES and ISAMS on January 10, 1992 and for LIMS on January 10, 1979, Near 29° S.

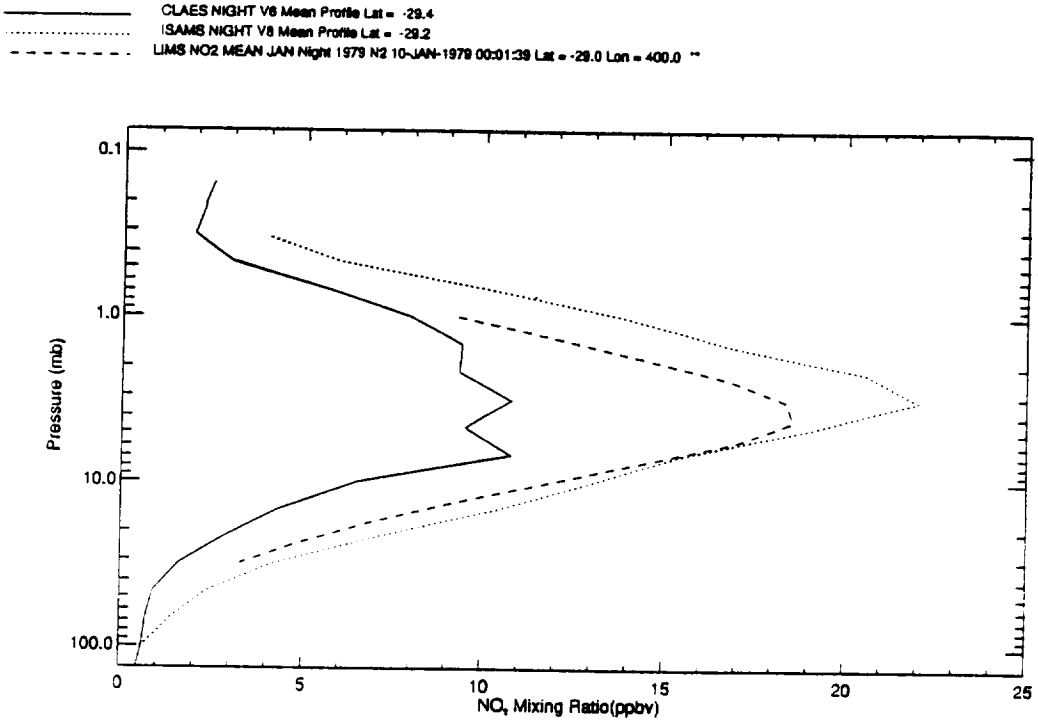

CLAES, ISAMS and LIMS Zonal Mean NO_2 Mixing Ratio Profiles, Nighttime from January near 29 S

Figure 9.2.2.1-14. Zonal Mean Profiles of Nighttime NO_2 for CLAES and ISAMS for January 10, 1992, and for LIMS on January 10, 1979, Near 29° S.

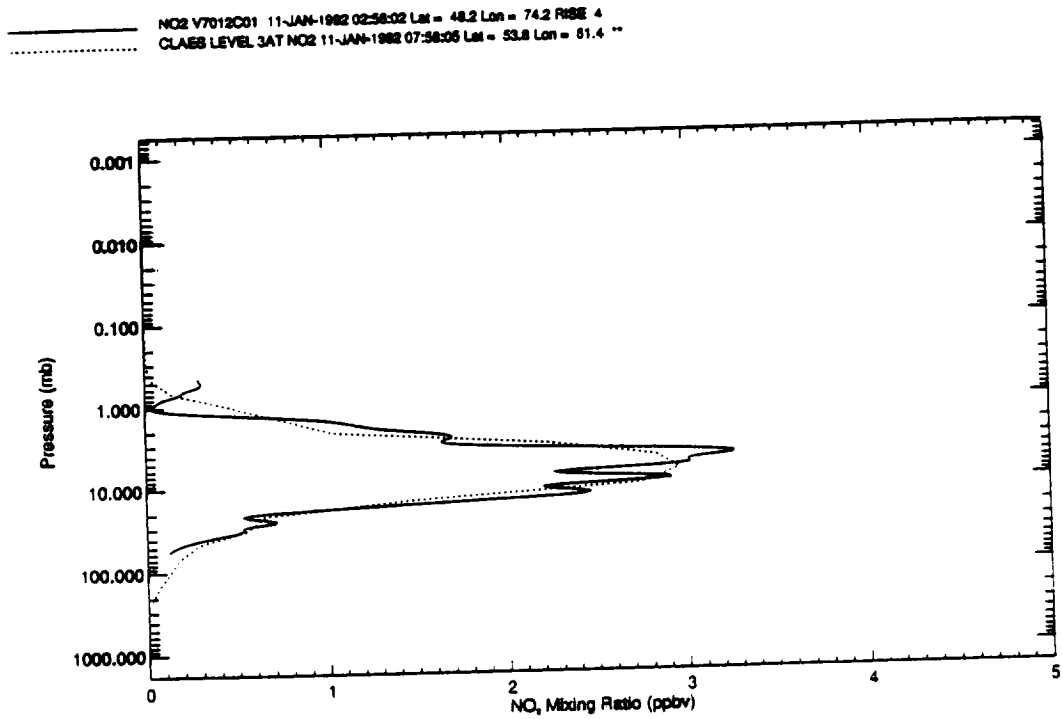

Figure 9.2.2.1-15. Profiles of Sunrise NO_2 for HALOE and CLAES on January 11, 1992.

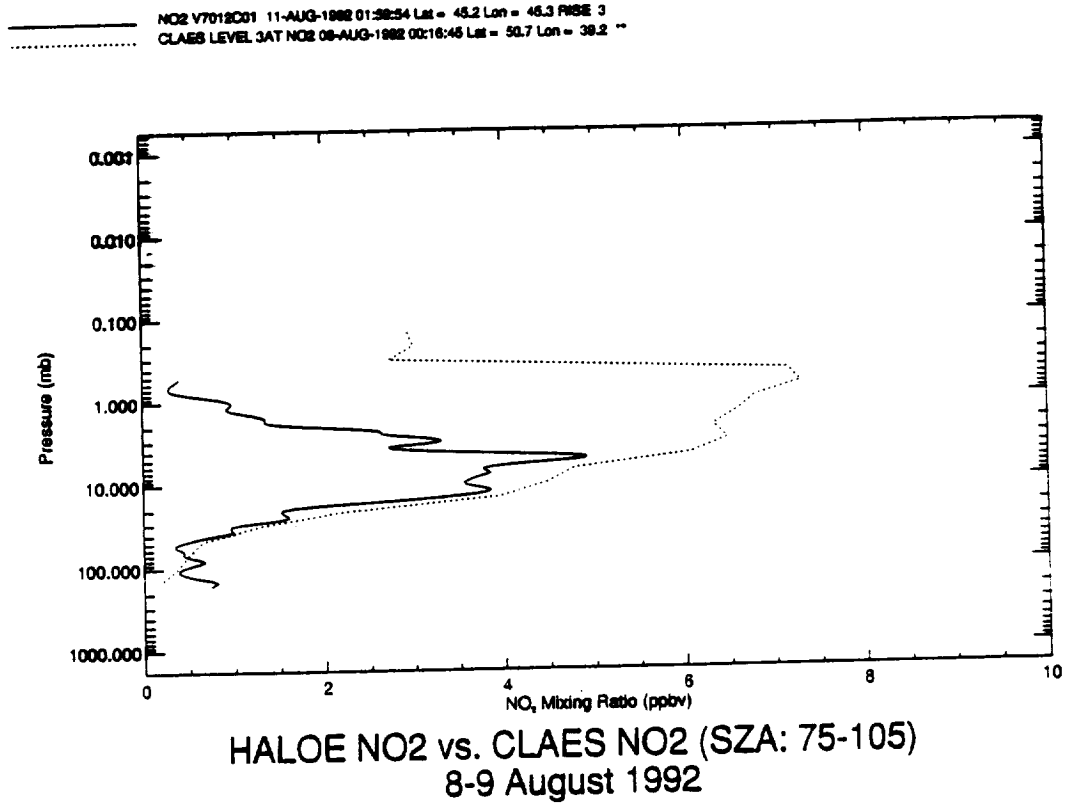

Figure 9.2.2.1-16. Profiles of Sunrise NO_2 for HALOE and CLAES on August 8-9, 1992.

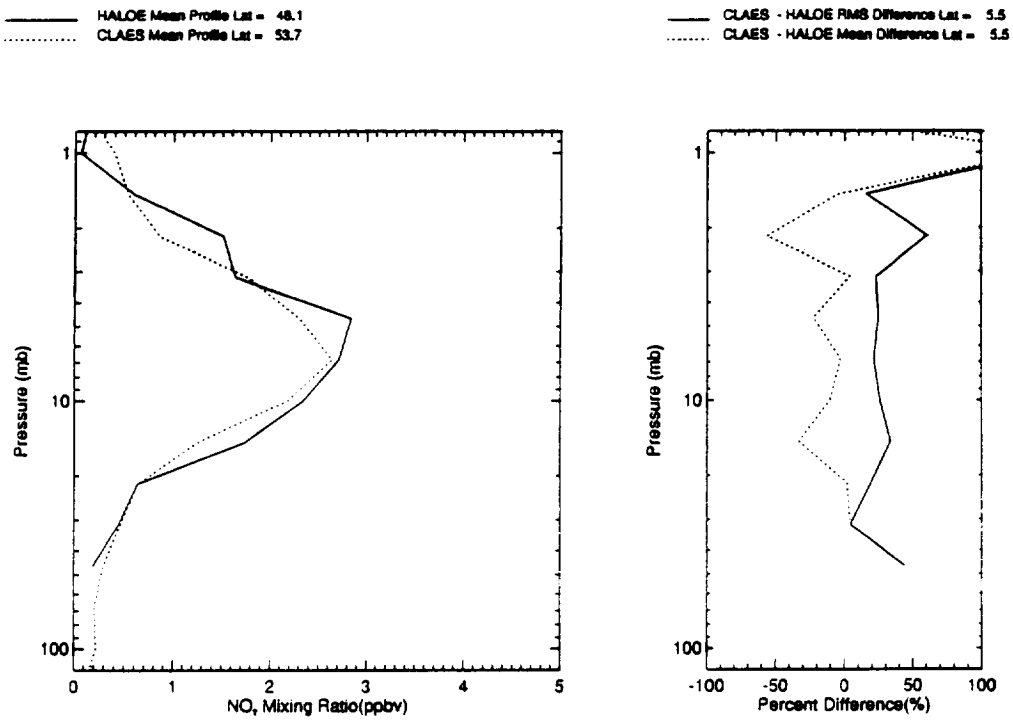

Figure 9.2.2.1-17. Profiles of Sunrise NO_2 for HALOE and CLAES, and CLAES - HALOE RMS Difference and Mean Difference on January 11, 1992.

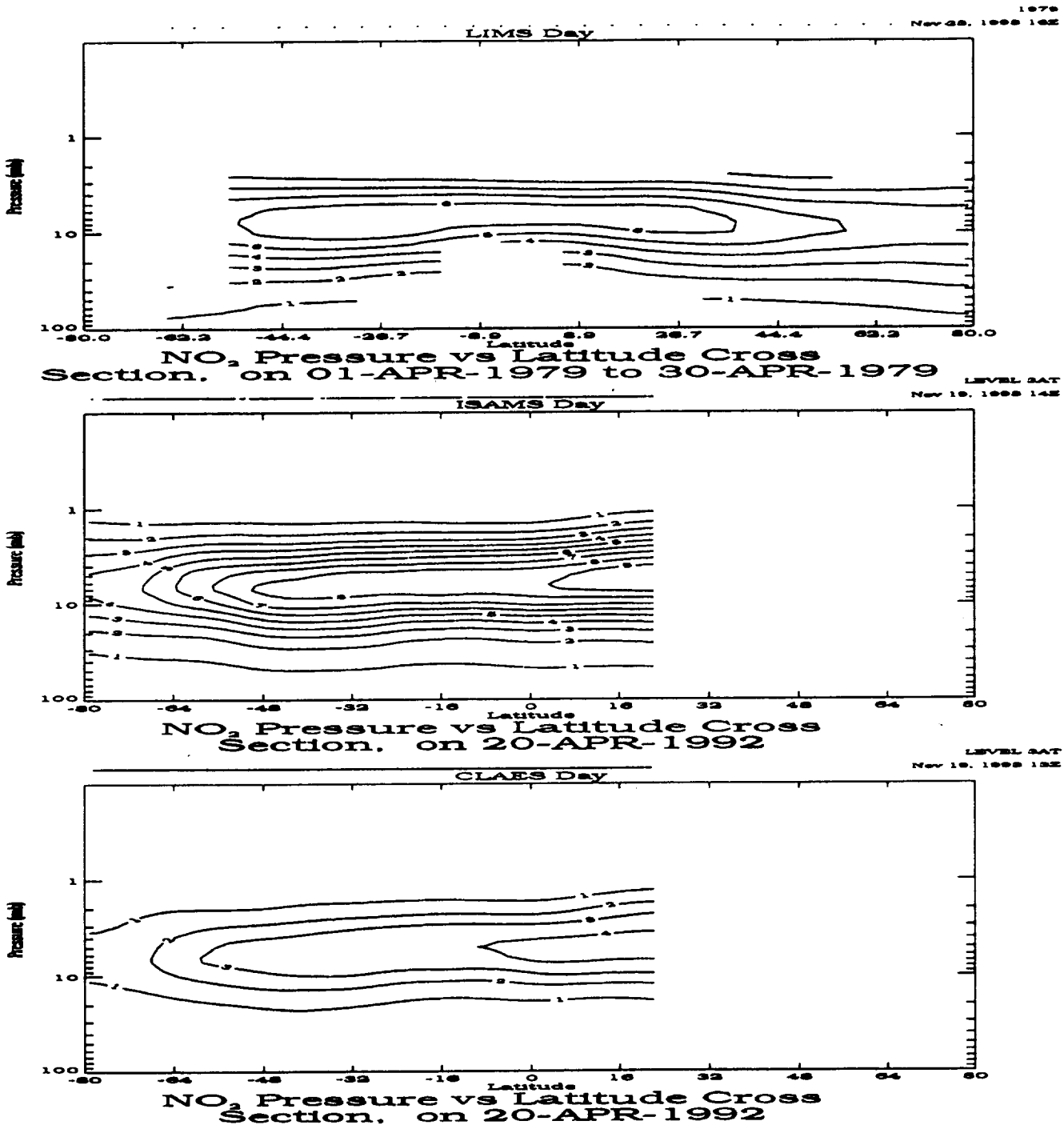

Figure 9.2.2.2-1. Daytime NO_2 Cross-Sections for LIMS on April 1-30, 1979 and for ISAMS and CLAES on April 20, 1992.

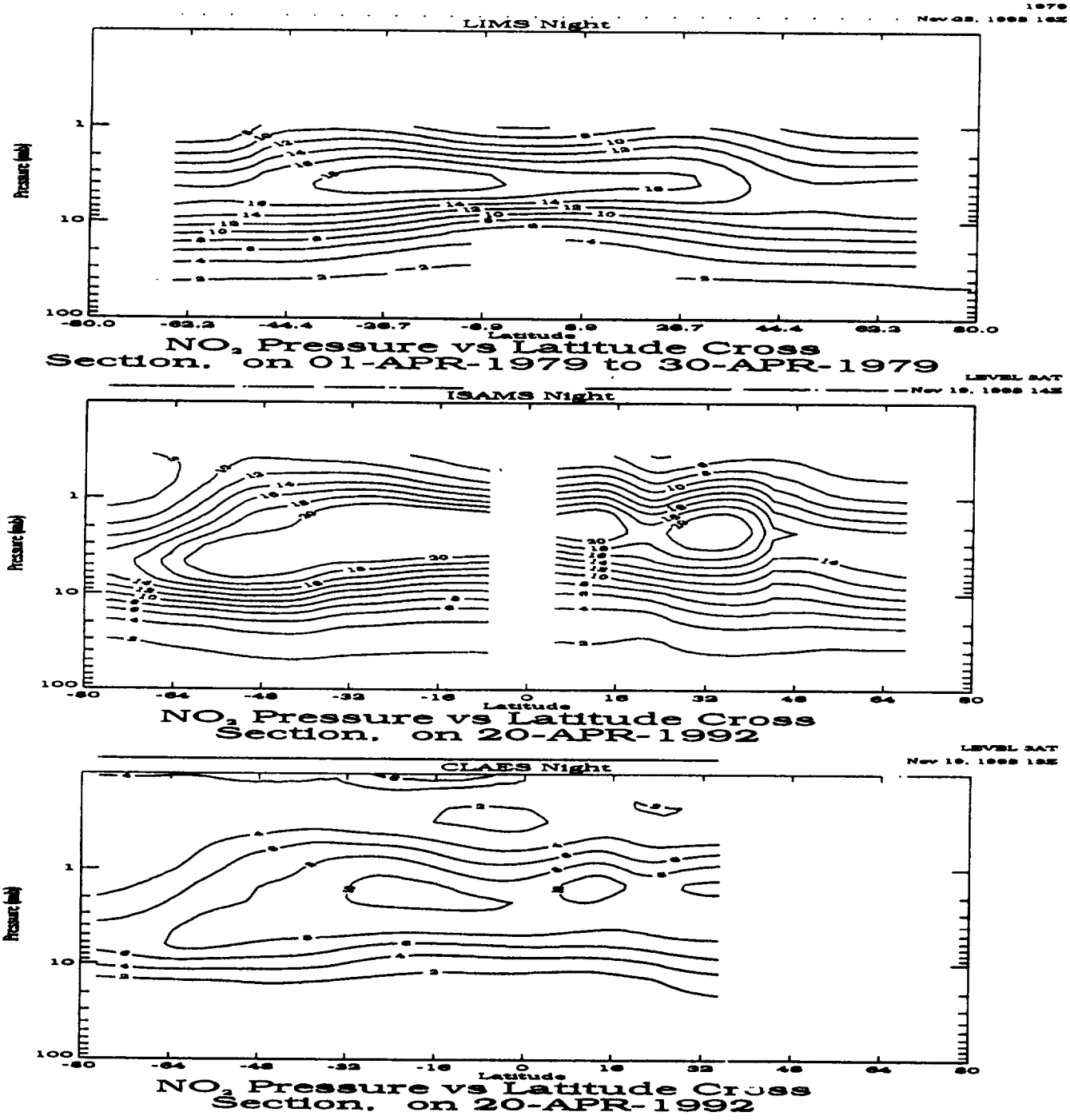

Figure 9.2.2.2-2. Night-time NO_2 Cross-Sections for LIMS on April 1-30, 1979 and for ISAMS and CLAES on April 20, 1992.

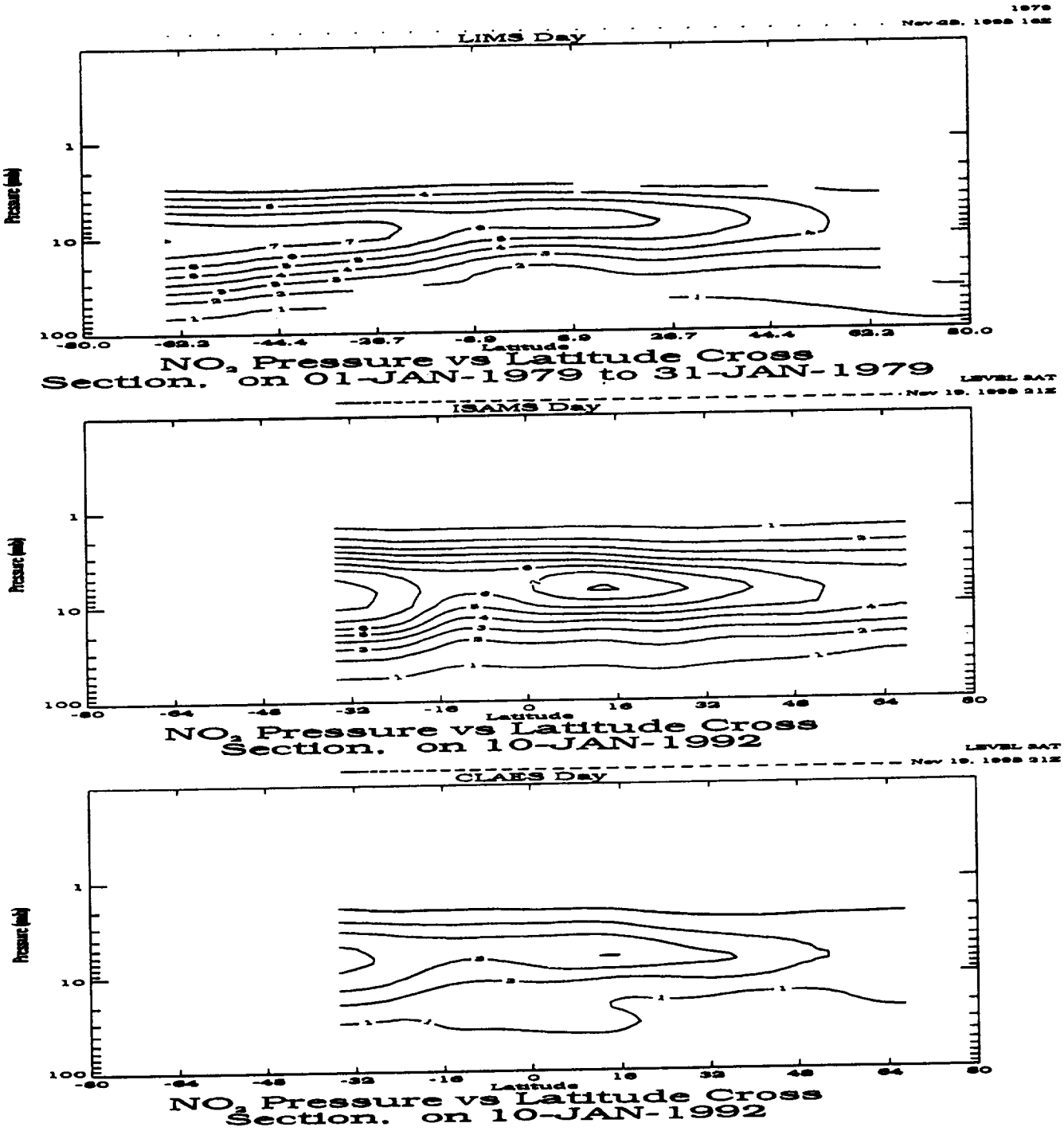

Figure 9.2.2.2-3. Daytime NO_2 Cross-Sections for LIMS on January 1-31, 1979 and for ISAMS and CLAES on January 10, 1992.

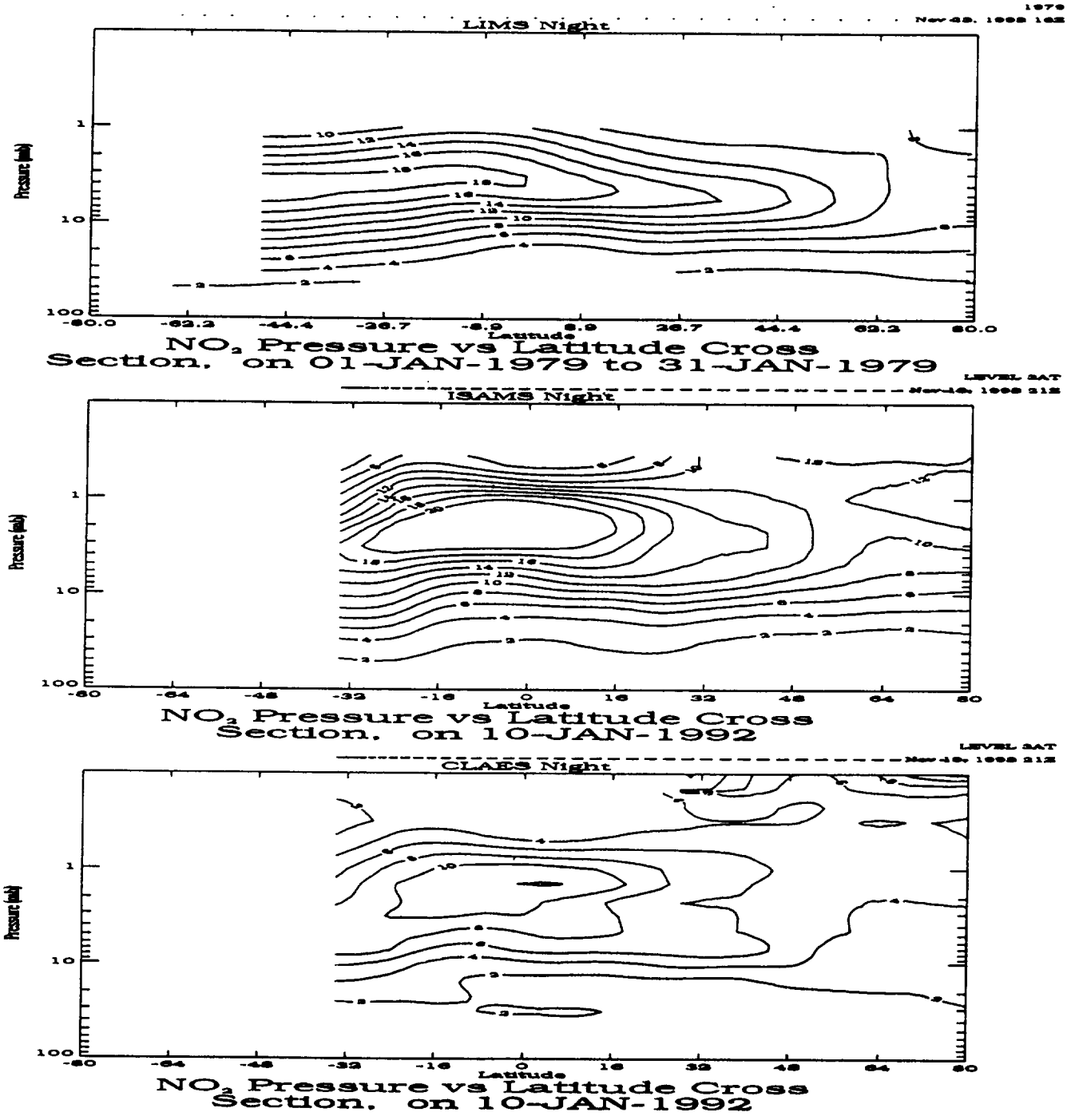

Figure 9.2.2.2-4. Night-time NO_2 Cross-Sections for LIMS on January 1-31, 1979 and for ISAMS and CLAES on January 10, 1992.

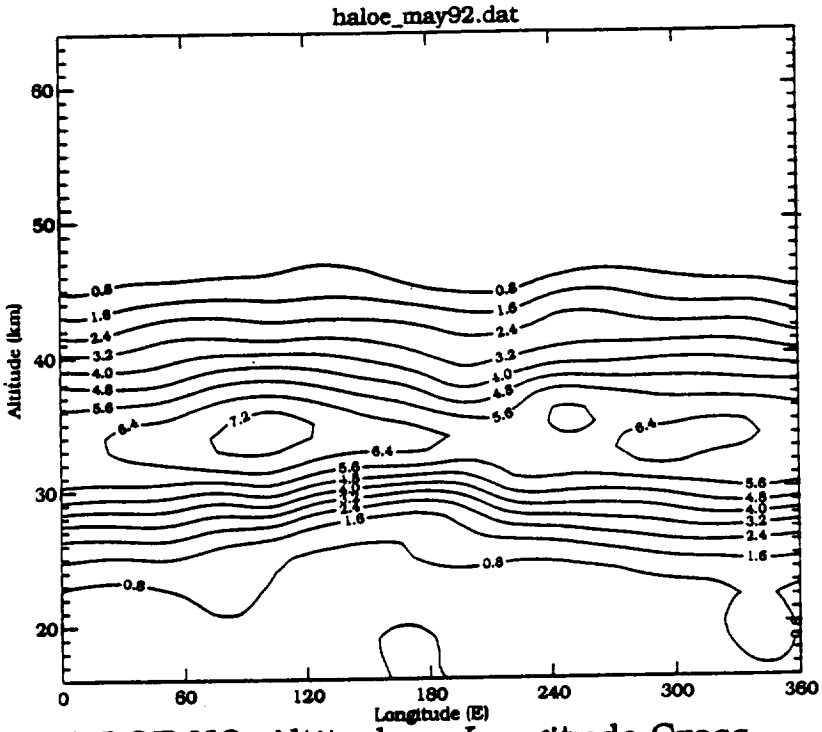

HALOE NO_2 Altitude vs Longitude Cross Section, Sunset on 23-MAY to 24-MAY-1992 at 39 S

Figure 9.2.2.2-5. HALOE Sunset NO_2 Cross-Section for May 23-24, 1992 at 39° S.

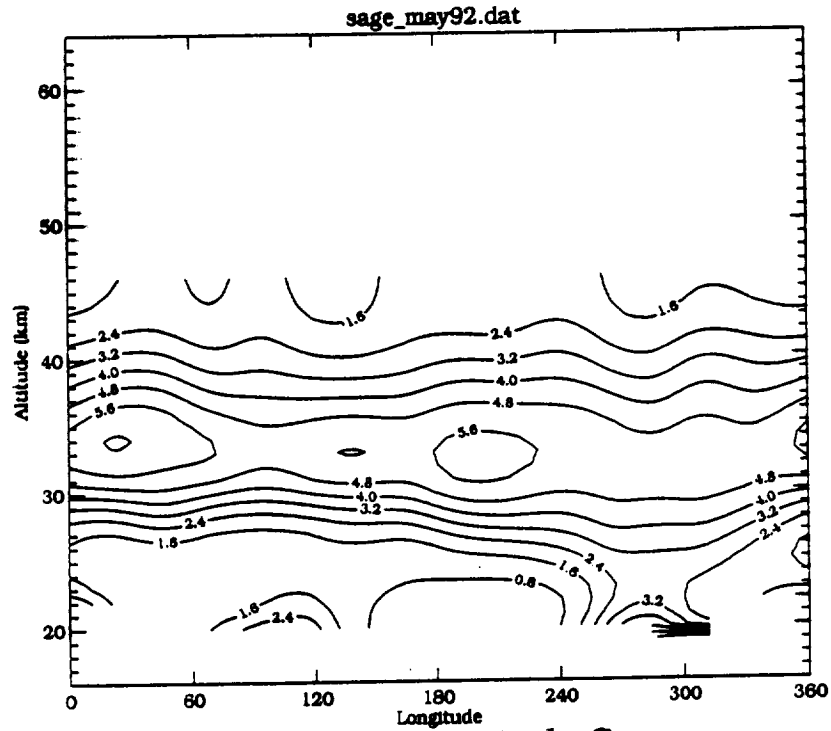

NO_2 Altitude vs Longitude Cross Section, on 20-MAY to 21-MAY-1992 at 39 S

Figure 9.2.2.2-6. SAGE II NO_2 Cross-Section for May 20-21, 1992, at 39° S.

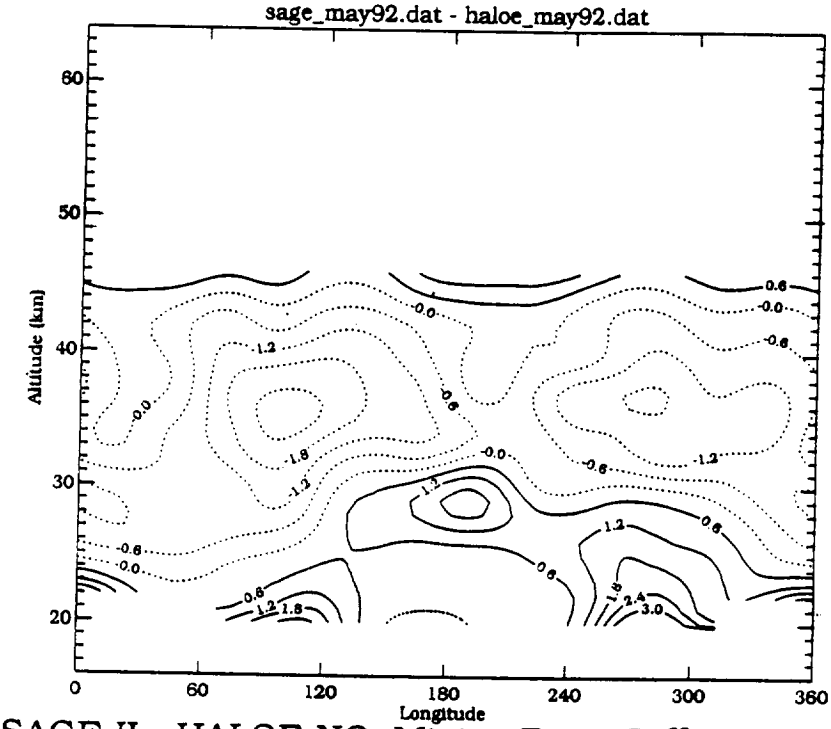

Figure 9.2.2.2-7. NO_2 Cross-Section of SAGE II - HALOE Differences for May 21-24, 1992 Near 37° S.

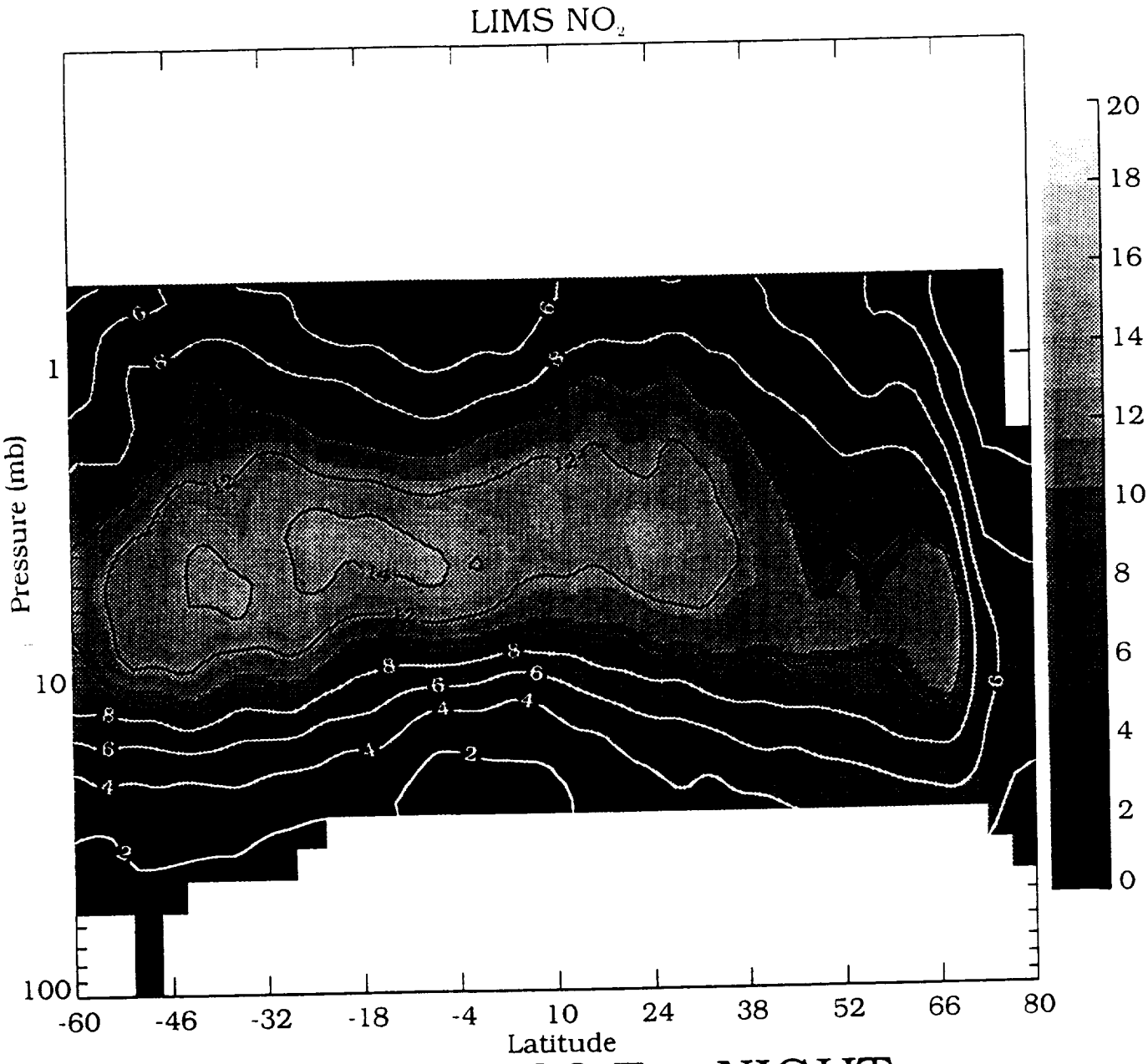

Figure 9.2.2.2-8. LIMS Night-time Zonal Mean NO_2 Cross-Section for May 5, 1979.

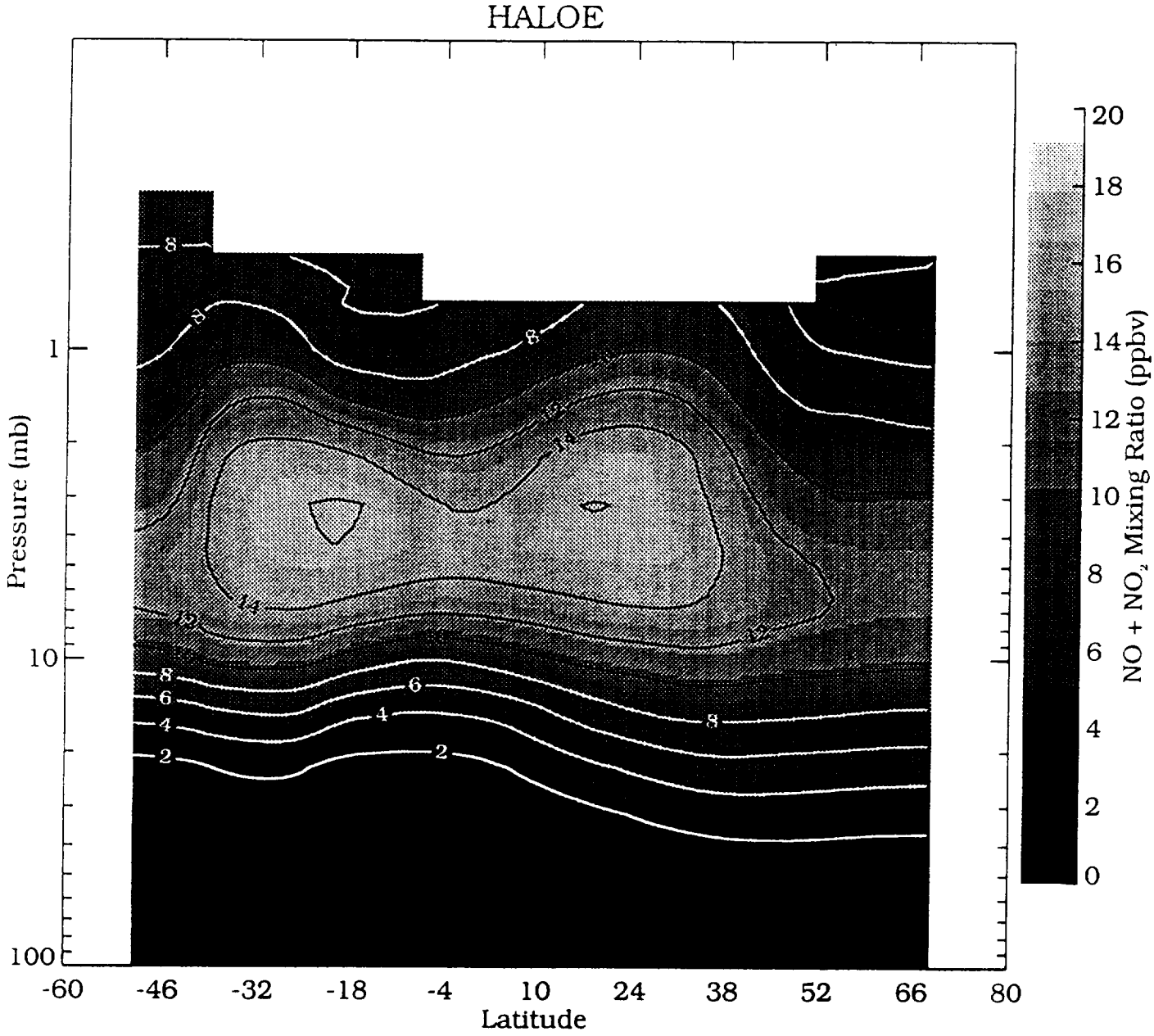

HALOE NO + NO_2 Pressure vs Latitude Cross Section, Sunset on 21-APR to 30-MAY-1993

Figure 9.2.2.2-9. HALOE Sunset NO + NO_2 Cross-Section for April 21 - May 30, 1993.

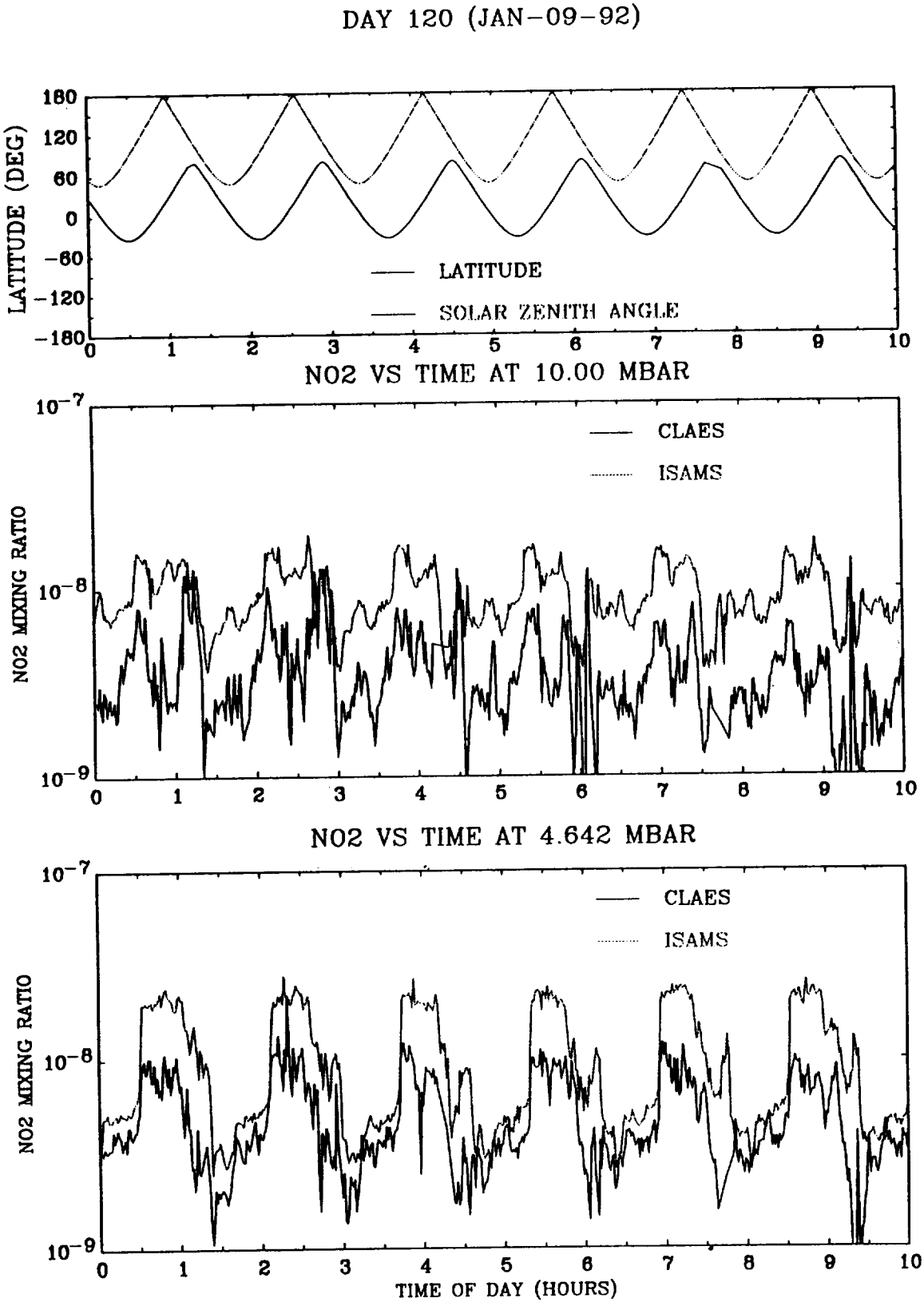

Figure 9.2.2.3-1. Time Series of NO_2 for CLAES and ISAMS on January 9, 1992 on the 10.0 and 4.64 mb Surfaces.

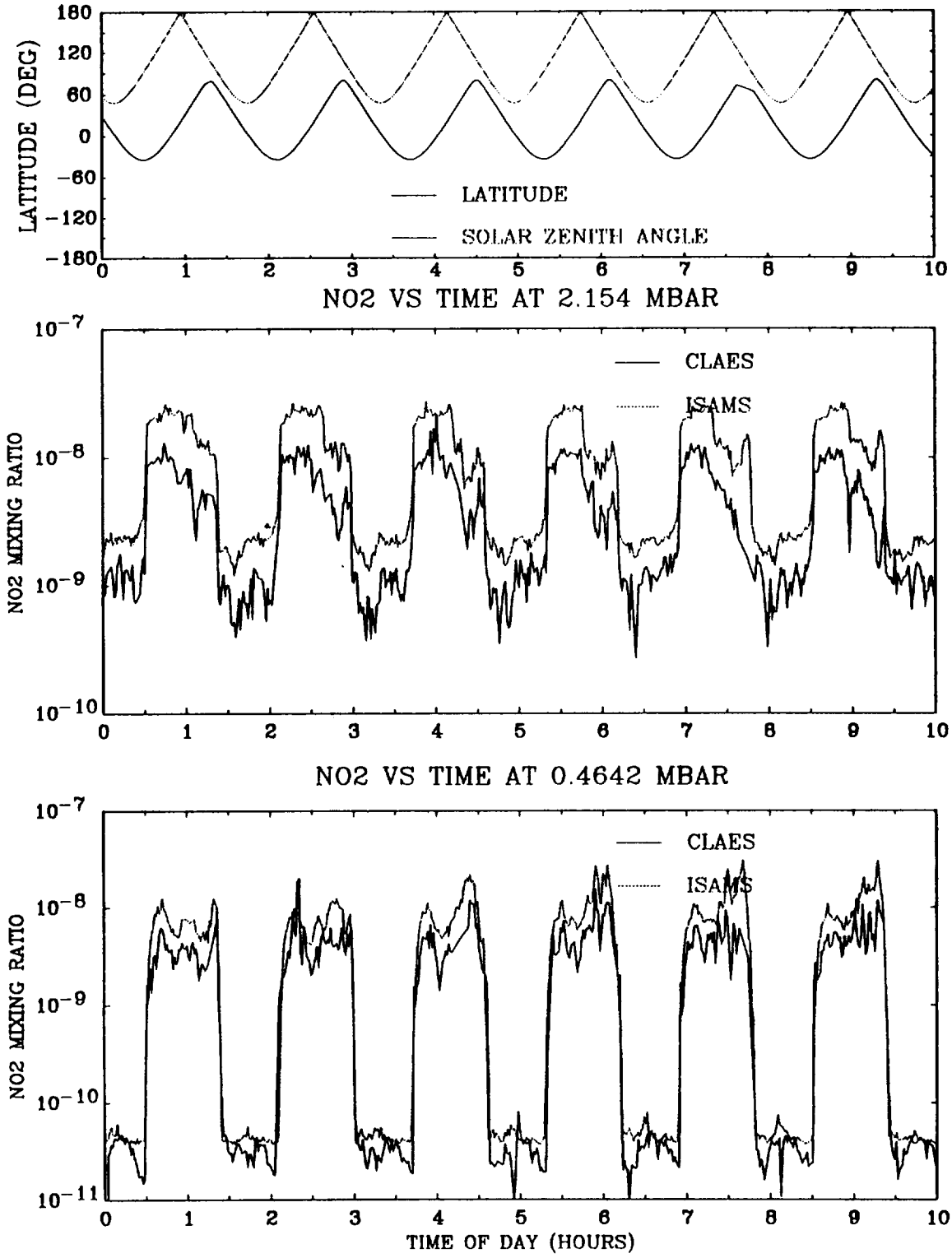

Figure 9.2.2.3-2. Time Series of NO_2 for CLAES and ISAMS on January 9, 1992 on the 2.154 and 0.464 mb Surfaces.

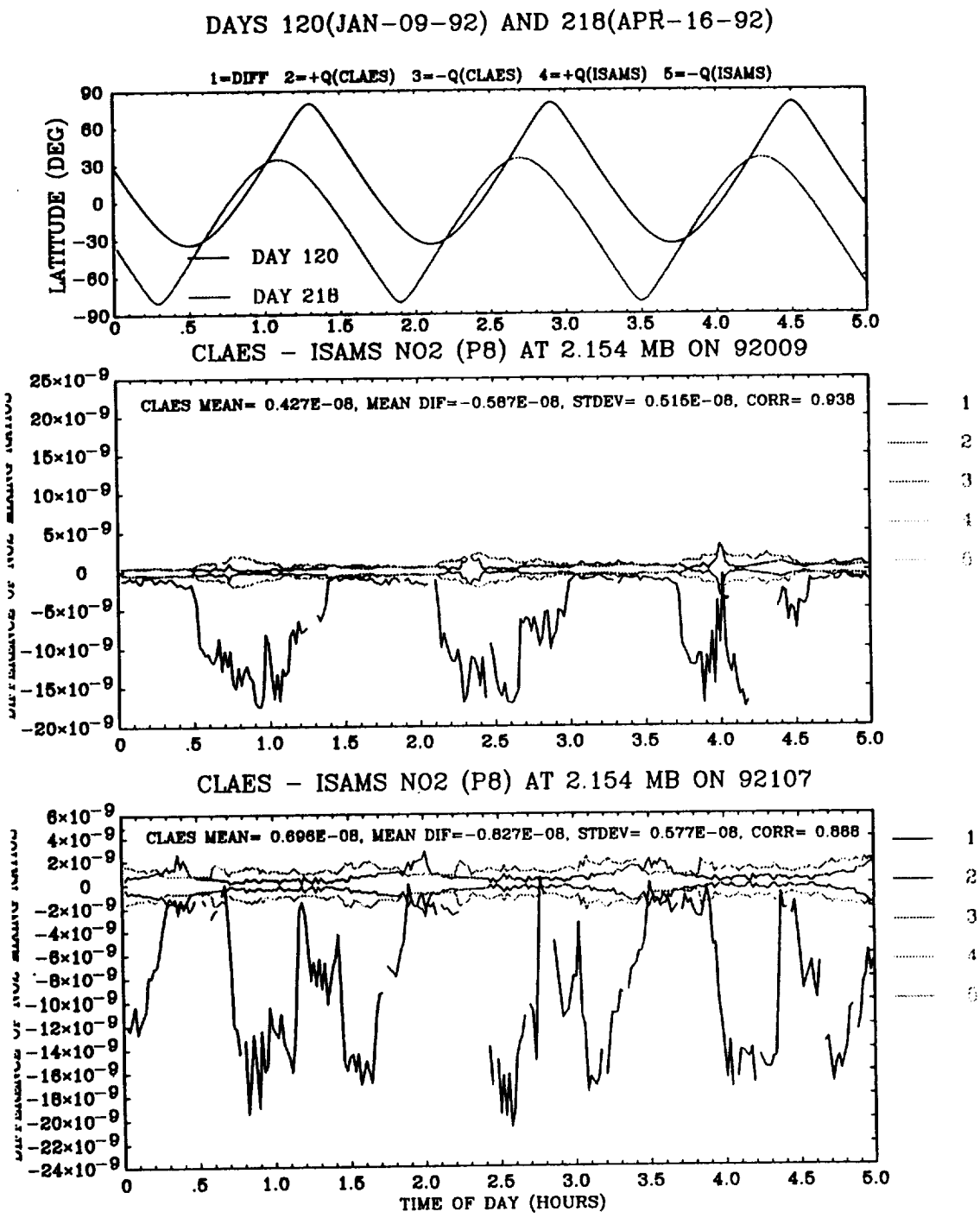

Figure 9.2.2.3-3. Time Series of CLAES - ISAMS NO_2 Differences at 2.154 mb on January 9, 1992 and April 16, 1992.

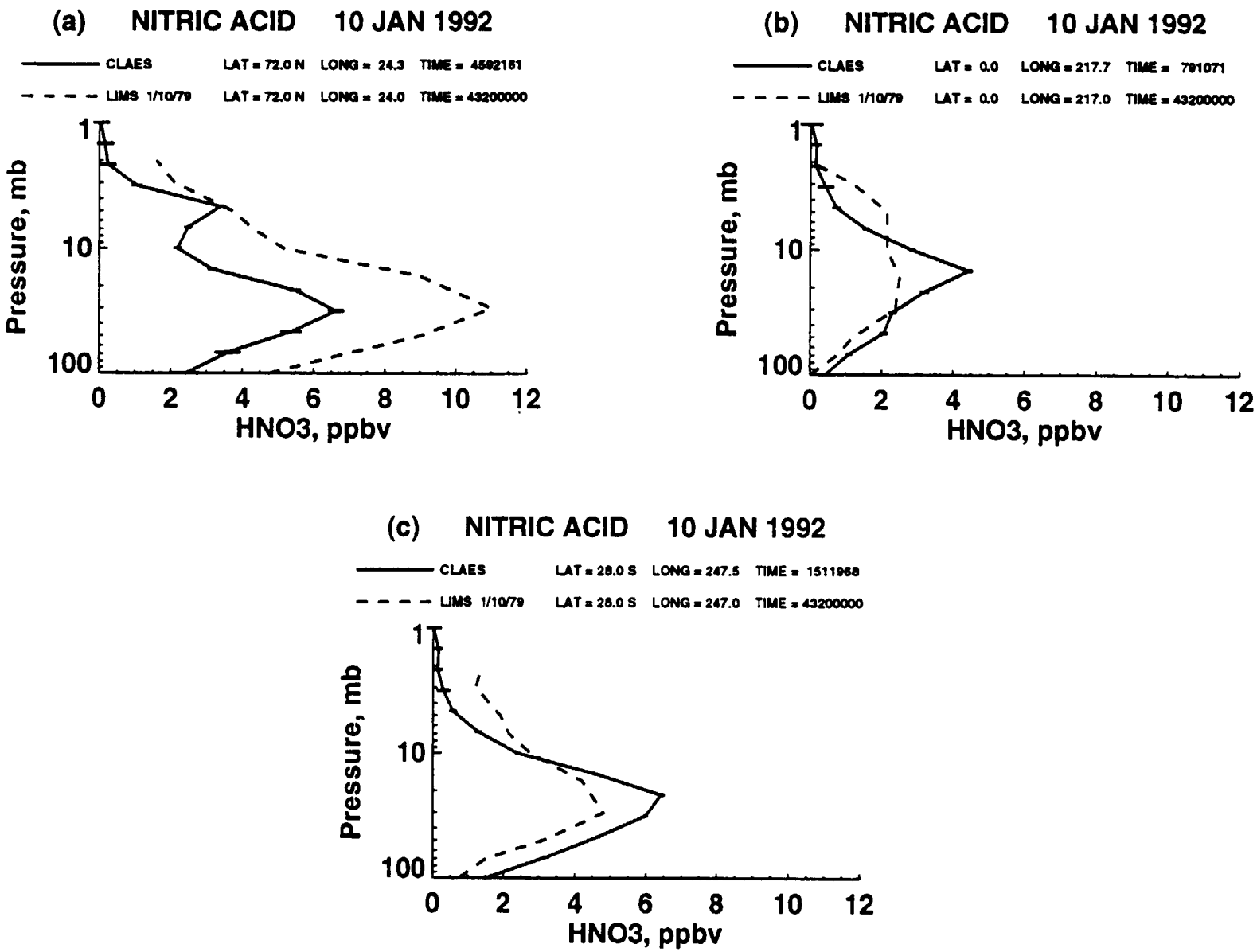

Figure 9.3.2.1-1. Profiles of HNO_3 for CLAES Level 3AL Data on January 10, 1992 and for LIMS Data on January 10, 1979 at (a) 72° N, (b) the Equator, and (c) 28° S.

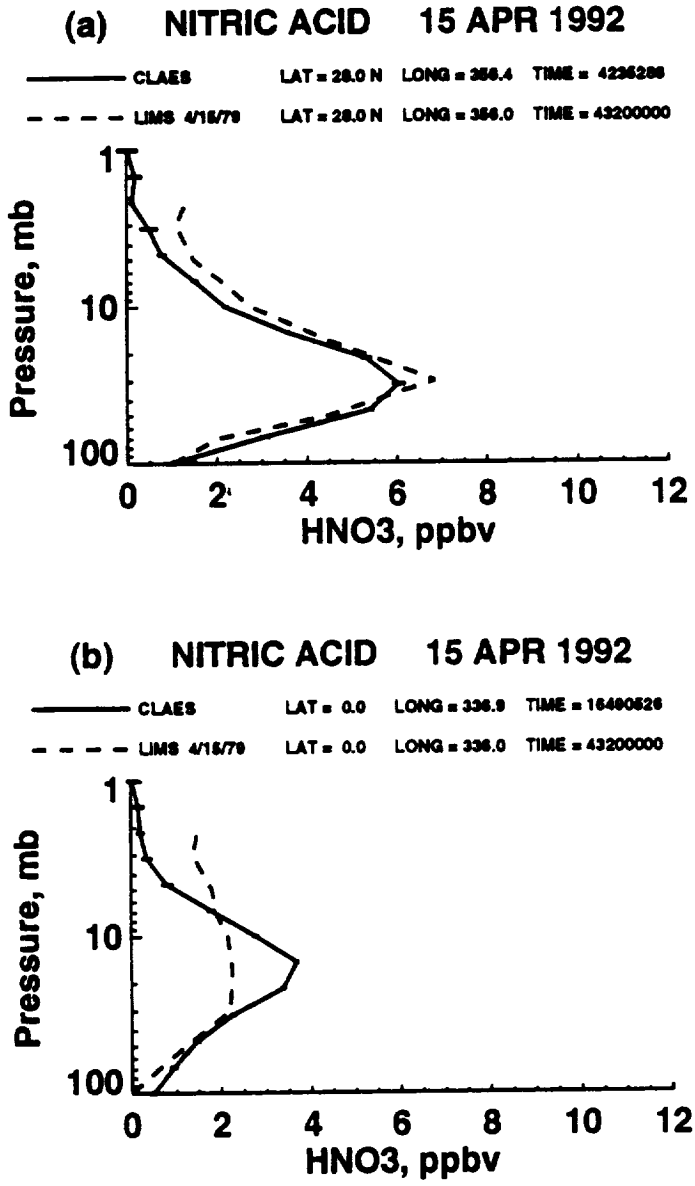

Figure 9.3.2.1-2. Profiles of HNO_3 for CLAES Level 3AL Data on April 15, 1992 and for LIMS Data on April 15, 1979 at (a) 28° N, and (b) the Equator.

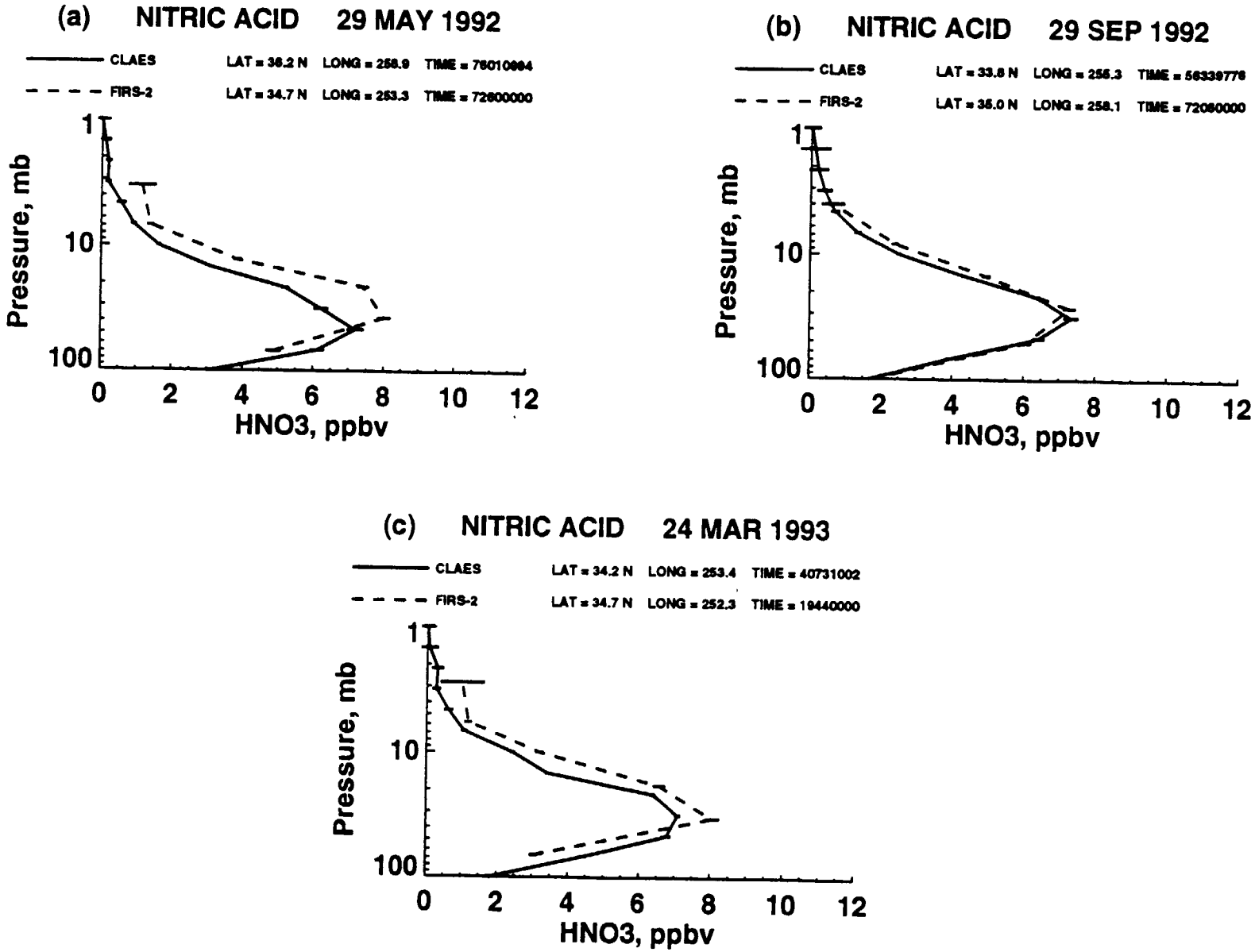

Figure 9.3.2.1-3. Profiles of HNO_3 for the CLAES Level 3AT Data and the Traub FIRS-2 Data on (a) May 29, 1992, (b) September 29, 1992, and (c) March 24, 1993.

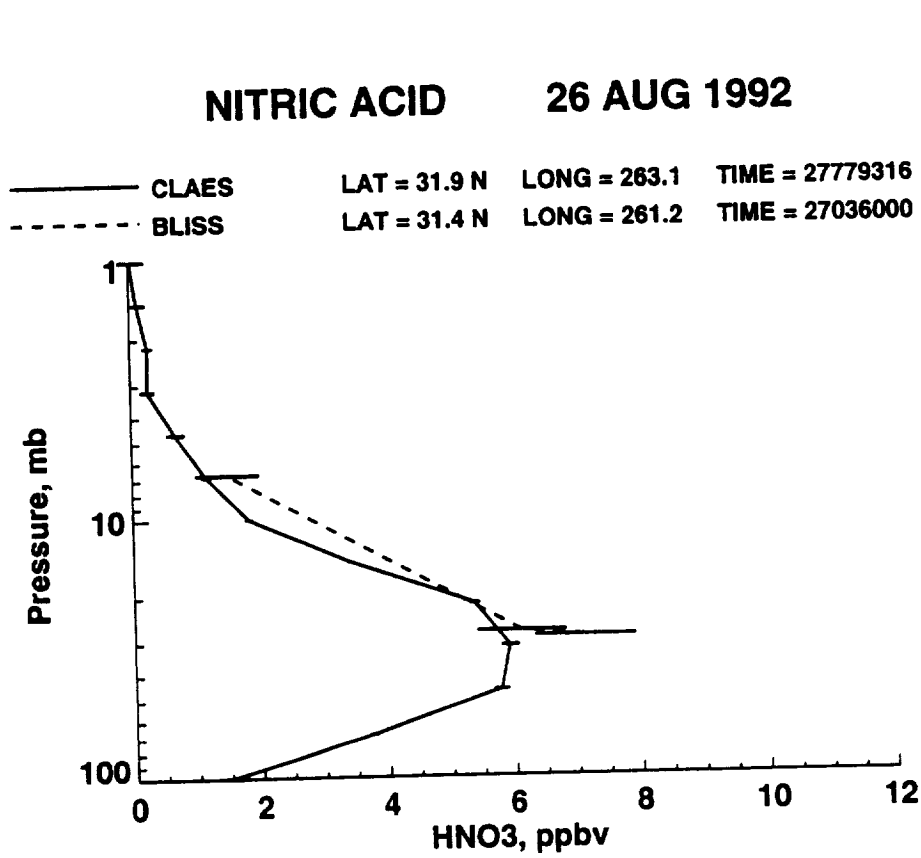

Figure 9.3.2.1-4. Profiles of HNO_3 for the CLAES Level 3AT Data and the Webster BLISS Data on August 26, 1992.

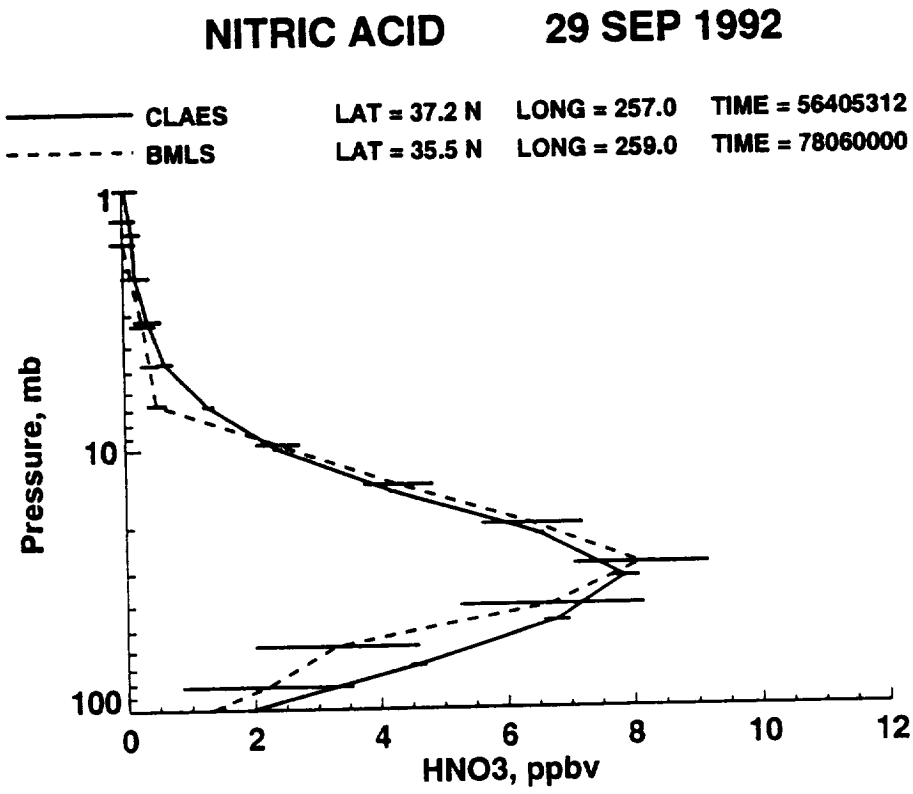

Figure 9.3.2.1-5. Profiles of HNO_3 for the CLAES Level 3AT Data and the Stachnik BMLS Data on September 29, 1992.

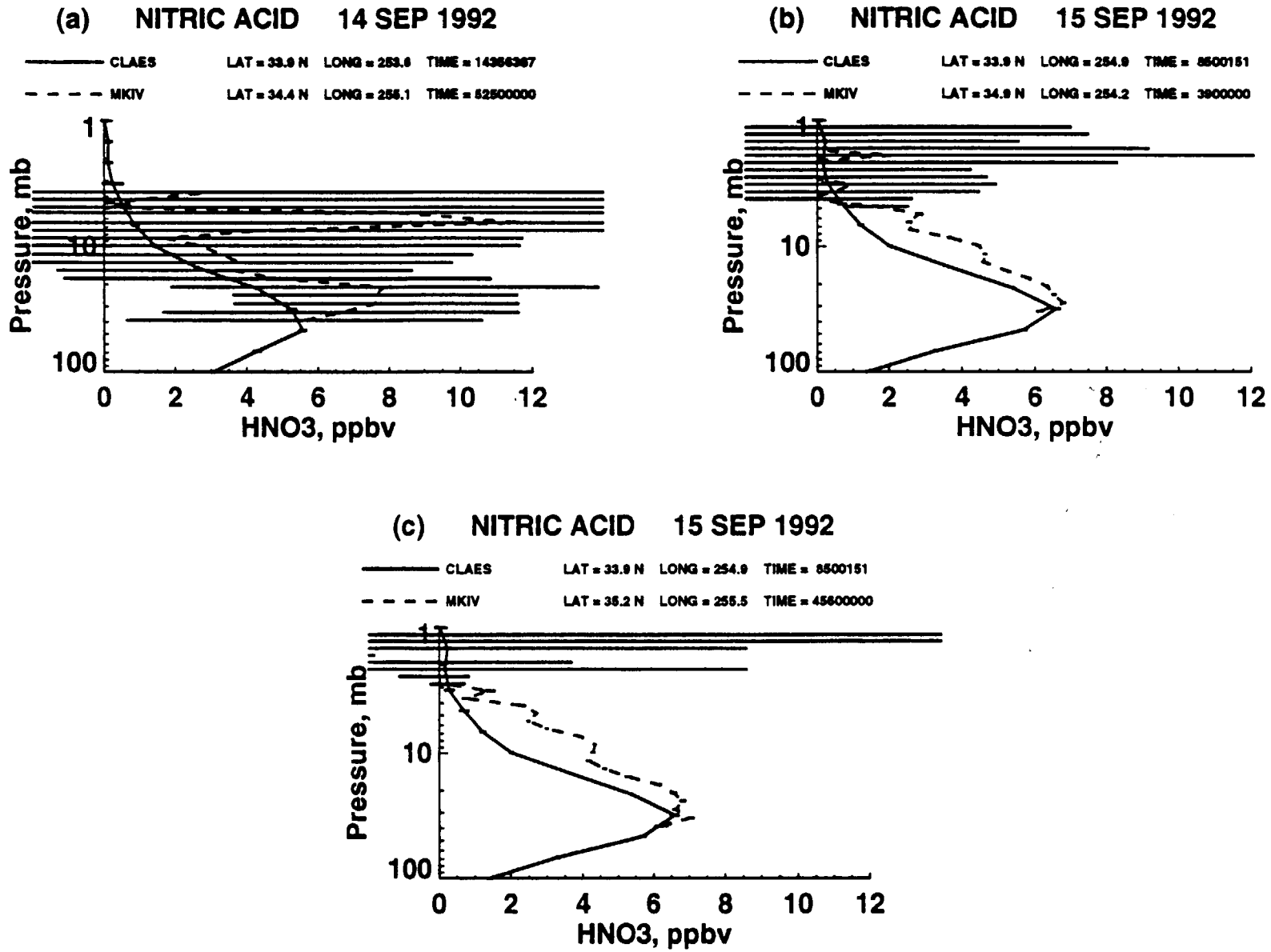

Figure 9.3.2.1-6. Profiles of HNO_3 for the CLAES Level 3AT Data and the Toon MKIV Data on (a) September 14, 1992, (b) September 15, 1992 (1st MKIV Data Set), and (c) September 15, 1992 (2nd MKIV Data Set). Note: Large error bars associated with the MKIV data.

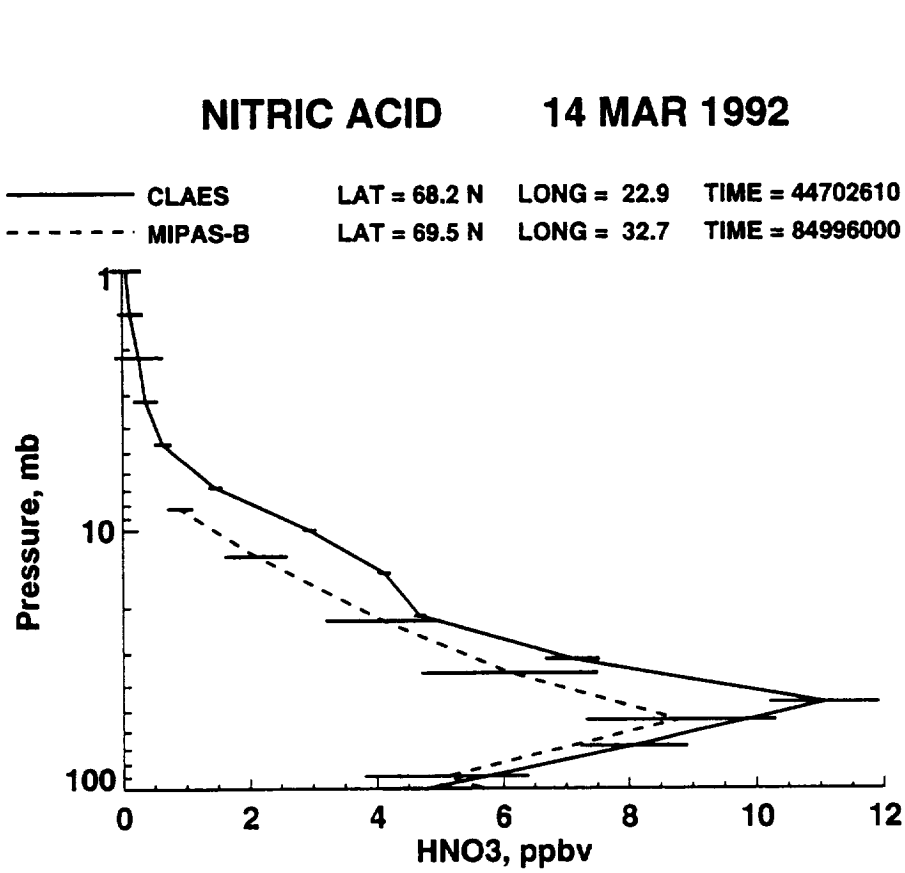

Figure 9.3.2.1-7. Profiles of HNO_3 for the CLAES Level 3AT Data and the Oelhaf MIPAS-B Data on March 14, 1992.

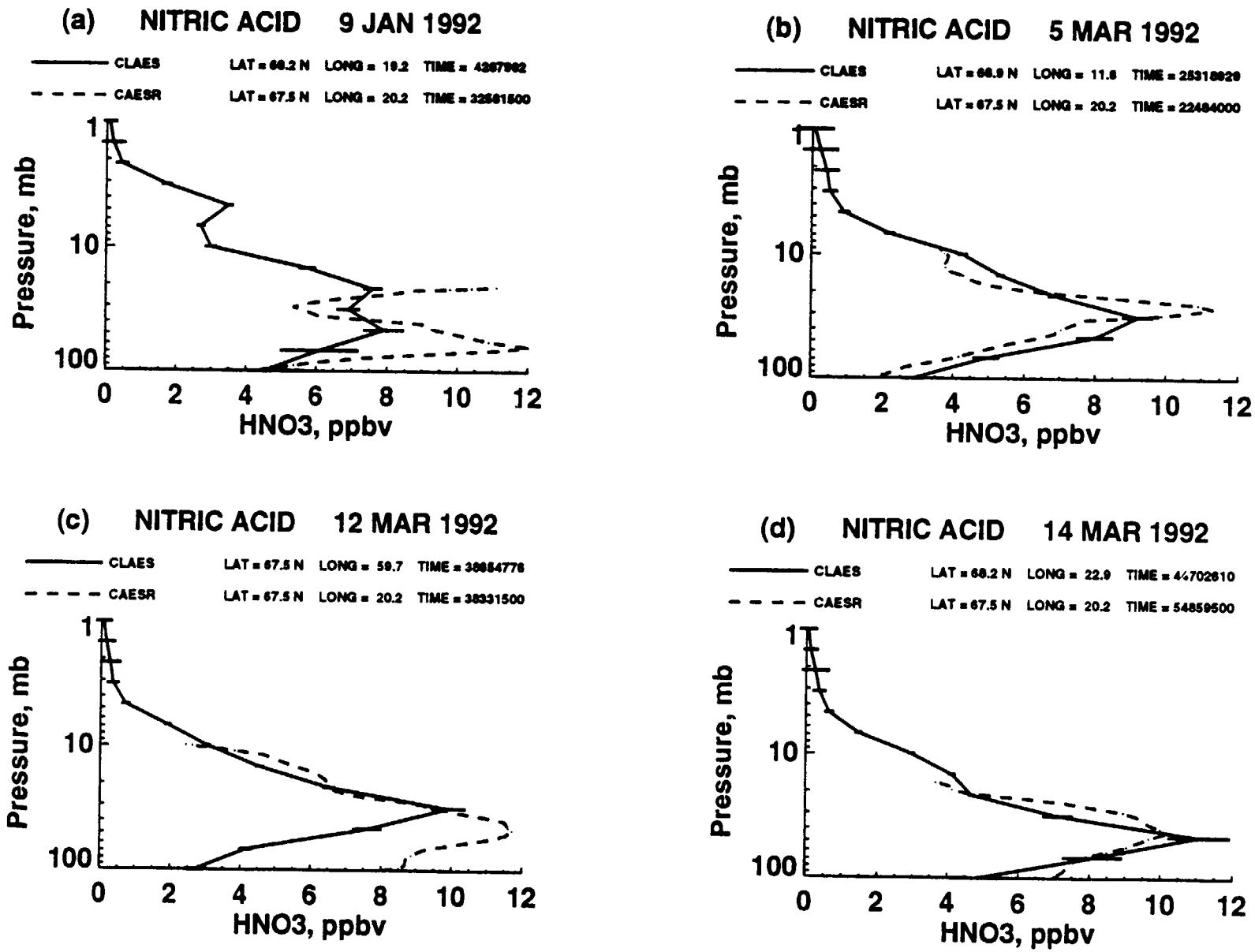

Figure 9.3.2.1-8. Profiles of HNO_3 for the CLAES Level 3AT Data and the Murcray CAESR Data on (a) January 9, 1992, (b) March 5, 1992, (c) March 12, 1992, and (d) March 14, 1992.

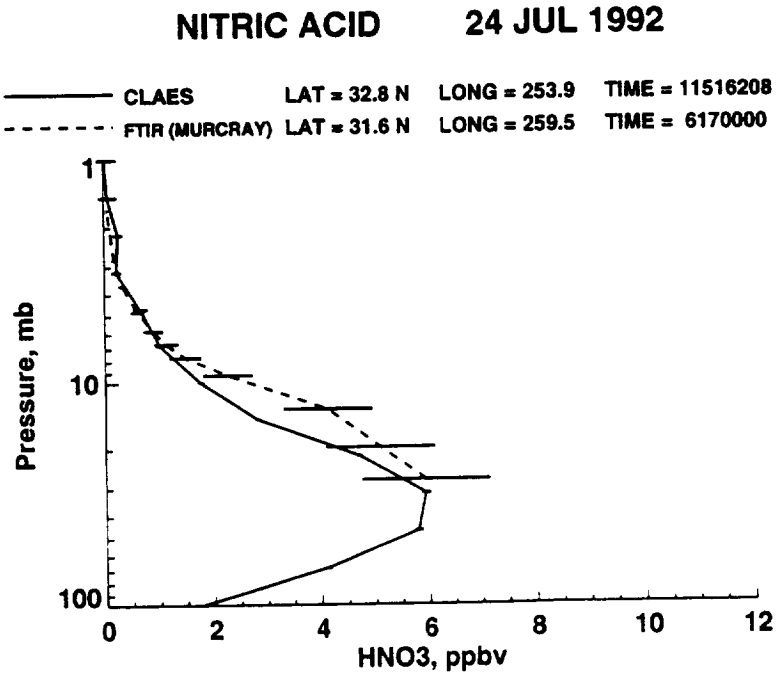

Figure 9.3.2.1-9. Profiles of HNO_3 for the CLAES Level 3AT Data and the Murcray FTIR Data on July 24, 1992.

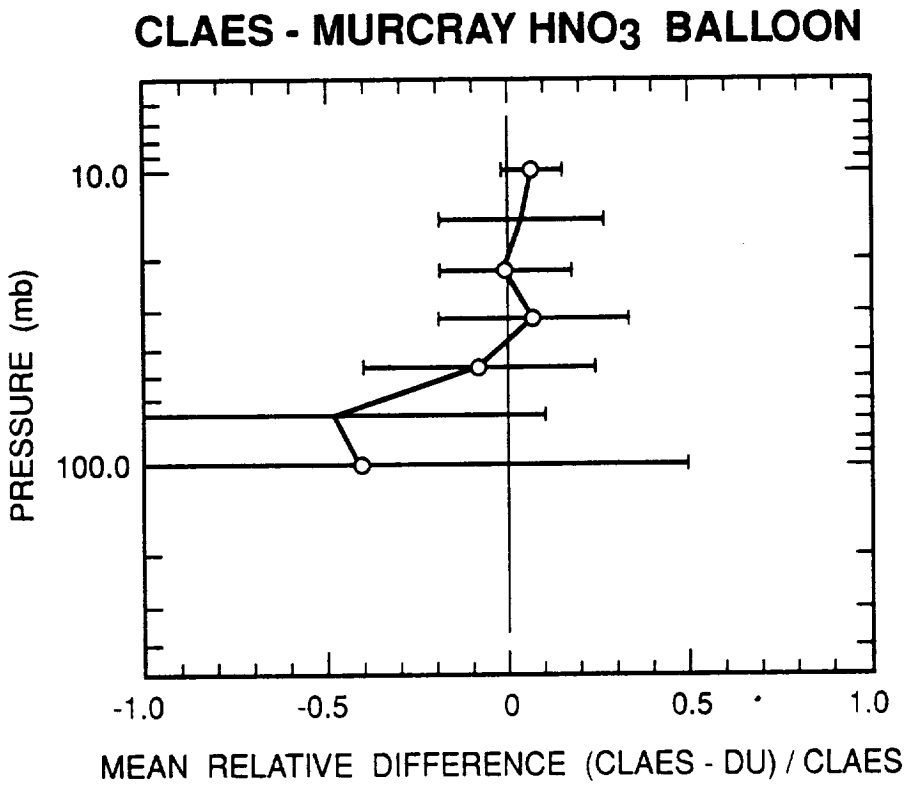

Figure 9.3.2.1-10. Mean Relative Difference Between the CLAES Level 3AT Data and the Murcray Data.

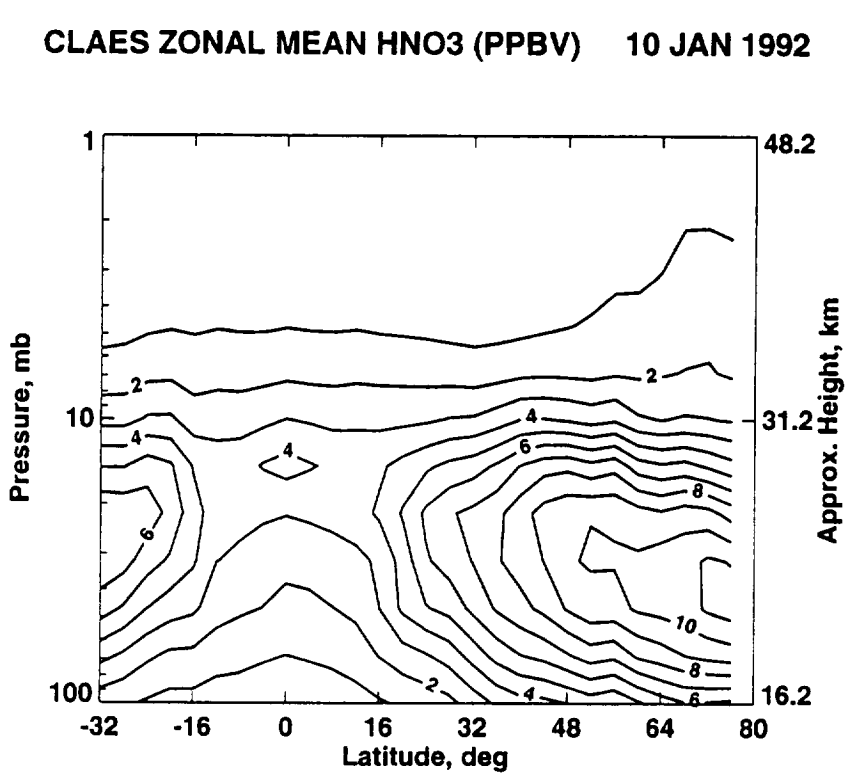

Figure 9.3.2.2-1. CLAES (Level 3AL) Zonal Mean HNO_3 Cross-Section for January 10, 1992 (1.0 ppbv Contour Interval).

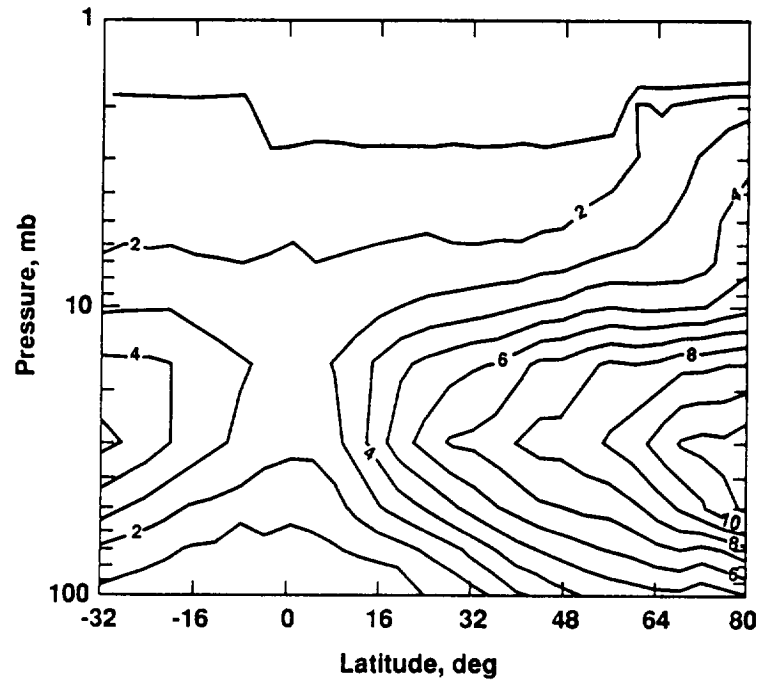

Figure 9.3.2.2-2. LIMS Zonal Mean HNO_3 Cross-Section for January 10, 1979 (1.0 ppbv Contour Interval).

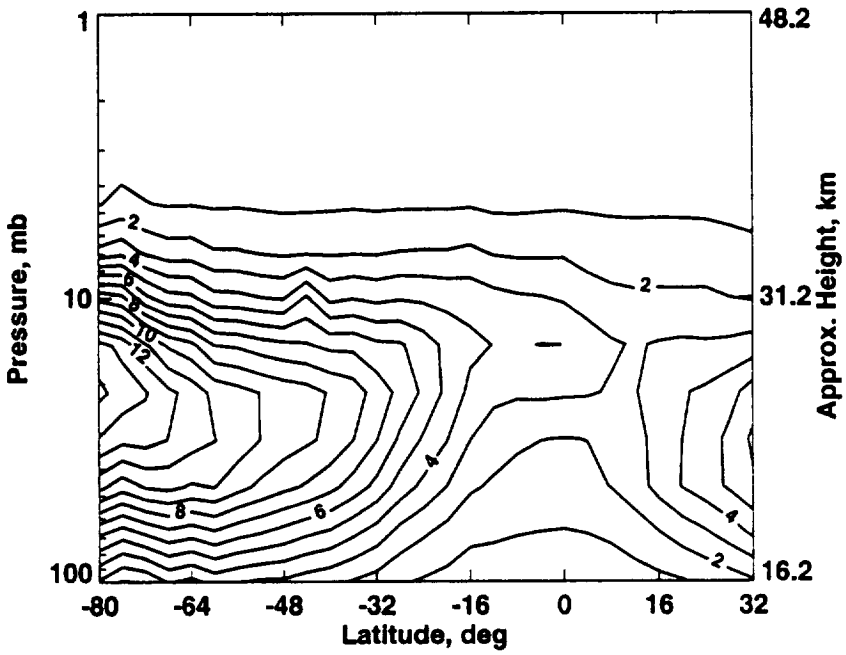

Figure 9.3.2.2-3. CLAES (Level 3AL) Zonal Mean HNO_3 Cross-Section for April 15, 1992 (1.0 ppbv Contour Interval).

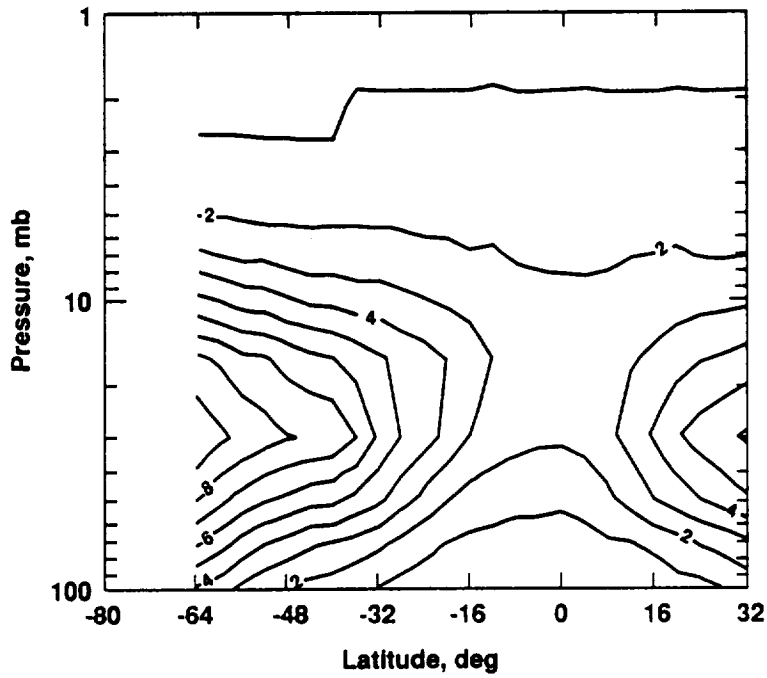

Figure 9.3.2.2-4. LIMS Zonal Mean HNO_3 Cross-Section for April 15, 1979 (1.0 ppbv Contour Interval).

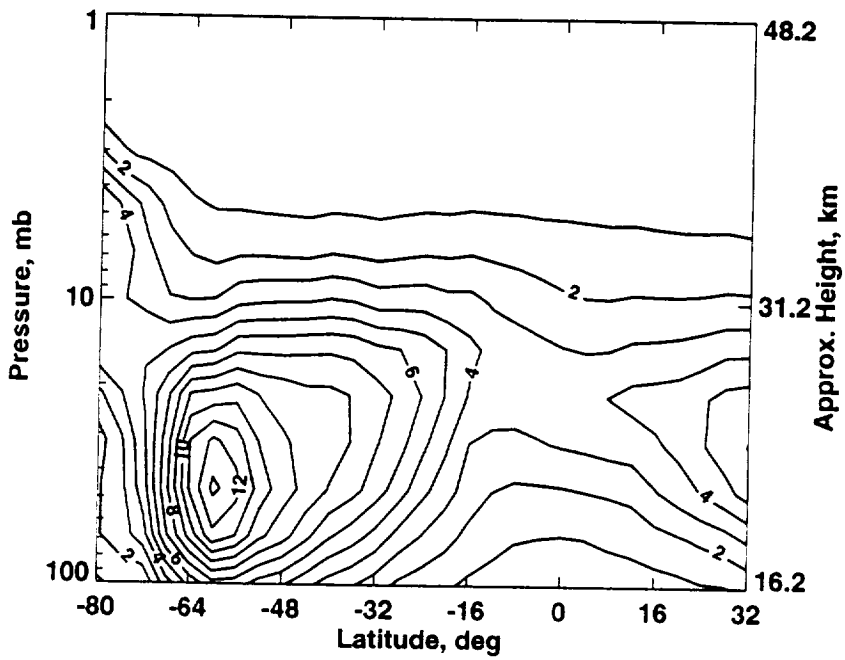

Figure 9.3.2.2-5. CLAES (Level 3AL) Zonal Mean HNO_3 Cross-Section for August 25, 1992 (1.0 ppbv Contour Interval).

APPENDIX A

Meteorological Overview for UARS Data Validation Periods

A.1 Data

The temperatures in this appendix are taken from analyzed fields produced by the National Meteorological Center's (NMC) Climate Analysis Center (CAC). Balanced wind estimates and inferred Ertel potential vorticity (EPV) fields were calculated at the NASA Goddard Space Flight Center. Potential vorticity is a dynamical variable that is approximately conserved for periods of several weeks in the lower stratosphere and as such can be a useful tracer for atmospheric motions. At upper stratospheric levels (~ 1 hPa and above) diabatic effects become more important and potential vorticity is not as well conserved. Regions of strong winds are located in regions where the potential vorticity gradient is large. Selected maps of temperature are presented for the lower (50 hpa), middle (10 hPa), and upper (1hPa) stratosphere. Maps of EPV are presented for the 460, 850, and1200 K potential temperature surfaces (nominally corresponding to the 50, 10, and 4 hPa levels, respectively). Some care must be exercised in interpreting the global EPV distributions. The balanced winds used to construct the EPV distributions are not expected to be accurate in the tropics, so that the EPV fields should be considered unreliable within 10 degrees of the equator. In addition, small scale features may be aliased because of the satellite sampling, and therefore only the larger-scale wavenumbers (wavenumbers 1-6) will be discussed.

January 9-11, 1992

The first UARS validation period is January 9-11,1992. An overview of the 91/92 winter stratosphere is given by Newman et al. (1993). A sudden warming is evident at the 10 hPa level during that period and can clearly be seen in the temperature-time section shown in Fig.1a. The maximum temperature increased by 20K in the Northern Hemisphere from the 9th to the 10th. This increase appeared in the warm air of the dominant wave one temperature pattern located at about 70N and 105E. The wave one pattern can be seen in Fig. 2. This wave one pattern exhibited a strong westward tilt with height. The peak-to-peak Northern Hemisphere temperature variation on January 10 was about 37, 50, and 60K at 50, 10, and 1 hPa, respectively.

As evident in Fig. 1a, the warming occurred slightly earlier at the 1 hPa level, and the maximum temperature at this level was decreasing at this time. Inspection of the temperature fields at this level shows about a 5K temperature decrease in both the warm and cold regions during the validation period.

The Ertel potential vorticity (EPV) distribution on the 850K isentropic surface (about 10 hPa) for January 10 is shown in Fig. 3. The polar vortex is displaced off the pole, and highest values of EPV are centered over the coldest air.

Like the temperature fields, the vortex was tilted westward with height. The large temperature changes from the 9th to the 10th were due to a combination of downward motion in the warming region and some horizontal advection occurring in the region where EPV contours cross the isotherms. If horizontal advection is neglected, a vertical velocity estimate of -1.5 cm/sec (-1.2 km/day) is required for vertical advection and adiabatic compression to balance the observed temperature change.

The minimum temperatures at the three selected levels for January 1992 are shown in Fig.1-b. The minimum 50 hPa temperature first fell below 195K (an approximate threshold for Type I PSC's at this level) on December 15, 1991, and except for a brief rise above 195K on December 24, continued to decrease well below 195K by the beginning of January, reaching 190K on January 9 and 10.

At the 10 hPa level, minimum temperatures were generally warmer than at 50 hPa, with January 10 being one of the exceptions. In contrast, between December 5-19, the 10 hPa minimum temperature was colder than the minimum at 50 hPa. During December 14-16, the minimum temperature at 10 hPa was below 190K.

April 15-20, 1992

The second UARS validation period is April 15-20, 1992. In the lower stratosphere (about 50 hPa or 460K) the remnants of the Northern Hemisphere vortex could still be seen, while the Southern Hemisphere vortex was deepening. The locations of these vortices are evident in the EPV distributionss shown in Fig. 4 for April 18, 1992. The main remnant of the N. H. vortex was located off the pole near 75N, 120E, while the S. H. vortex is centered near the pole.

The temperature fields are presented in Fig. 5. Examination of the temperature maps for April 15-20, shows that the warm air becomes more zonally symmetric in the N. H., while in the S. H. the cold air near the pole decreased by about 5K during this period. The cold air near the South Pole at this time can be described as a combination of zonal wavenumbers one and two. During this period, the cold air rotated eastward by 90 degrees from a 90W-90E orientation. The warm air between 30S and 60S displayed a zonal wavenumber three pattern with an amplitude of about 5K (215-220K).

In the middle stratosphere, comparison of the temperature fields for April 15 (Fig. 6) and April 20 (Fig. 7) shows that the S. H. cold pole was distorted by a wavenumber two pattern that was rotating to the east. In the N. H. a warm region at about 70N, 115E was decaying with time. The EPV distributions (Figs. 8 and 9) show the S. H. vortex growing slightly in area with time, as well as rotating eastward at the same rate as the temperature fields. The N. H. EPV maps are difficult to interpret. Their most striking feature is the strong gradient seen at about 30N.

The upper stratosphere EPV fields (Fig. 10) show the S. H. polar vortex and the lack of horizontal gradients in the N. H. The wavenumber two pattern of the S. H. vortex was rotating eastward at the same rate as the middle stratospheric vortex. The temperature field (Fig. 11) shows the coldest temperatures off the South Pole. These cold temperatures remained relatively constant in time over this period. The N. H. had a warm region that cooled by about 5K over this period.

A comparison of the zonally averaged temperatures for this validation period with the UARS reference climatology is shown in Fig. 12. At 50 hPa the temperatures for the validation period are similar to those from the climatology. At 10 hPa the temperatures north of 60N are warmer than those from the climatology. This difference arises from the warm region north of 60N at 10 hPa described above. In the S. H., poleward of 30S, the validation period temperatures are warmer than those of the UARS reference climatology. At 1 hPa the NMC/CAC temperatures are consistently about 5K colder than the climatology values. However, this difference may not be significant because corrections to the NMC/CAC temperatures which are usually made have not been applied.

August 8-11, 1992

The third UARS validation period is August 8-11, 1992. During this period the S. H. vortex changed from being nearly zonally symmetric on the 8th to a wavenumber 2 pattern on the 11th. This wavenumber two pattern can be seen in the 460K EPV fields (Fig. 13) and in the 50 hPa temperatures (Fig. 14) on the 11th. This change occurred at all three levels examined. During this validation period the vortex (as defined by EPV) was stacked vertically with little phase change with height. The temperature fields also were stacked in height, however the phase of the temperature field reversed at 1 hPa as shown in Fig. 15.

In the N. H. the EPV and temperature gradients were weak, being largest at the lowest levels (Figs. 13 and 14).

August 25-30, 1992

The fourth UARS validation period is August 25-30, 1992. A very minor warming occurred during late August in the S. H. which can be seen in the time series of maximum temperatures at 10 hPa (Fig. 16a). The maximum temperatures had been near 235K for most of the month, but began to rise on the 22nd and reached their maximum value on the 25th. The vortex remained nearly zonal during this time. Figure 17 presents a typical EPV distribution. In contrast, the temperature pattern at 10 hPa exhibited change during this period. At the height of the warming on the 25th, the warm region tilted westward with height, as can be seen by comparing the temperature maps in the lower (Fig. 18) and the middle (Fig. 19) stratosphere. Over the next six days the middle stratospheric warm region propagated eastward, decaying by the time it was above the stationary lower stratospheric warm region.. The remnant of this middle stratospheric warm region is the flat gradient area near 45N, 120W in Fig. 20.

Time series of the S. H. minimum temperature for August 1992 are shown in Fig. 16b. The minimum temperatures at 50 hPa were always below 185K during the third validation period, but rose above that value on August 27 and 28. Note that these temperatures are well below the approximate threshold temperature (195K) for the formation of Type I polar stratospheric clouds. As seen in the earlier August time period, polar temperatures at 1 hPa were warmer than middle latitude temperatures at this level (Fig. 21). During this time the coldest air at 1 hPa was located near 40N, 165E.

A comparison of the zonal average temperatures for this period with the August UARS reference climatology temperatures is shown in Fig. 22. There is a similarity to the climatology at 50 hPa, however the middle and upper stratosphere temperatures show larger differences from the climatology. At 10 hPa the tropical zonally-averaged temperature are similar to climatology, but at extratropical latitudes the N. H. is colder and the S. H. warmer than the climatology. At 1 hPa the NMC/CAC temperatures are about 5K colder than the climatology, except near the South Pole. Once again the usual corrections have not been applied to the NMC/CAC temperatures.

References

Newman, P., L. R. Lait, M. Schoeberl, E. R. Nash, K. Kelley, D. Fahey, R. Nagatani, D. Toohey, L. Avallone, and J. Anderson: Stratospheric meteorological conditions in the Arctic polar vortex, 1991 to 1992. *Science,* **261**, pp 1143-1146, 1993.

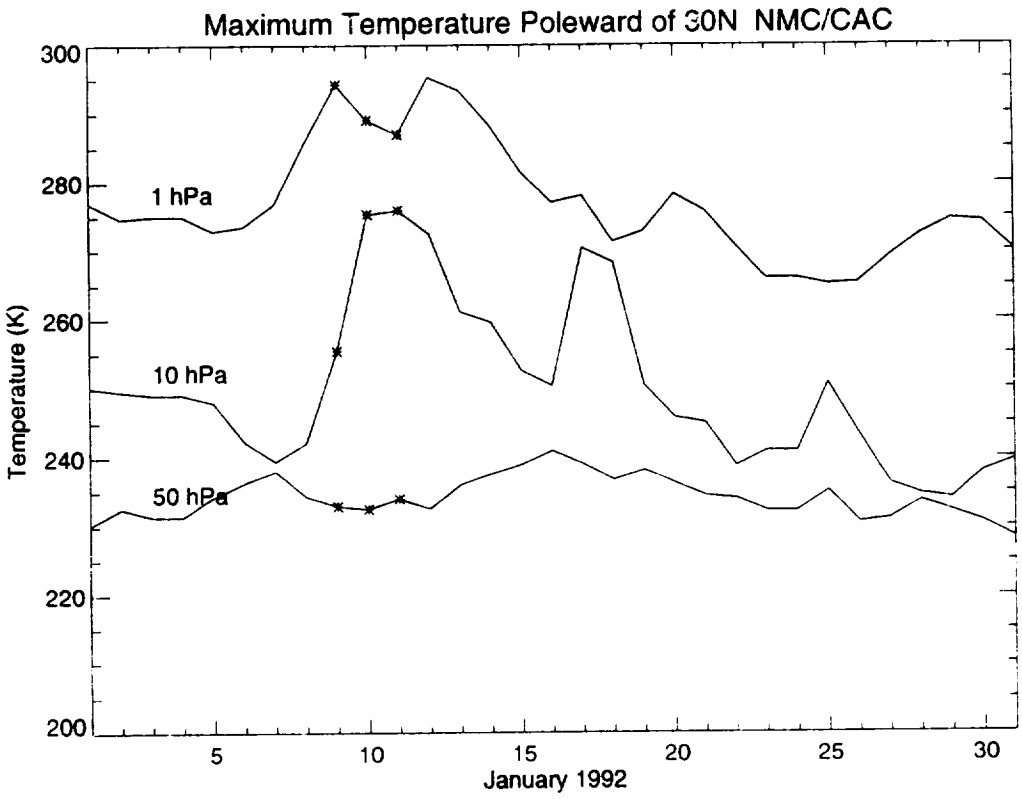

(a)

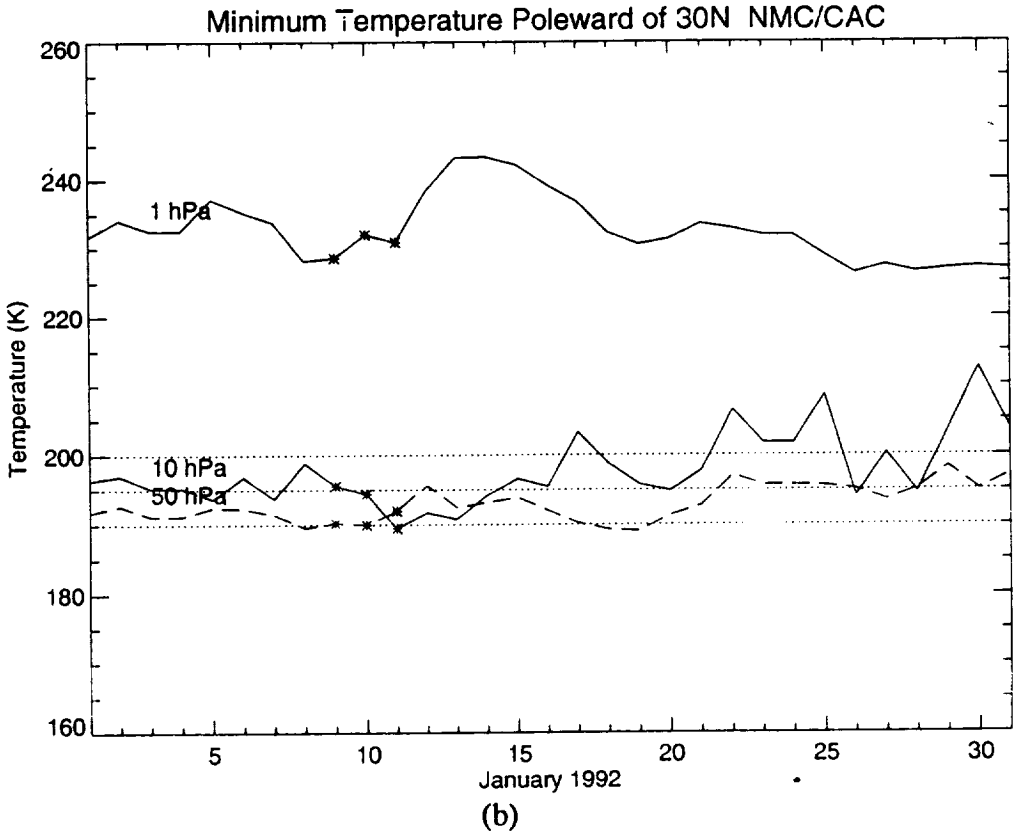

(b)

Figure 1 a) A time series of the maximum temperature poleward of 30N at 50, 10, and 1 hPa for January 1992. The star days correspond to the first UARS validation time period, January 9-11, 1992. b) A time series of the minimum temperature poleward of 30N at 50, 10, and 1 hPa for January 1992. The star days correspond to the first UARS validation time period January 9-11, 1992.

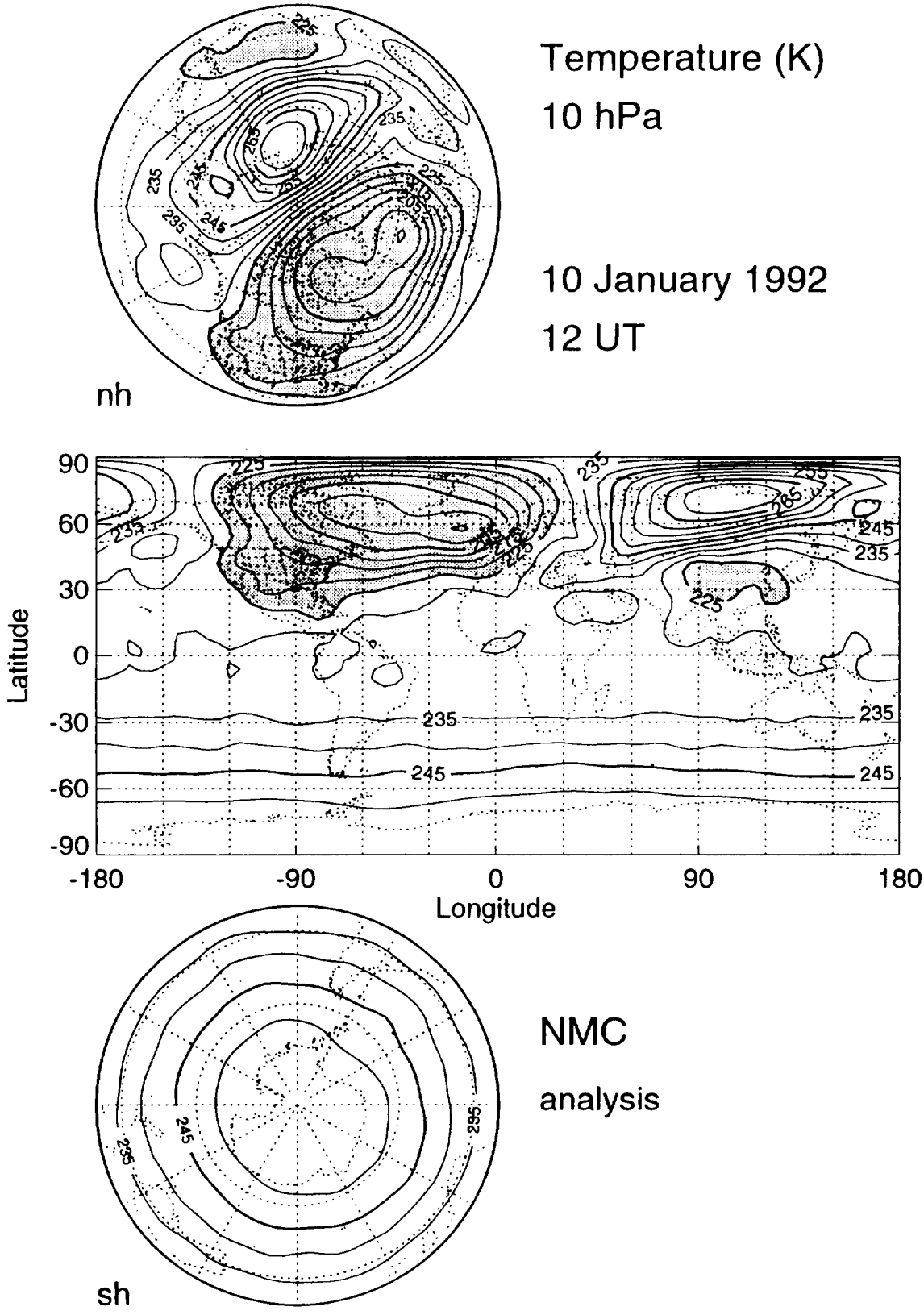

Figure 2 Three projections of the NMC/CAC temperature analyses at 10 hPa for January 10, 1992, 12 UT. Cold temperatures are shaded. The three projections in this and subsequent figures show orthographic projections of the Northern Hemisphere and the Southern Hemisphere, and a latitude/longitude projection showing the entire field.

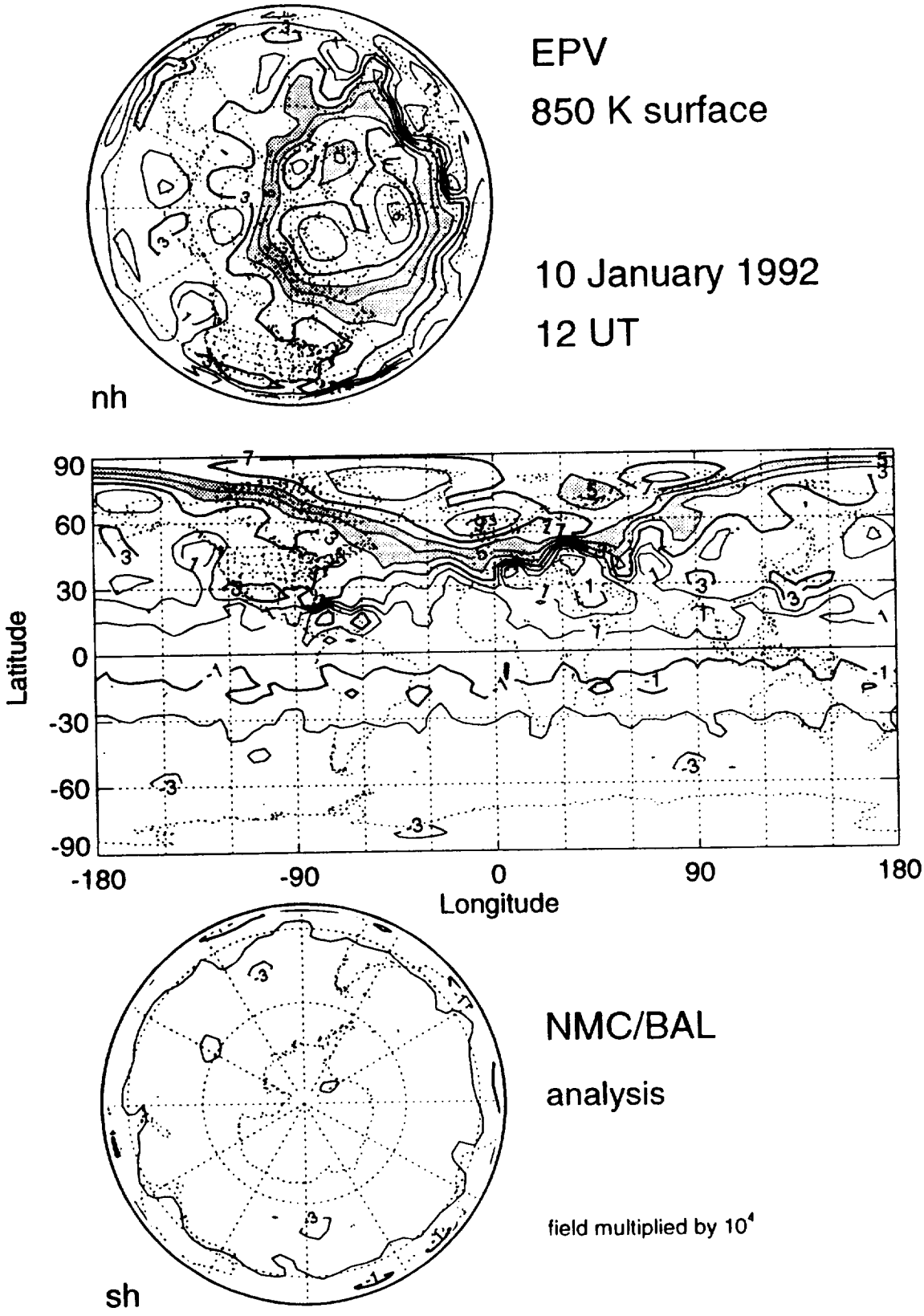

Figure 3 Three projections of the Ertel potential vorticity (EPV) field at 850 K for January 10, 1992, 12 UT. Values of EPV between 4.0 and 6.0×10^{-4} are shaded.

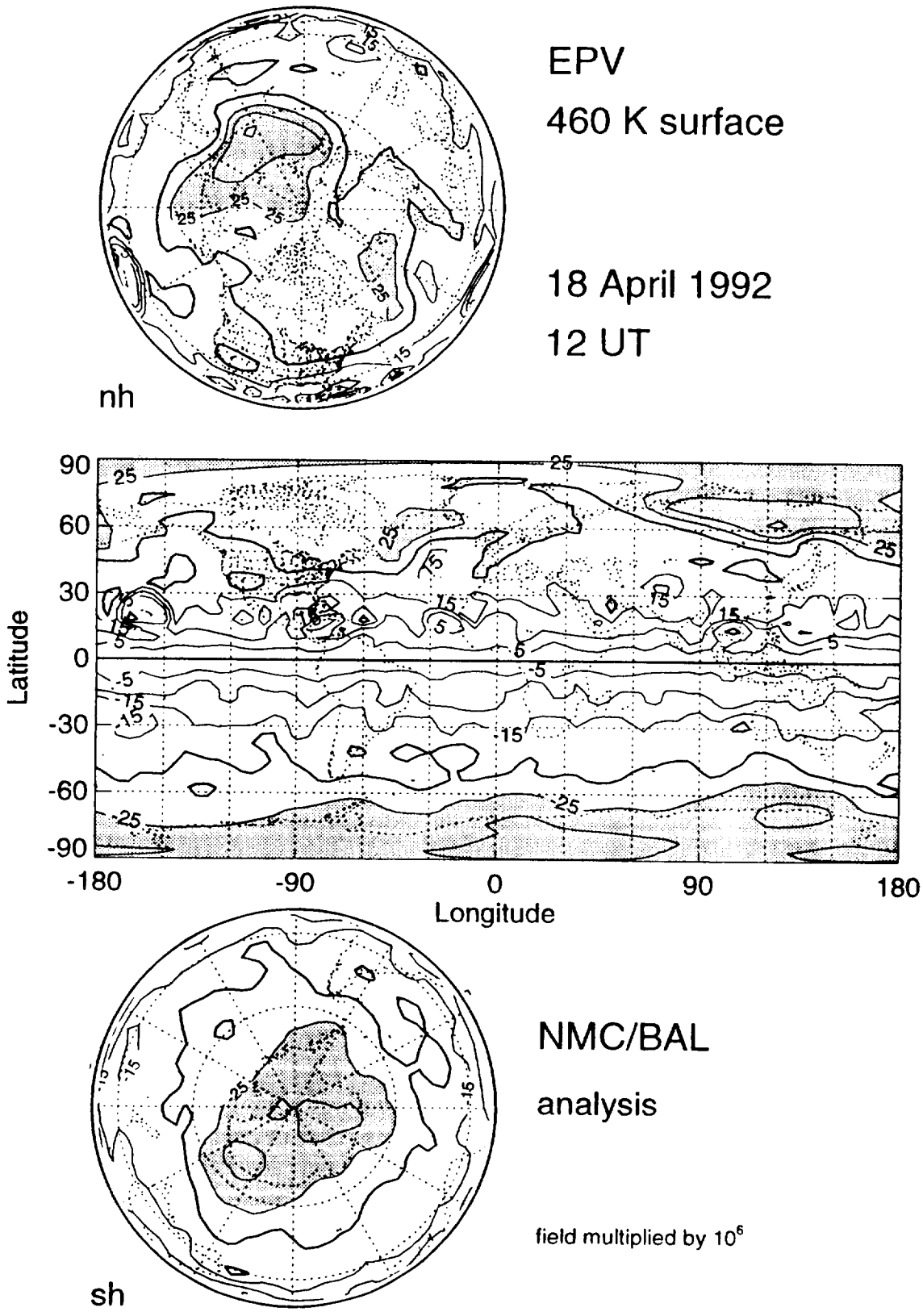

Figure 4 Three projections of the Ertel potential vorticity (EPV) field at 460 K for April 18, 1992, 12 UT. Values of EPV between 25.0 and 35.0 x10^{-6} are shaded.

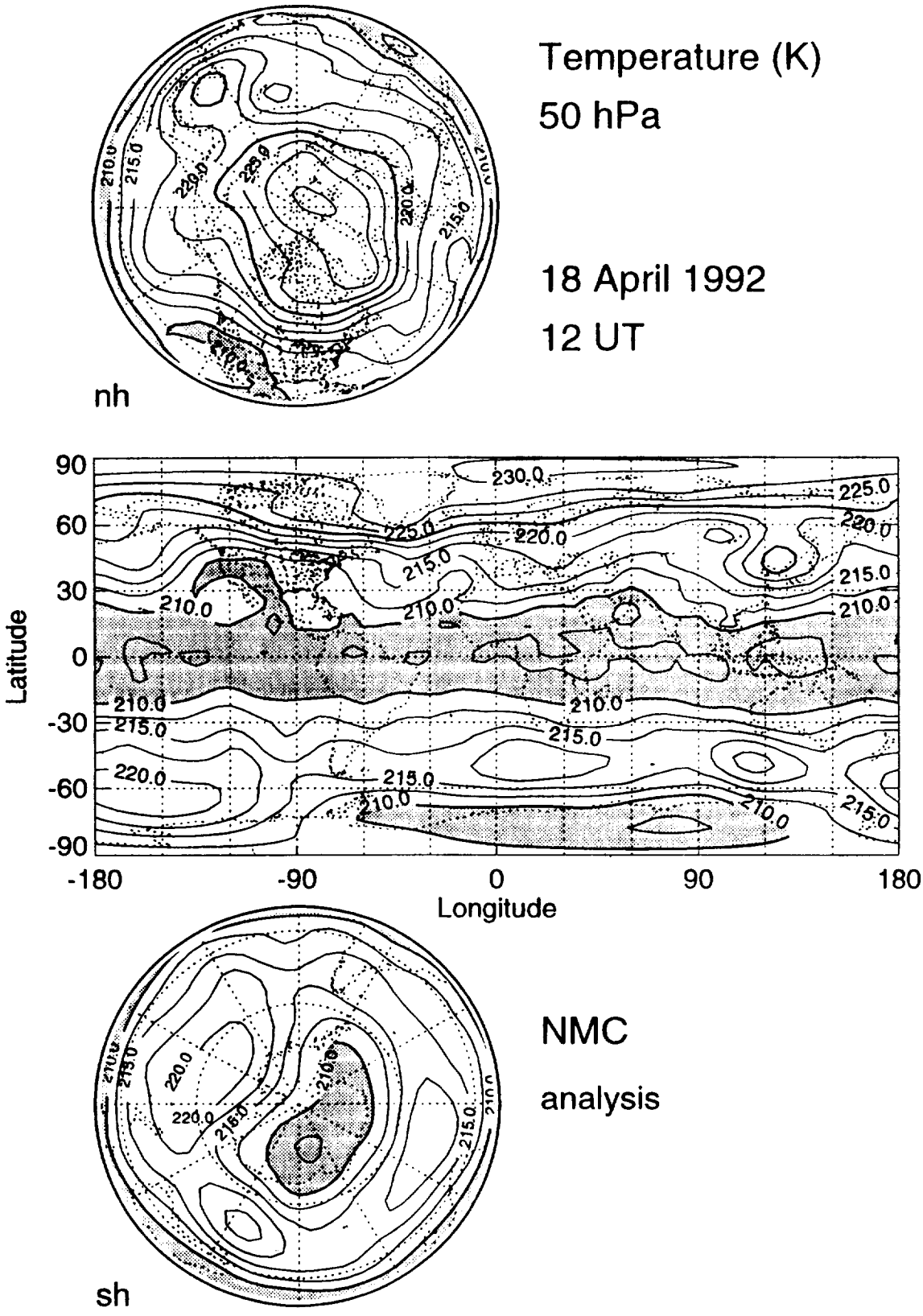

Figure 5 Three projections of the NMC/CAC temperature analyses at 50 hPa for April 18, 1992, 12 UT. Cold temperatures are shaded.

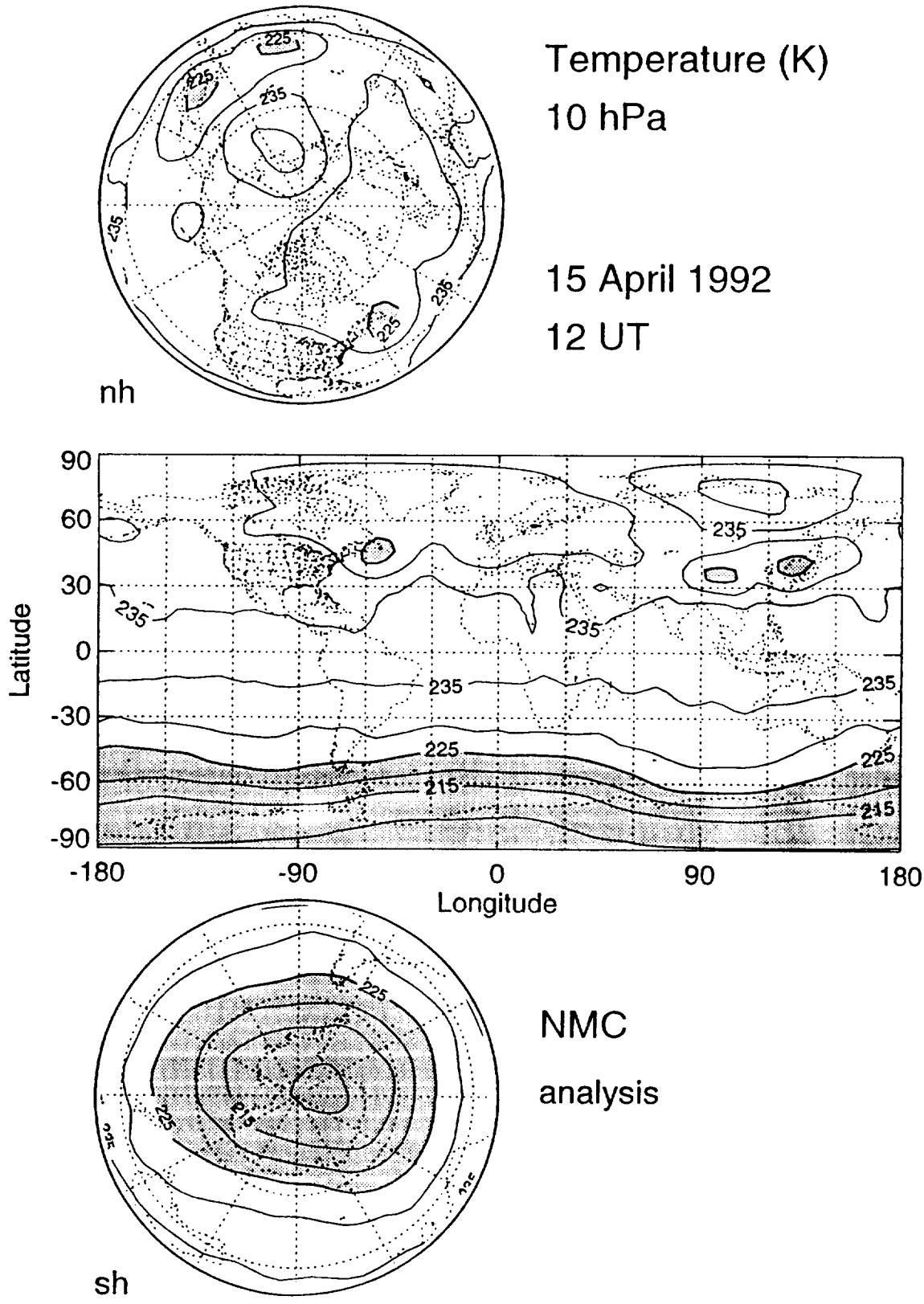

Figure 6 Three projections of the NMC/CAC temperature analyses at 10 hPa for April 15, 1992, 12 UT. Cold temperatures are shaded.

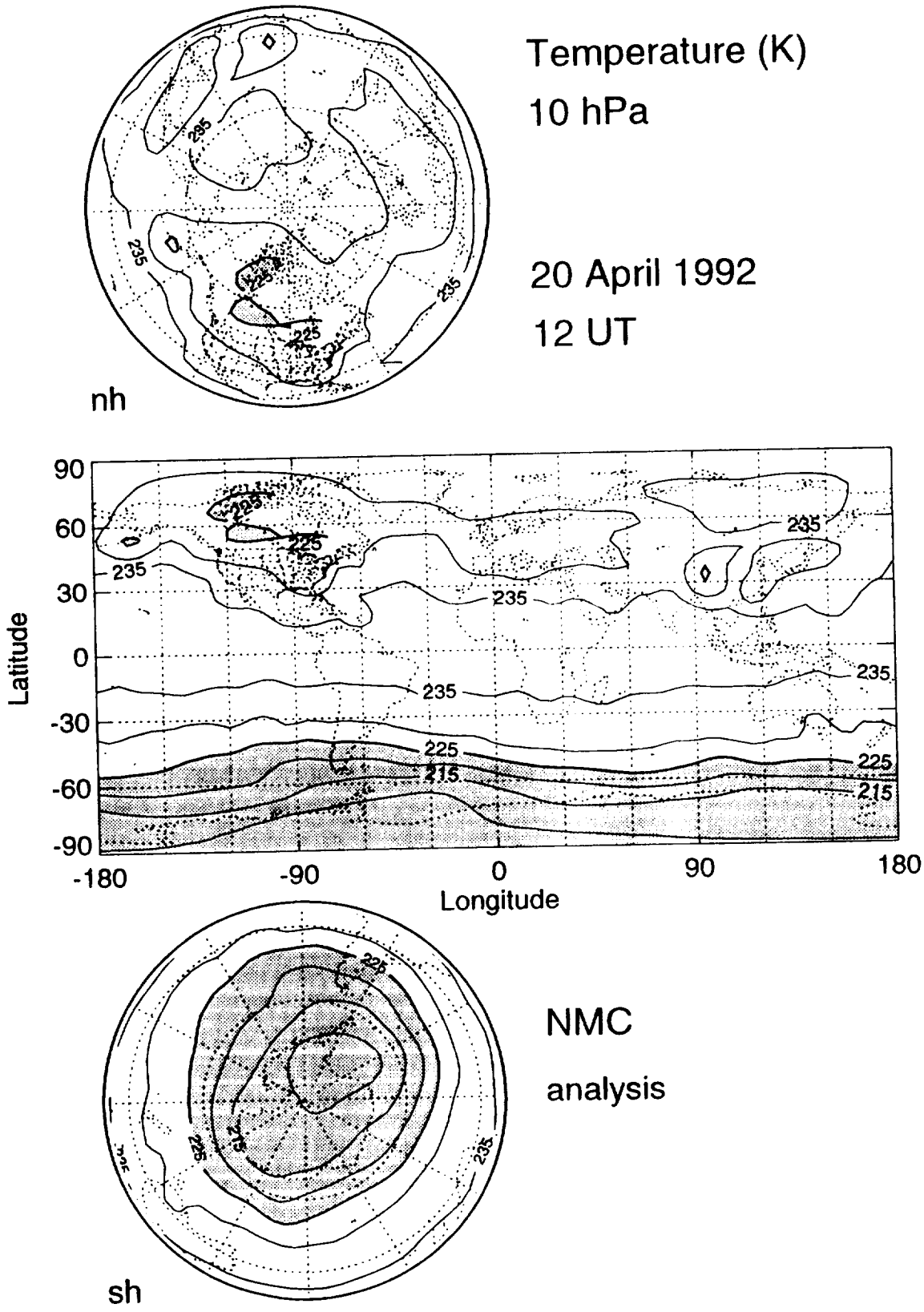

Figure 7 Three projections of the NMC/CAC temperature analyses at 10 hPa for April 20, 1992, 12 UT. Cold temperatures are shaded.

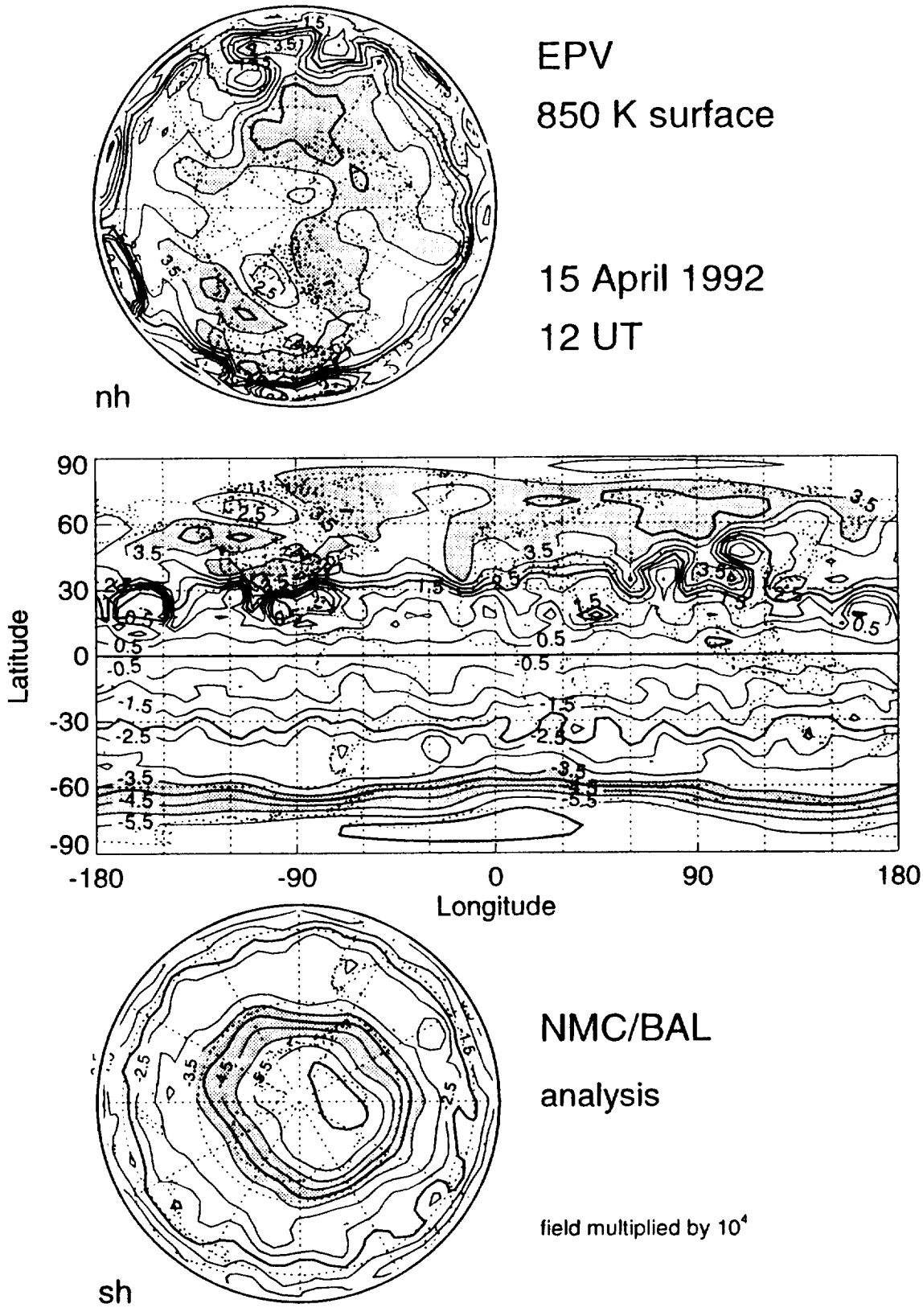

Figure 8 Three projections of the Ertel potential vorticity (EPV) field at 850 K for April 15, 1992, 12 UT. Values of EPV greater than 3.5×10^{-4} and between -3.5 and -5.5×10^{-4} are shaded.

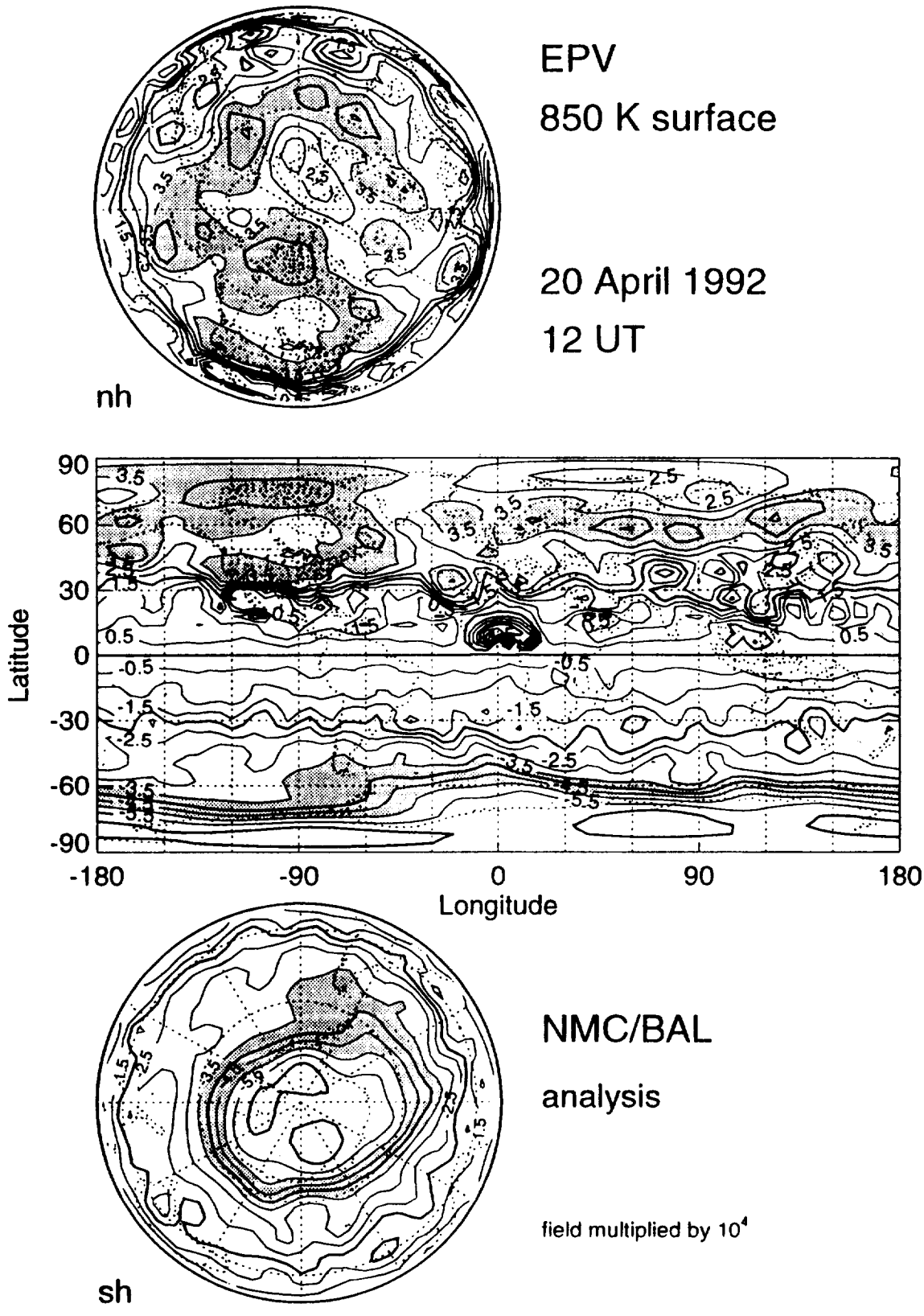

Figure 9 Three projections of the Ertel potential vorticity (EPV) field at 850 K for April 20, 1992, 12 UT. Values of EPV greater than 3.5×10^{-4} and between -3.5 and -5.5×10^{-4} are shaded.

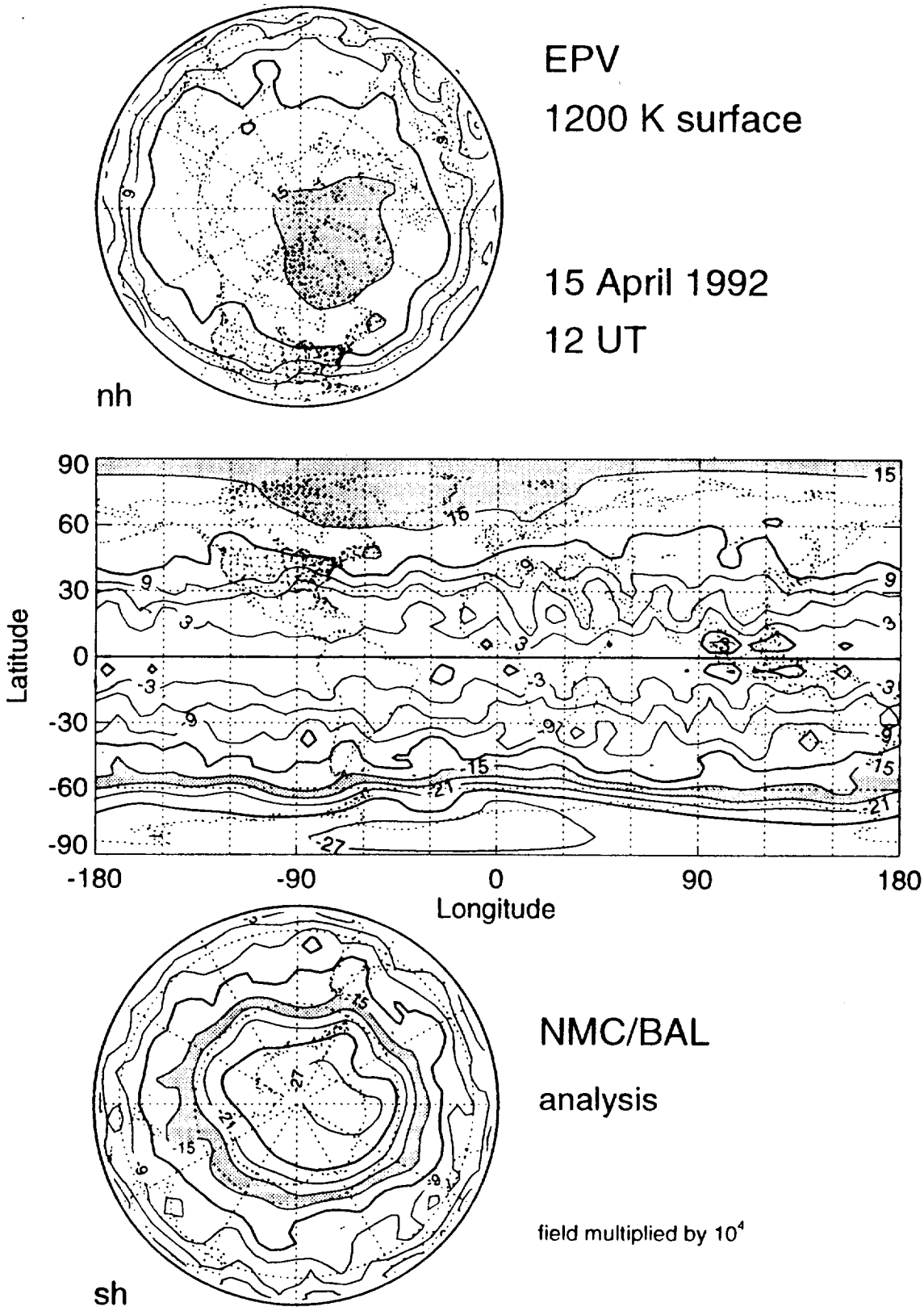

Figure 10 Three projections of the Ertel potential vorticity (EPV) field at 1200 K for April 15, 1992, 12 UT. Values of EPV greater than 15.0 x10^{-4} and between -15.0 and -18.0 x10^{-4} are shaded.

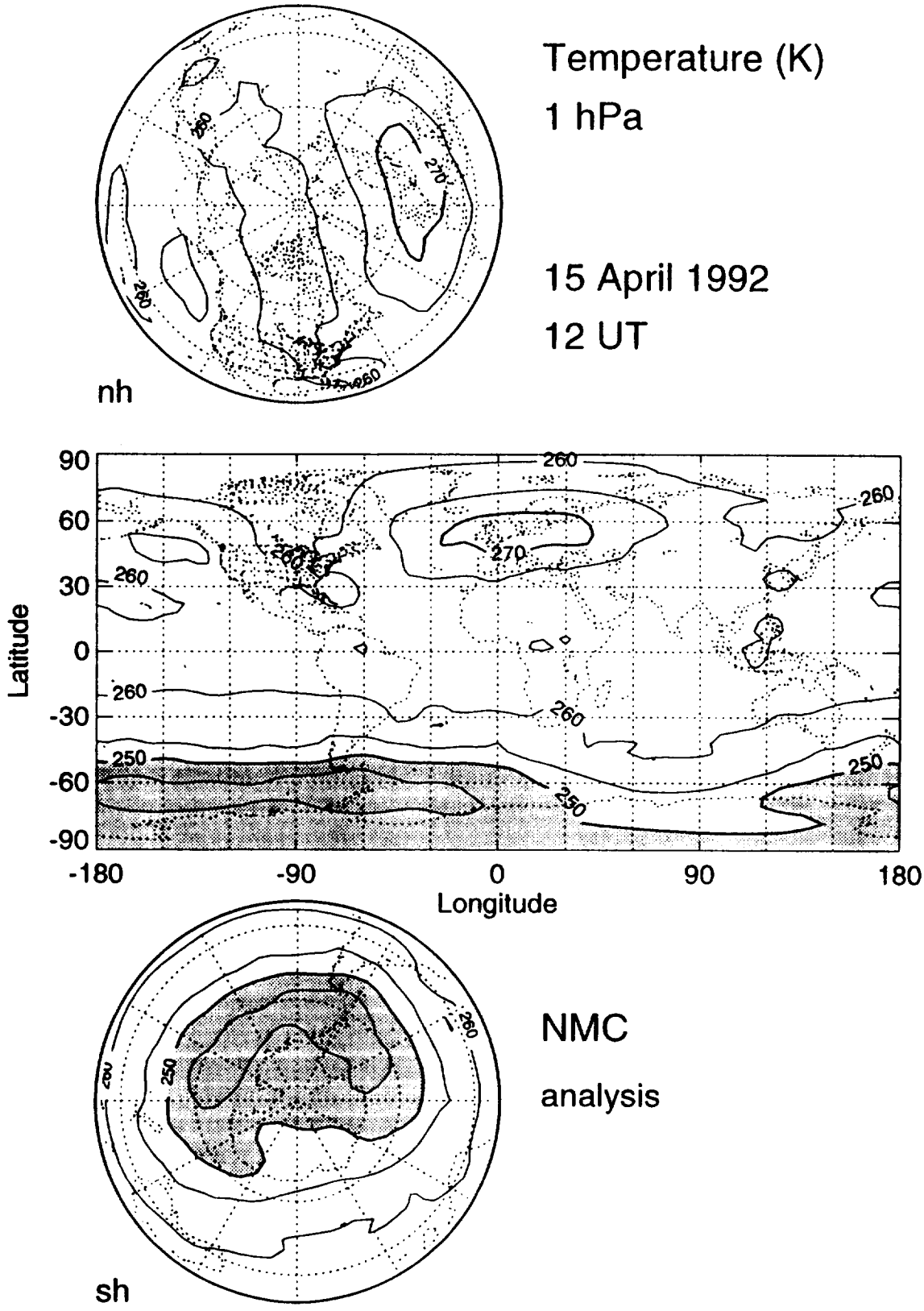

Figure 11 Three projections of the NMC/CAC temperature analyses at 1 hPa for April 15, 1992, 12 UT. Cold temperatures are shaded.

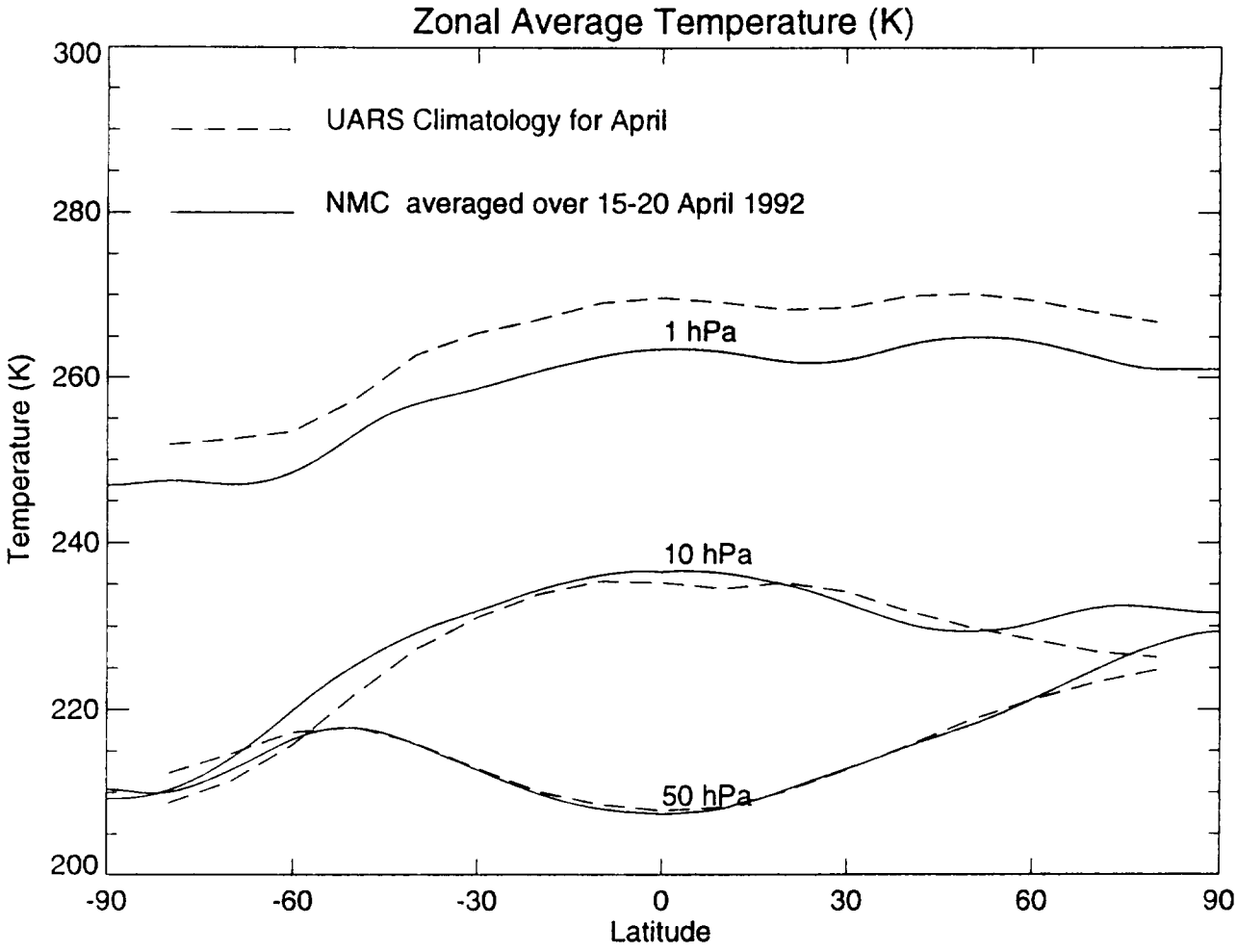

Figure 12 A comparison of the zonal averaged NMC/CAC temperatures for April 15-20, 1992 to the UARS April climatology at 50, 10, and 1 hPa. The UARS climatology temperatures were linearly interpolated in log pressure to the standard pressures.

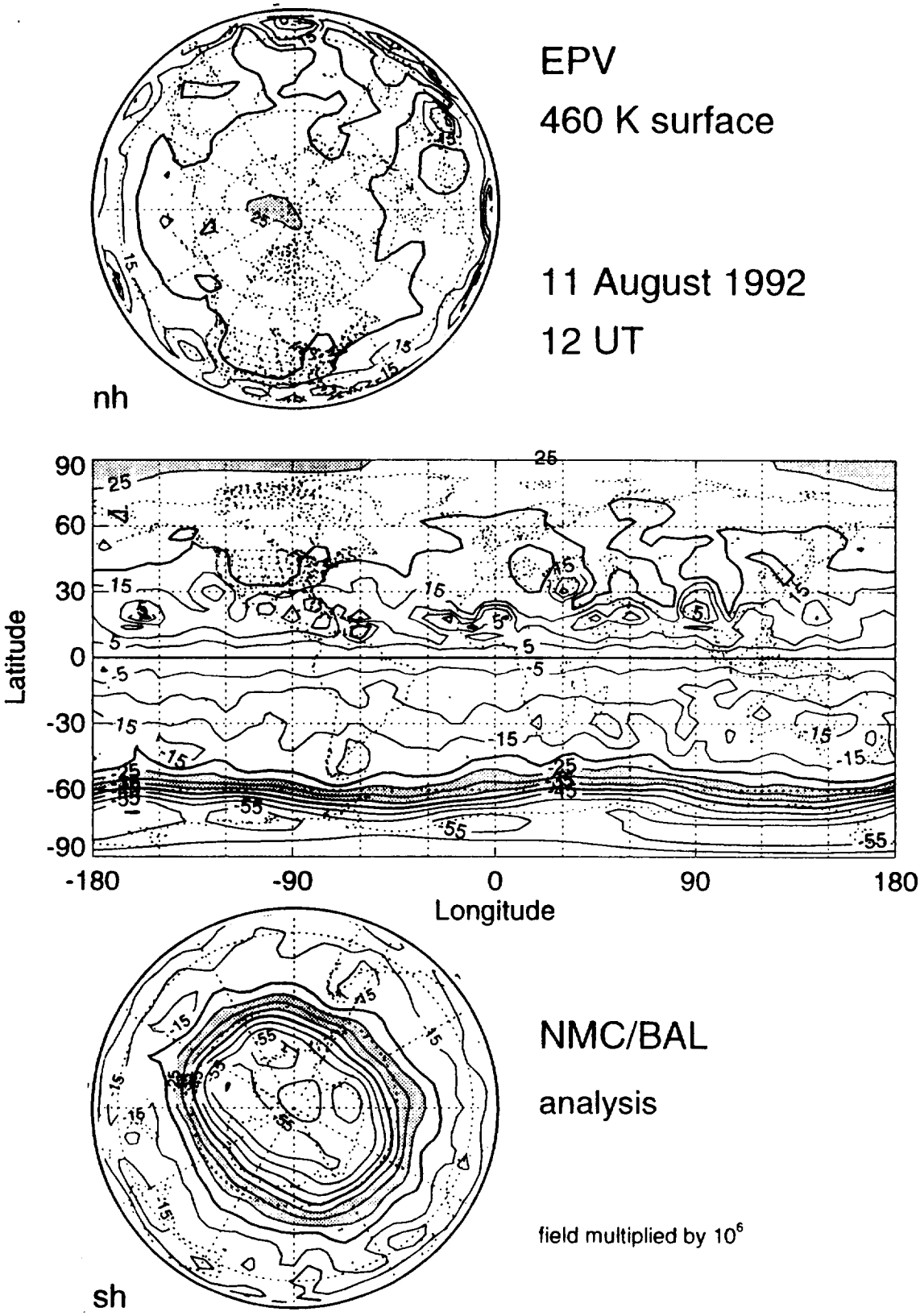

Figure 13 Three projections of the Ertel potential vorticity (EPV) field at 460 K for August 11, 1992, 12 UT. Values of EPV greater than 25.0x10^{-6} and between -25.0 and -35.0 x10^{-6} are shaded.

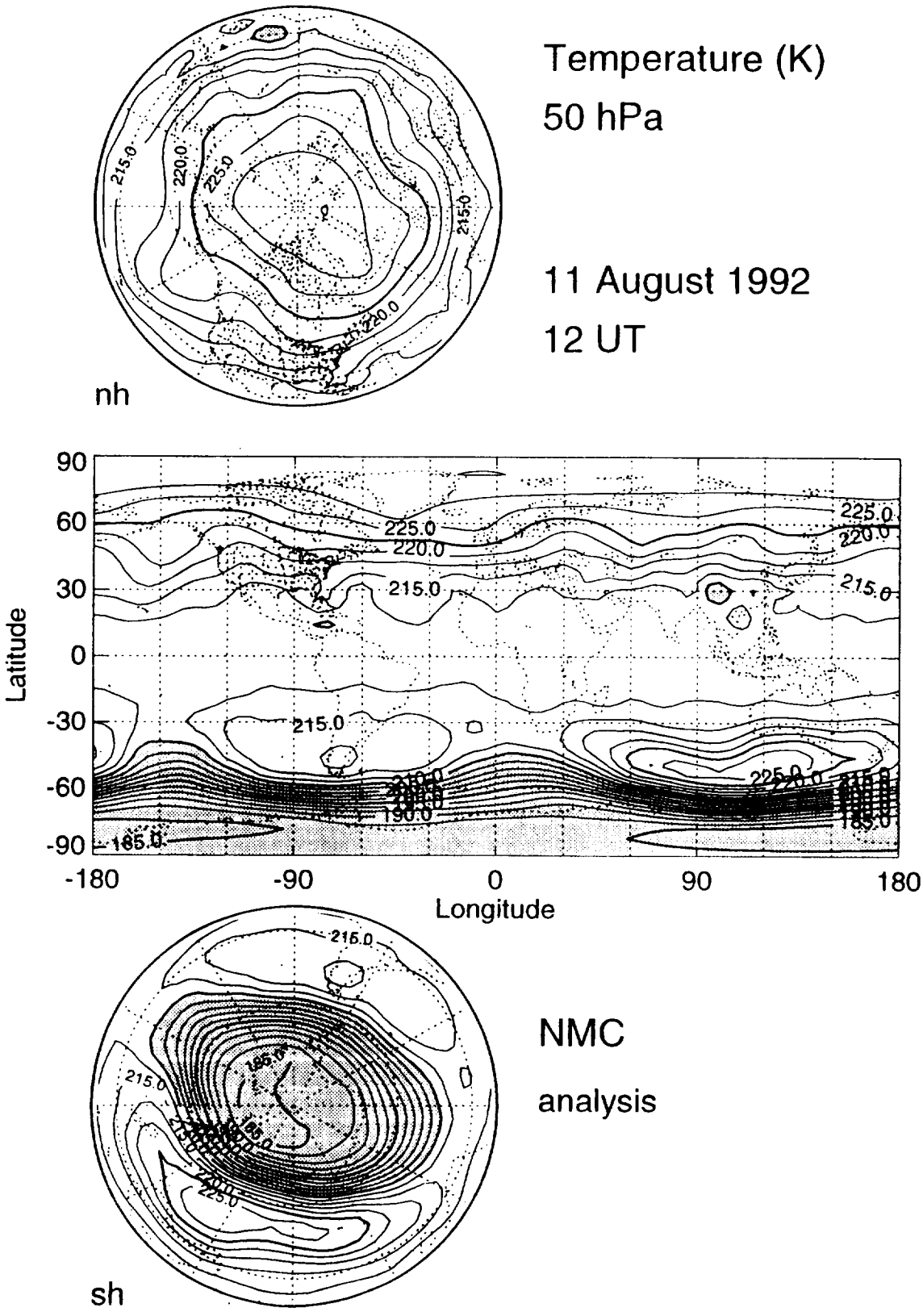

Figure 14 Three projections of the NMC/CAC temperature analyses at 50 hPa for August 11, 1992, 12 UT. Cold temperatures are shaded.

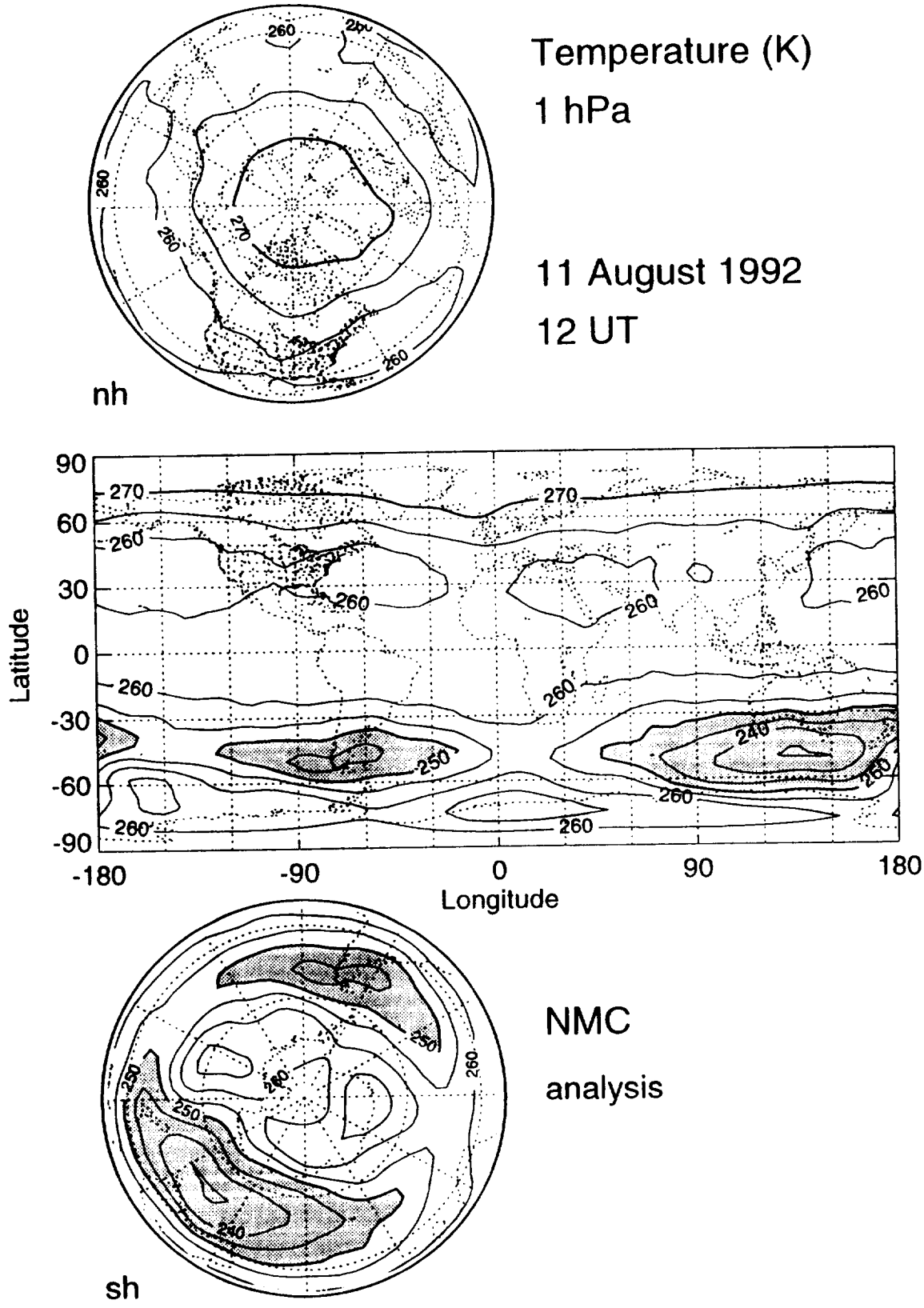

Figure 15 Three projections of the NMC/CAC temperature analyses at 1 hPa for August 11, 1992, 12 UT. Cold temperatures are shaded.

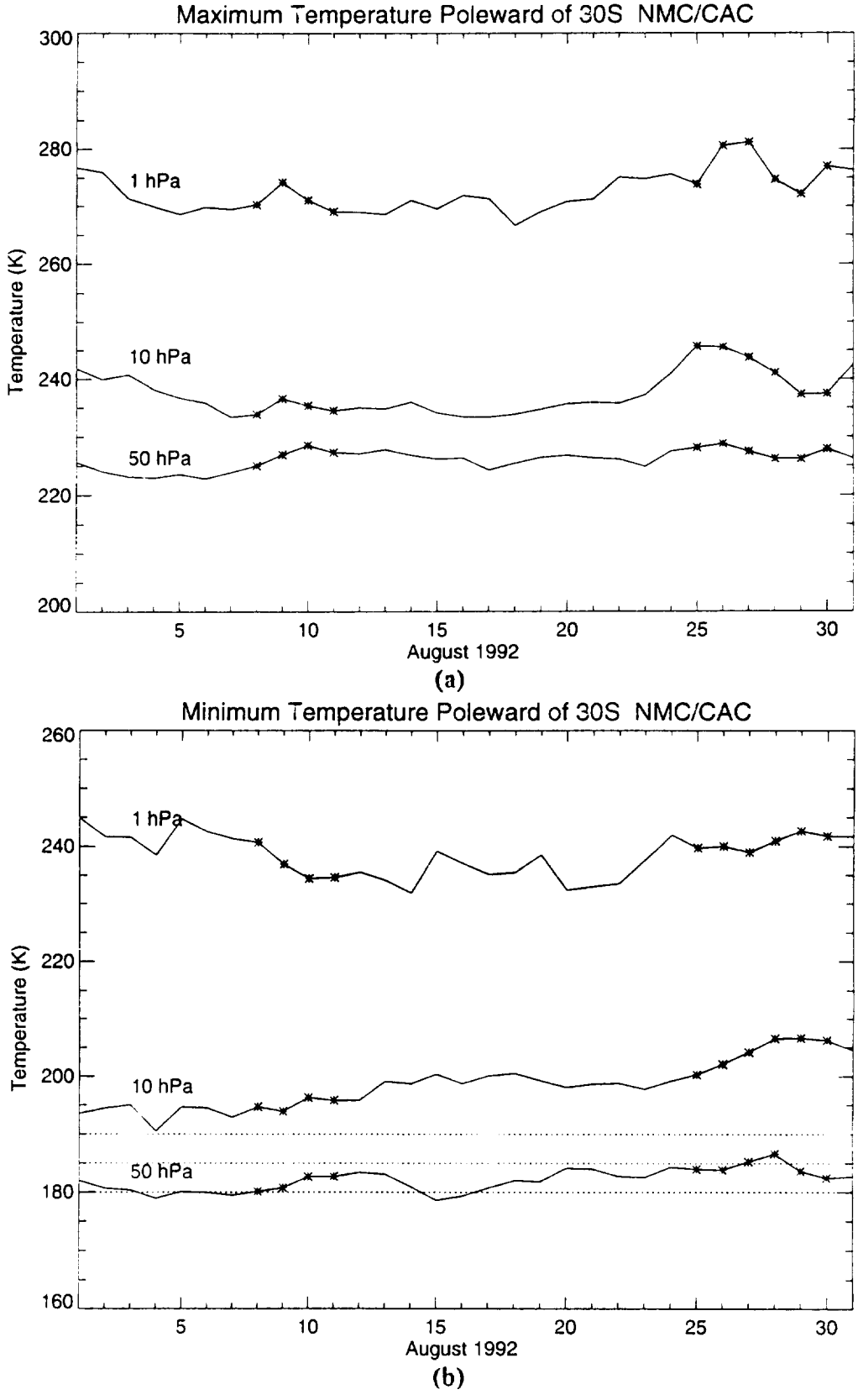

Figure 16 a) A time series of the maximum temperature poleward of 30S at 50, 10, and 1 hPa for August 1992. The star days correspond to the third and fourth UARS validation time periods, August 8-11 and 25-30, 1992. b) A time series of the minimum temperature poleward of 30S at 50, 10, and 1 hPa for August 1992. The star days correspond to the third and fourth UARS validation time periods, August 8-11 and 25-30, 1992.

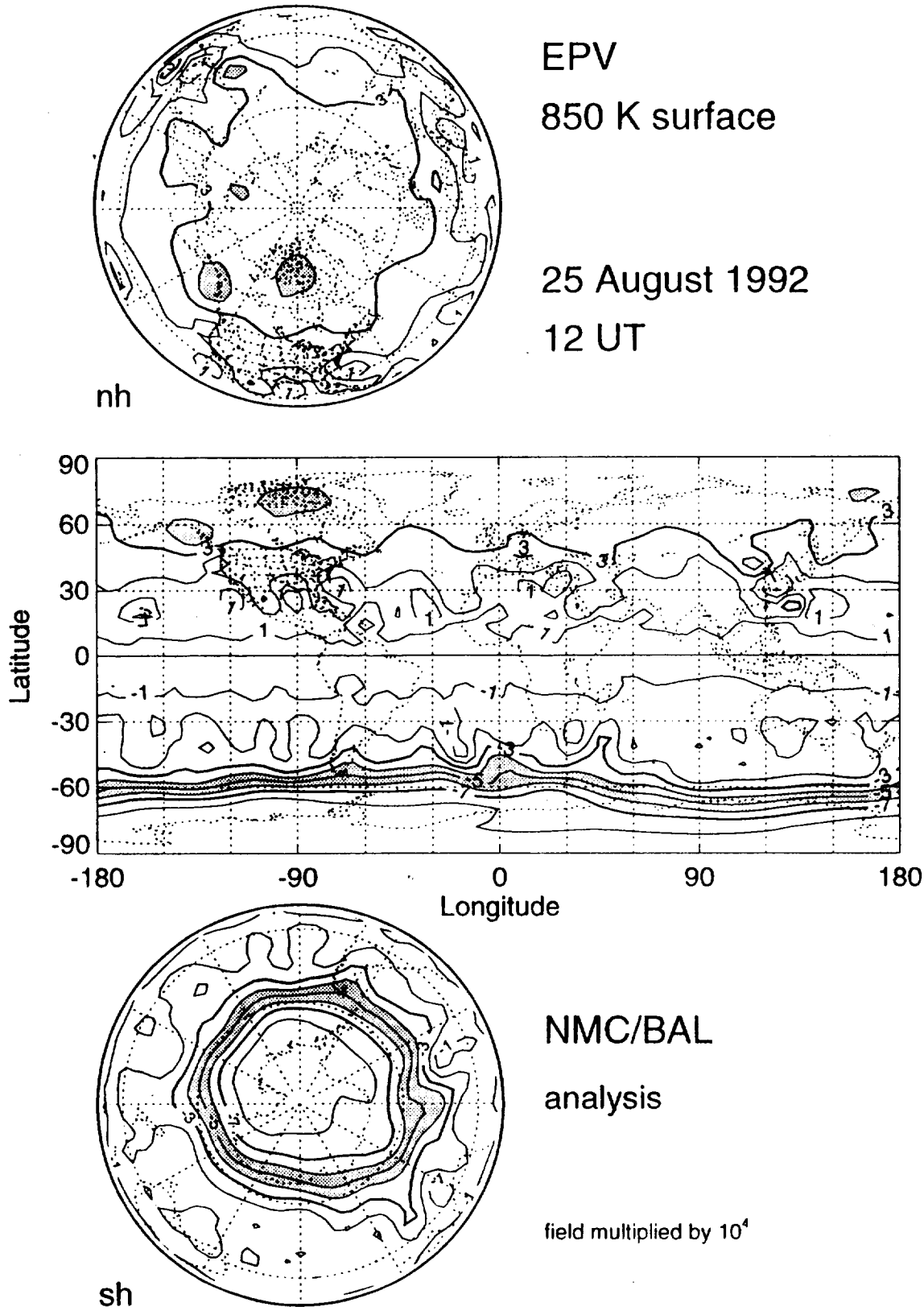

Figure 17 Three projections of the Ertel potential vorticity (EPV) field at 850 K for August 25, 1992, 12 UT. Values of EPV greater than 4.0×10^{-4} and between -4.0×10^{-4} and -6.0×10^{-4} are shaded.

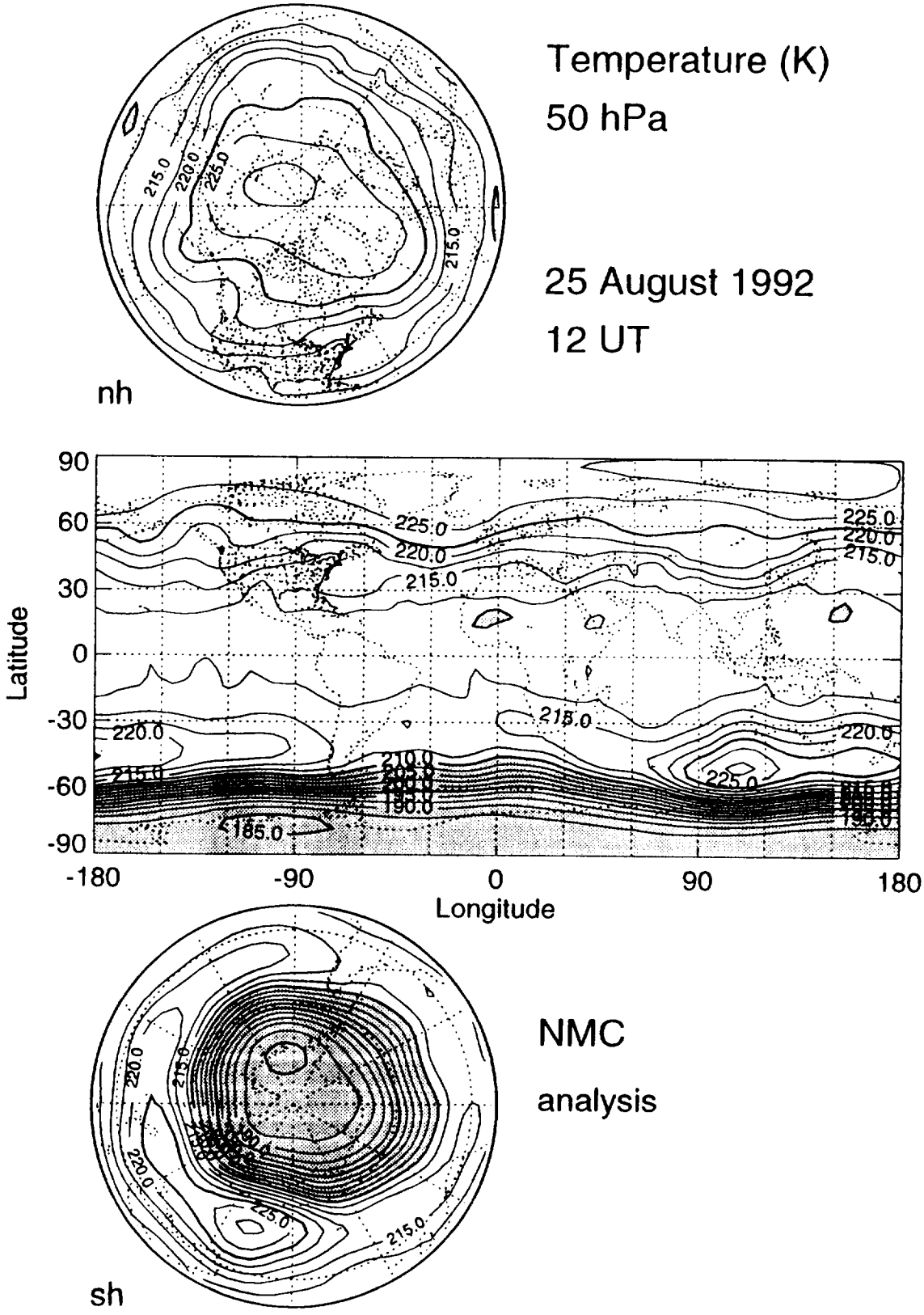

Figure 18 Three projections of the NMC/CAC temperature analyses at 50 hPa for August 25, 1992, 12 UT. Cold temperatures are shaded.

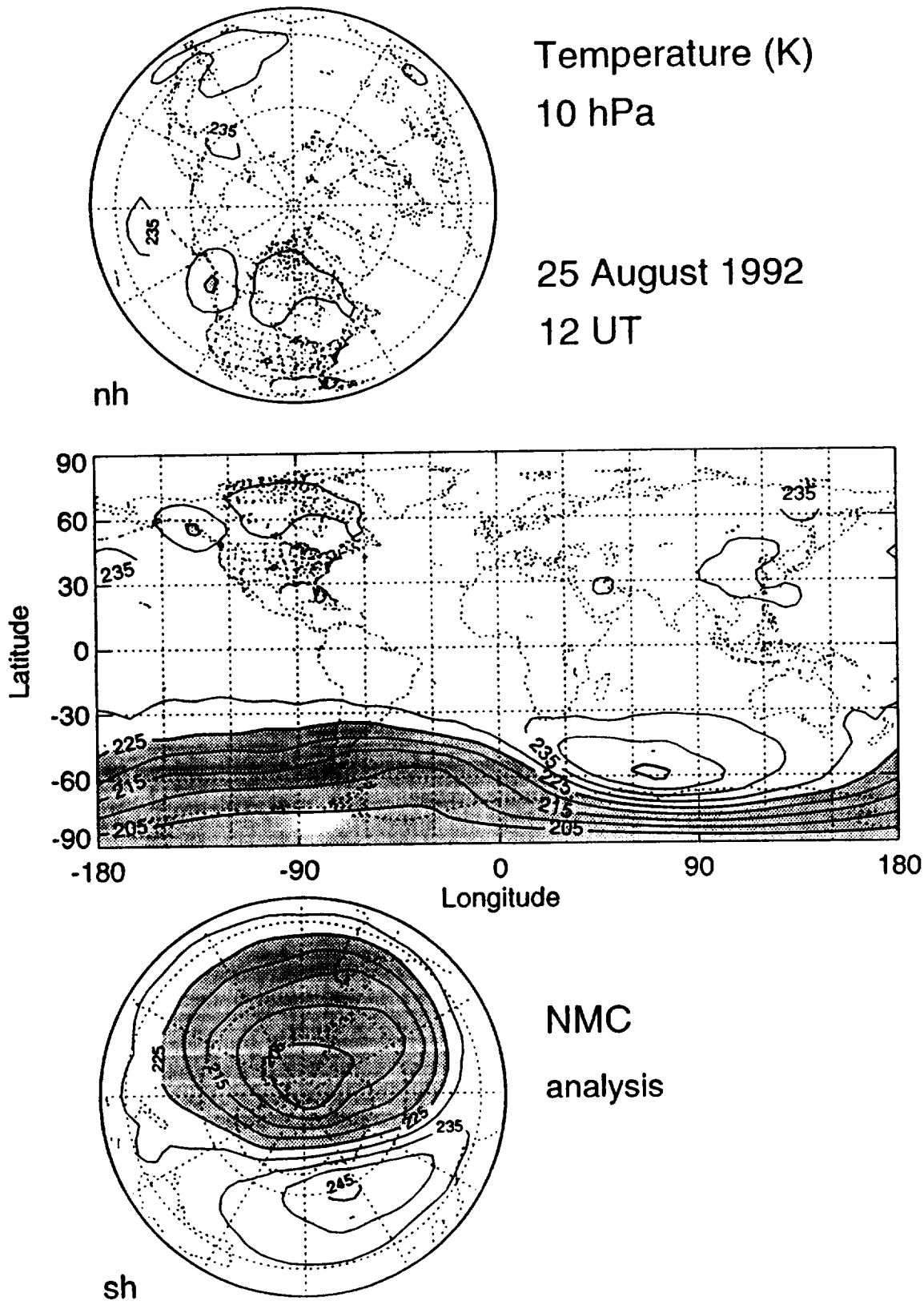

Figure 19 Three projections of the NMC/CAC temperature analyses at 10 hPa for August 25, 1992, 12 UT. Cold temperatures are shaded.

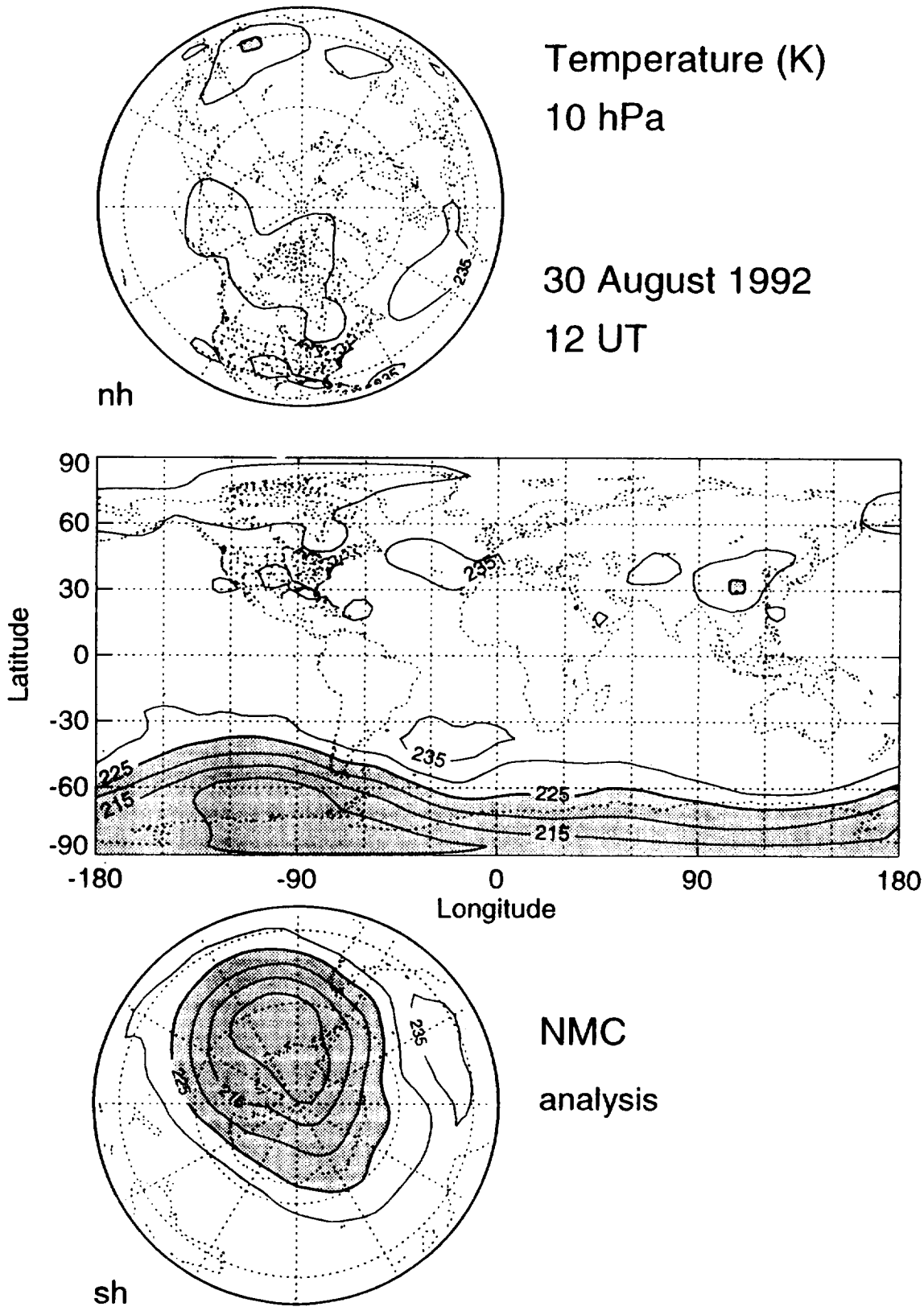

Figure 20 Three projections of the NMC/CAC temperatures analyses at 10 hPa for August 30, 1992, 12 UT. Cold temperatures are shaded.

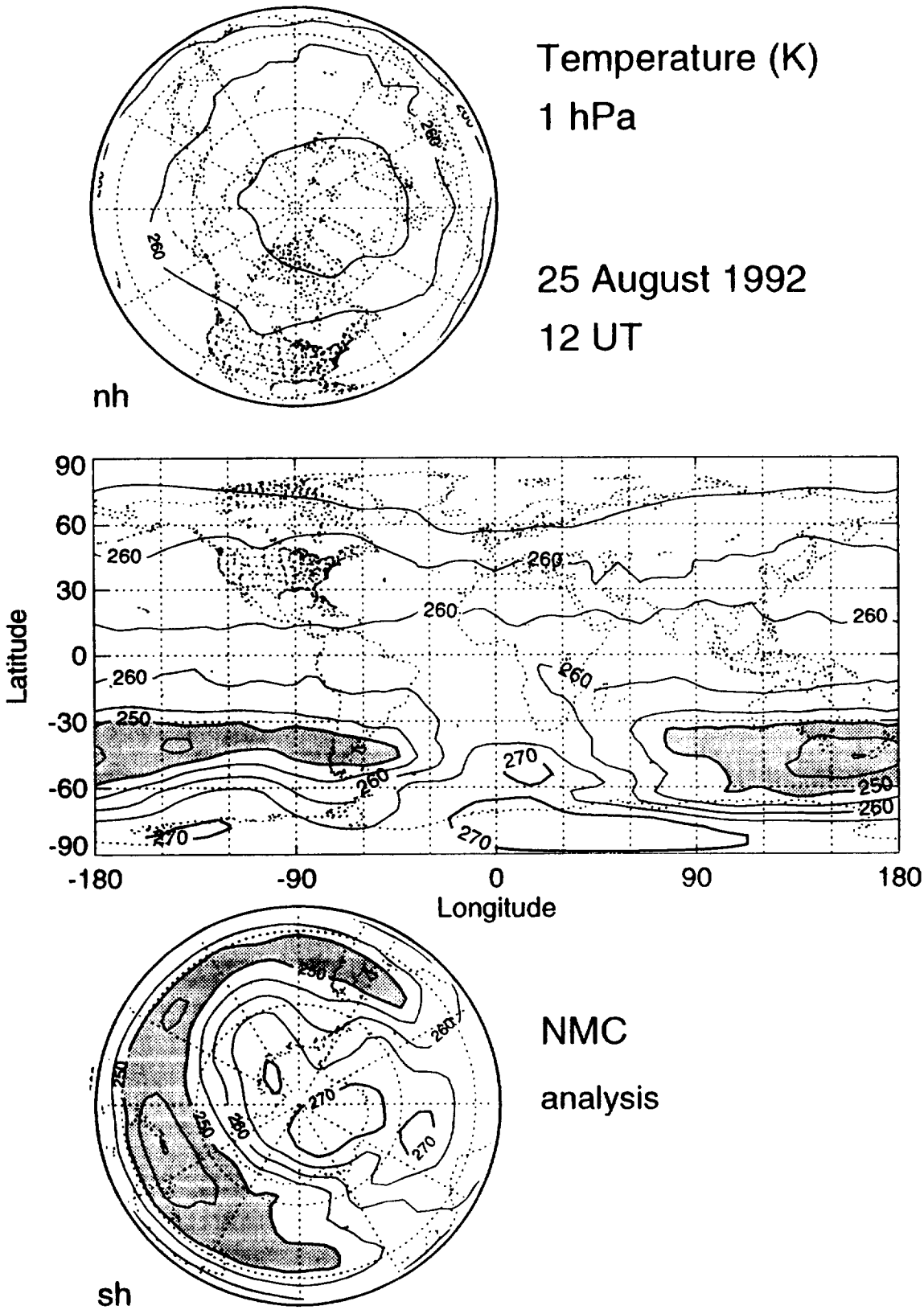

Figure 21 Three projections of the NMC/CAC temperature analyses at 1 hPa for August 25, 1992, 12 UT. Cold temperatures are shaded.

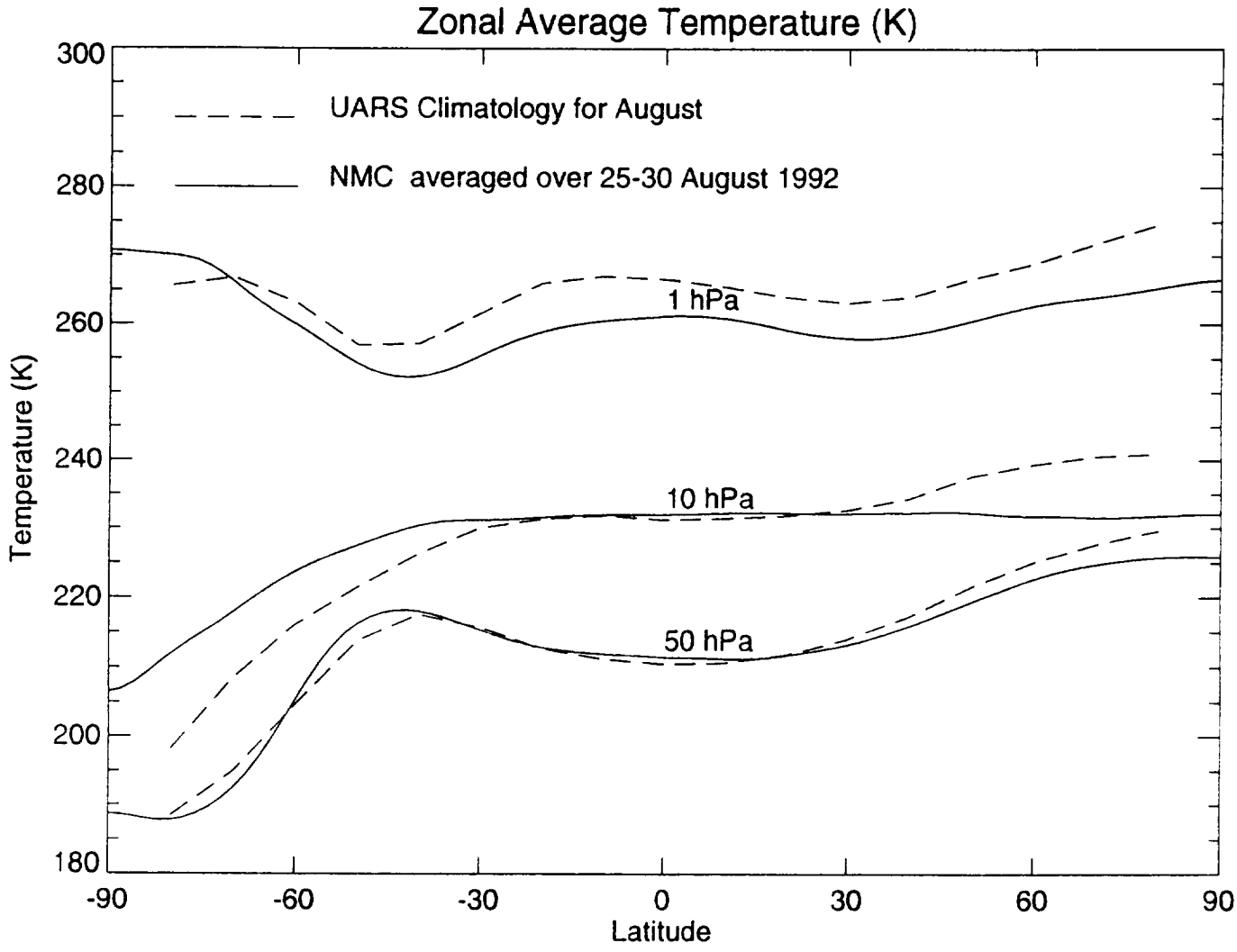

Figure 22 A comparison of the zonal averaged NMC/CAC temperatures for April 25-30, 1992 to the UARS April climatology at 50, 10, and 1 hPa. The UARS climatology temperatures were linearly interpolated in log pressure to the standard pressures.

APPENDIX B

HALOE V16 Retrievals

HALOE constituent and temperature comparisons included in the main body of this report have been replotted using Version 16 retrievals, and the updated results are included in this appendix. The main algorithm changes were made to correct for beta angle effects (angle between the Earth-Sun line and the orbit plane) in the data and to include an improved aerosol correction. The primary differences from the V12 results contained in the main body occur in the lower stratosphere mainly in the H_2O and CH_4 channels. Small effects are seen in the other channels.

No commentary on these data is provided since they were unavailable at the time of the workshop. Many of the figures contained in this appendix correspond to equivalent figures for Version 12 data set.

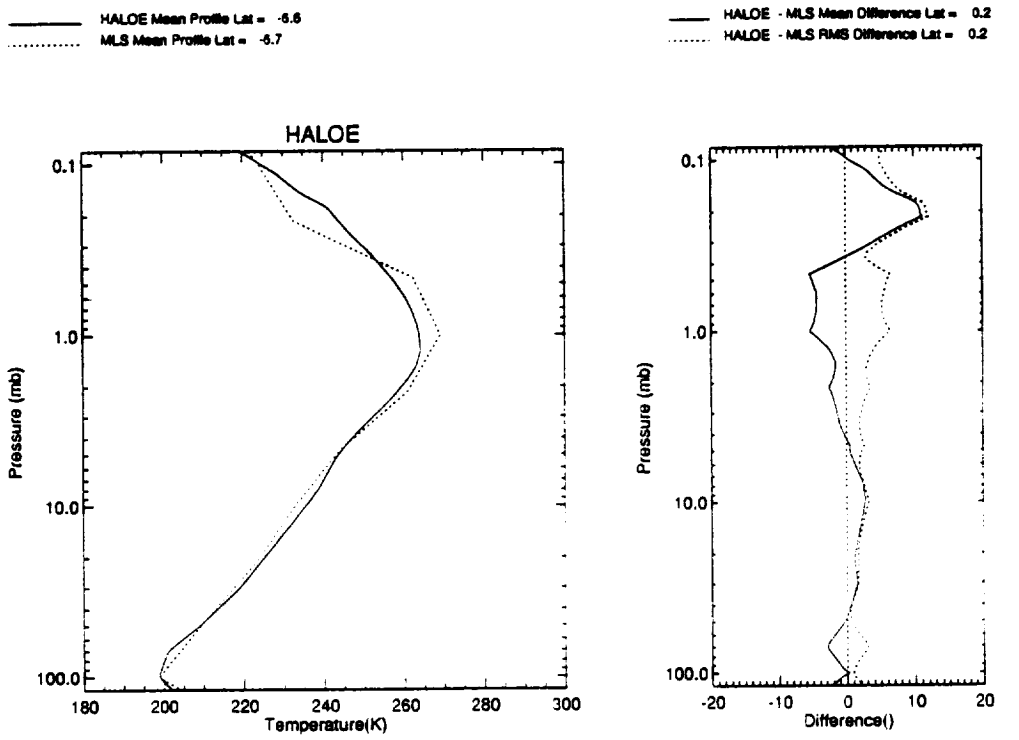

HALOE - MLS Temperature (K) differences
on 15-APR-1992 to 20-APR-1992 near 6 S using 73 profiles

Wed Jul 13 14:38:59 EDT 1994

Figure B-1

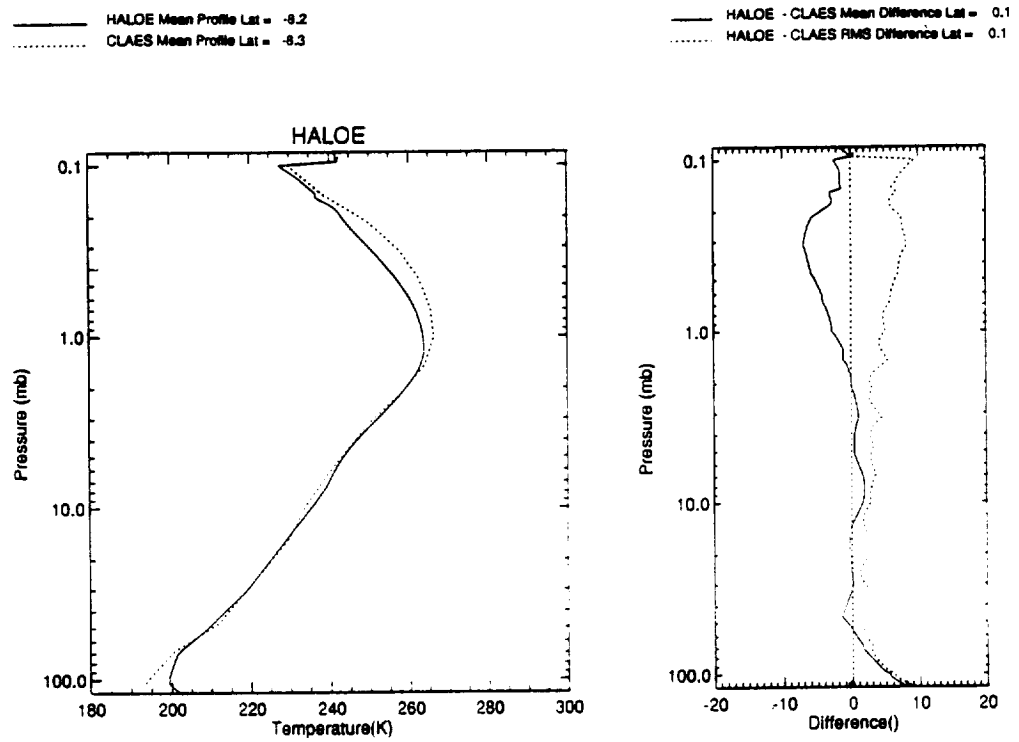

HALOE - CLAES Temperature (K) differences
on 15-APR-1992 to 20-APR-1992 near 8 S using 76 profiles

Wed Jul 13 14:40:15 EDT 1994

Figure B-2

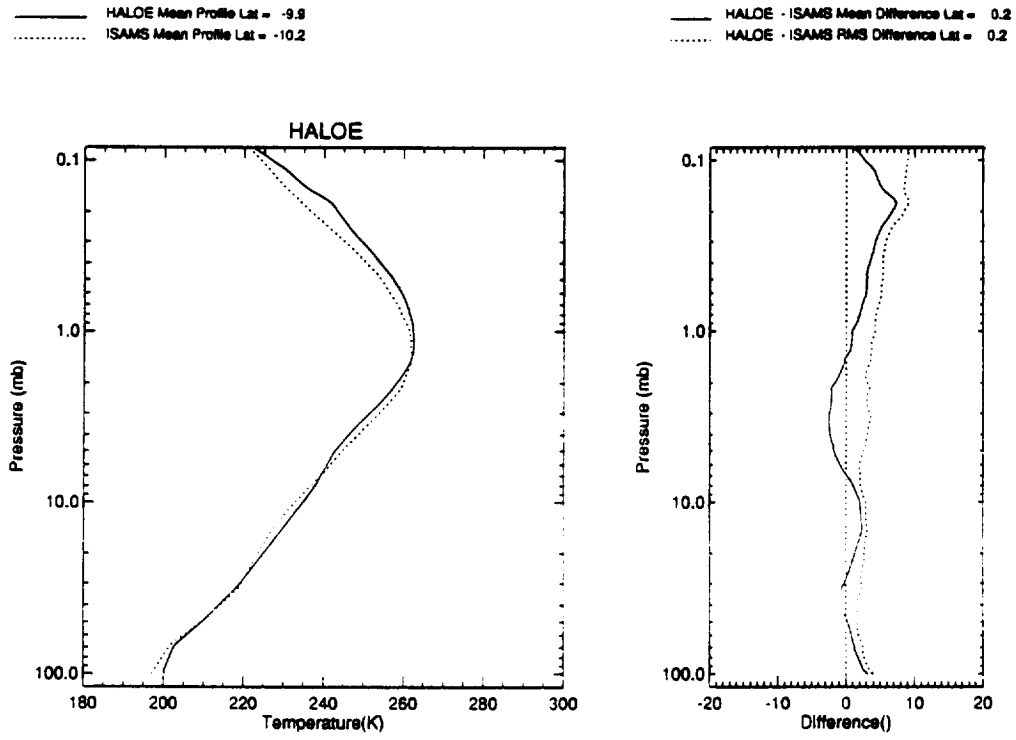

HALOE - ISAMS Temperature (K) differences
on 15-APR-1992 to 20-APR-1992 near 9 S using 69 profiles

Wed Jul 13 14:37:28 EDT 1994

Figure B-3

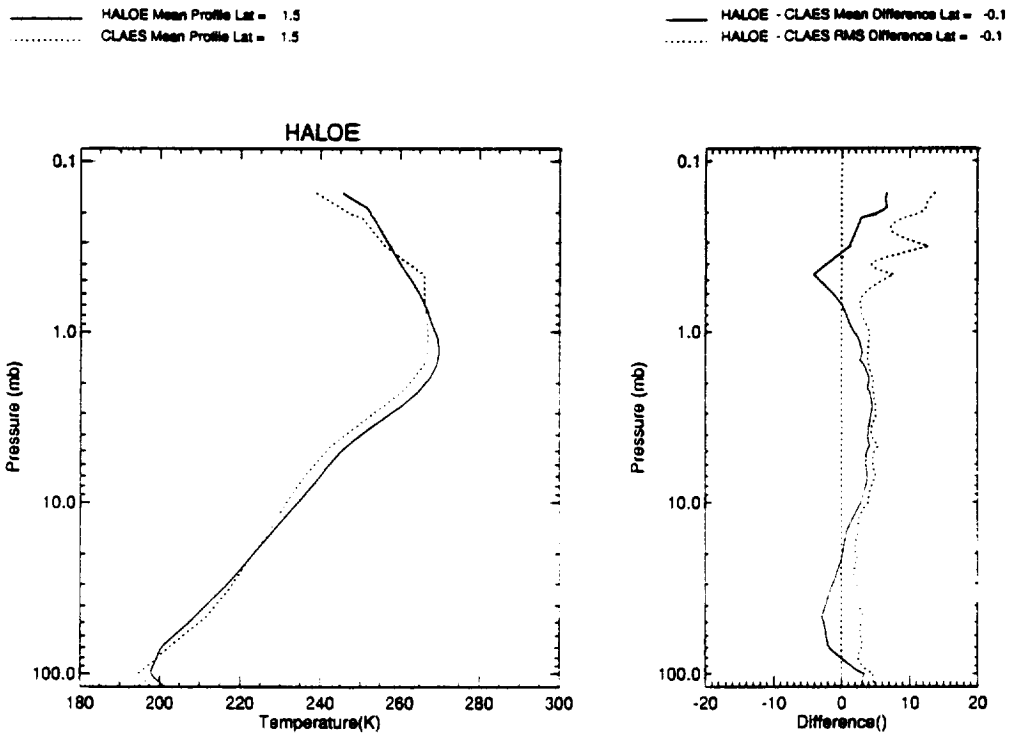

HALOE - CLAES Temperature (K) differences
on 1-APR-1993 to 3-APR-1993 near 1 N using 28 profiles

Wed Jul 13 14:42:58 EDT 1994

Figure B-4

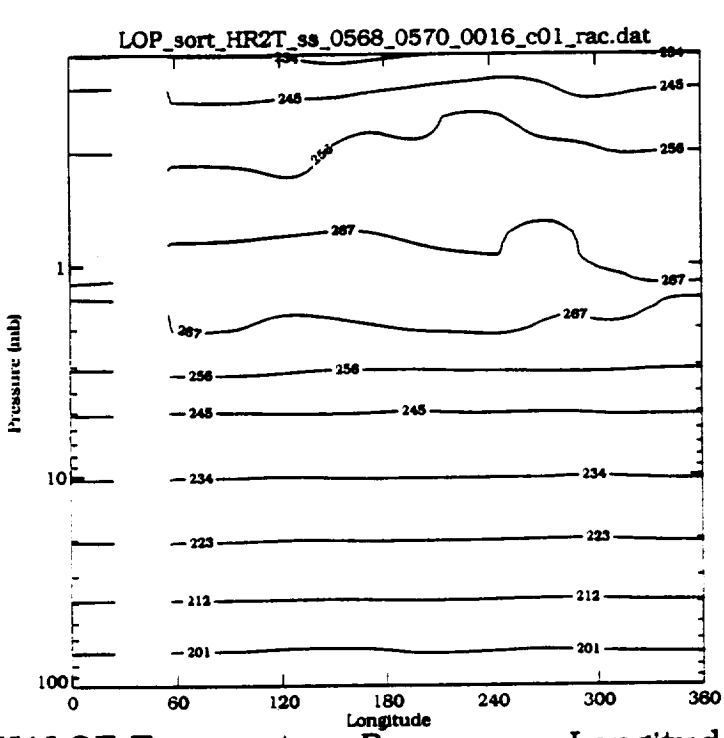

HALOE Temperature Pressure vs Longitude Cross Section, Sunset on 01-APR to 03-APR-1993 at 1 N

Figure B-5

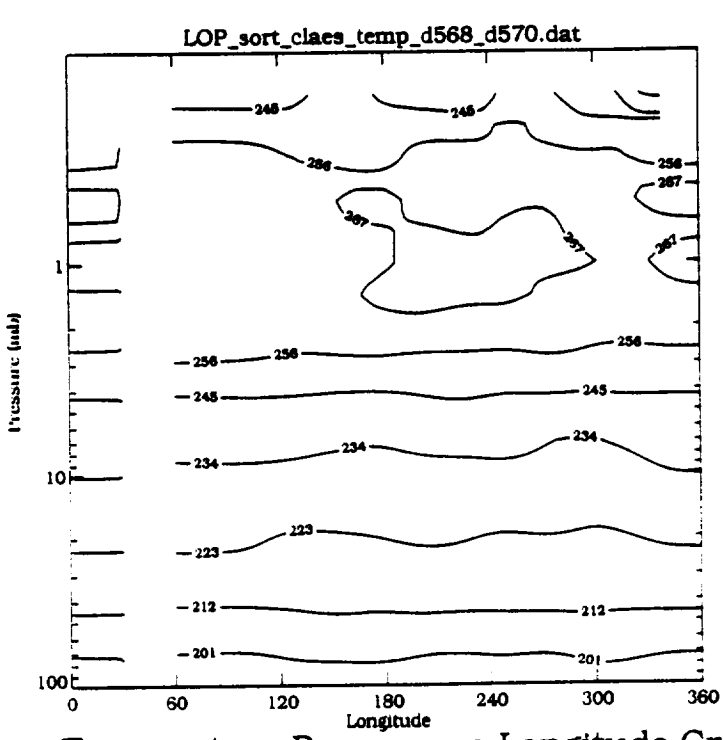

Temperature Pressure vs Longitude Cross Section, on 01-APR to 03-APR-1993 at 1 N

Figure B-6

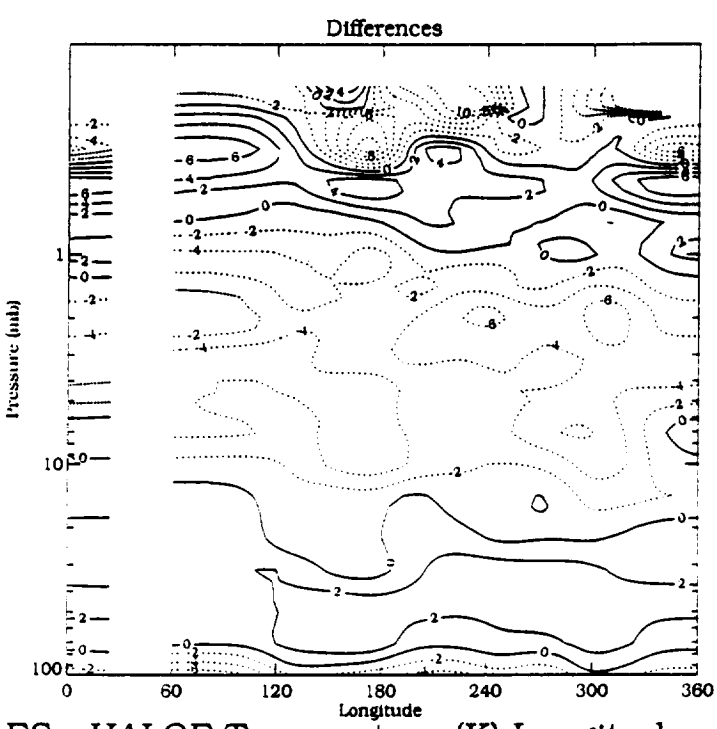

CLAES - HALOE Temperature (K) Longitude vs Pressure Cross Section on 1-APR-1993 to 3-APR-1993 near 1 N

Figure B-7

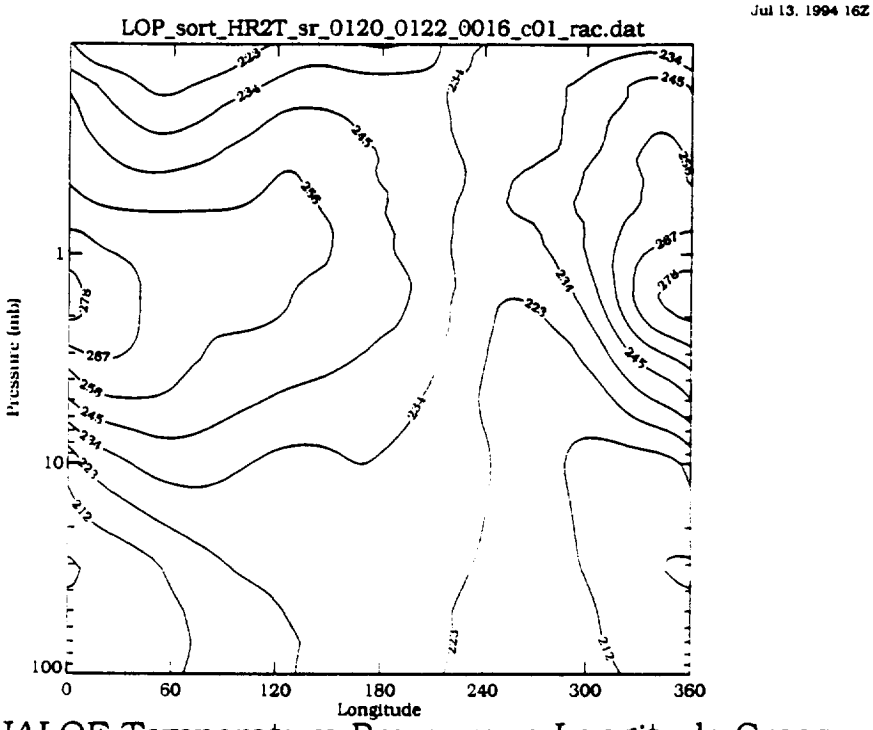

HALOE Temperature Pressure vs Longitude Cross Section, Sunrise on 09-JAN to 11-JAN-1992 at 47 N

Figure B-8

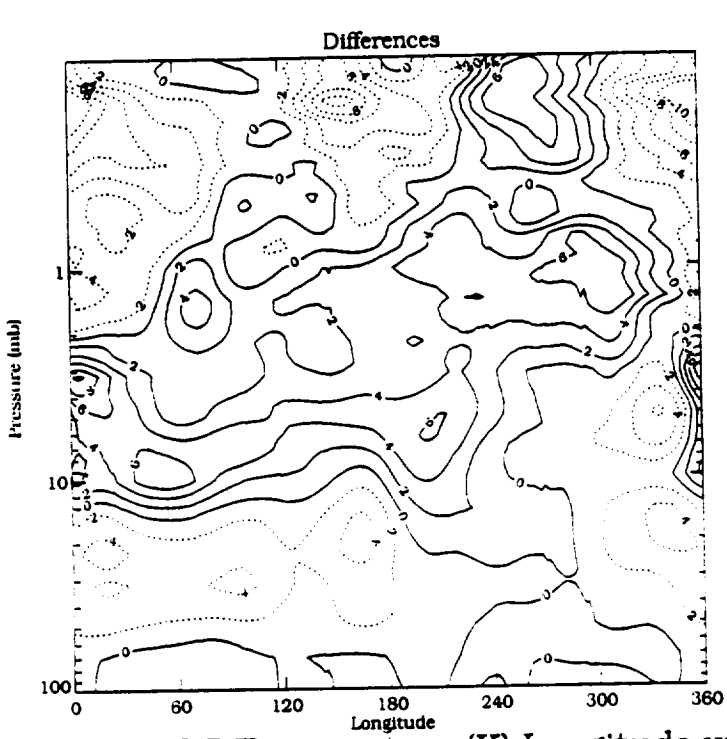

ISAMS - HALOE Temperature (K) Longitude vs Pressure Cross Section on 9-JAN-1992 to 11-JAN-1992 near 47 N

Figure B-9

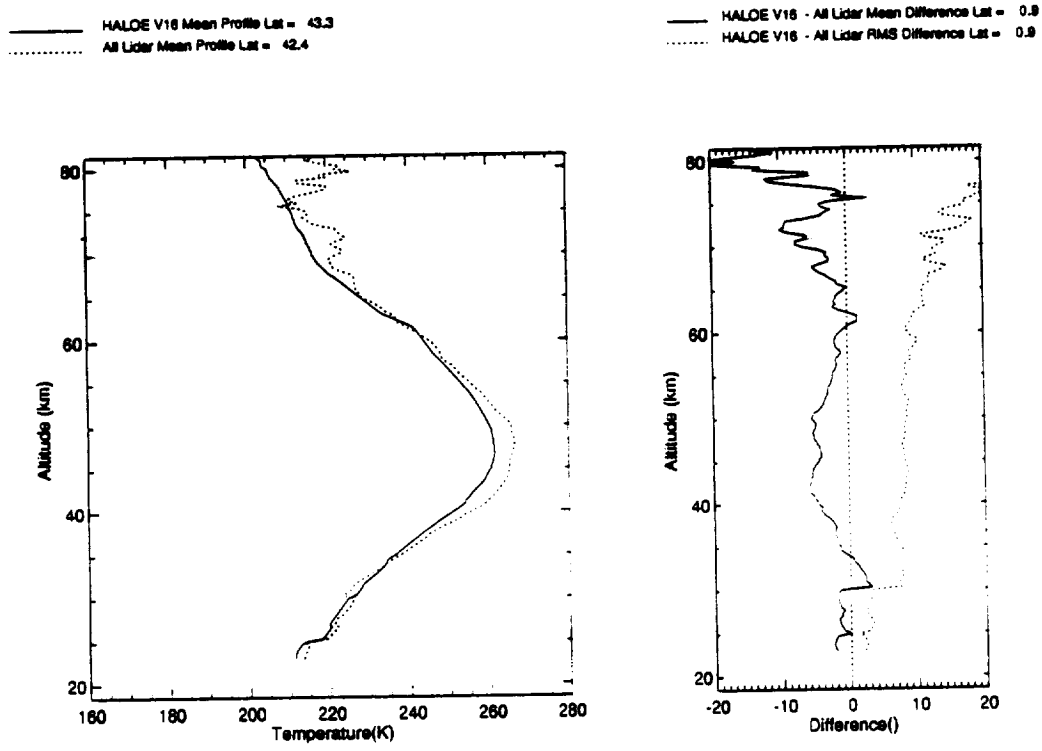

HALOE Temperature vs All LIDAR (92 profiles)

Figure B-10

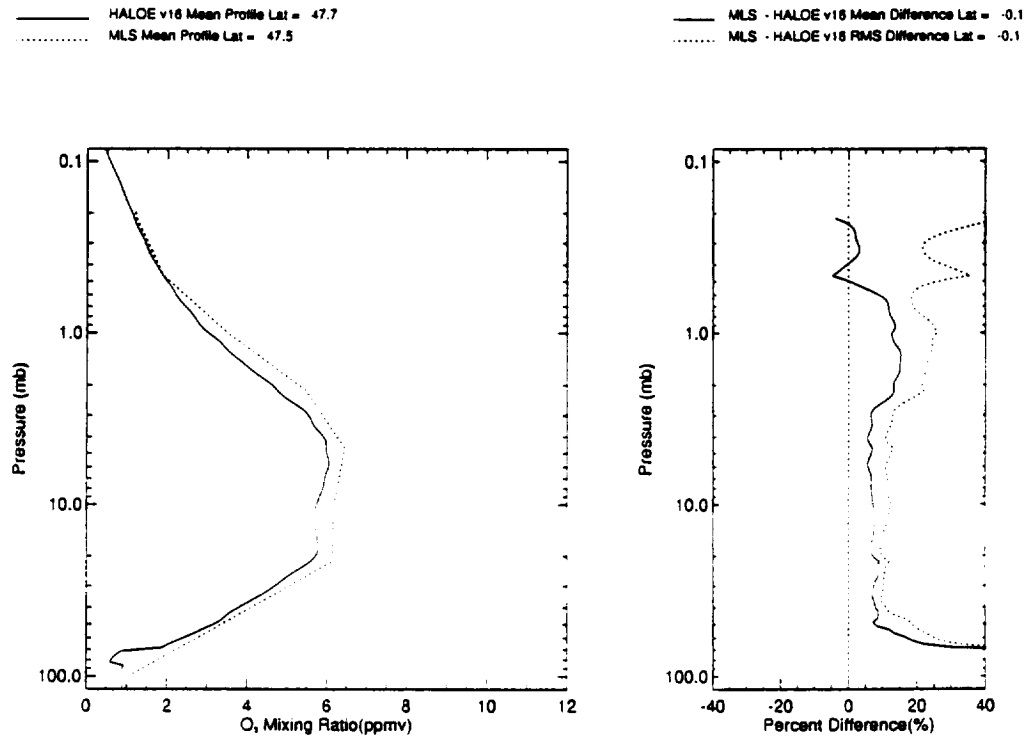

Figure B-11

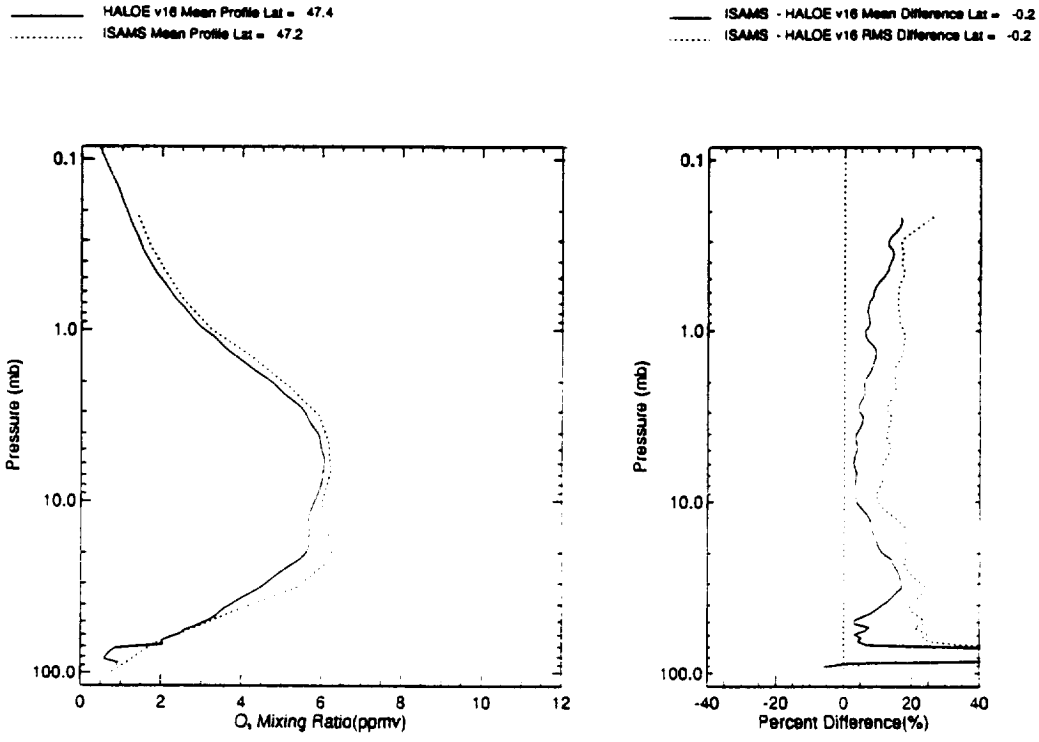

Figure B-12

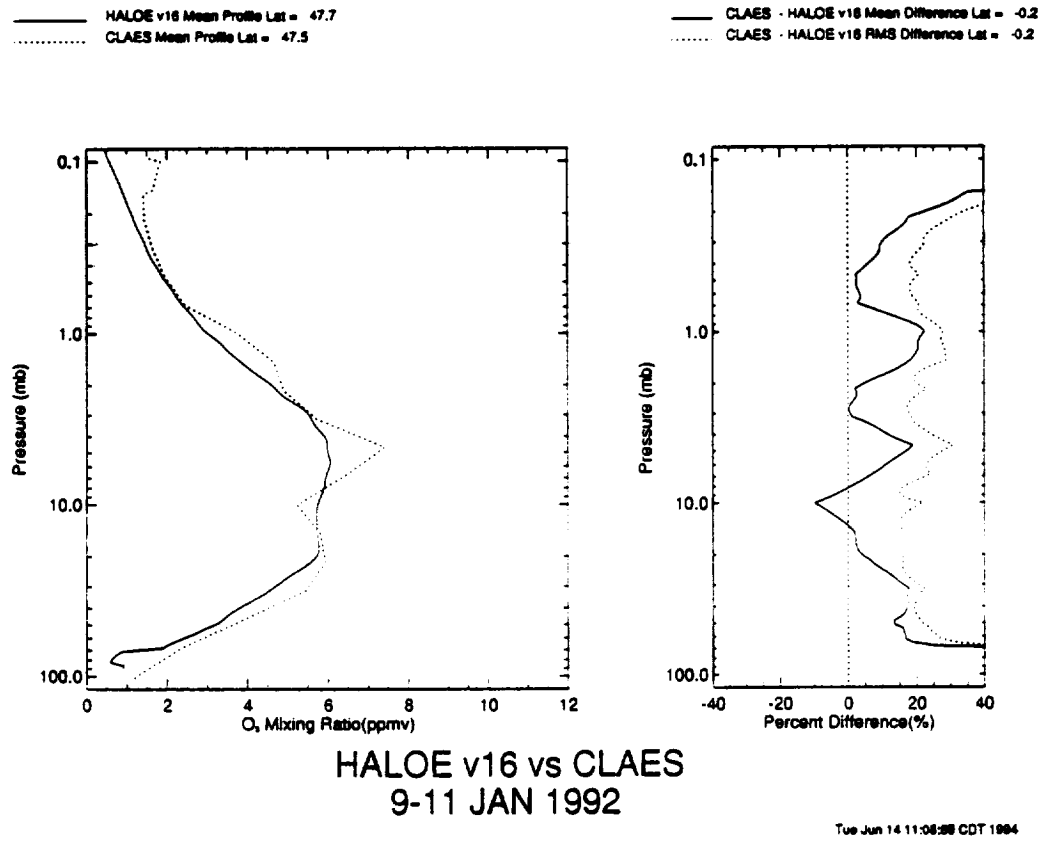

Figure B-13

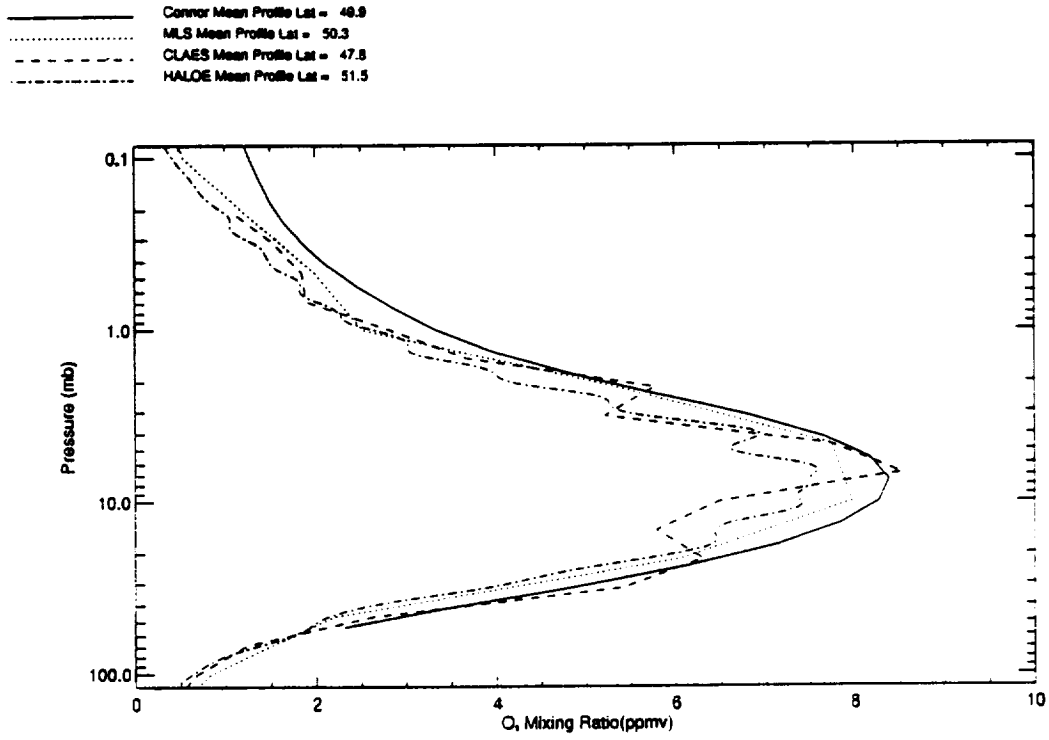

Figure B-14

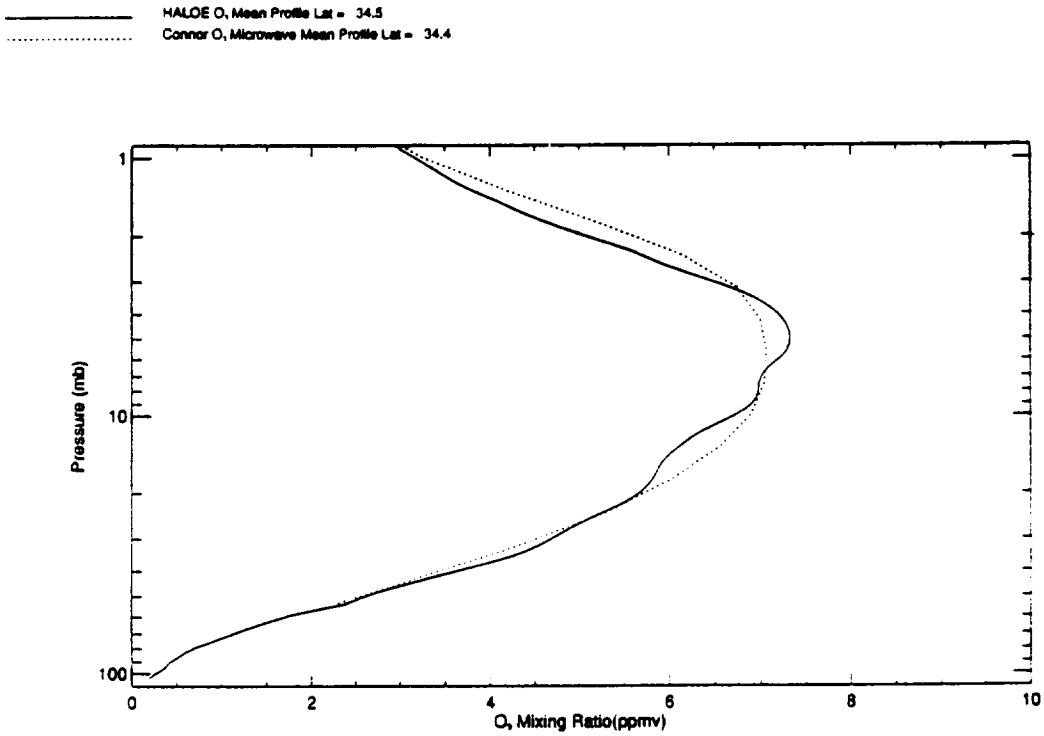

HALOE O_3 vs Table Mtn (MM) O_3
NOV 1991 - Mar 1992)

Mon Jun 13 09:46:07 CDT 1994

Figure B-15

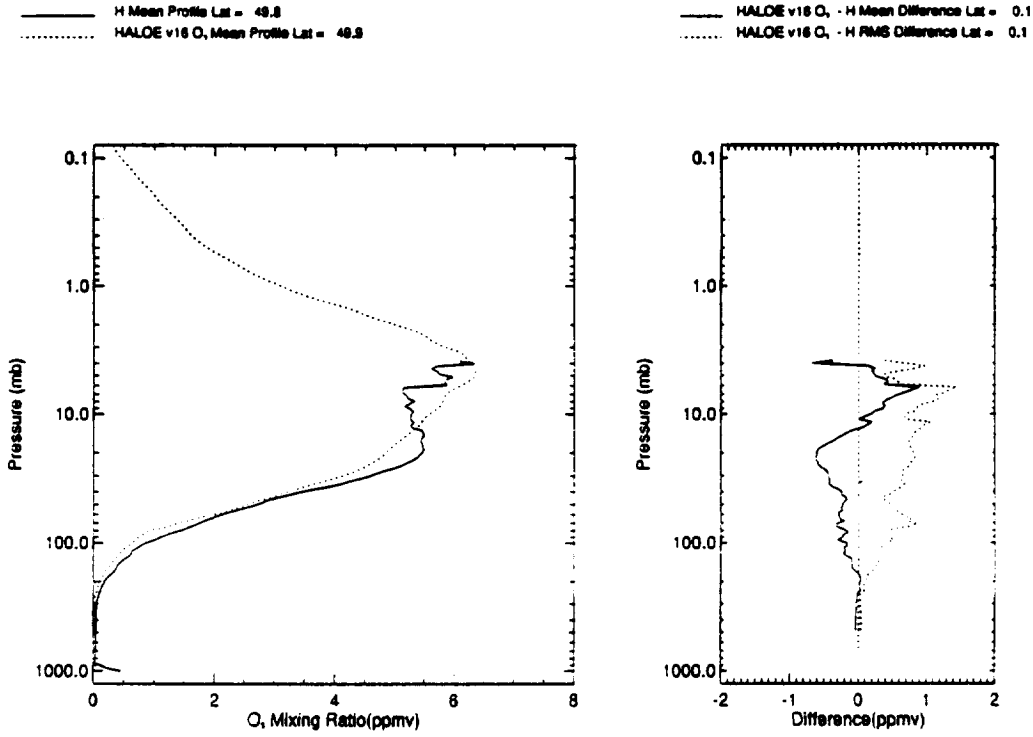

HALOE v16 O_3 vs German Ozone Sonde
Near 52.1 20 Events

Mon Jun 13 13:35:08 CDT 1994

Figure B-16

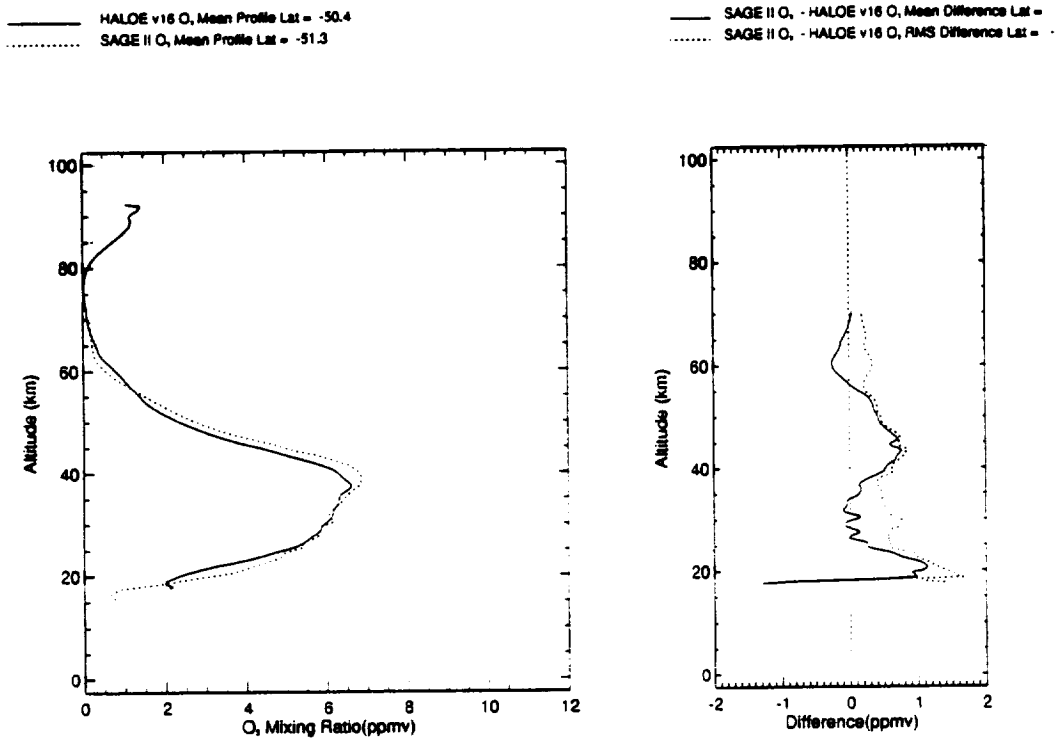

Figure B-17

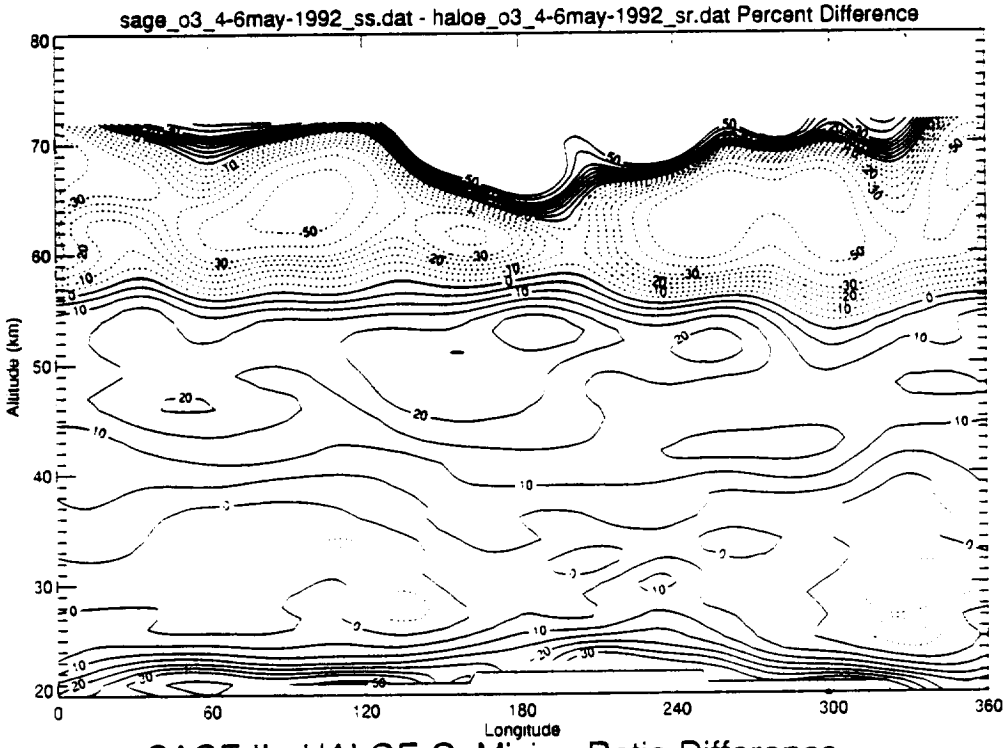

Figure B-18

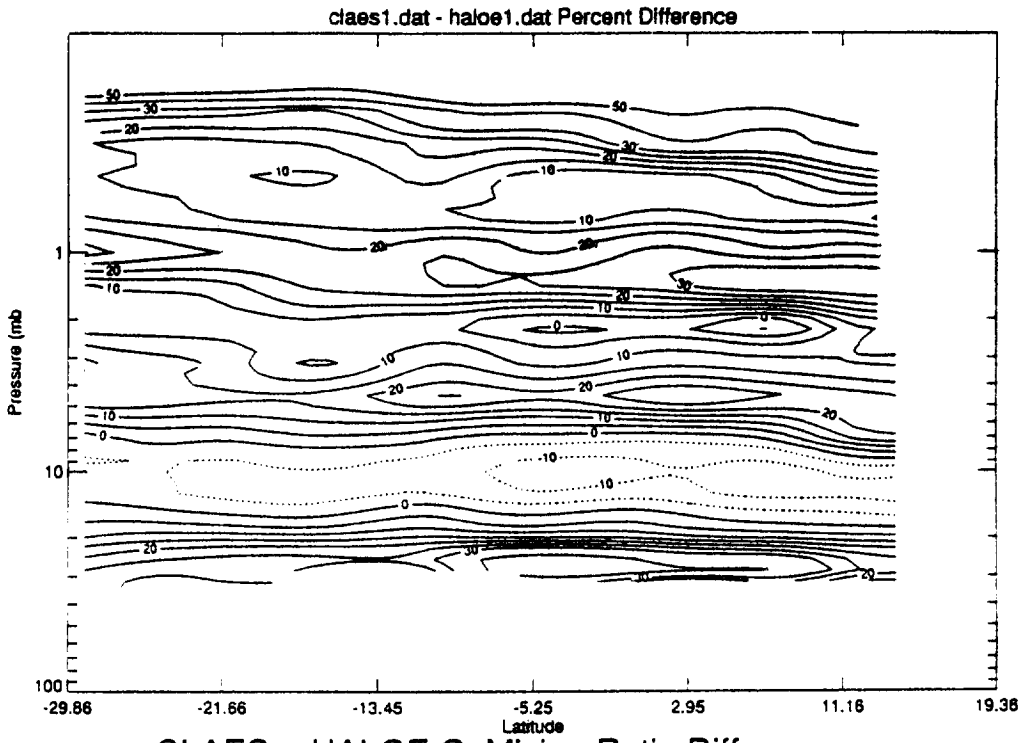

CLAES - HALOE O_3 Mixing Ratio Difference
on 15-20 Apr 1992

Figure B-19

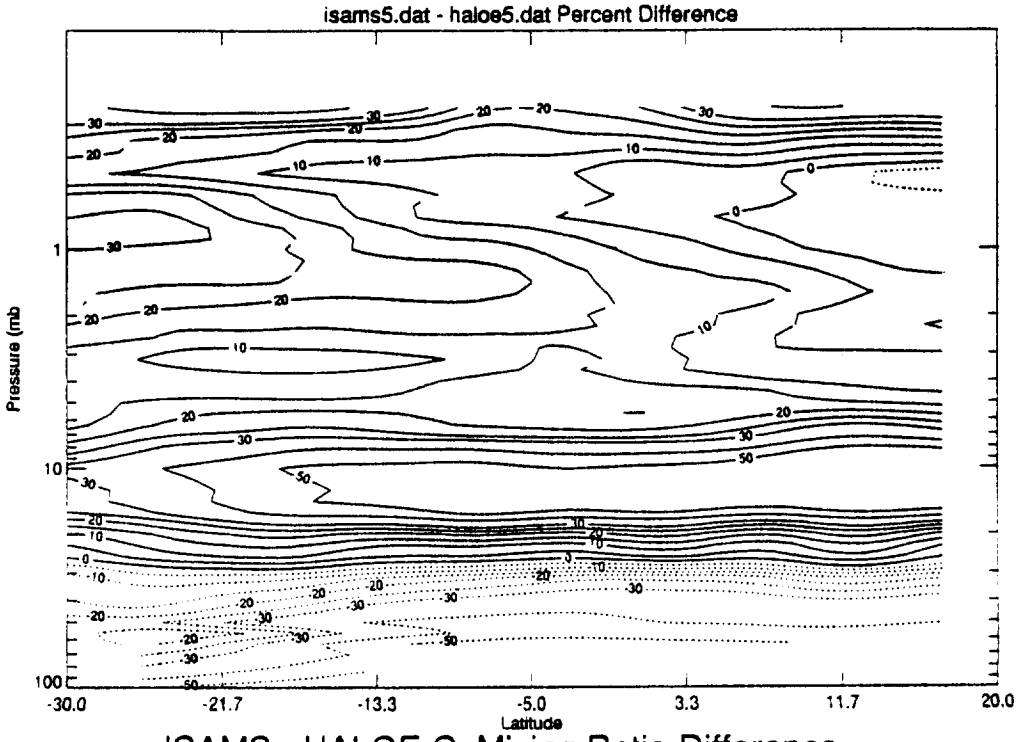

ISAMS - HALOE O_3 Mixing Ratio Difference
on 15-20 APR 1994

Figure B-20

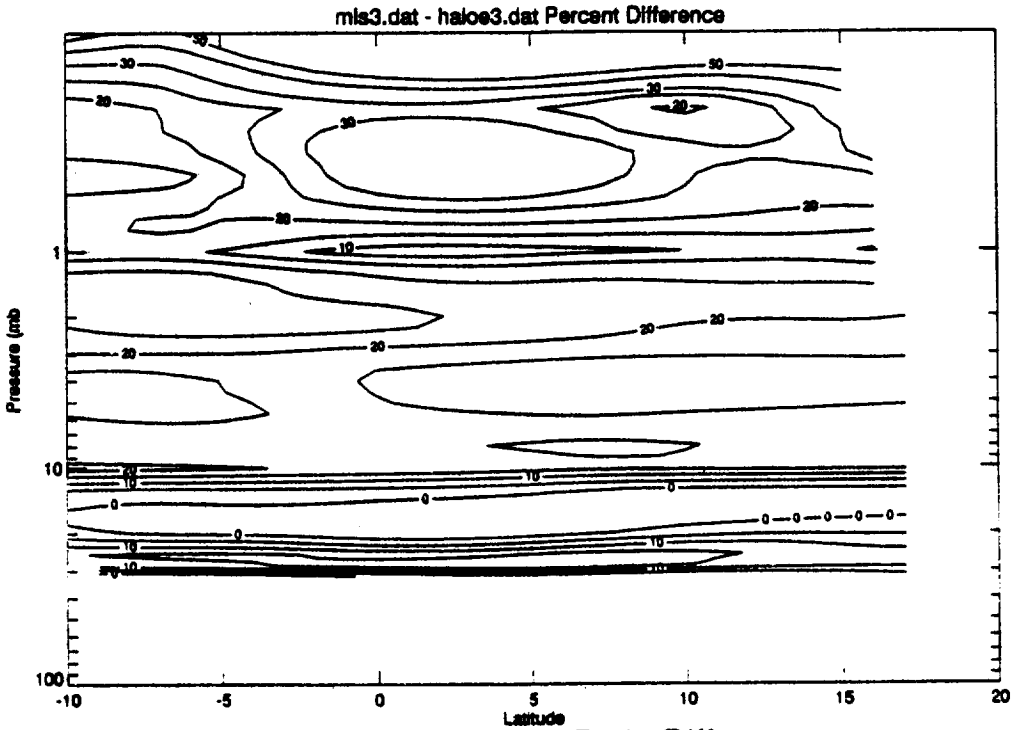

MLS - HALOE O_3 Mixing Ratio Difference
on 15-20 APR 1994

Figure B-21

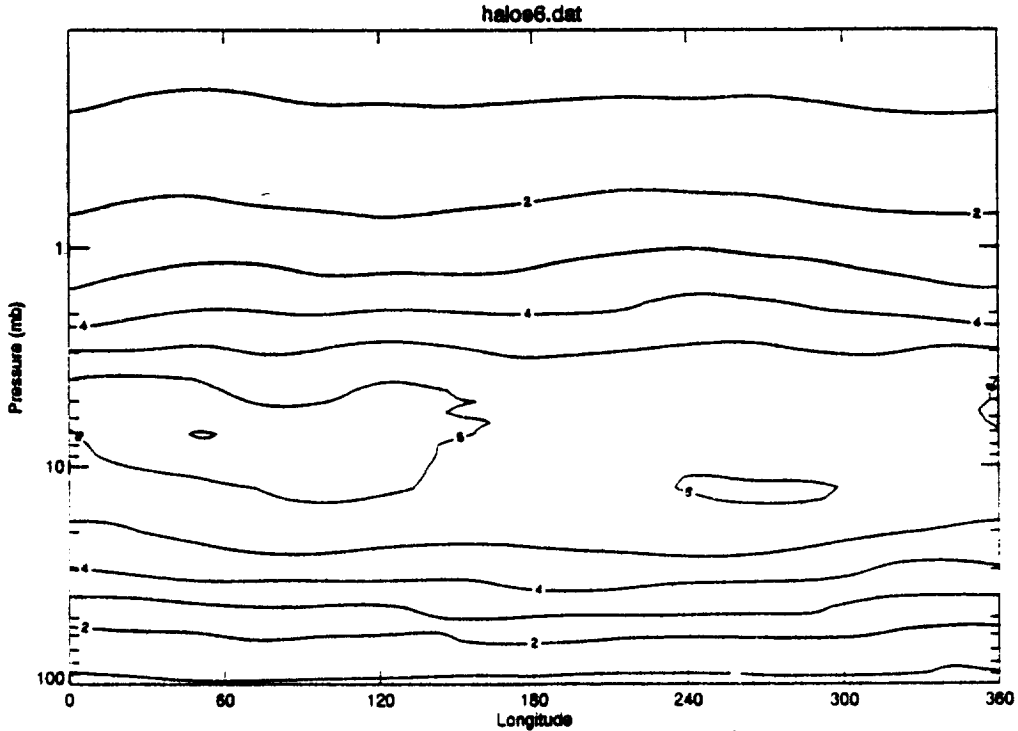

HALOE O_3 Pressure vs Longitude Cross
Section. Rise + Set on 09-JAN to 11-JAN-1992 at 7 S

Figure B-22

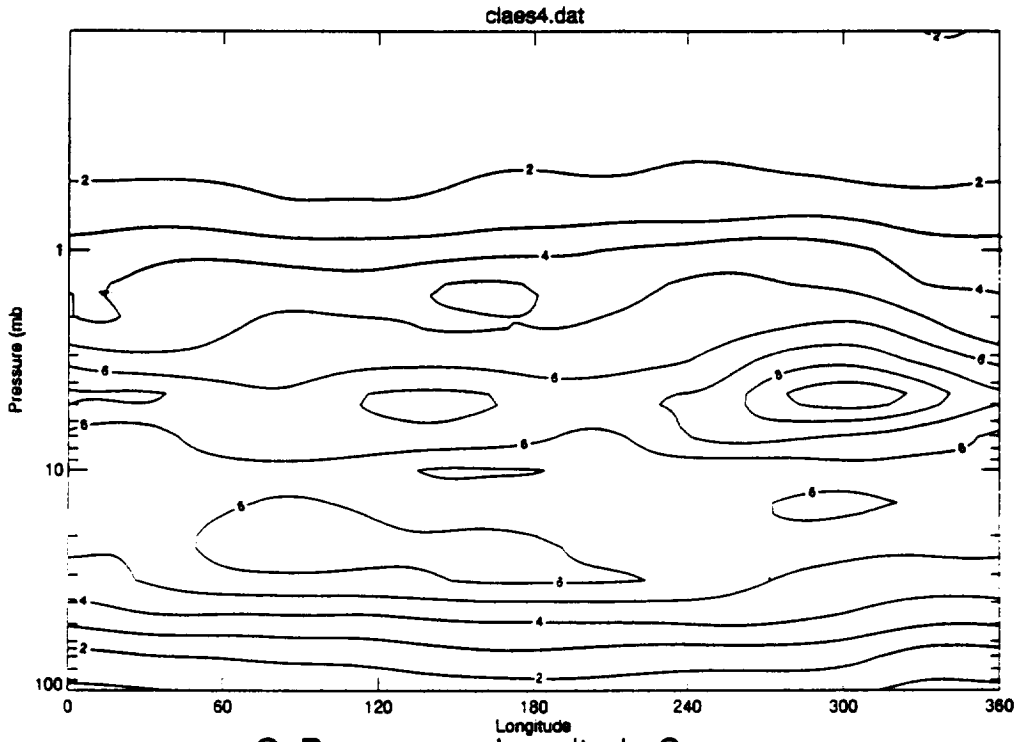

O_3 Pressure vs Longitude Cross Section. on 09-JAN to 11-JAN-1992 at 47 N

Figure B-23

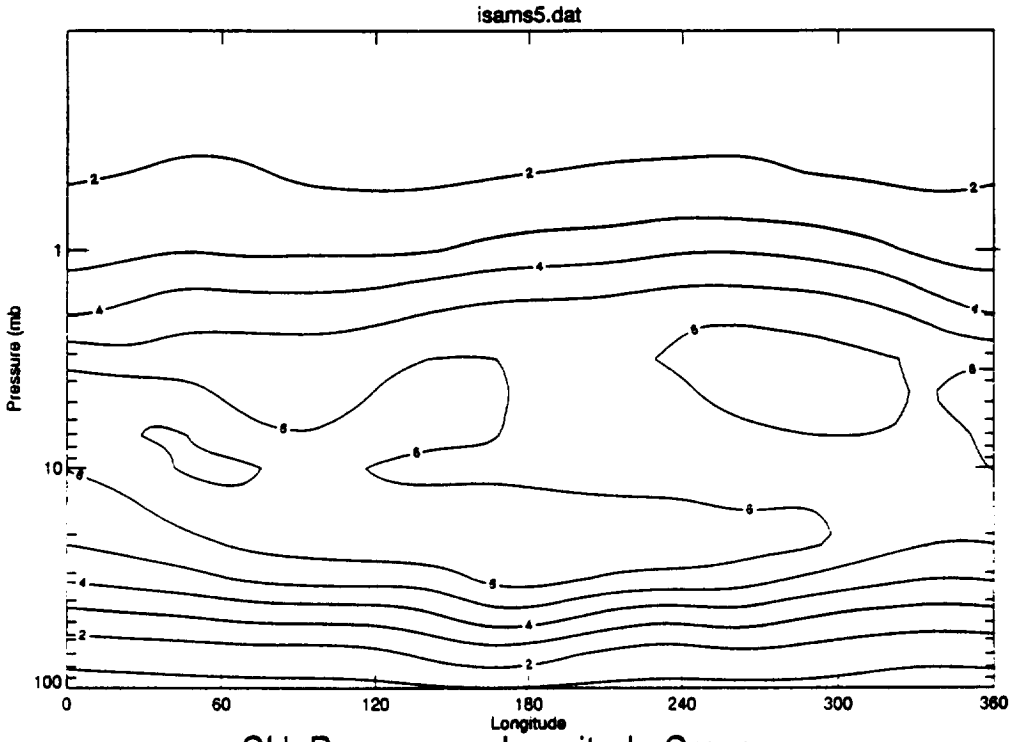

CH_4 Pressure vs Longitude Cross Section. on 09-JAN to 10-JAN-1992 at 47 N

Figure B-24

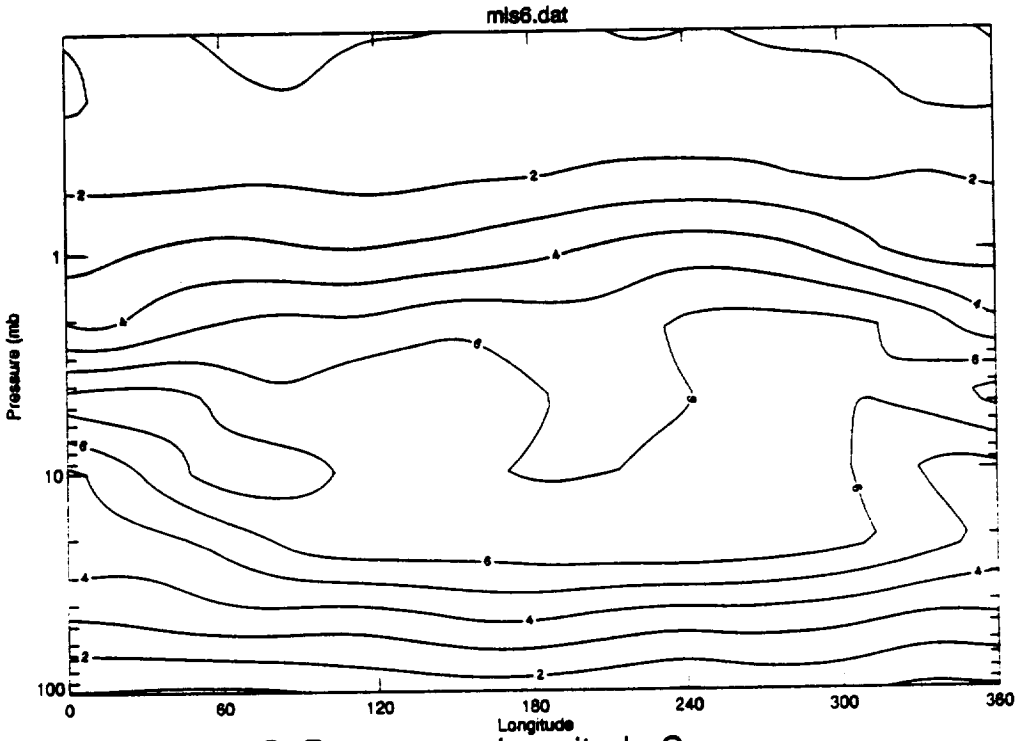

O_3 Pressure vs Longitude Cross Section. on 09-JAN to 12-JAN-1992 at 47 N

Figure B-25

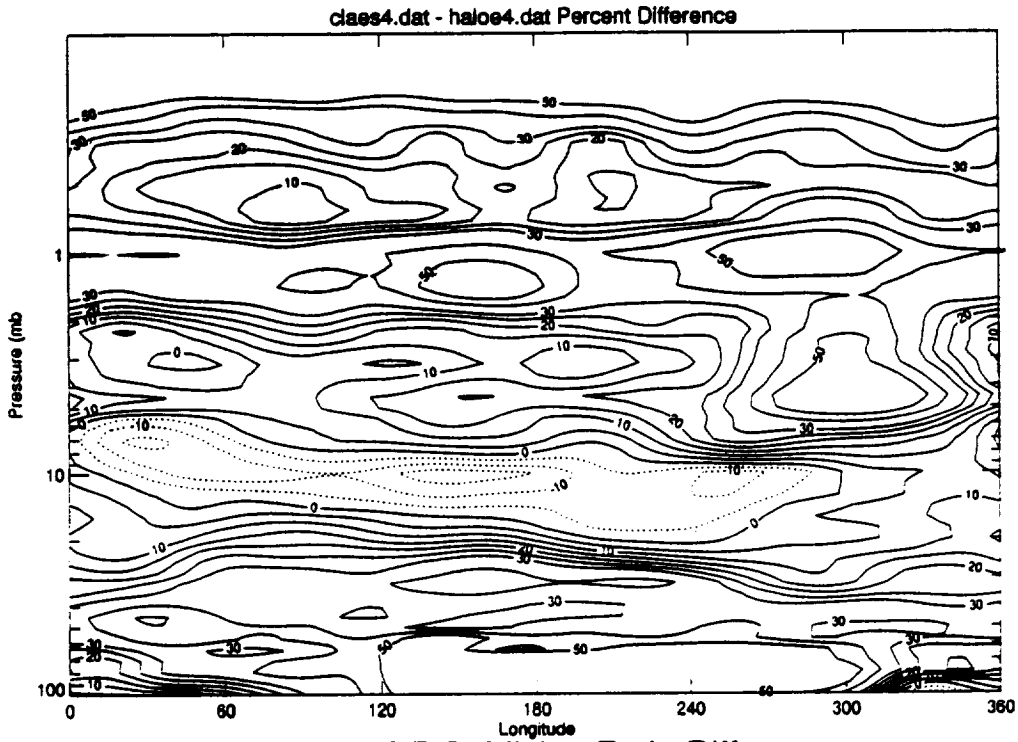

CLAES - HALOE O_3 Mixing Ratio Difference on 9-11 JAN 1994

Figure B-26

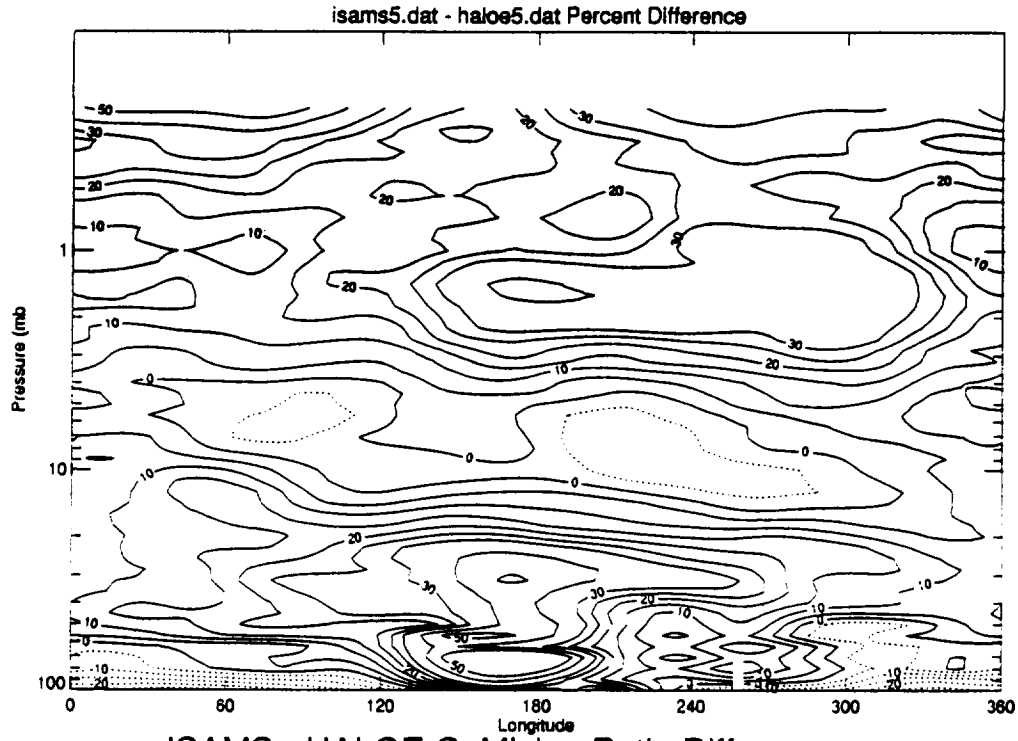

ISAMS - HALOE O_3 Mixing Ratio Difference
on 9-11 JAN 1994

Figure B-27

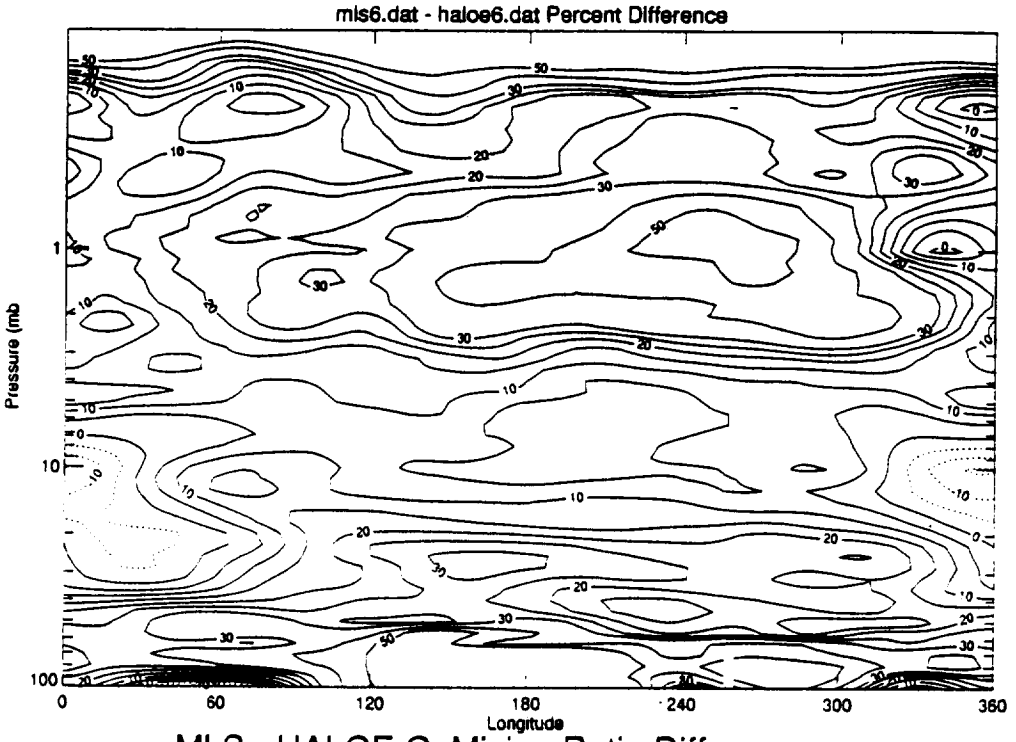

MLS - HALOE O_3 Mixing Ratio Difference
on 9-11 JAN 1994

Figure B-28

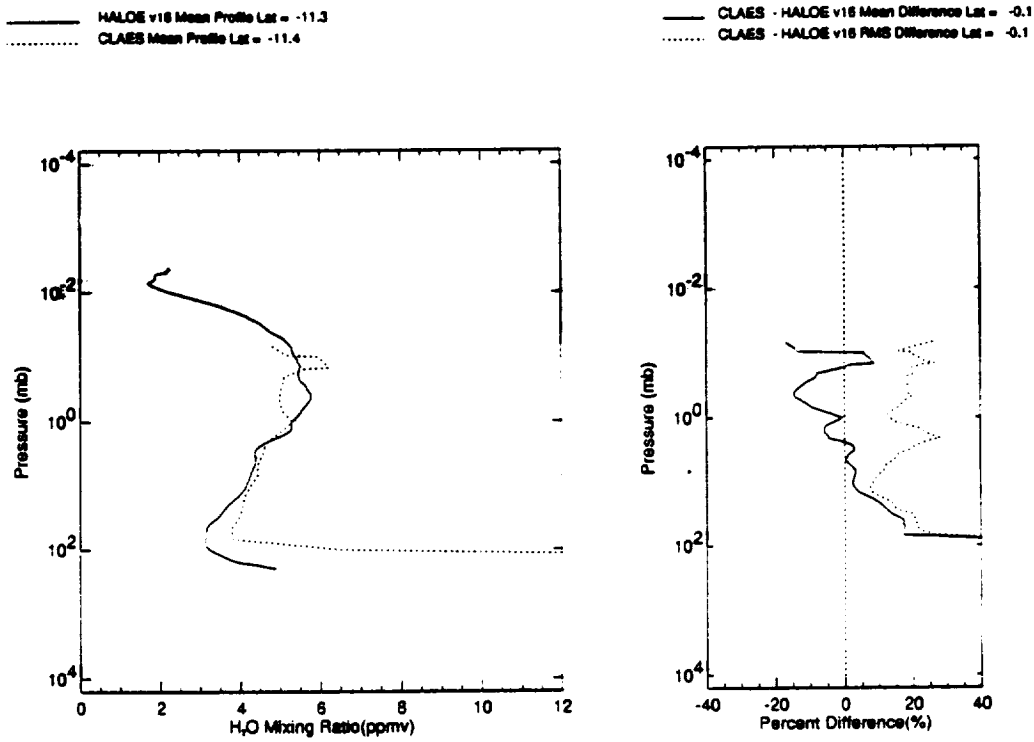

Figure B-29

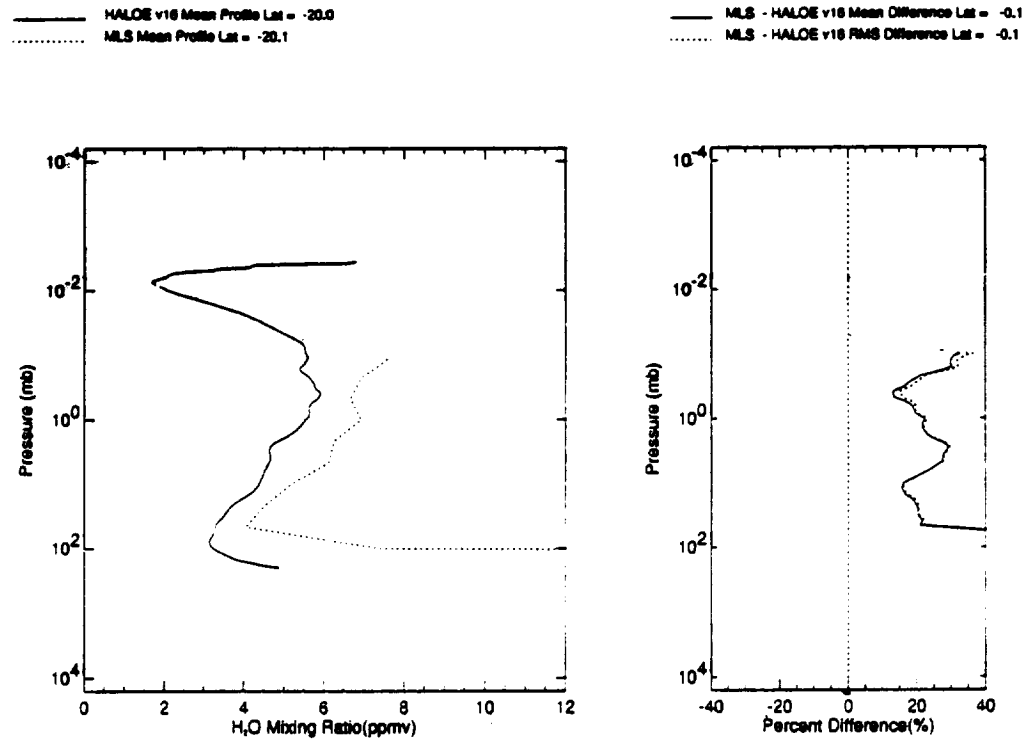

Figure B-30

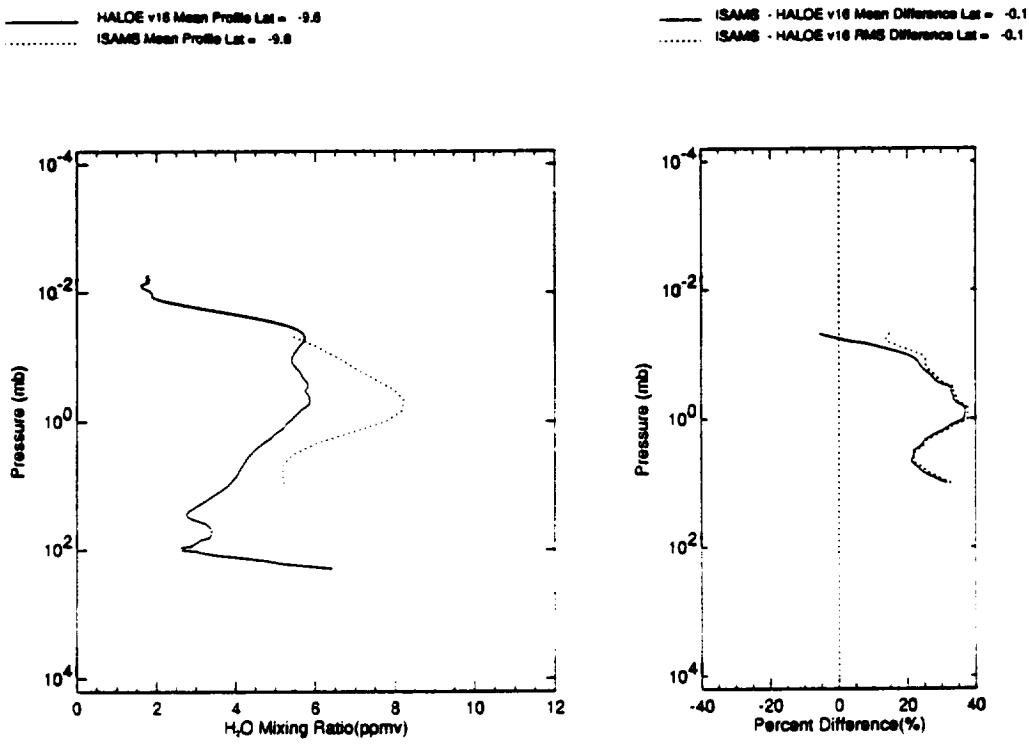

HALOE v16 H_2O vs ISAMS H_2O
15-20 APR 1992

Wed Jun 15 08:27:38 CDT 1994

Figure B-31

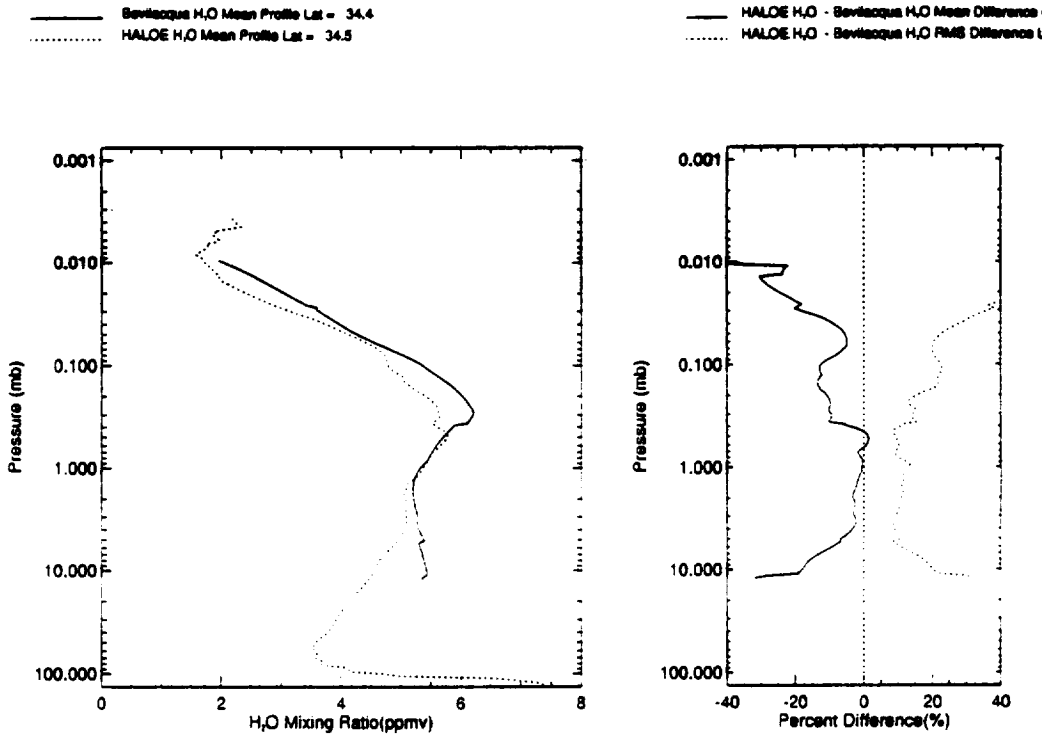

HALOE v16 H_2O vs Bevilacqua Microwave H_2O
Near 34.4 22 Events

Tue Jun 14 13:42:28 CDT 1994

Figure B-32

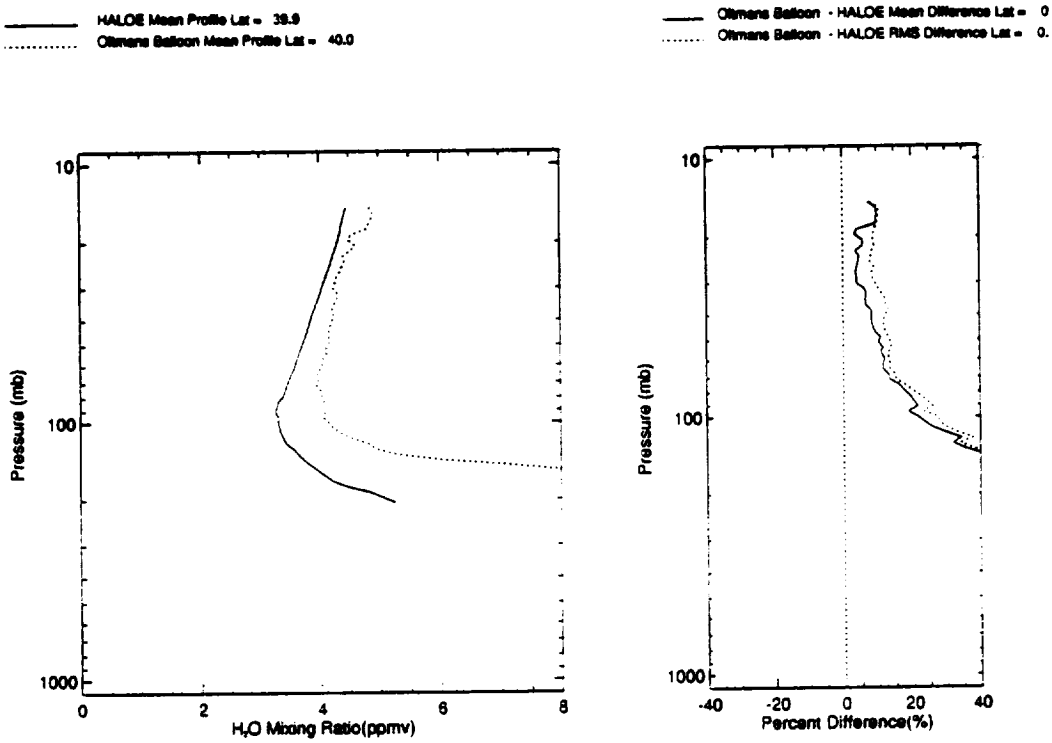

Figure B-33

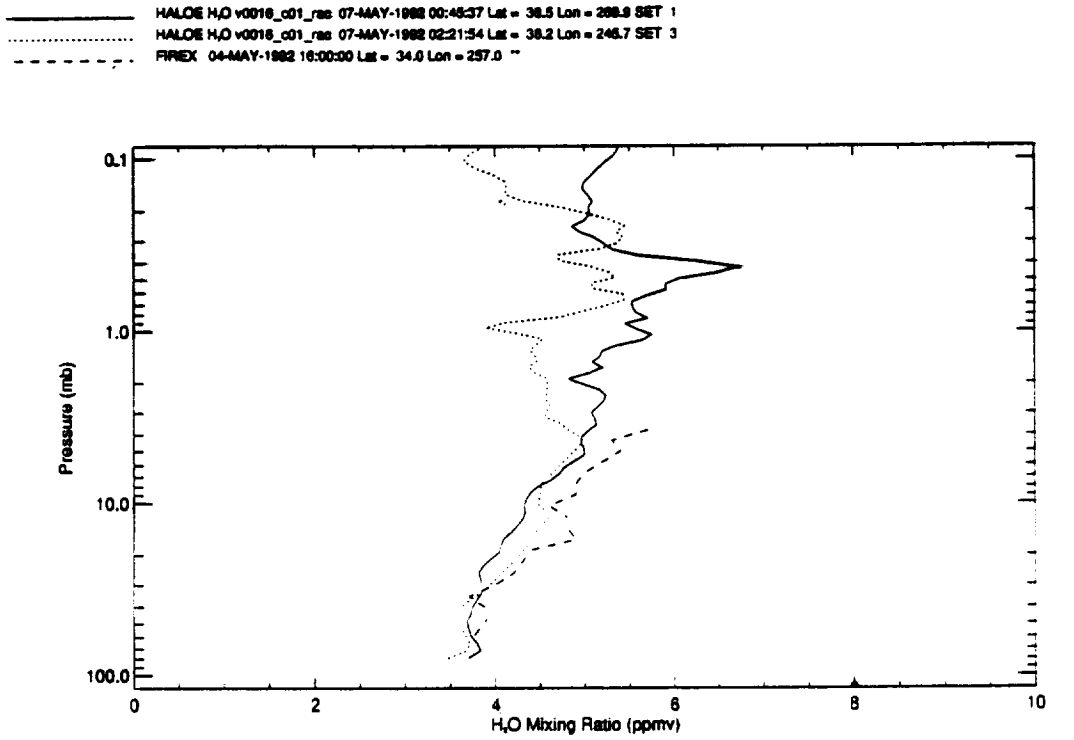

Figure B-34

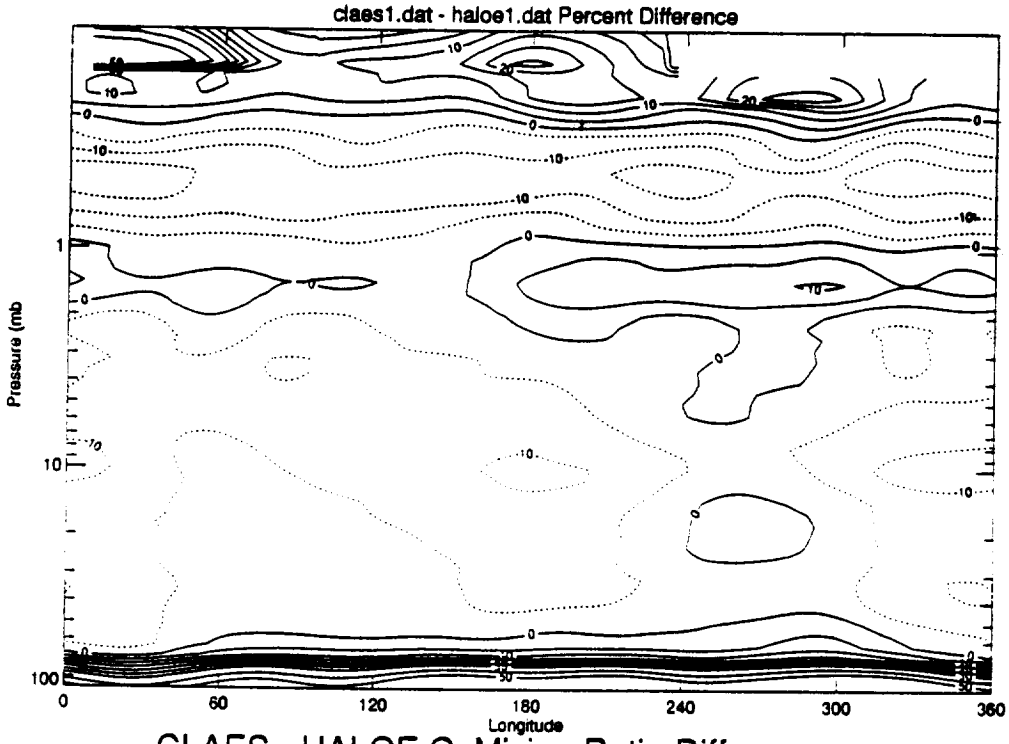

CLAES - HALOE O_3 Mixing Ratio Difference
on 8-10 AUG 1994

Figure B-35

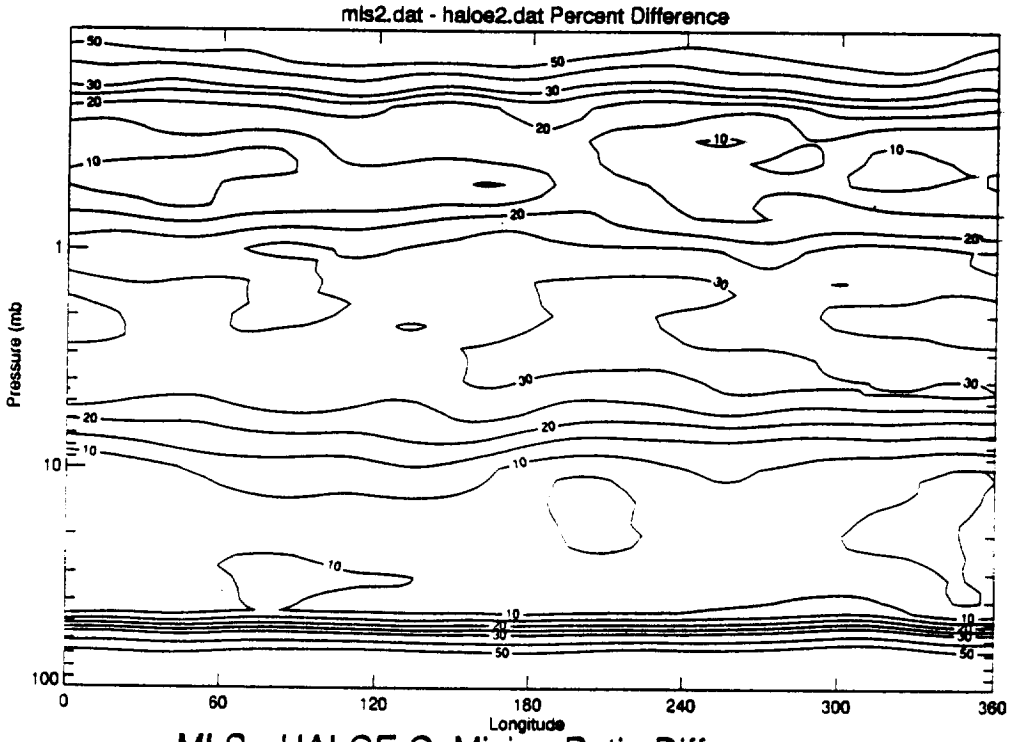

MLS - HALOE O_3 Mixing Ratio Difference
on 8-10 AUG 1994

Figure B-36

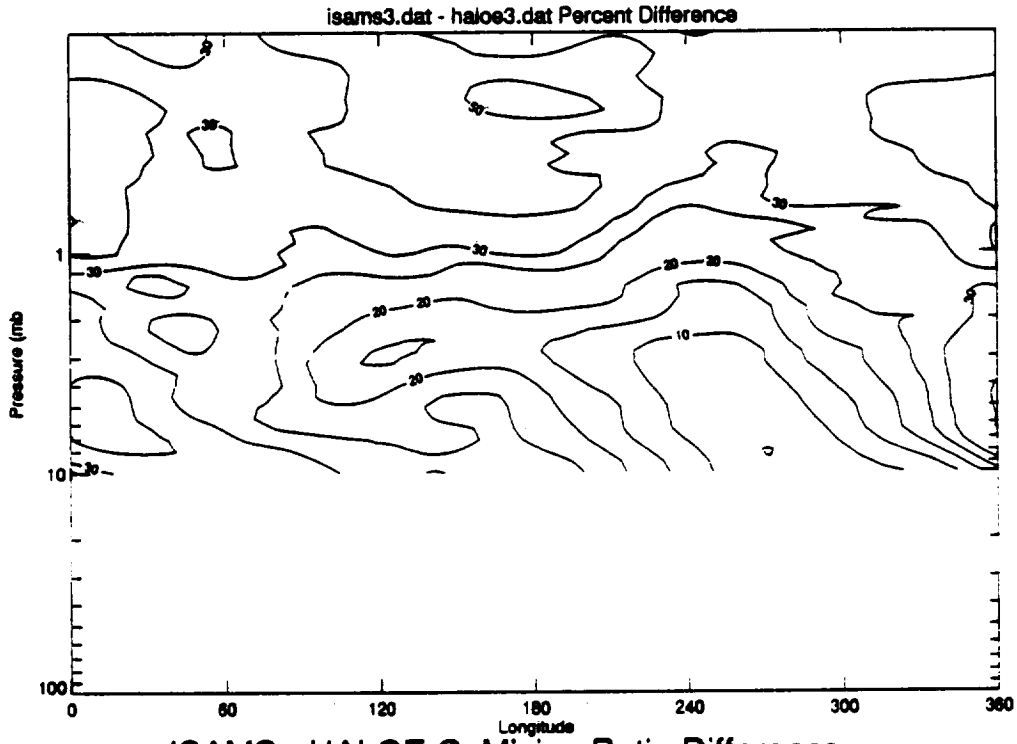

ISAMS - HALOE O_3 Mixing Ratio Difference
on 9-11 JAN 1992

Figure B-37

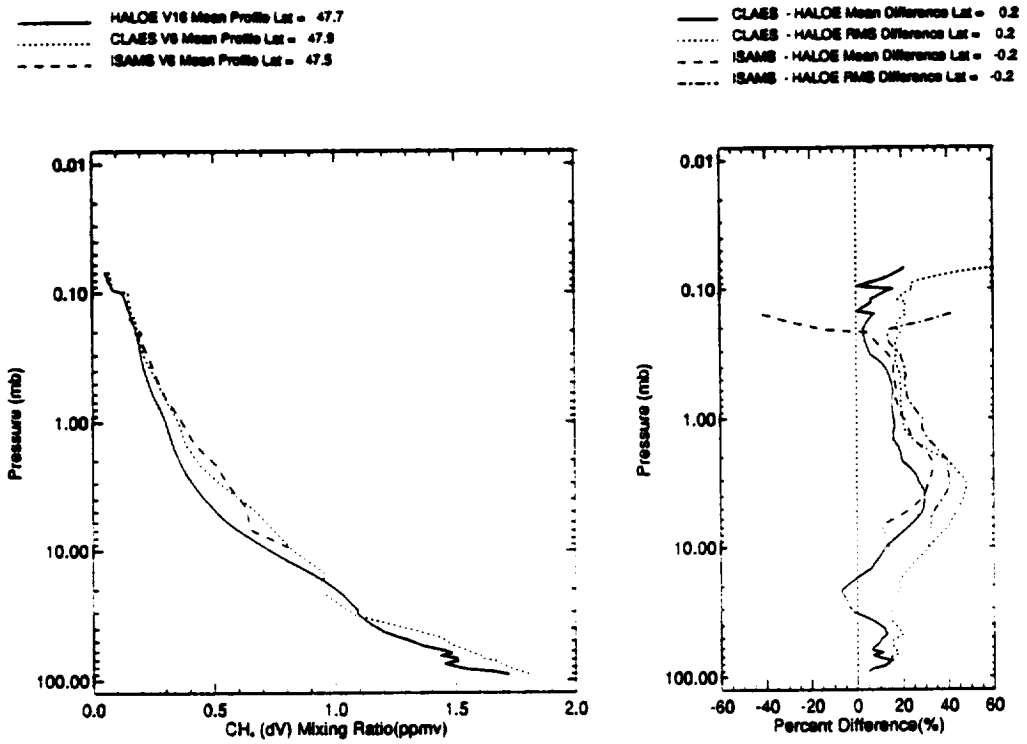

HALOE, CLAES, and ISAMS Mean CH_4 Mixing Ratio and Difference
on 9,10,11 January 1992 near 47N

Thu Jun 16 13:25:29 EDT 1994

Figure B-38

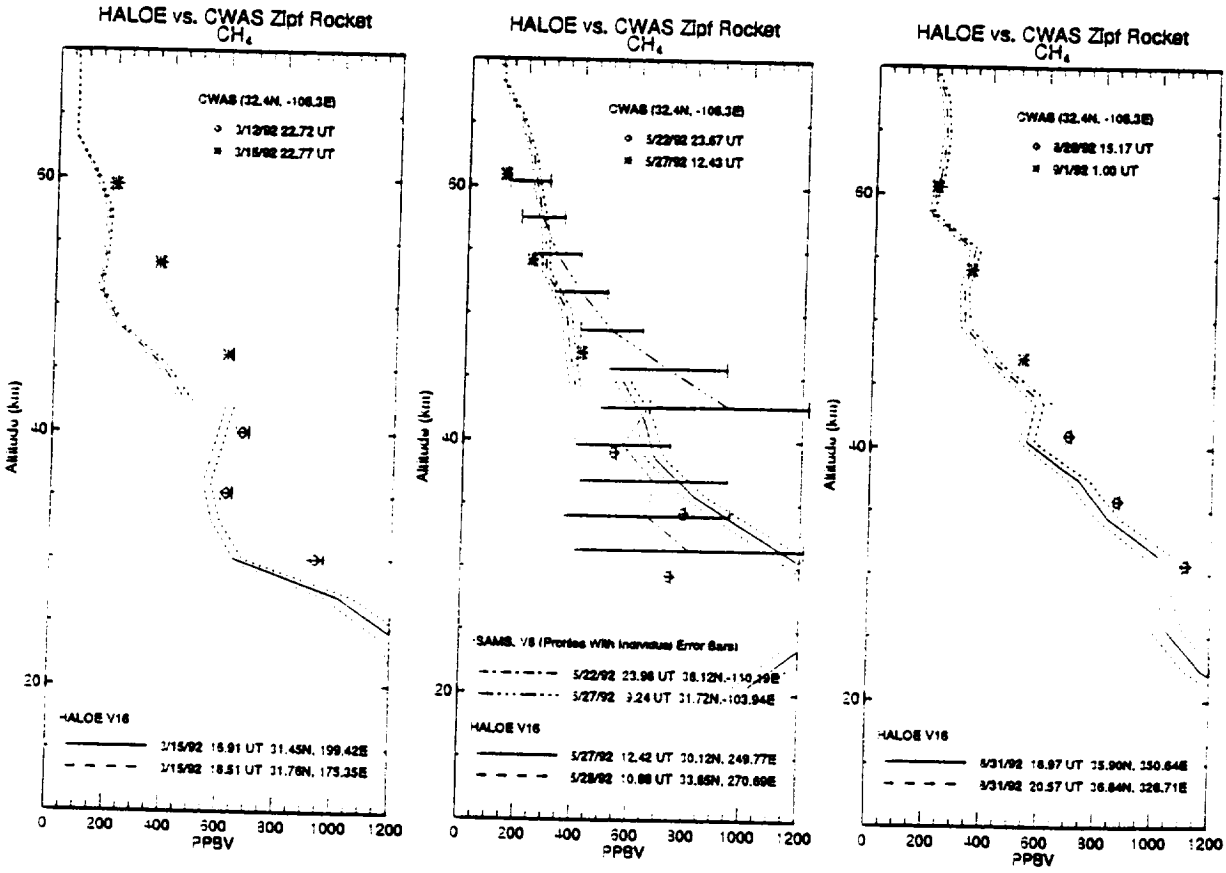

Figure B-39

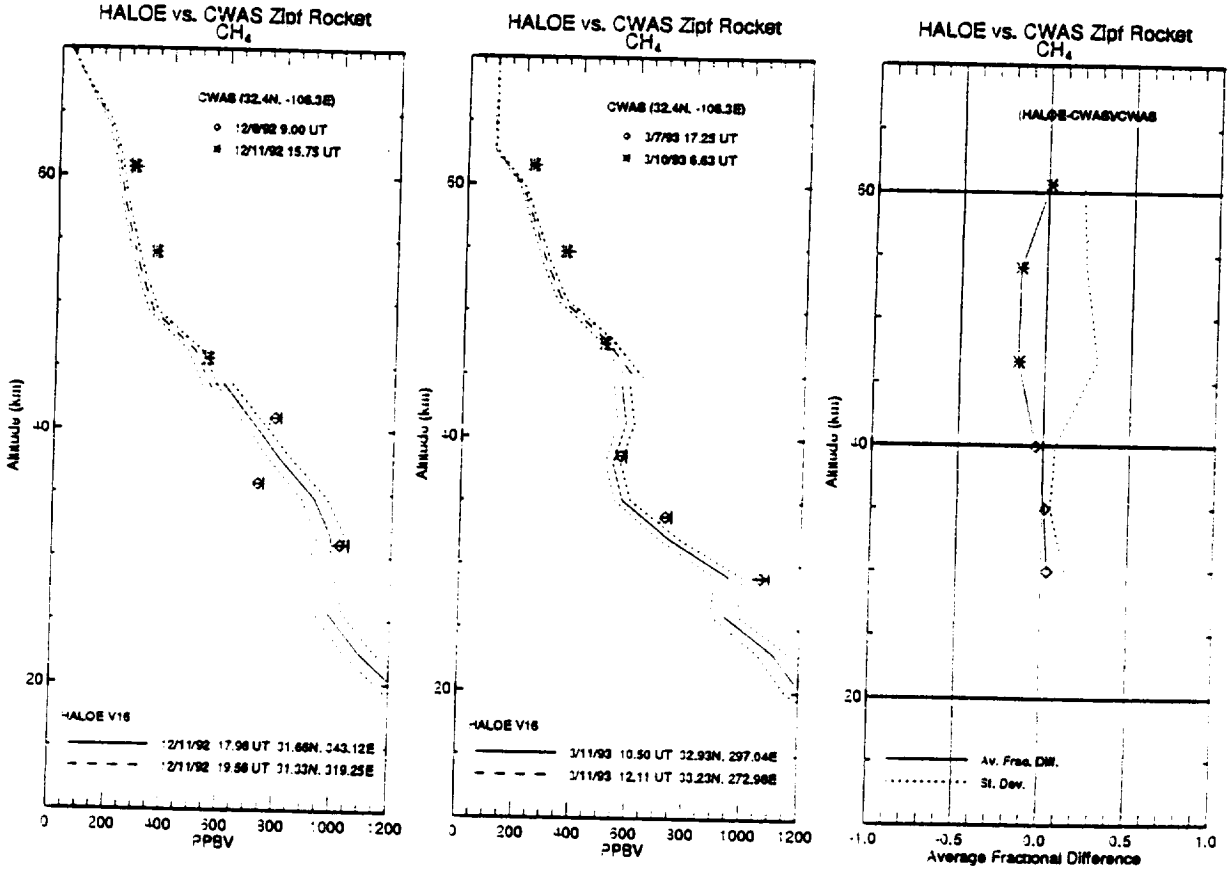

Figure B-40

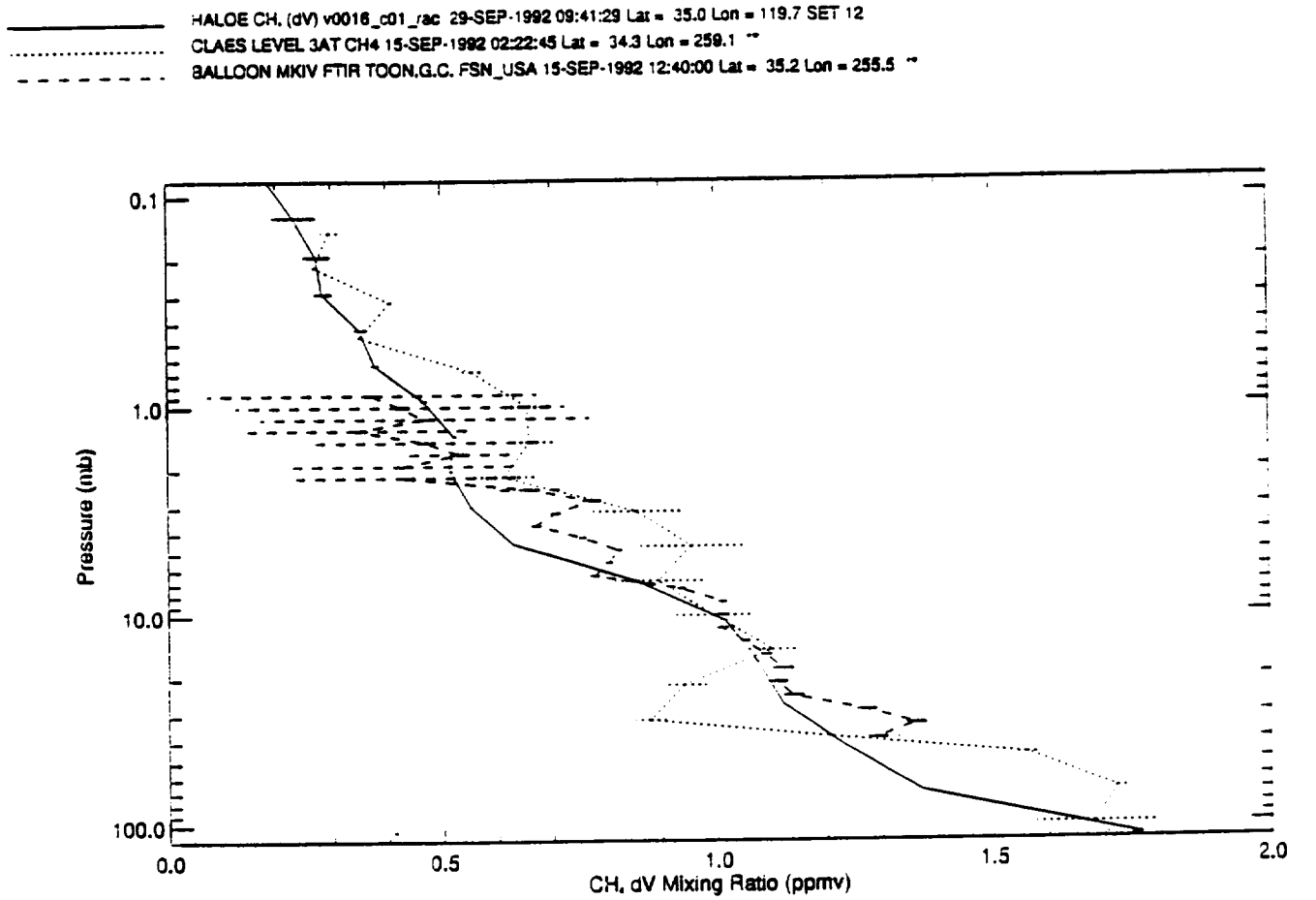
HALOE CH4 (dV) v0016_c01_rac 29-SEP-1992 09:41:29 Lat = 35.0 Lon = 119.7 SET 12
CLAES LEVEL 3AT CH4 15-SEP-1992 02:22:45 Lat = 34.3 Lon = 259.1 **
BALLOON MKIV FTIR TOON,G.C. FSN_USA 15-SEP-1992 12:40:00 Lat = 35.2 Lon = 255.5 **
Pressure (mb)
0.1
1.0
10.0
100.0
0.0
0.5
1.0
1.5
2.0
CH4 dV Mixing Ratio (ppmv)
HALOE(29-SEP), CLAES, and Toon Balloon CH4 Mixing Ratio vs Pressure on 15-SEP-1992 at 35N 255E
Thu Jun 16 15:03:19 EDT 1994

Figure B-41

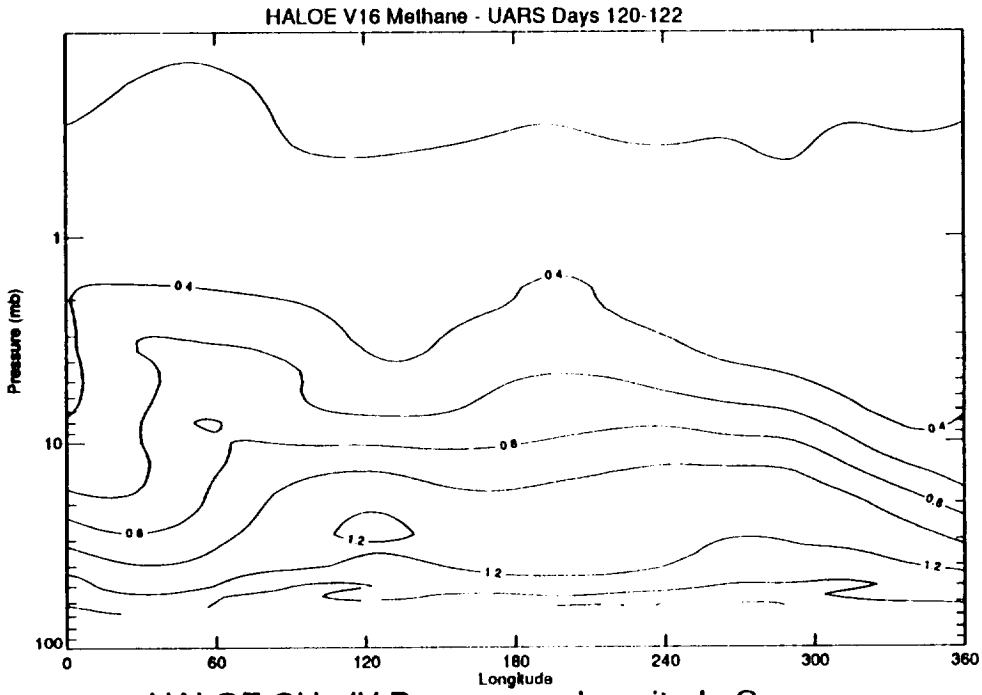

HALOE CH_4 dV Pressure vs Longitude Cross Section, Sunrise on 09-JAN to 11-JAN-1992 at 47 N

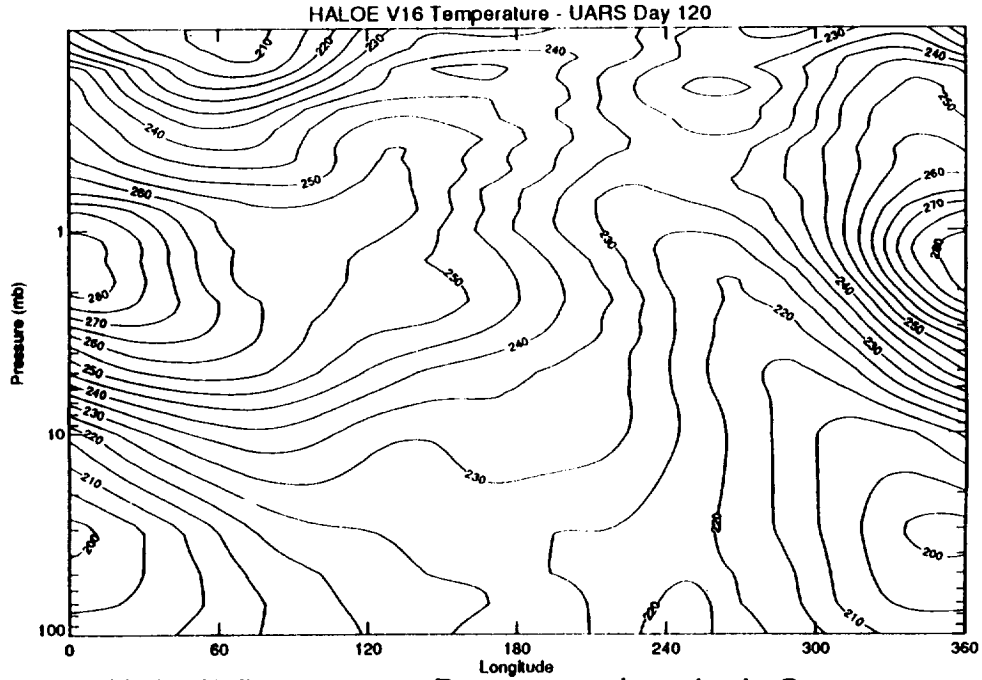

HALOE Temperature Pressure vs Longitude Cross Section, Sunrise on 09-JAN-1992 at 46 N

Figure B-42

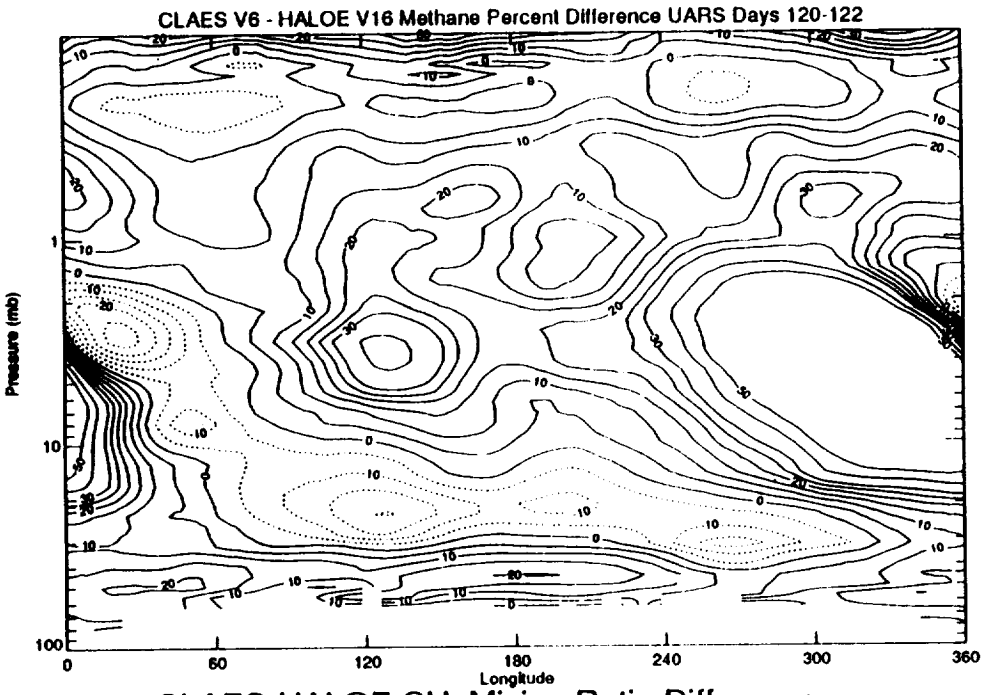

CLAES-HALOE CH_4 Mixing Ratio Difference
on 9-JAN-1992 to 11-JAN-1992

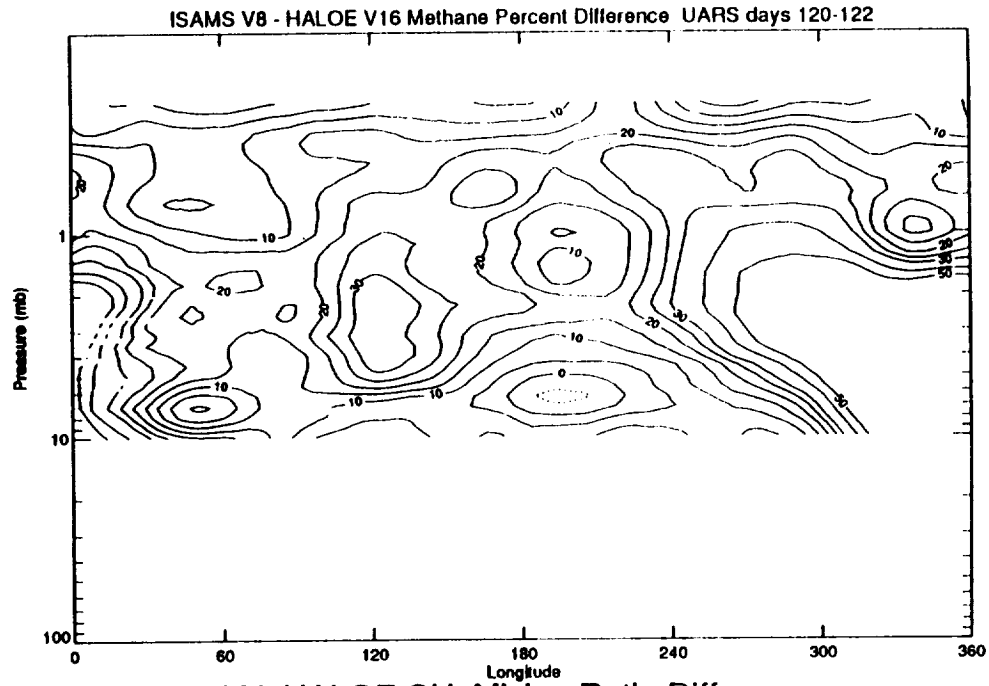

ISAMS-HALOE CH_4 Mixing Ratio Difference
on 9-JAN-1992 to 11-JAN-1992

Figure B-43

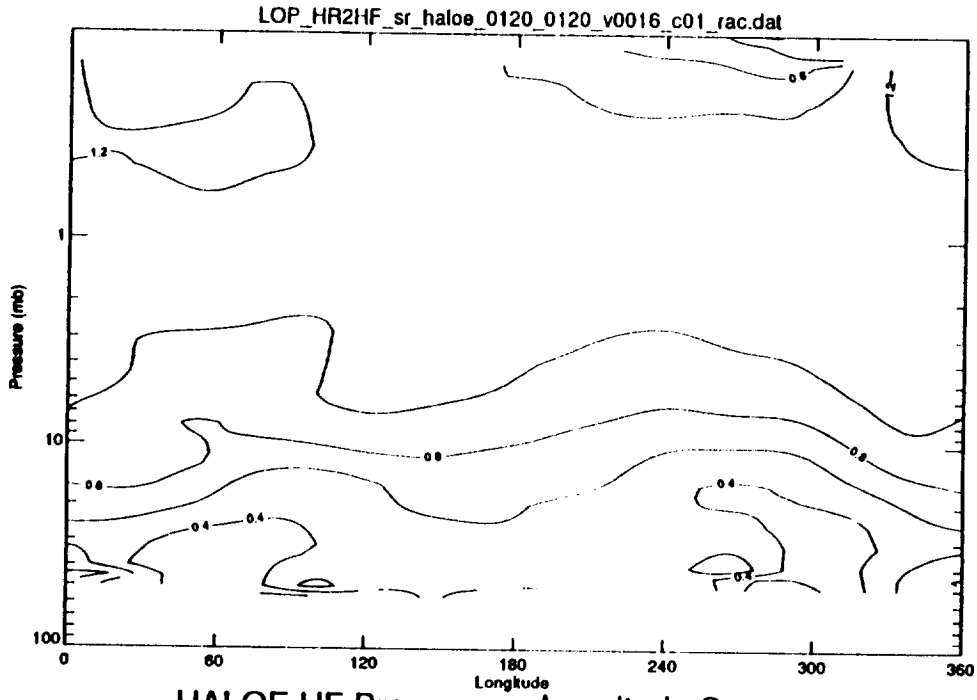

HALOE HF Pressure vs Longitude Cross Section, Sunrise on 09-JAN-1992 at 46 N

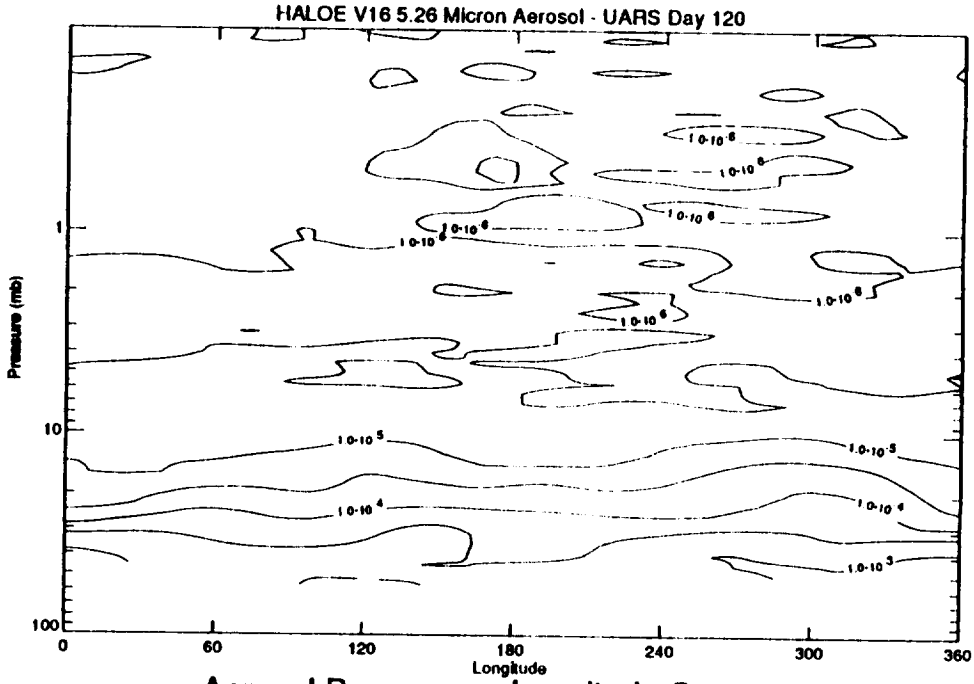

Aerosol Pressure vs Longitude Cross Section, Sunrise on 09-JAN-1992 at 46 N

Figure B-44

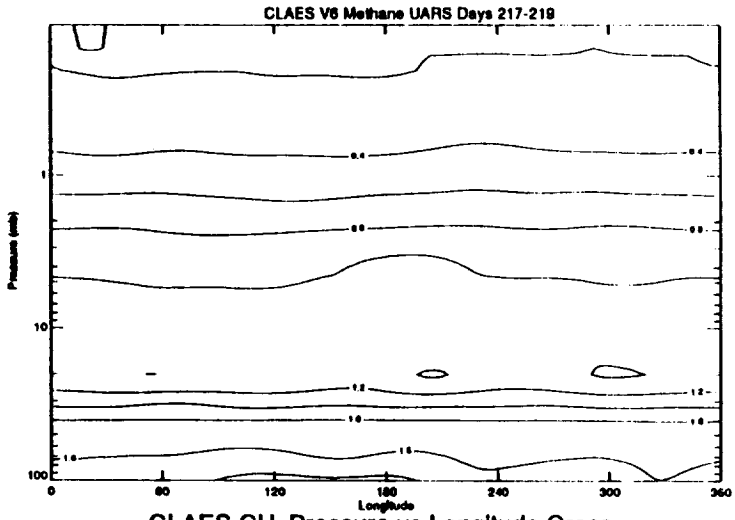

CLAES CH_4 Pressure vs Longitude Cross Section, on 15-APR to 17-APR-1992 at 8 N

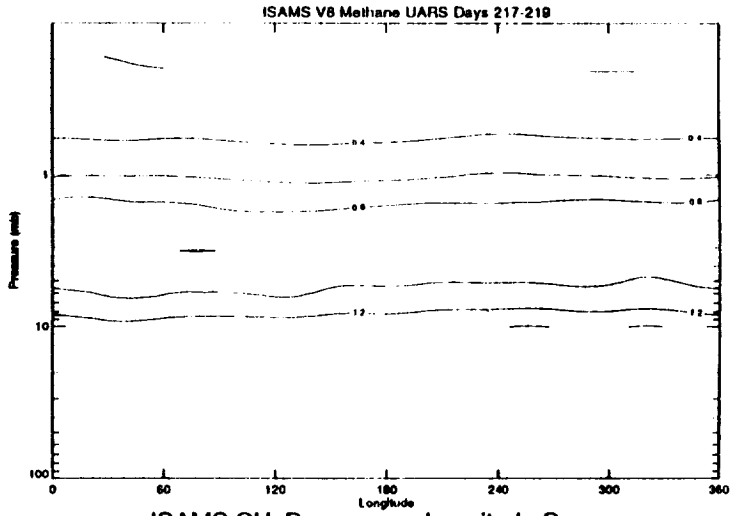

ISAMS CH_4 Pressure vs Longitude Cross Section, on 15-APR to 17-APR-1992 at 8 N

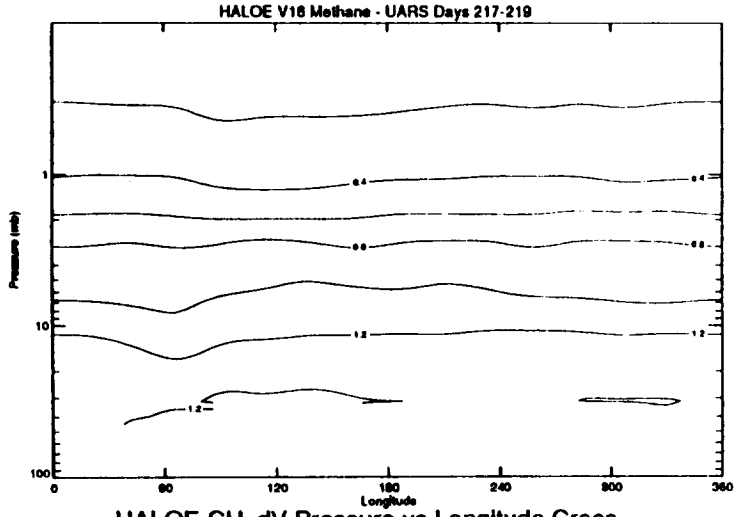

HALOE CH_4 dV Pressure vs Longitude Cross Section, Sunrise on 15-APR to 17-APR-1992 at 5 N

Figure B-45

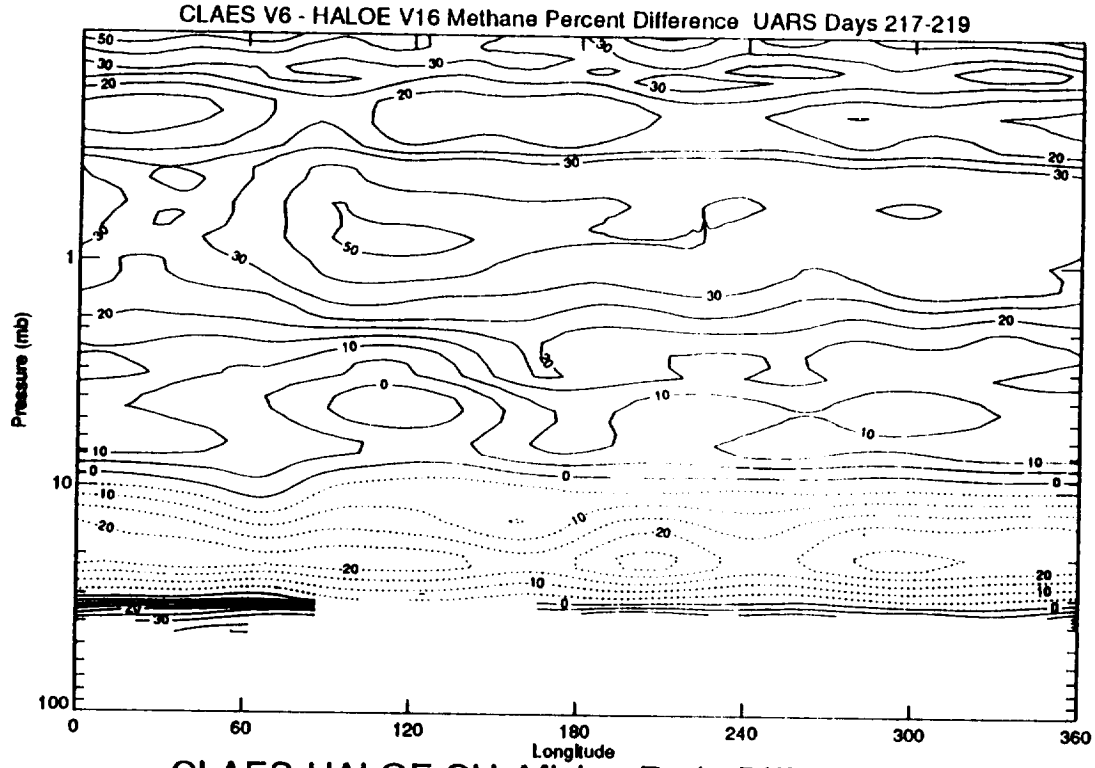

CLAES-HALOE CH_4 Mixing Ratio Difference
on 15-APR-1992 to 17-APR-1992

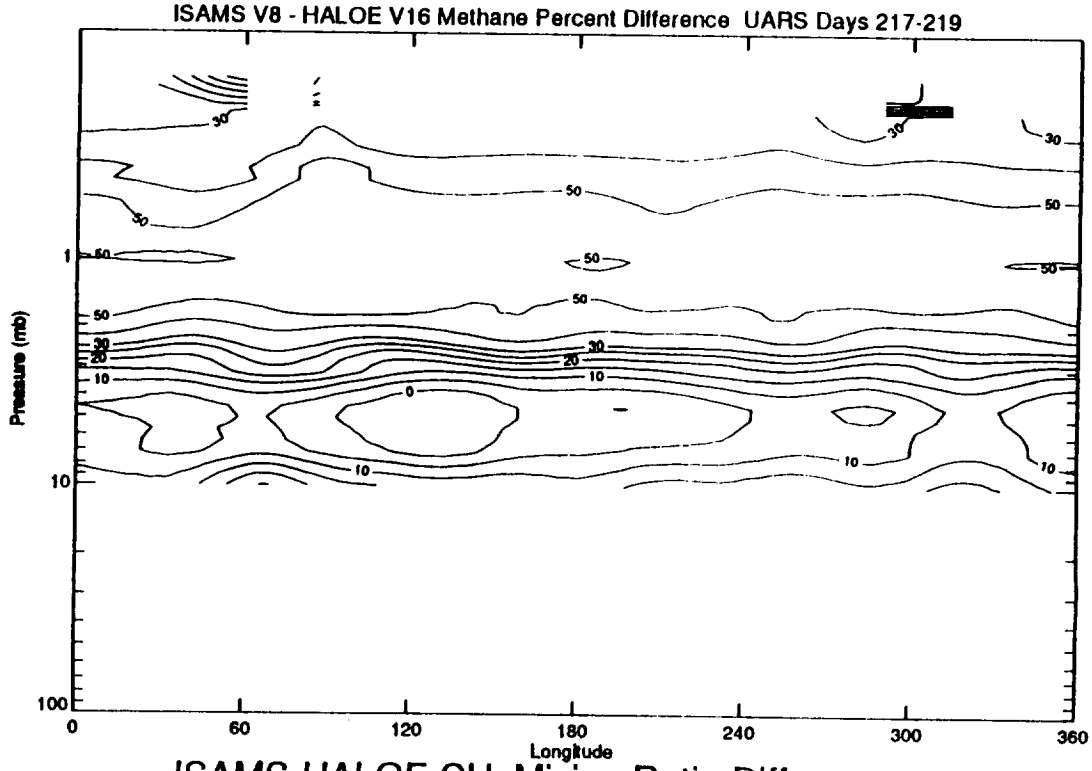

ISAMS-HALOE CH_4 Mixing Ratio Difference
on 15-APR-1992 to 17-APR-1992

Figure B-46

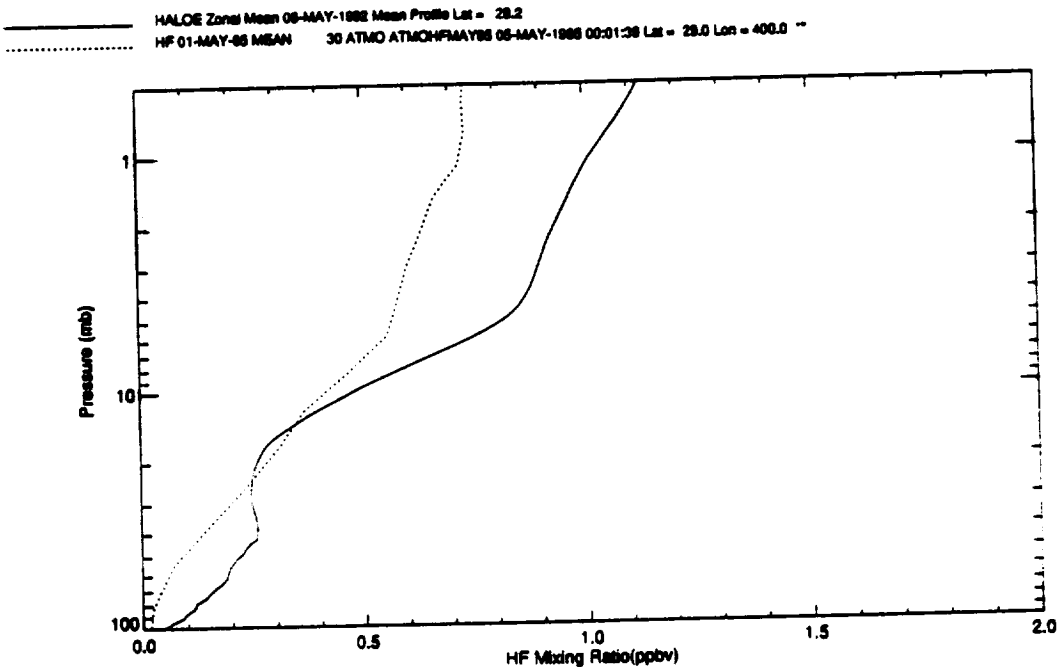

HALOE HF Zonal Mean Mixing Ratio Profiles and ATMOS 1985 Zonal Mean Mixing Ratio

Mon May 23 11:08:18 EDT 1994

Figure B-47

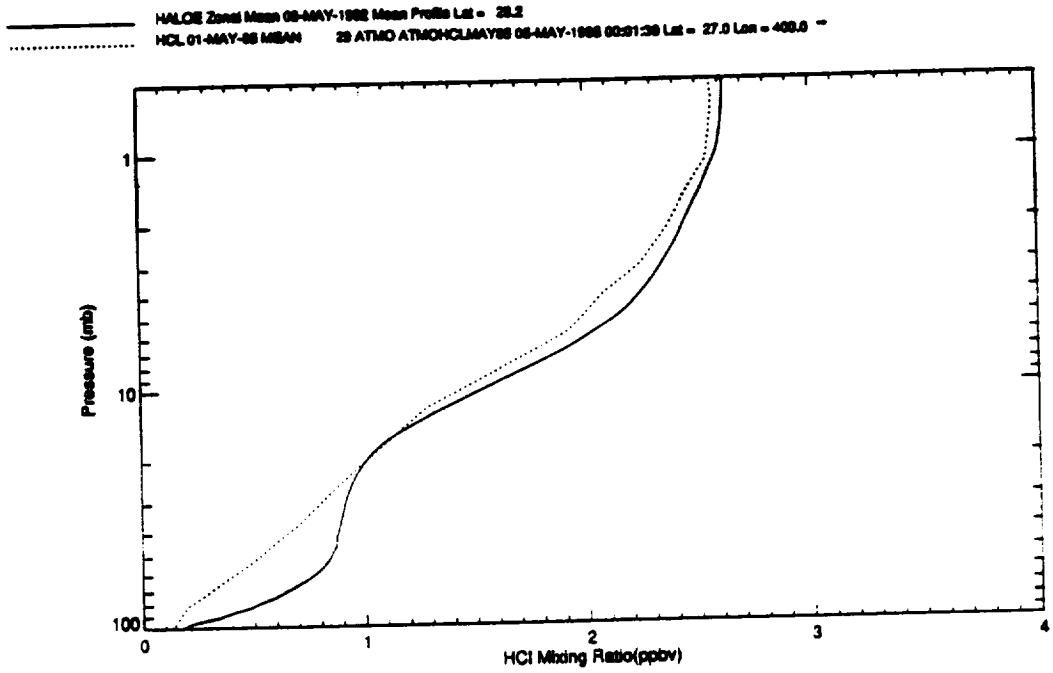

HALOE HCl Zonal Mean Mixing Ratio Profiles and ATMOS 1985 Zonal Mean Mixing Ratio

Mon May 23 11:14:12 EDT 1994

Figure B-48

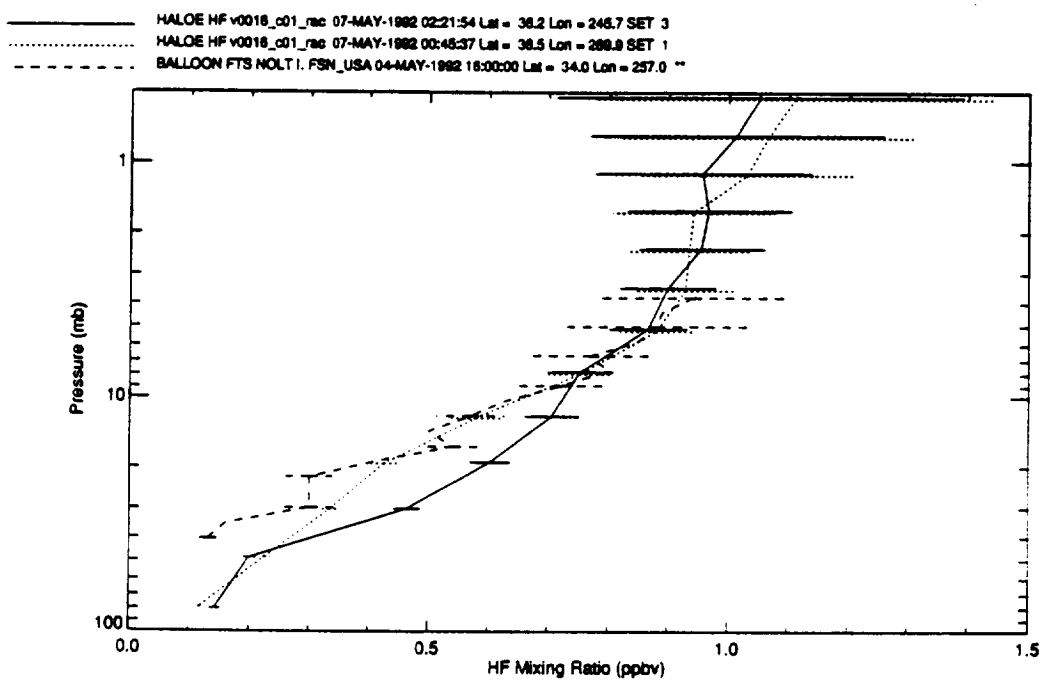

HALOE HF Mixing Ratio 07-MAY-92 and
FIREX HF Mixing Ratio 04-MAY-92

Mon May 23 12:00:03 EDT 1994

Figure B-49

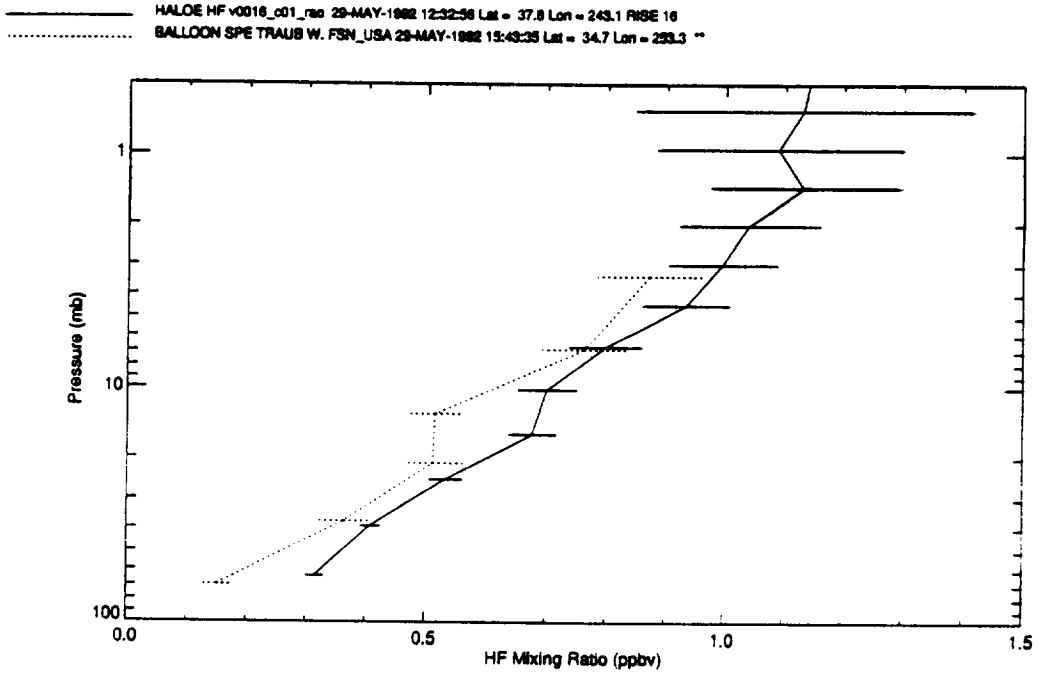

HALOE HF Mixing Ratio 29-MAY-92 and
FIRS-2 HF Mixing Ratio 29-MAY-92

Thu May 5 11:34:11 EDT 1994

Figure B-50

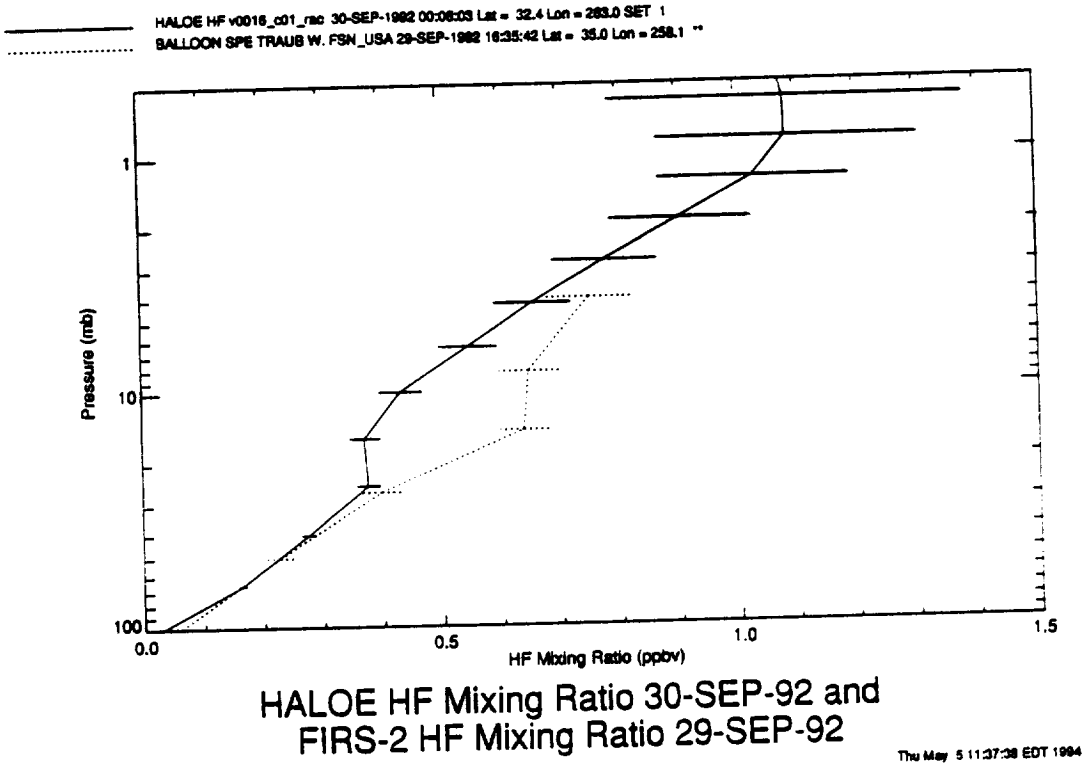

HALOE HF Mixing Ratio 30-SEP-92 and
FIRS-2 HF Mixing Ratio 29-SEP-92

Thu May 5 11:37:38 EDT 1994

Figure B-51

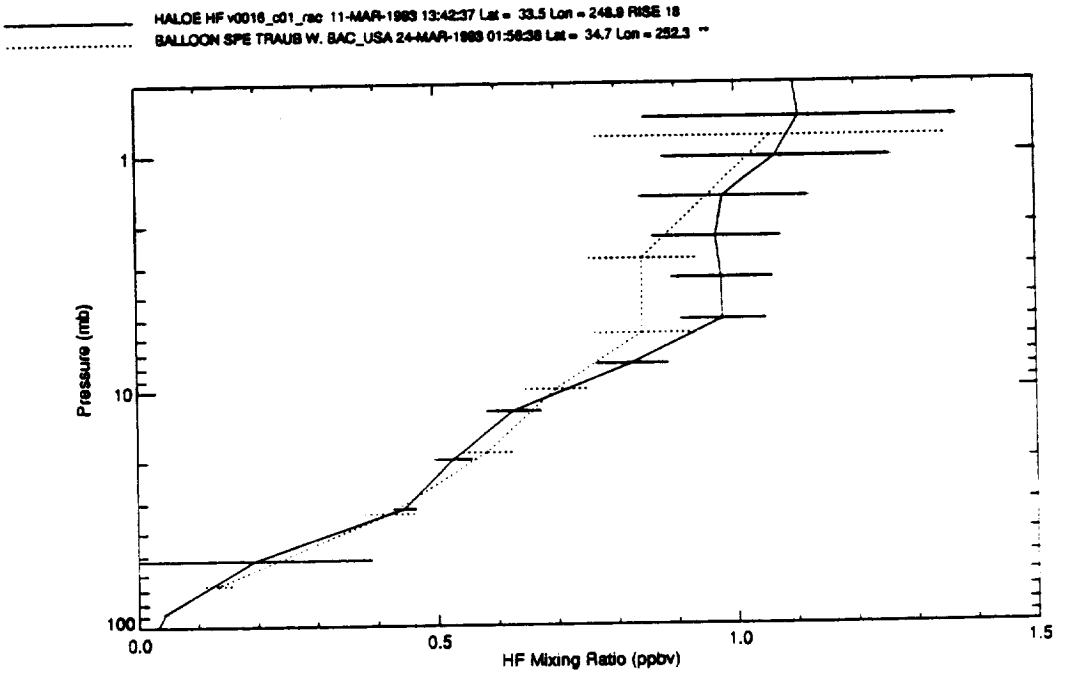

HALOE HF Mixing Ratio 11-MAR-93 and
FIRS-2 HF Mixing Ratio 24-MAR-93

Thu May 5 11:41:18 EDT 1994

Figure B-52

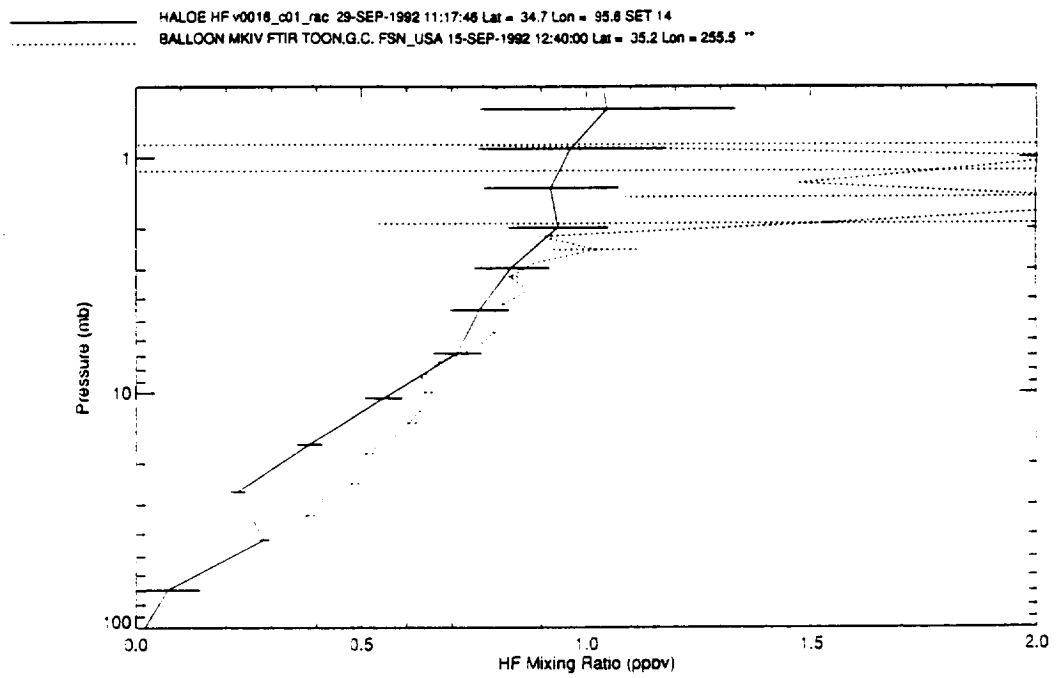

HALOE HF Mixing Ratio 29-SEP-92 and
MKIV FTIR HF Mixing Ratio 15-SEP-92

Fri Apr 15 19:57:09 CUT 1994

Figure B-53

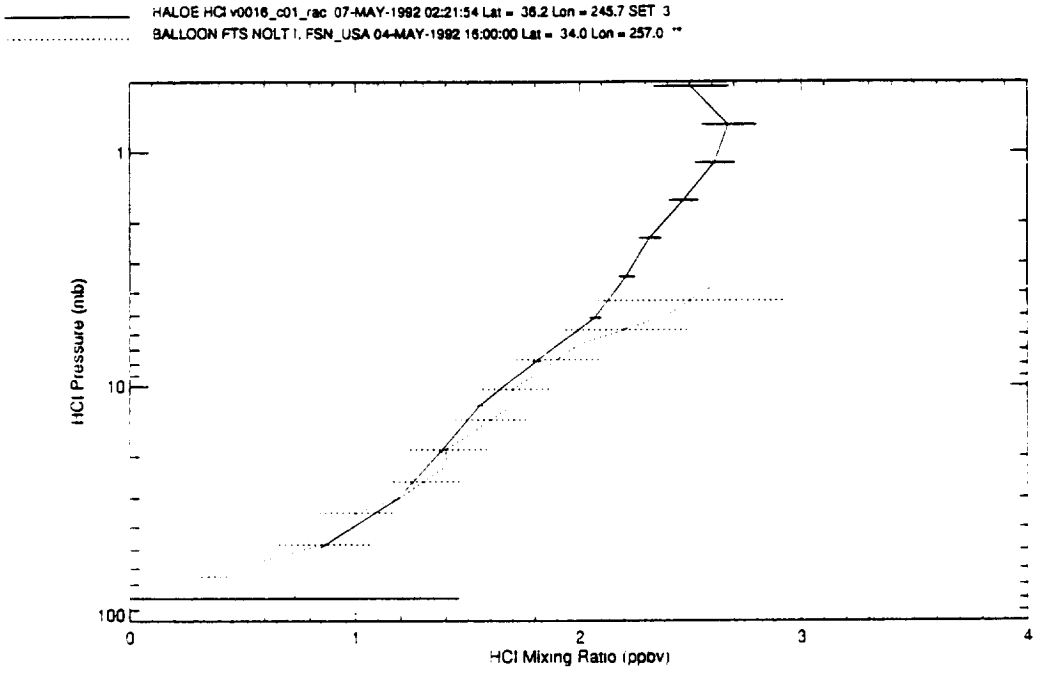

HALOE HCl Mixing Ratio 07-MAY-92 and
FIREX HCl Mixing Ratio 04-MAY-92

Wed May 4 17:41:51 CUT 1994

Figure B-54

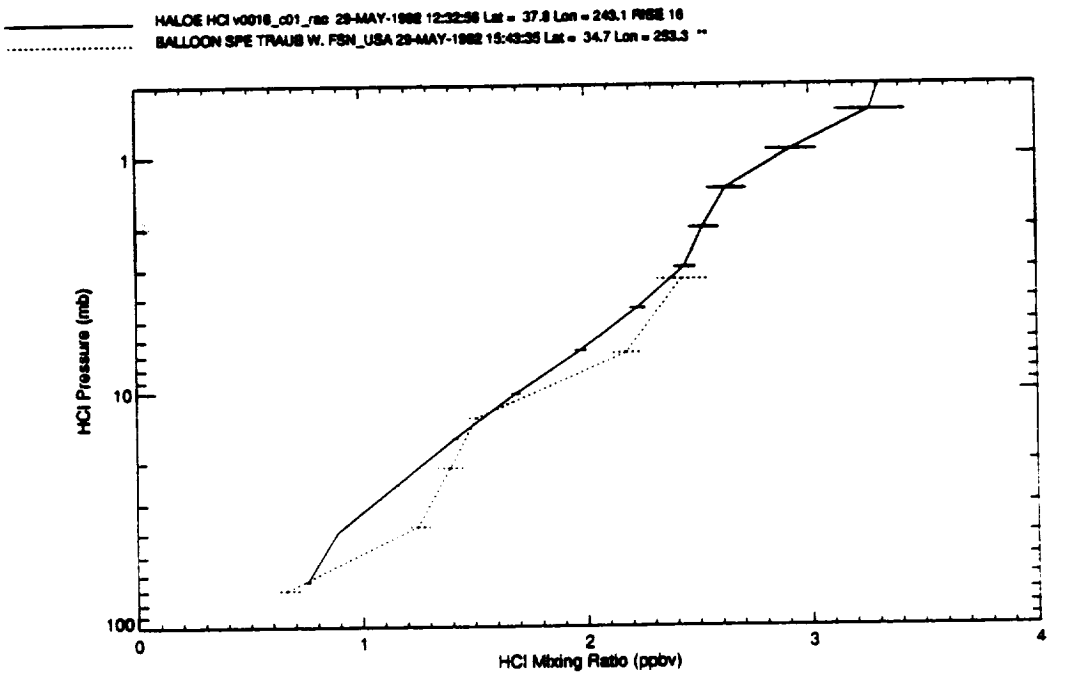

HALOE HCl Mixing Ratio 29-MAY-92 and
FIRS-2 HCl Mixing Ratio 29-MAY-92

Thu May 5 11:31:16 EDT 1994

Figure B-55

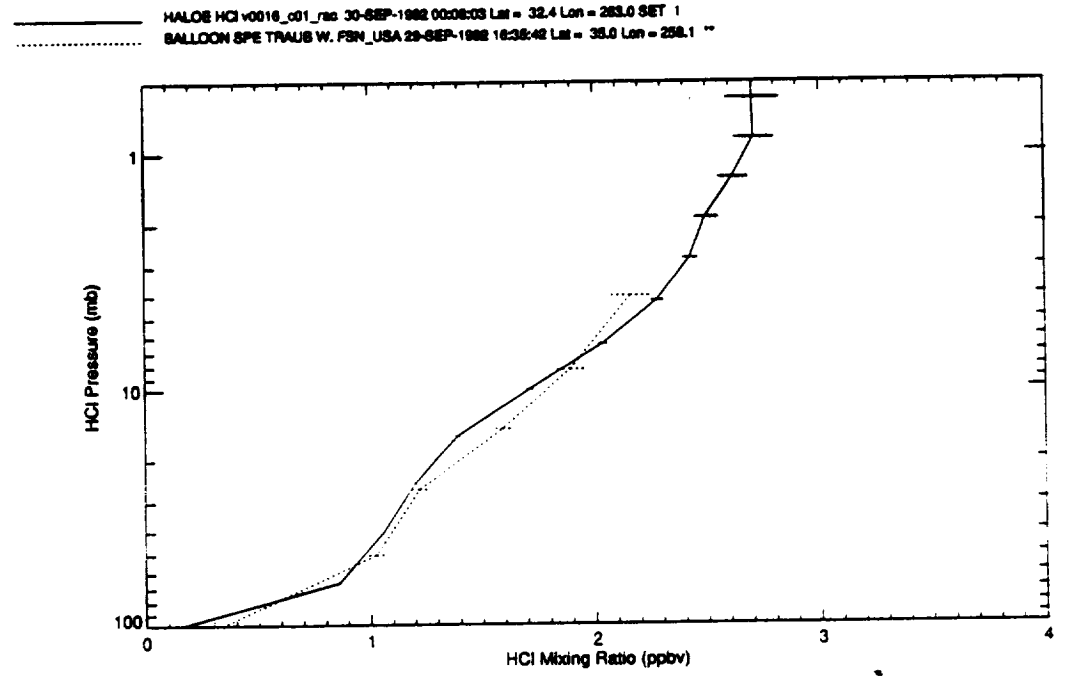

HALOE HCl Mixing Ratio 30-SEP-92 and
FIRS-2 HCl Mixing Ratio 29-SEP-92

Thu May 5 11:36:41 EDT 1994

Figure B-56

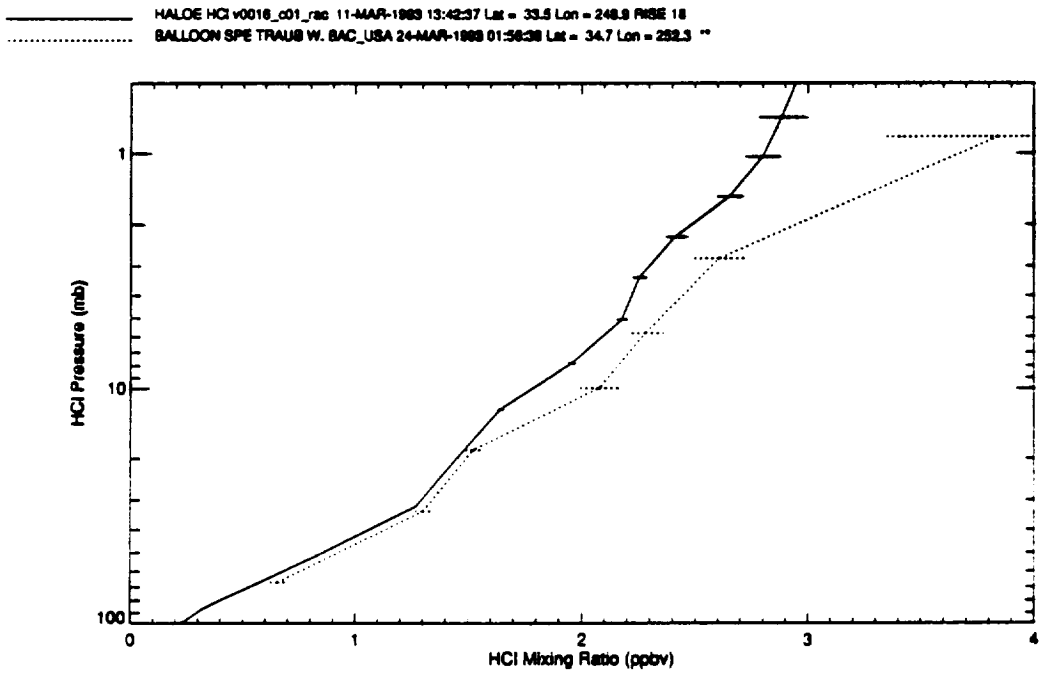

HALOE HCl Mixing Ratio 11-MAR-93 and
FIRS-2 HCl Mixing Ratio 24-MAR-93

Figure B-57

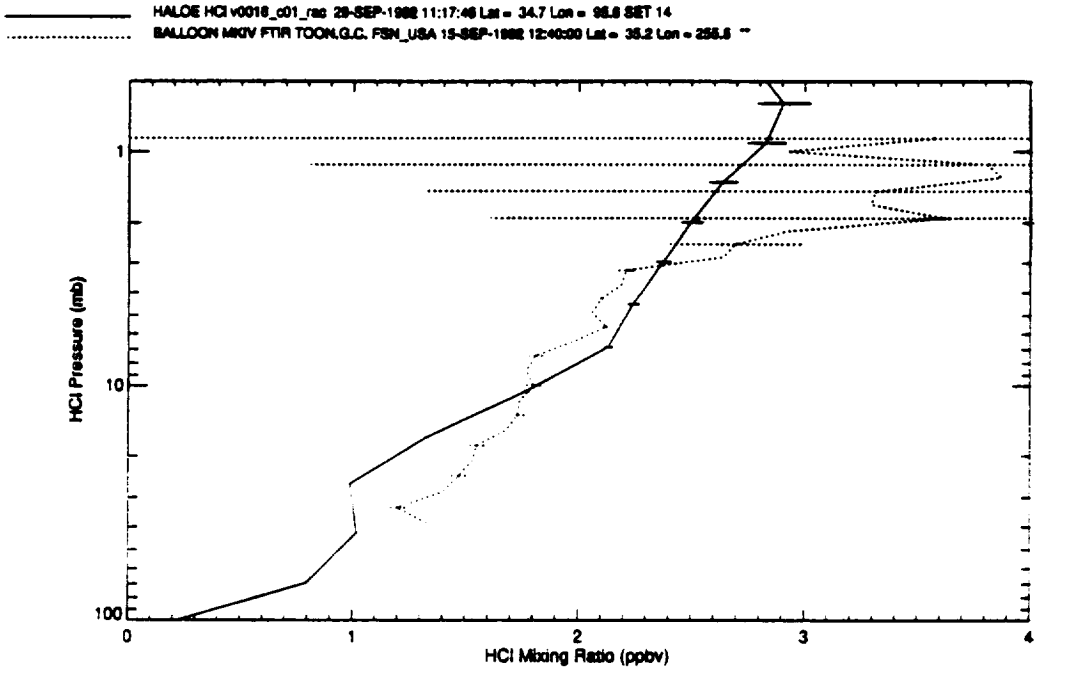

HALOE HCl Mixing Ratio 29-SEP-92 and
MKIV FTIR HCl Mixing Ratio 15-SEP-92

Figure B-58

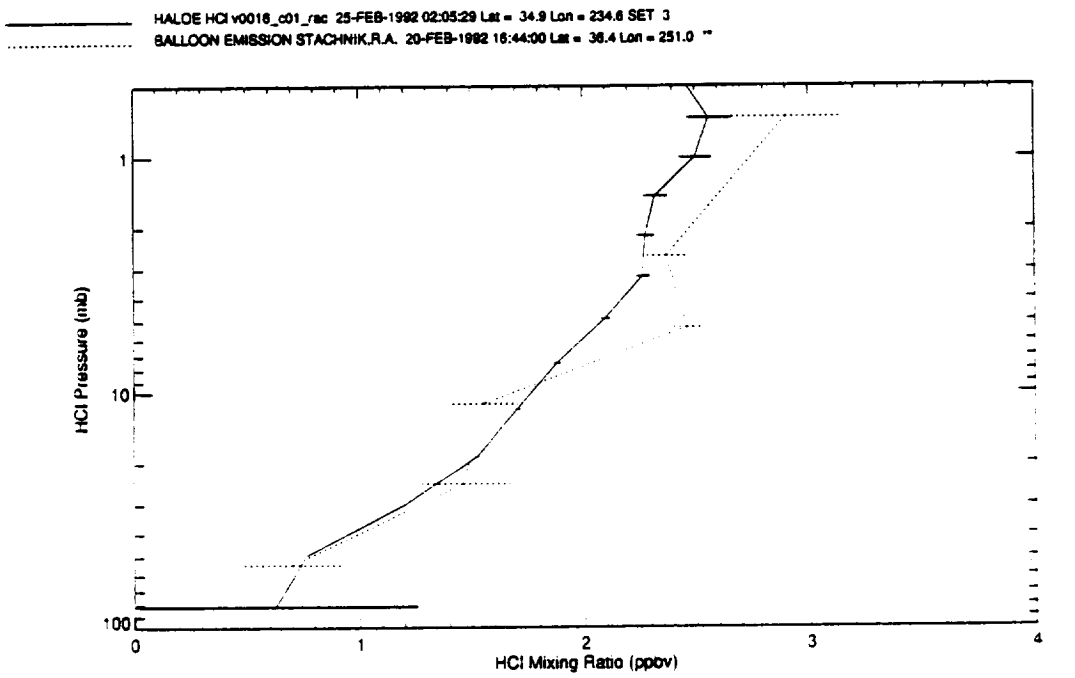

HALOE HCl Mixing Ratio 25-FEB-92 and
SLS HCl Mixing Ratio 20-FEB-92

Thu May 5 11:52:27 EDT 1994

Figure B-59

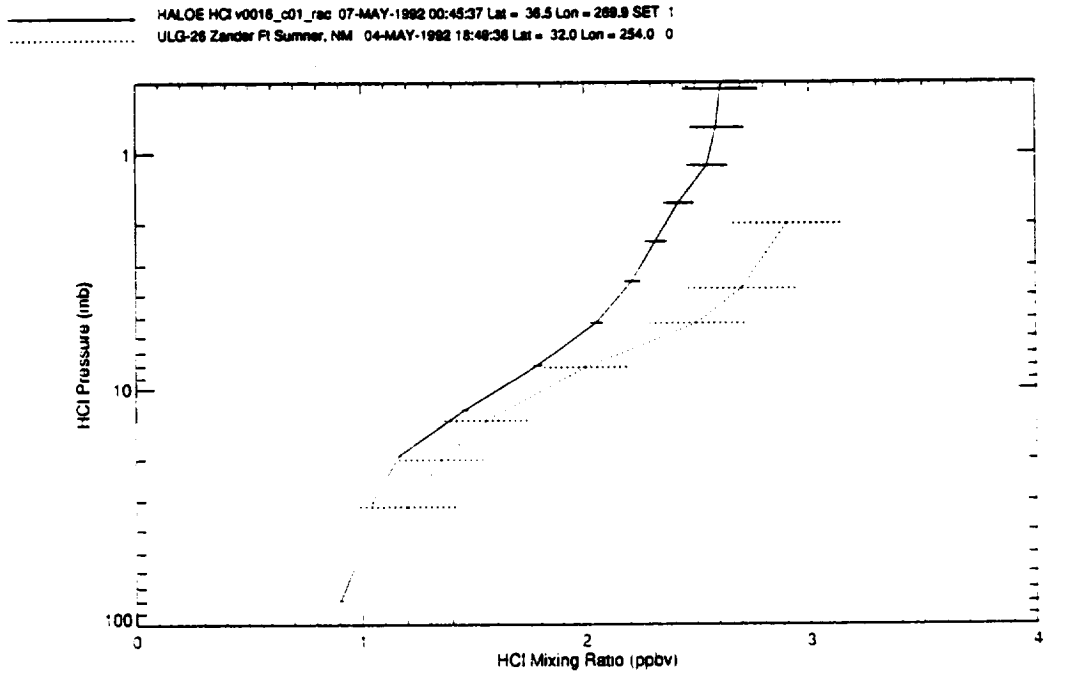

HALOE HCl Mixing Ratio 07-MAY-92 and
ULG-26 HCl Mixing Ratio 04-MAY-92

Tue May 31 10:04:46 EDT 1994

Figure B-60

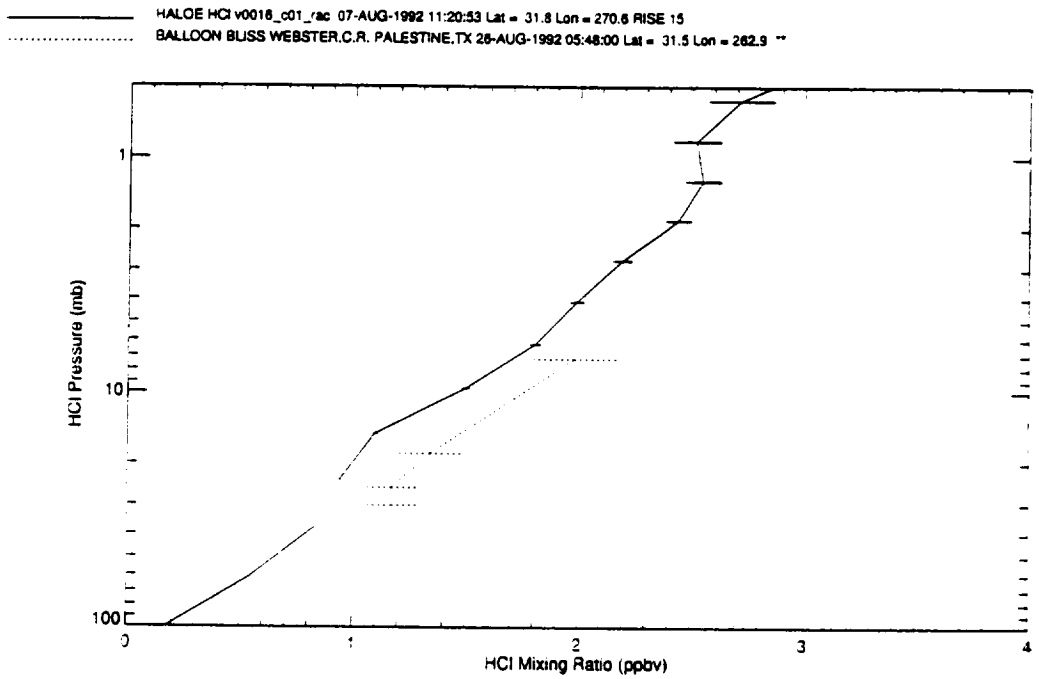

HALOE HCl Mixing Ratio 07-AUG-92 and
BLISS HCl Mixing Ratio 26-AUG-92

Wed May 4 17:44:19 CUT 1994

Figure B-61

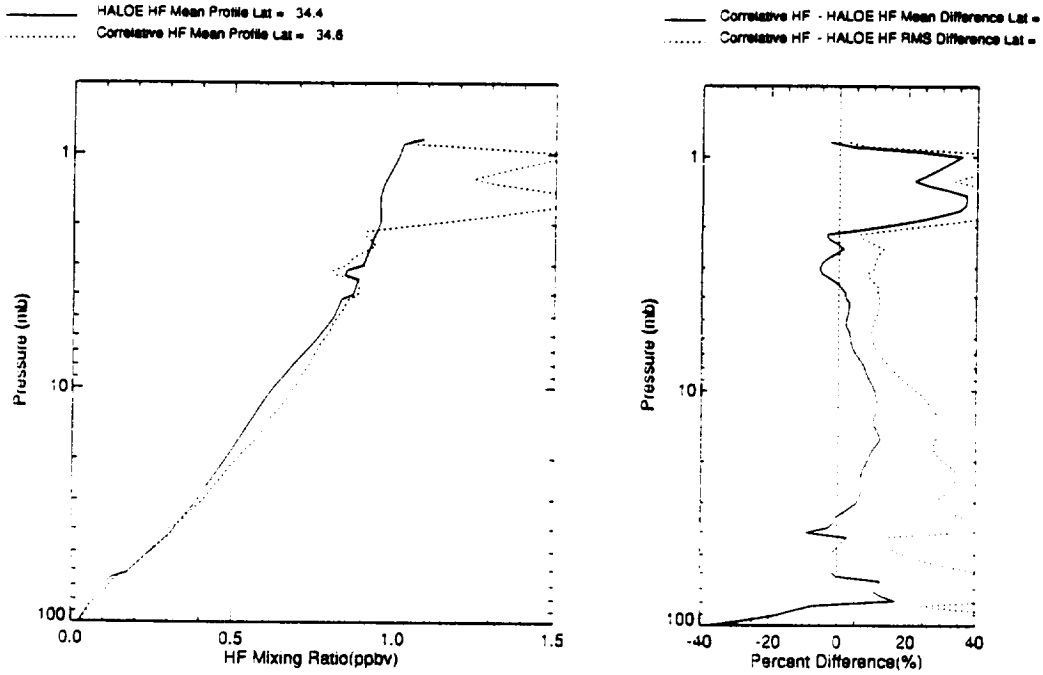

Version 16 HALOE HF Statistics from
7 Correlative Measurements

Wed May 25 08:45:32 EDT 1994

Figure B-62

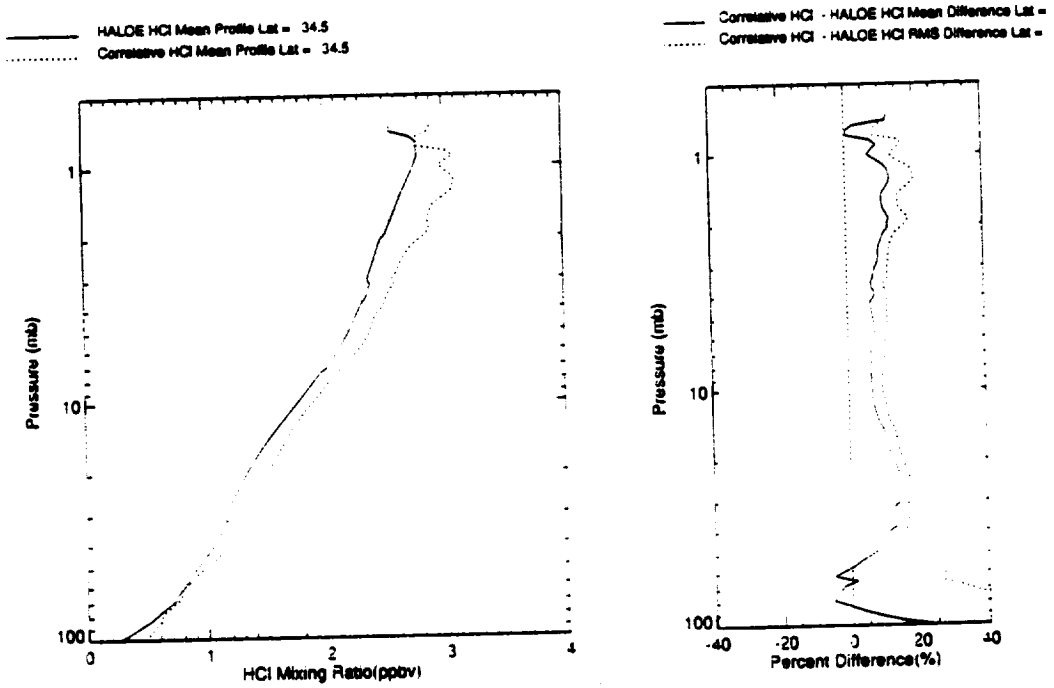

Figure B-63

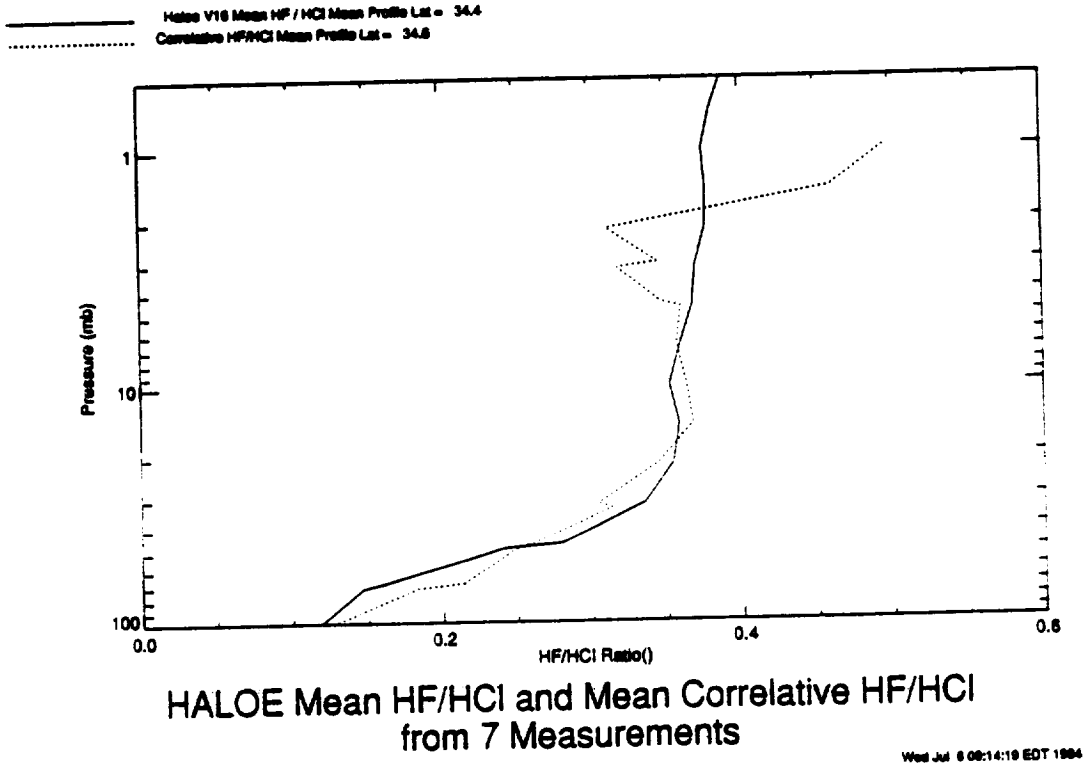

Figure B-64

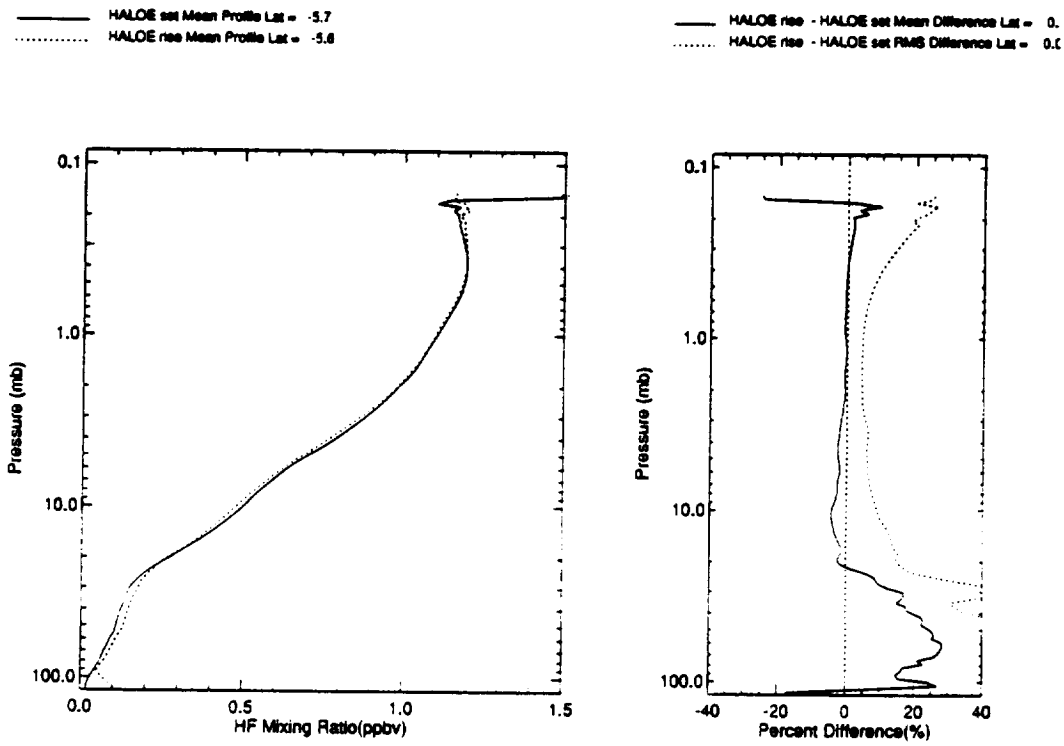

HALOE rise - HALOE set HF Differences
v16 for 19-NOV-1991 to 24-JUL-1993 near 5 S using 35 profiles

Sun Apr 24 14:21:23 CUT 1994

Figure B-65

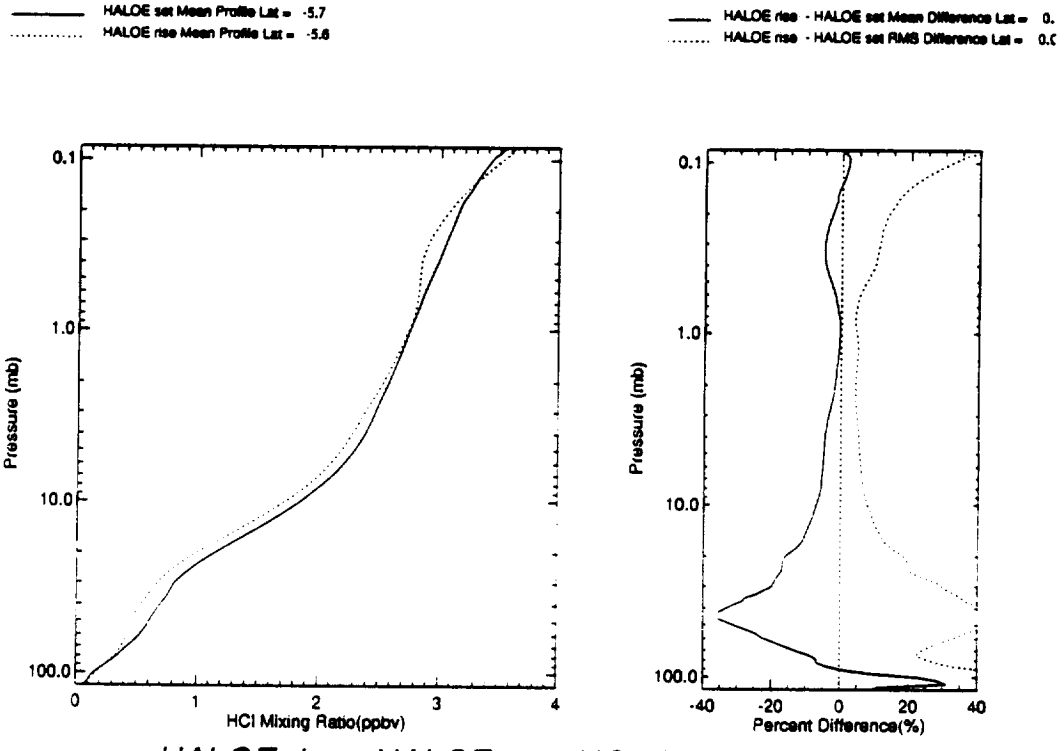

HALOE rise - HALOE set HCl Differences
v16 for 19-NOV-1991 to 24-JUL-1993 near 5 S using 35 profiles

Sun Apr 24 14:20:38 CUT 1994

Figure B-66

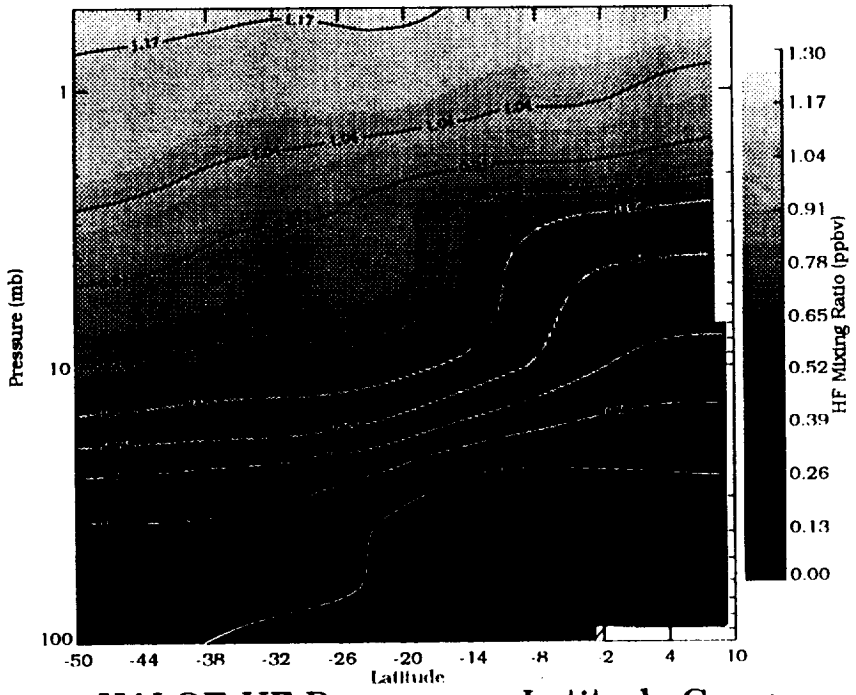

HALOE HF Pressure vs Latitude Cross Section, Sunset on 18-AUG to 29-AUG-1992

Figure B-67

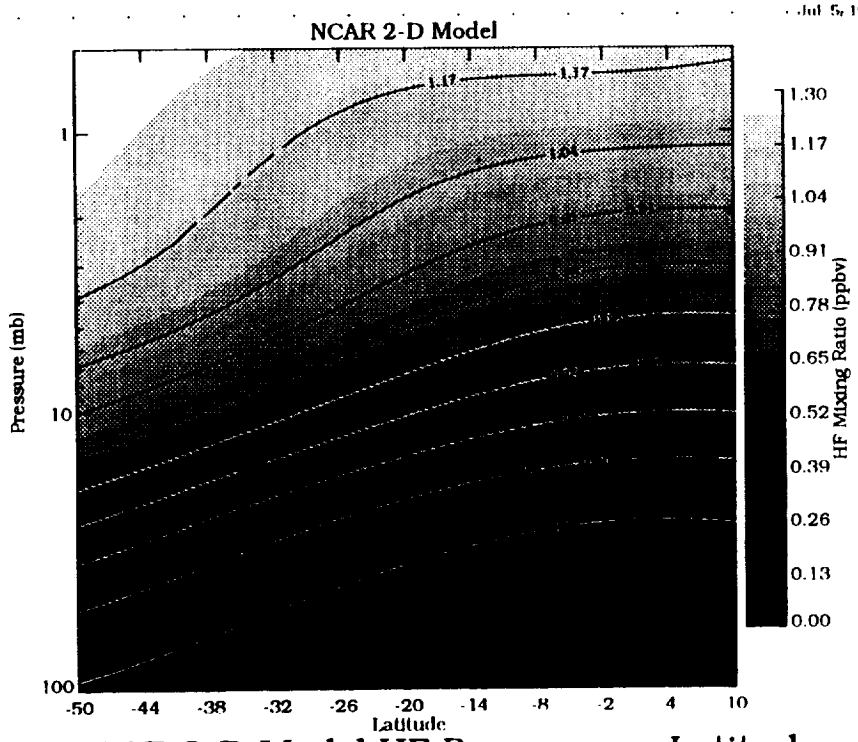

NCAR 2-D Model HF Pressure vs. Latitude Cross Section for August 15

Figure B-68

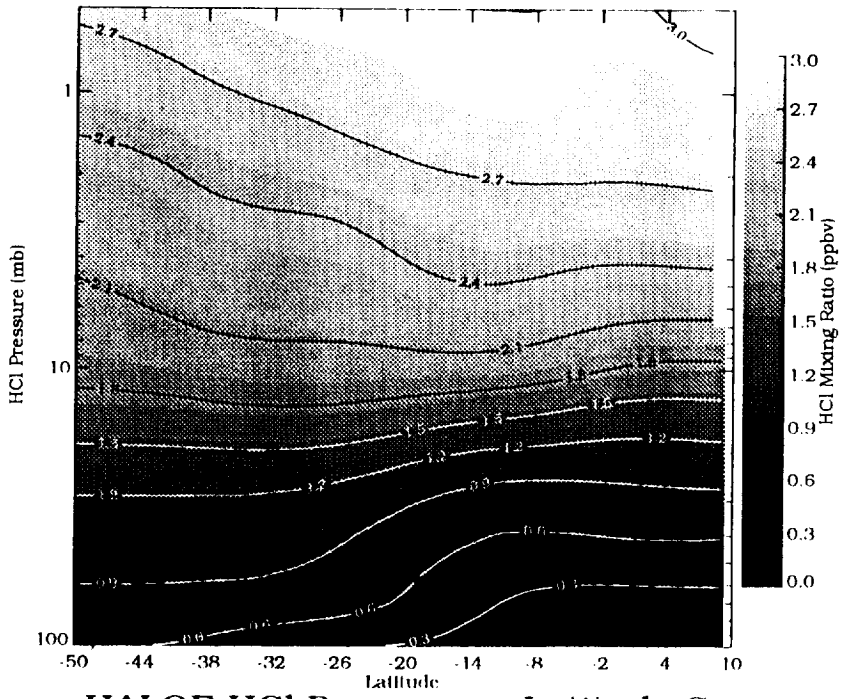

HALOE HCl Pressure vs Latitude Cross Section, Sunset on 18-AUG to 29-AUG-1992

Figure B-69

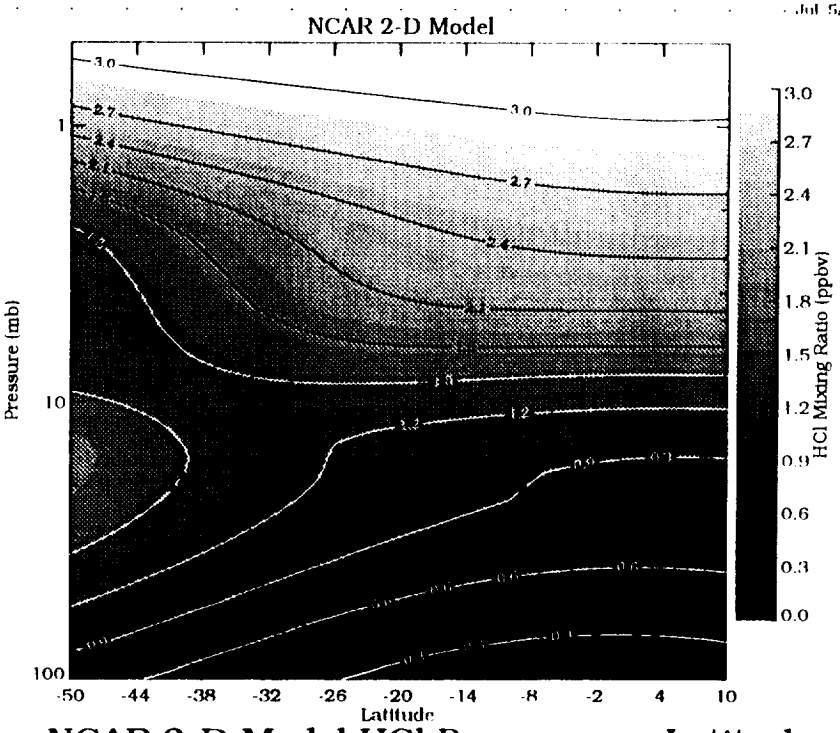

NCAR 2-D Model HCl Pressure vs. Latitude Cross Section for August 15

Figure B-70

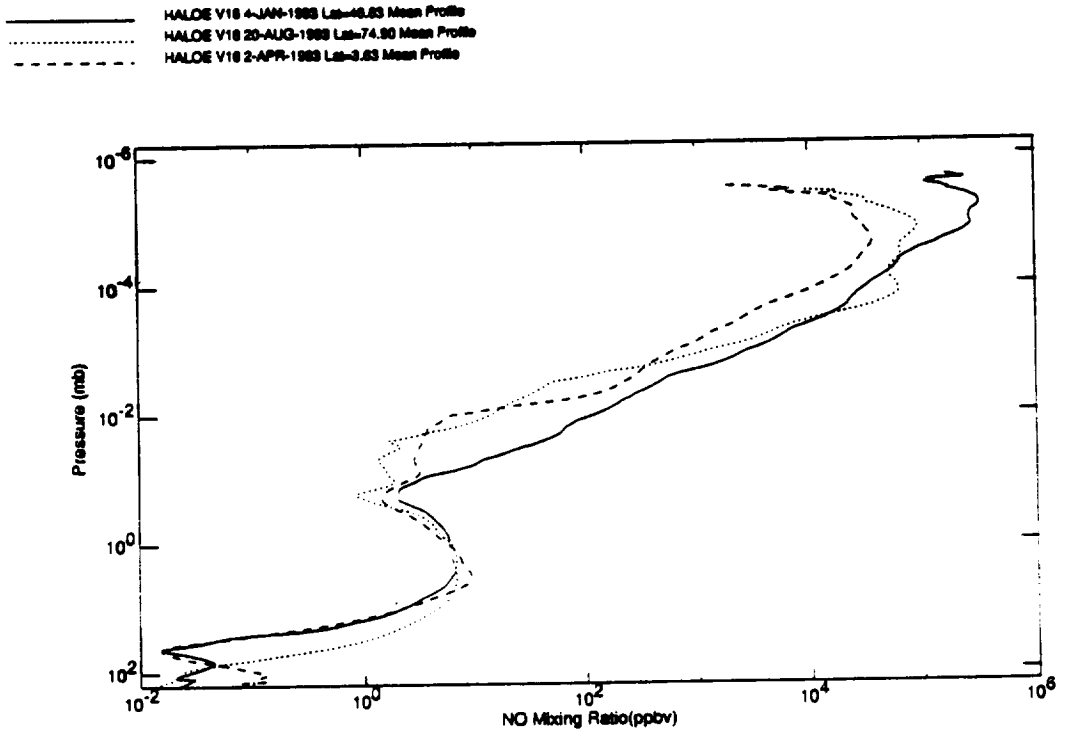

HALOE NO Mixing Ratio, High Latitude Winter,
High Latitude Summer, and Low Latitude Spring, 1993

Figure B-71

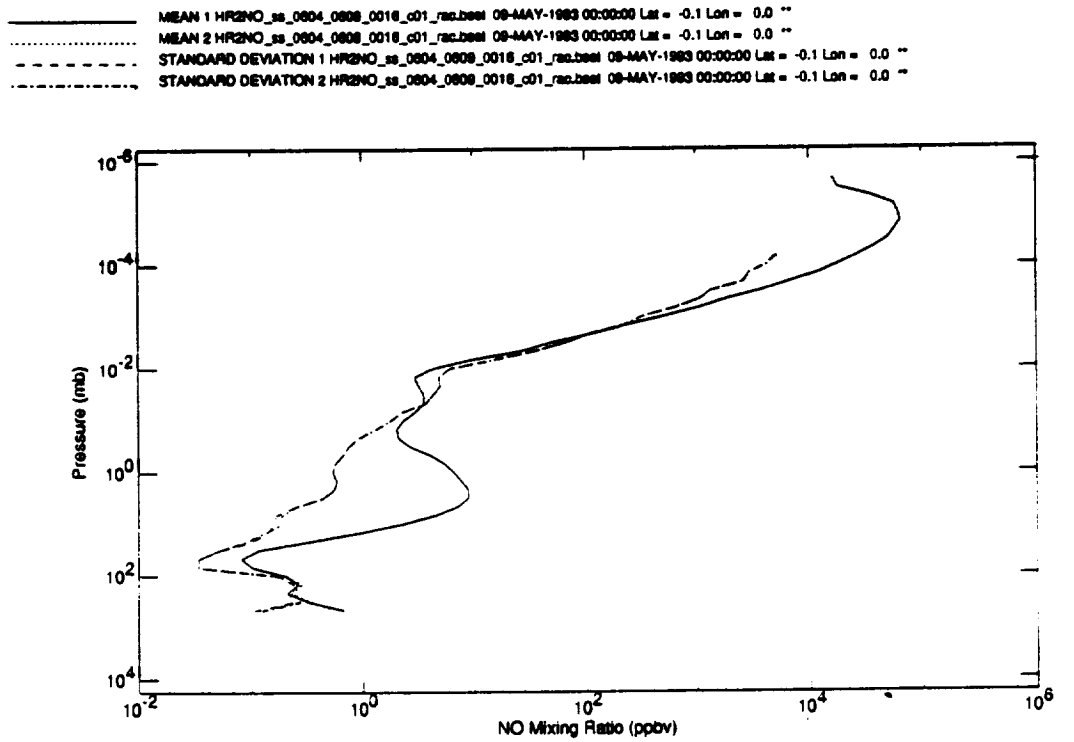

HALOE NO Mean and Instrument Noise Standard Deviation
07-MAY-1993 to 12-MAY-1993 14N to 14S - 89 Profiles

Figure B-72

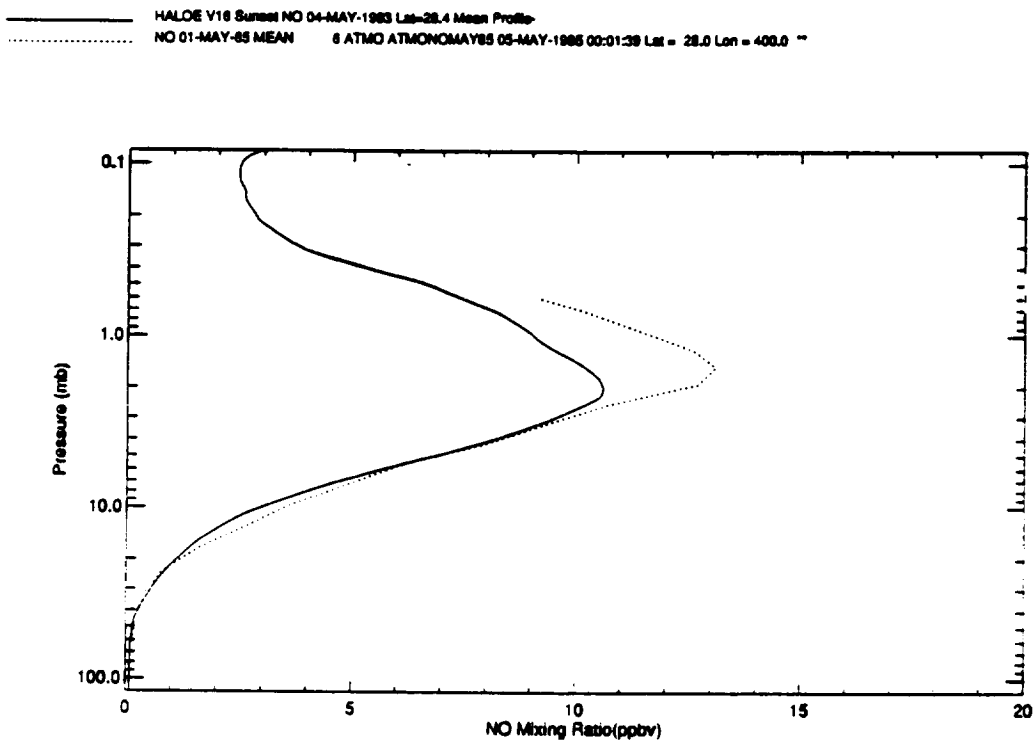

HALOE V16 04-MAY-1993 and ATMOS 01-MAY-1985
Sunset NO Mixing Ratio near 28N

Mon Jun 20 17:42:49 EDT 1994

Figure B-73

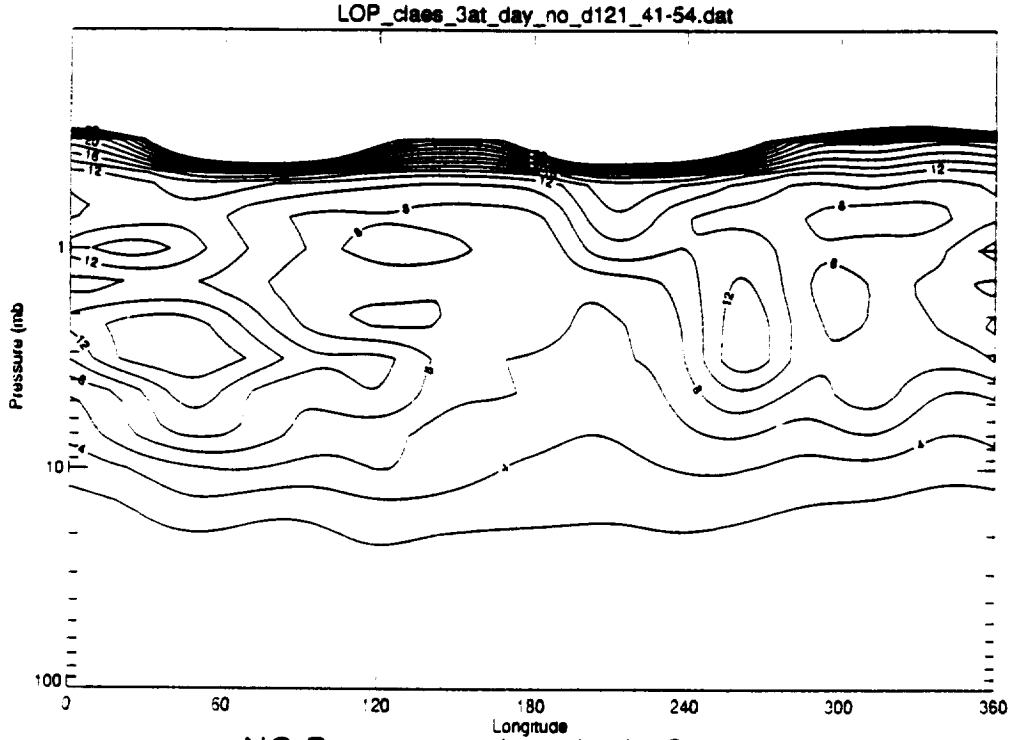

NO Pressure vs Longitude Cross
Section. on 10-JAN-1992 at 47 N

Figure B-74

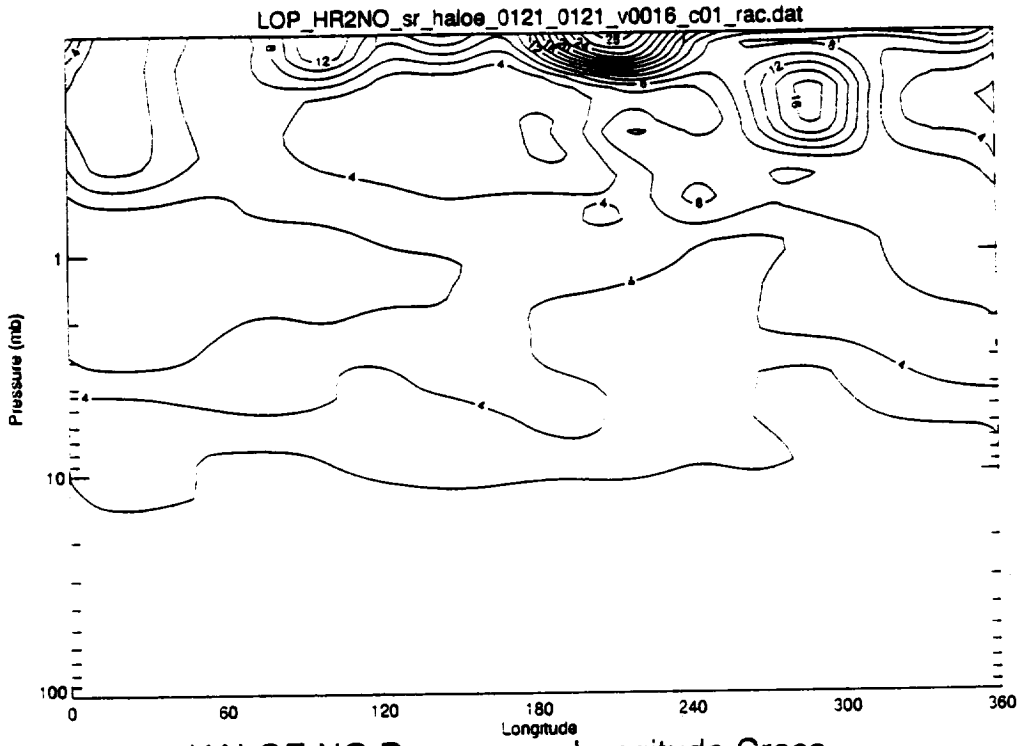

HALOE NO Pressure vs Longitude Cross Section. Sunrise on 10-JAN-1992 at 47 N

Figure B-75

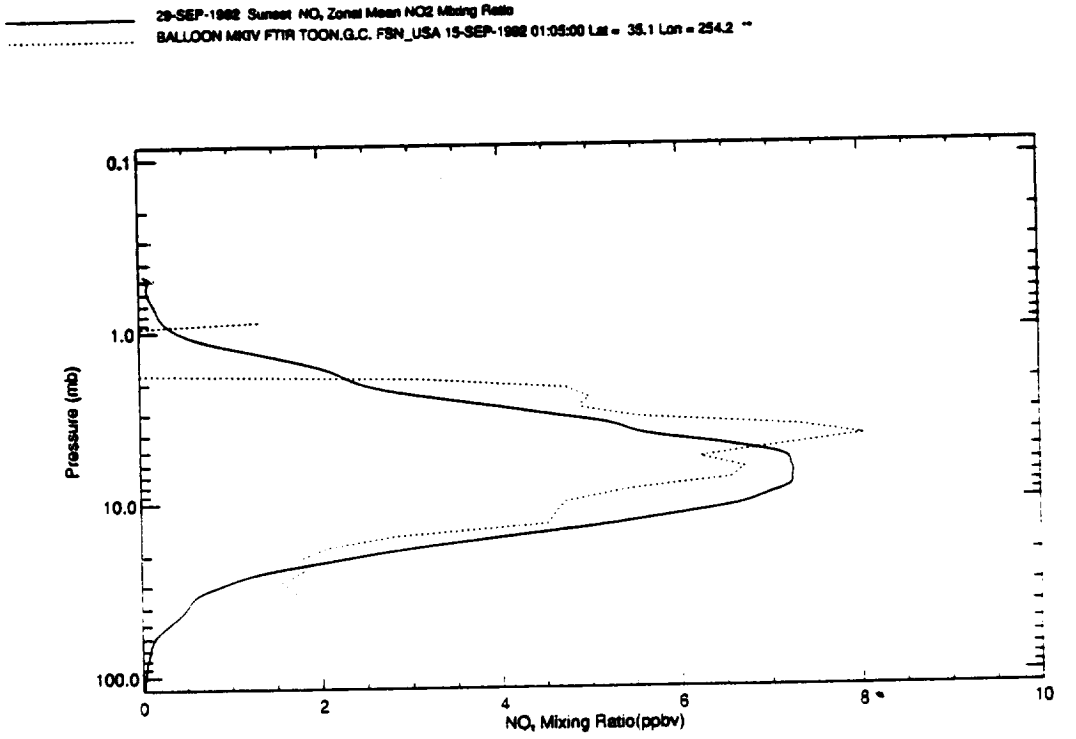

HALOE V16 on 29-SEP-1992 and Toon Balloon on 14,15-SEP-1992 NO_2 Mixing Ratio near 35N

Figure B-76

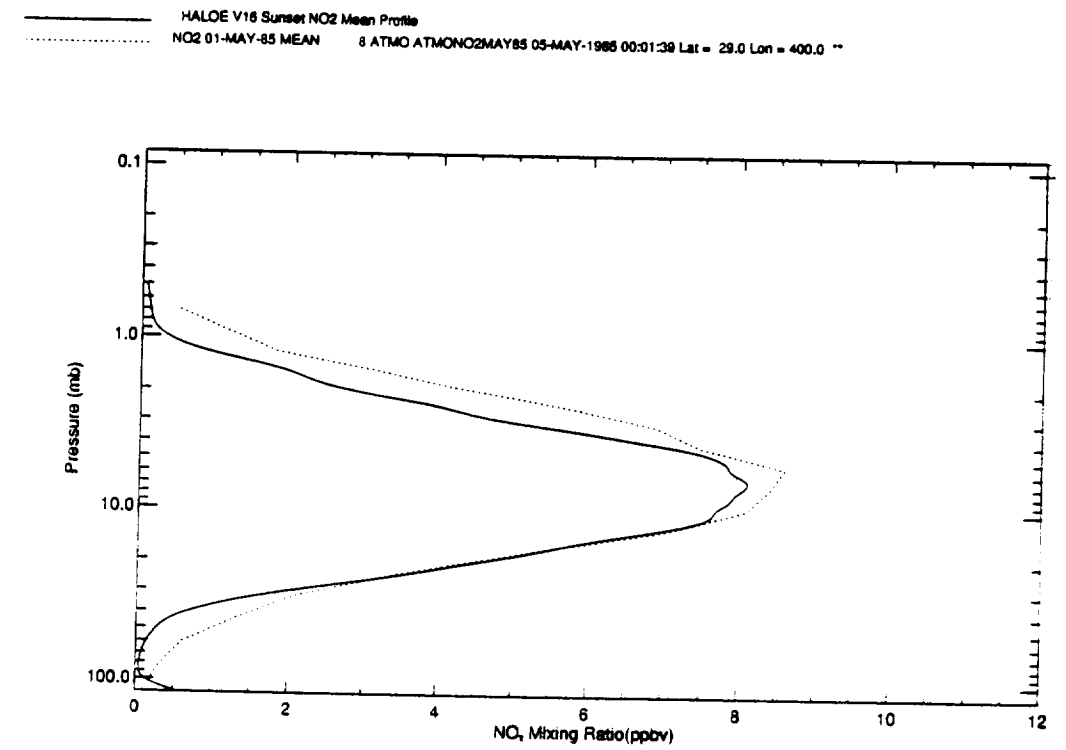

HALOE V16 04-MAY-1993 and ATMOS 01-MAY-1985
Sunset NO_2 Mixing Ratio near 28N

Tue Jun 21 08:27:11 EDT 1994

Figure B-77

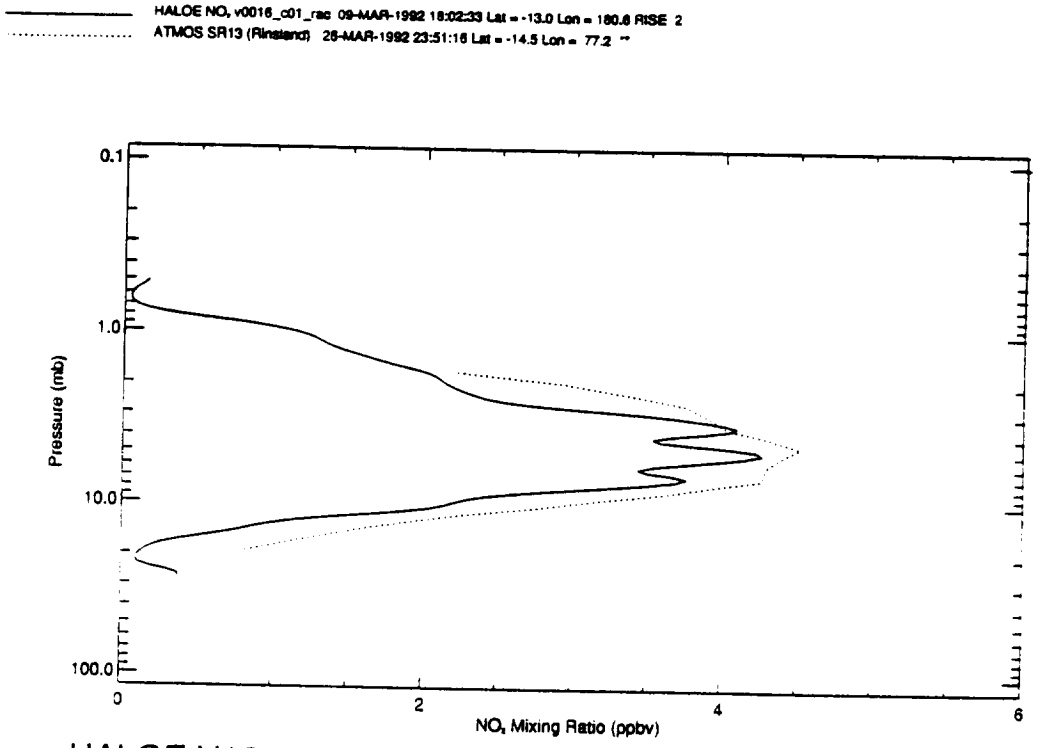

HALOE V16 on 09-MAR-1992 and ATMOS on 26-MAR-1992
NO_2 Mixing Ratio near 14S

Tue Jul 12 11:42:45 EDT 1994

Figure B-78

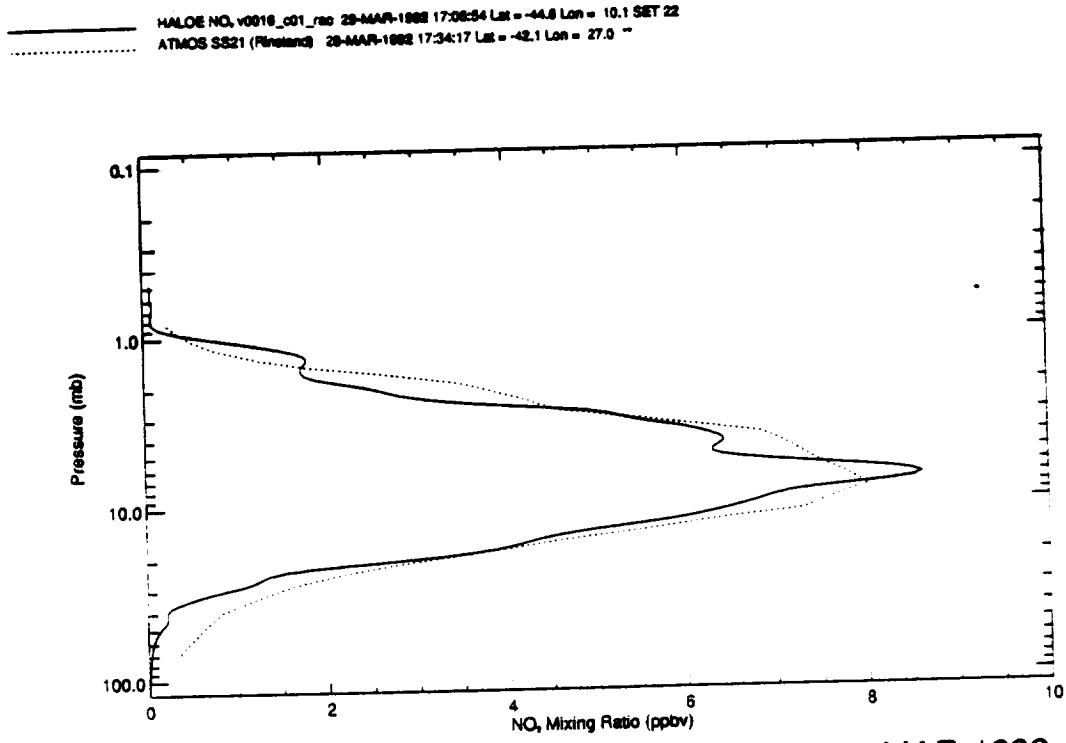

HALOE V16 on 29-MAR-1992 and ATMOS on 28-MAR-1992
NO_2 Mixing Ratio near 43S

Tue Jul 12 11:48:41 EDT 1994

Figure B-79

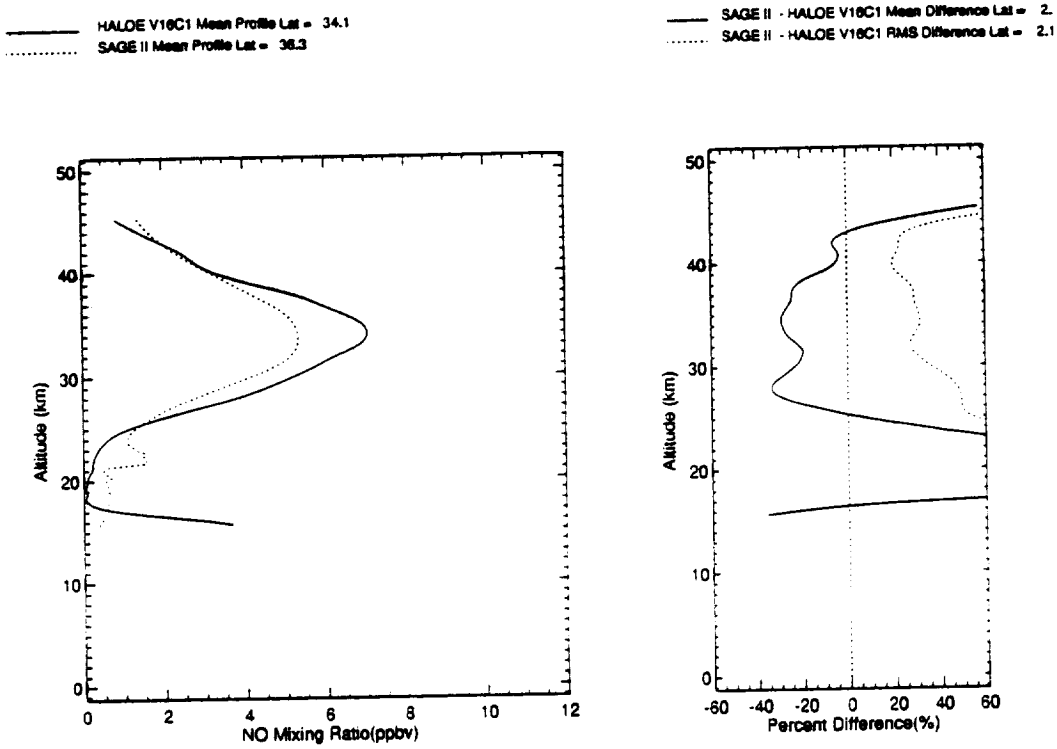

HALOE on 23-25NOV91 and SAGE II on 22-24NOV91
Sunset NO_2 near 34N

Tue Jul 12 07:44:58 EDT 1994

Figure B-80

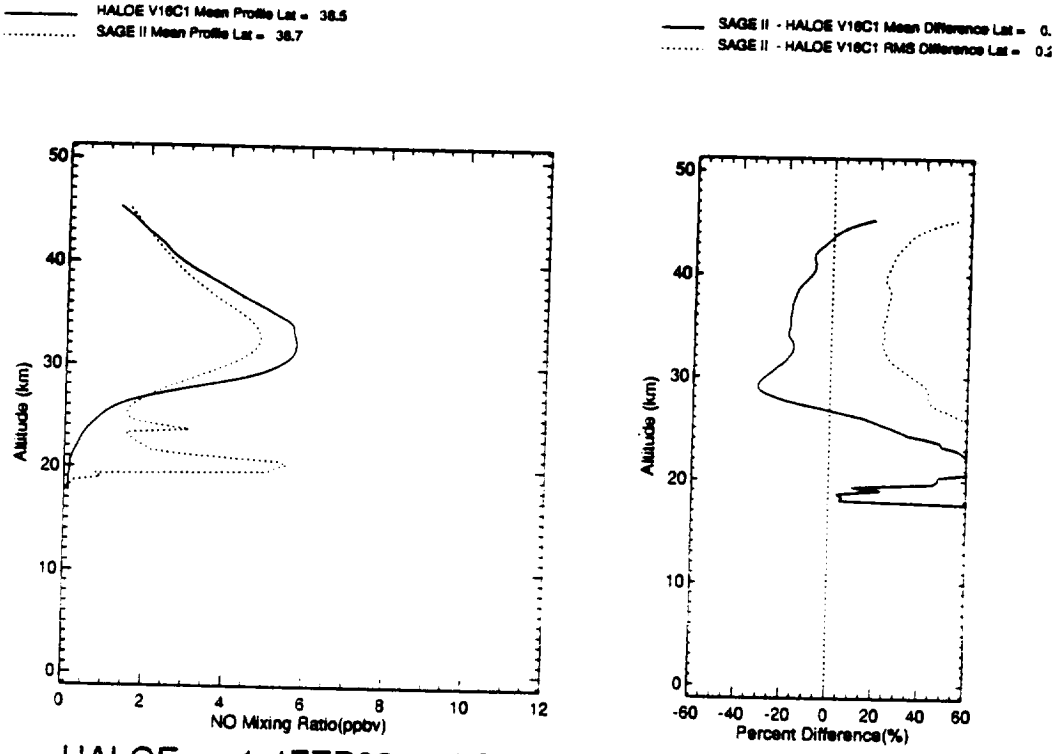

HALOE on 1-4FEB92 and SAGE II on 30JAN-4FEB92
Sunset NO_2 near 36N

Mon Jul 11 15:00:13 EDT 1994

Figure B-81

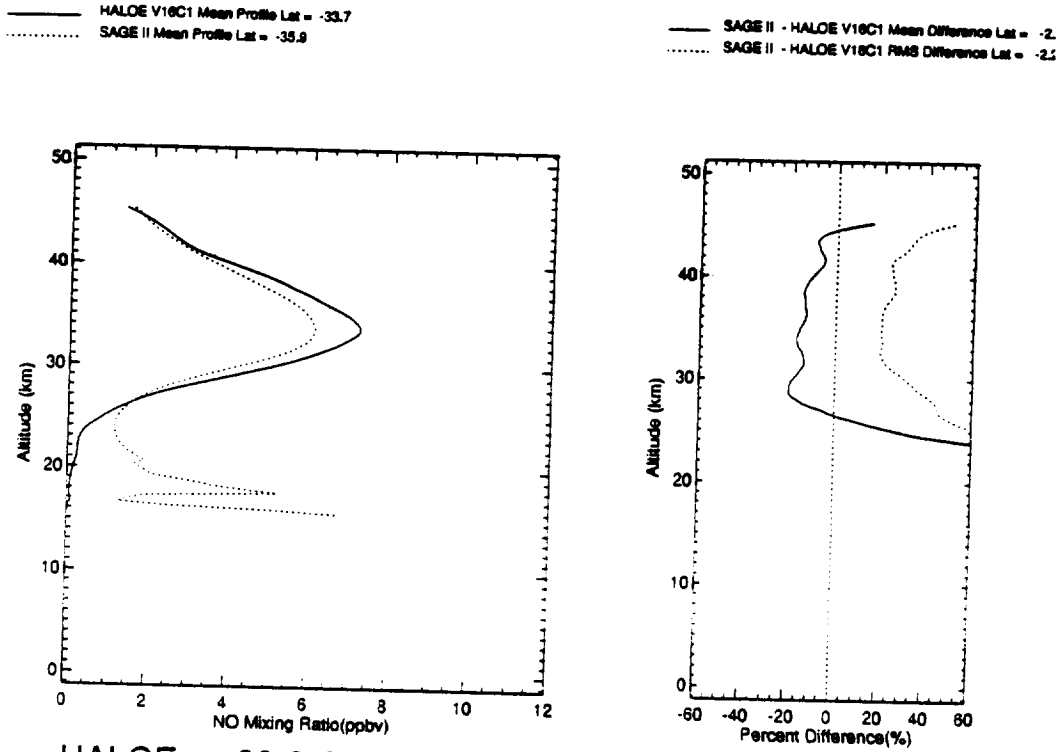

HALOE on 20-24MAY92 and SAGE II on 19-23MAY92
Sunset NO_2 near 35S

Mon Jul 11 13:34:28 EDT 1994

Figure B-82

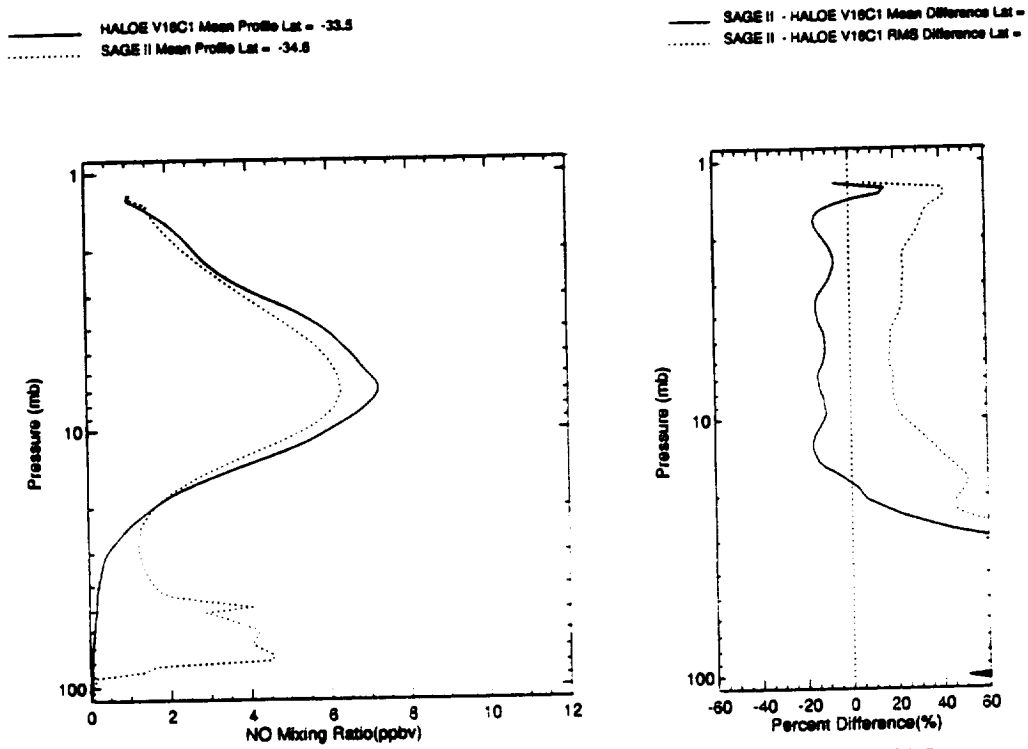

HALOE on 20-24MAY92 and SAGE II on 19-23MAY92
Sunset NO_2 near 36S - 1 day difference

Tue Jul 12 08:52:28 EDT 1994

Figure B-83

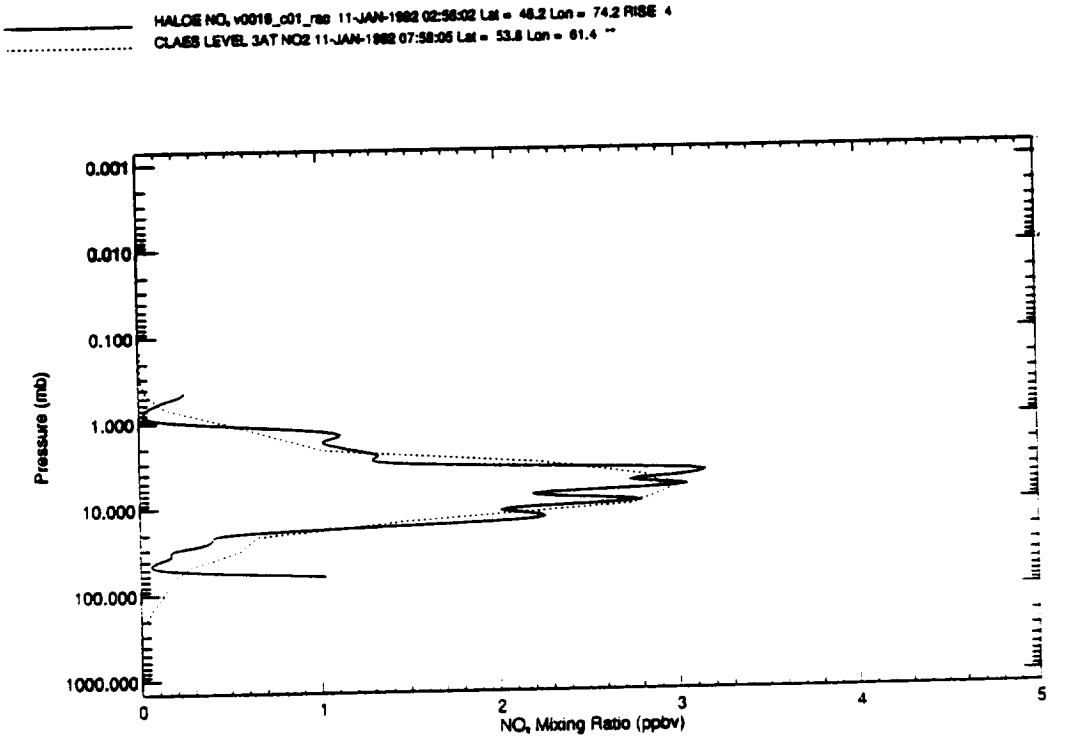

HALOE Sunrise and CLAES (SZA:75-105) NO_2 Mixing Ratio
on 11 January 1992 near 50N

Mon Jul 18 13:40:33 EDT 1994

Figure B-84

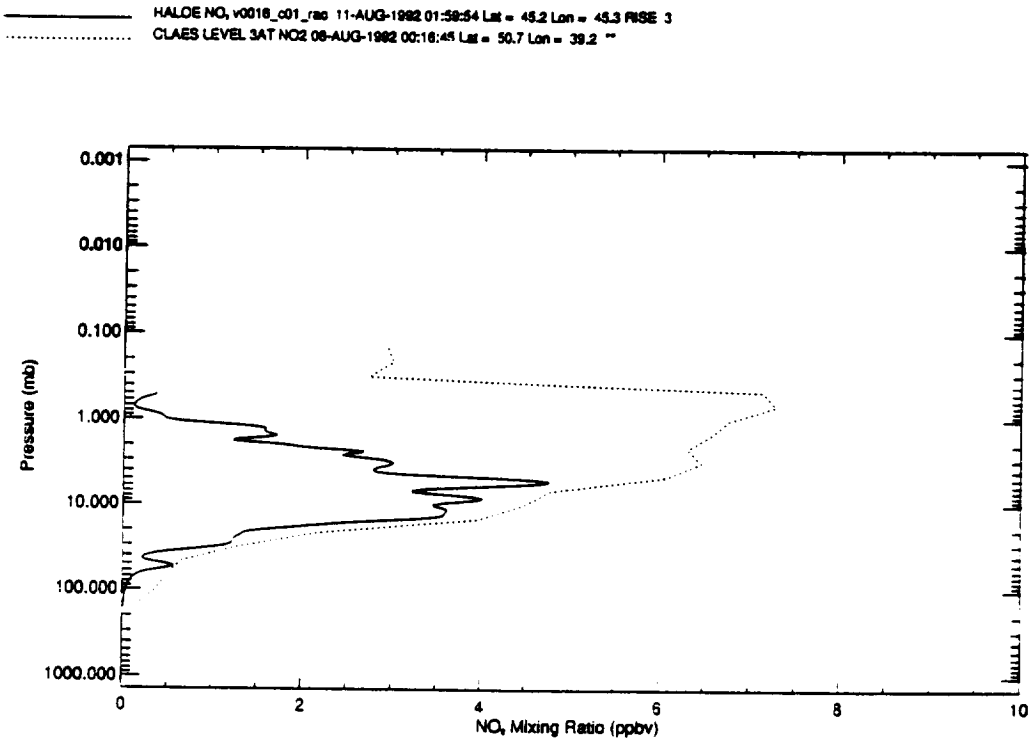

HALOE V16 and CLAES V6 (SZA:75-105) NO_2 Mixing Ratio on 8,11-August-1992

Mon Jul 18 14:46:43 EDT 1994

Figure B-85

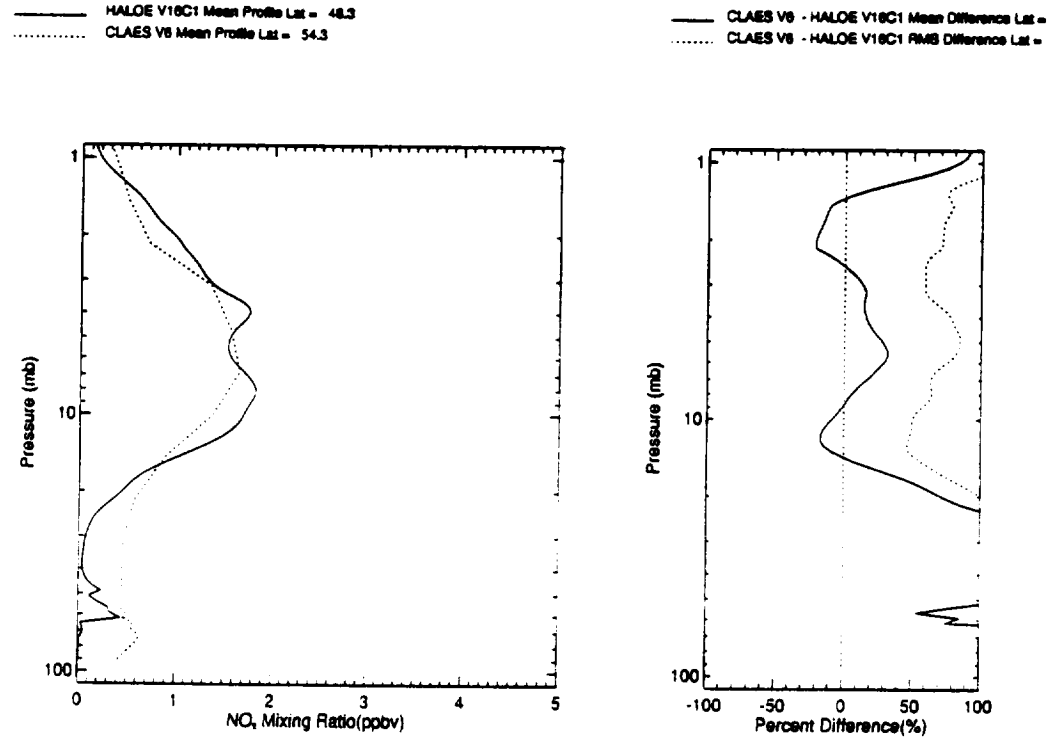

HALOE Sunrise and CLAES V6 (SZA:75-105) NO_2 Mixing Ratio Mean and Difference on 11-January-1992 - 11 Profiles

Mon Jul 18 14:22:98 EDT 1994

Figure B-86

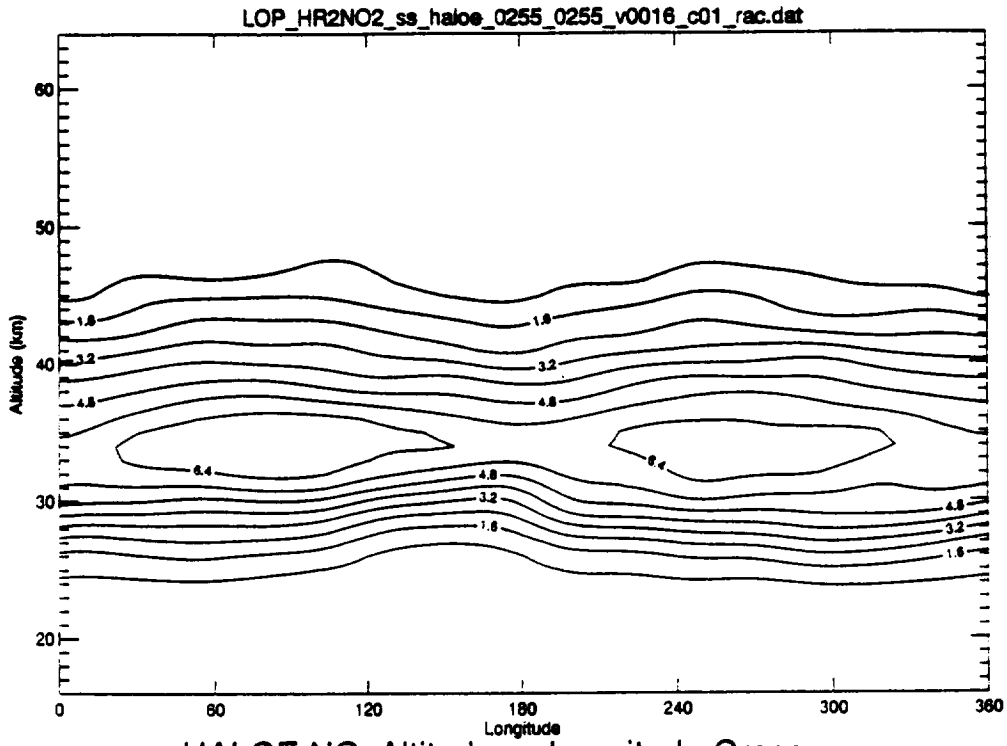

HALOE NO_2 Altitude vs Longitude Cross Section. Sunset on 23-MAY-1992 at 38 S

Figure B-87

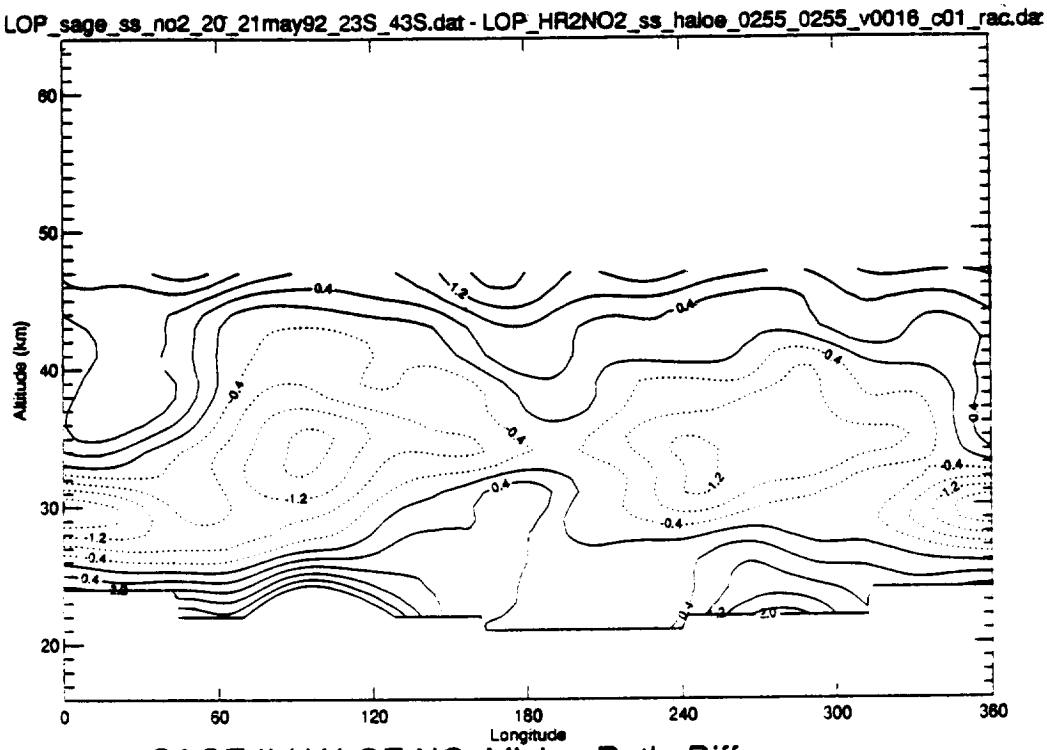

SAGE II-HALOE NO_2 Mixing Ratio Difference on 20-23 MAY 1992

Figure B-88

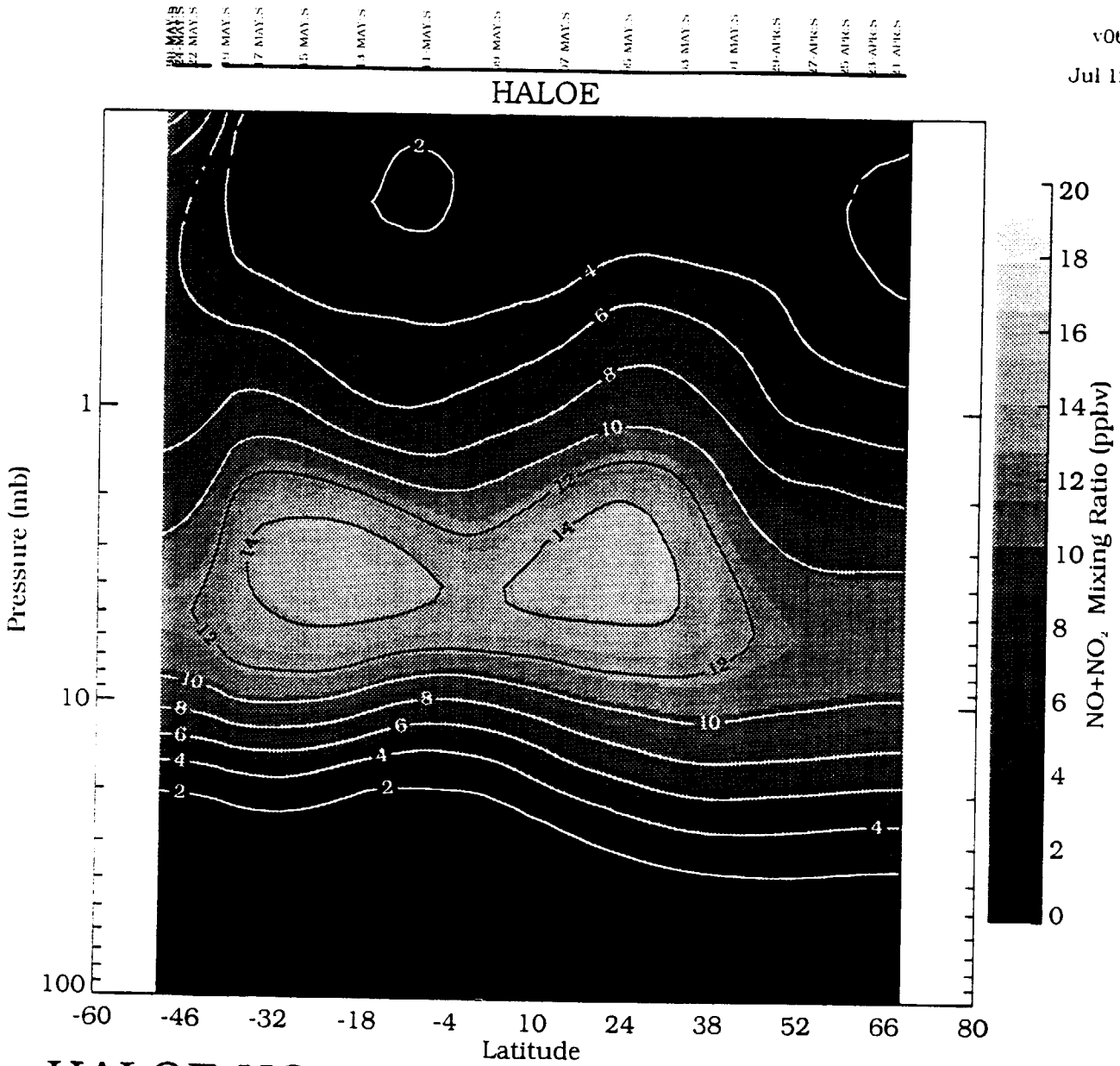

HALOE $NO+NO_2$ Pressure vs Latitude Cross Section, Sunset on 21-APR to 30-MAY-1993

Figure B-89

REPORT DOCUMENTATION PAGE

Form Approved
OMB No. 0704-0188

1. AGENCY USE ONLY *(Leave blank)*	2. REPORT DATE	3. REPORT TYPE AND DATES COVERED
	November 1995	Conference Publication

4. TITLE AND SUBTITLE
Upper Atmosphere Research Satellite Validation Workshop III: Temperature and Constituents Validation

5. FUNDING NUMBERS
RTR 665-70-01-02

6. AUTHOR(S)
William L. Grose and John Gille, Editors

7. PERFORMING ORGANIZATION NAME(S) AND ADDRESS(ES)
NASA Langley Research Center
Hampton, VA 23681-0001

8. PERFORMING ORGANIZATION REPORT NUMBER
L-17535

9. SPONSORING/MONITORING AGENCY NAME(S) AND ADDRESS(ES)
National Aeronautics and Space Administration
Washington, DC 20546-0001

10. SPONSORING/MONITORING AGENCY REPORT NUMBER
NASA CP-3317

11. SUPPLEMENTARY NOTES

12a. DISTRIBUTION/AVAILABILITY STATEMENT
Unclassified–Unlimited

Subject Category 46

12b. DISTRIBUTION CODE

13. ABSTRACT *(Maximum 200 words)*

The Upper Atmosphere Research Satellite (UARS) was launched in September 1991. Since that time data have been retrieved continuously from the various instruments on the UARS spacecraft. These data have been processed by the respective instrument science teams and subsequently archived in the UARS Central Data Handling Facility (CDHF) at the NASA Goddard Space Flight Center, Greenbelt, Maryland.

This report contains the proceedings from one of the three workshops held to evaluate the progress in validating UARS constituents and temperature data and to document the quality of that data. The first workshop was held in Oxford, England, in March 1992, five and one-half months after UARS launch. The second workshop was held in Boulder, Colorado in October 1992. Since launch, the various data have undergone numerous revisions. In many instances these revisions are a result of data problems identified during the validation workshops. Thus, the formal validation effort is a continually ongoing process.

14. SUBJECT TERMS	15. NUMBER OF PAGES
Satellite data; Stratospheric temperature and constituents; Upper atmosphere satellite	649
	16. PRICE CODE: A99

17. SECURITY CLASSIFICATION OF REPORT	18. SECURITY CLASSIFICATION OF THIS PAGE	19. SECURITY CLASSIFICATION OF ABSTRACT	20. LIMITATION OF ABSTRACT
Unclassified	Unclassified	Unclassified	